THE PROCEEDINGS OF THE PHYSICAL SOCIETY

Section A

VOL. 69, PART 1 — 1 January 1956 — No. 433A

EDITORIAL

Sections A and B of the Proceedings

Attention is drawn to a new assignment of papers between Sections A and B of the *Proceedings*. The new subdivision, which will take effect from January 1956, is as follows:

Section A (Physics of Elementary Processes)	Section B (Physics of Collective Processes)
Electrodynamics, Quantum Theory and Theory of Fields.	*Physics (including electron physics) of Solids and Fluids.
Molecular and Atomic Structure.	Thermodynamics and Statistical Mechanics.
Nuclear Physics.	Low Temperature Physics.
High Energy Particles and Cosmic Rays.	Aerodynamics, Hydrodynamics and Acoustics.
Atomic and Nuclear Collisions.	Optics and Electron Optics.
	*Physics of Biological Processes.
	*Astrophysics, Geophysics and Atmospheric Physics.
	*Electric Discharges.

*In certain circumstances where the main emphasis of the paper is on elementary processes a paper on this subject would appear in Section A.

Contributions to the *Proceedings* are divided into three categories: papers, research notes and letters to the editor.

Papers should be as concise as possible, and the publication of very long papers is discouraged. The presentation of work in a numbered series of separate papers is also usually discouraged.

Research Notes are intended for the communication of results where the work reported does not need a full paper. They should not normally exceed 4 printed pages, including diagrams, the equivalent length being about 2000 words if unaccompanied by diagrams.

Letters to the Editor are intended as a means of publication of new work which is of immediate importance to other workers in the field. They should not normally exceed 2 printed pages, including diagrams.

Further details of instructions to authors can be obtained from the Secretary-Editor at the offices of the Society.

The Equations of Motion of Rotating Bodies in General Relativity

By J. H. HAYWOOD
The Physical Laboratories, University of Manchester †

Communicated by L. Rosenfeld ; MS. received 27th May 1955

Abstract. This paper derives the equations of motion of two rotating bodies moving in the weak and quasi-static gravitational field of the bodies up to terms of the order $(v/c)^2$. The analysis is used to obtain the equations of motion of: (*a*) rotating bodies which remain spherically symmetric, (*b*) rotating fluid bodies which become spheroidal in form. In case (*a*) the equations of motion of one body depend directly on the rotation of the second body but not on its own rotation. In case (*b*) the equations of motion of the one body contain terms due to its own rotation which are dependent on its density distribution.

§ 1

Two independent methods have been developed recently for the derivation of the equations of motion of bodies in weak and quasi-static gravitational fields from the field equations of general relativity. The first method developed by Einstein and his co-workers (1938, 1940, 1949) uses the field equations of empty space surrounding the bodies, the bodies themselves being treated as spherically symmetric singularities. The second method introduced by Fock (1939) and later developed by Papapetrou (1951 a) employs the field equations inside the bodies as well as in empty space. This latter method has no restrictions on the symmetry of the bodies and therefore has considerable advantages over the first method.

Papapetrou has determined the equations of motion of spherically symmetric fluid bodies, these equations being identical to those obtained by Einstein and his co-workers. These results have limited application and cannot be used to determine the motion of stellar bodies where the oblateness caused by a rotation of these bodies becomes an important factor. In a relativistic treatment of the motion of rotating stellar bodies we must therefore depart from the assumption of spherical symmetry and develop the second method accordingly.

§ 2

In this section we state the physical assumptions on which the following calculations are based. The method developed by Papapetrou considers a system of bodies moving with velocities which are small compared with the velocity of light and assumes the gravitational field is weak. In addition to these fundamental assumptions we retain the simplifying assumption that the dimensions of the bodies are small compared with their material distances, i.e. if the dimensions are of the order of magnitude of length l and the distances of length L,

$$l \ll L. \qquad \ldots\ldots(2.1)$$

† Now in the Royal Naval Scientific Service.

Condition (2.1) ensures that the form of each body depends only on the conditions appertaining to that body, i.e. the oblateness of a stellar body, will be due only to the proper rotation of that body. We next introduce a new assumption for rotating bodies that the velocity of translation is at least of the same order of magnitude as the velocity of rotation: if we denote by $\dot{a}$ and ω the magnitude of the velocities of translation and rotation respectively, then

$$l\omega \simeq \dot{a}. \qquad \ldots\ldots(2.2)$$

This assumption is introduced so that the fundamental assumption referring to the quasi-static nature of the motion of the bodies is not violated. We shall also make use of the following symmetry properties of the bodies: (i) each body has axial symmetry about its axis of rotation; (ii) each body is symmetric with respect to the plane passing through the mass-centre normal to the axis of rotation. These symmetry properties also belong to both the mass density and the stress tensor of the bodies.

In the present paper we shall retain the coordinate condition†

$$\mathfrak{g}^{\mu\nu}{}_{,\nu}=0 \qquad \ldots\ldots(2.3)$$

so that the field equations given by Papapetrou can be adapted immediately to the case of the rotating bodies. The physical meaning of the coordinate condition is not at all clear and has been discussed from different viewpoints by Einstein and Infeld (1949) and Papapetrou (1951 b). According to the current interpretation of general relativity Infeld and Scheidegger (1951) have shown the equations of motion obtained by choosing different coordinate conditions are physically identical and merely different mathematical representations of the motion in different coordinate systems.

§ 3

In the following calculations the notation of Papapetrou (1951 a, to be referred to as I) is used throughout unless defined otherwise. We consider a system of discrete rotating bodies, the mass density of the body a being denoted by ρ_a. The velocity components of an element at x^i inside the body a are of the form

$$v_a{}^i=\dot{a}^i+\epsilon_{imk}\omega_a{}^m(x^k-a^k) \qquad \ldots\ldots(3.1)$$

where a^i is the spatial component of the centre of mass of the body and $\omega_a{}^m$ is the component of rotation about the axis x^m. ϵ_{imk} is the well known three-dimensional antisymmetric tensor, such that $\epsilon_{123}=\epsilon_{312}=\epsilon_{231}=1$, $\epsilon_{132}=-\epsilon_{123}$, etc. and is zero if any indices i, m, k are identical. We next take for the leading terms in $\mathfrak{T}_\nu^\mu$

$$\left.\begin{aligned} \mathfrak{T}_0{}^0&=\sum_a \rho_a c & \mathfrak{T}_i{}^0&=-\sum_a \rho_a v_a{}^i/c \\ \mathfrak{T}_0{}^k&=\sum_a \rho_a c v_a{}^k & \mathfrak{T}_i{}^k&=-\sum_a \rho_a v_a{}^i v_a{}^k/c-\sum_a p_a{}^{ik}/c \end{aligned}\right\} \qquad \ldots\ldots(3.2)$$

where $p_a{}^{ik}$ is the three-dimensional stress tensor of the body a.

Following the procedure in I the field equations in the first approximation are

$$U^{00}{}_{,ss}=\Delta U^{00}=-4\pi G\sum_a \rho_a \qquad U^{0k}{}_{,ss}=\Delta U^{0k}=-4\pi G\sum_a \rho_a v_a{}^k. \qquad \ldots\ldots(3.3)$$

With the help of (3.1) the solution of (3.3) is

$$U^{00}=\sum_a u_a \qquad U^{0k}=\sum_a (u_a \dot{a}^k+\epsilon_{kmn}\omega_a{}^m y_a{}^n) \qquad \ldots\ldots(3.4)$$

† As usual Latin indices take the values 1, 2, 3 only while Greek indices take the values 1, 2, 3 and 0.

with u_a and $y_a{}^n$ fulfilling the equations

$$\Delta u_a = -4\pi G\rho_a \quad \Delta y_a{}^n = -4\pi G\rho_a(x^n - a^n). \qquad \text{.....(3.5)}$$

We have for the dynamical equation up to the same approximation

$$\left.\begin{aligned} &\frac{d\rho_a}{dt} = 0 \\ &\frac{\partial}{\partial t}(\rho_a v_a{}^i) + (\rho_a v_a{}^i v_a{}^k)_{,k} + p_a{}^{ik}{}_{,k} = \rho_a U^{00}{}_{,i} \end{aligned}\right\} \qquad \text{.....(3.6)}$$

Because of (3.1) and (3.4) and by virtue of condition (2.1) equations (3.6) lead to the expressions

$$\left.\begin{aligned} &\ddot{a}^i = \sum_b (u_{b,i})_a \\ &p_a{}^{ik}{}_{,k} = \rho_a u_{a,i} + \rho_a \omega_a{}^k \omega_a{}^k x_a{}^i - \rho_a \omega_a{}^i \omega_a{}^k x_a{}^k - \rho_a \epsilon_{imk} \dot{\omega}_a{}^m x_a{}^k \end{aligned}\right\} \qquad \text{.....(3.7)}$$

with $x_a{}^k = (x^k - a^k)$. The summation Σ_b extends over all bodies except the body a and $(u_{b,i})_a$ refers to the value of $u_{b,i}$ at the centre of the body a. The first formulae in (3.7) are just the Newtonian equations of motion. The second formula is a condition determining the stress tensor inside each body. $\mathfrak{T}^{ik}$ must be symmetric in the indices i, k and we find, using the metric g^{mr} and (3.2) that $p_a{}^{ik}$ is also symmetric. This restriction on $p_a{}^{ik}$ and the symmetry properties of the body are used in Appendix 1 to obtain the results

$$\left.\begin{aligned} &\dot{\omega}_a{}^m = 0 \\ &p_a{}^{ik}{}_{,k} = \rho_a u_{a,i} + \rho_a \omega_a{}^k \omega_a{}^k x_a{}^i - \rho_a \omega_a{}^i \omega_a{}^k x_a{}^k \end{aligned}\right\} \qquad \text{.....(3.8)}$$

the first equation showing that the rotation of the bodies is constant. In Appendix 1 we also obtain an integral which we shall require in the next section,

$$\int_a p_a{}^{ik} dV = -\int_a \rho_a \{u_{a,i} x_a{}^k + \omega_a{}^m \omega_a{}^m x_a{}^i x_a{}^k - \omega_a{}^i \omega_a{}^m x_a{}^m x_a{}^k\}\, dV. \qquad \text{.....(3.9)}$$

§ 4

In this section we shall repeat the procedure in I in order to calculate the equations of motion from rotating bodies up to the second approximation. These equations of motion for the body a are obtained by integrating the dynamical equation over the volume of the body a, i.e.

$$\left.\begin{aligned} \frac{d}{dt}\int_a \mathfrak{T}^0 dV = &\int_a (\mathfrak{T}_s{}^s - \mathfrak{T}_0{}^0) U^{00}{}_{,i}\, dV + \frac{4}{c^2}\int_a \mathfrak{T}_0{}^k U^{0k}{}_{,i}\, dV \\ &- \frac{1}{c^2}\int_a \mathfrak{T}_0{}^0 (S^{kk} + S^{00} - 2U^{00}U^{00})_{,i}\, dV. \end{aligned}\right\} \qquad \text{.....(4.1)}$$

The $\mathfrak{T}_r{}^\mu$ in (4.1) contain first- and second-order terms and are determined by repeating the calculations in I using (3.1) for the velocity and retaining the general stress tensor $p_a{}^{ik}$. We find

$$\left.\begin{aligned} \mathfrak{T}_0{}^0 &= \sum_a \rho_a c \left(1 + \frac{v_a{}^2}{2c^2} - \frac{U^{00}}{c^2} + \frac{u_a}{2c^2}\right) \\ \mathfrak{T}_0{}^k &= \sum_a \rho_a c v_a{}^k \left(1 + \frac{v_a{}^2}{2c^2} - \frac{U^{00}}{c^2} + \frac{u_a}{2c^2}\right) + \sum_a p_a{}^{ks} \frac{v_a{}^s}{c} \\ \mathfrak{T}_i{}^0 &= -\frac{\mathfrak{T}_0{}^i}{c^2} - \frac{4}{c^3}\sum_a \rho_a (U^{00} v_a{}^i - U^{0i}) \\ \mathfrak{T}_i{}^k &= -\sum_a \rho_a v_a{}^i \frac{v_a{}^k}{c} - \sum_a \frac{p_a{}^{ik}}{c} \end{aligned}\right\} \qquad \text{.....(4.2)}$$

with $$d\rho_a/dt=0 \text{ and } v_a^2=v_a^s v_a^s. \qquad \ldots\ldots(4.3)$$

ρ_a in (4.2) and (4.3) is a different quantity from ρ_a in (3.2). We shall consider ρ_a in (4.2) and (4.3) as the first-order term in the expression for the mass density.

We shall now give some preliminary results which will be used in the subsequent claculations. For simplicity we shall henceforth consider the motion of two bodies only, i.e. the bodies a and b. Functions representing contributions to the field from the body b in the immediate neighbourhood of the body a are developed as a power series around the centre of mass of the body a,

$$\left.\begin{aligned} u_b &= U_a + U_{a,k}x_a^k + \ldots \\ y_b^i &= Y_a^i + Y_{a,k}^i x_a^k + \ldots \end{aligned}\right\} \qquad \ldots\ldots(4.4)$$

where $U_a=(u_b)_a$ $U_{a,k}=(u_{b,k})_a$ $Y_a^i=(y_b^i)_a$ $Y_{a,k}^i=(y_{b,k}^i)_a$. We shall find that the omitted terms in (4.4) are of no importance in this approximation because of condition (2.1). From the symmetry properties of the bodies we also find

$$\left.\begin{aligned} &\int_a \rho_a x_a^i dV=0 \\ &\int_a \rho_a x_a^i x_a^m x_a^n dV=0 \end{aligned}\right\} \qquad \ldots\ldots(4.5)$$

and†

$$\int_a p_a^{ik} x_a^m dV=0. \qquad \ldots\ldots(4.6)$$

From (4.3) we see that the bodies themselves are in a stationary state and therefore

$$\left.\begin{aligned} &\frac{d}{dt}\int_a \rho_a dV=0 && \frac{d}{dt}\int_a \rho_a u_a dV=0 \\ &\frac{d}{dt}\int_a \rho_a x_a^i x_a^k dV=0 && \frac{d}{dt}\int_a \rho_a u_a x_a^i dV=0 \\ &\frac{d}{dt}\int_a p_a^{ik} dV=0 && \frac{d}{dt}\int_a \rho_a y_a^i dV=0. \end{aligned}\right\} \qquad \ldots\ldots(4.7)$$

We also find by direct calculation

$$\frac{dU_a}{dt}=U_{a,s}(\dot{a}^s-\dot{b}^s), \qquad \frac{dY_a^i}{dt}=Y_{a,k}^i(\dot{a}^k-\dot{b}^k). \qquad \ldots\ldots(4.8)$$

Taking into account (4.2) to (4.8) and the conditions (2.1) and (2.2) we find‡

$$\begin{aligned} \frac{d}{dt}\int_a \mathfrak{H}^0 dV = &-\frac{\ddot{a}^i}{c}\int_a \rho_a dV + \frac{\ddot{a}^i}{2c^3}\int_a \rho_a u_a dV - \frac{\ddot{a}^s}{c^3}\int_a p_a^{si} dV - \frac{\ddot{a}^i}{2c^3}\omega_a{}^s\omega_a{}^s\int_a \rho_a r_a{}^2 dV \\ &+\frac{1}{c^3}\{(4\dot{b}^i-3\dot{a}^i)(\dot{a}^s-\dot{b}^s)U_{a,s}+(\ddot{a}^i-\ddot{b}^i)U_a-\tfrac{1}{2}\ddot{a}^i\dot{a}^s\dot{a}^s-\ddot{a}^s\dot{a}^s\dot{a}^i\}\int_a \rho_a dV \\ &+\frac{1}{c^3}\{\ddot{a}^s\omega_a{}^m\omega_a{}^p\epsilon_{imn}\epsilon_{skp}+\tfrac{1}{2}\ddot{a}^i\omega_a{}^n\omega_a{}^k\}\int_a \rho_a x_a^n x_a^k dV. \qquad \ldots\ldots(4.9) \end{aligned}$$

† This result is proved by taking

$$2\int_a p_a{}^{ik}x_a{}^m dV=\int_a p_a{}^{ms}{}_s x_a{}^i x_a{}^k dV-\int_a p_a{}^{ks}{}_{,s}x_a{}^i x_a{}^m dV-\int_a p_a{}^{is}{}_{,s}x_a{}^k x_a{}^m dV$$

substituting from (3.8) and integrating with the help of (4.5).

‡ In these calculations we use a result derived in appendix 2 according to which $U_a\simeq 1/L, Y_a{}^i\simeq(l/L)^2$. We omit all terms of the order $(l/L)^3$ and higher order terms.

$$\frac{1}{c^2}\int_a (\mathfrak{T}_a{}^s - \mathfrak{T}_0{}^0)U^{00}{}_{,i}dV$$
$$= -\frac{U_{a,i}}{c}\int_a \rho_a dV - \frac{1}{c}\int_a \rho_a u_{a,i}dV + \frac{U_{a,i}}{2c^3}\int_a \rho_a u_a dV - \frac{U_{a,s}}{c^3}\int_a p_a{}^{ss}dV$$
$$- \frac{1}{c^3}\{\tfrac{3}{2}\dot{a}^s\dot{a}^s U_{a,i} - U_a U_{a,i}\}\int_a \rho_a dV + \frac{1}{c^3}\{U_{a,n} - 3\dot{a}^s\epsilon_{smn}\omega_a{}^m\}\int_a \rho_a u_{a,i}x_a{}^n dV$$
$$+ \frac{U_a}{c^3}\int_a \rho_a u_{a,i}dV - \frac{3\dot{a}^s\dot{a}^s}{2c^3}\int_a \rho_a u_{a,i}dV - \frac{1}{c^3}\int_a p_a{}^{ss}u_{a,i}dV + \frac{1}{2c^3}\int_a \rho_a u_a u_{a,i}dV$$
$$+ \frac{3}{2c^3}\omega_a{}^s\omega_a{}^n U_{a,i}\int_a \rho_a x_a{}^s x_a{}^n dV - \frac{3}{2c^3}\omega_a{}^s\omega_a{}^s U_{a,i}\int_a \rho_a r_a{}^2 dV$$
$$+ \frac{3}{2c^3}\omega_a{}^s\omega_a{}^n\int_a \rho_a u_{a,i}x_a{}^s x_a{}^n dV - \frac{3}{2c^3}\omega_a{}^s\omega_a{}^s\int_a \rho_a u_{a,i}r_a{}^2 dV. \quad \ldots\ldots(4.10)$$

$$\frac{1}{c^4}\int_a \mathfrak{T}_0{}^s U^{0s}{}_{,i}dV = \frac{\dot{a}^s\dot{b}^s}{c^3}U_{a,i}\int_a \rho_a dV + \frac{\dot{a}^s}{c^3}\epsilon_{smn}\omega_a{}^m\int_a \rho_a y_a{}^n{}_{,i}dV$$
$$+ \frac{\dot{a}^s\dot{a}^s}{c^3}\int_a \rho_a u_{a,i}dV + \frac{\omega_a{}^s\omega_a{}^s}{c^3}\int_a \rho_a x_a{}^n y_a{}^n{}_{,i}dV$$
$$- \frac{\omega_a{}^s\omega_a{}^n}{c^3}\int_a \rho_a x_a{}^n y_a{}^s{}_{,i}dV + \frac{\dot{a}^s}{c^3}\epsilon_{smn}\omega_a{}^m\int_a \rho_a x_a{}^n u_{a,i}dV \quad \ldots\ldots(4.11)$$

where $r_a{}^2 = x_a{}^s x_a{}^s$. With the help of the field equations in I we obtain

$$-\frac{1}{c^4}\int_a (S^{kk} + S^{00} - 2U^{00}U^{00})_{,i}\mathfrak{T}_0{}^0 dV$$
$$= \frac{1}{c^3}\Big\{-\tfrac{3}{2}U_{a,i}\dot{b}^s\dot{b}^s + U_b U_{a,i} + \frac{(T_{b,i})_a}{2} - (F_{b,i})_a - (P_{b,i})_a - \tfrac{3}{2}\omega_b{}^s\omega_b{}^s(W_{b,i})_a$$
$$+ \tfrac{3}{2}\omega_b{}^m\omega_b{}^n(Z_b{}^{mn}{}_{,i})_a\Big\}\int_a \rho_a dV + \frac{1}{c^3}\Big\{U_a - \frac{3\dot{a}^s\dot{a}^s}{2}\Big\}\int_a \rho_a u_{a,i}dV$$
$$+ \frac{1}{2c^3}\int_a \rho_a T_{a,i}dV - \frac{1}{c^3}\int_a \rho_a F_{a,i}dV + \frac{1}{c^3}\{U_{a,n} - 3\dot{a}^s\epsilon_{smn}\omega_a{}^m\}\int_a \rho_a y_a{}^n{}_{,i}dV$$
$$- \frac{1}{c^3}\int_a \rho_a P_{a,i}dV - \frac{3}{2c^3}\omega_a{}^s\omega_a{}^s\int_a \rho_a W_{a,i}dV + \frac{3}{2c^3}\omega_a{}^m\omega_a{}^n\int_a \rho_a Z_a{}^{mn}{}_{,i}dV$$
$$\ldots\ldots(4.12)$$

where
$$\left.\begin{aligned} \Delta u_a &= -4\pi G\rho_a & \Delta W_a &= -4\pi G\rho_a r_a{}^2 \\ \Delta y_a{}^k &= -4\pi G\rho_a x_a{}^k & \Delta Z_a{}^{mn} &= -4\pi G\rho_a x_a{}^m x_a{}^n \\ \Delta T_a &= -4\pi G\rho_a u_a & \Delta P_a &= -4\pi G p_a{}^{ss} \end{aligned}\right\} \quad \ldots\ldots(4.13)$$

and
$$\Delta F_a = u_{a,00} = u_{a,mn}v_a{}^m v_a{}^n + u_{a,m}v_a{}^m{}_{,n}v_a{}^n - u_{a,m}v_a{}^m{}_{,0}. \quad \ldots\ldots(4.14)$$

In Appendix 2 we solve equations (4.13) and (4.14) outside the body a and find to our approximation

$$U_a = \frac{G}{r_{ab}}\int_b \rho_b^s dV \qquad U_b = \frac{G}{r_{ab}}\int_a \rho_a dV$$
$$U_{0,i} = G\frac{\partial}{\partial a^i}\left(\frac{1}{r_{ab}}\right)\int_b \rho_b dV \qquad (T_{b,i})_a = G\frac{\partial}{\partial a^i}\left(\frac{1}{r_{ab}}\right)\int_b \rho_b u_b dV$$
$$(W_{b,i})_a = G\frac{\partial}{\partial a^i}\left(\frac{1}{r_{ab}}\right)\int_b \rho_b r_b{}^2 dV \qquad (Z_b{}^{mn}{}_{,i})_a = G\frac{\partial}{\partial a^i}\left(\frac{1}{r_{ab}}\right)\int_b \rho_b x_b{}^m x_b{}^n dV$$
$$(P_{b,i})_a = G\frac{\partial}{\partial a^i}\left(\frac{1}{r_{ab}}\right)\int_b p_b{}^{ss}dV \qquad (F_{b,i})_a = \frac{G}{2}\left\{\dot{b}^m\dot{b}^n\frac{\partial^3 r_{ab}}{\partial a^i\partial a^m\partial a^n} - \ddot{b}^m\frac{\partial^2 r_{ab}}{\partial a^i\partial a^m}\right\}$$
$$\ldots\ldots(4.15)$$

where $r_{ab}^2=(a^s-b^s)(a^s-b^s)$.

Using the lemma of Appendix 3 we have the relations

$$\int_a \rho_a u_{a,i}dV=0 \qquad \int_a \rho_a\{T_{a,i}+u_a u_{a,i}\}dV=0$$

$$\int_a \rho_a x_a^s y_{a,i}^s dV=0 \qquad \int_a \rho_a\{W_{a,i}+r_a^2 u_{a,i}\}dV=0$$

$$\int_a \rho_a\{x_a^s y_{a,i}^n+x_a^n y_{a,i}^s\}dV=0 \qquad \int_a \rho_a\{Z_a^{mn}{}_{,i}+x_a^m x_a^n u_{a,i}\}dV=0$$

$$\int_a \rho_a\{y_{a,i}^s+x_a^s u_{a,i}\}dV=0 \qquad \int_a \{\rho_a P_{a,i}+p_a^{ss}u_{a,i}\}dV=0$$

$$\int_a \{\rho_a F_{a,i}-\frac{1}{4\pi G}u_{a,i}u_{a,00}\}dV=0. \qquad \text{.....(4.16)}$$

We also have the relation

$$\frac{\partial^2 r_{ab}}{\partial a^i \partial a^k}=\frac{\delta_{ik}}{r_{ab}}-\frac{(a^i-b^i)(a^k-b^k)}{r_{ab}^3}. \qquad \text{.....(4.17)}$$

Introducing (4.9) to (4.12) in (4.1) and using (4.15), (4.16) and (4.17) we obtain the equations of motion in the form

$$\begin{aligned}
&\left\{\ddot{a}^i-GM_b\frac{\partial}{\partial a^i}\left(\frac{1}{r_{ab}}\right)\right\}c^2GM_a\\
&=GM_a\left\{GM_b\left(\dot{a}^k\dot{a}^k+\tfrac{3}{2}\dot{b}^k\dot{b}^k-4\dot{a}^k\dot{b}^k-\frac{4GM_b}{r_{ab}}-\frac{5GM_a}{r_{ab}}\right)\frac{\partial}{\partial a^i}\left(\frac{1}{r_{ab}}\right)\right.\\
&\quad\left.+GM_b(4\dot{b}^i\dot{a}^k-4\dot{a}^i\dot{a}^k+3\dot{a}^i\dot{b}^k-4\dot{b}^i\dot{b}^k)\frac{\partial}{\partial a^k}\left(\frac{1}{r_{ab}}\right)+\frac{GM_b}{2}\dot{b}^k\dot{b}^s\frac{\partial^3 r_{ab}}{\partial a^i\partial a^k\partial a^s}\right\}\\
&\quad+GM_a\frac{\partial}{\partial a^i}\left(\frac{1}{r_{ab}}\right)\left\{\int_b p_b^{ss}dV-\tfrac{1}{2}\int_b p_b u_b dV+\tfrac{3}{2}\omega_b{}^s\omega_b{}^s\int_b \rho_b r_b^2 dV\right.\\
&\quad\left.-\tfrac{3}{2}\omega_b{}^s\omega_b{}^n\int_b \rho_b x_b^s x_b^n dV\right\}-G^2M_b\frac{\partial}{\partial a^s}\left(\frac{1}{r_{ab}}\right)\int_a p_a^{is}dV+G^2M_b\frac{\partial}{\partial a^i}\left(\frac{1}{r_{ab}}\right)\\
&\quad\times\left\{\int_a p_a^{ss}dV+\omega_a{}^s\omega_a{}^s\int_a \rho_a r_a{}^2dV\right\}-G^2M_b\left\{\omega_a{}^k\omega_a{}^m\epsilon_{skl}\epsilon_{imn}\frac{\partial}{\partial a^s}\left(\frac{1}{r_{ab}}\right)\right.\\
&\quad\left.+\omega_a{}^n\omega_a{}^l\frac{\partial}{\partial a^l}\left(\frac{1}{r_{ab}}\right)\right\}\int_a \rho_a x_a^n x_a^l dV+\frac{1}{4\pi}\int_a u_{a,i}u_{a,00}dV \qquad \text{.....(4.18)}
\end{aligned}$$

where $M_a=\int_a \rho_a dV$ is the leading term in the mass of the body a. The Newtonian approximation has been used in (4.18) for eliminating the quantities $\ddot{a}^i$ and $\ddot{b}^i$ in second order terms.

§ 5

The final step for the derivation of the equations of motion of rotating bodies in the second approximation is to define the conditions under which each body rotates and then evaluate the remaining integrals in (4.18). We shall investigate two cases. In the first case we shall examine the motion of rotating bodies which remain spherically symmetric. Such bodies cannot consist of matter in a fluid state and spherical symmetry must be ensured by a stress distribution $p_a{}^{ik}$ satisfying condition (3.8). In the second case we shall consider rotating bodies which consist of matter in a fluid state, the stress–strain tensor reducing to a

hydrostatic pressure, i.e. $p_a{}^{ik}=\delta_{ik}p_a$. Each body is in a stationary state and the form of the bodies will be a spheroidal one, in which the oblateness is due to a proper rotation of the body.

5.1. *Rotating Bodies with Spherical Symmetry*

Because of spherical symmetry of the bodies, the density ρ_a at a point inside the body a will be a function of the distance r_a between this point and the centre of the body a,

$$\rho_a=\rho_a(r_a). \qquad \ldots\ldots(5.1)$$

From (5.1) and (3.5) we see that u_a is a function of r_a only. For any such function $f(r_a)$ we have the relations

$$\left.\begin{aligned}\int_a f(r_a)x_a{}^i dV&=0\\ \int_a f(r_a)x_a{}^i x_a{}^k dV&=\frac{\delta_{ik}}{3}\int_a f(r_a)r_a{}^2 dV\end{aligned}\right\} \qquad \ldots\ldots(5.2)$$

therefore condition (3.9) reduces to

$$\int_a p_a{}^{ik}dV=-\frac{\delta_{ik}}{3}\int_a \rho_a\frac{\partial u_a}{\partial r_a}r_a dV-\frac{\delta_{ik}}{3}\omega_a{}^s\omega_a{}^s\int_a \rho_a r_a{}^2 dV+\frac{\omega_a{}^i\omega_a{}^k}{3}\int_a \rho_a r_a{}^2 dV. \qquad \ldots\ldots(5.3)$$

The next step is the evaluation of the integral

$$\frac{1}{4\pi}\int_a u_{a,i}u_{a,00}dV$$

in (4.18). From (4.14) we have

$$u_{a,00}=\frac{1}{r_a}\frac{\partial}{\partial r_a}\left(\frac{1}{r_a}\frac{\partial u_a}{\partial r_a}\right)x_a{}^s x_a{}^n\dot{a}^s\dot{a}^n+\frac{1}{r_a}\frac{\partial u_a}{\partial r_a}\dot{a}^s\dot{a}^s-\frac{1}{r_a}\frac{\partial u_a}{\partial r_a}x_a{}^s\ddot{a}^s \qquad \ldots(5.4)$$

in which all terms due to the rotation have vanished. Using (5.2) the integral becomes

$$\frac{1}{4\pi}\int_a u_{a,i}u_{a,00}dV=-\frac{\ddot{a}^i}{12\pi}\int_a\left(\frac{\partial u_a}{\partial r_a}\right)^2 dV=-\frac{\ddot{a}^i G}{3}\int_a \rho_a u_a dV \qquad \ldots\ldots(5.5)$$

the last relation following from Appendix IV of I.

After some simple calculations using equations (5.3) and (5.5) in (4.18) the equations of motion finally become

$$\begin{aligned}&\left\{\ddot{a}^i-GM_b\frac{\partial}{\partial a^i}\left(\frac{1}{r_{ab}}\right)\right\}\\ &=\frac{1}{c^2}\left\{GM_b\left(\dot{a}^k\dot{a}^k+\tfrac{3}{2}\dot{b}^k\dot{b}^k-4\dot{a}^k\dot{b}^k-\frac{4GM_b}{r_{ab}}-\frac{5GM_a}{r_{ab}}\right)\frac{\partial}{\partial a^i}\left(\frac{1}{r_{ab}}\right)\right.\\ &\quad+GM_b(4\dot{b}^i\dot{a}^k-4\dot{a}^i\dot{a}^k+3\dot{a}^i\dot{b}^k-4\dot{b}^i\dot{b}^k)\frac{\partial}{\partial a^k}\left(\frac{1}{r_{ab}}\right)\\ &\quad\left.+\frac{GM_b}{2}\dot{b}^k\dot{b}^s\frac{\partial^2 r_{ab}}{\partial a^i\partial a^k\partial a^s}\right\}+\frac{GA_b}{2c^2}\omega_b{}^s\omega_b{}^s\frac{\partial}{\partial a^i}\left(\frac{1}{r_{ab}}\right) \qquad \ldots\ldots(5.6)\end{aligned}$$

where $A_b=\frac{2}{3}\int_b\rho_b r_b{}^2 dV$ is the moment of inertia of the body b about any axis.

5.2. *Rotating Spheroidal Bodies*

The bodies will consist of matter in a fluid state with internal hydrostatic pressure $p_a(p_a{}^{ik}=\delta_{ik}p_a)$. Without loss of generality we shall assume the body a

rotates about an axis x_a^3 with angular velocity $\omega_a{}^3=\omega_a$, $\omega_a{}^1=\omega_a{}^2=0$. Equations (3.8) and (3.9) for body a reduce to

$$p_{a,i}=\rho_a u_{a,i}+\rho_a(\omega_a)^2(x_a{}^i-\delta_{i3}x_a{}^3) \qquad \ldots\ldots(5.7)$$

and

$$\int_a p_a dV=-\frac{1}{3}\int_a \rho_a u_{a,s}x_a{}^s dV-(\omega_a)^2\int_a \rho_a r_a{}^2 dV+\frac{(\omega_a)^2}{3}\int_a \rho_a x_a{}^3 x_a{}^3 dV. \qquad \ldots\ldots(5.8)$$

Equation (5.7) is just the condition for equilibrium of a fluid body in a stationary state, rotating about axis $x_a{}^3$ and is equivalent to a single total differential equation (Jeffreys 1924),

$$dp_a=\rho_a d\psi_a \qquad \psi_a=u_a+\tfrac{1}{2}(\omega_a)^2(x_a{}^1x_a{}^1+x_a{}^2x_a{}^2) \qquad \ldots\ldots(5.9)$$

with p_a, ρ_a functions of ψ_a only, and ψ_a is constant over the free surface of the body a and over all strata of equal density. The departure from spherical symmetry is described through the equation

$$r_a=s_a\{1+\epsilon_a(\tfrac{1}{3}-\cos^2\theta)\} \qquad \ldots\ldots(5.10)$$

where $\epsilon_a(s_a)$ is the ellipticity of a stratum of mean radius s_a and θ is defined by the spherical polar coordinates

$$x_a{}^1=r_a\sin\theta\sin\chi, \qquad x_a{}^2=r_a\sin\theta\cos\chi, \qquad x_a{}^3=r_a\cos\theta.$$

The density ρ_a inside the body a is a function of s_a only, $\rho_a=\rho_a(s_a)$.

Neglecting terms of the order $\epsilon_a{}^2$ and higher order, the solution of (3.5) is

$$\left.\begin{aligned} u_a=&\frac{4\pi G}{r_a}\int_0^{s_a}\rho_a s_a{}^2 ds_a+4\pi G\int_{s_a}^{\infty}\rho_a s_a ds_a+\frac{4\pi G}{5}(\tfrac{1}{3}-\cos^2\theta)\\ &\times\left\{\frac{1}{r_a{}^3}\int_0^{s_a}\rho_a\frac{d}{ds_a}(\epsilon_a s_a{}^5)ds_a+r_a{}^2\int_{s_a}^{\infty}\rho_a\frac{d\epsilon_a}{ds_a}ds_a\right\}\end{aligned}\right\} \qquad \ldots\ldots(5.11)$$

with the rotation related to the ellipticity by the equation

$$\frac{\epsilon_a}{s_a}\int_0^{s_a}\rho_a s_a{}^2 ds_a-\frac{1}{5s_a{}^3}\int_0^{s_a}\rho_a\frac{d}{ds_a}(\epsilon_a s_a{}^5)ds_a-\frac{s_a{}^2}{5}\int_{s_a}^{\bar{s}_a}\rho_a\frac{d\epsilon_a}{ds_a}ds_a=\frac{(\omega_a)^2 s_a{}^2}{8\pi G} \qquad \ldots\ldots(5.12)$$

where $\bar{s}_a$ is the mean radius of the body a.† In the final calculations we shall need the following relations which are derived using (5.11) in Appendices 4 and 5:

$$\begin{aligned}&\frac{1}{4\pi}\int_a u_{a,i}u_{a,00}dV\\ &=-\frac{\ddot{a}^i}{3}\int_0^{\bar{s}_a}\left\{\frac{4\pi G}{s_a}\int_0^{s_a}\rho_a s_a{}^2 ds_a\right\}^2 ds_a+\frac{2\ddot{a}^s}{45}(3\delta_{i3}\delta_{s3}-\delta_{is})\int_0^{\bar{s}_a}\left\{4\pi G\int_0^{s_a}\rho_a s_a{}^2 ds_a\right\}\\ &\times\left\{4\pi G\frac{d}{ds_a}\left(\frac{\epsilon_a}{s_a}\right)\int_0^{s_a}\rho_a s_a{}^2 ds_a-8\pi G s_a\int_{s_a}^{\infty}\rho_a\frac{d\epsilon_a}{ds_a}ds_a\right\}ds_a \qquad \ldots\ldots(5.13)\end{aligned}$$

$$\int_a \rho_a u_a dV=-2\int_a \rho_a u_{a,s}x_a{}^s dV=\frac{1}{G}\int_0^{\bar{s}_a}\left\{\frac{4\pi G}{s_a}\int_0^{s_a}\rho_a s_a{}^2 ds_a\right\}^2 ds_a. \qquad \ldots\ldots(5.14)$$

We now consider the terms

$$\int_b p_b dV-\tfrac{1}{2}\int_b \rho_b u_b dV+\tfrac{3}{2}\omega_b{}^s\omega_b{}^s\int_b \rho_b r_b{}^2 dV-\tfrac{3}{2}\omega_b{}^s\omega_b{}^n\int_b \rho_b x_b{}^s x_b{}^n dV$$

† (5.11) is obtained from Jeffreys (1924), p. 184, eqns 4 and 5, by taking the spherical harmonic $Y_2=\epsilon_a(\frac{1}{3}-\cos^2\theta)$ only. (5.12) is given by Jeffreys on p. 190.

appearing on the right-hand side of (4.18), which with the help of (3.9) become

$$-\int_b \rho_b u_{b,s} x_b{}^s dV - \tfrac{1}{2}\int_b \rho_b u_b dV + \frac{\omega_b{}^s \omega_b{}^s}{2}\int_b \rho_b r_b{}^2 dV - \frac{\omega_b{}^s \omega_b{}^n}{2}\int_b \rho_b x_b{}^s x_b{}^n dV. \quad \ldots\ldots(5.15)$$

Next we assume that the body b rotates about some axis $x_b{}^{3'}$ in a spatial system $x_b{}^{i'}$ with an angular velocity $\omega_b{}'$. The spatial system $x_b{}^{i'}$ is related to the original system $x_b{}^i$ by direction cosines l_{mn} where $x_b{}^{i'} = l_{ik} x_b{}^k$, $\omega_b{}' = l_{3k}\omega_b{}^k$. Then ρ_b is a function of $s_b{}'$ the mean radius of a stratum of body b, only. Remembering that $l_{is} l_{ks} = \delta_{ik}$ a simple transformation gives

$$-\int_b \rho_b \frac{\partial u_b}{\partial x^s} x_b{}^{s'} dV - \tfrac{1}{2}\int_b \rho_b u_b dV + \frac{(\omega_b{}')^2}{2} C_b{}' \quad \ldots\ldots(5.16)$$

where $C_b{}' = \int_b \rho_b (x_b{}^{1'} x_b{}^{1'} + x_b{}^{2'} x_b{}^{2'}) dV$ is the moment of inertia about $x_b{}^{3'}$. After a calculation similar to that for body a in Appendix 5, we have

$$\int_b \rho_b u_b dV = -2\int_b \rho_b \frac{\partial u_b}{\partial x^s} x_b{}^{s'} dV. \quad \ldots\ldots(5.17)$$

Using (5.8) and (5.13)–(5.17) in (4.18) the equations of motion for the fluid body a become,

$$\begin{aligned}
&\left\{\ddot{a}^i - GM_b \frac{\partial}{\partial a^i}\left(\frac{1}{r_{ab}}\right)\right\} \\
&= \frac{1}{c^2}\left\{GM_b\left(\dot{a}^k\dot{a}^k + \tfrac{3}{2}\dot{b}^k\dot{b}^k - 4\dot{a}^k\dot{b}^k - \frac{4GM_b}{r_{ab}} - \frac{5GM_a}{r_{ab}}\right)\frac{\partial}{\partial a^i}\left(\frac{1}{r_{ab}}\right)\right. \\
&\quad + GM_b(4\dot{b}^i\dot{a}^k - 4\dot{a}^i\dot{a}^k + 3\dot{a}^i\dot{b}^k - 4\dot{b}^i\dot{b}^k)\frac{\partial}{\partial a^k}\left(\frac{1}{r_{ab}}\right) + \frac{GM_b}{2}\dot{b}^k\dot{b}^s\frac{\partial^3 r_{ab}}{\partial a^i \partial a^k \partial a^s} \\
&\quad + \frac{(\omega_b{}')^2}{2} GC_b{}' \frac{\partial}{\partial a^i}\left(\frac{1}{r_{ab}}\right) + \frac{2M_b}{45M_a}(3\delta_{is}\delta_{s3} - \delta_{is})\frac{\partial}{\partial a^s}\left(\frac{1}{r_{ab}}\right) \\
&\quad \times \int_0^{\bar{s}_a}\left\{4\pi G\int_0^{s_a}\rho_a s_a{}^2 ds_a\right\}\left\{4\pi G\frac{d}{ds_a}\left(\frac{\epsilon_a}{s_a}\right)\int_0^{s_a}\rho_a s_a{}^2 ds_a - 8\pi G s_a\int_{s_a}^{\bar{s}_a}\rho_a\frac{d\epsilon_a}{ds_a}ds_a\right\}ds_a\Big\}
\end{aligned} \quad \ldots\ldots(5.18)$$

§ 6. Conclusion

We have derived in §5 the equations of motion for two kinds of rotating bodies: equation (5.6) for bodies which retain spherical symmetry during rotation, and equation (5.18) for perfectly fluid rotating bodies. When the rotation of the bodies is zero, both (5.6) and (5.18) reduce to the original equations of motion for two spherically symmetric bodies obtained by Einstein and Infeld (1949) and by Papapetrou (1951 a).

For the case of rotating spherically symmetric bodies, only the last term in (5.6) is due to the rotation of the bodies. This result shows that the motion of body a is influenced directly only by the rotation of body b and not by its own rotation.† Furthermore, the motion of body a is independent of the direction of the axis of rotation of body b.

We also find from (5.18) that the motion of a fluid body a is independent of the axis of rotation of the body b. Equation (5.18) contains terms due to the

† Indirectly the rotation of body a will be of importance: it influences the motion of body b which in turn also influences the motion of body a.

rotation of the body a, showing that the motion of a fluid body is influenced directly by its own rotation besides the rotation of other bodies. We notice that the mass and moments of inertia are not sufficient to derive the motion of bodies behaving as perfect fluids; the density distribution within the bodies must be defined. As an example we take a simple case of constant density throughout the body a. From (5.12) we obtain $4\epsilon_a M_a G = 5(\omega_a)^2 \bar{s}_a{}^2$ and the mass and moments of inertia A_a, B_a and C_a about the $x_a{}^1$, $x_a{}^2$ and $x_a{}^3$ axes respectively become

$$M_a = \frac{4\pi}{3}\rho_a \bar{s}_a{}^3, \qquad A_a = B_a = C_a(1-\epsilon_a), \qquad C_a = \frac{2}{5}M_a \bar{s}_a{}^2$$

where ϵ_a is constant. Then the additional terms on the right-hand side of (5.18) which are due to the rotation reduce to

$$\frac{(\omega_b')^2}{2} GC_b' \frac{\partial}{\partial a^i}\left(\frac{1}{r_{ab}}\right) + \frac{(\omega_a)^2}{36} GC_a \frac{M_b}{M_a}(\delta_{is} - 3\delta_{i3}\delta_{s3}) \frac{\partial}{\partial a^s}\left(\frac{1}{r_{ab}}\right).$$

Finally we remark that the order of magnitude of the ellipticity is given by (5.12), i.e.

$$\epsilon \simeq \frac{\omega^2 l^2}{MG} \simeq \frac{v^2 l}{MG} \simeq \frac{l}{L}$$

which is consistent with our omission in § 5.2 of terms of the order of ϵ^2. When obtaining the equations of motion up to terms in $(v/c)^2$, we have assumed that one body is independent of the other body. This has necessitated the omission of terms of the order $(l/L)^2$ in the Newtonian approximation (3.7). Therefore, for the equations of motion (5.18) to be complete, terms of this order on the left-hand side must be small compared with the right-hand side, i.e. $l/L \ll v/c$. In general, this condition will be satisfied in stellar systems where the distance between the bodies is large compared with their radii, i.e. condition (2.1).

Acknowledgment

The author wishes to thank Professor A. Papapetrou for his valuable advice and constant interest in this work.

References

Einstein, A., and Infeld, L., 1940 *Ann. Math.*, **41**, 455; 1949, *Canad. J. Math.*, **1**, 209.
Einstein, A., Infeld, L., and Hoffman, B., 1938, *Ann. Math.*, **39**, 65.
Fock, V. A., 1939, *J. Phys., U.S.S.R.*, **1**, 81.
Infeld, L., and Scheidegger, A. E., 1953, *Canad. J. Math.*, **3**, 195.
Jeffreys, H., 1924, *The Earth*, 1st Edn (Cambridge : University Press).
Papapetrou, A., 1951 a, *Proc. Phys. Soc.* A, **64**, 57; 1951 b, *Ibid.*, **64**, 302.

Appendix 1

We assume that the body a rotates about an axis, say $x_a{}^{3'}$, in a spatial system $x_a{}^{m'}$ with angular velocity $\omega_a{}^{3'}(\omega_a{}^{1'} = \omega_a{}^{2'} = 0)$. The spatial system $x_a{}^{m'}$ is related to the original system $x_a{}^m$ by direction cosines l_{mn}, where

$$x_a{}^{m'} = l_{mn} x_a{}^n \qquad x_a{}^n = l_{nm} x_a{}^{m'}$$

and

$$\omega_a{}^{3'} = l_{3n}\omega_a{}^n \qquad \omega_a{}^n = l_{n3}\omega_a{}^{3'}.$$

Equation (3.7) determining the stress tensor $p_a{}^{ik}$ in the spatial system $x_a{}^{i'}$ is

$$\frac{\partial p_a{}^{ik}}{\partial x^{k'}} = \rho_a \frac{\partial u_a}{\partial x^{i'}} + \rho_a(\omega_a{}^{3'})^2 x_a{}^{i'} - \rho_a(\omega_a{}^{3'})^2 \delta_{i3} x_a{}^{3'} - \rho_a \dot{\omega}^{3'} \epsilon_{i3k} x_a{}^{k'}. \qquad \ldots\ldots (A\,1)$$

Remembering that p_a^{ik} vanishes outside the body a, we have

$$\int_a p_a^{ik} dV = -\int_a \frac{\partial p_a^{is}}{\partial x^s} x_a^{k'} dV.$$

Introducing (A 1) we find

$$\int_a p_a^{ik} dV = -\int_a \rho_a \left\{ \frac{\partial u_a}{\partial x^i} x_a^{k'} + (\omega_a^{3'})^2 x_a^{1'} x_a^{k'} - \delta_{i3}\omega_a^{3'})^2 x_a^{3'} x_a^{k'} - \epsilon_{i3s}\dot{\omega}_a^{3'} x_a^{s'} x_a^{k'} \right\} dV.$$

Because $p_a^{12} = p_a^{21}$ and using the symmetric properties of the body a in the system $x_a^{s'}$ we obtain

$$\dot{\omega}_a^{3'} = 0 \quad \text{and} \quad \dot{\omega}_a^{n} = 0. \qquad \ldots\ldots (A\,2)$$

By taking $p_a^{13} = p_a^{31}$ we obtain the equation

$$\int_a \rho_a \frac{\partial u_a}{\partial x^3} x_a^{1'} dV = \int_a \rho_a \left\{ \frac{\partial u_a}{\partial x^1} x_a^{3'} + (\omega_a^{3'})^2 x_a^{1'} x_a^{3'} \right\} dV.$$

This condition will be of no importance because it is always satisfied by the form of the rotating bodies chosen in § 5.

Appendix 2

We consider the equation $\Delta A = -4\pi G\alpha$ where α is a function of x^i which vanishes outside volume V_α. The solution is

$$A = G\int_{V_\alpha} \frac{\alpha'}{R} dV'$$

where $R^2 = (x^s - x^{s'})(x^s - x^{s'})$ and α' is a function of $x^{i'}$. For large R we can expand about the point $x^{s'} = a^s$:

$$\frac{1}{R} = \frac{1}{r_a} + \frac{\partial}{\partial a^s}\left(\frac{1}{r_a}\right)(x^{s'} - a^s) + \ldots$$

with $r_a^2 = (x^s - a^s)(x^s - a^s)$ and therefore

$$A = \frac{G}{r_a}\int_{V_\alpha} \alpha' dV' + G\frac{\partial}{\partial a^s}\left(\frac{1}{r_a}\right)\int_{V_\alpha} \alpha' x_a^{s'} dV' + \ldots$$

Using this result we may solve (4.13) outside body a and obtain the expressions in (4.15). As an example we take $\Delta u_a = -4\pi G\rho_a$ so that at large distances from body a

$$u_a = \frac{G}{r_a}\int_a \rho_a dV + G\frac{\partial}{\partial a^s}\left(\frac{1}{r_a}\right)\int_a \rho_a x_a^s dV + \ldots.$$

The second integral vanishes from symmetry properties; higher order terms are neglected because of condition (2.1). We therefore find

$$U_{a,i} = (u_{b,i})_a = M_b G\frac{\partial}{\partial a^i}\left(\frac{1}{r_{ab}}\right), \qquad r_{ab}^2 = (a^s - b^s)(a^s - b^s).$$

The remaining expressions in (4.15) are calculated similarly. In particular, we notice that $(u_b)_a$ and $(y_b^s)_a$ are of the order of $1/L$ and $(l/L)^2$ respectively.

We next see that u_a can be evaluated inside or outside the body a and that F_a at large distances from the body a is obtained from (4.14) by taking the value for u_a outside the body a at large distances. Taking $u_a = GM_a/r_a$ and remembering $x_a^s v_a^s = x_a^s \dot{a}^s$ we find

$$\Delta F_a = GM_a\left\{\frac{\partial^2}{\partial x^s \partial x^n}\left(\frac{1}{r_a}\right)\dot{a}^s\dot{a}^n - \frac{\partial}{\partial x^s}\left(\frac{1}{r_a}\right)\ddot{a}^s\right\}, \qquad r_a \gg l.$$

The solution is

$$F_a = \frac{GM_a}{2}\left\{\frac{\partial^2 r_a}{\partial x^s \partial x^n}\dot{a}^s\dot{a}^n - \frac{\partial r_a}{\partial x^s}\ddot{a}^s\right\}, \qquad r_a \gg l$$

and to our approximation is identical to the result in I. Equation (4.15) follows immediately.

Appendix 3

We consider the equations $\Delta A = -4\pi G\alpha$, $\Delta B = -4\pi G\beta$ where A, B, α, β are functions of x^i and α, β are finite over volumes V_α, V_β respectively and vanish elsewhere. The solutions are

$$A = G\int_{V_\alpha}\frac{\alpha' dV'}{R}, \qquad B = G\int_{V_\beta}\frac{\beta' dV''}{R}$$

where $R^2 = (x^s - x^{s'})(x^s - x^{s'})$ and α', β' are functions of $x^{i'}$. We now form the integral

$$I = \int_V \{B_{,i}\Delta A + A_{,i}\Delta B\}dV$$

over volume V which encloses V_α and V_β. We prove the lemma that integral I vanishes.

Using the above solutions we have

$$I = -4\pi G^2\int_V\left\{\alpha\int_{V_\beta}\beta'\frac{\partial}{\partial x^i}\left(\frac{1}{R}\right)dV' + \beta\int_{V_\alpha}\alpha'\frac{\partial}{\partial x^i}\left(\frac{1}{R}\right)dV'\right\}dV.$$

Since α, β vanish outside V_α, V_β respectively, on reversing the order of integration in the first double integral we obtain

$$-\frac{I}{4\pi G^2} = \int_{V_\beta}\beta'\int_{V_\alpha}\alpha\frac{\partial}{\partial x^i}\left(\frac{1}{R}\right)dV dV' + \int_{V_\beta}\beta\int_{V_\alpha}\alpha'\frac{\partial}{\partial x^i}\left(\frac{1}{R}\right)dV' dV.$$

Remembering that

$$\frac{\partial}{\partial x^i}\left(\frac{1}{R}\right) = -\frac{\partial}{\partial x^{i'}}\left(\frac{1}{R}\right)$$

the right-hand side is zero and the lemma is proved.

We take as an example, $A = y_a{}^k$, $B = u_a$, $\alpha = \rho_a x_a{}^k$, $\beta = \rho_a$ and $V_\alpha = V_\beta = V_a$, V_a being the volume of the body a. The lemma states

$$\int_a \rho_a\{y_a{}^k{}_{,i} + u_{a,i}x_a{}^k\}dV = 0$$

which is given in (4.16). The remaining relations in (4.16) are obtained similarly.

In order to solve (4.14) inside the body a, we take the value of u_a inside body a only, then according to the lemma

$$\int_a\{\rho_a F_{a,i} - \frac{u_{a,i}}{4\pi G}u_{a,00}\}dV = 0$$

where $u_{a,00}$ refers to the value inside the body a.

Appendix 4

We express u_a in (5.11) in the form

$$u_a = \frac{P(s_a)}{r_a} + Q(s_a) + (\tfrac{1}{3} - \mu^2)\left\{\frac{R(s_a)}{r_a^3} + r_a{}^2 S(s_a)\right\} \qquad \ldots\ldots(A\,3)$$

with

$$P(s_a)=4\pi G\int_0^{s_a}\rho_a s_a{}^2 ds_a \qquad Q(s_a)=4\pi G\int_{s_a}^{\infty}\rho_a s_a ds_a$$

$$R(s_a)=\frac{4\pi G}{5}\int_0^{s_a}\rho_a\frac{d}{ds_a}(\epsilon_a s_a{}^5)ds_a \qquad S(s_a)=\frac{4\pi G}{5}\int_{s_a}^{\infty}\rho_a\frac{d\epsilon_a}{ds_a}ds_a$$

$\mu=\cos\theta$.

Then we find

$$\frac{\partial u_a}{\partial s_a}=0, \qquad u_{a,s}=\frac{\partial u_a}{\partial r_a}\frac{x_a{}^s}{r_a}+\left(\frac{\delta_{3s}}{r_a}-\frac{\mu x_a{}^s}{r_a{}^2}\right)\frac{\partial u_a}{\partial\mu}$$

and remembering $x_a{}^s v_a{}^s=x_a{}^s\dot{a}^s$ and $v_a{}^3=\dot{a}^3$,

$$u_{a,0}=-u_{a,s}\dot{a}^s$$

$$u_{a,00}=-u_{a,s}\ddot{a}^s+u_{a,sn}\dot{a}^s\dot{a}^n.$$

Accordingly we obtain

$$\int_a u_{a,00}u_{a,i}dV=-\ddot{a}^s\int_a u_{a,s}u_{a,i}dV+\dot{a}^s\dot{a}^n\int_a u_{a,sn}u_{a,i}dV. \qquad \ldots\ldots(A\,4)$$

Noting that $\partial u_a/\partial\mu$ is of the order of ϵ_a the first integral on the right-hand side of (A 4) becomes

$$-\ddot{a}^s\int_a\left\{\left(\frac{\partial u_a}{\partial r_a}\right)^2\frac{x_a{}^s x_a{}^i}{r_a{}^2}+\frac{1}{r_a{}^2}\frac{\partial u_a}{\partial r_a}\frac{\partial u_a}{\partial\mu}\left(x_a{}^s\delta_{3i}+x_a{}^i\delta_{3s}-\frac{2\mu x_a{}^i x_a{}^s}{r_a{}^2}\right)\right\}dV.$$

We next introduce the expressions

$$x_a{}^i=\delta_{i1}r_a(1-\mu^2)^{1/2}\sin\chi+\delta_{i2}r_a(1-\mu^2)^{1/2}\cos\chi+\delta_{i3}\mu r_a$$

$$\left(\frac{\partial u_a}{\partial r_a}\right)^2=\frac{P^2}{r_a{}^4}+2(\tfrac{1}{3}-\mu^2)\left(\frac{3PR}{r_a{}^6}-\frac{2PS}{r_a}\right)$$

$$\frac{\partial u_a}{\partial r_a}\frac{\partial u_a}{\partial\mu}=2\mu\left(\frac{PR}{r_a{}^5}+PS\right).$$

Now $P(s_a)=0$ when $s_a>\bar{s}_a$, $\bar{s}_a$ being the mean radius of body a, so we find on integrating over χ,

$$-\ddot{a}^s\pi\int_0^{\bar{s}_a}\int_{-1}^{1}\left\{\frac{P^2}{r_a{}^4}+2(\tfrac{1}{3}-\mu^2)\left(\frac{3PR}{r_a{}^6}-\frac{2PS}{r_a}\right)\right\}\{\delta_{i1}\delta_{s1}(1-\mu^2)+\delta_{i2}\delta_{s2}(1-\mu^2)+2\delta_{i3}\delta_{s3}\mu^2\}r_a{}^2 d\mu dr_a$$

$$-4\ddot{a}^s\pi\int_0^{\bar{s}_a}\int_{-1}^{1}\mu^2\left\{\frac{PR}{r_a{}^6}+\frac{PS}{r_a}\right\}\{2\delta_{i3}\delta_{s3}-[\delta_{i1}\delta_{s1}(1-\mu^2)+\delta_{i2}\delta_{s2}(1-\mu^2)+2\delta_{i3}\delta_{s3}\mu^2]\}r_a{}^2 d\mu dr_a.$$

We rewrite this in the form

$$-\ddot{a}^s\pi\int_0^{\bar{s}_a}\int_{-1}^{1}\frac{P^2}{r_a{}^2}\{\delta_{is}(1-\mu^2)+\delta_{i3}\delta_{s3}(3\mu^2-1)\}d\mu dr_a$$

$$-2\ddot{a}^s\pi\int_0^{\bar{s}_a}\int_{-1}^{1}\frac{PR}{r_a{}^2}\{\delta_{is}(1-\mu^2)(1-5\mu^2)+\delta_{i3}\delta_{s3}(12\mu^2-15\mu^4-1)\}d\mu dr_a$$

$$-\frac{4}{3}\ddot{a}^s\pi\int_0^{\bar{s}_a}\int_{-1}^{1}PSr_a\{\delta_{is}(\mu^2-1)+\delta_{i3}\delta_{s3}(3\mu^2+1)\}d\mu dr_a.$$

In order to integrate over μ we transform from r_a to s_a,† and obtain

† We could equally well transform s_a to r_a, noting that $\bar{s}_a$ is then a function of μ.

$$-\frac{4\pi\ddot{a}^a}{3}\int_0^{\bar{s}_a}\frac{P^2}{s_a^2}ds_a-\frac{8\pi}{45}\ddot{a}^a(\delta_{is}-3\delta_{i3}\delta_{s3})\int_0^{\bar{s}_a}\frac{P^2}{s_a^2}\left(s_a\frac{d\epsilon_a}{ds_a}-\epsilon_a\right)ds_a$$

$$+\frac{16\pi}{9}\ddot{a}^a(\delta_{is}-3\delta_{i3}\delta_{s3})\int_0^{\bar{s}_a}PSs_a ds_a.$$

By transforming from s_a to r_a in (A 3) we find u_a is of the form

$$\sum_{k=0,1}f_k(r_a)\mu^{2k}$$

and that

$$u_{a,sn}=\sum_{k=0,1}\{(a_k+b_k\cos^2\chi)\mu^{2k}+(c_k\cos\chi+d_k\sin\chi)\mu^{2k+1}\}$$

$$u_{a,i}=\sum_{k=0,1}\{(e_k+f_k\cos^2\chi)\mu^{2k+1}+(g_k\cos\chi+h_k\sin\chi)\mu^{2k}\}$$

where $a_k\ldots h_k$ are functions of r_a only. Introducing these equations into the last integral in (A 4) and integrating over χ, μ we find

$$\int_a u_{a,sn}u_{a,i}dV=0.$$

We have finally

$$\frac{1}{4\pi}\int_a u_{a,00}u_{a,i}dV$$

$$=-\frac{\ddot{a}}{3}\int_0^{\bar{s}_a}\left\{\frac{4\pi G}{s_a}\int_0^{s_a}\rho_a s_a^2 ds_a\right\}^2 ds_a+\frac{2}{45}\ddot{a}^a(3\delta_{i3}\delta_{s3}-\delta_{is})\int_0^{\bar{s}_a}\left\{4\pi G\int_0^{s_a}\rho_a s_a^2 ds_a\right\}$$

$$\times\left\{4\pi G\frac{d}{ds_a}\left(\frac{\epsilon_a}{s_a}\right)\int_0^{s_a}\rho_a s_a^2 ds_a-8\pi G s_0\int_{s_a}^{\infty}\rho_a\frac{d\epsilon_a}{ds_a}ds_a\right\}ds_a.$$

Appendix 5

Using the equation

$$-4\pi G\rho_a r_a^2=\frac{\partial}{\partial r_a}\left(r_a^2\frac{\partial u_a}{\partial r_a}\right)+\frac{\partial}{\partial\mu}\left[(1-\mu^2)\frac{\partial u_a}{\partial\mu}\right]$$

the following integral becomes

$$\int_a\rho_a u_{a,s}x_a^s dV=-\frac{1}{4G}\int_0^{\infty}\int_{-1}^{1}\left\{\frac{\partial}{\partial r_a}\left[r_a^3\left(\frac{\partial u_a}{\partial r_a}\right)^2\right]+r_a^2\left(\frac{\partial u_a}{\partial r_a}\right)^2\right.$$

$$\left.+2\frac{\partial u_a}{\partial r_a}\frac{\partial}{\partial\mu}\left[(1-\mu^2)\frac{\partial u_a}{\partial\mu}\right]\right\}d\mu dr_a.$$

The first term on the right-hand side vanishes because $\partial u_a/\partial r_a=0$ when $r_a=0$ and $\partial u_a/\partial r_a\simeq 1/r_a$ when $r_a\to\infty$, therefore introducing (A 3) and integrating we obtain

$$\int_a\rho_a u_{a,s}x_a^s dV=-\frac{1}{2G}\int_0^{\bar{s}_a}\frac{P^2}{s_a^2}ds_a.$$

A similar calculation shows that

$$\int_a\rho_a u_a dV=\frac{1}{G}\int_0^{\bar{s}_a}\frac{P^2}{s_a^2}ds_a$$

and we finally obtain the relation

$$\int_a\rho_a u_a dV=-2\int_a\rho_a u_{a,s}x_a^s dV.$$

An Investigation of Deuteron Induced Reactions by Magnetic Analysis I: Experimental Technique

By T. S. GREEN† and R. MIDDLETON
Nuclear Physics Research Laboratory, University of Liverpool

Communicated by H. W. B. Skinner; *MS. received* 29*th June* 1955, *and in final form* 14*th September* 1955

Abstract. A magnetic spectrograph has been constructed for the measurement of the angular distribution of charged particles emitted in the deuteron bombardment of nuclei. The spectrograph utilizes the focusing properties of an axially symmetrical field and is capable of focusing protons and α-particles of 3 to 18 MeV and deuterons of 1½ to 9 MeV on a 12 in. long photographic plate, with an energy resolution of 0·25%. The instrument has been used in conjunction with the Liverpool 37 in. cyclotron for measurements over an angular range of 5° to 60° at a bombarding energy of 9 MeV. Due to the energy spread of the deuteron beam and the effect of target thickness the total experimental resolution was 0·5 to 0·6%.

§ 1. Introduction

The measurement of the energy spectra and angular distributions of protons from (d, p) stripping reactions is now an established method of determining the excitation energies and parities of energy levels and as a means of assigning possible spin values to these levels. The shape of the angular distribution at small angles of emission is strongly characteristic of the angular momentum of the absorbed neutron, but measurements in this region are made difficult by the high background of elastically scattered deuterons. Thus in the extensive investigation of proton angular distributions by Burrows, Powell and Rotblat (1951), using a photographic plate scattering camera, measurements could not be made at angles less than 15°. This difficulty was overcome by Holt and Young (1950) and Holt and Marsham (1953) by using a gold absorber of sufficient thickness to stop the deuteron beam and observing the transmitted protons with a triple coincidence proportional counter. The energy resolution however, suffered due to the scattering and straggling of the protons in the absorber and measurements were confined to protons from reactions of positive Q-value. It was thus felt desirable to build a magnetic spectrograph similar in principle to that reported by Buechner (1954) which would separate the protons from the deuteron background and at the same time possess a high energy resolution. With this type of instrument it is possible to investigate the behaviour of protons from reactions of negative Q-values at small angles of emission. The need for such investigations arose from previous measurements of neutron angular distributions from (d, n) reactions of similar Q-values where occasional departures from theory were observed (Middleton, El-Bedewi and Tai 1953, Evans, Green and Middleton 1953). A further advantage is that inelastically scattered deuteron, triton and α-particle angular distributions can be measured with equal facility, none of these having previously been thoroughly investigated at small angles of emission.

† Now at the Atomic Energy Research Establishment, Harwell, Berks.

When measurements of spectra have to be made at several angles of emission, it is advantageous to record the whole spectrum simultaneously. For this purpose a magnetic spectrograph has been designed with a constant percentage energy resolution over a proton energy range of 3 to 18 MEV. The basic design of the instrument is similar in principle to that of the β-ray spectrograph used by Siday and Silverston (1952) and depends upon the focusing properties of an axially symmetrical field.

An existing magnet was adapted for use in this spectrograph and was fitted with 8 in. diameter semi-circular poles, across which a 16 000 gauss field could be maintained. It was calculated that this magnet would produce the desired dispersion, focusing protons and α-particles in the energy range 3 to 18 MEV and deuterons of $1\frac{1}{2}$ to 9 MEV on a 12 in. long photographic plate, with a momentum resolution of 0·1%. Although by modern standards this resolution is not very good it was considered to be sufficient in view of the energy spread of the cyclotron deuteron beam. In fact the total experimental energy resolution was between 0·5 and 0·6% depending upon the target thickness.

§ 2. EXPERIMENTAL TECHNIQUE

2.1. *General Arrangement*

A diagram of the general experimental arragement is shown in figure 1 (*a*). The external deuteron beam from the Liverpool 37 in. cyclotron was collimated by a system of three slits S_1, S_2 and S_3 and the resultant beam allowed to strike a thin target placed about five feet from the cyclotron tank. The spectrograph magnet was a little over 1 metre from the target and focused the charged particles, emitted within a narrow cone, on to the photographic plate. The magnet was mounted so that it could be moved about an arc of a circle centred on the target, allowing exposures to be made at angles from 0° to 60°. To minimize the effect

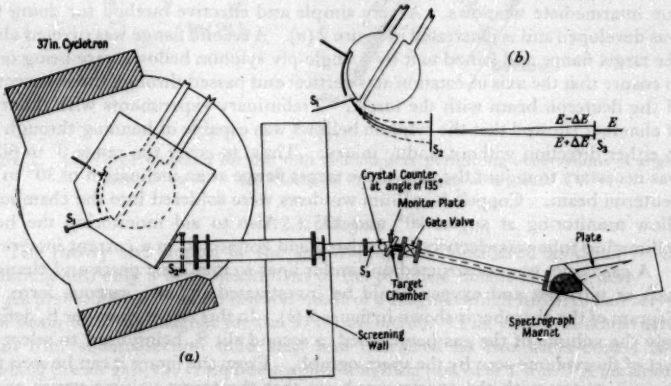

Figure 1. Diagram of general experimental arrangement and slit system.

of the γ-ray and neutron background from the cyclotron on the photographic plates and the scintillation counter monitor, a 2-foot thick concrete shielding wall was built between the apparatus and the cylotron.

2.2. *Slit System*

As shown in figures 1 (*a*) and (*b*) a system of three slits was used to collimate and reduce the energy spread of the deuteron beam. The first slit S_1 was placed close to the cyclotron deflector, the second S_2 a little beyond the boundary of the fringing field and the third S_3 4 inches in front of the target. The action of the fringing field between S_1 and S_2 resulted in a slightly divergent beam emerging from S_2, the deuterons of lowest energy being on the inside (i.e. on the same side as the cyclotron) and those of maximum energy on the outside. This effect is illustrated in figure 1 (*b*). The third slit S_3 was used to select deuterons of a particular energy. Slits S_1 and S_2 were both 1 mm wide and S_3 which defined the target size was $\frac{1}{2}$ mm wide by 3 mm high. The final energy spread of the beam was observed to be 30 kev, and was presumably due to radial oscillations in the cyclotron.

In order to obtain sufficient intensity it was necessary to run the cyclotron with a beam of 60 μA incident on S_1. Since this corresponds to a power dissipation of more than $\frac{1}{2}$ kilowatt, excessive heating and rapid deterioration of this slit occurred. This was finally overcome by forming the slit edges from $\frac{1}{8}$ in. diameter tungsten rod, hard soldered into a water-cooled copper block. Only 6 μA of beam were incident on S_2 so that no such difficulty was encountered and thin molybdenum edges sufficed. For convenience of operation of the cyclotron this slit was electrically insulated and the current displayed on a microammeter. S_3 was made from 0·005 in. gold sheet and was preceded by a slightly larger slit to prevent excessive heating and distortion occurring (see figure 2 (*a*)).

2.3. *Target Chambers*

The essential requirement imposed on the design of the target chamber was that it should permit exposures to be made over an angular range of 0° to 60° without intermediate windows. A very simple and effective method for doing this was developed and is illustrated in figure 2 (*a*). A second flange was pivoted about the target flange and joined to it by a single-ply sylphon bellows, care being taken to ensure that the axis of rotation was vertical and passed through the intersection of the deuteron beam with the target. Preliminary experiments with this type of chamber showed that the sylphon bellows was capable of bending through 30° in either direction without undue injury. Thus, to cover the range 0° to 60° it was necessary to mount the axis of the target flange at an inclination of 30° to the deuteron beam. Copper–beryllium windows were soldered into the chamber to allow monitoring at angles 90° and 135°. Also to aid monitoring the beam collimating tube was electrically insulated and connected to a current integrator.

A gas target was constructed on similar lines so that inert gases and elements such as nitrogen and oxygen could be investigated in pure gaseous form. A diagram of the chamber is shown in figure 2 (*b*). In this target chamber S_3 defined only the volume of the gas bombarded, a second slit S_4 being used to select the part of this volume seen by the spectrograph. From the figure it can be seen that this slit moves with the spectrograph, so that the target volume varies as the cosecant of the angle of observation. Due to the low yield from gas targets, it

was necessary to increase the width of the energy selector slit S_3 to 2½ mm and to make S_4 1 mm wide by 5 mm high. In addition it was necessary to use pressures up to 40 cm Hg, which required the use of aluminium windows of 2·2 mg cm^{-2} thickness mounted on these slits.

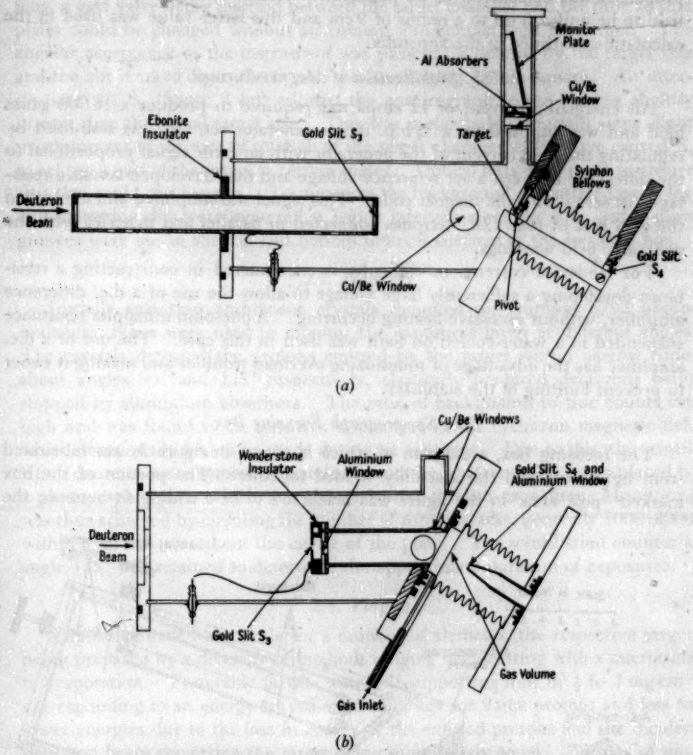

Figure 2. (*a*) Target chamber for use with solid targets, permitting observations at angles from 0° to 60°. (*b*) Modified version for use with gases.

2.4. *Magnet*

The theory and design of the spectrograph is considered in detail in the appendix and only a brief description of the practical details is given here.

As previously mentioned use was made of a magnet which hitherto had served as a beam focusing magnet for the 37 in. cyclotron. The yoke was constructed from 8 in. square section mild steel and energized by two water-cooled coils flanking the air gap, the complete magnet weighing just over 1 ton. A maximum field of 16 000 gauss could be maintained across an air gap of 1 inch with poles of roughly one third of the sectional area of the yoke.

Cylindrical poles of 20 cm diameter, half of which had been machined off at an angle of 45°, were fitted. Measurements made with a small search coil and Grassot fluxmeter showed the presence of slight azimuthal variations in the field arising from the unsymmetrical pole shape, but their effect on the focusing properties was considered to be negligible. Radial measurements showed the field to be uniform up to a radius of 9 cm and this latter value was used in the calculations outlined in the appendix.

2.5. *Stabilization of Magnet Current*

An energizing current of 12 amps was required to produce a 16 000 gauss field and was supplied by a 7½ h.p. motor-generator set. It was stabilized by regulating the field current of the generator with an error signal proportional to the difference between a set reference voltage and that developed across a resistance in series with the magnet coils. This signal was amplified and controlled the grid bias of four 12E1 tetrodes connected in parallel and in series with the generator field windings.

For moderate currents no difficulty is encountered in constructing a resistance developing a sufficiently large voltage to allow the use of a d.c. difference amplifier, without excessive heating occurring. A one-ohm minalpha resistance suspended in a water-cooled oil bath was used in this case. The use of a d.c. amplifier has the advantage of minimizing overload troubles and making it easier to prevent hunting of the stabilizer.

2.6. *Spectrograph Focusing Box*

The focusing box, a diagram of which is shown in figure 3, was fabricated from light alloy and the assembly welded together. The portion of the box marked 'pole area' in the figure was machined to be a sliding fit between the

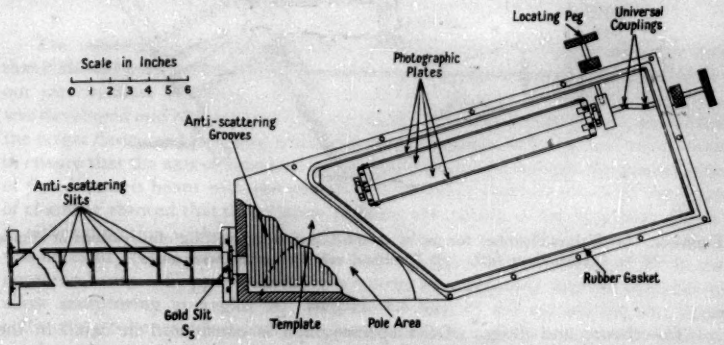

Figure 3. Spectrograph focusing box.

magnet poles and was precisely located by a template welded to the upper surface of the box matching the pole profile. Location was consistently achieved within 0·008 in. by checking the register of the template and the pole with a feeler gauge. The remaining portion of the box was made of deeper section to accommodate the hexagonal plate holder and was fitted with a lid to allow its removal. The plate holder was mounted on bearings bolted to the bottom of the box such that slight

adjustments of position could be made. Rotation was effected externally by a spindle, passing through a vacuum seal, connected to the plate holder via a pair of universal couplings. A locking device was provided to ensure that the plane of the emulsion of the plate being exposed was vertical.

The focusing box was joined to the target chamber by a brass tube 1 metre long, a gate valve being inserted between the target chamber and the tube so that plates could be changed without air coming into contact with the target. The angular acceptance of the instrument was principally defined by the target size and the slit marked S_5 in the figure, the latter being $4\frac{1}{2}$ mm square. An intermediate slit S_4 (figure 2 (*a*)) allowed the spectrograph to see an area slightly greater than the actual target size. This was particularly important since slight misalignment of the axis of rotation of the target chamber might have caused S_4 to eclipse a part of the target at certain angles. Optical tests were made to ensure that this could not happen. To minimize the background of scattered particles, anti-scattering slits were mounted at 3-inch intervals along the tube and shallow grooves were cut in the top and bottom internal surfaces of the focusing box.

2.7. *Monitors*

Initially two thin anthracene crystals mounted on Dumont 6292 photomultiplier tubes were used to monitor the exposures given at different angles. The crystals detected the protons emitted by the target within narrow cones about angles 90° and 135° respectively, elastically scattered deuterons being stopped by aluminium absorbers. The ratio of background to true counts was high and was found to be sensitive to changes in the cyclotron magnetic field which occasionally had to be made during an exposure. Due to this, the scintillation counters were somewhat unreliable and the counter at 90° was replaced by a photographic plate which was changed prior to each exposure. Monitoring was thus achieved by counting the number of proton tracks, generally 1000–2000, within a known area about the centre of the plate. The scintillation counter at angle 135° was retained to determine the approximate duration of exposures.

2.8. *Targets*

Exposures have been made for a number of elements, the respective targets being prepared by a diversity of methods ranging from cutting with a microtome to evaporation. Preferably targets were self-supporting foils of $\frac{1}{2}$ to 1 mg cm^{-2} corresponding to an energy spread of 15 to 30 kev for 9 MEV protons and less for lower energies due to the loss in energy of the emitted protons and the incident deuteron beam traversing the target being more nearly equal. Targets of non-metals and compounds which usually could not be obtained as self-supporting layers were generally backed by 0·78 mg cm^{-2} gold leaf. The latter was undesirable because of the increase in proton and particularly deuteron background it introduced.

Some elements, such as nitrogen and oxygen, were investigated in pure gaseous form using the gas target chamber described in §2.3. However, the energy resolution was much worse than that obtained from solid targets, principally due to the increased size of the energy selector slit S_3 and the straggling introduced by the gas outside the genuine target volume and the aluminium windows. It was thus found advantageous to use whenever possible a solid compound target containing the particular element as a constituent, despite the increased complexity of the spectrum.

2.9. *Plate Technique*

Ilford C2 photographic plates 12 in. long by 1 in. wide and 100 μ emulsion thickness were used in the spectrograph. Six plates could be mounted simultaneously on the faces of a hexagonal bar which could be rotated from outside the focusing box enabling separate exposures to be made without disturbing the vacuum. It was found advantageous to load no more than four plates at once since exposures were frequently long and the γ-ray fogging severe. After exposure, the plates were processed by standard methods and observations made with a Cooke, Troughton and Simms M 4000 microscope equipped with a $\times 20$ objective and $\times 10$ eyepieces. Since the particles are sorted according to energy by the magnet, range measurements are unnecessary and it remains to count the number of tracks per unit interval of length along the plate. The numbers of tracks within successive scans of width 220 μ and length 1 to 15 mm depending on the density, in a direction perpendicular to the length of the plate, were counted and recorded. For plotting purposes the numbers of protons and deuterons in two and four successive scans respectively were added and represented by a single point on the spectrum. The energy interval between points was the same in both cases and equal to about 25 kev. The conversion of the distance along the plate to an energy scale is shown for protons, deuterons and α-particles in figure 4 (*b*).

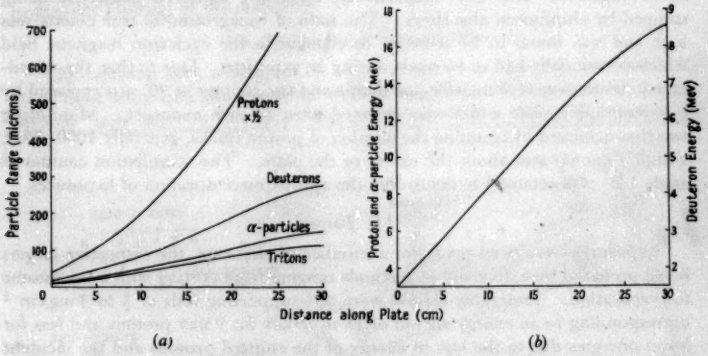

Figure 4. Curves showing the variation of range and energy of various particles as a function of distance along the photographic plate.

No difficulty was experienced in distinguishing between proton and deuteron tracks due to the large difference in range and initial ionization. For all except the lowest energies, inspection of the initial ionization was quite sufficient. In figure 4 (*a*) are shown the differences between the ranges of protons, deuterons, tritons and α-particles as functions of distance along the plate. It will be noticed that the difference in range of α-particles and tritons at any position along the plate is small but differentiation was reliable due to the difference in ionization and line width, triton groups generally being much broader than those of α-particles because of their greater energy dispersion.

APPENDIX

Theory and Design of the Magnetic Spectrograph

Theory of Axially Symmetrical Fields

(i) *Summary of results of Jennings' theory.* The theory of axially symmetrical fields developed by Jennings (1952) shows that the focusing properties can be represented by a lens with principal planes passing through the centre and perpendicular to the asymptotes to the initial and final particle directions, and with nodal points coincident with the centre. He further shows that the focal length f is equal to $1/2\lambda$, that the transverse aberration at the image is

$$\left\{\left(2\mu-\frac{b}{2u^3}\right)v-\frac{b}{v^2}\right\}x^2 \qquad \ldots\ldots\ (A1)$$

and that the energy dispersion D is $v\rho\,\partial\theta/\partial\rho$ where b is an impact parameter equal to the distance from the centre of the field to the asymptote to the initial particle direction, 2θ is the complement of the angle of deflection, u is the object distance, v is the image distance, x is the range of b-values of the particles accepted by the spectrograph, $\lambda=\partial\theta/\partial b$, and $2\mu=\partial^2\theta/\partial b^2$.

Siday (1947) also has developed expressions for these quantities and in addition indicates a method of calculating θ from the known field shape.

For our purpose both theories have been combined and extended to make it possible to calculate the focusing properties of a real field from the derivatives.

(ii) *Calculation of* λ, 2μ *and* $\partial\theta/\partial\rho$. It is a simple matter to calculate these derivatives for an ideal field i.e. when the field is uniform within the boundary $r=a$ and zero outside it. The particle then moves along a straight line outside the field and along a circular path of radius $(2mE)^{1/2}/He$ within it.

It is easily shown that

$$\theta=\tan^{-1}\frac{\rho+b}{(a^2-b^2)^{1/2}} \qquad \ldots\ldots(A2)$$

and the derivatives of θ with respect to b and ρ can be directly determined. In figure 5 (*a*) and (*b*) f/a and $2\mu a^2$ are plotted as functions of ρ/a for various values of b/a; $2\mu a^2$ is the principal term in equation (A1) for the transverse aberration.

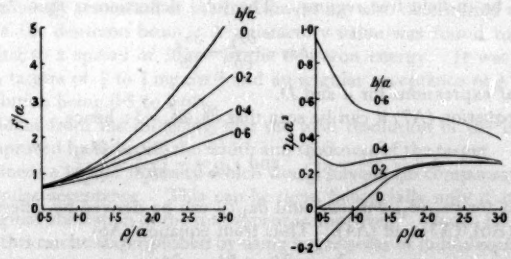

Figure 5. Curves showing the variation of the focal length and transverse aberration with the radius of curvature of the particles in the field for various impact parameters.

In a real field the motion is not so simple and it is not possible to derive analytical expressions for the derivatives. The equations of motion given by Siday are

$$r \sin \psi - b_1 = \frac{1}{H\rho} \int_u^r r H_z dr \qquad \ldots\ldots (A3)$$

and

$$\phi = \int_u^r \frac{\tan \psi}{r} dr \qquad \ldots\ldots (A4)$$

where ψ is the angle between the direction of the motion and the radius vector and ϕ is the angle of the rotation of the radius vector. The angle of deflection $\alpha\,(=180^\circ - 2\theta)$ is then given by

$$\alpha = \psi - \psi_1 - \phi. \qquad \ldots\ldots (A5)$$

Siday proceeds by considering the motion of the particle through half of the magnetic field i.e. to the nearest approach to the centre where $r = r_{\min}$ and $\psi = \pi/2$. This is done by calculating several values of ψ as a function of r by numerical integration of equation (A3) and by interpolation. The corresponding value of ϕ is then obtained by integration of equation (A4) to the limit $r = r_{\min}$ and finally the deflection of the particle in traversing half of the field is obtained by substituting this value into equation (A5). This procedure is difficult due to complications in the mathematics, the further determination of the derivatives of α being even more complex.

By approximating the real field to an ideal field bounded at $r = a$ and a fringing field at $r > a$ it is possible to carry out the calculations. Assume that the particle enters the fringing field with an impact parameter b_1, and that it is deflected through an angle α_1 in passing through this region, α_1 being given by

$$\alpha_1 = \psi_a - \psi_1 - \phi_a \qquad \ldots\ldots (A6)$$

where ψ_a and ϕ_a satisfy equations (A3) and (A4) for $r = a$. The particle then enters the ideal field with a new impact parameter b_2 given by

$$b_2 - b_1 = \frac{1}{H\rho} \int_u^a r H_z dr \qquad \ldots\ldots (A7)$$

and is further deflected through an angle $2\alpha_2$ obtained from equation (A2) by replacing $90^\circ - \theta$ by α_2, and finally re-enters the fringing field. Here it is again deflected through an angle α_1 if the initial and final points of motion can be considered to be in field-free regions. The total deflection is then $2\alpha_2 + 2\alpha_1$ and

$$\lambda = -\frac{\partial \alpha_1}{\partial b} - \frac{\partial \alpha_2}{\partial b}$$

with similar expressions for μ and D.

From equation (A7) it can be seen that $\partial b_1 / \partial b_2 = 1$; hence

$$\lambda = -\frac{\partial \alpha_1}{\partial b_1} - \frac{\partial \alpha_2}{\partial b_2} \quad \text{and} \quad \mu = -\frac{\partial^2 \alpha_1}{\partial b_1^2} - \frac{\partial^2 \alpha_2}{\partial b_2^2}.$$

Expressions for $\partial \alpha_1 / \partial b_1$, $\partial^2 \alpha_1 / \partial b_1^2$ and $\partial \alpha_1 / \partial \rho$ can be derived by differentiation of equations (A6), (A3) and (A4). Thus from equation (A6)

$$\frac{\partial \alpha_1}{\partial b_1} = \frac{\partial \psi_a}{\partial b_1} - \frac{\partial \psi_1}{\partial b_1} - \frac{\partial \phi_a}{\partial b_1}$$

and from equations (A3) and (A4)

$$\frac{\partial \alpha_1}{\partial b_1} = \frac{\sec \psi_a}{a} - \frac{\sec \psi_1}{u} - \int_u^a \frac{\sec^3 \psi}{r^2}\, dr \qquad \ldots\ldots\text{(A8)}$$

$$\frac{\partial^2 \alpha_1}{\partial b_1^2} = \frac{\tan \psi_a \sec^2 \psi_a}{a^2} - \frac{\tan \psi_1 \sec^2 \psi_1}{u^2} - 3\int_u^a \frac{\tan \psi \sec^4 \psi}{r^3}\, dr \qquad \ldots\text{(A9)}$$

and

$$\frac{\partial \alpha_1}{\partial \rho} = -\int_u^a \frac{\sec^3 \psi}{r^2 H \rho^2}\left\{\int_u^r H_z r\, dr\right\} dr - \frac{1}{H\rho^2}\,\frac{\int_u^a H_z r\, dr}{a \cos \psi}. \qquad \ldots\ldots\text{(A10)}$$

The derivatives of α_2 can be readily obtained from the results of the first paragraph of this section.

(iii) *Computation of derivatives.* Before computing the values of the derivatives it is necessary to decide where the boundary between the two field regions lies. It is difficult to apply any criterion in this decision but it is found not to be very critical and it is usually possible to make a reasonable estimate of a.

From the measurements made on the fringing field ψ_a and b are calculated by numerical integration of equations (A3) and (A7). Equations (A8), (A9) and (A10) then make it possible by further numerical integration to calculate the derivatives $\partial\alpha_1/\partial b_1$, $\partial^2\alpha_1/\partial b_1^2$ and $\partial\alpha_1/\partial\rho$. The corresponding derivatives for the ideal field region are obtained from equation (A2) using the calculated value of b_2.

The calculations can be repeated for various values of ρ to determine the focusing properties as a function of ρ. It should be noted however that if the particles entering the field are selected by a slit which is in the fringing field region then b_1 will vary slightly with ρ since the angle between the radius vectors to the source and slit is fixed. This correction is small but significant, especially in the design used where b is large and hence the properties vary rapidly with b.

(iv) *Choice of parameters.* The value of a was fixed at 9 cm by the magnet and further restrictions were imposed by the intention of using a photographic plate 12 in. long to cover a proton energy range of 3 to 18 Mev. This was achieved by using an impact parameter b of 6 cm and an object distance u of 120 cm.

The size and thickness of the target and the angular acceptance of the spectrograph were chosen as the best compromise between intensity and resolution. The choice of the target width was particularly important since it not only affected the intrinsic energy resolution of the instrument but also determined the spread in energy of the deuteron beam. A satisfactory value was found to be $\frac{1}{2}$ mm corresponding to a spread of 30 kev in the deuteron energy. It was also consistent with targets of $\frac{1}{2}$ to 1 mg cm^{-2} and an angular acceptance of $\frac{1}{4}°$, the total energy resolution being 0·5 to 0·6%.

It is evident from the foregoing that the total resolution of the instrument could be improved by reducing the width and thickness of the target. However, this would incur a loss of intensity which would have to be compensated for by a larger angular acceptance. This can be done beneficially only if at the same time the angular aberration of the instrument is improved. As can be seen from figure 5 (*b*) this can be accomplished by using larger poles of radius equal to $\bar{\rho}$ and a smaller impact parameter which would require a longer plate to cover the same energy range.

The design of a spectrograph must inevitably depend largely upon the accelerator in conjunction with which it is to be used. If a high intensity beam of low energy spread is available it is possible to use a relatively large object and the main design feature is strong focusing. If on the other hand the beam is not intense and well defined in energy, a small target has to be used and a large angular acceptance is desirable, and the spectrograph should be designed to produce a high degree of second order focusing.

(v) *Test of theory*. The calculations were tested for impact parameters of 1·5 and 6·0 cm, giving weak and strong focusing respectively, using the magnet previously described and α-particles from a thorium source. The natural energies of these α-particles are 6·0 and 8·8 MeV, but by using an absorber additional energies of 3·5 and 6·9 MeV were obtained. Measurements were made of the image distance v and the angle θ and a comparison of these values with those calculated is shown in figure 6 (*a*) and (*b*). Using the larger impact

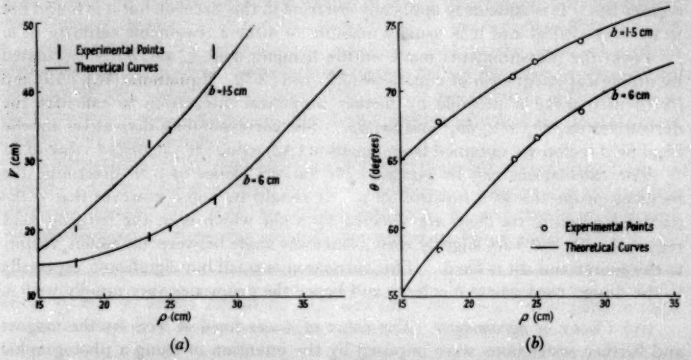

Figure 6. Theoretical curves showing the variation of the image distance and angle of deflection with the radius of curvature for impact parameters of 1·5 cm and 6·0 cm. Also shown are experimental points obtained using α-particles from a thorium source.

parameter, which was the one finally adopted, the observed half widths of the 6·0 and 8·8 MeV groups were 20 and 30 kev respectively as compared with the calculated values of 14 and 21 kev. The difference is probably due to field inhomogeneities and is small compared with the spread in energy of the cyclotron deuteron beam and the effect of target thickness.

Acknowledgments

The authors' thanks are due to Professor H. W. B. Skinner for his encouragement and advice. We should also like to express our gratitude to the cyclotron operator Mr. W. H. Ward for his co-operation. One of us (R.M.) wishes to make grateful acknowledgment to the Imperial Chemical Industries for a Research Fellowship and the other (T.S.G.) is grateful to the Department of Scientific and Industrial Research for a maintenance grant.

References

BUECHNER, W. W., 1954, *Proceedings of the Glasgow Conference on Nuclear and Meson Physics* (London : Pergamon Press), p. 52.
BURROWS, H. B., POWELL, C. F., and ROTBLAT, J., 1951, *Proc. Roy. Soc.* A, **209,** 461.
EVANS, W. H., GREEN, T. S., and MIDDLETON, R., 1953, *Proc. Phys. Soc.* A, **66,** 108.
HOLT, J. R., and MARSHAM, T. N., 1953, *Proc. Phys. Soc.* A, **66,** 249.
HOLT, J. R., and YOUNG, C. T., 1950, *Proc. Phys. Soc.* A, **63,** 833.
JENNINGS, J. C. E., 1952, *Proc. Phys. Soc.* B, **65,** 256.
MIDDLETON, R., EL-BEDEWI, F. A., and TAI, C. T., 1953, *Proc. Phys. Soc.* A, **66,** 95.
SIDAY, R. E., 1947, *Proc. Phys. Soc.* A, **59,** 905.
SIDAY, R. E., and SILVERSTON, D. A., 1952, *Proc. Phys. Soc.* A, **65,** 328.

Investigation of Deuteron Induced Reactions by Magnetic Analysis II : Results for ^{9}Be, ^{12}C, ^{14}N and ^{16}O

By T. S. GREEN† and R. MIDDLETON
Nuclear Physics Research Laboratory, University of Liverpool

Communicated by H. W. B. Skinner ; MS. received 29th June 1955

Abstract. Angular distributions have been measured of some of the proton, deuteron and α-particle groups emitted from targets of beryllium, carbon, nitrogen and oxygen when bombarded by 9 MeV deuterons. The proton angular distributions have been compared with those calculated from the stripping theories enabling assignments of spins and parities to be made to levels of the residual nuclei. Calculations have also been made of the relative capture probabilities and reduced widths and in the cases of carbon and nitrogen it was possible to express them in absolute units.

§ 1. Introduction

The apparatus described in the preceding paper (Green and Middleton 1956) has been used to measure the angular distributions of some of the proton, deuteron and α-particle groups emitted from targets of ^{9}Be, ^{12}C, ^{14}N and ^{16}O when bombarded by 9 MeV deuterons.

The angular distributions of the proton groups have been analysed using the stripping theories of Butler (1951) and Bhatia, Huang, Huby and Newns (1952). These theories show that the shape of the distribution depends principally on the angular momentum of the absorbed neutron, and that the cross section is proportional to the probability that the neutron is captured at the nuclear surface. Bhatia *et al.* define the latter as the 'particle capture probability' and Huby (1952) has shown that from this, using the Butler theory, it is possible to calculate the reduced level width. Both these quantities depend critically on the level configuration so that it is possible, in addition to determining the spin and parity, to obtain some knowledge of the structure of the level.

Attempts have been made to identify some of the levels, observed to have large reduced widths, with simple configurations expected on the bases of the shell model. In other cases the properties of levels have been compared with the predictions of calculations using the shell model with intermediate coupling (Lane 1953). It has also been possible to compare the measured reduced widths of some virtual levels with values determined from analysis of scattering data in an attempt to test the validity of the stripping theories.

§ 2. Targets

The beryllium target was a self-supporting foil of 0·6 mg cm^{-2} and like most targets prepared by evaporation contained impurities of carbon, oxygen and hydrogen. The latter was particularly troublesome since, at small angles of emission, it was responsible for the presence of three intense and broad groups in the spectra.

† Now at the Atomic Energy Research Establishment, Harwell, Berks.

A thin uniform target of carbon was prepared by smoking over burning camphor a leaf of 0·78 mg cm^{-2} gold mounted on a brass ring.

Two nitrogen exposures have been made, one using the gas target chamber filled with spectroscopically pure nitrogen at 40 cm Hg pressure and the other with a solid target prepared by evaporating a thin layer of adenine ($C_5N_5H_5$) on to a gold leaf.

Similarly two oxygen exposures were made, one with gas and the other with a fragment of a quartz bubble blown to a thickness of 0·8 mg cm^{-2}. To assist in the interpretation of the quartz spectra exposures were also made with a silicon target, prepared by evaporating the pure element on to a gold backing.

§ 3. Results: (d, p) Reactions

3.1. ^{9}Be(d, p)^{10}Be

(*a*) *Energy Spectrum.* A typical proton energy spectrum observed at an angle of 15° is shown in figure 1. The positions of the proton groups corresponding to the ground and excited states have been calculated from the results of Jung and Bockelman (1954) and are indicated by a letter P with an accompanying suffix describing the order of the state. Below the letter P and in brackets is the excitation energy of the corresponding level. Groups corresponding to impurities are marked with the chemical symbol of the residual nucleus and immediately below and in brackets is the energy of the corresponding state. As can be seen from the figure five prominent groups can be identified corresponding to the states in ^{10}Be. Three weak groups have also been identified due to carbon contamination and a fourth fairly strong group due to hydrogen either occluded or contained as hydride in the Be. A fifth fairly strong group is due to the elastic scattering of protons accelerated as molecular hydrogen together with the deuteron

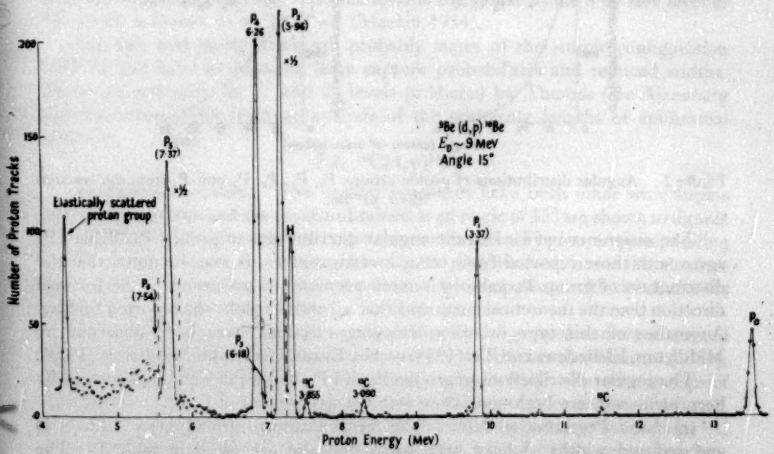

Figure 1. Proton energy spectrum at an angle of observation of 15° resulting from the deuteron bombardment of a thin self-supporting target of beryllium.

beam. No groups of significant intensity due to the levels in ^{10}Be at 6·18 and 7·54 MeV reported by Jung and Bockelman were observed. The former group, however, particularly if weak, may not have been resolved since it is separated from P_4 by only 80 kev, which is little greater than the experimental resolution. The 7·54 MeV level is virtual and has been observed in neutron scattering experiments (Bockelman, Miller, Adair and Barschall 1951).

(*b*) *Angular Distribution.* The angular distributions of the five proton groups associated with the ^{9}Be(d, p)^{10}Be reaction have been measured and are shown in figure 2, together with the curves calculated from the Butler theory. Good agreement was obtained in all cases using the conventional radius parameter of $4{\cdot}2 \times 10^{-13}$ cm except for the ground state which required an unusually large value of $5{\cdot}7 \times 10^{-13}$ cm. Holt and Marsham (1953) and Eby (1954) also report the need for a large radius, values of $5{\cdot}7 \times 10^{-13}$ cm and $5{\cdot}1 \times 10^{-13}$ cm respectively being used.

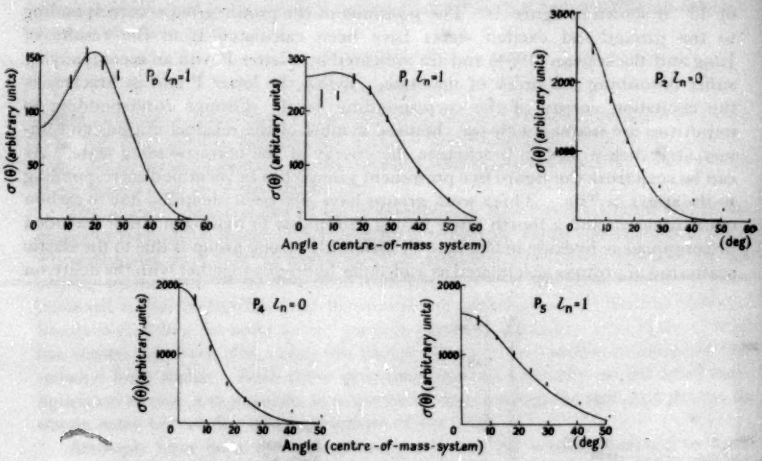

Figure 2. Angular distributions of proton groups P_0, P_1, P_2, P_4 and P_5 from the reaction ^{9}Be(d, p)^{10}Be.

The assignment of $l=1$ to the angular distributions of groups P_0, P_1 and P_5 agree with those reported from other investigations. It may be noted that the distribution of group P_1 exhibits a more pronounced minimum in the forward direction than the theoretical curve and that a similar result was reported by Eby. Anomalies of this type in other stripping reactions have been observed by Middleton, El-Bedewi and Tai (1955) and by Evans, Green and Middleton (1953).

The angular distributions of groups P_2 and P_4, neither of which has previously been measured, are both consistent with the assignment of $l=0$.

(*c*) *Level Properties of* ^{10}*Be.* The relative capture probabilities $\Lambda/(2J_f+1)$ and reduced widths γ^2 have been calculated and are listed in table 1. The spins of the ground and 3·37 MeV states were assumed to be 0 and 2 respectively. Also shown in the table are the absolute reduced widths of these two levels

calculated by Fujimoto, Kikuchi and Yoshida (1954) from the (d,p) data reported by Fulbright, Bruner, Bromley and Goldman (1952) and that of the 7·37 MeV level reported by Bockelman, Miller, Adair and Barschall (1951) from an investigation of neutron scattering by ^{9}Be.

Table 1

Group	Energy level (MeV)	l	Spin and parity	$A/(2J_t+1)$ (rel. units)	γ^2 (rel. units)	$\gamma^2/\frac{3\hbar^2}{2\mu a}$
P_0	0	1	0^+	45	22	0·055[a]
P_1	3·37	1	2^+	8	8	0·010[a]
P_2	5·96	0	1^-, 2^-	22, 13	110, 66	
P_4	6·26	0	1^-, 2^-	15, 9	103, 62	
P_5	7·37	1	2^+, 3^+	13, 9	9, 7	0·017[b]

[a] reduced width from (d, p) data (Fujimoto *et al.* 1954).
[b] reduced width from neutron scattering data (Bockelman *et al.* 1951).

The even parity levels, formed by the capture of a neutron with unit angular momentum, are presumably states of the $(1p)^6$ configuration. Inglis (1953) has shown that intermediate coupling predicts such states to be most probably in the order 0^+, $2,^+$ 2^+. The first two states are in agreement with this, but the third has been reported to be 3^+ (Adair, Barschall, Bockelman and Sala 1949). Our analysis allows either 2^+ or 3^+ but calculations show that the reduced width of a 3^+ level would be vanishingly small on either j–j or L–S coupling extremes (Lane 1954, Elliot, private communication), though the widths of 0^+ and 2^+ levels would be in the ratios 1:0·2 and 1:0·44 respectively. The experimental evidence shows that the reduced widths of the 3·37 and 7·37 MeV levels are about the same and thus favours an assignment of 2^+ to the latter level. This agrees with the suggestion that the 7·37 MeV level is the isobar of the 8·89 MeV level of ^{10}B which is known to be 2^+, $T=1$ (Mackin 1954).

The two odd parity levels are probably states of the simple configuration $(1p)^5$ 2s and have as expected large capture probabilities and reduced widths. These are probably the 1^- and 2^- levels predicted by Thomas (see Ajzenberg and Lauritsen 1952) from an analysis of the scattering lengths of epithermal neutrons.

3.2. ^{12}C(d, p)^{13}C

(*a*) *Energy Spectrum.* Two carbon exposures have been made with targets of soot and adenine and the spectra obtained at an angle of 15° are shown in figures 3(*a*) and 3(*b*). The pure carbon target was used to identify groups corresponding to ^{13}C and the latter to measure the angular distributions, since the absolute differential cross sections could be determined by comparison with the deuterons elastically scattered by the hydrogen in the target.

Four groups were identified corresponding to the ground and three excited states in ^{13}C, reported by Sperduto, Buechner, Bockelman and Browne (1954), and are designated by letter P_0, P_1, P_2 and P_3 in figure 3(*a*). No other groups of significant intensity, corresponding to levels in ^{13}C below an excitation of 6·8 MeV, were observed. Two groups were also observed corresponding to levels in ^{14}C at 6·091 and 6·723 MeV due to the presence of 1·1 % of ^{13}C in natural carbon. The remaining groups are due to oxygen and hydrogen contamination in the target and the presence of molecular hydrogen in the cyclotron beam.

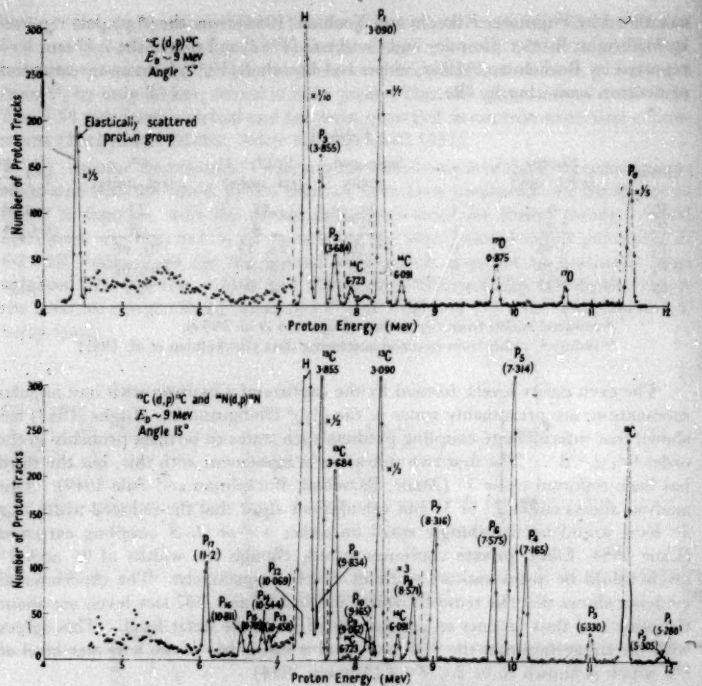

Figure 3. Proton energy spectra at angles of observation of 15° resulting from the deuteron bombardment of targets of (*a*) soot and (*b*) adenine ($C_5N_5H_5$).

(*b*) *Angular Distributions.* The angular distributions of groups P_0, P_1, P_2 and P_3 from ^{12}C have been measured and are shown together with the Butler curves in figure 4. The *l*-values are in agreement with those reported by Rotblat (1951 a, b). It may be noted that the angular distribution of group P_0 exhibits a similar anomaly to that observed for the 3·37 Mev level in ^{10}Be.

Since the adenine contained a known ratio of hydrogen to carbon it was possible to express the differential cross sections in terms of those for the scattering of deuterons by hydrogen. The latter was determined at 8·9 Mev deuteron energy by interpolation from the data of Sherr, Blair, Kratz, Bailey and Taschek (1947), Rosen and Allred (1951) and Allred, Armstrong, Bondelid and Rosen (1952). The cross sections determined in this way are considered accurate to within 10 %.

(*c*) *Level Properties of* ^{13}C. The absolute reduced widths have been calculated and are listed in table 2. The value obtained for the ground state is compared with that reported by Thomas (1952) from an analysis of thermal neutron scattering data, and those for the excited states with the values obtained by Jackson and Galonsky (1951) for the levels of the mirror nucleus ^{13}N from an

investigation of the resonance scattering of protons. A comparison is also made of the capture probabilities derived during the present investigation with those calculated by Holt and Marsham (1953) from the results of Rotblat (1951 a, b).

Table 2

Group	Energy level (Mev)	l	Spin and parity	$\gamma^2 / \frac{3\hbar^2}{2\mu a}$		$A/(2J_f+1)$	
				a	b	c	d
P_0	0	1	$1/2^-$	0·05	0·02	25	25
P_1	3·090	0	$1/2^+$	0·27	0·54	40	30
P_2	3·684	1	$3/2^-$	0·016	0·03	5	2
P_3	3·855	2	$5/2^+$	0·06	0·21	33	45

a and c, reduced widths and capture probabilities from present investigations.
b, reduced widths for ground state of ^{13}C (Thomas) and for corresponding states of mirror nucleus ^{13}N (Jackson and Galonsky).
d, relative capture probabilities calculated from the results of Rotblat.

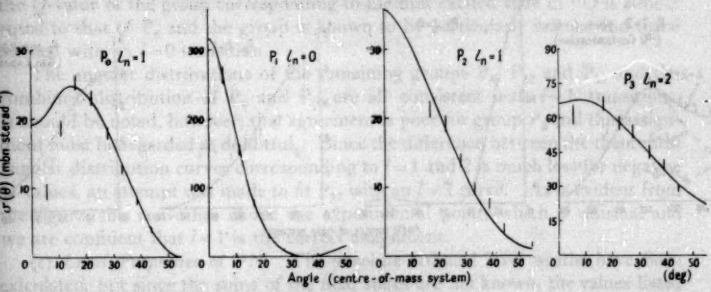

Figure 4. Angular distributions of proton groups P_0, P_1, P_2 and P_3 from the reaction $^{12}C(d, p)^{13}C$.

3.3. $^{14}N(d, p)^{15}N$

(*a*) *Energy Spectrum.* Proton groups in the spectrum shown in figure 3(*b*) were identified with transitions to the energy levels of ^{15}N reported by Sperduto *et al.* and are designated P_0, P_1, P_2 etc. The proton group P_0, corresponding to the ground state, was not observed because of its large Q-value and groups P_9 and P_{11} corresponding to levels at 9·062 and 9·834 Mev respectively were obscured by carbon groups. In the figure carbon is treated as if it were a contamination and the corresponding groups are designated by the chemical symbol accompanied by the excitation energy. Group P_{12} corresponding to a level in ^{15}N at 10·069 Mev is obscured by the hydrogen group, but this only occurs at this particular angle of observation. A new group of protons P_{17} was also observed corresponding to a level at approximately 11·2 Mev.

(*b*) *Angular Distributions.* The angular distributions of groups P_3, P_4, P_5, P_6, P_7, P_8, P_{12} and P_{17} have been measured and are plotted in the centre-of-mass system in figure 5. Also shown in the figure are the combined distributions of groups P_1 and P_2 which were beyond the resolution of the spectrograph and groups P_9 and P_{10}. The latter two groups could in principle be resolved using the adenine target, but at most angles of observation at least one, and sometimes both, were obscured by a carbon group. The combined distribution was

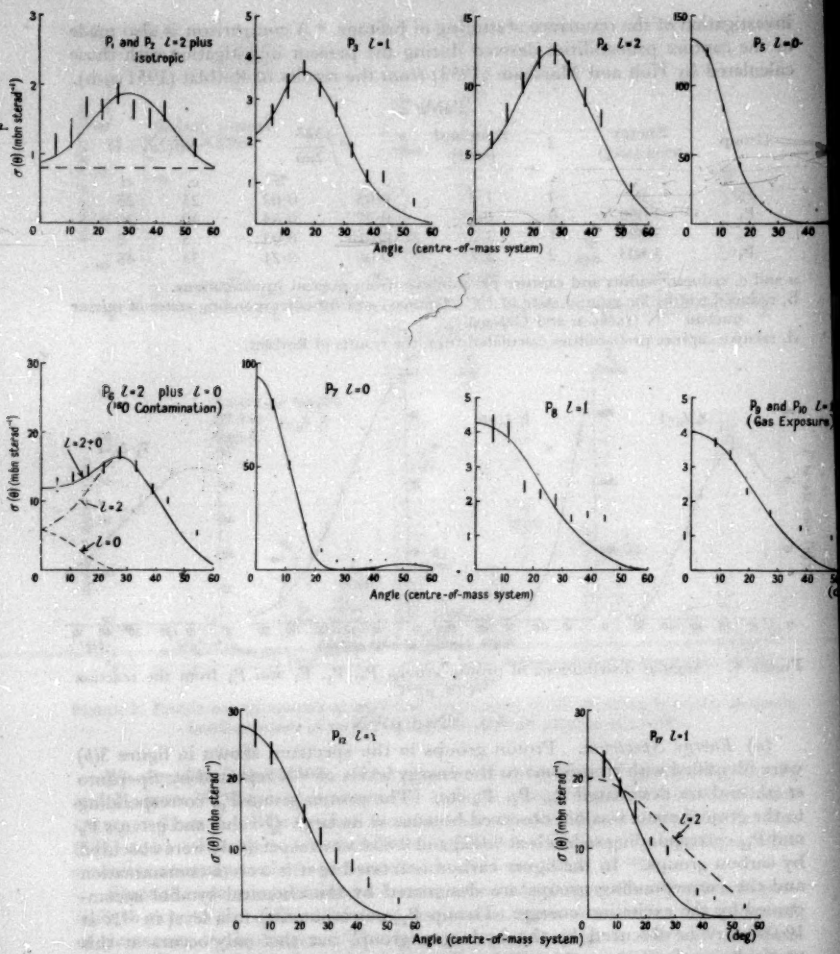

Figure 5. Angular distributions of proton groups P_3, P_4, P_5, P_6, P_7, P_8, P_{12} and P_{17} and the combined distributions of groups P_1, P_2 and P_9, P_{10} from the reaction $^{14}N(d, p)^{15}N$. The last mentioned combined distribution was obtained from the gas exposure.

obtained from the gas exposure, the resolution being worse in this case because of the poorer geometry and the straggling introduced by the gas and aluminium windows outside the genuine target volume. It was observed, however, that the group shape was symmetrical at all angles of observation and is consistent

with both groups being of approximately equal intensity and of similar angular distributions. The theoretical curves shown in the figure were calculated from the Butler theory, using a radius of $4{\cdot}7\times10^{-13}$ cm in all cases except for groups P_8 and P_{12} where better agreement was obtained with a radius of $5{\cdot}7\times10^{-13}$ cm.

The assignments of l-values of 1, 0 and 0 respectively to groups P_3, P_5 and P_7 agree with the values reported by Gibson and Thomas (1952), but, unlike these authors, we obtain an anisotropic combined distribution for groups P_1 and P_2. The latter distribution is consistent with one of these levels being formed by an $l=2$ transition and the other most probably isotropic. Eby also reports the combined angular distribution to be anisotropic.

The angular distributions of groups P_4 and P_6 are each consistent with $l=2$ transitions, but, as can be seen from the figure, P_6 does not exhibit as pronounced a minimum in the forward direction as either P_4 or the theoretical curves. This is thought to be due to the presence of a small oxygen impurity in the target, since the Q-value of the group corresponding to the first excited state in ^{17}O is almost equal to that of P_6 and the group is known to be particularly intense and to be formed with an $l=0$ transition.

The angular distributions of the remaining groups P_8, P_{12} and P_{17} and the combined distribution of P_9 and P_{10} are all consistent with $l=1$ transitions. It should be noted, however, that agreement is poor for group P_8 and this assignment must be regarded as doubtful. Since the difference between the theoretical angular distribution curves corresponding to $l=1$ and 2 is much less for negative Q-values, an attempt was made to fit P_{17} with an $l=2$ curve. As is evident from the figure, this curve lies above the experimental points which is unusual and we are confident that $l=1$ is the correct assignment.

(*c*) *Level Properties of* ^{15}N. The absolute reduced level widths have been calculated, but since the spins of the final states are not known, the values listed in table 3 contain the factor $2J_f+1$.

Several levels corresponding to $l=1$ transitions have been observed which can only have been formed by the addition of 1p or 2p neutrons to the ^{14}N core. The selection rules of the stripping theories predict these levels to be of odd parity and possible spin values of $\frac{1}{2}$, $\frac{3}{2}$ and $\frac{5}{2}$. If a 1p neutron is added to the ^{14}N core then the independent particle model would exclude the possibilities of a spin of $\frac{5}{2}$, the only possible values being $\frac{1}{2}$ and $\frac{3}{2}$.

Table 3

Group	Energy Level (Mev)	l	Parity	$(2J_f+1)\gamma^2\Big/\frac{3\hbar^2}{2\mu a}$
P_1, P_2	5·280/5·305	2	+	0·03
P_3	6·330	1	−	0·04
P_4	7·165	2	+	0·32
P_5	7·314	0	+	0·45
P_6	7·575	2	+	0·41
P_7	8·316	0	+	0·40
P_8	8·571	1?	−?	0·03
P_9, P_{10}	9·062/9·165	1	−	0·03
P_{12}	10·069	1	−	0·14
P_{17}	11·2	1	−	0·24

The ground state is presumably the $J=\frac{1}{2}$ component of this configuration and probably the 6·33 Mev level the $J=\frac{3}{2}$ component. In the limit of extreme j–j

coupling the latter level would have zero reduced width and since it is observed to have a small but finite reduced width it may be concluded that this extreme form of j–j coupling is not valid. This conclusion is consistent with the recent successes obtained from calculations based on intermediate coupling for certain light nuclei.

The odd parity levels at 10·069 and 11·2 MeV have large reduced widths and are probably states of the configuration $(1p)^{10}2p$. Similarly the even parity levels, having large reduced widths, are probably states with the configurations $(1p)^{10}2s$ and $(1p)^{10}1d$ predominating.

3.4. $^{16}O(d, p)^{17}O$

(*a*) *Energy Spectrum.* In figures 6(*a*) and 6(*b*) are shown typical proton energy spectra at angles of observation of 15° and 40° obtained using the oxygen gas and quartz targets respectively. It is evident from the figures that the

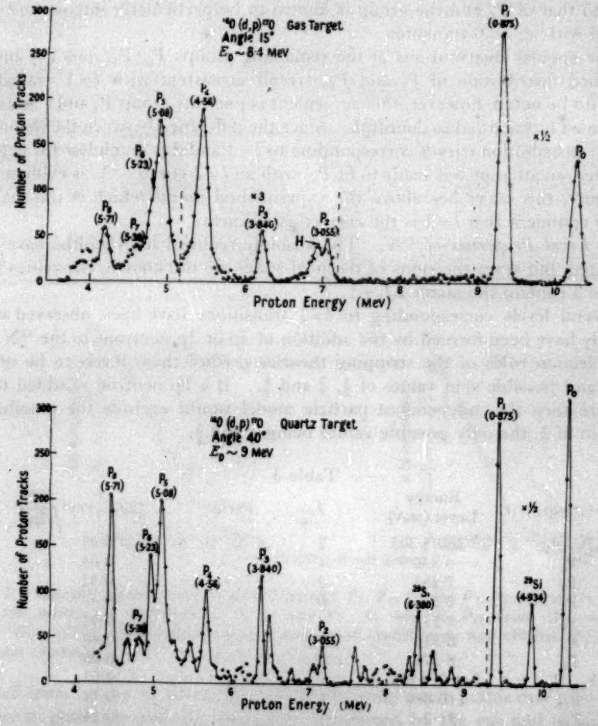

Figure 6. Proton energy spectrum at an angle of observation of : (*a*) 15° resulting from the bombardment of an oxygen gas target by 8·4 MeV deuterons ; (*b*) 40° resulting from the bombardment of a thin self-supporting target of quartz by 9 MeV deuterons.

resolution was better when using the quartz target but the spectrum was complicated by the presence of silicon. To facilitate the identification of the groups in the latter spectrum several exposures were made at different angles with a pure silicon target.

Groups have been identified corresponding to the levels in ^{17}O reported by Ajzenberg and Lauritsen (1955) and are designated P_0, P_1, P_2 etc. in both figures. A group (P_6) was observed corresponding to a level at 5·23 MeV which was reported by the above authors to be doubtful.

(*b*) *Angular Distributions.* The angular distributions of groups P_0 to P_5 have been measured and are shown in figure 7 together with the theoretical curves calculated from the Butler and Bhatia *et al.* stripping theories using radii of interaction of $4{\cdot}8 \times 10^{-13}$ cm and $5{\cdot}8 \times 10^{-13}$ cm respectively. One curve only is shown in each case for groups P_0, P_1 and P_5 since both theories predict very similar distributions. There is a slight difference between the curves calculated on the different theories in the case of group P_3 and for group P_4 agreement could only be obtained using the Bhatia *et al.* stripping theory. The lack of agreement with the Butler curve is probably due to the singularity in the theory for a negative Q-value numerically equal to the binding energy of the deuteron (Middleton *et al.* 1953), the Q-value of this group being $-2{\cdot}6$ MeV. Due to this lack of agreement it was not possible to calculate the reduced width of the level corresponding to group P_4. An attempt was also made to fit the distribution

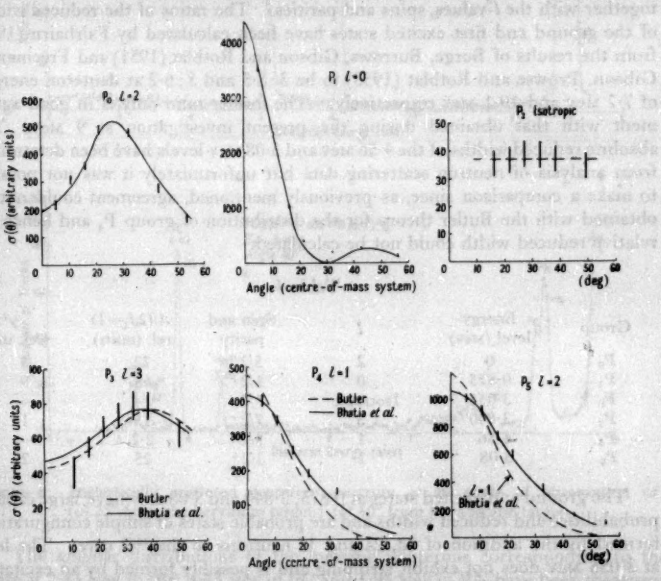

Figure 7. Angular distribution of proton groups P_0, P_1, P_2, P_3, P_4 and P_5 from the reaction $^{16}O(d, p)^{17}O$. Distributions of groups P_2 and P_5 were obtained from the gas exposure and the remainder from the quartz target.

of group P_5 with an $l=1$ curve in addition to the better fitting $l=2$ curve since for extreme negative Q-values the difference between theoretical curves corresponding to various l-values is small. Finally, it should be stated that the angular distributions of groups P_2 and P_3 were measured from the plates exposed to the gas target due to the interference of the silicon at small angles in the quartz exposure.

The l-values assigned to the transitions to the ground and excited states of ^{17}O agree with those reported by Burrows, Gibson and Rotblat (1950). The angular distribution of group P_2 does not appear to exhibit stripping, but this result is not conclusive, since the measurements at small angles were unreliable, due to the presence of a small amount of hydrogen in the gas target. The remaining groups, P_3, P_4 and P_5 were consistent with l-values of 3, 1 and 2 respectively. The former assignment is consistent with the reported spin and parity of $7/2^-$ of the mirror level in ^{17}F (Laubenstein and Laubenstein 1951) and the latter pair with the values of $3/2^-$ and $3/2^+$ for the 4·56 and 5·08 Mev levels in ^{17}O (Adair 1953).

It was not possible to make reliable measurements of the angular distributions of groups P_6, P_7 and P_8 due to the poor resolution and the presence of a large proton background.

(*c*) *Level Properties of* ^{17}O. The relative capture probabilities and reduced level widths have been calculated wherever possible and are listed in table 4 together with the l-values, spins and parities. The ratios of the reduced widths of the ground and first excited states have been calculated by Fairbairn (1954) from the results of Burge, Burrows, Gibson and Rotblat (1951) and Freemantle, Gibson, Prowse and Rotblat (1953) to be 3 : 8·5 and 3 : 6·2 at deuteron energies of 7·7 Mev and 19·1 Mev respectively. The former ratio only is in good agreement with that obtained during the present investigation at 9 Mev. The absolute reduced widths of the 4·56 Mev and 5·08 Mev levels have been determined from analysis of neutron scattering data but unfortunately it was not possible to make a comparison since, as previously mentioned, agreement could not be obtained with the Butler theory for the distribution of group P_4 and hence the relative reduced width could not be calculated.

Table 4

Group	Energy level (Mev)	l	Spin and parity	$A/(2J_f+1)$ rel. (units)	γ^2 (rel. units)
P_0	0	2	$5/2^+$	72	3
P_1	0·875	0	$1/2^+$	68	9
P_2	3·055	Isotropic	$1/2^-$	—	—
P_3	3·840	3	$7/2^-$	15	1
P_4	4·56	1	$3/2^-$	2·2	—
P_5	5·08	2	$3/2^+$	25	2

The ground and excited states at 0·875, 3·840 and 5·08 Mev have large capture probabilities and reduced widths and are probable states of simple configurations formed by the addition of 1d, 2s and 1f neutrons to the ^{16}O core. The level at 3·055 Mev does not exhibit stripping and is possibly formed by an excitation of the ^{16}O core. Similarly the level at 4·56 Mev which does exhibit stripping but has a small capture probability is also probably not a state of simple configuration.

§ 4. Inelastic Scattering of Deuterons

Limitations in the present technique prevented a systematic investigation of the inelastic scattering of deuterons. However, some preliminary measurements have been made for ^{9}Be, ^{12}C and ^{14}N. In figure 8(*a*) is shown the deuteron spectrum observed at an angle of 25° from the ^{9}Be target. Two elastically scattered groups due to ^{9}Be and H, and one inelastic group corresponding to a level in ^{9}Be at 2·43 Mev have been identified. No groups of significant intensity were observed corresponding to the levels at 1·8, 3·2 and 4·9 Mev (Moak, Good and Kunz 1954). In figure 8(*b*) is shown the deuteron spectrum from the adenine target observed at an angle of 40°. Three elastically scattered groups were identified corresponding to the gold target backing, carbon and nitrogen and also four inelastic groups corresponding to states at 3·95, 4·92 and 5·10 Mev in ^{14}N and at 4·43 Mev in ^{12}C.

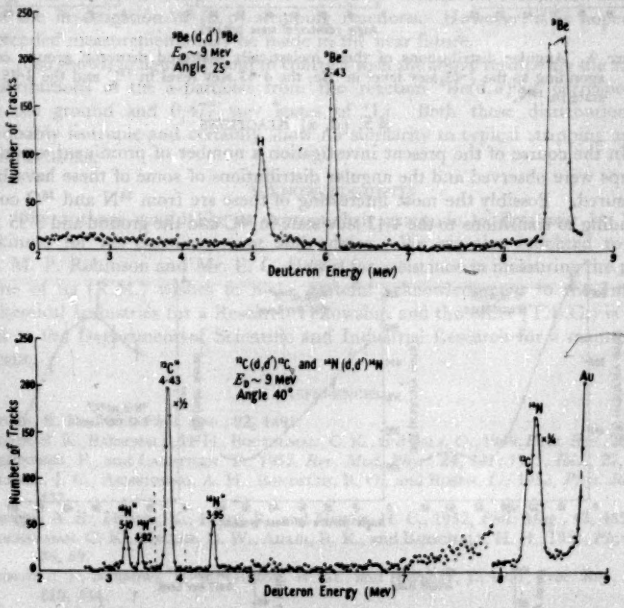

Figure 8. Inelastically scattered deuteron spectrum at an angle of observation of: (*a*) 25° from the beryllium target; (*b*) 40° from the adenine target.

The angular distributions of the inelastic deuterons corresponding to the state at 2·43 Mev in ^{9}Be, 4·43 Mev in ^{12}C and 3·95 Mev in ^{14}N have been measured and are shown in figure 9. The differential cross section of the ^{12}C and ^{14}N inelastic groups are presented in absolute units and those of ^{9}Be in the same relative units as the ^{9}Be (d, p)^{10}Be angular distributions. No attempt has been

made to fit the results with theoretical curves, since neither the ^{9}Be nor the ^{13}C distributions resemble typical stripping curves which are predicted by the theory of inelastic deuteron scattering reported by Huby and Newns (1951). It may be noted, however, that the differential cross sections are of the same order of magnitude as those of the corresponding (d, p) reactions.

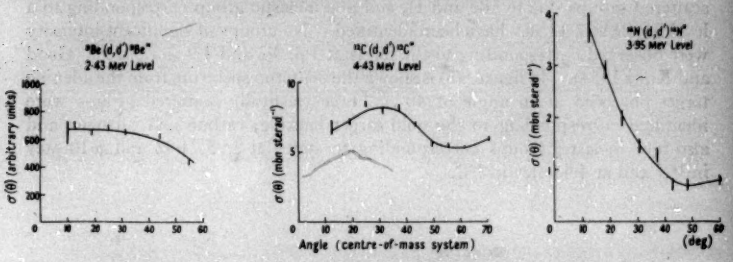

Figure 9. Angular distributions of three inelastically scattered deuteron groups corresponding to the 2·43 MeV level in ^{9}Be, the 4·43 MeV level in ^{13}C and the 3·95 MeV state in ^{14}N.

§ 5. (d, α) Reactions

In the course of the present investigation a number of prominent α-particle groups were observed and the angular distributions of some of these have been measured. Possibly the most interesting of these are from ^{14}N and ^{16}O corresponding to transitions to the 4·43 MeV state in ^{12}C and the ground and 3·95 MeV

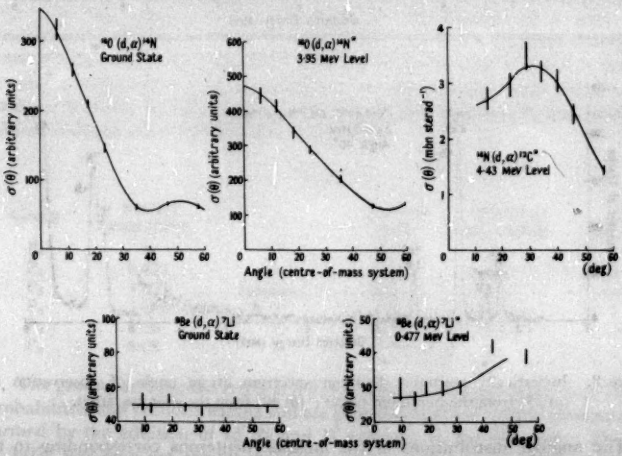

Figure 10. Angular distributions of two α-particle groups from the ^{16}O(d, α)^{14}N reaction corresponding to the ground and excited state at 3·95 MeV, one group from the ^{14}N(d, α)^{12}C reaction corresponding to an excited state at 4·43 MeV and two groups from ^{9}Be(d, α)^{7}Li reaction corresponding to the ground and excited state at 0·477 MeV.

states in ^{14}N. As can be seen from figure 10 the angular distributions at small angles of emission are similar to those obtained from (d, p) stripping reactions and those predicted by the theory of (d, t) pick-up reactions (Newns 1952). It therefore appears possible that the mechanism of (d, α) reactions at intermediate deuteron energies might be similar to that of (d, t) pick-up reactions, a deuteron or neutron and proton being picked up by the incident deuteron as opposed to a single proton in the latter type reaction. However, it is fairly evident that since measurements were made only over a limited angular range the observed distributions could be fitted with power series of cosines not exceeding the sixth power and the possibility that the reactions proceed via a compound nucleus stage cannot be ruled out. It is thought that extending measurements to backward angles to ascertain if the distribution is symmetrical about 90° may give some indication as to which of the above possible mechanisms may be correct. Unfortunately, this was not possible during the present investigation since the target chamber was designed not to exceed 60° which was considered adequate for the investigation of (d, p) stripping reactions. However, it is hoped that extended measurements may be made in the near future.

Also shown in figure 10, and in contrast with the above results, are the angular distributions of the α-particles from the reaction $^{9}Be(d,\alpha)^{7}Li$ corresponding to the ground and 0·477 MeV states of ^{7}Li. Both these distributions are probably isotropic and certainly show no similarity to typical stripping angular distributions.

Acknowledgments

The authors would like to express their gratitude to Professor H. W. B. Skinner for his encouragement and advice. We are also indebted to Miss P. M. P. Robinson and Mr. E. C. Hewitt for assistance in measuring the plates. One of us (R.M.) wishes to make grateful acknowledgment to the Imperial Chemical Industries for a Research Fellowship and the other (T.S.G.) is grateful to the Department of Scientific and Industrial Research for a maintenance grant.

References

Adair, R. K., 1953, *Phys. Rev.*, **92,** 1491.
Adair, R. K., Barschall, H. H., Bockelman, C. K., and Sala, O., 1949, *Phys. Rev.*, **75,** 1124.
Ajzenberg, F., and Lauritsen, T., 1952, *Rev. Mod. Phys.*, **24,** 321; 1955, *Ibid.*, **27,** 77.
Allred, J. C., Armstrong, A. H., Bondelid, R. O., and Rosen, L., 1952, *Phys. Rev.*, **88,** 433.
Bhatia, A. B., Huang, K., Huby, R., and Newns, H. C., 1952, *Phil. Mag.*, **43,** 485.
Bockelman, C. K., Miller, D. W., Adair, R. K., and Barschall, H. H., 1951, *Phys. Rev.*, **84,** 69.
Burge, E. J., Burrows, H. B., Gibson, W. M., and Rotblat, J., 1951, *Proc. Roy. Soc.* A, **210,** 534.
Burrows, H. B., Gibson, W. H., and Rotblat, J., 1950, *Phys. Rev.*, **80,** 1095.
Butler, S. T., 1951, *Proc. Roy. Soc.* A, **208,** 559.
Eby, F. S., 1954, *Phys. Rev.*, **96,** 1355.
Evans, W. H., Green, T. S., and Middleton, R., 1953, *Proc. Phys. Soc.* A, **66,** 108.
Fairbairn, W. M., 1954, *Proc. Phys. Soc.* A, **67,** 564.
Freemantle, R. G., Gibson, W. M., Prowse, D. J., and Rotblat, J., 1953, *Phys. Rev.*, **92,** 1268.
Fujimoto, Y., Kikuchi, K., and Yoshida, S., 1954, *Prog. Theor. Phys, Osaka*, **2,** 264.
Fulbright, H. W., Bruner, J. A., Bromley, D. A., and Goldman, L. M., 1952, *Phys. Rev.*, **88,** 700.

GIBSON, W. M., and THOMAS, E. E., 1952, *Proc. Roy. Soc.* A, **210,** 543.
GREEN, T. S., and MIDDLETON, R., 1956, *Proc. Phys. Soc.* A, **69,** 16.
HOLT, J. R., and MARSHAM, T. N., 1953, *Proc. Phys. Soc.* A, **66,** 1032.
HUBY, R., 1952, *Proc. Roy. Soc.* A., **215,** 385.
HUBY, R., and NEWNS, H. C., 1951, *Phil. Mag.*, **42,** 1442.
INGLIS, D. R., 1953, *Rev. Mod. Phys.*, **25,** 390.
JACKSON, H. L., and GALONSKY, A. I., 1951, *Phys. Rev.*, **84,** 401.
JUNG, J. J., and BOCKELMAN, C. K., 1954, *Phys. Rev.*, **96,** 1353.
LANE, A. M., 1953, *Proc. Phys. Soc.* A, **66,** 977; 1954, *Atomic Energy Research Establishment, Report T/R* 1289.
LAUBENSTEIN, R. A., and LAUBENSTEIN, J. W., 1951, *Phys. Rev.*, **84,** 18.
MACKIN, R. J., 1954, *Phys. Rev.*, **94,** 648.
MIDDLETON, R., EL-BEDEWI, F. A., and TAI, C. T., 1953, *Proc. Phys. Soc.* A, **66,** 95.
MOAK, C. D., GOOD, W. M., and KUNZ, W. E., 1954, *Phys. Rev.*, **96,** 1363.
NEWNS, H. C., 1952, *Proc. Phys. Soc.* A, **65,** 916.
ROSEN, L., and ALLRED, J. C., 1951, *Phys. Rev.*, **82,** 777.
ROTBLAT, J., 1951 a, *Nature, Lond.*, **167,** 1027; 1951 b, *Phys. Rev.*, **83,** 1271.
SHERR, R., BLAIR, J. M., KRATZ, H. R., BAILEY, C. L., and TASCHEK, R. F., 1947, *Phys. Rev.*, **72,** 662.
SPERDUTO, A., BUECHNER, W. W., BOCKELMAN, C. K., and BROWNE, C. P., 1954, *Phys. Rev.*, **96,** 1316.
THOMAS, R. G., 1952, *Phys. Rev.*, **88,** 1109.

Excitation Functions up to 980 MeV for Proton-Induced Reactions in ^{27}Al, relative to ^{12}C(p, pn)^{11}C

By G. A. CHACKETT, K. F. CHACKETT, P. REASBECK, J. L. SYMONDS and J. WARREN
Department of Physics, The University of Birmingham

MS. received 18*th April* 1955 *and in final form* 26*th October* 1955

Abstract. The activities produced in the bombardment of aluminium with protons in the energy range 200–980 MeV have been studied. The ratio of the cross section for the production of ^{11}C from polythene to that for both ^{18}F and ^{24}Na from aluminium are given in this energy range while cross section ratios of ^{27}Mg, ^{13}N and ^{11}C from aluminium are given at an energy of 980 MeV.

§ 1. Introduction

The activities produced by bombarding aluminium with protons have been studied by various authors from threshold up to about 400 MeV (Hintz and Ramsey 1952, Marquez and Perlman 1951, Marquez 1952), while the excitation function for reactions producing ^{11}C from ^{12}C when bombarded with protons has been the subject of much detailed study over this same energy range (Aamodt, Peterson and Phillips 1952). Recent results from Brookhaven (Wolfgang and Friedlander 1954a) have extended some of the work up to the region of 3 GeV, in the form of the ratio of the cross sections for the production of ^{11}C from polythene to that of ^{24}Na from aluminium. The results presented here for this ratio cover the energy range from 200 to 980 MeV. Results are also presented for the ratio of ^{18}F to ^{24}Na produced in the same aluminium specimen by bombardment with protons, while cross-section ratios for ^{27}Mg, ^{13}N and ^{11}C to ^{24}Na are given at an energy of 980 MeV. We shall denote by a subscript the chemical identity of the target, thus $\sigma_C(^{11}C)$ denotes the cross section for production of ^{11}C in carbon and $\sigma_{Al}(^{11}C)$ the cross section for production of ^{11}C in aluminium.

§ 2. Procedure

2.1. *Irradiation Technique*

The irradiations were carried out in the internal circulating proton beam of the Birmingham proton synchrotron, using a target on the maximum outer radius of the machine. Beam intensities of about 3×10^9 protons per pulse were obtained, at a repetition rate of one pulse every ten seconds. The desired proton energies below 980 MeV were achieved by driving the beam to the target at a given time in the normal acceleration cycle as described by Moon, Riddiford and Symonds (1955). For the irradiation at 980 MeV, the radio-frequency voltage was switched off at peak magnetic field, the beam moving out to the target as the magnetic field fell. When the protons struck the target, some, which were scattered from the machine, fell on a scintillation counter, the

output of which was displayed on an oscilloscope. An accurate knowledge of the magnetic field–time law enabled the energy of the incident protons to be determined from the field and target radius to better than 1%.

The targets generally consisted of three layers of polythene of thickness from 5 to 10 mg cm^{-2}, interleaved with layers of aluminium of thickness about 19 mg cm^{-2}.

The overall thickness of the foil stack was usually less than 80 mg cm^{-2} and it has been estimated that secondary reactions are unlikely to contribute in any great proportion to the activities produced. Tests were made with two types of target holder, one with a considerable amount of metal near the sample foils and one very little. No appreciable difference was indicated by the results.

After irradiation and while the foils were still clamped to the target holder, the stack was cut to remove foils of identical size (approximately 1 cm^2 in area).

2.2. *Beta Counting*

Active foils or chemically separated samples mounted on aluminium or copper trays were counted with a screened GM4 end-window (7 mg cm^{-2}) Geiger counter. If no chemical separation was to be carried out, the polythene foil was counted immediately to estimate the activity of the 20·5 minute ^{11}C. The aluminium foils were counted after about four half-lives of ^{11}C using the same carrier tray under the same counter, care being taken to ensure that the foils were placed in an identical position. Each aluminium foil was counted beforehand under the counter to be used for the chemically separated samples and a comparison foil counted under another counter over the same period.

All measured activities, extrapolated to midtime of bombardment, were corrected for counter background, dead-time losses, self-scattering and self-absorption in the foil or chemically separated material, back-scattering with different tray materials such as aluminium and copper (Burtt 1949), chemical yield if necessary, absorption in the counter window and bombardment time. No correction has been made to β^+-counting rates to make them comparable with β^--counting rates by allowing for the difference between the back-scattering of positrons and electrons in the sample trays (Seliger 1952). Furthermore, no correction has been applied for gamma and annihilation radiation. In § 4, a discussion of the corrections is given as they involve some doubtful factors which are still being investigated.

2.3. *Chemistry*

Chemical separations of the active products were undertaken to identify them chemically as well as from the gross decay measurements in the original foil. The foils were dissolved in acid or alkali containing measured amounts of appropriate carrier, e.g. sodium, fluorine, magnesium.

^{24}Na.

This activity was precipitated as sodium chloride and mounted on a copper tray. In all cases the activity of the sodium chloride corresponded with the activity in the original foil, after all the corrections mentioned in § 2 were made.

^{18}F.

Two separate methods were used for the chemical identification of this isotope.

(*a*) Distillation as silicon tetrafluoride from the dissolved foil in the presence of perchloric acid, fluoride ion carrier and excess silica, the gas being trapped in sodium carbonate solution. The silicic acid was precipitated with ammonium carbonate and the fluoride precipitated and mounted as calcium fluoride.

(*b*) Separation on a cation-exchange column, which had been developed chiefly for use with magnesium. The fluorine was eluted from the column in the first few drops of eluate, and precipitated as calcium fluoride. A discrepancy was observed between the yield of ^{18}F by chemical methods and that from the untreated foil as given by counting methods. This led to a search for other isotopes with a half-life close to that of ^{18}F with no result. Comparison of the three methods for estimating the fluorine activity showed that the distillation process gave about 30% of the ^{18}F activity estimated from the gross decay of untreated foils, and the ion-exchange method only about 10%. It would seem that the chemical state of the ^{18}F atoms at the time of dissolution is such that standard methods of separation are inadequate. A fuller investigation of this effect is to be undertaken.

^{27}Mg.

Since this isotope has a half-life of 9·6 minutes, chemical manipulations must be quite rapid. By the standard method of precipitation as magnesium ammonium phosphate, some ^{18}F contamination appeared, possibly due to fluophosphate formation. To overcome these difficulties, an ion-exchange column, using 'Dowex' cation-exchange resin, was employed. A pure magnesium fraction could be obtained within 5½ minutes from the commencement of foil dissolution, considerably increasing the speed of chemical processing. On precipitation as magnesium ammonium phosphate there was no sign of contamination.

^{13}N.

This activity appears in the gas phase on dissolution of the foil in boiling sodium hydroxide solution to which ammonia carrier has been added. It may be trapped on a filter pad moistened with dilute sulphuric acid and counted as ammonium sulphate.

^{11}C.

This activity also appears in the gas phase on dissolution of the foil in boiling sodium hydroxide solution. It is swept through a copper oxide combustion train, the carbon dioxide produced being trapped in caustic soda and counted as barium carbonate.

§ 3. Results

3.1. *Recoil Losses of ^{18}F and ^{24}Na from ^{27}Al*

By counting over a period of several hours those polythene foils which followed an aluminium foil in the direction of the beam, it was possible to estimate the recoil loss of ^{18}F and ^{24}Na from the aluminium. It was found that this loss was equivalent in activity to a thickness of aluminium of 1·6 μ and 0·7 μ for ^{18}F and ^{24}Na respectively. The relatively small momentum transfer indicated by these figures agrees with the results obtained by others (Fung and Perlman 1952, Wolfgang and Friedlander 1954 b). The correction to the activity produced in the foils used was therefore negligible.

3.2. ^{11}C *in Polythene—*^{18}F *and* ^{24}Na *in Aluminium*

These nuclei are readily identified by their characteristic half-lives. A bombardment time of ten minutes gave sufficient activity to obtain the ratios

$$\sigma_C(^{11}C)/\sigma_{Al}(^{24}Na) \quad \text{and} \quad \sigma_{Al}(^{18}F)/\sigma_{Al}(^{24}Na)$$

at any proton energy from 200 MeV to 980 MeV. The figure gives the combined results of several runs at each different energy for these ratios. On this same figure are plotted the results of experiments carried out elsewhere.

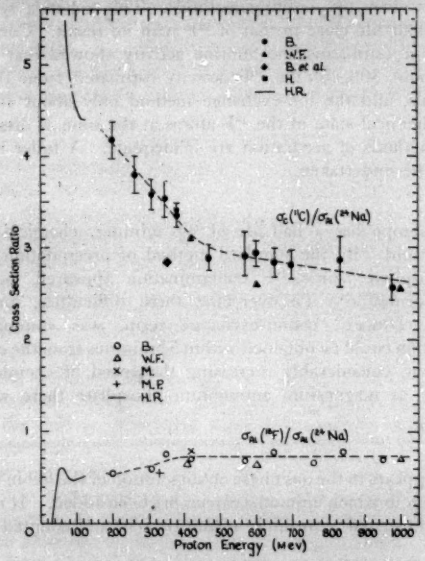

The cross section ratios $\sigma_C(^{11}C)/\sigma_{Al}(^{24}Na)$ and $\sigma_{Al}(^{18}F)/\sigma_{Al}(^{24}Na)$ as a function of energy. B, this paper; B. *et al.*, Birnbaum *et al.* 1954; H., Holt, preliminary result; H.R., Hintz and Ramsay 1952; M., Marquez 1952; M.P., Marquez and Perlman 1951; W.F. Wolfgang and Friedlander 1954 a, b.

Errors on $\sigma_C(^{11}C)/\sigma_{Al}(^{24}Na)$ are r.m.s. errors of all runs at each point.

3.3. ^{27}Mg, ^{13}N *and* ^{11}C *from aluminium*

A search for a reaction for the type $^{27}Al(p, p\pi^+)^{27}Mg$ was made [cf. $^{65}Cu(p, p\pi^+)^{65}Ni$ investigated by Fung and Turkevitch (1954)], since the cross section for π^+-meson production using 980 MeV protons should be quite appreciable. The difficulties experienced in extracting the 9·6 minute ^{27}Mg activity quickly are mentioned earlier and at least two half-lives elapsed before the extracted sample was placed under the counter. Evidence was found at 980 MeV for a small activity with approximately this half-life which enables us to set an upper limit for the ratio $\sigma_{Al}(^{27}Mg)/\sigma_{Al}(^{24}Na)$ of 3×10^{-2}. It is of course possible that this activity may be due in part to neutrons arising from $^{27}Al(n, p)^{27}Mg$; a small secondary neutron flux is undoubtedly produced in

the target. Similar runs at energies of about 400 MeV showed no sign of the 9·6 minute activity (ratio less than 10^{-3}).

Though the magnitudes of the cross sections at 980 MeV and 400 MeV are in agreement with the expected behaviour for this type of reaction, the evidence for it is still somewhat inconclusive. Reliable measurements of this ratio would need a proton beam whose mean intensity is larger by at least another order of magnitude. ^{11}C and ^{13}N were separated chemically from the aluminium foils. Further work is in progress to determine the relative excitation functions for the cross section for their production but preliminary figures for their cross section relative to $\sigma_{Al}(^{24}Na)$ at 980 MeV are :

$$\sigma_{Al}(^{11}C)/\sigma_{Al}(^{24}Na) = 0{\cdot}42 \pm 20\%$$
$$\sigma_{Al}(^{13}N)/\sigma_{Al}(^{24}Na) = 0{\cdot}13 \pm 20\%.$$

§ 4. Discussion

4.1. *Accuracy of Results*

Corrections to the measured counting rates to give absolute disintegration rates have some considerable importance as, in the worst cases, they are of the order of 10%. The self-scattering and self-absorption corrections used were taken from published data (Hintz and Ramsey 1952, Batzel *et al.* 1953) and from measurements made in this laboratory. The multiplying factors used on the counting rates to allow for self-scattering and self-absorption, taken together, were 1·036 for 5·5 mg cm^{-2} polythene and 1·086 for 19 mg cm^{-2} aluminium.

Since the shape of the curve for the cross section ratio $\sigma_C(^{11}C)/\sigma_{Al}(^{24}Na)$ as a function of proton energy was not affected by these considerations, it was felt that the results should be published while further work was in progress to determine these corrections more exactly. The ratio measurements relative to each other were considered to have errors of not more than $\pm 5\%$.

The difference between electron and positron scattering must lead to some difference in the corrections applicable to the observed counting rates for emitters of these particles. Seliger (1952) has found that, for sources of zero thickness mounted on aluminium backing, the multiplying factor for the ratio of positron to electron emitter counting rates in less than 2π geometry should be 1·12. However, for a source which is not of zero thickness, the back-scattering effect of the aluminium backing will be modified by the self-scattering and self-absorption in the source itself. Only the use of a 4π counter and an accurate set of measurements with Geiger counters, related to the results of the 4π measurements for various source thicknesses will resolve this difficulty. Taking all these possible factors into consideration the absolute values of the ratio are not certain to be better than $\pm 15\%$. On this basis the agreement with the results of Wolfgang and Friedlander (1954) is reasonable.

4.2. *Excitation Functions for ^{11}C and ^{24}Na Production*

The ratio of $\sigma_C(^{11}C)$ and to $\sigma_{Al}(^{24}Na)$ as a function of energy presents some interesting features. The relatively steep drop in the region from 200 MeV to 500 MeV is surprising as the recent results of Birnbaum *et al.* (1954) and Burcham *et al.* (1955) show only a slow change in $\sigma_C(^{11}C)$ in this region. The inference is that $\sigma_{Al}(^{24}Na)$ rises steadily in this same energy range although there appears to be evidence that this cross section is nearly constant from 120–200 MeV. A collection of the results of Hintz and Ramsey (1952), Aamodt *et al.* (1952),

Birnbaum *et al.* (1954) and Burcham *et al.* (1955) shows that the value of $\sigma_C(^{11}C)$ rises sharply with increasing energy up to about 100 mbn at 50 Mev, this being following by a rapid fall to about 34 mbn at 250 Mev. Subsequently the cross section decreases slowly to about 21 mbn at 950 Mev. Thus above 250 Mev, the value of $\sigma_{Al}(^{24}Na)$ deduced from these figures and the measured ratio figures rises from about 8·6 mbn to a maximum of 9·6 mbn at about 550 Mev and then decreases to about 7·8 mbn at 980 Mev. These results are lower than those given by Friedlander, Hudis and Wolfgang (1955). Their value of $\sigma_{Al}(^{24}Na)$ decreases steadily from about 11 mbn at 600 Mev (based on the result of Marquez (1952) of 10·8 mbn at 450 Mev) to 8·1 mbn at 3000 Mev. The discrepancy between all the figures for $\sigma_{Al}(^{24}Na)$ could be the result of discrepancies in any one or all of the results but it seems certain that the differences could be resolved to a great extent if the corrections to observed counting rates to give absolute disintegration rates were known more precisely.

Acknowledgments

The authors wish to thank the proton synchrotron staff for the help given in the preparation and irradiation of targets. They would thank also Professor W. E. Burcham and Mr. J. D. Young for helpful discussions on the $^{12}C(p, pn)^{11}C$ reaction, and Dr. J. R. Holt for preliminary figures on similar work with the Liverpool synchrocyclotron.

References

Aamodt, R., Peterson, V., and Phillips, R., 1952, *Phys. Rev.*, **88,** 739.
Batzel, R. E., Crane, W. W. T., and O'Kelley, G. D., 1953, *Phys. Rev.*, **91,** 939.
Birnbaum, W., Crandall, W E., Milburn, G. P., and Pyle, R. V., 1954, University of California, UCRL-2756.
Burcham, W. E., Symonds, J. L., and Young, J., 1955, *Proc. Phys. Soc.* A, **68,** 1001.
Burtt, B. P., 1949, *Nucleonics*, **5,** August, 28.
Friedlander, G., Hudis, J., and Wolfgang, R. L., 1955, *Phys. Rev.*, **99,** 263.
Fung, S., and Perlman, I., 1952, *Phys. Rev.*, **87,** 623.
Fung, S., and Turkevitch, A., 1954, *Phys. Rev.*, **95,** 176.
Hintz, F., and Ramsey, N., 1952, *Phys. Rev.*, **88,** 19.
Marquez, L., 1952, *Phys. Rev.*, **88,** 225.
Marquez, L., and Perlman, I., 1951, *Phys. Rev.*, **81,** 953.
Moon, P. B., Riddiford, L., and Symonds, J. L., 1955, *Proc. Roy. Soc.* A, **230,** 204.
Seliger, H. H., 1952, *Phys. Rev.*, **88,** 408.
Warshaw, S. D., Swanson, R. A., and Rosenfeld, A. H., 1954, *Phys. Rev.*, **95,** 649.
Wolfgang, R., and Friedlander, G., 1954 a, *Phys. Rev.*, **96,** 190; 1954 b, *Ibid.*, **94,** 775.

On the Method of Atoms in Molecules
II : An Intra-Atomic Correlation Correction

By A. C. HURLEY
Department of Theoretical Chemistry, University of Cambridge

Communicated by H. C. Longuet-Higgins; MS. received 11th August 1955

Abstract. The method of atoms in molecules is modified in such a way as to overcome difficulties encountered in previous calculations. The modified theory is applied to two calculations on the ground state of the hydrogen molecule. The more accurate of the two modified calculations leads to an energy curve accurate to within 0·05 electron volt in the range 1 to 4 atomic units of the nuclear separation.

---

§ 1. Introduction

In an earlier paper (Part I, Hurley 1955, to be referred to as I), the method of atoms in molecules developed by Moffitt (1951) was investigated in detail for the ground state of the hydrogen molecule. The results of the calculations were somewhat disappointing. It was found that, if the same screening constants were used for the ionic wave function as for the atomic wave function, the method broke down and did not give a good approximation to an exact calculation in terms of any wave functions. If a different screening constant was used for the ionic wave functions the method was successful inasmuch as it appeared to provide a good approximation to a calculation in terms of accurate atomic wave functions. However, the energy values obtained were much too high, indicating that the accurate atomic wave functions did not form a suitable basis for a molecular calculation. In the present paper a modification of Moffitt's correction is developed. The new correction gives excellent results for the hydrogen molecule and is immediately applicable to more complex systems.

§ 2. The Energies of Various Ionic Wave Functions

The reason for the breakdown of the method of atoms in molecules is most evident from a consideration of the energies of various ionic wave functions for the hydrogen molecule. We consider the three functions

$$\widetilde{\Psi}_{\mathrm{I1}} = 2^{-1/2}[a(1)\,a(2) + b(1)\,b(2)], \qquad \ldots\ldots(2.1)$$

$$\widetilde{\Psi}_{\mathrm{I2}} = 2^{-1/2}[a'(1)\,a'(2) + b'(1)\,b'(2)], \qquad \ldots\ldots(2.2)$$

and

$$\Psi_{\mathrm{I}} = 2^{-1/2}[\phi_a(1,2) + \phi_b(1,2)], \qquad \ldots\ldots(2.3)$$

where

$$a = \left(\frac{1}{\pi}\right)^{1/2} \exp(-r_a), \qquad b = \left(\frac{1}{\pi}\right)^{1/2} \exp(-r_b),$$

$$a' = \left(\frac{Z^3}{\pi}\right)^{1/2} \exp(-Zr_a), \quad b' = \left(\frac{Z^3}{\pi}\right)^{1/2} \exp(-Zr_b), \quad Z = 0{\cdot}6875$$

and ϕ_a, ϕ_b are exact were functions for the system H^-.

The energies $\widetilde{E}_{I1}(R)$ and $\widetilde{E}_{I2}(R)$ for the wave functions $\widetilde{\Psi}_{I1}$ and $\widetilde{\Psi}_{I2}$ are easily obtained by direct integration. That of the wave function Ψ_I is obtained by using the first form of the method of atoms in molecules, namely†

$$H=\widetilde{H}+\tfrac{1}{2}[\widetilde{M}(W-\widetilde{W})+(W-\widetilde{W})\widetilde{M}]. \qquad \ldots\ldots(2.4)$$

For the energy $E_I(R)$ of the ionic wave function (2.3) at nuclear separation R equation (2.4) gives simply

$$E_I(R)=\widetilde{E}_I(R)+W_I-\widetilde{W}_I, \qquad \ldots\ldots(2.5)$$

where $\widetilde{E}_I(R)$ is the energy of an orbital wave function $\widetilde{\Psi}_I$ approximating to Ψ_I, and W_I, $\widetilde{W}_I$ are the energies of an isolated H^- ion given by Ψ_I, $\widetilde{\Psi}_I$ respectively. For W_I we take the value $-0{\cdot}52756$ atomic unit (A.U.) ($=-14{\cdot}4$ ev) given by Chandrasekhar's (1944) eleven-term function.

Thus if we use $\widetilde{\Psi}_{I1}$ of (2.1) for $\widetilde{\Psi}_I$ we obtain for $E_I(R)$ the estimate

$$E_{I1}(R)=\widetilde{E}_{I1}(R)+W_I-\widetilde{W}_{I1}=\widetilde{E}_{I1}(R)-4{\cdot}2\,\text{ev}, \qquad \ldots\ldots(2.6)$$

whereas if we use $\widetilde{\Psi}_{I2}$ of (2.2) for $\widetilde{\Psi}_I$ we obtain

$$E_{I2}(R)=\widetilde{E}_{I2}(R)+W_I-\widetilde{W}_{I2}=\widetilde{E}_{I2}(R)-1{\cdot}5\,\text{ev}. \qquad \ldots\ldots(2.7)$$

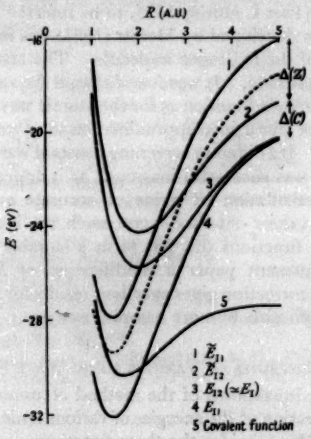

Figure 1. Energies of ionic wave functions for the hydrogen molecule.

The four energy curves $\widetilde{E}_{I1}(R)$, $\widetilde{E}_{I2}(R)$, $E_{I1}(R)$ and $E_{I2}(R)$ are shown in figure 1, together with the curve given by a covalent function with unit screening constant. Since the screening constant for $\widetilde{\Psi}_{I2}$ has the optimum value for the isolated ion H^-, the total charge density function given by $\widetilde{\Psi}_{I2}$ will be similar to that given by Ψ_I. Consequently the two functions should give nearly the same variation of energy

† Here we have simplified the notation of I by dropping the double tilde. The present H and $\widetilde{H}$ correspond to $\widetilde{H}_1$ and $\widetilde{\widetilde{H}}$ of I.

with nuclear separation, since this variation is largely due to Coulombic interaction. The $E_{I2}(R)$ curve will therefore be a good approximation to $E_I(R)$. It is now evident from figure 1 that $E_{I1}(R)$ is a very poor approximation to $E_I(R)$ for values of R less than about 3 A.U. At the equilibrium nuclear separation of 1·4 A.U. it leads to an error of 8·0 ev, a considerably larger error than the 4·2 ev of equation (2.6) which the method of atoms in molecules is designed to eliminate. It is also clear that Ψ_I is not a suitable function for a calculation of the energy of the ground state at equilibrium, since its energy $E_I(\simeq E_{21})$ is considerably higher than the energy $\widetilde{E}_{11}$ of the simple orbital function $\widetilde{\Psi}_{11}$.

§ 3. Modification of Moffitt's Correction

The gross error 8·0 ev which results from the substitution of $\widetilde{\Psi}_{11}$ into equation (2.5) arises from a failure to distinguish between two inaccuracies in the wave function $\widetilde{\Psi}_{11}$ at infinite nuclear separation. Firstly, we have the error

$$\Delta(Z)=\widetilde{W}_{12}-\widetilde{W}_{11}=-2{\cdot}7\,\text{ev}, \qquad \ldots\ldots(3.1)$$

which arises from the use of a non-optimum value of the screening constant Z, that is from the use of a wave function which gives an electronic charge cloud of the wrong size. Secondly, we have the error

$$\Delta(C)=W_I-\widetilde{W}_{12}=-1{\cdot}5\,\text{ev}, \qquad \ldots\ldots(3.2)$$

which is mainly due to the neglect of the correlation between the motions of the two electrons in H^-. As we have seen in § 2 it is not permissible to use an equation of the form (2.5) to eliminate the total error $\Delta(Z)+\Delta(C)$, since the behaviour of the term $\widetilde{E}_I(R)$ is strongly dependent on the value of the screening constant Z.

In the modified form of the theory we use the correlation correction $\Delta(C)$ in place of the total correction $\Delta(Z)+\Delta(C)$, whatever the value of the screening constant Z in the orbital function $\widetilde{\Psi}_I$. This procedure may be justified on the basis of two approximations.

(i) The correlation energy of the isolated ion H^- is independent of the value of the screening constant Z. That is, corresponding to each simple orbital function

$$\widetilde{\Psi}_{as}=a_s(1)\,a_s(2), \qquad \ldots\ldots(3.3)$$

with

$$a_s=\left(\frac{Z^3}{\pi}\right)^{1/2}\exp\,(-Zr_a),$$

giving energy $\widetilde{W}_s$, there exists a 'fully correlated' wave function Ψ_{as} giving the same total electronic charge density as $\widetilde{\Psi}_{as}$ and with energy W_s given by

$$W_s-\widetilde{W}_s=\Delta(C) \qquad \ldots\ldots(3.4)$$

where $\Delta(C)$ is independent of Z.

(ii) The energy $E_{1s}(R)$ of the ionic wave function

$$\Psi_{1s}=2^{-1/2}[\Psi_{as}+\Psi_{bs}], \qquad \ldots\ldots(3.5)$$

for the hydrogen molecule may be estimated from the equation

$$E_{1s}(R)=\widetilde{E}_{1s}(R)+W_s-\widetilde{W}_s, \qquad \ldots\ldots(3.6)$$

where $\widetilde{E}_{1s}(R)$ is the energy given by the orbital wave function

$$\widetilde{\Psi}_{1s}=2^{-1/2}[\widetilde{\Psi}_{as}+\widetilde{\Psi}_{bs}]. \qquad \ldots\ldots(3.7)$$

These two approximations enable us to determine $E_{1s}(R)$ for all values of Z and R. The value of the constant $\Delta(C)$ is obtained from equation (3.4) with $Z=0{\cdot}6875$, that is from equation (3.2)†. Since the charge densities of the two functions Ψ_{a2} and $\widetilde{\Psi}_{a2}$ are the same, approximation (ii) should be quite accurate. Approximation (i) seems reasonable in view of the almost exact equality of the correlation energies of the systems H^-, He and Li^+ (1·49, 1·51, 1·54 ev respectively). The behaviour of $E_{1s}(R)$ for $Z=1$ is given by the broken curve in figure 1.

The generalization of this procedure to more complex calculations is immediate. If, for any molecule, $\widetilde{H}$ and $\widetilde{M}$ are energy and overlap matrices with respect to a set of analytical approximate composite functions $\widetilde{\Psi}_1, \ldots \widetilde{\Psi}_n$ (Moffitt 1951), the corrected energy matrix H is given by equation (2.4) with $\widetilde{W}$ replaced by $\widetilde{W}'$,

$$H=\widetilde{H}+\tfrac{1}{2}[\widetilde{M}(W-\widetilde{W}')+(W-\widetilde{W}')\widetilde{M}]. \qquad \ldots\ldots(3.8)$$

Here $\widetilde{W}'$ is defined as the matrix obtained from $\widetilde{H}$ by first letting all internuclear separations tend to infinity and then minimizing each diagonal element with respect to the screening constants in the functions $\widetilde{\Psi}_1, \ldots \widetilde{\Psi}_n$. In a calculation involving many different atomic states this ideal procedure for determining $\widetilde{W}'$ would prove rather tedious. In practice it may prove sufficiently accurate to estimate $\widetilde{W}'$ by using the same values of the screening constants for all states of a given atom with the same ionicity and to determine these values from Slater's empirical rules. However, as we have seen in § 2 it is essential in estimating $\widetilde{W}'$ to use different values of the screening constants for atomic states of different ionicity.

A calculation based on equation (3.8) approximates to one in terms of the wave functions $\Psi_1, \ldots \Psi_n$, where $\Psi_r (r=1, \ldots n)$ is a wave function giving the same total charge density as $\widetilde{\Psi}_r$ (for infinite nuclear separation) but which makes full allowance for the correlation of the motions of the electrons within each of the separated atoms. For this reason equation (3.8) may be said to constitute an intra-atomic correlation correction (ICC).

If we use the same values of the screening constants in $\widetilde{\Psi}_1 \ldots \widetilde{\Psi}_n$ as in determining $\widetilde{W}'$, equation (3.8) reduces to the atoms in molecules correction (2.4). However, since we assume that the value of the ICC is independent of the screening constants in the wave functions, it is no longer necessary to use these same values for the parameters. Equation (3.8) applies for any choice of the parameters in $\widetilde{\Psi}_1 \ldots \widetilde{\Psi}_n$. Thus in estimating $\widetilde{H}$ and $\widetilde{M}$ of equation (3.8) we may use the same values for the screening constants for states of the same atom with different ionicity. This enables us to preserve the correspondence between the present theory and the ASMO theory and greatly simplifies the evaluation of the necessary integrals, especially for homonuclear molecules. Furthermore, it is now possible to vary these screening constants to minimize the energy. Such a variation has proved very important in calculating the energy of the hydrogen molecule (Weinbaum 1933, Altmann and Cohan 1954).

It is interesting to note that it is not possible to modify the alternative form of the method of atoms in molecules, namely

$$H=\tfrac{1}{2}[\widetilde{M}W+W\widetilde{M}]+\tfrac{1}{2}(\widetilde{V}+\widetilde{V}\dagger), \qquad \ldots\ldots(3.9)$$

‡ Here we neglect the difference between the total electronic charge densities associated with the optimum orbital function and the exact wave function for H^-.

in the same way as we have modified equation (2.4). Equation (3.9) depends essentially upon the separation of H into atomic and interaction terms (Moffitt 1951) and may only be used to approximate to a calculation in terms of accurate atomic functions. Equation (2.4), however, is simply an asymptotic adjustment of the energy matrix $\widetilde{H}$ and does not suffer from this limitation.

§ 4. Illustrative Calculations

We apply the ICC (3.8) to two calculations of the ground state energy curve for the hydrogen molecule. The calculation of Weinbaum (1933) is based on the wave function

$$\widetilde{\Psi} = \widetilde{\Psi}_0 + \widetilde{\gamma}\widetilde{\Psi}_I \qquad \ldots\ldots(4.1)$$

where

$$\widetilde{\Psi}_0 = 2^{-1/2}[a(1)b(2) + b(1)a(2)], \qquad \ldots\ldots(4.2)$$

$$\widetilde{\Psi}_I = 2^{-1/2}[a(1)a(2) + b(1)b(2)], \qquad \ldots\ldots(4.3)$$

with

$$a(1) = \left(\frac{Z^3}{\pi}\right)^{1/2} \exp(-Zr_{a1}), \text{ etc.}$$

The overlap matrix $\widetilde{M}(Z)$ and the energy matrix $\widetilde{H}(Z)$ were calculated in the usual way using the tables of integrals given by Hirschfelder and Linnett (1950). These authors also give the optimum values for the parameter Z determined from the equations

$$\det[\widetilde{H}(Z) - \widetilde{E}(Z)\widetilde{M}(Z)] = 0 \qquad \ldots\ldots(4.4)$$

and

$$\left(\frac{\partial \widetilde{E}(Z)}{\partial Z}\right)_R = 0. \qquad \ldots\ldots(4.5)$$

With the use of these optimum values of Z the ground state energy curve and the values of the parameter $\widetilde{\gamma}$ were calculated from the determinantal equation

$$\det(\widetilde{H} - \widetilde{E}\widetilde{M}) = 0, \qquad \ldots\ldots(4.6)$$

and the secular equations

$$\begin{aligned}(\widetilde{H}_{00} - \widetilde{E}\widetilde{M}_{00}) + \widetilde{\gamma}(\widetilde{H}_{01} - \widetilde{E}\widetilde{M}_{01}) &= 0,\\ (\widetilde{H}_{10} - \widetilde{E}\widetilde{M}_{10}) + \widetilde{\gamma}(\widetilde{H}_{11} - \widetilde{E}\widetilde{M}_{11}) &= 0. \qquad \ldots\ldots(4.7)\end{aligned}$$

The only non-zero element of the matrix $W - \widetilde{W}'$ of equation (3.8) is $W_{11} - \widetilde{W}'_{11}$ which from § 2 has the value $-1{\cdot}5$ ev. The modified energy matrix H is therefore given by the equations (ev),

$$\begin{aligned}H_{00} &= \widetilde{H}_{00},\\ H_{10} &= \widetilde{H}_{10} - 0{\cdot}75\,\widetilde{M}_{01},\\ H_{11} &= \widetilde{H}_{11} - 1{\cdot}5\,\widetilde{M}_{11}. \qquad \ldots\ldots(4.8)\end{aligned}$$

The modified values of the energy E and the parameter γ are then given by the equations

$$\det(H - E\widetilde{M}) = 0, \qquad \ldots\ldots(4.9)$$

and

$$\begin{aligned}(H_{00} - E\widetilde{M}_{00}) + \gamma(H_{01} - E\widetilde{M}_{01}) &= 0,\\ (H_{10} - E\widetilde{M}_{10}) + \gamma(H_{11} - E\widetilde{M}_{11}) &= 0. \qquad \ldots\ldots(4.10)\end{aligned}$$

In a similar way the ICC (3.8) was applied to the calculation of Hirschfelder and Linnett (1950), which is based on the wave function

$$\widetilde{\Psi} = \widetilde{\Psi}_0 + \widetilde{\alpha}\widetilde{\Psi}_s + \widetilde{\beta}\widetilde{\Psi}_c + \widetilde{\gamma}\widetilde{\Psi}_I, \qquad \ldots\ldots (4.11)$$

where, in their notation,

$$\Psi_s = 2^{-1/2}[a_s(1)\,b_s(2) + b_s(1)\,a_s(2)]\cos(\phi_2 - \phi_1),$$
$$\widetilde{\Psi}_c = 2^{-1/2}[a_c(1)\,b_c(2) + b_c(1)\,a_c(2)], \qquad \ldots\ldots (4.12)$$

with

$$a_c(1) = \left(\frac{Z^5}{\pi}\right)^{1/2} r_{a1}\cos\theta_{a1}\exp(-Zr_{a1}),$$
$$a_s(1) = \left(\frac{Z^5}{\pi}\right)^{1/2} r_{a1}\sin\theta_{a1}\exp(-Zr_{a1}), \qquad \text{etc.}$$

It is easily shown that for infinite nuclear separation the functions $\widetilde{\Psi}_s$ and $\widetilde{\Psi}_c$ each describe two hydrogen atoms in 2p states. If the parameter Z is now varied these wave functions become exact solutions of the Schrödinger equation for this system. Thus $W_{II} - \widetilde{W}'_{II}$ is again the only non-zero element of the matrix $W - \widetilde{W}'$ of equation (3.8). Furthermore, the wave functions $\widetilde{\Psi}_s$ and $\widetilde{\Psi}_c$ are each orthogonal to $\widetilde{\Psi}_I$ for all nuclear separations. Therefore the modified energy matrix H is given in terms of the unmodified matrix $\widetilde{H}$ by equations (4.8) supplemented by the equation

$$H_{0s} = \widetilde{H}_{0s},\quad H_{0c} = \widetilde{H}_{0c},\quad H_{ss} = \widetilde{H}_{ss},\quad H_{sc} = \widetilde{H}_{sc},\quad H_{sI} = \widetilde{H}_{sI},\quad H_{cc} = \widetilde{H}_{cc},\quad H_{cI} = \widetilde{H}_{cI}. \qquad \ldots\ldots (4.13)$$

In both modified calculations Z values given by Hirschfelder and Linnett (1950) were used. Since these values were obtained by minimizing the energies given by the wave functions (4.1) and (4.11) a slight reduction in the energies given by the modified calculations could be achieved by revarying Z according to the equation

$$\left(\frac{\partial E}{\partial Z}\right)_R = 0. \qquad \ldots\ldots (4.14)$$

It was found that for the modified Weinbaum calculation the use of equation (4.14) in place of (4.5) had a negligible effect on the calculated energy curve. In view of this the arduous task of revarying Z for the modified Hirschfelder–Linnett calculation was not attempted.

The energy curves and parameter values which result from the calculations are shown in figures 2, 3 and 4. In figure 2 the experimental values of Rydberg (1931) and Beutler (1934) are also shown. The calculated and experimental values of the equilibrium constants are given in the table. The values for the unmodified calculations differ slightly from those given by Hirschfelder and Linnett (1950). This is chiefly due to the use of a different method of interpolation. The values of the table were obtained by a quadratic interpolation of the electronic energy from calculated values at $ZR = 1{\cdot}5,\ 1{\cdot}75,\ 2{\cdot}0$ A.U. A quadratic interpolation of the total energy was found to give values very close to those of Hirschfelder and Linnett. From the exact equilibrium values for the Weinbaum function (4·03† ev and 1·42 A.U.) and the behaviour of the experimental values it appears that the former method of interpolation is considerably more accurate.

† Here we have recalculated the value given by Weinbaum (1933) using the conversion factor 1 A.U. = 27·206 ev.

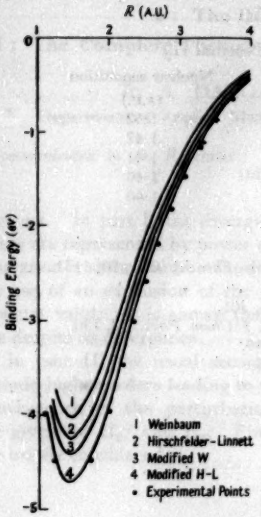

Figure 2. Binding energy of hydrogen molecule as function of nuclear separation.

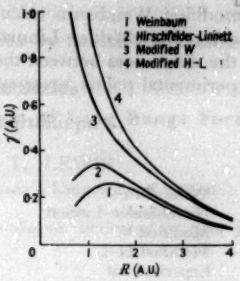

Figure 3. Behaviour of parameter γ.

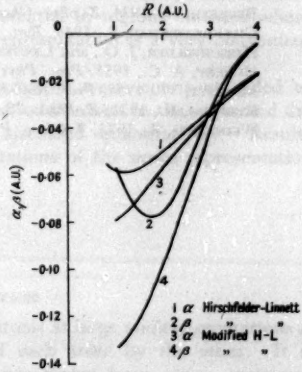

Figure 4. Behaviour of parameters α, β.

Several features of figures 2, 3 and 4 suggest that the modified calculations approximate quite closely to exact calculations in terms of an ionic wave function allowing for intra-atomic correlation. All calculated values of the energy are higher than the experimental values and the behaviour of all the parameters in the wave functions appears reasonable. The increase in the values of the parameter γ when the correlation correction is applied is to be expected from the decrease in the energy difference between the ionic and covalent states. The curves of figure 3 also suggest that for the modified calculations γ tends to infinity as R tends to zero. This is to be expected, since for $R=0$ the only difference between the covalent function and the modified ionic function is that the latter makes allowance for electron correlation. The increase in the absolute magnitudes of the parameters α and β shown in figure 4 is an indirect consequence of the increase in the value of γ; the functions $\widetilde{\Psi}_a$ and $\widetilde{\Psi}_c$ interact more strongly with the ionic function than with the covalent function.

The ICC leads to a substantial improvement in the calculated energy curves. The modified Weinbaum calculation is considerably more accurate than the unmodified Hirschfelder–Linnett calculation; while in the range of R from 1 to 4 A.U. the differences between the modified Hirschfelder–Linnett calculation and the experimental points never exceed 0·05 ev.

Equilibrium Constants for Normal H_2

	Binding energy (ev)	Nuclear separation (A.U.)
Weinbaum	4·03	1·42
Hirschfelder–Linnett	4·26	1·42
Modified W	4·42	1·41
Modified H–L	4·72	1·40
Experimental	4·74	1·40

References

ALTMANN, S. L., and COHAN, N. V., 1954, *Trans. Faraday Soc.*, **50**, 1151.
BEUTLER, H., 1934, *Z. phys. Chem.* B, **27**, 287.
CHANDRASEKHAR, S., 1944, *Rev. Mod. Phys.*, **16**, 301.
HIRSCHFELDER, J. O., and LINNETT, J. W., 1950, *J. Chem. Phys.*, **18**, 130.
HURLEY, A. C., 1955, *Proc. Phys. Soc.* A, **68**, 149.
MOFFITT, W., 1951, *Proc. Roy. Soc.* A, **210**, 245.
RYDBERG, R., 1931, *Z. Phys.*, **73**, 376.
WEINBAUM, S., 1933, *J. Chem. Phys.*, **1**, 593.

The Representation of Long Range Forces by Series Expansions

I : The Divergence of the Series

II : The Complete Perturbation Calculation of Long Range Forces

By A. DALGARNO and J. T. LEWIS
Department of Applied Mathematics, The Queen's University of Belfast

Communicated by D. R. Bates ; MS. received 5th August 1955 and in final form 16th September 1955

Abstract. In part I, the divergence which arises when long range inter-atomic forces are represented by power series expansions in the reciprocal of the nuclear separation is shown to be a fundamental property of such series and is *not* due to the use of an expansion of the perturbing potential in regions of space where it is not valid. It is shown that the series representation is a very convenient one despite its divergence.

In part II, the usual second order perturbation treatment is extended to include higher orders leading to the presence of odd powers in the series and the convergence of the perturbation series is discussed quantitatively. Results are given for H_2^+ and H_2. Finally the limitations of the series representation are briefly considered.

PART I

§ 1. Introduction

The dominant forces between a pair of atoms at large nuclear separations R arise from the mutual polarization of each atom by the other. It is customary to represent these long range forces by a series expansion in inverse powers of R, the series being obtained by the substitution of an expansion of the interaction potential into conventional first and second order perturbation theory. This yields an infinite series of powers of R^{-1} which is divergent at all R.

Various attempts have been made to remove the divergence. It is shown here that these attempts must necessarily prove fruitless in that the divergence must be accepted if a series expansion in powers of R^{-1} is to be retained; it is demonstrated however that the series representation is nevertheless a very convenient one.

§ 2. Theory

For simplicity, we shall examine the interaction of a proton A and a neutral hydrogen atom with nucleus B and an electron in the ground state. Then if $\mathbf{r}_a$ and $\mathbf{r}_b$ are the position vectors of the electron relative to A and B respectively and the distance AB equals R, the interaction potential is given in Hartree units by

$$V(\mathbf{r}, \mathbf{R}) = \frac{2}{R} - \frac{2}{r_a}. \qquad \ldots\ldots(1)$$

Denoting by $\psi_r(\mathbf{r}_b)$ the wave function of the rth excited state of hydrogen with binding energy E_r, conventional second order perturbation theory gives for the interaction energy

$$E(R) = \sum_r \frac{(0|V|r)(r|V|0)}{E_0 - E_r} \qquad \ldots\ldots(2)$$

where

$$(0|V|r) = \int \psi_0^* V \psi_r \, d\mathbf{r} \qquad \ldots\ldots(3)$$

and the summation excludes the $r=0$ term. To obtain a series representation of $E(R)$, V is expanded in Legendre polynomials

$$V \sim -\frac{2}{R} \sum_{n=1}^{\infty} (r_b/R)^n P_n(\cos\theta_b); \qquad \ldots\ldots(4)$$

the series (4) is valid for $r_b < R$. An approximate evaluation of (2) is obtained by following Unsöld's procedure (1927): $E_r - E_0$ is replaced by a non-zero constant ϵ and use is made of the summation formula

$$\sum_q (p|L|q)(q|M|r) = (p|LM|r) \qquad \ldots\ldots(5)$$

Thus

$$E(R) = -\frac{1}{\epsilon}\{(0|V^2|0) - (0|V|0)^2\}\dagger \qquad \ldots\ldots(6)$$

which on using (4) becomes

$$E(R) = -\frac{4}{\epsilon} \sum_{n=1}^{\infty} \frac{1}{R^{2n+2}} \frac{(2n+2)!}{(2n+1)2^{2n+1}}. \qquad \ldots\ldots(7)$$

The series (7) is divergent for all values of R.

Brooks (1952) has asserted that the divergence arises from the use of (4) in regions of space where it is not valid, the integrations in (5) being over all space; however (6) can easily be calculated using the exact form (1) of V (cf. Roe 1952) yielding the expression for $E(R)$:

$$E(R) = -\frac{2}{\epsilon R}\{(2R+1)\exp(-2R)\overline{\mathrm{Ei}}(2R) + (2R-1)\exp(2R)\mathrm{Ei}(-2R) - 2/R + 4(1+1/R)\exp(-2R) - 2R(1+1/R)^2\exp(-4R)\} \qquad \ldots\ldots(8)$$

where $\overline{\mathrm{Ei}}(x)$, $\mathrm{Ei}(-x)$ are the exponential integrals defined by

$$\overline{\mathrm{Ei}}(x) = \int_{-\infty}^{x} t^{-1}\exp(+t)dt, \quad -\mathrm{Ei}(-x) = \int_x^{\infty} t^{-1}\exp(-t)dt.$$

When (8) is expanded in powers of R^{-1} and exponentially decreasing terms are ignored, it reduces to the expression (7). It is clear that Brooks' explanation of the origin of the divergence is incorrect; the divergent series (7) arises whether or not the expansion (4) is used. Thus it is pointless to follow (as has recently been done) the laborious procedure of using the exact potential and then expanding the resulting expression.

Now, as Brooks pointed out, any real function $f(R)$ of a real variable which may be developed formally as

$$f(R) = \sum_{n=0}^{\infty} a_n/R^n \qquad \ldots\ldots(9)$$

† At any given R, (6) is exact for some value of ϵ such that $8/9 < \epsilon < 2$ (Dalgarno and Lewis 1956).

and is such that $\lim_{R\to\infty} R^N(f-f_N)=0$ for all positive N where

$$f_N=\sum_{n=0}^{N} a_n/R^n$$

is said to have an asymptotic expansion

$$f(R)\sim \lim_{N\to\infty} f_N(R)$$

and this expansion is *unique* (Bromwich 1942). Hence (7) is a unique expansion of (6) so that if a series representation in integral powers of R^{-1} is required, (7) is the appropriate one even though it diverges.

In practice, the series must be truncated at a particular value of N. The error involved is of the order of magnitude of the last term retained; provided R is sufficiently large that exponentially decreasing terms may be ignored, it may be shown (Whittaker and Watson 1935) that the error in truncating (7) at the Nth term is less than

$$(N+1)!/\epsilon 2^{N-1}R^N. \qquad \ldots\ldots(10)$$

By appropriate choice of N, (10) can usually be made very small. A convenient procedure to follow is to include for any given R all terms up to but excluding the smallest of the series plus half the smallest term (cf. Jeffreys and Jeffreys 1946). If this involves the computation of too great a number of terms, the methods described by Airey (1937) and Shanks (1955) may be employed.

§ 3. Numerical Data

In table 1 are listed the successive terms of the series (7) at a number of values of R together with their sums evaluated according to the method described above and the values of the exact expression (8). For all R at which the series representation can be expected to be useful (see part II), it is an excellent approximation to the exact value.

Table 1. Comparison of Series with Exact Values

	Contribution of term in							
R	R^{-4}	R^{-6}	R^{-8}	R^{-10}	R^{-12}	R^{-14}	Expression (7)	Exact (8)
4	0·0156	0·0044	0·0027	0·0030			0·0214	0·0226
5	0·00640	0·00115	0·00046	0·00032	0·00034		0·00817	0·00830
6	0·00309	0·00038	0·00011	0·00005	0·00004	0·00004	0·00365	0·00367
7	0·00167	0·00015	0·00003	0·00001	$0·00000_6$	$0·00000_5$	0·00187	0·00186
8	0·00098	0·00007	0·00001	$0·00000_3$	$0·00000_1$	$0·00000_1$	0·00106	0·00106

PART II

§ 1. Introduction

It is usual to obtain the series representation of long range forces between atoms from conventional first and second order perturbation formulae. For atoms in S states the first order term vanishes and the second order term yields an infinite series of *even* powers of R^{-1}. It is shown here that the third and higher order perturbations introduce odd powers into the series and a simple method of calculating them with sufficient accuracy is described; the convergence of the perturbation series is also discussed. Results are given for H_2^+ and H_2 and their accuracy is discussed.

§ 2. Higher Order Perturbations

The usual practice of selecting the first few terms of (7) whilst ignoring higher order perturbations is suspect in that the higher order approximations contribute terms which may be larger than those retained. The formulae for the third and fourth order approximations are (Niessen 1929)

$$E_3(R)=\sum_k\sum_j \frac{(0|V|k)(k|V|j)(j|V|0)}{(E_0-E_k)(E_0-E_j)}-\sum_k\frac{(0|V|k)(k|V|0)(0|V|0)}{(E_0-E_k)^2} \quad \ldots\ldots(11)$$

$$E_4(R)=\sum_l\sum_k\sum_j \frac{(0|V|k)(k|V|j)(j|V|l)(l|V|0)}{(E_0-E_k)(E_0-E_j)(E_0-E_l)}+\sum_k\frac{(0|V|0)^2(0|V|k)(k|V|0)}{(E_0-E_k)^3}$$
$$-\frac{1}{2}\sum_k\sum_j \frac{2(0|V|j)(j|V|k)(k|V|0)(0|V|0)+(0|V|j)(j|V|0)(0|V|k)(k|V|0)}{(E_0-E_j)^2(E_0-E_k)^2}$$
$$\times[E_0-E_j+E_0-E_k] \quad \ldots\ldots(12)$$

where none of j, k, l may equal zero.

Applying Unsöld's approximation and using (5), we readily obtain

$$E_3(R)=-\frac{1}{\epsilon_3^2}\{(0|V^3|0)-3(0|V^2|0)(0|V|0)+2(0|V|0)^3\} \quad \ldots\ldots(13)$$

$$E_4(R)=-\frac{1}{\epsilon_4^3}\{(0|V^4|0)-4(0|V^3|0)(0|V|0)+10(0|V^2|0)(0|V|0)^2$$
$$-2(0|V^2|0)^2-5(0|V|0)^4\}. \quad \ldots\ldots(14)$$

Although it is possible to evaluate (13) and (14) analytically using the exact form (1) of V and then expand as a series in R^{-1}, the same result is much more easily obtained by using directly the expansion (4) of V. Considerable simplification occurs and (13) and (14) become

$$E_3(R)=-\frac{1}{\epsilon_3^2}(0|V^3|0)$$

$$E_4(R)=-\frac{1}{\epsilon_4^3}\{(0|V^4|0)-2(0|V^2|0)^2\}.$$

2.1. *Series for* H_2^+

The numerical coefficients in the various orders are

$$E_1(R)=0$$

$$E_2(R)=-\frac{1}{\epsilon_2}\left[\frac{4}{R^4}+\frac{18}{R^6}+\frac{180}{R^8}+\frac{3150}{R^{10}}+O\left(\frac{1}{R^{12}}\right)\right]$$

$$E_3(R)=-\frac{1}{\epsilon_3^2}\left[\frac{72}{R^7}+\frac{1440}{R^9}+O\left(\frac{1}{R^{11}}\right)\right]$$

$$E_4(R)=-\frac{1}{\epsilon_4^3}\left[\frac{40}{R^8}+\frac{2880}{R^{10}}+O\left(\frac{1}{R^{12}}\right)\right]$$

$$E_5(R)=-\frac{1}{\epsilon_5^4}O\left(\frac{1}{R^{11}}\right).$$

Upper bounds to the coefficients are readily obtained in putting ϵ_2, ϵ_3^2 and ϵ_4^3 equal to their minimum values of 3/4, 2/3 and 27/64 respectively giving the series

$$E(R)=-\frac{16}{3R^4}-\frac{24}{R^6}-\frac{108}{R^7}-\frac{9040}{27R^8}-\frac{2160}{R^9}-\frac{33080}{3R^{10}}-O\left(\frac{1}{R^{11}}\right) \quad \ldots\ldots(15)$$

but owing to possible contributions from the continuum states no lower bounds can be given (other than that the coefficients cannot vanish).† The best choice of the ϵ's is a matter of some difficulty since they are functions of R. The usual practice when one of the interaction systems is ionic is to choose ϵ_2 so that the R^{-4} coefficient is correct, it being known from quantal calculations of the polarizability (cf. Unsold 1927): thus we take $\epsilon_2=\epsilon_3=\epsilon_4=8/9$ giving

$$E(R)=-\frac{9}{2R^4}-\frac{81}{4R^6}-\frac{729}{8R^7}-\frac{16605}{64R^8}-\frac{3645}{2R^9}-\frac{61155}{8R^{10}}-O\left(\frac{1}{R^{11}}\right). \quad \ldots\ldots(16)$$

Dalgarno and Lewis (1956) have recently described a sum rule technique which permits the exact evaluation of the summations (2), (11) and (12). The exact coefficients are given by

$$E_2(R)=-\frac{9}{2R^4}-\frac{15}{R^6}-\frac{525}{4R^8}-\frac{2835}{4R^{10}}-O\left(\frac{1}{R^{12}}\right) \quad \ldots\ldots(17)$$

$$E_3(R)=-\frac{213}{2R^7}-\frac{1773}{R^9}-O\left(\frac{1}{R^{11}}\right) \quad \ldots\ldots(18)$$

$$E_4(R)=-\frac{3555}{32R^8}-\frac{80379}{8R^{10}}-O\left(\frac{1}{R^{12}}\right). \quad \ldots\ldots(19)$$

The coefficients obtained from the sum of (17), (18) and (19) are identical to those derived by Coulson (1941) who employed a special perturbation method which does not distinguish explicitly between the successive orders; it is difficult to use his series numerically since the magnitudes of successive terms vary irregularly. With the series separated into the different orders, the terms of any given order decrease smoothly to a minimum and then increase; the separate orders may then be truncated at their smallest terms (cf. part I).

In table 2, the contributions from (17), (18) and (19) are compared as functions of R, each series being truncated as described in part I. The convergence is very rapid and even for R as small as 4 the second order term contributes more than half the sum.

Table 2. Comparison of the Second, Third and Fourth Order Approximations

R	4	5	6	7	8	9	10	11	12	13	14	15
$-E_2\times10^4$	233	85·7	38·8	20·3	11·6	7·17	4·66	3·16	2·22	1·61	1·19	0·903
$-E_3\times10^4$	33	18·2	5·6	1·7	0·8	0·29	0·12	0·06	0·01	0·00	0·00	0·001
$-E_4\times10^4$	8	1·4	0·3	0·1	0·0	0·01	0·01	0·01	0·00	0·00	0·00	0·000

2.1.1. *Contribution from continuum states.*

The correct values of ϵ_2, ϵ_3 and ϵ_4 corresponding to each term of (17), (18) and (19) are given in table 3. The continuum does not make a very significant contribution to the leading term of each order but becomes more important as the power of R^{-1} increases.

Table 3. Values of ϵ_2, ϵ_3, ϵ_4

Power of R^{-1}	4	5	6	7	8	9	10
ϵ_2	0·889	–	1·200	–	1·371	–	1·481
ϵ_3	–	–	–	0·822	–	0·901	–
ϵ_4	–	–	–	–	0·711	–	0·659

† The variational method can be used to obtain lower bounds (cf. Pauling and Wilson 1935) but a very complicated trial wave function would be required.

The approximate series (16), the upper bound (15) and the exact series are compared in table 4, the individual contributions from the different orders being truncated as described in part I. Close agreement of the approximate series (16) with the exact is expected at large R since the two series have the same leading term, but even for R as small as 4, agreement is still excellent and, although this may be due in some measure to chance, the position is nevertheless very satisfactory. Thus, although the continuum states are very important for the values of the coefficients of the higher terms, they are less so in calculations of the magnitude of the interaction energy. For many purposes, it would suffice to use the upper bound itself for it also provides a reasonably accurate approximation.

Table 4. Series Representation of $-E(R)$

R	4	5	6	7	8	9	10	11	12	13	14	15
Exact $\times 10^4$	274	105	44·7	22·1	12·4	7·47	4·79	3·23	2·23	1·61	1·19	0·904
Approximate $\times 10^4$	267	109	46·1	22·6	12·5	7·56	4·85	3·26	2·27	1·64	1·21	0·914
Upper bound $\times 10^4$	325	130	54·7	26·8	14·9	8·97	5·75	3·86	2·70	1·94	1·44	1·08

2.2. *Series Representation for* H_2

The detailed analysis need not be presented here; it suffices to mention that the appropriate expansion of the reciprocal of the distance between two electrons is either that of Heller (1941) or alternatively that of Carlson and Rushbrooke (1950). The results obtained are

$$E(R) = -\frac{1}{\epsilon_2}\left[\frac{24}{R^6} + \frac{540}{R^8} + \frac{15750}{R^{10}} + O\left(\frac{1}{R^{12}}\right)\right] - \frac{1}{\epsilon_3^2}\left[\frac{7452}{R^{11}} + O\left(\frac{1}{R^{13}}\right)\right]. \quad \ldots\ldots(20)$$

The minimum value of ϵ_2 is 3/2 and of ϵ_3^2 is 8/3 giving an upper bound

$$E(R) = -\frac{16}{R^6} - \frac{360}{R^8} - \frac{10{,}500}{R^{10}} - \frac{5589}{2R^{11}} - O\left(\frac{1}{R^{12}}\right) \quad \ldots\ldots(21)$$

but as before no lower bounds may be given. The usual choice of ϵ in the case of two neutral atoms is the sum of the ionization potentials of the two atoms and this gives a series

$$E(R) = -\frac{12}{R^6} - \frac{270}{R^8} - \frac{7875}{R^{10}} - \frac{1863}{R^{11}} - O\left(\frac{1}{R^{12}}\right). \quad \ldots\ldots(22)$$

Pauling and Beach (1935) have carried out an (apparently) accurate variational calculation and obtain

$$E(R) = -\frac{12{\cdot}99806}{R^6} - \frac{248{\cdot}798}{R^8} - \frac{2270{\cdot}42}{R^{10}} - O\left(\frac{1}{R^{11}}\right) \quad \ldots\ldots(23)$$

and the values of ϵ_2 corresponding to these terms are 1·846, 2·170 and 6·937. The first two values are much the same as twice the corresponding values for H_2^+ but the third value is very difficult to accept. It appears that Pauling and Beach have taken account of only the quadrupole–quadrupole contribution to the R^{-10} coefficient and have ignored the dipole–octupole contribution (cf. Heller 1941).

It is clear however that for sufficiently large R expression (22) provides a very good approximation to (23).

§ 3. Limitations of the Methods

It has been shown that a series expansion provides an accurate representation of the forces derived from perturbation theory, that the convergence of successive orders is rapid and that the approximations usually made in obtaining the series are sufficiently accurate for most purposes. However the degeneracy which arises because of the identity of the nuclei has been ignored; taking it into account gives rise to the so-called exchange forces which do *not* vanish when the expansion of the perturbing potential is used as do the direct forces arising from the overlap of the electron distributions of the interacting atoms. It is to be expected then that neglect of exchange forces is the major factor limiting the accuracy of the series representation.

The publication by Bates, Ledsham and Stewart (1953) and by Wallis and Hulburt (1954) of the exact interaction energies of the $1s\sigma_g$ and $2p\sigma_u$ states of H_2^+ allows a precise assessment of the importance of the exchange terms. Their values are given in table 5 together with the values obtained from the accurate series, which is an approximation to the energies of *both* the $1s\sigma_g$ and $2p\sigma_u$ states. It is seen that, due to exchange effects, the series cannot be accurate for R less than about 15 but it is essentially correct for R greater than 15.

Table 5. $-E(R)$

R	5	6	7	8	9
Exact					
(*a*) $1s\sigma$	$4{\cdot}88\times10^{-2}$	$2{\cdot}39\times10^{-2}$	$1{\cdot}12\times10^{-2}$	$5{\cdot}14\times10^{-3}$	$2{\cdot}39\times10^{-3}$
(*b*) $2p\sigma$	$-4{\cdot}54\times10^{-2}$	$-1{\cdot}87\times10^{-2}$	$-7{\cdot}45\times10^{-3}$	$-2{\cdot}79\times10^{-3}$	$-9{\cdot}10\times10^{-4}$
(*c*) Series	$1{\cdot}05\times10^{-2}$	$4{\cdot}47\times10^{-3}$	$2{\cdot}21\times10^{-3}$	$1{\cdot}26\times10^{-3}$	$7{\cdot}50\times10^{-4}$
(*d*) Arithmetic mean of (*a*) and (*b*)	$1{\cdot}71\times10^{-3}$	$2{\cdot}61\times10^{-3}$	$1{\cdot}87\times10^{-3}$	$1{\cdot}18\times10^{-3}$	$7{\cdot}40\times10^{-4}$
R	10	15	25	35	45
Exact		†	†	†	†
(*a*) $1s\sigma$	$1{\cdot}16\times10^{-3}$	$9{\cdot}79\times10^{-5}$	$1{\cdot}18\times10^{-6}$	$2{\cdot}80\times10^{-8}$	$1{\cdot}00\times10^{-9}$
(*b*) $2p\sigma$	$-1{\cdot}98\times10^{-4}$	$8{\cdot}41\times10^{-5}$	$1{\cdot}18\times10^{-5}$	$2{\cdot}80\times10^{-8}$	$1{\cdot}00\times10^{-6}$
(*c*) Series	$4{\cdot}79\times10^{-4}$	$9{\cdot}04\times10^{-5}$	$1{\cdot}16\times10^{-5}$	$3{\cdot}01\times10^{-8}$	$1{\cdot}10\times10^{-6}$
(*d*) Arithmetic mean of (*a*) and (*b*)	$4{\cdot}80\times10^{-4}$	$9{\cdot}10\times10^{-5}$	$1{\cdot}18\times10^{-6}$	$2{\cdot}80\times10^{-8}$	$1{\cdot}00\times10^{-6}$

† The last figures quoted in (*a*), (*b*) and (*d*) are not reliable.

It is of interest to compare the series with the exact interaction which would result if the identity of the nuclei were ignored. If we write the wave functions of the $1s\sigma_g$ and $2p\sigma_u$ states in the form

$$\chi(1s\sigma_g)=(\psi_a+\psi_b)/2^{1/2}$$
$$\chi(2p\sigma_u)=(\psi_a-\psi_b)/2^{1/2}$$

where ψ_a and ψ_b denote orbitals centred on nuclei A and B respectively and ignore the overlap integral $\int\psi_a\psi_b d\mathbf{r}$ since its square is small compared to unity, then the exact interaction ignoring exchange is given by

$$\int\psi_a H\psi_a d\mathbf{r}\simeq\tfrac{1}{2}\{E(1s\sigma)+E(2p\sigma)\}$$

where the notation is obvious. This energy is given in table 5 from which it is seen that the series gives a representation of the direct forces which is sufficiently accurate for most purposes for R at least as small as 7. For smaller R the overlap integral is no longer negligible and the comparison is not a valid one.

That the major factor limiting the accuracy of the series is neglect of the degeneracy had previously been recognized by Margenau (1939), whose work appears to have been overlooked by recent authors.

A comparison of the series with exact calculations in the case of a heteronuclear molecule such as HeH^{2+} would be of considerable interest and is in preparation.

References

Airey, J., 1937, *Phil. Mag.*, **24,** 521.

Bates, D. R., Ledsham, K., and Stewart, A. L., 1953 *Phil. Trans. Roy. Soc.* A, **246,** 215.

Bromwich, T. J., 1942, *An Introduction to the Theory of Infinite Series* 2nd edn, revised (London : Macmillan).

Brooks, F. C., 1952, *Phys. Rev.*, **86,** 92.

Carlson, B. C., and Rushbrooke, G. S., 1950, *Proc. Camb. Phil. Soc.*, **46,** 626.

Coulson, C. A., 1941, *Proc. Roy. Soc. Edinb.* A, **61,** 20.

Dalgarno, A., and Lewis, J. T., 1956, *Proc. Roy. Soc.* A, in the press.

Heller, R., 1941, *J. Chem. Phys.*, **9,** 156.

Jeffreys, H., and Jeffreys, B. S., 1946, *Methods of Mathematical Physics* (Cambridge : University Press), p. 472.

Margenau, H., 1939, *Phys. Rev.*, **56,** 1000.

Niessen, K. E., 1929, *Phys. Rev.*, **34,** 253.

Pauling, L., and Beach, J. Y., 1935, *Phys. Rev.*, **47,** 686.

Pauling, L., and Wilson, E. B., 1935, *Introduction to Quantum Mechanics* (New York : McGraw-Hill).

Roe, G. M., 1952, *Phys. Rev.*, **88,** 659.

Shanks, D., 1955, *J. Math. Phys.*, **34,** 1.

Unsöld, A., 1927, *Z. Phys.*, **43,** 563.

Wallis, R. F., and Hulburt, H. M., 1954, *J. Chem. Phys.*, **22,** 774.

Whittaker, E. T., and Watson, G. N., 1935, *Modern Analysis*, 4th edn (Cambridge : University Press).

The Calculation of Auto-ionization Probabilities III: Auto-detachment from the Negative Hydrogen Ion

By B. H. BRANSDEN† and A. DALGARNO‡

† Department of Physics and ‡ Department of Applied Mathematics, The Queen's University of Belfast

Communicated by D. R. Bates; MS. received 4th August 1955

Abstract. The probability of auto-detachment from $H^-(2s2p)^3P$ is calculated using both a time-dependent perturbation and a time-independent variational method. The values obtained are in essential agreement and are of the order 4×10^{12} sec^{-1}, about 100 times smaller than for the similar neutral case of auto-ionization of $He(2s2p)^3P$.

§ 1. Introduction

If an atom is in an excited level lying above the head of the lowest ionization continuum and certain selection rules are satisfied, a radiationless transition into this continuum may take place. Auto-ionization, as the phenomenon is termed, by reducing the lifetime of the level, will broaden the corresponding emission lines. In the first paper of this series (Bransden and Dalgarno 1953 a, paper I) the auto-ionization probabilities of a number of doubly excited states of the neutral helium atom were calculated using time-dependent perturbation theory; the predicted line widths appear to be too great to allow a satisfactory explanation of certain observations by Compton and Boyce (1928) and by Kruger (1930) in the vacuum ultra-violet.

The application of time-dependent perturbation theory to the calculation of auto-ionization probabilities has been criticized by a number of writers (cf. Wu and Ourom 1950). To provide a partial test of the validity of these criticisms a variational time-independent method which avoided most of the original difficulties was introduced in the second paper (Bransden and Dalgarno 1953 b, paper II). The results obtained by the two methods were found to be in essential agreement.

In this paper the probability of the auto-detachment process

$$H^-(2s2p)^3P \rightarrow H(1s) + e$$

is calculated. Besides giving additional data for assessing the accuracy of theoretical predictions, the results are of interest in connection with the possible magnitudes of the rate of dissociative attachment, and its inverse associative detachment, processes of considerable importance in studies on aeronomy (Bates 1950, Bates and Massey 1951) and gaseous discharges (Massey 1950).

§ 2. Theory

According to the general theory for the calculation of radiationless transition probabilities by variational methods, presented in paper II, the auto-detachment of electrons from the $(2s2p)\,^3P$ state of the negative hydrogen ion may be described by a wave function

$$\Phi(1,2) = \Psi_c(1,2) + \Psi_f(1,2) \qquad \ldots\ldots(1)$$

in which $\Psi_e(1,2)$ is an antisymmetrical normalized and closed wave function representing the excited state; and $\Psi_f(1,2)$ is an antisymmetrical wave function representing the final continuum state which is asymptotic to the correctly symmetrized product of $\chi(\mathbf{r})$, the ground state wave function of the hydrogen atom and $\mathcal{F}(\mathbf{r})$ a wave function containing at large radial distances only outgoing spherical waves:

$$\Psi_f(1,2)=\frac{1}{\sqrt{2}}\{\chi(\mathbf{r}_1)\mathcal{F}(\mathbf{r}_2)-\chi(\mathbf{r}_2)\mathcal{F}(\mathbf{r}_1)\} \qquad \ldots\ldots(2)$$

where

$$\chi(\mathbf{r})=\left(\frac{1}{\pi}\right)^{1/2}\exp(-r_1) \qquad \ldots\ldots(3)$$

and

$$\mathcal{F}(r)\sim dr_2^{-1}\exp(ikr_2)\,P_1(\cos\theta), \qquad \ldots\ldots(4)$$

k^2 being the energy of the detached electron.†

The probability of detachment per unit time γ is related to the amplitude d of the outgoing wave by

$$\gamma=\frac{8\pi k}{3}|d|^2. \qquad \ldots\ldots(5)$$

Suppose that $\Phi_t(1,2)$ is a trial wave function simulating $\Phi(1,2)$ and depending on p constants a_m and satisfying equations (1) to (4) with the exception that d_t replaces d, and write

$$I_1(a_m,d_t)=\int\Phi_t^*\,L[\Phi_t]\,d\tau+\frac{4\pi ik}{3}d_t^*\,d_t \qquad \ldots\ldots(6)$$

where $L\equiv H-E$, H being the Hamiltonian and E the total energy of the system. As shown in paper II, I_1 is a stationary expression to which the variational methods of Hulthén (1944, 1948), Hulthén and Olsson (1950) and Kohn (1948) may be applied. These give the two sets of equations:

$$\frac{\partial I_1}{\partial a_m}=0 \quad ; \quad I_1(a_m,d_t)=0, \qquad \ldots\ldots(7)$$

the Hulthén or H set, and

$$\frac{\partial I_1}{\partial a_m}=0 \quad ; \quad \frac{\partial I_1}{\partial d^*}=-\frac{4\pi ikd}{3}, \qquad \ldots\ldots(8)$$

the Kohn–Hulthén or KH set.

An arbitrary trial wave function will not in general satisfy the H and KH equations simultaneously, in particular solutions of (7) and (8) giving differing values for the parameter d_t. This property is conveniently used as a basis for discrimination between differing forms of trial wave function, the most acceptable trial wave function giving the best agreement between values of d_t calculated in the two ways. It should be noted that the form of the KH equations (8) is such that they can only be satisfied if d is a complex number, both d purely real and d purely imaginary being excluded. However the H equations (7) only provide a *single* relation between the real and imaginary parts of d and so could only completely define d in the excluded circumstances. Keeping this in mind an effective procedure for judging the suitability of a particular trial wave function has been evolved. The KH equations (8) are first solved for p and q, the real and imaginary parts of d. Taking the calculated KH value of p, the quadratic H equations (7) are solved to give two new values of q and hence d, and the process repeated by taking

† Atomic units are employed throughout.

the calculated KH value of q and solving for p. Of the four H values of d so obtained two can in general be excluded as differing in sign from the KH d, and of the remaining two values that most consistent with the KH d may be chosen, following the general practice in scattering problems (Massey and Moiseiwitsch 1951, Bransden and Dalgarno 1953 c).

2.1. *The Trial Wave Functions*

Some unpublished variational calculations of the scattering of electrons having unit angular momentum by hydrogen atoms in the ground state indicate that a suitable form of trial function for the continuum state is

$$\mathscr{F}(\mathbf{r}) = r\,[d\{j_1(kr) + (1-e^{-2kr})^3\, n_1(kr)\} + ar^2 e^{-3kr}]\, P_1(\cos\theta), \quad \ldots\ldots(9)$$

where j_1 and n_1 are spherical Bessel and Neumann functions of order one.

The closed wave function $\Psi_c(1,2)$ describing the doubly excited $(2s2p)\,^3P$ state of the negative hydrogen ion is written in a variational form due to Hylleraas (1950):

$$\Psi_c(1,2) = N\sum_n c_n\,[\phi_{n0}(\lambda \mathbf{r}_1)\,\phi_{21}(\lambda \mathbf{r}_2) - \phi_{21}(\lambda \mathbf{r}_1)\,\phi_{n0}(\lambda \mathbf{r}_2)] \quad \ldots\ldots(10)$$

where $\phi_{n0}(\mathbf{r})$, $\phi_{21}(\mathbf{r})$ are hydrogenic wave functions for the (ns) and (2p) states respectively, λ and c_n are variational parameters and N is the normalization factor. The numerical calculations are first performed using only the dominating term in series (10), that is the $n=2$ term. To illustrate the sensitivity of the results to the form of Ψ_c further calculations were made with the addition of the $n=1$ term, the numerical value of the scale factor λ and the energy E being found by minimizing the integral

$$I_c = \int \Psi_c L\,[\Psi_c]\, d\mathbf{r}.$$

When using the improved wave function with $n=1$ and $n=2$ terms, C_1 was found either by again minimizing I_c or alternatively treating C_1 as a variational parameter in I_1 and determining it by the solutions of (7) or (8). To anticipate, it may be stated that C_1 and E are insensitive to the addition of continuum terms to I_c so that the consistency of the procedure is fully confirmed.

The values of the constants appearing in expression (10) are found to be as follows:

Case (a). Single term.

$$(C_1=0),\ C_2=1{\cdot}0,\ \lambda=0{\cdot}734375,\ E=-0{\cdot}26965. \quad \ldots\ldots(11)$$

Case (b). Two terms.

$$C_1=0{\cdot}08894,\ C_2=1{\cdot}0,\ \lambda=0{\cdot}734375,\ E=-0{\cdot}26519. \quad \ldots\ldots(12)$$

§ 3. Numerical Results

Preliminary calculations with the trial wave function (9) show that most consistent results are obtained with the omission of the term containing the parameter a, in contrast to the corresponding scattering problem. In the table the values for the detachment probability γ obtained with (a) $\eta=2$ term only, (b) $n=1$ and $n=2$ terms with c_1 fixed to the value (12), and (c) $n=1$ and $n=2$ terms with c_1 varied, are given. The inconsistent and rejected H solutions are omitted, but the value of γ given by first order perturbation theory (cf. paper I) is included

for comparison. It is seen that the inclusion of a second term in the discrete wave function considerably improves the agreement between the H and KH solutions and gives slightly lower values of γ than the single term wave function. As values of the coefficients C_n alternate in sign and decrease in magnitude for $n>2$, the true value of γ should be between the two results, so that

$$3\times10^{12}\,\text{sec}^{-1}<\gamma<5\times10^{12}\,\text{sec}^{-1}. \qquad \ldots\ldots(13)$$

These limits are somewhat smaller than the value given by time-dependent perturbation theory, in harmony with what was found in the case of doubly excited helium, discussed in paper II.

		Probability of auto-detachment $\gamma(\text{sec}^{-1})$	
	Discrete trial wave function	KH	H
(*a*)	$C_1=0$	$4{\cdot}1\times10^{12}$	$6{\cdot}5\times10^{12}$
(*b*)	$C_1=0{\cdot}08894$	$3{\cdot}0\times10^{12}$	$3{\cdot}3\times10^{12}$
(*c*)	$C_1=$varied	$3{\cdot}0\times10^{12}$	$3{\cdot}3\times10^{12}$
Time-dependent perturbation theory		$1{\cdot}4\times10^{13}$.	

KH—Kohn–Hulthén values given by solution of equations (8).

H—Hulthén values given by solution of equations (7), the inconsistent Hulthén values being omitted (see text).

§ 4. Discussion

In view of the approximate nature of the calculations based upon the time-dependent method, the agreement between the results and those of the more complicated time-independent method must be regarded as very good; thus, provided serious cancellation does not occur, it would seem (in agreement with our previous conclusions, paper II) that auto-ionization probabilities calculated using the time-dependent theory are of the correct order of magnitude. Certainly high auto-ionization probabilities do sometimes occur (Shenstone 1940, Garton 1952, Marr 1954) and the experimental evidence on helium (Compton and Boyce 1928, Kruger 1930) is too imprecise to provide a real test of the theoretical predictions. The observations of Paschen and Kruger (1931) on beryllium are admittedly difficult to explain (cf. Wu and Ourom 1950) but the possibility of severe cancellation in the matrix element for this case cannot be excluded, the position being analogous to that occurring in photo-ionization (cf. Bates 1946). None of the other experimental evidence appears to yield satisfactory comparative data for it must be noted that the theory is as yet restricted to cases of L–S coupling. Further experimental work is very desirable.

The value of γ for $H^-(2s2p)\,^3P$ is about 100 times smaller than the value for the similar neutral case $He(2s2p)\,^3P$ (paper I) though the width of any line associated with $H^-(2s2p)\,^3P$ is still rather large, being at least 15 cm^{-1}, a value which is probably fairly typical of negative ions with L–S coupling.

As Bates (1950) has pointed out, the rate of dissociative recombination (attachment) is to a certain approximation directly proportional to the probability of auto-ionization (auto-detachment). It is to be expected therefore that dissociative attachment will proceed at a considerably slower rate than dissociative recombination, a conclusion that is in harmony with available experimental evidence (Massey 1950).

Acknowledgment

The authors wish to record their indebtedness to Professor D. R. Bates for many stimulating discussions.

References

Bates, D. R., 1946, *Mon. Not. Roy. Astr. Soc.*, **106**, 432; 1950, *Phys. Rev.*, **78**, 492.

Bates, D. R., and Massey, H. S. W., 1951, *J. Atmos. Terr. Phys.*, **2**, 1.

Bransden, B. H., and Dalgarno, A., 1953 a, *Proc. Phys. Soc.* A, **66**, 904; 1953 b, *Ibid.*, **66**, 911; 1953 c, *Ibid.*, **66**, 268.

Compton, K. T., and Boyce, J. C., 1928, *J. Franklin Inst.*, **205**, 497.

Garton, W. R. S., 1952, *Proc. Phys. Soc.* A, **65**, 268.

Hulthén, L., 1944, *K. Fysiogr. Sällsk. Lund Förh.*, **14**, No. 21; 1948, *Arkiv. Mat. Astr. Fys.*, **35A**, 25.

Hulthén, L., and Olsson, P. O., 1950, *Phys. Rev.*, **79**, 532.

Hylleraas, E., 1950, *Astrophys. J.*, **111**, 209.

Kohn, W., 1948, *Phys. Rev.*, **74**, 1763.

Kruger, P. G., 1930, *Phys. Rev.*, **36**, 853.

Marr, G. V., 1954, *Proc. Roy. Soc.* A, **224**, 83.

Massey, H. S. W., 1950, *Negative Ions*, 2nd edn (Cambridge: University Press).

Massey, H. S. W., and Moiseiwitsch, B. L., 1951, *Proc. Roy. Soc.* A, **205**, 483.

Paschen, F., and Kruger, P. G., 1931, *Ann. Phys. Lpz.*, **8**, 1005.

Shenstone, A. G., 1940, *Phys. Rev.*, **57**, 894.

Wu, T. Y., and Ourom, L., 1950, *Canad. J. Res.* A, **28**, 542.

RESEARCH NOTES

A High Energy Gamma Ray in the Decay of Barium 131

By R. K. GUPTA and S. JHA
Tata Institute of Fundamental Research, Apollo Pier Road, Bombay 1

MS. received 26*th August* 1955, *and in final form* 30*th September* 1955

From their studies of the γ-rays following K-capture in ^{131}Ba Lu, Kelly and Wiedenbeck (1955) have found that the excited states of ^{131}Cs occur at 122 kev, 274 kev, 371 kev and 619 kev. The energies of the observed γ-rays are 122 kev, 274 kev, 371 kev, 497 kev and 619 kev. They suspected the existence of a γ-ray at 1090 kev but they were not sure if it originated in the decay of ^{131}Ba.

The γ-rays from ^{131}Ba have been studied with our scintillation spectrometer (Gupta and Jha 1956). A thin deposit of ^{131}Ba, produced in the neutron-irradiation of 50 grammes of barium nitrate in the Harwell pile for a week, served as the source. For the summing technique, the source was enclosed in a brass tube before being introduced into the well of the crystal. The spectrum of the γ-rays with the source outside the well is given in figure 1 and that with the source inside the well of the crystal is shown in figure 2.

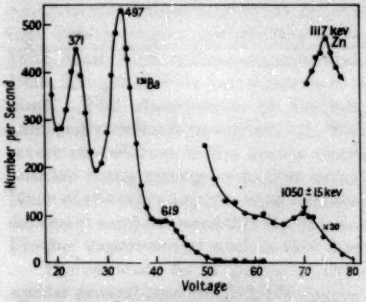

Figure 1. Scintillation spectrum of ^{131}Ba with the source away from the crystal, showing the photo-peaks of 371, 497, 619 and 1050 kev gamma rays.

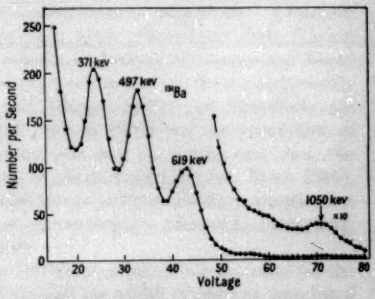

Figure 2. Scintillation spectrum of ^{131}Ba with the source inside the well of the crystal, showing the effect of summing.

One can see from figures 1 and 2 that there is a γ-ray of energy 1050 ± 15 kev being emitted by the barium source. The apparent intensity of this γ-ray is 1·5% of the intensity of the 497 kev γ-ray. When corrected for the difference in the efficiency of detection, the intensity comes out to be 4%. The apparent intensity of this line with the source inside the well was slightly higher, i.e. 2% of the intensity of the 497 kev γ-ray. This line persisted with the same relative intensity when sources of different strengths were placed outside the crystal, showing that it did not originate in the build-up processes.

In order to examine if this radiation originated in some isotope other than ^{131}Ba, the irradiated barium sample was purified from Ca, Sr, Fe, Pb, alkalies and lanthanum. In all cases, this line appeared with the same relative intensity. The intensity of this line relative to that of the 497 kev γ-ray was followed for about three weeks. The intensity ratio remained constant throughout this period, indicating that it decayed with the same half-life as the 497 kev γ-ray. The only other isotope of Ba which decays with about the same half-life is ^{140}Ba but it is very unlikely that this isotope can be formed in any appreciable quantity; secondly, $^{140}\text{Ba}\rightarrow{}^{140}\text{La}\rightarrow{}^{140}\text{Ce}$ chain has many γ-rays which have not been observed here. One feels thus reasonably justified in attributing this 1050 kev radiation to ^{131}Ba.

The presence of 1050 kev radiation suggests the existence of a level in ^{131}Cs at 1050 kev which de-excites itself by transition to the ground state. There are no radiations of appreciable intensity in the energy region 619 kev to 1050 kev. The fact that the intensity of the 1050 kev line seems to rise when the source is put inside the well points to the possibility that the 1050 kev level de-excites itself also by the emission of γ-rays in cascade, some of which, presumably, are not resolved in figures 1 and 2.

Further studies are in progress.

References

Lu, D. C., Kelly, W. H., and Wiedenbeck, M. L., 1955, *Phys. Rev.*, **97**, 139.
Gupta, R. K., and Jha, S., 1956, *J. Nuclear Physics*, in the press.

REVIEWS OF BOOKS

Operational Calculus based on the two-sided Laplace Integral, by B. VAN DER POL and H. BREMMER. 2nd Edn. Pp. xiv+415. (Cambridge: University Press, 1955.) 60*s*.

Physicists interested in the application of modern operational methods to the study of physical problems will already be familiar with the first edition of this book which appeared in 1950. In this work the authors base an operational calculus upon the properties of the bilateral Laplace transform

$$f(p)=p\int_{-\infty}^{\infty} e^{-pt}h(t)dt,$$

where it is assumed that p and hence $h(t)$ are such as to ensure the existence of the integral. The theory of such transforms is developed in the first half of the book and the second half is devoted to the solution of ordinary differential equations with constant and variable coefficients, of systems of simultaneous ordinary differential equations and of certain partial differential equations. There is a large number of examples drawn from a wide field in both physics and pure mathematics. The whole work is very well summarized in a 'Grammar' which is a collection of general formulae and rules of manipulation for the operational calculus, and a 'Dictionary' containing classified transform pairs.

The first edition of this book was distinguished by the high quality of the writing and the novel approach adopted by the authors. The concepts of Fourier theory are well explained and illustrated but the proofs of the basic theorems are omitted, reference being made to the classic treatises of Doetsch and Widder. This is probably the most effective method of treating the subject for readers whose main interest lies not in the theory but in its application to physical problems and there is no doubt that the authors have carried out their plan with signal success.

The new edition differs only slightly from the first. A number of corrections and improvements have been made at various places but only three sections of essentially new material have been added. Rules for the treatment of correlation functions have been added at the end of the chapter on 'Elementary Rules' (Chapter IV). The remarks on the Dirac delta function have been supplemented by a very brief paragraph which does no more than mention Schwarz's theory of distributions. A brief note on the operational interpretation of the Wiener–Hopf technique has been added to the chapter on integral equations (Chapter XIV). These additions are much too brief to add substantially to the stature of the work; this was already great and there is no doubt that this book will become a standard work on operational methods. I. N. SNEDDON.

Astrophysical Quantities, by C. W. ALLEN. Pp. xii+263. (London: Athlone Press, 1955.) 55*s*.

It is hard to express anything but the highest praise for this book. In 250 pages, Professor Allen has assembled in a coherent and orderly manner a most valuable collection of data covering almost the entire astrophysical sciences, and much of physics as well. In a short introduction the author explains

that the basis on which he has compiled the book is to present the quantitative framework on which astrophysics is being built. This is interpreted in a most generous manner, and the dividing line between modern physics and astrophysics is so thin that the reader is well past the hundredth page before he becomes conscious that the compilation has any such specialist bias.

The real business of the book begins in Chapter 2 devoted to General Constants and Units, followed by chapters on Atoms, Spectra and Radiation. Lists of elements with their stable isotopes and cosmic abundances, ionization potentials, data on fundamental particles, atomic configurations, line and multiplet intensities, wavelength standards, are all set out amongst a host of similar data. At Chapter 6 on the Earth the book becomes more specialized in its appeal, and the second half includes chapters on the Sun, Planets and Satellites, Interplanetary matter, Normal Stars, Stars with special characteristics, Star populations in the solar neighbourhood, Interstellar Space, Clusters and Galaxies, and ends with a series of incidental tables. The book is remarkably up to date—for example the Chapter on Interstellar Space contains three pages of data about the recent work in radio astronomy, and the radio work on the sun is treated as an integral part of that chapter.

There are few innovations to distract the seeker after data, and the symbolism is clear and consistent. Tables are everywhere preferred to graphs, since, as the author explains, the absolute values of astrophysical quantities constitute a live and ever changing subject and it is necessary to cater for numerical changes.

The compilation of a data book such as this requires an author with a wide and fundamental knowledge of his subject. Scientists of diverse interests will be grateful to Professor Allen for devoting his special gifts to this task.

A. C. B. LOVELL.

Elementary Theory of Nuclear Shell Structure, by M. GOEPPERT MAYER and J. H. D. JENSEN. Pp. xiv + 209. (London: Chapman and Hall; New York: John Wiley, 1955.) 62*s*.

It is seven years since Mrs. Mayer published her famous paper in which the magic numbers, representing nuclei having especially stable configurations of nucleons, became for the first time physical fact rather than wishful thinking. Shortly afterwards there appeared in coincidence papers by herself and by Professor Jensen and his colleagues. These papers explained the magic numbers in terms of an independent-particle, or shell, model of the nucleus, and at the same time accounted remarkably well for the observed sequence of spins and magnetic moments of odd mass nuclei.

Since those early papers a steadily increasing flow of work has been published confirming and extending the shell model which by now is generally recognized as giving a remarkably accurate picture of the properties of low lying states of nuclei. It is therefore entirely fitting that the two parents of this great advance in nuclear theory should at this time combine to give us the first comprehensive account in book form of the nuclear shell model.

The book, which is elementary throughout, confines itself to a discussion of the extreme j–j-coupling version of the shell model. Although this version is now known to be not at all appropriate to the lighter nuclei, the resulting simplicity justifies the approximation in a work of this kind. Much of the book

is devoted to a lucid exposition of the empirical facts, some of which have not been presented before. The treatment of the coupling together of several particles is presented too briefly for complete satisfaction, but a fuller discourse would certainly have taken the book out of the elementary class.

One serious criticism can be made. It is that the treatment of collective aspects of the shell model does not do justice to the important contributions of the Copenhagen group. It could hardly be deduced from this book that collective motions in nuclei are as important as the independent particle motions, and that the collective interpretation of certain phenomena is much less laboured than that of the pure shell model. It seems a pity that this has not been made the occasion to draw attention to the essential fact that the two approaches are complementary, even though the reasons for this are not yet properly understood.

Despite this fault, the book is a most welcome and valuable addition to the literature of nuclear physics and is recommended to all who wish to acquire a knowledge of the basic facts and theories of nuclear structure.

B. H. FLOWERS.

Boltzmann's Distribution Law, by E. A. GUGGENHEIM. Pp. 61. (Amsterdam: North-Holland Publishing Co., 1955.) 5*s*. 6*d*.

Although this booklet is written for "students of physics and chemistry in their first term at a university, provided only they have had an adequate training in elementary calculus", it will probably be the older students and their teachers who will benefit most from it.

Lucidly written, it derives properties of such systems as ideal diatomic gases, simple crystals, or a gas of electric dipoles, and discusses some of the assumptions used in the derivations.

It seems to me that the level is still too high for first-year students, but for students in their final honours year it should provide stimulating supplementary reading. The price is so low that it can become part of every student's library. One minor criticism is that figure 3 on p. 45 seems to me to need a caption.

D. TER HAAR.

An Introduction to Reactor Physics, by D. J. LITTLER and J. F. RAFFLE. Pp. viii + 196. (London: Pergamon Press, 1955.) 25*s*.

The rapidly increasing number of physicists and engineers whose work is concerned with nuclear energy has resulted in the introduction of specialized teaching in this subject in several institutions. The A.E.R.E. at Harwell has for some time provided such teaching in its Reactor School and the present book contains the basic material of the course.

The first five chapters present the relevant parts of atomic and nuclear physics for those new to the subject. This is a strictly practical section, whose impact on, for instance, the engineer, has presumably been found satisfactory; it is clearly written and provided with references for further reading. Chapters 6–12 contain the main body of specialized information which is throughout the book related to the design of thermal reactors of the type to be installed for power production in the United Kingdom. Most of the calculations are however of general application and good accounts are given of the progress of a chain reaction, of neutron diffusion and of the evaluation of the lattice

constants of a pile. The calculations are given in full and although their physical meaning is occasionally obscured by detail, they will be found useful by the student, particularly if his course also includes some examples for practice. The chapter entitled " Running a Pile at Power " is an interesting review of such problems as canning, coolants, and poisoning.

The last chapters deal with the passage of radiations through matter, particle detectors, radiation damage and diffusion length measurements; the appendices include a brief but useful account of radiation hazards. This part of the book, like the introductory section, is a very clear account of the main facts in the subjects treated, on which may be based both further study and practical experience.

The book gives a well-balanced survey of pile theory within its chosen limits, and should be very helpful to those about to teach, or to be taught, the subject of Reactor Physics. No mathematical knowledge beyond the theory of differential equations is required. There are a few minor errors; one is for instance a little surprised to learn (p. 140) that a heavy particle passing through matter may be ' absorbed ' when it has almost stopped. The use of the term ' nuclear interaction ' to describe the final stages of the reduction of the energy of a charged particle to the thermal value may also be misleading. The main theme is, however, developed authoritatively and the layout of the material is excellent. A short list of symbols with their definition would be a useful addition to the next issue of what should prove a very popular book.

W. E. BURCHAM.

BOOK NOTICES

La geométrie des groupes classiques, by J. DIEUDONNÉ. Pp. viii + 115. (Berlin, Göttingen, Heidelberg: Springer, 1955.) (Ergebnisse der Mathematik und ihrer Grenzgebiete, Neue Folge, Heft 5.) DM 19.60.

Méthodes d'algèbre abstraite en géométrie algébrique, by P. SAMUEL. Pp. x + 133. (Berlin, Göttingen, Heidelberg : Springer 1955.) (Ergebnisse der Mathematik und ihrer Grenzgebiete, Neue Folge, Heft 4.) DM 23.60.

L'exploitation des données empiriques. Actes du colloque tenu à Luxembourg en juillet 1953 dans le cadre du Congrès de l'Association Française pour l'Avancement des Sciences. Pp. 77. (Paris : Publications Scientifiques et Techniques du Ministère de l'Air, N.T. 52, 1955.) 850 *fr.*

L' interpolation idéale et son calcul numérique effectif, by P. VERNOTTE. Pp. iii + 74. (Paris : Publications Scientifiques et Techniques du Ministère de l'Air, No. 300.) 850 *fr.*

CONTENTS OF SECTION B

PAGE

Editorial 1

Dr. R. W. Crompton, Dr. J. Dutton and Dr. S. C. Haydon. Precision Measurements of Ionization Coefficients in Uniform Static Fields 2

Dr. M. J. Morant and Dr. H. House. The Work Function and Patch Field of an Irregular Metal Surface 14

Prof. H. Fröhlich and Mr. B. V. Paranjape. Dielectric Breakdown in Solids . 21

Dr. W. A. Prowse and Mr. P. E. Lane. The Breakdown of Gases subject to Crossed Electric Fields 33

Miss J. P. A. Tillett. Fracture of Glass by Spherical Indenters 47

Dr. F. C. Roesler. Indentation Hardness of Glass as an Energy Scaling Law . 55

Dr. D. W. Goodwin. Space Charge Phenomena in Liquid Dielectrics . . . 61

Dr. P. D. Fochs. The Measurement of the Energy Gap of Semiconductors from their Diffuse Reflection Spectra 70

Dr. R. Mansfield. Impurity Scattering in Semiconductors 76

Dr. I. C. Browne, Mr. K. Bullough, Dr. S. Evans and Dr. T. R. Kaiser. Characteristics of Radio Echoes from Meteor Trails—II : The Distribution of Meteor Magnitudes and Masses 83

Mr. E. R. Billam and Dr. I. C. Browne. Characteristics of Radio Echoes from Meteor Trails—IV : Polarization Effects 98

Research Notes :

Prof. K. G. Emeléus and Dr. N. R. Daly. Ion Oscillations in a Cathode Potential Minimum 114

Mr. I. M. Mackintosh. Photon-radiative Recombination in PbSe, PbTe and PbS 115

Letters to the Editor :

Ir. O. W. Memelink. The Distribution of Impurity in a Semi-infinite Solidified Melt 119

Prof. K. S. W. Champion. Radiation from Gaseous Arcs 120

Reviews of Books 122

Contents of Section A 128

The Photodisintegration of Nitrogen

By I. F. WRIGHT†, D. R. O. MORRISON‡,
J. M. REID and J. R. ATKINSON
Department of Natural Philosophy, University of Glasgow

Communicated by P. I. Dee; MS. received 11th July 1955 and in amended form 20th October 1955

Abstract. The (γ, p), (γ, pn), (γ, α), $(\gamma, \alpha\alpha)$ and $(\gamma, \alpha p)$ reactions in ^{14}N have been studied by passing the x-ray beam from a 23 Mev synchrotron through a Wilson cloud chamber. The range distribution of protons of energy up to 3 Mev shows sharp well-defined peaks at energies of 0·51, 1·63 and 2·92 Mev. These energies correspond closely to the energies of the resonances reported for the $^{13}C(p, \gamma)^{14}N$ (ground state) reaction. For these resonances the ratios of the cross sections for the (γ, p) and (p, γ) reactions are in good agreement with the predictions of the principle of detailed balancing. At higher energies the following measurements were made: (i) the (γ, p) process was investigated by measuring the range distribution of the ^{13}C nuclei, (ii) both (γ, p) and (γ, pn) processes were studied by measuring the numbers of events at three different synchrotron peak energies. These measurements showed that both the (γ, p) and (γ, pn) cross sections are small at energies up to 15 Mev and large in neighbourhood of 20 Mev. The estimated values of the integrated cross sections up to 23 Mev for the (γ, p) and the (γ, pn) reactions are both approximately 0·02 Mev barn. The (γ, α), $(\gamma, \alpha\alpha)$ and $(\gamma, \alpha p)$ cross sections are each about 0·1 millibarn. The implications of these results are discussed in some detail.

§ 1. Introduction

In recent years there has been a considerable amount of experimental work on photonuclear reactions and, as a result, it is becoming possible to draw some general conclusions about their behaviour. The most significant of these conclusions is the existence of the 'giant resonance', a feature of the photonuclear process which appears to be common to all nuclei. However it is also true that the experimental measurements made to date tend to be confined to limited sections of the field. Thus the most convincing evidence for the giant resonance all comes from (γ, n) cross section measurements which are experimentally much easier to measure than (γ, p) cross sections. Many (γ, n) reactions have been studied by measuring the activity of the product nucleus but, as many (γ, p) reactions lead to stable products, very few (γ, p) reactions have been, or can be, studied in this way. Measurements based on the detection of the particles emitted with counter techniques are also biased in favour of neutrons. Photoneutron yields can be measured quite readily by detecting the slowed down neutrons some time after the x-ray burst but photoprotons must be detected in

† Now at Department of Nuclear Physics, The Australian National University, Canberra.
‡ Now at Imperial Chemical Industries, Ltd., Ardeer, Scotland.

the presence of an intense x-ray background. As a result the measurement of absolute yields and energy distributions is difficult and uncertain. While the absence of detailed information on the (γ, p) reaction does not greatly affect the general picture in heavy nuclei where the (γ, n) cross section is much larger than the (γ, p) cross section, it is very important for light nuclei where the (γ, p) cross section may well be larger than the (γ, n) cross section.

Nuclear emulsions have been used to detect photoprotons ejected from a gas or foil target. This technique has been of value in establishing the anomalous yield of high energy protons but has the disadvantages that the resolution is limited by the unknown energy loss in the target and that there is no direct way of separating the protons from different reactions. The study of disintegrations in directly irradiated emulsions is very difficult except for reactions in which the products are all charged and of approximately equal mass.

This paper reports an investigation of the photodisintegration of ^{14}N by the study of the photonuclear disintegrations produced in the gas of a Wilson cloud chamber. When compared with the previous techniques the use of the cloud chamber has the following advantages for an investigation of the photonuclear process in light nuclei. The cloud chamber provides a very high degree of discrimination between the tracks of the particles being studied and the tracks due to the electron background. The energy distribution of photoprotons of energy up to a few Mev can be obtained with considerable accuracy from measurements of the proton ranges. Since the tracks of both the charged fragments and the recoil nucleus can be seen more information is available about the nature of each event. All reactions except (γ, n), (γ, 2n) and (γ, γ) lead to visible events and thus the cloud chamber provides the opportunity of studying the relative probabilities of a large number of reactions simultaneously. Thus in ^{14}N, the nucleus studied in this investigation, the (γ, p), (γ, d), (γ, pn), (γ, α), (γ, $\alpha\alpha$) and (γ, αp) reactions can all be studied in a cloud chamber irradiated with 23 Mev x-rays and, with the exception of events from the first two reactions, events of different kinds are easily distinguished from one another. Additional reasons for choosing ^{14}N are that the (γ, n) cross section has already been measured (Horsley *et al.* 1952) and that the thresholds for the (γ, p), (γ, n) and (γ, pn) reactions are all well below the energy of the giant resonance found in the (γ, n) cross section. Thus a study of these reactions might be expected to yield information about the change in the nature of the photonuclear process in going from energies below to energies in the vicinity of the giant resonance.

Gaerttner and Yeater have also reported cloud chamber measurements of photonuclear reactions in ^{4}He, ^{12}C, ^{14}N and ^{16}O using x-rays of energy up to 100 Mev (Gaerttner and Yeater 1951b, 1951a, 1950a, 1950b and 1950c respectively). Their work was of importance in showing that photonuclear events could be distinguished from the background of electrons produced by the x-ray beam and in indicating the relative importance of the (γ, p), (γ, pn) and the star producing reactions. The work described in this paper extends their results for ^{14}N by adding, for energies up to 23 Mev, a measurement of the energy distribution of the protons from the (γ, p) reaction, from which is obtained a detailed cross section for the (γ, p) reaction between 7·5 and 10·5 Mev: the work also gives the energy dependence of the (γ, p) and (γ, pn) reactions between 10·5 and 23 Mev and a measurement of the number of (γ, α), (γ, $\alpha\alpha$) and (γ, αp) events.

§ 2. Experimental Method

2.1. *Apparatus*

An investigation of this kind depends for its success on the attainment of a high standard of track quality so that the tracks of recoil nuclei as well as those of the lighter fragments can be clearly seen and measured. In addition the electron background must be kept down to a level where it does not obscure the photonuclear events. The production of good quality tracks is made easier by the fact that the synchrotron is a perfect shuttered source (the x-ray pulse is approximately 40 μsec long) so that, if the cloud chamber and synchrotron are correctly timed relative to one another and care is taken to keep all the cloud chamber conditions constant, the x-rays will always enter the chamber at the same supersaturation.

The cloud chamber used was a volume defined chamber of conventional design with a sensitive volume 12 in. in diameter by 2½ in. deep. It was filled with nitrogen saturated with water vapour, the expanded pressure being 1·4 atmospheres. The stopping power of the gas was calculated from its composition and the expanded pressure which was measured during each 6 hour run. The x-rays from the synchrotron were carefully collimated to give a rectangular beam (2½ cm high by 10 cm wide) which entered the cloud chamber through a window, 0·09 in. thick, made by thinning down the Perspex wall. The chamber was positioned so that the beam was accurately in the centre of the illuminated region (4 cm high). In order to estimate the energy of the photons responsible for the events observed, irradiations were made at three different values of the peak x-ray energy, these energies being approximately 19, 21 and 23 Mev.

The output from the synchrotron was restricted to single bursts of x-rays and the cloud chamber was triggered with a pulse derived from the synchrotron timing pulses. In the preliminary adjustment the delay between the opening of the cloud chamber expansion valve and the arrival of the x-rays was changed in 5-millisecond steps. The shortest delay that gave sharp tracks was chosen for use in the main experimental runs. If the delay is reduced below this value the tracks rapidly become diffuse. On the other hand the main effect of increasing the delay above the chosen value is to cause an increase in the chamber background. In this case there is no marked change in the sharpness of the tracks. Provision was made for the cloud chamber triggering pulse to turn off the electrostatic clearing field across the chamber. This effected an improvement in the sharpness of the tracks of recoil nuclei. Because of the large density of ions along these tracks some of the ions are dragged out by the clearing field. Tracks of electrons and protons were equally sharp no matter whether the field was left on or turned off.

The chamber was surrounded by a water-cooled aluminium cylinder which gave effective temperature stabilization so that once the expansion ratio was correctly adjusted it was not necessary to alter it during a 6 hour run. As can be seen from the examples in figures 1, 2 and 3 (Plates) the tracks of electrons, protons and recoil nuclei were all sharp and of high quality. The examples selected show two general views of the chamber and enlargements of a (γ, p) event, a (γ, pn) event and a (γ, $2\alpha^6$Li) star.

The output of the single pulse of x-rays was measured with an ionization chamber by observing the height of the output pulse on the screen of a cathode-ray

oscillograph. The ionization chamber was mounted behind a 3 in. lead wall and was placed in the beam behind the cloud chamber. The x-ray doses measured in this way were expressed in terms of the conventional '*r*-unit' by the following procedure. For each peak energy the ionization chamber response was compared with the activity induced in a copper disc irradiated in a standard position in front of the cloud chamber and counted in a standard geometry. The relative x-ray doses for the 19, 21 and 23 Mev runs were then calculated from the peak energies using the ^{62}Cu activation curve as measured at Saskatchewan (Katz and Cameron 1951). Absolute values were obtained by subsequently comparing (at a peak energy of 23 Mev) the activity induced in the copper disc with the response of a Victoreen thimble mounted at the centre of a Perspex cylinder 8 cm in outside diameter. This comparison is estimated to be accurate to 20%.

2.2. *Analysis*

The tracks were photographed with a stereographic set of three 60 mm cameras. One of these was mounted centrally above the chamber while the other two side cameras were separated from this top camera by 25½° in the vertical plane and from each other by 90° in azimuth. For both side cameras the plane of the film was tilted with respect to the axis of the lens and was at an angle of 30° to the horizontal. The images of all tracks of length greater than 3 mm were measured by each of the following techniques.

(i) The events were viewed under a low powered microscope, the final image being approximately seven times the original track size. (The microscope magnification was 40 and the chamber–film reduction ratio 1/6.) Each recoil length was measured with the eyepiece scale.

(ii) The length, direction in space and coordinates of the origin and end points of each track were measured by the usual method of stereographic analysis, i.e. the films were replaced in the cameras and the projected images of the tracks brought into coincidence on an adjustable table. The three films were brought into register using the images of the grid wires which were built into the chamber just above the velvet base. This automatically checked the accuracy of the reprojection system. Three cameras were used since, for a pair of cameras, it is sometimes impossible to get a satisfactory coincidence on a track lying more or less parallel to the line joining them. The measurements were made using the top camera and the side camera appropriate to the track in question with the third camera providing a useful check. Tests on artificial tracks showed that the length measurements were accurate to ½ mm for all lengths and that the angles were accurate to 1° for tracks within 60° of the horizontal.

The events were classified as:

(1) Collinear Flags—events in which the recoil and fragment were very nearly in a straight line for all three films. This group is intended to consist of events in which the recoil and fragment are the only two products of the reaction. For these events the momentum of the incident photon and the scattering of the recoil may both cause a small departure from exact collinearity. The criterion used was that events in which the recoil was within ± 10° of its expected direction were counted as collinear.

(2) Non-collinear Flags.

(3) Unclassified Flags—events with a visible recoil of uncertain direction (e.g. because of its short length).

(4) Singles—events without a visible recoil.
(5) Stars—events with three or more prongs.
(6) Tracks coming from the chamber wall.

The thresholds for the photonuclear reactions possible in ^{14}N are given in table 1, together with the expected classification of the events produced.

Table 1. Reaction Thresholds and Classifications

Photonuclear Reactions			Threshold (Mev)
$^{14}N+\gamma \rightarrow n+^{13}N$			10·54
$p+^{13}C$	Collinear	Flags	7·54
$d+^{12}C$	Collinear	Flags	10·26
$\alpha+^{10}B$	Collinear	Flags	11·6
$p+n+^{12}C$	Non-collinear	Flags	12·49
$\alpha+\alpha+^{6}Li$		Stars	16·07
$p+\alpha+^{9}Be$		Stars	18·2
Neutron Reactions			
$^{14}N+n \rightarrow p+^{14}C$	Non-collinear Flags (except for slow neutrons)		−0·63
$\alpha+^{11}B$	Non-collinear Flags (except for slow neutrons)		0·15

2.3. *Background Events*

Reactions initiated by the neutrons which accompany the x-ray beam will give rise to a background of unwanted tracks. In particular, since the $^{14}N(n, p)^{14}C$ reaction is exothermic there may be a relatively large number of proton tracks from disintegrations initiated by slow neutrons. These proton tracks have a characteristic length of 7½ mm (the range in the chamber of a proton of energy 0·58 Mev) and should occur uniformly throughout the chamber. The energy distribution of tracks stopping in the chamber shows that they form a distinctive group which is easily identified and hence eliminated (see figure 4 and discussion in § 3).

Fast neutrons produce both (n, p) and (n, α) events which will appear as non-collinear flags of length greater than 1 cm. The number of these background events was estimated from the number occurring outside the beam, and also from the number of tracks coming from the Perspex wall. Both estimates indicate that the correction required is small, the number (15) of tracks longer than 1 cm with origins outside the x-ray beam being only 2% of the number (660) of tracks within the beam, whereas the two volumes are equal.

The number and distribution of the tracks of recoil protons ejected from the Perspex wall by fast neutrons† confirms this estimate of the background and shows further that the fast neutron flux within the x-ray beam is not significantly greater than the fast neutron flux elsewhere in the chamber.

§ 3. Energy Distribution of Low Energy Protons

If it is assumed that the collinear flags (with (γ, α) events excluded), unclassified flags and singles stopping in the chamber are (γ, p) events, then the distribution of E_0, the total kinetic energy of the proton and recoil, is as given in figure 4. The proton kinetic energy was obtained directly from the measured track length and the recoil energy was then calculated using momentum conservation. Events occurring outside the x-ray beam are shaded and it can be seen that they are all

† This estimate was obtained from the data for the 19 and 21 Mev runs for which the number of tracks of photoprotons from the ^{12}C and ^{16}O in the Perspex is small and therefore easily allowed for.

due to slow (n, p) reactions. In figure 5 the slow (n, p) events have been subtracted and the classification of events is indicated. It can be seen that unclassified flags and singles only occur at proton energies for which recoils would be very short. (For a 1 MeV proton the recoil length is approximately $\frac{1}{3}$ mm.)

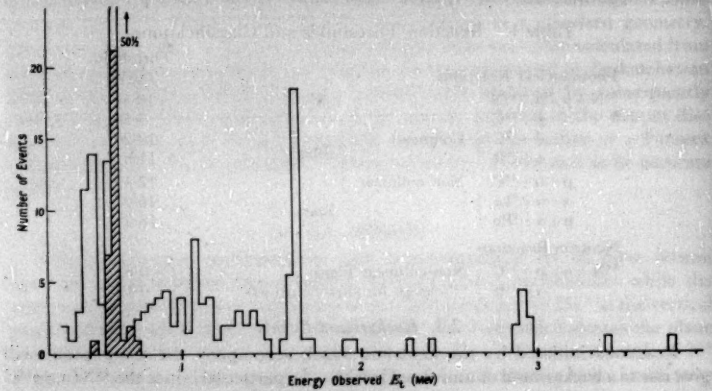

Figure 4. Distribution of the total energy (i.e. E_p+E_γ) of collinear flags, unclassified flags and singles stopping in the chamber, assuming these to be (γ, p) events. (See § 2.2 for description of the classification.) Events occurring outside the X-ray beam have been shaded.

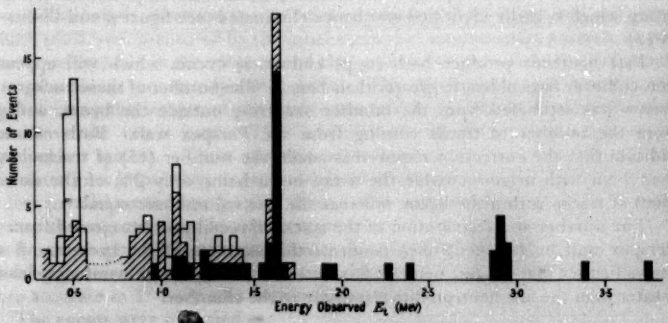

Figure 5. The energy distribution of figure 4 after subtraction of events due to the ^{14}N (n, p) ^{14}C reaction. Collinear flags are shown as solid rectangles, unclassified flags as shaded rectangles and singles as open rectangles.

Distinct groups are observed at $0{\cdot}51 \pm 0{\cdot}02$, $1{\cdot}63 \pm 0{\cdot}02$ and $2{\cdot}92 \pm 0{\cdot}03$ MeV, the latter group being few in number as most of the tracks leave the chamber, and a broad group centred at about $1{\cdot}15 \pm 0{\cdot}05$ MeV.

The occurrence of definite groups implies that these photoprotons arise from the resonance absorption of quanta into excited states of the ^{14}N nucleus. It is, therefore, of interest to compare these results with the information about

the excited states of ^{14}N derived from other reactions and, in particular, to make a comparison with the measurements made on the $^{13}C(p, \gamma)^{14}N$ reaction. This reaction has been studied by Seagrave (1952) and by Woodbury *et al.* (1953) using protons of energy up to 2·6 MeV and by Willard *et al.* (1955) who used protons of energy up to 3·2 MeV. These workers find that the $^{13}C(p, \gamma)^{14}N$ (ground state) reaction has resonances at centre-of-mass energies of 0·52, 1·64 and 2·89 MeV as well as a broad resonance at 1·16 MeV. In addition, other weak resonances (ground state) have been reported, but the additional contribution from these to the cross section is not significant. These energies correspond closely to the energies of the groups observed in this experiment and indicate that these proton groups come from the reaction $^{14}N(\gamma, p)^{13}C$ (ground state).

The comparison of the two reactions can be extended to cover the cross sections by using the principle of detailed balancing. The integrated (γ, p) cross sections for the resonances at 0·5, 1·6 and 2·9 MeV were calculated from the (p, γ) cross sections using this principle. The $^{13}C(p, \gamma)^{14}N$ (ground state) cross sections for the 0·5 and 1·6 MeV resonances were obtained by combining the results of Seagrave (1952) and Woodbury *et al.* (1953). The cross section for the 2·9 MeV resonance is a preliminary result obtained by Willard.† The expected number of tracks in each of the narrow groups was then calculated from the (γ, p) cross sections, the measured x-ray doses and an allowance for the percentage of tracks which do not stop in the chamber. In table 2 this estimate is compared with the number actually found. The agreement is very satisfactory and confirms the validity of applying the principle of detailed balancing to photonuclear reactions.

It may be added that there is, in this experiment, no way of deciding whether a proton is produced from the reaction $^{14}N(\gamma, p)^{13}C$ or the reaction $^{14}N(\gamma, p\gamma')^{13}C$; however, on the assumption that all the events may be represented by the $^{14}N(\gamma, p)^{13}C$ reaction, the close agreements with the details found from the inverse reaction have been established, thereby inferring that the contribution from the reaction $^{14}N(\gamma, p\gamma')^{13}C$ must be small.

Table 2. Comparison of the Observed Proton Groups with the Predictions from the $^{13}C(p, \gamma)^{14}N$ Reaction

(1)	(2)	(3)	(4)	(5)	(6)	(7)
8·06	0·52	0·065	0·603	0·99	34	32
9·18	1·64	0·044	0·813	0·62	24	26
10·43	2·89	0·040	±1·2	0·20	12	9

(1) ^{14}N energy of excitation (MeV); (2) energy of proton + recoil (MeV); (3) σ_{int}, (p, γ) (MeV mbn); (4) σ_{int}, (γ, p) (MeV mbn); (5) fraction of events stopping; (6) no. of tracks, calculated; (7) no. of tracks, observed.

A recent nuclear emulsion measurement (Spicer 1953) of the energy distribution of photoprotons from nitrogen irradiated with 11·5 MeV x-rays is in conflict with the present results. In this work a narrow beam of x-rays passed through a gas target chamber and the photoproton energy distribution was deduced from ranges measured in nuclear emulsions placed out of the beam, allowance being made for the energy lost by the proton before it reached the emulsion. The energy distribution reported by Spicer is a continuous energy distribution which decreases rapidly from 165 protons in the energy range 2·0–2·2 MeV to 19 protons in the energy range 3·0–3·2 MeV and has no sign of

† We are indebted to Dr. H. B. Willard for communicating this result to us.

a peak at 2·9 MEV. The distribution does not extend below 2 MEV since protons of energy less than this may fail to reach the emulsion. It is difficult to see how this result can be reconciled with the *absence* of tracks between 2·0 and 2·8 MEV which is such a striking feature of the distribution obtained in the present investigation and which is believed to be very reliable since, not only is the method inherently cleaner (e.g. (n, p) reactions are automatically eliminated since they either produce non-collinear flags or form a distinctive group), but also the results agree very well with all the data available from the inverse reaction. Until this discrepancy can be satisfactorily explained it would appear to be wise to treat the results of this and similar nuclear emulsion studies with some caution.

§ 4. STUDY OF THE (γ, p) AND (γ, α) REACTIONS AT HIGHER ENERGIES

For proton energies greater than 3 MEV the probability of a proton stopping in the chamber is very small and consequently the photoproton energy distribution cannot be determined from proton range measurements. However, since the proton momentum is directly related to the momentum of the recoiling ^{13}C nucleus this distribution can be determined from the range distribution of these recoils, which are from 1–4 mm long. These lengths can be determined quite readily from microscope measurements.

4.1. *Accuracy of Recoil Measurements*

The accuracy of these measurements was investigated by measuring the lengths of the recoils associated with the protons which stop in the chamber. These measurements were made for the recoils of collinear and unclassified flags of length greater than 1 cm. Since these tracks are either known or believed to be collinear, the recoil length was obtained from the lengths of the recoil and fragment images on the film and the fragment length measured by reprojection. Measurements were made on all three films and a mean taken, this being weighted according to the quality of the recoil track. The measurements on the film from the top camera generally had more weight than those from the side cameras.

These results are shown in figure 6 where these lengths are plotted as crosses. The abscissa in this plot is the recoil range calculated from the fragment range assuming this to be a proton. The necessary range–energy relationship for ^{13}C was chosen after a review of experimental range–velocity relations had been made. Practically all of the points group closely about the (γ, p) line and the accuracy of the recoil range measurements can be estimated from their spread. For the 1·64 and 2·89 MEV groups the root mean square deviations are 26% and 16% respectively. The expected range straggling is about 15% which indicates that the error introduced by the cloud chamber and in the measurement is less than 0·2 mm and is, therefore, comparable with or less than the unavoidable limitation imposed by straggling.

Since the range of a collinear flag recoil leads to a value of the fragment momentum this technique provides the same information as is obtained from measurements of magnetic curvature but has the advantage that a measurement can be made on practically all tracks whereas curvature measurements can only be made on long tracks. The error in momentum due to the range straggling of the recoil is comparable with the error in the curvature measurements arising from multiple scattering. (For a magnetic field of 5000 gauss and a chamber

filled with one atmosphere of nitrogen, the error in curvature for a 5 MeV proton—measured over a track length of 10 cm—is approximately 15%.)

In figure 6, a few (five) points are observed well off the expected (γ, p) line. These can only be (γ, d) events or (γ, pn) events where the neutron has been emitted in approximately the same direction as the proton. For comparison, the recoil ranges of some non-collinear (γ, pn) events which fall just outside the criterion for collinear flags are shown in the figure as circles. Since the distribution of these ranges completely overlaps the distribution of the five collinear recoils in question it is clear that these latter cannot be definitely identified and that the comparison of recoil and fragment ranges is an unsatisfactory method of identifying (γ, d) events when (γ, pn) events are also present.

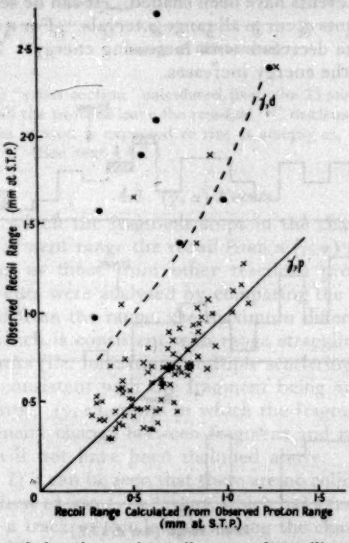

Figure 6. Comparison of the observed recoil ranges for collinear and unclassified flags stopping in the chamber with the ranges calculated from the range of the associated fragment track assuming this to be a proton. The dotted curve gives the expected ranges of the recoils from (γ, d) events.

4.2. *Recoil Range Measurements*

The accuracy of recoil range measurements and of the range–velocity data has been demonstrated for tracks which stop in the chamber. These events were of low energy, and had short recoils. Recoils from protons of energy greater than 3 MeV will be longer, and therefore the measurements will be more accurate.

For collinear flags in which the fragment leaves the illuminated region the fragment direction can be measured by reprojection and this gives the recoil direction. The recoil range can then be obtained from the microscopic measurement of the projected recoil image. These measurements were only made on

the film from the top camera as the geometrical calculations are extremely lengthy for the other films. The data for $(E_\gamma)_{max} = 23$ MeV was obtained from half of the films since the fragment directions of tracks leaving were not measured for the remainder. In order to avoid the errors inherent in measuring steeply inclined tracks only those within 45° of the horizontal were considered—this excluded 29% of the tracks (assuming an isotropic distribution). If unclassified flags are assumed to be collinear their recoil ranges correspond to protons of energy less than 3 MeV so that only collinear flags need be considered here.

The recoil range distribution for the three peak synchrotron energies is shown in figure 7. For the purposes of comparison the recoil ranges have been corrected to the values they would have if emitted at 90° to the γ-ray direction. The ranges of recoils from (γ, α) events have been shaded. It can be seen that approximately equal numbers of events occur in all range intervals. For a synchrotron spectrum the number of quanta decreases with increasing energy. Hence the (γ, p) cross section must rise as the energy increases.

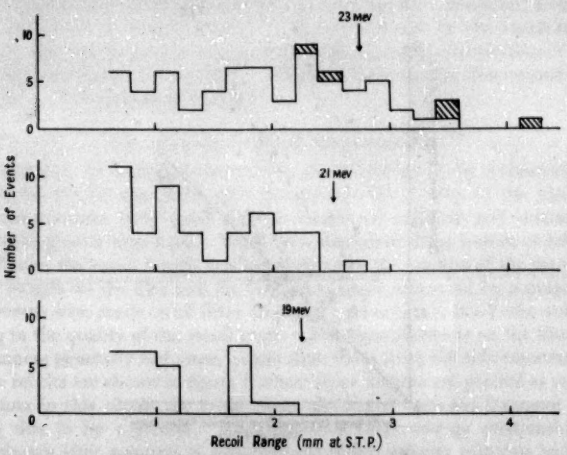

Figure 7. The range distribution of collinear flag recoils for the 19, 21 and 23 MeV runs. The shaded events are (γ, α) disintegrations.

In order to deduce the (γ, p) cross section from the above measurements it is necessary to know the number of protons leaving ^{13}C in an excited state and this information is not at present available. If it is assumed that in all cases the ^{13}C nucleus is left in the ground state, then the 'cross section', deduced from the data for the 23 MeV run, is shown in figure 8. If the residual ^{13}C nucleus is left in an excited state, the apparent value of E_γ calculated from the recoil range in this way will be too low. The true E_γ will be higher by between 3 MeV (the lowest excited state of ^{13}C) and 6 MeV (above which neutron emission produces non-collinear flags). It follows that the true (γ, p) cross section rises as steeply as, or more steeply than, the 'cross section' shown in figure 8.

A possible source of error is the presence of (γ, d) events which would tend to have longer recoils than (γ, p) events and, therefore, produce an artificial rise

in the (γ, p) cross section near the peak energy. No experimental evidence is available for or against the presence of (γ, d) events, but, on theoretical grounds (Gell-Mann and Telegdi 1953), their number is expected to be very small.

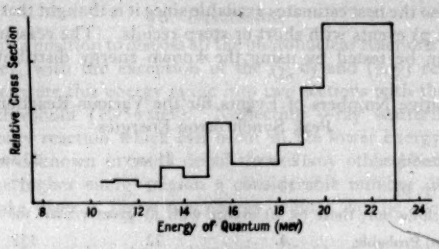

Figure 8. The (γ, p) ' cross section ' calculated from the 23 MeV recoil range distribution assuming that all the protons leave the residual ^{13}C nucleus in the ground state. The true (γ, p) cross section is expected to rise as steeply as, or more steeply than, this ' cross section '. (See text § 4.2.)

4.3. (γ, α) *Events*

(γ, α) events in which the fragment stops in the chamber can be identified since for a given fragment range the recoil from a (γ, α) reaction will be at least three times as long as those from other reactions producing collinear flags. Suspected (γ, α) events were analysed by comparing the measured recoil length with that calculated from the range, the maximum difference being 15% of the calculated range, which is consistent with range straggling. The 'appearance' of each of these tracks (i.e. ionization, multiple scattering and ionization change at the origin) was consistent with the fragment being an alpha particle. This gave five (γ, α) events. (γ, α) events in which the fragment leaves the chamber or in which the density change between fragment and recoil is too small to be detected visually will not have been included above. From the recoil range distribution (figure 7) it can be seen that there are no collinear events with longer recoils than the highest energy (γ, α) event, which has a fragment length of $2\frac{1}{8}$ cm. The probability of a track of this length leaving the chamber is less than 20%, so that it is very unlikely that any (γ, α) event will have been missed because its fragment does not stop in the chamber. Since the difference in density between the alpha and the ^{10}B track was not always very marked the 16 singles of appropriate range were carefully re-examined. The majority of these singles looked like protons (from track density and multiple scattering) there being only three of them which resemble alpha particles, so that we may take eight as an upper limit to the number of (γ, α) events.

§ 5. The Relative Probabilities of the Various Reactions

The relative numbers of events from the different reactions are listed in table 3.

In order to facilitate comparison with the (γ, n) reaction only (γ, p) events which occur at energies above the (γ, n) threshold (10·54 MeV) have been included. The number of such events was obtained from the measured recoil ranges of collinear flags. It was assumed that the number of (γ, d) events is negligible.

The numbers of (γ, pn) events have been taken as equal to the numbers of non-collinear flags. Since these numbers do not include any allowance for the possibility that some of the unclassified flags may be (γ, pn) events these numbers represent lower limits to the numbers of such events. However, it is believed that they are also the best estimates available since it is thought that the unclassified flags are all (γ, p) events with short or steep recoils. The reasonableness of this assumption can be tested by using the known energy distribution of protons

Table 3. Relative Numbers of Events for the Various Reactions at the Three Peak Synchrotron Energies

Reaction	19 MeV	21 MeV	23 MeV
(γ, p)	13	32	127
(These totals include only those (γ, p) events with E_γ greater than the (γ, n) threshold.)			
(γ, pn) Probable	4	22	132
Upper Limit (see text)	(13)	(27)	(147)
(γ, α)	0	0	5+?3
(γ, star)	0	0	8
(γ, n) (calc.)†	8±2	23±5	75
No. of r at 1 metre	0·014	0·024	0·050
No. of photos	304	265	333

† *Note.* The errors indicated in the number of (γ, n) disintegrations for the 19 and 21 MeV runs represent only the errors in the relative numbers at the three energies and arise from uncertainties in the synchrotron energy scale and in the monitoring arrangements. The absolute number of (γ, n) disintegrations may differ from these figures by a further ±20%.

of energy up to 3 MeV and the probability that a proton of a particular energy will stop in the chamber to calculate an expected value for the number of protons of energy less than 3 MeV which leave the chamber before stopping. This estimate can then be compared with the total of unclassified flags and collinear flags with short recoils which leave the chamber. All the unclassified flags have recoil lengths less than that corresponding to a 3 MeV proton. The estimated number of tracks is 58 ± 15 and the observed number is 73. Thus the assumption made is perfectly reasonable but, at the same time, the possibility that some of the unclassified flags may be (γ, pn) events cannot be ruled out. These considerations show that an upper limit of 30 may be given to the number of such events. The upper limits derived on this basis are given in brackets in table 3. It should be noted that the number of unclassified flags added to the 19 MeV total is probably abnormally high due to one of the films being of somewhat poorer quality.

The number of (γ, n) events was calculated from the induced activity measurements of the Saskatchewan group (Horsley *et al.* 1952).

It can be seen that the number of (γ, p) events increases with increasing x-ray energy as rapidly as the number of (γ, n) events, and that the number of (γ, pn) events increases rather more rapidly. Thus both the (γ, p) and (γ, pn) cross sections must have an energy dependence which is similar to that of the (γ, n) cross section (Horsley *et al.* 1952), i.e. they will be small at low energies and rise rapidly at about 20 MeV. The (γ, α) and (γ, star) cross sections are an order of magnitude lower, but have a similar energy dependence. Using the usual technique of momentum balance four of the eight star events were identified

as $(\gamma, \alpha p)$ events and three as $(\gamma, \alpha\alpha)$ events while one was too steeply inclined to permit accurate measurements. Thus the (γ, α), $(\gamma, \alpha p)$ and $(\gamma, \alpha\alpha)$ cross sections are all about $1\text{–}2 \times 10^{-28}$ cm^2.

§ 6. Discussion

We are now in a position to discuss all the photonuclear reactions in ^{14}N up to an energy of 23 Mev, with the exception of the (γ, d) and (γ, γ) reactions. It is convenient to separate this energy range into two sections with the dividing line at the (γ, n) threshold (10·54 Mev). Neglecting γ-ray scattering, the (γ, p) process is the only reaction which can occur in the lower energy region where its cross section is known in more detail than is any other photonuclear cross section. In the higher energy region a considerable number of photonuclear reactions can take place. These two energy regions will be considered in the reverse order.

It has been shown that the cross sections for both the (γ, p) and (γ, pn) reactions in ^{14}N have an energy dependence similar to that of the (γ, n) cross section, i.e. they are small below 15 Mev and large in the neighbourhood of 20 Mev. The cross sections of all other reactions are an order of magnitude smaller. The rise in the (γ, pn) cross section has also been established by the work of Ferguson *et al.* (1954) who measured the sum of the (γ, n) and (γ, pn) cross sections by observing the total yield of neutrons from ^{14}N. The (γ, pn) cross section, obtained by subtraction, resembles in shape the (γ, n) cross section obtained from measurements of the ^{13}N activity and is about three times as large. Thus the cross sections of all the principal reactions in ^{14}N reflect a pronounced increase

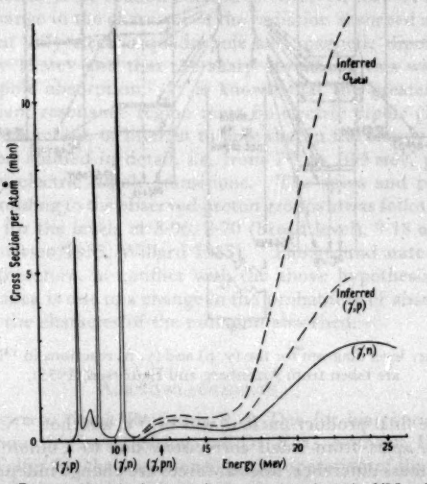

Figure 9. Measured and inferred photonuclear cross sections in ^{14}N. For fuller description see text (§ 5). For clarity the width of the narrow resonances below 10·5 Mev has been increased, but the integrated cross section remains correct.

N.B. The techniques used to obtain the cross sections above 10·5 Mev were incapable of resolving levels such as those observed below this energy.

in the nuclear photon absorption cross section in the vicinity of 20 MeV. This is shown in figure 9 which illustrates the characteristics of these cross sections but does not necessarily represent their exact values. This figure shows the (γ, p) cross section between 7·5 and 10·5 MeV together with the (γ, n) cross section as measured by the radioactive product technique (Horsley *et al.* 1952). Since it has been shown that, above 10·5 MeV, the (γ, p) cross section has the same general features as the (γ, n) cross section it is reasonable to suppose that it is a constant multiple of the (γ, n) cross section. Also, since the (γ, α) and the (γ, star) reactions have very small cross sections, the total cross section will be given by the sum of the (γ, n), (γ, p) and (γ, pn) cross sections. The (γ, pn) cross section was deduced in a manner similar to that used for the (γ, p) reaction except that, in accordance with the results discussed in § 5, the ratio of the (γ, pn) to the (γ, n) cross section was taken to increase somewhat with increasing photon energy.

From the relative yields of the (γ, p) and (γ, n) processes it is possible to draw some preliminary conclusions about the probability that the emission of a photoproton or photoneutron will leave the residual nucleus in its ground state. The number of events in which the emission of a neutron leaves the ^{13}N nucleus in its ground state is given by the (γ, n) yield deduced from the radioactive product measurements. This follows directly from the fact that the energy of the first excited state of ^{13}N is greater than the energy required for dissociation into ^{12}C + p (see figure 10) so that, in practically all cases in which ^{13}N is left in an

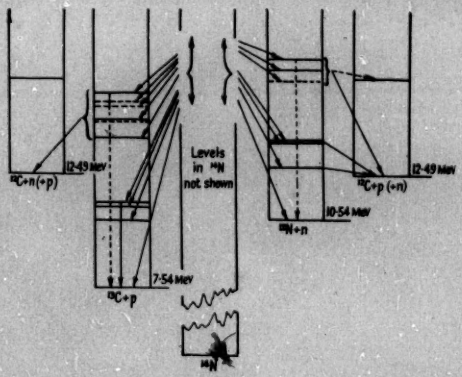

Figure 10. Energy level diagram for the (γ, p) and (γ, n) reactions in ^{14}N. Level positions are taken from Ajzenberg and Lauritsen (1955).

excited state, the final product nucleus will be ^{12}C and not ^{13}N. It is now well established that, apart from small corrections due to Coulomb forces and the proton–neutron mass difference, nuclear forces are change independent (Burcham 1955). Consequently it may be assumed that the probability for the emission of a neutron which leaves ^{13}N in a particular state differs only slightly from the probability for the emission of a proton which leaves ^{13}C in the corresponding state. Thus the number of (γ, n) events gives a good measure of the number

of events in which the emission of a proton leaves ^{13}C in its ground state. From figure 10 it can be seen that the number of (γ, p) events found in this experiment gives the number of events in which the proton leaves the ^{13}C nucleus in either the ground state or one of the first three excited states. From table 3 the number of (γ, n) events is just over half of the number of (γ, p) events and this, therefore, implies that the probability that the emission of a proton (or neutron) will leave ^{13}C (or ^{13}N) in its ground state is equal to the total probability that the nucleus will be left in any one of the first three excited states.

The range distribution of protons of energy up to 3 MeV (see figures 4 and 5) gives the (γ, p) cross section below 10·5 MeV with an energy resolution of approximately 50 kev. This is to be compared with the energy resolution of 1 MeV or more of other methods of measuring photonuclear cross sections. The results show that this cross section consists of a series of well-defined resonances and provide a convincing demonstration of level structure in photonuclear cross sections. The occurrence of such level structure has been suggested by Goward and Wilkins (1953), Titterton and Brinkley (1953) and Katz *et al.* (1954) from results obtained using methods of moderate energy resolution and, in the present case, would be anticipated from an application of the principle of detailed balancing to the measurements on the $^{13}C(p, \gamma)$ reaction. The present results completely confirm the predictions of the principle of detailed balancing and, therefore, show that the measurement of (p, γ) cross sections is a powerful method of studying, in detail, the characteristics of photonuclear cross sections within the range of proton energies available.

Blatt and Weisskopf (1952, p. 651) have suggested that an energy dependence of the total photonuclear cross section such as is observed for ^{14}N (see figure 9) might be due to a change in the character of the radiation absorbed above 15 MeV. They postulated that only electric quadrupole and magnetic dipole absorption were effective below 15 MeV and that the sharp rise above this was due to the onset of electric dipole absorption. It is known that the greater part of the absorption in the giant resonance region must be electric dipole (Levinger and Bethe 1950). It is, therefore, of interest to note that in the energy region where this process has been studied in detail, i.e. from 7·5 to 10·5 MeV, practically all the absorption is by electric dipole transitions. The spins and parities of the levels in ^{14}N corresponding to the observed proton groups are as follows: 1^-, 0^-, (2^-) and 2^- respectively for the levels at 8·06, 8·70 (broad level), 9·18 and 10·43 MeV (Ajzenberg and Lauritsen 1955, Willard 1955). The ground state of ^{14}N is 1^+. These results are, therefore, in conflict with the above hypothesis and suggest that the giant resonance is due to a change in the probability of absorption rather than to a change in the character of the radiation absorbed.

Acknowledgments

The authors desire to thank Professor P. I. Dee for his continued support and interest throughout this investigation, and Dr. K. G. McNeill, Dr. D. Greene and Mr. J. C. W. Telfer for their assistance in the operation of the synchrotron.

We also wish to acknowledge the award of a maintenance grant from the Department of Scientific and Industrial Research to one of us (D. R. O. M.), and of a scholarship from the Australian National University, and a grant from the Nuffield Foundation to another (I. F. W.).

References

AJZENBERG, F., and LAURITSEN, T., 1955, *Rev. Mod. Phys.*, **27**, 77.

BLATT, J. M., and WEISSKOPF, V. F., 1952, *Theoretical Nuclear Physics* (New York : John Wiley and Sons).

BURCHAM, W. E., 1955, *Progr. Nucl. Phys.*, **4**, 171.

FERGUSON, G. A., *et al.*, 1954, *Phys. Rev.*, **95**, 776.

GAERTTNER, E. R., and YEATER, M. L., 1950 a, *Phys. Rev.*, **77**, 570 (L); 1950 b, *Ibid.*, **77**, 714 (L),; 1950 c, *Ibid.*, **79**, 401 (L); 1951 a, *Ibid.*, **82**, 461 (L) ; 1951 b, *Ibid.*, **83**, 146.

GELL-MANN, M., and TELEGDI, V. L., 1953, *Phys., Rev.*, **91**, 169.

GOWARD, F. K., and WILKINS, J. J., 1953, *Proc. Roy. Soc.* A, **217**, 357.

HORSLEY, R. J., *et al.*, 1952, *Canad., J. Phys.*, **30**, 159.

KATZ, L., and CAMERON, A. G. W., 1951, *Canad. J. Phys.*, **29**, 518.

KATZ, L., *et al.*, 1954, *Phys. Rev.*, **95**, 464.

LEVINGER, J. S., and BETHE, H. A., 1950, *Phys. Rev.*, **78**, 115.

SEAGRAVE, J. D., 1952, *Phys. Rev.*, **85**, 197.

SPICER, B. M., 1953, *Aust. J. Phys.*, **6**, 391.

TITTERTON, E. W., and BRINKLEY, T. A., 1953, *Proc. Phys., Soc.*, A, **66**, 194.

WILLARD, H. B., *et al.*, 1955, *Bull. Amer. Phys. Soc.*, **30**, No. 1, p. 45, (also private communication from Dr. H. B. Willard).

WOODBURY, H. H., *et al.*, 1953, *Phys. Rev.*, **92**, 1199.

The $M_{IV,V}$ Spectra of ^{68}Er

By E. A. STEWARDSON and J. E. WILSON
Department of Physics, University College of Leicester

MS. received 29*th June* 1955 *and in final form* 30*th September* 1955

Abstract. The M_{IV} and M_V absorption spectra of Er_2O_3 have been studied in detail and a careful comparison made with the Mα, β emission lines. The M_V absorption spectrum possesses a number of well-defined absorption maxima. It is shown that the minima between these maxima coincide closely with components of the Mα multiplet and it is suggested that the main components of the emission line previously observed by Van der Tuuk and by Lindberg are not real but are produced by self-absorption in the target material. The line is probably accompanied by one or more real satellites however. The M_{IV} absorption spectrum is much weaker, but probably possesses a number of maxima also. The Mβ emission line probably possesses a satellite, but its form appears to be influenced by self-absorption.

§ 1. Introduction

The $M_{IV,V}$ emission spectrum of ^{68}Er was first observed by Stenström (1919) and later by Hjalmar (1923). In both cases the spectrum was described as consisting of two broad diffuse lines Mα and Mβ. In 1927 Van der Tuuk succeeded in resolving these lines into components (Mα into three main components and a satellite, Mβ into one main component and a satellite), while in 1931 Lindberg distinguished four main components and a satellite in Mα, but found only those already noticed by Van der Tuuk in Mβ. The β structure was also verified by Hirsch (1931) during an investigation of M satellite lines. Van der Tuuk and Lindberg further showed that the tendency to multiple components in Mα or Mβ or both was characteristic of the rare earth elements and the effect has usually been ascribed to coupling between the incomplete 4f sub-group and the (singly ionized) M_{IV} or M_V sub-groups (see for example Lindberg 1931, Borovski and Golovner 1953).

Lindberg also attempted an investigation of the corresponding absorption spectra. He failed to observe any M_{IV} absorption and in place of the normal M_V edge found two narrow absorption lines of wavelengths 8805, 8821 X.U. respectively. These lines he considered to 'correspond' to the emission lines $M\alpha_{III}$ and $M\alpha_{IV}$ ($\lambda\lambda$ 8810, 8832 X.U.) and suggested that where incomplete electron sub-groups are involved the radiation process may be reversible. In 1945 Rule suggested that Lindberg's result was due to his using too thin an absorbing screen and that heavier absorbing screens would probably show the usual edges. He based his argument on a study of the absorption in thin layers of Sm compounds. This conclusion was verified by Lee and Stewardson (1951) who found faint traces of apparently normal edges in an accidentally formed thick absorbing layer of Er_2O_3. Later Lee, Stewardson and Wilson (1952) suggested, from a study of the M_V absorption in Tm_2O_3 that Lindberg's two

absorption lines were really an absorption line accompanying an edge, the overall M_V absorption being similar to that found by Rule in Sm, and by Zandy (1952) in Pr, Nd, Sm and Eu where the normal edge is always accompanied by one or more absorption lines.

The experiments described in the present paper were carried out with a view to determining and measuring the absorption and emission structures in as great detail as possible and to making a close comparative study of the two spectra. As in all the earlier experiments described above, the erbium was used in the form of its oxide, Er_2O_3.

§ 2. Absorption Experiments

2.1. *Experimental Methods*

The bent crystal vacuum spectrograph described by Zandy (1952) was used both for the absorption and emission work. For some preliminary absorption experiments the absorption screens were prepared by spreading a paste of erbium oxide mixed with water on to thin Al foil, but later work was carried out entirely with oxide screens evaporated *in vacuo* on to Al foil as described by Zandy. The densities of the screens were estimated from the amount of oxide evaporated. The erbium was used sometimes in the form of spectrographically standardized oxide (*c.* 98% Er_2O_3) and sometimes as partially purified oxide mixtures of yttrium and erbium and of thulium and erbium. All were obtained from Messrs. Johnson, Matthey Ltd. A number of different screen densities ranging from 0·1 mg cm^{-2} to 1·0 mg cm^{-2} were employed and in a number of cases heavy equivalent densities were obtained by superimposing a number of layers of the erbium coated Al foil.

The absorption spectra were obtained by using the x-ray continuum from a platinum anti-cathode, the voltage being kept below twice the excitation potential for the $M_{IV,V}$ series for Er (*c.* 1500 v). Photographs were taken on x-ray film (Ilford Industrial C and G) as the short radius (*c.* 20 cm) made it difficult to bend glass plate to the focal circle. Microdensitometer recordings of the negatives however were made on photographic plates and all measurements were made on these.

Wavelength measurements of the more prominent features of the absorption spectra were made by using the first order spectra from mica and from gypsum and photographing alongside them high order K-spectra of Fe, Co, Zn, Mn. The wavelengths were determined relative to these K-lines, the wavelengths of the latter being taken from the wavelength tables of Cauchois and Hulubei (1947), and the grating constants for mica and gypsum from Siegbahn's *Spektroskopie der Röntgenstrahlen* (1931). All results are expressed in Siegbahn x.u. There is a tendency for our measurements made with gypsum to come out slightly higher than those made with mica but the difference of the means is somewhat less than the statistical error in either group and we give only the means of all determinations. The probable error is of the order of ± 1 to 2 x.u. This is purely statistical and does not take account of errors in grating constants or in wavelengths of standard lines.

The finer details of the absorption were observed by photographing with mica in the second order and the wavelengths measured using the previously determined points as standards. In a number of cases photographs were taken

with the absorbing screen (*a*) between x-ray source and crystal and (*b*) between crystal and photographic plate, and in some cases both types were recorded side by side on the same film. There was no detectable difference between the absorption photographs from the two types of exposure so that it is certain that all effects observed are genuine absorption effects unaffected by any possible fluorescent emission.

2.2. *Results*

Microdensitometer curves for four different thicknesses of absorber are shown in figures 1 and 2†. The thicknesses are: curve *a* (figure 1), 0·1 mg cm^{-2}; curve *b* (figure 1), 0·3 mg cm^{-2}; curve *c* (figure 2), 0·4 mg cm^{-2}; curve *d* (figure 2), 0·5 mg cm^{-2}. All are recordings of second order mica spectra. The most striking features are first the relatively large number of absorption maxima in the M_V spectrum and second the great weakness of the M_{IV} absorption as compared with M_V.

The M_V absorption maxima are indicated by the letters A...E on the microdensitometer curves. Of these maxima B is easily the most intense and A next in order of intensity. With a thin absorbing layer (curve *a*) these two are the only ones readily seen on the negative and they are evidently Lindberg's two absorption lines. This is confirmed by the wavelength measurements (see table 1).

Table 1. Absorption Spectra

		λ (x.u.)	ν/R			λ (x.u.)	ν/R
M_V	A	8819·(0)	103·3(3)	M_{IV}	a	8564·(9)	106·4(0)
	B_1	8808·(5)	103·4(5)		b	8561·(0)	106·4(4)
	B_2	8804·(2)	103·5(0)		A	8556·(0)	106·5(1)
	(B)	(8805·(2))	(103·4(9))		B	8547·(0)	106·6(2)
	C	8791·(4)	103·6(5)				
	D	8780·(1)	103·7(9)				
	E	8775·(4)	103·8(4)				

The weaker line C is imperceptible to the eye when the absorption produced by a thin layer is examined in the first order with a mica crystal. This accounts probably for its being overlooked by Lindberg. With thicker layers and using gypsum first order or mica second order it becomes very noticeable and two weaker absorption maxima at D and E come to light. With screens of medium density the absorption maximum B is resolved into two separate but close maxima B_1 and B_2. On some of the recordings of negatives taken with screens of medium density there is a slight hint of an inflection in the steeply falling curve on the long-wave side of A suggesting the possibility of an additional weak absorption maximum here also, but it has not been possible to measure its wavelength nor indeed to confirm that it really does exist.

The weak character of the M_{IV} absorption makes observation of its structure very difficult, and apart from the main maximum A the only other certain feature appears to be a second weaker maximum B revealing itself best as the rather sudden change in gradient shown in curve *c* obtained with the densest screens. As well as this two slight kinks a and b on the long-wave side of A have appeared sufficiently frequently to make it likely that they are real. The wavelengths and energies of all the points indicated on the microdensitometer curves are

† For figures see Plates at end of issue.

given in table 1. When the screen density is increased excessively the details, particularly in M_V, becomes submerged in the general background of absorption and there is every indication that ultimately the absorptions will tend to the form of the simple edges described by Lee and Stewardson.

§ 3. Emission Experiments

3.1. *Experimental Methods*

For production of the emission spectra a copper anti-cathode was used. In most cases this was coated mechanically with the powdered erbium oxide or with an erbium oxide paste. In a few cases the oxide was evaporated *in vacuo* on to the target in order to get a very thin uniform coating. From L data it appears that the excitation potential for the M_{IV} series for erbium is rather less than 1500 volts and photographs were taken with potentials ranging from this value up to several thousand volts.

As in the absorption experiments the more prominent features were measured by comparison with high order K lines of Fe, Co, Mn, Zn and with the Al $K\alpha_{1,2}$ line (first order) using a mica or gypsum crystal in the first order. Finer detail was studied with a mica crystal in the second order using the previously determined wavelengths as standards. All measurements were made from microdensitometer curves recorded on glass photographic plates.

3.2. *Results*

The general features of the emission lines $M\alpha$ and $M\beta$ noticed by Van der Tuuk and by Lindberg were readily confirmed. A typical microdensitometer curve obtained with an excitation energy of 3 kv is shown in figure 3. Wavelengths of the various components are given in table 2 which also includes the determinations of Van der Tuuk and Lindberg for comparison. The general agreement

Table 2. Emission Spectra

Line	Van der Tuuk	Lindberg	E.A.S. and J.E.W.
M α_{IV}	8835	8832	8831·(0)
α'_{III}	—	—	8824·(8)
α_{III}	8817	8810	8813·(2)
α_{II}	—	8794	8794·(7)
α_I	8781	8783	8785·(6)
α'	8751	8763	8774·(8)
α''	—	—	8771·(4)
M β	8571	8576	8571·(6)
β'	8540	8554†	8554·(0)
β''	—	—	*c.* 8520

† Hirsch gives $\beta' = 8548{\cdot}4$.

is quite good, particularly when it is borne in mind that while our measurements are made from microdensitometer recordings the earlier experimenters measured the rather diffuse lines directly on the negatives. There is however a rather large discrepancy in the wavelengths of the 'satellite' line α' and we can only account for this by assuming that visual observations of this line (which appears on the

negative as a rather long diffuse 'tail') tends to place its centre of gravity too much to the short wavelengths. It is noteworthy that Lindberg and Van der Tuuk differ fairly considerably in their estimates of this line. In identifying and labelling the lines we have used Lindberg's notation. This is an arbitrary enumeration in order from short to long wavelengths and is not intended to convey information about the relative intensities. In addition to the components given by Lindberg and Van der Tuuk we find a weak line α'_{III} between α_{III} and α_{IV}. This line is easily visible on negatives of the second order spectra taken with mica although, being very narrow, it often shows itself only as a slight inflection on the short-wave side of α_{IV} on the microdensitometer curves. The line α' also has a short-wave companion α'', and an additional line β'' seems to exist on the short-wave side of β'.

A feature of great interest is the way the profiles of the lines vary with the potential used to excite them. With low potentials the two lines Mα and Mβ are very diffuse and it is very difficult to distinguish the components present in each. As the potential is increased both lines broaden on the short wave side and develop a considerable 'skirt' on this side, the long-wave limit however remaining more or less fixed. In addition to this the components of each become much more distinct as the potential increases, while there is a considerable change in the relative intensities of the component of Mα. At low potentials (only slightly in excess of the critical excitation potential) the most prominent component is $M\alpha_{III}$, while at higher potentials the group composed of $\alpha_{II}\alpha_I\alpha'\alpha''$ is the most intense. These components also have their peaks displaced to shorter wavelengths as the potential increases, whereas $\alpha_{IV}\alpha'_{III}$ and α_{III} remain fixed in wavelength. All these features are noticeable in the two curves reproduced in figure 4. These are microdensitometer curves of two emission spectra taken side by side on the same film, the lower one being taken at 1·5 kv, the upper at 3·0 kv. Figure 5 shows an extreme case. Here the potential has been increased to 6 kv. The great increase of the group $\alpha_{II}\alpha_I\alpha'$ relative to the longer wave components is very apparent. The slight indication of additional short-wave components may be real or possibly due to high order K and L lines from impurities produced by the excessively high voltage. The possible significance of this variation is discussed in the next section.

§ 4. Comparison of Emission and Absorption Spectra

It is very striking that the wavelength ranges of the Mα and Mβ multiplets cover the wavelength ranges of the M_{IV} and M_V absorption regions respectively, instead of lying on the long-wave side of the absorption as is the case with elements possessing completed 4f electron groups ($Z>71$). In order to study more closely the relationship between absorption and emission a number of photographs of the absorption and emission spectra were taken side by side on the same negative. This was accomplished by photographing the continuous spectrum from a platinum target through an erbium oxide absorbing screen on the upper half of the photographic film, then removing the erbium screen, rotating the anode to bring a copper face coated with erbium into the electron beam and by movement of a shutter exposing the lower half of the film. All the operations were carried out without breaking the vacuum. An example of such a comparison between M_V absorption and Mα emission is shown in figure 6. The most surprising result is the apparently exact identity of the principal components of the Mα

multiplet with the dark lines separating the M_V absorption maxima. A similar result is found with M_{IV} and $M\beta$ where the absorption maximum seems to correspond to the emission minimum between $M\beta$ and $M\beta'$. Microdensitometer curves of the two photographs are shown (in exact register) in figure 7. It will be seen that the minima between the emission maxima in most cases correspond closely to the absorption maxima. The correspondence is not complete however as the emission minimum between α_{IV} and α'_{III} is not reproduced in the absorption (unless the suspected absorption maximum on the long-wave side of M_VA mentioned in §2.1 proves to be real) and the maximum M_VB_1 does not appear to be reproduced in the emission. Apart from these it is possible to draw up the following close correspondences:

Emission		Absorption
min. between α'_{III}	and α_{III} =	M_VA
,, ,, α_{III}	,, α_{II} =	$M_VB(B_2)$
,, ,, α_{II}	,, α_{I} =	M_VC
,, ,, α_{I}	,, α' =	M_VD
,, ,, α'	,, α'' =	M_VE

It seems impossible to avoid the conclusion that the 'components' of both $M\alpha$ and $M\beta$ as observed hitherto are produced by self-absorption in the target material, the true emission being a broad single line accompanied probably by true satellites as evidenced by the growth of the high frequency skirt when the excitation energy is increased. The conditions under which the emission lines are produced and observed would tend to favour such self-absorption as the face of the target is only a few degrees removed from being normal to the electron beam while the direction of observation is perpendicular to the electron beam and therefore nearly parallel to the target face, so that x-rays generated below the surface of the target material have a relatively long path within the material before emerging and travelling to the crystal.

Such self-absorption would help account for the variation of the emission structure with voltage (described in §2.2 above). For a simple extrapolation of the results of Williams (1931) on the ranges of low energy β particles in oxygen or of those of Schonland (1925) on the transmission of β particles through foils shows that the range of 2 kev electrons in matter is of the order of 10^{-5} to 10^{-4} g cm^{-2}. This is of the order of magnitude of the thickness of the erbium targets and it follows that variation of the electron energy over the range 1·5–3·5 kev can make an appreciable change in the depth in the target material at which the characteristic x-rays are produced. High energy tends to increase this depth and enhance the self-absorption thus resulting in greater definition of the apparent components. The shift in wavelength of the components α_{II} to α'' is presumably due to competition between increased self-absorption and the growth of the high-frequency satellite skirt, the latter tending to 'pull' the peaks of the curve to the shorter wavelengths. The effect probably takes place also in $M\beta$ but the much weaker nature of the M_{IV} absorption renders it less noticeable. An additional point of interest is that on many of our microdensitometer curves it is possible to distinguish a slight but rather sudden decrease in the gradient on the long wave side of the $M\alpha$ line. This seems to correspond fairly well with the onset of the M_V absorption.

§ 5. Discussion

5.1. *The Emission Structure*

From the results described in the previous section it seems reasonably certain that the structures of Mα and Mβ in erbium found by Van der Tuuk and by Lindberg and assumed to exist by Borovski and Golovner in their theory of the origins of the multiplets are due mainly if not entirely to self-absorption. It is possible that the lines *do* possess a fine structure but this must certainly be different from that hitherto observed and it has not been detected in the experiments described here. Indeed the only hope of detecting such structure would be to work under conditions where the self-absorption is reduced to a minimum, as for example by observation normal to a very thin target. Such a type of experiment is now under consideration in this laboratory.

The question naturally arises as to whether the structures observed in the M lines of other rare earth elements arise through the same process or whether it is peculiar to erbium. This can only be settled by experiment but from some preliminary experiments carried out here it seems very likely that it does occur in the case of ^{69}Tm and ^{67}Ho and probably also in ^{66}Dy and ^{64}Gd.

5.2. *The Emission and Absorption Transitions*

It is hoped to discuss the question of the origin of the absorption and emission lines in greater detail later when further experimental results (particularly for other members of the rare earths series) have been obtained. A brief general discussion only is attempted here.

The general nature of the absorption found for Er is similar to that found by Zandy for Nd, Pr and Eu and by Zandy and by Rule for Sm, but more complex, and it seems likely that in Er, as in these elements, the absorption structures arise, in part at least, through the transfer of an electron from the appropriate M group into vacancies available in the incomplete 4f group. Zandy appeals to the selection rules and the change in state of the single electron transferred to account for the appearance of line absorption in the M_{IV} and M_V absorption bands of Pr, Nd and Sm and in the M_V band of Eu and their absence in the M_{IV} band of the last named. Such a treatment of the matter would exclude the possibility of line absorption in the M_{IV} band of Er, while the results described in the present paper make it seem likely (although admittedly not certain) that such line absorption in the M_{IV} band of Er does occur. However Zandy's treatment, besides implicitly assuming strict j–j coupling between the 4f electrons, does not take account of the fact that the final state after absorption is one made up of two incomplete groups which may interact to give a configuration of the type $3d^9 4f^{x+1}$ for a rare earth ion possessing normally x 4f electrons. When this is taken into account it seems that 4f transitions may be associated with the M_{IV} band even for an element as far up the series as Er.

A point of greater immediate interest however is the possibility that the Mα, β emission lines of the rare earth elements may in actuality turn out to be broad single lines instead of the complex multiplets they have hitherto been thought to be. It has always been a matter for surprise that there should be such a profound change in the M line structure in passing from atoms of $Z>71$ to atoms of $Z<71$ and it seemed possible to account for the assumed structures only by assuming coupling between the M_{IV} or M_V group and the $4f^x$ group

to make possible transitions in which the final state of the atom is any of a number of possible $4f^{x-1}$ configurations (cf. Borovski and Golovner 1953). The present work makes it seem probable that the normal emission lines arise through transfer of a 4f electron into the M_{IV} and M_V vacancy, the atom being left in its lowest accessible $4f^{x-1}$ state, and the diffuseness of the line arising through broadening of the *initial* level due to coupling with the ionized M_{IV} or M_V group. The fine structure this coupling could give rise to would most likely be beyond the resolving power attainable with the usual x-ray techniques.

5.3. *The Energy Levels*

If we assume that each absorption maximum represents a transition to a definite energy level then by making use of the available observations of $L\alpha_1$, $L\alpha_2$ and the L_{III} edge we can compute the values of these energy levels relative to the lowest end level in the L_{III} absorption transition—the conventional zero energy level. The most recent L data on erbium is that of Sakellaridis (1954), and using his values for $L\alpha_{1,2}$ and the L_{III} edge the energies given in table 3 have been derived. The values for the M absorption levels, being the differences

Table 3. Energy Levels

Level		ν/R	ev
M_{IV}		−106·8(5)	−1452·(1)
M_V		−103·6(8)	−1409·(0)
End level of M_V	A transition	−0·3(5)	−4·(7)
,, ,, ,,	B_1 ,,	−0·2(3)	−3·(1)
,, ,, ,,	B_2 ,,	−0·1(8)	−2·(4)
,, ,, ,,	C ,,	−0·0(3)	−0·(4)
,, ,, ,,	D ,,	+0·0(9)	+1·(2)
,, ,, ,,	E ,,	+0·1(6)	+2·(1)
End level of M_{IV}	a transition	−0·4(5)	−6·(1)
,, ,, ,,	b ,,	−0·4(1)	−5·(6)
,, ,, ,,	A ,,	−0·3(4)	−4·(6)
,, ,, ,,	B ,,	−0·2(3)	−3·(1)

between two very nearly equal quantities, are subject to considerable uncertainty, and those for a and b are particularly doubtful. Nevertheless it does seem likely that M_VA and M_{IV}A involve transitions to the same end level as also do M_VB and M_{IV}B. It is interesting to note that the D and E levels appear to lie higher than the end level of the L_{III} transition, the latter of the two by an amount greater than one would expect to be due to experimental error. This scheme of levels is of course very tentative as slight adjustments in the values of the M_{IV} and M_V levels can bring about considerable changes in the scheme—indeed if the M_{IV} level is computed from Sakellaridis's measurements of $L\beta_1$ and the L_{II} edge or from his mean value for M_{IV} it becomes less certain that the end levels of M_VA and M_{IV}A are identical, and similarly for M_VB and M_{IV}B.

The initial energy levels in the transitions causing the $M\alpha, \beta$ emissions are still more uncertain as the self-absorption prevents measurement of the true wavelengths of the lines. From the lower curve in figure 4, where we assume self-absorption to be much reduced, the α line appears tolerably well distributed about α_{III}, the ν/R value for which is 103·40. That for Mβ in the same curve is

106·31. The difference between these is 2·91 which is appreciably less than the difference of 3·16 between $L\alpha_1$ and $L\alpha_2$ as measured by Sakellaridis. This suggests that the true peak of $M\alpha$ lies on the long-wave side of $M\alpha_{III}$ or that that of $M\beta$ lies on the short-wave side of the $M\beta$ peak found here. It is hoped to make this matter the subject of further investigation.

ACKNOWLEDGMENT

We wish to thank the Research Board of the University College of Leicester for a grant towards the cost of rare earth material.

REFERENCES

BOROVSKI, J. B., and GOLOVNER, T. M., 1953, *Dokl. Akad. Nauk. S.S.S.R.*, **88,** 233.
CAUCHOIS, Y., and HULUBEI, H., 1947, *Longueurs d'Onde des Emissions X et des Discontinuités d'Absorption X* (Paris : Hermann & Cie).
HIRSCH, F. R., JR., 1931, *Phys. Rev.*, **38,** 914.
HJALMAR, E., 1923, *Z. Phys.*, **15,** 65.
LEE, P. A., and STEWARDSON, E. A., 1951, *Proc. Phys. Soc.* A, **64,** 318.
LEE, P. A., STEWARDSON, E. A., and WILSON, J. E., 1952, *Proc. Phys. Soc.* A, **65,** 668.
LINDBERG, E., 1931, *Nova Acta Soc. Sci. Upsal. Ser. IV*, **7,** No. 7.
RULE, K. C., 1945, *Phys. Rev.*, **68,** 246.
SAKELLARIDIS, P., 1954, *C.R. Acad. Sci., Paris*, **238,** 2296.
SCHONLAND, B. F. J., 1925, *Proc. Roy. Soc.* A, **108,** 187.
SIEGBAHN, M., 1931, *Spektroskopie der Röntgenstrahlen* (Berlin : Springer).
STENSTRÖM, W., 1919, *Ann. Phys., Lpz.*, **57,** 347.
VAN DER TUUK, J. H., 1927, *Z. Phys.*, **44,** 737.
WILLIAMS, E. J., 1931, *Proc. Roy. Soc.* A, **130,** 310.
ZANDY, H. F., 1952, *Proc. Phys. Soc.* A, **65,** 1015.

Search for a Sidereal Variation of the Cosmic Ray Intensity at High Energies

By J. K. CRAWSHAW† and H. ELLIOT‡
Manchester University

Communicated by P. M. S. Blackett; MS. received 30th August 1955 *and in amended form 6th October* 1955

Abstract. Extensive air showers with energies of about 10^{16} ev and 10^{17} ev have been recorded at geographic latitude 53° N by means of counter sets separated by about 150 m and 300 m. Harmonic analysis of the shower frequencies has revealed no evidence for a sidereal daily variation with amplitude exceeding the statistical uncertainties, which are 2·5% and 6% respectively. No evidence has been found for a solar daily variation with amplitude exceeding 2·5% for 10^{16} ev showers. A solar daily variation has been found for 10^{17} ev showers with an amplitude of 19% and a time of maximum at about 1300 h. The interpretation of this result is briefly discussed.

§ 1. Introduction

It is known that the low-energy cosmic radiation is very nearly isotropic, there being no variation in intensity over the sidereal day as great as 0·1%. This is a remarkable result when considered in relation to the location of the solar system, which is very asymmetrically placed relative to the galactic centre, and this high degree of isotropy is usually ascribed to the existence of magnetic fields in the galaxy which scatter the primary radiation and trap it within the galaxy. Comparatively small fields are sufficient for this purpose at low energies, but the field strength necessary to produce isotropy increases as the energy of the particles under consideration increases. It might be expected, therefore, that if particles of sufficiently high energy could be recorded, a point should be reached where the magnetic fields can no longer produce complete isotropy. It is important, therefore, to look for variations in intensity with sidereal time at high energies. The present paper gives the results of such measurements on large air showers initiated by primary particles in the energy range 10^{16} to 10^{17} ev. The results of some similar measurements have recently been given by Cranshaw and Galbraith (1954).

§ 2. Experimental Arrangement

Extensive air showers were recorded during the period October 1951 to October 1953 by means of coincidence pulses between four counter sets placed at the corners of a quadrilateral of sides roughly equal to 150 m and 300 m (figure 1). Each counter set comprised three similar trays of Geiger–Müller counters placed in a horizontal plane and connected in three-fold coincidence. The sensitive area of each tray was 1600 cm² and the three-fold coincidence rate from each counter set was about one per minute. The coincidence pulses from the three distant counter sets were passed along private telephone lines to a mixing unit adjacent to the fourth counter set, where the pulse lengths were equalized.

† Now with Imperial Chemical Industries Ltd.
‡ Now at Imperial College of Science and Technology, London.

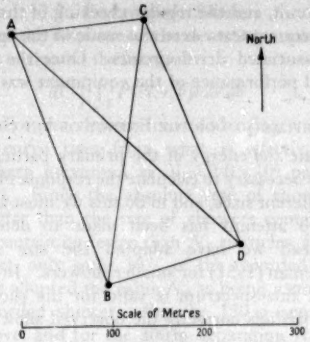

Figure 1.

The mixing unit recorded coincidences between each of the six different pairs of three-fold coincidence pulses; these six-fold coincidence pulses were recorded by electromechanical registers which, together with a 24-hour and a 7-day clock, were photographed each time any register was operated. Showers of nine-fold multiplicity were recorded by any one out of four possible combinations of three registers counting together, and were identified by subsequent inspection of the film record. Showers of twelve-fold multiplicity tripped all six registers.

Three of the counter sets were housed beneath roof windows on the top-most floors of various buildings, and the fourth was placed in a temperature-controlled hut made of a light alloy. There was about $3\,g\,cm^{-2}$ of material between the atmosphere and the sensitive volumes of the counters.

Measurements of the single coincidence counting rates between separated trays showed the resolving time of the mixing unit to be about $130\,\mu sec$. The casual coincidence rate between a pair of counter sets was therefore about 0·006 per day.

The low coincidence rates and the use of telephone lines in the equipment made it necessary to ascertain that the fraction of spurious counts caused by electromagnetic pick-up by the lines and the electronic circuits was negligible. This was done by reducing the voltages of the counters in one tray of a distant counter set to 1 kv, well below the Geiger threshold. In this state, a particular combination of registers was prevented from recording genuine showers. During a total period in which 140 counts would normally have been observed, none in fact was. If, say, 5% of normal counts were spurious, the probability of observing none during this time would be, for a Poisson distribution, $\exp(-7)$, or about 10^{-3}. Thus it is highly probable that at least one such count would have been observed, and hence fewer than 5% of the counts can have been spurious. The test was repeated at intervals for each distant counter set, with similar results. These tests also demonstrated the stability of the recording circuits and the coincidence circuits in each counter set.

Routine tests were carried out in order to ensure that the efficiency of the equipment remained constant. These included daily observation of the coincidence pulses appearing at the mixing unit, the regular testing of each counter

with its quenching circuit, and the regular checking of the coincidence rate from each counter set. Frequent tests were also made of the operation of the message registers and their associated drive circuits. Once the initial faults had been overcome, the general performance of the equipment was very satisfactory.

§ 3. Estimation of the Energy of the Showers

In order to estimate the energy of the primary particles responsible for the showers recorded, it is necessary to calculate the response of the detecting arrangement to showers of different sizes, and to do this we must know the size spectrum for the showers. No attempt has been made to determine this spectrum experimentally; instead we have adopted the size spectrum determined experimentally by Jakeman (1951) for smaller showers. In the next section, § 3.1, it will be shown that this spectrum is valid for the showers detected by our arrangement since it predicts correctly the observed shower rates.

3.1. *Calculated Shower Rates*

Take the origin of plane polar coordinates at the mid-point of a pair of counter units separated by a distance $2a$. For our experimental arrangement the probability of recording a shower containing N particles, the axis of which falls vertically at the point (r, θ) is

$$P(N, r, \theta) = \{1 - \exp[-NAf(r_1)]\}^3 \{1 - \exp[-NAf(r_2)]\}^3 \quad \ldots\ldots (1)$$

where $r_1^2 = r^2 + a^2 + 2ar\cos\theta$; $r_2^2 = r^2 + a^2 - 2ar\cos\theta$. A is the sensitive area of the counter trays and $f(r)$ is the lateral structure function of the showers defined in such a way that $Nf(r)$ is the particle density at the radial distance r from the shower axis.

If we now introduce the size spectrum given by Jakeman

$$dC = 10^5 N^{-2\cdot5} dN \mathrm{m}^{-2}\mathrm{h}^{-1} \quad \ldots\ldots (2)$$

where dC is the number of showers containing between N and $N + dN$ particles, the expected counting rate is given by

$$R(r, \theta, N) = \int\int\int P(N, r, \theta) r\, dr\, d\theta\, dC. \quad \ldots\ldots (3)$$

This integral has been evaluated numerically using the analytical form of the Molière structure function obtained by Bethe (Williams 1948)

$$f(r) = [(1 + 4r)/r][\exp(-4r^{2/3})]$$

where r is measured in units of the characteristic spread, r_0; in the notation of Rossi and Greisen (1941), $r_0 = X_0 E_s/\epsilon$ which, with $E_s = 21$ Mev and $\epsilon = 86$ Mev, is equal to 74 m at sea level.

The results are compared with the observed rates in table 1.

Table 1. Calculated and Observed Shower Rates

Counter separation (m)	150	300
Calculated rate (per day)	6·0	0·8
Observed rate (per day)	$6{\cdot}31 \pm 0{\cdot}17$	$0{\cdot}77 \pm 0{\cdot}05$

Errors are standard deviations calculated from total number of showers.

The close agreement between the observed and expected rates shows that the size spectrum given in (2) is valid for the showers recorded by the present arrangement and justifies its use in the next section, § 3.2, where the shower energies are estimated.

3.2. *Energy of the Showers*

In order to calculate the response of the detecting arrangement as a function of shower size we have evaluated the integral

$$dC \int_r \int_\theta P(N, r, \theta) r \, dr \, d\theta$$

as a function of N. For the showers recorded using a counter separation of 150 m this response curve rises from what is effectively zero response at $N_{\min} = 2 \times 10^5$ to a sharp maximum at $N_P = 2{\cdot}0 \times 10^6$ particles and then falls asymptotically to zero. Since the absolute rate of showers containing $N_{\min}$ particles is much greater than the rate of showers containing N_P particles, it follows that showers containing fewer than N_P particles are detected with very low efficiency. In fact, only some 10% of the recorded showers are of these sizes, and we therefore adopted the value N_P as being a reasonable figure for the minimum size of recorded shower. For the 150 m separation $N_P = 2{\cdot}0 \times 10^6$ particles as stated above, and for the 300 m separation $N_P = 1{\cdot}7 \times 10^7$ particles. Using these values for the sizes of the showers we can now estimate the energies of the primary particles which produce them.

It is generally believed that most of the electron photon component of extensive air showers is produced as a result of the nuclear interactions of cosmic radiation throughout the atmosphere. At energies up to about 10^{12} ev the soft component arises mainly from the photons produced by the decay of the π^0-meson; at much higher energies the processes of production are not yet known. In the absence of a detailed theory of air showers we shall assume that all the soft component originates in a small number of π^0-mesons produced in an energetic nuclear interaction near the top of the atmosphere and estimate this number using the theory of Fermi (1950). We then apply cascade theory to calculate the energy of the showers.

As shown above the minimum size of shower recorded using a counter separation of 150 m is one containing $2{\cdot}0 \times 10^6$ particles which will be assumed to be electrons of average energy equal to the critical energy ϵ, where $\epsilon = 86$ Mev. In order to get a rough idea of the shower energy we first suppose that these electrons have been produced by a single photon near the top of the atmosphere. On this basis cascade theory (neglecting ionization loss) requires the parent photon to have an energy of about 10^{16} ev. Now the Fermi theory predicts that about 15 π^0-mesons will be produced in a nuclear interaction by a proton of this energy, and using this multiplicity we find the energy of the soft component to be about 2×10^{16} ev, a figure which is not sensitive to the assumed multiplicity. Since the energy of the soft component is probably a large fraction of the total shower energy, we assume that the energy in the soft component is equal to the energy of the primary event, and conclude that the minimum energy of the primary particle responsible for the showers recorded by counters separated by 150 m is about 2×10^{16} ev.

For the counter separation of 300 m $N_P = 1{\cdot}7 \times 10^7$ particles; assuming a multiplicity of 20 π^0-mesons we obtain in this case a minimum primary energy of 10^{17} ev.

§ 4. Time Variations of the Showers

4.1. *Grouping the Showers*

It is apparent from figure 1 that the showers can conveniently be divided into two groups: those recorded by a pair of counter sets separated by distances

of about 150 m and those recorded by a pair of counter sets at separations of about 300 m.

The first group consists of all showers in which a coincidence count was observed between the counter sets A and C (figure 1), irrespective of whether either or both the sets at B and D were discharged. Time lost due to technical faults has been taken into account on the basis of faults which made this channel only unserviceable. A similar set of data has been formed for the showers recorded by the pair of counter sets B and D. The data from these two sets have been added together, with the exception of the showers which fired all four counter sets; these have been included once only. The results then refer to showers recorded by a pair of counter sets at separations of about 150 m.

The second group has been formed in a similar way and refers to showers recorded by a pair of counter sets at separations of 300 m. In neither group has any shower been included more than once. Showers of at least nine-fold multiplicity have not been analysed separately, since their number was too few and the increment in energy too small for useful results to be obtained.

4.2. *The Solar Daily Variation*

The bi-hourly values of the shower rates in solar time for the two groups described above are given in table 2. In table 3 are given the calculated amplitudes

Table 2. Bi-hourly Shower Rates in Solar Time

(*a*) Counter separation 150 m

Time	00	02	04	06	08	10	12	14	16	18	20	22
Rate	0·437	0·448	0·423	0·503	0·470	0·441	0·476	0·427	0·474	0·451	0·509	0·456
S.D.	0·026	0·026	0·026	0·028	0·028	0·028	0·028	0·025	0·028	0·027	0·028	0·027

(*b*) Counter separation 300 m

Time	00	02	04	06	08	10	12	14	16	18	20	22
Rate	0·044	0·041	0·033	0·048	0·051	0·054	0·052	0·058	0·064	0·043	0·042	0·042
S.D.	0·006	0·006	0·005	0·006	0·006	0·006	0·007	0·007	0·007	0·006	0·006	0·006

S.D. = Standard deviation.

of the first and second harmonics derived from harmonic analysis of the data, expressed as a percentage of the mean counting rate, for both groups of showers.

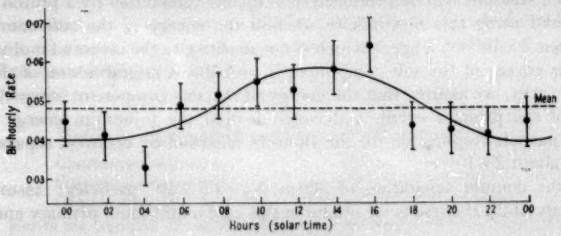

Figure 2.

The results in table 3 show no significant variation for showers recorded at separations of 150 m. For the 300 m separation, however, the amplitude of the first harmonic (19·3%) is statistically significant. The bi-hourly rates for these

Table 3. Amplitudes of Solar Daily Variation

Energy (ev)	$>2\times10^{16}$	$>1\times10^{17}$
Counter separation (metres)	150	300
1st harmonic amplitude (%)	1·0	19·3
2nd harmonic amplitude (%)	4·5	3·4
Number of showers	3414	711

showers are shown in figure 2, where the curve is the sum of the first and second harmonics of the Fourier series fitted to the points. In order to investigate the statistical significance of this variation the showers have been divided into eight independent groups of seventy-two showers. The 24-hour wave of best fit has been calculated for each group and these are shown plotted on a harmonic dial in figure 3 together with their centroid C. This diagram can be used to test

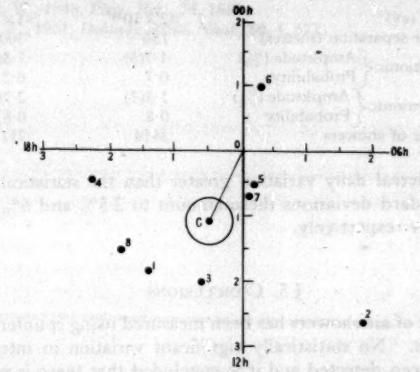

Figure 3.

the significance of the amplitude of the calculated solar daily variation given in table 3. The probability that the amplitude $R=\mathrm{OC}$ be exceeded, if it is due to random fluctuations, is given by (Chapman and Bartels 1940)

$$W(>R)=\exp\left[-R^2/4m^2\right].$$

In this equation m, the standard deviation of the average of the eight vectors CP_β, is given for this case by $2m=E_2/\sqrt{8}$ where E_2 is the square root of the average of the squared vectors CP_β. For the points in figure 3, $R=\mathrm{OC}=1{\cdot}194$ and $E_2=2{\cdot}715$, whence $W(>1{\cdot}194)=0{\cdot}01$. That is to say, there is only a 1% chance that the observed variation is the result of a statistical fluctuation. A variance ratio test (Kendall 1946) leads to the same result. It appears, therefore, that a solar daily variation may exist for extensive air showers of energies of about 10^{17} ev.

4.3. *The Sidereal Daily Variation*

The bi-hourly rates in sidereal time are given in table 4 for both groups of showers. Harmonic analysis of these data gives the amplitudes shown in table 5, which also shows the probabilities that the calculated amplitudes arise as a result of random fluctuations in the measurements. None of the calculated amplitudes in table 5 is significant and we conclude therefore that the present data give no

Table 4. Bi-hourly Shower Rates in Sidereal Time

(*a*) Counter separation 150 m

Time	00	02	04	06	08	10	12	14	16	18	20	22
Rate	0·493	0·458	0·487	0·425	0·486	0·455	0·414	0·489	0·443	0·481	0·446	0·448
S.D.	0·027	0·027	0·028	0·026	0·028	0·027	0·026	0·028	0·027	0·028	0·027	0·027

(*b*) Counter separation 300 m

Time	00	02	04	06	08	10	12	14	16	18	20	22
Rate	0·043	0·038	0·047	0·051	0·046	0·049	0·054	0·053	0·043	0·053	0·043	0·052
S.D.	0·006	0·006	0·006	0·006	0·006	0·006	0·007	0·007	0·006	0·006	0·007	0·006

S.D. = standard deviation.

Table 5. Amplitudes of Sidereal Daily Variation

Energy (ev)		$>2\times10^{16}$	$>1\times10^{17}$
Counter separation (metres)		150	300
1st harmonic	Amplitude (%)	1·7(5)	7·5(4)
	Probability	0·7	0·2
2nd harmonic	Amplitude (%)	1·3(3)	2·7(3)
	Probability	0·8	0·8
Number of showers		3414	711

evidence for a sidereal daily variation greater than the statistical uncertainties. Expressed as standard deviations these amount to 2·5% and 6% at energies of 2×10^{16} and 10^{17} ev respectively.

§ 5. Conclusions

The frequency of air showers has been measured using counter sets separated by 150 and 300 m. No statistically significant variation in intensity over the sidereal day has been detected and it is concluded that there is no evidence for any anisotropy of the primary radiation greater than 2·5% at energies of 2×10^{16} ev and 6% at energies of 10^{17} ev.

There is no significant variation in intensity over the solar day for showers of 2×10^{16} ev, but there appears to be a variation at 10^{17} ev with an amplitude of 19%. This variation could be a statistical fluctuation but it seems more likely that it is either a genuine effect or an undetected instrumental defect although none of the tests described earlier in the paper revealed the presence of spurious counts which could account for the variation.

There is no *a priori* reason for expecting a solar variation at these energies since it is highly improbable that daily atmospheric pressure or temperature changes could be responsible for so large a variation in shower frequency. The terrestrial atmosphere apart, only two other mechanisms have been suggested whereby the intensity of primary cosmic ray particles of this energy could conceivably be influenced by the Sun. There is the possibility of radiation by the primary particles in the solar magnetic field (Pomeranchuk 1940, Blackett 1947) or of the photo-disintegration by solar photons of heavy nuclei of high energy (Zatsepin 1951). However, neither of these processes would appear to be capable of accounting for so large a variation and in the absence of independent confirmation we must conclude that the reality of the solar daily variation is in doubt.

ACKNOWLEDGMENTS

We are indebted to Professor P. M. S. Blackett for providing the facilities for this work and for his constant interest and encouragement. We also wish to thank Dr. D. Jakeman for the benefit of many helpful discussions.

REFERENCES

BLACKETT, P. M. S., 1947, *Phys. Soc. Cambridge Conference Report*, p. 79.
CHAPMAN, S., and BARTELS, J., 1940, *Geomagnetism* (Oxford : University Press).
CRANSHAW, T. E., and GALBRAITH, W., 1954, *Phil. Mag.*, **45**, 1109.
FERMI, E., 1950, *Progr. Theor. Phys., Osaka*, **5**, 570.
JAKEMAN, D., 1951, *Ph.D. Thesis*, University of Manchester.
KENDALL, M. G., 1946, *Advanced Theory of Statistics* Vol. 2 (London : Griffin).
POMERANCHUK, I., 1940, *J. Phys. U.S.S.R.*, **2**, 65.
ROSSI, B., and GREISEN, K., 1941, *Rev. Mod. Phys.*, **13**, 240
WILLIAMS, R. W., 1948, *Phys. Rev.*, **74**, 1689.
ZATSEPIN, G. T., 1951, *Doklady Adad. Nauk*, **80**, 4, 577.

Observations of the Nuclear Interactions of a 315 MeV Bremsstrahlung γ-ray Beam

By E. P. GEORGE

The F.B.S. Falkiner Nuclear Research and Adolph Basser Computing Laboratories, School of Physics,† University of Sydney

Communicated by H. Messel; MS. received 6th June 1955 and in amended form 27th September 1955

Abstract. The γ-ray beam was incident normally on Ilford G5 nuclear research emulsions, and events occurring in the emulsion were studied. The events have been analysed, and particular attention paid to interactions in which charged mesons leave tracks of length greater than 1·5 mm at right angles to the γ-ray beam. About 50% of the observed photo-mesons are not accompanied by visible nuclear disintegration 'stars'. The energy spectrum of the emulsion photo-mesons has been measured. The ratio of stars to mesons is found to be 11·4 : 1. These results are all consistent with a theoretical model proposed by Butler, in which meson production is considered to take place preferentially on the surface of atomic nuclei. Several high-energy electrons and electron-pairs moving at right angles to the γ-ray beam have been observed, and are accounted for.

The observed cross section for the production of stars with three or more prongs is $2{\cdot}9 \times 10^{-27}$ cm² nucleus$^{-1}Q^{-1}$ in agreement with the result of Miller and disagreement with that of Kikuchi. The relation of these results to observations of the electromagnetic excitation of nuclei by fast charged particles is considered.

§ 1. Introduction

The production of charged π-mesons by photons was discovered by McMillan, Peterson and White (1949) who used carbon absorbers. The observations of these workers have since been extended by many others. Mozley (1951) and Littauer and Walker (1951) showed that the cross section for π-meson production varied as $A^{2/3}$, where A is the atomic number of the parent nucleus, and Steinberger and Bishop (1952) determined the energy and angular distributions of the mesons produced in carbon and hydrogen.

Another feature of the interaction of photons with atomic nuclei is the production of nuclear disintegrations or 'stars'. These were investigated by Kikuchi (1952) and by Miller (1951) whose values for the cross section for the production of 'stars' by photons were in disagreement.

From 1949 onwards, my colleagues and I have made a series of observations of the nuclear interactions of the penetrating cosmic radiation observed at great depths below ground. It was found possible to explain the main features of these observations in terms of the nuclear excitations produced by the virtual photons of the μ-mesons assumed to form the penetrating component at these underground depths.

† Also supported by the Nuclear Research Foundation within the University of Sydney.

This directed my attention to the need for further investigations of some aspects of the photo-nuclear effects in order to obtain a better understanding of the underground observations. In particular, no observations had been reported on the events occurring when photons produce mesons in complex nuclei.

In order to analyse such events, and also to decide between the two discordant results on photo-'star' production, nuclear research emulsions were exposed to high-energy gamma rays. The observations made in these emulsions are reported in this paper.

§ 2. Experimental

Ilford G5 nuclear research emulsions, 200 μ thick, were exposed with their planes perpendicular to the bremsstrahlung γ-ray beam of the Cornell University electron synchrotron, which was operated at an energy of 315 Mev. The energy distribution of the γ-rays was approximately of the form dE/E up to 315 Mev, and zero thereafter. The arrangement of equipment during the exposure is shown in figure 1. The dimensions of the plates were 3 in. × 1 in., but the area exposed along the centre line of the plate to the γ-ray beam was 15 mm × 8 mm.

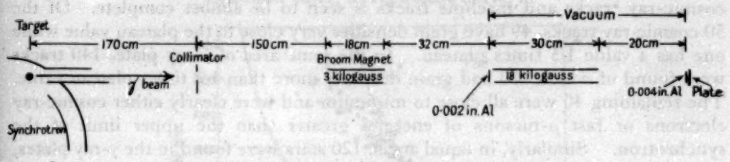

Figure 1. General arrangement during exposure.

Each area received a flux of $1{\cdot}45 \times 10^8 Q$ and there were twelve areas in all. Q is the number of equivalent quanta in the beam, defined as the energy flux divided by the maximum energy. The exposed areas were examined using × 45 oil-immersion objectives. In the first two areas searched the following events were noted: (*a*) all tracks starting in the emulsion, whether in stars or starting as single tracks in the emulsion whatever their length, (*b*) all single tracks passing through the emulsion whose projected lengths were greater than 1·5 mm. On all tracks longer than 1·5 mm, whether straight through or starting in the emulsion, measurements were made of the grain density and mean angle of multiple scattering by the Bristol method (Fowler 1950). In this way, the particles responsible for the tracks were identified as electron, light meson, or proton or deuteron.

In the two areas scanned exhaustively, some 800 'stars' with three or more prongs and about 400 long straight-through tracks were obtained, as well as 20 mesons starting in the emulsion. It took eight months to scan one small area. The number of stars and straight tracks obtained was thought to be sufficiently large to be representative. In order to improve the statistics on the mesons starting in the emulsion, the remaining areas were searched specifically for such events; the stars without long mesons and the background tracks were not recorded. In this way a further 80 meson tracks starting in the emulsion and with length greater than 1·5 mm were found. The searching time was six weeks per area.

The cosmic-ray contribution to the events observed was determined by examining a plate from the same batch which had the same history except that it was not exposed to the γ-ray beam. The emulsions were manufactured on 10th November 1953, exposed on 9th December 1953, processed the next day at Ithaca and sent to Sydney for examination.

§ 3. Results—General

The results for the tracks in the background plate are plotted out in figure 2 (*a*) and for an equal area of γ-ray plate in figure 2 (*b*). The results for all the tracks observed in this investigation are given in figure 2 (*c*). The curves drawn in these figures are the theoretical curves for ionization density given by the Bethe–Bloch theory, modified at high energies to allow for polarization. The plateau value of grain density was determined by averaging the value for several electron tracks. The value so found was 240 grains per millimetre. In drawing the theoretical curves, the magnitude of the increase in grain density from the minimum to the plateau value was taken to be 10%, the mean of the values reported by Daniel *et al.* (1952) and Stiller and Shapiro (1953).

From the comparison of equal areas in figure 2 (*a*) and (*b*) the separation between cosmic-ray tracks and machine tracks is seen to be almost complete. Of the 50 cosmic-ray tracks, 49 have grain densities very close to the plateau value while one has a value 1·5 times plateau. In the same area of γ-ray plate, 140 tracks were found of which 100 had grain densities more than 1·2 times plateau value. The remaining 40 were all close to minimum and were clearly either cosmic-ray electrons or fast μ-mesons of energies greater than the upper limit of the synchrotron. Similarly, in equal areas, 120 stars were found in the γ-ray plates, and none in the control plate. Thus we conclude that the cosmic-ray effects are easily distinguishable in the γ-ray plates, and that the error introduced by the cosmic-ray background is negligible.

§ 4. Results on Photo-Mesons

In this section we discuss the results obtained from all tracks longer than 1·5 mm starting in the emulsion which were classified as meson-tracks from their values of grain density and multiple scattering. From the thickness of the emulsion and the minimum track-length required, it follows that our observations refer to mesons emitted at $90 \pm 5°$ to the γ-ray beam. At least one half of the photo-mesons produced started all alone in the emulsion, unaccompanied by any other visible tracks.

4.1. *The Distribution in Prong-number of the Stars accompanying Meson Production*

The number and energies of the slow, heavy tracks accompanying meson production were noted. The energies were determined from grain or gap counts depending on the grain density. The energy measurements are reported in § 5. The frequency distribution of the star prong-numbers is given in figure 3. A striking feature of these observations is the relatively large number, 50%, of events with zero prongs, characteristic of low values of nuclear excitation (Le Couteur 1950, 1952).

In his analysis of nuclear photo-disintegrations, Kikuchi (1952) reported the occasional occurrence of meson production unaccompanied by stars. However, Kikuchi did not make any systematic survey of these events. The present

work confirms the events reported by Kikuchi and makes a systematic study of them. For comparison, the prong distribution for the stars initiated by 45 MeV protons reported by Hodgson (1953) have been included in figure 3.

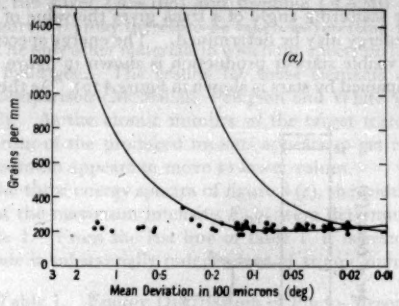

Figure 2 (*a*). g plotted against $\bar{\alpha}_{100}$ for tracks in control plate. Left-hand curve, π; right-hand curve, P.

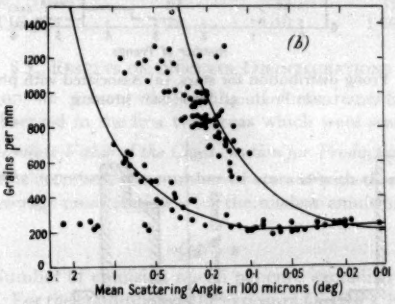

Figure 2 (*b*). g plotted against $\bar{\alpha}_{100}$ for an area of γ-ray plate equal to that in figure 2 (*a*). Left-hand curve, π; right-hand curve, P.

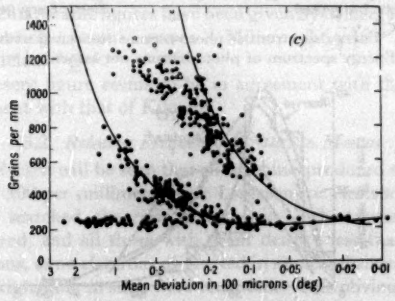

Figure 2 (*c*). g plotted against $\bar{\alpha}_{100}$ for all tracks in γ-ray plates. Left-hand curve, π; right-hand curve, P.

The two distributions are seen to exhibit the same general features. The significance of these results will be discussed later in § 7.

4.2. *The Energy Spectrum of the Produced Mesons*

The multiple scattering angle of a track gives the value of $p\beta$ of the particle from which the energy may be determined. The energy spectrum of the mesons accompanied by visible stars at production is shown in figure 4 (*a*), and that for mesons unaccompanied by stars is shown in figure 4 (*b*). As there is no significant

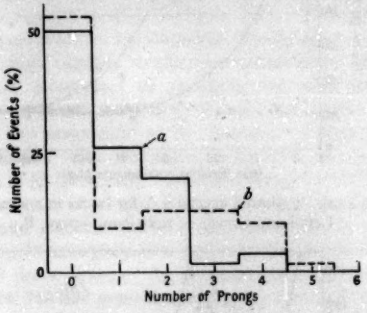

Figure 3. Prong distribution for stars. (*a*) Associated with photo mesons. (*b*) Produced by 45 MeV protons.

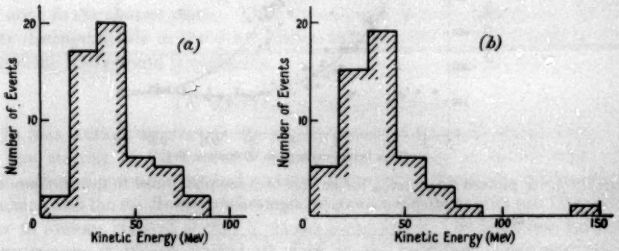

Figure 4 (*a*). Energy spectrum of photo-mesons associated with visible stars.
Figure 4 (*b*). Energy spectrum of photo-mesons not associated with visible stars.

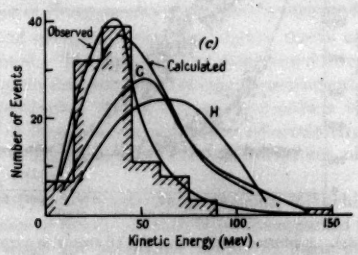

Figure 4 (*c*). Energy spectrum of all π-meson tracks together.

difference between these histograms, the two sets of results have been lumped together and are shown in figure 4 (*c*). From the $A^{2/3}$ dependence of the cross section for meson production, it follows that 80% of the observed mesons will have come from the silver ($A=108$) and bromine ($A=80$) in the emulsion. The results of figure 4 (*c*) may therefore be taken as referring to medium heavy nuclei ($A=90$). The only other materials in which the spectrum has been measured are carbon and hydrogen. The results for these elements are also given in figure 4 (*c*) for comparison (McMillan, Peterson and White 1949, Steinberger and Bishop 1952). As the atomic number of the target material is increased, the energy spectrum of the produced mesons appears to get narrower, and the energy at the maximum appears to move to lower values.

For each of the three energy spectra of figure 4 (*c*), the width at half-height Γ and the energy at the maximum intensity E_{max} were determined. The results are given in table 1. From the last line of table 1, it is seen that the ratio of half-width to mode is substantially independent of atomic number.

Table 1. Energy Distribution of Photo-Mesons

A	1	12	90
Γ(MeV)	79	57	38
E_{max}(MeV)	67	52	35
Γ/E_{max}	1·18	1·10	1·09

§ 5. Results on Nuclear Disintegrations

In this section we present the results of measurements on the nuclear disintegrations observed in the first two areas which were searched completely.

5.1. *The Absolute Value of the Cross Section for Production of 'Stars'*

In the two areas searched, the number of stars n with three or more prongs was 817. The average cross section σ for the nuclear emulsion was found from the formula

$$\sigma QN = n \qquad \ldots\ldots(1)$$

where N is the number of emulsion nuclei per cm², excluding hydrogen, and Q is defined in § 2. For the conditions of the exposure $Q=2{\cdot}9\times10^{8}$, $N=9{\cdot}88\times10^{20}$ giving

$$\sigma = 2{\cdot}9\times10^{-27}\ \text{cm}^2\ \text{nucleus}^{-1}\,Q^{-1}. \qquad \ldots\ldots(2)$$

Previously, very comparable figures have been given by Miller (1951) and Kikuchi. Their corresponding results were: Miller, $2{\cdot}6\times10^{-27}$, and Kikuchi, $6{\cdot}2\times10^{-27}$ cm² nucleus^{-1} Q^{-1}.

Thus the present figure seems to be in agreement with the result of Miller and in disagreement with that of Kikuchi.

5.2. *Relative Frequency of Stars to Mesons*

From figure 2 (*c*), it will be seen that all machine-produced tracks with a grain density less than 500 per millimetre were L-mesons or electrons. In one of the areas completely searched, the grain densities in all the tracks originating from stars was measured, and all those with grain density less than 500 mm^{-1} were classed as π-mesons, as no electrons originated in nuclear disintegrations. In this way 22 mesons originating in stars were recorded. It is obvious from figure 2 (*c*) that some 15% of the π-mesons have a grain density greater than 500 mm^{-1}, and would not have been recorded by the previous method. However, such

meson tracks are easily identified in view of their excessive scattering. Five additional π-mesons from stars with $g > 500\,\mathrm{mm}^{-1}$ were identified by inspection, making a total of 27 mesons from stars in the same area in which 410 stars with three or more prongs were found. From the results of § 4.1 we know that there would have been an equal number of mesons not associated with stars, making a total of 54 π-mesons in all.

At excitation energies around 200 MeV, the work of Gardner and Peterson (1949) and of Bernardini and Levy (1951) has shown that two-thirds of the stars have three or more heavy prongs, and that this fraction does not vary rapidly with energy. Therefore, for events produced by photons above the meson-producing energy threshold, the ratio

$$\frac{\text{All visible stars}}{\text{Mesons produced}} = \frac{\cdot 1 \cdot 5 \times 410}{54} = 11 \cdot 4.$$

This parameter turns out to be an important one for comparison with theory. The comparison is made in § 7.

5.3. *Energy Measurements on the Visible Tracks accompanying Meson Production*

The energies of the tracks in the visible stars were measured by grain or gap-counting, depending on the grain density. The visible kinetic energies released in the meson-associated 'stars' found in this way varied from 5 MeV to 23 MeV, the mean value being 13 MeV.

§ 6. Results of Observations on Electron Tracks

From figure 2 (*c*) it will be observed that there were many tracks of low momentum and low grain density. These were classified as electron tracks. In all the γ-ray plates, twenty-three electron tracks longer than 1·5 mm were observed to start in the emulsion, whereas, in the control plates, no electrons starting in the emulsion were observed. These electron tracks, starting almost at right angles to direction of the γ-rays were an unexpected aspect of the observations, and their main features will be reported. Ten of the electron tracks started in electron pairs, the other thirteen started alone in the emulsion.

The total energies of the electron pairs, determined from scattering measurements on each track, or, in one case, from the angle between them when one track was too short to measure were: 66, 89, 92, 118 and 172 MeV, the mean value being 107 MeV. The energy distribution of the single electrons is shown in table 2.

Table 2

Energy interval (MeV)	10–20	20–30	30–40	40–50	50–60
Number observed	6	1	3	2	1

It follows from the Bethe–Heitler formula for pairs, and the Klein–Nishina formula, that these pairs and single electrons could not be produced by the main stream of γ-rays perpendicular to the emulsion plane, but rather from a flux of γ-rays lying almost in the plane of the emulsion.

Also, because of the energies involved, it is unlikely that a fraction of the original beam could be deflected through 90°.

On the other hand, we know that there is a substantial flux of charged π-mesons in the plane of the emulsion, to wit, those starting in stars, those starting alone and those passing straight through from glass to surface as mentioned in § 3.

Now, the cross section for the production of neutral π-mesons is known to be about one half of the value for charged π-mesons. The neutral π-mesons decay immediately into two photons and therefore we must expect a path-length of γ-rays arising from π^0-decay approximately equal to that of the charged π-mesons. The total path-length of charged mesons of length greater than 1·5 mm was 41·6 cm. The theoretical value for the mean free path for pair-production in the emulsion is 5·75 cm at 100 MeV. Thus, it follows that $41{\cdot}6/5{\cdot}75 = 7{\cdot}2$ pairs will be expected satisfying the length criterion. The number observed, 5, is in sufficiently good agreement to justify the interpretation of the emulsion-plane γ-rays as arising from the decay of π^0-mesons produced by the main γ-ray beam.

Since the Klein–Nishina cross section varies approximately inversely as the energy, the Compton recoils will arise, in general, from photons of lower energy than the pairs do. The mean free path in emulsion for the production of Compton recoil electrons is about 5 cm in the energy region 10–20 MeV. Thus the number of single electron tracks starting in the emulsion should be comparable with the number of pairs. The actual numbers were 13 single electrons as against 5 pairs. The difference hardly seems worth worrying about. Both the single electrons and the electron pairs seem to be adequately explained in terms of photons moving in the plane of the emulsion, these photons arising from the decay of the neutral photo-mesons produced by the bremsstrahlung beam.

§ 7. Discussion

The main experimental results arising from this investigation are as follows: (*a*) about one half of the photo-mesons are not accompanied by any visible nuclear disintegration, (*b*) the energy spectrum of the mesons from heavy nuclei like silver and bromine reaches its maximum at lower energies than that of mesons produced from carbon and from hydrogen, (*c*) the cross section for the production of stars with three or more prongs is $2{\cdot}9 \times 10^{-27}$ cm^2 nucleus^{-1} Q^{-1}, and (*d*) for events produced by photons above the meson-production threshold, the ratio of the frequency of stars to that of mesons is 11·4. These results will now be discussed in greater detail.

7.1. *Photo-Mesons*

(*a*) *Relative frequency of isolated mesons.*

Photo-meson production in complex nuclei is usually interpreted using the optical model (Brueckner, Serber and Watson 1951). On this model, the nucleus is regarded as a sphere possessing a refractive index and an attenuation constant. The attenuation constant is usually expressed in terms of λ_π, the mean free path for the absorption of π-mesons in nuclear matter. The value of λ_π is known to depend on the π-meson energy (Tenney and Tinlot 1953) varying from 22×10^{-13} cm at 10 MeV to about 4×10^{-13} cm at 80 MeV. From figure 2 (*c*), it is seen that energies in the region 30 to 50 MeV are the important ones in our present consideration, and we have assumed $\lambda_\pi = \text{const.} = 4 \times 10^{-13}$ cm or 8×10^{-13} cm. The results turn out to be not critically dependent on the value of λ_π (Reff 1954).

It was pointed out by Butler (1952) that the well-known $A^{2/3}$ dependence of the photo-meson cross section on atomic number A could not be explained on the optical model if it was assumed that all nucleons contributed equally to meson production, and the measured values of λ_π were inserted in the calculation.

This led Butler to postulate that mesons were produced preferentially on the surface, meson production in the nuclear core being suppressed by some such mechanism as that proposed by Wilson (1951). Wilson postulated that a photo-meson produced in the core is immediately reabsorbed by its parent nucleon and another nucleon with which it is interacting at that moment. The relevant calculations to be compared with the observations reported in this paper have accordingly been performed both for the optical model and for the Butler model of surface production.

In the primary act, the production of a meson in the field of a nucleon, the nucleon recoils with an energy which depends on the angle and energy of the produced meson. For the bremsstrahlung spectrum under consideration, the average energy of the nucleon is close to 40 MeV, and according to Serber (1947) the mean free path for absorption at this energy is $\lambda_n = 2{\cdot}1 \times 10^{-13}$ cm. The probability of escape of a particle produced at an arbitrary point inside a nucleus of radius R has been given by Brueckner, Serber and Watson (1951) as

$$f = 3\left\{\frac{1}{2x} - \frac{1}{x^3} + \frac{1}{x^3}(1+x)e^{-x}\right\} \qquad \ldots\ldots(3)$$

where $x \equiv 2R/\lambda$.

This has been evaluated separately for the nucleon and the meson, using the stated values of λ for the emulsion nuclei C, N, O, Ag and Br. The results have been averaged over the emulsion constituents to give the average probabilities of escape of nucleons f_N and mesons f_π. From these figures the probability of both escaping, one or other escaping or both being absorbed have been calculated.

Table 3. Summary of Calculations on Photo-Meson Production

Occurrence	Appearance	Probability			
		Optical model		Butler model	
	$\lambda_\pi = 10^{-13}$cm ×	4	8	4	8
1. Meson and nucleon escape without interaction, nucleon as neutron	Isolated meson track	0·16	0·20	0·09	0·09
2. Meson escapes, nucleon absorbed	Isolated meson track	0·18	0·23	0·27	0·30
3. Meson escapes, nucleon absorbed	Meson emerging from star	0·16	0·20	0·24	0·25
4. Meson and nucleon escape without interaction, nucleon as proton	Meson emerging from star with one heavy prong	0·16	0·20	0·09	0·09
5. Meson absorbed, nucleon escapes	Star without meson	0·16	0·08	0·19	0·13
6. Meson and nucleon absorbed	Star without meson	0·18	0·08	0·13	0·10

The results of these calculations are given in table 3. It will be noted that six different possibilities are considered in table 3, whereas only four different occurrences are possible. The reason for this is that two of the occurrences can each appear in two different forms in the emulsion. For example, if the

meson escapes and the nucleon is absorbed, there may or may not be a visible star since the nuclear excitation will be quite low, of order 40 Mev. Stars produced in emulsion by 45 Mev protons have been studied by Hodgson. From his results it follows that at this excitation only 47% of the nuclear interactions result in visible stars, in the remaining 53%, only neutrons are emitted. Rows 2 and 3 take into account these two possibilities. Similarly, if both meson and nucleon escape, then in 50% of the cases the nucleon will be neutral and hence invisible (row 1) while for the remainder it will be a proton and hence classified as a star (row 4).

For the Butler model, the geometrical averaging was found to be more difficult and recourse was made to an analogue computer. A ball of plasticine was made and two needles representing the nucleon and meson meeting at the surface at the appropriate angle for photo-meson production were inserted, and the path-lengths read off. This was repeated for many orientations of the nucleon–meson plane, and for 25 different positions on the surface. The results were further averaged over the emulsion nuclei by the use of scale factors. In this way the probabilities were calculated for the Butler model, the results being given in the last two columns of table 2.

From these individual probabilities, we can calculate probabilities to be compared with the observations. In particular, the ratio of stars with mesons to isolated meson tracks is given by {rows 3 plus 4}/{rows 1 plus 2}. The results are given in table 4 together with the experimental figure.

Table 4. Ratio of Mesons accompanied by Stars to Mesons not accompanied by Stars

	Optical model		Butler model		Observed
λ_π (cm)	4.10^{-13}	8.10^{-13}	4.10^{-13}	8.10^{-13}	
Ratio	0·94	0·93	0·92	0·88	$1{\cdot}0 \pm 0{\cdot}1$

The results are seen to be extremely insensitive to the value of λ_π, and the predictions of both models are consistent with observation. Thus, this particular parameter is no help in deciding between the two models.

If the meson escapes, then the energy of the recoil nucleon is about 40 Mev. It is of interest to compare the prong distribution of the meson associated stars with that for the stars produced by 45 Mev protons (Hodgson 1953). Hodgson's results are drawn for comparison in figure 3. The two distributions are seen to be in reasonable agreement. The only serious discrepancy occurs for $N_n = 1$, but there should be an excess in the photo-meson stars precisely at this point on account of those cases where both π-mesons and nucleon escape, the nucleon in proton form (row 4, table 3). The large number of photo-meson tracks which are not associated with visible stars is thus simply explained in terms of the relatively large probability of pure neutron emission at the low value of 40 Mev for the corresponding excitation.

Other effects that could contribute to the 'starless' meson events are the production of π^+-mesons on the hydrogen in the emulsion, and the sudden disappearance of π^--mesons in flight through the emulsion. The production in hydrogen can be evaluated from the known $A^{2/3}$ dependence of the photo-meson cross section and it turns out that between 1 and 2 of the 50 'starless' mesons may be attributed to hydrogen. The effect of the sudden stops is less, since

Bernardini, Booth and Lederman (1951) have shown that the mean free path in emulsion for stopping is of the order of 200 cm at 30–50 Mev. Since the total path-length of background meson track is 41·6 cm, this means that the probable number of events due to stopping is of the order of 0·2.

Similarly, interactions of the background π-mesons resulting in stars would have been classified as meson production accompanied by a star. Again, the mean free path for this process is given by Bernardini *et al.* (1951) as 57 cm for π^+ and 43 cm for π^- indicating that about one of the fifty star-accompanied meson productions may be an interaction due to an incoming π-meson. This is further supported by the low mean energy (13 Mev) of the stars accompanying meson production. A significant number of π-meson produced stars would certainly have pushed this up to a much higher value.

(*b*) *Energy spectrum of photo-mesons.*

The problem we must now consider is the following: given that the spectrum of the photo-mesons from free nucleons is as indicated in curve H in figure 4 (*c*), how can we account for the observed squeezing up of the spectrum to lower energies with increasing atomic number of the target nuelei?

One factor that might come into play is the variation with energy of the mean free path for absorption of π-mesons in nuclear matter. Recent measurements have been summarized by Tenney and Tinlot (1953), who show that λ_π decreases monotonically from a value of about 22×10^{-13} cm at 10 Mev to about 4×10^{-13} cm at 100 Mev. This will clearly favour the escape of low-energy mesons, thus weighting the spectrum for complex nuclei in the desired direction. However, on working out the spectrum expected from heavy nuclei like silver and bromine, taking into account only the energy dependence of λ_π, the resulting curve, while quite different from the hydrogen spectrum, was not in even approximate agreement with the observed spectrum. This suggested that some other factor must come into play. This additional factor is probably the internal motion of the nucleons. Henley and Huddlestone (1951) have already shown the importance of this factor by discussing the spectrum of mesons produced by protons incident on carbon nuclei. Best agreement was obtained assuming a gaussian energy distribution in nuclear matter with the mean equal to 19·3 Mev. Following Henley and Huddlestone the effect of internal motion has been evaluated, and the spectrum calculated when an allowance is made both for the variation in λ_π and the effect of internal motion is shown in figure 4 (*c*). The agreement is not perfect, but these two effects clearly go a long way to explain the observed spectrum. The calculations are only approximate and it would be necessary to do them more carefully before deciding whether the discrepancy occurring at high energies is significant or not.

Other factors that could come in are emulsion distortion, the possibility of a systematic loss of high-energy tracks by the scanners and the slight difference in maximum energy of the γ-rays used in determining the hydrogen spectrum (325 Mev). These are all thought to play a minor role for the following reasons: The emulsion distortion was measured by Major's method (Major 1952). The distortion vector was found to be 10 μ for the 200-micron plates corresponding to a distortion of 250 covans. This is negligible for tracks of 80 to 100 Mev, in fact many cosmic-ray tracks of much higher energy were observed, the maximum energy measured being 5·3 Gev. Since the scanners picked up about the right

number of Compton electrons, which were of course at minimum ionization, the possibility of a serious loss of meson tracks around 80 Mev corresponding to a grain density $1{\cdot}15\,g_{plateau}$ may be discounted. The difference in energies of the two beams is only 10 Mev, and any modification of the spectrum could only amount to a shift of 10 Mev at the upper end of the spectrum, and to a smaller shift at lower energies.

7.2. *Photonuclear Disintegration 'Stars'*

(*a*) *Absolute cross section for star production.*

The absolute cross section obtained here for stars with three or more prongs is $2{\cdot}9\times10^{-27}$ cm^2 nucleus^{-1} Q^{-1}, where the value of Q is simply the total energy in the beam divided by the maximum energy. The result is in good agreement with the value of Miller, $2{\cdot}6\times10^{-27}$ cm^2 nucleus^{-1}, when allowance is made for the fact that Miller used C2 plates which are not sensitive to tracks at minimum ionization. Page (1950) has compared the frequency of cosmic-ray stars in G5 and C2 emulsions, and finds the ratio to be 1·1. A corresponding correction of 10% applied to Miller's result would bring it into excellent agreement with the value obtained here. The discrepancy with Kikuchi's figure has already been noted by Kikuchi (1952) and attributed by him to errors in the calibration of the γ-ray beam in the determination of the value of Q. Kikuchi's and the present value were obtained using the same γ-ray beam from the same synchrotron.

The cross section may also be given per nucleon. Multiplying the answer by 1·5, as before, in order to extrapolate for the inclusion of one- and two-pronged stars, we obtained for the cross section for the production of stars by photons in the range 150 to 315 Mev: $\sigma=0{\cdot}95\times10^{-28}$ cm^2 nucleon^{-1} Q^{-1}. Of interest in the application of this result is the cross section per photon, not the cross section per Mev. Since the bremsstrahlung energy distribution is very closely QdE/E, the number of photons in the interval 150 to 315 Mev is $Q\log_e(315/150)=0{\cdot}725Q$. Thus the photonuclear cross section obtained here may also be expressed as

$$\sigma=1{\cdot}3\times10^{-28}\text{ cm}^2\text{ nucleon}^{-1}\text{ quantum}^{-1} \qquad \ldots\ldots(4)$$

in the energy interval $150>E>315$ Mev.

(*b*) *Relative frequency of stars to mesons.*

Above the photo-meson threshold, the ratio of visible stars to mesons was found to be 11·4 : 1. This is not inconsistent with Kikuchi's figure for the ratio of three-pronged stars to mesons starting in stars which was 16 (Kikuchi 1952). My figure for this same ratio is 15 but in obtaining the figure quoted (i.e. 11·4) all the mesons found starting in the emulsion alone have been included, and so has the factor for one- and two-pronged stars, since this is the figure that must be compared with theoretical prediction. For the optical model the figure is found from table 2 by taking all the star events (rows, 3, 4, 5 and 6) and dividing by all the meson events (rows 1, 2, 3 and 4). Further, one must increase the numerator by 50% to allow for the effect of the neutral π-mesons, which will of course contribute to star production, if re-absorbed, but will not leave visible meson tracks. The figure of 50% comes from the known ratio of the photo-production cross sections for charged and neutral mesons (Silverman and Stearns 1952, Steinberger and Bishop 1952), and also from cosmic-ray data (Carlson, Hooper and King 1950). The results of this calculation are given in table 5.

On the Butler model one proceeds slightly differently. The nucleus is divided into two parts—a core region in which photon absorption in the energy interval 150–315 MeV always results in a nuclear disintegration with no free meson production, and a surface region in which the nucleons may be treated as if they are free.

Table 5. Ratio of Stars to Mesons

	Optical model		Butler model		Observed
λ_π (cm)	4.10^{-13}	8.10^{-13}	4.10^{-13}	8.10^{-13}	
Ratio	1·5	1·0	15	9·6	11·4

Of the mesons produced at the nuclear surface, approximately 50% are re-absorbed and 50% escape as free mesons.

For the nuclei in question, the ratio of the number of nucleons in the core to those in the surface is 4 : 1 (Butler, private communication) and hence it follows that the relative probabilities of a photon interacting in the core and surface are in the same ratio. This means that the ratio of stars from charged meson re-absorption to free charged mesons is approximately 8 : 1 and multiplying by 1·5 for neutral π-mesons, the final ratio becomes approximately 12 : 1. The results of a more detailed calculation for the usual values of λ_π are given in table 5.

It will be seen from table 5 that the theoretical results based on the optical model are lower than the observed value by an order of magnitude, whereas the values based on the Butler model are close to the observed value.

7.3. *Bearing on Electromagnetic Nuclear Interactions observed below Ground*

In this section the present results will be briefly related to underground observations of the nuclear interactions of the penetrating component of the cosmic radiation. These have been summarized by George (1952). The underground observations were interpreted in terms of the nuclear interactions of the virtual photons associated with the Coulomb charge of these fast particles, following Williams and von Weizsäcker. One parameter that has to be inserted in the calculations is the value of the cross section for star production by photons. The value that I had used previously, based on the work of Miller, was $\sigma_{\lambda\gamma} = 10^{-28}$ cm^2 nucleon^{-1}. It was found that the observed cross sections were all some 30 to 40% larger than the calculated values. It is seen that using the value given in equation (4) this discrepancy is now largely removed.

Finally, the large number of events (50%) in which photo-mesons are not accompanied by heavy evaporation tracks means that there could have been a loss of up to 50% of events in the underground emulsions in which fast μ-mesons create π-mesons via their virtual photons, since only events associated with heavy tracks were searched for. The final figure of George and Evans (1955) for shower production by fast μ-mesons is $(1{\cdot}7 \pm 0{\cdot}3) \times 10^{-30}$ cm^2 nucleon^{-1}. If we now double this figure to allow for the cases where the 'stars' were invisible, we get as the upper limit for shower production the value $(3{\cdot}4 \pm 0{\cdot}6) \times 10^{-30}$ cm^2 nucleon^{-1}. This means that it is not possible to explain in terms of nuclear electromagnetic interactions the large cross section ($\sim 5 \times 10^{-29}$ cm^2 nucleon^{-1}) at one time reported for the production of penetrating secondary particles (A.P.P.) underground by fast μ-mesons (Braddick, Nash and Wolfendale 1951, George, Redding and Trent 1953). Later work has shown this cross section to have been over-estimated (Braddick and Leontic 1954). The present work, while showing

that the total cross section for the production of secondary π-mesons by fast μ-mesons may be higher than that determined from the underground emulsion work, it certainly cannot be larger than by a factor two. The increased value of $3{\cdot}4 \times 10^{-30}$ cm^2 nucleon^{-1} is consistent with the latest cloud-chamber data of Braddick and Leontic, whose cross section for the nuclear interaction of cosmic rays underground is $3{\cdot}2 \pm 1{\cdot}8 \times 10^{-30}$ cm^2 nucleon^{-1}.

§ 8. Conclusions

The following conclusions have been drawn from the observations reported in this paper:

(i) Some 50% of the photo-mesons produced by bremsstrahlung photons in the energy range 150 to 315 Mev are not accompanied by visible nuclear disintegration 'stars'.

(ii) The energy spectrum of the photo-mesons, produced mostly in Ag and Br is bunched up to lower energies compared with that of mesons produced in C or H.

(iii) In the γ-ray energy range 150 to 315 Mev, the ratio of stars to mesons produced by the bremsstrahlung γ-ray beam is 11·4 : 1.

(iv) In the same energy range, the mean value of the photo-nuclear cross section is $1{\cdot}3 \times 10^{-28}$ cm^2 nucleon^{-1} quantum^{-1}. The observed cross section for the production of stars with three or more prongs is $2{\cdot}9 \times 10^{-27}$ cm^2 nucleus^{-1} Q^{-1}, in agreement with Miller's value and disagreeing with that of Kikuchi.

(v) The observed electrons and electron pairs travelling at right angles to the main γ-ray beam can be explained in terms of γ-rays arising from the decay of neutral photo-mesons produced by the main beam.

(vi) The observed photo-meson spectrum can be explained in terms of combined effects of internal motion of nucleons in the parent nucleus, and of the energy dependence of the mean free path for absorption of π-mesons in nuclear matter.

(vii) The fraction of mesons not accompanied by visible stars and the ratio of stars to mesons can both be explained on the Butler model, whereas only the former result can be explained on the optical model.

(viii) The cross section in (iv) above is in good agreement with the value required to account for underground observations of electromagnetic interactions of fast μ-mesons.

(ix) The large fraction of mesons escaping unaccompanied by other visible tracks makes it possible that the previously reported figure of $1{\cdot}7 \times 10^{-30}$ cm^2 nucleon^{-1} for the cross section for underground shower production should be raised to $3{\cdot}4 \times 10^{-30}$ cm^2 nucleon^{-1}.

Acknowledgments

I would like to thank Professor Messel for the excellent facilities provided for doing this work. I am grateful to Professor Dale Corson for exposing the plates to the Cornell synchrotron. Many stimulating conversations with Dr. S. T. Butler are gratefully acknowledged. Thanks are due to our scanners whose painstaking observations contributed materially to the completion of this investigation: Mrs. Chartres, Mrs. Docherty, Mrs. Landers and Jennifer O'Brien. I would also like to thank the Research Committee of the University of Sydney for supporting this work.

References

Bernardini, G., Booth, E. T., and Lederman, L., 1951, *Phys. Rev.*, **83**, 1075.
Bernardini, G., and Levy, F., 1951, *Phys. Rev.*, **84**, 610.
Braddick, H. J. J., and Leontic, B., 1954, *Phil. Mag.*, **45**, 1287.
Braddick, H. J. J., Nash, W. F., and Wolfendale, A., 1954, *Phil. Mag.*, **42**, 1277.
Brueckner, K. A., Serber, R., and Watson, K. M., 1951, *Phys. Rev.*, **84**, 258.
Butler, S. T., 1952, *Phys. Rev.*, **87**, 1117.
Carlson, A. G., Hooper, J. E., and King, D. T., 1950, *Phil. Mag.*, **41**, 701.
Daniel, R. R., Davies, J. H., Mulvey, J. H., and Perkins, D. H., 1952, *Phil. Mag.*, **43**, 753.
Fowler, P. H., 1950, *Phil. Mag.*, **41**, 169.
Gardner, E., and Peterson, V., 1949, *Phys. Rev.*, **75**, 364.
George, E. P., 1952, *Progress in Cosmic Ray Physics* (Amsterdam : North-Holland Publishing Co.).
George, E. P., and Evans, J., 1955, *Proc. Phys. Soc.* A, **68**, 829.
George, E. P., Redding, J. L., and Trent, P. T., 1953, *Proc. Phys. Soc.* A, **66**, 533.
Henley, E. M., and Huddlestone, R. H., 1951, *Phys. Rev.*, **82**, 754.
Hodgson, P. E., 1953, *Phil. Mag.*, **44**, 1113.
Kikuchi, S., 1952, *Phys. Rev.*, **86**, 41.
Le Couteur, K. J., 1950, *Proc. Phys. Soc.* A, **63**, 259; 1952, *Proc. Phys. Soc.* A, **65**, 718.
Littauer, R. M., and Walker, D., 1951, *Phys. Rev.*, **82**, 746.
Major, J. V., 1952, *Brit. J. Appl. Phys.*, **3**, 309.
McMillan, E. M., Peterson, J. M., and White, R. S., 1949, *Science*, **110**, 579.
Miller, R. D., 1951, *Phys. Rev.*, **82**, 260.
Mozley, R. F., 1951 *Phys. Rev.*, **80**, 493.
Page, N., 1950, *Proc. Phys. Soc.* A, **63**, 250.
Reff, I., 1954, *Phys. Rev.*, **91**, 150.
Serber, R., 1947, *Phys. Rev.*, **72**, 1114.
Silverman, A., and Stearns, M., 1952, *Phys. Rev.*, **88**, 1225.
Steinberger, J., and Bishop, A. S., 1952, *Phys. Rev.*, **86**, 171.
Stiller, B., and Shapiro, M. M., 1953, *Phys. Rev.*, **92**, 735.
Tenney, F. H., and Tinlot, J., 1953, *Phys. Rev.*, **92**, 974.
Wilson, R. R., 1951, *Phys. Rev.*, **86**, 125.

The Polarization of γ-Radiation from the Reactions $^{27}Al(p, \gamma)^{28}Si$, $^{26}Mg(p, \gamma)^{27}Al$, $^{23}Na(p, \gamma)^{24}Mg$

BY I. S. HUGHES AND D. SINCLAIR
Department of Natural Philosophy, The University of Glasgow

Communicated by P. I. Dee; MS. received 27th July 1955, and in amended form 19th October 1955

Abstract. Measurements of the polarization of some of the high energy γ-rays from the reactions $^{27}Al(p,\gamma)^{28}Si$, $^{26}Mg(p,\gamma)^{27}Al$ and $^{23}Na(p,\gamma)^{24}Mg$ have been made using nuclear emulsions impregnated with heavy water. The results obtained enable assignments of even parity to be made to the ground and first excited states of ^{27}Al and to the ground state of ^{23}Na. A range–energy relation for protons up to 5 MeV in wet emulsions is given in an appendix.

§ 1. INTRODUCTION

THE photodisintegration of deuterium provides a useful method of studying the polarization of γ-rays which have an energy greater than about 5 MeV, whereas the Compton effect is rather insensitive to polarization at such energies. For γ-rays with energies in the range 5–50 MeV the disintegration takes place almost entirely by an electric dipole mechanism (Bethe 1947, p. 56). Bethe and Bacher (1936) have calculated the azimuthal angular distribution of the ejected photoprotons which, for plane polarized radiation, is of the form $\cos^2\psi$, where ψ is the azimuthal angle of the ejected photoproton, measured with respect to the direction of the electric vector of the γ-ray. The form of this distribution has been confirmed experimentally by Wilkinson (1952), and the effect has been used to measure the polarization of the γ-rays from the reaction $^{19}F(p,\gamma)^{20}Ne$ (Fagg and Hanna 1953), and the polarization of the γ-ray beam from a betatron (Phillips 1953, Tzara 1954, Muirhead and Mather 1954).

The present paper describes measurements of the polarization of γ-rays from the reactions $^{27}Al(p,\gamma)^{28}Si$, $^{26}Mg(p,\gamma)^{27}Al$, and $^{23}Na(p,\gamma)^{24}Mg$, using nuclear emulsions impregnated with heavy water. The results enable assignments of parity to be made to the ground states of ^{27}Al and ^{23}Na which are in agreement with the predictions of the shell model. A measurement of the polarization of the 7·6 MeV γ-ray from the reaction $^{26}Mg(p,\gamma)^{27}Al^*$ enables an assignment of even parity to be made to the first excited level of the ^{27}Al nucleus.

The results for the reaction $^{27}Al(p,\gamma)^{28}Si$ have already been briefly reported in this journal (Hughes and Grant 1954).

§ 2. EXPERIMENTAL PROCEDURE

The reactions were produced using the resolved proton beam from the Glasgow H.T. set.

Ilford G5 nuclear emulsions, usually 300 μ but also 400 μ in thickness, were used throughout the series of exposures. G5 rather than C2 emulsions were chosen in order to give well-defined tracks in the swollen emulsion and also since, in the long exposures required, it was important to avoid fading of the tracks. The density of background grains was not high when the plates were screened

against soft x-rays. The method of introducing the heavy water into the emulsion was to place a plate, cut to 1 in. × 1·5 in., in a Perspex box, insert a U-shaped glass spacer to prevent the emulsion resting against the inside of the box, and then to add sufficient water to cover the plate. Four plates were exposed simultaneously, three in heavy, and one in ordinary water. Preliminary measurements showed that swelling virtually ceased after immersion for fifteen hours if the temperature was maintained below 18°C or 19°C; at least this length of time was, therefore, allowed to elapse between immersion and exposure.

The Perspex boxes were held in a container which fitted round the target in such a way that the γ-rays at 90° to the proton beam were incident normally at the centre of the plates. A shield of $\frac{1}{8}$ in. copper was effective in stopping soft x-rays from the target from blackening the plates. In later exposures the temperature of the container was held constant to within one centigrade degree with a consequent improvement in the energy resolution of the photoprotons.

Since the H.T. set is frequently used to accelerate deuterons, the accelerating tube and the resolving chamber tend to become contaminated with deuterium. This gives rise to a background of knock-on protons produced by neutrons from the reaction $^{2}H(d,n)^{3}He$. The emulsion impregnated with ordinary water is, however, an extremely efficient detector of neutrons since, with the swellings normally used, it contains about eight times as much hydrogen per square centimetre of surface area as does an emulsion impregnated with heavy water.

Targets were made by condensing a suitable vapour upon a brass or copper backing. To produce targets of ^{27}Al, pure aluminium vapour was condensed upon brass. For the targets of ^{23}Na, sodium chloride was normally used, but in the last exposure it was replaced by sodium sulphate. The targets of sodium sulphate lasted better under bombardment and are less likely to contain fluorine as an impurity. For the $^{26}Mg(p,\gamma)^{27}Al$ reaction, targets of the separated isotope were obtained from the Atomic Energy Research Establishment, Harwell. All the targets were of such a thickness that only one resonance could be excited. A modification during later exposures was to heat the target electrically to about 230°C. This proved completely effective in preventing the deposition of carbon on the target.

The proton beam current was normally about 40 μA, and the exposures were made for about 20 hours. The results for γ-rays from the bombardment of ^{27}Al and ^{26}Mg were obtained from one exposure for each element, but the results quoted for ^{23}Na represent the data from four exposures.

An area of about 4·5 cm^2, centred on the level of the target and clear of the edges, was scanned on each plate. Only tracks which started and ended in the emulsion and which had a dip of less than 45° in the unprocessed emulsion were accepted for measurement. The length of each track was calculated from measurements of its horizontal and vertical projections. The azimuthal angle of ejection ϕ, of each photoproton was measured with respect to the direction of the beam of protons incident on the target.

The plates were processed in two ways; by the normal temperature development method using amidol as the developing agent (Dainton, Gattiker and Lock 1951), and by a modification of the hydroquinone–pyrogallol development suggested by Bonnet (1954). The second method proved the more satisfactory, giving well-defined tracks with a low density of background grains. This

developer appears, however, to deteriorate rapidly, and it was found necessary to make up and cool the solutions quickly immediately prior to use. The development was carried out on a hot plate at 25°c for 45 minutes.

§ 3. Results

The range distributions of the photo-protons for each of the reactions studied are shown in figure 1. In the distributions for the reactions $^{27}Al(p,\gamma)^{28}Si$ and $^{23}Na(p,\gamma)^{24}Mg$ tracks with a length less than 80 μ have not been included. The

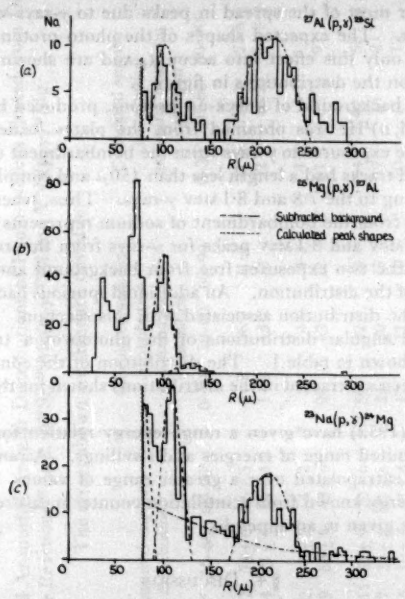

Figure 1. Range distributions in emulsions impregnated with heavy water of photo-protons ejected by (*a*) 7·5 MeV and 10·4 MeV γ-rays from the reaction $^{27}Al(p,\gamma)^{28}Si$, (*b*) 7·6 MeV and 8·6 MeV γ-rays from the reaction $^{26}Mg(p,\gamma)^{27}Al$, (*c*) 7·2 MeV, 8·1 MeV and 10·8 MeV γ-rays from the reaction $^{23}Na(p,\gamma)^{24}Mg$, (*b*) also shows peaks corresponding to the 6·04 MeV and 8·78 MeV α-particles from thorium.

distribution for the reaction $^{26}Mg(p,\gamma)^{27}Al$ shows two prominent peaks in the region 25 μ to 80 μ. These peaks are also present in the distributions for the other reactions when measurements of the range are extended to this region. Tracks of this range are also observed in plates soaked in ordinary and heavy water, but not exposed to γ-radiation. Since the track of an α-particle is indistinguishable from that of a proton in a swollen G5 emulsion, they are assumed to arise from a contamination of thorium, and the observed ranges correspond to the 6·04 MeV α-particle from thorium A, and the 8·78 MeV α-particle from thorium C.

The resolution of the peaks in the range distributions is influenced by the following effects: (*a*) Observational and microscope errors in track measurement, including the uncertainty in fixing the end points of a track: It is estimated that

such errors are responsible for a maximum spread of about 15 μ in the range distribution. (*b*) Changes in the swelling of the emulsion produced by temperature variations during the exposure: During the exposure to γ-rays from the bombardment of ^{27}Al the temperature varied by as much as seven centigrade degrees. In the exposure to γ-rays from the bombardment of ^{26}Mg and the later exposures to γ-rays from the ^{23}Na(p, γ)^{24}Mg reaction the temperature was held constant to within one centigrade degree. (*c*) The dependence of the energy of the photo-proton on the angle it makes with the incident γ-ray: This effect accounts for most of the spread in peaks due to γ-rays with an energy of 7·5 MeV or greater. The expected shapes of the photo-proton peaks have been calculated taking only this effect into account, and are shown by broken lines superimposed upon the distributions in figure 1.

Evidence of a background of knock-on protons, produced by neutrons from the reaction ^{2}H(d, n)^{3}He was obtained from the plates loaded with ordinary water in two of the exposures to γ-rays from the bombardment of ^{23}Na. Almost all the background tracks had a length less than 150 μ and completely masked the peaks corresponding to the 7·8 and 8·1 MeV γ-rays. Thus, whereas the 10·8 MeV peak for the γ-ray from the bombardment of sodium represents tracks from four exposures the 7·0 MeV and 8·1 MeV peaks for γ-rays from this reaction represent tracks from only the two exposures free from background and are normalized to the remainder of the distribution. An additional spurious background appears to be present in the distribution associated with this reaction.

The measured angular distributions of the photoproton tracks from each of the peaks are shown in table 1. The distribution of the continuous spurious background has been subtracted in the distributions shown for the ^{23}Na(p, γ)^{24}Mg reaction.

Gibson *et al.* (1952) have given a range–energy relation for protons in wet emulsions for a limited range of energies and swellings. A range–energy curve close to this, but extrapolated over a greater range of values, was found to fit all the peaks of energy known from scintillation counter measurements. Details of this relation are given in an appendix.

§ 4. Discussion

Hamilton (1948) has derived relations between the coefficients of the angular correlation for a cascade of two successive γ-rays and the degree of elliptical polarization of one of them. The theory is directly applicable to the case of absorption of a particle by the nucleus and the subsequent emission of a γ-ray if the coefficients of the angular correlation for the γ–γ cascade are replaced by the coefficients of the polar angular distribution of the emitted γ-rays with respect to the direction of the incident particle beam. The polarization may be described in terms of R, the ratio of the intensity of radiation, plane polarized in the plane of the incident proton and the emitted γ-ray, to the intensity of radiation plane polarized at right angles to this plane. If the polar angular distribution is of the form

$$1+a_2\cos^2\theta+a_4\cos^4\theta+\ldots,$$

then Hamilton has shown that for electric dipole radiation

$$R=\frac{1+a_2\cos 2\theta}{1+a_2}=\frac{1-a_2}{1+a_2}\quad\text{for}\quad\theta=90^\circ$$

Table 1. Measured and Calculated Azimuthal Angular Distributions of Photo-protons ejected from Deuterium by γ-rays from the Reactions $^{27}Al(p,\gamma)^{28}Si$, $^{26}Mg(p,\gamma)^{27}Al$ and $^{23}Na(p,\gamma)^{24}Mg$

The errors shown are standard deviations

Reaction	γ-Ray energy (MeV)	Measured angular distribution			Calculated angular distribution assuming electric radiation			Calculated angular distribution assuming magnetic radiation			Assignment
		0–30°	30–60°	60–90°	0–30°	30–60°	60–90°	0–30°	30–60°	60–90°	
$^{27}Al(p,\gamma)^{28}Si$	10·4	49±7	35±6	26±5	51·8	36·7	21·4	21·4	36·7	51·8	Electric
	7·5	18±4	21±5	16±4	14·8	18·2	22	22	18·2	14·8	Undetermined
$^{26}Mg(p,\gamma)^{27}Al$	8·6	5±2	5±2	4±2	5	4·7	4·3	4·3	4·7	5	Undetermined
	7·6	88±9	64±8	38±6	94	63	32	31	62	92	Electric
$^{23}Na(p,\gamma)^{24}Mg$	10·8	70±11	36±9	20±6	50	42	34	34	42	50	Electric
	8·1	19±7	20±5	21±5	23	20	17	17	20	23	Undetermined
	7·2	12±5	10±4	11±4	12	11	10	10	11	12	Undetermined

and for magnetic dipole radiation

$$R=\frac{1+a_2}{1+a_2\cos 2\theta}=\frac{1+a_2}{1-a_2}\quad\text{for}\quad\theta=90°.$$

For electric quadrupole radiation

$$R=\frac{(1+a_2+a_4)-\frac{1}{2}a_4\sin^2 2\theta}{1+(a_2+a_4)\cos 2\theta}$$

and the inverse for magnetic quadrupole radiation. Thus if the polar angular distribution of the γ-rays is known the polarization may be predicted as having one of two complementary forms. The azimuthal angular distributions of the photo-protons are then given in terms of R by the expression $1+(R-1)\cos^2\phi$.

The azimuthal angular distributions of the photo-proton tracks were calculated from the polar angular distributions of the corresponding γ-rays measured by Rutherglen *et al.* (1954) for the reaction ^{27}Al(p, γ)^{28}Si, Grant *et al.* (1955) for the reaction ^{23}Na(p, γ)^{24}Mg, and Rutherglen, Deuchars and Wallace (private communication) for the reaction ^{26}Mg(p, γ)^{27}Al. These calculated values are shown in table 1, together with the measured distributions. The measured distributions can be accounted for by these calculations in all cases except for the 10·8 MeV γ-ray from the reaction ^{23}Na(p, γ)^{24}Mg, and, where an assignment of the nature of the radiation had been possible, the distributions are shown in figures 2, 3 and 4.

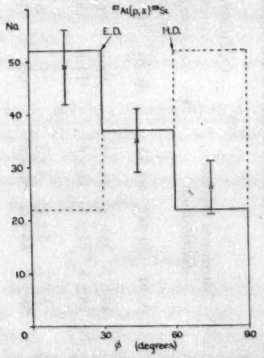

Figure 2. Azimuthal angular distribution of photo-protons ejected by the 10·4 MeV γ-ray from the reaction ^{27}Al(p, γ)^{28}Si. The errors indicated in this and the following figures are standard deviations. The continuous and broken lines represent the calculated distributions assuming electric dipole and magnetic dipole radiations respectively.

§ 5. Parity Assignments

For all three of the reactions the gamma rays which have been studied are anisotropic. Since the resonance energy is in no case sufficiently high to make it likely that d-wave protons are responsible for the reaction, we may therefore assume that all the reactions are due to p-wave protons. The polar angular distribution measurements of Rutherglen *et al.* (1954), Grant *et al.* (1955) and

Rutherglen, Deuchars and Wallace (private communication) indicate a dipole transition, and the present measurements an electric rather than a magnetic radiation, in each case. Thus each reaction involves a double change of parity and therefore the parity of the ground state of the initial nucleus and of the final excited state of the product nucleus will be the same.

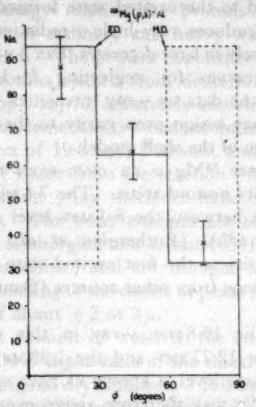

Figure 3. Azimuthal angular distribution of photo-protons ejected by the 7·6 MeV γ-ray from the reaction $^{26}Mg(p, \gamma)^{27}Al$.

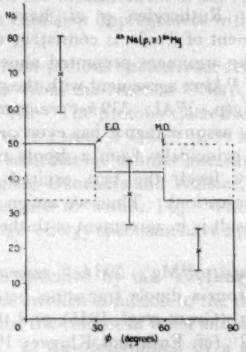

Figure 4. Azimuthal angular distribution of photo-protons ejected by the 10·8 MeV γ-ray from the reaction $^{23}Na(p, \gamma)^{24}Mg$.

We shall now consider each of the reactions in detail.

$^{27}Al(p, \gamma)^{28}Si$; *652 keV resonance.* The 10·5 MeV γ-ray from the reaction arises from a dipole transition between the 12·23 MeV and the 1·8 MeV levels in ^{28}Si (Rutherglen *et al.* 1954) (figure 5). At the 404 keV resonance in this reaction

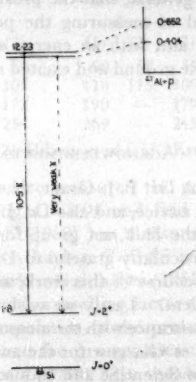

Figure 5.

Rutherglen *et al.* have shown that there is no α-particle emission to the ground state of ^{24}Mg which has spin zero with even parity. Since anisotropic γ-rays are emitted at this resonance it must, therefore, have spin and parity 2^-, 4^- or 1^+, 3^+ according as the ground state parity of ^{27}Al is even or odd. No ground state transition and only a very weak transition to the first excited state at 1·8 MeV is observed and so $J=4^-$ or 3^+ is assigned to the excited state formed at this resonance. Since the 404 kev resonance produces very little γ-radiation to the 1·8 MeV excited level in ^{28}Si this level is unlikely to have J greater than 2 with even parity. Rutherglen *et al.* have given reasons for neglecting $J=1$. The assignment of $J=2^+$ is consistent with all the data on γ-ray intensities. Thus, from the argument presented above, we may assign even parity to the ground state of ^{27}Al in agreement with the prediction of the shell model.

^{26}Mg(p, γ)^{27}Al; 339 *keV resonance*. Since ^{26}Mg is an even–even nucleus, we may assume that it has even parity in its ground state. The 7·6 MeV γ-ray results principally from a dipole transition between the 8·5 MeV level and the 0·84 MeV level, the first excited state in ^{27}Al (Rutherglen *et al.*, private communication). Thus we assign even parity to the first excited state of ^{27}Al. This result is in agreement with the indications from other sources (Daniel *et al.* 1953).

^{23}Na(p, γ)^{24}Mg; 593 *keV resonance*. The 10·8 MeV γ-ray in this reaction arises from a dipole transition between the 12·27 MeV and the 1·38 MeV levels in ^{24}Mg, (Grant *et al.* 1955), and the 1·38 MeV level is known to have spin and parity 2^+ (cf. Endt and Kluyver 1954). We may therefore assign even parity to the ground state of ^{23}Na. This is again in agreement with the accepted assignment.

It has not been found possible to explain the discrepancy between the measured angular distribution for the photo-protons produced by the 10·8 MeV γ-ray from ^{23}Na and the distribution as calculated from the polar angular distribution of the γ-ray. The difficulty may arise, in part, from the very low γ-ray yield in this reaction and the consequent increase in the importance of background effects.

The results indicate, in general, that the present method is an effective and comparatively rapid method of measuring the polarization of γ-rays having a moderate or high intensity, and with an energy above about 7 MeV, and hence of assigning the parities of the ground and excited states of nuclei.

Acknowledgments

The authors wish to thank Dr. P. J. Grant, who suggested these experiments, for invaluable assistance and advice, and also Dr. J. G. Rutherglen, Mr. A. Ward, and the other members of the H.T. set group for considerable help during the exposures. We are also particularly grateful to Dr. H. Muirhead for his advice and supervision during the course of this work, and to Professor P. I. Dee for his interest and encouragement. Lastly we wish to thank Miss W. Green and Miss M. McCann for their assistance with the measurements. One of us (I. S. H.) is grateful to the University of Glasgow for the award of a studentship, and one (D. S.) to the Department of Scientific and Industrial Research for the award of a maintenance grant.

APPENDIX

Range–Energy Relation for Protons in an Emulsion Impregnated with Water

Several authors have reported measurements and calculations bearing on the range–energy relation for protons in nuclear emulsions containing different amounts of ordinary and heavy water. These results do not show complete agreement. The present experiment involved the measurement of the ranges of photoprotons ejected from deuterium, in an emulsion impregnated with heavy water, by γ-rays of accurately known energy.

Measurements were made of the range of photo-protons ejected from deuterium by γ-rays of 10·8 Mev, 8·09 Mev, and 7·01 Mev from the reaction $^{23}Na(p,\gamma)^{24}Mg$ and of 7·6 Mev from the reaction $^{26}Mg(p,\gamma)^{27}Al$. The protons ejected at 90° to the incident γ-ray therefore have energies of 4·3 Mev, 2·93 Mev, 2·39 Mev and 2·7 Mev. The γ-ray energies are based on scintillation counter measurements (Flack, Rutherglen and Grant 1954, Rutherglen, Deuchars and Wallace, private communication) and are thought to be accurate to within 1%. The ranges corresponding to the centre of peaks in the range–energy spectrum have a probable error of about ± 2 or 3μ.

The amount of water in the emulsion is specified by the 'swelling factor' C, where C is the ratio of the thickness of the swollen emulsion to the thickness of the original dry emulsion. It is assumed that the volume of water and emulsion add without any overall change in density. C was determined by a series of measurements made at specified points on the emulsion using a cover plate and a micrometer screw gauge. The values obtained for C have a probable error of about $\pm 4\%$.

The results are presented in table 2 in which the calculated values of Gibson *et al.* (1952) and of Krohn and Schrader (1952) are shown for comparison. Those obtained from the present work have been extrapolated from 4·3 Mev to 5 Mev and from 2·39 Mev to 2 Mev for convenience of presentation.

Table 2. Ranges (microns)

Energy	$C=2{\cdot}8$			$C=3{\cdot}3$			$C=3{\cdot}8$		
(Mev)	(1)	(2)	(3)	(1)	(2)	(3)	(1)	(2)	(3)
2	60	57·5	54	60	58	56	64	59	57
3	115	112	105	116	115	109	125	117	112
4	185	—	172	190	—	179	197	—	185
5	263	—	254	269	—	265	284	—	277

(1) Present work; (2) Gibson *et al.*; (3) Krohn and Schrader.

Gibson *et al.* (1952) have also measured the range of 2·0 Mev and 2·4 Mev protons in an emulsion having $C=3{\cdot}94$ and find close agreement with their own calculated curve. Hough (1950) has measured the range of 2·0 Mev and 2·4 Mev protons in an emulsion having $C=3{\cdot}85$ and obtains values in precise agreement with the present work. Goldhaber (1951) has measured the range of protons of the same energies with a swelling factor $C=1{\cdot}7$ and obtains values in rough agreement with an extrapolation of the present work although a detailed comparison is not possible since the present measurements only extend down to $C=2{\cdot}8$. Waffler and Younis (1949) have measured ranges at a number of proton energies, but obtain values considerably larger than those of other workers.

References

Bethe, H. A., 1947, *Elementary Nuclear Theory* (New York : John Wiley).
Bethe, H. A., and Bacher, R. F., 1936, *Rev. Mod. Phys.*, **8,** 122.
Bonnet, A., 1954, *J. Phys. Radium*, **15,** 587.
Dainton, A. D., Gattiker, A. R., Lock, W. O., 1951, *Phil. Mag.*, **42,** 396.
Daniel, H., Koester, L., and Mayer-Kuchuk, T., 1953, *Z. Naturf.*, **8a,** 447.
Endt, P. M., and Kluyver, J. C., 1954, *Rev. Mod. Phys.*, **26,** 103.
Fagg, L. W., and Hanna, S. S., 1953, *Phys. Rev.*, **92,** 372.
Flack, F. C., Rutherglen, J. G., and Grant, P. J., 1954, *Proc. Phys. Soc.* A, **67,** 973.
Gibson, W. M., Grotdal, T., Orlin, J. J., and Trumpy, B., 1952, *Phil. Mag.*, **43,** 457.
Goldhaber, G., 1951, *Phys. Rev.*, **81,** 930.
Grant, P. J., Rutherglen, J. G., Flack, F. C., and Hutchinson, G. W., 1955, *Proc. Phys. Soc.* A, **68,** 369.
Hamilton, D. R., 1948, *Phys. Rev.*, **74,** 782.
Hough, P. V. C., 1950, *Phys. Rev.*, **80,** 1069.
Hughes, I. S., and Grant, P. J., 1954, *Proc. Phys. Soc.* A, **67,** 481.
Krohn, V. E., and Schrader, E. F., 1952, *Phys. Rev.*, **86,** 393.
Muirhead, E. G., and Mather, K. B., 1954, *Aust. J. Phys.*, **7,** 527.
Phillips, K., 1953, *Metropolitan Vickers Research Report.*
Rutherglen, J. G., Grant, P. J., Flack, F. C., and Deuchars, W. M., 1954, *Proc. Phys. Soc.* A, **67,** 101.
Tzara, C., 1954, *C.R. Acad. Sci., Paris.*, **239,** 44.
Waffler, H., and Younis, S., 1951, *Helv. Phys. Acta*, **24,** 483.
Wilkinson, D. H., 1952, *Phil. Mag.*, **43,** 659.

The Effect of Finite Nuclear Size on Electron Pair Production

By E. H. S. BURHOP
Physics Department, University College, London

MS. received 3rd October 1955

Abstract. Calculations have been carried out of the energy and angular distribution of the electrons produced in the process of pair production by incident quanta using Born's approximation and assuming different forms for the distribution of electric charge on the nucleus.

The effect of the finite charge distribution is large for large angle pairs produced by quanta of energy above 20 MeV, but there are only small differences between the effects to be expected for different distributions.

§ 1. Introduction

The finite extension of the nuclear charge distribution will influence the cross section for the production of electron pairs by γ-rays and a rough estimate of the magnitude of this effect made by Hough (1948) showed that it can become large if one member of the pair is emitted at a comparatively large angle to the direction of the incident quantum. In view of the possibility of the detection of this effect owing to the development of high energy electron accelerators, the previous calculations of the effect of finite nuclear size on bremsstrahlung production (Biel and Burhop 1955, to be referred to as I) have been extended to the discussion of pair production.

§ 2. Theory

As in the case of the bremsstrahlung calculation, Born's approximation has been used. The effect of the finite extension of the nuclear charge is then represented by multiplying the Bethe–Heitler formula for the differential cross section for pair production by γ-rays incident on a point charge (Heitler 1954, p. 257) by a quantity $|F(q)|^2$ where q is the magnitude of the momentum transmitted to the nucleus and

$$F(q)=\frac{4\pi}{Ze}\int_0^\infty \rho(r)\frac{\sin\kappa r}{\kappa r}r^2dr$$

is the form factor for a nucleus of charge Z, and is determined by the distribution of nuclear charge density $\rho(r)$, and $\kappa\hbar=q$.

Three forms of nuclear charge distribution have been used in the present calculation, viz.

(i) *Uniform spherical nucleus*:

$$\rho=\rho_0, \qquad r<R;$$
$$\rho=0, \qquad r>R;$$
$$R=1{\cdot}20\times10^{-13}A^{1/3}\text{ cm}.$$

(ii) *Uniform spherical shell* of radius $R=0{\cdot}924\times10^{-13}A^{1/3}$ cm.

(iii) *Uniform spherical nucleus with exponential fall-off near boundary (two parameter distribution)*:

$$\rho=\rho_0,\quad r<R;$$
$$\rho=\rho_0\exp\{-(r-R)/R_0\},\quad r>R;$$
$$R=0{\cdot}995\times10^{-13}A^{1/3}\text{ cm};$$
$$R_0/R=1/7.$$

The expressions for $F(q)$ in these cases are given in I.

These values of the radii are chosen as those which best fit the data on the elastic scattering of 16 MeV electrons in the case of (i) and (ii) while (iii) is chosen to fit the data on high energy elastic scattering by gold as well.

The differential cross section for pair production in which the electron is ejected in a direction θ_- to the incident quantum per unit solid angle and per unit energy range of the electron, was calculated by integrating the modified Bethe–Heitler formula over the angles θ_+, ϕ_+ which specify the direction of ejection of the positron.

§ 3. Angular Distribution of the Electrons of the Pair

The integrations that have to be performed are of the same type as those in the earlier bremsstrahlung calculation. If k, E_+, E_- are respectively the energies (in units of mc^2) of the incident quantum and of the positron and electron, and if p_+, p_- are the momenta of the positron and the electron (in units of mc), the approximation $E_+, E_-\gg1$ has been made so that the relations $E_+=p_+$, $E_-=p_-$ can be used. Writing $\gamma=E_+/E_-$, $\sigma=\{\gamma^2+4(1+\gamma)\sin^2\frac{1}{2}\theta_-\}^{1/2}$ the cross section $d\Phi_-$ for pair production in which the electron is ejected in a solid angle $d\omega_-$ in a direction making an angle θ_- to the direction of the incident quantum and having energy between E_- and E_-+dE_- is obtained in the following form:

$$d\Phi_-=\frac{Z^2r_0^2}{137k^3}\frac{d\omega_-\,dE_-}{4\pi}\left[\frac{(1+\gamma^2)C^2}{S^4}\ln\frac{2\gamma k}{1+\gamma}F\left(\frac{2kRS}{r_C(1+\gamma)}\right)\right.$$
$$+f_0+\alpha_1\left(\frac{kR}{r_C(1+\gamma)}\right)^2f_1+\alpha_2\left(\frac{kR}{r_C(1+\gamma)}\right)^4f_2$$
$$\left.+\alpha_3\left(\frac{kR}{r_C(1+\gamma)}\right)^6f_3+\alpha_4\left(\frac{kR}{r_C(1+\gamma)}\right)^8f_4+\dots\right]\qquad\dots\dots(1)$$

where $r_0=e^2/mc^2$, the classical electron radius, $r_C=\hbar/mc$, the Compton wavelength, $C=\cos\frac{1}{2}\theta_-$, $S=\sin\frac{1}{2}\theta_-$, F is the form factor defined above, α_1, α_2, α_3, α_4 are constants which depend on the shape of the nuclear charge distribution and whose values for the charge distributions assumed in this calculation have been given in paper I, and the quantities f take the following forms:

$$f_0=-\frac{(1+\gamma^2)C^2}{S^4}\ln(1+\gamma)+\frac{\gamma(5-2\gamma)}{4S^4}+\frac{\gamma^2-2\ln(1+\gamma)}{S^2}$$
$$+\frac{\gamma^2}{8S^6}\left\{\frac{\gamma(2S^2+\gamma)}{\sigma^2}-1\right\}-\frac{\{3\sigma^2-\gamma(2+\gamma)\}(1+\gamma)}{2\sigma^3S^2}\ln\frac{\sigma-\gamma}{\sigma+\gamma}.$$

$$f_1=4(1+\gamma)^2\ln(1+\gamma)+\frac{8\gamma C^2}{S^2}-\frac{2\gamma(1+\gamma)^2(\gamma+2S^2)}{\sigma^2S^2}$$
$$-\frac{4(1+\gamma)^2\{-\gamma+2(1+\gamma)S^2\}}{\sigma^3}\ln\frac{\sigma-\gamma}{\sigma+\gamma}.$$

$$f_2 = \frac{4\gamma^2(1+\gamma^2)}{S^2} + 16\gamma(2-\gamma)S^2 + 16\gamma(2+\gamma^2).$$

$$f_3 = \frac{16}{3}\frac{\gamma^4(1+\gamma^2)}{S^2} + 16\gamma^2\left(5 + \frac{14}{3}\gamma + 5\gamma^2 + \frac{10}{3}\gamma^3\right)$$
$$+ \frac{64\gamma}{3}(14 - 4\gamma + \gamma^2 + 4\gamma^3)S^2 - 128\gamma\left(3 - \frac{2\gamma^2}{3}\right)S^4.$$

$$f_4 = \frac{32}{3}\frac{\gamma^6(1+\gamma^2)}{S^2} + \frac{128\gamma^4}{3}(5 + 7\gamma + 5\gamma^2 + 2\gamma^3)$$
$$+ \frac{64\gamma^2}{3}(33 + 64\gamma + 57\gamma^2 + 24\gamma^3 + 4\gamma^4)S^2 + \frac{256\gamma}{3}(15 - 2\gamma^2 - 6\gamma^3 - 2\gamma^4)S^4$$
$$- \frac{128\gamma}{3}(30 + 9\gamma - 12\gamma^2 - 22\gamma^3)S^6. \qquad \ldots\ldots(2)$$

The quantities $f_0 \ldots f_4$ can in fact be obtained from the quantities $h_0 \ldots h_4$ of the bremsstrahlung calculation by replacing γ by $-\gamma$ throughout. At high energies and provided γ is not too small the terms involving the f's in (1) can be neglected in comparison with the first term inside the square bracket. In these circumstances the effect of the finite size connection is simply to multiply the point nucleus cross section by $F\{2kRS/r_C(1+\gamma)\}$.

§ 4. Numerical Calculations

The quantities f are given in the table for a series of values of γ and θ_-. From these quantities the distribution in angle and energy of the ejected electron for incident quanta of any energy can be readily obtained by calculating $\ln\{2\gamma k/(1+\gamma)\}$ and using equation (1) with the appropriate values of α_1, α_2, α_3, α_4 as given in table 1 of paper I.

θ_-	γ	f_0	f_1	f_2	f_3	f_4
10°	0·2	$-5{\cdot}743\times10^{3}$	$-9{\cdot}390\times10$	$2{\cdot}848\times10$	5·536	0·8726
	0·5	$-9{\cdot}995\times10^{3}$	$-7{\cdot}488\times10$	$1{\cdot}8265\times10^{2}$	$9{\cdot}188\times10$	$5{\cdot}747\times10$
	1·0	$-2{\cdot}3060\times10^{4}$	$-1{\cdot}155\times10$	$1{\cdot}1013\times10^{3}$	$1{\cdot}6946\times10^{3}$	$3{\cdot}649\times10^{3}$
	2·0	$-1{\cdot}0199\times10^{5}$	$-2{\cdot}486\times10^{2}$	$1{\cdot}0724\times10^{4}$	$6{\cdot}009\times10^{4}$	$4{\cdot}873\times10^{5}$
	5·0	$-9{\cdot}360\times10^{5}$	$-3{\cdot}990\times10^{3}$	$3{\cdot}444\times10^{5}$	$1{\cdot}1638\times10^{7}$	$5{\cdot}816\times10^{8}$
	10·0	$-4{\cdot}854\times10^{6}$	$-2{\cdot}0220\times10^{4}$	$5{\cdot}335\times10^{6}$	$7{\cdot}154\times10^{8}$	$1{\cdot}429\times10^{11}$
15°	0·2	$-5{\cdot}719\times10^{2}$	0·2497	$1{\cdot}6393\times10$	5·406	1·2676
	0·5	$-1{\cdot}6552\times10^{3}$	$-1{\cdot}3348\times10$	$9{\cdot}157\times10$	$6{\cdot}272\times10$	$4{\cdot}656\times10$
	1·0	$-4{\cdot}339\times10^{3}$	2·939	$5{\cdot}178\times10^{2}$	$9{\cdot}195\times10^{2}$	$2{\cdot}129\times10^{3}$
	2·0	$-1{\cdot}985\times10^{4}$	$-9{\cdot}434\times10$	$4{\cdot}888\times10^{3}$	$2{\cdot}898\times10^{4}$	$2{\cdot}388\times10^{5}$
	5·0	$-1{\cdot}837\times10^{5}$	$-1{\cdot}6503\times10^{3}$	$1{\cdot}5476\times10^{5}$	$5{\cdot}316\times10^{6}$	$2{\cdot}655\times10^{8}$
	10·0	$-9{\cdot}537\times10^{5}$	$-8{\cdot}399\times10^{3}$	$2{\cdot}388\times10^{6}$	$3{\cdot}224\times10^{8}$	$6{\cdot}434\times10^{10}$
20°	0·2	$-6{\cdot}218\times10$	$1{\cdot}6262\times10$	$1{\cdot}2220\times10$	5·875	1·941
	0·5	$-4{\cdot}006\times10^{2}$	9·216	$5{\cdot}982\times10$	$5{\cdot}375\times10$	$4{\cdot}736\times10$
	1·0	$-1{\cdot}2805\times10^{3}$	$1{\cdot}2058\times10$	$3{\cdot}138\times10^{2}$	$6{\cdot}511\times10^{2}$	$1{\cdot}6356\times10^{3}$
	2·0	$-6{\cdot}152\times10^{3}$	$-3{\cdot}732\times10$	$2{\cdot}845\times10^{3}$	$1{\cdot}811\times10^{4}$	$1{\cdot}524\times10^{5}$
	5·0	$-5{\cdot}7570\times10^{4}$	$-8{\cdot}2934\times10^{2}$	$8{\cdot}838\times10^{4}$	$3{\cdot}104\times10^{6}$	$1{\cdot}549\times10^{8}$
	10·0	$-2{\cdot}995\times10^{5}$	$-4{\cdot}260\times10^{3}$	$1{\cdot}3561\times10^{6}$	$1{\cdot}849\times10^{8}$	$3{\cdot}683\times10^{10}$

θ_-	γ	f_0	f_1	f_2	f_3	f_4
30°	0·2	$1·1791\times10$	$1·4673\times10$	9·398	7·527	4·281
	0·5	$-3·401\times10$	$1·930\times10$	$3·746\times10$	$5·052\times10$	$6·168\times10$
	1·0	$-2·075\times10^2$	$2·058\times10$	$1·685\times10^2$	$4·673\times10^2$	$1·3910\times10^3$
	2·0	$-1·1473\times10^3$	6·815	$1·3863\times10^3$	$1·039\times10^4$	$9·213\times10^4$
	5·0	$-1·1065\times10^4$	$-2·401\times10^2$	$4·096\times10^4$	$1·526\times10^6$	$7·601\times10^7$
	10·0	$-5·7868\times10^4$	$-1·3008\times10^3$	$6·193\times10^5$	$8·669\times10^7$	$1·719\times10^{10}$
45°	0·2	4·990	8·410	8·508	$1·0663\times10$	$1·3377\times10$
	0·5	2·179	$1·5705\times10$	$2·829\times10$	$5·487\times10$	$6·033\times10$
	1·0	$-1·6548\times10$	$2·177\times10$	$1·0497\times10^2$	$4·013\times10^2$	$3·920\times10^2$
	2·0	$-1·989\times10^2$	$2·789\times10$	$7·383\times10^2$	$7·078\times10^3$	$6·860\times10^4$
	5·0	$-2·048\times10^3$	$2·438\times10$	$1·988\times10^4$	$8·281\times10^5$	$4·120\times10^7$
	10·0	$-1·0840\times10^4$	$1·651\times10$	$2·920\times10^5$	$4·313\times10^7$	$8·477\times10^9$
60°	0·2	1·892	5·155	8·634	$1·3377\times10$	$2·246\times10$
	0·5	2·305	$1·1268\times10$	$2·600\times10$	$6·033\times10$	$1·6425\times10^2$
	1·0	−2·217	$1·909\times10$	$8·400\times10$	$3·920\times10^2$	$1·8900\times10^3$
	2·0	$-5·154\times10$	$3·420\times10$	$5·120\times10^2$	$6·053\times10^3$	$6·395\times10^4$
	5·0	$-5·841\times10^2$	$1·1765\times10^2$	$1·250\times10^4$	$5·890\times10^5$	$2·931\times10^7$
	10·0	$-3·154\times10^3$	$4·781\times10^2$	$1·776\times10^5$	$2·799\times10^7$	$5·448\times10^9$
90°	0·2	0·4132	2·473	9·741	$1·3244\times10$	$5·127\times10$
	0·5	0·9117	6·447	$2·650\times10$	$5·950\times10$	$3·158\times10^2$
	1·0	0·9208	$1·4068\times10$	$7·200\times10$	$3·947\times10^2$	$2·875\times10^3$
	2·0	−3·869	$3·565\times10$	$3·520\times10^2$	$5·632\times10^3$	$6·690\times10^4$
	5·0	$-7·536\times10$	$1·827\times10^2$	$7·240\times10^3$	$4·312\times10^5$	$2·138\times10^7$
	10·0	$-4·478\times10^2$	$8·053\times10^2$	$9·648\times10^4$	$1·744\times10^7$	$3·322\times10^9$
120°	0·2	0·3036	1·5041	$1·1070\times10$	3·609	$6·197\times10$
	0·5	0·4439	4·430	$2·867\times10$	$3·656\times10$	$4·252\times10^2$
	1·0	1·0424	$1·1322\times10$	$7·067\times10$	$3·742\times10^2$	$3·901\times10^3$
	2·0	1·958	$3·463\times10$	$2·987\times10^2$	$5·769\times10^3$	$7·003\times10^4$
	5·0	−2·397	$2·029\times10^2$	$5·447\times10^3$	$3·900\times10^5$	$1·900\times10^7$
	10·0	$-4·785\times10$	$9·137\times10^2$	$6·923\times10^4$	$1·410\times10^7$	$2·631\times10^9$
150°	0·2	0·06182	1·1136	$1·2081\times10$	−9·475	$4·394\times10$
	0·5	0·2921	3·575	$3·054\times10$	5·483	$4·453\times10^2$
	1·0	0·9375	$1·0033\times10$	$7·150\times10$	$3·380\times10^2$	$4·654\times10^3$
	2·0	2·938	$3·336\times10$	$2·777\times10^2$	$5·959\times10^3$	$6·951\times10^4$
	5·0	$1·3074\times10$	$2·100\times10^2$	$4·723\times10^3$	$3·802\times10^5$	$1·806\times10^7$
	10·0	$4·050\times10$	$9·556\times10^2$	$5·843\times10^4$	$1·287\times10^7$	$2·366\times10^9$
180°	0·2	0·04546	1·0053	$1·2454\times10$	$-1·5539\times10$	$2·965\times10$
	0·5	0·2548	3·333	$3·125\times10$	−8·917	$4·349\times10^2$
	1·0	0·8965	9·566	$7·200\times10$	$3·200\times10^2$	$4·928\times10^3$
	2·0	3·083	$3·302\times10$	$2·720\times10^2$	$6·037\times10^3$	$6·852\times10^4$
	5·0	$1·603\times10$	$2·119\times10^2$	$4·520\times10^3$	$3·788\times10^5$	$1·778\times10^7$
	10·0	$5·800\times10$	$9·670\times10^2$	$5·544\times10^4$	$1·255\times10^7$	$2·294\times10^9$

By including terms up to f_4 it is possible to obtain the distribution of the ejected electrons in an angular range up to 120° for an incident quantum of energy 50 MeV and up to 60° for an incident quantum of energy 100 MeV.

§ 5. Results of the Calculation

Figures 1–3 show the effect of the nuclear charge distribution of the electrons on pairs produced by incident γ-ray quanta of energy 10, 20, 50 and 100 MeV.

The effect consists of a marked decrease of the proportion of electrons ejected at a large angle. Since however the proportion of large angle pairs is so small this will be a difficult effect to measure although it should be possible with the incident gamma-ray intensities now available from electron accelerators.

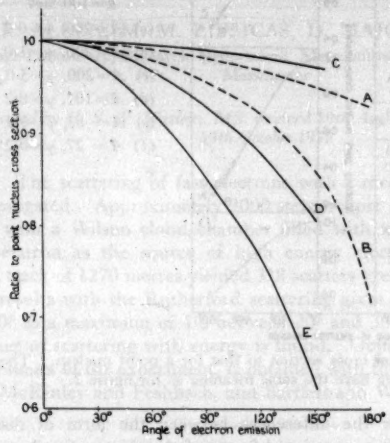

A k=10 MeV, γ=1·0
B k=10 MeV, γ=0·2
C k=20 MeV, γ=5·0
D k=20 MeV, γ=1·0
E k=20 MeV, γ=0·2

Figure 1. Ratio of differential cross section for electron pair production to that from a point nucleus for different angles of emission of the electron. These curves refer to a uniform spherical distribution of charge for the case A=200, radius=$1{\cdot}2\times10^{-13}A^{1/3}$. k is the incident gamma-ray energy and γ=the ratio of the positron to electron energy. At these energies the curves are insensitive to the detailed shape of the charge distribution.

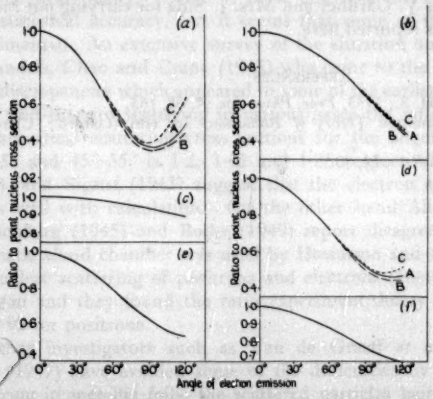

k=50 MeV
(*a*) A=200, γ=0·2
(*b*) A=200, γ=1·0
(*c*) A=200, γ=5·0
(*d*) A=107, γ=0·2
(*e*) A= 63, γ=0·2
(*f*) A= 27, γ=0·2

Figure 2. Ratio of differential cross section for electron pair production to that from a point nucleus for different angles of emission of the electron. A, spherical charge distribution; B, spherical shell; C, two-parameter distribution. Curves A, B, and C are indistinguishable for (*c*), (*e*) and (*f*).

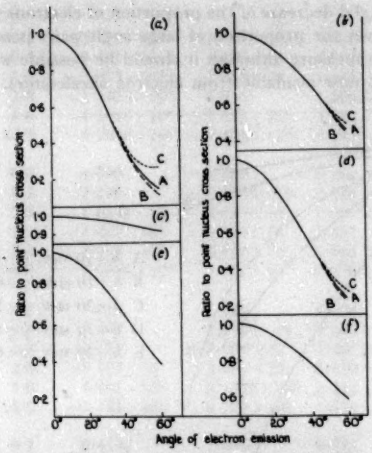

k=100 MeV
(*a*) A=200, γ=0·2
(*b*) A=200, γ=1·0
(*c*) A=200, γ=5·0
(*d*) A=101, γ=0·2
(*e*) A= 63, γ=0·2
(*f*) A= 27, γ=0·2

Figure 3. Ratio of differential cross section to that for a point nucleus. The markings on the curve have the same meaning as for figure 2.

Unfortunately however the differences between the form of distribution to be expected for the different assumed forms of the charge distribution are so small that it will scarcely be possible to use this method to obtain any more detailed information about the nuclear charge distribution than can be obtained from a study of the elastic scattering of fast electrons.

Acknowledgments

I am indebted to Miss V. Gardner and Mrs. J. Sida for carrying out most of the numerical calculations reported here.

References

Biel, S. J., and Burhop, E. H. S., 1955, *Proc. Phys. Soc.* A, **68**, 165.
Heitler, W., 1954, *The Quantum Theory of Radiation*, 3rd edn (Oxford: Clarendon Press).
Hough, P. V. C., 1948, *Phys. Rev.*, **74**, 80.

The Scattering of Fast Charged Particles
I : On the Single Scattering of 13·5 MeV Electrons in Xenon

By K. R. ALLEN, M. M. LIPSICAS, D. MAJOR and K. PHILLIPS
High Voltage Laboratory, Research Department, Metropolitan-Vickers Electrical Co. Ltd., Manchester

Communicated by H. S. W. Massey; *MS. received* 10*th August* 1955 *and in amended form* 19*th October* 1955

Abstract. The scattering of fast electrons with a mean energy of 13·5 MeV has been investigated. Approximately 3000 stereoscopic pairs of photographs were obtained with a Wilson cloud chamber filled with xenon and helium using a 20 MeV betatron as the source of high energy electrons. A total length of corrected track of 1270 metres yielded 318 scatters greater than 5°. Comparison of these results with the Rutherford scattering gives a ratio which varies from unity at 0° to a maximum of 1·6 between 20° and 30°. An inverse square law dependence of scattering with energy is found. General agreement, within the statistical limits of the experiment, is obtained with the theoretical cross sections of Curr, McKinley and Feshbach, and Bartlett and Watson.

§ 1. Introduction

Within the last two decades a considerable amount of experimental data on the scattering of electrons in gases has become available. Perhaps the most noticeable feature about all these results is the considerable disagreement between the separate experiments and also the variance with theory. Some of these discrepancies may be due, partially, to poor statistical accuracy, but it seems that some of the difficulties are purely experimental. An extensive survey of the situation up to 1945 has been given by Randels, Chao and Crane (1945) who came to the conclusion that the very large discrepancies which appeared in some of the earlier work are not significant. They find that for scattering in various gases the ratio of the experimental to the theoretical scattering cross sections for the angular intervals of 25°–35°, 35°–45° and 45°–55° is 1·2, 1·45 and 1·25 respectively. Champion and Roy (1948), and Sigrist (1943) suggest that the electron scattering at large angles agrees well with calculation. On the other hand Alichanian, Alichanow and Weissenberg (1945) and Bothe (1949) report disagreement with theory. An automatic cloud chamber was used by Howatson and Atkinson (1951) to study the nuclear scattering of positrons and electrons (energy approximately 1 MeV) in argon and they found the ratio experiment/theory to be 1·02 for electrons and 0·92 for positrons.

Other investigators such as Van de Graaff *et al.* (1946) and Beuchner *et al.* (1947) have avoided some of the difficulties by confining themselves to scattering in metallic foils, the scattered particles being detected by means of ionization chambers or counters. More recently a very elegant experiment studying the nuclear scattering of 15·7 MeV electrons in foils has been described

by Lyman, Hanson and Scott (1951). They find that the results are in good agreement with theory if the nuclear charge is assumed to be distributed uniformly throughout the nucleus. Scattering in foils up to 150 MeV has been investigated by Hofstadter, Fechter and McIntyre (1953). Although the cloud chamber method cannot hope to compete in statistical accuracy with counter experiments it possesses certain important advantages. For instance, scattering in gases can be investigated and there is no need to apply the Wentzel (1922) criterion for scattering. Each scatter can be assumed to be single as each track can be observed, and there is little likelihood of confusion with background effects. Some of the discrepancies in the cloud chamber method are undoubtedly due to difficulties in sampling the gas in the chamber and in measuring the absolute angle of scattering. Techniques have been developed by the authors in an attempt to overcome some of these problems and it is the purpose of this paper to describe work which extends the previous cloud chamber work to higher energies.

§ 2. Experimental Arrangement

A 20 MeV betatron was used as the source of high-energy electrons. The accelerated particles were scattered out of the doughnut by means of a target welded to the end of the electron gun. The fast electrons were deflected to one side by the stray betatron guide field and were collimated into a narrow beam by a series of lead bricks and finally directed into the cloud chamber by a magnetic channel. This allowed electrons with energies from 10 to 18 MeV to enter the chamber. The bremsstrahlung beam which comes out of the betatron in the forward direction was blocked off. In order to reduce the stray x-ray background to a workable limit an 8-foot thick wall of barytes concrete bricks was constructed between the betatron and the chamber. The cloud chamber was 28 cm diameter by 8 cm deep and was mounted between a pair of Helmholtz coils, each coil consisting of a series arrangement of three flat 'pancakes' made of $\frac{3}{8}$ in. wide by 0·032 in. thick copper strip, insulated with varnished paper. The coils were energized from the 500 volt, 60 amp d.c. mains and produced a magnetic field of 1200 oersteds in the median plane of the chamber. This field was uniform to within 2% across the sensitive volume of the chamber.

The system used for recording the tracks was similar to the one described by Allen *et al.* (1953). Briefly, it consists of two 35 mm cameras mounted as a stereoscopic pair on an accurately machined support. Visual observations were made at intervals during a series of photographs to check the track quality. The importance of good track quality cannot be over-emphasized since scatters can easily be missed if the tracks are diffuse. The light source consisted of two flash tubes type LSD 15 and cylindrical glass lenses mounted on opposite sides of the chamber. The beam of light was restricted to a depth of 4·5 cm by a system of slits and sufficient light was available for photography with a lens aperture of F/4. The film was located by means of a fiduciary line etched on the glass clamping plate in the camera.

In all cloud chamber experiments the gas filling must be chosen so that there is a good yield of large angle deflections but that the measurement of angle and curvature of the tracks is not seriously affected by multiple scattering. The chamber filling used in this experiment was approximately 20% xenon and 80% helium, which introduced a multiple scattering error of less than 10%.

The gas mixture was contained in a 2 litre reservoir and could be transferred to the chamber with a glass Töppler pump. Before filling, the chamber was evacuated to remove traces of air. The alcohol–water mixture was introduced via a liquid trap. For cleaning purposes the complete filling could be quickly transferred to the reservoir.

The concentration of xenon in the chamber was checked every few days by analysing a small gas sample with a mass spectrometer (Type M.S. 3). It was found that the relative proportions of each gas remained practically constant over a considerable period. By using this sampling method the contents of the chamber could be determined with an accuracy to one per cent. This method was adopted since the estimation of the concentration of the scattering gas is liable to be in error if pressure measurements alone are used.

The betatron and cloud chamber cycle was as follows: (*a*) The betatron magnet was energized and the x-ray output obtained by switching on the injector gun filament, all the other controls having been set previously at their optimum position. (*b*) The expander modulator was switched off by a single shot control circuit. (*c*) The cloud chamber magnetic field was switched on. (*d*) The cloud chamber was triggered. (*e*) The expander modulator was pulsed. (*f*) The magnetic field and the betatron were switched off. (*g*) The film was advanced in each camera. (*h*) The chamber was cleaned by several slow expansions. After each cleaning cycle the cloud chamber was allowed one minute waiting time to return to thermal equilibrium. This process was assisted by a water-cooled metal pad attached to the outside wall of the chamber. The complete cycle was repeated every two minutes and it was found possible to take up to 150 photographs in a day. To avoid overheating the chamber and consequent thermal distortion, it was necessary to cool the magnetic field coils with forced air. The power consumption of these coils was 30 kilowatts.

§ 3. Analysis of the Photographs

In order to avoid any errors due to optical distortion, the films were re-projected through the stereoscopic pair of cameras used for taking the photographs. They were mounted on a vertical stand in a position identical to that which they occupied during photography. The images of the tracks were projected on a white plastic screen mounted on a ball and socket joint. This joint could be magnetically clamped at the required angle of tilt. The reprojection system was illuminated from a high pressure mercury lamp. This served both cameras by means of a suitable arrangement of mirrors and condenser lenses. The illumination was sufficient to permit scanning of tracks in a normally lit room provided no stray light was allowed to fall on the projection table. The apparent brightness of the stereoscopic images could be increased by viewing successively each member of a pair. A rotating disc which allowed alternate images to be projected was fitted below the cameras. When the speed of rotation of the disc was correctly adjusted very little flicker was observed and it was easy to detect non-coincidence of the stereoscopic images. To increase the rate of scanning a duplicate projector was used. The optical system of the second projector was carefully compared with the first and no detectable differences were observed.

Unless a rigid set of rules for track acceptance is adopted, considerable errors are likely to arise. The first requisite for satisfactory scanning is that only sharply defined tracks with a minimum of distortion should be accepted. This criterion

is difficult to apply and becomes a matter of personal judgment since the observer tends to accept bad track quality when confronted by a large angle scatter. The following additional rules were also applied. (i) Only scatters which occurred at a distance greater than 5 cm from the edge of the chamber were accepted. Although this rule reduced the total track length it avoided the difficulty of measuring the true scattering angle and energy on a portion of track less than 5 cm in length. It also eliminated effects due to thermal distortion which often occurs at the edge of the chamber. (ii) Accepted tracks had to show no sign of distortion, whether due to local alpha particles or thermal distortion. This distortion could be detected by observing the shape of adjacent tracks and could be readily distinguished from true scattering. (iii) All tracks had to appear on both members of a stereoscopic pair of photographs. (iv) Only tracks within the radius limits of 30 to 50 cm were accepted. (v) Scatters observed to be less than 5° were rejected.

The photographs were projected to normal size and the tracks observed stereoscopically. The length of track was measured with a map measurer and the curvature obtained by fitting arcs of circles inscribed on thin Perspex sheets. All the radii were measured in a plane perpendicular to the vertical component of the cloud chamber magnetic field. For convenience of handling, the measuring arcs were grouped on two separate 7 in. square sheets of Perspex, with arcs of 30 to 40 cm in 0·5 cm steps on one, and 40 to 50 cm on the other. It was found that unless great care was taken an observer tended to weight the radii near the edge of each sheet, i.e. on the 30 to 40 cm sheet there was a tendency to read 40 cm rather than change to the other sheet. This would have introduced a peak in the energy distribution at 40 cm radius.

The scattering angles were measured in three dimensions by means of a protractor system shown in figure 1. It consisted of a geometrical protractor, with a fixed orientation relative to the projector framework, which could be placed at any point on the projector table. The latter was tilted until the incident track was aligned stereoscopically. The best fitting arc was then adjusted to coincide with the track and the tangent to this was drawn, at the point of scatter, on the

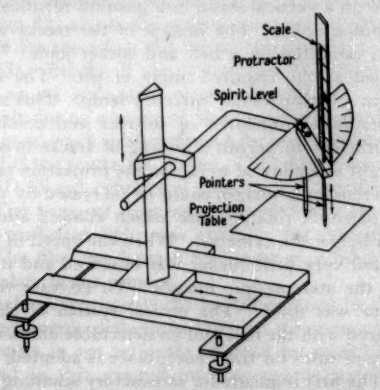

Figure 1. The angle measuring apparatus showing the protractor and vertical scale.

table. The horizontal projected angle between this tangent and a fixed horizontal line was then measured with the protractor. The angular tilt of the table along the tangent was also measured by means of the movable pointer and a vertical scale. This procedure was repeated for the scattered portion of the track. Thus for each scatter, three angles were measured—the projected scattering angle Ω, and the two direction cosines of the tangents at the point of scatter. The true scattering angle could be determined from the spherical trigonometrical formula,

$$\cos\theta = \cos\Omega\cos\phi_1\cos\phi_2 + \sin\phi_1\sin\phi_2 \qquad \ldots\ldots(1)$$

where θ is the true angle of scatter, Ω is the projected angle of scatter, ϕ_1 is the angle between the tangent to the incident track at the point of scatter and the horizontal plane and ϕ_2 is the corresponding angle for the scattered portion of the track.

The accuracy of this method of measuring the true angle of scatter by different observers was checked by repeated measurements on the same scatter and the measured angle was found to agree in each case to within $\pm 0{\cdot}5°$.

In order to correct the number of scatters observed, for those which are not measurable, it is necessary to know the illuminated depth of the chamber. The most satisfactory method was to take height measurements on the stereoscopic images of tracks in the chamber. The apparatus used consisted of an arm pivoted over the projection table. A pointer could be moved to any position along the arm and the vertical height of the projection table could be measured on an attached scale.

From a total number of 3000 stereoscopic pairs of photographs approximately 3000 metres of electron track were scanned. This length reduced to 1270 metres when the 5 cm correction was applied to each track. A length–energy histogram is shown in figure 2 with a mean electron energy of 13·5 Mev. A total number of 318 scatters was observed in the angular interval from 5 to 80°.

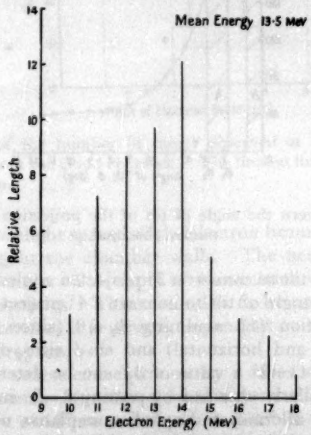

Figure 2. Histogram of the electron track length plotted against the energy, indicating a mean energy of 13·5 Mev.

§ 4. Corrections and Assessment of Experimental Errors

In an experiment of this type it is obvious that certain corrections must be applied to the results. One of the main objectives of the technique employed was to reduce the magnitude of the correction factors to a minimum. Corrections have been applied to take account of the following: (i) small angle scatters whose projected angle is less than 5°, (ii) scatters which are not measurable due to the finite depth of illumination, (iii) effect of the partial pressure of the water–alcohol vapour on the xenon concentration measurement, (iv) effect of multiple scattering on angle and energy measurements.

The minimum detectable angle of scatter was taken as 5°. Since a scatter whose true angle is greater than 5° may have a projected angle of less than 5° and is therefore rejected during scanning, a correction to allow for these scatters is estimated as follows.

The distribution of the angle of tilt of the projection table is plotted in figure 3.

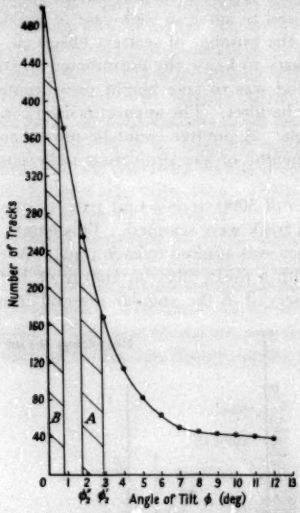

Figure 3. Relation between the angle of tilt of the projection table and the number of tracks observed.

Let ϕ_2' be the angle of tilt to convert a 3° projected angle to a true angle between 5° and 6°. ϕ_2'' is the angle of tilt to convert a 4° projected angle to between 5° and 6°. From equation (1), assuming $\phi_1 \to 0$ (since the incident beam of electrons was narrow and horizontal) and $\sin\phi_1 \sin\phi_2 \ll 1$, $\cos\phi_2 = \cos\theta/\cos\Omega$. By putting $\theta = 5°$ and $\Omega = 3°$ a value of ϕ_2' can be determined from the above expression. ϕ_2'' is similarly obtained by putting $\theta = 5°$ and $\Omega = 4°$.

It is assumed that all tracks accepted as coplanar were measured with an error of ± 1 mm in the projection table tilt, this being the error in the estimation of the difference in the vertical positions of the tips of the pointers shown in

figure 1. The area B (figure 3) contains the numbers of scatters which are measured as coplanar to within ± 1 mm or 0·7° slope of the projection table.

Referring to figure 3, AN/B is the number of scatters which have a projected angle lying between 3° and 4° but a true angle between 5° and 6°. N is taken as the number of coplanar scatters observed between 5° and 6°. This fraction AN/B was summed for the angular interval 2°–5° for true angles from 5°–10°. It was found that few scatters with a projected angle of less than 5° contributed to the number above 8°. For projected angles between 5° and 8°, however, the correction factor is 1·84.

Since the illuminated depth was restricted to 4·5 cm the number of measurable scatters was less than the number of scatters occurring within this depth. Some authors have taken this fact into consideration but the correction factors have been as high as 3. It was considered that some of these large corrections combined with poor statistics may have caused the large discrepancies previously observed. One way of reducing this correction is to use a narrow electron beam well within the limits of the illuminated region. This can be achieved by good collimation of the incident electrons. A method of checking the height of the electron beam has been described in §3 and a histogram of these measurements is shown in figure 4. From this it can be seen that the effective electron beam

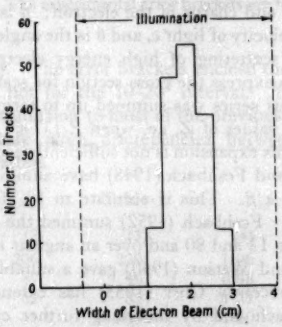

Figure 4. Histogram of the number of tracks observed at specified levels within the illuminated depth of the cloud chamber. The broken line indicates the limits of the illuminated region.

height is 1·2 cm. The slight spread of the electron beam to 2 cm can be ascribed to multiple scattering in the chamber walls. The height correction factor is calculated in the Appendix. The depth of illumination was measured on steeply inclined cosmic-ray particles. This method is to be preferred to a geometrical measurement of height since it is directly dependent on the variation of scattered light intensity from droplets.

In measuring the xenon concentration by a mass spectrometer no account was taken of the presence of water–alcohol vapour. The vapour pressure of water–alcohol mixture at 18° was obtained from tables (Das Gupta and Ghosh 1946), and was found to affect the scattering cross section by only 4%. Multiple scattering corrections have been discussed at length by Bethe (1946), and the

particular application to angle measurement has been dealt with by Randels, Chao and Crane (1945). These corrections have been kept below 10% by limiting the xenon content to less than 20% of the total gas mixture. The bulk of the mixture was helium, whose contribution to multiple scattering is negligible.

An overall check on the consistency of the scanning was made by counting the relative number of ogival and cusped scatters, as it is obvious that an equal number of both types of scatters should occur. In the present work, out of a sample of 178 scatters above 8°, 94 were ogival and 84 cusped giving a ratio of ogival to cusped scatters of almost unity. An observer might detect more cusped scatters than ogival particularly at small angles and the value of almost unity obtained lends support to the consistency of scanning.

§ 5. Discussion of the Results and Comparison with Theory

The theoretical cross section for Coulomb scattering from a point nucleus was originally given by Rutherford. Taking into consideration the variation of mass with velocity we have the well-known equation

$$\sigma_R = \left(\frac{Ze^2}{2m_0c^2}\right)^2 (1-\beta^2)\,\mathrm{cosec}^4\,\tfrac{1}{2}\theta$$

where σ_R is the cross section, Z is the atomic number of the scattering element and m_0, e are the mass and charge of the electron; β is the ratio of the velocity of the particle to the velocity of light c, and θ is the angle of scatter. Mott (1929, 1931) considered the scattering of high energy electrons and used quantum mechanical methods to express the cross section for scattering as a conditionally convergent series. This series was summed up to terms of the order of α^2 and is applicable for small values of Z, i.e. when $Z/137 \ll 1$, where 1/137 is the fine structure constant. This expansion is not sufficiently accurate for xenon ($Z=54$, $\alpha=0{\cdot}39$). McKinley and Feshbach (1948) have summed the Mott series as a power series in α and α/β. This is accurate to 1% for elements with Z less than 40 and for $\beta \sim 1$. Feshbach (1952) summed the Mott series numerically for values of Z between 13 and 80 and over an angular range of 30 to 150°. For small angles Bartlett and Watson (1940) gave a suitable approximation for the Mott series. More recently Curr (1955) has extended the calculations of McKinley and Feshbach and by including further coefficients up to α^6 has calculated the cross section for heavy elements with greater accuracy.

It is usual to express the results in terms of the calculated Rutherford cross section. The corresponding theoretical values have been determined for the theories of (*a*) Curr, (b) McKinley and Feshbach and (*c*) Bartlett and Watson, for a mean energy of 13·5 Mev and $Z=54$, and are shown in figure 5.

The variation of scattering with angle is shown in table 1. The number of scatters is divided into groups of 5–8°, 8–10°, and in 10° intervals up to 80° and comparison made with the number of scatters calculated from the Rutherford formula. The values corrected for depth, water–alcohol vapour and helium content are given in column (3). The ratio of experimental to Rutherford scattering is shown in column (4). The experimental ratio increases from almost unity t small values of θ to 1·6 at 25°. In the angular group from 30 to 80° a ratio of 1·2 is obtained. The errors in the last column are statistical and are taken as plus and minus twice the standard error $0{\cdot}67/\sqrt{n}$ where n is the number of scatters in each angular interval. The probability that the true value lies within these

limits is approximately 20 to 1. The ratios with their respective error brackets are also shown in figure 5. There is an increase in the ratio to Rutherford scattering with increasing angle as indicated by theory. There is a slight tendency for the experimental values to be greater than the theoretical values in the 10–30° range. This difference, however, is hardly significant because of the

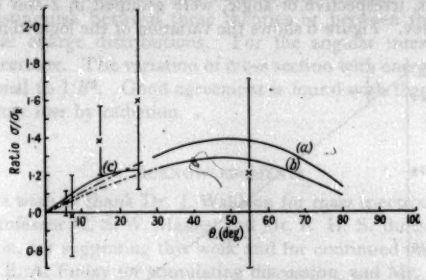

Figure 5. Ratio of various cross section values to the Rutherford cross section for different scattering angles θ. (*a*) Curr (1955), (*b*) McKinley and Feshbach (1948), (*c*) Bartlett and Watson (1940). The experimental error brackets are taken as twice the standard error.

statistical errors involved. The error brackets enclose the theoretical values for the 20–30° interval but not for the 10–20° interval. The general agreement with the theory is in contradiction to most of the previous cloud chamber results which in general indicate large discrepancies between the observed and theoretical number of scatters.

Table 1

(1)	(2)	(3)	(4)	(5)
5–8	206	220	1·06	± 9
8–10	47	46	0·98	± 19
10–20	62	85	1·37	± 14
20–30	11·6	19	1·60	± 30
30–40	5·1	4		
40–50	1·9	2·2		
50–60	0·99	2·3	1·2	± 45
60–70	0·60	1·2		
70–80	0·37	1·2		

(1) Angle of scatter (°); (2) theoretical number of scatters (Rutherford); (3) experimental number of scatters; (4) ratio (experimental/Rutherford); (5) error 2 $(0{\cdot}67/\sqrt{n})$ (%).

A check was made on the variation of the scattering cross section with energy. Substituting $mc^2\beta/e(1-\beta^2)^{1/2}=H\rho$ in the Mott formula the number of scatters $N(\theta)$ is given by an equation of the form

$$N(\theta)=\frac{NZ^2e^4}{4}\left(\frac{1}{H\rho}\right)^2 f(\theta)$$

where H is the magnetic field in oersteds, ρ the radius of curvature of the track in cm and N the number of atoms per cm^3.

The energy of the electron in MEV is given by

$$H = \frac{1}{300}\{E(E+1{\cdot}02)\}^{1/2}$$

and when E is large compared with 1·02 MEV $N(\theta)$ varies inversely as the square of the energy.

The scatters, irrespective of angle, were grouped in 2-MEV energy intervals from 10 to 18 MEV. Figure 6 shows the variation of the logarithm of the number

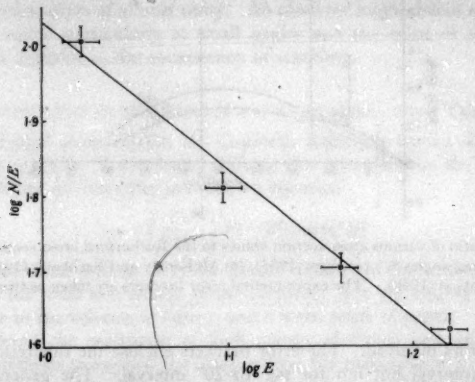

Figure 6. A plot of the logarithm of the number of scatters N normalized per unit length L against the logarithm of the energy E of the scattered track, giving a straight line of slope of 2.

of scatters N normalized per unit length L plotted against the logarithm of the energy E. The graph is a straight line with a slope of almost two confirming the approximate inverse square law dependence on energy.

The loss of energy of scattered electrons due to bremsstrahlung was also studied and a total of 12 events with an energy loss greater than 10% was observed. The theory of Bethe and Heitler (1934) predicts a total of 11 events indicating reasonable agreement between experiment and theory. Previous workers using gases as the scattering elements in cloud chambers have in general found disagreement with theory. For instance, Bleuler (1942) found evidence for an excessive number of cases of energy loss in fluorine; 19 samples were observed with apparent loss of more than 10% of their initial energy and 25 examples with an apparent gain of energy of more than 10%. The expected number of inelastic scatters was about three. Bleuler explained this apparent increase in energy as being due to multiple scattering errors in measurement. Davies and Shaw (1951) attempted to extend the work of Bleuler and their experiment suffered from a similar fault in that any measurement of change in energy made by fitting radii to the tracks was impossible due to the large amount of multiple scattering which is to be expected from the theory of Williams (1939). They found 70 examples of energy change, both positive and negative, whereas the Bethe–Heitler theory predicted only one such event. Randels, Chao and Crane also using xenon found only two examples of bremsstrahlung with more than 50% energy loss for electrons compared with a predicted total of eight.

§ 6. Conclusions

The number of observed scatters shows reasonable agreement with that expected theoretically in the range of 5°–80°. The ratio of the experimental scattering to the Rutherford value indicates an increase from unity above 10°. These results agree within the statistical accuracy with the theoretical results of Curr, McKinley and Feshbach, and Bartlett and Watson. It is impossible, however, to distinguish between these theories or between theories based on different nuclear charge distributions. For the angular interval 30°–80° the ratio tends to decrease. The variation of cross section with energy was confirmed to be proportional to $1/E^2$. Good agreement is found with theory of Bethe and Heitler for energy loss by radiation.

Acknowledgments

The authors wish to thank Dr. J. Waldron for mass spectrometer analysis of gas samples, Professor H. S. W. Massey and Dr. E. H. S. Burhop of University College, London, for suggesting this work and for continued interest, Mr. F. R. Perry and Mr. E. A. Finlay for stimulating discussion, and Mr. B. G. Churcher, Manager of Research Department, and Dr. Willis Jackson, Director of Research and Education, for permission to publish this paper.

APPENDIX

Correction for Finite Illumination Depth

Referring to figure 7, d is the depth of illumination, h is the height of the electron beam, θ is the true scattering angle, b is the accepted minimum track length and $r = b \sin\theta$.

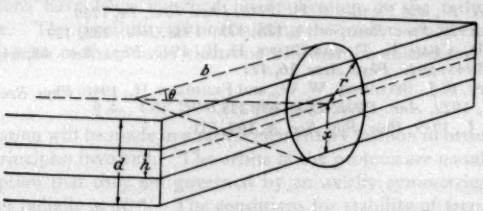

Figure 7. Schematic diagram of the illuminated depth of the chamber and the electron beam showing the acceptance cone for a scattering angle θ.

The fraction of the tracks lying within the conical envelope which are not measurable is

$$a = \frac{2r\cos^{-1}(x/r) + 2r\cos^{-1}\{(d-x)/r\}}{2\pi r},$$

Integrating for all values of x the average value of a is

$$\bar{a} = \frac{1}{h\pi}\left[x\cos^{-1}\frac{x}{r} - (r^2-x^2)^{1/2} - (d-x)\cos^{-1}\frac{d-x}{r} + \{r^2-(d-x)^2\}^{1/2}\right].$$

Taking limits $\frac{1}{2}(d+h)$, $\frac{1}{2}(d-h)$ we get

$$\bar{a} = \frac{2}{h\pi}\left[\frac{d+h}{2}\cos^{-1}\frac{d+h}{2r} - \left\{r^2-\left(\frac{d+h}{2r}\right)^2\right\}^{1/2} + \left\{r^2-\left(\frac{d-h}{2}\right)^2\right\}^{1/2} - \frac{d-h}{2}\cos^{-1}\frac{d-h}{2}\right].$$

Values of $(1-\bar{a})^{-1}$ are given in table 2.

Table 2

θ (deg)	<20	<30	<40	<50	<60	<70
$(1-\bar{a})^{-1}$	1·00	1·3	1·83	2·17	2·48	2·65

References

Alichanian, A. I., Alichanow, A. I., and Weissenberg, A., 1945, *J. Phys. U.S.S.R.*, **9**, 280.

Allen, K. R., Lipsicas, M., Williams, W. F., and Fotheringham, D., 1953, *Rev. Sci. Instrum.*, **24**, 501.

Bartlett, J. H., and Watson, R. E., 1940, *Proc. Amer. Acad. Arts Sci.*, **74**, 53.

Bethe, H. A., 1946, *Phys. Rev.*, **70**, 821.

Bethe, H. A., and Heitler, W., 1934, *Proc. Roy. Soc.* A, **146**, 83.

Beuchner, W. W., Van de Graaff, R. J., Sperduto, A., Burrill, E. A., Jr, and Feshbach, H., 1947, *Phys. Rev.*, **72**, 678.

Bleuler, E., 1942, *Helv. Phys. Acta*, **15**, 613.

Bothe, W., 1949, *Z. Naturf.* **4a**, 88.

Champion, F. C., and Roy, R. R., 1948, *Proc. Phys. Soc.* A, **61**, 532.

Curr, R. M., 1955, *Proc. Phys. Soc.* A, **68**, 156.

Das Gupta, N. N., and Ghosh, S. K., 1946, *Rev. Mod. Phys.*, **18**, 225.

Davies, W. T., and Shaw, D. F., 1951, *Proc. Phys. Soc.* A, **64**, 1006.

Feshbach, H., 1952, *Phys. Rev.*, **88**, 295.

Hofstadter, R., Fechter, H. R., and McIntyre, J. A., 1953, *Phys. Rev.*, **92**, 978.

Howatson, A. F., and Atkinson, J. R., 1951, *Phil. Mag.*, **42**, 1136.

Lyman, E. M., Hanson, A. O., and Scott, M. B., 1951, *Phys. Rev.*, **84**, 626.

McKinley, W. A., and Feshbach, H., 1948, *Phys. Rev.*, **74**, 1759.

Mott, N. F., 1929, *Proc. Roy. Soc.* A, **124**, 425; 1931, *Ibid.*, **135**, 429.

Randels, R. B., Chao, K. T., and Crane, H. R., 1945, *Phys. Rev.*, **68**, 64.

Sigrist, W., 1943, *Helv. Phys. Acta*, **16**, 471.

Van de Graaff, R. J., Beuchner, W. W., and Feshbach, H., 1946, *Phys. Rev.*, **69**, 452.

Wentzel, G., 1922, *Ann. Phys., Lpz.*, **69**, 335.

Williams, E. J., 1939, *Proc. Roy. Soc.* A, **169**, 531.

Space Charge and Ionization Phenomena in Constant-gradient Proton Synchrotrons

By P. B. MOON
Department of Physics, University of Birmingham

MS. received 21*st September* 1955

Abstract. The stability of small oscillations of protons circulating in a synchrotron is investigated on the assumption of a uniform space charge in addition to the magnetic field of constant radial gradient.

If the space charge is that of the protons themselves, the greatest number that can be held in a uniform beam of cross section A is $VB_zA/2e$, where V is the velocity of the protons, B_z is the magnetic field on the equilibrium orbit and the units are electrostatic. One third of this number might be held in a bunched beam of 120° azimuthal length, but existing synchrotrons fall far short of this.

Consideration is given to the effects of ionization in the residual gas, and to the possibility that the space charge could be neutralized by the continuous injection of electrons.

§ 1. Introduction

The high-energy circulating current in a proton synchrotron is usually determined mainly by the number of protons that can be injected into stable orbits. If, however, many more protons could be injected, the number that are trapped would be limited by the space charge of the circulating beam. For alternating-gradient machines this limit has been discussed in privately circulated reports and in at least one published paper (Barden 1954), but it seems useful to give the simpler calculation for a constant-gradient synchrotron and to consider how the ionization of the residual gas by the circulating protons may affect the space charge. It will be shown that any effect is likely to disappear once the protons have been bunched by application of the radio-frequency driving voltage. The possibility of neutralizing the proton space charge by the continuous injection of thermionic electrons will then be considered.

§ 2. The Space-charge Limit

The calculation will be made in a rather elementary fashion in order to display the physical principles involved. The orbits of the protons are usually analysed on the assumption that they are governed by an axially symmetrical magnetic field decreasing radially as R^{-n}. The conditions for stability of free oscillations about the equilibrium orbit may then be written as $0<n<1$.

To find what modifications arise from the electrostatic field caused by the space charge, let us consider the dynamical principles upon which the two inequalities rest. They are firstly that if a proton departs upwards (downwards) from the equilibrium orbit, it shall meet a downward (upward) force; secondly, that if the orbit is displaced radially outwards (inwards) the inward radial force on the proton shall become greater (less) than is required for equilibrium. If F_z, F_R

are the mechanical forces in the directions of Z and R, measured vertically upwards and radially outwards from the equilibrium orbit, then on the equilibrium orbit $F_Z=0$ and $-RF_R=MV^2$, where M and V are the mass and velocity of the proton. The orbit will therefore be stable if

$$-dF_Z/dZ>0 \qquad \text{.....(1)}$$

and $$(d/dR)(-RF_R)>0 \quad \text{or} \quad -dF_R/dR>F_R/R. \qquad \text{.....(2)}$$

Now $$F_Z=eVB_R+eE_Z \qquad \text{.....(3)}$$

and $$F_R=-eVB_Z+eE_R \qquad \text{.....(4)}$$

where B_Z, B_R, E_Z, E_R are the components of magnetic induction and electric field. We combine these equations with (1) and (2) respectively, and remember that $dB_R/dZ=dB_Z/dR$ and that $dE_Z/dZ+dE_R/dR=4\pi\rho$ where ρ is the charge density.† The conditions for stability then emerge in the form

$$-(d/dR)(VB_Z-E_R)>4\pi\rho \qquad \text{.....(5)}$$

$$-(d/dR)(VB_Z-E_R)<(VB_Z-E_R)/R. \qquad \text{.....(6)}$$

If the electrostatic terms are zero, these give

$$-dB_Z/dR>0 \quad \text{and} \quad -dB_Z/dR<B_Z/R,$$

which are the differential forms of the familiar conditions $0<n<1$.

Stability fails when the right-hand sides of (5) and (6) become equal, i.e. when $\rho=(VB_Z-E_R)/4\pi R$ or, very closely, $VB_Z/4\pi R$ since $VB_Z\gg E_R$. If the cross section of the beam has area A so that the volume of the beam is $2\pi RA$, the maximum number of ions that can be stably held is thus $VB_ZA/2e$. If the beam is bunched and occupies a length l instead of $2\pi R$ the number will be $VB_ZAl/4\pi Re$.

If more particles are injected the beam must spread, to give a greater value of A. In most accelerators, $n>\frac{1}{2}$ and the vertical magnetic focusing is stronger than the horizontal, so it might be thought that horizontal instability would set in first. However, if $n>\frac{1}{2}$ the beam (and the vacuum box) is naturally wider than it is high and dE_Z/dZ will exceed dE_R/dR. It thus seems likely that the beam will adjust itself as between radial and vertical stability and that, if space charge were the only limitation, the limit calculated above would be quite closely approachable.

For the Birmingham proton synchrotron the following values apply to the time immediately following injection, when space-charge effects should be most serious: $V=c/30$, $B_Z=225$ gauss, $R=450$ cm, $A=330$ cm^2 (10 cm × 33 cm). In these circumstances, the greatest number of protons within a uniform circulating beam should be about 3×10^{12}; for a bunched beam of 120° azimuthal length the limit is 1×10^{12}. Allowance must be made for oscillations and other factors that may cause part of the beam to strike the walls of the vacuum box but it seems likely that more than 10^{11} protons could be accelerated to full energy. At present, less than 10^{10} reach full energy.

For the Brookhaven cosmotron, the space-charge limit and the actual beam are both higher by a factor of about ten.

† At this stage it becomes necessary to specify the system of units. Electrostatic units have been chosen; in e.m.u. the right-hand side of the previous equation would become $4\pi\rho c^2$ and the final formulae would require division by c^2.

If V_1 is the injection voltage, V and B_z are each proportional to $V_1^{1/2}$. For a given machine the space-charge limit to the number of protons accelerated is therefore proportional to the first power of the injection voltage.† For machines of the same shape but different sizes, the limit is proportional to the product of injection voltage and linear dimensions.

§ 3. Effects of Ionization‡

The circulating beam will ionize the residual gas and it is necessary to consider the possible effects of this. To assess orders of magnitude, estimates will be made for the Birmingham machine, in which the mean orbit circumference is about 3×10^8 cm and the average pressure is about 8×10^{-7} mm Hg, measured on an ionization gauge calibrated for air; though the residual gas is certainly a mixture, no large error will be involved in reckoning it to be nitrogen. The mean free path for ionization by protons of the injection energy (500 kev) is then about 1×10^5 cm; since the proton's velocity is 1×10^9 cm sec^{-1}, the average time taken for each proton to produce an electron–ion pair is 10^{-4} sec, which happens to be about equal to the duration of injection.

If the initial energies of the ions and electrons exceed those that can be provided by the electric field of the circulating space charge of protons, the ionization will immediately be lost to the walls; if the reverse is true, the positive ions will be repelled to the walls but the electrons will oscillate within the proton space charge, their movements being closely confined to the lines of magnetic force. To estimate the rate of repulsion of ions and the frequency of oscillation of electrons, we shall consider only vertical motions and shall regard the proton space charge as a uniform sheet 10 cm high and infinitely wide, though in fact it cannot exceed the width of the vacuum box (33 cm). If x be the distance from the median plane of an ion or electron at time t, it having been generated with negligible velocity at $x=x_0$ and $t=0$, the equations of motion are $d^2x/dt^2 = +4\pi e\rho x/M$ for the positive ion and $d^2x/dt^2 = -4\pi e\rho x/m$ for the electron, M and m being their masses. The respective solutions are $x = x_0 \cosh t(4\pi\rho e/M)^{1/2}$ and $x = x_0 \cos t(4\pi\rho e/m)^{1/2}$.

To proceed any further we must assume a value for the proton space-charge density ρ, and this will be chosen to correspond to 3×10^{11} protons in the whole volume of the vacuum box—a number that has been estimated above to be attainable, though not attained. It is then found than an ion (N^+) starting midway between the median plane and the top or bottom of the box will be ejected in a time of less than 10^{-5} second, while an electron will remain oscillating with a frequency of about 5×10^6 c/s.

Since it takes about 10^{-4} second for a proton to make an ion pair, a substantial neutralization of space charge will occur. However, as soon as the proton beam becomes bunched, the oscillating electrons will strike the upper or lower walls of the box during the intervals of about 2×10^{-6} second when no protons are passing over them. The neutralization thus suddenly fails, and indeed there is a small

† Barden (1954) states that the current is proportional to $V_1^{3/2}$. This is true in respect of the injected current but not of the high energy beam; the further factor of $V_1^{1/2}$ represents merely the velocity of the injected protons.

‡ The phenomena considered in this section are essentially similar to those studied by Bernas, Kaluszyner and Druaux (1954) with linear beams of ions at somewhat lower energies and higher pressures in the presence of an intermittent electrostatic field.

adverse effect because the slow-moving positive ions, now being ejected by an electric field whose time-average is only a third of that for the continuous beam, take a longer time to reach the walls. For the typical ion starting midway between the median plane and the wall, this time is about $1{\cdot}2 \times 10^{-5}$ second; since the time taken for each proton to generate another ion is about 10^{-4} second, equilibrium will be attained when the total positive space charge is of the order of 12% greater than that due to the protons alone.

It seems, therefore, that ionization should play only a temporarily important part in the performance of the machine. Transients are apt to leave troubles in their wake even when, as in this instance, they are favourable while they last; so this conclusion should not be regarded as final.

§ 4. Space-charge Reduction by the Introduction of Thermionic Electrons

If electrons from, say, thermionic sources are introduced into the top and/or bottom of the vacuum box, they will be attracted into the proton space charge and pass through it to the opposite wall. It is interesting to estimate the electron current that would be required to neutralize the positive space charge, which as before will be assumed to correspond to 3×10^{11} protons in a total volume of about $10^6\,\text{cm}^3$, or $3 \times 10^5\,\text{per cm}^3$. The centre of this space charge would be at a potential of about 7 volts with respect to the walls. It is remarkable that so low a voltage can seriously affect the beam.

If this voltage were to be neutralized by an equal concentration of, say, 25-volt electrons, their flux would be 9×10^{13} electrons per second. The surface area of the top or bottom of the vacuum box being about $10^5\,\text{cm}^2$, the total current would be about 9×10^{18} electrons per second or about $1\frac{1}{2}$ amperes. When designing a new machine it would seem possible to provide for considerably larger electron currents and thus to neutralize even greater proton beams.

References

Barden, S. E., 1954, *Phys. Rev.*, **93**, 1378.

Bernas, R., Kaluszyner, L., and Druaux, J., 1954, *J. Phys. Radium*, **15**, 273.

The Structures of the Ground Multiplets of Certain Rare-Earth Ions

By B. R. JUDD
The Clarendon Laboratory, Oxford

Communicated by B. Bleaney; MS. received 17th October 1955 and in final form 16th November 1955

Abstract. Departures from the Landé interval rule in the ground multiplets of certain rare-earth ions are examined. It is found that magnetic spin–spin interactions between the 4f electrons are much too small to account for the apparent distortions, but that by allowing for the partial breakdown of Russell–Saunders coupling it is possible to obtain satisfactory agreement between experiment and theory. Values of the spin–orbit constant ζ are given for several rare-earth ions, and the positions of a number of excited multiplets are tabulated.

§ 1. Introduction

It is well known that the 4f electrons in ions of the rare-earth elements exhibit a type of spin–orbit coupling that follows the Russell–Saunders (RS) approximation fairly closely. The energy level system for any ion thus consists of a number of multiplets, each of which can be described by two quantum numbers L and S corresponding to the total orbital and total spin angular momentum respectively. The individual levels that make up a multiplet are characterized in addition by different values of J, corresponding to the total angular momentum. For spin–orbit coupling of the RS type, the spacings between the various levels that comprise a multiplet are given by the Landé interval rule, which states that the energy separation between two neighbouring levels is proportional to the higher J value of the pair.

Although the study of the energy level structure of excited multiplets has not yet progressed very far, the positions of many of the levels of the ground multiplets are known from experiments with rare-earth salts. For some of the more extended multiplets, the positions of the upper components have been found by infra-red absorption, while many of the lower levels can be found from the fluorescence spectra of various salts. The observed multiplet structures may be conveniently compared with those calculated on the basis of RS coupling by arranging the latter to have the same overall splittings as the former (see, for instance, Gobrecht 1938). In most cases the agreement is moderately good, but it is noticeable that the discrepancies, although comparatively small, are systematic. The inner levels of a multiplet are consistently found to lie above their counterparts in the RS coupling scheme, the effect being most pronounced in the centre of the multiplet. This is just as apparent for elements in the second half of the rare-earth series, where the multiplets are inverted, as it is for those in the first half. The question now arises as to what modifications in the theory are required to account for these deviations from the simple RS coupling model, and this problem forms the subject of this paper.

§2. Spin–Spin Interaction

A few years ago, Araki (1948a, b) made a study of the multiplet structures that occur in a large number of atoms and ions. He attributed the deviations from the Landé interval rule to magnetic spin–spin interactions, and showed that the inclusion of this effect in the theory produced an extra term in the expression for the energy spacings of adjacent levels that is of the correct form to account for these deviations.

In the usual notation, neglecting the term representing the contact interaction of the spins (since it does not affect the splitting of a multiplet), the contribution to the Hamiltonian of the magnetic interactions of the spins of the electrons can be written as

$$4\beta^2\sum\left[\frac{\mathbf{s}_j\cdot\mathbf{s}_k}{r_{jk}^3}-\frac{3(\mathbf{r}_{jk}\cdot\mathbf{s}_j)(\mathbf{r}_{jk}\cdot\mathbf{s}_k)}{r_{jk}^5}\right].$$

Within a particular LS multiplet, this can be replaced by

$$-\rho[(\mathbf{L}.\mathbf{S})^2+\tfrac{1}{2}(\mathbf{L}.\mathbf{S})-\tfrac{1}{3}L(L+1)S(S+1)]$$

where ρ is at present an undetermined constant. This leads to the following expression for Δ_J, the difference between the energy displacements of levels J and $J-1$ due to spin–spin interactions:

$$\rho[L(L+1)+S(S+1)-\tfrac{1}{2}]J-\rho J^3.$$

(The formulae quoted here have been given by Araki (1948a).) In view of the Landé interval rule, it can be seen that the term linear in J provides a contribution that combines with the normal spin–orbit effect. The cubic term, however, gives rise to a distortion in the energy level scheme, and Araki (1948b) found that the observed departures from the Landé interval rule in most of the multiplets he analysed could be quite accurately accounted for by choosing suitable values for ρ.

An examination of the ground multiplets of the rare-earth ions shows that this is equally true in these cases; the next problem (and one that Araki did not investigate in detail) is to decide whether the values of ρ that are required are realistic ones. Unfortunately, it is impossible to determine them accurately without precise knowledge of the shape of the single 4f electron radial eigenfunction $R(r)$. The results can, however, be put in the form

$$\rho=\beta^2(q_2I_2+q_4I_4+q_6I_6)$$

where

$$I_n=\int_0^\infty\frac{1}{r_1^{n+1}}[R(r_1)]^2\int_0^{r_1}r_2^{n-2}[R(r_2)]^2\,dr_2\,dr_1.$$

The numerical coefficients q_n have been calculated for all the multiplets that can be built from configurations of the form $4f^n$ and that possess the maximum multiplicity of their configuration. The results are given in table 1. By Hund's rule, the ground multiplet of a particular configuration is the one that possesses the largest value of L.

Estimates of I_n may be obtained by assuming the radial eigenfunction is of hydrogenic form. In the calculations, there occur integrals of the type

$$\int_0^\infty x^a e^{-x}\int_0^x y^b e^{-y}\,dx\,dy$$

where the integers $a,\ b \geqslant 1$. Similar integrals appear elsewhere (e.g. in the calculation of F_k, mentioned later in this paper). By integrating by parts, one obtains the recurrence relation

$$bI(a, b-1) - aI(a-1, b) = (a+b)!/2^{a+b}.$$

This equation may be used to relate any integral to one whose parameter b is zero, in which case the integration is elementary. In this way the integrals I_n

Table 1. Values of q_n

Configuration	Multiplet	q_2	q_4	q_6
f^2, f^{12}	^3P	12/5	24/5	60/11
	^3F	4/45	−32/45	160/99
	^3H	−4/45	136/495	1060/(39 . 363)
f^3, f^{11}	^4D	−136/315	184/315	580/693
	^4F	4/45	4/45	−50/99
	^4G	4/1155	1996/(77 . 165)	850/(77 . 363)
	^4I	−8/495	232/(33 . 165)	14860/(13 . 33 . 363)
f^4, f^{10}	^5D	34/105	−44/315	−50/693
	^5F	−1/15	2/15	−5/33
	^5G	−1/385	1042/(77 . 165)	535/(77 . 363)
	^5I	2/165	28/(33 . 165)	4570/(13 . 33 . 363)
f^5, f^9	^6P	−24/25	36/25	18/11
	^6F	−8/225	−8/225	20/99
	^6H	8/225	−4/495	−466/(39 . 363)
f^6, f^8	^7F	4/45	−16/225	−8/99

can be found. The results are suitably expressed in terms of $\langle r^{-3} \rangle$, the mean value of r^{-3} for a single 4f electron:

$$I_2 = \frac{3473}{16384} \langle r^{-3} \rangle, \qquad I_4 = \frac{2115}{16384} \langle r^{-3} \rangle, \qquad I_6 = \frac{1485}{16384} \langle r^{-3} \rangle.$$

Consider now a particular rare-earth ion, say Sm^{3+}. Using a formula due to Elliott and Stevens (1953), $\langle r^{-3} \rangle = 52\ \text{Å}^{-3}$, and with the aid of Table 1, it is found that $\rho(^6H) = 0{\cdot}078\ \text{cm}^{-1}$. Although this result must be regarded as only an approximate one, yet the value of ρ is quite inadequate to account for the observed deviations from the Landé interval rule. Calculations for the multiplets of other rare-earth ions support this view; in some cases ρ is too small by a factor of 50 or more. It is thus apparent that the spin–spin interactions between the electrons play only a very small part in distorting the multiplets.

§ 3. Intermediate Coupling

Another mechanism that can produce deviations from the Landé interval rule is not difficult to find; indeed it seems rather more obvious and is certainly less sophisticated than spin–spin interaction. The validity of RS coupling rests on the assumption that the spin-orbit interaction energy is much smaller than the energy associated with the Coulomb interactions of the electrons, thus allowing each multiplet to be treated as an isolated system. But this is only an approximation, and it is natural to inquire whether it is a sufficiently accurate one. The answer to this question can be found by using perturbation theory to calculate the second and higher order corrections to the first order positions of the energy levels, the relative importance of these contributions being a measure of the deviation from RS coupling.

The spin–orbit coupling is written in the usual way as $\zeta \Sigma \mathbf{l}.\mathbf{s}$, the summation being taken over all the electrons. Most configurations of the type $4f^n$ are extremely complex, and for this reason it is usually not practicable to carry the

§2. Spin–Spin Interaction

A few years ago, Araki (1948 a, b) made a study of the multiplet structures that occur in a large number of atoms and ions. He attributed the deviations from the Landé interval rule to magnetic spin–spin interactions, and showed that the inclusion of this effect in the theory produced an extra term in the expression for the energy spacings of adjacent levels that is of the correct form to account for these deviations.

In the usual notation, neglecting the term representing the contact interaction of the spins (since it does not affect the splitting of a multiplet), the contribution to the Hamiltonian of the magnetic interactions of the spins of the electrons can be written as

$$4\beta^2 \sum \left[\frac{\mathbf{s}_j \cdot \mathbf{s}_k}{r_{jk}^3} - \frac{3(\mathbf{r}_{jk} \cdot \mathbf{s}_j)(\mathbf{r}_{jk} \cdot \mathbf{s}_k)}{r_{jk}^5} \right].$$

Within a particular LS multiplet, this can be replaced by

$$-\rho[(\mathbf{L}.\mathbf{S})^2 + \tfrac{1}{2}(\mathbf{L}.\mathbf{S}) - \tfrac{1}{2}L(L+1)S(S+1)]$$

where ρ is at present an undetermined constant. This leads to the following expression for Δ_J, the difference between the energy displacements of levels J and $J-1$ due to spin–spin interactions:

$$\rho[L(L+1)+S(S+1)-\tfrac{1}{2}]J - \rho J^3.$$

(The formulae quoted here have been given by Araki (1948 a).) In view of the Landé interval rule, it can be seen that the term linear in J provides a contribution that combines with the normal spin–orbit effect. The cubic term, however, gives rise to a distortion in the energy level scheme, and Araki (1948 b) found that the observed departures from the Landé interval rule in most of the multiplets he analysed could be quite accurately accounted for by choosing suitable values for ρ.

An examination of the ground multiplets of the rare-earth ions shows that this is equally true in these cases; the next problem (and one that Araki did not investigate in detail) is to decide whether the values of ρ that are required are realistic ones. Unfortunately, it is impossible to determine them accurately without precise knowledge of the shape of the single 4f electron radial eigenfunction $R(r)$. The results can, however, be put in the form

$$\rho = \beta^2(q_2 I_2 + q_4 I_4 + q_6 I_6)$$

where

$$I_n = \int_0^\infty \frac{1}{r_1^{n+1}} [R(r_1)]^2 \int_0^{r_1} r_2^{n-2} [R(r_2)]^2 \, dr_2 \, dr_1.$$

The numerical coefficients q_n have been calculated for all the multiplets that can be built from configurations of the form $4f^n$ and that possess the maximum multiplicity of their configuration. The results are given in table 1. By Hund's rule, the ground multiplet of a particular configuration is the one that possesses the largest value of L.

Estimates of I_n may be obtained by assuming the radial eigenfunction is of hydrogenic form. In the calculations, there occur integrals of the type

$$\int_0^\infty x^a e^{-x} \int_0^x y^b e^{-y} \, dx \, dy$$

where the integers a, $b \geqslant 1$. Similar integrals appear elsewhere (e.g. in the calculation of F_k, mentioned later in this paper). By integrating by parts, one obtains the recurrence relation

$$bI(a, b-1) - aI(a-1, b) = (a+b)!/2^{a+b}.$$

This equation may be used to relate any integral to one whose parameter b is zero, in which case the integration is elementary. In this way the integrals I_n

Table 1. Values of q_n

Configuration	Multiplet	q_2	q_4	q_6
f^2, f^{12}	^3P	12/5	24/5	60/11
	^3F	4/45	−32/45	160/99
	^3H	−4/45	136/495	1060/(39 . 363)
f^3, f^{11}	^4D	−136/315	184/315	580/693
	^4F	4/45	4/45	−50/99
	^4G	4/1155	1996/(77 . 165)	850/(77 . 363)
	^4I	−8/495	232/(33 . 165)	14860/(13 . 33 . 363)
f^4, f^{10}	^5D	34/105	−44/315	−50/693
	^5F	−1/15	2/15	−5/33
	^5G	−1/385	1042/(77 . 165)	535/(77 . 363)
	^5I	2/165	28/(33 . 165)	4570/(13 . 33 . 363)
f^5, f^9	^6P	−24/25	36/25	18/11
	^6F	−8/225	−8/225	20/99
	^6H	8/225	−4/495	−466/(39 . 363)
f^6, f^8	^7F	4/45	−16/225	−8/99

can be found. The results are suitably expressed in terms of $\langle r^{-3} \rangle$, the mean value of r^{-3} for a single 4f electron:

$$I_2 = \frac{3473}{16384} \langle r^{-3} \rangle, \qquad I_4 = \frac{2118}{16384} \langle r^{-3} \rangle, \qquad I_6 = \frac{1485}{16384} \langle r^{-3} \rangle.$$

Consider now a particular rare-earth ion, say Sm^{3+}. Using a formula due to Elliott and Stevens (1953), $\langle r^{-3} \rangle = 52\,\text{Å}^{-3}$, and with the aid of Table 1, it is found that $\rho(^6H) = 0{\cdot}078\,\text{cm}^{-1}$. Although this result must be regarded as only an approximate one, yet the value of ρ is quite inadequate to account for the observed deviations from the Landé interval rule. Calculations for the multiplets of other rare-earth ions support this view; in some cases ρ is too small by a factor of 50 or more. It is thus apparent that the spin–spin interactions between the electrons play only a very small part in distorting the multiplets.

§3. Intermediate Coupling

Another mechanism that can produce deviations from the Landé interval rule is not difficult to find; indeed it seems rather more obvious and is certainly less sophisticated than spin–spin interaction. The validity of RS coupling rests on the assumption that the spin-orbit interaction energy is much smaller than the energy associated with the Coulomb interactions of the electrons, thus allowing each multiplet to be treated as an isolated system. But this is only an approximation, and it is natural to inquire whether it is a sufficiently accurate one. The answer to this question can be found by using perturbation theory to calculate the second and higher order corrections to the first order positions of the energy levels, the relative importance of these contributions being a measure of the deviation from RS coupling.

The spin–orbit coupling is written in the usual way as $\zeta \Sigma \mathbf{l}.\mathbf{s}$, the summation being taken over all the electrons. Most configurations of the type $4f^n$ are extremely complex, and for this reason it is usually not practicable to carry the

analysis beyond second order. To this approximation, it can be shown that the analysis becomes restricted to a study of those multiplets that differ by zero or unity in L and S from the ground multiplet of the ion under consideration; for it is only between such multiplets and the ground multiplet that $\Sigma \mathbf{l}.\mathbf{s}$ can form non-zero matrix elements. This can be proved by using the technique for deducing selection rules as described by Dirac (1947). Because of this, all the excited multiplets exhibiting maximum multiplicity are immediately excluded from the analysis, since they differ from the corresponding ground multiplets by two or more in L.

The spin–orbit interaction $\zeta \Sigma \mathbf{l}.\mathbf{s}$ commutes with $\mathbf{J}$, and this fact implies that all matrix elements between different J levels vanish. Hence in dealing with the perturbation of an excited multiplet on the ground multiplet, it is only necessary to examine the interactions between those pairs of levels possessing the same J. By transforming from $LSJJ_z$ to LSL_zS_z quantization, the dependence on J of the matrix elements can be separated out, and this enables the form of the distortion of a ground multiplet by second order interactions to be determined. For convenience, $\Sigma \mathbf{l}.\mathbf{s}$ is replaced by Λ:

$$\langle L,S,J\,|\Lambda|\,L-1,S-1,J\rangle = -\frac{1}{4}\sqrt{\frac{(L+S-J)(L+S-J-1)(L+S+J)(L+S+J+1)}{L(2L-1)S(2S-1)}} \times \langle L,S,L_z=L,S_z=S\,|\Sigma l_+ s_+|\,L-1,S-1,L_z=L-1,S_z=S-1\rangle, \quad ..(1)$$

$$\langle L,S,J\,|\Lambda|\,L,S-1,J\rangle = -\frac{1}{2L}\sqrt{\frac{(S+L-J)(S+L+J+1)(L-S+J+1)(S-L+J)}{2S(2S-1)}} \times \langle L,S,L,S\,|\Sigma l_z s_+|\,L,S-1,L,S-1\rangle, \quad .....(2)$$

$$\langle L,S,J\,|\Lambda|\,L+1,S-1,J\rangle = \frac{1}{4}\sqrt{\frac{(S-L+J)(S-L+J-1)(L-S+J+1)(L-S+J+2)}{S(2S-1)(L+1)(2L+1)}} \times \langle L,S,L,S\,|\Sigma l_- s_+|\,L+1,S-1,L+1,S-1\rangle, \quad .....(3)$$

where $l_+ = l_x + il_y$, $l_- = l_x - il_y$, etc. Although these equations differ in detail, it may be shown by the conventional methods of perturbation theory that the contribution of any excited level to Δ_J, the difference between the second order corrections to the levels J and $J-1$ of the ground multiplet, consists of a term linear in J together with one proportional to J^3. Summing over all the relevant excited multiplets, the result

$$\Delta_J = aJ + bJ^3$$

is obtained. This is similar to the corresponding expression given previously for spin–spin interaction; indeed, if the method one adopts for analysing the observed structure of a multiplet consists solely of fitting the spacings between adjacent levels with an expression of the form $aJ + bJ^3$, it is clearly impossible to distinguish the effects of spin–spin interaction from a slight deviation from RS coupling. Araki, by using just this method, has clearly been presumptuous in supposing that spin–spin interaction alone is responsible for the distortions in the multiplets he examined.

Estimating the magnitude of the deviation from RS coupling involves, in the first place, finding the positions of the required multiplets in the energy

level scheme, and secondly, the evaluation of the appropriate matrix elements. If these multiplets could actually be identified from a study of the relevant absorption spectra, then the first problem would soon be dealt with; however, the opportunity to do this occurs in only a few isolated cases, and hence the positions of the majority of them must be calculated. Just as the effect of spin–spin interaction depends on I_2, I_4 and I_6, so the energies of the centres of gravity of the multiplets depend on three similar integrals, F_2, F_4 and F_6, defined by Condon and Shortley (1935). The writer has recently made a detailed study of the lowest ^5D multiplet of Eu^{3+} (Judd 1955), and has shown that the assumption of a hydrogenic 4f radial eigenfunction leads to theoretical positions for the energy levels that fit the observations quite well. The same assumption is made here. As a consequence of this, the integrals F_k are interrelated through the equations

$$F_4/F_2 = 41/297 \quad \text{and} \quad F_6/F_2 = 7.25/(81.143). \qquad \ldots\ldots (4)$$

In his recent work on rare-earth ions, Jørgensen (1955 b) has used the tentative values 0·2 and 0·02 for these ratios. Unlike those given in equations (4), they are not related to a specific eigenfunction, and for this reason it was felt preferable to adopt the former set in the present calculations. (For a discussion of Jørgensen's values, see Satten (1955) and Jørgensen (1955 a, b).)

The procedure now is to calculate energies in terms of F_2. One would expect this parameter to vary slightly from one rare-earth ion to the next, and the following formula has been used:

$$F_2 = 12{\cdot}4(Z-34)\ \text{cm}^{-1} \qquad \ldots\ldots (5)$$

where Z is the atomic number of the ion. An equation expressing a similar variation in F_2 has been given by Satten (1953). Sufficient data are now available for the positions of all the multiplets and the nature of their states to be determined, the calculations proceeding in a way similar to that described by Judd (1955). In a few cases, it is possible to compare the experimental and theoretical positions of a multiplet, and the agreement that is obtained supports the use of equations (4) and (5) in the analysis.

The calculation of the matrix elements is often rather lengthy. A suitable check on the working can be obtained by making use of the equation

$$\langle L,S,J\,|\Lambda^2|\,L,S,J\rangle = \sum_{L',S'} \langle L,S,J\,|\Lambda|\,L',S',J\rangle\langle L',S',J\,|\Lambda|\,L,S,J\rangle.$$

Within a manifold of states of constant L and S, Λ^2 can be replaced by

$$u(\mathbf{L}.\mathbf{S})^2 + v(\mathbf{L}.\mathbf{S}) + w.$$

Hund's rule enables the L and S of the lowest term in a configuration to be found, and in this case the simple nature of the states allows the parameters u, v and w to be found in a straightforward way:

$$v = \tfrac{1}{2}u - \frac{1}{4S},$$

$$w = -\tfrac{1}{2}L(L+1)S(S+1)\left(u - \frac{1}{4S^2}\right) + \frac{1}{12S}(L+S^2)(4S^2-1),$$

and

$$u = \frac{L+S}{2S^2(2L-1)}$$

provided $S \neq \frac{1}{2}$. In the special case of $S = \frac{1}{2}$ (which is of no interest here),

$$u = 1, \qquad v = 0, \qquad w = 0.$$

§4. Comparison with Experiment

Having found the positions of the excited multiplets and the matrix elements of Λ, the energy of a particular J level of a ground multiplet can now be expressed as the sum of two terms. The first, linear in ζ, derives from the first-order spin–orbit effect, and is equal to $\zeta\langle L,S,J\,|\Lambda|\,L,S,J\rangle$. The second is quadratic in ζ, involving second-order contributions from the excited multiplets. The procedure now is to consider each rare-earth ion in turn and attempt to fit the entire structure of the ground multiplet with a single value of ζ.

Most of the experimental data have been obtained from the absorption and fluorescence spectra of rare-earth crystals. The system of charges surrounding a rare-earth ion produces a splitting of the levels, and lines that would otherwise be single show a structure. This effect, which often makes it difficult to find the exact centres of gravity of the levels, is not present in the spectra of rare-earth ions in solution. The structure in these cases becomes smoothed out, usually leaving fairly well defined maxima. In view of the influence which the surroundings of a rare-earth ion have on the spectrum, it is not surprising to find that the energies of the levels vary slightly according to the experimental conditions.

Theory and experiment are compared in table 2. The wave numbers followed by (G) have been given by Gobrecht (1938), who has also tabulated in detail the fluorescence spectra of several rare-earth octohydrosulphates (Gobrecht 1937). Assuming that each line is of equal weight, the structures due to the charges surrounding the rare-earth ions can be replaced by single lines at their centres of gravity, and this enables the positions of many levels to be obtained. The results are rounded off to the nearest $100\,\mathrm{cm}^{-1}$ and indicated by (G′). Further information has been drawn from Rosenthal (1939), Zeidel, Larionov and Philippov (1939), Hellwege and Kahle (1951), and Geisler and Hellwege (1953). These sources are referred to by (R), (Z), (K) and (H) respectively. In order to appreciate the importance of second-order effects, the positions of the levels calculated on the basis of pure RS coupling are also given, the value of ζ being chosen to allow the highest and lowest levels of each multiplet to coincide with experiment.

Table 2 begins with Sm^{3+}, since, apart from the trivial case of Ce^{3+}, this is the first rare-earth ion for which the entire ground multiplet is known. As one advances along the rare-earth series, deviations from RS coupling become progressively more serious, and third and higher order effects cease to be comparatively unimportant. Overlapping between the ground multiplet and the lower excited multiplets begins to take place, and this makes it difficult to be certain about the identification of the upper levels of the former. (Jørgensen (1955 b) has discussed this problem.) For these reasons, no ion beyond Ho^{3+} is considered.

An examination of table 2 shows that the inclusion of second-order effects produces a considerable improvement on the simple RS coupling scheme. In many cases, the difference between the calculated and observed positions of a level is reduced to less than $100\,\mathrm{cm}^{-1}$, the order of magnitude of the splitting caused by the crystal field. When discrepancies are larger than this, the reasons are often apparent. In Tb^{3+}, for instance, the lowest ^5D multiplet has an unusually extended structure, and this can be shown to have the effect of depressing $^7F_4$ and $^7F_3$ while elevating $^7F_0$, $^7F_1$ and $^7F_2$. Although this would clearly improve the agreement between experiment and theory, it was felt that

it would be rather improper to take this interaction into account without including all third-order effects.

Table 2. A Comparison between Theory and Experiment

Ion	Level	Pure RS coupling	Theory	Observed		
	$^6H_{15/2}$	6600	6650	6600(G),	6550(R)	
	$^6H_{13/2}$	4800	5160	5000(G'),	4920(R)	
Sm^{3+},	$^6H_{11/2}$	3240	3670	3600(G')		
	$^6H_{9/2}$	1920	2270	2300(G')		
$4f^5$	$^6H_{7/2}$	840	1030	1100(G')		
	$^6H_{5/2}$	0	0	0		
	$^7F_6$	5110	5100	5100(G)		
	$^7F_5$	3650	3990	3900(G')		
	$^7F_4$	2430	2850	2900(G')		
Eu^{3+},	$^7F_3$	1460	1800	1900(G')		
	$^7F_2$	730	940	1100(G'),	1000(K)	
$4f^6$	$^7F_1$	240	320	300(G'),	350(K)	
	$^7F_0$	0	0	0		
	$^7F_6$	5670	5470	5660(H),	5765(Z),	5800(G')
	$^7F_5$	5400	5340	5430(H),	5525(Z),	5600(G')
	$^7F_4$	4860	5020	4975(H),	5018(Z),	5100(G')
Tb^{3+},	$^7F_3$	4050	4460	4325(H),	4347(Z),	4400(G')
	$^7F_2$	2970	3540	3330(H),	3472(Z),	3400(G')
$4f^8$	$^7F_5$	1620	2120	2080(H),	2101(Z),	2100(G')
	$^7F_6$	0	0	0		
	$^6H_{5/2}$	10230	10200	10200(R),	10200(G)	
	$^6H_{7/2}$	8930	9320	9340(R),	9200(G)	
Dy^{3+},	$^6H_{9/2}$	7250	8010	8032(R),	7800(G)	
	$^6H_{11/2}$	5210	6140	6078(R),	6000(G)	
$4f^9$	$^6H_{13/2}$	2790	3530	3200(G')		
	$^6H_{15/2}$	0	0	0		
	$^5I_4$	13330	13270	13300(G)		
Ho^{3+},	$^5I_5$	10760	11440	11200(G)		
	$^5I_6$	7690	8790	8500(G),	8470(R),	8747(R)
$4f^{10}$	$^5I_7$	4100	5070	5050(G),	5090(R)	
	$^5I_8$	0	0	0		

The values of ζ that were used to obtain the results given in table 2 are listed below. They are regarded as being accurate to within 5%. In parenthesis, it might be added that the absorption band in neodymium bromate observed by Satten (1953) at 5880 cm^{-1}, which corresponds to the transition $^4I_{9/2} \rightarrow {}^4I_{15/2}$, leads to a value of 860 cm^{-1} for ζ in Nd^{3+}, allowing for second-order effects.

Table 3. Values of ζ

Ion	Sm^{3+}	Eu^{3+}	Tb^{3+}	Dy^{3+}	Ho^{3+}
ζ (cm^{-1})	1180	1360	1720	1920	2080

These values are only slightly different from those used to obtain the column headed 'Pure RS coupling' in table 2. This is due to the fact that the second-order corrections to the highest and lowest levels of a multiplet are often roughly the same, a result that justifies taking the overall splitting of a multiplet to give approximate values of ζ, as has been recently done by Bleaney (1955).

The positions of the excited multiplets required in the calculations are also of some interest. Their energies above the ground multiplet are given to the nearest integral multiple of F_2 in table 4.

Table 4. The Positions of Certain Excited Multiplets

Sm^{3+}, Dy^{3+}, Eu^{3+}, Tb^{3+}	^4G : 51, 72, 107, 197 ;	^4H : 65, 107, 143 ;	^4I : 50, 85, 166.
	^5D : 52, 100, 180 ;	^5F : 79, 149 ;	^5G : 61, 97, 177.
Ho^{3+}	^3H : 51, 93, 118, 201 ;	^3I : 71, 133 ;	^3K : 41, 114

In his analysis of Eu^{3+} (Judd 1955), the writer assumed perfect RS coupling and used the observed positions of $^7F_0$, $^7F_1$ and $^7F_2$ to give a value of 2100 cm^{-1} for ζ. This is now seen to be too large, and hence the theoretical spacings of $^5D_0$, $^5D_1$ and $^5D_2$ given in that paper must be proportionately reduced. While this tends to spoil the agreement with the observed positions of these levels, it must be remembered that the multiplet ^5D is probably even more susceptible to second-order interactions than the ground multiplet ^7F, since it is not in such an isolated position in the configuration as the latter.

§5. Conclusion

In this paper it has been shown that the observed deviations from the Landé interval rule in the ground multiplets of certain rare-earth ions can be satisfactorily explained in terms of a partial breakdown in RS coupling. The assumption of a hydrogenic 4f radial eigenfunction to calculate the energies of the excited multiplets is not as drastic a step as it might appear, for the ratios of the integrals F_k are comparatively insensitive to the shape of the eigenfunction. Because of the uncertainties in the positions of the multiplets, however, there seems little point at this stage either of carrying the perturbation treatment to a higher order or of including the comparatively small effects of spin–spin interaction in the theory.

Acknowledgment

Finally, I should like to express my gratitude to Dr. B. Bleaney for drawing my attention to this problem and for the interest he has taken in my work.

References

Araki, G., 1948 a, *Prog. Theor. Phys.*, **3**, 152 ; 1948 b, *Ibid.*, **3**, 262.
Bleaney, B., 1955, *Proc. Phys. Soc.* A, **68**, 937.
Condon, E. U., and Shortley, G. H., 1935, *The Theory of Atomic Spectra* (Cambridge : University Press).
Dirac, P. A. M., 1947, *The Principles of Quantum Mechanics* (Oxford : University Press).
Elliott, R. J., and Stevens, K. W. H., 1953, *Proc. Roy. Soc.* A, **218**, 553.
Geisler, H. F., and Hellwege, K. H., 1953, *Z. Phys.*, **136**, 293.
Gobrecht, H., 1937, *Ann. Phys., Lpz.*, **28**, 673 ; 1938, *Ibid.*, **31**, 755.
Hellwege, K. H., and Kahle, H. G., 1951, *Z. Phys.*, **129**, 62.
Jørgensen, C. Klixbüll, 1955 a, *J. Chem. Phys.*, **23**, 399 ; 1955 b, *K. Danske vidensk. Selsk. Mat. Fys. Medd.*, **29**, No. 11.
Judd, B. R., 1955, *Proc. Roy. Soc.* A, **228**, 120.
Rosenthal, G., 1939, *Phys. Z.*, **40**, 508.
Satten, R. A., 1953, *J. Chem. Phys.*, **21**, 637 ; 1955, *Ibid.*, **23**, 400.
Zeidel, A., Larionov, J., and Philippov, A., 1939, *J. Exp. Theor. Phys., U.S.S.R.*, **9.1**, 17.

Measurement of γ-Transition Lifetimes by Recoil Methods
II: M1 Transitions in ^{7}Li and ^{7}Be

By D. St. P. Bunbury†, S. Devons†, G. Manning‡ and J. H. Towle
Department of Physics, Imperial College, London

MS. received 12*th August* 1955, *and in amended form* 16*th September* 1955

Abstract. The methods described in a previous paper have been applied to the measurement of the mean lifetimes of the first excited states of the mirror nuclei ^{7}Li and ^{7}Be. The experimental results are, respectively, $7{\cdot}7 \pm 0{\cdot}8 \times 10^{-4}$ sec and $2{\cdot}7 \pm 1{\cdot}0 \times 10^{-13}$ sec. The accuracy of these results is limited, particularly in the latter case, by inadequate knowledge of the range–velocity relationship for these nuclei in their passage through solid materials.

§ 1. Introduction

Methods of utilizing the recoil motion of excited nuclei to obtain estimates of the half-lives of these states have been reviewed and described in a previous paper (Devons, Manning and Bunbury 1955, to be referred to as I). The present paper describes the application of such methods to the determination of the half-lives of the first excited states of the mirror nuclei ^{7}Li and ^{7}Be, from which transitions go to the ground states by emission of M1 radiation of energies 478 and 430 kev respectively.

These levels were known or expected to have half-lives in the region 10^{-13} to 10^{-14} sec, so that the most suitable methods were Doppler shift measurements described in § 2.2 of I. Such methods are particularly appropriate for such light nuclei as ^{7}Be and ^{7}Li, which can easily be produced with large recoil velocities. Indeed it turns out that measurement of the Doppler shift of the γ-radiation due to recoil motion can be made with sufficient precision for the limitation in the accuracy of the lifetime determination to be due to inexact knowledge of the range–velocity relations for such nuclei in their passage through matter.

§ 2. 478 kev Mγ Transition in ^{7}Li

Several attempts have been made previously to measure the half-life for this transition (Rasmussen *et al.* 1949, Elliott and Bell 1948, 1949, Bell 1955, Zhpinel 1954). Most of these measurements resulted in upper limits in the region 10^{-12} to 10^{-13} sec. The most accurate value, as reported by Bell (1955), is $7{\cdot}5 \pm 2{\cdot}5 \times 10^{-14}$ sec, but in arriving at this result some assumptions were apparently made about the range–velocity relationship for ^{7}Li ions in various materials.

For our measurements we used a modified form of the coincidence apparatus described in I. The gas-filled proportional counter used previously was replaced

† Now at The Physical Laboratories, The University, Manchester.
‡ Now at the English Electric Company, Stafford.

by a ZnS (Ag-activated) screen in conjunction with a 14-stage EMI photomultiplier (Type 6262), which made possible the use of shorter coincidence resolving times ($\sim 2 \times 10^{-8}$ sec). This change, together with the use of larger acceptance solid angles for both particle and γ-detectors, greatly speeded the accumulation of accurate data. The arrangement is shown diagrammatically in figure 1, and a block diagram of the modified electronic equipment is shown in figure 2. Two reactions were used to excite the 478 level of ^{7}Li: ^{9}Be(d, α)^{7}Li with deuteron energy of 450 kev, and ^{6}Li(d, p)^{7}Li with deuteron energy of 500 kev.

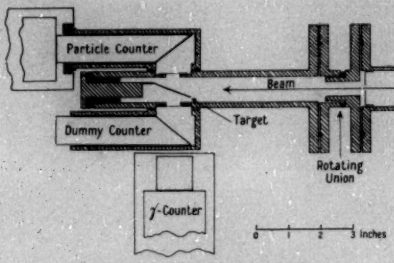

Figure 1. Coincidence apparatus.

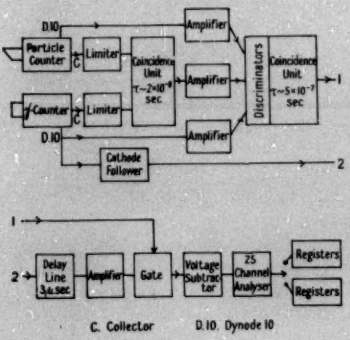

Figure 2.

2.1. ^{9}Be(d, α)^{7}Li

In addition to measurement of the Doppler shift, as described in I, with the Be layer deposited on a 'thick' copper backing, measurements were also made of the shifts when the recoil motion was into thin layers of copper, with thicknesses $13{\cdot}5 \pm 1{\cdot}5$, 25 ± 2, 28 ± 2 and $56 \pm 3 \times 10^{-6}$ cm. Further measurements were made when the recoil occurred into 'vacuum'.

The target for these last measurements was prepared by evaporating a thin layer ($\sim 10^{-6}$ cm) of beryllium on to an aluminium foil of about 0·2 mg cm^{-2} thickness, and observing the α-particles from the (d, p) reaction through the aluminium foil, so that apart from a small correction for the finite Be target

thickness, the Li nuclei recoiled into vacuum with their full initial velocity. The targets used for measurement of the recoil through the two thinnest copper layers were made by evaporating copper on to the Be of the aluminium supported targets described above. In order to measure the thicknesses of these copper layers, calcium fluoride targets were placed adjacent to the Be targets during the evaporation of the copper layers, and energy loss of protons in passing through the copper could be determined by examining a convenient resonance in the $^{19}F(p,\alpha,\gamma)^{16}O$ reaction.

The targets for recoil into the thicker copper layers were prepared by evaporating Be on to self-supporting copper films, since it was found that when using the previous technique for thick copper films, the copper and aluminium layers were liable to separate when the target was bombarded. If this occurred the Doppler shift measured would be different according as the Be layer adhered to the copper or the aluminium. The thicknesses of the self-supporting copper layers were measured by bombarding CaF_2 targets with protons through the actual targets.

Great care was taken that conditions at the γ-detector were as nearly identical as possible when the particle detector was in each of its two positions. In particular the apparatus was adjusted so that the rotation through 180° about the beam axis did not cause appreciable changes in the mean counting rates in either detector, and especially in the γ-detector. This latter was carefully examined to determine the effect of mean counting rate on pulse height for a γ-line of particular energy, and the circuits used with the photomultiplier were adjusted so as to reduce this variation to a minimum. In the actual measurements, the counting rates employed were never such as to make the apparent change in γ-energy with fluctuations in γ-intensity a serious source of error.

The results of Doppler shift measurements in six different targets are shown in figure 3. A typical pair of γ-spectra obtained in coincidence with α-particles moving towards and away from the γ-detector is shown in figure 4. The computed full shift for recoil motion into vacuum is $\delta E/E = 0{\cdot}0545$.

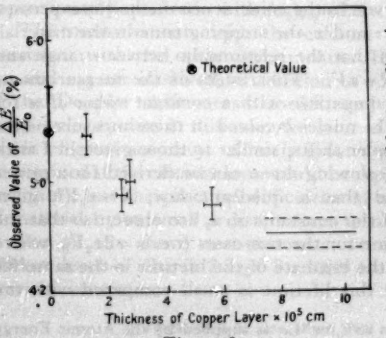

Figure 3.

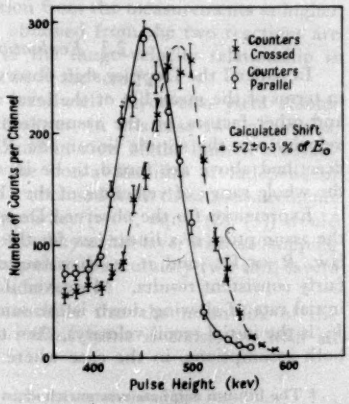

Figure 4.

2.2. $^6Li(d, p)^7Li$

The shifts in this reaction are rather smaller than in the previous case, so that measurements were made mainly of the recoil motion into 'thick' backings of copper and calcium, using evaporated layers of $^6Li_2SO_4$ as targets.† One set of measurements was also made using a layer of calcium, of thickness $2{\cdot}0 \pm 0{\cdot}1 \times 10^{-4}$ cm, 'sandwiched' between the lithium sulphate target layer and the 'thick' backing of copper. The results of these measurements are given in the table. The computed full shift for recoil into vacuum is $\delta E/E = 0{\cdot}0264$.

Measured Values of the Doppler Shift using the Coincidence Method and the $^6Li(d, p)^7Li^*$ Reaction for Copper, Calcium and a Calcium–Copper Sandwich, Target Backings

Material of target backing†	Cu_∞	Ca_∞	Ca–Cu
Measured values of $\delta E/E_0$ (%)	$1{\cdot}4 \pm 0{\cdot}4$	$1{\cdot}7 \pm 0{\cdot}3$	$2{\cdot}2 \pm 0{\cdot}4$
	$1{\cdot}4 \pm 0{\cdot}3$	$2{\cdot}0 \pm 0{\cdot}6$	$2{\cdot}2 \pm 0{\cdot}3$
	$1{\cdot}6_5 \pm 0{\cdot}3$	$2{\cdot}3 \pm 0{\cdot}3$	$1{\cdot}95 \pm 0{\cdot}4$
	$1{\cdot}3 \pm 0{\cdot}3$	$2{\cdot}5 \pm 0{\cdot}3$	$1{\cdot}6 \pm 0{\cdot}4$
	$1{\cdot}7 \pm 0{\cdot}3$	$2{\cdot}1 \pm 0{\cdot}3$	$1{\cdot}5 \pm 0{\cdot}4$
	$1{\cdot}3 \pm 0{\cdot}4$	$2{\cdot}3 \pm 0{\cdot}3$	$1{\cdot}9 \pm 0{\cdot}3$
	$1{\cdot}35 \pm 0{\cdot}3$		$2{\cdot}1 \pm 0{\cdot}3$
	$2{\cdot}2 \pm 0{\cdot}3$		$2{\cdot}4 \pm 0{\cdot}4$
	$1{\cdot}5 \pm 0{\cdot}3$		$2{\cdot}1 \pm 0{\cdot}3$
			$1{\cdot}7 \pm 0{\cdot}3$
			$1{\cdot}5 \pm 0{\cdot}4$
			$1{\cdot}6 \pm 0{\cdot}4$
			$2{\cdot}8 \pm 0{\cdot}5$
			$1{\cdot}8 \pm 0{\cdot}4$
			$2{\cdot}3 \pm 0{\cdot}4$
Weighted average values of $\delta E/E_0$ (%)	$1{\cdot}50 \pm 0{\cdot}11$	$2{\cdot}16 \pm 0{\cdot}14$	$1{\cdot}96 \pm 0{\cdot}10$

† Cu_∞ = 'infinite' Cu; Ca_∞ = 'infinite' Ca; Ca–Cu = calcium–copper sandwich : thickness of calcium layer $2 \pm 0{\cdot}1 \times 10^{-4}$ cm.

2.3. *Evaluation of the Half-lives*

In paper I the Doppler shift observed in the coincidence method is expressed in terms of the mean life of the level τ and α, the stopping time in the material, and other factors, on the assumption that the relationship between range and velocity was the simple linear one $R = \alpha V$. The results of the measurements described above are found to be incompatible with a constant value of α for the whole range of velocities of the ^7Li nuclei involved in these measurements.

Expressions for the observed Doppler shifts, similar to those given in I with the assumption of a linear law for the slowing down can be derived for a power law, $R = \alpha_n V^n$, and it is then found that a quadratic law, $R = \alpha_2 V^2$, gives fairly consistent results. Moreover if the constants α, α_2 are chosen so that the initial rate of slowing down is the same for the two cases (i.e. $\alpha = 2\alpha_2 V_0$, where V_0 is the initial recoil velocity), then the estimate of the lifetime is the same for both assumptions, in the case where this lifetime is small compared with the

† The lithium sulphate was enriched to 98% in ^6Li, as supplied by the Atomic Energy Research Establishment, Harwell.

slowing-down time in the stopping material. (For lifetimes large compared with the slowing-down time the estimated lifetime is dependent on the range–velocity relationship assumed, e.g. the quadratic law gives an estimate of half of that of the corresponding linear law with $\alpha = 2\alpha_2 V_0$.)

Since the observed Doppler shifts indicated a lifetime short compared with the slowing-down time in the present case, a determination of the *initial* rate of slowing down is clearly the significant quantity to be determined. It can easily be shown that the rate of change of Doppler shift S with thickness of copper t (see figure 3) for *very thin* layers depends on the constant assumed in the range–velocity relation and is independent of the lifetime of the level being measured. Using the values of the shifts observed for the thinnest copper layers ($<3\times10^{-5}$ cm) for ^{9}Be(d, α), together with the calculated value of V_0, a first approximation to the values of α_{Cu}, for ^{7}Li nuclei, of $3{\cdot}6\pm0{\cdot}6\times10^{-13}$ sec and of $(\alpha_2)_{Cu}$ of $2{\cdot}1\pm0{\cdot}4\times10^{-22}$ sec^2 cm^{-1} are obtained. Using these values we obtained estimates for the mean life τ of $6{\cdot}3\pm1{\cdot}6\times10^{-14}$ and $5{\cdot}5\pm1{\cdot}3\times10^{-14}$ sec respectively, which justifies the assumption that $\alpha_{Cu}\gg\tau$. These values of τ can now be used to correct the estimates of α, α_2, which are inaccurate on account of the finite thicknesses of Cu involved. A few steps of successive approximation yield a more accurate value of τ and α:

$$\tau = 7{\cdot}4\pm1{\cdot}8\times10^{-14}\text{ sec}, \qquad \alpha_{Cu} = 4{\cdot}2\pm0{\cdot}7\times10^{-13}\text{ sec}.$$

In principle, then, it is clear that measurement of the Doppler shift in several layers of a material with suitable thicknesses can yield information about both τ and α, but the accuracy of the final result is less than would be obtained from the same number of observations of the Doppler shift in a single layer, if independent, precise knowledge of α was available. Measurements of the range–velocity relationship for ^{7}Li nuclei were therefore made, for velocities in the range 8·6 to $5{\cdot}4\times10^8$ cm sec^{-1}, by an entirely independent method.† These gave a value of α_{Cu} at the velocities relevant to the ^{9}Be(d, α)^{7}Li experiments of $4{\cdot}4\pm0{\cdot}3\times10^{-13}$ sec, and the corresponding value of the mean life τ is $7{\cdot}8\pm1{\cdot}0\times10^{-14}$ sec. These measurements of the range–velocity relationship have not been extended to small enough velocities to be applicable directly to the ^{6}Li(d, p)^{7}Li experiments, but extrapolation from the measurements at higher velocities indicates that the estimates of τ obtained from the two reactions are in good agreement. The general shape of the range–velocity relationship is approximately quadratic with $(\alpha_2)_{Cu} = 2{\cdot}6\times10^{-22}$ sec^2 cm^{-1}.

The measurements with the calcium 'sandwich' layer also yield results consistent with the other experiments. However, in this case two quantities, α_{Cu} and α_{Ca} are involved, in addition to τ, and in view of the limited accuracy of the Doppler shift measurements, and the non-availability of independent range–velocity data in this case, the value of τ obtained from these measurements is not of great accuracy. Clearly greater accuracy (cf. I, eqns. (2), (3)) would be obtained if the calcium layer could be replaced by a thin layer with no stopping (vacuum), but the practical difficulties of separating accurately two thin layers of material by so small a distance are formidable.

For all the above measurements we conclude that the mean life of the 478 kev level of ^{7}Li is $7{\cdot}7\pm0{\cdot}8\times10^{-14}$ sec. This value is consistent with all previous estimates.

† These will be described in a separate communication.

§ 3. 430 kev Level of ^{7}Be

The experimental procedure used in this case was the 'target rotation' method described in I, and the apparatus and technique were essentially the same as described in that paper.

The reaction used to excite the 430 kev level was $^{10}B(p,\alpha)^7Be$, with protons of 1·45 Mev energy. The targets were prepared by evaporating boric acid, enriched to 99% in ^{10}B, on to 'thick' backings of copper and calcium. The γ-ray spectrum produced by proton bombardment was carefully examined for γ-radiation other than that from the excited ^7Be, such as was produced from the copper and calcium backings, and for positron-annihilation radiation from the $^{12}C(p,\gamma)$ reaction resulting from traces of carbon deposit on the targets. This latter was particularly serious since it is close in energy to the Be radiation, and could vary in amount with rotation of the target. In the actual measurements, these extraneous effects were reduced to very small magnitudes, and where appropriate small corrections were made to allow for residual effects.

The Doppler shifts were measured using the 'magnification' method described in I. The weighted average of ten measurements of the shift using 'thick' copper backings was $\delta E/E = 0{\cdot}0049 \pm 0{\cdot}0003$, and that for eight measurements using thick calcium backings was $\delta E/E = 0{\cdot}0025 \pm 0{\cdot}0004$.

In order to deduce the lifetime from these measurements it is necessary to know the angular distribution of the α particles in the (p,α) reaction, in addition to the range–velocity relationship for the recoiling ^7Be nuclei. In the absence of other information the (p,α) distribution was assumed isotropic, and this assumption is not likely to introduce an error of more than 10% in the estimate for τ. The computed full shift, with this assumption, is $\delta E/E = 0{\cdot}0075$.

In the absence of any independent information regarding the range–velocity relationship for ^7Be nuclei in solids, the relationship was assumed to be quadratic as in the case of ^7Li nuclei. This assumption gives, for the two measurements, values of the mean life, τ, in terms of $(\alpha_2)_{Cu}$ and $(\alpha_2)_{Ca}$:

$$\tau = 9{\cdot}7 \pm 1{\cdot}5 \times 10^8 (\alpha_2)_{Cu},$$
$$\tau = 3{\cdot}3 \pm 0{\cdot}5 \times 10^8 (\alpha_2)_{Ca}.$$

These results give, for the ratio $(\alpha_2)_{Ca}/(\alpha_2)_{Cu}$ a value of $3{\cdot}0 \pm 0{\cdot}7$ which is consistent with the value that is obtained on the assumption that the *relative* stopping power of the two materials is the same as for protons with the same initial velocity as the ^7Be recoil nuclei. (The data for protons is that given by Allison and Warshaw 1953.) This ratio is also in agreement with measurements, by an independent method, of the slowing of ^7Li nuclei in various metals.

To obtain an absolute value of τ, values must be assumed for $(\alpha_2)_{Cu}$ or $(\alpha_2)_{Ca}$. Assuming a value of $(\alpha_2)_{Cu}$ in this case of $2{\cdot}6 \times 10^{-22}$ sec^2 cm^{-1}, i.e. the same as for ^7Li nuclei, we obtain an estimate of τ of $2{\cdot}5 \pm 1{\cdot}0 \times 10^{-13}$ sec, where an uncertainty of some 30% has been attributed to the value of α_2. From the observed trend of the slowing down of heavy ions in gases one would expect the value of α_2 for Be to be somewhat larger than that for Li, and indeed, an attempt to estimate α_2 from such data and the relative stopping powers of air and metals for protons of comparable velocity confirms this indication.

We estimate, therefore, that $\tau = 2{\cdot}7 \pm 1{\cdot}0 \times 10^{-13}$ sec. An independent measurement of the range–velocity relation would reduce this error limit considerably.

§ 4. Discussion

Detailed calculations of the expected lifetimes for these M1 γ-transitions in ^{7}Li and ^{7}Be have been made by Lane (1955). The absolute transition probability is expressed in terms of the transition strength Λ, which is related to the mean lifetime by $\Lambda = \Gamma/(2{\cdot}76E^3 \times 10^{-3})$ and $\tau = \hbar/\gamma$ where Γ is the width in ev, γ is in ergs, and E is the transition energy in Mev. Lane's results are shown in figure 5, which gives the variation in the calculated values of Λ as a function of y, the coupling parameter expressing the relative strengths of central and spin–orbit forces involved in the intermediate-coupling calculations. It will be seen that the value of Λ for the ^{7}Li transition is definitely larger than the maximum theoretical value, which corresponds to a value of y of about 0·2, i.e. close to L–S coupling. The value of Λ for ^{7}Be is less precise but seems to depart, if anything, in the opposite direction, i.e. it seems smaller than the theoretical value with $y \sim 0{\cdot}2$. The theoretical ratio $\Lambda_{Li}/\Lambda_{Be}$ varies very little at all for values of $y < 0{\cdot}5$ and is approximately 1·33, whereas the experimental value is $2{\cdot}5 \pm 1$.

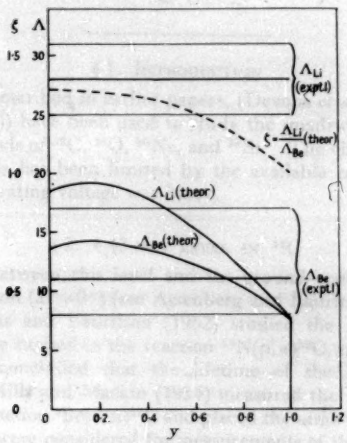

Figure 5.

This disagreement may well be due to the neglect of the motion of the ^{4}He core in the shell-model calculations, as discussed by Lane, and also to the contribution to the M1 transition strength from exchange currents. It may be significant that the static-dipole moment of ^{7}Li is also larger (by about 5%) than the calculated value, for $y \sim 0{\cdot}2$, on the intermediate-coupling model. Any refinements in the theory to improve the agreement with experiment in the case of either M1 transition could be readily checked by its predicted effect on the value of the strength of the other transition. In this connection, a more accurate value of α_2 for Be nuclei, and hence of τ_{Be}, would be very useful.

ACKNOWLEDGMENTS

We would like to express our thanks to Dr. A. Folkierski for technical assistance, and one of us (J. H. T.) is indebted to the Department of Scientific and Industrial Research for a maintenance grant.

REFERENCES

ALLISON, S. K., and WARSHAW, S. D., 1953, *Rev. Mod. Phys.*, **25**, 779.

BELL, R. E., 1955, *β and γ Spectroscopy* (Ed. K. Siegbahn), (Amsterdam : North-Holland), p. 518.

DEVONS, S., MANNING, G., and BUNBURY, D. St. P., 1955, *Proc. Phys. Soc.* A, **68**, 18.

ELLIOTT, L. G., and BELL, R. E., 1948, *Phys. Rev.*, **74**, 1869; 1949, *Ibid.*, **76**, 168.

LANE, A. M., 1955, *Proc. Phys. Soc.* A, **68**, 189.

RASMUSSEN, V. K., LAURITSEN, C. C., and LAURITSEN, T., 1949, *Phys. Rev.*, **75**, 199.

ZHPINEL, 1954, *Izvest. Akad. Nauk, S.S.S.R.*, **18**, 65.

Measurement of γ-Transition Lifetimes by Recoil Methods
III : E2 Transitions in some Even–Even Nuclei

BY S. DEVONS†, G. MANNING‡ AND J. H. TOWLE
Department of Physics, Imperial College, London

MS. received 29th August 1955

Abstract. The mean lives of the first 2^+ states of ^{12}C, ^{16}O, ^{20}Ne, and ^{28}Si have been measured using recoil methods with following results:

^{12}C $\tau = 2{\cdot}6 \pm 0{\cdot}9 \times 10^{-14}$ sec.
^{16}O $\tau \lesssim 2{\cdot}5 \times 10^{-14}$ sec.
^{20}Ne $\tau = 7{\cdot}6 \pm 3{\cdot}3 \times 10^{-13}$ sec.
^{28}Si $9 \times 10^{-13} \lesssim \tau$ (or $\tau \lesssim 3 \times 10^{-14}$).

§ 1. INTRODUCTION

THE methods described in earlier papers, (Devons *et al.* 1955 (I), Bunbury *et al.* 1956 (II)) have been used to study the quadrupole transitions from the first 2^+ levels of ^{12}C, ^{16}O, ^{20}Ne, and ^{28}Si. The choice of reaction used to excite these levels has been limited by the available equipment, for which the maximum accelerating voltage was 2 MeV.

§ 2. 4·43 MeV LEVEL IN ^{12}C

The transition between this level and the ground state is well established as a pure E2 transition ($2^+ \rightarrow 0^+$) (see Ajzenberg and Lauritsen 1955 for detailed references). Thomas and Lauritsen (1952) studied the Doppler broadening of the 4·43 MeV γ-line excited in the reaction $^{15}N(p,\alpha)^{12}C$, using a magnetic lens spectrometer, and concluded that the lifetime of the level was less than 3×10^{-13} second. Mills and Mackin (1954) measured the Doppler shift in this line excited in the reaction $^{9}Be(\alpha,n)^{12}C$ and placed the same limits on the lifetime.

Three reactions were considered for measurements of this transition lifetime, $^{14}N(d,\alpha)$, $^{15}N(d,p)$, and $^{9}Be(\alpha,n)$. With the available bombarding energies the first of these reactions would have yielded the largest Doppler shifts, and although some measurements were made with this reaction using the coincidence method, the relative convenience of beryllium as opposed to nitrogen targets led to the final choice of the third reaction for detailed measurements. The technique employed was that appropriate to endo-momental reactions, with stationary γ-detector as described in I, § 2.2 (*a*). The arrangement of the targets and detector is shown schematically in figure 1. The targets were thin ($\sim 7\,\mu g\,cm^{-2}$) layers of metallic beryllium evaporated (*a*) on to 'solid' backings of copper, (*b*) on to thick ($\gtrsim 10^{-4}$ cm) layers of calcium, which were evaporated

† Now at The Physical Laboratories, The University, Manchester.
‡ Now at The English Electric Company, Stafford.

on to copper backings, (*c*) on to thin self-supporting layers of copper. Doppler shifts were measured using the method described in I. A typical spectrum 'gated' by the wide and narrow channels respectively is shown in figure 2.

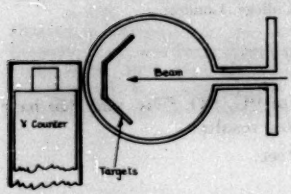

Figure 1. Apparatus used for endomomental method.

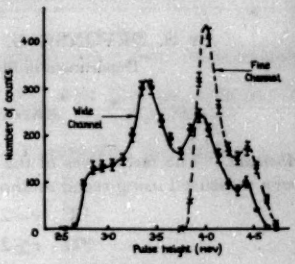

Figure 2. Typical gated spectra for measurement of lifetime of 4·43 Mev level of ^{12}C.

Two sets of measurements were made. In the first, the energy of the γ-radiation from excited ^{12}C nuclei recoiling into the copper backing was compared with that from ^{12}C nuclei recoiling into the 'thick' calcium layer. An α-particle energy of 1·9 Mev was used in these measurements. In the second set of measurements, the γ-radiation from nuclei recoiling into copper was compared with that from nuclei recoiling into vacuum, by bombarding, in the latter case, the Be target deposited on the thin copper film through the copper film. This second measurement yields a unique estimate of the lifetime, and is in principle a better comparison than the first, since it involves only the range–velocity relationship for one material, copper. However, the loss of energy of the α-particles when bombardment was made *through* the supporting film led to a reduction in yield and consequent loss of accuracy in the measurements, and with the actual maximum available α-particle energy of about 2 Mev, the first measurement was the more accurate. In comparing γ-energies from different targets many precautions were taken, as described in I and II, to ensure that the observed changes were due to genuine Doppler shifts and no other causes. This was particularly important in the present case where shifts of the order of a few parts in 10^5 were significant.

The mean result of twelve sets of measurements with 'thick' copper and calcium backings was a difference, $E_{Ca}-E_{Cu}=\delta E=(0{\cdot}00078\pm 0{\cdot}00008)E$.

The mean result for six comparisons with copper and vacuum backings was $E_0-E_{Cu}=\delta' E=(0\pm 0{\cdot}001)E$.

The computed full Doppler shift for the comparison of a vacuum and a perfect stopping material (stopping time, $\alpha \ll \tau$) was $\Delta E=0{\cdot}009E$. In order to interpret these results, some assumptions had to be made about the neutron, α-particle and γ-neutron angular correlations. In the absence of other information both were assumed isotropic, and the inaccuracy introduced by this assumption is unlikely to be serious in comparison with the uncertainty in the range–velocity relationship for carbon nuclei in solid materials.

Estimates of the stopping times for recoil into copper and calcium (α_{Cu} and α_{Ca}) were made by comparison of the range of ^{12}C nuclei in gases (Wrenshall 1940, Feather 1933) with our own measurements (see below) of the stopping of oxygen nuclei in copper, and approximate values of α_{Cu} for ^{12}C of $1{\cdot}4 \pm 0{\cdot}4 \times 10^{-13}$ sec and α_{Ca} of $5{\cdot}6 \pm 1{\cdot}6 \times 10^{-13}$ sec at the relevant velocities, were obtained.

From these values of α_{Cu} and α_{Ca} and the measured Doppler shift with these two targets, we obtain, neglecting the finite thickness of the Be layer, two possible values for the mean lifetime of the excited state: $\tau = 1{\cdot}9 \pm 0{\cdot}7 \times 10^{-14}$ sec and $\tau = 4{\cdot}3 \pm 1{\cdot}5 \times 10^{-12}$ sec. The rough comparison of the γ-radiation with copper and vacuum backings is sufficient to show that τ is less than about 3×10^{-14} sec so that the smaller of the above two values is the correct one.

The correction for the finite thickness of the beryllium target was quite appreciable with so short a lifetime. The final estimate for the mean lifetime is $2{\cdot}6 \pm 0{\cdot}9 \times 10^{-14}$ sec. The large error is largely due to the uncertainties in the range–velocity relationships.

§ 3. 6·9 MeV LEVEL IN ^{16}O

An upper limit for the lifetime of this level has been obtained by Doppler shift methods, as described in I, § 3.2. The estimate of this limit required some assumption regarding the range–velocity relation for ^{16}O nuclei in copper. We have, since these measurements were made, determined this range–velocity relationship by a Doppler-shift technique.

The lifetime of the 6·13 MeV level of ^{16}O is of the order 10^{-11} sec, which is much longer than the slowing down time α_{Cu} for such excited ^{16}O nuclei produced in the $^{19}F(p,\alpha)^{16}O$ reaction, recoiling into copper. It is a simple matter then to choose suitable copper layers (thickness $\lesssim 5 \times 10^{-5}$ cm) in which the excited ^{16}O nuclei will be slowed down, but will have negligible probability of radiating. By measuring the Doppler shifts for various thicknesses of copper, using the target rotation method described in I, the range–velocity relationship can be determined without any precise knowledge of the lifetime of the excited state.

Targets of this sort were prepared by evaporating copper on to thin CaF_2 targets, which were themselves evaporated on to thick copper backings. The thickness of the copper layers was determined by the energy shift in the resonances of the $^{19}F(p,\alpha)$ reaction.

The expected Doppler shift, for an average proton energy at the CaF_2 target of 1·38 MeV was computed, on the basis of a linear range–velocity relation, $R = \alpha_{Cu} V$, to be

$$\delta E/E = 0{\cdot}0049(1 - d/R_0)^2, \quad \text{for} \quad d < R_0,$$

where d is the thickness of the copper layer covering the CaF_2 target, and R_0 is the range in copper for an initial velocity of $2{\cdot}8 \times 10^8$ cm. For $d > R_0$, $\delta E/E = 0$ of course.

Measurements of this Doppler shift were made for copper layers of thickness 12 ± 2, 26 ± 3, and $55 \pm 3 \times 10^{-6}$ cm, and also for an uncovered target. The mean values of $\delta E/E$ were $0{\cdot}0032 \pm 0{\cdot}0006$, $0{\cdot}0014 \pm 0{\cdot}0006$, $-0{\cdot}0003 \pm 0{\cdot}0006$, and $0{\cdot}0056 \pm 0{\cdot}0006$ respectively. Figure 3 shows a graph of $(\delta E/E \times 0{\cdot}0049)^{1/2}$ plotted against d, from which it is seen that these results are consistent with a linear range–velocity relationship, with a value of α_{Cu} of $1{\cdot}8 \pm 0{\cdot}2 \times 10^{-13}$ second.

This is to be compared with the value $1{\cdot}3 \times 10^{-13}$ which was assumed in paper I. The estimate for the mean life of this state is consequently changed to $\tau \lesssim 2{\cdot}5 \times 10^{-14}$ second.

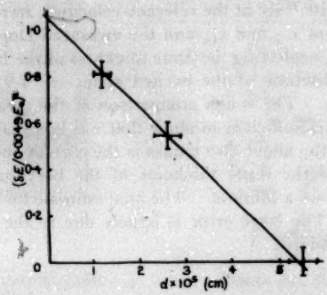

Figure 3. Results of experiments on the range of ^{16}O nuclei in copper.

§ 4. 1·62 MeV LEVEL OF ^{20}Ne

This level was excited by means of the reaction $^{23}Na(p,\alpha)^{20}Ne$ using protons of energy 1·22 MeV. Doppler shift measurements were made with the 'target-rotation' technique, as used for ^{16}O and as described in I. Targets used were thin evaporated layers of NaCl on 'thick' backings of calcium and gold.

The mean shifts measured were $\delta E/E = 0{\cdot}0012 \pm 0{\cdot}00015$, and $0{\cdot}0021 \pm 0{\cdot}0003$ for calcium and gold backings respectively. The angular correlation of α-particles with protons and γ-radiation with α-particles are known in this case (Seed 1953) so that the Doppler shift corresponding to a perfect stopping material could be calculated as $\delta E/E = 0{\cdot}0029$.

There is no direct information regarding the range–velocity relationship for ^{20}Ne nuclei in solids. Assuming a linear relationship we obtained the following estimate for the mean life: $\tau = (0{\cdot}69 \pm 0{\cdot}19)\alpha_{Ca}$ and $\tau = (2{\cdot}6 \pm 1{\cdot}1)\alpha_{Au}$. These results indicate a ratio of about 4 for α_{Ca}/α_{Au}, which is consistent with the estimate obtained from the ratio of stopping powers of the two metals for protons of the same velocity as the Ne recoil nuclei.

The range of Ne nuclei in gases has been measured (McCarthy 1938), and by using these results, and assuming the relative stopping powers of gases and solids are similar for Ne and O nuclei, we estimate α_{Ca} for Ne nuclei of relevant velocities to be $1{\cdot}1 \pm 0{\cdot}4 \times 10^{-12}$ second. This gives an estimate of the mean life of the 1·63 level of ^{20}Ne of $7{\cdot}6 \pm 3{\cdot}3 \times 10^{-13}$ second.

§ 5. 1·78 MeV LEVEL OF ^{28}Si

This level was excited by means of the reaction $^{27}Al(p,\gamma)^{28}Si$, using protons of energy 990 kev corresponding to a prominent resonance for the reaction. It was assumed that the lifetime for cascade of γ-rays from the resonance level to the 1·78 MeV was much shorter than the lifetime of the level itself. The small momentum given to the ^{28}Si nuclei by these cascade γ-rays was also neglected, and the recoil motion attributed entirely to the bombarding protons.

Doppler shift measurements were made in a similar manner to those described above for ^{12}C. Thin targets of aluminium were made by evaporation on to 'thick' backings of calcium and tantalum. The difference in the γ-energy δE for these two targets was found to be less than $0{\cdot}0003E$, whereas the computed difference in Doppler shift for a vacuum and a perfect stopping material is $0{\cdot}0017E$.

Assuming a linear range–velocity relationship for ^{28}Si nuclei, and that $\alpha_{Ca} \simeq 4\alpha_{Ta}$, we obtain two possible interpretations of the small measured shift: (*a*) γ-transition fast: $\tau \lesssim \frac{1}{3}\alpha_{Ta}$, (*b*) γ-transition slow: $\tau \gtrsim 3\alpha_{Ca}$. We can only make rough estimates of the limits for α_{Ta} and α_{Ca}, for recoil nuclei of these low velocities (5×10^7 cm sec^{-1}), and these we take to be $\alpha_{Ta} \simeq 10^{-13}$ and $\alpha_{Ca} \simeq 3 \times 10^{-13}$. The corresponding limits for the γ-lifetime are $\tau \lesssim 3 \times 10^{-14}$ or $\tau \gtrsim 9 \times 10^{-13}$. For an E2 transition of this energy, the second limit is more likely to be the correct one. Of course a direct comparison of the energy shift with recoil into vacuum and one of the above materials would remove this ambiguity, but this involves bombardment through a supporting layer, a technique which presents some difficulty when the exciting reaction has so sharp a resonance.

§ 6. Discussion

In the absence of detailed knowledge of the wave functions of the nuclear states involved in the above measurements, we give below a comparison of the measured lifetimes with those predicted for a single-proton transition in a fixed potential well. Assuming 'constant-density' radial wave functions and a nuclear radius of $1{\cdot}45 \times 10^{-13}A^{1/3}$ cm, Moszkowski (1955) gives the expression $1/\tau = 1{\cdot}6 \times 10^8 A^{4/3}E^5S$ (where S is a factor of the order unity and depends on initial and final spins). Using a smaller value of $1{\cdot}3 \times 10^{-13}A^{1/3}$ reduces the numerical factor to 10^8. Using this value we get for the ratio, $r = \tau_{theor}/\tau_{exp}$:

^{12}C: $r = (8{\cdot}0 \pm 2{\cdot}8)S^{-1}$; ^{16}O: $r \gtrsim 0{\cdot}8S^{-1}$

^{20}Ne: $r = (21 \pm \frac{15}{7})S^{-1}$; ^{28}Si: $r \lesssim 6{\cdot}5S^{-1}$.

The large quadrupole transition moments indicated by these results are of interest in connection with estimating the extent of correlated nuclear motion in light nuclei, but more extensive results are clearly desirable before definite conclusions are made. The methods described in this and the previous papers should enable such results to be obtained, particularly if particles of higher energy than those used in the present experiments are employed.

References

Ajzenberg, F., and Lauritsen, T., 1955, *Rev. Mod. Phys.*, **27**, 77.

Bunbury, D. St. P., Devons, S., Manning, G., and Towle, J. H., 1956, *Proc. Phys. Soc.* A, **69**, 165.

Devons, S., Manning, G., and Bunbury, D. St. P., 1955, *Proc. Phys. Soc.* A, **68**, 18.

Feather, N., 1933, *Proc. Roy. Soc.* A, **141**, 194, **142**, 689.

Mills, W. R., and Mackin, R. J., 1954, *Phys. Rev.*, **95**, 1206.

McCarthy, J. T., 1938, *Phys. Rev.*, **53**, 30.

Moszkowski, S. A., 1955, *Beta and Gamma-Ray Spectroscopy* (Ed. K. Siegbahn) (Amsterdam: North-Holland).

Seed, J., 1953, *Phil. Mag.*, **44**, 921.

Thomas, R. G., and Lauritsen, T., 1952, *Phys. Rev.*, **88**, 969.

Wrenshall, G. A., 1940, *Phys. Rev.*, **57**, 1095.

RESEARCH NOTES

The Identification of a Band System, $B(^2\Sigma^+) - A^2\Sigma^+$, in OH and OD

By R. F. BARROW and A. R. DOWNIE
Physical Chemistry Laboratory, Oxford

MS. received 4th October 1955

Schüler and Woeldike (1943) were the first to record a band-system, excited by a discharge in water vapour, which lies in the region 4200 to 6000 Å. The emitter of this system has not yet been identified, although it has at one time or another been suggested that it is H_2O, OH^+, OH or OH^-. The purpose of this note is to show that the bands arise from a transition $B(^2\Sigma^+)$–$A^2\Sigma^+$ in OH.

Rotational analyses of the new bands of O^1H have been published (Schüler, Reinebeck and Michel 1954, Benoist 1955) which are in satisfactory agreement, although the precision of neither set of measurements is high. We have evaluated the constants anew from the published figures, making some attempt to take account of centrifugal stretching terms, which are important. The results are given in table 1. The first lower state vibrational interval is 1916 cm^{-1}. Now

Table 1. Constants for B–$A^2\Sigma^+$ system of O^1H

v', v''	ν_0		B	D
1, 5	23703	$v''=5$	$12{\cdot}60_4$	$2{\cdot}_8\times10^{-3}$
0, 5	23043	6	$11{\cdot}53_8$	$2{\cdot}_9\times10^{-3}$
1, 6	21790	7	$10{\cdot}19_6$	$3{\cdot}_7\times10^{-3}$
0, 6	21126	8	$8{\cdot}3_8$	$(5{\cdot}_5)\times10^{-3}$
0, 7	19502	$v'=0$	$5{\cdot}19_3$	$1{\cdot}_5\times10^{-3}$
0, 8	18227	1	$4{\cdot}18_3$	$(2)\times10^{-3}$

$T_0=68366$ cm^{-1}

for $A^2\Sigma^+$ of OH, Gaydon (1953) gives $\Delta G(0–1)=2987$, (1–2) 2793, (2–3) 2593, (3–4) 2384 cm^{-1}. A natural extrapolation gives $\Delta G(4–5)=2163$, (5–6) = 1927 cm^{-1}. The agreement between the extrapolated interval, 1927, and the observed value 1916 cm^{-1} is suggestive. If we now consider the values of B_v for $A^2\Sigma^+$ of OH, we find that Tanaka and Koana (1934) give the equation

$$B_v = 17{\cdot}351 - 0{\cdot}796_9(v+\tfrac{1}{2}) - 0{\cdot}0123_5(v+\tfrac{1}{2})^2,$$

valid for $0 \leqslant v \leqslant 4$. By extrapolation, $B_5 = 12{\cdot}595$, in excellent agreement with the value of B'' for the band at 23044 cm^{-1} (table 1) 12·60 cm^{-1}. We may reasonably conclude that the lower state of the system is $A^2\Sigma^+$: further evidence in support of this conclusion appears below. The way in which ΔG and B vary with vibrational quantum number is illustrated in the figure.

The extrapolation of the vibrational intervals in $A^2\Sigma^+$ to the convergence point is short, and amounts only to some 1230 cm^{-1}. We obtain $D_e(A^2\Sigma^+)=20532$ cm^{-1}, which with $T_e(A–X)=32861$ cm^{-1}, leads to

$D_0''(x^2\Pi) = 35501\,cm^{-1}$, or $101{\cdot}4_8$ kcal. If it is assumed that the extrapolation is correct to about $\pm 10\%$, then the limits of error in D_0'' are about $\pm 0{\cdot}5$ kcal. The agreement with the thermal value obtained by Dwyer and Oldenberg (1944), $D_0'' = 100{\cdot}2 \pm 0{\cdot}9$ kcal (see Gaydon 1953), is satisfactory.

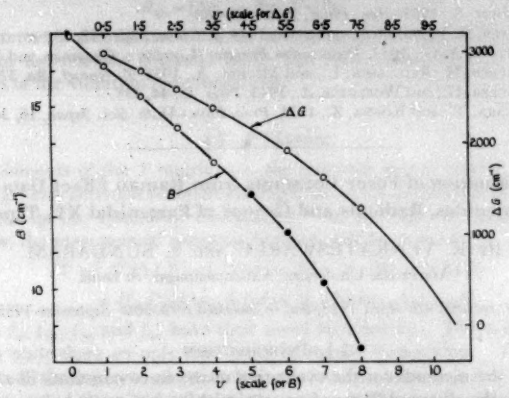

The variation of ΔG and of B with v in the state $A^2\Sigma^+$ of OH.

Corresponding bands of O^2H have been photographed by Schüler, Reinebeck and Michel (1954), and the vibrational scheme which they propose is correct. They also give rotational analyses of three bands which are erroneous. We have, however, been able to carry out acceptable analyses, using their measurements, by shifting appropriately the numbering in the branches. The constants for the O^2H bands are given in table 2. The values of ΔG and of B fit well with extrapolated constants for $A^2\Sigma^+$ of O^2H, if the band at 23014 cm^{-1} has as its lower state $v = 7$. Proceeding as before, we find $D_e(A^2\Sigma^+) = 20619\,cm^{-1}$, in good agreement with the more precise value obtained from the O^1H bands.

Table 2. Constants for B–$A^2\Sigma^+$ system of O^2H

v', v''	ν_0		B	D
0, 7	23014	$v''=7$	$6{\cdot}68_7$	$(7{\cdot}5 \times 10^{-4})$
0, 9	20303	9	$5{\cdot}78_7$	$8{\cdot}9 \times 10^{-4}$
0, 10	19186	10	$5{\cdot}22_3$	10×10^{-4}
		$v'=0$	$2{\cdot}74_3$	$2{\cdot}6 \times 10^{-4}$

$T_0 = 68669\,cm^{-1}$

$\Delta G'(0\text{–}1) = 546$, $\Delta G'(1\text{–}2) = 360\,cm^{-1}$ (Schüler *et al.* 1954)

The upper state B calls for some comment. Since only two branches have been observed in each band, it is probable that it is a $^2\Sigma^+$ state. The vibrational intervals in this state converge very rapidly, and it seems certain that it correlates with $O(^1S_0) + H$. Information is not yet available to verify in detail the expected isotope relations in $B^2\Sigma^+$ of O^1H and O^2H, but it appears that the lowest observed vibrational levels for each molecule have $v = 0$. The values for D_0' are about 930 and 985 cm^{-1} for O^1H and O^2H respectively.

It is clear that a detailed investigation of these bands, with higher resolution than hitherto, is likely to prove of some interest, and should in particular lead to a very precise determination of the dissociation energy of OH. This work is now in progress.

REFERENCES

BENOIST, S., 1955, *Ann. Phys., Paris*, **10**, 363.
DWYER, R. J., and OLDENBERG, O., 1944, *J. Chem. Phys.*, **12**, 351.
GAYDON, A. G., 1953, *Dissociation Energies* (London: Chapman and Hall).
SCHÜLER, H., REINEBECK, L., and MICHEL, A., 1954, *Z. Naturf.*, **9a**, 279.
SCHÜLER, H., and WOELDIKE, A., 1943, *Phys. Z.*, **44**, 435.
TANAKA, T., and KOANA, Z., 1934, *Proc. Phys.-Math. Soc. Japan*, **16**, 365.

Evaluation of Force Constants from Raman Effect Data: Molecules, Radicals and Groups of Pyramidal XY_3 Type

BY K. VENKATESWARLU AND S. SUNDARAM

Annamalai University, Annamalainagar, S. India

MS. received 4th April 1955, and in amended form 30th September 1955

§ 1. INTRODUCTION

Of all the methods for the evaluation of the force constants of a molecule from the observed Raman frequencies, the more recent and comparatively simpler method is the one introduced by Wilson (1939, 1941) utilizing the symmetry coordinates. The chief advantages of this Wilson's *F–G* matrix method, as it is usually called, are (i) the method requires no separate coordinate system but instead makes use of the internal coordinates which are the changes in the bond distances and the inter-bond angles in a molecule, and (ii) the solution of the secular equation in the form of an expanded algebraic equation becomes easier than in a determinantal form.

In the present investigation, the *F–G* matrix method is used to evaluate the force constants in the case of some molecules, radicals and groups of the pyramidal XY_3 type. It can be seen from the available literature (Herzberg 1951) that the force constants in the case of some of these pyramidal molecules have previously been worked out by other methods but a rigorous application of this group-theoretical method has been attempted here for the first time to evaluate the force constants of several pyramidal structures, some of which have not been worked out by any of the methods so far.

§ 2. SYMMETRY COORDINATES

These pyramidal structures belong to the point group C_{3v} and as such give rise to two nondegenerate A_1 type and two doubly degenerate E type Raman frequencies. As there are six vibrations in all, the six internal coordinates used in constructing the symmetry coordinates are Δd_1, Δd_2, Δd_3 indicating the changes in the X–Y bond distances and $\Delta\alpha_{12}$, $\Delta\alpha_{23}$, $\Delta\alpha_{31}$ the changes in the Y–X–Y inter-bond angles. For the two types of vibrations, the six symmetry coordinates which are the linear combinations of the above internal coordinates are

for the A_1 type,
$$R_1=(\Delta d_1+\Delta d_2+\Delta d_3)/\sqrt{3}$$
$$R_2=(\Delta\alpha_{12}+\Delta\alpha_{23}+\Delta\alpha_{31})/\sqrt{3}$$

and for the E type,

$$R_{3a} = (2\Delta d_1 - \Delta d_2 - \Delta d_3)/\sqrt{6}$$
$$R_{3b} = (\Delta d_2 - \Delta d_3)/\sqrt{2}$$
$$R_{4a} = (2\Delta\alpha_{12} - \Delta\alpha_{23} - \Delta\alpha_{31})/\sqrt{6}$$
$$R_{4b} = (\Delta\alpha_{23} - \Delta\alpha_{31})/\sqrt{2}.$$

These symmetry coordinates form an orthonormal set and further it may be seen, from the relevant character table, that they transform according to the characters of the vibration type concerned.

§ 3. *F* Matrix

The elements of the *F* matrix, viz. the potential energy matrix, are derived from the general potential function assumed, using the coefficients of the internal coordinates in the symmetry coordinates. In the case of these pyramidal structures, the most general potential function will be of the form

$$2V = f_d[\Sigma(\Delta d_1)^2] + f_\alpha[\Sigma(d\Delta\alpha_{12})^2] + 2f_{dd}[\Sigma(\Delta d_1)(\Delta d_2)] + 2f_{d\alpha}[\Sigma(d\Delta\alpha_{12})](\Delta d) + 2f_{\alpha\alpha}[\Sigma(d\Delta\alpha_{12})(d\Delta\alpha_{23})]$$

where f_d, f_α, f_{dd}, $f_{d\alpha}$ and $f_{\alpha\alpha}$ have their usual significance. There are five force constants while there are only four observed Raman frequencies. Thus in order to evaluate all the five force constants from the four frequencies, it may be necessary to assume one of them and calculate the remaining four. In case no reported data are available to assume one of the force constants, one of the five constants which contributes very little to the potential energy is neglected and in those cases four force constants are evaluated. Accordingly, when the above most general quadratic potential function is assumed, the matrix elements are for the A_1 type,

$$F_{11} = (f_d + 2f_{dd}), \quad F_{12} = F_{21} = 2df_{d\alpha}, \quad F_{22} = d^2(f_\alpha + 2f_{\alpha\alpha})$$

and for the E type,

$$F_{33} = (f_d - f_{dd}), \quad F_{34} = F_{43} = \tfrac{1}{2}df_{d\alpha}, \quad F_{44} = d^2(f_\alpha - f_{\alpha\alpha}).$$

For those cases where $f_{d\alpha}$ is neglected, $F_{12} = F_{21} = 0$, $F_{34} = F_{43} = 0$, all the other elements remaining the same.

§ 4. *G* Matrix

The elements of the kinetic energy matrix are obtained from Wilson's general expressions, assuming unit vectors directed along the bonds in terms of the reciprocal masses of the atoms, bond distances and inter-bond angles. For the A_1 type vibrations they are :

$$G_{11} = \mu_y + \mu_x(1 + 2\cos\alpha)$$
$$G_{12} = G_{21} = [-2\mu_x(1 - \cos\alpha)(1 + 2\cos\alpha)]/d\sin\alpha.$$
$$G_{22} = 2[\mu_y(1 + \cos\alpha - 2\cos^2\alpha) + 2\mu_x(1 - \cos\alpha)^2(1 + 2\cos\alpha)]/d^2\sin^2\alpha$$

and for the E type vibrations,

$$G_{33} = \mu_y + \mu_x(1 - \cos\alpha)$$
$$G_{34} = G_{43} = [-\mu_x(1 - \cos\alpha)^2]/2d\sin\alpha$$
$$G_{44} = [\mu_y(2 - \cos\alpha - \cos^2\alpha) + \mu_x(1 - \cos\alpha)^2]/d^2\sin^2\alpha.$$

	Y–X–Y angle (°)	Observed frequencies A_1		E		$f_d \times 10^{-5}$ (dyn cm^{-1})	$f_{dd} \times 10^{-5}$ (dyn cm^{-1})	$f_\alpha \times 10^{-5}$ (dyn cm^{-1})	$f_{\alpha\alpha} \times 10^{-5}$ (dyn cm^{-1})	$f_{d\alpha} \times 10^{-5}$ (dyn cm^{-1})	X–Y distance (Å) (Badger's rule)
NH_3	109	950	3334	1630	3415	6·3500	0·0278	0·5463	−0·0478	0·1325	
ND_3	111	748	2410	1191	2528	6·5100	0·0281	0·5727	−0·0068	0·1375	1·00
PH_3	99	979	2306	1115	3428	3·2400	−0·0750	0·3379	0·0007	0·1008	1·30
PF_3	104	531	890	486	840	4·5900	0·3823	1·0050	0·1815	−0·1191	
PCl_3	101	258	511	190	484	2·1200	0·2591	0·2840	0·0710	0·0116	
PBr_3	101·5	162	380	115	400	1·6300	0·1244	0·1995	0·0723	0·0307	
$SbCl_3$	96	152	355	126	318	1·7800	0·2534	0·1676	0·0225	0·1751	
$BiCl_3$	100	130	288	100	242	1·1900	0·1699	0·1260	0·0246	−0·0034	
AsF_3	97	341	707	273	644	3·9200	0·3300	0·3987	0·0586	−0·1114	
$AsCl_3$	103	194	405	158	370	2·0300	0·1822	0·1941	0·0341	−0·0695	
$AsBr_3$	100	129	276	98	220	1·0827	0·2836	0·1780	0·0295		
ClO_3	89	625	933	480	963	5·3167	−0·6293	1·3573	0·3839		1·60
BrO_3	89	442	800	350	828	5·2260	−0·1680	0·5944	0·0528		1·68
IO_3	89	357	780	326	809	5·3447	−0·1463	0·4834	0·0024		1·79
$SiCl_3$	110	249	489	179	587	2·7177	0·2107	0·2285	0·1105		
$SiBr_3$	110	166	362	115	470	2·0113	0·0833	0·2470	0·0778		
CF_3	109	697	937	508	1116	3·8463	0·2203	1·6970	−0·5090		

The secular equations obtained from the above elements of the F and G matrices are

$$\lambda^2-\lambda(F_{11}G_{11}+2F_{12}G_{12}+F_{22}G_{22})+(F_{11}F_{22}-F_{12}^2)(G_{11}G_{22}-G_{12}^2)=0$$

and

$$\lambda^2-\lambda(F_{33}G_{33}+2F_{34}G_{34}+F_{44}G_{44})+(F_{33}F_{44}-F_{34}^2)(G_{33}G_{44}-G_{34}^2)=0$$

for the A_1 type and E type vibrations respectively. $\lambda=4\pi^2c^2\nu^2$, ν being the frequency in cm^{-1}.

§ 5. Results

The theoretical considerations developed above have been applied to the evaluation of force constants of some molecules, radicals and groups having the pyramidal structure and belonging to the point group C_{3v}. As mentioned earlier, there are five force constants in the most general quadratic potential function as against four observed frequencies from which they have to be evaluated. There are ten cases out of the 17 discussed in this paper, for which reported values of f_d are available (Herzberg 1951), and in those cases, the remaining four constants have been evaluated. For the remaining seven cases where f_d values are not available, the uniform procedure of neglecting $f_{d\alpha}$ and calculating the other four has been followed, as in these cases using $f_{d\alpha}$ and neglecting $f_{\alpha\alpha}$ led to the quadratics in $f_{d\alpha}$ having no real roots.

The observed Y–X–Y interbond angles, the observed frequencies (taken from Landolt–Börnstein Tables, 1951 edn) and the most probable sets of the force constants obtained for the various cases are given in the table. Also the X–Y distances calculated by Badger's rule (1935) from the f_d values obtained in the present investigation for some cases where such data are not available are given in the last column of the table. The frequencies calculated using the force constants obtained in the present investigation are in exact agreement with the observed frequencies.

References

Badger, R. M., 1935, *J. Chem. Phys.*, **3**, 710.

Herzberg, G., 1951, *Infra-red and Raman Spectra of Polyatomic Molecules* (New York: van Nostrand), p. 177.

Wilson, E. B., 1939, *J. Chem. Phys.*, **7**, 1047; 1941, *Ibid.*, **9**, 76.

LETTERS TO THE EDITOR

Spherical Harmonics with the Symmetry of the Close-Packed Hexagonal Lattice

In using the cellular method, expansions in spherical harmonics are necessary which reproduce the symmetry of the group of the **k** vector. A method to obtain these expansions has been given by von der Lage and Bethe (1947) and recently extended by Bell (1954). In this method, however, the spherical harmonics are expressed in Cartesian coordinates, which makes it difficult to apply recurrence and other relations between them. We have therefore developed a general, group-theoretical, technique to obtain these expansions in polar coordinates. We use the representations of the rotation group given by Wigner (1931), which we have put in a convenient form for computation. Some theorems, which simplify the representations for the finite rotation groups, have also been obtained. A full account of the method will be published elsewhere. We have considered it convenient, however, to publish in advance our results for the representations with the full symmetry of the close-packed hexagonal lattice ($\mathbf{k}=0$), as they are at variance with similar expansions recently given by Schiff (1955).

Our results are summarized in the table where, to facilitate comparison, we use the same notation as Schiff for the irreducible representations. This is the one given by Herring (1942).

Representation		l† (mod 2)	m‡ (mod 6)	ϕ-dependence	sign
Γ_1^+,	Γ_4^-	0	0	cos	+, −
		3	3	cos	−, +
Γ_1^-,	Γ_4^+	4	3	sin	−, +
		7	6	sin	+, −
Γ_2^+,	Γ_3^-	6	6	sin	+, −
		3	3	sin	−, +
Γ_2^-,	Γ_3^+	4	3	cos	−, +
		1	0	cos	+, −
Γ_5^+,	Γ_6^-	2	1, 5	$\begin{Bmatrix}\sin\\ \cos\end{Bmatrix}$	+, −
		3	2, 4	$\begin{Bmatrix}\sin\\ \cos\end{Bmatrix}$	−, +
Γ_5^-,	Γ_6^+	2	2, 4	$\begin{Bmatrix}\sin\\ \cos\end{Bmatrix}$	−, +
		1	1, 5	$\begin{Bmatrix}\sin\\ \cos\end{Bmatrix}$	+, −

† See the text for the notation for l and m. For example, $l=6$ (mod 2) means here the succession of values 6, 8, 10 . . . .

‡ For example, $m=1, 5$ (mod 6) means here the succession of values 1, 5, 7, 11, 13, 17 . . .

The following notes are necessary for the understanding of our table. As there are two atoms per unit cell, our expansions must be given in terms of spherical harmonics centred around each of the two atoms of the basis. If these are denoted respectively with Y_l^m and $'Y_l^m$ they will appear in pairs of the form $Y_l^m \pm {}'Y_l^m$. The sign to be used in this linear combination is given in the fifth column of the table, the first sign to the left corresponding to the first representation given in the first column. For non-degenerate representations the spherical harmonics reduce to the form $P_l^m(\cos\theta)\sin m\phi$ or $P_l^m(\cos\theta)\cos m\phi$. Both these forms appear in pairs in the degenerate representations. This ϕ-dependence is given in the fourth column and in the second and third the permissible values of l and m, modulo 2 and 6 respectively, are listed. In each case we give the smallest integer, modulo 2 or modulo 6, which can appear in the expansions. The definition which we use for the functions P_l^m is that given by Margenau and Murphy (1943).

I am grateful to Dr. B. Schiff for correspondence and discussion.

Mathematical Institute, S. L. Altmann.
Oxford.
6th December 1955.

Bell, D. G., 1954, *Rev. Mod. Phys.*, **26**, 311.
Herring, C., 1942, *J. Franklin Inst.*, **233**, 525.
von der Lage, F. C., and Bethe, H. A., 1947, *Phys. Rev.*, **71**, 612.
Margenau, H., and Murphy, G. M., 1943, *The Mathematics of Physics and Chemistry* (New York : Van Nostrand).
Schiff, B., 1955, *Proc. Phys. Soc.* A, **68**, 686.
Wigner, E., 1931, *Gruppentheorie und ihre Anwendung auf die Quantenmechanik der Atomspektren* (Braunschweig : Vieweg und Sohn).

The Cellular Method for Close-Packed Hexagonal Titanium

In a recent paper (Schiff 1955) the author has given the expansions in spherical harmonics for the symmetry types belonging to the centre of the zone in a close-packed hexagonal lattice. Some of the expansions and the corresponding boundary conditions given in the paper are incorrect, due to the use of incorrect irreducible representations. Altmann (1956) has tabulated the correct expansions for each type belonging to the zone centre, and a corrected table of boundary conditions is given below. The notation of Herring (1942) is used to denote the symmetry types, and the boundary conditions are given for the section of the atomic polyhedron shown in figure 2(*b*) of the author's paper. Altmann's table, together with that given below, replaces tables 1 and 2 of the paper respectively.

Of the eigenvalues given in table 3, those for the states Γ_1^+ and Γ_4^- are unaffected, but those given for the states Γ_4^+, Γ_6^+, Γ_5^+ and Γ_6^- must be considered as incorrect. Thus the conclusion that the eigenvalue of the lowest d-like state in close-packed hexagonal titanium lies above that of the lowest s-like state cannot be relied upon. The eigenvalues for the body-centred cubic modification given in table 4 are, of course, unaffected.

Boundary Conditions for the Symmetry Types at Γ

Non-Degenerate Types: Type	Face CDE ψ	Face CDE ψ'	Line BC ψ	Line BC ψ'
Γ_1^+		0	s	a
Γ_1^-	0		s	a
Γ_2^+	0		a	s
Γ_2^-		0	a	s
Γ_3^+		0	s	a
Γ_3^-	0		s	a
Γ_4^+	0		a	s
Γ_4^-		0	a	s

Degenerate Types: Type	ϕ-dependence	Face CDE ψ	Face CDE ψ'	Line BC ψ	Line BC ψ'
Γ_5^+	$\cos m\phi$		0	s	a
Γ_5^+	$\sin m\phi$	0		a	s
Γ_5^-	$\cos m\phi$		0	a	s
Γ_5^-	$\sin m\phi$	0		s	a
Γ_6^+	$\cos m\phi$		0	s	a
Γ_6^+	$\sin m\phi$	0		a	s
Γ_6^-	$\cos m\phi$		0	a	s
Γ_6^-	$\sin m\phi$	0		s	a

Note.—The boundary conditions for the two components of a degenerate function, being different, are given separately.

I am grateful to Dr. S. Altmann for pointing out the errors in the expansions, and to Professor H. Jones and to Dr. Altmann for correspondence and discussion on the subject.

Department of Mathematics,
Imperial College,
London, S.W.7.
6th December 1955.

B. SCHIFF.

ALTMANN, S., 1956, *Proc. Phys. Soc.* A, **69**, 184.
HERRING, C., 1942, *J. Franklin Inst.*, **233**, 525.
SCHIFF, B., 1955, *Proc. Phys. Soc.* A, **68**, 686.

REVIEWS OF BOOKS

Methoden und Anwendungen der Massenspektroskopie, by H. EWALD and H. HINTENBERGER. Pp. 288. (Weinheim: Verlag Chemie, 1953.) DM 25.60

Modern Mass Spectrometry, by G. P. BARNARD. Pp. 326. (London: Institute of Physics, 1953.) 50*s*.

The first of these two books has the more comprehensive scope. It discusses methods in which the deflection of ion beams is used either to determine atomic masses with very high accuracy by the use of photographic techniques or to find the abundances of atomic or molecular species with electrometric methods. In addition it contains short chapters on the use of ion beams for separating isotopes and the employment of time-of-flight techniques in accurate mass measurement.

After a brief historical chapter and one about ion production there follows a detailed discussion of the various types of magnetic and electric field combinations which have been developed by ingenious experimenters in order to achieve a maximum of resolution in mass spectrographs. A good deal of mathematics has been condensed into this chapter, which should prove valuable to readers interested otherwise in the deflection of charge particles in electric and magnetic fields; it is made intelligible by many well-conceived and well-drawn diagrams. There follows a chapter on ion detection, general construction principles and auxiliary equipment. Almost one half of the book is given to the description of precision mass determinations (with many beautiful reproductions) and to a large number of applications of abundancy measurements to the study of nuclear transformations, geological problems, problems of ion formation, analysis of gas mixtures and the use of stable isotopes as tracers.

Modern Mass Spectrometry by G. P. Barnard is on the whole a more down-to-earth kind of book. As the title indicates it is more limited to electronic methods for studying abundances of ionic species. Accordingly the theoretical chapter is simpler and less condensed, and more space is devoted to the discussion of practical details, sources of error and so on. Again nearly half the volume is devoted to the discussion of applications, in this case including a considerable bulk of applications to industrial analysis (as would be expected from a book in the series 'Physics in Industry').

Both books are very well printed, having a good index and extensive lists of references.

O. R. FRISCH.

CONTENTS OF SECTION B

PAGE

Mr. B. D. Saksena and Mr. S. Viswanathan. Principal Lattice Frequency of MgO 129

Mr. H. Pursey. The Power Radiated by an Electromechanical Wave Source . 139

Prof. L. F. Bates and Dr. D. H. Martin. Ferromagnetic Domain Nucleation in Silicon Iron 145

Dr. B. K. P. Scaife. On the Molecular Theory of Electrostriction 153

Dr. S. C. Mossop. Sublimation Nuclei 161

Dr. S. C. Mossop. The Nucleation of Supercooled Water by Various Chemicals 165

Dr. R. Cade and Mr. D. O. Vickers. The Electrostatic Centre of a Conductor . 175

Dr. H. D. Keith. An X-ray Study in High Vacuum of the Structure of Evaporated Copper Films 180

Mr. J. Busby and Dr. E. G. Richardson. The Propagation of Ultrasonics in Suspensions of Particles in a Liquid 193

Mr. H. J. Goldsmid. The Thermal Conductivity of Bismuth Telluride . . . 203

Dr. J. W. Leech and Dr. A. J. Manuel. Magnetic Properties of some Anhydrous Chlorides of the Iron Group—I : Magnetic Resonance 210

Dr. J. W. Leech and Dr. A. J. Manuel. Magnetic Properties of some Anhydrous Chlorides of the Iron Group—II : Interpretation of the Cryomagnetic Anomalies in $CoCl_2$, $FeCl_2$, $NiCl_2$ and $CrCl_3$ 220

Mr. F. J. Hyde. Measurement of Noise Spectra of a Germanium p–n Junction Diode 231

Research Notes :

Mr. F. J. Hyde. Excess Noise Spectra in Germanium 242

Dr. V. G. Bhide, Mr. J. N. Das and Mr. P. V. Khandekar. Analysis of H_2S Treated PbS Point Contact Rectifiers 245

Mr. A. J. Mortlock and Dr. D. H. Tomlin. The Diffusion of Chromium in Titanium studied by an Autoradiographic Method 248

Mr. A. J. Mortlock and Dr. D. H. Tomlin. A Comparison of Three Radioactive Tracer Methods for studying the Diffusion of Chromium in Titanium 250

Mr. J. S. Dryden and Mr. R. J. Meakins. Absence of Radio Frequency Resonance Absorption in Triethylamine with an addendum by M. Davies and A. H. Price 252

Dr. R. Fürth. Temperature Dependence of Coherent Light Scattering in Monocrystals and Intrinsic Block Structure 255

Mr. H. Goldenberg. Some Numerical Evaluations of Heat Flow in the Region Bounded Internally by a Circular Cylinder 256

Dr. R. I. Garrod. Anomalous Interplanar Spacings in Evaporated Deposits of Face-centred Cubic Metals 260

Reviews of Books 264

Contents of Section A 268

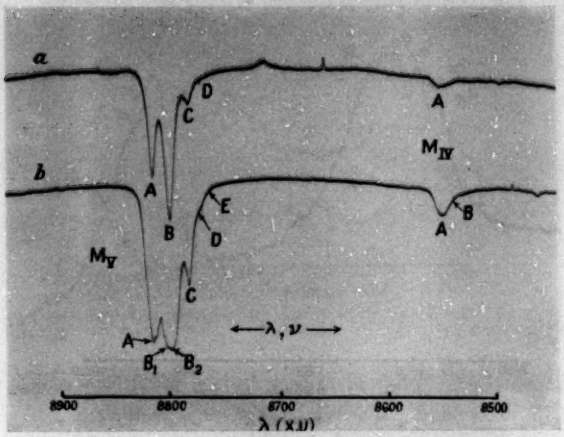

Figure 1.

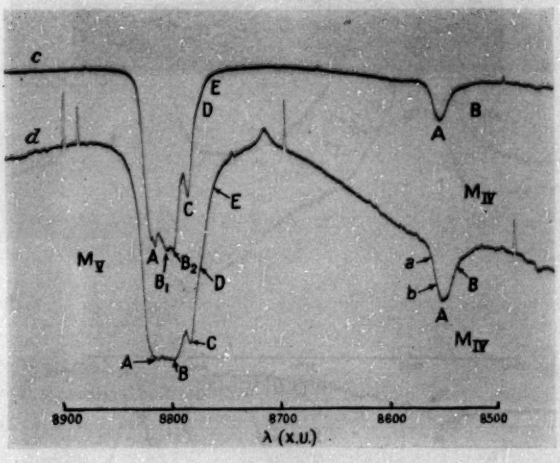

Figure 2.

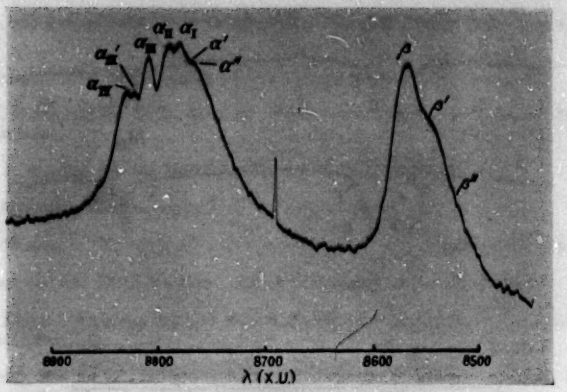

Figure 3.

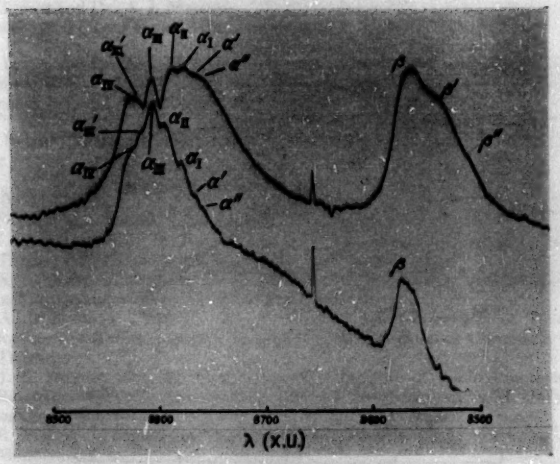

Figure 4.

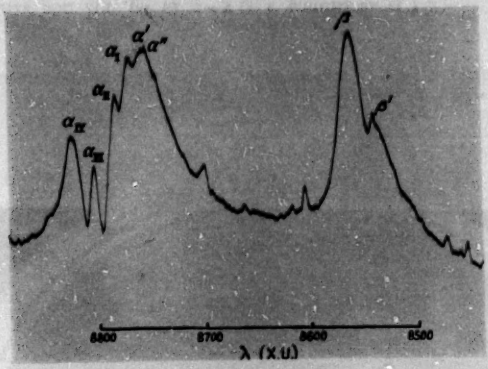

Figure 5.

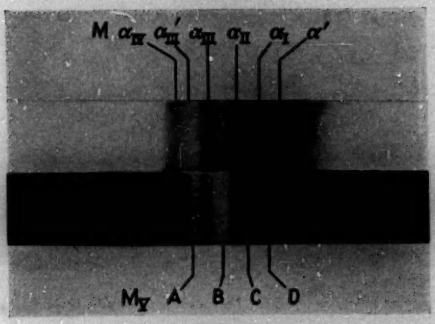

Figure 6.

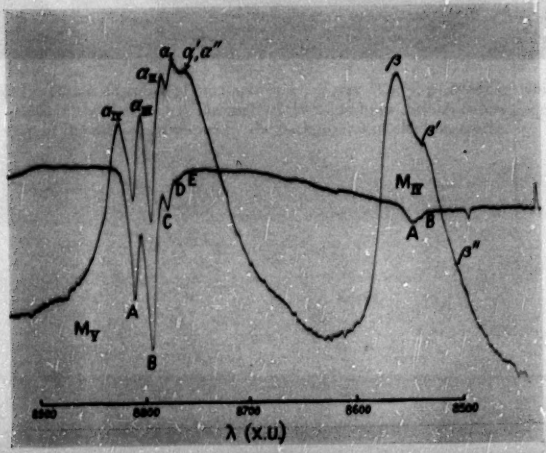

Figure 7.

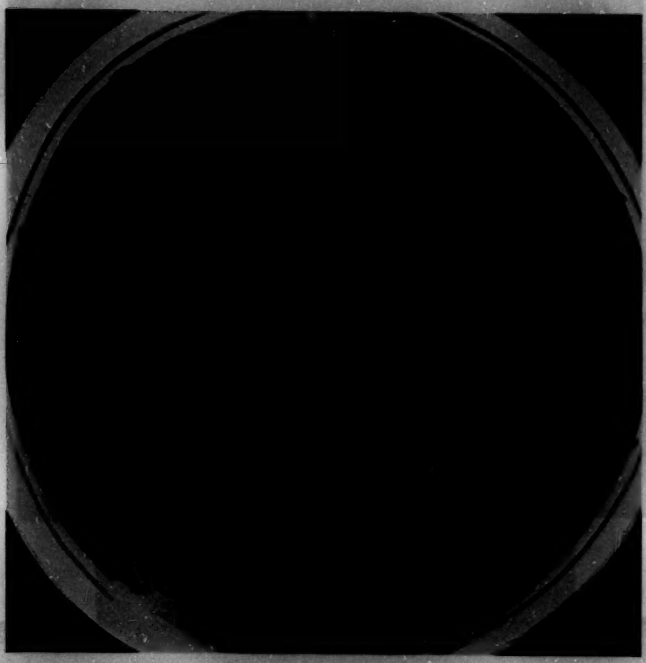

Figure 1. Cloud chamber photograph of a 2·9 Mev ^{14}N (γ, p) event in which the proton stops in the chamber. The path of the x-ray beam, which enters the chamber at the top of the picture, is shown by the background of electron tracks.

(*a*)

(*b*)

Figure 2. A ^{14}N (γ, p) (or (γ, d)) event which has been enlarged to show the detail of the recoil track.

(*a*)

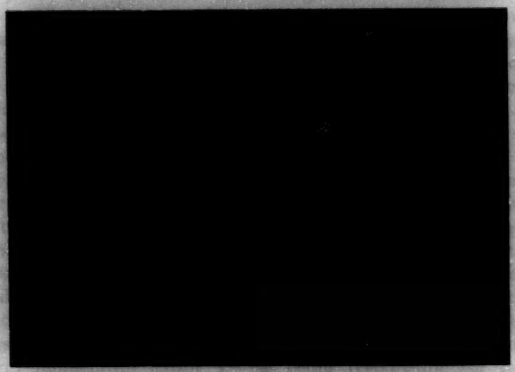

(*b*)

Figure 3. Enlargements of
(*a*) a ^{14}N $(\gamma, 2\alpha)^{6}Li$ event,
(*b*) a ^{14}N (γ, np) event.

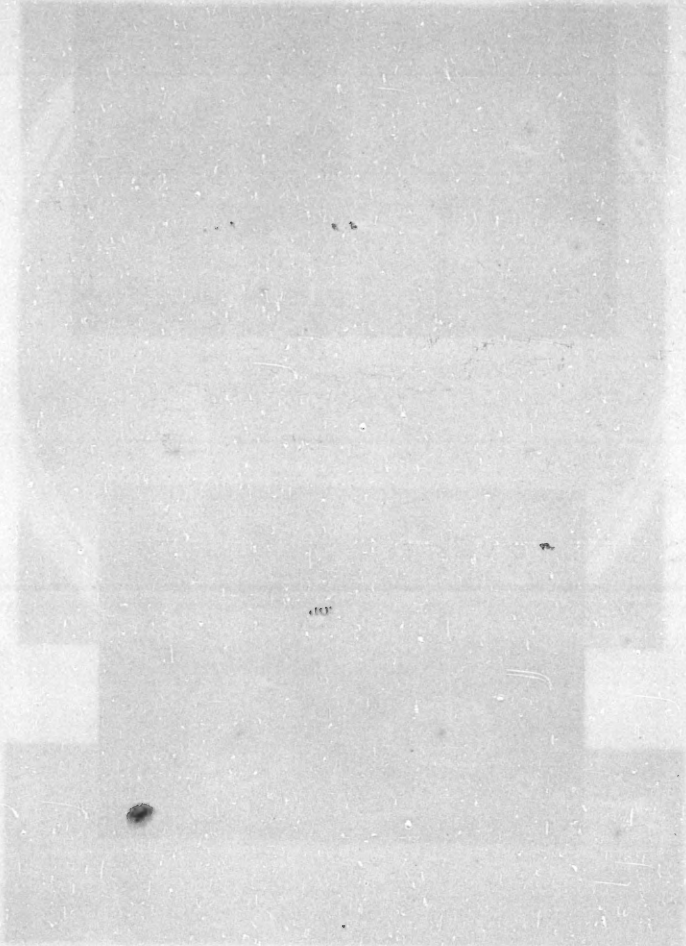

The Two-body Problem in the Theory of the Quantized Gravitational Field †

By E. CORINALDESI ‡
Dublin Institute for Advanced Studies

Communicated by L. Rosenfeld ; MS. received 7th June 1955 and in amended form 17th November 1955

Abstract. The equations of the two-body problem of general relativity are derived by a Hamiltonian method based on an expansion of the general covariant Lagrangian in powers of the gravitational constant and by employing the techniques and the viewpoint of quantum field theory. It is found that, within the approximation in which they have so far been calculated, the equations could have been obtained identically from a linear theory of gravitation.

§ 1. Introduction

The equations of the two-body problem in general relativity were derived long ago by Einstein and his co-workers (Einstein *et al.* 1938, 1949) from the assumption that the bodies can be regarded as singularities of the gravitational field. Though the work of these authors is a classic of completeness and mathematical rigour, it leads to equations containing only the first few terms of an expansion in powers of the gravitational constant and of the velocities of the bodies. It appears therefore conceivable that an alternative simplified derivation should be possible.

A way of proceeding which suggests itself consists in starting from the general relativistic Lagrangian corresponding to the field equations $R^{\mu\nu} - \frac{1}{2}Rg^{\mu\nu} = -\frac{1}{2}\kappa^2 T^{\mu\nu}$, where $T^{\mu\nu}$ describes the bodies as spinless particles obeying general covariant equations. The Lagrangian is then expanded in powers of the gravitational constant and is taken as the basis for a Hamiltonian derivation of the equations of motion, in analogy with a similar calculation performed thirty-five years ago by Darwin (1920) for the electromagnetic interaction between charged particles. This approach differs from that of Einstein, Hoffmann and Infeld in that the bodies have, so to speak, to be put into the equations at the outset, though in a way that satisfies the requirements of general covariance. In other words, we regard the energy–momentum tensor $T^{\mu\nu}$ as being responsible for the non-vanishing value of the left-hand term of the Einstein field equations, while Einstein and his co-workers tend rather to regard the left-hand term as a definition of $T^{\mu\nu}$.

A definite advantage of the method we propose to employ is its ease of manipulation and the insight it gives into the relationship between the equations of motion according to the general theory of relativity and those which would result from a linear theory of gravitation.

† A short account of this work has already appeared in the June 1955 number of the Italian journal *Il Nuovo Cimento*.

‡ Now at Department of Natural Philosophy, The University, Glasgow.

In this work we have found it convenient to develop our approach along the lines afforded by the theory of the quantized gravitational field.

It was Rosenfeld (1930) who first had the idea of quantizing the linearized Einstein equations. More recently Gupta (1952, 1954) was able to give a general treatment of the quantization of the complete gravitational field, which is amenable to actual calculations. His approach amounts to re-interpreting the general theory as an ordinary field theory in flat space with a Lagrangian consisting of an infinite number of terms. Thus the linear part of the gravitational field is isolated and regarded as the free field, whose quanta are the gravitons, while the non-linearity is interpreted as an interaction among the gravitons, and between the gravitons and the various matter fields which are present. When formulated in this fashion, the theory of the gravitational field shows a very close similarity to quantum electrodynamics and meson theory.

In these latter theories, the two-body problem has been the object of the greatest interest for many years. The first step was made by Breit (1929, 1932), who used the retarded Møller interaction between two electrons, derived from quantum electrodynamics, as a 'potential' in order to calculate the relativistic corrections to the energy levels of the helium atom. The Breit method will be sufficient for our purpose, and we shall not need to mention any of the more recent developments of the two-body problem in field theory.

In the theory of the quantized gravitational field, it is easy to derive a velocity dependent interaction between two particles, which is the analogue of the Møller formula. Such an interaction is then inserted in a two-particle Hamiltonian of the type used by Breit, and by the help of this it is possible to evaluate the second time derivative of the operator representing the coordinate of one of the particles. Taking the average value of this for a wave function describing two wave packets for the two interacting particles, the Einstein, Infeld and Hoffmann equations have been found to hold.

As pointed out before, the use of quantum-mechanical techniques has been suggested by reasons of convenience rather than necessity. Genuine quantum field theoretical features, such as the occurrence of divergencies, would only make their appearance in an approximation higher than that pursued here, so that it should not be difficult to translate our calculations into a completely classical language, should one incline towards a more traditional description of nature.

§ 2. Preliminaries

We consider two fields $\psi^{(1)}$ and $\psi^{(2)}$ of scalar particles of mass m_1 and m_2 in the presence of the gravitational field. The field equations

$$\frac{1}{\sqrt{(-g)}}\frac{\partial}{\partial x^\mu}\left(g^{\mu\nu}\sqrt{(-g)}\frac{\partial\psi^{(i)}}{\partial x^\nu}\right)+m_i^2\psi^{(i)}=0 \qquad (i=1,2) \qquad \ldots\ldots(1)$$

can be derived from the Lagrangian

$$L_g=\tfrac{1}{2}\sqrt{(-g)}\sum_{i=1,2}(g^{\mu\nu}\psi^{(i)}_{,\mu}\psi^{(i)}_{,\nu}-m_i^2\psi^{(i)2}). \qquad \ldots\ldots(2)$$

Following Gupta we shall put $g^{\mu\nu}=\epsilon^{\mu\nu}-\kappa\gamma^{\mu\nu}$, where $\epsilon^{\mu\nu}$ is the Minkowskian tensor, and expand L_g in powers of κ. Similarly the Lagrangian of the gravitational field can be taken over from Gupta's work in the form of an expansion. Reverting to the coordinates x_1, x_2, x_3, $x_4=it$, and therefore

neglecting the distinction between covariant and contravariant indices, we have the Lagrangian

$$L=-\tfrac{1}{4}(\gamma_{\mu\nu,\lambda}\gamma_{\mu\nu,\lambda}-\tfrac{1}{2}\gamma_{,\lambda}\gamma_{,\lambda})+\sum_{i=1,2}(L^{(i)}-\tfrac{1}{2}\kappa h_{\mu\nu}T_{\mu\nu}^{(i)})+\mathrm{O}(\kappa^2), \quad \ldots\ldots(3)$$

where $\gamma=\gamma_{\mu\mu}$, $h_{\mu\nu}=\gamma_{\mu\nu}-\frac{1}{2}\gamma\delta_{\mu\nu}$, while

$$L^{(i)}=\tfrac{1}{2}\left[\left(\frac{d\psi^{(i)}}{dt}\right)^2-(\operatorname{grad}\psi^{(i)})^2-m_i^2\psi^{(i)2}\right], \quad \ldots\ldots(4)$$

$$T_{\mu\nu}^{(i)}=\psi_{,\mu}^{(i)}\psi_{,\nu}^{(i)}+\delta_{\mu\nu}L^{(i)}. \quad \ldots\ldots(5)$$

In (3) $\mathrm{O}(\kappa^2)$ denotes terms of the second and higher order in κ, which would make a contribution to the final result lying outside the approximation pursued. Note that the linear approximation (3) corresponds to the field equations

$$\Box^2\gamma_{\mu\nu}=\kappa T_{\mu\nu}, \qquad \Box^2\gamma=\kappa T_{\mu\mu} \quad \ldots\ldots(6)$$

with

$$T_{\mu\nu}=T_{\mu\nu}^{(1)}+T_{\mu\nu}^{(2)}. \quad \ldots\ldots(7)$$

From the Lagrangian it is easy to derive the interaction Hamiltonian in the interaction representation,

$$H_{\mathrm{int}}=\tfrac{1}{2}\kappa h_{\mu\nu}T_{\mu\nu}+\mathrm{O}(\kappa^2). \quad \ldots\ldots(8)$$

The element of the S-matrix

$$S=1+(-i)\int_{-\infty}^{\infty}H_{\mathrm{int}}(x)\,dx+\tfrac{1}{2}(-i)^2\int_{-\infty}^{\infty}dx\int_{-\infty}^{\infty}dx'\;P\{H_{\mathrm{int}}(x)H_{\mathrm{int}}(x')\}+\ldots \quad \ldots\ldots(9)$$

for the scattering of a particle 1 by a particle 2 can be calculated by standard methods with the help of the equation

$$\langle P\{h_{\mu\nu}(x)h_{\lambda\rho}(x')\}\rangle_0=\tfrac{1}{2}(\delta_{\mu\lambda}\delta_{\nu\rho}+\delta_{\mu\rho}\delta_{\nu\lambda}-\delta_{\mu\nu}\delta_{\lambda\rho})D_{\mathrm{F}}'(x-x') \quad \ldots\ldots(10)$$

for the vacuum expectation value of the P-bracket of two gravitational field operators. Here

$$D_{\mathrm{F}}'(x)=\frac{-2i}{(2\pi)^4}\int(k^2+\rho^2)^{-1}\exp(ikx)\,dk \qquad (\rho\to 0) \quad \ldots\ldots(11)$$

is Feynman's singular function for the gravitational field.

Denoting by $p\equiv(\mathbf{p},p_0)$, $p'\equiv(\mathbf{p}',p_0')$ the initial and final momenta of particle 1, and by $q\equiv(\mathbf{q},q_0)$ and $q'\equiv(\mathbf{q}',q_0')$ those of particle 2, the scattering matrix element is found to be

$$\frac{i\kappa^2}{32}\frac{1}{(2\pi)^8}\frac{\delta(p+q-p'-q')}{(q-q')^2}\frac{1}{(p_0p_0'q_0q_0')^{1/2}}[(pq)(p'q')+(pq')(p'q) -(pp')(qq')-m_1^2(qq')-m_2^2(pp')-2m_1^2m_2^2], \quad \ldots\ldots(12)$$

where $\delta(p)$ is a four-dimensional δ-function. It is convenient at this stage to make an expansion of the last two factors in powers of the velocities, which gives

$$\frac{1}{(p_0p_0'q_0q_0')^{1/2}}[\ldots]=\frac{1}{m_1m_2}[m_1^2m_2^2+\tfrac{3}{4}m_1^2(\mathbf{q}^2+\mathbf{q}'^2)+\tfrac{3}{4}m_2^2(\mathbf{p}^2+\mathbf{p}'^2) -m_1m_2(\mathbf{pq}+\mathbf{p}'\mathbf{q}'+\mathbf{pq}'+\mathbf{p}'\mathbf{q})]+\ldots. \quad \ldots\ldots(13)$$

A velocity dependent potential is defined by Fourier transformation of the scattering matrix element, and results in

$$(\mathbf{r}_1\mathbf{r}_2|V|\mathbf{r}_1'\mathbf{r}_2') = -\frac{2\kappa^2}{(2\pi)^8 m_1 m_2}\Big[m_1^2m_2^2 - \tfrac{3}{4}m_1^2(\Delta_2+\Delta_2') - \tfrac{3}{4}m_2^2(\Delta_1+\Delta_1') + m_1m_2\Big(\frac{\partial}{\partial\mathbf{r}_1}\frac{\partial}{\partial\mathbf{r}_2} + \frac{\partial}{\partial\mathbf{r}_1'}\frac{\partial}{\partial\mathbf{r}_2'} - \frac{\partial}{\partial\mathbf{r}_1}\frac{\partial}{\partial\mathbf{r}_2'} - \frac{\partial}{\partial\mathbf{r}_1'}\frac{\partial}{\partial\mathbf{r}_2}\Big)\Big] \times \int \exp[i(\mathbf{p}\mathbf{r}_1+\mathbf{q}\mathbf{r}_2-\mathbf{p}'\mathbf{r}_1'-\mathbf{q}'\mathbf{r}_2')] \times \frac{\delta(\mathbf{p}+\mathbf{q}-\mathbf{p}'-\mathbf{q}')}{(\mathbf{q}-\mathbf{q}')^2-(q_0-q_0')^2}\,d\mathbf{p}\,d\mathbf{q}\,d\mathbf{p}'\,d\mathbf{q}' \qquad \ldots\ldots(14)$$

with $\Delta_1 \equiv (\partial/\partial\mathbf{r}_1)(\partial/\partial\mathbf{r}_1)$ etc. It is to be noted that this potential is not diagonal in the coordinate representation. Only the Newton potential enjoys this property, and it is obtained by neglecting all terms except $m_1^2m_2^2$ in the square bracket (i.e. neglecting the velocity dependent part), and also neglecting $(q_0-q_0')^2$ in the denominator of the integral (i.e. neglecting retardation). Otherwise the full expression of the potential reads

$$(\mathbf{r}_1\mathbf{r}_2|V|\mathbf{r}_1'\mathbf{r}_2') = -\frac{\kappa^2}{m_1m_2}\Big[m_1^2m_2^2 - \tfrac{3}{4}m_1^2(\Delta_2+\Delta_2') - \tfrac{3}{4}m_2^2(\Delta_1+\Delta_1') + m_1m_2\Big(\frac{\partial}{\partial\mathbf{r}_1}\frac{\partial}{\partial\mathbf{r}_2} + \frac{\partial}{\partial\mathbf{r}_1'}\frac{\partial}{\partial\mathbf{r}_2'} - \frac{\partial}{\partial\mathbf{r}_1}\frac{\partial}{\partial\mathbf{r}_2'} - \frac{\partial}{\partial\mathbf{r}_1'}\frac{\partial}{\partial\mathbf{r}_2}\Big)\Big] \times (\mathbf{r}_1\mathbf{r}_2|N+R|\mathbf{r}_1'\mathbf{r}_2'), \qquad \ldots\ldots(15)$$

where

$$(\mathbf{r}_1\mathbf{r}_2|N|\mathbf{r}_1'\mathbf{r}_2') = \frac{1}{|\mathbf{r}_1-\mathbf{r}_2'|}\delta(\mathbf{r}_1-\mathbf{r}_1')\delta(\mathbf{r}_2-\mathbf{r}_2') \qquad \ldots\ldots(16)$$

and

$$(\mathbf{r}_1\mathbf{r}_2|R|\mathbf{r}_1'\mathbf{r}_2') = \frac{2}{(2\pi)^8}\int \frac{(q_0-q_0')^2}{[(\mathbf{q}-\mathbf{q}')^2]^2}\exp[i(\mathbf{p}\mathbf{r}_1+\mathbf{q}\mathbf{r}_2-\mathbf{p}'\mathbf{r}_1'-\mathbf{q}'\mathbf{r}_2')] \times \delta(\mathbf{p}+\mathbf{q}-\mathbf{p}'-\mathbf{q}')\,d\mathbf{p}\,d\mathbf{q}\,d\mathbf{p}'\,d\mathbf{q}' \qquad \ldots\ldots(17)$$

is the retardation correction obtained by expanding the integrand in powers of q_0-q_0'.

It is important to notice that there is no contribution of the order of κ^3 to the matrix element. This is due to the fact that terms in κ^3 can only induce processes in which three emissions or absorptions of gravitons occur, while in the scattering process in question there must be an even number of such emissions and absorptions.

§ 3. The Two-particle Hamiltonian

Following Breit we now define the two-particle Hamiltonian

$$H = K + \Delta K + V, \qquad \ldots\ldots(18)$$

where

$$K = \frac{1}{2m_1}\mathbf{p}_1^2 + \frac{1}{2m_2}\mathbf{p}_2^2 \qquad \ldots\ldots(19)$$

and

$$\Delta K = -\frac{1}{8m_1^3}(\mathbf{p}_1^2)^2 - \frac{1}{8m_2^3}(\mathbf{p}_2^2)^2 \qquad \ldots\ldots(20)$$

is a relativistic correction to the classical kinetic energy.

Consider now the operator r_1^i representing the ith coordinate of particle 1. Its time derivative is given by

$$\frac{dr_1^i}{dt} = i[H, r_1^i]. \qquad \ldots\ldots(21)$$

If V did commute with r_1^i as is the case for the Newton potential, we would have simply $dr_1^i/dt = p_1^i/m_1 - (\mathbf{p}_1^2)p_1^i/2m_1^3 + \ldots$. But in the present instance a contribution from V is also to be added. We proceed now to evaluate the second time derivative of r_1^i,

$$\frac{d^2r_1^i}{dt^2} = -[H, [H, r_1^i]] \qquad \ldots\ldots(22)$$

and to express the resulting operator by means of its matrix element in the coordinate representation. We have

$$\begin{aligned}\left(\mathbf{r}_1\mathbf{r}_2\left|\frac{d^2r_1^i}{dt^2}\right|\mathbf{r}_1'\mathbf{r}_2'\right) = i\int d\mathbf{r}_1''\,d\mathbf{r}_2''\Big[&(\mathbf{r}_1\mathbf{r}_2|K|\mathbf{r}_1''\mathbf{r}_2'')i(r_1^{i\prime}-r_1^{i\prime\prime})(\mathbf{r}_1''\mathbf{r}_2''|V|\mathbf{r}_1'\mathbf{r}_2')\\ &-i(r_1^{i\prime\prime}-r_1^i)(\mathbf{r}_1\mathbf{r}_2|V|\mathbf{r}_1''\mathbf{r}_2'')(\mathbf{r}_1''\mathbf{r}_2''|K|\mathbf{r}_1'\mathbf{r}_2')\\ &+(\mathbf{r}_1\mathbf{r}_2|V|\mathbf{r}_1''\mathbf{r}_2'')\left(\mathbf{r}_1''\mathbf{r}_2''\left|\frac{p_1^i}{m_1}\right|\mathbf{r}_1'\mathbf{r}_2'\right)\\ &-\left(\mathbf{r}_1\mathbf{r}_2\left|\frac{p_1^i}{m_1}\right|\mathbf{r}_1''\mathbf{r}_2''\right)(\mathbf{r}_1''\mathbf{r}_2''|V|\mathbf{r}_1'\mathbf{r}_2')\\ &+(\mathbf{r}_1\mathbf{r}_2|V|\mathbf{r}_1''\mathbf{r}_2'')\left(\mathbf{r}_1''\mathbf{r}_2''|-\frac{1}{2m_1^3}(\mathbf{p}_1^2)p_1^i|\mathbf{r}_1'\mathbf{r}_2'\right)\\ &-\left(\mathbf{r}_1\mathbf{r}_2|-\frac{1}{2m_1^3}(\mathbf{p}_1^2)p_1^i|\mathbf{r}_1''\mathbf{r}_2''\right)(\mathbf{r}_1''\mathbf{r}_2''|V|\mathbf{r}_1'\mathbf{r}_2')\\ &+i(r_1^i+r_1^{i\prime\prime}-2r_1^{i\prime\prime})(\mathbf{r}_1\mathbf{r}_2|V|\mathbf{r}_1''\mathbf{r}_2'')(\mathbf{r}_1''\mathbf{r}_2''|V|\mathbf{r}_1'\mathbf{r}_2')\Big].\end{aligned} \qquad \ldots\ldots(23)$$

In this formula, we have neglected a correction, amounting to the replacement of K by $K+\Delta K$ in the first two terms. It would, in fact, give a contribution to the final result lying outside the approximation required.

It could be objected that a contribution in κ^4 to (22) might arise from the interplay of terms of H of the order of κ and κ^3. We have however previously stressed that V is proportional to κ^2 in the first approximation, the next term being of the order of κ^4, so that the above situation cannot arise.

§ 4. Average Value of $d^2r_1^i/dt^2$

Consider now the wave function $\Psi(\mathbf{r}_1, \mathbf{r}_2)$ representing two non-overlapping wave packets for the two particles. To calculate the average value of $d^2r_1^i/dt^2$

$$\left\langle\frac{d^2r_1^i}{dt^2}\right\rangle = \int \Psi^*(\mathbf{r}_1, \mathbf{r}_2)\frac{d^2r_1^i}{dt^2}\Psi(\mathbf{r}_1, \mathbf{r}_2)\,d\mathbf{r}_1\,d\mathbf{r}_2 \qquad \ldots\ldots(24)$$

for this wave function is a simple, if somewhat lengthy, matter. The method to be used consists in performing a number of partial integrations, bearing in mind that $\langle d^2r_1^i/dt^2\rangle$ is sought in a form which shows at sight that it is the average value of a Hermitian operator. Denoting by [1]...[7] the terms in the right-hand member of equation (23), the following partial results are obtained.

Neglecting retardation: $(\mathbf{r}=\mathbf{r}_1-\mathbf{r}_2)$

$$
\begin{aligned}
&[1]+[2]+[3]+[4]\\
&=\kappa^2\int\Psi^*(\mathbf{r}_1,\mathbf{r}_2)\left\{\left(\frac{m_2}{r}\right)_{,i}\left[1-\frac{3}{2m_1{}^2}\Delta_1-\frac{3}{2m_2{}^2}\Delta_2+\frac{4}{m_1m_2}\frac{\partial^2}{\partial r_1{}^s\partial r_2{}^s}\right]\right.\\
&\quad+\left(\frac{m_2}{r}\right)_{,s}\left[\frac{3}{m_1{}^2}\frac{\partial^2}{\partial r_1{}^i\partial r_1{}^s}+\frac{4}{m_2{}^2}\frac{\partial^2}{\partial r_2{}^i\partial r_2{}^s}-\frac{4}{m_1m_2}\frac{\partial^2}{\partial r_1{}^s\partial r_2{}^i}-\frac{3}{m_1m_2}\frac{\partial^2}{\partial r_1{}^i\partial r_2{}^s}\right]\\
&\quad\left.+\left(\frac{1}{r}\right)_{,is}\frac{1}{2}\left(\frac{1}{m_1}-\frac{1}{m_2}\right)\frac{\partial}{\partial r_2{}^s}\right\}\Psi(\mathbf{r}_1,\mathbf{r}_2)\,d\mathbf{r}_1\,d\mathbf{r}_2,\\
&[5]+[6]\\
&=\kappa^2\int\Psi^*(\mathbf{r}_1,\mathbf{r}_2)\left\{-\left(\frac{m_2}{r}\right)_{,i}\frac{1}{2m_1{}^2}\Delta_1-\left(\frac{m_2}{r}\right)_{,s}\frac{1}{m_1{}^2}\frac{\partial}{\partial r_1{}^i}\frac{\partial}{\partial r_1{}^s}\right.\\
&\quad\left.+\left(\frac{m_2}{r}\right)_{,is}\frac{i}{m_1{}^2}\frac{\partial}{\partial r_1{}^s}\right\}\Psi(\mathbf{r}_1,\mathbf{r}_2)\,d\mathbf{r}_1\,d\mathbf{r}_2. \qquad\ldots\ldots(25)
\end{aligned}
$$

Retardation correction affecting only [3] and [4] in the approximation required:

$$
\begin{aligned}
([3]+[4])_{\text{ret}}&=\kappa^2m_2\int\Psi^*(\mathbf{r}_1,\mathbf{r}_2)\left\{\left(\frac{1}{r}\right)_{,i}\frac{1}{2m_2{}^2}\Delta_2\right.\\
&\quad\left.+\left(\frac{1}{r}\right)_{,is}\frac{i}{2m_2{}^2}\frac{\partial}{\partial r_2{}^s}\right\}\Psi(\mathbf{r}_1,\mathbf{r}_2)\,d\mathbf{r}_1\,d\mathbf{r}_2\\
&\quad-\frac{\kappa^2}{2m_2}\int\Psi^*(\mathbf{r}_1,\mathbf{r}_2)\frac{\partial}{\partial r_2{}^s}\left[\frac{\partial}{\partial r_1{}^i}\left(\frac{r^sr^n}{(r)^3}\right)\frac{\partial\Psi(\mathbf{r}_1,\mathbf{r}_2)}{\partial r_2{}^n}\right]d\mathbf{r}_1\,d\mathbf{r}_2. \qquad\ldots\ldots(26)
\end{aligned}
$$

Thus the terms from [1] to [6], including retardation, yield

$$
\begin{aligned}
\left\langle\frac{d^2r_1{}^i}{dt^2}\right\rangle&=\kappa^2\int\Psi^*(\mathbf{r}_1,\mathbf{r}_2)\left\{\phi_{,i}+v_1{}^s\phi_{,i}v_1{}^s-2[v_1{}^s\phi_{,s}v_1{}^i+v_1{}^i\phi_{,s}v_1{}^s]\right.\\
&\quad-2[v_1{}^s\phi_{,i}v_2{}^s+v_2{}^s\phi_{,i}v_1{}^s]+2[v_1{}^s\phi_{,s}v_2{}^i+v_2{}^i\phi_{,s}v_1{}^s]\\
&\quad+\tfrac{3}{2}[v_1{}^i\phi_{,s}v_2{}^s+v_2{}^s\phi_{,s}v_1{}^i]+2v_2{}^s\phi_{,i}v_2{}^s-2[v_2{}^i\phi_{,s}v_2{}^s+v_2{}^s\phi_{,s}v_2{}^i]\\
&\quad\left.-\frac{m_2}{2}v_2{}^s\left[\frac{\partial}{\partial r_1{}^i}\left(\frac{r^sr^n}{(r)^3}\right)\right]v_2{}^n\right\}\Psi(\mathbf{r}_1,\mathbf{r}_2)\,d\mathbf{r}_1\,d\mathbf{r}_2, \qquad\ldots\ldots(27)
\end{aligned}
$$

where $\phi\equiv m_2/r$, $\phi_{,i}\equiv\partial\phi/\partial r_1{}^i$, and $v_1{}^s\equiv(1/im_1)\partial/\partial r_1{}^s$ and $v_2{}^s\equiv(1/im_2)\partial/\partial r_2{}^s$, wherever occurring, are supposed to operate on all the factors to their right.

This expression is in agreement with the Einstein, Infeld and Hoffmann equations, but for two velocity independent terms of the order of κ^4.† It is remarkable that two such terms do not arise from the radiative corrections to the potential, due to Feynman diagrams of a higher order of complexity than a single graviton exchange, but only from the term [7] of equation (23). Though a superficial inspection might point to the contrary, actual calculation shows that [7] gives

$$
[7]=\kappa^4\int\Psi^*(\mathbf{r}_1,\mathbf{r}_2)\left\{-\phi_{,i}\left(\frac{4m_2}{r}+\frac{5m_1}{r}\right)\right\}\Psi(\mathbf{r}_1,\mathbf{r}_2)\,d\mathbf{r}_1\,d\mathbf{r}_2 \qquad\ldots\ldots(28)
$$

where the contribution $(-m_2\phi_{,i}/r)$ arises from cross terms which are the product of the Newton part of the potential with the retardation correction, and the remainder from the velocity dependent part of the potential.

Thus the Einstein, Infeld and Hoffmann equations are found to hold in their full form for the motion of wave packets, and therefore, in the classical limit of wave mechanics, also for the motion of macroscopic bodies.

† The reader who has not access to the mathematical journals may find it useful to consult the paper by Bertotti (1954) on the subject.

It is clear that an attempt to extend the present calculation to an approximation higher than κ^4 would meet with difficulties. In fact, the next approximation for the potential would be affected by the usual divergences and the success of the renormalization method is doubtful. On the other hand, it is precisely in this higher approximation that the quantization of the gravitational field may be expected to yield results essentially different from those of the classical theory. This is, however, outside the scope of this study, from which one important physical result emerges; that is, the conclusion that even if the data on the motion of planets were known with greater accuracy than they are at the present time, so that effects in $\kappa^2 v^2$ and κ^4 were detectable, it would still be impossible to decide in favour of either the general theory of relativity or of a theory of gravitation based only on the linear interaction as in equation (3).

References

Bertotti, B., 1954, *Nuovo Cim.*, **12,** 226.

Breit, G., 1929, *Phys. Rev.*, **34,** 553 ; 1932, *Ibid.*, **39,** 616.

Darwin, C. G., 1920, *Phil. Mag.*, **39,** 537.

Einstein, A., and Infeld, L., 1949, *Canad. J. Math.*, **1,** 209.

Einstein, A., Infeld, L., and Hoffmann, B., 1938, *Ann. Math.*, **39,** 66.

Gupta, S. N., 1950, *Proc. Phys. Soc.* A, **63,** 681 ; 1952, *Ibid.*, **65,** 608 ; 1954, *Phys. Rev.*, **96,** 1683.

Rosenfeld, L., 1930, *Z. Phys.*, **65,** 589.

Single Scattering of Fast Electrons by Atomic Nuclei

By K. K. DAMODARAN† and R. M. CURR‡
Department of Physics, University College, London

Communicated by E. H. S. Burhop; MS. received 29th August 1955 and in amended form 25th October 1955

Abstract. An attempt has been made to check the validity of Mott's theory of single scattering of electrons by heavy nuclei such as silver, platinum and uranium at various angles of scattering and thus to investigate whether there is any marked deviation from theory at large angles of scattering as observed by some previous workers in this field. An electron beam from the 4·5 Mev microtron at University College, London, was used for the experiment and the scattered electrons were detected in Ilford G5-50 micron emulsions. It has been found from these measurements that the scattering of 4·33 Mev electrons by the above mentioned nuclei agrees with Mott's theory within the experimental accuracy of a few per cent for angles of scattering from 45° to 90°. Measurements made at angles of scattering of 120° and 135° were found to have been affected by the presence of spurious scattering from the walls of the apparatus so that no definite conclusions can be drawn regarding the scattering at these angles.

§ 1. Introduction

The study of the elastic scattering of fast electrons by nuclei provides the most direct method for determining the forces between electrons and nuclei at close distances of approach and much research work has been performed in this field. The scattering of relativistic electrons by atomic nuclei was investigated theoretically by Mott (1929, 1932) on the basis of Dirac's theory of the electron. Early experimental investigators (Champion 1936, Zuber 1938, Sen Gupta 1939, Bleuler *et al.* 1942) in this field found values of the scattering cross sections differing widely from those predicted by Mott's theory. Recently, however, further investigations have been carried out under improved experimental conditions. The experimental results of Sigrist (1943), Randels *et al.* (1945), Van de Graaff *et al.* (1946), Buechner *et al.* (1947) and Champion and Roy (1948) agree with Mott's theory within the limits of experimental error. However, insufficient work has been done to test the validity of Mott's theory for nuclei of very high atomic number especially at large angles of scattering. Paul and Reich (1951) measured the elastic scattering of 2·2 Mev electrons for elements of atomic numbers up to 78 at angles of scattering of 60°, 90° and 120° and found that the scattering cross sections for heavy nuclei at angles above 60° were smaller than the values predicted by Mott's theory. Kinzinger and Bothe (1952) and Kinzinger (1953) also have observed significant deviations from the theory for heavy nuclei at angles greater than 70°, using 245 kev electrons and found that the scattering for gold at 120° was about 25% less than the theoretical predictions. These observed deviations from theory in the case of heavy elements

† Now Research Fellow at the Department of Physics, University of Birmingham.
‡ Now at the G.E.C. Research Laboratories, Stanmore, Middlesex.

at large angles of scattering demand further investigation. Bayard and Yntema (1954, 1955) have reported good agreement with Mott's theory in the large angle scattering of 0·6, 1·0, and 1·7 Mev electrons for gold nuclei.

In the present work relative cross sections at angles of scattering of 45°, 60° and 90° were measured for silver and platinum, and at 45° and 60° for uranium and aluminium. Measurements of absolute values of the cross sections were also made for uranium at 50°, 60°, 90° and 120° and for aluminium at 60° and 90°. The measurements on aluminium served as a check on the validity of the method of measurements because, in the case of light elements such as aluminium, previous workers have found that the scattering agrees with the theory.

§ 2. Apparatus and Procedure

The scattering chamber used for the experiment was a brass cylinder 5 in. in diameter and 24 in. long. One end of the chamber was connected to the beam extractor of the microtron, the chamber resting horizontally on two supports. The other end of the chamber was removable, being bolted on and sealed by means of a rubber gasket. The electron beam from the microtron was passed through aluminium and lead collimators as shown in figure 1 and emerged from the chamber through a 0·002 in. thick aluminium window.

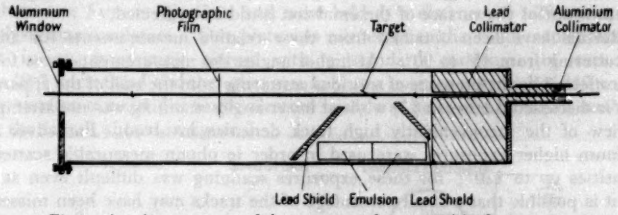

Figure 1. Arrangement of the apparatus for group (*a*) of exposures.

The camera contained the target holder, plate holder and the lead shielding for the photographic plates. The target holder was fixed vertically on a brass platform of length 6½ in. and breadth 4 in. The plane of the scattering foil mounted on the target holder was inclined at an angle of 30° to the direction of the incident beam. (The measurements could thus be made on the transmission side of the foil, minimizing the effect of double scattering.) The holder for the emulsions was of brass and was mounted horizontally on the brass platform with its longer side parallel to the direction of the incident beam. For each exposure two plates each of size 3 in. × 1 in. were used. The near side of the emulsion was at a distance of 2½ in. from the vertical plane containing the incident beam. The surface of the emulsion was 0·75 in. below the horizontal plane containing the incident beam, except in the small-angle relative exposures with uranium and aluminium where this distance was increased to 1·1 in. The camera was located reproducibly with respect to the scattering chamber and the beam position was found with photographic film.

Scattering foils of silver, platinum and aluminium of a high degree of purity were supplied by Johnson, Matthey Ltd. and were beaten to the required thickness

by Geo. M. Whiley Ltd. Scattering foils of uranium were prepared by evaporating uranium in high vacuum and depositing it on thin backing foils of aluminium (thickness 0·18 mg cm^{-2}). The variation in thickness of the uranium foils was measured by counting the alpha and beta radiations from the various parts of the foils, using a Geiger–Müller counter. The percentage purity of uranium in the scattering foils was determined by chemical analysis.†

Exposures were made for (*a*) relative measurements of the scattering cross sections for silver, platinum, uranium and aluminium, (*b*) absolute measurements of the scattering cross sections for uranium and aluminium. (The method of absolute measurement was developed only after the group (*a*) measurements had been completed.)

In the relative measurements for silver and platinum the angular range 45° to 120° was covered in each exposure. For platinum two exposures were made with foils of different thickness in order to confirm that the corrections applied for multiple scattering were not seriously in error. The relative exposures for uranium and aluminium were divided into two groups, one for angles less than 90° and the other for angles from 90° to 135°. As mentioned above, the surface of the emulsions was lowered to 1·1 in. below the plane of the incident beam for the small-angle group of these exposures. This step was taken in order to maintain an angle of entry of the electrons into the emulsion greater than about 10°, for angles of scattering down to 30°, so that scattering of the electrons out of the surface of the emulsion could be neglected.

Results have been obtained from these relative measurements for angles of scattering from 45° to 90°. At higher angles the measurements were found to be affected by the presence of spurious scattering from the wall of the apparatus (this is discussed further in § 3) while at lower angles scanning was not attempted in view of the inconveniently high track densities involved. For silver and platinum higher exposures were used in order to obtain measurable scattering intensities up to 120°; for these exposures scanning was difficult even at 45° and it is possible that a small percentage of the tracks may have been missed at this angle of scattering.

For group (*a*) of exposures, the arrangement as shown in figure 1 was used. The camera was placed close to the beam entrance end of the scattering chamber and the position of the plates with respect to the target was varied according to the angular range to be investigated. To obtain a measure of the intensity of the primary electron beam in each of these exposures an x-ray film mounted at right angles to the direction of the primary electron beam at a distance of about 8 in. from the target was exposed simultaneously with the emulsions. The relative intensities of the primary electron beams in these exposures were determined by scanning the exposed photographic film by means of a microphotometer and by measuring the distribution of the density due to the electrons which struck the various points of the film. Two types of photographic film were used, Ilford Line film and Ilford fine grain ordinary film. These films were calibrated for sensitivity of fast electron detection using an ionization chamber. The maximum density on the film was in most cases less than 1·0 rising to 1·3 in some cases. The calibration is not very reliable at the higher densities but the accuracy achieved (to the order of 10%) was considered sufficient for estimation of the background correction for which exposures without target foil were made.

† An account of the method of preparation, measurement of thickness and analysis of the uranium foils is to be published elsewhere.

For the group (*b*) of exposures which covered angles of scattering from 50° to 120°, the camera was placed close to the removable end of the scattering chamber as shown in figure 2. The primary electron beam emerging from the target foil passed through the aluminium window at the end of the chamber and through an air-filled parallel plate ionization chamber. The ionization chamber was

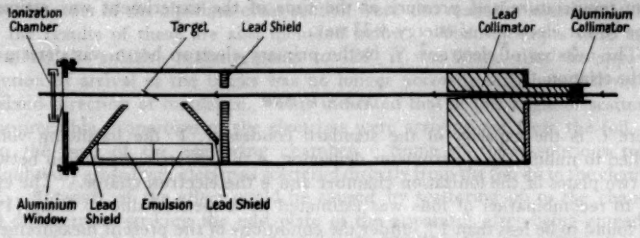

Figure 2. Arrangement of the apparatus for group (*b*) of exposures.

built to a design in use by the Hammersmith Hospital M.R.C. Group. We are indebted to Dr. P. Howard-Flanders for drawing our attention to this design. The centres of the target foil, the aluminium window and the ionization chamber were adjusted to be in the same horizontal line. The plates of the ionization chamber were 5 cm in diameter and were held at a distance of 1·29 mm apart by polystyrene insulators. One plate was connected to the Lindemann electrometer in an integrating circuit with a standard condenser of capacity $1{\cdot}02 \times 10^{-3}$ microfarad and the other was held at a positive potential of 240 volts. The ionization current due to the electron beam was measured by a null method using the circuit shown in figure 3.

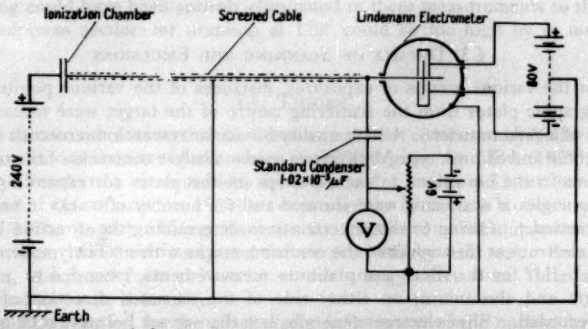

Figure 3. Circuit used for monitoring the electron beam in absolute measurements.

The number of ion pairs produced by an electron per cm path in air under the conditions of the experiment was computed from the experimental results of Ovadia *et al.* (1952), making use of the Bethe–Bloch (1933) theory. According to this theory the ionization produced by a moving charged particle can be written as

$$S = \frac{A}{\beta^2}\left\{\log K + \log \frac{\beta^2}{(1-\beta^2)} - \beta^2\right\} \qquad \ldots\ldots(1)$$

where S is the total number of ion pairs produced per cm path, β the ratio of the velocity of the ionizing particle to that of light and A and K are constants for the medium. Using the values of the total specific ionization in air for electrons of energies 17·5 MeV and 9 MeV measured by Ovadia *et al.* the constants in equation (1) have been determined and hence the number of ion pairs S per cm path in air at room temperature and pressure at the time of the experiment was estimated to be 56 for electrons of energy 4·33 MeV.

The number of electrons N_1 in the primary electron beam was determined by the relation

$$N_1 = CV/Sde \qquad \ldots\ldots(2)$$

where C is the capacity of the standard condenser, V the balancing voltage applied to nullify the electrometer deflection, d the effective separation between the two plates of the ionization chamber and e the electron charge. The effect due to recombination of ions was estimated by a method due to Boag (1950) and found to be less than 1% under the conditions of the present measurements.

Processing of the G5 Plates and Photographic Films.

The developing solution used for processing the G5 plates consisted of one part of Johnson's Azol developer, one part of 1% potassium bromide solution and 50 parts of water. The emulsions were developed for 40 minutes at a temperature of 19°C. The plates were then transferred to a stop bath of ½% solution of acetic acid for about 15 minutes. They were then fixed in plain hypo solution until clear and were finally washed in running water for several hours.

The photographic films used for relative intensity measurements, were developed for 5½ minutes at 19°C in Kodak D19B developer, fixed in plain hypo solution and washed in running water.

§ 3. Details of Scanning the Emulsions

For the various groups of exposures, distances of the various points on the photographic plates from the scattering centre of the target were measured by means of a cathetometer. A high quality binocular research microscope (Cooke, Troughton and Simms, type M4005) was used to analyse the tracks of the scattered electrons in the emulsions. Narrow strips on the plates corresponding to the various angles of scattering were scanned and the number of tracks in each strip was counted.† Owing to the uncertainty in determining the direction of entry of the electrons at the surface of the emulsion, tracks within a fairly wide range of angles ($\pm 11°$ for the silver and platinum measurements, extended to $\pm 14°$ for uranium and aluminium) on either side of the expected direction of arrival were recorded. Slow electrons (energies less than about 1–2 MeV, such as might be due to electron–electron scattering) which could easily be recognized by the excessive amount of multiple scattering were ignored. Some plates were exposed without any foil in position in order to estimate the effect of background. These were scanned in the same way and enabled the appropriate corrections to be applied.

† These strips should have been parabolic to maintain a constant angle of scattering. Actually straight strips were used. The error made in so doing was less than 1% in all cases.

The relative measurements using silver and platinum foils were made first. A study of the apparent direction of arrival of tracks for these exposures showed that these directions are approximately normally distributed about the expected direction of incidence. Absolute measurements were made of the scattering from the uranium foil at 50°, 60° and 90° and for the aluminium foil at 60° and 90°. Measurements of the absolute cross section were also made for uranium at 120° and the results of these are also included below. When attempts were made to extend the relative measurements to 120° it was found that the apparent direction of arrival of the tracks was no longer normally distributed about the expected direction of incidence. This indicated that at this angle of scattering an appreciable proportion of the electrons were arriving not from the foil, but from the wall of the scattering chamber. Some of these spurious tracks undoubtedly arose from electrons scattered directly from the foil on to the chamber wall. But part of the effect could be caused by scattering on to the chamber wall of electrons striking the end plate of the apparatus after being spread by small angle multiple scattering in the foil. At 120° the distortion of the distribution in direction of arrival of tracks suggested an excess scattering from the wall of $25 \pm 10\%$ for Pt and $40 \pm 15\%$ for Ag. There is no evidence of such spurious scattering at angles of 90° and less and a rough estimate of its magnitude suggests that it would not exceed a few per cent at these angles. In the absolute measurements on uranium at 120° no marked distortion in the distribution of the tracks about the expected direction of entry into the emulsion was observed. This suggests that there was less spurious back scattering from the wall in this case. This could be associated with the different geometry used in these measurements. The camera was located close to the removable end of the chamber so that a much smaller proportion of the beam struck the end plate after undergoing small angle multiple scattering in the foil. Nevertheless it seems unlikely that wall scattering could have been entirely eliminated in these measurements so that the measured cross section for uranium at 120° could be too high by as much as 10%.

§ 4. Theory

The theoretical cross section for uranium has been computed by Yadav (1955) by numerical summation of the series expression given by Mott (1929, 1932). From his results the cross sections for electrons of energy 4·33 MeV have been computed. One of us (Curr 1955) has expanded the Mott cross section in powers of $\alpha = Z/137$ up to α^8.† Using this series the cross sections for aluminium, silver and platinum have been computed for electron energy 4·33 MeV. Results for uranium, computed from this series at this energy differ from Yadav's more exact results by only about 1%.

A small correction for the effect of the finite extent of the nucleus has been applied to the above results. This correction has been estimated by using Born approximation formulae given by Rose (1948). Corrections for the effect of multiple scattering on the scattering by a thin foil in the case of oblique incidence have been estimated by one of us (R. M. C. in course of publication) and corrections computed on the basis of this theory are given in the next section.

† The term $(-)^{k+1}[3\alpha^4/8k^4]/k$ has been omitted from the expansion (7) of D_k in this paper. The correct expression was used in the calculations however.

§ 5. Results

If N_1 is the number of electrons in the incident beam and N the number scattered into a small solid angle Ω about the angle of scattering θ, then σ the scattering cross section per unit solid angle, is given by

$$\sigma = \frac{N}{ntN_1\Omega} \qquad \ldots\ldots(3)$$

where n is the number of nuclei per unit volume of the scattering material and t the path length of the primary beam in the scattering foil. In the present experiment the scattering foil was inclined at an angle of 30° to the incident beam, so that t is equal to twice the actual thickness of the foil.

Table 1. Results of Relative Measurements (group (*a*) of exposures)

(1)	(2)	(3)	(4)	(5)	(6)	(7)	(8)		(9)		(10)	(11)
							(*a*)	(*b*)	(*a*)	(*b*)		
	45	392	9	1·86	7	0	29·4	29·0	1·26	1·256	+1	6
Ag 7·74	60	785	25	12·5	5	0	8·9	9·70	1·12	1·226	−8	5
	90	607	29	45·4	4	1	(1·89)	1·89	(0·952)	0·952	–	–
	45	2025	48	11·0	4	0	97	103	1·52	1·62	−6	3
Pt 3·83	60	1105	30	14·9	3	1	38·7	39·5	1·78	1·81	−2	4
	90	1813	50	99·0	3	2	(9·70)	9·70	(1·78)	1·78	–	–
Pt 9·57	45	1942	19	11·6	11	0	97	103	1·53	1·62	−6	3
	90	1518	17	94·5	6	2	(9·70)	9·70	(1·78)	1·78	–	–
U 3·18	45	452	10	5·18	4	0	157	150	1·78	1·70	+5	7
	60	522	12	15·0	3	1	(63·6)	63·6	(2·10)	2·10	–	–
Al 18·08	45	434	14	6·25	7	0	1·81	1·65	1·03	0·936	+9	6
	60	515	21	26·8	5	0	(0·509)	0·509	(0·839)	0·839	–	–

(1) Foil thickness (mg cm^{-2}); (2) angle of scattering θ (°); (3) observed number of tracks; (4) background tracks; (5) solid angle $\Omega \times 10^8$ (sterad); (6) multiple scattering correction (%); (7) correction due to finite size of nucleus (%); (8) $\sigma \times 10^{24}$ (cm^2 sterad^{-1}) : (*a*) experiment, (*b*) theory; (9) R : (*a*) experiment, (*b*) theory; (10) deviation from theory (%); (11) probable error (%).

The results obtained from the relative measurements (group (*a*) of exposures) are given in table 1, together with the values predicted by theory. The value of σ is given, in addition to the ratio R to the Rutherford cross section

$$\sigma_{\text{Ruth}} = Z^2nt\left(\frac{e^2}{2mc^2}\right)^2 \frac{(1-\beta^2)}{\beta^4}\operatorname{cosec}^4\theta/2 \qquad \ldots\ldots(4)$$

where β is the ratio of the velocity of the electrons to the velocity of light and m the rest mass of the electron. The experimental cross sections have been fitted to the theoretical values at 90° except for the small angle uranium and aluminium measurements, where they were fitted at 60°.

The results obtained from the absolute measurements of cross sections for uranium and aluminium are compared with the theoretical values in table 2.

In tables 1 and 2 the values of the corrections applied for background scattering, multiple scattering and finite nuclear size are also given.

§ 6. Discussion

At small angles of scattering sources of error are mainly statistical but for angles of scattering of 90° and above other effects may be important. The multiple scattering theory referred to above does not take into account double scattering of the type discussed by Goertzel and Cox (1943). The intensity at large angles of scattering may be increased by a few per cent by this effect. In calculating the theoretical cross sections radiative effects have not been taken into account. It is estimated, however, that the error due to neglecting radiative effects is at the most of the order of 1 or 2%.

Table 2. Results of Absolute Measurements (group (*b*) of exposures)

(1)	(2)	(3)	(4)	(5)	(6)	(7)	(8)	(9)		(10)		(11)	(12)
								(*a*)	(*b*)	(*a*)	(*b*)		
		50	462	11	7·54	4	0	101	109	1·71	1·84	−7	5
U 3·03	$3{\cdot}71\times10^{9}$	60	543	17	13·4	3	1	66·9	63·6	2·21	2·10	+5	5
		90	436	30	38·5	3	2	18·0	18·4	2·39	2·43	−2	5
		120	250	22	62·5	4	2	6·15	5·95	1·82	1·76	+3	6
		60	542	37	47·6	5	0	0·497	0·509	0·822	0·839	−2	4
Al 18·08	$2{\cdot}53\times10^{9}$	90	251	53	104	3	0	0·091	0·088	0·596	0·579	+3	6

(1) Foil thickness (mg cm^{-2}); (2) incident electron intensity (N_0); (3) angle of scattering θ (°); (4) observed number of tracks; (5) background tracks; (6) solid angle $\Omega\times10^{5}$ (sterad); (7) multiple scattering correction (%); (8) correction due to finite size of nucleus (%); (9) $\sigma\times10^{24}$ (cm^{2} sterad^{-1}) : (*a*) experiment, (*b*) theory; (10) R : (*a*) experiment, (*b*) theory; (11) deviation from theory (%); (12) probable error (%).

For angles of scattering of 90° and below, the results are in satisfactory agreement with the theory both in the relative and the absolute measurements. The only case in which there is a discrepancy appreciably greater than that expected from statistical considerations is the 45° scattering by the platinum foils which is 6–7% low relative to the scattering at 90°. The high track density in these scans makes the reliability of these measurements less certain than at larger angles so that this deviation is probably not significant.

The results of the absolute measurements on uranium at 120° also appear to agree with the theory although in assessing the significance of this agreement one should bear in mind the remarks made above about the importance of wall scattering.

Acknowledgments

The authors have great pleasure in expressing their sincere thanks to Professor H. S. W. Massey for his continued interest in the problem, to Dr. E. H. S. Burhop, for his guidance and encouragement throughout the course of the work, to Drs. C. Henderson, F. F. Heymann and R. E. Jennings of the microtron group for their co-operation, to the late Professor H. Terrey of the Chemistry Department for the analysis of the uranium foils and to Miss M. Kurz for assistance in the scanning of the plates. One of us (K.K.D.) is also indebted to the S.N.D.P. Yogam and the management of the Sree Narayana College, Quilon, Travancore-cochin, India, and to the University of Travancore, for financial assistance. The other (R.M.C.) is grateful to the Department of Scientific and Industrial Research for the award of a maintenance allowance.

References

Bayard, R. T., and Yntema, J. L., 1954, *Phys. Rev.*, **93,** 1412 ; 1955, *Ibid.*, **97,** 372.

Bethe, H. A., 1933, *Handbuch der Physik*, **24,** 523.

Bleuler, E., Scherrer, P., and Zunti, W., 1942, *Phys. Rev.*, **61,** 95.

Bloch, F., 1933, *Ann Phys., Lpz.*, **16,** 285.

Boag, J. W., 1950, *Brit. J. Radiol., N.S.* **23,** 601.

Buechner, W. W., Van de Graaff, R. J., Sperduto, A., Burrill, E. A. and Feshbach, H., 1947, *Phys. Rev.*, **72,** 678.

Champion, F. C., 1936, *Proc. Roy. Soc.* A, **153,** 353.

Champion, F. C., and Roy, R.R., 1948, *Proc. Phys. Soc.*, **61,** 532.

Curr, R. M., 1955, *Proc. Phys. Soc.* A, **68,** 156.

Goertzel, G., and Cox, R. T., 1943, *Phys. Rev.*, **63,** 37.

Kinzinger, E., 1953, *Z. Naturf.*, **8a,** 312.

Kinzinger, E., and Bothe, W., 1952, *Z. Naturf.*, **7a,** 390.

Mott, N. F., 1929, *Proc. Roy. Soc.* A, **124,** 426 ; 1932, *Ibid.*, **135,** 429.

Ovadia, J., Laughlin, J. S., Beattie, J. W., and Henderson, W. J., 1952, *Bull. Amer. Phys. Soc.*, **27,** 14.

Paul, W., and Reich, H., 1951, *Z. Phys.*, **131,** 326.

Randels, R. B., Chao, K. T., and Crane, H. R., 1945, *Phys. Rev.*, **68,** 64.

Rose, M. E., 1948, *Phys. Rev.*, **73,** 279.

Sen Gupta, R. L., 1939, *Proc. Phys. Soc.*, **51,** 355.

Sigrist, W., 1943, *Helv. Phys. Acta*, **16,** 471.

Van de Graaff, R. J., Buechner, W. W., and Feshbach, H., 1946, *Phys. Rev.*, **69,** 452.

Yadav, H. N., 1955, *Proc. Phys. Soc.* A, **68,** 348.

Zuber, K., 1938, *Helv. Phys. Acta*, **11,** 370.

Nuclear Scattering of High Energy Electrons on the Independent-particle Model

By L. J. TASSIE
Physics Department, University of Melbourne

Communicated by L. H. Martin; MS. received 15*th July* 1955 *and in final form* 11*th October* 1955

Abstract. A simple independent-particle model is used to treat the elastic and inelastic scattering of electrons by light nuclei at high energies, using the relativistic first Born approximation. The matrix elements are calculated for a harmonic oscillator nucleus and a spherical box nucleus. Comparison is made with experiment for the scattering of 190 MeV electrons by ^{9}Be.

§ 1. Introduction

The use of the electron as a nuclear probe for obtaining information about the charge distribution of the nucleus, and also for excitation of the nucleus has been demonstrated by the experimental work of Hofstadter and collaborators (Hofstadter *et al.* 1953, 1954, McIntyre *et al.* 1954). The theory of the elastic scattering of high-energy electrons by nuclear models with different charge distributions has been dealt with by several authors (Yennie *et al.* 1954, Brenner *et al.* 1954), and the theory of electron excitation of nuclei at energies less than about 50 MeV has been developed by considering the first term in the multipole expansion of the interaction between the electron and the nucleus (Sneddon and Touschek 1948, Thie *et al.* 1952). Schiff (1954) has developed a more general theory of electron excitation and has applied this to the collective model of the nucleus. The elastic and total inelastic scattering has been calculated by Amaldi *et al.* (1950 b) for the independent-particle model of the nucleus, using a harmonic oscillator potential, but their results are not directly applicable to the inelastic scattering of electrons with a single discrete energy loss. This problem will be considered here for the independent-particle model.

The transitions of a nucleon from one state to another in the nucleus can be divided into two types: inter-shell transitions where the nucleon jumps from one shell to another, and, since there will be several states in each shell corresponding to different couplings between the nucleons (Inglis 1953), intra-shell transitions between these states. The theory developed here should be adequate for the inter-shell transitions, but because a crude independent-particle model is used neglecting all couplings between the spins and angular momenta of the nucleons, the cross sections obtained here for the intra-shell transitions must be regarded as only a very rough first approximation, as it would be expected that the coupling would affect the transition probabilities for these transitions (Lane and Radicati 1954).

No method exists as yet for calculating the inelastic scattering accurately, but for light elements first order perturbation theory can be used with plane waves for the scattered electron, i.e. the Born approximation. The spin and

retardation are taken into account by using the Møller potentials (Møller 1931). It is assumed that the electrons interact only with the protons in the nucleus, and the effect of the finite size of the proton and the contribution due to the neutrons considered by Amaldi *et al.* (1950 a, b) are neglected.

§ 2. General Theory for Independent-particle Model

Using the theory of the retarded interaction of two charged Fermi particles developed by Møller (1931), the following expression can be derived for the differential cross section for electrons exciting the nuclear proton from the nth to the n'th state (Amaldi *et al.* 1950 b),†

$$\begin{aligned} d\sigma_{nn'}(\theta)/d\omega = (4e^4/c^4)(p/p_0)[&|\mathbf{p}-\mathbf{p}_0|^2-(E_0-E)^2/c^2]^{-2} \\ &\times \tfrac{1}{2}\tfrac{1}{2}SS_0\{|\rho_{nn'}|^2[c^2\mathbf{p}\cdot\mathbf{p}_0+\mu^2+EE_0] \\ &-2\mathscr{R}(\rho_{nn'}{}^*[c\mathbf{J}_{nn'}\cdot\mathbf{p}E_0+c\mathbf{J}_{nn'}\cdot\mathbf{p}_0E]) \\ &+2c^2\mathscr{R}[(\mathbf{J}_{nn'}{}^*\cdot\mathbf{p})(\mathbf{J}_{nn'}\cdot\mathbf{p}_0)]-\mathbf{J}_{nn'}{}^*\cdot\mathbf{J}_{nn'}[c^2\mathbf{p}\cdot\mathbf{p}_0+\mu^2-E_0E]\}, \end{aligned} \quad \ldots\ldots(1)$$

where

$$\rho_{nn'}=\int \Phi(\mathbf{R})\psi_n(\mathbf{R})\psi_{n'}(\mathbf{R})\,dV, \quad \ldots\ldots(2)$$

$$\mathbf{J}_{nn'}=\int \Phi(\mathbf{R})\psi_n(\mathbf{R})\boldsymbol{\alpha}\psi_{n'}(\mathbf{R})\,dV, \quad \ldots\ldots(3)$$

$$\Phi(r)=\exp(i\mathbf{K}.\mathbf{r}), \qquad \mathbf{K}=\mathbf{k}-\mathbf{k}_0, \qquad \mu=m_0c^2. \quad \ldots\ldots(4)$$

$\mathbf{k}_0=\mathbf{p}_0/\hbar$, $\mathbf{k}=\mathbf{p}/\hbar$, and E_0, E are the initial and final wave vectors and energies respectively of the scattered electron. ψ_n, $\psi_{n'}$ are the initial and final wave functions of the nuclear proton, and S_0 and S refer to summation over initial and final proton spin states. In equation (3) no account is taken of the anomalous magnetic moment of the proton and this effect will be considered later (§ 5).

Accurate Dirac wave functions cannot be used for the nuclear protons (Plesset 1932), but, since the energy of the protons in the nucleus is much smaller than their rest energy, the Darwin approximation can be used (Darwin 1928, Amaldi *et al.* 1950 b). The proton wave function is written

$$\psi_n=a_s\phi_n \quad \ldots\ldots(5)$$

where ϕ_n is the Schrödinger wave function, and a_s is either of the two spin functions

$$a_s=\begin{Bmatrix} \tfrac{1}{2}r_m(i\partial/\partial x+\partial/\partial y) \\ -\tfrac{1}{2}r_m i\partial/\partial z \\ 0 \\ 1 \end{Bmatrix}, \quad a_s=\begin{Bmatrix} \tfrac{1}{2}r_m i\partial/\partial z \\ \tfrac{1}{2}r_m(i\partial/\partial x-\partial/\partial y) \\ 1 \\ 0 \end{Bmatrix} \quad \ldots\ldots(6)$$

where $r_m=\hbar/Mc$ and M is the rest mass of the proton. The Darwin approximation can be used only to terms of the order r_m in the charge and current density, as terms of order $r_m{}^2$ in the charge density must be neglected for the orthogonality and normalization conditions to be satisfied. If the $r_m{}^0$ terms in $\rho_{nn'}$ do not vanish, $|\rho_{nn'}|^2$ gives rise to terms of order $r_m{}^2$ which are neglected; and thus since $J_{nn'}$ is of order r_m, the $|J_{nn'}|^2$ terms in (1) must also be neglected. Thus,

† The derivation of equation (1) is given by Amaldi *et al.* (1950 b), but the expression itself is stated incorrectly. Since they neglect the last two terms, this did not affect their results. Their equation (26) is also incorrect, and would slightly modify their results for inelastic scattering.

for transitions where r_m^0 terms in $\rho_{nn'}$ do not vanish, equation (1) reduces to equation (20) of Amaldi *et al.* (1950 b),

$$d\sigma_{nn'}/d\omega = (4e^4/c^4)(p/p_0)[|\mathbf{p}-\mathbf{p}_0|^2-(E_0-E)^2/c^2]^{-2} \times \tfrac{1}{2}\{|\rho_{nn'}|^2[c^2\mathbf{p}\cdot\mathbf{p}_0+\mu^2+EE_0] - 2\mathscr{R}(\rho_{nn'}{}^*[c\mathbf{J}_{nn'}\cdot\mathbf{p}E_0+c\mathbf{J}_{nn'}\cdot\mathbf{p}_0E])\}. \quad \ldots\ldots(7)$$

These transitions will be referred to as 'allowed' transitions and for the crude independent-particle model they are far more probable than transitions involving higher orders of r_m in the cross sections, which will be referred to as 'forbidden' transitions. Since Amaldi *et al.* (1950 b) are concerned only with the total inelastic scattering, they neglect the 'forbidden' transitions and deal only with the 'allowed' transitions. The 'allowed' transitions have selection rules $\Delta s=0$, $\Delta m=0$, and are thus inter-shell transitions, e.g. 1s→2p, 2p→3d etc.; whereas the 'forbidden' transitions include the intra-shell transitions, e.g. 2p→2p, which are more important in the theory of light nuclei (Inglis 1953).

For 'forbidden' transitions, the r_m^0 terms in $\rho_{nn'}$ vanish, and the $\rho_{nn'}$ terms in (1) contribute terms of order r_m^3 and r_m^4. Thus, taking terms of order r_m^2, we obtain for 'forbidden' transitions

$$d\sigma_{nn'}/d\omega = (4e^4/c^4)(p/p_0)[|\mathbf{p}-\mathbf{p}_0|^2-(E_0-E)^2/c^2]^{-2} \times \tfrac{1}{2}\tfrac{1}{2}SS_0\{2c^2\mathscr{R}[(\mathbf{J}_{nn'}{}^*\cdot\mathbf{p}_0)(\mathbf{J}_{nn'}\cdot\mathbf{p})] - \mathbf{J}_{nn'}{}^*\cdot\mathbf{J}_{nn'}[c^2\mathbf{p}\cdot\mathbf{p}_0+\mu^2-E_0E]\}, \quad \ldots\ldots(8)$$

Since the positions of the energy levels in the nucleus cannot be calculated accurately, we cannot determine the energy loss E_0-E. However, for the scattering of electrons with energies of the order of 100 Mev, it can be safely assumed that this energy loss is small in comparison with the incident energy E_0. Thus, E_0-E can be neglected except for scattering through small angles (Smith 1954). Then $k=k_0$, and $K=2k\sin\theta/2$, where θ is the angle of scattering.

For convenience we take $\mathbf{K}$ as pointing along the z axis and $\mathbf{k}_0$ and $\mathbf{k}$ in the xz plane. Also, in dealing with high-energy electrons, we take $v/c=1$, $E=pc$. Then equation (7) becomes

$$d\sigma_{nn'}/d\omega = \tfrac{1}{4}(e^2/\hbar c)^2k^{-2}\cos^2\tfrac{1}{2}\theta\,\mathrm{cosec}^4\tfrac{1}{2}\theta\,|\rho_{nn'}|^2, \quad \ldots\ldots(9)$$

$$\rho_{nn'} = \int \exp(iKz)\phi_n{}^*(\mathbf{R})\phi_{n'}(\mathbf{R})\,dV, \quad \ldots\ldots(10)$$

For $n=n'$, this is the usual form of the first Born approximation for the elastic scattering by a charge distribution $e|\phi_n|^2$ (Rose 1948).

Equation (8) becomes

$$d\sigma_{nn'}/d\omega = (e^4/c^2)\,|\Delta\mathbf{p}|^{-4}SS_0\{2p^2|J_{nn',z}|^2+|J_{nn',y}|^2|\Delta\mathbf{p}|^2/2\}. \quad \ldots\ldots(11)$$

For transitions involving change of orientation of the proton spin ($\Delta s=\pm1$)

$$|J_{nn',z}|^2 = |J_{nn',y}|^2 = |\tfrac{1}{2}ir_m\int \exp(iKz)\frac{\partial}{\partial z}(\phi_n{}^*\phi_{n'})\,dV|^2, \quad \ldots\ldots(12)$$

and for no spin change ($\Delta s=0$)

$$J_{nn',z} = ir_m\int \exp(iKz)\phi_n{}^*(\partial\phi_{n'}/\partial x)\,dV,$$

$$J_{nn',y} = ir_m\int \exp(iKz)\phi_n{}^*(\partial\phi_{n'}/\partial y)\,dV. \quad \ldots\ldots(13)$$

For elastic scattering, ρ_{nn} is summed over all protons in the nucleus, giving

$$d\sigma_e/d\omega = \tfrac{1}{4}(e^2/\hbar c)^2k^{-2}(\cos^2\tfrac{1}{2}\theta\,\mathrm{cosec}^4\tfrac{1}{2}\theta)\,|\mathscr{F}|^2. \quad \ldots\ldots(14)$$

$|\mathcal{F}|^2$ is the nuclear form factor, the ratio to point charge scattering. We have

$$\mathcal{F}=\Sigma_n \rho_{nn}=z_1\rho_{1s1s}+z_2\rho_{2p2p}+\text{etc.}, \qquad \ldots\ldots(15)$$

where z_1 is the number of protons in the first shell, etc. When the ρ_{nn} given in § 3, equations (17) and (18) for the harmonic oscillator model, and in § 4, figure 1 for the spherical box model, are substituted in equation (15), the elastic scattering nuclear form factors are obtained for these models for nuclei up to $Z=8$.

For excitation of a particular nuclear transition, the inelastic cross section must be summed over all protons which can give rise to that particular transition, giving

$$z_n(1-z_{n'}/\zeta_{n'})\,d\sigma_{nn'}/d\omega \qquad \ldots\ldots(16)$$

where $\zeta_{n'}$ is the number of protons required to fill the n'th level.

§ 3. Harmonic Oscillator Model

The elastic and total inelastic scattering of high-energy fermions by a harmonic oscillator nucleus have been calculated by Amaldi *et al.* (1950 b) and Gatto (1953). The proton wave functions are separable in Cartesian coordinates:

$$\left.\begin{aligned}&\phi_n(\mathbf{R})=X_{n_1}(x)Y_{n_2}(y)Z_{n_3}(z),\\&\rho_{nn'}=\delta_{n_1n_1'}\delta_{n_2n_2'}I_{n_3n_3'},\\&I_{n_3n_3'}=\int_{-\infty}^{\infty}\exp(iKz)Z_{n_3}{}^*(z)Z_{n_3'}(z)\,dz.\end{aligned}\right\} \qquad \ldots\ldots(17)$$

The $I_{nn'}$ are given by Amaldi *et al.* (1950 a). The harmonic oscillator energy levels are highly degenerate and this does not permit calculation of the scattering cross sections for different discrete energy losses. This difficulty can be overcome by using the spherical box model as in § 4. However, suitable linear combinations of the harmonic oscillator wave functions corresponding to particular values of l may be used, assuming some deviation from the harmonic oscillator potential which splits up these states without appreciably altering the wave functions. It is also assumed that the order of the states is the same as for the spherical box.

In this manner, and using the $I_{n_3n_3'}$ of Amaldi *et al.* (1950 a), we obtain the following matrix elements (averaged over all values of the magnetic quantum number m) which are needed for treating nuclei with incomplete 2p shells.

$$\left.\begin{aligned}&I_{1s1s}=I_{00}=\exp(-\tfrac{1}{2}x)\\&I_{2p2p}=\tfrac{1}{3}I_{11}+\tfrac{2}{3}I_{00}=\exp(-\tfrac{1}{2}x)(1-\tfrac{1}{3}x)\\&|I_{1s2p}|^2=|I_{01}|^2=x\exp(-x)\\&|I_{2p3d}|^2=\tfrac{2}{3}[|I_{01}|^2+\tfrac{1}{2}|I_{12}|^2]=\tfrac{2}{3}x\exp(-x)\{1+\tfrac{1}{6}(x-2)^2\}\\&|I_{2p2s}|^2=\tfrac{1}{3}|I_{12}|^2=\tfrac{1}{3}x\exp(-x)(x-2)^2\\&|I_{1s3d}|^2=\tfrac{2}{5}|I_{02}|^2=\tfrac{1}{5}x^2\exp(-x)\\&|I_{1s2s}|^2=\tfrac{1}{3}|I_{02}|^2=\tfrac{1}{6}x^2\exp(-x),\end{aligned}\right\} \qquad \ldots\ldots(18)$$

where $x=\frac{1}{2}Q^2$, $Q=Ka$, $a=(\hbar^2/Mw)^{1/2}$. w is the energy interval between successive states of the harmonic oscillator; a is then the parameter determining the size of the nucleus.

'Forbidden' Transitions.

For proton wave functions separable in Cartesian coordinates, equation (11) becomes for transitions with spin change ($\Delta s = \pm 1$)

$$d\sigma_{nn'}/d\omega = \tfrac{1}{4}(e^2/\hbar c)^2 k^{-2}(E/Mc^2)^2(1+\sin^2\tfrac{1}{2}\theta)\operatorname{cosec}^2\tfrac{1}{2}\theta\,\delta_{n_1n_1'}\delta_{n_2n_2'}|I_{n_3n_3'}|^2, \quad \ldots.(19)$$

since $r_m k = E/Mc^2$. The probability of spin change transitions is thus roughly $(E/932)^2$ times that of 'allowed' transitions, where E is in MeV. This justifies the use of the term 'forbidden' unless the energy of the incident electron is comparable with 932 MeV. This result will be modified by the effect of the anomalous magnetic moment of the proton (§ 5), and also by the coupling between nucleons. Equation (13) for no spin change ($\Delta s = 0$), becomes

$$J_{nn',x} = ir_m \int_{-\infty}^{\infty} X_{n_1}^*(x)\frac{dX_{n_1'}(x)}{dx}\,dx\,\delta_{n_2n_2'}I_{n_3n_3'}. \quad \ldots\ldots(20)$$

For harmonic oscillator wave functions,

$$\int_{-\infty}^{\infty} X_n \frac{dX_{n'}}{dx}\,dx = a[(\tfrac{1}{2}n')^{1/2}\delta_{n,n'-1} - \{\tfrac{1}{2}(n'+1)\}^{1/2}\delta_{n,n'+1}] \quad \ldots\ldots(21)$$

thus giving for 'forbidden' transitions with $\Delta s = 0$

$$(d\sigma_{nn'}/d\omega)_{(x)} = \tfrac{1}{4}(e^2/\hbar c)^2 k^{-2}\operatorname{cosec}^4\tfrac{1}{2}\theta(r_m/2a)^2$$

$$\times\{\tfrac{1}{2}n_1'\delta_{n_1,n_1'-1} + \tfrac{1}{2}(n_1'+1)\delta_{n_1,n_1'+1}\}\delta_{n_2n_2'}|I_{n_3n_3'}|^2 \quad \ldots\ldots(22a)$$

$$(d\sigma_{nn'}/d\omega)_{(y)} = \tfrac{1}{4}(e^2/\hbar c)^2 k^{-2}\operatorname{cosec}^2\tfrac{1}{2}\theta(r_m/2a)^2$$

$$\times\delta_{n_1n_1'}\{\tfrac{1}{2}n_2'\delta_{n_2,n_2'-1} + \tfrac{1}{2}(n_2'+1)\delta_{n_2,n_2'+1}\}|I_{n_3n_3'}|^2 \quad \ldots\ldots(22b)$$

$r_m = \hbar/Mc = 2{\cdot}11\times10^{-14}$ cm. Since a is of the order 10^{-13} cm, $(r_m/2a)^2$ is of the order 10^{-2} and thus the probability of these 'forbidden' transitions is very much smaller than that of the 'allowed' transitions. Using wave functions for particular values of l, both (22*a*) and (22*b*) can contribute towards the same transition and their contributions must be added for these cases.

§ 4. Spherical Box Nucleus

Since the probabilities of the 'forbidden' transitions are very much smaller than those of the 'allowed' transitions, only 'allowed' transitions will be considered for the spherical box nuclear model. Writing the proton wave functions in terms of spherical polar coordinates, it is seen from equation (10) that $\Delta m = 0$ is a selection rule for 'allowed' transitions. Using the expansion (Blatt and Weisskopf 1952)

$$\exp(iKr\cos\theta) = \sum_{\nu=0}^{\infty} i^\nu(2\nu+1)\mathrm{j}_\nu(Kr)\mathrm{P}_\nu(\cos\theta), \quad \ldots\ldots(23)$$

where

$$\mathrm{j}_\nu(x) = (\pi/2x)^{1/2}\mathrm{J}_{\nu+1/2}(x)$$

is the spherical Bessel function, then

$$\rho_{nn'} = \sum_{\nu=0}^{\infty}\mathscr{A}_\nu(l,l',m)\mathscr{B}_\nu(n,n',l,l'), \quad \ldots\ldots(24)$$

where

$$\mathscr{A}_\nu = \left\{\left(\frac{2l+1}{2}\frac{(l-|m|)!}{(l+|m|)!}\right)\left(\frac{2l'+1}{2}\frac{(l'-|m|)!}{(l'+|m|)!}\right)\right\}^{1/2} \times i^\nu(2\nu+1)\int_{-1}^{1} \mathrm{P}_\nu^0(z)\mathrm{P}_l^m(z)\mathrm{P}_{l'}^m(z)\,dz \qquad \ldots\ldots(25)$$

$$\mathscr{B}_\nu = \int_0^\infty u_n^*(r)u_{n'}(r)\mathrm{j}_\nu(Kr)\,dr, \qquad \ldots\ldots(26)$$

where $u_n(r)/r$ is the radial part of the proton wave function. The integral in $\mathscr{A}_\nu$ vanishes except for

$$\nu = |l'-l|,\ |l'-l|+2,\ \ldots,\ l'+l,$$

and can be expressed in terms of a finite hypergeometric series (Gaunt 1929). The values of $\mathscr{A}_\nu$ obtained are tabulated below in table 1.

Table 1

l	l'	m	ν	$\mathscr{A}_\nu$
0	0	0	0	1
0	1	0	1	$i\sqrt{3}$
0	2	0	2	$-\sqrt{5}$
1	1	0	0	1
			2	-2
		1	0	1
			2	1
1	2	0	1	$i2\sqrt{(3/5)}$
			3	$-i3\sqrt{(3/5)}$
1	2	1	1	$i\sqrt{(3/5)}$
			3	$i3/\sqrt{5}$

Taking the nucleus as a spherical box of radius a the normalized proton wave functions are

$$u_n(r) = (2/a)^{1/2}\{\mathrm{j}_{l-1}(\alpha a)\}^{-1}(r/a)\mathrm{j}_l(\alpha r), \qquad r \leqslant a;$$
$$= 0, \qquad r \geqslant a; \qquad \ldots\ldots(27)$$

where $\alpha = (8\pi^2 Me/h^2)^{1/2}$ and has the value such that $\mathrm{j}_l(\alpha a) = 0$. Inserting these wave functions in equation (26), the following $\mathscr{B}_\nu$ were obtained:

$$\mathscr{B}_0(1\mathrm{s},\ 1\mathrm{s}) = X(\alpha)/K,$$
$$\mathscr{B}_0(2\mathrm{p},\ 2\mathrm{p}) = 3\{K\mathrm{j}_1(K) + (2\beta^2 - K^2)X(\beta)/K\beta\sin 2\beta\}/\beta^2, \qquad \ldots\ldots(28)$$

where

$$X(\alpha) = \mathrm{Si}(K) - \tfrac{1}{2}\mathrm{Si}(2\alpha + K) + \tfrac{1}{2}\mathrm{Si}(2\alpha - K).$$

On averaging over m, $\mathscr{B}_2(2\mathrm{p},\ 2\mathrm{p})$ is not required.

$$\mathscr{B}_1(\mathrm{ns},\ \mathrm{n'p}) = 2\{\alpha\sin K\cos\alpha\sin\beta/2\beta K + (\alpha^2 - K^2 - \beta^2)Y(\alpha,\beta)/8\beta K\}/K\sin\beta,$$
$$\mathscr{B}_1(\mathrm{np},\ \mathrm{n'd}) = \{9K^3\mathrm{j}_1(K)/\gamma^2 + 3(\gamma^2 - 3\beta^2)K\mathrm{j}_1(K)/\gamma^2 - (3\beta^2 + \gamma^2)\mathrm{j}_0(K) - 3K^2\mathrm{j}_0(K) + 3[(\gamma^2 - \beta^2)(\gamma^2 + 3\beta^2)/2K + (\gamma^2 + 3\beta^2)K - 3K^3/2]Y(\beta,\gamma)/2\gamma^2\sin\beta\sin\gamma\}/4K\beta\gamma,$$
$$\mathscr{B}_2(\mathrm{np},\ \mathrm{n'd}) = 3\{-\mathrm{j}_1(K)[\tfrac{1}{3}K^3 + K(2\beta^2 + \gamma^2) + 5(3\gamma^2 - \beta^2)(\gamma^2 + 3\beta^2)/6K]/\gamma^2 + \mathrm{j}_0(K)[\tfrac{1}{6}K^2 + \tfrac{1}{3}(3\beta^2 + \gamma^2) + 5(\beta^2 - \gamma^2)^2/6K^2] + [K^3 + (3\beta^2 + \gamma^2)K + 3(\gamma^2 - \beta^2)(\gamma^2 + 3\beta^2)/K + 5(\beta^2 - \gamma^2)^3/K^3]Y(\beta,\gamma)/8\gamma^2\sin\beta\sin\gamma\}/4K\beta\gamma, \qquad \ldots\ldots(29)$$

where

$$Y(\alpha,\beta) = \mathrm{Si}(\alpha - \beta + K) + \mathrm{Si}(\alpha + \beta - K) + \mathrm{Si}(\beta + K - \alpha) - \mathrm{Si}(\alpha + \beta + K),$$

where a is used as the unit of length, i.e. K is equivalent to Ka, and α, β, γ are such that $j_0(\alpha)=0$, $j_1(\beta)=0$, $j_2(\gamma)=0$.

As $K\to 0$, equations (28) become

$$\mathscr{B}_1'(\mathrm{ns, n'p})=4K\alpha\beta/3(\beta^2-\alpha^2)^2,$$
$$\mathscr{B}_1'(\mathrm{np, n'd})=4K\beta\gamma/3(\gamma^2-\beta^2)^2, \qquad \ldots\ldots(30)$$

$\mathscr{B}_3$ is of order K^3. Equation (30) is the usual electric dipole approximation for small K.

ρ_{nn} and $|\rho_{nn'}|^2$ are averaged over m for elastic and inelastic scattering respectively and the results so obtained are shown in figure 1.

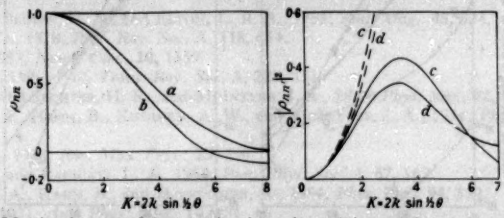

Figure 1. Matrix elements for scattering by spherical box nucleus. *a*, ρ_{1s1s}; *b*, ρ_{2p2p}; *c*, $|\rho_{1s2p}|^2$; *d*, $|\rho_{2p3d}|^2$. Broken line dipole approximation as given by equations (30).

§ 5. Effect of Anomalous Magnetic Moment of the Proton

The anomalous magnetic moment of the proton can be considered by adding the term

$$s_k'-s_k=l\frac{\partial}{\partial x_l}(\psi^\dagger i\tfrac{1}{2}(\gamma_k\gamma_l-\gamma_l\gamma_k)\psi) \qquad \ldots\ldots(31)$$

to the Dirac current charge four-vector (Pauli 1941). For small particle velocity this gives an additional term in the magnetic moment of the form $-l(\hbar c)^{1/2}$. Thus

$$l=-\tfrac{1}{2}(\gamma-1)(e^2/\hbar c)^{1/2}r_\mathrm{m} \qquad \ldots\ldots(32)$$

where γ is the magnetic moment of the proton in units of $e\hbar/2Mc$. l is of the first order in r_m, and on applying the Darwin approximation all terms in $\psi^\dagger\gamma_k\gamma_l\psi$ of the first or higher order in r_m are neglected. The remaining terms occur only for transitions involving change of the proton spin, and the effect of these terms is the same as multiplying the right-hand sides of equations (12) and (19) by $\gamma_\mathrm{p}^2=7{\cdot}76$.

If the magnetic moment of the neutron is also described by such a term as (31), then the electrons could also excite neutrons in the nucleus, the cross sections being given by equation (19) multiplied by γ_n^2.

§ 6. Scattering of Electrons by ^{9}Be

^{9}Be has a proton configuration $(1s)^2(2p)^2$ and the elastic scattering is given by equation (14) with

$$\mathscr{F}=2\rho_{1s1s}+2\rho_{2p2p}. \qquad \ldots\ldots(33)$$

The parameters a_HO and a_SB for the harmonic oscillator and spherical box model respectively can be determined by comparison with the experimental results of Hofstadter *et al.* (1953) for the elastic scattering of 125 Mev electrons by ^{9}Be. The values obtained are

$$a_\mathrm{HO}=1{\cdot}64\times10^{-13}\ \mathrm{cm}; \qquad a_\mathrm{SB}=3{\cdot}94\times10^{-13}\ \mathrm{cm}.$$

The elastic and inelastic scattering was calculated for 190 MeV electrons by ^{9}Be, for which $ka_{HO}=1{\cdot}58$, $ka_{SB}=3{\cdot}8$, and the results are shown in figure 2. The unit on the ordinate scale is $\frac{1}{4}(e^2/\hbar c)^2k^{-2}=1{\cdot}43\times10^{-31}$ cm^2. The results have been summed over final values of m and averaged over initial values of m.

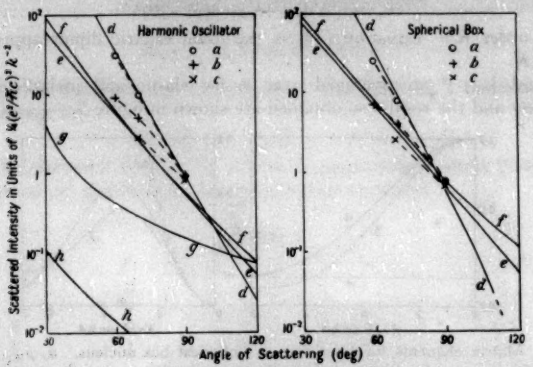

Figure 2. Scattering of 190 MeV electrons by ^{9}Be. *d*, elastic ; *e*, 1s→2p inelastic ; *f*, 2p→3d inelastic ; *g*, 2p→2p, $\Delta s=1$, inelastic ; *h*, 2p→2p, $\Delta m=1$, inelastic. Experimental results of McIntyre *et al.* (1954) : *a*, elastic ; *b*, inelastic, 2·54 MeV energy loss ; *c*, inelastic, 6·96 MeV energy loss.

Equation (19) has been used for the 'spin–flip' transition, modified for the anomalous magnetic moment of the proton as in § 5. The experimental results shown in these figures are those of McIntyre *et al.* (1954). Since no measurements of absolute scattering cross section were made, the experimental results can be translated up or down as a whole in figure 2. The experimental energy losses are 2·54 MeV and 6·96 MeV. The nuclear model used here gives no estimate of the energy loss for intra-shell transitions. For the inter-shell transitions the crude independent particle model gives the energy losses shown below. These figures would be altered considerably by the effect of the actual internucleon forces and by spin–orbit coupling.

Table 2. Associated Energy Loss

	Harmonic oscillator	Spherical box
1s→2p	15·4 MeV	13·9 MeV
2p→3d	15·4 MeV	17·2 MeV

The experimental transitions can hardly be identified with any of the inter-shell transitions, because of the large difference in the values of the energy loss. Also, the 1s→2p and 2p→3d transitions involve a parity change, whereas Ribe and Seagrave (1954) have shown that the 2·43 MeV level has the same parity as the ground state. The scattered intensities predicted here for the intra-shell transitions are much smaller than the experimental intensities, but further refinements to the theory, such as including the coupling between angular momenta and spin of the nucleons, are necessary before any conclusion can be reached.

ACKNOWLEDGMENTS

I should like to express my thanks to Associate-Professor C. B. O. Mohr for his advice and encouragement in this work, and to Mr. J. W. G. Wignall for useful discussions. I am indebted also to the Commonwealth Scientific and Industrial Research Organisation for an Australian Studentship.

REFERENCES

AMALDI, E., FIDECARO, G., and MARIANI, F., 1950 a, *Nuovo Cim.*, **7**, 553; 1950 b, *Ibid.*, **7**, 758.
BLATT, J. M., and WEISSKOPF, V. F., 1952, *Theoretical Nuclear Physics* (New York : Wiley), p. 784.
BRENNER, S., BROWN, G. E., and ELTON, L. R. B., 1954, *Phil. Mag.*, **45**, 524.
DARWIN, C. G., 1928, *Proc. Roy. Soc.* A, **118**, 654.
GATTO, R., 1953, *Nuovo Cim.*, **10**, 1559.
GAUNT, J. A., 1929, *Phil. Trans. Roy. Soc.* A, **228**, 151.
HOFSTADTER, R., FECHTER, H. R., and MCINTYRE, J. A., 1953, *Phys. Rev.*, **92**, 978.
HOFSTADTER, R., HAHN, B., KNUDSEN, A. W., and MCINTYRE, J. A., 1954, *Phys. Rev.*, **95**, 512.
INGLIS, D. R., 1953, *Rev. Mod. Phys.*, **25**, 390.
LANE, A. M., and RADICATI, L. A., 1954, *Proc. Phys. Soc.* A, **67**, 167.
MCINTYRE, J. A., HAHN, B., and HOFSTADTER, R., 1954, *Phys. Rev.*, **94**, 512.
MØLLER, C., 1931, *Ann. Phys., Lpz.*, **14**, 531.
PAULI, W., 1941, *Rev. Mod. Phys.*, **13**, 203.
PLESSET, M. S., 1932, *Phys. Rev.*, **41**, 278.
RIBE, F. L., and SEAGRAVE, J. D., 1954, *Phys. Rev.*, **94**, 934.
ROSE, M. E., 1948, *Phys. Rev.*, **73**, 279.
SCHIFF, L. I., 1954, *Phys. Rev.*, **96**, 765.
SMITH, J. H., 1954, *Phys. Rev.*, **95**, 271.
SNEDDON, I. N., and TOUSCHEK, B. F., 1948, *Proc. Roy. Soc.* A, **193**, 344.
THIE, J. A., MULLIN, C. J., and GUTH, E., 1952, *Phys. Rev.*, **87**, 962.
YENNIE, D. R., RAVENHALL, D. G., and WILSON, R. N., 1954, *Phys. Rev.*, **95**, 500.

Experiments on the Inelastic Scattering of Neutrons by Uranium

By R. BATCHELOR
Atomic Energy Research Establishment, Harwell, Berks.

Communicated by W. J. Whitehouse; MS. received 5th September 1955 and in final form 7th November 1955

Abstract. A helium 3 neutron spectrometer has been used to study the spectrum of neutrons inside a spherical uranium shell, 3 cm thick, when the latter is bombarded with monoenergetic neutrons of various energies between 500 kev and 1·0 Mev. The spectra of neutrons scattered inelastically and also the cross sections for this process have been derived, and the results compared with those predicted by current nuclear theory. Evidence for the existence of the low-lying rotational levels of uranium 238 is presented, and at least one new level at 700 kev (and possibly more at higher energies) has been found. Qualitative confirmation has been obtained by measuring the spectrum of neutrons from a uranium shell, 11·5 cm thick, with a neutron source in the centre.

§ 1. Introduction

Although inelastic scattering of neutrons by nuclei has been reported by many observers, it is only in a few cases that the energy spectrum of the scattered neutrons has been observed. For example Poole (1952, 1953) has studied inelastic scattering by several materials using a source of (d, d) neutrons and an anthracene scintillation counter as the neutron spectrometer, and from the measured spectra has deduced the energies of levels of the bombarded nuclei. The recently developed helium 3 neutron spectrometer (Batchelor 1952, Batchelor, Aves and Skyrme 1955) is ideally suited to the measurement of neutron spectra below 1 Mev, a region for which no reliable technique has previously existed. It consists of a proportional counter containing helium 3 which measures the total energy released in the reaction

$$^{1}_{0}\mathrm{n} + ^{3}_{2}\mathrm{He} \rightarrow ^{1}_{1}\mathrm{H} + ^{3}_{1}\mathrm{H} + 770\ \mathrm{kev}.$$

The resolution, defined as the relative standard deviation of a peak produced by monoenergetic neutrons, is 3%. This communication describes experiments using this spectrometer on inelastic scattering by uranium, a material chosen primarily for its importance in reactor design. Experiments of the sphere transmission type, as discussed by Barschall (1952) have been made to establish the nature of the scattered neutron spectra and to obtain crude values of the inelastic scattering cross sections at various incident neutron energies.

The only experimental information which exists on the uranium 238 level structure is that obtained from Coulomb excitation studies by Heydenburg and Temmer (1954) and Newton (1955, private communication). They find a level at 45 kev, a value which is in good agreement with that predicted by the Bohr–Mottelson nuclear model (1953) for a rotational state of spin 2. On this

model a heavy even-even nucleus should have low-lying levels at excitation energies E given by

$$E = \frac{\hbar^2 J}{2I}(J+1) \qquad J = 0, 2, 4 \ldots \qquad \ldots\ldots(1)$$

where I is the effective moment of inertia of the nucleus and J is the spin of the state, and the ratio $\hbar^2/2I$ for uranium is about 8 kev.

In 1953, Flowers, in a private communication, pointed out that this level scheme would lead to a scattered neutron spectrum of different character from the Maxwellian distribution expected with the previous assumption that the density of contributing levels in a heavy nucleus rises exponentially with excitation energy. On the new model the level density at low excitation energy decreases with increasing energy and the requirements of angular momentum conservation imply that only the first one or two levels can contribute to the inelastic scattering. Consequently a peak is expected in the scattered neutron spectrum at high energy. Assuming a 'black' nucleus, Flowers also made crude estimates of the inelastic scattering cross sections; from the threshold at 45 kev it rises to about $\frac{1}{2}\pi R^2$ at 250 kev, where R is the nuclear radius, and is then constant up to the energy where other levels begin to contribute to the process. It is then expected to rise again to a limiting value of πR^2. More recently Brink (1955) has calculated for various nuclei the inelastic cross section for a 0^+ to 2^+ rotational state transition using the 'cloudy crystal ball' model of the nucleus. The scattering is subdivided into two incoherent components, one resulting from the formation of a compound nucleus and one from direct interaction, each of cross section about 1 barn for uranium 238. The two theories therefore predict roughly the same cross sections for this nucleus although widely different values are predicted for many other elements.

§ 2. Experiments with a Thin Uranium Shell

2.1. *Experimental Method*

Neutrons were produced by accelerating protons with the Harwell Van de Graaff machine on to either a lithium fluoride or zirconium tritide target. Although the former gave a greater yield, it is known that a less intense group of low energy neutrons is also emitted when the main group exceeds about 700 kev (Willard and Preston 1951), and consequently the latter was used above this energy. The beam current was monitored with a current integrator. A spherical shell of uranium, 3 cm thick, $11\frac{1}{2}$ in. outside diameter was placed with its centre at a distance 25 in. in the forward direction from the target, and the helium 3 counter, completely surrounded with cadmium to eliminate thermal neutron disintegrations, was placed in the centre of the shell with its axis perpendicular to the direction of the incident neutrons. The neutrons incident on the sphere were not truly monoenergetic due to target thickness and angular variation, but these effects were less than the resolution of the detector.

A 30-channel kicksorter was used to measure the pulse height distributions from the helium 3 counter, with and without the uranium shell, at various bombarding energies. In addition a similar measurement at 500 kev was made with a 2 in. thick lead shell (for convenience a cube instead of a sphere was used) the purpose of which is mentioned in §2.2.

The neutron spectrum inside the shell is composed of unmoderated neutrons and those which have been elastically or inelastically scattered. Unmoderated and elastically scattered neutrons will not be resolved by the helium 3 detector, but the inelastic spectrum should be clearly seen. It will be distorted by multiple collisions but since the shell thickness is only one neutron mean free path, the effect should be small.

The inelastic cross section can be calculated from the observed transmission, which is taken to be the ratio of the unmoderated plus elastically scattered neutrons recorded with the shell to the number of neutrons of incident energy recorded without the shell. Bethe, Beyster and Carter (1955) have recently derived transmission formulae which allow for multiple scattering effects and have also calculated the corrections to be applied for finite counter–source separation, angular asymmetry of the counter efficiency, absorption by the counter and finite counter size. In order to apply these formulae it is necessary to know the total and elastic transport cross sections. The former are well known but values of the latter have only been reported for incident neutron energies of 0·5 and 1·0 Mev (Walt 1955). For intermediate energies interpolated values have been used.

Fission neutrons, which can arise from spontaneous fission, thermal fission of uranium 235 and fast fission of uranium 238 above the threshold ($\simeq$920 kev) will produce backgrounds to the observed pulse distributions. Since a large proportion of the fission neutron spectrum lies above 1 Mev, helium 3 disintegration pulses and recoil pulses from elastic collisions between neutrons and helium 3 will contribute to this background.

Spontaneous fission was shown to be completely negligible by observing the background pulse distribution with the detector inside the shell. Fission of uranium 235 by thermal neutrons produced by wall scattering etc. was also shown to be negligible by making observations with and without a cadmium shield around the shell. The effect of fast fission of uranium 238, which is expected to increase with increasing neutron energy above threshold, cannot be separately measured. The following crude argument shows, however, that it is not significant for bombarding energies less than 1 Mev. If fission does not occur the total number of neutrons recorded will be independent of the presence of the shell. Experimentally there was found to be no significant difference in the number of neutrons recorded with and without the shell for bombarding energies up to 1170 kev. Allowing a fair margin or error, results with bombarding energies up to 1 Mev only are considered reliable.

2.2. *Results*

2.2.1. *The scattered neutron spectrum with* 500 kev *incident neutrons.*

Figure 1 shows the pulse height distributions obtained with uranium when bombarded with 500 kev neutrons. In figure 2, the 'without shell' distribution is normalized so that the high-energy side of the peak fits the corresponding section of the 'with shell' distribution. The difference between these two curves is interpreted as the combined effect of inelastically scattered neutrons and those which have lost a significant amount of energy by multiple elastic collisions. That the latter effect is small is demonstrated by the distribution obtained with the lead shell which is also shown in figure 2. Inelastic scattering

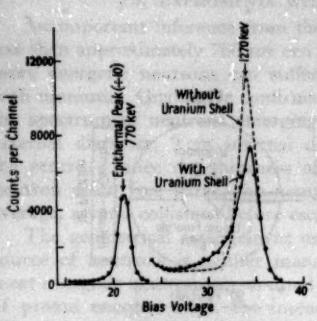

Figure 1. Pulse height distributions with and without uranium shell at 500 kev bombarding energy.

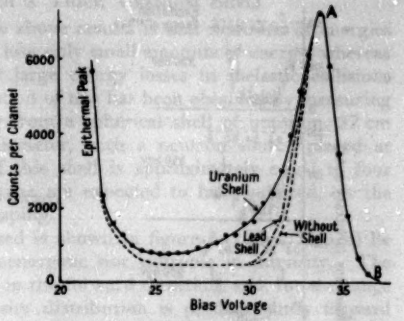

Figure 2. Pulse height distributions with 500 kev neutrons. Distribution with shell removed normalized to fit distribution with shell over section AB.

by lead is known to be rather improbable (Walt and Barschall 1954); therefore it can be assumed that the difference between 'without shell' and 'lead shell' curves is due to multiple elastic scattering only. This result can therefore be used as a rough correction for the small effect of multiple elastic scattering by uranium since the thicknesses of both shells are approximately equal to one neutron mean free path. The inelastically scattered neutron spectrum has been calculated by making additional corrections for the variations of $^3He(n, p)^3H$ cross section and counter wall effect with energy, and is shown in figure 3.

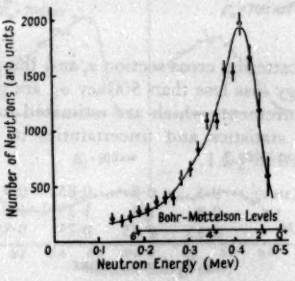

Figure 3. The spectrum of neutrons scattered inelastically by uranium at 500 kev bombarding energy.

2.2.2. *The scattered neutron spectra with higher incident energy neutrons.*

Figure 4 shows the inelastically scattered neutron spectra for various bombarding energies between 800 kev and 1 MeV. First one group, and then possibly several unresolved groups of low-energy neutrons, which provide evidence for inelastic scattering to a level or a group of levels at 700 kev excitation energy, can be seen.

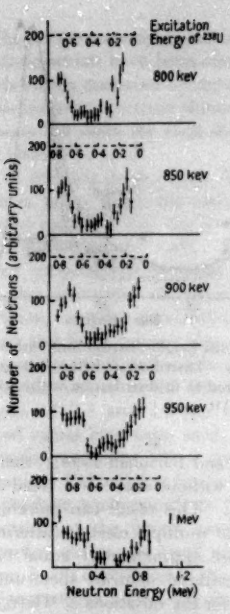

Figure 4. The spectra of neutrons scattered inelastically at various bombarding energies.

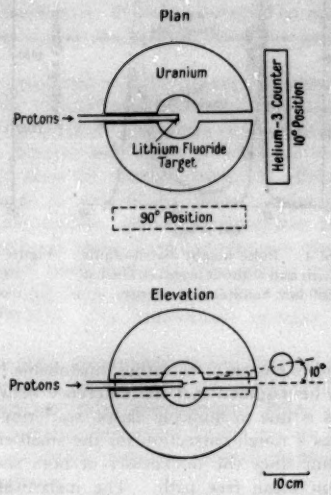

Figure 5. Geometrical arrangement of thick shell experiment.

2.2.3. *Cross sections.*

The total inelastic scattering cross section σ_1 and the cross section for inelastic scattering with an energy loss less than 500 kev σ_1' are given in the table.

The errors of measurement, which are estimated to be about $+20\%$, arise mainly from counting statistics and uncertainties in the corrections applied for the effects mentioned in § 2.1.

Neutron energy (Mev)	0·5	0·8	0·85	0·9	0·95	1·0
σ_1 (barns)	0·8	1·3	1·35	1·8	1·5	1·7
σ_1' (barns)	0·85	0·75	0·75	0·85	0·8	0·6

2.3. *Conclusions*

The following conclusions can be drawn from this experiment:

(*a*) Although the results give no information on the level structure, the shape of the inelastically scattered neutron spectrum at low incident neutron energy is in reasonable qualitative agreement with the Bohr–Mottelson level scheme.

(*b*) With incident neutrons of higher energy, at least one level (at an excitation energy of 700 kev) and possibly more (at higher excitation energies) contribute to the inelastic scattering process.

(*c*) The observed values of the inelastic scattering cross sections are in reasonable agreement with theoretical expectations and with other reported results (Walt 1955).

§ 3. Experiments with a Thick Uranium Shell

An important inference from the above results is that neutrons of energies less than approximately 700 kev can lose only small amounts of energy, whereas more energetic neutrons can suffer large energy losses in inelastic collisions with uranium. Qualitative confirmation of this has been obtained by measuring the spectrum of neutrons emerging from a spherical shell of uranium, 32 cm external diameter, 9 cm internal diameter, with a neutron source placed at the centre. Since the thickness of this shell is approximately equal to four neutron mean free paths, the neutrons are expected to have suffered, on the average, several collisions before escaping.

The geometrical arrangement used is shown in figure 5. The ^{7}Li(p, n)^{7}Be source of neutrons is neither monoenergetic nor isotropic in intensity. The most energetic neutrons are emitted in the forward direction, and, for the range of proton energies used, the intensity distribution is predominantly forward (Taschek and Hemmendinger 1948). Measurements were made with the spectrometer placed in the two positions shown in figure 5 (labelled 10° and 90° positions). Three different proton energies were used which correspond to the emission of neutrons in the forward direction with energies of 500, 700 and 900 kev.

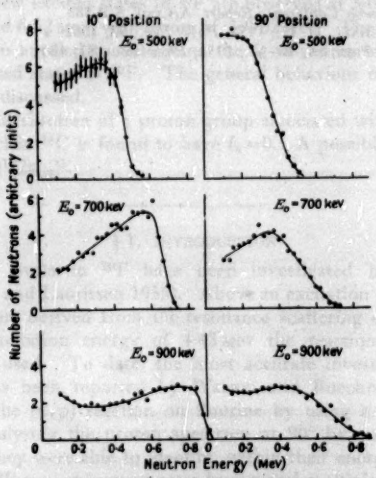

Figure 6. Spectra of neutrons emerging from thick uranium shell with ^{7}Li(p, n) ^{7}Be source placed at centre.

The observed spectra are shown in figure 6, where E_0 refers to the energy of the neutrons emitted from the source in the forward direction. For $E_0 \leqslant 700$ kev the peaks of the spectra at high energy are consistent with the energy loss in an inelastic collision being small. For $E_0 = 900$ kev, however, the shapes of the spectra have changed and the distributions quite clearly rise at low energy. This agrees with the assumption that collisions involving large energy losses

can take place at this energy. The rise at low energy is not as marked as would be expected from the previous results, but this can be understood in terms of the increasing probability of neutron capture in uranium with decreasing neutron energy.

ACKNOWLEDGMENTS

I am indebted to Dr. M. J. Poole and Dr. B. H. Flowers for their suggestions and advice. I also wish to thank Mr. G. C. Morrison who collaborated in the second experiment, Mr. M. J. Elliott for his help in making the measurements and Dr. W. D. Allen and the operating crew for the use of the Van de Graaff machine.

REFERENCES

BARSCHALL, H. H., 1952, *Rev. Mod. Phys.*, **24,** 120.
BETHE, H. A., BEYSTER, J. R., and CARTER, R. E., 1955, *United States Atomic Energy Report* LA–1429.
BOHR, A., and MOTTELSON, B. R., 1953, *Phys. Rev.*, **89,** 316.
BATCHELOR, R., 1952, *Proc. Phys. Soc.* A, **65,** 674.
BATCHELOR, R., AVES, R., and SKYRME, T. H. R., 1955, *Rev. Sci. Instrum.*, **26,** 1037.
BRINK, D. M., 1955, *Proc. Phys. Soc.* A, **68,** 994.
HEYDENBERG, N. P., and TEMMER, G. M., 1954, *Phys. Rev.*, **93,** 906.
POOLE, M. J., 1952, *Phil. Mag.*, **43,** 1060 ; 1953, *Ibid.*, **44,** 1398.
TASCHEK, R., and HEMMENDINGER, A., 1948, *Phys. Rev.*, **74,** 373.
WALT, M., 1955, *Geneva Conference Report*, A/Conf. 8/P/588.
WALT, M., and BARSCHALL, H. H., 1954, *Phys. Rev.*, **93,** 1062.
WILLARD, H. B., and PRESTON, W. M., 1951, *Phys. Rev.*, **81,** 480.

Magnetic Analysis of the Inelastically Scattered Deuterons and Disintegration Protons from the Deuteron Bombardment of Fluorine

By F. A. EL BEDEWI†
Nuclear Physics Research Laboratory, University of Liverpool

Communicated by H. W. B. Skinner: MS. received 29th June 1955, *and in amended form* 11*th October* 1955

Abstract. A magnetic spectrograph with photographic detection has been used to analyse the spectra of charged particles emitted from the bombardment of a thin teflon target by 8·9 MeV deuterons. Angular distribution measurements are also reported for several proton and deuteron groups produced in this bombardment.

Two inelastically scattered deuteron groups corresponding to excited states in ^{19}F at 1·60 ± 0·02 MeV and 2·83 ± 0·02 MeV have been observed. The angular distribution of the former group is compared with a theory proposed by Huby and Newns. A number of proton groups have been assigned to the ^{19}F(d, p)^{20}F reaction. Eight new excited states in ^{20}F are observed at 5·04, 5·19, 5·27, 5·72, 5·87, 5·95, 6·25 and 6·52 MeV, with errors of ± 0·02 MeV. The deuteron stripping theories have been applied to determine the l_n-values as well as the reduced widths of 21 excited states in ^{20}F. The general behaviour of the energy levels of this nucleus is discussed.

The angular distribution of a proton group associated with the transition to the 6·091 MeV level in ^{14}C is found to have $l_n = 0$. A possible configuration for this state is $(1p_{1/2})^1 (2s_{1/2})^1$.

§ 1. Introduction

The energy levels in ^{20}F have been investigated by several authors (Ajzenberg and Lauritsen 1955). Above an excitation energy of 6·63 MeV, the levels are derived from the resonance scattering of neutrons by ^{19}F and below an excitation energy of 4·43 MeV the reactions ^{19}F(d, p)^{20}F and ^{22}Ne(d, α)^{20}F are used. To date, the most accurate investigation of the low energy region has been reported by Watson and Buechner (1952). These authors studied the (d, p) reaction on fluorine by using a 2 MeV electrostatic generator and analysing the proton spectrum at 90° by an annular magnetic spectrograph. They were able to identify, within their energy region, eighteen excited states in ^{20}F spaced in most cases by integral multiples of 165 kev. This regular repetition of the spacing between the levels is of particular interest and suggests further search for such regularity among higher excitation levels.

In the present work, a deuteron beam of energy 8·9 MeV was employed to investigate the energy spectra and the angular distributions of the proton and deuteron groups emitted from the bombardment of a teflon (CF_2) target. The particles were analysed by a magnetic spectrograph and detected by photographic plates. Up to date, no deuteron groups inelastically scattered by ^{19}F have been

† Now at the Faculty of Science, University of Alexandria, Egypt.

reported. The angular distribution of the ground state protons has been measured with 14·3 Mev deuterons by Black (1953) and with 3·6 Mev deuterons by Bromley, Bruner and Fulbright (1953). Although the latter authors were able to fix the spin of ^{20}F ground state as 1^+ their apparatus was inadequate to resolve the complex spectrum of ^{20}F. So far, no assignments of the spins and parities of the individual excited states have been reported. The properties of these levels are of considerable interest as illustrating the competition between the $2s_{1/2}$ and $1d_{5/2}$ shells of Mayer's model. These two shells are found to be nearly coincident in the case of ^{19}F which has spin $\frac{1}{2}^+$ (Ajzenberg and Lauritsen 1955). A calculation by Elliott and Flowers (1955) shows that the configuration of the ^{19}F ground state is mainly $(d^2_{5/2}s^1_{1/2})$ mixed with $d^3_{5/2}$ and $s^3_{1/2}$.

§ 2. Procedure

2.1. *Method*

A thin teflon target of 1 mg cm^{-2} surface density was prepared by cutting thin slices from a teflon block by a microtome. The target was mounted at an angle 60° to the collimated deuteron beam provided by the Liverpool 37 inch cyclotron. The collimation was achieved by a three-slit system and the cross section of the beam was defined to a rectangular area $\frac{1}{2}$ mm wide and 3 mm high. The energy spread of the incident beam is estimated to be less than 30 kev. The charged particles emitted at a certain angle were recorded by means of a heavy particle magnetic spectrograph. This instrument is described in detail by Green and Middleton (1956 a). In the present investigation seven plates were used, each corresponding to one of the following angles of observation: 5°, 10°, 15°, 20°, 30°, 40° and 50°. The relative beam intensities at these different exposures were monitored by small photographic plates (1·2 cm × 5 cm) placed on one side of the target at an angle of 90° with respect to the incident beam. Rough monitoring to indicate the relative exposures during the performance of the experiment was done by a current integrator attached to an insulated slit just in front of the target.

2.2. *Measurements*

A Cooke, Troughton and Simms binocular microscope with × 10 eyepieces and × 20 objective was used for scanning a strip of width 8 mm centred about the axis of the plate. For each scan (0·23 mm × 8 mm) the number of protons and deuterons starting at the surface of the emulsion in the right direction were noted. Discrimination between protons, deuterons and other charged particles was made on the basis of differences in track length. In presenting the proton spectrum the number of tracks recorded in each pair of scans was plotted against the distance along the plate. In the case of the deuteron spectrum the number of tracks in four consecutive scans was used.

2.3. *Energy Calibration*

An oil immersion objective × 45 was used for measuring the lengths of deuteron tracks which lay wholly in the emulsion. The energy of the incident deuteron beam was thus obtained from range measurements of the elastically scattered deuterons from carbon and fluorine at various angles of observation. After correcting for the emulsion shrinkage, the deuteron energy was calculated

using the range–energy relation of El Bedewi (1951). The mean value for the energy of the deuteron beam at the centre of the target was found to be $8{\cdot}90 \pm 0{\cdot}02$ MeV. The loss of particle energy in escaping from the target was taken into consideration for accurate determination of the energy levels.

Owing to the scattering of the beam by the edges of the defining slits, a general deuteron background was observed over the whole length of the plate. A preliminary calibration curve was plotted from range measurements of these deuterons. This curve showed that the energy–distance relation is linear for proton energies below 12 MeV and the gradient dE/dx decreases gradually for higher energies. The gradient of the linear portion of the calibration curve was more accurately determined as 11·68 kev/0·23 mm from the positions of the proton groups emitted from the $^{12}C(d, p)^{13}C$ reaction. The Q-values corresponding to these groups had been accurately measured by Sperduto, Buechner, Bockelman and Browne (1954).

§ 3. Measurements of Cross Sections and Reduced Widths

The fact that a teflon molecule (CF_2) contains carbon and fluorine in the ratio of 1 : 2 suggests the possibility of measuring the absolute cross sections for the particles emitted from fluorine if those due to carbon are known. Rotblat (1951 a, b) and Green and Middleton (1956 b) have measured the angular distributions of the carbon proton groups in absolute units. Their mean result for the ground state proton group was used for the present calibration. The angular distributions of the protons and the deuterons emitted from fluorine are all presented in the same arbitrary units. They can be converted to millibarns per steradian by multiplying by 0·0085. The error in this multiplication factor is estimated to be $\pm 20\%$.

The cross section for deuteron stripping can also provide a direct experimental measurement of the reduced level width $\gamma_l^2{}_n$ which is proportional to the probability of finding the stripped-off nucleon at the surface of the residual nucleus (Huby 1953). The reduced width is generally denoted by θ^2 when it is expressed in units of the sum rule limit $3\hbar^2/2m_0R$, where m_0 is the mass of the captured nucleon and R the nuclear radius. The numerical value of θ^2 is regarded as a measure of the degree of purity of the state configuration. On the single-particle picture θ^2 is expected to be close to unity whereas it should be considerably smaller for levels of complicated structure formed by multiple excitation (Teichmann and Wigner 1952).

§ 4. Results and Discussion

4.1. *Deuterons*

(*a*) *Spectrum.*

The deuteron spectrum at an angle of observation of 40° is shown in figure 1(*a*). Groups denoted by F and C are due to elastically scattered deuterons from fluorine and carbon respectively. The position of the arrow at O shows the possible contribution of oxygen contamination. The first level in ^{12}C is known to be at 4·43 MeV (Ajzenberg and Lauritsen 1955) and the inelastically scattered deuterons from this state are represented by the group C*. Groups denoted by A and B are thus due to inelastically scattered deuterons from fluorine.

The Q-values corresponding to these groups are calculated from range measurements at various angles of observation and the mean values are found to be $-1{\cdot}60 \pm 0{\cdot}02$ Mev and $-2{\cdot}83 \pm 0{\cdot}02$ Mev. These results are in

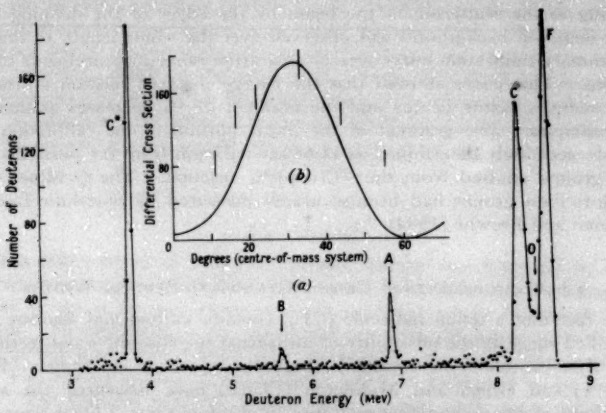

Figure 1. (*a*) Spectrum of deuteron groups from the deuteron bombardment of teflon at an angle of observation of 40°.
(*b*) Angular distribution of inelastically scattered deuterons from the 1·60 Mev level (A) in ^{19}F.

good agreement with those determined from the ^{19}F(p, p)^{19}F* reaction by Arthur, Allen, Bender, Hausman and McDole (1952). They observed few energy levels in ^{19}F and their data on the Q-values of groups corresponding to the present measurements are $-1{\cdot}59 \pm 0{\cdot}03$ Mev and $-2{\cdot}82 \pm 0{\cdot}03$ Mev respectively. The corresponding levels from the ^{18}O(d, n)^{19}F reaction are reported by Seale (1953) as $1{\cdot}6 \pm 0{\cdot}1$ Mev and $2{\cdot}75 \pm 0{\cdot}1$ Mev respectively. Bullock and Sampson (1951) observed a level in ^{19}F at $2{\cdot}67 \pm 0{\cdot}05$ Mev from the ^{16}O(α, p)^{19}F reaction.

(*b*) *Angular distribution.*

The angular distribution of the inelastically scattered deuteron group A from the 1·60 Mev level is shown plotted in the centre-of-mass system in figure 1(*b*). The experimental errors are the statistical standard deviation. The maximum cross section is 1·6 mbn sterad^{-1} at 32° (centre-of-mass). The curve shown in this figure was calculated by Newns to represent the best fit according to the theory of Huby and Newns (1951). An angular momentum transfer $l=2$ and a radius of interaction $R=7{\cdot}0\times10^{-13}$ cm were used. This assignment suggests that this state has even parity and a half-integer spin of value between 1/2 and 7/2. A possible assignment of $3/2^+$ for this level is reported by Jones, Phillips, Johnson and Wilkinson (1954) from the β-decay of ^{19}O. This value is in good agreement with that determined by Elliott and Flowers (1955) from a computation of the low-lying levels in ^{19}F.

It should be mentioned that the agreement between the experimental and theoretical curves is not yet satisfactory since the width of the latter is smaller than that of the experiment. This broadening in the experimental curve is found to be more serious in the case of the carbon inelastically scattered deuteron group C*. It shows similar behaviour to that group from ^{19}F but its maximum cross section is about seven times greater. Similar distributions have been observed by Green and Middleton (1956 b).

It is unfortunate that the inelastically scattered group B corresponding to the 2·83 Mev level in ^{19}F is so weak that it could not be distinguished above the deuteron background for angles less than 30°. At an angle of observation of 40° it has a cross section of the order of 0·2 mbn sterad^{-1}. The assignment of this level is of particular interest to check the theory of Elliott and Flowers which predicts a spin of $9/2^+$ for this level. If this value is correct an even angular momentum transfer of at least $l=4$ is required.

4.2. *Protons*

(*a*) *Spectrum.*

A typical proton spectrum is shown in figure 2 (*a*) for an angle of observation of 15°. The width at half-height of a single proton group is found to be less than 60 kev. The position of a group is taken to be the weighted mean of the points defining it. Identification of each group is made by assuming a given reaction and calculating, at all angles of observation, the corresponding Q-value. The procedure of sorting out these groups is simplified by comparing the variation of the energy shift of each group with angle and then locating the groups belonging to carbon from their known Q-values (Sperduto *et al.* 1954). These groups are denoted in the figure by C_0, C_1, C_2 and C_3.

In previous investigations of the ^{19}F(d, p)^{20}F reaction, Burrows, Powell and Rotblat (1951) reported a level at $2{\cdot}55 \pm 0{\cdot}05$ Mev which agrees with the level observed at $2{\cdot}52 \pm 0{\cdot}04$ Mev by Allen and Rall (1951). This level was found neither by Shull (1951) nor by Watson and Buechner (1952). In the present investigation, the group denoted by O_0 at 10·65 Mev, if attributed to fluorine, gives an unsatisfactory set of Q-values calculated from the various angles of observation. The mean value is found to be 2·49 Mev. Another group O_1 is also observed at 9·77 Mev which may correspond to a level in ^{20}F at 3·36 Mev. The fact that this group has not been previously observed in spite of its significant intensity suggests that both groups may possibly belong to some oxygen contamination in the target. On that assumption, the mean Q-values are found to be 1·89 Mev and 1·05 Mev which agree with the values ($1{\cdot}915 \pm 0{\cdot}01$ Mev and $1{\cdot}040 \pm 0{\cdot}010$ Mev) reported by Sperduto *et al.* (1954) for the ground and first excited states in ^{17}O. Also, the angular momenta transferred by the captured neutron at these states are found to be $l_n=2$ and $l_n=0$ respectively using Butler's formula (1951) and a radius of interaction $5{\cdot}0 \times 10^{-13}$ cm. These results agree with those determined for ^{16}O(d, p)^{17}O reaction by Burrows, Gibson and Rotblat (1950). Moreover, when a slightly thicker fresh target was used a large decrease in the intensity of these two groups was found as shown in figure 2 (*b*). For these reasons it seems certain that these two groups are due to some oxygen contamination and no evidence is thus found for a level at about 2·5 Mev in ^{20}F. Possible contributions from other levels in ^{17}O are shown by the arrows at O_2, O_3 and O_4,

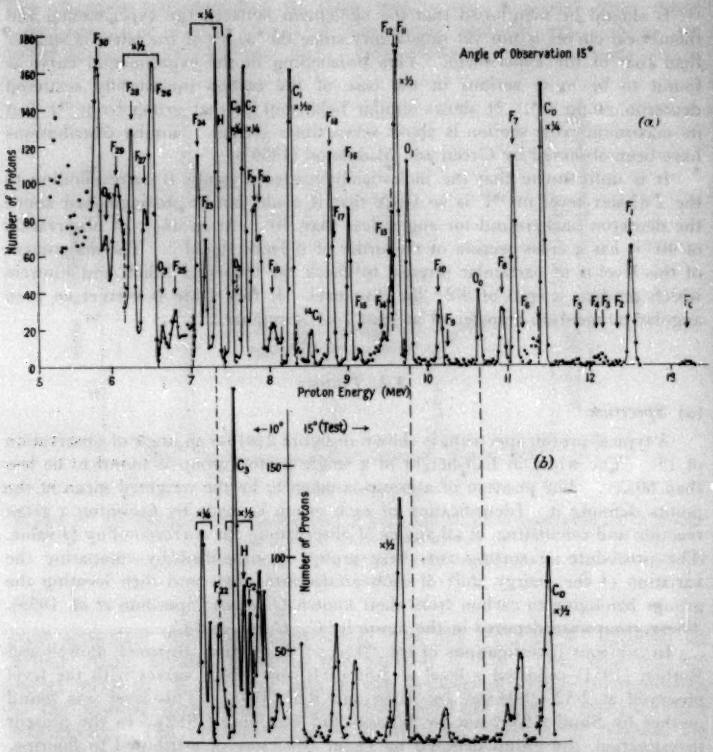

Figure 2. Spectrum of proton groups from the deuteron bombardment of teflon.

the positions of which are derived from their known Q-values (Ajzenberg and Lauritsen 1955).

Within the energy region of the present work, two more groups are found belonging to different reactions. The group at 8·52 MeV denoted by $^{14}C_1$ is attributed to the $^{13}C(d, p)^{14}C$ reaction leaving the residual nucleus in its first excited state. The mean Q-value is found to be $-0{\cdot}15 \pm 0{\cdot}02$ MeV which agrees well with the value $-0{\cdot}149 \pm 0{\cdot}007$ MeV reported by Sperduto *et al.* (1954). The other group, denoted by H, at an energy of 7·35 MeV, is attributed, from its considerable energy shift with angle, to some hydrogen contamination in the target. This elastically scattered proton group has been observed in all the targets investigated so far with the present arrangement.

With regard to the proton groups emitted from the $^{19}F(d, p)^{20}F$ reaction thirty energy levels have been observed. The well-separated group at 13·19 MeV is due to the ground state of ^{20}F and the mean Q-value of the reaction is calculated as $4{\cdot}38 \pm 0{\cdot}03$ MeV which is in good agreement with the value $4{\cdot}373 \pm 0{\cdot}007$ MeV

reported by Watson and Buechner (1952). It is found that the position of the group F_1 (0·652 MeV level) could be more accurately estimated at all angles of observation than that of F_0. The energy levels are thus calculated with respect to F_1 and then increased by 0·65 MeV. The position of the arrows shown at F_1, F_2, ..., F_{18} are derived from the results of Watson and Buechner and they are found to agree well with the intense groups observed in the present work. The group at 9·59 MeV corresponds to a level of mean energy of $3{\cdot}51 \pm 0{\cdot}02$ MeV which is intermediate between F_{11} (3·491 MeV) and F_{12} (3·528 MeV). The symmetrical shape of this group suggests that if it is in fact a doublet both components have about the same intensity.

Watson and Buechner (1952) reported also an uncertain level of energy $5{\cdot}062 \pm 0{\cdot}011$ MeV which corresponds to the group F_{19}. The associated level has an energy of $5{\cdot}04 \pm 0{\cdot}02$ MeV. The groups denoted by F_{20}, F_{21}, ..., F_{30} were outside the range of Watson and Buechner's measurements. The corresponding excited states in ^{20}F are at 5·19, 5·27, 5·72, 5·87, 5·95, 6·25, 6·52, 6·63, 6·81, 6·98 and 7·20 MeV with errors of $\pm 0{\cdot}02$ MeV. The group denoted by F_{22} is obscured by the elastically scattered proton group in the presented spectrum. It is observed at other angles and its position at an angle of observation of 10° is shown in figure 2 (*b*). Above an excitation energy of 6·63 MeV the following levels are reported from the ^{19}F(n, n)^{19}F reaction (Ajzenberg and Lauritsen 1955): 6·63, 6·65, 6·70, 6·86, 6·92, 7·00, 7·08 and 7·17 MeV. Some of these levels probably correspond to those observed in the present work. It is probable that some groups in this region could not be observed due to their low intensity.

(*b*) *Angular distributions.*

The reaction ^{12}C(d, p)^{13}C. The angular momenta of the captured neutron for the transitions to the ground state and the three low-lying levels in ^{13}C nucleus have been determined by Rotblat (1951 a, b) and the corresponding level configurations are discussed by Holt and Marsham (1953). During the course of the present investigation, angular distribution measurements on these four groups lead to similar results. The reduced width θ^2 for each level is calculated and the results are given in table 1. It is of interest to compare the reduced widths of the single-particle levels in ^{13}C with the values calculated, in the present work, for levels in ^{14}C and ^{20}F.

Table 1

Energy level (MeV)	γ^2 (10^{-13} MeV cm)	θ^2(%)	Configuration
0	0·8	7	$1\,p_{1/2}$
3·090	2·4	21	$2\,s_{1/2}$
3·684	0·3	2	
3·855	1·6	14	$1\,d_{5/2}$

The reaction ^{13}C(d, p)^{14}C. The angular distribution of protons associated with the transition to the 6·091 MeV state in ^{14}C nucleus had been measured by Benson (1953) using 3·89 MeV deuterons to bombard an enriched carbon target. His experimental resolution was inadequate to separate this group from the protons associated with the first excited state in ^{13}C which is known to have $l_n = 0$.

However, Benson suggested a value $l_n=0$ for the level in ^{14}C. The angular distribution of this proton group determined in the present work is represented in figure 3. The Butler theoretical curve which gives the best fit has $l_n=0$ and $r_0=4{\cdot}6\times10^{-13}$ cm.

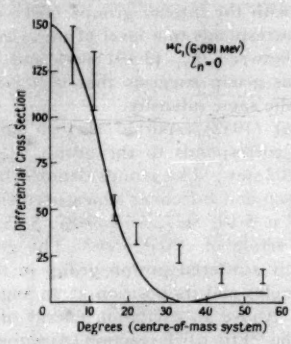

Figure 3.

Since the ground state of ^{13}C is known to have $J=\frac{1}{2}$ and odd parity, the 6·091 Mev state in ^{14}C must have odd parity and spin 0 or 1. The γ-ray transition which has been observed from this state to the ground state (Thomas and Lauritsen 1952) excludes spin 0 and accordingly this state must have $J=1^-$. This assignment is of interest for a comparison between levels of the same isotopic spin $T=1$. The analogous level in ^{14}N is known to be at 8·06 Mev, and according to Milne (1954) it has $J=1^-$.

To calculate the reduced width, the differential cross section has been converted to absolute units by making use of the isotopic abundance ratio 98·9 : 1·1 for ^{12}C and ^{13}C and the known cross sections for $^{12}C(d, p)^{13}C$ reaction. A multiplication factor 1·52 mbn sterad^{-1} is used. The maximum cross section is thus found to be 0·23 bn sterad^{-1} at an angle 0°. The reduced width θ^2 is 32% of the sum rule limit which is much higher than those corresponding to single particle levels in ^{13}C nucleus.

On the basis of the shell model, the ground state configuration of ^{13}C is known to be $1p_{1/2}$. The deuteron stripping reaction on ^{13}C shows that the l_n value for the ground state of ^{14}C is equal to 1 (Benson 1953, Koudijs, Valckx and Endt 1953). This state is known to have $J=0^+$ and its configuration is probably $(1p_{1/2})^2$. The fact that $l_n=0$ for the first excited state shows that the $2s_{1/2}$ level is lower in ^{14}C than the $1d_{5/2}$ shell. A possible configuration for this state is $(1p_{1/2})^1(2s_{1/2})^1$ coupled together to give spin 1. This configuration can also lead to spin 0 which suggests the existence of a neighbouring state having that spin.

The reaction $^{19}F(d, p)^{20}F$. The angular distributions of 21 proton groups associated with the transition to various excited states in the ^{20}F nucleus in the centre-of-mass system are shown in figure 4. The experimental errors are the statistical standard deviations. The theoretical curves are calculated from

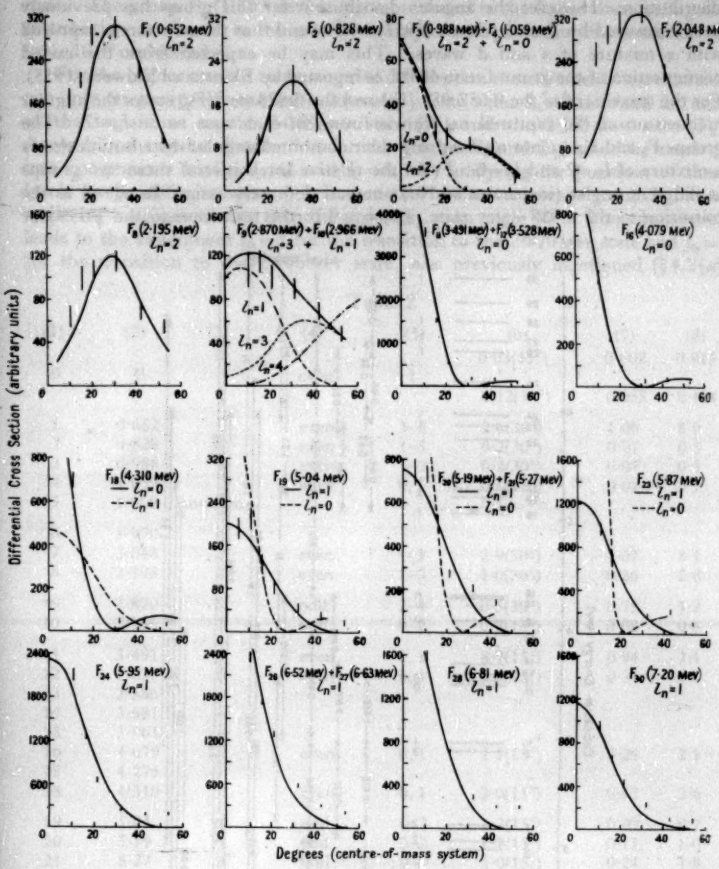
F1 (0·652 MeV) ln=2
F2 (0·828 MeV) ln=2
F3 (0·988 MeV)+F4 (1·059 MeV) ln=2 + ln=0
F7 (2·048 MeV) ln=2
F8 (2·195 MeV) ln=2
F9 (2·870 MeV)+F10 (2·966 MeV) ln=3 + ln=1
F11 (3·431 MeV)+F12 (3·528 MeV) ln=0
F16 (4·079 MeV) ln=0
F18 (4·310 MeV) ln=0 ln=1
F19 (5·04 MeV) ln=1 ln=0
F20 (5·19 MeV)+F21 (5·27 MeV) ln=1 ln=0
F23 (5·87 MeV) ln=1 ln=0
F24 (5·95 MeV) ln=1
F26 (6·52 MeV)+F27 (6·63 MeV) ln=1
F28 (6·81 MeV) ln=1
F30 (7·20 MeV) ln=1
Differential Cross Section (arbitrary units)
Degrees (centre-of-mass system)

Figure 4.

Butler's formula (1951) using a radius of interaction of $5{\cdot}01 \times 10^{-13}$ cm and the value of the angular momentum l_n transferred by the captured neutron is chosen to give the best fit. The results are consistent with those derived from the Born approximation stripping theory (Bhatia, Huang, Huby and Newns 1952) using a radius of about $6{\cdot}0 \times 10^{-13}$ cm.

With regard to the low-lying levels F_0, F_2, $F_3 \ldots F_5$ the proton intensity is quite low and measurement was carried out for all the tracks in the whole width of the plate and then normalized to the same scale. The relative intensities of the ground state group F_0 are not adequate to establish a definite shape for the

distribution. However the angular distribution for this group has previously been measured by Bromley *et al.* (1953) who found that the neutron is captured with a mixture of s and d waves. This may be expected from the mixed configuration of the ground state of ^{19}F as reported by Elliott and Flowers (1955). For the transitions to the 0·652 Mev (F_1) and the 0·828 Mev (F_2) states the angular momentum of the captured neutron is found in each case to be $l_n=2$. The groups F_3 and F_4 are not resolved and their combined angular distribution shows a mixture of $l_n=2$ and $l_n=0$. From the relative intensities of these two groups at different angles (in particular 10°) one can definitely assign the $l_n=2$ to the transition to the 0·988 = Mev state, and $l_n=0$ to the transition to the 1·059 Mev

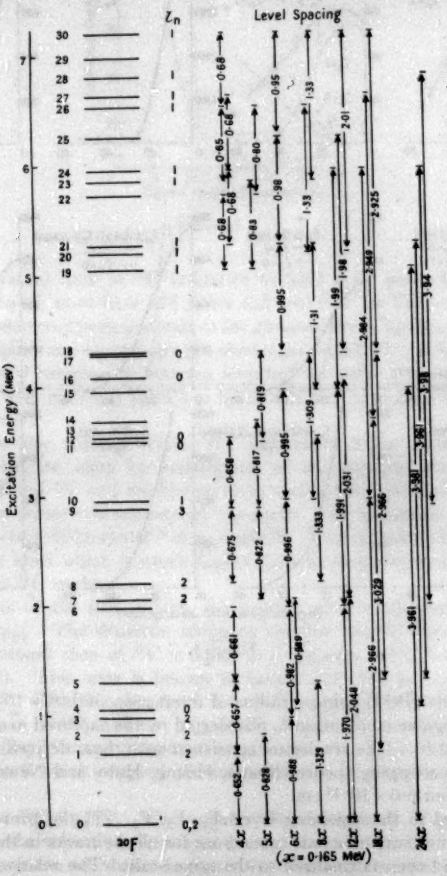

Figure 5. Energy level diagram for ^{20}F.

state. The group F_5 (1·309 MeV) is not represented in the figure since its angular distribution is found to be nearly isotropic with a mean cross section of $0{\cdot}9 \times 10^{-28}$ cm^2 sterad^{-1}.

For the higher excited states angular distribution measurements were carried out only on groups of reasonable intensity. The value $l_n = 2$ is found for each of the transitions to the 2·048 MeV state (F_7) and the 2·195 MeV state (F_8). A combined angular distribution for the groups F_9 and F_{10} could be resolved into components having $l_n = 1$ and $l_n = 3$. By analysing the positions of these levels in the different spectra, it is seen that the more intense group F_{10} at an angle 15° becomes weaker than the group F_9 at an angle 40°. This observation leads to the assignment $l_n = 3$ for the transition to the 2·870 MeV state and $l_n = 1$ for the transition to the 2·966 MeV state. As previously mentioned (§ 4.2(*a*))

Table 2

(1)	(2)	(3)	(4)	(5)	(6)	(7)	(8)
		0			0·03(15°)	0·002	0·015
0	0		even	1			
		2			0·12(30°)	0·055	0·414
1	0·652	2	even	1–3	2·6(30°)	1·06	8·0
2	0·828	2	even	1–3	0·2(30°)	0·07	0·5
3	0·988	2	even	1–3	0·2(30°)	0·07	0·5
4	1·059	0	even	0, 1	0·4(15°)	0·02	0·1
5	1·309	isotropic			0·1		
6	1·970	–					
7	2·048	2	even	1–3	2·9(30°)	1·07	8·1
8	2·195	2	even	1–3	1·0(30°)	0·36	2·8
9	2·870	3	odd	2–4	0·5(30°)	0·75	5·7
10	2·966	1	odd	0–2	0·9(15°)	0·08	0·6
11	3·491	0	even	0, 1	8·9(15°)	0·94	7·1
12	3·528	0	even	0, 1	8·9(15°)	0·94	7·1
13	3·586	–					
14	3·681	–					
15	3·961	–					
16	4·079	0	even	0, 1	2·1(15°)	0·28	2·1
17	4·275	–					
18	4·310	0	even	0, 1	3·0(15°)	0·47	3·6
19	5·04	1	odd	0–2	1·2(15°)	0·09	0·7
20	5·19	1	odd	0–2	1·7(15°)	0·13	1·0
21	5·27	1	odd	0–2	3·0(15°)	0·24	1·8
22	5·72	–					
23	5·87	1	odd	0–2	6·8(15°)	0·58	4·4
24	5·95	1	odd	0–2	13·6(15°)	1·2	9
25	6·25	–					
26	6·52	1	odd	0–2	11·5(15°)	1·2	9
27	6·63	1	odd	0–2	5·5(15°)	0·6	5
28	6·81	1	odd	0–2	10·2(15°)	1·0	7
29	6·98	–					
30	7·20	1	odd	0–2	5·9(15°)	0·5	4

(1) Group number ; (2) excitation energy (MeV) ; (3) l_n–value ; (4) parity ; (5) possible spins of the final nucleus J_f ; (6) absolute cross sections (mbn sterad^{-1}) at the angle shown ; (7) reduced width $\gamma^2(2J_f+1)$ in units of 10^{-13} MeV cm ; (8) reduced width $\theta^2(2J_f+1)$ in percentage of the sum rule limit.

the unresolved groups F_{11}(3·491 MeV) and F_{12}(3·528 MeV) may have nearly equal intensities characterized in both cases by $l_n=0$. Each of the transitions to the 4·079 MeV (F_{16}) and 4·310 MeV (F_{18}) states has $l_n=0$. A p-wave neutron capture is found for each of the remaining states. This applies as well to each component of the combined angular distributions of the groups $F_{20}+F_{21}$ and $F_{26}+F_{27}$ since the relative intensity shown by the shape of their spectra is the same for all angles of observation.

4.3. *Nuclear Structure of* ^{20}F

The application of a magnetic analyser to the study of deuteron stripping reactions is proved to be a powerful technique in nuclear spectroscopy. In addition to reliable identification of energy levels in the residual nuclei, the use of the stripping theories can fix the parity, limit the spin and give information about the level capture probability or reduced width.

An energy level diagram for the ^{20}F nucleus is shown in figure 5 and the results concerning these levels are summarized in table 2. From an analysis of the level structure of this nucleus one can point out the following striking features:

1. *Level spacing.* Seven sets of nearly equal level spacings are shown beside the energy diagram. The energy separation of each set has a mean value equal to an integral multiple of $x=0·165$ MeV. These integers are 4, 5, 6, 8, 12, 18 and 24. It is rather surprising that starting from the ground state, levels corresponding to these sets are observed.

2. *Parity.* Above an excitation energy of about 5 MeV only odd parity levels are observed. Below this excitation even parities predominate. The only two odd parity levels in this region appear at about 2·9 MeV.

3. *Group nature.* The levels are found to appear in groups of the same parity separated from each other by an energy of about 0·6 MeV ($\sim 4x$). It is interesting to note that each group contains a low-lying level of relatively high reduced width.

Acknowledgments

The author is grateful to Professor H. W. B. Skinner for his encouragement and advice and to Dr. R. Huby and Dr. H. C. Newns for information regarding the theories of the stripping process. Thanks are also due to Dr. J. R. Holt, Dr. R. Middleton, Mr. T. Green and Mr. S. Hinds for their willing assistance and helpful discussions.

References

Ajzenberg, F., and Lauritsen, T., 1955, *Rev. Mod. Phys.*, **27**, 77.
Allen, R. C., and Rall, W. R., 1951, *Phys. Rev.*, **81**, 60.
Arthur, J. C., Allen, A. J., Bender, R. S., Hausman, H. J., and McDole, C. J., 1952, *Phys. Rev.*, **88**, 1291.
Benson, R. E., 1953, *Phys. Rev.*, **90**, 420.
Bhatia, A. B., Huang, K., Huby, R., and Newns, H. C., 1952, *Phil. Mag.*, **43**, 485.
Black, C. F., 1953, *Phys. Rev.*, **90**, 381 A.
Bromley, D. A., Bruner, J., and Fulbright, H. W., 1953, *Phys. Rev.*, **89**, 396.
Bullock, M. L., and Sampson, M. B., 1951, *Phys. Rev.*, **84**, 967.
Burrows, H. B., Gibson, W. M., and Rotblat, J., 1950, *Phys. Rev.*, **80**, 1095.
Burrows, H. B., Powell, C. F., and Rotblat, J., 1951, *Proc. Roy. Soc.* A, **209**, 478.
Butler, S. T., 1951, *Proc. Roy. Soc.* A, **208**, 559.
El Bedewi, F. A., 1951, *Proc. Phys. Soc.* A, **64**, 1079.
Elliott, J. P., and Flowers, B. H., 1955, *Proc. Roy. Soc.* A, **536**, 229.

GREEN, T., and MIDDLETON, R., 1956 a, *Proc. Phys. Soc.* A, **69**, 16; 1956 b, *Ibid.*, **69**, 28.
HOLT, J. R., and MARSHAM, T. N., 1953, *Proc. Phys. Soc.* A, **66**, 1032.
HUBY, R., 1953, *Progr. Nucl. Phys.*, **3**, 177.
HUBY, R., and NEWNS, H. C., 1951, *Phil. Mag.*, **42**, 1442.
JONES, G. A., PHILLIPS, W. R., JOHNSON, C. M. P., and WILKINSON, D. H., 1954, *Phys. Rev.*, **96**, 547.
KOUDIJS, B., VALCKX, F. P. G., and ENDT, P. M., 1953, *Physica*, **19**, 1133.
MILNE, E. A., 1954, *Phys. Rev.*, **93**, 762.
ROTBLAT, J., 1951 a, *Nature, Lond.*, **167**, 1027; 1951 b, *Phys. Rev.*, **83**, 1271.
SEALE, R. L., 1953, *Phys. Rev.*, **92**, 389.
SHULL, F. B., 1951, *Phys. Rev.*, **83**, 875 A.
SPERDUTO, A., BUECHNER, W. W., BOCKELMAN, C. K., and BROWNE, C. P., 1954, *Phys. Rev.*, **96**, 1316.
TEICHMANN, T., and WIGNER, E. P., 1952, *Phys. Rev.*, **87**, 123.
THOMAS, R. G., and LAURITSEN, T., 1952, *Phys. Rev.*, **88**, 969.
WATSON, H. A., and BUECHNER, W. W., 1952, *Phys. Rev.*, **88**, 1324.

The Band Structure of Mixed Linear Lattices†

By E. H. KERNER
Physics Department, University of Buffalo, New York

MS. received 11*th July* 1955, *and in amended form* 24*th October* 1955

Abstract. A reformulation of Saxon and Hutner's scattering matrix method for lattices is introduced, and a connection shown between the characteristic matrix for going across a cell in the lattice and proper Lorentz transformations. This provides a convenient geometrical model for analysing mixed lattices of A and B atoms. Luttinger's proof of a theorem on the persistence of forbiddenness, in the mixed lattice, of energies forbidden in the pure component lattices is generalized. It is shown also that there are energy levels in mixed lattices whose forbidden or allowed character is invariant to any re-arrangement of lattice atoms, and that there are physically distinguishable lattices having identical band structures. The major problem of finding the probability that a given energy is allowed or forbidden in a random mixed lattice is taken up. A method for finding the moments of the relevant random variable is provided, and the complete analysis for the Poisson limit of a few B atoms sprinkled in a long A lattice is given, with quantitative conclusions as to the persistence of allowedness in mixed lattices, the effect of strong forbiddenness in the pure B lattice on the band structure of the mixed lattice, and the like.

§ 1. Introduction

The problem of deducing the band structure of linear mixed lattices, in which groups of different species of atoms are connected in a chain of greater or lesser complexity, has been approached in a practical way by James and Ginzbarg (1953) and by Landauer and Helland (1954). The question as to what properties of a mixed lattice can be inferred from a knowledge of the separate band structures of pure lattices has been answered to some extent by a theorem of Saxon and Hutner (1949) and Luttinger (1951). This states that the common forbidden energies of two pure delta-function lattices A and B remain forbidden in any mixture of A and B. As has recently been shown (Kerner 1954), the theorem is peculiar to delta-functions and fails in less special cases. Luttinger's proof really contains a general criterion ($\kappa > 0$ in his notation, which is always satisfied for delta functions) for the persistence of forbiddenness in the mixed lattice, but the restriction to symmetrical cells for A and B leaves something to be desired.

The basic question, raised so clearly by Saxon and Hutner, as to what is the probability that a given energy is allowed or forbidden in a random mixed lattice, has remained largely unanswered.

One of our principal aims here is to answer this question. After preliminaries, we shall show how to calculate the moments of the relevant stochastic variable describing a random lattice, and in the particular case of a sprinkling of a few

† A summary of the main results of this report was presented at the Toronto meeting of the American Physical Society, June 23, 1955.

B atoms in an otherwise pure A lattice shall find explicitly the probability that a given energy is allowed. One result of the latter calculation suggests another side to the Saxon–Hutner theorem, namely, that under some conditions a common allowed energy of A and B lattices remains allowed in any mixed lattice.

We begin with a reformulation of Saxon–Hutner's scattering matrix method that brings out its connection with more familiar methods of analysis, and that offers a useful geometric model for describing mixed lattices. In practical applications this can provide a perhaps simpler alternative to the node-counting or phase-advance techniques heretofore employed. Luttinger's result will be somewhat broadened, and we shall show that whole blocs of atoms may sometimes be interchanged in a mixed lattice without affecting its band structure, i.e. that there are physically distinguishable lattices that yet are equivalent electronically. This conclusion is foreshadowed by Landauer's numerical analysis, but is much less general than the result found by Landauer. It will also be pointed out that there are circumstances, rather special, in which certain energies (either forbidden or allowed) in a mixed lattice are invariant in position and character under any rearrangement whatever of atoms in the lattice.

§ 2. General Lattices

For lattices of square wells, matrices of the form

$$H=\begin{pmatrix} F & G^* \\ G & F^* \end{pmatrix}, \quad |H|=1 \qquad \ldots\ldots(1)$$

were exhibited earlier (Kerner 1954) which give the connection between linear combinations of independent solutions of the wave equation at the ends of the cell that is repeated indefinitely in the lattice. These H-matrices, fundamental to the discussion of the band structure, will be seen later to form a group, isomorphic to the group of Lorentz transformations in two space and one time dimensions, much as the group of 2×2 unitary matrices in the Cayley–Klein parameters is isomorphic to the group of ordinary space rotations. It is of interest to bring out the basic role of H-matrices for any kind of lattice before going on to mixed lattices.

In the wave equation for the motion of an electron in the periodic potential $V(x)$, having the period b, let the zero of energy be selected sufficiently low that only energies E greater than zero need be considered, all energies less than zero being forbidden. When we introduce a small interval of zero potential of width a (later to vanish) between the cells of size b we may represent the wave function ψ in $(0, a)$ as a superposition of right- and left-going plane waves with amplitudes, say, a_0 and b_0. In $(a, a+b)$, ψ is a superposition of any real linearly independent solutions u_1, u_2 of Schrödinger's equation for the potential V, $\psi=a_1u_1+b_1u_2$; the Wronskian $W=u_1u_2'-u_1'u_2$ is different from zero. Again, in $(a+b, 2a+b)$, ψ is specified by plane wave amplitudes a_2, b_2. Using

$$A_i=\begin{pmatrix} a_i \\ b_i \end{pmatrix}$$

the matching of ψ and ψ' at a and $a+b$ may be summarized by writing $A_1=T_1A_0$, $A_2=T_2A_1$, $A_2=(T_2T_1)A_0=fA_0$, with T-matrices similar to those used earlier, but containing the u's and their derivatives rather than just exponential functions. Since ψ is to be of the Floquet form, $\phi\exp(ikx)$, with periodic ϕ of period $c\equiv b+a$, we must also have $A_2=S(c)\exp(ikc)A_0$, S being the diagonal matrix with elements

$\exp(\mp ikc)$, ϵ being $(2mE/\hbar^2)^{1/2}$. That is, calling H the matrix $S^{-1}f$, we require $HA_0 = \exp(ikc)A_0$, from which a non-trivial A_0 exists only when (I being the unit matrix)

$$|H - \exp(ikc)I| = 0 = |H| - \exp(ikc)\,\mathrm{Tr}\,H + \exp(2ikc). \quad \ldots\ldots(2)$$

The calculation of H gives, upon letting a tend to zero, the form in equation (1) with

$$\left.\begin{aligned} F &= \frac{1}{2W}\left\{\begin{vmatrix} u_{1b} & u_{2b} \\ u_{10}' & u_{20}' \end{vmatrix} + \begin{vmatrix} u_{10} & u_{20} \\ u_{1b}' & u_{2b}' \end{vmatrix} + i\left(\epsilon\begin{vmatrix} u_{10} & u_{20} \\ u_{1b} & u_{2b} \end{vmatrix} + \frac{1}{\epsilon}\begin{vmatrix} u_{10}' & u_{20}' \\ u_{1b}' & u_{2b}' \end{vmatrix}\right)\right\} \\ G &= \frac{1}{2W}\left\{\begin{vmatrix} u_{1b} & u_{2b} \\ u_{10}' & u_{20}' \end{vmatrix} - \begin{vmatrix} u_{10} & u_{20} \\ u_{1b}' & u_{2b}' \end{vmatrix} + i\left(\epsilon\begin{vmatrix} u_{10} & u_{20} \\ u_{1b} & u_{2b} \end{vmatrix} - \frac{1}{\epsilon}\begin{vmatrix} u_{10}' & u_{20}' \\ u_{1b}' & u_{2b}' \end{vmatrix}\right)\right\} \end{aligned}\right\} \quad .(3)$$

Also, $|H| = 1$ by direct computation, so that the characteristic equation (2) for the energy becomes $\cos kb = \frac{1}{2}\,\mathrm{Tr}\,H = \mathscr{R}F$, the well-known result of Kramers (1935). The values of F and G and the form of H are of course independent of the choice of basic solutions u_1, u_2.

What we have in effect done above by using the artifice of regions of zero potential is, as will be evident from Saxon and Hutner's work, to calculate reflection and transmission coefficients for a cell in terms of any linearly independent solutions of the wave equation for the cell. This serves to connect the scattering-matrix viewpoint with the more conventional techniques (James 1949, Kramers 1935); and it provides a means for computing practically the matrix elements of H (which has the same form for any sort of cell) in particular cases.

The H-matrices have some properties akin to the Cayley–Klein unitary matrices. That they form a group will be evident after a moment's inspection. Under a similarity transformation with $H(F, G)$ as transformation matrix, matrices of the type $H(it, x+iy)$ are form invariant, $H(it, x+iy) \rightarrow H(it', x'+iy')$, and have an invariant determinant, $t^2 - x^2 - y^2 = t'^2 - x'^2 - y'^2$. The H-matrices indeed are isomorphic to (x, y, t) Lorentz transformations (L3 transformations). This is a special case of van der Waerden's (1944) representation of proper Lorentz transformations as linear groups.

The connections between x', y', t' and x, y, t when written out in terms of F and G and then in the usual way for L3 transformations (Møller 1952) provide the identification

$$F = \cosh\tfrac{1}{2}\psi \exp(\tfrac{1}{2}i\theta), \qquad G = i\sinh\tfrac{1}{2}\psi \exp\{i(\phi - \tfrac{1}{2}\theta)\},$$

where ψ, ϕ, θ are the parameters of L3 given by $\cosh\psi = (1-v^2)^{-1/2}$, $v_x = v\cos\phi$, with $c = 1$ and θ the angle of the purely spatial rotation of x, y axes with respect to x', y' axes. This representation of F and G by means of the Lorentz parameters allows a description of the electron motion in terms of the relative motion of coplanar sets of cartesian axes; the electron motions are allowed or forbidden according as $|\cosh\tfrac{1}{2}\psi\cos\tfrac{1}{2}\theta|$ is less or greater than 1, i.e. according as the relative motion of axes is, roughly speaking, a low or high velocity motion of parallel axes, or a high or low velocity motion with axes anti-parallel. In short, we have a sort of physical isomorphism between the actual electronic motions and the rectilinear motions of coordinate frames in special relativity theory.

Any $H(\psi, \theta, \phi)$ can be decomposed into

$$H = R(\theta)R(-\phi)L_0(\psi)R(\phi) \equiv R(\theta)L(\phi, \psi), \quad \ldots\ldots(4)$$

with

$$R(\lambda)=\begin{pmatrix}\exp(-\frac{1}{2}i\lambda) & 0\\ 0 & \exp(\frac{1}{2}i\lambda)\end{pmatrix},\qquad L_0(\psi)=\begin{pmatrix}\cosh\frac{1}{2}\psi & -i\sinh\frac{1}{2}\psi\\ i\sinh\frac{1}{2}\psi & \cosh\frac{1}{2}\psi\end{pmatrix}.$$

Here $R(\theta)$ represents the purely rotational part of H, and L represents a pure Lorentz transformation. Under the similarity transformation $PHP^{-1}=\bar{H}$ with $P_{22}=i/2^{1/2}=-P_{11}$, $P_{21}=1/2^{1/2}=-P_{12}$, which diagonalizes L_0 and which leaves $\mathrm{Tr}\,H$ unchanged, any rotational factor $R(\lambda)$ in H goes into a real planar rotation $\bar{R}_{11}=\bar{R}_{22}=\cos\frac{1}{2}\lambda$, $\bar{R}_{12}=-\bar{R}_{21}=\sin\frac{1}{2}\lambda$, while L_0 goes into a real distortion $\bar{L}_{011}=\exp(\frac{1}{2}\psi)$, $\bar{L}_{022}=\exp(-\frac{1}{2}\psi)$, $\bar{L}_{012}=\bar{L}_{021}=0$, which stretches the X-component of a vector X, Y and shrinks the Y-component by the same factor. This further isomorphism of H with products of simple rotations and distortions in a plane is without particular significance for a pure lattice but is of some interest in providing a geometrical model for studying mixed lattices.

§ 3. Mixed Lattices

Consider first an arbitrary binary lattice of the form $\ldots[(n_1\mathrm{A})(n_2\mathrm{B})\ldots(n_k\mathrm{B})]\ldots$ in which n_1 A-cells of width b_1 are followed by n_2 B-cells of width b_2, etc., and then the whole configuration is repeated indefinitely. Following the earlier procedure and sandwiching small intervals a of zero potential between all cells, we can find the connection between the vectors A_l and A_r at the field-free regions to the left and right of any atom in the form (when $a\to 0$) $A_r=g(F_j,G_j,\alpha)A_l$, where j is A or B for an A or B atom and α is the distance of the right end of the atom from the beginning of the chain. The A-vectors at the beginnings of the second and first $n_1\mathrm{A}\ldots n_k\mathrm{B}$ chains are then connected by a product M of g-matrices, one for each atom in the first chain. Through use of the property that $g(\alpha+x)=S(x)g(\alpha)S^{-1}(x)$, S being the diagonal matrix introduced before, one may show that

$$M=S(l)S(b_0)H_{\mathrm{B}}{}^{n_k}S^{-1}(b_0)H_{\mathrm{A}}{}^{n_{k-1}}\ldots S(b_0)H_{\mathrm{B}}{}^{n_2}S^{-1}(b_0)H_{\mathrm{A}}{}^{n_1},$$

with $b_0=\frac{1}{2}(b_2-b_1)$ and l the total chain length. Now the periodicity condition $\phi(x+l)=\phi(x)$ gives, in the same way as for equation (2), the eigenvalue equation

$$\cos kl=\tfrac{1}{2}\,\mathrm{Tr}\,S(b_0)B^{n_k}\ldots S(b_0)B^{n_2}S(-b_0)A^{n_1}\equiv\tfrac{1}{2}\,\mathrm{Tr}\,H_l\equiv\tfrac{1}{2}Z,\quad\ldots\ldots(5)$$

in which the characteristic pure-lattice H-matrices are specified always by equations (1) and (3). Here and in what follows we change the names of $H_{\mathrm{A}}, H_{\mathrm{B}}$ to A, B.

The effect of having different sizes for A and B cells is only to introduce extra 'rotations' $S(b_0)$ or $S(-b_0)$ at the junctions of neighbouring groups of A's and B's. In the general case of a mixed lattice of many different species of atoms having arbitrary cell lengths, H_l will always be a sequence of H-matrices similar in form to the atomic sequence, with appropriate junction rotations separating the H-groups. The junction rotations may be incorporated, using equation (4), into the ϕ parts of A or B: this does not affect $\mathrm{Tr}\,A$ or $\mathrm{Tr}\,B$. We may therefore omit the junction rotations with impunity.

To reduce any H^n to a simpler form, the similarity transformation W used earlier (Kerner 1954) which diagonalizes H is useful. The result is

$$H^n=\frac{\sin n\beta}{\sin\beta}H-\frac{\sin(n-1)\beta}{\sin\beta}I\qquad\ldots\ldots(6)$$

$$\cos\beta\equiv\tfrac{1}{2}\,\mathrm{Tr}\,H=\mathscr{H}F.$$

The representation of H in terms of the parameters of L3 may be used, though clumsily, to reduce H_l. First, all the rotations in H_l may be brought together, using the inversion rule $R(\theta)L(\phi,\psi)=L(\phi-\theta,\psi)R(\theta)$, so that H_l is put in the form of a product of a rotation and a chain of pure L-matrices (pure Lorentz transformations). Grouping the latter in pairs, each pair may then be written as a rotation times a pure Lorentz transformation using the well-known rule for combining two such transformations. Then the rotations can be brought together again and the process repeated until H_l is represented as a pure single rotation followed by a pure single Lorentz transformation.

A much more convenient scheme, affording a simple geometrical or mechanical model for finding $\mathrm{Tr}\,H_l$, is to carry out a similarity transformation of H_l with the transformation P. If we take two vectors $(1,0)$ and $(0,1)$ and allow H_l to transform them in a succession of rotations and deformations we shall have always

$$\mathrm{Tr}\,\dot{H}_l=\mathrm{Tr}\,H_l=\left[\dot{H}_l\begin{pmatrix}1\\0\end{pmatrix}\right]_X+\left[\dot{H}_l\begin{pmatrix}0\\1\end{pmatrix}\right]_Y.$$

A ruler and compass suffice for conducting the sequence of operations in $\dot{H}_l$. This motion of two points in the plane allows a description of a random lattice in terms of a pair of random walks, with the novel characteristic that the different permissible steps in the walks are non-commutative.

We examine now some properties of H_l without explicitly evaluating this matrix.

First, it is worth noticing that for a binary lattice H_l is insensible to the ordering of the sequence when, and only when, A and B commute (Kerner and Logan 1955). In this case, n_A and n_B being the total numbers of A and B atoms, the diatomic lattice $\ldots(n_A A)(n_B B)\ldots$, which is relatively easy to investigate, is a sort of fundamental mixed lattice from which some properties of the disordered lattice may be found. The commutability of A and B requires that $G_A{}^*G_B=G_AG_B{}^*$, $G_A\mathscr{I}F_B=G_B\mathscr{I}F_A$. For square-wells of potential height V_1, potential width w, and separation s between wells, we have

$$F=\exp(i\epsilon s)\left(\cosh\epsilon_1 w-i\frac{\epsilon_1{}^2-\epsilon^2}{2\epsilon_1\epsilon}\sinh\epsilon_1 w\right),$$

$$G=i\frac{\epsilon_1{}^2+\epsilon^2}{2\epsilon_1\epsilon}\sinh\epsilon_1 w\exp(i\epsilon s),\quad \epsilon_1\equiv(V_1-E)^{1/2},\quad \frac{2m}{\hbar^2}=1,$$

and these conditions read for example

$$\sin\epsilon(s_1-s_2)=0$$

$$\frac{V_1}{\epsilon_1}\cos\epsilon(s_1-s_2)\left(\sin\epsilon s_2\coth\epsilon_2 w_2-\frac{\epsilon_2{}^2-\epsilon^2}{2\epsilon_2\epsilon}\cos\epsilon s_2\right)$$
$$=\frac{V_2}{\epsilon_2}\left(\sin\epsilon s_1\coth\epsilon_1 w_1-\frac{\epsilon_1{}^2-\epsilon^2}{2\epsilon_1\epsilon}\cos\epsilon s_1\right).$$

For energy levels E satisfying these conditions for prescribed well parameters (or for well parameters satisfying these conditions for prescribed E), the value of $\mathrm{Tr}\,H_l$ may be determined from that for the fundamental diatomic lattice, and the levels classified as 'super-forbidden' or 'super-allowed' in view of the invariance of their character to the ordering of the sequence. The existence or non-existence of such super-*levels* would seem to imply the existence or non-existence of super-*bands* surrounding them which persist with greater or smaller width no matter how the lattice is arranged.

A simple special case that illuminates this result is that for which the commutability of A and B is assured through $G_A = 0 = G_B$ or, for square wells, $\sinh \epsilon_1 w_1/\epsilon_1 = 0 = \sinh \epsilon_2 w_2/\epsilon_2$. These can be satisfied only if E is greater than V_1 and V_2, when they may be written $E = V_1 + (N_1\pi/w_1)^2$, $E = V_2 + (N_2\pi/w_2)^2$, N_1 and N_2 being integers different from zero. All these levels are allowed levels for pure A and pure B lattices, and for appropriate well parameters some will be common allowed levels of the lattices. Such levels are also super-allowed, as a computation of H_l shows.

Next, we restate the Saxon–Hutner–Luttinger theorem without restrictions on the A and B atoms.

Since only the magnitude, and not the sign, of $\cos\beta = \frac{1}{2}\operatorname{Tr} H$ controls whether an energy is allowed or forbidden in a lattice, we may restrict β to the principal values $0 \leqslant \beta \leqslant \frac{1}{2}\pi$ for an allowed energy and $\beta = iv$ (v real) for a forbidden energy; this entails at most a change in sign of Z in equation (5) when, to conform to the use of principal values for β, we must replace an H-matrix by its negative.

In equation (6), because of the way n enters into the expanded form of H^n we may consider n to be continuously variable. Moreover, it is clear that Z is an analytic function of its arguments. Let us examine the Maclaurin expansion of Z. Using $H^{-1} = 2\cos\beta - H$, it is easy to show that H^n may also be written in the form, similar to that introduced by Luttinger (1951),

$$H^n = \cos n\beta + Ui \sin n\beta = \exp(in\beta U)$$

$$U \equiv \frac{H - H^{-1}}{2i\sin\beta} \equiv \frac{1}{i\sin\beta}\begin{pmatrix} i\mathscr{I}F & G^* \\ G & -i\mathscr{I}F \end{pmatrix}, \qquad \ldots\ldots(7)$$

where the fact that $U^2 = I$ has been used in the second equality. We have now $Z = \operatorname{Tr}\exp(in_1\beta_1 U_1)\ldots\exp(in_k\beta_2 U_2) = \operatorname{Tr} H_l$, and $Z(0) = 2$. The operations of differentiating H_l with respect to the n_i and taking the trace of H_l are commutable. Since $\operatorname{Tr} U_i = 0$ and $U_i^2 = 1$ we have that the origin-values ($n_i = 0$) of all odd-order derivatives of Z are zero.

If there is a common forbidden energy for both the pure A and pure B lattices ($\beta_1 = iv_1, \beta_2 = iv_2$), then the even-order derivatives of Z at $n_i = 0$ involve taking the trace of a polynomial in U_1U_2 whose numerical coefficients are positive numbers. Since U_1U_2 is an H-matrix, it may be diagonalized to a form having diagonal elements $\exp(\pm i\gamma)$. Hence, when $\operatorname{Tr} U_1U_2 = 2\cos\gamma \geqslant 2$, $\operatorname{Tr}(U_1U_2)^n$ will be positive and Z will be $Z = (2 + \text{positive terms}) > 2$ for all n_i. That is, in any mixed lattice, a common forbidden energy of the component-atom lattices remains forbidden whenever

$$\Lambda \equiv \tfrac{1}{2}\operatorname{Tr} U_1U_2 = \frac{\mathscr{R}G_1G_2^* - \mathscr{I}F_1\mathscr{I}F_2}{\sinh v_1 \ \sinh v_2} \geqslant 1.$$

The angles ϕ_1 and ϕ_2 are unimportant for a discussion of the separate pure lattices, but, as may be seen by writing Λ in terms of the Lorentz parameters, are crucial in the mixed lattice. The quantity Λ will be seen presently to be of basic significance for random lattices.

A final remark before taking up the random lattice. This is that Z is insensitive to the interchange of whole A groups of atoms or of B groups of atoms whenever the lattice is the four-group one $\ldots(n_1A)(n_2B)(n_3A)(n_4B)\ldots$. To verify this it is only necessary to write out H_l explicitly using equation (7) for the separate groups of H-matrices, (or else to write out the Maclaurin expansion of Z) whence Z comes out to be symmetric under the interchange of n_1 and n_3 or of n_2 and n_4.

It follows that whenever some mixed lattice of A's and B's may be represented as $(N_1\overline{A})(N_2\overline{B})(N_3\overline{A})(N_4\overline{B})$, where $\overline{\mathrm{A}}$ and $\overline{\mathrm{B}}$ are sub-lattices of the original lattice, comprising any grouping of A's and B's, we have a band structure invariant to the exchange of $\overline{\mathrm{A}}$ groups or of $\overline{\mathrm{B}}$ groups. It appears that the four-group lattice is the only one strictly having this symmetry property, though it is not ruled out that a more general kind of near-symmetry holds, at least for certain kinds of A and B atoms, as suggested by Landauer and Helland's (1954) results.

§ 4. Random Lattices

Consider now a lattice of n atoms $\ldots(X_1X_2\ldots X_n)\ldots$ where X_i is with probability p an A-atom and with probability $q=1-p$ a B-atom; the probabilities are independent of position in the lattice (i.e. of the index i). We ask for the properties of such a random lattice. More particularly, the relevant question is, in what fraction of the ensemble of all possible chains of n atoms is a given energy allowed or forbidden (a chain having ν A-atoms and μ B-atoms being assigned a statistical weight $p^\nu q^\mu$). This is a statistical question superimposed on the quantum-mechanical one asking for the band structure of any particular mixed lattice. Of special interest is the case that n is large.

We start with the stochastic matrix

$$h_n=\alpha_1\alpha_2\ldots\alpha_n$$

where $\alpha_i=\epsilon_iA+(1-\epsilon_i)B$, with $\epsilon_i=1$ or 0 with probability p or q, and want to know, for a fixed energy, with what probability $|\operatorname{Tr}h_n|<2$; this is the desired probability that the given energy is allowed.

It is natural, therefore, to ask for the moments of the random variable $Z_n=\operatorname{Tr}h_n$. The first moment, or average trace, is simply

$$M_1\equiv\overline{Z}_n=\overline{\operatorname{Tr}h_n}=\operatorname{Tr}\overline{h}_n=\operatorname{Tr}(pA+qB)^n.$$

For the higher moments the appropriate tool to use is the direct matrix product (Macduffee 1946) defined through $[a\,.\,b]_{ij}=ab_{ij}$, where the square bracket designates a matrix of matrices. The two basic properties of the direct product that are useful to us are that $\operatorname{Tr}a\,.\,b=(\operatorname{Tr}a)(\operatorname{Tr}b)$ and that $ab\,.\,cd=(a\,.\,c)(b\,.\,d)$. The second moment of Z_n is

$$\begin{aligned}M_2&=\overline{(\operatorname{Tr}h_n)^2}=\overline{\operatorname{Tr}h_n\,.\,h_n}=\overline{\operatorname{Tr}\alpha_1h_{n-1}\,.\,\alpha_1h_{n-1}}\\&=\operatorname{Tr}\overline{(\alpha_1\,.\,\alpha_1)(h_{n-1}\,.\,h_{n-1})}=\operatorname{Tr}\overline{(\alpha_1\,.\,\alpha_1)(\alpha_2\,.\,\alpha_2)\ldots(\alpha_n\,.\,\alpha_n)}\\&=\operatorname{Tr}(pA\,.\,A+qB\,.\,B)^n,\end{aligned}$$

and for the Nth moment we find similarly

$$M_N=\operatorname{Tr}(pA_N+qB_N)^n,$$

where A_N is $A\,.\,A\ldots.A$ to N direct factors.

This result is also obtainable, in perhaps a more direct way, as follows. The matrix

$$G=(pA+qB)^n=p^nA^n+p^{n-1}q(A^{n-1}B+A^{n-2}BA+\ldots)+\ldots+q^nB^n$$

generates all possible chains and gives them the correct statistical weight, so we have the earlier result $M_1=\operatorname{Tr}G$ at once. For the second moment we have, from its definition,

$$\begin{aligned}M_2&=p^n(\operatorname{Tr}A^n)^2+\ldots=p^n\operatorname{Tr}A^n\,.\,A^n+\ldots\\&=p^n\operatorname{Tr}(A\,.\,A)^n+\ldots=\operatorname{Tr}(pA\,.\,A+qB\,.\,B)^n,\end{aligned}$$

the terms beyond the leading one being easily condensed into the proper form by using the multiplication rule $ab \,.\, cd = (a \,.\, c)(b \,.\, d)$; and similarly for the higher moments.

The first moment is readily found and shows an important characteristic of Z_n. If λ_1, λ_2 be the latent roots of $pA+qB$, M_1 is $\lambda_1{}^n+\lambda_2{}^n$. When the roots are complex conjugates, for example, M_1 is of the form $2r^n \cos n\sigma$, so that if $r>1$ the first moment tends to no definite limit as n becomes infinite. This appears to be true for the higher moments too. The distribution of the random variable Z_n, in short, apparently depends strictly on the chain length n and has no well-defined asymptotic form. This suggests the importance of introducing a grand ensemble of chains of different lengths and averaging $M_N(n)$ over the grand ensemble.

A rough bound for the moments may be found as follows. For the absolute moments μ_N of order N we have

$$\begin{aligned}\mu_N &= p^n \,|\operatorname{Tr} A_N{}^n| + \ldots + q^n \,|\operatorname{Tr} B_N{}^n| \\ &\geqslant 2^N (p^n \,|\cos^N n\beta_1| + q^n \,|\cos^N n\beta_2|)\end{aligned}$$

($A_N{}^n$ is $(A^n)_N$ or $(A_N)^n$, which are equal). Hence, if an energy is forbidden in at least one of the pure lattices ...A... or ...B... all absolute moments can diverge in the limit of large n.

The practical task of evaluating the moments, and an approximate distribution function, involves finding the latent roots of a $2^N \times 2^N$ matrix (for the Nth moment). This problem we bypass for the present in favour of going to the Poisson limit where a full analytical discussion is possible.

Suppose then that the chain length n is very large, but the number α of B atoms in the chain is small, so that $q=\alpha/n$ is a small number and $p=1-\alpha/n$ is nearly unity. The Nth moment may be written

$$M_N = \operatorname{Tr}\left[A_N + \frac{\alpha}{n}(B_N - A_N)\right]^n.$$

To a sufficient approximation we can diagonalize the matrix in brackets, call it J, by diagonalizing A_N and dropping the off-diagonal elements in the 'perturbation' $\alpha(B_N - A_N)/n$. If W is the similarity transformation matrix which diagonalizes A, then W_N diagonalizes A_N, and we have

$$J' = W_N J W_N{}^{-1} = d_N + \frac{\alpha}{n}(R_N - d_N),$$

where d is just

$$\begin{pmatrix} \exp(-i\beta_1) & 0 \\ 0 & \exp(i\beta_1) \end{pmatrix},$$

and R stands for WBW^{-1} with its off-diagonal terms placed equal to zero. Then

$$J' = d_N \left\{ I_N + \frac{\alpha}{n}\left[\begin{pmatrix} R_{11}\exp(i\beta_1) & 0 \\ 0 & R_{22}\exp(-i\beta_1) \end{pmatrix}_N - I_N \right] \right\}$$

$$\begin{aligned} J'^n &= \begin{pmatrix} \exp(-in\beta_1) & 0 \\ 0 & \exp(in\beta_1) \end{pmatrix}_N \exp\alpha \left[\begin{pmatrix} R_{11}\exp(i\beta_1) & 0 \\ 0 & R_{22}\exp(-i\beta_1) \end{pmatrix}_N - I_N \right] \\ &= e^{-\alpha} D_N \exp\alpha E_N, \end{aligned}$$

where D, E are abbreviations for the first and second matrices in the second line, and I_N is the 2^Nth order unit matrix.

Rather than calculate the moments explicitly let us write them as the series

$$M_N = \mathrm{Tr} J'^n = e^{-\alpha} \mathrm{Tr}\, D_N \sum_\nu \frac{\alpha^\nu E_N{}^\nu}{\nu!}$$
$$= e^{-\alpha} \sum_\nu \frac{\alpha^\nu [\mathrm{Tr}\ DE^\nu]^N}{\nu!}.$$

The reason for doing so is to make easy the calculation of the characteristic function f of the distribution:

$$f(u) = \sum_N \frac{(iu)^N M_N}{N!} = e^{-\alpha} \sum_{N,\nu} \frac{(iu)^N \alpha^\nu Q_\nu{}^N}{\nu! N!}$$
$$= e^{-\alpha} \sum_\nu \exp(iuQ_\nu) \frac{\alpha^\nu}{\nu!}$$
$$Q_\nu \equiv \mathrm{Tr}\, DE^\nu.$$

Writing f in this way presupposes that all moments exist, which will be the case if n, though large, is finite. The final series representing $f(u)$ is absolutely convergent since Q_ν is always real.

For the distribution function $F(t)$ itself, giving the probability that $Z_n < t$, we find now

$$F(t) = -\frac{1}{2\pi} \int_{-\infty}^{\infty} \frac{\exp(-iut)}{iu} f(u)du$$
$$= e^{-\alpha} \sum_\nu \frac{\alpha^\nu}{\nu!} \int_0^\infty \frac{\sin u(t - Q_\nu)}{\pi u} du.$$

The last integral is Dirichlet's integral having the value 1/2, 0, $-1/2$ according as t is greater than, equal to or less than Q_ν.

Finally, for the probability that $|Z_n| < 2$, i.e. the probability that a given energy is allowed in the random lattice, we obtain

$$P(E_{\text{alld}}) = F(2) - F(-2) = \tfrac{1}{2} e^{-\alpha} \sum C_\nu \frac{\alpha^\nu}{\nu!}$$
$$C_\nu = 2, \qquad |Q_\nu| < 2$$
$$C_\nu = 1, \qquad |Q_\nu| = 2$$
$$C_\nu = 0, \qquad |Q_\nu| > 2.$$

If, then, $|Q_\nu| \leqq 2$ for all ν the energy is certainly allowed or certainly forbidden in the A lattice infected with a few B atoms.

To obtain the physical information contained in the preceding result we must examine Q_ν in detail. This quantity is

$$Q_\nu = \exp(-in\beta_1)\{R_{11} \exp(i\beta_1)\}^\nu + \exp(in\beta_1)\{R_{22} \exp(-i\beta_1)\}^\nu.$$

By suitably arranging W in $WBW^{-1} = R$ an algebraic reduction yields

$$R_{11} = \cos\beta_2 + i \frac{\mathscr{R}G_1 G_2{}^* - \mathscr{I}F_1 \mathscr{I}F_2}{\sin\beta_1} = \cos\beta_2 - i\Lambda \sin\beta_2$$

$$R_{22} = \cos\beta_2 - i \frac{\mathscr{R}G_1 G_2{}^* - \mathscr{I}F_1 \mathscr{I}F_2}{\sin\beta_1} = \cos\beta_2 + i\Lambda \sin\beta_2,$$

A being the same quantity, $\frac{1}{2}\,\mathrm{Tr}\, U_1 U_2$, used to prove the Saxon–Hutner theorem.

Suppose now that we have an energy which is allowed in the pure A lattice. Then β_1 is real, R_{11} and R_{22} are complex conjugates, say $R \exp \pm i\rho$, and

$$Q_\nu = 2R^\nu \cos(\nu\beta_1 - n\beta_1 + \nu\rho)$$
$$R \equiv (\cos^2\beta_2 + \Lambda^2 \sin^2\beta_2)^{1/2}.$$

Hence, if this energy is also allowed in the pure B lattice (real β_2), and if also $|\Lambda|<1$, $|Q_\nu|<2$ for all ν and $P(E_{\text{alld}})=1$. One finds, however, from the Lorentz representation of Λ, that $|\Lambda|\geqslant 1$; the equality can hold only if $|\sin\beta_1/\sinh\tfrac{1}{2}\psi_1| = |\sin\beta_2/\sinh\tfrac{1}{2}\psi_2|$. In this case, $Q_\nu = 2\cos(\nu\beta_1 - n\beta_1 \pm \nu\beta_2)$, and for $|Q_\nu|$ to be always less than 2, it suffices that β_1 and β_2 be irrational multiples of π. When they are rational multiples, some $|Q_\nu|$ will equal 2 and it is less than certain that the energy is allowed; ordinarily, however, $P(E_{\text{alld}})$ will be close to 1. We may say, to characterize this too delicate distinction, that if $|\Lambda|=1$ a common allowed energy of the pure lattices is almost certainly allowed in the Poisson mixed lattice. Since we may reverse the roles of A and B in this argument, it would appear that this result is valid for any mixed lattice (or at least for lengthy ones). This would be the other face of the Saxon–Hutner theorem. If the energy is allowed in A but forbidden in B, the energy is never certainly allowed in the Poisson lattice.

For an allowed energy in A and either simultaneous allowedness in B with $|\Lambda|>1$ or simultaneous forbiddenness in B with any Λ, R exceeds unity and oscillates beyond the range $(+2,-2)$. Here we must consider that, as before remarked, the distribution of Z_n has no definite limit with increasing n: Q_ν contains n even though n has been taken to be large. If we fix ν and watch Q_ν and then C_ν as functions of n, it will be evident that $C_\nu(n)$ is a periodic step function with period π/β_1 and steps of height 2 and width $2\sin^{-1}R^{-\nu}$ ($\sin^{-1}$ referring only to the principal value between 0 and $\pi/2$). It is sensible now, for want of a definite value of $C_\nu(n)$, to take its average over a grand ensemble of chains of different length. For a uniform ensemble, in which the relative number of chains $h(n)dn$ with length between $n, n+dn$ is simply a constant for $n_0<n<n_1$ and zero otherwise, one finds

$$\overline{C_\nu(n)} = \int C_\nu(n)h(n)dn = \frac{4}{\pi}\sin^{-1}R^{-\nu}.$$

This result depends insensitively on the exact choice of $h(n)$ within fairly wide limits.

Now we calculate

$$\overline{P}(E_{\text{alld}}) = \tfrac{1}{2}e^{-\alpha}\sum\frac{\alpha^\nu}{\nu!}\overline{C_\nu(n)}.$$

Using the power series expansion for the $\sin^{-1}$ function gives

$$\overline{P}(E_{\text{alld}}) = \frac{2}{\pi}e^{-\alpha}\left(\exp\frac{\alpha}{R} + \frac{1}{6}\exp\frac{\alpha}{R^3} + \frac{3}{40}\exp\frac{\alpha}{R^5} + \dots\right).$$

When $R\gg 1$, i.e. for energies strongly forbidden in the B lattice ($\cosh v_2$ large) or for energies close to a band edge in the A lattice ($\sin\beta_1$ small) or for $\mathscr{B}G_1G_2^* - \mathscr{I}F_1\mathscr{I}F_2$ large, we have more simply, replacing $\sin^{-1}R^{-\nu}$ by its argument,

$$\overline{P}(E_{\text{alld}}) = e^{-\alpha}\left(1 - \frac{2}{\pi}\left[1 - \exp\frac{\alpha}{R}\right]\right).$$

If also $R\gg\alpha$ this is just $\exp(-\alpha)$: the energy is practically forbidden for even a small total number α of B atoms strewn in the A lattice; while if $\alpha\gg R$, $\overline{P}=(2/\pi)\exp(-\alpha)\simeq 0$.

In the case where R is small, $R=1+\sigma$, $\sigma\ll 1$, we get

$$\overline{P}(E_{\text{alld}}) = \frac{2}{\pi}\sin^{-1}e^{-\alpha\sigma}.$$

Turning, in conclusion, to the case in which the energy is forbidden in the A lattice, let us write, for example, $\beta_1 = iv_1$, and thence

$$Q_\nu = \exp\{(n-\nu)v_1\}R_{11}{}^\nu + \exp\{-(n-\nu)v_1\}R_{22}{}^\nu.$$

Here, for any ν when we go to large n we find $Q_\nu \to \infty$ in general, so that the forbiddenness in the pure A lattice dominates and the energy is forbidden certainly in the Poisson lattice, irrespective of forbiddenness or allowedness in the B lattice. An exception occurs when R_{11} vanishes. Then

$$\overline{P}(E_{\text{alld}}) = \tfrac{1}{2}e^{-\alpha}\sum_{\nu=1}^{\infty} 2\frac{\alpha^\nu}{\nu!} = 1 - e^{-\alpha},$$

and for a moderate value of α the energy is practically allowed in the random lattice. This will occur at single, isolated energy levels. It is easy to show that this exceptional case never conflicts with the Saxon–Hutner theorem.

ACKNOWLEDGMENT

The author is indebted to Professor M. Kac and to Mr. H. Lawrence for valuable discussions of probability questions.

REFERENCES

JAMES, H. M., 1949, *Phys. Rev.*, **76**, 1602.
JAMES, H. M., and GINZBARG, A. S., 1953, *J. Phys. Chem.*, **57**, 840.
KERNER, E. H., 1954, *Phys. Rev.*, **95**, 687.
KERNER, E. H., and LOGAN, J. G., 1955, *Bull. Amer. Phys. Soc.*, **30**, 26.
KRAMERS, H. A., 1935, *Physica*, **2**, 483.
LANDAUER, R., and HELLAND, J. C., 1954, *J. Chem. Phys.*, **22**, 1655.
LUTTINGER, J. M., 1951, *Philips Res. Rep.*, **6**, 303.
MACDUFFEE, C. C., 1946, *The Theory of Matrices* (New York : Chelsea Publishing Co.).
MØLLER, C., 1952, *The Theory of Relativity* (Oxford : Clarendon Press).
SAXON, S. D., and HUTNER, R. A., 1949, *Philips Res. Rep.*, **4**, 82.
VAN DER WAERDEN, B. L., 1944, *Die Gruppentheoretische Methode in der Quantenmechanik* (Ann Arbor, Michigan : Edwards Bros.).

The Intensities of the Symmetry-forbidden Electronic Bands of Benzene

By J. N. MURRELL and J. A. POPLE
Department of Theoretical Chemistry, Cambridge

MS. received 11*th October* 1955, *and in final form* 4*th November* 1955

Abstract. The molecular orbital method is used to calculate the intensities of the symmetry-forbidden bands of benzene. Both the bands at 2650 Å and 2000 Å derive intensity by interaction with the upper state of the 1800 Å band. The states of symmetry B_{1u} and B_{2u} are made accessible by e_{2g} vibrations of the benzene framework at 606 cm^{-1} and 1595 cm^{-1}. The 606 cm^{-1} vibration is most important in making the transition to the B_{2u} state (at 2650 Å) allowed, whereas that at 1595 cm^{-1} is most important for the $A_{1g} \rightarrow B_{1u}$ transition. The alternative assignments B_{1u} and E_{2g} are considered for the 2000 Å band, but the calculated total intensities cannot differentiate between them.

§ 1. Introduction

To a first approximation, the intensity of an absorption band which arises from an electronic transition is proportional to the square of the transition electric dipole moment measured with the nuclei in their equilibrium configuration. If by virtue of the symmetry of the states involved this dipole moment is zero, the transition is said to be symmetry-forbidden. That such transitions do often give rise to weak bands is primarily due to the effect of vibrations on the symmetry of the molecule, for in the course of a vibration there may be a non-zero instantaneous (but not average) transition dipole moment. The band which results usually has considerable vibrational fine structure.

The general theory of the absolute intensity of these symmetry-forbidden bands (and the relative intensity of the vibrational components), was developed by Herzberg and Teller (1933). They outlined the principles that decide which normal vibrations make the transition allowed, and they showed how the absolute intensity of the resulting band could be calculated from a knowledge of the electronic wave functions of the molecule in its equilibrium nuclear configuration. At that time, however, so little was known quantitatively about the electronic wave functions of the excited states of molecules, that it was not possible to carry out any detailed calculations. Recent developments in the molecular orbital theory, and in other approximate methods for handling many electron wave functions, have made an extension of Herzberg and Teller's work possible.

Benzene is one of the simplest molecules for which there is accurate experimental data about symmetry-forbidden transitions. There are three bands in the near ultra-violet region of the spectrum, at 2650, 2000 and 1800 Å. Of these the 1800 Å band is generally accepted to arise from a symmetry-allowed transition, with a transition moment in the plane of the molecule. Polarization measurements on crystals of hexamethylbenzene (Craig and Lyons 1952, Nelson and Simpson 1955), suggest that the other two transitions also have moments in

this plane, and being much weaker than the 1800 Å band are probably symmetry-forbidden. Extensive work has been carried out on the structure of the 2650 Å band (Garforth and Ingold 1948), and there is general agreement for the assignment B_{2u} to the upper state. The symmetry of the upper state of the 2000 Å band, however, is still uncertain.

The aim of this paper is to use the general features of the Herzberg–Teller method in conjunction with recent molecular orbital theories of excited states (Göppert-Mayer and Sklar 1938, Pariser and Parr 1953, Dewar and Longuet-Higgins 1954, Pople 1955) to calculate the intensities of these bands. Craig (1950) has examined the intensity of the longest wavelength band using the valence bond method.

§ 2. General Theory of the Intensity of Vibrationally Allowed Transitions

To introduce the molecular orbital treatment of the intensities of symmetry-forbidden bands, we shall outline the relevant parts of the general theory of Herzberg and Teller.

The Born–Oppenheimer adiabatic approximation enables us to write the total wave function as a product of functions,

$$\Psi_{kl}(x, q) = \Theta_k(x, q)\Phi_{kl}(q), \qquad \ldots\ldots(2.1)$$

where $\Theta_k(x, q)$ is a solution of the electronic Schrödinger equation for a fixed nuclear configuration. x and q are collective symbols for the electronic and nuclear coordinates, and k, l are quantum numbers (or sets of quantum numbers) describing the electronic and vibration–rotation states respectively. The nuclear coordinates will be taken as a set of normal coordinates $q_1, q_2, \ldots$, together with a set describing translation and rotation.

For each nuclear configuration q, we may define a variable electronic transition moment

$$\mathbf{M}_{kk'}(q) = \int \Theta_k^*(x, q)\mathbf{M}(x)\Theta_{k'}(x, q)\, dq, \qquad \ldots\ldots(2.2)$$

where $\mathbf{M}$ is the electronic dipole moment operator. The oscillator strength $f_{kl\to k'l'}$ of a single component $kl\to k'l'$ of an electronic transition $k\to k'$ is then given by

$$f_{kl\to k'l'} = \frac{8\pi^2 mc}{3h^2e^2} E_{kl\to k'l'} \left| \int \Phi_{kl}^*(q)\mathbf{M}_{kk'}(q)\Phi_{k'l'}(q)\, dq \right|^2, \qquad \ldots\ldots(2.3)$$

where $E_{kl\to k'l'}$ is the energy of the transition.

An approximate expression for the total intensity of the whole band can be obtained if we suppose that only the lowest vibrational state Ψ_{k0} is populated. If we replace the energy $E_{k0\to k'l'}$ by a mean value $E_{k\to k'}$ for the band as a whole, and sum over l', we get

$$f_{k\to k'} = \sum_{l'} f_{k0\to k'l'} = \frac{8\pi^2 mc}{3h^2e^2} E_{k\to k'} \overline{M_{kk'}^2}, \qquad \ldots\ldots(2.4)$$

where $\overline{M_{kk'}^2}$ is the mean square of the variable transition moment $\mathbf{M}_{kk'}(q)$ in the ground state.

The transitions we are concerned with are those for which $\mathbf{M}_{kk'}(q)$ vanishes in the equilibrium configuration ($q_1 = q_2 = \ldots = 0$). Expanding $\mathbf{M}_{kk'}(q)$ in powers of $q_1, q_2 \ldots$ and neglecting all but the linear terms, we have

$$\overline{M_{kk'}^2} = \sum_a \left(\frac{\partial \mathbf{M}_{kk'}}{\partial q_a}\right)_0^2 \overline{q_a^2}, \qquad \ldots\ldots(2.5)$$

$(\partial \mathbf{M}_{kk'}/\partial q_a)_0$ being evaluated for the equilibrium configuration. The individual terms in this sum measure the relative effects of the various normal vibrations in making the transition allowed. The mean square displacements $\overline{q_a^2}$ are easily calculated if the oscillations are assumed to be harmonic. For a system of nuclei all of mass μ, the ground vibrational state wave function gives

$$\overline{q_a^2} = h/8\pi^2\mu\nu_a, \qquad \ldots\ldots(2.6)$$

where ν_a is the frequency of the normal vibration corresponding to q_a. The coordinates q_a are normalized so that the sum of the squares of the nuclear displacements is unity.

It remains to find the change of transition moment during a vibration as given by $(\partial \mathbf{M}_{kk'}/\partial q_a)_0$. This can be done by a perturbation method, expanding the electronic wave functions of both states in terms of those for the equilibrium configuration. Thus

$$\Theta_k(x, q) = \Theta_k(x, 0) + \sum_s \lambda_{ks}(q)\Theta_s(x, 0) \qquad \ldots\ldots(2.7)$$

and similarly for $\Theta_{k'}$. The coefficients $\lambda_{ks}(q)$ and $\lambda_{k's}(q)$ show the amount of mixing between the electronic states produced by the vibration. The required derivative is then given by

$$\left(\frac{\partial \mathbf{M}_{kk'}}{\partial q_a}\right)_0 = \sum_s \left(\frac{\partial \lambda_{ks}^*}{\partial q_a}\right)_0 (\mathbf{M}_{sk'})_0 + \sum_s \left(\frac{\partial \lambda_{k's}}{\partial q_a}\right)_0 (\mathbf{M}_{ks})_0, \qquad \ldots\ldots(2.8)$$

where $(\mathbf{M}_{sk'})_0$ and $(\mathbf{M}_{ks})_0$ are evaluated for the equilibrium configuration.

The coefficients λ_{ks} can be evaluated by first order perturbation theory

$$\lambda_{ks} = \frac{1}{E_k - E_s} \int \Theta_k^*(x, 0) H_a \Theta_s(x, 0)\, dx, \qquad \ldots\ldots(2.9)$$

where H_a is the change in the Hamiltonian which occurs during the vibration q_a. This change is manifest in the terms $-Z_\sigma e^2/r_{i\sigma}$ where Z_σ is the charge of nucleus σ and $r_{i\sigma}$ the distance of electron i from this nucleus. Then for small displacements q_a

$$H_a = -q_a \frac{\partial}{\partial q_a} \sum_i \sum_\sigma \frac{Z_\sigma e^2}{r_{i\sigma}} = \sum_i \sum_\sigma Z_\sigma e^2 \frac{\partial \mathbf{r}_\sigma}{\partial q_a} \frac{\mathbf{r}_{i\sigma}}{r_{i\sigma}^3} q_a, \qquad \ldots\ldots(2.10)$$

where $\mathbf{r}_\sigma$ is the position vector of nucleus σ. It follows that

$$\left(\frac{\partial \lambda_{ks}}{\partial q_a}\right)_0 = \frac{1}{E_k - E_s} \int \Theta_s^*(x, 0) h_a \Theta_k(x, 0)\, dx, \qquad \ldots\ldots(2.11)$$

where $h_a = (\partial H_a/\partial q_a)_0$. The Hamiltonian h_a is equivalent to the interaction energy of a set of dipoles $eZ_\sigma(\partial \mathbf{r}_\sigma/\partial q_a)$ with the electrons i. Since h_a is a sum of identical one-electron operators, the integration can be carried out over all electrons but one, and the integral in (2.11) then reduces to the interaction energy of this set of dipoles and a single electron density

$$\rho_{sk} = N \int \Theta_s^* \Theta_k\, dx', \qquad \ldots\ldots(2.12)$$

where the integration dx' is over $N-1$ of the N electrons. As we shall see in the next section, this transition density takes a simple form when molecular orbital wave functions are used and it then becomes possible to attempt quantitative estimates of the integral in (2.11) and consequently of the absolute intensity.

§ 3. Application to the Symmetry-forbidden Bands of Benzene

In molecular orbital theory, the lowest excited states of an aromatic hydrocarbon are attributed to the excitation of electrons in the delocalized molecular orbitals which have a node in the plane of the molecule. For benzene, in the usual LCAO approximation, the molecular orbitals have the form

$$\left.\begin{aligned}
\theta_6 &= \sqrt{\tfrac{1}{6}}(\omega_1-\omega_2+\omega_3-\omega_4+\omega_5-\omega_6)\\
\theta_5 &= \sqrt{\tfrac{1}{12}}(2\omega_1-\omega_2-\omega_3+2\omega_4-\omega_5-\omega_6)\\
\theta_4 &= \tfrac{1}{2}(-\omega_2+\omega_3-\omega_5+\omega_6)\\
\theta_3 &= \tfrac{1}{2}(\omega_2+\omega_3-\omega_5-\omega_6)\\
\theta_2 &= \sqrt{\tfrac{1}{12}}(2\omega_1+\omega_2-\omega_3-2\omega_4-\omega_5+\omega_6)\\
\theta_1 &= \sqrt{\tfrac{1}{6}}(\omega_1+\omega_2+\omega_3+\omega_4+\omega_5+\omega_6)
\end{aligned}\right\} \quad \ldots\ldots(3.1)$$

where $\omega_1 \ldots \omega_6$ are $2p\pi$ atomic orbitals for the carbon atoms. The pairs of orbitals θ_2, θ_3 and θ_4, θ_5 are degenerate.

In the ground state the total wave function for the π-electron is written as a determinant

$$\Theta_0 = \sqrt{\frac{1}{6!}}\,|\theta_1\bar{\theta}_1\theta_2\bar{\theta}_2\theta_3\bar{\theta}_3|. \qquad \ldots\ldots(3.2)$$

Following the method of Dewar and Longuet-Higgins (1954) and Pople (1955), the wave functions for the excited states are written as sums or differences of those for degenerate excited configurations χ_k^l in which one electron has been removed from the orbital θ_k and placed in θ_l.

The wave functions assigned to the upper states of the three lowest transitions in benzene by Göppert-Mayer and Sklar, Pariser and Parr (1953) and by Dewar and Longuet-Higgins (1954) are shown in table 1. There is still some uncertainty

Table 1. Wave Functions for the Lowest Excited States of Benzene and Possible Assignment

Symbol	Configuration	Symmetry	Energy of band (cm^{-1})	Obs Int. (f)
Θ_α	$\sqrt{\tfrac{1}{2}}(\chi_3^5-\chi_2^4)$	B_{2u}	39400 (α-band)	0·0014[1]
Θ_p	$\sqrt{\tfrac{1}{2}}(\chi_3^4+\chi_2^5)$	B_{1u}	49500 (p-band)	0·094[2]
Θ_β	$\sqrt{\tfrac{1}{2}}(\chi_3^5+\chi_2^4)$	E_{1u}	54400 (β-band)	0·88[2]
$\Theta_{\beta'}$	$\sqrt{\tfrac{1}{2}}(\chi_3^4-\chi_2^5)$			
Θ_γ	$\sqrt{\tfrac{1}{2}}(\chi_1^5-\chi_2^6)$	E_{2g}		
$\Theta_{\gamma'}$	$\sqrt{\tfrac{1}{2}}(\chi_1^4-\chi_3^6)$			
Θ_δ	$\sqrt{\tfrac{1}{2}}(\chi_1^5+\chi_2^6)$	E_{2g}		
$\Theta_{\delta'}$	$\sqrt{\tfrac{1}{2}}(\chi_1^4+\chi_3^6)$			

1. Klevens and Platt (1954).
2. Hammond and Price (1955).

about the intermediate band at 49 500 cm^{-1}, however, and the alternative assignment E_{2g} has been proposed. The wave functions for possible E_{2g} states have been included in this table.

In applying the theory developed in § 2 to the calculation of the intensities of the symmetry-forbidden bands we shall neglect the mixing of the ground state Θ_0, of symmetry A_{1g}, with any excited state. This is justified to some extent by the large difference in energy between the ground and excited states. It follows from (2.8) that the only electronic states Θ, which contribute to the intensity of the transition $\Theta_0 \rightarrow \Theta_k$, are those of symmetry E_{1u}. Furthermore,

for $(\partial\lambda_{ks}/\partial q_\sigma)_0$ to be non-zero, the perturbing vibration must belong to the same representation of the symmetry group D_{6h} as the density function ρ_{sk}. Detailed examination shows that B_{1u} and B_{2u} states are made accessible by e_{2g} vibrations, whilst transitions to E_{2g} states are allowed by e_{1u} vibrations. The intensities of the bands of table 1 will now be considered in detail.

α-band.

There are four pairs of e_{2g} vibrations which contribute to the intensity of this band. To simplify the calculations we will ignore those vibrations which arise mainly from the C–H bending and stretching. The two e_{2g} frequencies for a hexagonal framework arise from a superposition of the radial and tangential vibrations shown in figure 1. A complete set of normal coordinates has been

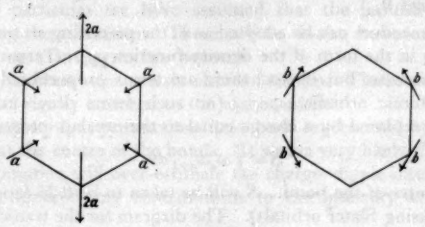

Figure 1.

given by Whiffen (1955). For the two skeletal e_{2g} vibrations he gives: frequency 606 cm^{-1}, $a=0{\cdot}243$, $b=0{\cdot}273$; 1595 cm^{-1}, $a=-0{\cdot}127$, $b=0{\cdot}450$. (The normal coordinates are normalized so that the sum of the squares of the displacements is unity.) The two coordinates defined in this way are not strictly orthogonal because the complete vibrations involve some motion of the C–H bonds. The Hamiltonian H_a consists of the interaction of the π-electrons with dipoles $eZ_\sigma\mathbf{r}_\sigma$ where $\mathbf{r}_\sigma$ is the displacement of nucleus σ given by these normalized coordinates. Z_σ will be taken as unity, it being supposed that each carbon core behaves bodily as a unit charge.

By carrying out the partial integration of equation (2.12), it is easily shown that the transition density $\rho_{\alpha\beta}$ is equal to $\frac{1}{2}(\theta_2^2+\theta_5^2-\theta_3^2-\theta_4^2)$. If this is expanded in terms of atomic orbitals using (3.1) and if product terms $\omega_\sigma\omega_\tau$ $(\sigma\neq\tau)$, are omitted, then $\rho_{\alpha\beta}$ can be represented schematically as in figure 2, each coefficient measuring a density $-e\omega_\sigma^2$ at position σ. The interaction of this density function with the perturbing set of dipoles is conveniently estimated by replacing the distribution $-\kappa e\omega_\sigma^2$ by a point charge $-\kappa e$ at position σ and evaluating its energy

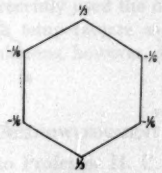

Figure 2.

in the field of the dipoles. (There will be no interaction between the dipole at centre σ and the charge distribution ω_σ^2.) The interaction energies are found to be $0{\cdot}643e^2/R^2$ and $0{\cdot}493e^2/R^2$ for the 606 cm^{-1} and 1595 cm^{-1} vibrations respectively, R being the bond length (1·39 Å). There will be identical contributions due to mixing of the states Θ_α and Θ_β. Substituting in the formulae of the last section, we have for the ratio of the oscillator strengths

$$\frac{f_\alpha}{f_\beta} = \frac{E_\alpha}{E_\beta(E_\beta - E_\alpha)^2} \frac{he^4}{8\pi^2\mu R^4} \left\{ \frac{(0{\cdot}643)^2}{606} + \frac{(0{\cdot}493)^2}{1595} \right\} = 0{\cdot}0135.$$

One important result emerging from these figures is that the 606 cm^{-1} vibration is 4·5 times as effective in contributing to the intensity of the α-band as is the 1595 cm^{-1} vibration.

p-*band* (*assignment* B_{1u}).

The same procedure can be adopted as in the preceding section, the principal difference being in the form of the density function $\rho_{p\beta}$. Terms of the type ω_σ^2 all vanish in this case, but instead there are terms proportional to products of neighbouring atomic orbitals $\omega_\sigma\omega_{\sigma+1}$ (no such terms occur in $\rho_{\alpha\beta}$). Such a product will be replaced by a charge equal to the overlap integral

$$S = \int \omega_\sigma \omega_{\sigma+1}\, dx, \qquad \ldots\ldots (3.4)$$

placed at the centre of the bond. S will be taken to be 0·25 (approximately the value obtained using Slater orbitals). The diagram for the transition density $\rho_{p\beta}$ is then as figure 3. The intensity of the band is given by

$$\frac{f_p}{f_\beta} = \frac{E_p}{E_\beta(E_\beta - E_p)^2} \frac{he^4S^2}{8\pi^2\mu R^4} \left\{ \frac{(2{\cdot}283)^2}{606} + \frac{(6{\cdot}829)^2}{1595} \right\} = 0{\cdot}452.$$

p-*band* (*assignment* E_{2g}).

Here the appropriate vibration is e_{1u} (frequency 1480 cm^{-1}), see figure 4. The transition densities are of similar form to those described above and are represented in figure 5. The complete results are collected in table 2.

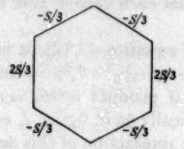

Figure 3.

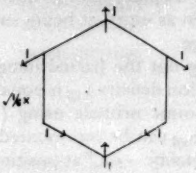

Figure 4.

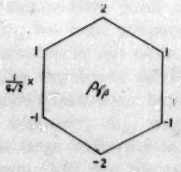

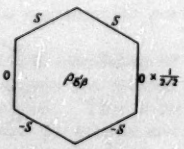

Figure 5.

Table 2. Comparison of Observed and Calculated Intensities

Band and assignment	Calculated ratio f_x/f_β due to vibration 606 cm^{-1}	1595 cm^{-1}	Total	Observed f_x/f_β
α-band B_{2u}	0·0110	0·0025	0·0135	0·0016
p-band B_{1u}	0·103	0·349	0·452	
$E_{2g}(\gamma)$			0·066	0·107
$E_{2g}(\delta)$			0·210	

§ 4. Discussion of Results

Before attempting to draw any conclusions from the results we have obtained, it would be useful to list the approximations which have been made.

(1) Only the mixing of the excited state with the lowest E_{1u} state has been considered. In particular we have assumed that the ground state remains unchanged during the vibrations. There is little doubt, however, that we have taken the most important terms into account.

(2) Benzene has been taken as a six-electron system. The remaining electrons are assumed to be rigidly attached to the carbon nuclei.

(3) The transition density functions have been represented by point charges at the nuclei or at the centre of the bonds. It seems very likely that in the latter case this approximation will over-estimate the charge–dipole interaction.

(4) We have ignored any contributions to the intensity arising from the C–H vibrations.

The absolute intensity of the α-band which we calculate is considerably too large. This may well be due to the first approximation we have listed. Limiting the number of terms in the expansion of the wave functions of the ground and excited states prevents complete readjustment of the electronic structure in the distorted molecule. The relative contributions of the two vibrations are supported by experimental work on the fine structure of the α-band (Garforth and Ingold 1948). They find no vibrational lines which can be attributed to the 1595 cm^{-1} vibration. The conclusion that the 606 cm^{-1} vibration was the more important was reached by Craig (1950) using a valence-bond method. He found a much higher value for the ratio of contributions, but his method of obtaining matrix elements is not based on a direct evaluation of the interaction between the perturbing dipoles and the transition density.

The calculated intensities are also too large for either assignment of the *para* band. The calculations do not, therefore, give any direct evidence in favour of one assignment or the other. The relative contributions of the two e_{2g} vibrations on the B_{1u} hypothesis are of some interest, however, They show that, unlike the α-band, the 1595 cm^{-1} vibration makes the principal contribution to the intensity. This is estimated to be 3·4 times as effective as the 606 cm^{-1} mode. Dunn and Ingold (1955) have recently used the non-appearance of a Boltzmann (1→0) vibrational band at high temperatures as an argument against the B_{1u} assignment. The present calculations, however, suggest that such a band would only be expected to be weak.

Acknowledgment

The authors are indebted to Professor H. C. Longuet-Higgins for valuable discussions on this topic.

References

Craig, D. P., 1950, *J. Chem. Soc.*, 59.

Craig, D. P., and Lyons, L. E., 1952, *Nature, Lond.*, **169,** 1102.

Dewar, M. J. S., and Longuet-Higgins, H. C., 1954, *Proc. Phys. Soc.* A, **67,** 795.

Dunn, T. M., and Ingold, C. K., 1955, *Nature, Lond.*, **176,** 65.

Garforth, F. M., and Ingold, C. K., 1948, *J. Chem. Soc.*, 4170

Göppert-Mayer, M., and Sklar, A. L., 1938, *J. Chem. Phys.*, **6,** 645.

Hammond, V. J., and Price, W. C., 1955, Trans. Faraday Soc., **51,** 605.

Herzberg, G., and Teller, E., 1933, *Z. Phys. Chem.* B, **21,** 410.

Klevens, H. B., and Platt, J. R., 1953–1954, *Technical Report of the Laboratory of Molecular Structure and Spectra*, University of Chicago.

Nelson, R. C., and Simpson, W. T., 1955, *J. Chem. Phys.*, **23,** 1146.

Pariser, R., and Parr, R. G., 1953, *J. Chem. Phys.*, **21,** 767.

Pople, J. A., 1955, *Proc. Phys. Soc.* A, **68,** 81.

Whiffen, D. H., 1955, *Phil. Trans. Roy. Soc.* A, **248,** 131.

r-Centroids : Average Internuclear Separations Associated with Molecular Bands

By R. W. NICHOLLS and W. R. JARMAIN
Department of Physics, University of Western Ontario, London, Canada

MS. received 8th September 1955

Abstract. The r-centroid $\bar{r}_{v'v''}$ of a molecular band is defined by

$$\int \psi_{v'} r \psi_{v''} dr \Big/ \int \psi_{v'} \psi_{v''} dr$$

and is an average internuclear separation which may be associated with the $v' \rightarrow v''$ transition. $\psi_{v'}$ and $\psi_{v''}$ are vibrational wave functions. The physical meaning of r-centroids is discussed and it is shown that the average internuclear separation $\bar{r}_{v'}$ in the level v' may be represented by the weighted mean of r-centroids with respect to Franck–Condon factors $q_{v'v''}$; i.e. $\bar{r}_{v'} = \Sigma_{v''} q_{v'v''} \bar{r}_{v'v''}$. Methods for evaluating arrays of r-centroids are developed and values are reported for ten band systems. The smooth relationship between r-centroid and wavelength is described and illustrated. A knowledge of r-centroids has been found very useful in the discussion of variation with internuclear separation of the electronic transition moment and it may reasonably be expected to have value in the study of other molecular properties.

§ 1. Introduction

The internuclear separation r is an important quantity in terms of which to describe the structure and properties of diatomic molecules. The range of internuclear separations which are encountered by a molecule in the emission or absorption of light is determined by the form of the potential functions of the upper and lower states of the transition and by the separation between their minima. These factors also determine which of the classical turning points of the vibrational levels in the two potentials occur at about the same internuclear separations and thus, by the application of the Franck–Condon principle (Condon 1928), which of the transitions between the vibrational levels have the highest probability of occurrence.

It is well known (Herzberg 1950) that the probability of a $v' \rightarrow v''$ vibrational transition in emission is proportional to

$$E_{v'v''}^3 \left| \int \psi_{v'}(r) R_e(r) \psi_{v''}(r) dr \right|^2 = E_{v'v''}^3 p_{v'v''} \qquad \ldots\ldots(1)$$

where $E_{v'v''}$ is the energy involved in the transition, $\psi_{v'}(r)$ and $\psi_{v''}(r)$ are the vibrational wave functions and $R_e(r)$ is the electronic transition moment of the transition. $p_{v'v''}$ which is defined by equation (1) is called the relative vibrational transition probability. If $R_e(r)$ is substantially independent of r, then the Franck–Condon factor

$$q_{v'v''} = \left| \int \psi_{v'}(r) \psi_{v''}(r) dr \right|^2 \qquad \ldots\ldots(2)$$

will control the value of $p_{v'v''}$. On the other hand if $R_e(r)$ is not independent of r in the range of r encountered in the transition its effect will have to be taken into account.

Because of the part played by the internuclear separation r in the definition and description of such molecular parameters as $R_e(r)$, $q_{v'v''}$ and $p_{v'v''}$, it is of interest to consider whether one of a set of specific values of r, which extend across the whole range of r experienced by the molecule, may be assigned to each transition. In this way experimental observations upon discrete transitions may be associated with specific values of r and may be used to describe molecular properties as a function of r. It is therefore the purpose of this paper (i) to discuss how an internuclear separation $\bar{r}_{v'v''}$ (the r-centroid) may be assigned to each band of a transition and what physical meaning may be attached to it, (ii) to review the methods which have so far been developed to calculate values of $\bar{r}_{v'v''}$ and to present values so far obtained, (iii) to discuss and explain the relationship which has been found between $\bar{r}_{v'v''}$ and wavelength.

A further paper (Nicholls 1956, to be published) describes one application of r-centroids, namely, how they may be employed to find the variation of electronic transition moment with internuclear separation for a number of band systems for which intensity measurements are available.

§ 2. The r-Centroids

It was originally noticed during the numerical evaluation of integrals of the form $\int \psi_{v'}\psi_{v''}dr$, $\int \psi_{v'}r\psi_{v''}dr$, $\int \psi_{v'}r^2\psi_{v''}dr$, $\int \psi_{v'}r^{-1}\psi_{v''}dr$ for bands of the First Positive system of N_2 that the following equations hold quite closely:

$$\frac{\int \psi_{v'}r^2\psi_{v''}dr}{\int \psi_{v'}r\psi_{v''}dr} = \frac{\int \psi_{v'}r\psi_{v''}dr}{\int \psi_{v'}\psi_{v''}dr} = \frac{\int \psi_{v'}\psi_{v''}dr}{\int \psi_{v'}r^{-1}\psi_{v''}dr}. \qquad \ldots\ldots(3)$$

The middle ratio in equation (3) is an expression for the r-coordinate of a centroid. The r-centroid of the $v'\rightarrow v''$ transition is thus defined by

$$\bar{r}_{v'v''} = \frac{\int \psi_{v'}r\psi_{v''}dr}{\int \psi_{v'}\psi_{v''}dr}. \qquad \ldots\ldots(4)$$

As a consequence of equation (3) an analytical investigation was made of the conditions under which equations (5), (6) and (7) would hold for molecular band systems in general (Fraser 1954 a):

$$\bar{r}_{v'v''} = \frac{\int \psi_{v'}r^n\psi_{v''}dr}{\int \psi_{v'}r^{n-1}\psi_{v''}dr}; \quad n=0, 1, 2\ldots \qquad \ldots\ldots(5)$$

$$\int \psi_{v'}r^n\psi_{v''}dr = (\bar{r}_{v'v''})^n \int \psi_{v'}\psi_{v''}dr \qquad \ldots\ldots(6)$$

$$\int \psi_{v'}f(r)\psi_{v''}dr = f(\bar{r}_{v'v''}) \int \psi_{v'}\psi_{v''}dr. \qquad \ldots\ldots(7)$$

It was found that these equations were valid provided that (i) $\mu_A\omega_e \sim 10^4$ for the molecule under consideration; μ_A is the reduced mass of the molecule in atomic weight units and ω_e is the vibrational quantum in kaysers; (ii) $0{\cdot}01\text{ Å} < |r_{e1} - r_{e2}| < 0{\cdot}25\text{ Å}$ where r_{e1} and r_{e2} are the two equilibrium internuclear separations concerned in the transition; (iii) v' and v'' do not exceed about 10; (iv) if $f(r)$ is a polynomial in r, the highest power of r should not exceed about 10.

Equation (7) has a number of important applications one of which is found in equation (17) and another of which is discussed by Nicholls (1956).

It is natural to enquire into what physical meaning may be attached to the r-centroid. From equation (4) it is seen to be a weighted average with respect to $\psi_{v'}\psi_{v''}$ of the range of r values experienced by the molecule in both states of the $v'\rightarrow v''$ transition. It is also the r-coordinate of the centroid of the area represented by the overlap integral from which its suggested name is derived. A simple relationship between r-centroids and the average or expectation value of r experienced by a molecule in a specific vibrational level v' or v'' may be developed as follows.

The average value $\bar{r}_{v'}$ of the internuclear separation in the level v' is

$$\bar{r}_{v'} = \int \psi_{v'}^2 r dr. \qquad \ldots\ldots(8)$$

Now $\psi_{v'}$ may be expanded in an orthogonal series of $\psi_{v''}$, the coefficients of which may be easily shown, by using the orthogonality properties of $\psi_{v''}$,† to be the overlap integrals (v', v'') where

$$(v', v'') = \int \psi_{v'}\psi_{v''} dr. \qquad \ldots\ldots(9)$$

Thus

$$\psi_{v'} = \sum_{v''} (v', v'')\psi_{v''}. \qquad \ldots\ldots(10)$$

From equations (8) and (10)

$$\bar{r}_{v'} = \sum_{v''} (v', v'') \int \psi_{v'} r \psi_{v''} dr. \qquad \ldots\ldots(11)$$

Also from equations (4) and (11)

$$\bar{r}_{v'} = \sum_{v''} (v', v'') . (v', v'')\bar{r}_{v'v''} = \sum_{v''} q_{v'v''}\bar{r}_{v'v''}. \qquad \ldots\ldots(12)$$

Similarly it may be shown that

$$\bar{r}_{v''} = \sum_{v'} q_{v'v''}\bar{r}_{v'v''}. \qquad \ldots\ldots(13)$$

Equations (12) and (13) clearly indicate that the average internuclear separation $\bar{r}_v$ experienced by a molecule while in a vibrational level v' or v'' may be considered as a weighted average, with respect to the Franck–Condon factors $q_{v'v''}$, of the r-centroids $\bar{r}_{v'v''}$ taken over all transitions which involve the level. It will be recalled that $q_{v'v''}$ is a measure of the relative probability that the $v'\rightarrow v''$ transition takes place. Thus $q_{v'v''}\bar{r}_{v'v''}$ is the appropriate contribution from the $v'\rightarrow v''$ transition to each of $\bar{r}_{v'}$ and $\bar{r}_{v''}$.

An alternative form for $\bar{r}_{v'v''}$ to equation (4) may be readily derived by expansion of $\psi_{v'}$ in the numerator of this equation as an orthogonal series of $\psi_{w''}$ as in equation (10). Thus

$$\bar{r}_{v'v''} = \frac{\sum_{w''}(v', w'')(v'', rw'')}{(v', v'')} \qquad \ldots\ldots(14)$$

where

$$(v'', rw'') = \int \psi_{v''} r \psi_{w''} dr. \qquad \ldots\ldots(15)$$

The implications of equation (14) are discussed in the next section.

An array of r-centroids for a band system is a set of discrete values of r over the range experienced by the molecule in all the levels of both potentials. It has been found that the r-centroids vary slowly from band to band of a system following the extension in r of $\psi_{v'}\psi_{v''}$.

† Fraser (1954b) has discussed the application of equations (9) and (10) to the evaluation of Franck–Condon factors $q_{v'v''} = (v', v'')^2$.

§ 3. The Evaluation of r-Centroids

The methods so far developed for the evaluation of r-centroids are: 1, direct methods, 2, mean-value method, 3, difference method.

1. *Direct Methods*

Direct application of equation (4) is the most obvious method of evaluation of an array of r-centroids. This presupposes knowledge of $\psi_{v'}$ and $\psi_{v''}$ either in numerical form or in such an analytic form that the integrals may be evaluated. The numerical approach is very tedious although it was used originally. The analytic approach is also possible by an approximate method (Fraser and Jarmain 1953, Jarmain and Fraser 1953, Fraser 1954 c) which allows the evaluation of the integrals $\int\psi_{v'}r\psi_{v''}dr$ and $\int\psi_{v'}\psi_{v''}dr$ for Morse potentials. The methods described below, however, are easier to apply.

The same analytic methods are available for evaluation of the integrals (v', w'') and (v', v'') in equation (14). Other methods (e.g. Fraser 1954 b) may be used to evaluate the integrals (v'', rw'') in this equation. No direct application of this equation has yet been made, however, as the methods described below have been entirely adequate for the band systems studied. Equation (14) would nevertheless probably afford a useful method for band systems whose Condon parabolae were sufficiently narrow that the major contribution in the sum over w'' is vested in a few terms yet not so narrow that the condition $|r_{c1}-r_{c2}|<0{\cdot}01$Å is invalidated.

2. *The Mean Value Method*

The reduced one-dimensional Schrödinger equations which describe the molecule in levels v' and v'' respectively lead readily to the relation

$$(E_{v'}-E_{v''})\int\psi_{v'}\psi_{v''}dr=\int\psi_{v'}[V_1(r)-V_2(r)]\psi_{v''}dr \qquad \ldots\ldots(16)$$

where $V_1(r)$ and $V_2(r)$ are the potentials of the upper and lower states respectively and $E_{v'}$ and $E_{v''}$ are the vibrational energies concerned. As $V_1(r)-V_2(r)$ is a slowly and smoothly varying function of r over the significant range of integration it follows from equations (7) and (16) that

$$E_{v'}-E_{v''}=V_1(\bar{r}_{v'v''})-V_2(\bar{r}_{v'v''}). \qquad \ldots\ldots(17)$$

If, as is often true, V_1 and V_2 may be adequately represented by Morse functions, equation (17) becomes

$$E_{v'}-E_{v''}=D_1[1-\exp\{-\alpha_1(\bar{r}_{v'v''}-r_{e1})\}]^2-D_2[1-\exp\{-\alpha_2(\bar{r}_{v'v''}-r_{e2})\}]^2 \qquad \ldots\ldots(18)$$

which may be solved for $\bar{r}_{v'v''}$. In equation (18)

$$D=\omega_e{}^2/4(\omega_e x_e), \qquad E_v=\omega_e(v+\tfrac{1}{2})-(\omega_e x_e)(v+\tfrac{1}{2})^2 \ldots\ldots(19)$$

The symbols have their conventional spectroscopic meanings (Herzberg 1950). Equation (18) is suitable for evaluation of r-centroids in many cases. Two methods for its solution will be discussed.

(*a*) *The graphical method.* The right-hand side of equation (18) may be computed and plotted as a function of r over the significant range of r. Similarly the difference between $E_{v'}$ and $E_{v''}$ on the left-hand side of the equation may be calculated for each band of the system. Values of $\bar{r}_{v'v''}$ appropriate to these energy differences may then be read from the graph. It has been found that $\bar{r}_{00}$ is usually slightly greater than $(r_{e1}+r_{e2})/2$ for systems whose potentials are not very anharmonic.

(*b*) *The quadratic equation method.* Equation (18) may be considered as a quadratic equation in $x = \exp(-\alpha \bar{r}_{v'v''})$ after a simple approximation has been applied. This approximation is the replacement of α_1 and α_2 by a mean α (preferably the arithmetic mean) together with equivalent adjustment of all α-dependent parameters. The same approximation has also been employed in methods for the analytical determination of Franck–Condon factors (Fraser and Jarmain 1953, Jarmain and Fraser 1953, Fraser 1954 c). The approximate form of equation (18) is then

$$E_{v'}' - E_{v''}' = D_1'[1 - \exp\{-\alpha(\bar{r}_{v'v''} - r_{e1})\}]^2 - D_2'[1 - \exp\{-\alpha(\bar{r}_{v'v''} - r_{e2})\}]^2 \quad \ldots\ldots(20)$$

where primed quantities have been adjusted with respect to α.

Equation (20) is equivalent to

$$Px^2 - 2Qx + R_{v'v''} = 0 \quad \ldots\ldots(21)$$

where

$$\left.\begin{aligned} P &= F_1^2 D_1' - F_2^2 D_2', & F_1 &= \exp(\alpha r_{e1}) \\ Q &= F_1 D_1' - F_2 D_2', & F_2 &= \exp(\alpha r_{e2}) \\ R_{v'v''} &= D_1' - D_2' - (E_{v'}' - E_{v''}'), & x &= \exp(-\alpha \bar{r}_{v'v''}) \end{aligned}\right\} \quad \ldots\ldots(22)$$

Equation (21) has two roots of which often one (x_1) is positive and the other (x_2) is negative. Thus

$$\bar{r}_{v'v''} = -\frac{1}{\alpha} \ln x_1. \quad \ldots\ldots(23)$$

An array of *r*-centroids may be determined by solving equation (21) as a quadratic and interpreting each positive root according to equation (23). In cases where both roots are positive, the physically meaningful $\bar{r}_{v'v''}$ is that which lies within the range r_{e1}, r_{e2} or in the neighbourhood thereof. When both roots are negative or complex, the conditions under which equation (7) holds do not obtain. Thus neither equation (20), nor its more general form, equation (17), follows from equation (16) and the quadratic equation method is not applicable.

The difference between values of $\bar{r}_{v'v''}$ derived from equations (18) and (20) is small (less than 1%) when $\Delta v = v' - v''$ is less than about five, for a system where the use of a mean α is a small distortion, e.g. N_2 First Positive System.

3. *The Difference Method*

During the development of the above methods it was observed that nearly linear trends existed in $\bar{r}_{v'v''}$ along *sequences* $\Delta v =$ constant. The constant difference in *r*-centroids along a sequence suggested that a further method of obtaining arrays of $\bar{r}_{v'v''}$ would be to compute the value for the leading member of each sequence by, say, the quadratic equation method, and then successively to apply the appropriate constant difference to build up the rest of the sequence.

An expression for this approximately constant difference may be derived as follows:

Let $\bar{r} = \bar{r}_{v'v''}$, $\alpha = \frac{1}{2}(\alpha_1 + \alpha_2)$ and let all α-dependent quantities be adjusted suitably. Using the standard expressions for the vibrational energies of the v', v'', $v'+1$, $v''+1$ levels it is easily found that

$$(E_{v'+1} - E_{v''+1}) - (E_{v'} - E_{v''}) = \omega_e' - \omega_e'' - 2\Delta v \omega_e x_e = W, \text{ say.} \quad \ldots\ldots(24)$$

Now in Morse potentials

$$E_{v'+1}-E_{v''+1}=D_1[1-F_1\exp(-\alpha\bar{r}_1)]^2-D_2[1-F_2\exp(-\alpha\bar{r}_1)]^2 \quad \ldots\ldots(25)$$

$$E_{v'}-E_{v''}=D_1[1-F_1\exp(-\alpha\bar{r})]^2-D_2[1-F_2\exp(-\alpha\bar{r})]^2 \quad \ldots\ldots(26)$$

where $\bar{r}_1=\bar{r}_{v'+1,\,v''+1}$. W is clearly the difference between right-hand members of equations (25) and (26).

For most systems so far examined $\bar{r}_1-\bar{r}\sim 0{\cdot}01$ Å. This difference depends basically upon the width of the potential curves, as the change $\bar{r}_1-\bar{r}$ in the r-centroid is determined by how much the wave functions are spread as quantum numbers are increased. $\bar{r}_1-\bar{r}$ would exceed 0·01 Å only if the potentials were very wide. For cases where $\bar{r}_1-\bar{r}$ is not much greater than 0·01 a good approximation is

$$\left.\begin{aligned} W=D_1[2F_1x\alpha(\bar{r}_1-\bar{r})-2F_1^2x^2\alpha(\bar{r}_1-\bar{r})] \\ -D_2[2F_2x\alpha(\bar{r}_1-\bar{r})-2F_2^2x^2\alpha(\bar{r}_1-\bar{r})]. \end{aligned}\right\} \quad \ldots\ldots(27)$$

This represents a first order approximation in

$$\exp\{-\alpha(\bar{r}_1-\bar{r})\} \qquad \text{and} \qquad \exp\{-2\alpha(\bar{r}_1-\bar{r})\}.$$

Thus

$$\bar{r}_1-\bar{r}=\Delta\bar{r}=\frac{W}{2\alpha x(Q-Px)}. \quad \ldots\ldots(28)$$

P, Q and x are defined in equations (22) above. Equation (28) enables a constant difference in r-centroids to be obtained for each sequence $\Delta v=$ constant. Data for the complete sequence can then rapidly be built up once $\bar{r}_{v'v''}$ for one member, usually the leading member, is known.

§ 4. Results

Tables 1–10 present arrays of $\bar{r}_{v'v''}$ and $\lambda_{v'v''}$ for the following band systems.

1. CN	Red	$A^2\Pi\rightarrow X^2\Sigma^+$	(Difference)	$r_{eA}=1.2327$ $r_{eX}=1{\cdot}1718$
2. N_2	Second Positive	$C^3\Pi_u\rightarrow B^3\Pi_g$	(Graphical)	$r_{eC}=1{\cdot}1482$ $r_{eB}=1{\cdot}2123$
3. N_2^+	First Negative	$B^2\Sigma_u^+\rightarrow X^2\Sigma_g^+$	(Graphical)	$r_{eB}=1{\cdot}075$ $r_{eX}=1{\cdot}116$
4. N_2	First Positive	$B^3\Pi_g\rightarrow A^3\Sigma_u^+$	(Graphical)	$r_{eB}=1{\cdot}2123$ $r_{eA}=1{\cdot}293$
5. CN	Violet	$B^2\Sigma^+\rightarrow X^2\Sigma^+$	(Direct Numerical)	$r_{eB}=1{\cdot}1506$ $r_{eX}=1{\cdot}1718$
6. C_2	Swan	$A^3\Pi_g\rightarrow X^3\Pi_u$	(Quadratic)	$r_{eA}=1{\cdot}2660$ $r_{eX}=1{\cdot}3117$
7. NO	γ	$A^2\Sigma^+\rightarrow X^2\Pi$	(Quadratic)	$r_{eA}=1{\cdot}0637$ $r_{eX}=1{\cdot}1508$
8. OH	Violet	$A^2\Sigma^+\rightarrow X^2\Pi$	(Difference)	$r_{eA}=1{\cdot}0121$ $r_{eX}=0{\cdot}9706$
9. O_2	Schumann–Runge	$B^3\Sigma_u^-\rightarrow X^3\Sigma_g^-$	(Graphical)	$r_{eB}=1{\cdot}604$ $r_{eX}=1{\cdot}2074$
10. O_2	Herzberg	$A^3\Sigma_u^+\rightarrow X^3\Sigma_g^-$	(Graphical)	$r_{eA}=1{\cdot}521$ † $r_{eX}=1{\cdot}2074$

† The value of r_{eA} for the Herzberg system is that recommended by Pillow (1953).

The above values of r_e (Herzberg 1950) are in ångström units and the method used in each case is indicated.

Tables 1 and 2 are each presented as a conventional v'–v'' array and, as illustrated in figures 1 and 2, are examples of the two forms of behaviour of $\bar{r}_{v'v''}$ with $\lambda_{v'v''}$ which are discussed more fully in the next section. To conserve space however, tables 3–10 inclusive are presented in an abbreviated form. Entries of $\bar{r}_{v'v''}$ and $\lambda_{v'v''}$ are made for each of the leading members of the sequences usually $(0, v'')$ or $(v', 0)$. The constant difference $\Delta\bar{r}$ for each sequence (equation (28)) is also given where known so that the reader may rapidly construct a more complete table for himself. The third figure after the decimal point quoted for each $\bar{r}_{v'v''}$ in these tables is, of course, only suggestive of trends. This implies that $\bar{r}_{v'v''}$ is probably correct to one percent. The wavelengths were taken from the compilations of Pearse and Gaydon (1951) and Rosen (1952). These wavelengths were usually of the band heads. However, for the CN Red and OH Violet

Table 1. *r*-Centroids and Wavelengths: CN Red Band System

v' \ v''	0	1	2	3	4	5	6
0	1·204						
	9140·5						
1	1·166	1·211					
	7874	9393					
2	1·131	1·172					
	6927·6	8067					
3	1·099	1·138	1·179				
	6191·7	7119	8272				
4	1·071	1·106	1·144	1·185			
	5606·7	6332·2	7259	8485			
5	1·043		1·113	1·150	1·192		
	5129·7		6478·7	7435	8708		
6	1·019			1·119			
	4732·7			6631·6			
7					1·125		
					6792·5		
8						1·132	
						6961	
9							
10							1·111
							6432·7

Upper figure $\bar{r}_{v'v''}$, lower figure $\lambda_{v'v''}$.

Table 2. *r*-Centroids and Wavelengths: N_2 Second Positive Band System

v' \ v''	0	1	2	3	4	5	6	7	8	9
0	1·182	1·148	1·116	1·086	1·058					
	3371·3	3576·9	3804·9	4059·4	4344					
1	1·228	1·189	1·154	1·122	1·092	1·065	1·039	1·014		
	3159·3	3339	3536·7	3755·4	3998·4	4269·7	4574	4916·8		
2	1·280	1·234	1·195	1·160	1·129	1·099	1·072	1·046	1·021	
	2976·8	3136	3309	3500·5	3710·5	3943	4200·5	4490·2	4814·7	
3	1·344	1·287	1·241	1·202	1·166	1·135	1·106	1·079	1·054	1·032
	2819·8	2962	3116·7	3285·3	3469	3671·9	3894·6	4141·8	4416·7	4723·3
4	1·426	1·351	1·294	1·247	1·208	1·173	1·141	1·113	1·086	1·061
		2814·3	2953·2	3104	3268·1	3446	3641·7	3857·9	4094·8	4355

Upper figure $\bar{r}_{v'v''}$, lower figure $\lambda_{v'v''}$.

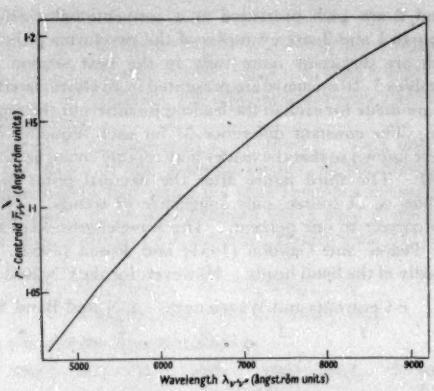

Figure 1. Variation of r-centroid with wavelength for the CN Red($A^2\Pi \rightarrow X^2\Sigma^+$) band system. $r_{eA}=1{\cdot}2327$ Å, $r_{eX}=1{\cdot}1718$ Å.

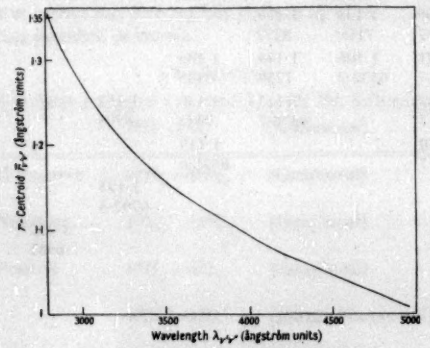

Figure 2. Variation of r-centroid with wavelength for the N_2 Second Positive ($C^3\Pi_u \rightarrow B^3\Pi_g$) band system. $r_{eC}=1{\cdot}1482$ Å, $r_{eB}=1{\cdot}2123$ Å.

systems wavelengths of R_2 branch heads are quoted and wavelengths of P_2 branch heads are quoted for the NO γ bands. $\bar{r}_{v'v''}$ and $\lambda_{v'v''}$ are both expressed in ångström units.

Comparison between the calculated values of $\bar{r}_{v'v''}$ of a band system and the ranges of r between the classical turning points for each of the levels v' and v'' has shown that $\bar{r}_{v'v''}$ lies within, or close to, the region which is common to both ranges.

It may be noted from equations (4) and (6) that an array of $|\int\psi_{v'}r\psi_{v''}dr|^2$, or in general of $|\int\psi_{v'}r^m\psi_{v''}dr|^2$ may readily be computed, if required, from arrays of $q_{v'v''}$ and $\bar{r}_{v'v''}$.

Table 3. *r*-Centroids and Wavelengths: N_2^+ First Negative Band System

Band	$\lambda_{v'v''}$	$\bar{r}_{v'v''}$	$\Delta\bar{r}$
$0 \rightarrow 0$	3914·4	1·097	0·004
$0 \rightarrow 1$	4278·1	1·053	0·004
$0 \rightarrow 2$	4709·3	1·013	0·004
$0 \rightarrow 3$	5228·3	0·974	0·006
$1 \rightarrow 0$	3582·1	1·159	0·004
$2 \rightarrow 0$	3308	1·265	—

Table 4. *r*-Centroids and Wavelengths: N_2 First Positive Band System

Band	$\lambda_{v'v''}$	$\bar{r}_{v'v''}$	$\Delta\bar{r}$
$0 \rightarrow 0$	10387	1·255	0·007
$0 \rightarrow 1$	12211	1·222	0·007
$0 \rightarrow 2$	14375	1·193	0·007
$1 \rightarrow 4$	17199	1·173	0·007
$5 \rightarrow 9$	16948	1·177	0·007
$1 \rightarrow 0$	8851	1·297	0·007
$2 \rightarrow 0$	7694	1·346	0·007
$3 \rightarrow 0$	6824	1·403	0·007
$4 \rightarrow 0$	6171	1·469	0·007
$5 \rightarrow 0$	5633	1·552	0·008

Table 5. *r*-Centroids and Wavelengths: CN Violet Band System

Band	$\lambda_{v'v''}$	$\bar{r}_{v'v''}$	$\Delta\bar{r}$
$0 \rightarrow 0$	3883·4	1·166	0·010
$0 \rightarrow 1$	4216	1·046	0·000
$0 \rightarrow 2$	4606·1	0·966	0·016
$1 \rightarrow 0$	3590·4	1·291	0·014
$3 \rightarrow 1$	3333	1·556	—

Table 6. *r*-Centroids and Wavelengths: C_2 Swan Band System

Band	$\lambda_{v'v''}$	$\bar{r}_{v'v''}$	$\Delta\bar{r}$
$0 \rightarrow 0$	5165·2	1·292	0·006
$0 \rightarrow 1$	5635·5	1·229	0·005
$0 \rightarrow 2$	6191·2	1·171	0·006
$0 \rightarrow 3$	6852	1·110	0·007
$1 \rightarrow 0$	4737·1	1·379	0·006

Table 7. *r*-Centroids and Wavelengths: NO γ Band System

Band	$\lambda_{v'v''}$	$\bar{r}_{v'v''}$	$\Delta\bar{r}$
$0 \rightarrow 0$	2262·8	1·107	0·006
$0 \rightarrow 1$	2363·3	1·080	0·005
$0 \rightarrow 2$	2471·1	1·067	0·005
$0 \rightarrow 3$	2587·5	1·049	0·005
$0 \rightarrow 4$	2713·2	1·031	0·006
$0 \rightarrow 5$	2849·8	1·015	0·005
$0 \rightarrow 6$	2997·6	1·000	0·005
$0 \rightarrow 7$	3171	0·984	0·006
$0 \rightarrow 8$	3376	0·968	0·006
$1 \rightarrow 10$	3459	0·963	0·005
$1 \rightarrow 0$	2152	1·135	0·006
$2 \rightarrow 0$	2047·5	1·165	0·005
$3 \rightarrow 0$	1956·1	1·196	—

Table 8. r-Centroids and Wavelengths: OH Violet Band System

Band	$\lambda_{v'v''}$	$\bar{r}_{v'v''}$	$\Delta\bar{r}$
$0 \rightarrow 0$	3063·6	1·01	0·04
$0 \rightarrow 1$	3428·1	1·27	0·03

Table 9. r-Centroids and Wavelengths: O_2 Schumann–Runge Band System

Band	$\lambda_{v'v''}$	$\bar{r}_{v'v''}$	Band	$\lambda_{v'v''}$	$\bar{r}_{v'v''}$
$0 \rightarrow 0$	2026	1·372	$8 \rightarrow 0$	1845·8	1·327
$1 \rightarrow 0$	1997·5	1·365	$9 \rightarrow 0$	1830·1	1·323
$2 \rightarrow 0$	1971·4	1·359	$10 \rightarrow 0$	1815·6	1·318
$3 \rightarrow 0$	1946·7	1·353	$11 \rightarrow 0$	1803·1	1·314
$4 \rightarrow 0$	1923·5	1·348	$12 \rightarrow 0$	1792	1·310
$5 \rightarrow 0$	1901·9	1·343	$13 \rightarrow 0$	1782·3	1·306
$6 \rightarrow 0$	1881·7	1·337	$14 \rightarrow 0$	1774·3	1·302
$7 \rightarrow 0$	1863	1·332	$15 \rightarrow 0$	1767·7	1·298

Table 10. r-Centroids and Wavelengths: O_2 Herzberg Band System

Band	$\lambda_{v'v''}$	$\bar{r}_{v'v''}$	$\Delta\bar{r}$
$0 \rightarrow 6$	3840	1·448	0·008
$0 \rightarrow 7$	4064	1·467	0·007
$0 \rightarrow 8$	4309	1·486	—
$0 \rightarrow 9$	4577	1·506	—
$0 \rightarrow 10$	4880	1·527	—
$1 \rightarrow 5$	3542	1·422	0·007
$1 \rightarrow 6$	3734	1·438	0·008
$2 \rightarrow 4$	3285	1·399	0·007
$2 \rightarrow 5$	3453	1·414	0·007
$3 \rightarrow 2$	2931	1·365	0·007
$3 \rightarrow 3$	3066	1·378	0·008
$3 \rightarrow 4$	3211	1·392	0·008
$4 \rightarrow 2$	2873	1·360	0·007
$5 \rightarrow 2$	2820	1·355	0·008
$6 \rightarrow 2$	2775	1·351	0·007
$7 \rightarrow 1$	2622	1·336	—
$7 \rightarrow 2$	2734	1·347	—

§ 5. Relationship between r-Centroid and Wavelength

As will be seen in tables 1–10, $\bar{r}_{v'v''}$ varies systematically from band to band of a system following the extension in r of $\psi_{v'}\psi_{v''}$. The band wavelengths also vary in a systematic way from band to band, and thus a relationship may be expected between wavelength and r-centroid. If r-centroids are plotted as a function of wavelength for the band systems of tables 1–10, smooth curves are in fact obtained. In some of them $\bar{r}_{v'v''}$ is an increasing function of $\lambda_{v'v''}$, while in others $\bar{r}_{v'v''}$ is a decreasing function of $\lambda_{v'v''}$. Examples of both types of behaviour are shown respectively in figures 1 and 2 for the CN Red and the N_2 Second Positive systems.

The dependence of $\bar{r}_{v'v''}$ upon wavelength or wave number may be shown analytically as follows: It will be recalled that $R_{v'v''}$ is defined in equations (22) as $D_1' - D_2' - (E_{v'}' - E_{v''}')$. To a high degree of approximation

$$E_{v'}' - E_{v''}' = E_0' - E_0'' + \nu_{v'v''} - \nu_{00}. \qquad \ldots\ldots(29)$$

E_0' and E_0'' are the adjusted vibrational energies of the zeroth vibrational levels of the upper and lower states. $\nu_{v'v''}$ and ν_{00} are the wave numbers of the $v'\rightarrow v''$ and $0\rightarrow 0$ bands.

Thus equation (21) may be written

$$Px^2-2Qx+S=1/\lambda_{v'v''}=\nu_{v'v''} \qquad \ldots\ldots(30)$$

where $S=D_1'-D_2'-E_0'+E_0''+1/\lambda_{00}$, and $x=\exp(-\alpha\bar{r}_{v'v''})$. Equation (30) shows how the wavelength and r-centroid of a band are related. The two forms of variation of $\bar{r}_{v'v''}$ with wavelength mentioned above are consistent with this equation. $\bar{r}_{v'v''}$ increases or decreases as λ increases according as $r_{e1}>r_{e2}$ or $r_{e1}<r_{e2}$. This may be shown as follows.

Equation (30) provides in general two sets of values of x corresponding to a known series of $\lambda_{v'v''}$, one set arising from each limb of the parabola. The valid array of $\bar{r}_{v'v''}$ arises from the limb which covers the range of r including r_{e1} and r_{e2}. The variation of $\bar{r}_{v'v''}$ with $\lambda_{v'v''}$ will then be monotonic, and the sign of the slope of the appropriate limb of the curve will determine whether $\bar{r}_{v'v''}$ is an increasing or a decreasing function of $\lambda_{v'v''}$. From equation (30) the slope $d\nu_{v'v''}/dx$ is readily seen to be $2(Px-Q)$. From equations (22)

$$Px-Q=D_2'\exp(\alpha r_{e2})\{1-\exp[\alpha(r_{e2}-r_{e1})]\} \qquad \ldots\ldots(31)$$

where $x=\exp(-\alpha r_{e1})$ for convenience.

Thus $d\nu_{v'v''}/dx$ is negative when $r_{e1}<r_{e2}$ and is positive when $r_{e1}>r_{e2}$. The sign of $d\lambda_{v'v''}/d\bar{r}_{v'v''}$ obviously obeys the same conditions. When $x=\exp(-\alpha r_{e2})$ the same conclusions are drawn.

For the band systems of tables 1–10, $\bar{r}_{v'v''}$ increases with $\lambda_{v'v''}$ for the CN Red, OH Violet, O_2 Schumann–Runge and O_2 Herzberg systems, in all of which $r_{e1}>r_{e2}$. For the other six systems $\bar{r}_{v'v''}$ decreases as $\lambda_{v'v''}$ increases and $r_{e1}<r_{e2}$. Any small scatter about a smooth curve which is noted on large scale plots of $\bar{r}_{v'v''}$ against $\lambda_{v'v''}$ made from tables 1–10 may possibly be attributed to the band-head wavelength (which has usually been employed) not being a comparable average for the band to the r-centroid.

The smooth relationship between r-centroids and wavelengths should provide a useful bridge between experimental measurements, which are often expressed as a function of wavelength, and theoretical studies, which are often made in terms of internuclear separation.

§ 6. Conclusions

The concept of the r-centroid $\bar{r}_{v'v''}$ of a band which has been introduced enables an average internuclear separation to be assigned to each band of a system.

A variety of straightforward methods is available to determine the r-centroids. Knowledge of $\bar{r}_{v'v''}$ for a band enables measured molecular quantities (e.g. intensity, wavelength, transition probability) associated with the $v'\rightarrow v''$ transition also to be associated with a specific internuclear separation. In particular, Nicholls (1956) discusses one way in which the variation of electronic transition moment with internuclear separation may be studied by using r-centroids, intensities and transition probabilities of molecular bands.

Acknowledgments

The authors would like to acknowledge much helpful discussion and correspondence on this subject with Dr. P. A. Fraser. They would also like

to acknowledge the assistance of Dr. R. G. Turner and Mr. L. M. Hyde with some of the computations.

This work has been made possible through the support of the Air Force Cambridge Research Centre by Contract No. AF19(122)–470.

References

Condon, E. U., 1928, *Phys. Rev.*, **32,** 858.

Fraser, P. A., 1954a, *Canad. J. Phys.*, **32,** 515 ; 1954b, *Scientific Report No.* 16, Dept. of Physics, University of Western Ontario ; 1954c, *Proc. Phys. Soc.* A, **67,** 939.

Fraser, P. A., and Jarmain, W. R., 1953, *Proc. Phys. Soc.* A, **66,** 1145.

Herzberg, G., 1950, *Molecular Spectra and Molecular Structure.* Vol. I, 22nd Edn (New York : D. Van Nostrand).

Jarmain, W. R., and Fraser, P. A., 1953, *Proc. Phys. Soc.* A, **66,** 1153.

Pearse, R. W. B., and Gaydon, A. G., 1951, *The Identification of Molecular Spectra*, 2nd Edn (London : Chapman and Hall).

Pillow, M. E., 1953, *Proc. Phys. Soc.* A, **66,** 1064.

Rosen, B. (Ed.), 1952, *Données Spectroscopiques Concernant Les Molecules Diatomiques* (Paris : Herman et Cie).

The Cross Section and Angular Distributions of the D–D Reactions between 40 and 90 keV

By D. L. BOOTH, G. PRESTON and P. F. D. SHAW
The Clarendon Laboratory, Oxford

MS. received 23rd September 1955

Abstract. A thin gas target was used for measurements of the cross sections and angular distributions of the ^{3}He and ^{3}H disintegration products at bombarding energies of 52 and 87 kev, two symmetrically placed proportional counters being used as detectors. The angular range covered was from 18° to 150° in the laboratory coordinate frame. In addition, the ratio of the differential cross sections of the reactions was measured for a laboratory angle of 48° at bombarding energies of 39 and 65 kev.

The results obtained are consistent with earlier measurements using the same technique, and show that the neutron-producing reaction has the greater anisotropy, and that the ratio of the total cross sections is energy dependent.

§ 1. Introduction

The angular distributions of the neutron and proton reactions D(d,n)^{3}He and D(d,p)^{3}H can be expressed in the form

$$\frac{d\sigma(\theta)}{d\omega} = \frac{d\sigma(\pi/2)}{d\omega}\{1 + A\cos^2\theta + B\cos^4\theta + \ldots\}$$

where $d\sigma(\theta)/d\omega$ is the differential cross section per steradian at the gravicentric angle θ. Below 200 kev terms of higher order than $\cos^2\theta$ have been assumed to be insignificant (see Preston, Shaw and Young 1954).

Below 100 kev values for the asymmetry coefficient and cross section for the proton reaction have been obtained by Huntoon, Ellett, Bayley and Van Allen (1940), Bretscher, French and Seidl (1948), Moffatt, Roaf and Sanders (1952), Wenzel and Whaling (1952), and Davenport, Jeffries, Owen, Price and Roaf (1953).

Measurements by Bartholdson (1951), Baker and Waltner (1952), Timm, Neuert and Elsner (1954), and Fuller and Ralph (1955) show that the asymmetry of the two reactions is similar, but Eliot, Roaf and Shaw (1953), and Preston (unpublished), using gas target techniques, found a greater anisotropy for the neutron reaction; their results for the proton reaction were consistent with the distributions of other authors. A similar disagreement has been found at higher energies (Preston *et al.* 1954).

The present work was undertaken to provide results between those of the latter authors and of Eliot *et al.* (1953).

§ 2. Apparatus

A transformer with a half-wave rectifying circuit supplied the accelerating voltage, which was measured by comparing it with the e.m.f. of a Weston cadmium cell, by means of a resistance chain. The uncertainty in the calibration of this

voltmeter was estimated to be 0·25%. The 50 c/s ripple voltage varied between 120 and 180 v peak to peak, depending on the current taken from the generator. The accelerating voltage was controlled to within ± 50 v of the mean value.

The deuterium-ion beam from a radio-frequency ion source was analysed by an 11° magnetic analyser, and the D^+ ions were allowed to enter the gas target. This target, fully described in a previous paper (Preston *et al.* 1954), consisted of a cylindrical volume across a diameter of which the beam was accurately collimated. The target gas pressure was measured with a McLeod gauge and the beam current by the calorimetric method used previously.

Two proportional counters were used to count disintegration products at angles symmetrical with respect to the beam direction, their plane of rotation containing the plane of magnetic deflection of the beam. In the plane normal to this, another similar proportional counter was placed at a fixed angle of 90° with respect to the beam, and used as a monitor. If the mean count of the two rotatable counters is normalized to a standard monitor count, this arrangement is insensitive to a first order to beam movement due to change of beam energy, but is sensitive to displacement towards the monitor counter. To detect such displacements the calorimeter was modified; it was constructed with two slightly overlapping semi-circular copper heads which were supported on copper stems from a common water-cooled base. The cross sectional areas of the stems were adjusted relative to their lengths so that the thermal resistance of the stems, and hence the sensitivities of the calorimeters, were equal. Constantan wires were soldered to the heads of the calorimeter and the e.m.f's of the thermocouples so formed were opposed, so that any difference was detected by a sensitive galvanometer. A 0·1 mm movement of the beam towards the monitor counter, which would increase the counting rate by 0·35%, would produce a 6% change in the ratio of the rate of production of heat in the calorimeter heads. During measurements, the maximum off-balance current observed corresponded to a change in the monitor counting rate of 0·05% at 87 kev and 0·17% at 52 kev.

The voltage pulses from the proportional counters were fed through cathode followers and pulse-shaping circuits to linear amplifiers. Pulse height discriminators with integral scalers and a single-channel pulse height analyser were used for the identification and separation of the output pulses due to ^3He, ^3H, ^1H and scattered D particles in the counters. Thin foils in front of the counter windows were used to remove the more heavily ionizing ^3He and the low energy D particles from the counters when detecting ^3H particles. The counts due to the neutron flux through the counters were estimated by placing thick absorbers in front of the counter windows.

§ 3. Angular Distributions

The response of each proportional counter to ^3He particles had been previously investigated by taking a differential pulse height spectrum, with background subtracted, at 300 kev bombarding energy; it was shown that an integral bias could be chosen so that 99·9% of the ^3He pulses were greater than this bias. At each angle, the position of this bias was redetermined by using the single channel pulse height analyser; the accuracy of the redetermination was such that the errors in the number of ^3He and ^3H counts were respectively ± 0·2% and ± 0·3%.

A beam was passed through the target containing deuterium gas at a pressure of about 150 microns of mercury, and with the integral biases set as above, the number

of ^{3}He particles entering the rotating counters was recorded; the number of counts obtained was normalized to the number of counts in the monitor counter. After a determination of the background, a count was made of the ^{3}H particles, with the monitor running under the same conditions.

Corrections were made to the recorded counts for the change of solid angle subtended by the counters at the beam when converting from laboratory to gravicentric coordinates, and also for the change in the length of the beam viewed by the counters through their collimating slits as their angle to the beam was altered.

The differential cross sections $d\sigma(\theta)/d\omega$ were calculated after the calibration of the monitor counter described in the next section, a range of angles from 18° to 150° to the beam in the laboratory system being covered. The asymmetry coefficient A for both reactions was found from a least squares fit to the formula

$$d\sigma(\theta)/d\omega = d\sigma(\pi/2)/d\omega\{1 + A\cos^2\theta\}.$$

The differential cross sections as a function of $\cos^2\theta$ are shown in figures 1 and 2. Despite the large change of gravicentric solid angle subtended by the counters

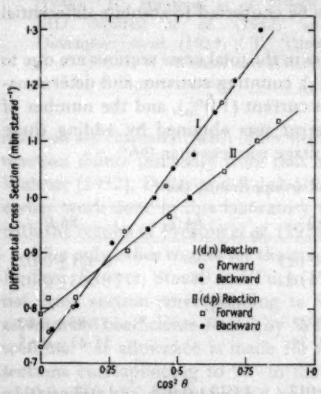

Figure 1. The differential cross sections at 87 kev as a function of $\cos^2\theta$.

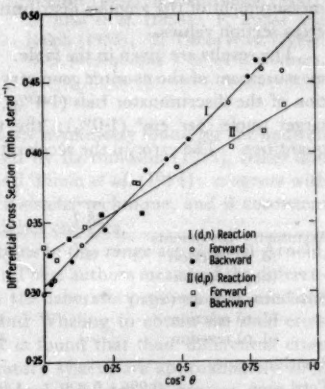

Figure 2. The differential cross sections at 52 kev.

at the beam, points in the forward and backward hemispheres show no systematic deviation from the curves. This is a necessary consequence of the symmetry of the D–D reactions, and affords a valuable test of the apparatus. The statistical errors of counting associated with the points shown in figures 1 and 2 are approximately $\pm 1{\cdot}5\%$. Errors due to the standardization of the monitor counter, and hence the absolute differential cross section scale, will be discussed later.

The errors for the asymmetry coefficients A in the table were calculated from the deviations of the individual points from the least squares fit.

§ 4. Cross Sections

The total cross sections for the reactions were obtained from the differential cross sections measured at 48° to the beam. Over the energy range investigated, the total cross section is close to 4π times the differential cross section at this angle,

which was chosen so that the corrections for the asymmetry of the reaction were small.

To obtain these differential cross sections, the beam current was measured by a previously calibrated calorimeter and the target gas pressure was reduced to 90 μ Hg. A sample of the gas was taken for mass spectrometric analysis.

The data of Reynolds, Dunbar, Wenzel and Whaling (1953) was used to make allowance for the energy loss of the beam in reaching the effective target volume, and also to correct the beam energy at the calorimeter. The currents used, which were about 120 and 200 μA at 87 and 52 kev respectively, were obtained from the observed heat dissipation in the calorimeter and the corrected beam energy. The gas temperature was taken to be that of the walls of the target chamber.

Counts were made of the ^{3}He particles at 52 kev and of the ^{3}H particles at 87 kev. In each case the gas pressure and temperature were recorded at 5 minute intervals and the calorimeter readings at 1 minute intervals, the duration of the experiments being approximately 1 hour. Meanwhile the monitor counter was run under its usual conditions, so enabling the counts taken during the measurement of the angular distributions to be converted to absolute differential cross section values.

The results are given in the table. Errors in the total cross sections are due to measurement of the counter geometry (2·3%), counting statistics and determination of the discriminator bias (1·4%), beam current (1·0%), and the number of target nuclei per cm^3 (1·0%); the total error was obtained by adding these quantities. The error in the accelerating voltage was less than 0·6%.

	Bombarding Energy (kev)			
	38·7	52·2	64·7	86·9
Asymmetry coefficients				
(d, n) reaction	—	0·654 ± 0·023	—	0·931 ± 0·026
(d, p) reaction	—	0·360 ± 0·023	—	0·503 ± 0·017
Total cross sections (mbn)				
(d, n) reaction	—	4·64 ± 0·27	—	11·85 ± 0·83
(d, p) reaction	—	4·59 ± 0·34	—	11·41 ± 0·65
Branching ratios				
Total σ_n/σ_p	0·996 ± 0·020	1·008 ± 0·017	1·030 ± 0·018	1·038 ± 0·013
$d\sigma_n/d\sigma_p$ at 90°	—	0·926 ± 0·014	—	0·925 ± 0·011

Ratios of the total cross sections, and of the differential cross sections at 90° were obtained from the least squares fits to the angular distribution data at 87 and 52 kev.

The total branching ratio of the reactions was also determined at 65 and at 39 kev by measuring the relative yields at 48° to the beam. The asymmetry coefficients used to convert the corrected counts to a ratio of total cross sections were obtained from the curves shown in figures 3 and 4. The errors in the ratios of the total cross sections include those due to the statistics of counting (about 1·2%), and the assumed asymmetry coefficients (0·1%).

§ 5. Discussion

The results in the table and figures 1 and 2 show that both the asymmetry and the total cross sections of the two D–D reactions are different.

The present results for the asymmetry coefficients, together with those of other authors, are shown in figures 3 and 4. The present data for the proton

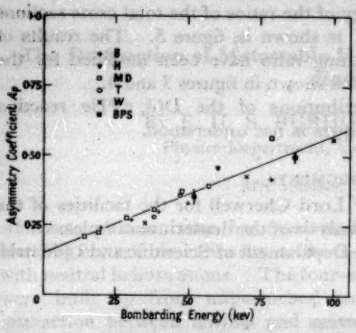

Figure 3. The asymmetry coefficient A_p for the (d, p) reaction as a function of bombarding energy. B, Bretscher *et al.* (1948); H, Huntoon *et al.* (1940); MD, Moffatt *et al.* (1952) and Davenport *et al.* (1953); T, Timm *et al.* (1954); W, Wenzel and Whaling (1952); BPS, present data.

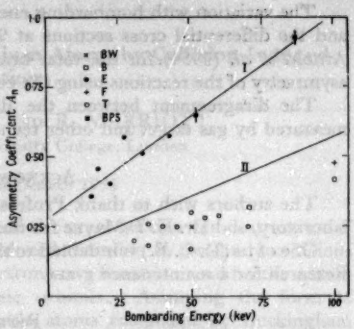

Figure 4. The asymmetry coefficient A_n for the (d, n) reaction as a function of bombarding energy. BW, Baker and Waltner (1952); B, Bartholdson (1951); E, Eliot *et al.* (1953); F, Fuller and Ralph (1955); T, Timm *et al.* (1954); BPS, present data. Curve I is arbitrary, curve II is the same as shown in figure 3.

reaction are consistent with other work, but the asymmetry found for the neutron reaction differs markedly from that observed by Bartholdson (1951), Baker and Waltner (1952), Fuller and Ralph (1955), and Timm *et al.* (1954); it agrees with earlier work done in this laboratory using a similar technique, and is consistent with the results of Preston *et al.* (1954) at higher energies.

The only other results for the cross sections in this range are those of Arnold, Phillips, Sawyer, Stovall and Tuck (1954). These authors measured the differential cross section corresponding to 90° in the laboratory system and used the asymmetry coefficients found by Wenzel and Whaling to obtain the total cross sections. If allowance is made for this, it is found that their differential cross sections corresponding to 90° in the laboratory system are approximately 10% greater than the corresponding quantities calculated from the present data.

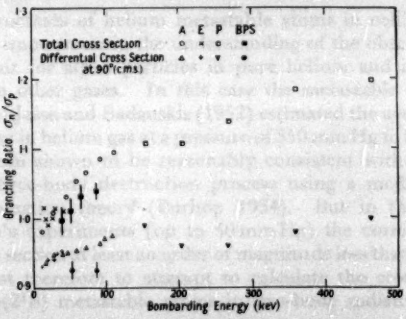

Figure 5. The branching ratios σ_n/σ_p as a function of bombarding energy. A, Arnold *et al.* (1954); E, Eliot *et al.* (1953); P, Preston *et al.* (1954); BPS, present data.

The variation with bombarding energy of the ratios of the total cross sections and the differential cross sections at 90° is shown in figure 5. The results of Arnold *et al.* (1954) for the total branching ratio have been modified for the asymmetry of the reactions using the curves shown in figures 3 and 4.

The disagreement between the distributions of the D(d, n)^{3}He reaction measured by gas target and other techniques is not understood.

Acknowledgments

The authors wish to thank Professor Lord Cherwell for the facilities of the laboratory, and Dr. K. I. Mayne for the analysis of the deuterium samples.

One of us (D. L. B.) is indebted to the Department of Scientific and Industrial Research for a maintenance grant.

References

Arnold, W. R., Phillips, J. A., Sawyer, G. A., Stovall, E. J., and Tuck, J. L., **1954**, *Phys. Rev.*, **93**, 483.

Baker, P., and Waltner, A., 1952, *Phys. Rev.*, **88**, 1213.

Bartholdson, I., 1951, *Ark. Fys.*, **2**, 271.

Bretscher, E., French, A. P., and Seidl, F. G. P., 1948, *Phys. Rev.*, **73**, 815.

Davenport, D. A., Jeffries, T. O., Owen, M. E., Price, F. V., and Roaf, D., 1953, *Proc. Roy. Soc.* A, **216**, 66.

Eliot, E. A., Roaf, D., and Shaw, P. F. D., 1953, *Proc. Roy. Soc.* A, **216**, 57.

Fuller, J. C., and Ralph, D. C., 1955, *Phys. Rev.*, **98**, 248.

Huntoon, R. D., Ellett, A., Bayley, D. S., and Van Allen, J. A., 1940, *Phys. Rev.*, **58**, 97.

Moffatt, J., Roaf, D., and Sanders, J. H., 1952, *Proc. Roy. Soc.* A, **212**, 220.

Preston, G., Shaw, P. F. D., and Young, S. A., 1954, *Proc. Roy. Soc.* A, **226**, 206.

Reynolds, H. K., Dunbar, D. N. F., Wenzel, W. A., and Whaling, W., 1953, *Phys. Rev.*, **92**, 742.

Timm, U., Neuert, H., and Elsner, B., 1954, *Z. Phys.*, **139**, 425.

Wenzel, W. A., and Whaling, W., 1952, *Phys. Rev.*, **88**, 1149.

The Destruction of Metastable Helium Atoms by Collision-Induced Radiation

By E. H. S. Burhop and R. Marriott
Physics Department, University College, London

MS. received 31*st October* 1955

Abstract. A calculation has been made of the cross section for destruction of He(2^1S) metastable atoms by collision-induced radiation in two-body collisions with neutral helium atoms. The four-electron wave functions used for the system were built up from unperturbed atomic orbitals. Assuming the form of interaction between normal and metastable atoms calculated by Buckingham and Dalgarno which exhibits a repulsive barrier of a height of 0·26 ev at separations greater than $2{\cdot}1 \times 10^{-8}$ cm, the calculated cross section was 9×10^{-26} cm^2 at a temperature of 300°K. However, even if no barrier was assumed the cross section increased only to 5×10^{-22} cm^2, still much too small to account for the value of 3×10^{-20} cm^2 measured by Phelps for the destruction cross section.

§ 1. Introduction

In some recent experiments using a very elegant optical absorption technique Phelps (1955) has studied the time variation of the concentration of helium metastable atoms in the afterglow of a discharge in helium. He has obtained striking evidence of the destruction of He(2^3S) metastable atoms in three-body collisions which result in the formation of $He_2(2^3\Sigma_u)$ molecules. Measurements of the destruction of He(2^1S) metastable atoms are more difficult to make because these metastable atoms are rapidly converted to the 2^3S state by super-elastic collisions with electrons in the afterglow. However, using afterglows with very low electron densities he has obtained data which seem to indicate that He(2^1S) metastable atoms are destroyed mainly in two-body collisions with other helium atoms. Under the conditions of his experiment at a gas temperature of 300°K Phelps obtained for the average cross section of this destruction process a value of 3×10^{-20} cm^2.

Destruction processes of helium metastable atoms in collision with normal helium are also of importance in the understanding of the observed values of the energy per ion pair for alpha particles in pure helium and in helium slightly contaminated with other gases. In this case the metastable atoms are mainly in the 2^1S state and Jesse and Sadauskis (1952) estimated the average cross section for their destruction in helium gas at a pressure of 850 mm Hg to be $1{\cdot}5 \times 10^{-20}$ cm^2. This value has been shown to be reasonably consistent with the cross section estimated for a three-body destruction process using a modified form of the Thomson recombination theory (Burhop 1954). But in the pressure range covered by Phelp's experiments (up to 50 mm Hg) the corresponding process would have a cross section at least an order of magnitude less than that he observed.

It is of interest therefore to attempt to calculate the cross section for the destruction of He(2^1S) metastable atoms in two-body radiative collisions with normal helium.

§ 2. Theory

The form of the interaction between He(2^1S) metastable atoms and normal He atoms has been calculated by Buckingham and Dalgarno (1952). Molecule formation is possible in the $2^1\Sigma_u$ state. Radiative transitions are then possible from this state to the ground $^1\Sigma_g$ state. If then a calculation is made of the transition rate to the dissociating ground state at different stages of a two-body collision between He(2^1S) and normal He, it is possible to estimate the average cross section for the destruction of such metastable atoms by collision-induced radiation.

Buckingham and Dalgarno showed the existence of a potential barrier in the interaction curve which would have to be surmounted to enable a close approach of the two atoms. Unfortunately they were not able to estimate exactly either the height ΔE or the critical separation r_c corresponding to the top of the potential barrier. They give for the interaction energy

$$U^*(r) = V_1(r) - C/r^6 \qquad \ldots\ldots (1)$$

where $V_1(r)$ is the interaction given by the first-order calculation which they carry out completely and C/r^6 is a polarization term. The value of the constant C, which is uncertain, has little effect on the separation r_c but a marked effect on the barrier height ΔE. The form of $V_1(r)$ is shown in figure 1.

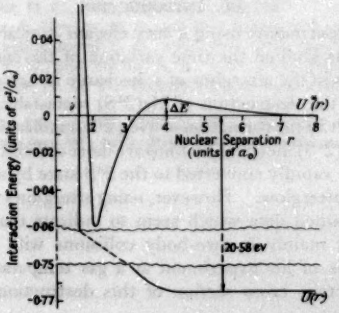

Figure 1. Radial variation of the interaction energy between He*(2^1S) and a normal He atom $U^*(r)$ and between two normal He atoms $U(r)$. The form of $U^*(r)$ is that given by Buckingham and Dalgarno for the $2^1\Sigma_u$ state and does not allow for polarization. It is called $V_1(r)$ in the text.

Account has to be taken of the actual path of the collision and the cross section obtained from a weighted average of the probability of transition during the impact averaged over all possible paths. This averaging was done using a method due to Bates (1951) who corrected an earlier calculation of Kramers and ter Haar (1946).

Let $U^*(r)$ be the interaction energy between the metastable and normal helium atoms when the separation between their nuclei is r and $U(r)$ the corresponding interaction energy between two normal helium atoms in the dissociating ground $^1\Sigma_g$ state of He_2. We suppose further that both normal and metastable atoms have the same temperature T.

Then assuming a Maxwellian distribution at temperature T it may be shown that (Kramers and ter Haar 1946)

$$\gamma = \frac{32\pi^2 g}{3c^3h^4}\left(\frac{M}{2\pi kT}\right)^{3/2}\int_0^\infty r^2(\mathfrak{C}(r))^2 I(r)\{U^*(r)-U(r)\}^3 dr \ldots \quad \ldots\ldots(2)$$

where
$$I(r) = \int_{v_{\min}}^{\infty} v\exp(-Mv^2/2kT) \times\left\{\left(v^2-\frac{2U^*(r)}{M}\right)^{1/2}-\left(v^2-\frac{2U^*(r)}{M}-\frac{v^2}{r^2}p_m^{\,2}\right)^{1/2}\right\}dv.. \quad \ldots\ldots(3)$$

M, the reduced mass of the system, is half the mass of a helium atom; v is the relative velocity of a normal and metastable atom, g is a statistical weighting factor. In this case $g=\frac{1}{2}$ since the initial state is either $2^1\Sigma_u$ or $2^1\Sigma_g$; $\mathfrak{C}(r)$ is the dipole moment corresponding to the transition to the $^1\Sigma_g$ ground state of the system when the separation is r; p_m is the maximum value of the impact parameter consistent with the chosen v and r; and γ is defined by the equation

$$\frac{dN^*}{dt} = -\gamma NN^*$$

where N is the number of ground state atoms cm^{-3} and N^* the number of metastable atoms cm^{-3}. It may easily be shown that the mean cross section for the destruction of He(2^1S) metastables and the coefficient γ are connected by the equation

$$\gamma = 2\sigma\left(\frac{2kT}{\pi M}\right)^{1/2} \qquad \text{assuming} \qquad N \gg N^*. \qquad \ldots\ldots(4)$$

Hence from (2) and (4)

$$\sigma = \frac{4\pi g}{3c^3h^4}\frac{M^2}{k^2T^2}\int_0^\infty r^2(\mathfrak{C}(r))^2 I(r)\{U^*(r)-U(r)\}^3 dr. \qquad \ldots\ldots(5)$$

For the interaction $U^*(r)$ two forms were used. Calculations were first carried out using

$$U^*(r) = V_1(r) \qquad \ldots\ldots(6)$$

i.e. neglecting the polarization term in the Buckingham and Dalgarno calculations. This certainly overestimates the height of the potential barrier. Calculations were also carried out using the following form for $U^*(r)$

$$\left.\begin{aligned} U^*(r) &= V_1(r), \qquad r<r_1 \\ U^*(r) &= 0, \qquad\quad r>r_1 \end{aligned}\right\} \qquad \ldots\ldots(7)$$

where r_1 is the larger zero of $V_1(r)$ (see figure 1). This neglects the effect of the potential barrier altogether. The magnitude of the mean cross section for an intermediate barrier height can then be estimated approximately by a suitable interpolation.

The limit $v_{\min}$ of the integration in (3) was taken as the greater of $(2\Delta E/M)^{1/2}$ and $(2U^*(r)/M)^{1/2}$ for a value of $r<r_c$. For $r>r_c$, $v_{\min}$ was taken as $(2U^*(r)/M)^{1/2}$. Some care is needed in deciding the value to be chosen for p_m the maximum impact parameter consistent with a given v and r. Since one obtains from the dynamics of the problem the relation

$$\frac{dr}{dt} = \left\{v^2-\frac{p^2v^2}{r^2}-\frac{2U^*(r)}{M}\right\}^{1/2}$$

earlier writers took

$$p_m^{\,2} = \left\{r^2-\frac{2U^*(r)r^2}{Mv^2}\right\} \qquad \ldots\ldots(8)$$

which ensures that $dr/dt=0$ at an internuclear separation r so that this should represent a perihelion point.

Bates pointed out however that if p is known, the value of r that makes dr/dt vanish is not uniquely determined, so that if for a given r, p_m is determined from (8), the given value of r may actually be inaccessible owing to the fact that dr/dt vanishes also for a larger value of r. This will in fact be the case if $U^*(r)$ falls off more rapidly than r^{-2}.

The value of p_m to be taken in (3) can be seen by reference to figure 2 which shows, for a number of different values of v, a plot of $r^2\{1-2V_1(r)/Mv^2\}$ against r^2. For a given value of v, if $r^2\{1-2V_1(r)/Mv^2\}$ passes through a minimum value ($=C^2$) when $r=b$ and if it again takes the value C^2 when $r=a(<b)$ then, following Bates, we must take $p_m=C$ for $a<r<b$; $p_m=r\{1-2V_1(r)/Mv^2\}^{1/2}$ for $r<a$ and $r>b$.

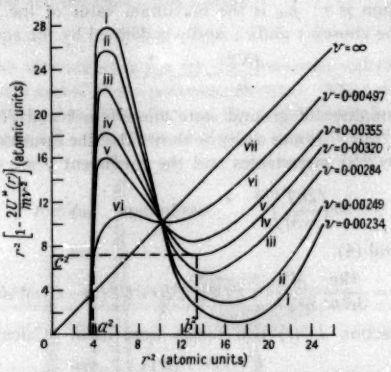

Figure 2. Plot of $r^2\left[1-\dfrac{2U^*(r)}{Mv^2}\right]$ against r^2 for different values of the velocity v. The following values of v (in 10^{-3} atomic units) are appropriate to the respective curves: (i) 2·34; (ii) 2·49; (iii) 2·84; (iv) 3·20; (v) 3·55; (vi) 4·97; (vii) ∞.

For the interaction energy $U(r)$ between two helium atoms in their ground states the expression $U(r)=21{\cdot}2(e^2/a_0)\exp(-2{\cdot}33r/a_0)$ due to Rosen (1950) was used. (e, a_0 are the electronic charge and radius of lowest Bohr orbit respectively).

§ 3. Calculation of the Dipole Moment

The major part of the calculation lies in the evaluation of $\mathfrak{C}(r)$.

Let Φ_i, Φ_f, be the total wave functions of the initial and final states of the system and $\mathbf{r}_m$ ($m=1, 2, 3, 4$) the position vectors of the electrons of the two atoms.

Then
$$\mathfrak{C}(r)=eN_fN_i\int\Phi_f^*(\mathbf{r}_1+\mathbf{r}_2+\mathbf{r}_3+\mathbf{r}_4)\Phi_i d\tau_{(1,2,3,4)} \qquad \ldots\ldots(9)$$

where the integration has to be taken over the coordinates of all four electrons and the integral sign is taken to include also summation over their spin coordinates. N_i, N_f are normalization factors for the initial and final states respectively.

The notation used in this calculation can be understood by reference to figure 3, where A and B are taken to denote the two nuclei and 1, 2, 3, 4 the four electrons The separation between the two nuclei is written as $2r_0$.

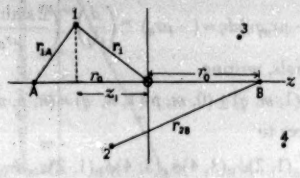

Figure 3.

For the initial $^1\Sigma_u$ state we write

$$\Phi_i = \frac{1}{2\sqrt{3}}(I - P_{AB})(I + P_{13}P_{24} - P_{13} - P_{24} - P_{14} - P_{23})\psi_A(1, 2)\phi_B(3, 4) \quad \ldots\ldots(10)$$

where I is the identity operator, P_{AB} a permutation operator that interchanges nuclei A and B, and P_{mn} a permutation operator that interchanges electrons m and n ($m, n = 1, 2, 3, 4$).

$\psi_A(1, 2)$, $\phi_B(3, 4)$ are respectively the wave functions for a helium atom in a metastable 2^1S state and the ground 1^1S state.

For the final $^1\Sigma_g$ ground state of the system we write

$$\Phi_f = \frac{1}{2\sqrt{3}}(I + P_{AB})(I + P_{13}P_{24} - P_{13} - P_{24} - P_{14} - P_{23})\psi_A(1, 2)\phi_B(3, 4). \quad \ldots\ldots(11)$$

The molecular wave functions $\psi_A(1, 2)$, $\phi_B(3, 4)$ were built up from unperturbed atomic orbitals.

Thus
$$\left.\begin{aligned} \phi_A(1, 2) &= \frac{1}{\sqrt{2}}(\alpha_1\beta_2 - \alpha_2\beta_1)a^A(1)a^A(2) \\ \psi_A(1, 2) &= \tfrac{1}{2}(\alpha_1\beta_2 - \alpha_2\beta_1)\{\bar{a}^A(1)b^A(2) + \bar{a}^A(2)b^A(1)\} \end{aligned}\right\} \quad \ldots\ldots(12)$$

where $a^A(1)$, $\bar{a}^A(1)$, $b^A(2)$, etc.... are functions given by Morse, Young and Haurwitz (1935), viz.

$$\left.\begin{aligned} a^A(m) &= \left(\frac{\mu^3 a^3}{\pi}\right)^{1/2} \exp(-\mu a r_{mA}) \\ \bar{a}^A(m) &= \left(\frac{\mu^3 \bar{a}^3}{\pi}\right)^{1/2} \exp(-\mu \bar{a} r_{mA}) \\ b^A(m) &= \left(\frac{\mu^5}{3\pi\nu}\right)^{1/2} \left\{ r_{mA} \exp(-\mu r_{mA}) - \left(\frac{3\lambda}{\mu}\right) \exp(-\mu b r_{mA}) \right\} \end{aligned}\right\} \quad \ldots\ldots(13)$$

and the functions $a^B(m)$, $\bar{a}^B(m)$, $b^B(m)$ are similarly defined.

The constants appearing in (13) are given by

$$\left.\begin{aligned} \mu a &= 1{\cdot}69/a_0 \qquad \lambda = 0{\cdot}59661 \\ \mu \bar{a} &= 2{\cdot}00/a_0 \qquad \nu = 0{\cdot}8866 \\ \mu b &= 1{\cdot}57/a_0 \qquad \mu = 0{\cdot}61/a_0 \end{aligned}\right\} \quad \ldots\ldots(14)$$

In calculating (9) above, having summed over the spins all the integrals may be evaluated by transforming to prolate spheroidal coordinates.

The component integrals are of the types

$$\left.\begin{aligned}(0,n,p)&=\int_1^\infty \xi^n \exp(-\mu r_0 p\xi)d\xi=(-\mu r_0)^{-n}\left(\frac{d}{dp}\right)^n\left(\frac{\exp(-\mu r_0 p)}{\mu r_0 p}\right)\\(1,m,q)&=\int_{-1}^1 \eta^m \exp(-\mu r_0 q\eta)d\eta=(-\mu r_0)^{-m}\left(\frac{d}{dq}\right)^m\left(\frac{2\sinh\mu r_0 q}{\mu r_0 q}\right).\end{aligned}\right\} \quad \ldots\ldots(15)$$

In terms of these integrals, writing

$$(0,n,p)(1,m,q)\pm(0,m,p)(1,n,q)=(n,p,m,q)^{\pm}$$

equation (9) then reduces to

$$\mathfrak{E}(r)=16eN_1N_f\begin{bmatrix}\int \phi_A(1,2)\psi_B(3,4)\phi_A(3,4)\phi_B(1,2)z_{(3)}d\tau_{(1,2,3,4)}\\-\int \phi_A(1,2)\psi_B(3,4)\phi_A(3,1)\phi_B(2,4)z_{(3)}d\tau_{(1,2,3,4)}\end{bmatrix} \quad \ldots\ldots(16)$$

$$\begin{aligned}&=\frac{256eN_1N_f}{(6\nu)^{1/2}}\mu^7a^6\bar{a}^{3/2}r_0^7[(0,2,2a)-\tfrac{1}{3}(0,0,2a)]\\&\times\Big\{r_0^6\mu^6a^3[(0,2,2a)-\tfrac{1}{3}(0,0,2a)][r_0(3,a+\bar{a},1,a-\bar{a})^-\\&\times\{(3,a+1,0,a-1)^+-(1,a+1,2,a-1)^+\}\\&+r_0(2,a+\bar{a},0,a-\bar{a})^-\{(4,a+1,1,a-1)^+-(2,a+1,3,a-1)^+\}\\&-\frac{3\lambda}{\mu}\{(2,a+b,0,a-b)^-(3,a+\bar{a},1,a-\bar{a})^-+(2,a+\bar{a},0,a-\bar{a})^-\\&\times(3,a+b,1,a-b)^-\}]-\frac{3}{\mu}\left[\frac{1}{(a+1)^4}-\frac{\lambda}{(a+b)^3}\right](3,a+\bar{a},1,a-\bar{a})^-\\&-\frac{r_0}{(a+\bar{a})^3}[(4,a+1,1,a-1)^+-(2,a+1,3,a-1)^+]\\&+\frac{3\lambda}{\mu(a+\bar{a})^3}(3,a+b,1,a-b)^-\Big\} \quad \ldots\ldots(17)\end{aligned}$$

where

$$N_1=\left[\int|\Phi_1|^2\,d\tau_{(1,2,3,4)}\right]^{-1/2} \quad \ldots\ldots(18)$$

has been calculated by Buckingham and Dalgarno (1952).

$$\begin{aligned}N_f&=\left[\int|\Phi_f|^2\,d\tau_{(1,2,3,4)}\right]^{-1/2}\\&=2^{-1/2}\{1-4\mu^6a^6r_0^6[(0,2,2a)-\tfrac{1}{3}(0,0,2a)]^2\\&\quad+64\mu^{12}a^{12}r_0^{12}[(0,2,2a)-\tfrac{1}{3}(0,0,2a)]^4\}^{-1/2}. \quad \ldots\ldots(19)\end{aligned}$$

It is interesting to note that in (16)

$$\int \phi_A(1,2)\psi_B(3,4)\phi_A(3,1)\phi_B(2,4)z_3d\tau_{(1,2,3,4)}$$

is the dominant term. This provides some justification of the use of the unperturbed atomic orbitals in forming the molecular wave function since it indicates that the dipole moment arises essentially from the exchange of one electron between the two helium atoms. The magnitude of $\mathfrak{E}(r)$ is therefore determined chiefly by the inter-nuclear separation and would not be expected to depend critically on the finer details of the electron wave functions.

The magnitude of the dipole moment $\mathfrak{E}(r)$ as calculated from equations (16)–(19) is shown in figure 4. It is seen to decrease rapidly as the nuclear separation increases.

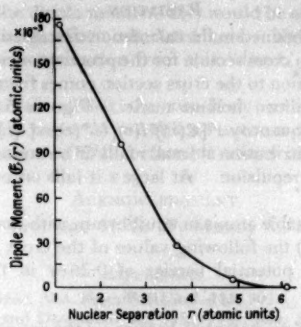

Figure 4. Dipole moment for the transition $2'\Sigma_u \rightarrow 1^1\Sigma_g$ for different nuclear separations r.

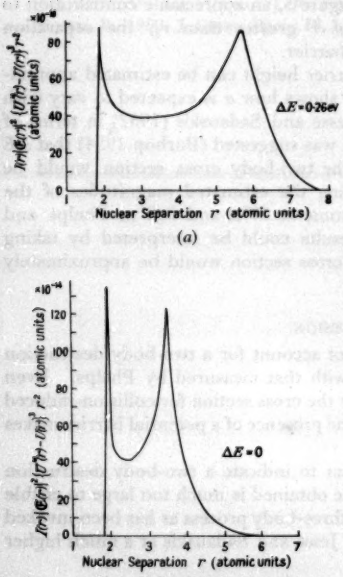

Figure 5. Plot of $r^3[\mathfrak{E}(r)]^2 I(r) \{U^*(r)-U(r)\}^3$ against r. (*a*) case I of text, $\Delta E=0{\cdot}26$ ev. (*b*) case II of text, $\Delta E=0$.

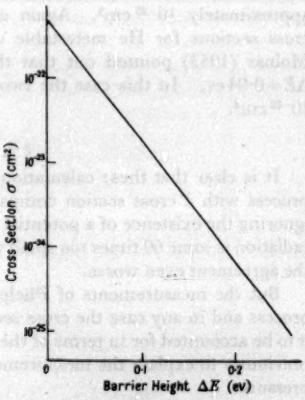

Figure 6. Estimated variation of σ with ΔE.

§ 4. Calculation of the Mean Cross Section for Collision-Induced Radiation

The values of $\mathfrak{C}(r)$ obtained in the calculation described above were substituted in (2) to obtain the mean cross section for the process considered. It is of interest to see how the contribution to the cross section comes from different values of the separation between the two helium nuclei. Figures 5 (*a*) and 5 (*b*) show the variation with r of the quantity $r^2[\mathfrak{C}(r)]^2 I(r)\{U^*(r)-U(r)\}^3$ which occurs in the integral of (2). The contribution at small r falls off on account of the inaccessibility of this region of strong repulsion. At large r it falls off on account of the fall in $\mathfrak{C}(r)$.

For $He^+(2^1S)$ metastable atoms in equilibrium with normal He atoms at room temperature ($T=300°K$) the following values of the cross section are obtained:

Case I: Assuming potential barrier of 0·26 ev in the interaction energy,

$$\sigma = 9\times10^{-26}\,\text{cm}^2.$$

Case II: Assuming no potential barrier in the interaction,

$$\sigma = 5\times10^{-22}\,\text{cm}^2.$$

For this temperature the factor $\exp(-\Delta E/kT)$ comes to be $4{\cdot}5\times10^{-5}$ for $\Delta E = 0{\cdot}26$ ev, while the ratio of the two calculated cross sections ($=18\times10^{-5}$) is greater than this since, as is seen from figure 5, an appreciable contribution to the cross section comes from values of r greater than r_c, the separation corresponding to the top of the potential barrier.

The value of σ for an intermediate barrier height can be estimated approximately from these calculations. Figure 6 shows how σ is expected to vary with ΔE. In order to explain the results of Jesse and Sadauskis (1952) in terms of a three-body recombination mechanism, it was suggested (Burhop 1954) that ΔE should be about 0·115 ev. In this case the two-body cross section would be approximately $10^{-23}\,\text{cm}^2$. Again comparing the estimated magnitudes of the cross sections for He metastable destruction at 77°K and 300°K, Phelps and Molnar (1953) pointed out that these results could be interpreted by taking $\Delta E = 0{\cdot}04$ ev. In this case the two-body cross section would be approximately $10^{-22}\,\text{cm}^2$.

§ 5. Discussion

It is clear that these calculations cannot account for a two-body destruction process with a cross section comparable with that measured by Phelps. Even ignoring the existence of a potential barrier the cross section for collision-induced radiation is some 60 times too small while the presence of a potential barrier makes the agreement even worse.

But the measurements of Phelps appear to indicate a two-body destruction process and in any case the cross section he obtained is much too large to enable it to be accounted for in terms of the same three-body process as has been invoked previously to explain the measurements of Jesse and Sadauskis at a much higher pressure.

It should be remembered however, that in the calculations described in this paper the molecular wave functions have been formed from unperturbed atomic orbitals. If the perturbation of the orbitals had been taken into account another term would have appeared in (16) corresponding to the direct transition of the excited electron to the 1s state of motion about the same nucleus. Unfortunately

the labour involved in calculating this term is considerable and it appears unlikely that its contribution to the dipole moment $\mathscr{C}(r)$ would be of an order of magnitude different from the exchange effect calculated here. Nevertheless a calculation of the magnitude of the contribution from this 'direct' transition process is at present being carried out.

It is concluded therefore that the two-body collision-induced radiation process discussed in this paper is not able to account for the measured cross sections for the destruction of 2^1S metastable atoms in collision with neutral helium atoms.

ACKNOWLEDGMENT

We are indebted to Professor H. S. W. Massey for stimulating discussions.

REFERENCES

BATES, D. R., 1951, *Mon. Not. Roy. Astr. Soc.*, **111,** 303.
BUCKINGHAM, R. A., and DALGARNO, A., 1952, *Proc. Roy. Soc.* A, **213,** 327.
BURHOP, E. H. S., 1954, *Proc. Phys. Soc.* A, **67,** 276.
JESSE, W. P., and SADAUSKIS, J., 1952, *Phys. Rev.*, **88,** 417.
KRAMERS, H. A., and TER HAAR, D., 1946, *Bull. Astr. Insts. Netherlands*, **10,** 137.
MORSE, P. M., YOUNG, L. A., and HAURWITZ, E. S., 1935, *Phys. Rev.*, **48,** 948.
PHELPS, A. V., 1955, *Phys. Rev.*, **99,** 1307.
PHELPS, A. V., and MOLNAR, J. P., 1953, *Phys. Rev.*, **89,** 1202.
ROSEN, P., 1950, *J. Chem. Phys.*, **18,** 1182.

RESEARCH NOTE

Energy Levels of π-mesic Atoms

By D. J. THOULESS
Cavendish Laboratory, Cambridge

Communicated by H. A. Bethe ; MS. received 30th November 1955

THE effect of the nuclear absorption of a π-meson on the 1S level of a π-mesic atom has been studied by Brueckner in a recent paper (1955). He considers only the effect of an intermediate state in which there is no meson present and two nucleons have been excited. There is also an intermediate state in which there are two mesons in the orbit and two nucleons have been excited, and this contributes

$$\frac{|\phi(0)|^2}{(2\pi)^3}\int\frac{\psi^2(p)\,|R(p)|^2}{-E-p^2/M}\,d^3p$$

to the energy, using Brueckner's assumptions and notation. Adding this to his expression for the energy shift ΔE_R gives

$$\Delta E_R=\frac{|\phi(0)|^2}{(2\pi)^3}P\int\frac{\psi^2(p)\,|R(p)|^2\,2p^2/M}{(E^2-p^4/M^2)}\,d^3p.$$

In Brueckner's expression there would be an energy shift if $\psi(p)$ were a δ-function, that is if the nucleons were not interacting, and so he had to subtract that part of the expression which he asserts is due to single-nucleon scattering. In the expression derived here, there is no effect from uncorrelated nucleons, which is as one would expect. Brueckner's ΔE_R* is only identical with this when $|R(p)|^2=R_0+R_1p^2$, and $R_1=R_0/ME$. Using the gaussian form assumed by Brueckner for $\psi(p)$,

$$\Delta E_R/R_{abs}=(1{\cdot}45R_0+0{\cdot}71MER_1)/(R_0+MER_1).$$

The value of this expression does depend on the ratio of R_0 and R_1, contrary to Brueckner's result.

To find what effect the nuclear model chosen had on the result, $\psi(p)$ was taken to be of the form assumed by Chew and Goldberger (1950)

$$\psi(p)=N/(\alpha^2+p^2)^2$$

with $\alpha^2/M=35$ MEV, or a quarter of the meson energy E (Chew and Goldberger took $\alpha^2/M=36$ MEV). This gave

$$\Delta E_R/R_{abs}=(1{\cdot}06R_0+0{\cdot}28MER_1)/(R_0+MER_1)$$

which is somewhat less than the value obtained with the gaussian distribution, particularly if MER_1/R_0 is large. This is because the high-momentum part of $\psi(p)$ gives a negative contribution to the energy, and the second distribution has a larger high-momentum part.

It is clear that the value of this effect cannot be predicted as precisely as Brueckner supposed, as it depends too much on the models used, but the order of magnitude is probably correct.

The author wishes to thank Professor H. A. Bethe for several helpful discussions on this subject.

References

Brueckner, K. A., 1955, *Phys. Rev.*, **98**, 769.
Chew, G. F., and Goldberger, M. L., 1950, *Phys. Rev.*, **77**, 470.

LETTER TO THE EDITOR

Nuclear Spins and Magnetic Moments of ^{161}Dy, ^{163}Dy, ^{171}Yb and ^{173}Yb

We have observed paramagnetic resonance absorption in crystals of dysprosium acetate, ytterbium acetate, and in the same salts diluted with yttrium acetate. Working with the diluted salts at a wavelength of 3·1 cm and a temperature of 4·2°K we were able to observe the hyperfine structure due to the nuclear moments of the odd isotopes, and to determine their nuclear spins.

These salts of the formula $R(CH_3COO)_3.4H_2O$, form triclinic crystals in which all the rare earth ions are magnetically equivalent. The principal g-values are all different, and there is no approximation to axial symmetry. We have investigated the spectra with the magnetic field in the direction of maximum g-value. In this direction the intensity of absorption is low, but the hyperfine structure is particularly clear, since the lines are narrow, and quadrupole and higher order effects are small. The spectrum of dysprosium acetate diluted

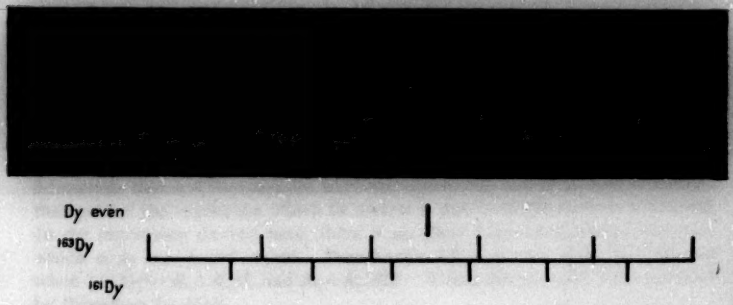

1 : 150 with yttrium acetate is shown in the figure. (The oscillograph deflection is not accurately proportional to field; the fields at which absorption occurred were measured by proton magnetic resonance.) The main line due to the isotopes of even mass number is flanked on each side by three lines due to ^{161}Dy and three due to ^{163}Dy, corresponding to a spin of 5/2 for each of these nuclei. The innermost hyperfine lines are not fully resolved from the main line, but their presence is clearly indicated.

The spin Hamiltonian may be written in the form (Bleaney 1951)

$$\mathscr{H} = \beta(g_x H_x S_x + g_y H_y S_y + g_z H_z S_z) + A_x S_x I_x + A_y S_y I_y + A_z S_z I_z.$$

Our measurements fit this Hamiltonian with
$g_x = 13{\cdot}60 \pm 0{\cdot}06$, $^{161}A_x = 0{\cdot}0381 \pm 0{\cdot}0005\ \text{cm}^{-1}$, $^{163}A_x = 0{\cdot}0540 \pm 0{\cdot}0005\ \text{cm}^{-1}$, giving for the ratio of the nuclear magnetic moments $^{163}\mu/^{161}\mu = 1{\cdot}41 \pm 0{\cdot}02$. The signs of the moments are not determined by our experiments. Their magnitudes can be estimated using the theory of Elliott and Stevens (1953) provided we assume that the ground state of Dy^{3+} in the acetate is spanned by the $J = 15/2$ manifold. (The ground state of the free ion is $^6H_{15/2}$.) The value of A_x/g_x is

then independent of the particular state, and is simply related to the nuclear magnetic moment. This assumption is likely to be valid if the higher free ion states are well removed from the ground state. For example it holds for erbium ($\Delta E = 8000\,\text{cm}^{-1}$) and praseodymium ($\Delta E = 2000\,\text{cm}^{-1}$) and very nearly for neodymium ($\Delta E = 1800\,\text{cm}^{-1}$). The energy of the first excited state of the free Dy^{3+} ion is estimated at $3300\,\text{cm}^{-1}$. Using the values of $\langle r^{-3} \rangle$ for the 4f orbits given by Bleaney (1955) we obtain $^{161}\mu = 0{\cdot}38 \pm 0{\cdot}05$ n.m. and $^{163}\mu = 0{\cdot}53 \pm 0{\cdot}05$ n.m.

From an examination of the hyperfine structure of the 3968 Å line of the Dy II spectrum, Murakawa and Kamei (1953) concluded that the nuclear spin of each of these nuclei is probably 7/2. However, this conclusion was reached from an experiment made under difficult conditions in which the lines due to the two isotopes were not separately identified.

The spectrum of ytterbium acetate diluted 1:100 with yttrium acetate consists of a main line due to the even isotopes, with one satellite on each side due to ^{171}Yb, corresponding to a spin of 1/2 for this nucleus, and three on each side due to ^{173}Yb, corresponding to a spin of 5/2. These spins agree with the values found by Schüler, Roig and Korsching (1938) from the hyperfine structure of lines of the Yb I spectrum. We find $g_x = 4{\cdot}57 \pm 0{\cdot}02$, $^{171}A_x = 0{\cdot}122 \pm 0{\cdot}001\,\text{cm}^{-1}$, $^{173}A_x = 0{\cdot}0341 \pm 0{\cdot}0003\,\text{cm}^{-1}$. The ratio of the nuclear magnetic moments is then $^{173}\mu/^{171}\mu = 1{\cdot}39 \pm 0{\cdot}01$. The $^2F_{7/2}$ ground state of the free Yb^{3+} ion is separated by $10\,300\,\text{cm}^{-1}$ from the first excited state, so that we may assume with confidence that the ground state in the crystal is spanned by the $J = 7/2$ manifold. We then obtain for the nuclear magnetic moments $|^{171}\mu| = 0{\cdot}43 \pm 0{\cdot}05$ and $|^{173}\mu| = 0{\cdot}60 \pm 0{\cdot}05$, compared with $^{171}\mu = 0{\cdot}4_5$ and $^{173}\mu = -0{\cdot}6_5$ obtained by Schüler and Korsching (1938).

Clarendon Laboratory,
Oxford.
22nd December 1955.

A. H. Cooke.
J. G. Park.

Bleaney, B., 1951, *Phil. Mag.*, **42**, 441 ; 1955, *Proc. Phys. Soc.* A, **68**, 937.
Elliott, R. J., and Stevens, K. W. H., 1953, *Proc. Roy. Soc.* A, **218**, 553.
Murakawa, K., and Kamei, T., 1953, *Phys. Rev.*, **92**, 325.
Schüler, H., and Korsching, H., 1938, *Z. Phys.* **111**, 386.
Schüler, H., Roig, J., and Korsching, H., 1938, *Z. Phys.* **111**, 165.

CONTENTS OF SECTION B

PAGE

Prof. H. S. Green. Molecular Theory of Irreversible Processes in Fluids . . 269

Dr. J. G. Powles. Nuclear Magnetic Resonance Absorption in Polyisobutylene 281

Dr. R. O. Davies and Dr. J. Lamb. On the Description of Rate Processes by Means of Relaxation Times 293

Dr. H. A. Whale. Effective Tilts of the Ionosphere at Places about 1000 km apart 301

Dr. H. A. Whale and Dr. W. J. Ross. An Automatic Direction Finder for recording Rapid Fluctuations of the Bearing of Short Radio Waves . . 311

Dr. J. S. Hey and Mr. S. J. Parsons. The Radar Measurement of Low Angles of Elevation 321

Mr. I. G. Austin and Dr. R. Wolfe. Electrical and Optical Properties of a Semiconducting Diamond 329

Dr. L. Ward. The Variation with Temperature of the Spectral Emissivities of Iron, Nickel and Cobalt 339

Dr. A. D. Buckingham. Birefringence Resulting from the Application of an Intense Beam of Light to an Isotropic Medium 344

Dr. S. P. F. Humphreys-Owen. The Scattering of Light by Single Crystals . 350

Mr. G. T. Wright. Scintillation Decay Times of Organic Crystals . . . 358

Mr. R. H. Bromley. Two-dimensional Strain Measurement by Moiré . . 373

Dr. T. F. W. Embleton. The Propagation and Reflection of Sound Pulses of Finite Amplitude 382

Mr. J. Ewles and Mr. J. C. Stead. Luminescence and Electrical Conductivity associated with Defects in Alkali Halide Crystals 396

Research Notes:

Mr. I. M. Mackintosh. Low Temperature Magnetoresistance Anomalies in Indium Antimonide 403

Dr. K. W. H. Stevens. Population Changes with Magnetic Field . . 406

Mr. Bipin Kumar Agarwal. The Influence of ^{3}He on the Lambda Point 408

Dr. H. B. Dyer and Mr. P. T. Wedepohl. Electrical Measurements on Type IIb Diamonds 410

Reviews of Books 413

Contents of Section A 416

Approximate Molecular Orbitals
IV: The $3p\sigma_u$ and $4f\sigma_u$ states of H_2^+

By A. DALGARNO and J. T. LEWIS
Department of Applied Mathematics, Queen's University of Belfast

Communicated by D. R. Bates; MS. received 10th November 1955

Abstract. A variational method is used to obtain approximate wave functions for the $3p\sigma_u$ and $4f\sigma_u$ states of H_2^+ and their accuracy is assessed by comparing various quantities computed using them with the exact values of these quantities. The dependence of the kinetic and potential energies on the nuclear separation is discussed. A brief summary of the conclusions of this series of papers is presented.

---

§ 1. Introduction

Previous papers of this series have used the Rayleigh–Ritz variational principle to determine approximate molecular orbitals of H_2^+ for the $1s\sigma_g$ and $2p\sigma_u$ states (Dalgarno and Poots 1954, to be referred to as I), the $2p\pi_u$ and $3d\pi_g$ states (Moiseiwitsch and Stewart 1954, to be referred to as II) and for the $2s\sigma_g$ and $3d\sigma_g$ states (Carson and Dalgarno 1955, to be referred to as III); the accuracy of these orbitals was assessed by using them to evaluate various molecular properties which had been or could be determined exactly. This paper deals in a similar way with the $3p\sigma_u$ and $4f\sigma_u$ states.†

The procedure followed is closely analogous to that adopted for the investigation of the $2s\sigma_g$ and $3d\sigma_g$ states (paper III) and only a very brief description will be given.

§ 2. Wave Functions and Method

Although there have been qualitative discussions of approximate wave functions of the $3p\sigma_u$ and $4f\sigma_u$ states (Morse and Stueckelberg 1929, Lennard-Jones 1929, Gilbert 1933), the only quantitative treatment appears to be that of Pritchard and Skinner (1951) who used the LCAO approximations to the wave functions

$$\Psi\begin{Bmatrix}3p\sigma\\4f\sigma\end{Bmatrix} = a_1\{(1-r_a/2)\exp(-r_a/2)-(1-r_b/2)\exp(-r_b/2)\} + a_2\{r_a\cos\theta_a\exp(-r_a/2)-r_b\cos\theta_b\exp(-r_b/2)\} \quad \ldots\ldots(1)$$

where $\mathbf{r}_a$ and $\mathbf{r}_b$ are the position vectors of the electron relative to the nuclei A and B respectively and the ratios $a_1 : a_2$ are determined by minimizing the energy

$$E = -\int \Psi^*\left(\nabla^2 + \frac{2}{r_a} + \frac{2}{r_b}\right)\Psi \mathbf{dr} \Big/ \int \Psi^*\Psi \mathbf{dr}. \quad \ldots\ldots(2)$$

The function (1) has the correct form when the nuclear separation R is infinite; it is however very inaccurate even at large values of R (cf. tables 3 and 4).

† In the separated-atoms notation these are both designated σ^* (2s, $2p_z$).

It has been shown in earlier papers that united atom wave functions of the form (paper I)

$$\psi(3p\sigma) = (2\alpha R\lambda - \alpha^2 R^2\lambda^2)\exp(-\alpha\lambda R)\mu \qquad \ldots\ldots(3)$$

$$\psi(4f\sigma) = \lambda^3 R^3 \exp(-\alpha\lambda R)(5\mu^3 - 3\mu) \qquad \ldots\ldots(4)$$

where $\lambda = (r_a + r_b)/R$, $\mu = (r_a - r_b)/R$, are usually superior to the LCAO wave functions; further (3) and (4) may readily be improved by the introduction of a variable screening parameter and it then becomes desirable and in the case of (3) necessary to ensure their orthogonality to the lower $2p\sigma$ state (cf. paper III). Thus we choose

$$\Psi(3p\sigma) = \psi(3p\sigma) + q\Psi(2p\sigma) \qquad \ldots\ldots(5)$$

and for consistency

$$\Psi(4f\sigma) = \psi(4f\sigma) + q'\Psi(2p\sigma) \qquad \ldots\ldots(6)$$

where q and q' are determined by the conditions

$$\int \Psi^*(3p\sigma)\Psi(2p\sigma)\mathbf{dr} = \int \Psi^*(4f\sigma)\Psi(2p\sigma)\mathbf{dr} = 0 \qquad \ldots\ldots(7)$$

and α and α' are varied to obtain minimum energies.

§ 3. Description of Calculations

The functions used were of the types (5) and (6) with

(i) $\alpha = \frac{1}{3}$, $q = 0$; $\alpha' = \frac{1}{4}$, $q' = 0$.

(ii) $\alpha = \frac{1}{3}$, q determined by (7); $\alpha' = \frac{1}{4}$, q' determined by (7).

(iii) α variable, q determined by (7); α' variable, q' determined by (7).

The orbital $\Psi(2p\sigma)$ was taken as wave function (VI) of paper I, where it was shown to be very accurate at all values of R.

Using the three functions (i), (ii) and (iii) the $3p\sigma$–$1s\sigma$ and $4f\sigma$–$1s\sigma$ transition integrals Q were computed, the wave functions for the $1s\sigma$ state being obtained from paper I. Both the dipole length and dipole velocity forms of Q were used:

$$Q_L\mathbf{t} = \int \chi_i \mathbf{r}\chi_f \mathbf{dr} \qquad \text{(dipole length)} \qquad \ldots\ldots(8)$$

$$Q_V\mathbf{t} = -\frac{2}{\Delta E}\int \chi_i \nabla\chi_f \mathbf{dr} \qquad \text{(dipole velocity)} \qquad \ldots\ldots(9)$$

where χ_i and χ_f are the initial and final wave functions, ΔE is the photon energy of the radiation in rydbergs and $\mathbf{t}$ is some unit vector. The exact values have been computed by Bates, Darling, Hawe and Stewart (1954).

In addition, the potential energy of the electron in the field of the nuclei has been computed:

$$V = -\int \Psi^*\left(\frac{2}{r_a} + \frac{2}{r_b}\right)\Psi\mathbf{dr} \Big/ \int \Psi^*\Psi\mathbf{dr}. \qquad \ldots\ldots(10)$$

Exact values of V have been calculated from the exact values of E (Bates, Ledsham and Stewart 1953) using the quantal virial theorem (Slater 1933) and provide additional information on the differences between bonding and non-bonding orbitals.

§ 3. Results

The values of α, α', q and q' obtained for (ii) and (iii) are given in table 1 for the $3p\sigma$ state and in table 2 for the $4f\sigma$ state. The total and potential energies

corresponding to (i), (ii) and (iii) are compared with the exact values in tables 3, 4, 5 and 6 respectively whilst in tables 7 and 8 are compared the $3p\sigma$–$1s\sigma$ and $4f\sigma$–$1s\sigma$ transition integrals Q_L and Q_V computed using (i), (ii) and (iii) in (8) and (9) with the exact values.

A comparison of the LCAO energies with the exact has previously been made by Bates *et al.* (1953). Their results and some additional values are included in tables 3 and 4.

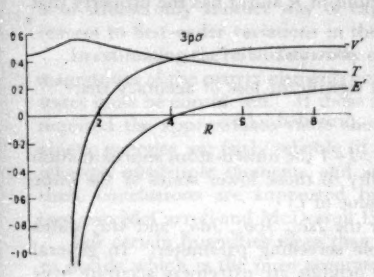

Figure 1.

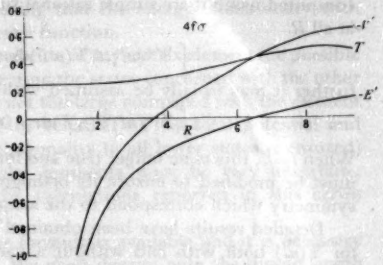

Figure 2.

§ 5. Discussion

The united-atom approximation introduced in paper I is again found to be extremely accurate. Indeed for the $4f\sigma$ state the error in the predicted energy at $R=5a_0$ is less than 2% even when orthogonality is ignored and no variation made in the screening parameter. It is necessary to make the $3p\sigma$ function orthogonal to the lower $2p\sigma$ orbital in order that the derived energies be not greater than the exact values and when this is done an accuracy of 98% is achieved. Energies predicted by the commonly used LCAO approximation are in error by a factor of over four for the $4f\sigma$ state but by only a few per cent in the $3p\sigma$ state, the accuracy in the latter case being probably fortuitous.

Variation of the screening parameters and the imposing of orthogonality leads generally to a marked improvement in all quantities. The accuracy is high especially in view of the sensitivity of the transition integrals to the detailed nature of the wave functions. For most but not all values of R the dipole velocity formula is to be preferred.

The variations with R of the potential energy $V'=V+2/R$ and the kinetic energy T of the $3p\sigma$ and $4f\sigma$ states are illustrated in figures 1 and 2. The curves are similar to those obtained earlier for the promoted $3d\sigma$, $2p\sigma$ and $3d\pi$ orbitals (papers III, I and II). It is not possible to say whether or not T does not pass through a minimum, as was the case for the antibonding $2p\sigma$ and $3d\pi$ states.

§ 6. Summary

The most significant conclusion that may be drawn from the calculations reported in this series of papers is that excited orbitals are much more accurately represented by a united-atom type of approximation than by a separated-atoms type of approximation. The latter type, when written as is customary in the

simple LCAO form, is indeed so seriously in error even for large nuclear separations that predictions based upon it may not possess even qualitative accuracy.

Amongst the various possible forms of united-atom approximation the simplest appears to be obtained according to

$$\phi_{nl}(r, \theta) \rightarrow \phi_{nl}(\lambda R/2, \cos^{-1}\mu) = \Psi(nl) \quad \text{say,}$$

where $\phi_{nl}(r, \theta)$ is the atomic wave function at $R=0$ and n and l are respectively the principal and azimuthal quantum numbers. Most molecular quantities computed using it are simple rational functions of R and it has the property that at all R

$$\int \Psi^*(nl)\mathscr{H}\Psi(n'l')\mathbf{dr} = 0 \quad \text{provided} \quad l \neq l';$$

further it may usually be assumed without significant loss of accuracy that

$$\int \Psi^*(nl)\Psi(n'l')\mathbf{dr} = 0 \qquad \text{provided} \quad l \neq l'.$$

When $l=l'$, this is no longer true and for $n>l+1$ the united-atom approximation must be modified to ensure its orthogonality to those lower states of the same symmetry which correspond to the same value of l.

Detailed results have been obtained for the $2s\sigma_g$, $3p\sigma_u$, $3d\sigma_g$ and $4f\sigma_u$ states for $\Psi(nl)$ both with and without a variable screening parameter. In general predictions based upon these approximate orbitals are extremely accurate over a wide range of R. The exceptions involve those states which possess a node in λ-space, some molecular quantities being rather sensitive to its position so that care is required in assessing the accuracy of any predictions. For the $1s\sigma_g$, $2p\sigma_u$, $2p\pi_u$ and $3d\pi_g$ states, the united-atom approximation has been improved by mixing it with the LCAO approximation. Attention is drawn to the high accuracy of the simple representation of the $1s\sigma_g$ orbital as

$$\Psi(1s\sigma) = \exp\{-\alpha(r_a + r_b)/2\} + p\{\exp(-\alpha r_a) + \exp(-\alpha r_b)\}$$

α and p being variable parameters.

The estimation of the accuracy of the calculation of any atomic or molecular quantity is a matter of considerable importance and although no criterion can be given which is generally applicable some progress can be made through a consideration of the expansion of the *approximate* orbital in terms of the complete set of *exact* wave functions χ_i. Suppose Ψ_1 and Ψ_2 are approximations to the exact orbitals χ_1 and χ_2 respectively. Then we may write

$$\Psi_1 = a_{11}\chi_1 + \sum_{i\neq 1} a_{1i}\chi_i \qquad \ldots\ldots(11)$$

$$\Psi_2 = a_{22}\chi_2 + \sum_{i\neq 2} a_{2i}\chi_i. \qquad \ldots\ldots(12)$$

The diagonal matrix element of any dynamical variable L is given by

$$\int \Psi_1^* L \Psi_1 d\tau = a_{11}^2(1|L|1) + 2a_{11}\sum_{i\neq 1} a_{1i}(1|L|i) + \sum_{i\neq 1}\sum_{j\neq 1} a_{1i}a_{1j}(i|L|j) \quad \ldots.(13)$$

and the non-diagonal element by

$$\int \Psi_1^* L \Psi_2 d\tau = a_{11}a_{22}(1|L|2) + a_{11}\sum_{i\neq 2} a_{2i}(1|L|i) + a_{22}\sum_{i\neq 1} a_{1i}(i|L|2) + \sum_{i\neq 1}\sum_{j\neq 2} a_{1i}a_{2j}(i|L|j). \qquad \ldots\ldots(14)$$

Provided that a_{ij} may be supposed small the approximations may be regarded as reasonably accurate and the double summations can be ignored. Expression (14) shows that if $\Psi_1 \equiv \chi_1$, a_{12} is effectively equal to the departure from orthogonality

and emphasizes the importance of ensuring orthogonality to lower states for variational calculations of the energy. Unfortunately, for calculations of other quantities it may not be the lower states for which the matrix element is large so that a wave function which yields an accurate energy value may be grossly in error in predicting other quantities.

The higher accuracy usually achieved in predicting energies than in predicting other quantities is explained by (13) for the single summation vanishes identically for the energy and for no other quantity (except by chance cancellation). This is of course only another way of expressing that the energy is stationary with respect to first-order variations in the wave function.

In estimating the reliability of the calculation of any matrix element the possible magnitudes of the matrix elements connecting the states concerned with the other states must be considered. If those are not too large compared with the element required the approximate value should be reliable. Thus total potential and kinetic energies are fairly reliable (if orthogonality to all lower states is ensured) whereas quadruple moments and angular momenta must be very uncertain; these conclusions are supported by the calculations reported in this series (see also McCarroll and McDowell 1955).

For certain quantities more than one formula is available and it is necessary to decide which is the most accurate. We shall discuss only the dipole length and dipole velocity forms of the transition integrals Q_{12}, say. Then from (14),

$$Q_{12}{}^{\mathrm{L}} \sim a_{11}a_{22}Q_{12} + a_{11}\sum_{i\neq 2} a_{2i}Q_{1i} + a_{22}\sum_{i\neq 1} a_{1i}Q_{i2}$$

$$Q_{12}{}^{\mathrm{V}} \sim a_{11}a_{22}Q_{12} + a_{11}\sum_{i\neq 2} a_{2i}\frac{(E_1-E_i)}{(E_1-E_2)}Q_{1i} + a_{22}\sum_{i\neq 1} a_{1i}\frac{(E_i-E_2)}{(E_1-E_2)}Q_{i2}.$$

It is clear that $Q_{12}{}^{\mathrm{L}}$ may equal $Q_{12}{}^{\mathrm{V}}$ without being equal to their exact value Q_{12} and the agreement of the two approximate forms cannot be accepted as a reliable criterion for their accuracy (cf. $2p\sigma_u - 2s\sigma_g$ transition at $R=2a_0$ (Bates, Darling, Hawe and Stewart 1954)). Though cancellation may occur in the summations so that in any particular case no completely definite choice can be made, it appears that if the photon energy associated with the transition is larger than that associated with any other possible strong transition from either of the states then the dipole velocity form is to be preferred and if the photon energy is smaller then the dipole length is to be preferred. For example the $2s\sigma$–$2p\pi$ transition has a small photon energy and Q_{L} is much superior to Q_{V}, the opposite being the case for the $1s\sigma$–$4f\sigma$ transition where the photon energy is large.

Table 1. Parameters of the $3p\sigma_u$ Wave Functions

Internuclear distance R		0·0	0·4	0·8	1·2	1·6	2·0	3·0	4·0	5·0
Function (ii)	q	0·0000	−0·0099	−0·0501	−0·0997	−0·1289	−0·0638	−0·0018	0·0681	0·1282
Function (iii)	α	0·333	0·341	0·360	0·381	0·393	0·394	0·388	0·356	0·343
	q	0·0000	0·0133	0·0236	0·0237	0·0386	0·0495	0·0653	0·0870	0·1375

Table 2. Parameters of the $4f\sigma_u$ Wave Functions

Internuclear distance R		0·0	0·4	0·8	1·2	1·6	2·0	3·0	4·0	5·0
Function (ii)	q'	0·0000	0·2202	0·6560	1·0190	0·7481	−0·1729	−1·6312	−4·8382	−8·3013
Function (iii)	α'	0·250	0·250	0·251	0·252	0·253	0·254	0·260	0·271	0·288
	q'	0·0000	0·2202	0·6531	1·0143	0·7662	−0·1010	−1·3532	−3·6152	−4·9633

Table 3. Total Electronic Energies E of the $3p\sigma_u$ State

Function \ R	0·0	0·4	0·8	1·2	1·6	2·0	3·0	4·0	5·0
(1)	—	—	0·394	0·467	0·492	0·500	0·495	0·480	0·464
(i)	0·44444	0·45020	0·46311	0·47615	0·48499	0·48862	0·48614	0·49552	0·53171
(ii)	0·44444	0·45007	0·46115	0·46962	0·47110	0·47409	0·48609	0·48160	0·46873
(iii)	0·44444	0·45051	0·46604	0·48443	0·49914	0·50646	0·50503	0·48473	0·46940
Exact	0·44444	0·45081	0·46805	0·48872	0·50380	0·51083	0·50636	0·49022	0·47214

Table 4. Total Electronic Energies E of the $4f\sigma_u$ State

Function \ R	0·0	0·4	0·8	1·2	1·6	2·0	3·0	4·0	5·0
(1)	—	—	1·042	1·163	1·246	1·297	1·335	1·306	1·230
(i)	0·25000	0·25013	0·25051	0·25115	0·25205	0·25321	0·25736	0·26339	0·27134
(ii)	0·25000	0·25013	0·25051	0·25115	0·25205	0·25321	0·25775	0·26335	0·27114
(iii)	0·25000	0·25013	0·25051	0·25116	0·25208	0·25328	0·25776	0·26487	0·27550
Exact	0·25000	0·25013	0·25051	0·25116	0·25208	0·25329	0·25777	0·26491	0·27587

Table 5. Electronic Potential Energies V of the $3p\sigma_u$ State

Function \ R	0·0	0·4	0·8	1·2	1·6	2·0	3·0	4·0	5·0
(i)	0·889	0·890	0·890	0·884	0·867	0·842	0·763	0·708	0·702
(ii)	0·889	0·881	0·845	0·792	0·722	0·742	0·760	0·790	0·792
(iii)	0·889	0·922	0·988	1·036	1·071	1·069	0·987	0·855	0·823
Exact	0·889	0·914	0·978	1·034	1·051	1·039	0·974	0·909	0·855

Table 6. Electronic Potential Energies V of the $4f\sigma_u$ State

Function \ R	0·0	0·4	0·8	1·2	1·6	2·0	3·0	4·0	5·0
(1)	0·500	0·500	0·501	0·502	0·503	0·505	0·510	0·518	0·528
(ii)	0·500	0·500	0·501	0·502	0·503	0·505	0·510	0·518	0·528
(iii)	0·500	0·500	0·503	0·506	0·509	0·513	0·532	0·565	0·619
Exact	0·500	0·501	0·502	0·505	0·508	0·513	0·532	0·565	0·619

Table 7. The $3p\sigma_u$–$1s\sigma_g$ Transition Integrals

Function \ R	0·0	0·4	0·8	1·2	1·6	2·0	3·0	4·0	5·0
(i) Q_L	0·149	0·170	0·181	0·176	0·168	0·132	−0·067	−0·428	−0·913
(i) Q_V	0·149	0·160	0·167	0·159	0·134	0·094	−0·050	−0·199	−0·293
(ii) Q_L	0·149	0·166	0·156	0·121	0·068	0·063	−0·072	−0·699	−1·650
(ii) Q_V	0·149	0·157	0·148	0·116	0·073	0·059	−0·051	−0·153	−0·238
(iii) Q_L	0·149	0·167	0·179	0·149	0·104	0·043	−0·310	−0·484	−0·262
(iii) Q_V	0·149	0·166	0·177	0·153	0·111	0·058	−0·085	−0·182	−0·184
Exact $Q_L=Q_V$	0·149	0·164	0·174	0·148	0·097	0·038	−0·097	−0·210	−0·316

Table 8. The $4f\sigma_u$–$1s\sigma_g$ Transition Integrals

Function \ R	0·0	0·4	0·8	1·2	1·6	2·0	3·0	4·0	5·0
(i) Q_L	0·00	$1·23\times10^{-4}$	$6·97\times10^{-4}$	$2·10\times10^{-3}$	$4·80\times10^{-3}$	$9·37\times10^{-3}$	$3·36\times10^{-2}$	$8·69\times10^{-2}$	$1·59\times10^{-1}$
(i) Q_V	0·00	$1·14\times10^{-4}$	$6·24\times10^{-4}$	$1·86\times10^{-3}$	$4·21\times10^{-3}$	$8·14\times10^{-3}$	$2·78\times10^{-2}$	$6·62\times10^{-2}$	$9·50\times10^{-2}$
(ii) Q_L	0·00	$4·33\times10^{-5}$	$3·94\times10^{-4}$	$1·52\times10^{-3}$	$4·26\times10^{-3}$	$9·54\times10^{-3}$	$3·74\times10^{-2}$	$1·03\times10^{-1}$	$1·22\times10^{-1}$
(ii) Q_V	0·00	$5·22\times10^{-5}$	$4·10\times10^{-4}$	$1·49\times10^{-3}$	$3·93\times10^{-3}$	$8·21\times10^{-3}$	$2·88\times10^{-2}$	$6·86\times10^{-2}$	$9·20\times10^{-2}$
(iii) Q_L	0·00	$4·33\times10^{-5}$	$3·97\times10^{-4}$	$1·54\times10^{-3}$	$4·36\times10^{-3}$	$9·83\times10^{-3}$	$4·02\times10^{-2}$	$1·12\times10^{-1}$	$2·20\times10^{-1}$
(iii) Q_V	0·00	$5·22\times10^{-5}$	$4·15\times10^{-4}$	$1·53\times10^{-3}$	$4·06\times10^{-3}$	$8·57\times10^{-3}$	$3·19\times10^{-2}$	$7·99\times10^{-2}$	$1·63\times10^{-1}$
Exact $Q_L=Q_V$	0·00	$1·07\times10^{-4}$	$5·83\times10^{-4}$	$1·74\times10^{-3}$	$4·01\times10^{-3}$	$7·91\times10^{-3}$	$2·91\times10^{-2}$	$7·76\times10^{-2}$	$1·65\times10^{-1}$

ACKNOWLEDGMENT

The authors take pleasure in recording their thanks to Professor D. R. Bates for his interest and encouragement.

REFERENCES

BATES, D. R., DARLING, R. T. S., HAWE, S. C., and STEWART, A. L., 1954, *Proc. Phys. Soc.* A, **67,** 533.
BATES, D. R., LEDSHAM, K., and STEWART, A. L., 1953, *Phil. Trans. Roy. Soc.* A, **246,** 215.
CARSON, T. R., and DALGARNO, A., 1955, *Proc. Phys. Soc.* A, **68,** 569.
DALGARNO, A., and POOTS, G., 1954, *Proc. Phys. Soc.* A, **67,** 343.
GILBERT, C., 1933, *Phil. Mag.*, **16,** 929.
LENNARD-JONES, J. E., 1929, *Trans. Faraday Soc.*, **25,** 668.
MOISEIWITSCH, B. L., and STEWART, A. L., 1954, *Proc. Phys. Soc.* A, **67,** 457.
MORSE, P. M., and STUECKELBERG, E. C. G., 1929, *Phys. Rev.*, **33,** 932.
MCCARROLL, R. W., and MCDOWELL, M. R. C., 1955, *Proc. Phys. Soc.* A, **68,** 810.
PRITCHARD, H. O., and SKINNER, H. A., 1951, *J. Chem. Soc.*, **2,** 945.
SLATER, J. C., 1933, *J. Chem. Phys.*, **1,** 687.

On Neutron–Proton Pairing Interaction in Heavy Nuclei

By S. N. GHOSHAL and A. N. SAXENA

Institute of Nuclear Physics, Calcutta

MS. received 12*th October* 1955 *and in amended form* 7*th December* 1955

Abstract. The effect of neutron–proton pairing interaction between the last odd neutron and the last odd proton in the outermost neutron and proton shells of a nucleus has been demonstrated by the last neutron binding energy and the last proton binding energy plots in the heavy nuclei. The n–p pairing interaction has been estimated for nuclei in the region $Z>82$ and $N>126$ and it has been successfully used to explain the neutron and proton binding energy plots. The interaction energy seems to decrease with increase in the difference between neutron and proton numbers in the outermost neutron and proton shells respectively for nuclei in the region of $Z>82$ and $N>126$.

§ 1. Introduction

The effect of neutron–proton pairing interaction between an odd neutron and an odd proton in the outermost neutron and proton shells of a nucleus on the last nucleon binding energy in nuclei has been investigated by Feather (1953), Green and Edwards (1953) and Edmonds (1953). Feather has estimated the average value of the n–p pairing energy in the region of heavy nuclei ($Z>82$, $N>126$).

The effect of n–p pairing interaction becomes very clear when the last neutron binding energy B_n for a system of nuclei with constant neutron number N (isotones) is plotted against the proton number Z. Similarly a plot of the last proton binding energy B_p for a system of nuclei with constant Z (isotopes) against N brings out this effect clearly. This can be easily seen if we write down the nuclear mass formula for various even–odd combinations of protons and neutrons. Assuming both Z and N to be even, we write,

$$\left.\begin{aligned}
M(Z,N) &= f(Z,N) - 2\sum_{j}^{Z/2}\pi_j - 2\sum_{k}^{N/2}\nu_k && \text{(even–even)}\\
M(Z+1,N) &= f(Z+1,N) - 2\sum_{j}^{Z/2}\pi_j - 2\sum_{k}^{N/2}\nu_k && \text{(odd–even)}\\
M(Z,N+1) &= f(Z,N+1) - 2\sum_{j}^{Z/2}\pi_j - 2\sum_{k}^{N/2}\nu_k && \text{(even–odd)}\\
M(Z+1,N+1) &= f(Z+1,N+1) - 2\sum_{j}^{Z/2}\pi_j - 2\sum_{k}^{N/2}\nu_k - \lambda(Z+1,N+1) && \text{(odd–odd)}
\end{aligned}\right\} \quad \ldots\ldots(1)$$

where $f(Z, N)$ expresses the functional dependence of nuclear mass on Z and N; π_j and ν_k are the pairing energies per nucleon of proton and neutron respectively, the suffixes j and k denoting respectively the different proton and neutron pairs. The sum of the pairing energies of all the proton and neutron pairs have been considered in the above equations. The last odd proton or neutron does not

contribute to these pairing energy terms (Mayer 1950). In the case of the odd–odd nuclei, we have introduced a new term λ to take into account the effect of the n–p pairing interaction between the 'last' odd neutron and the 'last' odd proton. It is the behaviour of λ which has been investigated in the present work. λ is positive, since it lowers the energy of the odd–odd nucleus. Equations (1) are slightly modified forms of the mass equation introduced by Kumar and Preston (1955).

From equations (1) we may write, for a series of *isotones* containing even number of neutrons,

$$B_n^{ee}(Z, N) = \Delta f_n(Z, N) + 2\nu_{N/2} \quad \ldots\ldots(2a)$$

$$B_n^{oe}(Z+1, N) = \Delta f_n(Z+1, N) + 2\nu_{N/2} - \lambda(Z+1, N-1) \quad \ldots\ldots(2b)$$

$$B_n^{ee}(Z+2, N) = \Delta f_n(Z+2, N) + 2\nu_{N/2}. \quad \ldots\ldots(2c)$$

For the case of odd neutron *isotones*,

$$B_n^{eo}(Z, N-1) = \Delta f_n(Z, N-1) \quad \ldots\ldots(3a)$$

$$B_n^{oo}(Z+1, N-1) = \Delta f_n(Z+1, N-1) + \lambda(Z+1, N-1) \quad \ldots\ldots(3b)$$

$$B_n^{eo}(Z+2, N-1) = \Delta f_n(Z+2, N-1). \quad \ldots\ldots(3c)$$

Here Δf_n gives the contribution to the neutron binding energy from the differences between the various terms of $f(Z, N)$ in the mass equation between the nuclei (Z, N) and $(Z, N-1)$ together with the neutron mass (Feather 1953). Δf_n is an almost linearly increasing function of Z (or N) for constant N (or Z) when $f(Z, N)$ is calculated by taking the usual parameters in the Fermi–Weizsäcker mass equation over small ranges of A. These plots of Δf_n against Z for different N give a set of almost linearly increasing curves with nearly equal slopes. As has been shown by various workers, the 'theoretically' derived parameters in the Fermi–Weizsäcker mass formula give mass values (or mass differences) which depart considerably from observed masses (or mass differences) (for references see Coryell 1953). A thorough investigation of the parameters which will give a better representation of the masses has been carried out by Suess and Jensen (1951), Coryell (1953), Ghoshal and Saxena (1955), Glass *et al.* (1955), Kumar and Preston (1955), and the values of the various parameters involved (e.g. Z_A, B_A, etc.) have been estimated accurately for different values of A in the different shell regions. If Δf_n is calculated using these new parameters, its variations with Z or N will also be more or less linear. Only the slopes and the absolute values will be different. This is due to the fact that the modified parameter Z_A (Coryell 1953) is a linear function of A in a particular shell region, while the other modified parameter B_A is almost constant for heavy nuclei (Glass *et al.* 1955).

While evaluating the contribution of neutron pairing energy to the binding energy of the last neutron, we have made the assumption that the shell configuration of the existing neutron pairs is not affected by the addition of an extra neutron to a given nucleus. This assumption cancels out the contribution of the neutron pairing energy to the binding energy of the last neutron in the odd N nuclei (see equations (3)).

The neutron pairing energy terms in the equations (2) refer to the last, i.e. the $(\frac{1}{2}N)$th neutron pair in the nuclei involved. These should normally be the same for all the three nuclei considered, since the neutron number is constant and their shell assignments are expected to remain unaltered. However, there

may be variation of the neutron pairing energy terms due to the perturbation of the shell assignments of a constant number of neutrons owing to the presence of different proton numbers in different nuclei.

Equations similar to (2) and (3) can be written for the binding energy of the last proton.

For a series of *isotopes* containing even numbers of protons,

$$B_p^{ee}(Z+2, N-2) = \Delta f_p(Z+2, N-2) + 2\pi_{(Z+2)/2} \quad \ldots\ldots(4a)$$

$$B_p^{eo}(Z+2, N-1) = \Delta f_p(Z+2, N-1) + 2\pi_{(Z+2)/2} - \lambda(Z+1, N-1) \quad \ldots\ldots(4b)$$

$$B_p^{ee}(Z+2, N) = \Delta f_p(Z+2, N) + 2\pi_{(Z+2)/2}. \quad \ldots\ldots(4c)$$

For the case of odd proton *isotopes*,

$$B_p^{oe}(Z+1, N-2) = \Delta f_p(Z+1, N-2) \quad \ldots\ldots(5a)$$

$$B_p^{oo}(Z+1, N-1) = \Delta f_p(Z+1, N-1) + \lambda(Z+1, N-1) \quad \ldots\ldots(5b)$$

$$B_p^{oe}(Z+1, N) = \Delta f_p(Z+1, N). \quad \ldots\ldots(5c)$$

Behaviour of Δf_p is analogous to that of Δf_n. As in the case of neutron binding energies, we have assumed that the addition of an extra proton does not affect the shell configuration of the existing proton pairs.

If we examine equations (2) we find that for a constant even value of N, the even–even and odd–even neutron binding energies should fall on a smooth curve (approximately linear), increasing with increasing proton number Z, if the n–p pairing energy term λ were zero and the perturbing influence of the differing proton numbers on the neutron pairing energy terms can be neglected. Such perturbations in the shell assignments of a constant number of neutrons due to the variation of the number of protons in different nuclei are not very frequent (Klinkenberg 1952). In the region of heavy nuclei considered, very meagre data of shell assignments are available. Hence it is not possible to predict how and in which cases such perturbations will affect the neutron pairing energy terms, and we will neglect the effect of these perturbations in the present work. Presence of λ will *depress* the o–e points below the line through the e–e points and a zig-zag line will result. The amount of depression of the o–e points below the smooth curve is determined by the value of λ. For smaller values of λ departure from the smooth line will be small.

A similar behaviour will be shown by the (B_n, Z) plot for a constant odd N. Here the o–o points will be *raised* by λ above the line through the e–o points (see equations (3)).

Similarly equations (4) show that for a constant Z, the last proton binding energies B_p of the e–o nuclei will be *lowered* by λ below the line through the e–e points. This will be true again if the perturbing influence of differing neutron numbers on the shell assignments of a constant number of protons in the different nuclei are neglected. Finally, the last proton binding energies B_p of the o–o nuclei will be *raised* by λ above the line through the o–e points (see equations (5)).

§ 2. Estimation of λ

In figures 1 and 2 we have plotted the known binding energies of the last neutron and proton, B_n and B_p, against Z (at constant N) and N (at constant Z) respectively, for $Z>82$ and $N>126$. The binding energy values have been mostly taken from the compilations of Feather (1953) and Glass *et al.* (1955).

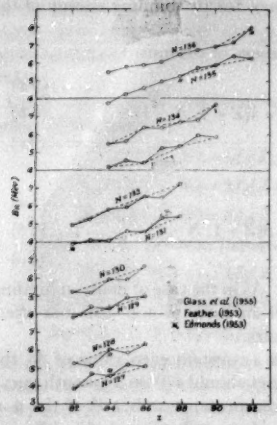

Figure 1. Last neutron binding energies B_n plotted against the proton number Z for constant neutron numbers N.

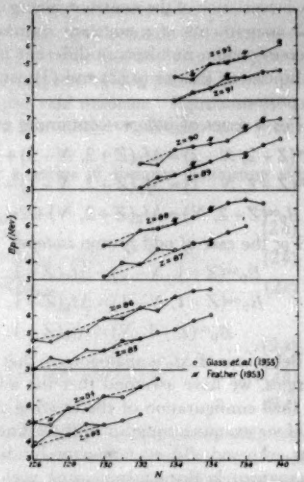

Figure 2. Last proton binding energies B_p plotted against the neutron number N for constant proton numbers Z.

In a few cases where the binding energies given in the two compilations do not agree, we have tried to check the binding energy values using the latest compilations of beta disintegration energies (King 1954), nuclear reaction Q values (Van Patter and Whaling 1954) and α-disintegration energies (Asaro and Perlman 1954). In general the binding energies compiled by Glass *et al.* (1955) have been plotted. Where the binding energies compiled by Feather depart significantly from these values, the former have also been shown.

In figure 1, where B_n has been plotted against Z for different values of N ranging from $N=127$ to 136, broken lines have been drawn through the e–o (for odd N) and e–e (for even N) points for the different values of N. Similarly, in figure 2, the o–e (for odd Z) and e–e (for even Z) points have been joined by broken lines in the (B_p, N) plots for different constant Z values from $Z=83$ to 92. In figure 1, the B_n curve for an odd N has been grouped with the B_n curve for the next *higher* even N. This has been done because λ terms involved refer to the same odd–odd nuclei for definite (odd) Z values in both the curves (see equations (6) and (7)). Likewise, in figure 2, the B_p curves for a given odd Z and for the next *higher* even Z have been grouped together for similar reasons (see equations (8) and (9)).

From figure 1, the regularity in the neutron binding energies as predicted by the equations (2) and (3) in § 1 is well illustrated. The dashed lines through the e–o points (for the odd N case) and through the e–e points (for the even N case) increase nearly linearly up to the isotonic series 132. (The value of B_n

for $Z=82$, $N=131$ is estimated by Glass *et al.* (1955), to be 3·9 MEV. However, the same binding energy computed from the data plotted by Edmonds (1953) is 3·6 MEV. As can be seen from figure 1, the latter value would make the dashed line through the even Z points for $N=131$ more nearly linear. Beyond $N=132$, the trend in the dashed curve is to increase with increasing Z, but not very regularly. This irregularity may be due to the errors in the estimation of the neutron binding energy in this region (Feather 1953) and also due to the differences in the neutron–neutron pairing energy term for the different neutron pairs in the same shell due to their being in different sub-shells (see discussions in § 1 following equations (2) and (3)). For the isotonic series 135 and 136, the points are quite irregular; only at $Z=91$ the effect of n–p pairing interaction is prominent. As we shall see in the next section, this is to be expected.

Similarly, figure 2 illustrates the regularity in the proton binding energies as expected from the equations (4) and (5). The dashed lines through the o–e points (for the odd Z case) and the e–e points (for the even Z case) vary almost linearly up to the isotopic series 88. λ effect is pronounced for the isotopic series 89 and 90 at $N=133$ and for the isotopic series 91 and 92 at $N=135$. As we shall see later, this is to be expected. At higher values of N, the irregularities in the observed B_p curves for the higher isotopic series may be due to the larger errors in the determination of B_p (Feather 1953), as also due to the differences in the p–p pairing energy term for the different proton pairs in the same shell due to their being in different sub-shells.

For still higher values of N and Z, little regularity in the B_n and B_p curves are observed. The reasons are probably the same as those discussed above. These have not been, therefore, included in figures 1 and 2.

The elevation or the depression of the B_n values at odd Z (or of the B_p values at odd N) from the corresponding broken lines through the even Z (or even N in case of B_p) points gives λ. This can be estimated in the following manner. From equations (2),

$$B_n^{ee}(Z,N)+B_n^{ee}(Z+2,N)-2B_n^{oe}(Z+1,N)$$
$$=\Delta f_n(Z,N)+2\nu_{N/2}+\Delta f_n(Z+2,N)+2\nu_{N/2}$$
$$-2[\Delta f_n(Z+1,N)+2\nu_{N/2}-\lambda(Z+1,N-1)].$$

Assuming a linear increase in Δf_n with Z at constant N, we get

$$\lambda(Z+1,N-1)=\tfrac{1}{2}[B_n^{ee}(Z,N)+B_n^{ee}(Z+2,N)-2B_n^{oe}(Z+1,N)]. \quad \ldots\ldots(6)$$

Similarly from equations (3),

$$\lambda(Z+1,N-1)=-\tfrac{1}{2}[B_n^{eo}(Z,N-1)+B_n^{eo}(Z+2,N-1)-2B_n^{oo}(Z+1,N-1)]. \quad \ldots\ldots(7)$$

Again from equations (4) and (5),

$$\lambda(Z+1,N-1)=\tfrac{1}{2}[B_p^{ee}(Z+2,N-2)+B_p^{ee}(Z+2,N)-2B_p^{eo}(Z+2,N-1)] \quad \ldots\ldots(8)$$

$$\lambda(Z+1,N-1)=-\tfrac{1}{2}[B_p^{oe}(Z+1,N-2)+B_p^{oe}(Z+1,N)-2B_p^{oo}(Z+1,N-1)]. \quad \ldots\ldots(9)$$

§ 3. Discussion

Equations (6) to (9) give four independent evaluations of λ as a function of Z and N. It is not possible to decide whether these evaluations of λ give pure n–p pairing energies and do not contain any contributions from the n–n and

p–p pairing energies, unless the shell assignments of the nucleon pairs of all the nuclei involved are known. Even if the precise shell assignments were known, it would be difficult to estimate the contributions from the n–n and p–p pairing energies because the errors in the estimations of λ are quite large. Its evaluation involves three different binding energy values. The errors in the binding energy values are included in the compilation of Feather (1953). However, in the present work, binding energies of a large number of nuclei, not included in this compilation, have been used for which the errors are not given. Hence the errors in the λ values could not be calculated for all the nuclei considered. The lowest value of the error in λ calculated from Feather's compilation comes out to be about 10 per cent and that only in very few cases. In most of the cases, the errors are much higher. We have, therefore, taken the average value of λ from these four independent evaluations. In figure 3, this average value of λ has been plotted against N for different Z values. The curves are not smooth. However, the decreasing trend of λ with increasing N is evident from the figure. In figure 4, we have plotted λ as a function of Z for different N values. Here again the increasing trend of λ with increasing Z is evident, except at $N=127$ and 129. This general behaviour of the average values of λ is discernible even in the various independent evaluations of λ in spite of their large errors.

From figures 3 and 4, it seems that λ is dependent upon the differences between the proton and neutron numbers in the outermost proton and neutron shells ($Z>82$, $N>126$) respectively. To demonstrate this more clearly, we have plotted λ against the difference between the numbers of neutrons and protons $n-z$ in the *outermost* neutron and proton shells, for various values of the proton number z in the outermost proton shell in figure 5. Though the points are widely scattered, the decrease in λ with increasing $n-z$ is quite clear. *λ reaches the highest value when the numbers of neutrons and protons in the outermost shells are equal.*

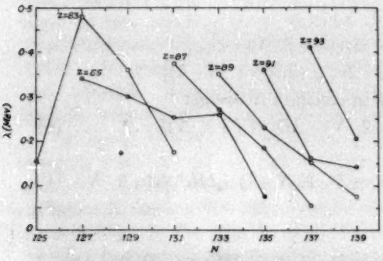

Figure 3. Plot of λ against neutron number N for constant proton numbers Z.

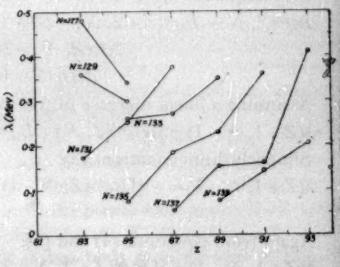

Figure 4. Plot of λ against proton number Z for constant neutron numbers N.

This behaviour of λ would explain its observed variations with N and Z at constant Z and N respectively, as shown in figures 3 and 4. For, at a definite value of Z, increasing N means an increase in the value of $n-z$. Hence λ should decrease with increasing N for a constant value of Z. On the other hand, at a definite value of N, $n-z$ decreases with increase in Z, thus causing an increase in the value of λ. The behaviour of the lines for $N=127$ and 129 in figure 4

needs explanation. In both these cases, λ decreases as Z increases from 83 to 85, instead of increasing with increasing Z, as is the case at all other N. This is to be expected in the case of $N=127$ where, at $Z=83$, the numbers of protons and neutrons in the outermost shells are each equal to unity, and hence λ for this nucleus (^{210}Bi) should be the maximum, for the line $N=127$. In the case of $N=129$, the numbers of protons and neutrons in the outermost shells are equal at $Z=85$ (each being equal to three). So, λ for this nucleus (^{214}At) should have the highest value for the line $N=129$. However, in figure 4, λ for ^{212}Bi ($Z=83$, $N=129$) is somewhat greater than that for ^{214}At. This may be due to errors in the estimated value of λ or due to the contributions of n–n or p–p pairing energies appearing in it, as discussed above.

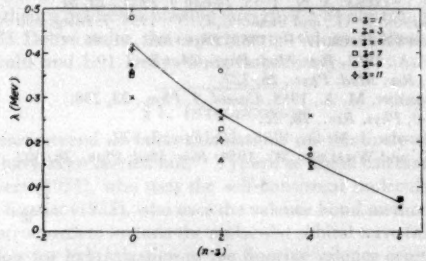

Figure 5. Plot of λ against $n-z$, the difference between the number of neutrons in excess of the closed neutron shell at $N=126$ and the number of protons in excess of the closed proton shell at $Z=82$. The solid line has no significance except that it shows the decreasing trend of λ.

The pronounced λ effects in the otherwise irregular lines for the isotonic series 135 and 136 at $Z=91$, about which reference has been made earlier, can easily be seen to be due to the equality of numbers of neutrons and protons in the outermost shells at these points ($n=z=9$). Similarly, the prominent λ effects in the otherwise irregular B_p lines for the isotopic series 89 and 90 at $N=133$ and for the isotopic series 91 and 92 at $N=135$ are due to the equality of the n and z values at these points ($n=z=7$ in the first case, and $n=z=9$ in the second case).

Edmonds (1953) has calculated the effect of pairing interaction between the last neutron and last proton on the last proton binding energies in heavy nuclei ($Z>82$, $N>126$) by making the simplified assumption that the last neutron and the last proton occupy the same sub-shell. His results indicate a constant value of λ for different values of $n-z$, in contrast with the observed behaviour of λ as reported above. If the pairing interaction between the last odd neutron and the last odd proton depends only upon their angular momenta, as in the case of n–n or p–p pairing interaction (Mayer 1950), then the above result is difficult to understand. The above results seem to indicate that the n–p pairing interaction is influenced by the nature of the neutron and proton cores in the outermost shells.

There are very few binding energy values available just below $Z=82$ and $N=126$ so that it was not possible to investigate the behaviour of λ at shell crossing.

However, the only one point ($Z=83$ and $N=125$) which is available in this region seems to indicate a large increase in λ when the neutron shell is crossed.

Acknowledgments

We are indebted to Professor M. N. Saha for the kind interest in our work. Thanks are due to Mr. B. Baliga for performing some calculations for us.

References

Asaro, F., and Perlman, I., 1954, *Rev. Mod. Phys.*, **26,** 456.
Coryell, C. D., 1953, *Ann. Rev. Nuclear Sci.*, **2,** 305.
Edmonds, A. R., 1953, *Proc. Phys. Soc.* A, **66,** 793.
Feather, N., 1953, *Advanc. Phys.*, **2,** 141.
Ghoshal, S. N., and Saxena, A. N., 1955, *Indian J. Phys.*, **29,** 81.
Glass, R. A., Thompson, S. G., and Seaborg, G. T., 1955, *J. Inorg. and Nucl. Chem.*, **1,** 3.
Green, A. E. S., and Edwards, D. F., 1953, *Phys. Rev.*, **91,** 46.
Klinkenberg, P. F. A., 1952, *Rev. Mod. Phys.*, **24,** 63.
King, R. W., 1954, *Rev. Mod. Phys.*, **26,** 327.
Kumar, K., and Preston, M. A., 1955, *Canad. J. Phys.*, **33,** 298.
Mayer, M. G., 1950, *Phys. Rev.*, **78,** 22.
Suess, H. E., and Jensen, J. H. D., 1951, *Ark. Fys.*, **3,** 577.
Van Patter, D. M., and Whaling, W., 1954, *Rev. Mod. Phys.*, **26,** 402.

On the Method of Atoms in Molecules
III: The Ground State of Hydrogen Fluoride

By A. C. HURLEY

Department of Theoretical Chemistry, University of Cambridge

Communicated by H. C. Longuet-Higgins ; MS. received 11th November 1955, and in final form 12th December 1955

Abstract. Techniques suggested by the results of calculation on the hydrogen molecule are used to calculate the properties of hydrogen fluoride. The most satisfactory results are obtained using an intra-atomic correlation correction theory. This theory predicts a binding energy of 5·84 electron volts and a dipole moment of 2·33 Debye units, the experimental values of these quantities being 6·08 electron volts and 1·91 Debye units respectively.

§ 1. Introduction

In recent years several *ab initio* calculations on relatively complex diatomic molecules have been carried out. Typical of these calculations are those on N_2 by Scherr (1955), who uses the self-consistent molecular orbital method and on HF by Kastler (1953), who uses the valence bond method with sufficiently many valence structures to include the molecular orbital wave function as a special case and to allow for hybridization of the fluorine valence orbitals. The results of the calculations have been somewhat disappointing, especially in respect to the predicted binding energies. It is clear that much more accurate wave functions must be used in order to obtain useful estimates of these important quantities. Although wave functions of sufficient accuracy are not at present available, Moffitt (1951) has suggested how such a calculation may be approximated using the results of atomic spectroscopy.

Moffitt's technique, the method of atoms in molecules, and a related procedure employing an intra-atomic correlation correction, which was suggested by calculation on the hydrogen molecule (Hurley 1955, 1956), are here applied to Kastler's calculation of the ground state of hydrogen fluoride.

§ 2. The Orbital Approximation

We consider the second of the orbital calculations of Kastler (1953), which is based on the orthonormal fluorine orbitals

$$\left.\begin{aligned}
1s &= \left(\frac{a^3}{\pi}\right)^{1/2} \exp(-ar) \\
2s &= N\left[\left(\frac{\mu^5}{3\pi}\right)^{1/2} r\exp(-\mu r) - K.1s\right] \\
2p_x &= \left(\frac{\mu^5}{\pi}\right)^{1/2} x\exp(-\mu r) \\
2p_y &= \left(\frac{\mu^5}{\pi}\right)^{1/2} y\exp(-\mu r) \\
2p_z &= \left(\frac{\mu^5}{\pi}\right)^{1/2} z\exp(-\mu r)
\end{aligned}\right\} \quad \ldots\ldots(2.1)$$

with $$a = 8{\cdot}67, \qquad \mu = 2{\cdot}6 \qquad \ldots\ldots(2.2)$$

$$K = 3^{1/2}a^{-3/2}\mu^{5/2}(2a)^3(a+\mu)^{-4} = 0{\cdot}239\,0105$$

$$N = \{1 + K^2 - 16(3)^{1/2}Ka^{3/2}\mu^{5/2}(a+\mu)^{-4}\}^{-1/2} = 1{\cdot}029\,8481 \qquad \ldots\ldots(2.3)$$

and the normalized hydrogen orbital

$$h = \left(\frac{1}{\pi}\right)^{1/2} \exp(-r'). \qquad \ldots\ldots(2.4)$$

Here x, y, z are Cartesian axes centred on the fluorine nucleus with the z axis directed towards the hydrogen nucleus, $r = (x^2+y^2+z^2)^{1/2}$ and r' is the distance from the hydrogen nucleus. The internuclear separation ρ is given the experimental equilibrium value of 1·733(154) atomic units.

The following normalized Slater determinants are built up from the orbitals (2.1):

$$\left.\begin{aligned}
\tilde{\Psi}_1 &= (10!)^{-1/2} \det\{1s(1)_\alpha, 1s(2)_\beta, 2s(3)_\alpha, 2s(4)_\beta, 2p_x(5)_\alpha, 2p_x(6)_\beta, \\
&\qquad 2p_y(7)_\alpha, 2p_y(8)_\beta, 2p_z(9)_\alpha, 2p_z(10)_\beta\} \\
\tilde{\Psi}_{p\alpha} &= \frac{(10!)^{-1/2}}{A} \det\{1s(1)_\alpha, 1s(2)_\beta, 2s(3)_\alpha, 2s(4)_\beta, 2p_x(5)_\alpha, 2p_x(6)_\beta, \\
&\qquad 2p_y(7)_\alpha, 2p_y(8)_\beta, 2p_z(9)_\alpha, h(10)_\beta\} \\
\tilde{\Psi}_j &= \frac{(10!)^{-1/2}}{A^2} \det\{1s(1)_\alpha, 1s(2)_\beta, 2s(3)_\alpha, 2s(4)_\beta, 2p_x(5)_\alpha, 2p_x(6)_\beta, \\
&\qquad 2p_y(7)_\alpha, 2p_y(8)_\beta, h(9)_\alpha, h(10)_\beta\} \\
\tilde{\Psi}_{s\alpha} &= \frac{(10!)^{-1/2}}{B} \det\{1s(1)_\alpha, 1s(2)_\beta, 2p_z(3)_\alpha, 2p_z(4)_\beta, 2p_x(5)_\alpha, 2p_x(6)_\beta, \\
&\qquad 2p_y(7)_\alpha, 2p_y(8)_\beta, 2s(9)_\alpha, h(10)_\beta\} \\
\tilde{\Psi}_{l\alpha} &= \frac{(10!)^{-1/2}}{AB} \det\{1s(1)_\alpha, 1s(2)_\beta, 2s(3)_\alpha, 2p_z(4)_\beta, 2p_x(5)_\alpha, 2p_x(6)_\beta, \\
&\qquad 2p_y(7)_\alpha, 2p_y(8)_\beta, h(9)_\alpha, h(10)_\beta\} \\
\tilde{\Psi}_k &= \frac{(10!)^{-1/2}}{B^2} \det\{1s(1)_\alpha, 1s(2)_\beta, 2p_z(3)_\alpha, 2p_z(4)_\beta, 2p_x(5)_\alpha, 2p_x(6)_\beta, \\
&\qquad 2p_y(7)_\alpha, 2p_y(8)_\beta, h(9)_\alpha, h(10)_\beta\},
\end{aligned}\right\} \qquad \ldots\ldots(2.5)$$

together with $\tilde{\Psi}_{p\beta}$, $\tilde{\Psi}_{s\beta}$ and $\tilde{\Psi}_{l\beta}$, which are obtained from $\tilde{\Psi}_{p\alpha}$, $\tilde{\Psi}_{s\alpha}$, $\tilde{\Psi}_{l\alpha}$ by interchanging the symbols $2p_z$ and h, 2s and h, 2s and $2p_z$, respectively. The symbols A and B are normalization constants.

From these functions the normalized bond eigenfunctions

$$\tilde{\Psi}_{\tilde{p}} = [2\{1 + (\tilde{\Psi}_{p\alpha} | \tilde{\Psi}_{p\beta})\}]^{-1/2}(\tilde{\Psi}_{p\alpha} + \tilde{\Psi}_{p\beta})$$

$$\tilde{\Psi}_{\tilde{s}} = [2\{1 + (\tilde{\Psi}_{s\alpha} | \tilde{\Psi}_{s\beta})\}]^{-1/2}(\tilde{\Psi}_{s\alpha} + \tilde{\Psi}_{s\beta})$$

and the unnormalized bond eigenfunction

$$\tilde{\Psi}_{\cdot} = 2^{-1/2}(\tilde{\Psi}_{l\alpha} + \tilde{\Psi}_{l\beta})$$

are constructed.

The resulting non-orthogonal wave functions will be denoted by the row vector $\widetilde{\Psi}$;

$$\widetilde{\Psi} = (\widetilde{\Psi}_1, \widetilde{\Psi}_{\bar{p}}, \widetilde{\Psi}_j, \widetilde{\Psi}_{\bar{s}}, \widetilde{\Psi}_l, \widetilde{\Psi}_p). \qquad \ldots\ldots(2.6)$$

In order to avoid the appearance of multiple exchange integrals, a set of orthonormal wave functions $\widetilde{\Psi}_1^0$, $\widetilde{\Psi}_{\bar{p}}^0$, $\widetilde{\Psi}_j^0$, $\widetilde{\Psi}_{\bar{s}}^0$, $\widetilde{\Psi}_l^0$, $\widetilde{\Psi}_k^0$ is also considered. This set of wave functions is obtained from the set (2.6) by replacing the orbital h wherever it appears by the orbital

$$c = \{1 - (1s\,|\,h)^2 - (2s\,|\,h)^2 - (2p_s\,|\,h)^2\}^{-1/2}\{h - (1s\,|\,h)1s - (2s\,|\,h)2s - (2p_s\,|\,h)2p_s\}$$

which is normalized and orthogonal to all the fluorine orbitals. We will denote this orthonormal set of wave functions by the row vector $\widetilde{\Psi}^0$:

$$\widetilde{\Psi}^0 = (\widetilde{\Psi}_1^0, \widetilde{\Psi}_{\bar{p}}^0, \widetilde{\Psi}_j^0, \widetilde{\Psi}_{\bar{s}}^0, \widetilde{\Psi}_l^0, \widetilde{\Psi}_k^0). \qquad \ldots\ldots(2.7)$$

Kastler shows that the wave functions (2.7) are linear combinations of the wave functions (2.6) and gives explicit formulae for transforming from one set to the other. This transformation may be written as the matrix equation†

$$\widetilde{\Psi}^0 = \widetilde{\Psi} T \qquad \ldots\ldots(2.8)$$

where

$$T = \begin{bmatrix} 1, & -0{\cdot}5108, & 0{\cdot}1305, & -0{\cdot}8070, & -0{\cdot}2915, & 0{\cdot}3256 \\ ., & 1{\cdot}1229, & -0{\cdot}5736, & . \;, & 0{\cdot}6408, & . \\ ., & . \;, & 1{\cdot}1305, & . \;, & . \;, & . \\ ., & . \;, & . \;, & 1{\cdot}2850, & 0{\cdot}4642, & -1{\cdot}0370 \\ ., & . \;, & . \;, & . \;, & 1{\cdot}2242, & . \\ ., & . \;, & . \;, & . \;, & . \;, & 1{\cdot}3256 \end{bmatrix} \qquad \ldots(2.9)$$

Kastler also gives numerical values for the matrices of the Hamiltonian $\mathscr{H}$ and the quantity

$$\xi = \sum_{i=1}^{10} z_i,$$

which represents the sum of the z coordinates of the ten electrons, with respect to the orthonormal wave functions. In the representation (2.7) these matrices are, in atomic units

$$\widetilde{H}^0 = \begin{bmatrix} 0{\cdot}3855, & -0{\cdot}4566, & 0{\cdot}0340, & 0{\cdot}2562, & -0{\cdot}0388, & 0{\cdot}0277 \\ & 0{\cdot}4541, & -0{\cdot}2886, & 0{\cdot}1420, & 0{\cdot}0892, & 0{\cdot}0267 \\ & & 1{\cdot}0968, & 0{\cdot}0047, & -0{\cdot}0324, & 0{\cdot}1994 \\ & & & 1{\cdot}3758, & 0{\cdot}1945, & -0{\cdot}0324 \\ & & & & 2{\cdot}1605, & -0{\cdot}0324 \\ & & & & & 2{\cdot}9022 \end{bmatrix} \qquad (2.10)$$

and

$$\widetilde{\xi}^0 = \begin{bmatrix} . \;, & 0{\cdot}3756, & . \;, & 0{\cdot}1600, & . \;, & . \\ & 1{\cdot}9791, & 0{\cdot}3756, & -0{\cdot}5597, & -0{\cdot}1131, & . \\ & & 3{\cdot}9583, & . \;, & 0{\cdot}7915, & . \\ & & & 1{\cdot}9791, & -0{\cdot}2656, & 0{\cdot}1600 \\ & & & & 3{\cdot}9583, & 0{\cdot}7915 \\ & & & & & 3{\cdot}9583 \end{bmatrix} \qquad (2.11)$$

† The values in the fifth column of T differ from those given by Kastler (1953). His expression for Ψ_l' (p. 565) is in error. Fortunately this error does not affect his results, except for the final expression of the wave function in the non-orthogonal representation.

both matrices being symmetrical about the leading diagonal. In equation (2.10) the origin of the energy scale is the energy at infinite nuclear separation given by the wave function $\widetilde{\Psi}_{\bar{p}}$. Since the functions $\widetilde{\Psi}^0$ form an orthonormal set, the overlap matrix in this representation is equal to the unit matrix

$$\widetilde{M}^0 = I. \qquad \ldots\ldots(2.12)$$

The normalized wave function $\widetilde{\Phi}$, binding energy $\widetilde{E}$ and dipole moment $\widetilde{m}$ of the ground state of HF are now given by the equations:

$$\left.\begin{aligned} \widetilde{\Phi} &= \widetilde{\Psi}^0\widetilde{\Gamma}^0, \\ \det(\widetilde{H}^0 - \widetilde{E}I) &= 0, \qquad \text{(lowest root)} \\ (\widetilde{H}^0 - \widetilde{E}I)\widetilde{\Gamma}^0 &= 0, \\ \widetilde{\Gamma}^{0\dagger}\widetilde{\Gamma}^0 &= 1, \\ \widetilde{m} &= \rho - \widetilde{\Gamma}^{0\dagger}\widetilde{\xi}^0\widetilde{\Gamma}^0, \end{aligned}\right\} \qquad \ldots\ldots(2.13)$$

where $\widetilde{\Gamma}^0$ is a column vector with Hermitian conjugate $\widetilde{\Gamma}^{0\dagger}$.

The corresponding equations in the non-orthogonal representation (2.6) are the following

$$\left.\begin{aligned} \widetilde{\Phi} &= \widetilde{\Psi}\widetilde{\Gamma}, \\ \det(\widetilde{H} - \widetilde{E}\widetilde{M}) &= 0, \qquad \text{(lowest root)} \\ (\widetilde{H} - \widetilde{E}\widetilde{M})\widetilde{\Gamma} &= 0, \\ \widetilde{\Gamma}^{\dagger}\widetilde{M}\widetilde{\Gamma} &= 1, \\ \widetilde{m} &= \rho - \widetilde{\Gamma}^{\dagger}\widetilde{\xi}\widetilde{\Gamma} \end{aligned}\right\} \qquad \ldots\ldots(2.14)$$

where the matrices $\widetilde{H}$, $\widetilde{M}$ and $\widetilde{\xi}$ are given in terms of the matrices (2.9), (2.10) and (2.11) by the equations

$$\left.\begin{aligned} \widetilde{H} &= S^{\dagger}\widetilde{H}^0 S, \\ \widetilde{M} &= S^{\dagger}S, \\ \widetilde{\xi} &= S^{\dagger}\widetilde{\xi}^0 S \end{aligned}\right\} \qquad \ldots\ldots(2.15)$$

with $S = T^{-1}$.

§ 3. Atomic Excitation Energies

In order to apply Moffitt's correction and the intra-atomic correlation correction to the calculation of § 2, we must consider the asymptotic behaviour of the basic wave functions (2.6). For large nuclear separations these wave functions yield the following valence states:

$$\widetilde{\Psi}_{\bar{1}} \to F^-(1s)^2(2s)^2(2p)^6 V_0 + H^+ V_0 \qquad \ldots\ldots(3.1)$$

$$\widetilde{\Psi}_{\bar{p}} \to F(1s)^2(2s)^2(2p_x)^2(2p_y)^2(2p_z)V_1 + H(1s)V_1 \qquad \ldots\ldots(3.2)$$

$$\widetilde{\Psi}_{\bar{j}} \to F^+(1s)^2(2s(^2(2p_x)^2(2p_y)^2 V_0 + H^-(1s)^2 V_0 \qquad \ldots\ldots(3.3)$$

$$\widetilde{\Psi}_{\bar{\varepsilon}} \to F(1s)^2(2s)(2p)^6 V_1 + H(1s)V_1 \qquad \ldots\ldots(3.4)$$

$$\widetilde{\Psi}_{\bar{1}} \to F^+(1s)^2(2s)(2p_x)^2(2p_y)^2(2p_z)V_0 + H^-(1s)^2 V_0 \qquad \ldots\ldots(3.5)$$

$$\widetilde{\Psi}_{\bar{k}} \to F^+(1s)^2(2p)^6 V_0 + H^-(1s)^2 V_0. \qquad \ldots\ldots(3.6)$$

The energies of the above fluorine valence states were calculated for the orthogonalized Slater functions (2.1) using Dirac's vector formula. Three sets of values were used for the screening constants a and μ:

(1) The values $a=8{\cdot}67$, $\mu=2{\cdot}6$ of the orbital calculation (cf. equation (2.2)).

(2) The values F^+ $a=8{\cdot}7$, $\mu=2{\cdot}775$,

F $a=8{\cdot}7$, $\mu=2{\cdot}6$,

F^- $a=8{\cdot}7$, $\mu=2{\cdot}425$,

given by Slater's rules (Slater 1930).

(3) Optimum values obtained by minimizing the total energy for each valence state.

The results of these calculations are shown in table 1 together with the experimental values of Pritchard and Skinner (1953). The state

$$F(1s)^2(2p_x)^2(2p_y)^2(2p_z)V_1$$

is taken as the origin of energy. Because of their very high excitation energies no experimental estimates are possible for the states $F^+(1s)^2(2s)(2p)^5V_2$ and $F^+(1s)^2(2p)^6V_0$.

Table 1. Calculated and Experimental Excitation Energies (ev)

State	Calculated energies			Experiment
	(1)	(2)	(3)	
$F(sp^6, V_1)$	26·83	26·83	26·70	20·95
$F^-(s^2p^6, V_0)$	11·67	6·90	6·99	$-3{\cdot}65\pm(0{\cdot}10)$
$F^+(s^2p^4, V_0)$	16·01	15·56	15·30	20·88
$F^+(sp^5, V_0)$	37·72	37·06	36·93	—
$F^+(p^6, V_0)$	66·96	66·56	66·36	—

From table 1 it is clear that all the wave functions considered are incapable of providing accurate estimates of atomic and ionic excitation energies. The errors in the calculated values of the electron affinity are particularly large. Consequently the results of a calculation by the method of atoms in molecules or one using the intra-atomic correlation correction will differ markedly from those of the simple orbital theory (§ 2). Furthermore, because of the difference of 5 ev in the estimates which calculation (1) and calculations (2) and (3) provide for the electron affinity of fluorine the atoms in molecules and the intra-atomic correlation correction calculations will lead to significantly different results.

On the other hand we see that the differences between calculations (2) and (3) are insignificant, especially in view of the uncertainty in the experimental value of the electron affinity. For practical purposes, Slater's rules may be regarded as giving the optimum parameter values for each valence state.

§ 4. The Modified Energy Matrix

In a calculation by the method of atoms in molecules the basic functions (2.6) of the orbital theory are regarded as approximations to a more accurate set of functions

$$\Psi=(\Psi_{\bar{i}}, \Psi_{\bar{p}}, \Psi_{\bar{j}}, \Psi_{\bar{s}}, \Psi_{\bar{i}}, \Psi_{\bar{k}}), \qquad \ldots\ldots(4.1)$$

which are constructed from exact wave functions for the valence states (3.1)–(3.6) (Moffitt 1951). The energy matrix H with respect to the functions (4.1) is estimated from the formula

$$H=\widetilde{H}+\tfrac{1}{2}[\widetilde{M}(W-\widetilde{W})+(W-\widetilde{W})\widetilde{M}], \qquad \text{(AIM theory)} \ldots\ldots (4.2)$$

where $\widetilde{H}$ and $\widetilde{M}$ are the energy and overlap matrix of the orbital theory (equation (2.15)), W is a diagonal matrix formed from the experimental energies of the valence states (3.1)...(3.6), and $\widetilde{W}$ is the asymptotic form of $\widetilde{H}$ for large nuclear separations.

To evaluate the matrix $W-\widetilde{W}$, cf. equation (4.2), we use the values given in table 1 (calculation (1) and experiment), the accurate value 0·75 ev for the electron affinity of the hydrogen atom (Chandrasekhar 1944), and the value −3·40 ev predicted by the function (2.4). From these values we obtain the matrix

$$\begin{aligned} W-\widetilde{W} &= \text{diag}\{-15{\cdot}32,\ 0,\ 0{\cdot}72,\ -5{\cdot}88,\ (0{\cdot}72),\ (0{\cdot}72)\}\ \text{(ev)} \\ &= \text{diag}\{-0{\cdot}5632,\ 0,\ 0{\cdot}0265,\ -0{\cdot}2161,\ (0{\cdot}0265)\ (0{\cdot}0265)\}\ \text{(A.U.)} \ldots . (4.3) \end{aligned}$$

Here the lowest energy valence state dissociation products (3.2) have been chosen as the origin of the energy scale. Because of the effects of spin orbit interaction this energy origin is very slightly ($\simeq$0·02 ev) above the energy of the dissociation products in their ground states (Pritchard and Skinner 1953).

In constructing the matrix (4.3) we have assumed that the corrections for the unobservable states (3.5) and (3.6) are the same as that for the observed state (3.3) of the same ionicity. These corrections for the unobservable states have been included for the sake of completeness. Because of their high excitation energies these states play a very minor role in the calculations and changes in their energies of up to 5 ev have a negligible effect on the results.

For numerical purposes it is convenient to transform equation (4.2) into the orthogonal representation (2.7) by means of the matrix T of equation (2.9). In this representation we have

$$H^0=\widetilde{H}^0+\tfrac{1}{2}[(W-\widetilde{W})^0+(W-\widetilde{W})^{0\dagger}], \qquad \text{(AIM theory)} \ldots\ldots (4.4)$$

with

$$(W-\widetilde{W})^0=T^{-1}(W-\widetilde{W})T. \qquad \text{(AIM theory)} \qquad \ldots\ldots (4.5)$$

The normalized wave function Φ, binding energy E, and dipole moment m of the ground state of HF according to the theory of atoms in molecules are now given by the equations

$$\left.\begin{aligned} \Phi &= \Psi^0\Gamma^0 \\ \det(H^0-EI) &= 0 \qquad \text{(lowest root)} \\ (H^0-EI)\Gamma^0 &= 0 \\ \Gamma^{0\dagger}\Gamma^0 &= 1 \\ m &= \rho-\Gamma^{0\dagger}\tilde{\xi}^0\Gamma^0. \end{aligned}\right\} \ldots\ldots (4.6)$$

Detailed calculations on the hydrogen molecule (Pauncz 1954, Hurley 1955, 1956) show that the basic equation (4.2) of the theory of atoms in molecules is quite inaccurate when applied to a calculation such as that of § 2 which employs the same orbitals to approximate the neutral and ionic valence states (3.1)–(3.6). Two methods have been suggested for overcoming this difficulty. The first consists in using different screening constants for the ionic valence states in the orbital calculation. With this modification equation (4.2) provides an accurate

approximation. This has been shown by Pauncz (1954) who has carried out a complete calculation on the H_2 molecule using the accurate wave functions of Hylleraas (1930) for the ion H^-. The results of this calculation are in complete agreement with those of the atoms in molecules theory using different screening constants for H and H^- (Hurley 1955). However there are two serious disadvantages in this approach. Firstly the computational difficulties are greatly increased, and secondly it appears that, at least for the hydrogen molecule, the accurate atomic and ionic wave functions do not form a suitable basis for expanding the molecular wave function.

The second method of eliminating the errors from equation (4.2) consists in re-interpreting the accurate wave functions (4.1). These are now taken to represent the best possible (lowest energy) wave functions for the valence states (3.1)–(3.6) subject to the restriction that the total charge density for each valence state shall be the same as that given by the wave functions of the orbital calculation §2. The energies corresponding to the wave functions (4.1) are now estimated by assuming that the correlation energy for each valence state wave function is independent of the screening constants. We are thus led to the approximation

$$H=\widetilde{H}+\tfrac{1}{2}[\widetilde{M}(W-\widetilde{W}')+(W-\widetilde{W}')\widetilde{M}], \qquad \text{(ICC theory)} \quad \ldots\ldots(4.7)$$

in place of equation (4.2) (Hurley 1955 b). Here $\widetilde{W}'$ is obtained from $\widetilde{W}$ by minimizing the energy of each valence state with respect to variations in the screening constants. From the results of § 3 it is apparent that the tedious task of varying the screening constants for each valence state may be avoided, without introducing significant errors, by the use of Slater's rules. We therefore base the calculation of the matrix $\widetilde{W}'$ on column (2) of table 1 rather than on column (3). From these values and the electron affinity of the hydrogen atom predicted by optimum hydrogenic functions ($-0{\cdot}74$ ev) we obtain the matrix

$$\begin{aligned} W-\widetilde{W}' &= \text{diag}\{-10{\cdot}55,\ 0,\ 3{\cdot}83,\ -5{\cdot}88,\ (3{\cdot}83),\ (3{\cdot}83)\}\ \text{(ev)},\\ &= \text{diag}\{-0{\cdot}3876,\ 0,\ 0{\cdot}1408,\ -0{\cdot}2161,\ (0{\cdot}1408),\ (0{\cdot}1408)\},\ \text{(A.U.)} \end{aligned} \quad \ldots\ldots(4.8)$$

where as before the corrections for the unobservable states (3.5) and (3.6) have been assumed to be the same as that for the state (3.3).

It is again convenient to transform to the orthogonal representation (2.7). Equations (4.4) and (4.5) now become

$$H^0=\widetilde{H}^0+\tfrac{1}{2}[(W-\widetilde{W}')+(W-\widetilde{W}')^0], \qquad \text{(ICC theory)} \quad \ldots\ldots(4.9)$$

with $$(W-\widetilde{W}')^0=T^{-1}(W-\widetilde{W}')T. \qquad \text{(ICC theory)} \quad \ldots\ldots(4.10)$$

The ground state wave function, energy and dipole moment in the intra-atomic correlation correction theory are given by equations (4.6) with H^0 given by equation (4.9).

§ 5. Numerical Results

The values of the binding energy D_e and dipole moment m of hydrogen fluoride predicted by various calculations are shown in table 2 together with the experimental values. The table includes calculations using all six valence states (3.1)–(3.6) and simpler calculations based on the two most important states

(3.1) and (3.2). The results of the orbital calculations and Kastler's modified calculation were taken from Kastler (1953). The experimental value of the binding energy D_e was obtained from the now generally accepted value of 37·7 kcal for the heat of dissociation of F_2 (Doescher 1952), the heat of dissociation of H_2, the heat of formation of HF (Rossini 1947) and the zero point vibrational energy of HF (Herzberg 1950). The experimental value of the dipole moment m was taken from Hannay and Smyth (1946).

Table 2. Calculated and Experimental Properties of Hydrogen Fluoride

	Orbital (2 terms)	Orbital (6 terms)	AIM (2 terms)	KM (2 terms)	KM (6 terms)	ICC (2 terms)	ICC (6 terms)	Experiment
D_e(ev)	1·03	1·96	8·33	5·05	5·77	5·39	5·84	6·08
m (Debye)	1·13	0·93	3·01	3·03	2·75	2·44	2·33	1·91

AIM=atoms in molecules; KM=Kastler's modified theory; ICC=intra-atomic correlation correction.

It is apparent from table 2 that the unmodified orbital calculation is much too crude to provide a useful estimate of either the binding energy or the dipole moment of hydrogen fluoride. It is also clear that the atoms in molecules theory based on equation (4.2) is not satisfactory, even though the results are a considerable improvement on those of the orbital theory. A calculation by this method, based on the first two wave functions of the set (4.1), leads to a binding energy considerably greater than the experimental value. Although such a result would not necessarily invalidate an orbital calculation based on approximate atomic functions, it is inconsistent with the basis (4.1) of the atoms in molecules theory, which includes the exact wave functions for the separated atoms. The principal source of this error is clearly the same as in the case of the hydrogen molecule (Hurley 1956); the use of too large a value for the screening constant in the F^- orbitals leads to a serious over-estimation of the interaction energy of the ions F^- and H^+. Consequently, equation (4.2) introduces serious errors, and the atoms in molecules calculation is not a good approximation to an accurate calculation in terms of the basis (4.1). This is reflected in the large value of the calculated dipole moment, which indicates an over-estimation of the importance of the ionic structure H^+F^-.

The modification employed by Kastler avoids the most serious error of the atoms in molecules theory by using the results of a self-consistent field calculation on F^- (Hartree 1933) to estimate the interaction energy of F^- and H^+. In as much as some of the interaction terms are estimated using a realistic approximation to the exact wave function for F^-, Kastler's modification may be regarded as a very incomplete version of a calculation by the atoms in molecules theory using different screening constants for atomic and ionic states.

The results of the intra-atomic correlation correction theory appear satisfactory. Although some 20% too high, the estimated dipole moment is considerably better than for any of the other calculations. The greater part of the error may well be due to neglect of the polarization of the non-bonding $2p_\pi$ electrons of the fluorine atom. The binding energy given by the six-term intra-atomic correlation correction calculation is rather better than might be expected in view of the fact that the values of the screening constants for the fluorine and hydrogen orbitals have not been varied to minimize the total energy. It appears that such a variation is less important here than in the case of the hydrogen molecule (Altmann and Cohan 1954, Hurley 1956).

References

ALTMANN, S. L., and COHAN, N. V., 1954, *Trans. Faraday Soc.*, **50**, 1151.
CHANDRASEKHAR, S., 1944, *Rev. Mod. Phys.*, **16**, 301.
DOESCHER, R. N., 1952, *J. Chem. Phys.*, **20**, 330.
HANNAY, N., and SMYTH, C., 1946, *J. Amer. Chem. Soc.*, **68**, 171.
HARTREE, D. E., 1933, *Proc. Roy. Soc.* A, **41**, 282.
HERZBERG, G., 1950, *Spectra of Diatomic Molecules* (New York : Van Nostrand).
HURLEY, A. C., 1955, *Proc. Phys. Soc.* A, **68**, 149 ; 1956, *Ibid.*, **69**, 49.
HYLLERAAS, E. A., 1930, *Z. Phys.*, **60**, 624.
KASTLER, D., 1953, *J. Chem. Phys.*, **50**, 556.
MOFFITT, W., 1951, *Proc. Roy. Soc.* A, **210**, 245.
PAUNCZ, R., 1954, *Acta Phys. Hung.*, **4**, 237.
PRITCHARD, H. O., and SKINNER, H. A., 1953, *Trans. Faraday Soc.*, **49**, 1254.
ROSSINI, F. D., *et al.*, 1947, *Circ. U.S. Bur. Stand.*, 461, *Tables of Selected Values of Pyoperties of Hydrocarbons.*
SCHERR, C. S., 1955, *J. Chem. Phys.*, **23**, 569.
SLATER, J. C., 1930, *Phys. Rev.*, **36**, 57.

An Investigation of Deuteron Induced Reactions by Magnetic Analysis III : Results for Neon and Argon

By H. B. BURROWS, T. S. GREEN†, S. HINDS and R. MIDDLETON‡
Nuclear Physics Research Laboratory, University of Liverpool

Communicated by H. W. B. Skinner ; MS. received 24th October 1955 and in final form 6th December 1955

Abstract. The energy spectra of the protons emitted from targets of natural neon and argon when bombarded by 8·5 MeV deuterons have been measured by magnetic analysis and in both cases several levels not previously reported have been observed. The angular distributions of nine proton groups from ^{20}Ne, two groups from ^{22}Ne and eight groups from ^{40}A have been measured. In most cases these have been fitted with theoretical stripping curves enabling the spin and parity assignments listed below to be made:

^{21}Ne ground state (isotropic) 0·35 MeV (3/2 or 5/2$^+$), 2·78(1/2$^+$), 4·58(3/2 or 5/2$^+$) 4·81(1/2, 3/2$^-$), 5·43(3/2, 5/2$^+$), 5·63(3/2, 5/2$^+$), 5·78(1/2, 3/2$^-$), 6·72(3/2, 5/2$^+$)
^{23}Ne ground state (3/2, 5/2$^+$), 0·98(1/2$^+$).
^{41}A ground state (5/2, 7/2$^-$), 0·57, 1·39, 2·46, 2·79, 3·01, 3·36, 3·98 (all 1/2, 3/2$^-$).

§ 1. Introduction

The apparatus and method of procedure described in papers I and II (Green and Middleton 1956 a, b) has been used to measure the proton energy spectra and the angular distributions of the prominent groups emitted by neon and argon when bombarded by 8·5 MeV deuterons. Attempts have been made to fit the angular distributions with theoretical curves calculated from the stripping theory of Bhatia, Huang, Huby and Newns (1952) enabling the parities and possible spins to be assigned to the states of the residual nuclei. Since ^{20}Ne and ^{40}A have zero spin the ambiguity usually present in the spin assignment is restricted to $l \pm \frac{1}{2}$, where l is the orbital angular momentum of the absorbed neutron.

Both exposures were made using the gas target chamber described in paper I filled respectively with spectroscopically pure neon and argon gas of normal isotopic abundance to a pressure of about 40 cm Hg. Due to the presence of about 9% of ^{22}Ne in natural neon it was possible to identify and measure the angular distributions of two proton groups corresponding to states in ^{23}Ne.

The energy levels of ^{21}Ne have previously been investigated below an excitation energy of about 3 MeV by Sperduto (1951) and Ahnlund (1954 a, b), magnetic analysis being used in both cases, and below 9 MeV by Middleton and Tai (1951 a). Middleton and Tai (1951 b) used a photographic plate scattering camera and were also able to measure the angular distributions of most proton groups. However, on account of the interference of elastically scattered deuterons at small angles of emission, the l-value assignments were uncertain except for the ground, first and third excited states.

†Now at the Atomic Energy Research Establishment, Harwell, Berks.
‡Now at the Atomic Weapons Research Establishment, Aldermaston, Berks.

The proton energy spectrum from the ^{40}A(d, p)^{41}A reaction has previously been measured by Davison, Buchanan and Pollard (1949) below an excitation energy of about 4 MeV using an absorption method. The angular distributions of the proton groups corresponding to the ground and an excited state of ^{41}A at 1·34 MeV have also been measured by Gibson and Thomas (1952). These authors assigned $l=3$ for the transition to the ground state but were unable to make a unique assignment to the transition to the 1·34 MeV state.

§ 2. Results

(a) Neon.

A typical proton energy spectrum obtained at an angle of observation of 15° is shown in figure 1. It may be noticed that the energy resolution is poorer than usually obtained from solid targets (paper II). This is principally due to the increased size of the target, necessitated by intensity considerations, and the straggling of the incident deuterons and emitted protons in the gas outside the actual target volume.

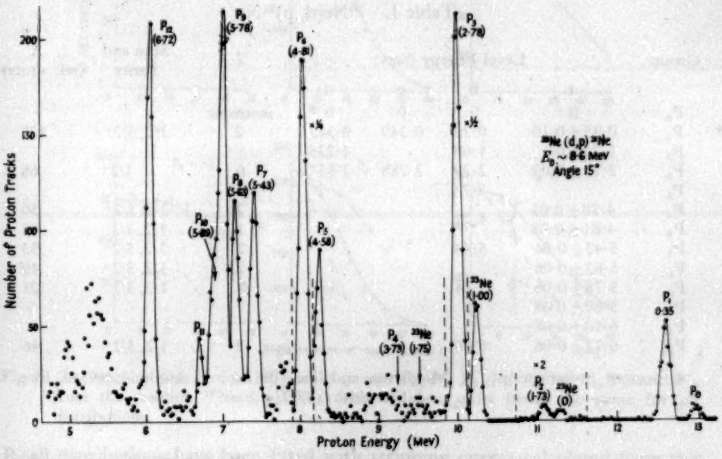

Figure 1. Energy spectrum of protons emitted from the deuteron bombardment of a target of natural neon, obtained at an angle of observation of 15°.

The energy of the incident deuteron beam was calculated from the Q-value of the first excited state reported by Ahnlund and found to be 8·60 MeV. This state was used rather than the ground state since the corresponding proton group was considerably more intense, enabling a more accurate determination of its position on the plate and hence of its energy to be made. Since measurements of spectra were made over a limited angular range it was not possible to identify proton groups corresponding to the less abundant isotope ^{22}Ne by measuring their shift in position relative to groups definitely identified as

corresponding to ^{20}Ne. However, two groups were positively identified corresponding to transitions from ^{22}Ne to the ground and an excited state at 0·98 MeV of ^{23}Ne by calculating their positions on the plates at different angles from their known Q-values (Zucker and Watson 1950) and the previously determined beam energy. These are marked in figure 1 by the symbol ^{23}Ne as distinct from groups due to ^{20}Ne which are marked P_0, P_1, P_2, etc. Further evidence in favour of assigning these two groups due to the ^{22}Ne(d, p)^{23}Ne reaction was obtained from the measurement of their angular distributions but this will be discussed later.

The remaining proton groups have all been assumed to be due to the more abundant isotope ^{20}Ne, though it is not possible to be completely certain of this, particularly in the cases of weak groups such as P_{11}. The Q-values of these groups have been calculated at different angles from their energies, determined from the position along the plate, and the calculated deuteron energy. It may be noted that any small error in the beam energy affects only the Q-values and has a negligible effect on the energy levels which are listed in column a of table 1. Also listed

Table 1. ^{20}Ne(d, p)^{21}Ne

Group	Level Energy (MeV)				l	Spin and Parity	Λ (rel. units)
	a	b	c	d			
P_0	0	0	0	0	isotropic		
P_1	0·35 ± 0·10	0·33	0·349	0·343	2	3/2, 5/2$^+$	128
P_2	1·73 ± 0·1	1·68		1·735			
P_3	2·78 ± 0·05	2·79	2·788	2·852	0	1/2$^+$	68
P_4		3·73					
P_5	4·58 ± 0·05	4·71			2	3/2, 5/2$^+$	50
P_6	4·81 ± 0·05				1	1/2, 3/2$^-$	98
P_7	5·43 ± 0·06	5·44			2	3/2, 5/2$^+$	53
P_8	5·63 ± 0·06	5·74			2	3/2, 5/2$^+$	49
P_9	5·78 ± 0·06				1	1/2, 3/2$^-$	21
P_{10}	5·89 ± 0·08						
P_{11}	6·10 ± 0·08						
P_{12}	6·72 ± 0·06	6·66			2	3/2, 5/2$^+$	46

a, present investigation ; b, Middleton and Tai (1951a) ; c, Ahnlund (1954a, b) ; d, Sperduto (1951).

in columns b, c and d are the energy levels reported by Middleton and Tai, Ahnlund and Sperduto, the last mentioned being determined from an investigation of the ^{23}Na(d, α)^{21}Ne reaction. Good agreement is obtained in the positions of the first, second and third excited states, but no group of significant intensity was observed corresponding to the level at 3·73 MeV reported by Middleton and Tai. The levels at 4·71 and 5·74 MeV reported by the latter authors have been resolved into two and three groups respectively. A group P_{11} was also observed corresponding to a level at 6·10 MeV which has not previously been reported. However, as mentioned above, it is not possible to state with certainty if this is due to ^{20}Ne. Group P_{12} was calculated to correspond to a level at 6·72 MeV which is in good agreement with the level at 6·66 MeV reported by Middleton and Tai.

The angular distributions of groups P_0, P_1, P_3, P_5, P_6, P_7, P_8, P_9 and P_{12} have been measured and are plotted in the centre-of-mass system in figure 2, the differential cross sections being in arbitrary units. Except in the case of group

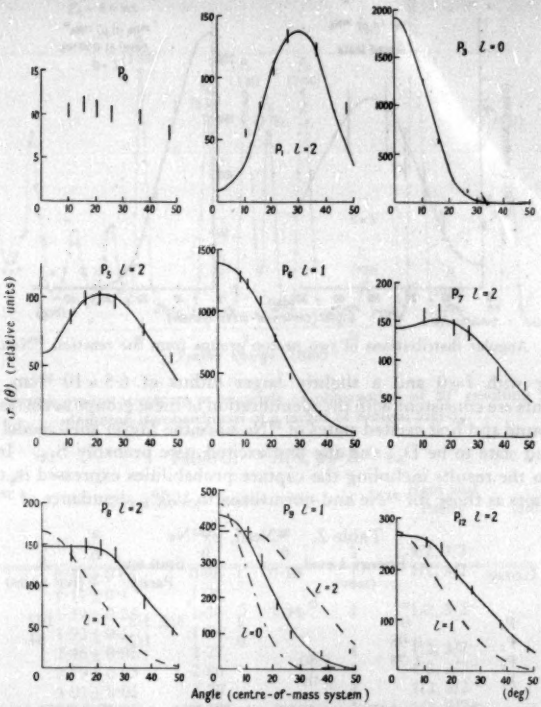

Figure 2. Angular distributions of proton groups P_0, P_1, P_3, P_5, P_6, P_7, P_8, P_9, and P_{12} from the reaction $^{20}Ne(d, p)^{21}Ne$. The ordinate units being the same for all distributions.

P_0 all distributions have been fitted with stripping curves calculated from the theory of Bhatia *et al.* and the *l*-value assignments are listed in table 1. Also shown in the figure are some alternative curves of different *l*-values. These were drawn for groups P_8, P_9 and P_{12} since they have small *Q*-values and the difference between the theoretical curves corresponding to various *l*-values is minimum. For most groups a radius of interaction of $6{\cdot}0 \times 10^{-13}$ cm was used, which is equal to the Gamow radius plus 1×10^{-13} cm, this radius having been reported by Holt and Marsham (1953) as being the most satisfactory. Better fits were obtained from groups P_1, P_3 and P_9 with radii of 7·0, 6·5 and $6{\cdot}5 \times 10^{-13}$ cm respectively. Also listed in table 1 are the parities and possible spins of the various states of ^{21}Ne obtained assuming ^{20}Ne to have zero spin and even parity and the relative neutron capture probabilities Λ.

The angular distributions of the two groups assigned to the formation of ^{23}Ne in the ground and an excited state at 0·98 Mev are shown in figure 3. The former has been fitted with an $l=2$ curve calculated using a radius of $6{\cdot}1\times10^{-13}$ cm and

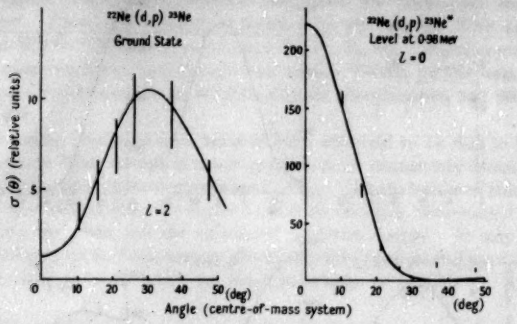

Figure 3. Angular distributions of two proton groups from the reaction ^{22}Ne(d, p)^{23}Ne.

the latter with $l=0$ and a slightly larger radius of $6{\cdot}5\times10^{-13}$ cm. These assignments are consistent with the identification of these groups as corresponding to the ground and first excited states of ^{23}Ne since the Meyer shell model predicts the ground state to be $D_{5/2}$ and the first excited state probably $S_{1/2}$. In table 2 are shown the results including the capture probabilities expressed in the same relative units as those for ^{21}Ne and normalized to 100% abundance of ^{22}Ne.

Table 2. ^{22}Ne(d, p)^{23}Ne

Group	Energy Level (Mev) a	Energy Level (Mev) b	l	Spin and Parity	Λ (rel. units)
P_0	0		2	3/2, $5/2^+$	102
P_1	0·98		0	$1/2^+$	84
P_2	1·75	1·80			
P_3		3·01			

a, Zucker and Watson (1950) ; b, Middleton and Tai (1951a).

(*b*) *Argon.*

In figure 4 is shown a proton energy spectrum obtained at an angle of observation of 20°. As in the case of neon, the energy of the incident deuteron beam was calculated from a known Q-value. For this purpose the Q-value of 3·90 Mev reported by Gibson and Thomas for the transition to the ground state was used, which gave a beam energy of 8·39 Mev. Using this value and the energies of proton groups deduced according to their position along the plate the corresponding Q-values and energy levels were calculated. Since natural argon contains 99·6% of ^{40}A, all groups were assumed to be due to this isotope. The energy levels of ^{41}A determined in this way are listed in table 3 together with those reported by Davison *et al.* and Gibson and Thomas. As is evident from the table the positions of levels obtained during the present investigation are in moderately good agreement with those of Davison *et al.* except for groups P_5, P_7 and P_8.

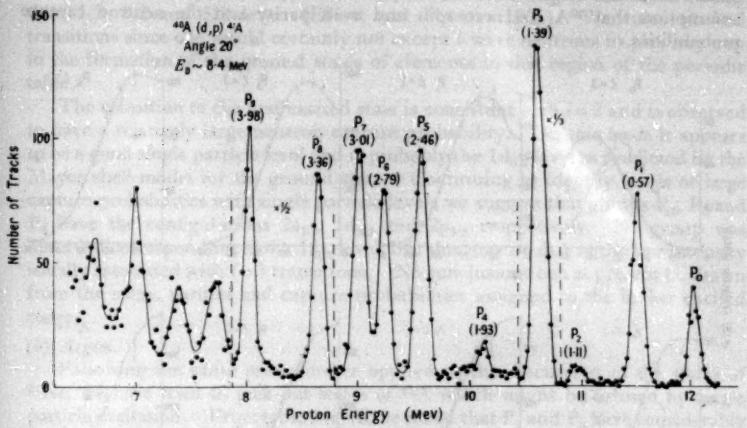

Figure 4. Proton energy spectrum at an angle of observation of 20° resulting from the deuteron bombardment of a target of natural argon.

Table 3. ^{40}A(d, p)^{41}A

Groups	Level Energy (Mev)			l	Spin and Parity	A (rel. units)
	a	b	c			
P_0	0	0	0	3	5/2, 7/2$^-$	130
P_1	0·57 ± 0·05	0·66	0·50	1	1/2, 3/2$^-$	20
P_2	1·11 ± 0·1	1·21				
P_3	1·39 ± 0·05	1·34	1·34	1	1/2, 3/2$^-$	100
P_4	1·93 ± 0·1	1·94				
P_5	2·46 ± 0·05	2·27		1	1/2, 3/2$^-$	19
P_6	2·79 ± 0·05	2·80		1	1/2, 3/2$^-$	17
P_7	3·01 ± 0·05	3·29		1	1/2, 3/2$^-$	18
P_8	3·36 ± 0·05	3·69		1	1/2, 3/2$^-$	28
P_9	3·98 ± 0·05	4·01		1	1/2, 3/2$^-$	27

a, present investigation ; b, Davison, Buchanan and Pollard (1949) ; c, Gibson and Thomas (1952).

The angular distributions of all groups, except P_2 and P_4 which were too weak, have been measured and are plotted in the centre-of-mass system in figure 5 together with the curves calculated from the stripping theory of Bhatia *et al.* Apart from the ground state which is known to correspond to an $l=3$ curve, the remaining groups are all consistent with $l=1$ transitions. The poor fit of the theoretical curve in the case of the ground state is not unusual for an $l=3$ transition and is probably due to a relatively large percentage of the reaction proceeding via a compound nucleus stage. As for neon a radius of interaction equal to the Gamow radius plus 1×10^{-13} cm was used whenever possible in the calculation of the theoretical curves. However, better fits were obtained for groups P_3, P_5, P_6, P_7, P_8, P_9 where a slightly smaller radius equal to $6{\cdot}6\times10^{-13}$ cm was used.

Listed in table 3 are the *l*-values, the parities and possible spins deduced on the assumption that ^{40}A has zero spin and even parity and the neutron capture probabilities.

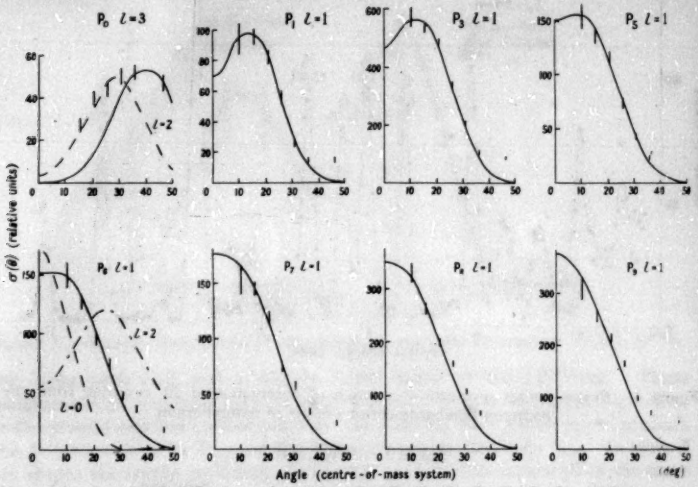

Figure 5 Angular distributions of proton groups P_0, P_1, P_3, P_5, P_6, P_7, P_8 and P_9 from the reaction ^{40}A(d, p)^{41}A.

§ 3. Discussion

(*a*) *Neon.*

The lack of stripping and the small differential cross section observed in the transition to the ground state of ^{21}Ne implies a small capture probability for the stripping process. The cross section for the formation of this state is therefore almost entirely due to the formation and decay of a compound nucleus. A possible explanation would be that ^{21}Ne is a shell model anomaly similar to ^{23}Na in having three nucleons in a sub-shell coupled to give a total spin of 3/2 instead of 5/2. The formation of this state by stripping would therefore involve a rearrangement of the parent nucleus and consequently imply a small capture probability. The spin assignment of 3/2 to ^{21}Ne is favoured by the direct determination of Koch and Rasmussen (1949), who report a most probable value of 3/2 but do not rule out the possibility of a larger value. An investigation of the reaction ^{21}Ne(d, p)^{22}Ne would be of interest since if ^{22}Ne is a normal shell model nucleus and ^{21}Ne is as suggested above, then one would again expect little stripping occurring in the ground state transition. It is also of interest to note that the reaction ^{23}Na(d, n)^{24}Mg has recently been investigated by Calvert, Jaffe, Litherland and Maslin (1955) who report that transition to the ground state of ^{24}Mg to be very weak.

An alternative explanation would arise if ^{21}Ne had a spin $\geqslant 7/2$ in which case the stripping selection rules would not allow its formation by an $l=2$ transition. However, this is unlikely since analysis of the levels of a neighbouring

nucleus ^{19}F indicates that a 7/2 level would occur at a higher excitation energy than 1/2, 3/2 and 5/2 levels (Elliott and Flowers 1955). We rule out $l \geqslant 3$ transitions since one would certainly not except f-wave neutrons to play any part in the formation of the ground states of elements in this region of the periodic table.

The transition to the first excited state is consistent with $l=2$ and is observed to have a relatively large neutron capture probability. On this basis it appears to be a good single particle level and is probably the $1d_{5/2}$ level as predicted by the Mayer shell model for the ground state. Continuing to identify levels of large capture probabilities with single particle levels we suggest that groups P_3, P_5 and P_6 have the configurations $2s_{1/2}$, $1d_{3/2}$ and $2p_{3/2}$ respectively. No group was observed corresponding to the $1f_{7/2}$ level, but this may be due to the low intensity usually associated with $l=3$ transitions. No conclusions can at present be drawn from the spins, parities and capture probabilities assigned to the higher excited states.

(*b*) *Argon.*

Following the same procedure as applied to the discussion of the states of ^{21}Ne, we have tried to pick out states of ^{41}A which might be formed by single particle excitation. From table 3 it will be noted that P_0 and P_3 have considerably larger capture probabilities than the other groups. It seems therefore that the ground state transition corresponds to the capture of a neutron in the $1f_{7/2}$ orbit as predicted by the Mayer shell model. Similarly P_3 may correspond to the capture of a neutron in the $2p_{3/2}$ orbit. The large number of other $l=1$ transitions with similar but smaller capture probabilities is difficult to understand. A possible explanation may be the rearrangement of the ^{40}A core but this would result in a small stripping cross section. However, since these are $l=1$ transitions (unlike the $l=2$ transition to the ground state of ^{21}Ne) they are considerably more intense than the background at small angles of emission and therefore retain their characteristic forward peaks.

Acknowledgments

We are grateful to Professor H. W. B. Skinner for his encouragement and advice and we would also like to thank Dr. H. C. Newns for helpful discussions. One of us (R.M.) wishes to make acknowledgment to the Imperial Chemical Industires for a Research Fellowship and two of us (S.H. and T.S.G.) are grateful to the Department of Scientific and Industrial Research for maintenance grants.

References

Ahnlund, K., 1954a, *Ark. Fys.*, **7**, 155 ; 1954b, *ibid*, **9**, 39.
Bhatia, A. B., Huang, K., Huby, R., and Newns, H. C., 1952, *Phil. Mag.*, **43**, 485.
Calvert, J. M., Jaffe, A. A., Litherland, A. E., and Maslin, E. E., 1955, *Proc. Phys. Soc.* A, **68**, 1008.
Davison, P. W., Buchanan, J. O., and Pollard, E., 1949, *Phys. Rev.*, **76**, 890.
Elliott, J. P., and Flowers, B. H., 1955, *Proc. Roy. Soc.* A, **229**, 536.
Gibson, W. M., and Thomas, E. E., 1952, *Proc. Roy. Soc.* A, **210**, 543.
Green, T. S., and Middleton, R., 1956 a, *Proc. Phys. Soc.* A, **69**, 16; 1956b, *Ibid.*, **69**, 28.
Holt, J. R., and Marsham, T. N., 1953, *Proc. Phys. Soc.* A, **66**, 1032.
Koch, J., and Rasmussen, E., 1949, *Phys. Rev.*, **76**, 1417.
Middleton, R., and Tai, C. T., 1951a, *Proc. Phys. Soc.* A, **64**, 801 ; 1951b, *Ibid.*, **65**, 752.
Sperduto, A., 1951, *Massachusetts Institute of Technology Prog. Report* (May, 1951).
Zucker, A., and Watson, W. W., 1950, *Phys. Rev.*, **78**, 14.

The Relativistic Theory of the Specific Primary Ionization and Stopping Power and its Application in Helium

By H. S. PERLMAN
Physics Department, University of Melbourne

Communicated by L. H. Martin; MS. received 28th November 1955

Abstract. Using a relativistic Born approximation due to Bethe, an expression is derived for the collision cross section of relativistic electrons with an atomic shell in terms of Schrödinger wave functions. Then, by comparison with Møller's work for hydrogen, the stopping power and specific primary ionization are obtained as functions of a number of atomic parameters. These parameters are calculated for the case of helium and the results compared with experiment.

§ 1. Introduction

The original contributions to the theory of the extra-nuclear interaction of relativistic charged particles with matter were made over twenty years ago by Bethe (1932, 1933) and Møller (1932). And while the original non-relativistic theory has recently been improved by Brown (1950) and Walske (1952) no corresponding refinements have been made to the relativistic theory. That such improvements in the latter need to be initiated separately and cannot be obtained from improved lower energy theory may be seen from the following.

Consider the mean ionization energy $\bar{I}$, where $\bar{I}$ is defined as that parameter which allows the non-relativistic stopping power to be written

$$-(dT/dx)=(4\pi e^4 z^2 Z/m_0 v^2)\ln(2m_0 v^2/\bar{I})$$

irrespective of the order of approximation (and what follows is true of the parameters in the specific primary ionization expression also). This parameter merely represents a convenient way of lumping together the terms in the stopping power expression which are dependent on the struck atom. Now Møller, modelling his relativistic calculations on Bethe's non-relativistic work, made approximations radical enough to obtain an expression for $\bar{I}$ identical with Bethe's. But obviously, this does not ensure that the $\bar{I}$ obtained non-relativistically to a higher order approximation than Bethe's, for example Brown's and Walske's, can be substituted into Møller's relativistic stopping power expression without impairing the order of the non-relativistic approximation.

We have therefore derived, *ab initio*, the relativistic differential cross section —and hence the relativistic stopping power and specific primary ionization— of a many-electron shell, examining the approximations made at each step. The formulae obtained are applied to helium.

§ 2. General Theory

2.1. *Derivation of Relativistic Differential Cross Section*

The relativistic differential cross section for electron collisions with hydrogen was obtained by Møller (1932) using the method of variation of constants. Møller, by considering the interaction between incident electrons (specified by the Dirac wave functions for a free electron) and the atomic electrons as a time-independent perturbation applied to the total system 'atom and non-interacting incident electron', obtained the transition probability, and hence the differential cross section, in terms of the interaction matrix element which he derived in the following way.

He calculated the interaction with the atomic electron of the electromagnetic field produced by the transition of the incident electron from initial to final state, by substituting the Dirac charge and current densities associated with this transition into the expressions of classical electromagnetic theory for the potentials due to these densities, and forming the Dirac interaction between the field defined by these potentials and the atomic electron. On symmetrizing, Møller obtained a plausible expression for the interaction matrix element.

Bethe (1933) has extended this method to a many-electron atom and has given an explicit expression for the resultant differential cross section in terms of relativistic atomic wave functions and Dirac spin matrices.

For inelastic collisions with an atomic shell containing Z electrons, Bethe's expression reduces to

$$d\Phi_{mn}(q) = 8\pi e^4 E_1^1 E_1^0 \hbar^{-4} c^{-4} (k_1^0)^{-2} q[q^2 - (\alpha_{mn}^2/2\kappa)^2]^{-2} |\zeta|^2 dq \quad \ldots\ldots(1)$$

where

$$|\zeta|^2 = \left| \int \Psi_n^*(\mathbf{r}_1, \ldots, \mathbf{r}_Z) \{\sum_{j=1}^{Z} \exp(i\mathbf{q}\cdot\mathbf{r}_j)[A - \mathfrak{A}\cdot\boldsymbol{\alpha}^{(j)}]\} \Psi_m(\mathbf{r}_1, \ldots, \mathbf{r}_Z) d\tau \right|^2.$$

The symbols in (1) have the following connotations: $\Psi_m(\mathbf{r}_1, \ldots, \mathbf{r}_Z)$, $\Psi_n(\mathbf{r}_1, \ldots, \mathbf{r}_Z)$ are the relativistic atomic wave functions for the initial and final states m and n respectively, before and after the collision; E_m and E_n are the energies of these states respectively; E_1^0 and E_1^1 are the energies of the initial and final states of the incident electron and $\omega_1^0 = E_1^0/\hbar$, $\omega_1^1 = E_1^1/\hbar$; $\mathbf{r}_i$ is the position vector of the ith atomic electron relative to the nucleus; $\mathbf{k}_1^0$ and $\mathbf{k}_1^1$ represent the propagation vector of the incident electron before and after collision; $\mathbf{q}$, κ and α_{mn} are defined by $\mathbf{q} = \mathbf{k}_1^0 - \mathbf{k}_1^1$, $\kappa = m_0 c/\hbar$ and $\alpha_{mn}^2 = 2m_0(E_n - E_m)/\hbar^2$ respectively; $\alpha^2 = 2m_0|I|/\hbar^2$ where I is the first ionization energy of the shell; for continuous states, $\alpha_{mk}^2 = \alpha^2 + k^2$ and $E_k = E_i + (\hbar^2/2m_0)k^2$ where E_i is the ground state energy of the singly ionized shell; and A, $\mathfrak{A}$ are defined by $A = N_1^1 N_1^0 a^{1*} a^0$, $\mathfrak{A} = N_1^1 N_1^0 a^{1*} \boldsymbol{\alpha}^{(1)} a^0$, the a's being the Dirac wave functions for a free electron and N the normalizing factor (Mott and Sneddon 1948); the components of the vector $\boldsymbol{\alpha}^{(1)}$ are the Dirac matrices, the exponent 1 in brackets indicates they operate only on the incident electron.

The general expression (1) has never been applied. The work of Brown and Walske is based on a non-relativistic differential cross section.

To proceed, we classify the collisions as distant or close according to whether $k < \eta$ or $k > \eta$ respectively where η satisfies the inequalities

$$\eta^2 \ll \kappa^2, \qquad \eta^2 \gg \alpha^2. \quad \ldots\ldots(2)$$

An expression for the differential cross section for distant collisions is obtained as follows, it being observed that by virtue of conservation of energy and the restriction to distant collisions, the limits of $\mathbf{q}$ in (1) are given by

$$q_{\min} \simeq \alpha_{m_n}{}^2\gamma/2k_1{}^0, \qquad q_{\max} \simeq 2k_1{}^0, \qquad \ldots\ldots(3)$$

where $\gamma=(1-v^2/c^2)^{-1/2}$ and v is the velocity of the incident electron.

We assume that to a first order approximation—which is sufficiently good for relativistic effects—the atomic electrons do not interact.

Accordingly, the relativistic atomic wave functions can be represented by

$$\Psi_n(\mathbf{r}_1,\ldots,\mathbf{r}_Z)=(Z!)^{-1/2}\sum_P(-1)^{P'}P'\prod_\mu\Psi_{n_\mu}(\mathbf{r}_\mu)$$

$$\Psi_m(\mathbf{r}_1,\ldots,\mathbf{r}_Z)=(Z!)^{-1/2}\sum_{P''}(-1)^{P''}P''\prod_\nu\Psi_{m_\nu}(\mathbf{r}_\nu), \qquad \ldots\ldots(4a)$$

where the $\Psi(\mathbf{r}_\nu)$ are relativistic hydrogenic wave functions. The n_i and m_i denote both the three spatial quantum numbers N_i and M_i and the spin quantum numbers S_{n_i} and S_{m_i} respectively. Also, $n_i=m_i$ for $i=1, 2, \ldots, Z-1$ and $n_Z\neq m_Z$; while for all i, j; $m_i\neq m_j$, and $n_i\neq n_j$, if $i\neq j$.

For the relativistic hydrogenic wave functions, since the restriction to distant collisions precludes states other than those for which $E_0\ll m_0c^2$, good approximations are given by (Mott and Sneddon 1948, p. 319)

$$\Psi_{n_i}(\mathbf{r}_\nu)=b_{Sn_i}(\mathbf{r}_\nu)\phi_{n_i}(\mathbf{r}_\nu)$$

$$\Psi_{m_i}(\mathbf{r}_\nu)=b_{Sm_i}(\mathbf{r}_\nu)\phi_{m_i}(\mathbf{r}_\nu), \qquad \ldots\ldots(4b)$$

where $\phi_{n_i}(\mathbf{r}_\nu)$ and $\phi_{m_i}(\mathbf{r}_\nu)$ are Schrödinger hydrogenic wave functions including spin. The operators $b_S(\mathbf{r}_\nu)$ corresponding to the two opposite spin orientations are defined by Mott and Sneddon (1948, p. 319); call them $(4c)$. The subscript ν here implies they operate only on the coordinates of the νth electron.

On account of the indistinguishability of different spins for a given energy, $|\zeta|^2$ may be written as the sum over the different spin states, divided by the number of states, of the terms $|\zeta_{S_nS_m\sigma'\sigma''}|^2$ where $\zeta_{S_nS_m\sigma'\sigma''}$ is defined by

$$\zeta_{S_nS_m\sigma'\sigma''}=\int\Psi_n{}^*(\mathbf{r}_1,\ldots,\mathbf{r}_Z)O_{\sigma'\sigma''}\Psi_m(\mathbf{r}_1,\ldots,\mathbf{r}_Z)d\tau, \qquad \ldots\ldots(5)$$

where

$$O_{\sigma'\sigma''}=\sum_{j=1}^{Z}O_{\sigma'\sigma''}{}^j=\sum_{j=1}^{Z}\exp(i\mathbf{q}\cdot\mathbf{r}_j)(A_{\sigma'\sigma''}-\mathfrak{A}_{\sigma'\sigma''}\cdot\boldsymbol{\alpha}^{(j)}).$$

On substituting $(4a)$ into (5) and reducing the double summation, we find that

$$\zeta_{S_nS_m\sigma'\sigma''}=\sum_P(-1)^P\int\prod_\mu\Psi_{n_\mu}{}^*(\mathbf{r}_\mu)O_{\sigma'\sigma''}P\prod_\nu\Psi_{m_\nu}(\mathbf{r}_\nu)d\tau. \qquad \ldots\ldots(6)$$

By virtue of orthogonality, all the terms in the summation in (6) vanish except the term involving the identity permutation. The vanishing terms can therefore be replaced by the terms

$$(-1)^P\int\prod_\mu\phi_{n_\mu}{}^*(\mathbf{r}_\mu)\overline{O}_{\sigma'\sigma''}P\prod_\nu\phi_{m_\nu}(\mathbf{r}_\nu)d\tau$$

(where $\overline{O}_{\sigma'\sigma''}$ is an operator which acts on the spatial coordinates and is defined later), since these all vanish also, except when P is the identity permutation.

For similar reasons, the term in (6) involving the identity permutation can be replaced by

$$\sum_{j=1}^{Z-1}\int\prod_{\mu=1}^{Z}\phi_{n_\mu}{}^*(\mathbf{r}_\mu)\overline{O}_{\sigma^1\sigma^0}{}^j\prod_{\nu=1}^{Z}\phi_{m_\nu}(\mathbf{r}_\nu)d\tau+\int\Psi_{n_Z}{}^*(\mathbf{r}_Z)O_{\sigma^1\sigma^0}{}^Z\Psi_{m_Z}(\mathbf{r}_Z)d\tau_Z$$
$$\left\{\prod_{\mu=1}^{Z-1}\int\phi_{n_\mu}{}^*(\mathbf{r}_\mu)\phi_{m_\mu}(\mathbf{r}_\mu)d\tau_\mu\right\}.$$

The first factor in the second term is easily evaluated if it is noted that by choice of coordinate system, $\mathbf{k}_1{}^0\simeq(0,\,0,\,k_1{}^0{}_z)$. For then, by virtue of energy conservation and the restriction to distant collisions, it is found that $O_{\sigma^1\sigma^0}{}^j$ vanishes unless $\sigma^1=\sigma^0$ in which case

$$O_{\sigma^1\sigma^0}{}^j=\exp(i\mathbf{q}\,.\,\mathbf{r}_j)\left\{1+\left(\frac{\gamma+1}{\gamma-1}\right)^{1/2}\left(\frac{4(\gamma^2-1)\kappa^2-q^2}{4(\gamma+1)\gamma\kappa^2-q^2}\right)\alpha_z{}^{(j)}\right\}\left(\frac{4m_0{}^2c^2\gamma(\gamma+1)-\hbar^2q^2}{4m_0\hbar\omega_1{}^0(\gamma+1)}\right). \quad \ldots\ldots(7)$$

Hence, using (7), the operators (4 *c*) the magnitudes of the first and second matrix elements of which are small compared with those of the third and fourth (Mott and Sneddon 1948) and the fact that the wave functions vanish at infinity, we obtain

$$\int\Psi_{n_Z}{}^*(\mathbf{r}_Z)O_{\sigma^1\sigma^0}{}^Z\Psi_{m_Z}(\mathbf{r}_Z)d\tau_Z=\int\phi_{n_Z}{}^*(\mathbf{r}_Z)\overline{O}_{\sigma^1\sigma^0}{}^Z\phi_{m_Z}(\mathbf{r}_Z)d\tau_Z, \quad \ldots\ldots(8\,a)$$

where $\overline{O}_{\sigma^1\sigma^0}{}^j$ vanishes for $\sigma^1\neq\sigma^0$ while for $\sigma^1=\sigma^0$ it is defined by

$$\overline{O}_{\sigma_0\sigma^0}{}^j=\frac{m_0c^2\gamma}{\hbar^2\omega_1{}^0}\left\{\exp(i\mathbf{q}\,.\,\mathbf{r}_j)\left[1+\frac{1}{\kappa}\left(\frac{\gamma+1}{\gamma-1}\right)^{1/2}\left(\frac{4(\gamma^2-1)\kappa^2-q^2}{4(\gamma+1)\gamma\kappa^2-q^2}\right)\left(i\frac{\partial}{\partial z_j}-\frac{q_z}{2}\right)\right]\right\}, \quad \ldots\ldots(8\,b)$$

q_z being the component of $\mathbf{q}$ along $\mathbf{k}_1{}^0$.

Thus, on collecting the equivalents of the terms that constitute (7) and reversing the procedure leading from (5) to (6), it is evident that $\zeta_{S_{n_s}S_{m^s\sigma^s\sigma^s}}$ may be written

$$\zeta_{S_{n_s}S_{m^s\sigma^s\sigma^s}}=\sum_{j=1}^{Z}\int\Theta_n{}^*\overline{O}_{\sigma^s\sigma^s}{}^j\Theta_m d\tau, \quad \ldots\ldots(9)$$

where
$$\Theta_n=(Z!)^{-1/2}\sum_P(-1)^{P'}P'\prod_\mu\phi_{n_\mu}(\mathbf{r}_\mu)$$

and Θ_m is defined similarly.

To obtain a better approximation, the wave functions Θ are replaced by products of the Schrödinger wave functions for the shell (which include electronic interactions) and the respective spin functions, the former being denoted by Φ_M and Φ_N where M, N henceforth signify the spatial quantum numbers $(n_0,\,l_0,\,m_0)$ and $(n,\,l,\,m)$ respectively. By the orthogonality of the spin functions (9) becomes

$$\zeta_{S_{m_s}S_{m^s\sigma^s\sigma^s}}=\sum_{j=1}^{Z}\int\Phi_N{}^*\overline{O}_{\sigma^s\sigma^s}{}^j\Phi_M d\tau. \quad \ldots\ldots(10)$$

Hence, with the help of (8 *b*) and (10), averaging $|\zeta_{S_{m_s}S_{m^s\sigma^s\sigma^s}}|^2$ over the different spin states, substituting into (1) and summing over the different l, m corresponding to the same n leads to the result

$$d\Phi_{n_s,n}(q)=8\pi e^4\hbar^{-2}v^{-2}(q^2-\rho_{n_s,n}{}^2)^{-2}qdq\sum_{l,\,m}\Big|\sum_{j=1}^{Z}\int\Phi_{n,l,m}{}^*(\mathbf{r}_1,\ldots,\mathbf{r}_Z)$$
$$\times\exp(i\mathbf{q}\,.\,\mathbf{r}_j)\left\{1+\kappa^{-1}\left(\frac{\gamma+1}{\gamma-1}\right)^{1/2}\left(\frac{4(\gamma^2-1)\kappa^2-q^2}{4(\gamma+1)\gamma\kappa^2-q^2}\right)\left(i\frac{\partial}{\partial z_j}-\frac{1}{2}q_z\right)\right\}$$
$$\times\Phi_{n_s,l_s,m_s}(\mathbf{r}_1,\ldots,\mathbf{r}_Z)d\tau\Big|^2 \quad \ldots\ldots(11)$$

where $\rho_{n_s n} = \alpha_{n_s n}^2/2\kappa$. Equation (11) gives the differential cross section presented by a Z electron shell to electrons with relativistic energies. If q is considered negligible compared with κ and if the wave functions Φ are replaced by those for a single-electron system, it reduces to the expression given by Møller.

For close collisions, Møller (1932) showed that in the case of hydrogen, the differential cross section becomes that for the collision between two free electrons where one is initially at rest and the other is incident with relative velocity v.

Extended to a Z electron shell, Møller's expression for the total cross section for collisions in which one of the electrons loses an energy between Q and $Q+dQ$ may be written

$$\Phi(Q)dQ = 2\pi e^4 Z m_0^{-1} v^{-2} Q^{-2} dQ (1 - QT^{-1})^{-2} \times \{1 - [3 - (1-\gamma^{-1})^2](1 - QT^{-1})QT^{-1} + (1+\gamma^{-1})^2(1 - QT^{-1})^2 (QT^{-1})^2\}, \quad \ldots\ldots(12)$$

where T is the kinetic energy of the incident electron. The upper and lower limits of Q are given by $Q_{\max} = T/2$ and $Q_{\min} \simeq T_\eta \simeq \hbar^2\eta^2/2m_0$ respectively.

2.2. *Expressions for Stopping Power and Specific Primary Ionization for Electrons (to a first order approximation)*

We may now obtain first-order expressions for the stopping power and specific primary ionization of a Z electron shell for relativistic electrons as explicit functions of the wave function of the shell. The derivation is essentially similar to that of Møller for hydrogen, the only difference being that a higher degree of generality is maintained here.

The total stopping power $-(dT/dx)$ may be written

$$-\left(\frac{dT}{dx}\right) = -\left(\frac{dT}{dx}\right)_{k<\eta} - \left(\frac{dT}{dx}\right)_{k>\eta}, \quad \ldots\ldots(13a)$$

with

$$-\frac{1}{N}\left(\frac{dT}{dx}\right)_{k<\eta} = \sum_{n=n_s+1}^{\eta} Q\Phi(Q), \quad \ldots\ldots(13b)$$

$$-\frac{1}{N}\left(\frac{dT}{dx}\right)_{k>\eta} = \int_{Q\min}^{Q\max} Q\Phi(Q)dQ, \quad \ldots\ldots(13c)$$

where Q is the energy transferred by the incident electron; $\Phi(Q)$ is the total cross section for a given Q; in (13 b), $\Phi(Q)$ is the integral over q of equation (11;) in (13 c), $\Phi(Q)$ is given by equation (12); N is the number of atoms per cm^3 at S.T.P.; and $\Sigma_{n=n_s+1}^{\eta}$ denotes summation over all discrete states from $n = n_0 + 1$ and integration over all continuous states to $k = \eta$.

For convenience, equation (13 b) is separated into four expressions J_1, J_2, J_3 and J_4 in which the limits of the integration over q implicit in (13 b) are $(q_{\min}, q_0)$, $(q_0, \eta/2)$, $(\eta/2, 2\eta)$ and $(2\eta, q_{\max})$ respectively, q_0 being defined by the inequalities $q_0 \ll \alpha$ and $q_0^2 \gg t(\alpha^2/2\kappa)^2$ where $t \simeq 500$.

In each of these ranges, the integrand, i.e. the expression (11) for $d\Phi_{n_s n}(q)$, simplifies considerably.

It is found (the derivation is substantially the same as that due to Møller) that for $q \ll \alpha$

$$d\Phi_{n_s n}(q) = 8\pi e^4 \hbar^{-2} v^{-2} (q^2 - \rho_{n_s n}^2 - \rho_{n_s n}^2/\gamma^2)(q^2 - \rho_{n_s n}^2)^{-2} q dq \, |x_{n_s n}|^2, \quad \ldots\ldots(14a)$$

where

$$|x_{n_s n}|^2 = \sum_{l,m} |x_{n_s; nlm}|^2 = \sum_{l,m} \Big| \sum_{j=1}^{Z} z_j \Phi_{nlm}{}^* \Phi_{n_s l_s m_s} d\tau \Big|^2;$$

for $q \geqslant \alpha$

$$d\Phi_{n_s n}(q) = 8\pi e^4 \hbar^{-2} v^{-2} (q^2 - \rho_{n_s n}{}^2)^{-2} q\, dq\, |\mathrm{E}_{n_s n}(q)|^2,$$

where

$$|\mathrm{E}_{n_s n}(q)|^2 = \sum_{l,m} |\mathrm{E}_{n_s; nlm}(q)|^2 = \sum_{l,m} \Big| \sum_{j=1}^{Z} \int \exp(i\mathbf{q} \cdot \mathbf{r}_j) \Phi_{nlm}{}^* \Phi_{n_s l_s m_s} d\tau \Big|^2; \quad \ldots\ldots(14b)$$

for $q \geqslant 2\eta$

$$d\Phi_{n_s n}(q) \simeq 0. \quad \ldots\ldots(14c)$$

With the help of (14), $-(1/N)(dT/dx)_{k<\eta}$ eventually reduces to

$$-\frac{1}{N}\left(\frac{dT}{dx}\right)_{k<\eta} = \left(\frac{2\pi e^4 Z}{m_0 v^2}\right)\left[\ln\left(\frac{2m_0 v^2 \gamma^2 T_\eta}{\bar{I}^2}\right) - \frac{v^2}{c^2}\right] \quad \ldots\ldots(15a)$$

where $\bar{I} = 2Ia/b$ and

$$\ln a = (2m_0/\hbar^2 Z) \sum_{n=n_s+1}^{k=\infty} (E_n - E_{n_s}) |x_{n_s n}|^2 \ln(\alpha_{n_s n}{}^2/\alpha^2),$$

$$\ln b = (2m_0/\hbar^2 Z) \sum_{n=n_s+1}^{\eta} \int_{\eta/2}^{2\eta} (E_n - E_{n_s}) q^{-3} |\mathrm{E}_{n_s n}(q)|^2 dq.$$

Addition of $-(1/N)(dT/dx)_{k>\eta}$, obtained from equations (12) and (13), to (15*a*) finally yields the following first-order approximation for the stopping power of a Z electron shell for very fast electrons:

$$-\frac{dT}{dx} = 2\pi e^4 N Z m_0{}^{-1} v^{-2} \left\{ \ln\left(\frac{2m_0 \gamma^2 v^2 T}{\bar{I}^2}\right) + \frac{(\gamma-1)^2}{8\gamma^2} - \left[3 - \frac{(\gamma-1)^2}{\gamma^2}\right] \ln 2 + 1 - \frac{v^2}{c^2} \right\}. \quad \ldots\ldots(15b)$$

If S denotes the specific primary ionization and Φ_c, Φ_1 and Φ_e denote the total cross sections for all collisions, all ionizing collisions and all excitation collisions respectively, then

$$S = N\Phi_1 = N(\Phi_c - \Phi_e). \quad \ldots\ldots(16)$$

To the order of approximation adopted here, Φ_e and the contribution to Φ_c from distant collisions may be derived in much the same way as was $-(1/N)(dT/dx)_{k<\eta}$, while the contribution to Φ_c from close collisions can be shown to be vanishingly small.

Using (16) it is found the specific primary ionization of a Z electron shell for relativistic electrons is given by

$$S = 2\pi r_0{}^2 m_0 c^4 Z N a' I^{-1} v^{-2} \{\ln(2m_0 v^2 \gamma^2 / I) + b' - v^2/c^2\}, \quad \ldots\ldots(17)$$

where $a' = (2m_0 I / Z\hbar^2) a_1'$, $b' = 2(b_1' + b_2' + b_3')/a_1'$,

and

$$a_1' = \int_{k=0}^{\infty} |x_{n_s k}|^2 dk,$$

$$b_1' = \int_{k=0}^{\eta} \int_{q=\eta/2}^{2\eta} |\mathrm{E}_{n_s k}(q)|^2 q^{-3} dq dk + a_1' \ln(q_0 \alpha^{-1}),$$

$$b_2' = -\int_{k=0}^{\eta} |x_{n_s k}|^2 \ln(\alpha_{n_s k}{}^2/\alpha^2),$$

$$b_3' = \int_{k=0}^{\eta} \int_{q=\eta/2}^{2\eta} |\mathrm{E}_{n_s k}(q)|^2 q^{-3} dq dk, \qquad (r_0 = e^2/m_0 c^2).$$

2.3. *Extension to Incident Particles other than Electrons*

The previous results for electrons can be easily modified to apply to any incident charged particle of arbitrary mass M_0 and charge $\pm ze$ which obeys Dirac's equation (if $M_0 \gg m_0$, call such particles 'heavy electrons') since the differential cross section (11) for distant collisions (apart from the charge factor z^2) is exactly the same for all such particles.

Hence, since the total cross section for close collisions is negligible compared with that for distant collisions, it is apparent that the specific primary ionization for electrons, positrons and 'heavy electrons' is given by (17) (apart from the additional factor z^2).

But though the stopping power for distant collisions remains the same as (15 *a*) (but for the factor z^2) for Dirac particles of different masses, the stopping powers for close collisions—and these cannot be neglected—will be different in so far as the cross sections for close collisions differ.

The relevant close collision cross sections have been calculated by Bhabha (1938). With their help, the following expressions are obtained for the stopping power:

For 'heavy electrons':

$$-\left(\frac{dT}{dx}\right) = 2\pi e^4 z^2 Z N m_0^{-1} v^{-2}\left\{\ln\left(\frac{4m_0^2 v^4 \gamma^4}{\bar{I}^2}\right) - \frac{v^2}{c^2}\right\}, \quad \ldots\ldots(18)$$

For positrons:

$$-\left(\frac{dT}{dx}\right) = 2\pi e^4 Z N m_0^{-1} v^{-2}\left\{\ln\left(\frac{m_0 v^2 \gamma^2 T}{\bar{I}^2}\right) - \frac{v^2}{c^2} - \frac{133\gamma^4 - 36\gamma^3 + 330\gamma^2 + 236\gamma - 3}{192\gamma^2(\gamma+1)}\right\}, \quad \ldots\ldots(19)$$

where the $\bar{I}$ in both (18) and (19) is defined by (15 *a*).

Now by comparing the cross sections for free electron collisions with heavy particles of the same arbitrary mass $M_0 \gg m_0$ but with different spin quantum numbers it is seen (Rossi 1952) that for collisions of the energy type considered here, these close collisions are independent of the spin of the independent particle. Thus in effect, the results obtained here for 'heavy electrons' are valid for protons, alpha particles and mesons.

§ 3. The Stopping Power and Specific Primary Ionization of Helium

The stopping power and specific primary ionization for the particular case of helium may now be obtained by computing the atomic parameters $\bar{I}$, a' and b' using helium wave functions.

3.1. *The Form of the Helium Wave Functions*

To an approximation sufficient for most of the atomic parameters involved, the initial and final helium wave functions (only singlet states are considered) can be represented respectively by

$$\Phi_{n_s l_s m_s} = \phi_0(Z' \mid \mathbf{r}_1)\phi_0(Z' \mid \mathbf{r}_2), \qquad Z' = 1{\cdot}687; \quad \ldots\ldots(20\,a)$$

$$\Phi_{nlm} = 2^{-1/2}\{\phi_0(Z''' \mid \mathbf{r}_1)\phi_{nlm}(Z'' \mid \mathbf{r}_2) + \phi_0(Z''' \mid \mathbf{r}_2)\phi_{nlm}(Z'' \mid \mathbf{r}_1)\}, \quad \ldots\ldots(20\,b)$$

where $Z'' = 1$, $Z''' = 2$ for both discrete and continuous states, except S states,

and $\phi_{nlm}(Z|\mathbf{r}_i)$ denotes the wave function of the ith electron (the two orbital electrons being distinguished by suffixes 1, 2) in the state n, l, m in the Coulomb field due to a charge Z. For discrete states, the ϕ's are merely hydrogenic wave functions with the effective nuclear charges indicated. We call these (21 *a*). For S states, wave functions of the type (20 *b*) are not orthogonal to the ground state wave function (20 *a*). Suitable wave functions for S states have been devised by Vinti (1932). These are used here.

The continuous wave functions $\phi_k(Z'|\mathbf{r})$, which are the solutions of the Schrödinger equation

$$\nabla^2\phi + [k^2 + 2m_0V/\hbar^2]\phi = 0 \qquad \ldots\ldots(21')$$

where $V = 2Z'e^2/r$, are given by Schrödinger (1926) and, in a different form, by Wentzel (1929). We call these (21 *b*) and (21 *c*) respectively.

Now as suggested, these wave functions suffice for most of the parameters. But a and a', upon which the stopping power and specific primary ionization depend fairly critically, are themselves rather sensitive to the type of wave function employed (cf. figure 1). For this reason a and a^1 are also calculated from more accurate wave functions ϕ_0 and ϕ_k, namely the Hartree wave function for an electron in the ground state in the field due to a normal singly ionized helium atom (Lindsay 1935) and the continuous wave function obtained by numerical integration of equation (21′) with V given by

$$V = -e^2r^{-1}[1 + (1 + 2ra_0^{-1})\exp(-4ra_0^{-1})],$$

this being the Hartree potential for an electron in the field of a normal singly ionized helium atom. We call these wave functions (22 *a*) and (22 *b*) respectively.

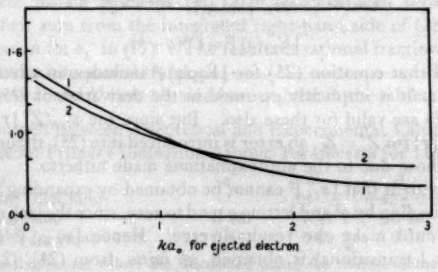

Figure 1. Illustrating the dependence of the dipole matrix elements on the type of wave functions used.

(1) The ratio of $|x_{1k}|^2$ calculated from the wave functions (26′) to $|x_{1k}|^2$ calculated from the wave functions (26).

(2) The ratio of $|x_{1k}|^2$ calculated using a 6 parameter Hylleraas wave function in (26) to $|x_{1k}|^2$ calculated from the wave functions (26).

The normalization of both (21 *b*) and (22 *b*) is given by the condition

$$\int \phi_k^1(\mathbf{r})\phi_k(\mathbf{r})d\tau = \delta(k - k'), \qquad \ldots\ldots(23\,a)$$

but to effect the practical normalization of the wave functions (22 *b*) it is necessary to determine the asymptotic form of the radial functions R implied by the condition (23 *a*). It is found (Fues 1926, Hargreaves 1929) that (23) is equivalent to taking

$$R = (\pi k a_0)^{-1/2}r^{-1}\cos(kr - \gamma). \qquad \ldots\ldots(23\,b)$$

3.2. *Evaluation of the Matrix Elements*

On substituting (20 *a*) and (20 *b*) into equation (14 *b*), we see, by virtue of symmetry, orthogonality and the choice of the z axis of the coordinate system along $\mathbf{q}$ (this excludes all transitions in m), that the generalized matrix elements for transitions to all states, discrete and continuous (except S states) are of the form

$$|\mathrm{E}_{1n}(q)|^2 = C\sum_l \left|\int \exp(i\mathbf{q}\cdot\mathbf{r})\phi_{nl0}^*(Z''|\mathbf{r})\phi_0(Z'|\mathbf{r})d\tau\right|^2, \qquad \ldots\ldots(24)$$

where $C = 1{\cdot}956$.

For transitions to continuous states, we find by modifying Wentzel's work (in which $Z' = Z''$) and using a contour integration due to Bethe (1930) that the expressions (24), (21 *a*) and (21 *c*) finally lead to the result

$$|\mathrm{E}_{1k}(q)|^2 = \frac{C2^8\alpha_1^5\alpha_2 q^2 k\{\frac{1}{3}(\alpha_2^2+k^2)+[(\alpha_1+\alpha_2)q^2+(\alpha_1-\alpha_2)(k^2+\alpha_1^2)]^2(2\alpha_1 q)^{-2}\}}{[(q+k)^2+\alpha_1^2]^3[(q-k)^2+\alpha_1^2]^3[1-\exp(-2\pi\alpha_2 k^{-1})]}$$
$$\times \exp\{-2\alpha_2 k^{-1}\arctan[2k\alpha_1(q^2-k^2+\alpha_1^2)]\}, \qquad \ldots\ldots(25)$$

where $\alpha_1 = Z'/a_0$, $\alpha_2 = Z''/a_0$.

For $q \gg \alpha_1$, $q \gg \alpha_2$, (25) reduces to

$$|\mathrm{E}_{1k}(q)|^2 = (8C/3\pi)\alpha_1^5[(q-k)^2+a_1^2]^{-3},$$

the right-hand side of which, as Møller points out, behaves like the Dirac delta function.

Putting

$$N\delta(q-k) = (8C/3\pi)\alpha_1^5[(q-k)^2+\alpha_1^2)^{-3},$$

it is found that

$$N = (8C/3\pi)\alpha_1^5\int_{-\infty}^{\infty}[(q-k)^2+\alpha_1^2]^{-3}dk = C,$$

so that

$$|\mathrm{E}_{1k}(q)|^2 = C\delta(q-k). \qquad \ldots\ldots(25')$$

It is noted that equation (25) for $|\mathrm{E}_{1k}(q)|^2$ includes, in effect, a summation over s states, as it is implicitly assumed in the derivation of (25) that the wave functions (20 *b*) are valid for these also. But since the $\phi_{k00}(Z''|\mathbf{r})$ are not orthogonal to $\phi_0(Z'|\mathbf{r})$ for $Z'' \neq Z'$, an error is introduced into (25), though it is probably smaller than those due to the approximations made hitherto.

Also it is evident that $|x_{1k}|^2$ cannot be obtained by expanding the exponential in $|\mathrm{E}_{1k}(q)|^2$, dividing by q^2 and letting q tend to zero, since the lack of orthogonality referred to would make the result diverge. Hence $|x_{1,\,k10}|^2$ (selection rules prohibit other l transitions) is obtained, *ab initio*, from (24), (21 *a*) and (21 *b*). The required integration has been accomplished by Vinti (1934), and separately by Wheeler (1933), and the result, suitably modified, is

$$|x_{1k}|^2 = \frac{2^8 C\alpha_2(2\alpha_1-\alpha_2)^2\alpha_1^3(\alpha_2^2+k^2)k\exp[-4\alpha_2 k^{-1}\arctan(k\alpha_1^{-1})]}{(\alpha_1^2+k^2)^6[1-\exp(-2\pi\alpha_2 k^{-1})]}. \qquad \ldots\ldots(26)$$

The matrix elements for discrete state transitions are calculated separately for a number of different transitions, this being more convenient than using a modified form of the general expression derived by Massey and Mohr (1931). The corresponding $|x_{1,\,n10}|^2$ are derived from these by means of the relation

$$|x_{1,\,nlm}|^2 = \lim_{q\to 0} q^{-2}|\mathrm{E}_{1,\,nlm}(q)|^2. \qquad \ldots\ldots(27)$$

A more accurate version of (26), the use of which is to be preferred in the calculation of a and a' can be obtained from the improved wave functions (22)

by numerical integration. We call such matrix elements (26′). Figure 1 provides a comparison between (26), (26′) and matrix elements due to Wheeler (1933) which make use of Hylleraas' six-parameter function for ϕ_0 and the wave function (21 *c*) for ϕ_k, over the relevant range of k.

3.3. *The Calculation of* $\bar{I}$, a' *and* b'

The calculation of the contributions to a and b from the transitions to the continuum, for helium, may be effected without difficulty by substituting the matrix elements (26) or (26′), and (25′) into (15 *a*) and integrating numerically. Addition of the respective discrete contributions (their calculation is trivial: in the case of b it is negligible) yields a and b and hence $\bar{I}$.

The following are the results finally obtained:

Approximate (analytical) wave functions: $\bar{I}=49$ ev.

Accurate (numerical) wave functions: $\bar{I}=40$ ev.

Similarly, evaluation of the parameters a' and b_2' is accomplished with the help of (26), or (26′) in the case of a', by numerical integration of the relevant expressions in (17). Also the integration of (25′) in b_3' indicates that the latter term is negligible compared with b_2'.

The parameter b_1' is obtained with the aid of the summation theorem (for helium)

$$2+\int [\exp\{i\mathbf{q}.(\mathbf{r}_1-\mathbf{r}_2)\}+\exp\{i\mathbf{q}.(\mathbf{r}_2-\mathbf{r}_1)\}]\Phi_0^*\Phi_0 d\tau=\sum_{n=1}^{k=\infty}|E_{1n}(q)|^2. \quad \ldots\ldots(28)$$

The discrete matrix elements $|E_{1n}(q)|^2$ are calculated separately and the difference of their sum from the integrated right-hand side of (28) is substituted into the expression for b_1' in (17). The resultant rational fractions are integrated over q by resolving into partial fractions.

The values of a' and b' thus obtained are quoted in the table.

Comparison between Theoretical and Experimental Values of the Specific Primary Ionization Atomic Parameters for Helium

Parameter	a'	b'	A	C
Exptl. value (McClure)			$0{\cdot}42\pm0{\cdot}04$	4·0
Theoretical value	0·46	0·41	0·26	2·9
Theor. value for impure He†	0·64	0·06	0·36	3·8

†These theoretical values are calculated using the matrix elements (26).

§ 4. Discussion of Results

The most recent stopping power experiments (Reynolds *et al.* 1953) for protons suggest, by extrapolation, a mean ionization energy of 36 ev for protons with energies greater than 1 MeV.

The energy dependence of $\bar{I}$ exhibited in these results does not appear in the present approximation, but would undoubtedly do so in a higher approximation, just as it appears in the $\bar{I}$ obtained by recasting the non-relativistic results of Brown and Walske.

But disregarding this effect, which is fairly small, we see that while the better of the values obtained here ($\bar{I}=40$ ev) is too large by some 10% compared with experiment, it coincides exactly with the value calculated by Halpern and Hall (1948) using an entirely different procedure.

It appears therefore that the best theoretical results hitherto differ from the best experimental data by about 10%. In the present work, an error of this magnitude could arise from the approximations utilized in the derivation of the stopping power expression (15) from a differential cross section (11). And although this discrepancy is small for stopping power computations, since $\bar{I}$ occurs in the log term, it does indicate the need for more refined approximations. Another point of interest emerging from the present calculations is the high sensitivity of $\bar{I}$ to the accuracy of the wave functions employed.

The most recent and reliable specific primary ionization measurements are those of McClure (1953) for electrons with energies in the neighbourhood of 1 Mev (at such incident velocities, the approximations used in the calculations here are particularly justified).

McClure expresses his results in the following way: For equation (17) by means of the substitution $v^2/c^2=(p/M_0c)^2[(p/M_0c)^2+1]^{-1/2}$, where p is the momentum of the incident particle and M_0 its rest mass, he obtains the expression

$$S=A\{(p/M_0c)^2\ln(p/M_0c)^2[(p/M_0c)^2+1]-1\}+C(p/M_0c)^{-2}[(p/M_0c)^2+1],$$

where the lumped constants A and C are defined by

$$A=2\pi r_0^2 m_0c^2Nz^2Za'/I, \qquad C=A[b'+\ln(2m_0c^2/I)].$$

From his experimental results McClure determined A and C empirically by least square fits. His values for helium together with the values obtained here for A and C (using the calculated values of a' and b') are given in the table. Since a', unlike a, is largely unaffected by the use of more accurate wave functions, to the order of accuracy of the present calculations (the internal error is less than 5% here) it is immaterial which value is used for the purpose of comparison with experiment.

Comparison of theoretical and experimental parameters suggests that $S_{\text{theor}}\simeq 0{\cdot}7S_{\text{exp}}$. But this result is not disquieting in the light of the recent experiments by Jesse and Sadauskis (1952), who observed that the addition in minute quantities of certain contaminating gases to helium depresses the value of the energy per ion pair very considerably. Moreover the energy per ion pair continues to decrease with increase in concentration of contaminant until a saturation value is reached.

To account for this effect, they suppose that collisions between excited helium atoms and atoms of the contaminating gas (the ionization energy of which is smaller than the least excitation energy of helium) lead to the production of ion pairs and that, eventually, every excited helium atom is de-activized in this manner. Hence, in the presence of a saturation concentration of contaminant, every excited helium atom can be counted as an ion pair. This hypothesis is borne out by recent calculations due to Erskine (1954).

It is likely, therefore, that because of admitted impurities, McClure's experiment furnishes the total cross section for all collisions rather than the specific primary ionization of helium.

The total cross section for all collisions has been calculated here. The corresponding atomic parameters are quoted in the table. Comparing these results with McClure's data, it is seen that the calculated specific primary ionization parameters (modified in the light of the Jesse and Sadauskis hypothesis) agrees to within 10% with the experimental values (see figure 2).

It is hoped to extend the work initiated here by deriving stopping power and specific primary ionization expressions from the differential cross section (11) akin to the Brown–Walske non-relativistic theory in degree of refinement, and applying the results obtained to other light elements.

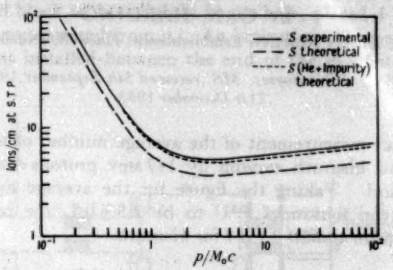

Figure 2. Comparison between experimental and theoretical values of the specific primary ionization for helium for different energies of the incident electrons.

Acknowledgment

I would like to express my deep gratitude to Associate Professor C. B. O. Mohr for suggesting this topic and for his guidance throughout the course of the work.

References

Bethe, H., 1930, *Ann. Phys., Lpz.*, **5**, 325; 1932, *Z. Phys.*, **76**, 293; 1933, *Handbuch der Physik*, **24**, 273.
Bhabha, H., 1938, *Proc. Roy. Soc.* A, **164**, 257.
Brown, L., 1950, *Phys. Rev.*, **79**, 297.
Erskine, G., 1954, *Proc. Phys. Soc.* A, **67**, 640.
Fues, E., 1926, *Ann. Phys., Lpz.*, **81**, 295.
Halpern, O., and Hall, H., 1948, *Phys. Rev.*, **73**, 477.
Hargreaves, J., 1929, *Proc. Camb. Phil. Soc.*, **25**, 75.
Jesse, W., and Sadauskis, J., 1952, *Phys. Rev.*, **88**, 417.
Lindsay, R., 1935, *Phys. Rev.*, **47**, 681.
McClure, G., 1953, *Phys. Rev.*, **90**, 796.
Massey, H., and Mohr, C., 1931, *Proc. Roy. Soc.* A, **132**, 605.
Møller, C., 1932, *Ann. Phys., Lpz.*, **14**, 531.
Mott, N., and Sneddon, I., 1948, *Wave Mechanics and its Applications* (Oxford: University Press).
Reynolds, H., *et al.*, 1953, *Phys. Rev.*, **92**, 742.
Rossi, B., 1952, *Higher Energy Particles*, (New York: Prentice-Hall).
Schrödinger, E., 1926, *Ann. Phys., Lpz*, **79**, 361.
Vinti, J., 1932, *Phys. Rev.*, **42**, 632; 1934, *Ibid.*, **44**, 524.
Walske, M., 1952, *Phys. Rev.*, **88**, 1283.
Wentzel, G., 1929, *Z. Phys.*, **58**, 349.
Wheeler, J., 1933, *Phys. Rev.*, **43**, 258.

A Measurement of the Average Number of Neutrons per Fission from Uranium and Bismuth when Bombarded with 147 MeV Protons

By G. N. HARDING
Atomic Energy Research Establishment, Harwell, Didcot, Berks.

Communicated by W. J. Whitehouse; MS. received 5th September 1955, *and in final form* 21*st December* 1955.

Abstract. A direct measurement of the average number of neutrons per fission from uranium and bismuth excited by 147 MeV protons has been made by a coincidence method. Taking the figure for the average number of neutrons per thermal neutron fission of ^{235}U to be $2{\cdot}5 \pm 0{\cdot}1$, the results obtained are $13{\cdot}1 \pm 1{\cdot}6$ for uranium and $10{\cdot}0 \pm 2{\cdot}7$ for bismuth.

§ 1. Introduction

The yields of fission and spallation products obtained in radiochemical studies of fission induced by high-energy particles can be explained by assuming that the emission of a large number of neutrons accompanies this process. The most simply interpreted evidence on this subject is that of Goeckermann and Perlman (1949), who obtained a yield curve from the fission of bismuth bombarded with 190 MeV deuterons which is symmetrical about mass number 100. Since the compound nucleus formed in this process is ^{211}Po, each fission should be accompanied by the emission of an average number of 11–12 neutrons. Similar measurements by Biller (1953), who bombarded bismuth with 340 MeV protons, would lead one to expect the emission of about 18 neutrons. With uranium the evidence is not quite so clear, but the measurements of O'Connor and Seaborg (1948) using 380 MeV α-particles, and of Folger *et al.* (1955) using 340 MeV protons, suggest that the emission of 20 neutrons per fission may occur.

These results, however, only give an indirect measure of the average number emitted, and up to the present no direct measurement of this quantity has been reported. The present experiment was therefore undertaken to obtain direct information about the emission of neutrons.

§ 2. Experimental Arrangement

Fission was induced in thin films of uranium and bismuth by the 147 MeV external proton beam from the Harwell cyclotron. The films formed a coating on the electrodes of an electron-collection ionization chamber. A second electron-collection ionization chamber, made in the form of an annulus surrounding the first, detected the neutrons by means of the recoil protons which they ejected from a 10 mg cm^{-2} polyethylene foil. The pulses produced by the two chambers, after amplification, were fed via discriminators to a coincidence unit having a resolving time of 4×10^{-7} second. Thus only neutrons were recorded which were coincident with a fission event.

A diagram of the general arrangement is shown in figure 1. The external proton beam was passed down a 3 in. diameter evacuated tube located in a 12 ft concrete wall which shielded the ionization chambers from radiation from the cyclotron tank. The beam was collimated by means of a brass block 5 cm thick having a hole 1 cm square at its centre, placed about 5 metres from the fission chamber. A second block with a slightly larger hole, placed 4 metres from the first, absorbed protons scattered from it. An ionization chamber for monitoring the proton beam was installed between the end of the evacuated tube and the fission chamber.

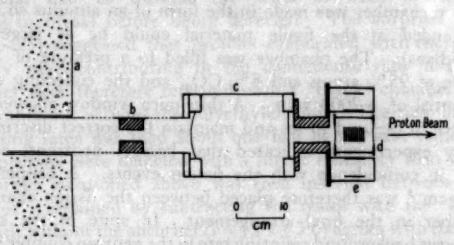

Figure 1. General arrangement: a, shielding wall; b, second aperture of collimator; c, proton monitor; d, fission chamber; e, neutron chamber.

The ionization chambers are shown in detail in figures 2 and 3. The fission chambers had ten electrodes of 0·001 in. aluminium foil, which were spaced 5 mm apart and connected alternately, one set to a potential of -1000 volts, and the other to the amplifier. Excepting the end electrodes, the foils were coated

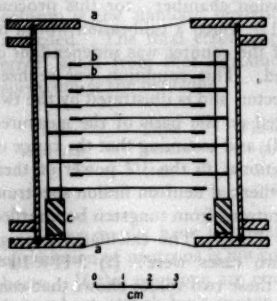

Figure 2. Fission chamber, diagrammatic section: a, 0·001 in. duralumin windows; b, 0·001 in. aluminium foils coated with fissile material; c, polytetrafluorethylene insulators.

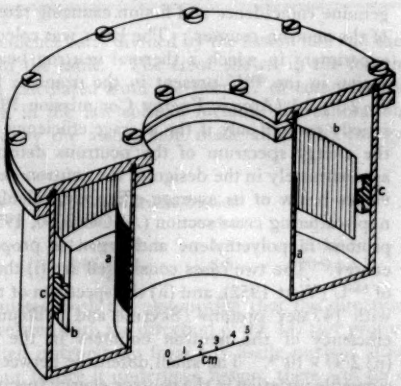

Figure 3. Neutron chamber, diagrammatic section: a, 10 mg cm^{-2} polyethylene foil; b, collector electrode; c, polytetrafluorethylene insulators.

on both sides with uranium oxide by the Zapon painting technique, or with bismuth by electroplating, over a central area 3 cm in diameter, the thickness of the deposit being 2 mg cm^{-2} in both cases. The filling was a mixture of 95% argon and 5% CO_2, the total pressure being 50 cm Hg. This filling, and the dimensions of the chamber, were chosen because it was necessary to discriminate between pulses due to fission fragments on the one hand, and on the other hand pulses due to α-particles (in the case of uranium) and to the passage of the proton beam through the chamber. For the same reason the time constant of the amplifier was made short ($3{\cdot}2 \times 10^{-8}$ sec).

The neutron chamber was made in the form of an annulus so that the solid angle it subtended at the fissile material could be as large as possible ($0{\cdot}4 \times 4\pi$ steradians). The chamber was filled to a pressure of 1 atmosphere with a mixture of 95% argon and 5% CO_2, and the collecting electrode was held at a potential of +2000 volts. A thin mica window allowed an external α-particle source to be used to set and maintain the correct discriminator level.

Preliminary experiments indicated that besides neutrons, some protons were detected in coincidence with the fission events. A copper absorber of thickness 2·8 g cm^{-2} was therefore placed between the fission chamber and the neutron chamber in the final arrangement. In spite of the shielding and collimation, a large background counting rate in the neutron counter was recorded. The random coincidence rate was determined in separate measurements with a delay line of 1·2 μsec connected between the neutron counter and the coincidence unit.

§ 3. Calibration

The average number of neutrons per fission $\bar{\nu}$ is given by the ratio of the genuine coincidence and fission counting rates, divided by the average efficiency of the neutron counter. The latter was calculated from the results of a separate experiment in which a thermal neutron beam from the Harwell pile induced fission in the ^{235}U present in the uranium fission chamber; for this process, $\bar{\nu} = 2{\cdot}5 \pm 0{\cdot}1$ (Atomic Energy Commission 1951). Such a calibration would be strictly correct only if the average efficiency of the counter was independent of the energy spectrum of the neutrons detected. This condition was realized approximately in the design of the neutron detector, and is illustrated by the two values below of its average efficiency, calculated on the basis of the measured n–p scattering cross section (AECU 2040, 1952), and assuming that the range of protons in polyethylene and argon is proportional to the 3/2 power of their energy. The two cases considered are (i) the thermal neutron fission spectrum of ^{235}U (Watt 1952), and (ii) the spectrum of neutrons from tungsten bombarded with 147 Mev protons (Skyrme and Williams 1951). The calculated average efficiency of the neutron counters in the two cases were: (i) $3{\cdot}11 \times 10^{-4}$, (ii) $2{\cdot}99 \times 10^{-4}$. The small difference between these two values shows that considerable variation in the neutron energy spectrum is possible without invalidating the calibration.

In view of the assumptions made in the efficiency calculations, an attempt was made to verify them by measuring the efficiency of the neutron counter in two energy regions: (*a*) using coincident emission of neutrons and γ-rays from Po–Be (Harding 1955); the neutrons have all energies between zero and 6 Mev

with maximum intensity at about 4 MeV; (*b*) using neutrons of energy 0·5–0·8 MeV from the reaction ^{7}Li(p, n)^{7}Be. The results obtained were sufficiently close to the calculated values to give confidence in the calculations, although the experimental errors were large.

§ 4. Preliminary Tests

4.1. *Evaporation Protons*

In the first measurements with uranium, particles evaporated from the fissile material had to traverse the walls of both ionization chambers ($\frac{1}{16}$ in. Al + $\frac{1}{16}$ in. brass) before being detected. The surprisingly large result obtained ($\bar{\nu}\sim25$) suggested that protons evaporated with energy greater than about 30 MeV were contributing to the coincidence rate in this way. The measurements were therefore repeated with a 'blank' chamber, similar to the neutron chamber but without the polyethylene foil. The ratio of coincidence to fission counting rates was then about one half of the first value, showing that evaporated protons were detected with a higher efficiency than neutrons. The copper absorber mentioned above was then inserted between the chambers. The value for $\bar{\nu}$ obtained by subtracting the result with the 'blank' chamber from the result without the absorber ($\bar{\nu}=13{\cdot}1\pm3{\cdot}0$) agrees with the result obtained with the absorber.

4.2. *Non-fission Events*

Using a chamber similar to the fission chambers except that the electrodes were not coated, the operating conditions of the fission chamber and its amplifier were set so that only pulses due to fission fragments were recorded. Thus the recording of neutrons from events other than fission was avoided.

§ 5. Results

The genuine and random coincidence rates divided by the fission rate and the resulting values for $\bar{\nu}$ are given in the table. The error shown in the fourth column is the standard deviation calculated from the number of coincidences recorded. The total error shown in the last column includes the calibration error, apart from that introduced by the assumption made about the energy spectrum of the neutrons.

Fissile material	Time (min.)	Fission rate (sec^{-1})	Coincidences/Fission genuine	random	$\bar{\nu}$
U	460	2·56	11·6 ± 1·4	1·7	13·1 ± 1·8
Bi	587	2·58	8·85 ± 2·2	8·8	10·0 ± 2·7

These results have been calculated with the assumption that the direction of emission of neutrons is not correlated with the direction of the 147 MeV proton beam. If the neutrons are emitted isotropically from the fissile nucleus after it has been struck by a proton but before it undergoes fission, there will be a slightly higher probability of emission in the forward hemisphere due to the motion of the heavy nucleus. Since the present measurement was made at 90° to the direction of the proton beam, where this will have the least effect, the error introduced by assuming an isotropic distribution is negligible. The value obtained for $\bar{\nu}$, however, does not include any very energetic 'knock-on' neutrons

emitted at a small angle to the proton beam. On the other hand, a correlation between the directions of emission of fission fragments and neutrons would not invalidate these results, since the fission fragments were not collimated in any particular direction.

Acknowledgments

I am grateful to Mr. W. J. Whitehouse for suggesting this measurement and for discussion, to Dr. E. Bretscher, head of the Nuclear Physics division, Atomic Energy Research Establishment, Harwell, to Mr. B. Rose and the Harwell cyclotron team, and to Mr. Ralph Jackson for help with the construction of apparatus and measurements.

References

A.E.C., 1951, Official release by U.S., U.K., and Canadian Atomic Energy Commissions, *Atomics*, **2**, 15.

A.E.C.U. 2040, 1952, *Neutron Cross-sections*, compiled by the A.E.C. Neutron Cross-section Advisory Group.

Biller, W. F., 1953, University of California, U.C.R.L. 2067.

Folger, R. L., Stevenson, P. C., and Seaborg, G. T., 1955, *Phys. Rev.*, **98**, 107.

Goeckermann, R. H., and Perlman, I., 1949, *Phys. Rev.*, **76**, 628.

Harding, G. N., 1955, *Proc. Phys. Soc.* A, **68**, 52.

O'Connor, P. R., and Seaborg, G. T., 1948, *Phys. Rev.*, **74**, 1189.

Skyrme, D. M., and Williams, W. S. C., 1951, *Phil. Mag.*, **42**, 1187.

Watt, B. E., 1952, *Phys. Rev.*, **87**, 1037.

The Energy Levels of ^{26}Al

By L. L. GREEN, J. J. SINGH and J. C. WILLMOTT
Nuclear Physics Research Laboratory, University of Liverpool

Communicated by Professor H. W. B. Skinner; *MS. received* 14*th November* 1955
and in final form 24*th January* 1956

Abstract. The ^{25}Mg(p, γ)^{26}Al reaction has been studied at six resonances in the region of 675 kev to 960 kev. New levels have been located at 2·32 Mev, 3·16 Mev, 3·76 Mev and 4·55 Mev, and the level at 2·09 Mev is shown to be a close doublet. Spins and parities have been assigned on the basis of angular distribution measurements. The resonances are shown to be reasonably pure isotopic spin states with the main transitions being E 1 transitions satisfying the isotopic spin selection rules.

§ 1. Introduction

The nucleus ^{26}Al is one of the series of nuclei of mass $A=4n+2$ which form isobaric triplets, the centre member of each possessing states with isotopic spin $T=0$ or 1. In work on the reaction ^{25}Mg(p, γ)^{26}Al, Kluyver, van der Leun and Endt (1954) have observed a level at 230 kev above the ground state which was not observed by Browne (1954) in a study of the reaction ^{28}Si(d, α)^{26}Al. Only $T=0$ states can be formed in this latter reaction and hence, as was pointed out by Browne, this 230 kev state is the analogue of the ground state of ^{26}Mg. This 230 kev state is the short lived β^+ emitter which decays to the ground state of ^{26}Mg. Kluyver *et al.* have also ascribed spins and parities to levels of energy up to 2 Mev in ^{26}Al on the basis of transition strengths in the reaction ^{25}Mg(p, γ)^{26}Al, but recent work by Elliott and Flowers (1955) has shown this procedure to be of doubtful validity due to the very mixed configurations which occur.

The present work was undertaken to extend the range of resonances in this reaction in the hope of extending the level scheme to high energies, elucidating the decay of some of the low-lying levels and assigning spins and parities on the basis of angular distribution measurements.

§ 2. Experimental Procedure

A 60 μA beam of protons bombarded a target of electromagnetically separated ^{25}Mg which had been evaporated on to a 0·01 in. thick copper backing. The γ-rays were detected in a cylinder of NaI 2 in. in diameter by 2 in. high mounted on a Dumont 6292 photomultiplier. The pulses produced were shaped and amplified and then analysed by a Hutchinson and Scarrott type pulse analyser.

The γ-ray spectra were observed in the forward direction and also, in some cases, at 90° to the proton beam direction. The spectra were analysed and the intensity measurements made in the same manner as described in a previous paper (Green, Singh and Willmott 1955). From these energy and intensity measurements a decay scheme was drawn up for each resonance and coincidence work undertaken to verify the cascades.

For the coincidence work the 2 in. × 2 in. crystal was placed at 90° to the beam direction on one side of the target and a NaI crystal 1½ in. in diameter by 1 in. thick was placed on the opposite side of the target. The target was set at 45° to the beam in a ½ in. diameter tube so that the crystals could be placed as close to the target as possible. Figure 1 shows in diagrammatic form the electronic system used. A single channel pulse analyser was set to straddle a particular peak in the spectrum given by the 1½ in. × 1 in. crystal and coincidences between these pulses and those from the 2 in. × 2 in. crystal were used to open the gate of the multichannel pulse analyser. In this way the spectrum of pulses in coincidence with the pulses occurring within the range of the single channel analyser was obtained. Naturally any particular peak was superimposed on the continuous Compton spectrum due to the higher energy γ-rays. This means that the coincidence spectrum for any particular peak in the γ-ray spectrum will include contributions from higher energy γ-rays through these Compton distributions. It is thus necessary to know which γ-rays are in coincidence with higher energy γ-rays before a particular coincidence spectrum can be interpreted. Hence it was necessary to take coincidence spectra with the single channel analyser set across the various peaks in descending order of energy.

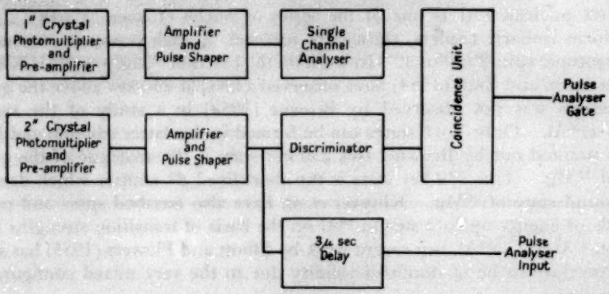

Figure 1.

For the angular distribution measurements the 2 in. × 2 in. crystal was mounted on a movable arm approximately 6 in. from the target. The 1½ in. × 1 in. crystal was used as a monitor at 135° to the beam, and the spectra were taken at six different angles between 0° and 90° in a random order. Angular distribution measurements were only taken on the higher energy γ-rays owing to the complexity of the spectra at the lower energies.

§ 3. Results

3.1. *Energy Levels*

Resonances were observed and spectra taken at 675 kev, 720 kev, 777 kev, 820 kev, 940 kev and 960 kev. The results are summarized in table 1 where the γ-ray energies observed are shown together with the relative intensities and the transitions to which they have been ascribed. This table contains all the γ-rays observed at all the resonances except at the 960 kev resonance where γ-rays of 3·27 Mev and 2·07 Mev also occurred which could not be fitted into the scheme.

These discrepancies are discussed later. In addition annihilation radiation was observed at all the resonances. The level scheme deduced is shown in figure 2 together with the decay schemes of the resonance levels.

Table 1

γ-ray energy (MeV)	Transition Initial level	Transition Final level	Relative Intensity† 675 kev	720 kev	777 kev	820 kev	940 kev	960 kev
6·73–7·00	Resonance	1	—	—	—	—	70	—
6·54–6·81	,,	2	32·5	4·3	3·1	8·7	—	—
5·20–5·47	,,	4	43	—	—	—	—	—
4·87–5·14	,,	6 & 7	—	50	37	50	33·5	80
4·64–4·91	,,	8	7	—	12	—	—	—
4·42–4·69	,,	9	—	7	—	17	—	13
3·80–4·07	,,	10	—	<4	60	—	—	—
3·29–3·56	,,	11	17	—	—	—	—	8
3·20–3·47	,,	12	‡	—	6	21	—	‡
2·41–2·68	,,	13	—	36	—	—	—	—
4·14	13	2	—	16	—	—	—	—
3·50	13	3	—	16	—	—	—	—
2·74	10	2	—	<5	37	—	—	—
2·54	9	0	—	<3	—	10	—	5
2·32	8	0	~2	—	20	—	—	—
2·12	9	2	—	2	—	9	—	‡
2·09	10	3	—	‡	18	—	—	—
1·88	12	5	2	—	6	23	—	2·5
	5	0	2	—	6	23	—	2·5
1·66	6	2	—	15	12	28	7	80
1·60	11	7	21	—	—	—	—	‡
1·40	10	4	—	<5	8	—	—	—
1·34	4	2	42	<5	8	—	—	—
1·07	10	7	—	—	5	—	—	—
1·02	7	3	15	42	20	15	24	4
0·840	3	1	15	62	33	17	24	4
0·420	2	0	85	44	51	30	8	87

† The intensities have been normalized so that the sum of the intensities of γ-rays originating at each resonance level is approximately 100. These γ-rays are to be found in the top half of the table.

‡ In these cases the γ-ray in question is not observed due to its proximity to another intense γ-ray, but other members of the cascade to which it belongs are observed at the resonance.

For the purposes of discussion the levels of ^{26}Al can be divided into three groups: (i) The levels up to 2·08 MeV, except for the level at 1·86 MeV. These are the levels already found by Browne, plus the level at 0·230 MeV which has been observed by Kluyver, van der Leun and Endt. The level at 1·86 MeV was completely resolved by Browne at only one bombarding energy and, therefore, could not be ascribed with certainty to ^{26}Al. (ii) Those of the remaining levels which are fed from more than one resonance level. In this case the slight shift in γ-ray energy at the different resonances identifies a particular γ-ray as a primary γ-ray which may be used to determine an energy level value. These include the levels at 2·32 MeV, 2·54 MeV, 3·67 MeV, and 3·76 MeV. Strictly this also includes the level at 2·09 MeV, but as the γ-ray feeding this level was not separable in energy from the γ-ray feeding the 2·08 MeV level this requires special discussion.

(iii) The remaining levels, namely, those at 1·86 MeV, 2·09 MeV, 3·16 MeV and 4·55 MeV.

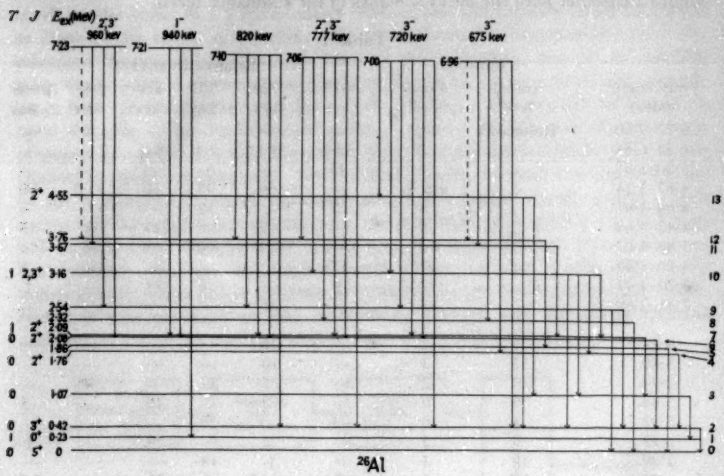

Figure 2.

The 1·86 MeV *level.*

At four of the six resonances a rather broad peak was observed corresponding to a γ-ray of mean energy 1·88 MeV, and at the 820 kev resonance it was stronger than any other low energy γ-ray. Coincidence measurements with the single channel analyser set on this peak showed that the only γ-rays in coincidence with it were the 3·34 MeV γ-ray which feeds the 3·76 MeV level, and the 1·88 MeV γ-ray itself. The total intensity of the 1·88 MeV γ-ray was quite closely twice that of the 3·34 MeV γ-ray, so if the assumption is made that the 3·76 MeV level decays by a double cascade to the ground state, both γ-rays being close to 1·88 MeV in energy, the intensity and coincidence measurements are both satisfied. Because of Browne's measurements, we have placed the lower level at 1·86 MeV.

The 2·09 MeV *level.*

The γ-rays leading to the level at 2·09 MeV are not separable in energy from the transitions to the 2·08 MeV level, but proof that this is a doublet comes from the cascades which follow the high energy γ-rays to these states; these are a 1·66 MeV γ-ray and a 0·420 MeV γ-ray in cascade, ending at the ground state, and a 1·02 MeV γ-ray and 0·84 MeV γ-ray in cascade ending at the 0·230 MeV level. The ratio of these two modes of decay varies from resonance to resonance. The mean energy of the level determined from the cascade 2·08 MeV level→0·420 MeV level→ground state is 10 kev lower than that determined from the cascade, 2·09 MeV level→1·07 MeV level→0·230 MeV level. So we associate the cascade through the 1·07 and 0·230 MeV levels with the upper member of the doublet. The resolution of the spectrometer in this energy region is approximately 7% but the energy of a peak can be fixed to slightly better than 10 kev. Although

the absolute accuracy of the spectrometer may not be as good as 10 kev, on a particular spectrum relative energies can probably be determined to this accuracy. These results are in agreement with the recent work of Kavanagh, Mills and Sherr (1955), who suggest that levels exist at 2·064 Mev and 2·074 Mev. The results of Browne on the $^{28}Si(d, \alpha)^{26}Al$ reaction using a high resolution magnetic spectrometer show only one level at 2·06 Mev. This reaction leads only to $T=0$ states, and hence the second of these levels must be a $T=1$ level.

The 3·16 Mev *level.*

A transition from a resonance level to the 3·16 Mev level occurs with certainty only at the 777 kev resonance where the 3·89 Mev γ-ray is by far the strongest. Coincidence measurements showed the 3·89 Mev, 2·74 Mev and 0·420 Mev γ-rays to be in cascade, and the 3·89 Mev, 2·09 Mev and 0·84 Mev γ-rays to be in cascade. The intensities of the 2·74 Mev γ-ray and the 2·09 Mev γ-ray are together approximately equal to the intensity of the 3·89 Mev γ-ray, so presumably the 3·89 Mev γ-ray is the primary γ-ray, feeding a level at 3·16 Mev and this level then decays by branching, mainly to the 1·07 Mev level and the 0·420 Mev level. Other much weaker γ-rays branch from this level and these will be discussed later. Confirmation that a level is to be expected at about this excitation is provided by the fact that the second excited state in ^{26}Mg occurs at 2·97 Mev, which would correspond to a level in ^{26}Al at 3·2 Mev. Presumably, then, the 3·16 Mev level is the third $T=1$ state.

The 4·55 Mev *level.*

The level at 4·55 Mev occurs only at the 720 kev resonance. Its existence is necessary to explain the fact that the strong 2·46 Mev γ-ray is in coincidence with the 4·14 Mev and 3·50 Mev γ-rays found at this resonance, and with the 0·840 Mev and 0·420 Mev γ-rays. A level at 4·55 Mev decaying in equal proportions to the 0·420 Mev level, and the 1·07 Mev level satisfies these measurements. An alternative explanation requires levels at 2·86 Mev and 3·50 Mev. Apart from the first explanation invoking fewer new levels, support for a level at 4·55 Mev comes from the existence of a level in ^{26}Mg at 4·35 Mev suggesting that a $T=1$ level should exist in ^{26}Al at about 4·6 Mev.

3.2. *The Cascade Scheme*

The 4·55 Mev *level* decays in equal proportions to the 1·07 Mev level and the 0·420 Mev level. The evidence is presented in the previous section.

The 3·76 Mev *level* decays to the 1·86 Mev level and the evidence is presented in the section above on the 1·86 Mev level.

The 3·67 Mev *level* decays to the 2·09 Mev level giving a γ-ray of measured energy 1·60 Mev. This is indicated by the intensity measurements at the 675 kev resonance, where the 1·60 Mev γ-ray has approximately the same intensity as the 3·28 Mev γ-ray from the resonance level to the 3·67 Mev level. Coincidence measurements with the single channel analyser set on the 3·28 Mev γ-ray showed the 1·60 Mev γ-ray and the 1·02 Mev and 0·84 Mev γ-rays to be in coincidence with the 3·28 Mev γ-ray, verifying the above conclusion. At the 960 kev resonance the 1·60 Mev γ-ray was lost under the very strong 1·66 Mev γ-ray, but the high energy spectrum in coincidence with this latter γ-ray was found to contain the 3·56 Mev γ-ray leading to the 3·67 Mev level.

The 3·16 MeV *level.* As discussed above, in the section on its existence, this level decays mainly to the 0·420 MeV level and the 1·07 MeV level. It also decays partially to the 1·76 MeV level giving a γ-ray of 1·40 MeV. At the 777 kev resonance at which this level occurs strongly, there is a weak 1·07 MeV γ-ray indicating, possibly, a partial decay to the 2·09 MeV doublet. This is confirmed by the intensity of the cascade from the 2·09 MeV level, which is too great unless it is also fed from the 3·16 MeV level.

The 2·54 MeV *level.* γ-rays leading to this level are observed at three resonances, the strongest occurring at the 820 kev resonance. At the 820 kev resonance a 2·54 MeV γ-ray is observed of approximately half the strength of the 4·56 MeV γ-ray leading to this state, so approximately half of the transitions from this level are to the ground state. A 2·12 MeV γ-ray of almost the same strength shows that the remainder of the transitions are to the 0·420 MeV level. At the 960 kev resonance there is a serious discrepancy involving this cascade. Instead of observing a 2·12 MeV γ-ray, we observe a 2·07 MeV γ-ray of approximately four times the correct intensity. Coincidence measurements with the single channel analyser set on the 2·07 MeV peak showed γ-rays of 4·68 MeV, 3·27 MeV and possibly 1·86 MeV in coincidence with this peak. The last γ-ray is so very weak that no reliable measurements can be made on it. The 4·68 MeV γ-ray is to be expected due to the 2·12 MeV γ-ray which is presumably lying partially underneath the 2·07 MeV γ-ray. The 3·27 MeV γ-ray, as mentioned earlier, does not fit into our level scheme; it is approximately half the strength of the 2·07 MeV γ-ray. These γ-rays must involve a level not observed at the other resonances.

The 2·32 MeV *level.* This appears to decay directly to the ground state, but there are some uncertainties. The γ-rays involved appear fairly strongly at the 777 kev resonance, but rather weakly at the 675 kev resonance. Coincidence measurements at the 777 kev resonance show the 2·32 MeV γ-ray to be in coincidence with the spectrum between 4·04 MeV and 5·02 MeV, and there is a high energy γ-ray of 4·72 MeV giving the correct total excitation energy. The intensity measurements, however, give poor agreement, particularly at the 675 kev resonance. This may be due, in the latter case, to a weak 4·87 MeV γ-ray, in which case the 4·65 MeV γ-ray would have an appreciably lower intensity than is recorded in table 1.

The 2·09 MeV *level* decays to the 1·07 MeV level and is discussed in the section above on its existence.

The 2·08 MeV *level* decays to the 0·420 MeV level as is shown clearly at the 960 kev resonance by intensity and coincidence measurements.

The 1·86 MeV *level* decays to the ground state and is discussed in the section on the existence of this level.

The 1·76 MeV *level* decays to the 0·420 MeV level giving a γ-ray of 1·34 MeV. This is shown by the intensities of the 5·15 MeV and 1·34 MeV γ-rays at the 675 kev resonance and was checked by coincidence measurements.

The 1·07 MeV *level* decays to the 0·230 MeV level, the corresponding γ-ray being observed at all the resonances.

The 0·420 MeV *level* decays directly to the ground state, the corresponding γ-rays being observed at all the resonances.

The 0·230 MeV *level.* This decays by β^+ emission to the ground state of ^{26}Mg, as discussed by Endt, Kluyver and van der Leun (1954).

§ 4. The Angular Distributions

Angular distribution measurements were made on the two most energetic γ-rays at each of the resonances at 675 kev, 720 kev, 777 kev and 940 kev, and on the single, strong high energy γ-ray occurring at the 960 kev resonance. At the 720 kev resonance the angular distribution of the transition to the 4·55 Mev level was also measured.

Table 2 gives the theoretical distributions required for the discussion of these results, together with the experimental distributions. One of these angular distributions is shown in figure 3.

Table 2.

Theoretical Angular Distributions

Transition	Channel Spin 2	Channel Spin 3
$2^- \to 2^+$	$1-0{\cdot}35\ P_2$	$1+0{\cdot}1\ P_2$
$2^- \to 3^+$	$1+0{\cdot}1\ P_2$	$1-0{\cdot}03\ P_2$
$2^- \to 4^+$	$1-0{\cdot}14\ P_2$	$1+0{\cdot}04\ P_2$
$3^- \to 2^+$	$1-0{\cdot}24\ P_2$	$1+0{\cdot}3\ P_2$
$3^- \to 3^+$	$1+0{\cdot}3\ P_2$	$1-0{\cdot}375\ P_2$
$3^- \to 4^+$	$1-0{\cdot}1\ P_2$	$1+0{\cdot}125\ P_2$
$4^- \to 4^+$	—	$1+0{\cdot}275\ P_2$

Experimental Angular Distributions

Resonance	γ-ray	Final State	Angular Distribution (by least squares)
675 kev	6·52 Mev	0·420 Mev level	$1-(0{\cdot}10\pm0{\cdot}02)\ P_2$
	5·15 Mev	1·76 Mev level	$1+(0{\cdot}10\pm0{\cdot}02)\ P_2$
720 kev	6·60 Mev	0·420 Mev level	$1+(0{\cdot}08\pm0{\cdot}02)\ P_2$
	4·93 Mev	2·09 Mev doublet	$1-(0{\cdot}05\pm0{\cdot}02)\ P_2$
	2·45 Mev	4·55 Mev level	$1-(0{\cdot}03\pm0{\cdot}03)\ P_2$
777 kev	6·64 Mev	0·420 Mev level	$1-(0{\cdot}01\pm0{\cdot}02)\ P_2$
	4·97 Mev	2·09 Mev doublet	$1+(0{\cdot}03\pm0{\cdot}02)\ P_2$
940 kev	6·96 Mev	0·230 Mev level	$1-(0{\cdot}21\pm0{\cdot}02)\ P_2$
	5·11 Mev	2·09 Mev doublet	$1-(0{\cdot}05\pm0{\cdot}03)\ P_2$
960 kev	5·11 Mev	2·09 Mev doublet	$1-(0{\cdot}24\pm0{\cdot}02)\ P_2$

The 940 kev resonance is the simplest case to consider, since it is the only resonance at which the $T=1$ level at 230 kev is formed by a direct transition from the resonance level, and this transition is very strong, the only other γ-ray of comparable strength going to the state at 2·09 Mev. Consequently it is almost certain that these transitions are E 1 transitions, and that it is the upper level of the doublet at 2·09 Mev, which decays via the 1·07 Mev level to the 0·230 Mev level, which is the $T=1$ state. If this is so, and the 3·16 Mev level and 4·55 Mev level are identified as $T=1$ levels by comparison with the level scheme of ^{26}Mg, then the transitions from the resonance levels go either predominantly to $T=1$ levels or $T=0$ levels. Table 3 gives the relative intensities at the various resonances. It seems clear from these arguments that the resonance levels

Table 3

Resonance	675 kev	720 kev	777 kev
Transitions	100% to $T=0$	75% to $T=1$	80% to $T=1$
Resonance	820 kev	940 kev	960 kev
Transitions	85% to $T=0$	95% to $T=1$	95% to $T=0$

have T as a fairly good quantum number and that the strong transitions from these states are E1 transitions satisfying the isotopic spin selection rule for selfconjugate nuclei $\Delta T = \pm 1$. As the 0·230 MeV state is the analogue of the ground state of ^{20}Mg, and therefore has spin and parity 0^+, we can assign 1^- as the spin and parity of the 940 kev resonance level. The 2·09 MeV level is 2^+ or 3^+ as the analogue level at 1·83 MeV in ^{24}Mg is known to be 2^+ or 3^+ (Holt and Marsham 1953) and since this state is also presumably formed by an E1 transition, it must be 2^+.

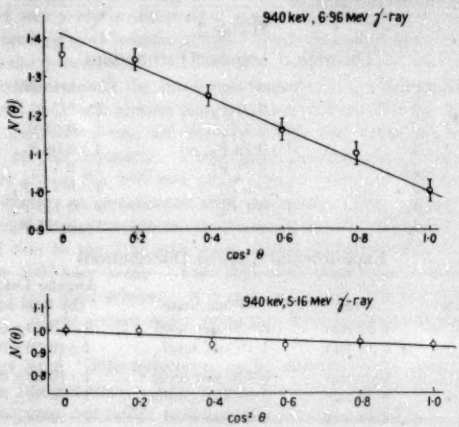

Figure 3.

The angular distribution for the transition from the 940 kev resonance level to the 0·230 MeV level cannot be fitted by assuming ingoing p-waves. Only one channel spin occurs in this case, and a unique solution of $1 - 0{\cdot}14\cos^2\theta$ is found, compared with the experimental result of $1 - 0{\cdot}28\cos^2\theta$. Hence it is necessary to consider f-waves. At 940 kev the barrier penetrability of f-waves is only 0·4% of that of p-waves, so the main contribution is to be expected from the interference term. A calculation was carried out using the phase factors for the components of the ingoing waves calculated from the formulae given by Blatt and Biedenharn (1952). In order to fit the experimental results the f-wave intensity was required to be 6·3% of the p-wave intensity, i.e. 16 times the ratio given by penetrability alone, suggesting that this resonance has a strong f-wave character. The angular distribution of the transition to the 2·09 MeV doublet agreed with that calculated, under these conditions, for a transition to a 2^+ state.

At the 720 kev resonance the two most energetic γ-rays are the transitions to the 0·420 MeV level and the 2·09 MeV doublet. The transition to the 0·420 MeV level has a very different angular distribution from that to the 2·09 MeV doublet, 75% of which is to the 2^+, $T = 1$ level, as is shown by the decay of the 2·09 MeV doublet. The 0·420 level is not, therefore, 2^+. As it decays to the ground state, which is 5^+, it is 3^+, or possibly 4^+. The resonance level decays strongly to the 4·55 MeV level which is the analogue of the 4·35 MeV level in ^{28}Mg, which is

known to be 2^+ or 3^+, and, of course, $T=1$. The angular distribution of the transition to this level was also measured. Such a strong decay to a highly excited state would not be likely to take place unless it were an electric dipole transition satisfying the isotopic spin selection rule. This consideration, together with the strong transition to the 2^+, $T=1$ state at 2·09 Mev, and the absence of any transition to the 0^+, $T=1$ state fixes the resonance level as 2^- or 3^-. Hence the transitions to the 0·420 Mev level are 2^- or 3^- to 3^+ or 4^+ and the transitions to the 4·55 Mev level are 2^- or 3^- to 2^+ or 3^+. To fit the angular distributions with a unique value of the channel spin mixing ratio it is necessary to assume that the resonance level is 3^-, the 0·420 Mev level is 3^+ and the 4·55 Mev level is 2^+. The observed angular distribution for the transition to the 2·09 Mev doublet is, within the limit of error, that calculated for a 3^- to 2^+ angular distribution using this channel spin ratio. 75% of the γ-ray to the 2·09 Mev doublet is due to a transition to the 2^+ $T=1$ state and 25% to the $T=0$ state. It follows that the angular distribution for the transition to the $T=0$ state cannot be very different from that for the $T=1$ state. The transition 3^- to 4^+ is also a very weak angular distribution so that the spin of the $T=0$ state is either 2^+ or 4^+. 4^+ is less likely due to the fact that the $T=0$ state decays to the 0·420 Mev level which has been shown to be 3^+, and not at all to the ground state which is 5^+, though it cannot be ruled out on these grounds.

At the 960 kev resonance almost the entire strength of the resonance is concentrated to the $T=0$ member of the 2·09 Mev doublet and hence on the same grounds as before we assume this to be an E 1 transition. If the level at 2·08 Mev is assumed to be 2^+ the observed angular distribution can be accounted for by assuming the resonance level is either 2^- or 3^-. If we assume the 2·08 Mev level is 4^+ it is not possible to fit the observed angular distribution for any value of the spin of the resonance level even if ingoing f-waves are included in the calculation. Thus the 2·08 Mev level is also 2^+.

If we assume that the main transitions at the 777 kev resonance are E 1 then the resonance may be fixed as 2^- or 3^-. Both these assignments for the resonance level can lead to angular distributions for the transitions to the 0·420 Mev level and the 2·09 Mev level which are in agreement with the observed angular distributions within the experimental error.

The 675 kev resonance decays exclusively to $T=0$ states. It is, however, a strong resonance and its radiation width is in no way smaller than for any other resonance and hence the main transitions should thus be electric dipole transitions. The strong transition to the 3^+ state at 0·420 Mev fixes the resonance level at 2^-, 3^- or 4^- and of these only 3^- can fit the observed angular distribution of the γ-ray to this level. The channel spin ratio required for this gives the correct angular distribution for the transition to the 1·76 Mev level if this is assumed to be 2^+, thus fixing the spin of this level.

§ 5. Radiation Widths

From the thick target yield of γ-rays from the resonance level the corresponding radiation width multiplied by $2J+1$ can be calculated if the detection efficiency of the crystal is known. Table 4 gives the radiation width Γ_γ calculated from the results at each resonance. These are approximately two orders of magnitude smaller than the single particle level widths.

Table 4

Resonance (kev)	675	720	777	820	940	960
$(2J+1)\Gamma_\gamma$ (ev)	3·5	2·8	1·9	1·2	1·5	3·8
J	3	3	2	—	1	2,3
Γ_γ (ev)	0·5	0·4	0·4	—	0·5	0·6

Acknowledgments

We should like to thank Professor H. W. B. Skinner for much helpful discussion of this paper and Dr. B. Collinge and Mr. K. Aitchison for technical assistance. One of us (J. J. S.) is indebted to the Punjab Government for leave of absence. Our thanks are due to A.E.R.E. for preparing the separated ^{25}Mg target.

References

Blatt, J. M., and Biedenharn, L. C., 1952, *Rev. Mod. Phys.*, **24**, 241.
Browne, C. P., 1954, *Phys. Rev.*, **95**, 860.
Elliott, J. P., and Flowers, B. H., 1955, *Proc. Roy. Soc.* A, **229**, 536.
Endt, P. M., Kluyver, J. C., and van der Leun, C., 1954, *Physica*, **20**, 1299.
Green, L. L., Singh, J. J., and Willmott, J. C., 1955, *Phil. Mag.*, **46**, 982.
Holt, J. R., and Marsham, T. N., 1953, *Proc. Phys. Soc.* A, **66**, 527.
Kavanagh, R. W., Mills, W. R., and Sherr, R., 1955, *Phys. Rev.*, **97**, 248.
Kluyver, J. C., van der Leun, C., and Endt, P. M., 1954, *Physica*, **20**, 1287.

RESEARCH NOTES

Range Velocity Relationship for ^{7}Li Ions in Solids

By S. DEVONS† and J. H. TOWLE
Department of Physics, Imperial College, London

MS. received 24*th November* 1955, *and in final form* 19*th December* 1955

In measurements of the lifetimes of excited states of nuclei using recoil methods, it is frequently necessary to know the range velocity relationships for recoil nuclei passing through solid materials (see for example Devons *et al.* 1955). The present note describes measurements of the relationship for ^{7}Li ions. This information has been used in the estimate of the lifetime of the first excited state in ^{7}Li (Bunbury *et al.* 1956). The only data available on the stopping of ions in solids in the velocity region of interest ($V \lesssim 10^9$ cm sec^{-1}) is for hydrogen and helium ions and is summarized in the review article by Allison and Warshaw (1953). At these low velocities the slowing down of an ion in matter is a very complex process. Theoretical or semi-theoretical estimates of the stopping cross section entail many approximations, and are not sufficiently reliable.

The ^{7}Li ions were produced in the nuclear reaction ^{9}Be(d, α)^{7}Li at a deuteron energy of 1 Mev. The velocity V_0 of the ^{7}Li ions recoiling in a direction making an angle of 90° with the direction of motion of the incident particles is $8{\cdot}6 \times 10^8$ cm sec^{-1}. The velocity of the recoil ions was measured using a magnetic analyser with a deflection of 40°. The analyser was calibrated against particle groups of known energy. Absorbing foils of various thicknesses could be placed in the path of the recoil ions. The apparatus is shown schematically in figure 1.

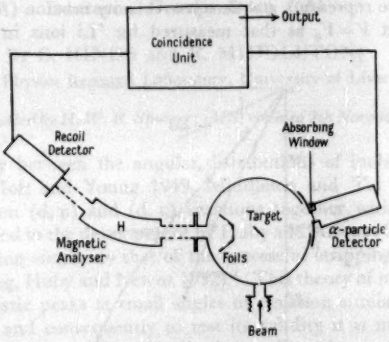

Figure 1. Apparatus.

Various particles other than ^{7}Li recoil ions emerge at the exit of the analyser, in particular the alpha particles produced in the reaction ^{9}Be(d, α)^{7}Li, which, if

† Now at the Physical Laboratories, University of Manchester.

emitted in the same direction as the recoil ions, i.e. 90° to the incident beam, have approximately the same momentum. In order to obtain a spectrum of recoil ions only, the following coincidence method was used. An alpha particle detector was placed at the correct angle to receive all the alpha particles corresponding to ^{7}Li recoils which entered the analyser. The alpha particles traversed the thin target backing (aluminium equivalent to 1·5 mm air). An absorbing foil of sufficient thickness to absorb the scattered deuterons and recoil ions was placed in front of the alpha particle detector. Pulses from the alpha particle detector and the analyser detector were fed to a coincidence unit of resolving time one microsecond. Owing to the unique angle between the alpha particle and ^{7}Li recoil ion, together with the coincidence discrimination, the pulses appearing at the output of the coincidence unit were due only to the detection of ^{7}Li recoil ions. Both recoil ion and alpha particle detectors consisted of an activated zinc sulphide screen with an E.M.I. photomultiplier. The advantage of this coincidence technique lies in the fact that it introduces little reduction in the essential counting rate, whilst making the recoil spectrum much easier to interpret. The velocity of the recoil ions was measured after traversing foils of aluminium, copper and gold of various thicknesses up to one milligramme per square centimetre. The thickness of the absorbers was measured by observing with the analyser the loss in energy of protons scattered from a thin layer of gold, due to their passage through the foils, and using the stopping data for protons given by Allison and Warshaw (1953).

The results are shown in figure 2. The initial slopes of the curves are in the ratio Au 1 : Cu 2·5 : Al 4. This is the ratio of stopping powers (per mg cm^{-2}) at the velocity V_0 which is $8{\cdot}6 \times 10^8$ cm sec^{-1}. For *protons* of this velocity, from the data given by Allison and Warshaw, the stopping powers of gold, copper and aluminium are in the ratio Au 1 : Cu 2·3 : Al 3·3. Over the limited range of velocities used, the range–velocity relationship does not deviate very much from the linear one which has been assumed in some nuclear lifetime measurements. The broken curve represents a square law velocity relation ($R-x=\beta V^2$) having the same slope at $V=V_0$ as that measured for ^{7}Li ions in copper, and with

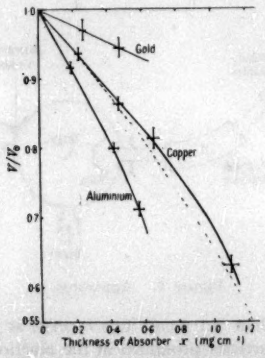

Figure 2. Results. ^{7}Li ions. $V_0=8{\cdot}6\times10^8$ cm sec^{-1}.

$\beta = 2{\cdot}65 \times 10^{-22}\,\mathrm{cm^{-1}\,sec^2}$. Reduction in counting rate due to straggling and scattering in the absorbing foils prevented the further extension of the curves using recoil ions from the reaction $^9\mathrm{Be(d, \alpha)^7Li}$.

Some information was obtained about the charge state of the ^{7}Li ions but this was limited to the Li^{3+} and Li^{2+} ions since the spectrometer was not large enough to focus the Li^+ ions properly. Also for low recoil energies measurements were limited by the presence of a large background of scattered particles. For recoil ions leaving the target directly, with a mean energy of 2·74 MeV, the relative number of Li^{2+} to Li^{3+} was $0{\cdot}65 \pm 0{\cdot}05$. The relative number of Li^+ ions was probably less than 0·3. The Be target thickness was $25\,\mu\mathrm{g\,cm^{-2}}$ so that it cannot be asserted that charge equilibrium was reached. After passage through either gold or copper foils sufficient to reduce their energy to 2·4 MeV ($V/V_0 = 0{\cdot}94$), the ratio Li^{2+}/Li^{3+} was increased to $0{\cdot}83 \pm 0{\cdot}07$, and it is very probable that for these foils charge equilibrium has been reached.

We intend to extend these measurements to lower velocities and to obtain data for the stopping of other ions in solids using this technique.

ACKNOWLEDGMENT

One of us (J.H.T.) is indebted to the Department of Scientific and Industrial Research for a maintenance grant.

REFERENCES

ALLISON, S. K., and WARSHAW, S. D., 1953, *Rev. Mod. Phys.*, **25**, 779.
BUNBURY, D. ST. P., DEVONS, S., MANNING, G., and TOWLE, J. H., 1956, *Proc. Phys. Soc.* A, **69**, 165.
DEVONS, S., MANNING, G., and BUNBURY, D. ST. P., 1955, *Proc. Phys. Soc.* A, **68**, 18.

Angular Distributions of Some Inelastically Scattered Deuteron Groups from ^{27}Al

BY S. HINDS AND R. MIDDLETON†
Nuclear Physics Research Laboratory, University of Liverpool

Communicated by H. W. B. Skinner; *MS. received 9th November* 1955

THE similarity between the angular distributions of inelastically scattered deuterons (Holt and Young 1949, Middleton and Tai 1952) and those obtained from (d, p) and (d, n) reactions together with the large cross sections reported, led to the development by Huby and Newns (1951 a) of a theory of inelastic scattering similar to that of the successful stripping theories (Butler 1951, Bhatia, Huang, Huby and Newns 1952). This theory of inelastic scattering predicts characteristic peaks at small angles of emission similar to those of the stripping theories and consequently to test its validity it is most important to measure this region of the angular distributions. Experimentally this is difficult owing to the high intensity of elastically scattered deuterons at small angles. However, this difficulty can be overcome to a large extent by using magnetic analysis, so separating the considerably less intense inelastically scattered deuterons

† Now at the Atomic Weapons Research Establishment, Aldermaston, Berks.

from those elastically scattered. In this communication results are reported obtained from the bombardment of ^{27}Al with 9 MeV deuterons, using the magnetic spectrograph described by Green and Middleton (1956 a).

A deuteron spectrum is shown in figure 1 obtained at an angle of observation of 45°. Groups have been identified corresponding to the ground and excited states of ^{27}Al at 0·84, 1·01, 2·23, 2·75 and 3·04 MeV, which are the mean values obtained from many investigations reported by Endt and Kluyver (1954). Elastically scattered deuteron groups due to oxygen and carbon have been identified and also an inelastic group corresponding to the 4·43 MeV level of ^{12}C. Inelastic deuteron groups from ^{27}Al have previously been observed by Greenlees, Kempton and Rhoderick (1949), Holt and Young (1949), Boyer (1950) and Keller (1951); none of these investigators resolved the doublet corresponding to the states at 0·84 and 1·01 MeV, also the group due to the transition to the 2·75 MeV level has not previously been observed. No groups of significant intensity were observed corresponding to excited states in ^{27}Al between 3·04 MeV and about 6 MeV.

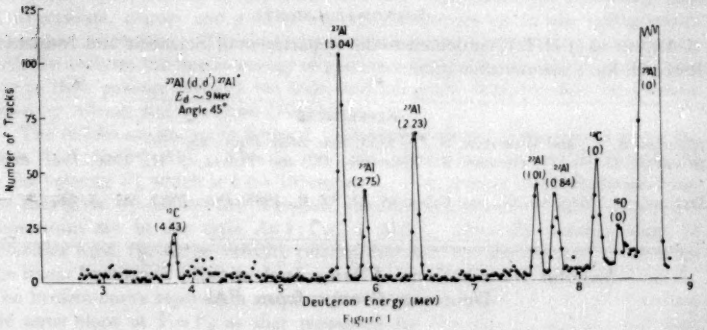

Figure 1

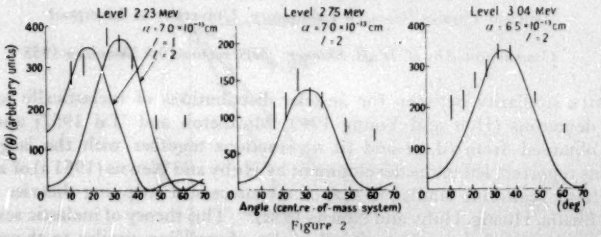

Figure 2

Angular distributions are shown in figure 2 for groups corresponding to the 2·23, 2·75 and 3·04 MeV levels together with the appropriate theoretical curves calculated from the theory of Huby and Newns. It may be noticed that although a magnetic spectrograph was used it was not possible to make measurements at angles less than 10° due to a background of deuterons extending along the length of the plate but tailing off in intensity towards the low energy end. This

background almost certainly arises from edge effects of the beam collimating slit and it is hoped that it may be reduced in the future by using an improved slit. The extremely high intensity of the background at the high energy end of the plate made it impossible to measure the angular distributions of the two most energetic deuteron groups.

The parameter a occurring in the theory is the affective radius of interaction and for ^{27}Al a reasonable value is $7{\cdot}0 \times 10^{-13}$ cm (Huby and Newns 1951 a). The value of the orbital angular momentum l which the nucleus receives during the interaction has been chosen so that the peaks of the theoretical and experimental distributions approximately coincide. The agreement obtained is very poor compared with that usually found in stripping reactions. However, the agreement is even worse for the inelastically scattered deuterons exciting the 2·429 MeV state of ^{9}Be and the 4·43 MeV state of ^{12}C (Green and Middleton 1956 b), though for the 1·38 MeV state of ^{24}Mg (Huby and Newns 1951 a) the agreement is good. It is to be noticed that the background in inelastic deuteron angular distributions is much larger than is usual in normal stripping reactions. One possible explanation is that the approximation introduced by the use of plane waves in this theory has much more serious consequences than in the stripping theory. Certainly some modification of the theory is required to explain these results.

Another possibility is that the inelastic scattering may be due to electrical excitation of the nucleus (Huby and Newns 1951 b). This has previously been ruled out since it predicts cross sections which were thought to be too small, but if the ratios of the inelastic to elastically scattered deuteron groups from ^{27}Al and ^{12}C are compared (see figure 1) the ratio for ^{27}Al is considerably smaller than that for ^{12}C. Therefore it appears possible that the inelastic cross section for ^{27}Al may be of the same order of magnitude as that predicted by the theory. Unfortunately a more detailed comparison is not possible since the angular distributions at these energies have only been calculated using the Born approximation which is not adequate for the electric interaction.

Acknowledgments

We would like to thank Professor H. W. B. Skinner for his encouragement and advice and also Dr. H. C. Newns for helpful discussions. One of us (R. M.) wishes to make acknowledgment to the Imperial Chemical Industries for a Research Fellowship and the other (S. H.) is grateful to the Department of Scientific and Industrial Research for a maintenance grant.

References

Bhatia, A. B., Huang, K., Huby, R., and Newns, H. C., 1952, *Phil. Mag.*, **43**, 485.
Boyer, K., 1950, *Massachusetts Institute of Technology Progress Report* (*L.N.S.E.*) July, 1950.
Butler, S. T., 1951, *Proc. Roy. Soc.* A, **208**, 559.
Endt, P. M., and Kluyver, J. C., 1954, *Rev. Mod. Phys.*, **26**, 95.
Green, T. S., and Middleton, R., 1956 a, *Proc. Phys. Soc.* A, **69**, 16; 1956 b, *Ibid.*, **69**, 28.
Greenlees, G. W., Kempton, A. E., and Rhoderick, E. H., 1949, *Nature, Lond.*, **164**, 663.
Holt, J. R., and Young, C. T., 1949, *Nature, Lond.*, **164**, 1000.
Huby, R., and Newns, H. C., 1951 a, *Phil. Mag.*, **42**, 1442; 1951 b, *Proc. Phys. Soc.* A, **64**, 619.
Keller, K. K., 1951, *Phys. Rev.*, **84**, 884.
Middleton, R., and Tai, C. T., 1952, *Proc. Phys. Soc.* A, **65**, 752.

Excitation Curve for the Reaction ^{10}B (p, α)^{7}Be

By H. R. ALLAN, M. GOVINDJEE and N. SARMA
Department of Physics, Imperial College, London

MS. received 16*th December* 1955

The yield of α-particles from the reaction $^{10}B(p, \alpha)^{7}Be$, has been investigated at an angle of 46° to the incident proton beam at bombarding energies of from 800 kev to 1·8 Mev. The target material was pure ^{10}B, 20 $\mu g\,cm^{-2}$ thick, deposited on a gold-plated copper foil. A double focusing magnetic spectrometer was used to separate the alpha particles from the scattered protons. The spectrometer had an angle of deviation of 37°, a resolving power of about 5% in energy, and a collection efficiency of about 1 in 2×10^{4}. A proportional counter was used as detector; it also served to discriminate between the alpha particles and the small number of protons which entered the counter after being scattered in the analyser. It was not possible to make reliable measurements on the short range group of alpha particles leading to the excited state of ^{7}Be, because at the appropriate energy setting a very large number of protons entered the counter causing pile-up.

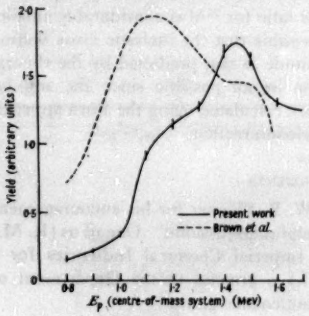

Figure 1.

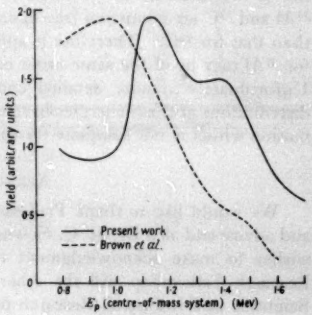

Figure 2.

The results are shown in figure 1 together with the excitation curves obtained by Brown *et al.* (1951) for the alpha particles at an angle of 138°. Penetrability factors for the incident protons and the emergent alpha particles were calculated using the graphs of Coulomb functions given by Sharp *et al.* (1953). Figure 2 gives the form of the excitation curves obtained after correction for penetrabilities. Both the corrected excitation curves show resonances at about 1·1 Mev ($\Gamma > 300$ kev) and 1·5 Mev ($\Gamma \sim 200$ kev). These resonances are asymmetric about their maximum; this is especially evident at 1·1 Mev. Moreover, the positions of the maxima show a shift in energy at the two angles of observation which is characteristic of interference between levels of the compound nucleus ^{11}C.

The table shows possible assignments of spins and parities of the levels in the compound nucleus for the two resonances and the background, made on the basis of the values of the penetrabilities P_pP_α and the observed widths. The fact that the short range alpha particles leading to the excited state $^7Be^*$ were not observed by Brown *et al.*, except at the 1·5 MeV resonance, is consistent with these assignments.

	(1) E_p	(2) S_i	(3) l_i	(4) J_π	(5) S_f	(6) l_f	(7) $P_p \times P_\alpha$
(1)	b'gnd	5/2	1	$3/2^-$	3/2	0	0·013
(2)	1·1	5/2	0	$5/2^+$	3/2	1	0·037
(3)	1·5	5/2	1	$5/2^-$	3/2	2	0·003
(4)	1·5	7/2	0	$7/2^+$	3/2	3	0·001

Columns : (1), E_p (MeV) incident proton resonance energy in centre-of-mass coordinates; (2), S_i incident channel spin; (3), l_i incident proton orbital angular momentum; (4), J_π spin and parity of level in the compound nucleus; (5), S_f final channel spin; (6), l_f orbital angular momentum of emergent α-particle; (7), $P_p \times P_\alpha$ product of proton and α-particle penetrabilities.

Comparison of the yields of the two curves may be effected by adjusting the scales of the ordinates so that at the upper and lower limits of observation the yields indicated are about the same; this has been done in figure 2. The reason for this procedure is that the angles of observation are symmetric about 90°, and interference effects should be small away from the resonance peaks.

The shift of the 1·5 MeV resonance by about 100 keV, and the very different amplitudes obtained at the two angles of observation indicate that this level interferes with the background, or with the 1·1 MeV resonance, or with both. Thus an assignment of $5/2^-$ for the relevant level in the compound nucleus, as in row 3 of the table, is more probable than the $7/2^+$ assignment of row 4. Brown *et al.* (1951), while suggesting both these possibilities, were unable to make a choice between them.

Acknowledgments

We are grateful to Professor S. Devons for suggestions and advice offered during the experiment, and to the Atomic Energy Research Establishment, Harwell, for supplying the ^{10}B target.

Note added in proof. Further measurements have been reported by J. W. Cronin, *Phys. Rev.*, 1956, **101**, 298.

References

Brown, A. B., Snyder, C. W., Fowler, W. A., and Lauritsen, C. C., 1951, *Phys. Rev.*, **82**, 159.

Sharp, W. T., Gove, H. E., and Paul, E. B., 1953, TPI–70 (Atomic Energy of Canada Ltd., Chalk River, Ontario).

LETTERS TO THE EDITOR

The Ionization of Fast Neutral Deuterium Atoms

It has been shown (Fremlin and Spiers 1955) that a cyclotron gives rise to numbers of fast-moving neutral atoms. The majority of these are produced by the break-up of accelerated molecular ions, such as H_2^+, or of negative ions, such as D^-, by residual gas.

The energy of the molecular ion H_2^+ or of the negative ion D^- will be identical with the known energy of the simple positive ion D^+ at the same radius. The neutral atoms obtained are not deflected appreciably by the collisions producing them, and hence travel along tangents to the orbits in which they were moving at the instant of collision. At any point in the cyclotron, therefore, the energies of the neutral atoms arriving depend in a calculable way on the direction from which they come.

A small camera was constructed in which two 0·1 mm slits, parallel to the lines of magnetic field and 1 cm apart, defined an approximately mono-energetic beam of neutral deuterium atoms. When the camera was placed in the cyclotron, on the axis of the dee gap, at a radius of 70 cm (beyond the reach of the charged beam) and with the camera's own axis at an angle of 45° to the axis of the dee gap, deuterium atoms of energy about 10 Mev were accepted. About 4 cm behind the slit system, the beam struck a C2 nuclear plate, held at an angle of about 20° to the beam and perpendicular to the median plane of the cyclotron. The camera slit nearest to the plate was covered along part of its length by a Formvar film prepared as described by Revell and Agar (1955). Uncharged atoms thus passed through the camera in a straight line and struck the plate along a well-defined strip about 1·5 mm wide. Atoms which were ionized by their passage through the foil, however, were deflected by the magnetic field and gave a similar, almost equally well-defined strip displaced by about 4 mm along the plate.

Hence, behind the open part of the slit system, a single strip of tracks due to the undeflected beam was observed, while behind the part covered by the Formvar two strips were found. One of these, less densely covered by tracks, was in line with the single strip due to the untouched beam and was due to atoms which had traversed the Formvar without ionization. The second and denser area was due to ions formed by electron loss during this traversal.

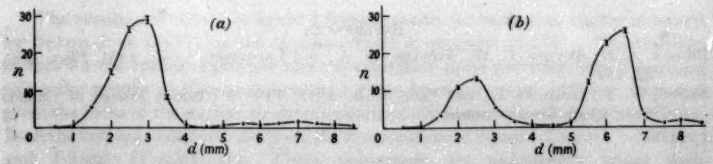

In the figure is shown the average number n of deuteron tracks per unit area as a function of distance d across the plate, (*a*) in the open and (*b*) in the Formvar-covered area. It can be seen that the background (due to particles

scattered from the slit edges) is small and that the proportion traversing the film un-ionized can be determined with good accuracy.

In our first experiment this proportion was $0{\cdot}35 \pm 0{\cdot}03$, the deuteron energy being $9{\cdot}7 \pm 0{\cdot}3$ Mev and the Formvar 'thickness' being $1{\cdot}2 \pm 0{\cdot}25\ \mu g\ cm^{-2}$. This gives a mean free path before an ionizing collision of $0{\cdot}88 \pm 0{\cdot}2\ \mu g\ cm^{-2}$. To this accuracy we may probably consider the Formvar film as being equivalent to a carbon film of similar weight per unit area and hence we find a cross section for ionization of 10 Mev deuterium atoms by carbon to be $2{\cdot}4 \pm 0{\cdot}4 \times 10^{-17}\ cm^2$. In other words, the average deuterium atom manages to traverse the surprising number of 30 carbon atoms before its electron is removed.

Department of Physics,
The University,
Birmingham 15.

L. P. Chalklin.
J. H. Fremlin.

22nd November 1955,
and in final form 4th January 1956.

Fremlin, J. H., and Spiers, V. M., 1955, *Proc. Phys. Soc.* A, **68**, 398.
Revell, R. S. H., and Agar, A. W., 1955, *Brit. J. Appl. Phys.*, **6**, 23.

Nuclear Spins and Magnetic Moments of Cobalt 56 and 57

The earlier paramagnetic resonance experiments on radioactive cobalt (Baker, Bleaney, Bowers, Shaw and Trenam 1953) have been repeated using apparatus of higher sensitivity, and crystals of lower specific activity, which give better resolution because of reduced line width. The nuclear spin $I = 7/2$ for ^{57}Co is confirmed, and the magnetic moment is found to be $4{\cdot}65 \pm 0{\cdot}05$ n.m. For ^{56}Co the values $I = 4$ and $\mu = 3{\cdot}848 \pm 0{\cdot}015$ n.m. are determined in agreement with the result of Jeffries (unpublished) of which we were informed while these experiments were in progress. This lies just outside the range $2{\cdot}8 \pm 0{\cdot}9$ n.m., obtained from nuclear alignment experiments by Gallaher, Whittle, Beun, Diddens, Gorter and Steenland (1955).

The radioactive cobalt was prepared by (d, n) and (d, 2n) reactions on an iron target in the Birmingham cyclotron, and the preparation of crystals of $ZnK_2(SO_4)_2 . 6D_2O$ containing the cobalt was similar to that in the previous work. If the specific activity of the solution from which the crystals are grown is too high, the paramagnetic resonance lines are abnormally broad, presumably owing to defects in the crystal structure which distort the crystal field acting on the cobalt ions. A good compromise between the desiderata of small line width (8 gauss) and good signal/noise ratio was obtained from a 40 mg crystal with 0·2 mc and 0·1 mc activity due to ^{56}Co and ^{57}Co respectively (corresponding to about 6×10^{-9} g of the former isotope and 10^{-8} g of the latter). The paramagnetic resonance spectrum was observed at 3 cm wavelength and 20°K in a system where the magnetic field was modulated at 115 kc/s (to reduce excess rectifier noise); the output from a phase-sensitive detector (time constant 1 sec) was traced on a recording milliammeter. Lines due to ^{56}Co were about 10 times greater than noise and fell inside a pattern of eight lines whose intensity was about 20–25 times greater. These lines are principally due to ^{59}Co, which has the same spin and whose moment is the same within 5% as ^{57}Co (Baker *et al.*).

The relative intensities of the outermost and innermost of these lines were found to be $1{\cdot}00 \pm 0{\cdot}02$; hence the separation of components due to ^{57}Co and ^{59}Co in the outermost line must be less than 4 gauss, and the moments must be equal to within $\pm 1\%$.

Seven well-resolved lines were obtained from ^{56}Co and from their spacing it was apparent that two other lines were masked by the much stronger ^{59}Co spectrum. A careful search showed no indication of a further line at the place where it should appear if the nuclear spin were 5; hence the value $I = 4$ is assigned to this isotope. From measurements of the position of the outermost lines in the ^{56}Co spectrum relative to the nearest lines in the ^{59}Co spectrum, the ratio of the moments is found to be $0{\cdot}828 \pm 0{\cdot}003 : 1$, after allowing for small deviations from equal spacing of the lines. Taking the nuclear moment of ^{59}Co as 4·648 n.m. (with diamagnetic correction), we obtain the values given above for the other moments.

Our thanks are due to the Nuffield cyclotron team of Birmingham University who carried out the irradiation, and to Dr. M. A. Grace and Mr. R. T. Taylor, who made measurements of the activity. We are also indebted to Professor C. D. Jeffries of the University of California, Berkeley, for advance information of his results.

Clarendon Laboratory,
Oxford.
8th December 1955.

J. M. Baker.
B. Bleaney.
P. M. Llewellyn.
P. F. D. Shaw.

Baker, J. M., Bleaney, B., Bowers, K. D., Shaw, P. F. D., and Trenam, R. S., 1953, *Proc. Phys. Soc.* A, **66**, 305.
Gallaher, L. J., Whittle, C., Beun, J. A., Diddens, A. N., Gorter, C. J., and Steenland, M. J., 1955, *Physica*, **21**, 117.

An Examination of Observed Regularities in Nuclear Energy Levels

Grant (1952) surveyed the known excitation energy levels of atomic nuclei, and concluded that they obeyed a simple numerical relation. If y denotes an observed energy level, Grant's hypothesis is that

$$y = 2r\delta + \epsilon$$

where r is a positive integer, 2δ the basic energy level or quantum appropriate to the nucleus observed and ϵ the error of observation. The value of the quantum 2δ was deduced from examination of the available measurements.

Whether Grant's data are strong evidence in favour of his hypothesis or whether the data are consistent with some other distribution of energy levels are questions which require statistical examination. Grant himself concluded that if his observations had been randomly distributed the probability of his observed integral sequences was approximately 10^{-30}. The calculation of this figure does not appear to take into account the fact that Grant chose the various quanta 2δ after inspecting the data. In other words the data used to test the hypothesis had also suggested the constants asserted in the hypothesis. A simple analogy will help to make the position clear. I toss an unbiased coin 100

times and observe the sequence say HHT . . . I then calculate the *a priori* probability of obtaining just the sequence HHT . . . and find it is 2^{-100} (which approximately equals 10^{-30}). I cannot then assert the coin is biased in some way because it has just produced a sequence which is *a priori* so very unlikely.

Suppose we wish to test whether data support a quantum hypothesis and the quantum proposed in the hypothesis has been deduced from the data to be used in the test. Then we must compare the agreement between data and hypothesis with the agreement between observations drawn from some other distribution (such as the rectangular distribution) and a quantum law chosen after examining these observations. It is only this comparison which can assure us that, for example, a rectangular parent distribution is not as reasonable as a quantum law.

In some experiments recently completed at the National Physical Laboratory samples were drawn from rectangular distributions and then 'quanta' were fitted to the observations. For example the following sample of 20 observations was obtained, and is compared with integer multiples of 0·02497 :

Exp.	0·025	0·048	0·054	0·108	0·177	0·178	0·205	0·268	0·321	0·356
Calc.	0·025	0·050	0·050	0·100	0·175	0·175	0·200	0·275	0·325	0·350
Exp.	0·402	0·458	0·673	0·690	0·747	0·776	0·996	0·998	1·000	1·000
Calc.	0·400	0·449	0·674	0·699	0·749	0·774	0·999	0·999	0·999	0·999

The agreement appears good but is of course entirely spurious.

These sampling experiments suggest that the agreement which Grant obtained between experimental and calculated values can equally well be explained by the hypothesis that nuclear energy levels are randomly distributed. Further, the discrepancy between Grant's calculated values and those observed is frequently greater than the experimental accuracy reported. These conclusions do not of course disprove the hypothesis proposed; they are merely a warning that a simpler explanation is possible.

A general examination of quantum hypotheses has appeared in *Biometrika* (Broadbent 1955) and in the same journal the National Physical Laboratory sampling experiments and a detailed study of Grant's data are to be reported.

British Coal Utilisation Research Association,
Leatherhead.
18th October 1955.

S. R. Broadbent†.

Grant, P. J., 1952, *Proc. Phys. Soc.*, **65**, 150.
Broadbent, S. R., 1955, *Biometrika*, **42**, 45.

† Now at United Glass Bottle Manufacturers Ltd., London, W.C.2.

On a Supposed Predissociation in the Spectrum of AlO

The best-known feature in the spectrum of AlO is a band system in the visible region which arises from a $^2\Sigma$–$^2\Sigma$ transition. Rotational analyses of some bands of this system have been carried out by Pomeroy (1927) and by Sen (1937). Dehalu (1937) extended the analysis of the 0, 0 band to higher rotational quantum numbers, and reported anomalous intensities in lines of the P-branch. She found that although the intensities of the P lines were normal as far as P(128), at higher K-values the P lines appeared to be unexpectedly weak. This observation was supported by the reproduction of a microphotometer trace. The effect was believed to arise from a predissociation.

In later work, Rosen (1944, 1945, 1946) maintained the view that the lower $^2\Sigma$ state is predissociated. From the variation of apparent intensity in the spectrum, without rotational analysis, he concluded that the predissociation starts at $K=60$ in $v''=6$, at $K=44$ in $v''=7$ and at $K=18$ in $v''=8$: bands with $v''\geqslant 9$ were said to be absent. He considered that the apparent predissociation at $K=129$ in $v''=0$ probably belongs to the same limiting curve of predissociation.

It is, however, only possible to decide with certainty if the lower state of AlO is predissociated or not by carrying out a rotational analysis. We have, to this end, photographed the spectrum in a Bausch and Lomb plane grating (dispersion about 3·3 mm Å^{-1}, resolving power ~300 000) and a Wood concave grating (dispersion about 0·8 mm Å^{-1}, resolving power ~100 000).

Examination of the 0, 0 band shows that there is no predissociation here. We have studied the variation of intensity among the P lines. The temperature of the aluminium arc was estimated to be 4000°K, using the method of Knauss and McCay (1937). This value agrees well with those of Brinkman (1937) and of Coheur and Coheur (1946). Microphotometric measurements of the relative intensities of the P lines are in complete harmony with a Boltzmann distribution for an equilibrium temperature of 4000°K.

If however, microphotometer traces are taken with a wide slit of the spectra photographed with the lower resolution instrument, we obtain results which approach those of Dehalu (see figure). We conclude that the supposed

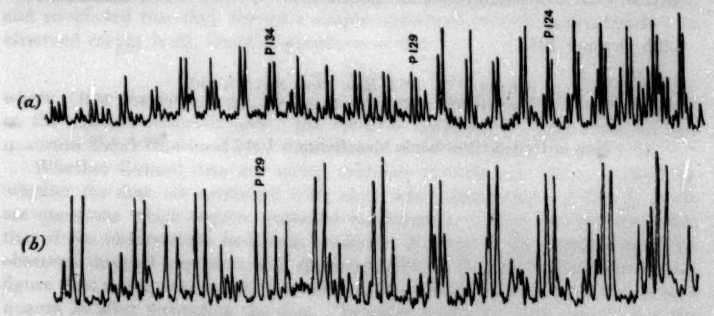

Reproductions of microphotometer traces of part of the 0, 0 band of AlO
(*a*) from concave grating (resolving power ~ 100 000)
(*b*) from echelle grating (resolving power ~ 300 000).

predissociation is in fact an instrumental effect arising from the use of inadequate resolving power.

There is thus no evidence that the 0, 0 band is predissociated. It may well be that the other predissociations reported by Rosen in $v''=6$, 7, 8 and 9 are equally illusory. We shall return to a study of this point later.

† Physics Department,
University of Stockholm.
‡ Physical Chemistry Laboratory,
University of Oxford.

† A. Lagerqvist.
† N. E. Lennart Nilsson.
‡ R. F. Barrow

13th January 1956.

Brinkman, H., 1937, *Thesis*, University of Utrecht.
Coheur, F. P., and Coheur, P. M., 1946, *Phys. Rev.*, **69**, 240.
Dehalu, F. P., 1937, *Bull. Acad. Belg. Cl. Sci.*, **23**, 604.
Knauss, H. P., and McCay, M. S., 1937, *Phys. Rev.*, **52**, 1143.
Pomeroy, W. C., 1927, *Phys. Rev.*, **29**, 59.
Rosen, B., 1944, *Bull. Soc. Sci. Liége*, **13**, 176; 1945, *Phys. Rev.*, **68**, 124; 1946, *Physica*, **12**, 184.
Sen, M. K., 1937, *Indian J. Phys.*, **11**, 251.

REVIEWS OF BOOKS

Mesons and Fields, Vol. II, *Mesons*, by H. A. BETHE and F. DE HOFFMANN. Pp. xiii + 446. (Evanston, Ill.: Row, Peterson & Co., 1955.) 65*s*.

The two volumes of this book have been eagerly awaited by nuclear physicists, whose appetities have been sharpened by frequent references in the current literature to pre-publication texts. The first volume, which is not yet available here, deals with field theory. The second volume, now published, is primarily concerned with the survey and analysis of the present experimental situation in 'low energy' pion physics. As such it is particularly well timed, for the last year or so has seen the completion of a preliminary experimental survey of nearly the whole field. Experimental data are now available on most of the possible processes involving pions, nucleons, and γ-rays at energies up to about 400 MeV. Most of this work is not very precise, but nearly all the data can be collated, with a minimum of arbitrary constants, by a simple phenomenological theory based on charge independence, and to a lesser extent on the dominance of the $P_{3/2}$, $T=\frac{3}{2}$ state of the pion–nucleon interaction.

In this book the experimental data are collected carefully, systematically and thoroughly. The phenomenological interpretation provided is sometimes of the same standard, but there are some uneven patches. For example, the deduction of zero spin for the neutral pion from the existence of the $\pi_0 \rightarrow 2\gamma$ process is set out clearly and at length, but the short argument which leads to zero spin for the charged pions is not given in detail. The chapter on production of pions in nucleon–nucleon collisions is excellent, whereas the various photoproduction cross sections are not so well discussed. Possibly this uneven quality of presentation arises from last minute revisions, which have certainly resulted in the inclusion of nearly all the information available.

As might be expected from these authors, the physics is rarely at fault. One of the few criticisms is that too much weight is put on the use of pion mesic atom spectral shifts to derive the difference between the $T=\frac{1}{2}$ and $T=\frac{3}{2}$ S wave phase-shifts in pion–nucleon scattering. It seems very dubious to assume that the effects of the several protons and neutrons in the nucleus are merely additive, especially since the analysis of nuclear emulsion stars seems to show a strong interaction between pions and pairs of nucleons in the nucleus.

On the other hand, the authors have little experimental evidence to go on when they argue against the existence of D wave interaction in pion–nucleon scattering up to 200 MeV, and very recent experimental results seem to be showing that they are quite right.

The properties of pions, and related topics such as nuclear forces, are also discussed in terms of field theory. The discussion assumes a knowledge of basic field theory, for example of the technique of second quantization, which is usually lacking in experimental physicists in this country. There is not very much provided here to help readers of this kind, and it is to be hoped that Volume I of the set will put this right. A clear explanation of the ground work would make this part of Volume II very valuable to experimenters. Fermi, in his well-known short book on elementary particles, showed how much can be done quite simply to convey to the non-specialist reader the spirit of field theory calculations.

The book is completed by chapters on very high energy collisions, on muon physics, admittedly very briefly surveyed, and on the more recently discovered heavy mesons and hyperons. This last field is still rapidly expanding and a survey in book form is necessarily obsolescent almost as soon as published. However, the authors make the point that these particles probably have little relevance to the problem of nuclear forces because their Compton wavelengths are shorter than the radius of the very short range repulsive core in the nucleon–nucleon interaction. Such a core is predicted by the strong-coupling field theory of pions, and has probably been observed in high energy nucleon–nucleon scattering.

The book is attractively printed and produced, and the price is not unreasonably high in these inflated days. It is as up to date as a book can possibly be, and no meson physicist should be without his own copy. J. M. CASSELS.

Molecular Beams, by K. F. SMITH. Pp. x + 133. (London : Methuen's Monographs on Physical Subjects.) 8*s*. 6*d*.

Dr. Smith's monograph replaces the earlier volume in this series by Dr. Fraser, published in 1937. Few subjects can have developed so rapidly in the interval. The introduction of radio-frequency resonance methods, by which very small multiplet intervals are measured directly, has transformed the technique, and has enabled measurements of nuclear magnetic moments to be made with an extraordinary precision.

The book covers a very wide field of work, from the use of molecular beams as sources for optical spectroscopy to the most refined of the resonance experiments. The author is to be congratulated on dealing with all this material without losing touch with the needs of students, for whom this series is primarily intended. The long section on magnetic deflection, with its detailed consideration of effective magnetic moments in low and high fields, is especially useful in clearing up many points that students find difficult. The book is well produced, and with 133 pages, including 37 figures and 12 tables, is commendably cheap.

A. H. COOKE.

Foundations of Quantum Theory, by A. LANDÉ. Pp. viii + 106. (New Haven : Yale University Press; London : Cumberlege, 1955.) 32*s*.

The purpose of this book is to deduce the basic principles and laws of quantum mechanics from classical thermodynamics. The author dislikes the usual approach to quantum theory based on experiments with atoms, electrons and photons ; he prefers to use what he calls the fundamental axiom of entropy continuity. This axiom is put forward to avoid a paradox, due to Gibbs, which appears in discussing the entropy of mixing of two gases. Suppose a vessel is divided into two equal parts by a wall, one part containing n mols of a perfect gas A and the other containing n mols of a perfect gas B. On removing the wall the gases diffuse, and if the diffusion is isothermal the work done by the gases is $2nRT \log 2$; the molecules of A have to be different, or in a different state, from those of B. If A and B are identical there is no work done, and no entropy change. Dr. Landé states the paradox in the form that if the molecules of A and B are spheres of radii a and b respectively, there is a change of entropy on mixing which is independent of the size of $a-b$ provided $a \neq b$; when $a = b$ there is no

change of entropy. The author suggests that the entropy discontinuity is the result of applying the narrow alternative ' either like or unlike ' to states of a gas, and he proposes to make the entropy change continuous by making it a continuous function of the ' degree of likeness ' between the two states A and B of the gas. The ' degree of likeness ' is defined to be the fraction of the number of molecules in state B which passes through a filter designed to select state A; this connects the degrees of likeness to the coefficients of the superposition relation which, for example, express a photon state of arbitrary polarization in terms of states with polarization in two given orthogonal directions. Arguments along these lines are used to set up what is in effect a complete set of commuting dynamical variables for a physical system, and the author claims that the requirement of entropy continuity also leads to the indistinguishability of individual particles. $\hbar$ has to be introduced by assuming the usual commutation rule for coordinate and momentum.

The reviewer prefers to base quantum theory on inferences from atomic phenomena rather than inferences from macroscopic phenomena. The closer the region of usefulness of the theory to the phenomena on which the theory is based, the less likely are we to make mistakes in our derivation of the theory. It is also difficult to see why the concepts of classical mechanics and classical thermodynamics are regarded as being fundamentally easier to understand than those of quantum mechanics.

The Gibbs paradox is very much a product of classical concepts. No one could have invented the paradox once it was realized that atoms and molecules have discrete, rather than continuously varying, properties. If we do not have continuously varying properties, then there is no paradox to be explained away, and it is hard to see why thermodynamics suggests that ' either like or unlike ' must be replaced by ' degrees of likeness '. J. HAMILTON.

Classical Electricity and Magnetism, by W. K. H. PANOFSKY and M. PHILLIPS. Pp. xi + 400. (Cambridge Mass. : Addison-Wesley, 1955.) $8.50

The student of electromagnetism has at his disposal textbooks of rare excellence : Becker's revision of the old classic ' Abraham–Föppl ', Sommerfeld's inspiring lectures and, in a more formalistic vein, the recent treatise by Landau and Lifshitz. In a domain so thoroughly and authoritatively worked out it would be hard to innovate. Indeed, one wonders whether there is any real need for yet another textbook of comparable scope.

The book under review appears to respond to some specific requirement of the American University curriculum, and makes no ambitious claims to originality. It follows in an eclectic way the well-established lines, with judicious emphasis on the more modern aspects. Besides the fundamental laws comprehended in Maxwell's equations, it covers the special theory of relativity, the theory of waveguides, the radiation field of accelerated charges, the elementary theory of scattering and dispersion, and the treatment of electromagnetic interactions from the Hamiltonian point of view. It thus brings together in a clear, logical disposition a most felicitous selection of topics, which is perhaps not found so nicely balanced in the other treatises. An excellent feature is the list, at the end of each chapter, of books recommended for further reading, with brief indications of what is to be looked for in them. The examples are made interesting by being often taken from 'actual life', i.e. from problems met with in the discussion of experiments in atomic and nuclear physics.

The treatment is throughout clear and concise, but surprisingly abstract, in the sense that the physical aspect of the problems is only just evoked in laconic sentences rather than properly explained.† It seems that the authors have in mind an audience who has already been taught the basic facts without mathematics, and has only to be shown how to translate them into the mathematical language. From the latter point of view, they again presuppose a rather solid knowledge of vector analysis in the Gibbsian notation, which is used from the beginning without explanation. The book is therefore not self-contained, but for the student who has the required physical and mathematical preparation, it may be recommended as a reliable and practical introduction. It has good diagrams and the printing of text and formulae is of exquisite neatness.

L. ROSENFELD.

Multipole Fields, by M. E. ROSE. Wiley's Structure of Matter Series. Pp. viii + 99. (New York: John Wiley; London: Chapman and Hall, 1955.) 40*s*.

This useful little monograph sets out in an elegant manner the angular momentum and parity properties of the electromagnetic field, applying to their discussion some of the recent developments in the algebra of irreducible tensors. After setting out Maxwell's equations of the electromagnetic field in a time-independent form and discussing the properties of angular momentum operators, the author goes on to construct the potentials of a 2^L pole field in terms of irreducible tensors of rank L and to a study of the properties of these multipole fields.

The final two chapters discuss the application of the theory to the problems of the emission of gamma radiation from nuclei and to its internal conversion.

The presentation is lucid, unnecessary formalism is avoided and very little previous knowledge of group theory is assumed. The book will be found to fill a very real need of those interested in questions of the emission and absorption of electromagnetic radiation, beta decay, angular correlations of nuclear radiations and similar fields.

E. H. S. BURHOP.

Introduction to Stochastic Processes, with special reference to Methods and Applications, by M. S. BARTLETT. Pp. xiv + 312. (Cambridge: University Press, 1955.) 35*s*.

This book is intended for 'applied mathematicians' and statisticians. However, it can be recommended to engineers and physicists interested in fluctuations, communication theory, or one of the many other processes changing with time and containing a random element which, in turn, influences what happens next. (This is a rough definition of a stochastic process.) For the mathematics is presented as a tool for solving problems. This is in contrast to much published work on stochastic processes by mathematicians for mathematicians—only. There is a similar contrast in papers on quantum theory, as many physicists know to their cost.

† For some reason, the authors make an exception in favour of Michelson's experiment, of which they give a detailed and interesting account.

Until recently theoretical physicists have been more active in advancing fluctuation theory than statisticians, but neither group can escape the many formulae. The reader who knows some statistics (and not statistical mechanics only) may then vaguely feel that he has seen some of them before, with different notation, and that it could all be simplified. Has it been mentioned anywhere, for example, after nearly 30 years, that the uncertainty principle is about the product of two standard deviations? Of course it is not as simple as this and more than notation is involved. In the older problems the number of independent units varying at random is so large that the probability arguments are simple and besides this it can often be assumed that the process is continuous. The statistician can hardly ever do this. So although he can learn from the physicist it is not surprising that he should have developed different methods. Professor Bartlett is a leading mathematical statistician and those he gives, including some of his own, succeed where older methods would fail. He describes his exposition as (relatively) elementary; in fact the mathematics is about as advanced and difficult as in, say, Mott and Sneddon's *Wave Mechanics:* it does not go beyond Laplace transforms or matrices.

Choosing which parts of the subject to include must have been difficult. About two thirds of them come under probability theory and the rest can be classed as statistics. These proportions are more nearly reversed in almost every other recent book by a statistician, and this shows how new the subject is. The statistical sections outline modern methods of estimation, inference and goodness of fit tests, and then deal with autoregressive series and periodogram analysis. The new techniques often succeed in describing a time series simply when this looks as if it has cycles, better than by Fourier analysis which may be wholly misleading in geophysics and in economics. Probability problems considered are the random walk, Markoff chains and continuous processes. Two more general chapters on limiting stochastic operations and stationary processes are followed by an introduction to prediction and communication theory.

Applications discussed include turbulence, queues, growth of bacteria, epidemics, and first passage times. The random walk of a point in a sampling inspection diagram is omitted, since sequential analysis is becoming a subject on its own with an extensive literature. Chemical reactions, the growth of polymers, co-operative phenomena and order–disorder are not mentioned in either the text or the reference list, nor are some recent papers on Brownian motion. This list may have been confined as far as possible to papers illustrating modern statistical methods, but it still gives nearly 300 titles. Professor Bartlett also points out that a systematic discussion of stochastic processes in physics would require another volume, which he hopes J. E. Moyal will write.

Even without this discussion the book contains a great deal for its size and price. The prose style is often condensed and some passages contain too many abstract nouns and too many afterthoughts to make pleasurable reading. Improving all these might lengthen the book. As it is, much of it seems more like notes. But if so these notes are excellently arranged, co-ordinated and indexed. In short this is a good book for anyone with problems to solve in this wide field of research.

M. E. WISE.

Nuclear Physics, by I. KAPLAN. Pp. xi + 609. (Cambridge, Mass.: Addison-Wesley Publishing Co., 1955.) $10.00

The author of this book sets out as his aim, in the preface, to provide a book that will be useful " in an advanced undergraduate course in nuclear physics, to engineers interested in the large-scale applications of nuclear physics . . . and anyone else with the indicated preparation who might be interested in nuclear physics ". In this preparation " the reader is assumed to have had no previous exposure to atomic and nuclear physics ".

In order to fulfil this aim, Dr. Kaplan devotes the first quarter of the book to a rapid survey of atomic physics which includes chapters on the electron, quantum theory, and the special theory of relativity, as well as those dealing with atomic structure and spectra. Naturally such a treatment has to be greatly compressed, and it is, to the reviewer, doubtful whether they are sufficiently thorough to provide an adequate basis for the extensive account of nuclear physics which comprises the remainder of the book.

The chapters on nuclear physics cover such topics as isotopes, α- and β-radioactivity, γ-radiation, nuclear reactions, nuclear forces and structure, fission, reactors and accelerators. The treatment is mainly descriptive, but the author has made a definite attempt to indicate " the physical ideas contained in the results " of quantum-mechanical theories even though the theories are beyond the scope of the book. It is hard to believe that the meaning of these physical ideas will always be intelligible to a reader who has met atomic physics for the first time in the first part of the book. The steps from, say, Avogadro's number to the theory of β-decay are far too many and substantial to be covered in 250 pages of even the most lucid exposition, and the student who meets the term 'matrix-element' for the first time in the theory of β-decay will, surely, not derive much enlightenment from it. The attempt to provide an elementary treatment of nuclear physics which goes beyond a recital of facts or description of experimental methods is surely to be encouraged, but to do so successfully in a book of reasonable size (and price) must assume at the outset a more thorough preparation of the background physics. There are many excellent textbooks that already cover the material in the first part of Dr. Kaplan's book, and had this been omitted more space could have been devoted to the overcompressed elementary interpretations of the nuclear phenomena described.

Most of the chapters are followed by a collection of elementary problems and a large collection of references. The latter include textbooks, review articles, original papers of historical interest, and other papers containing detailed accounts of theory and experiment. Again it is hard to believe that many of the detailed references would be suitable for the reader of this book. The gap between them and the elementary standard of the book is far too great.

The choice and arrangement of subject matter may reflect the style of undergraduate teaching in the United States, which differs, no doubt, from the general pattern in this country. For undergraduates here, the value of the book would be enhanced if the author had taken more for granted from the reader at the beginning and less towards the end.

S. DEVONS.

CONTENTS OF SECTION B

PAGE

Prof. J. Reekie and Dr. Y. L. Yao. Magnetic Anisotropy and Cold Worked Texture of Titanium 417

Dr. R. C. Newman. The Lattice Spacings of Thin Electrodeposits of Cobalt and Nickel on a Copper Single Crystal 432

Mr. F. J. Bradshaw and Mr. S. Pearson. The Electrical Resistivity of Sodium between 78°K and 372°K 441

Mr. R. Englman and Dr. E. H. Sondheimer. The Electrical Conductivity of Anisotropic Thin Films 449

Mr. N. Louat. The Effect of Temperature on Cottrell Atmospheres . . 459

Dr. R. J. Bickerton and Dr. A. von Engel. The Positive Column in a Longitudinal Magnetic Field 468

Research Notes:

Dr. J. A. Rayne. Heat Capacity of Silver below 4·2°K 482

Mr. D. [illegible] Bradley, Dr. J. S. Halliday and Dr. W. Hirst. Stereoscopic Reflection Electron Microscopy 484

Letters to the Editor:

Prof. C. Domb and Mr. M. F. Sykes. On High Temperature Expansions in the Heisenberg Theory of Ferromagnetism 486

Mr. J. D. [illegible]ixon and Dr. P. C. Banbury. Time Dependent Changes of Surface Lifetime in Germanium in the presence of Electric Fields . 487

Dr. A. F. Gibson. The Absorption of 39 kMc/s (39 Gc/s) Radiation in Germanium 488

Dr. R. Stratton. The effect of Field Emission on the Behaviour of Semiconductor Contacts 491

Reviews of Books 493

Contents of Section A 496

Calculations with the Optical Model of the Nucleus

By C. B. O. MOHR and B. A. ROBSON
Physics Department, University of Melbourne

Communicated by L. H. Martin ; MS. received 5th December 1955

Abstract. The optical model of the nucleus has been used with the phase shift method to calculate the scattering of 340 MeV neutrons and protons in carbon and lead, and of 4, 14, 36 and 100 MeV neutrons in nitrogen, for different forms of potential well and with different amounts of nuclear absorption. The results are used to establish the range of validity of the approximations of Born, of Montroll and Greenberg, and of Fernbach, Serber and Taylor. The latter gives remarkably accurate values over a wide energy range for the total elastic and absorption cross sections and forward elastic scattering. It is the only approximation which gives a satisfactory account of the effect of absorption. Unfortunately it does not give the angular distribution simply, and the most accurate approximation which does so, that of Montroll and Greenberg, has a very limited range of validity. Comparison with the experimental angular distributions of 340 MeV protons in carbon and lead leads to limited conclusions about the nuclear potential. An approximate calculation of the angular distribution of the scattering of 22 MeV α-particles in silver and lead indicates that the optical model can account for the observed results in terms of a rounded-off potential well.

§ 1. Introduction

While the theory of the compound nucleus has been widely successful, there is evidence that a particle entering a nucleus does not always share its energy among the nucleons composing it. Studies of the form of the energy distributions of disintegration particles indicate that the incident particle interacts strongly with surface nucleons, and in stripping and pick-up reactions the interaction is with individual nucleons.

Particles may traverse a nucleus without losing energy to any of the component nucleons, and be observed as elastically scattered particles. Here the nucleus may be treated as a homogeneous sphere refracting the incident particle-wave; and the possibility of energy loss in the nucleus is taken into account by using a complex refractive index whose imaginary component corresponds to absorption. In terms of wave mechanical theory the nucleus is represented by a potential well with complex depth. Since experimental evidence indicates that the radius R of a nucleus is proportional to $A^{1/3}$, the nuclear density—and hence the real component of the well depth—is the same for all nuclei. In a more sophisticated theory of the nucleus, the real well depth will change with the incident energy (e.g. Brueckner 1955). The imaginary well depth depends on the absorption coefficient in nuclear matter, and varies with the energy of the incident particle, since the target area presented by the separate particles in the struck nucleus varies with energy.

This model has been used for a considerable number of calculations of elastic scattering by nuclei, mostly for energies below 30 MeV. While the general form of the angular distribution of the scattering is accounted for broadly by a rectangular potential well of radius proportional to $A^{1/3}$, a few attempts at more precise fitting of the experimental curves have required a potential well rounded off near the edge. However a calculation of the scattering of 340 MeV protons by light nuclei, based on the Born approximation, suggested an approximately exponential potential (Gatha *et al.* 1954).

It seemed of interest to examine this discrepancy and to extend the calculations for 340 MeV protons to heavy nuclei; also to consider the scattering of α-particles. Both these problems have been tackled (Izumo 1954, Kawaguchi *et al.* 1954) with the aid of the Montroll and Greenberg approximation, whose accuracy is at least open to doubt. Systematic calculations were therefore carried out with the phase shift method for neutrons and protons over a wide energy range, to test the accuracy of existing approximations as well as to gain information about nuclear potentials.

§ 2. Method of Calculation

For incident neutrons of velocity v, 2π times the wave number outside the nucleus is $k=\gamma mv/\hbar$, and inside $K=K_r+iK_i$ where

$$K^2=k^2+2\gamma m\hbar^{-2}V_0(r)(1+i\zeta), \quad \text{with} \quad \gamma=(1-v^2/c^2)^{-1/2},$$

$V_0(r)$ being the nuclear potential. The absorption coefficient in nuclear matter is $2K_i$. The differential cross section for elastic scattering $\sigma_{sc}(\theta)$, and the total cross sections for elastic scattering and absorption σ_{sc} and σ_{abs} respectively, are given by the usual expressions (Mott and Massey 1949 a) but with the relativistic mass γm, in terms of phase shifts which are now complex instead of real.

For a uniform nucleus, V_0 was taken constant for r less than $1{\cdot}45\times10^{-13}A^{1/3}$ cm, and the phase shifts were found by fitting the interior and exterior wave functions at the nuclear boundary. The radial wave functions involve Bessel functions of complex argument, which were calculated by expansion in a Taylor series of powers of K_iR.

For other forms of nuclear potential, the phase shifts were calculated at the lower energies by numerical integration of the radial wave equation; and at the higher energies by use of the WKB and Born approximations for the low and high order phases respectively, after the accuracy of these approximations had been tested for the case of the rectangular well. The Born phases for the rectangular well were obtained from the zero order phase by a recurrence relation, and for other forms of well by numerical integration using the extensive tables available of Bessel functions of large order (Harvard University 1951).

For charged particles, the potential outside the nucleus $V_c=Zze^2/r$, and inside $V=V_0+(3R^2-r^2)Zze^2/2R^3$ for a uniform nucleus. At high energies, the lower order phases κ_l due to V alone were obtained by the WKB Method, taking the difference of two integrands of the usual form containing $V+V_c$ and V_c respectively. The difference between corresponding phases for protons and neutrons, which is relatively small, was extrapolated to large l and added on to the Born phases for neutrons to give the higher order phases for protons. The

total phase shift η_l is then $\xi_l+\kappa_l$, where ξ_l is the phase shift produced by the Coulomb field alone, and $\sigma_{sc}(\theta)$ is then calculated in terms of the η_l and ξ_l (Mott and Massey 1949 b).

For charged particles of low energy, the tedious joining of wave functions of complex argument to Coulomb wave functions is necessary in general, but a simpler and reasonably accurate procedure was adopted for the calculations on 22 MEV α-particles on heavy nuclei. Here the strong Coulomb repulsion prevents the α-particles from penetrating far below the nuclear surface, so that the wave function is small where the nuclear potential becomes large (for a rounded-off potential well), and one may use the Born approximation for the phases κ_l without too great error. The required values of the Coulomb wave functions of large argument are given by asymptotic expressions (Biedenharn *et al.* 1955) for certain values of r, and were obtained for other values of r by numerical integration of the wave function inwards and outwards.

§ 3. Approximate Methods

The phase shift method is lengthy in application, especially at high energies and for large nuclei. It is therefore worth while determining the region of validity of the available approximate methods viz. the well-known Born approximation (Mott and Massey 1949 c), the variational method of Montroll and Greenberg (1952), and the semi-classical impact parameter method of Fernbach, Serber and Taylor (1949).

The FST method gives convenient closed formulae for σ_{sc}, σ_{abs} and $\sigma_{sc}(0)$; but $\sigma_{sc}(\theta)$ is approximated merely by replacing the numerical summation of the phase shift formula by a numerical integration, and using an approximate form of the WKB formula for the phase shifts, and the reduction of numerical work is not great. The Born and the MG approximations have the advantage of giving closed formulae for σ_{sc} and $\sigma_{sc}(\theta)$ when one of the usual analytic forms is adopted for $V(r)$, but they are incapable of giving a value for σ_{abs} in the optical model.

For charged particles the MG method may be used, but not the Born or FST unless the Coulomb scattering is small compared with the nuclear force scattering, as at high enough energies and sufficiently large angles.

The results given by the three approximations are easily shown to approach each other as the energy increases, provided there is no absorption. Each may therefore be expected to become inadequate below a certain energy depending on the size of the nucleus.

§ 4. Accuracy of the Approximations for σ_{sc}, $\sigma_{sc}(0)$ and σ_{abs} for Neutrons

The regions of applicability of these approximate methods and their accuracy in these regions are indicated by the table. Let us discuss first the case of no absorption (V real). Below 100 MEV in nitrogen the approximations become increasingly unsatisfactory. The Born approximation gives values many times too large, the FST a few times too small for $\sigma_{sc}(0)$ though less in error for σ_{sc}, while the MG method gives values correct to within a factor of 2. The disagreement is always greater for $\sigma_{sc}(0)$ than for σ_{sc}—the angular distribution is a more severe test of the theory than the integrated scattering. At 340 MEV the

Born approximation is still poor, particularly for the largest nucleus, and the FST is now best.

Neutron Cross Sections for a Rectangular Well

	E	V	σ_{sc} Exact	FST	MG	Born	$\sigma_{sc}(0)$ Exact	FST	MG	Born	σ_{abs} Exact	FST
C	340	35	0·43	0·38	0·41	0·51	6·1	4·6	8·1	9·0	0	0
		$35+7i$	0·36	0·34	0·43	0·53	5·1	4·5	8·4	9·4	0·113	0·123
		$35+\infty i$	—	0·35	∞	∞	—	5·1	∞	∞	—	0·35
		42	0·58	0·55	0·54	0·72	7·9	7·0	11·5	13·0	0	0
		$42+42i$	0·32	0·30	0·65	1·44	4·8	4·1	13·8	26·0	0·34	0·31
		$42+\infty i$	—	0·35	∞	∞	—	5·1	∞	∞	—	0·35
Pb	340	42	6·6	6·9	7·4	32	535	590	850	3530	0	0
		$42+8·4i$	4·0	4·0	7·8	33	382	406	900	3670	1·59	1·67
		$42+42i$	2·35	2·34	45	64	272	285	5120	7060	2·37	2·27
		$42+\infty i$	—	2·31	∞	∞	—	262	∞	∞	—	2·31
N	100	43	1·18	0·96	1·35	1·9	5·2	3·7	7·1	9·3	0	0
	36	43	1·69	1·16	1·18	5·4	3·1	1·5	4·2	8·3	0	0
	14	43	1·41	0·87	1·03	14·0	1·59	0·34	1·77	7·9	0	0
	4	43	0·93	0·57	0·60	49	0·21	0·041	0·48	7·7	0	0

Comparison of values of σ_{sc} and σ_{abs} the elastic scattering and absorption cross sections, and $\sigma_{sc}(0)$ the forward scattering cross section, as given by the exact phase shift calculation, and by the approximations of Fernbach, Serber and Taylor, of Montroll and Greenberg, and of Born. E is the energy of the incident neutrons in MEV and V the depth of the potential well in MEV. The cross sections are in barns. The radius of the well $R=1·45A^{1/3}\times10^{-13}$ cm.

With increasing absorption (increasing V_i) the FST values decrease by about the same amount as the 'exact' values, for the approximation includes a coefficient of absorption for the neutron waves. The MG and Born values, however, increase indefinitely with increasing V_i, for in both approximations the scattering is given by the square of the modulus of an integral containing $V=V_r+iV_i$; and this feature makes the methods completely unsatisfactory for dealing with the effect of absorption. Increasing absorption causes σ_{sc} to decrease and σ_{abs} to increase asymptotically towards the same ultimate value of πR^2, the geometrical cross section.

§ 5. Accuracy of the Approximations for $\sigma_{sc}(\theta)$ for Neutrons

The FST method does not give a closed formula for $\sigma_{sc}(\theta)$, and the MG and Born approximations are unsatisfactory for complex V. Angular distributions given by these two approximations for real V are shown in figure 1 for neutrons in nitrogen. Comparing them with the curves obtained with the phase shift method, we see that both approximations are entirely unsatisfactory for energies as low as 4 MEV. At 14 MEV the MG approximation gives a reasonable fit, both for a rectangular potential well and for an exponential well; but the Born approximation is unsatisfactory even at 36 MEV.

At 340 MEV in carbon (figure 2) the approximations give much better predictions, though the logarithmic scale used in this figure greatly emphasizes differences near the low minimum which occurs for a rectangular well. The MG approximation is little improvement on the Born: both give curves of similar form, the main differences being in absolute magnitude and in the position of the minima. The fit of the Born curve is best for the most slowly varying potential.

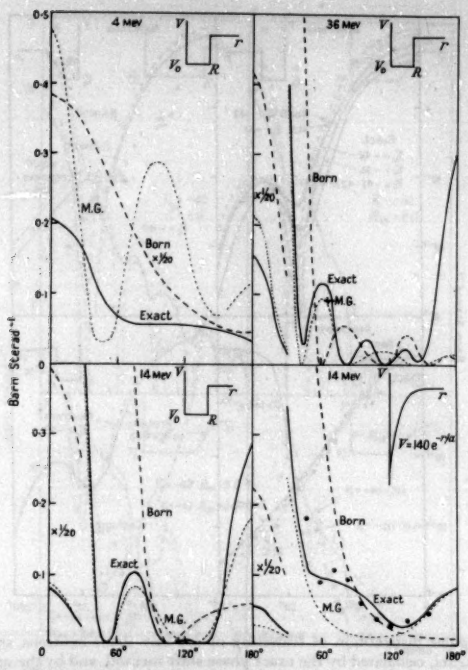

Figure 1. Angular distribution of scattering of 4, 14 and 36 Mev neutrons by nitrogen nuclei, calculated by the exact phase shift method, and by the approximations of Born, and Montroll and Greenberg. The inset diagrams show the form of nuclear potential used ($V_0 = -42$ Mev, $R = 3{\cdot}49 \times 10^{-13}$ cm, $a = 1{\cdot}16 \times 10^{-13}$ cm.) The points for 14 Mev neutrons are experimental values (relative magnitude only).

In the phase shift calculation for the rectangular well, the ratio of the scattered intensity at small angles for $V_0 = -42$ Mev to that for $V_0 = -35$ Mev is approximately proportional to the ratio of the squares of these well depths; in the MG and Born formulae the proportionality is exact. In the phase shift calculation, absorption reduces the scattering in approximately the same ratio at all angles of scattering.

For the larger nucleus, lead, at 340 Mev (figure 3) the Born approximation is less satisfactory, even for the rounded-off rectangular well. It may be more satisfactory for an exponential well, but one would not expect the interior of a large nucleus to depart so strongly from uniformity. The MG approximation gives more nearly correct values at the small angles which contribute most to σ_{sc}, but is little better than the Born approximation at larger angles. Rounding off the potential well produces a much greater reduction in the large angle scattering for lead than for carbon, though the thickness of the nuclear 'rim' is taken the same for both nuclei.

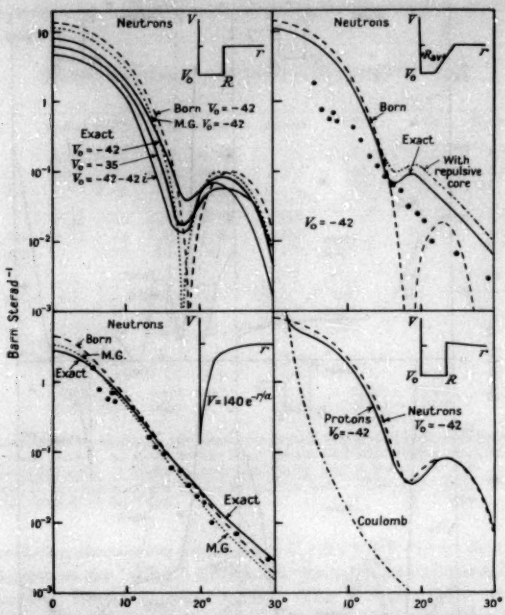

Figure 2. Angular distribution of scattering of 340 MeV (lab.) neutrons and protons by carbon nuclei, calculated by the exact phase shift method, and by the approximations of Born, and Montroll and Greenberg. The inset diagrams show the form of nuclear potential used. Well depths are in MeV. $R=R_{av}=3{\cdot}32\times10^{-13}$ cm, $a=1{\cdot}16\times10^{-13}$ cm.

§ 6. Comparison of $\sigma_{sc}(\theta)$ with Experiment for 340 MeV Protons

6.1. *Carbon*

For 340 MeV protons on carbon the nuclear force scattering greatly exceeds the Coulomb scattering beyond 5°, and then the scattered intensity is nearly the same as for neutrons (figure 2). We may therefore compare the experimental values of Richardson *et al.* (1952) for protons with the calculated values for neutrons. The experimental points show no sign of the convexity below 13°, terminating in a kink, which is present in the theoretical curve for a rounded-off well, but fit fairly satisfactorily the theoretical curve for a suitably chosen exponential well.

Other potentials than those shown in figure 2 were tried. A repulsive core of radius $0{\cdot}6\times10^{-13}$ cm was added to the rounded-off rectangular well to take account, in an *ad hoc* manner, of the repulsion between protons at small separations; for 340 MeV protons have a wavelength comparable with the dimensions of the individual nuclear protons, and can 'see' them as separate particles. This modification is seen to increase the scattering beyond 15°, but not to smooth

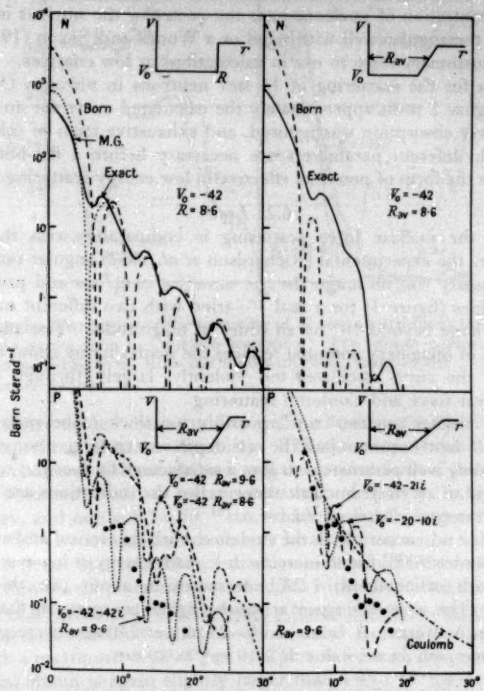

Figure 3. Angular distribution of scattering of 340 Mev neutrons (top two diagrams) and protons (bottom two diagrams) by lead nuclei, calculated by the exact phase shift method, and by the approximations of Born, and Montroll and Greenberg. The inset diagrams show the form of nuclear potential used. The well depths are in Mev, and radii in 10^{-13} cm. The points for protons are experimental values.

out the kink. A potential also tried was V constant out to $r = b$ and then falling exponentially, and this gave a curve without noticeable convexity only when b was appreciably less than the nuclear radius.

Spin–orbit coupling slightly reduces the depth of the minimum in the curve for a rounded-off potential well, and may smooth it out completely for a parabolic well (Sternheimer 1955), but it hardly affects the convexity at smaller angles. There seems to be no way of avoiding the conclusion that the well for carbon is approximately exponential.

A similar conclusion was previously arrived at by Gatha *et al.* (1954) using the Born approximation with a complex V. They obtained best fit with experiment for V equal to the sum of three gaussians, the resultant being approximately exponential in form. We note in this connection that the sensitivity of the angular distribution to the form of V is spuriously high in the Born approximation.

This concentration of nucleons near the centre of the nucleus is surprising, and in fact a rectangular well with a tail or a Woods and Saxon (1954) well has become the customary form to use in calculations at low energies. But experimental values for the scattering of 14 MeV neutrons in nitrogen (Smith 1954) are seen in figure 1 to fit approximately the calculated curve for an exponential well. However absorption was ignored, and exhaustive trials of other forms of potential with different parameters are necessary before a flat-bottomed well is ruled out as the form of potential effective in low energy scattering.

6.2. *Lead*

For lead the nuclear force scattering is comparable with the Coulomb scattering over the experimental (Richardson *et al.* 1952) angular range, and the scattered intensity will no longer be the same for neutrons and protons. The calculated values (figure 3) for a real V—tried with two different mean nuclear radii—is too large beyond 10° by an order of magnitude. The addition of an equal amount of imaginary potential reduces the scattering by about the required amount, but the curve oscillates too violently, largely through interference between nuclear force and Coulomb scattering.

A slightly thicker nuclear 'rim', possibly too thick to be realistic, and an imaginary well depth equal to half the real depth is seen to give somewhat better results. Finding well parameters to give a satisfactory fit does not seem feasible without the aid of an electronic calculator. But the indications are that a value of V_i of 20–40 MeV may be required.

Such a value is in accord with the evidence, both theoretical and experimental (Lane and Wandel 1955), for an increase in V_i with energy at low energies. The mean free path of nucleons, $1/2K_i$, decreases to about one third between 0 and 20 MeV, but increases again at much higher energies, so that it reaches a minimum in between. A value of $V_i = 25$ MeV at 340 MeV corresponds to the same mean free path as the value $V_i = 10$ MeV at 20 MeV.

§ 7. Comparison of $\sigma_{sc}(\theta)$ with Experiment for 22 MeV α-particles

Experiments on the scattering of 22 MeV α-particles in silver, gold and lead have recently been carried out by Wall *et al.* (1955). Using a simplified model of the nucleus, in which the first few order waves are assumed to be completely absorbed, they obtain reasonable agreement with experiment for lead, less satisfactory agreement for gold, and no agreement at all at large angles for silver (figure 4). Izumo (1954) has used the MG method to calculate the variation of scattering with energy at 60° and 95° for 20–40 MeV α-particles in gold. To agree with experiment he finds it necessary to use different values of V_i at the two angles. This inconsistency may arise from the inaccuracy of the MG method (see § 5) and its inadequacy in dealing with the effect of absorption (see § 4).

In using the optical model, the nuclear well depth for α-particles is uncertain: it will be greater than for protons, since the nuclear attraction acts on four times as many particles, but to take it four times greater may be unrealistic; for before the α-particle can reach the region of maximum V it may be broken up into its constituents. It has, in any case, a quite small probability of reaching this region in nuclei of high atomic number because of the strong Coulomb repulsion.

The perturbation method used to compute the phases (see § 2) gives values which, for a given form of potential, are proportional to its absolute magnitude.

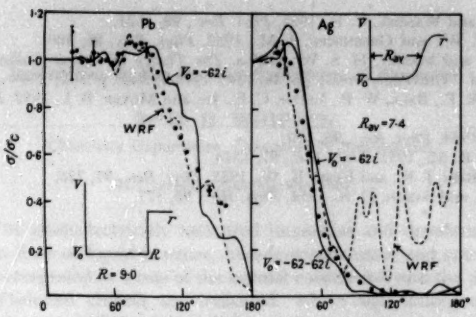

Figure 4. Angular distribution of the scattering of 22 MeV α-particles in lead and in silver, expressed as the ratio to Coulomb scattering. The broken curves are theoretical curves obtained by Wall, Rees and Ford with their 'fuzzy model'. The points are experimental values.

This circumstance made it easier to find well parameters giving an approximate fit with the experimental curves (figure 4). The case of lead was found not to be critical to the choice of well parameters, and the general form of the experimental curve was obtained with a rectangular well of purely imaginary depth $V_0 = -62i$ MeV, and radius $9{\cdot}1 \times 10^{-13}$ cm, which is slightly larger than the value of $1{\cdot}45 \times 10^{-13} A^{1/3}$ by an amount which may be attributed to the finite size of the α-particle. A better fit may be obtained with somewhat different well parameters; and a proportion of real potential may be added without spoiling the fit.

The case of silver was more critical, and a reasonable fit could not be obtained without using a rounded-off well. A Woods and Saxon (1954) potential was adopted, with a maximum depth V_0 of -62 MeV as for lead, and a mean radius of $7{\cdot}4 \times 10^{-13}$ cm, which is again slightly larger than $1{\cdot}45 \times 10^{-13} A^{1/3}$ cm. Most of the experimental points lie between the curves for $V_0 = -62i$ MeV and $V_0 = -62 - 62i$ MeV.

For neither lead nor silver could satisfactory results be obtained for $V_i < V_r$, and this implies a much smaller mean free path for α-particles in nuclear matter than for nucleons, as is to be expected, since the α-particle may break up before penetrating far into the nucleus. The implication that V_r is less than 62 MeV, say, may be avoided by using a larger value of V_r and a larger radius for the imaginary well than for the real well.

References

Biedenharn, L. C., Gluckstern, R. L., Hull, M. H. Jr., and Breit, G., 1955, *Phys. Rev.*, **97**, 542.

Brueckner, K. A., 1955, *Phys. Rev.*, **97**, 1353.

Fernbach, S., Serber, R., and Taylor, T. B., 1949, *Phys. Rev.*, **75**, 1352.

Gatha, K. M., Shah, G. Z., and Patel, N. J., 1954, *Proc. Phys. Soc.* A, **67**, 773.

Harvard University, 1951, *Annals of the Computation Laboratory* (Harvard: University Press).

Izumo, K., 1954, *Prog. Theor. Phys.*, **12**, 549.

Kawaguchi, O., Kaway, M., Nishida, Y., Sano, M., and Uji, H., 1954, *Prog. Theor. Phys.*, **12**, 99.

LANE, A. M., and WANDEL, C. F., 1955, *Phys. Rev.*, **98**, 1524.
MONTROLL, E. W., and GREENBERG, J. M., 1952, *Phys. Rev.*, **86**, 889.
MOTT, N. F., and MASSEY, H. S. W., 1949 a, *The Theory of Atomic Collisions*, 2nd Edn (Oxford : University Press), pp. 24, 134; 1949 b, *Ibid.*, p. 302; 1949 c, *Ibid.*, p. 183.
RICHARDSON, R. E., BALL, W. P., LEITH, C. E., Jr., and MOYER, B. J., 1952, *Phys. Rev.*, **86**, 29.
SMITH, J. R., 1954, *Phys. Rev.*, **95**, 730.
STERNHEIMER, R. M., 1955, *Phys. Rev.*, **97**, 1314.
WALL, N. S., REES, J. R., and FORD, K. W., 1955, *Phys. Rev.*, **97**, 726.
WOODS, R. D., and SAXON, D. S., 1954, *Phys. Rev.*, **95**, 577.

Intensities in the Raman Spectrum of Benzene

By D. H. WHIFFEN
Chemistry Department, University of Birmingham

MS. received 25th January 1956

Abstract. The photoelectrically measured intensities and depolarization ratios of the Raman lines of liquid benzene, hexadeuterobenzene and *sym.*-trideuterobenzene are interpreted in terms of the normal coordinates and the polarizability gradients. Preferred choices are indicated, where sign ambiguities lead to alternative solutions, and the polarizability gradients are:

$$\partial\alpha_{xx}/\partial S_1 = +6{\cdot}7A^2, \quad \partial\alpha_{zz}/\partial S_1 = +1{\cdot}9A^2, \quad \partial\alpha_{xx}/\partial S_2 = +4{\cdot}7A^2,$$
$$\partial\alpha_{zz}/\partial S_2 = +0{\cdot}3A^2, \quad \partial\alpha_{xx}/\partial S_{6a} = +1{\cdot}16A^2, \quad \partial\alpha_{xx}/\partial S_{7a} = +1{\cdot}17A^2,$$
$$\partial\alpha_{xx}/\partial S_{8a} = -1{\cdot}14A^2, \quad \partial\alpha_{xx}/\partial S_{9a} = +0{\cdot}25A^2, \quad \partial\alpha_{x^*z^*}/\partial\alpha_{10a} = +0{\cdot}050A^2.$$

Tables show the agreement between experiment and calculation. Bond polarizability gradients are deduced and the reasons for incomplete agreement are discussed.

§ 1. Introduction

In a recent paper, Allen and Bernstein (1955) have presented photoelectrically recorded values for the relative intensities of the Raman lines of liquid C_6H_6, C_6D_6 and *sym.*-$C_6H_3D_3$. They discussed the A_{1g} class intensities in terms of the normal coordinates of Lord and Teller (1937) and obtained partial agreement between observed and calculated intensities and depolarization ratios. More complete normal coordinates, including the E_{1g} and E_{2g} classes, are now known (Whiffen 1955, Kovner 1954) and the present contribution examines the interpretation of the experimental results of Allen and Bernstein using the coordinates of Whiffen (1955). The general treatment and the symbols follow this paper.

§ 2. E_{1g} Class

It is preferable to consider first the E_{1g} symmetry class since from it the scale factor may be determined and since the class contains only one frequency each for C_6H_6 and C_6D_6, and as a result there is no sign ambiguity of importance. The vibration involved is the degenerate Raman-active out-of-plane C–H deformation. Lord and Teller (1937) have pointed out that the rotation in this class affects the Raman intensities. The intensity S of the Raman line as defined by Allen and Bernstein (1955) is given by

$$S/2 = 7\nu K^2\gamma'^2 = 21\nu K^2\left[\frac{\partial\alpha_{x^*z^*}}{\partial S_{10a}}S_{10a}' + (\alpha_{zz}-\alpha_{xx})\omega_y\right]^2. \quad \ldots\ldots(1)$$

x^*, y^*, z^* are coordinates bound to the median carbon plane as defined earlier (Whiffen 1955), S_{10a}' is the derivative of the symmetry coordinate with respect to the normal coordinate and ω_y is the rotation in radians of the median plane in space. The factor ν appears by virtue of the normalization to $h\nu/2$, K is the scale constant which depends on the intensity of the CCl_4 (458 cm^{-1}) reference line,

and the expression is equated to $S/2$, rather than S, to allow for the two-fold degeneracy. The equilibrium molecular polarizabilities have been given by Stuart and Volkmann (1933) as $\alpha_{xx}=12{\cdot}31A^3$ and $\alpha_{zz}=6{\cdot}35A^3$. There remain two unknowns, K and $\partial\alpha_{x^0x^0}/\partial S_{10a}$, and these may be chosen to give the correct experimental values for both C_6H_6 and C_6D_6. The values required are $K=0{\cdot}0326\times10^{24}$ if ν is in cm^{-1}, and $\partial\alpha_{x^0x^0}/\partial S_{10a}=+0{\cdot}050A^2$. The positive sign of the latter quantity is opposite to that obtained previously (Whiffen 1955) with more approximate intensity measurements and the new sign agrees with the expectation that the C–H bonds should be more polarizable along their length than in the perpendicular direction. The intensities of the E″ class of *sym.*-$C_6H_3D_3$ may now be predicted and the agreement between experiment and calculation is given in table 1. Formally there is a second solution to the C_6H_6 and C_6D_6 intensity equations, but this predicts the 713 cm^{-1} shift of *sym.*-$C_6H_3D_3$ to be easily the weakest of the three E″ frequencies and the second solution is therefore quite unacceptable.

Table 1. Raman Line Intensities for the E_{1g} and Related Classes

	Observed		Calculated	
	ν	S	ν	S
C_6H_6 (E_{1g})	849	0·105	851	0·105
C_6D_6 (E_{1g})	661	0·204	661	0·204
$C_6H_3D_3$ (E″)	374	0·013	375	0·013
	710	0·101	713	0·131
	—	—	939	0·083

§ 3. A_{1g} Class

The totally symmetric class, A_{1g}, contains a C–C stretching motion described by the symmetry coordinate S_1 and a C–H stretching motion described by S_2. In this class the intensities and the depolarization ratios are related to the normal coordinates by

$$S=K^2\nu(45\bar{\alpha}'^2+7\gamma'^2) \qquad \ldots\ldots(2)$$

$$\rho=6\gamma'^2/(45\bar{\alpha}'^2+7\gamma'^2) \qquad \ldots\ldots(3)$$

$$9\bar{\alpha}'^2=\left[\left(2\frac{\partial\alpha_{xx}}{\partial S_1}+\frac{\partial\alpha_{zz}}{\partial S_1}\right)S_1'+\left(2\frac{\partial\alpha_{xx}}{\partial S_2}+\frac{\partial\alpha_{zz}}{\partial S_2}\right)S_2'\right]^2 \qquad \ldots\ldots(4)$$

$$\gamma'^2=\left[\left(\frac{\partial\alpha_{xx}}{\partial S_1}-\frac{\partial\alpha_{zz}}{\partial S_1}\right)S_1'+\left(\frac{\partial\alpha_{xx}}{\partial S_2}-\frac{\partial\alpha_{zz}}{\partial S_2}\right)S_2'\right]^2. \qquad \ldots\ldots(5)$$

In order to introduce the experimental values and solve for the four quantities in round brackets, it is necessary to know the signs of the square roots of both S and ρ for each of the two vibrations in the class. These are unknown, but by taking all permutations it would be possible to obtain four distinct solutions to fit the C_6H_6 results exactly: the observed and calculated intensities for C_6D_6 and *sym.*-$C_6H_3D_3$ would then be compared and the most satisfactory solution chosen, since the isotopic intensities give sufficient extra quantities, in principle, for selecting the relative signs. In practice, the experimental values and the normal coordinates are hardly accurate enough for this to be done. It therefore seemed preferable to spread the errors by calculating the polarizability derivatives to fit exactly the sums of $(S/\nu)^{1/2}$ and $\rho^{1/2}$ for the corresponding vibrations of

C_6H_6 and C_6D_6. The resulting agreement for the four distinct solutions is shown in table 2. It can be seen that solutions 2 and 3 give unsatisfactory depolarization ratios and that solutions 2 and 4 give unsatisfactory intensities and so solution 1 must be strongly preferred. This solution is

$$2\frac{\partial\alpha_{xx}}{\partial S_1}+\frac{\partial\alpha_{zz}}{\partial S_1}=\pm 15{\cdot}20A^2 \qquad 2\frac{\partial\alpha_{xx}}{\partial S_2}+\frac{\partial\alpha_{zz}}{\partial S_2}=\pm 9{\cdot}75A^2$$

$$\frac{\partial\alpha_{xx}}{\partial S_1}-\frac{\partial\alpha_{zz}}{\partial S_1}=\pm\ 4{\cdot}81A^2 \qquad \frac{\partial\alpha_{xx}}{\partial S_2}-\frac{\partial\alpha_{zz}}{\partial S_2}=\pm 4{\cdot}38A^2$$

where in each line the upper or the lower sign must be taken consistently.

Table 2. Raman Line Intensities and Depolarization Ratios for the A_{1g} and Related Classes

	Observed			Calculated							
				Solution 1			Solution 2		Solution 3		Solution 4	
	ν	S	ρ	ν	S	ρ	S	ρ	S	ρ	S	ρ
C_6H_6	992	4·406	0·11	992	4·19	0·11	4·64	0·10	4·29	0·13	4·74	0·12
(A_{1g})	3061	16·505	0·21	3073	17·80	0·20	13·80	0·26	16·91	0·17	12·90	0·22
C_6D_6	945	4·041	0·12	943	4·29	0·12	3·88	0·13	4·20	0·10	3·78	0·12
(A_{1g})	2292	7·702	0·21	2286	6·98	0·22	9·66	0·16	7·55	0·27	10·14	0·20
$C_6H_3D_3$	955	2·785	0·12	951	2·92	0·12						
(A_1')	1003	0·804	0·11	1004	1·34	0·11						
	2283	2·422	0·22	2285	3·44	0·22						
	3054	—	—	3070	8·89	0·20						
(A_1' +E')	3054	7·730	0·36		10·93	0·36						

The natures of the remaining sign choices are such that they cannot be determined by isotopic intensity measurements but they can be inferred in the following manner. S_1 corresponds to an expansion of the carbon skeleton and S_2 to the stretching of C–H bonds and, since polarizability normally increases with size, it is very probable that both $\partial\alpha_{xx}/\partial S_1$ and $\partial\alpha_{xx}/\partial S_2$ are positive. It is also probable that bond stretching changes the polarizability along the bond more than that in the perpendicular directions and so probably

$$\partial\alpha_{xx}/\partial S_1>|\partial\alpha_{zz}/\partial S_1| \quad \text{and} \quad \partial\alpha_{xx}/\partial S_2>|\partial\alpha_{zz}/\partial S_2|.$$

All these expectations are simultaneously true if positive signs are taken throughout, but the other sign arrangements lead to at least two false expectations. In the favoured case $\partial\alpha_{xx}/\partial S_1=+6{\cdot}7A^2$, $\partial\alpha_{zz}/\partial S_1=+1{\cdot}9A^2$, $\partial\alpha_{xx}/\partial S_2=+4{\cdot}7A^2$ and $\partial\alpha_{zz}/\partial S_2=+0{\cdot}3A^2$.

§ 4. E_{2g} Class

The symmetry coordinates of the E_{2g} class, S_6, S_7, S_8 and S_9, refer to the ring angle deformation, the C–H stretching, the C–C stretching, and the C–H in-plane deformation respectively and the additional subscript a indicates that component of the degenerate motions which is symmetrical with respect to the yz plane. For this class the intensity of the shifts is given by

$$S/2=7\nu K^2\gamma'^2=21\nu K^2\left(\frac{\partial\alpha_{xx}}{\partial S_{6a}}S_{6a}'+\frac{\partial\alpha_{xx}}{\partial S_{7a}}S_{7a}'+\frac{\partial\alpha_{xx}}{\partial S_{8a}}S_{8a}'+\frac{\partial\alpha_{xx}}{\partial S_{9a}}S_{9a}'\right)^2. \quad \ldots(6)$$

Again numerical values of the polarizability gradients have been taken to fit exactly the sum of $(S/\nu)^{1/2}$ for the corresponding vibrations of C_6H_6 and C_6D_6. There are eight distinct sign permutations and there is no solution which can unambiguously be stated to be the most satisfactory though solutions numbered 1, 3 and 8 were superior to the other five, and the intensities calculated with these solutions are indicated in table 3. At the foot of table 3 are given the corresponding polarizability gradients for which the upper or lower signs must be taken consistently in each column.

Table 3. Raman Line Intensities for the E_{2g} and Related Classes

	Observed			Calculated for Solution No.		
				1	3	8
	ν	S	ν	S	S	S
C_6H_6	606	0·181	610	0·21	0·20	0·14
(E_{2g})	1178	0·584	1179	0·45	0·58	0·62
	1584, 1606	1·084	1599	0·98	1·15	1·07
	3045	4·608	3044	4·76	3·66	5·12
C_6D_6	577	0·146	574	0·12	0·13	0·19
(E_{2g})	867	0·305	868	0·40	0·31	0·28
	1560	0·979	1545	1·09	0·92	0·99
	2264	2·470	2275	2·38	3·15	2·17
$C_6H_3D_3$	594	0·180	590	0·16	0·16	0·17
(E')	832	0·133	841	0·18	0·12	0·09
	1102	0·169	1087	0·29	0·24	0·28
	1396	0·049	1427	0·04	0·12	0·05
	1576	0·925	1574	1·11	1·03	1·13
	2273	0·523	2282	1·23	1·64	1·12
	3054	—	3062	2·34	2·04	2·51
$\partial\alpha_{xx}/\partial S_{6a}$ (units of A^2)				$\pm 0·71$	$\pm 1·16$	$\pm 0·26$
$\partial\alpha_{xx}/\partial S_{7a}$ (units of A^2)				$\pm 1·68$	$\pm 1·17$	$\mp 1·90$
$\partial\alpha_{xx}/\partial S_{8a}$ (units of A^2)				$\pm 1·59$	$\mp 1·14$	$\mp 0·05$
$\partial\alpha_{xx}/\partial S_{9a}$ (units of A^2)				$\pm 0·66$	$\pm 0·25$	$\mp 0·91$

Of these three solutions, 1 is not very satisfactory for the C_6H_6 shift at 1178 cm^{-1} or the C_6D_6 shift at 867 cm^{-1} and is especially poor for the ratio of these two intensities. Solution 3 is poor for the frequencies above 2000 cm^{-1} and solution 8 erroneously predicts the 606 cm^{-1} shift in C_6H_6 to be weaker than that at 577 cm^{-1} in C_6D_6. The author prefers solution 3. Firstly, because the frequencies above 2000 cm^{-1} are overlapped by the adjacent, stronger, A_{1g} lines and are consequently liable to greater experimental error. Secondly, the force field is less satisfactory for the hydrogen stretching frequencies and no interaction constants involving hydrogen stretching coordinates were included in the determination of the normal modes. And thirdly, if bond stretching increases the polarizability along the bond direction more than in the perpendicular direction, which is probable, then $\partial\alpha_{xx}/\partial S_{7a}$ ought to be positive and $\partial\alpha_{xx}/\partial S_{8a}$ ought to be negative: this is only true if solution 3 with the upper sign is adopted.

§ 5. Bond Polarization Derivatives

The polarizability derivatives in terms of the symmetry coordinates are difficult to visualize, and it may be clearer to evaluate bond polarizabilities and their derivatives (Long 1953), even though it is difficult to define a bond satisfactorily and to apportion the unshared electrons. For benzene the assumption

of cylindrical bond symmetry would not be valid and the bond polarizabilities are not determinable from the data available. But it is possible to compute the polarizability derivatives with respect to the stretching of individual bonds.

If r is the C–H bond length, the $\partial\alpha/\partial\Delta r$ are defined for the stretching motion in which only one H atom moves. If R is the C–C bond length then $\partial\alpha/\partial\Delta R$ will depend on the way in which the ring angles are allowed to readjust themselves. The equations below refer to the motion for which S_6 remains zero; this is necessarily true if the ring angles at C_1 and C_4 remain 120° when stretching of the bond C_2–C_3 is considered. If $\alpha_{\parallel}$ is written for the polarizability parallel to the bond which stretches, $\alpha_{\perp}$ for that perpendicular to the bond in the plane of the ring and α_z for the polarizability perpendicular to the ring, then for the C–C bonds

$$\frac{\partial\alpha_{\parallel}}{\partial\Delta R} = 6^{-1/2}\left(\frac{\partial\alpha_{xx}}{\partial S_1} - 2^{1/2}\frac{\partial\alpha_{xx}}{\partial S_{8a}}\right) = +3{\cdot}4A^2 \qquad \ldots\ldots(7)$$

$$\frac{\partial\alpha_{\perp}}{\partial\Delta R} = 6^{-1/2}\left(\frac{\partial\alpha_{xx}}{\partial S_1} + 2^{1/2}\frac{\partial\alpha_{xx}}{\partial S_{8a}}\right) = +2{\cdot}5A^2 \qquad \ldots\ldots(8)$$

$$\frac{\partial\alpha_z}{\partial\Delta R} = 6^{-1/2}\frac{\partial\alpha_{zz}}{\partial S_1} = +0{\cdot}8A^2 \qquad \ldots\ldots(9)$$

and for the C–H bonds

$$\frac{\partial\alpha_{\parallel}}{\partial\Delta r} = 6^{-1/2}\left(\frac{\partial\alpha_{xx}}{\partial S_2} + 2^{1/2}\frac{\partial\alpha_{xx}}{\partial S_{7a}}\right) = +2{\cdot}6A^2 \qquad \ldots\ldots(10)$$

$$\frac{\partial\alpha_{\perp}}{\partial\Delta r} = 6^{-1/2}\left(\frac{\partial\alpha_{xx}}{\partial S_2} - 2^{1/2}\frac{\partial\alpha_{xx}}{\partial S_{7a}}\right) = +1{\cdot}2A^2 \qquad \ldots\ldots(11)$$

$$\frac{\partial\alpha_z}{\partial\Delta r} = 6^{-1/2}\frac{\partial\alpha_{zz}}{\partial S_2} = +0{\cdot}1A^2. \qquad \ldots\ldots(12)$$

The most favoured solutions have been introduced to obtain the numerical values. It must be emphasized that the changes of α are strictly those of the whole molecular polarizability and it is uncertain to what extent the changes can be considered as localized in the bond whose length is varying, as implied by the term ' bond polarizability derivatives '.

§ 6. Discussion

The overall agreement between calculation and prediction in tables 1–3 is only moderate. The reasons for the discrepancies include

(i) Experimental errors. These are largest for the overlapping A_{1g} and E_{2g} C–H stretching modes. The agreement between the sum of the intensities for the two shifts is much better. For C_6H_6 near 3050 cm^{-1}, $S_{\text{total}} = 21{\cdot}113$ (observed) and 21·46 (calculated) and for C_6D_6 near 2280 cm^{-1}, $S_{\text{total}} = 10{\cdot}172$ (observed) and 10·13 (calculated). It may be that the intensity distribution between the two lines is in error in each case.

(ii) Errors in the normal coordinates arising from errors in the force field. If this were the only trouble the intensity sum rules would be valid and a better agreement than that of Allen and Bernstein (1955) would be expected.

(iii) Neglect of cubic and higher terms in the force field. This neglect means that Fermi resonance is neglected; its inclusion would be expected to vitiate the sum rules for fundamentals. With a near degeneracy, intensity may be

exchanged between a fundamental and an overtone Raman shift. There are many places, especially in *sym.*-$C_6H_3D_3$, where this may be occurring. In the absence of experimental knowledge of the overtone or combination tone intensities and in ignorance of the higher order force constants, a detailed discussion is not feasible.

In conclusion it may be said that there are many points where some doubt remains, but that the agreement is close enough to indicate that the chosen polarizability gradients are probably essentially correct.

References

Allen, G., and Bernstein, H. J., 1955, *Canad. J. Chem.*, **33,** 1137.
Kovner, M. A., 1954, *Dokl. Akad. Nauk SSSR.*, **97,** 65.
Long, D. A., 1953, *Proc. Roy. Soc.* A, **217,** 203.
Lord, R. C., and Teller, E., 1937, *J. Chem. Soc.*, 1728.
Stuart, H. A., and Volkmann, H., 1933, *Z. Phys.*, **80,** 107.
Whiffen, D. H., 1955, *Phil. Trans. Roy. Soc.* A, **248,** 131.

Elastic Scattering of Gamma Rays

By S. MESSELT and A. STORRUSTE
Department of Physics, University of Oslo, Blindern, Norway

Communicated by P. B. Moon ; MS. received 21st September 1955, and in revised form 24th January 1956

Abstract. When measuring elastic scattering of gamma rays, the secondary radiation from the scatterer, such as bremsstrahlung from photo- and Compton electrons and annihilation radiation, must be considered. It is shown that this secondary radiation is predominant in many experiments reported on elastic scattering of gamma rays.

A measurement of the large angle scattering of 1·33 MeV gamma rays by lead is described. It is found that the elastic scattering cross sections at 90° and 120° are, without corrections, $1{\cdot}7\times10^{-28}$ cm^2 sterad^{-1} and $1{\cdot}6\times10^{-28}$ cm^2 sterad^{-1} respectively.

The first result is already below the combined effect of Rayleigh and Thomson scattering as calculated by Bethe, and both must contain contributions from bremsstrahlung etc. that can be estimated only roughly but are appreciable. The present experiments therefore support the destructive interference of Delbrück scattering with the Rayleigh and Thomson components.

§ 1. Introduction

The development of scintillation counters has made it possible to measure the Rayleigh scattering of gamma rays with some confidence, at least for energies below 1 MeV (Moon 1950, Storruste 1950), but the Thomson scattering by the nuclear charge and the Delbrück scattering by virtual pair formation in the potential field of the nucleus remain to be experimentally proved. Since these processes are elastic and therefore inseparable by measurement of the energy of the scattered photons their disentanglement requires reliable theories and reliable measurements of intensities, angular distribution, variation with energy and atomic number, etc.

The main experimental difficulties result from hard rays created by secondary processes; they will be dealt with later in this paper.

Since the Rayleigh scattering is usually much larger than the others, it is important that it should be precisely calculated. The calculations of Franz (1935) are non-relativistic and based on the Thomas–Fermi approximation to the electron distribution in the atom. According to Wilson (1953), Bethe has made similar calculations, but using relativistic wave functions for the K-electrons. His calculations predict a lower cross section at large angles than the one obtained by the theory of Franz, and show that the scattering may be proportional to Z^8 or Z^{10} in the energy region of 1·3 MeV, while the theory of Franz predicts a Z^3 dependence. The calculation of the Thomson component is extremely simple.

An exact calculation of Delbrück scattering has been made only for zero angle of scatter by Rohrlich and Gluckstern (1952) who predict a value of $0{\cdot}6\times10^{-27}$ cm^2 sterad^{-1} for 1·33 MeV gamma rays scattered by lead. The cross

section is proportional to Z^4 and the scattering is mainly at small angles (Bethe and Rohrlich 1952). While Rayleigh and Thomson scattering should interfere constructively (Moon 1950) they should both interfere destructively with the Delbrück scattering.

§ 2. Previous Investigations

A thorough analysis of some ten papers dealing with the search for elastic scattering of energetic gamma rays has been made (Storruste 1951), the results stated by the authors being recalculated using the latest information regarding counter efficiencies etc. Some of the results are shown in table 1.

Table 1.

(1)	(2)	(3)	(4)	(5)
Meitner and Kösters (1933)	Thorium	3	90	90
Gray and Tarrant (1934)	Thorium	16	90–150	10
Ketelaar (1936)	Radium	7	120	10
Pollard and Alburger (1948)	^{24}Mg	4	135	9

(1) Author ; (2) source ; (3) thickness of lead filter (cm) ; (4) scattering angle (°) ; (5) ratio of experiment to theory.

The results indicate insufficient suppression of inelastic components, such as bremsstrahlung created by photo- and Compton electrons, hard annihilation radiations created by positrons in flight and, for relatively small angles, double Compton scattered rays.

The relative intensity of the disturbing components in the scattered radiation depends very much on the primary energies and on the atomic number of the atoms in the scatterer. Thus, for 0·41 Mev gamma rays scattered by lead at large angles, not more than 5% of the scattered radiation behind a filter of 10 g cm^{-2} is bremsstrahlung created by photoelectrons, the other processes being even less disturbing. Measurements of Rayleigh scattering can, therefore, be performed with comparative ease for gamma rays of this energy.

Much better energy discrimination can be obtained with a scintillation spectrometer and such measurements have now been reported in the energy region above 1 Mev, where Delbrück scattering might be expected to become prominent.

Wilson (1953) has measured elastic scattering by lead at various angles for 1·33 Mev and 2·6 Mev gamma rays, while Strickler (1953) has measured elastic scattering at 135° by lead, tin, copper and aluminium at an energy of 1·33 Mev. Davey (1953) has measured elastic scattering by lead for gamma rays at 1·33 Mev at scattering angles between 40° and 120°. Before discussing the various results obtained by this method, a similar experiment performed by the present authors is described in § 3.

§ 3. Elastic Scattering of 1·33 Mev Gamma Rays

The general arrangement of the apparatus is shown in the figure.

The whole apparatus was suspended by wires, first in the middle of a large room and later out of doors. The ^{60}Co source, having a strength of about 100 mc, was placed in a glass tube which could be drawn up to the ceiling or lowered to fit accurately into an outer glass tube fastened to the suspension system, the joint between the tubes being a ground cone. A cone of lead prevented the direct

beam from reaching the phosphor, the distance from the top of the cone to the phosphor being 25 cm. The scatterers were made of 0·25 cm thick sheets of lead formed into appropriate figures of revolution about the line joining the source and the phosphor, so as to give mean scattering angles of 90° and 120°. The weight of the scatterers was 4800 g and 8800 g respectively.

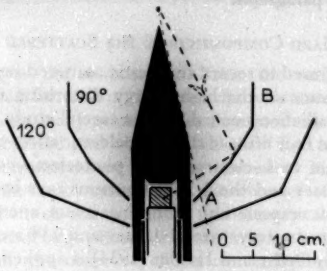

Diagram of the apparatus to measure the elastic scattering.

The scintillation spectrometer consisted of a NaI(T1) crystal, 1½ inches in diameter and height, mounted directly on an EMI 6260 photomultiplier tube in conjunction with a cathode follower. The detector was placed in a drilled hole 5·5 cm diameter in the middle of the lead cone. The lead around the phosphor, being 2 cm thick, served both as a light-tight box and as an energy filter preventing the Compton scattered rays and much of the low energy bremsstrahlung from reaching the counter.

The pulses were fed through an amplifier to a single channel sweep type discriminator. For 1·2 MeV gamma rays the ratio of half width to pulse height for the photo-peak was about 0·08 without lead around the phosphor. With the lead cone in place the ratio increased to about 0·12.

Before measuring the scattering, it was necessary to determine the pulse–height distribution using the direct radiation from a small ^{60}Co source. The bias and width of the channel were then set up to record rays in the energy intervals 0·95–1·10 MeV, 1·10–1·25 MeV and 1·25–1·40 MeV respectively. To eliminate fatigue effects, the observations were taken in the following sequence: (*a*) The source at a fixed large distance, (*b*) source in place but scatterer still removed, (*c*) scatterer in place, (*d*) scatterer removed and (*e*) source at the large distance. With this method it was not necessary to know the absolute strength of the source or the efficiency of the detector, because the scattering cross section could be calculated from the relative counting rates and the geometry of the arrangement. In order to find the numerical value of the cross section, the scatterer was divided into zones *ds* where *ds* is an element of the arc measured from A to B (see figure). Thus, a zone *ds* represents a ring. From the geometry of the arrangement the scattered intensity due to the ring could be found and corrected for absorption in the scatterer. The absorption in the lead around the phosphor of rays scattered by different rings *ds* varied with *s*, and had to be compared with the absorption of the primary rays from the source when placed at the fixed large distance. Corrections for this variation were measured directly with a small source placed at different angles with the line through the source and the phosphor.

After applying these corrections, the contributions from the zones *ds* could be integrated. In this way a relation between the scattering cross section and the counting rates was obtained.

The most difficult problem was to find corrections for the counting rates due to the disturbing components in the scattered radiation. These difficulties are discussed in the next paragraph.

§ 4. The Hard Components in the Scattered Radiation

At the bias setting used to record the elastic scattered rays, there was a certain chance of counting some of the high energy disturbing radiation. Therefore the intensity of this radiation needed a more careful study.

If it is assumed that four fifths of the photoelectric effect was due to K-electrons and one fifth was due to L-electrons, the photoelectrons created in the lead scatterer by the 1·33 MeV and the 1·17 MeV gamma rays had average energies of 1·26 MeV and 1·10 MeV respectively. The maximum energ. f the Compton electrons created by the two rays were 1·12 MeV and 0·96 MeV. Usually the Born approximation used by I e and Heitler (1934) is applied when calculating the bremsstrahlung created by electrons of these energies. At the high energy limit, a more exact calculation by Jaeger (1937) gives somewhat higher results, and Guth (1941) has given a correction to the Born approximation. Here, values in accordance with Guth and Jaeger were used at the high energy limit, while at lower energies of the emitted quanta, the fo mula given by Heitler (1949, e n (16), p. 165) was used. A numerical calculation owed that the bremsstrahlu om the photoelectrons was by most troublesome component in the sca l radiation. The result of tne calculations for the various contributions t counting rate is shown in table 2, § 5.

Another process which had to be considered was annihilation of positrons created by pair production in the scatterer, although the cross section for pair production for 1·33 MeV gamma rays is small, being for lead $1{\cdot}8 \times 10^{-26}$ cm² sterad^{-1} (Dayton 1953). Of interest here were the two-quantum and one-quantum annihilations of the positrons in flight, because these processes give rise to harder quanta than the ordinary 0·51 MeV annihilation radiation. The probability for annihilation in flight depends on the energy. Owing to the small primary gamma energy and the large atomic weight, there will be a rather big asymmetry in the energy distribution of the positron spectrum. By taking this into account and using the formula given by Bethe (1935), the probability for two-quantum and one-quantum annihilation in flight was estimated to be respectively 8×10^{-3} and 5×10^{-4} for the positrons created by the 1·33 MeV gamma rays. The intensity of the harder quantum from the two-quantum process, having an energy of 0·66 MeV on the average, corresponded to an over-all cross section of $1{\cdot}5 \times 10^{-28}$ cm², while the one-quantum process corresponded to a cross section of $0{\cdot}9 \times 10^{-29}$ cm² with an average energy of 1·18 MeV.

The result of the calculation was that the rays created by the two-quantum process having an energy above, for example, 0·8 MeV were so few in number that they could be neglected. By the one-quantum process a few rays were produced with energies between the primaries of 1·17 MeV and 1·33 MeV. These could, if recorded, have contributed about $0{\cdot}5 \times 10^{-29}$ cm² to the cross section.

Through multiple Compton scattering a few quanta with higher energy than the single scattered ones could reach the phosphor. A rough estimation of the

double Compton process gave for the 90° arrangement the following result: The double scattered rays, having energies of 0·1 MeV or more in excess of the single scattered rays, had an average energy of 0·5 MeV (maximum energy of 0·514 MeV) and in number amounted to about 5% of the single scattered ones. They were effectively ruled out by the scintillation spectrometer.

§ 5. Results

The contributions to the counting rate from the various processes in the scatterer were calculated for each of the three channels used in the arrangement. There were, however, so many uncertainties that good agreement could not be expected between calculated and observed values. For example, the theories for the creation of bremsstrahlung and the numerical integrations were only approximate. Also, the exact variation of the counter efficiency with energy for each of the three channels was difficult to find theoretically, especially because double processes in such a large phosphor contributed so much to the photo-peak.

On the other hand, the observed effects can easily be reconciled with the calculated data. The large increase in counting rate from channel I to channel III was clearly caused by bremsstrahlung. When the resolving power of the spectrometer was reduced, the 1·33 MeV photo-peak was flattened, and relatively more high energy bremsstrahlung were counted at the highest bias setting. This explains the effect observed that the measured elastic scattering decreased with increasing resolving power of the spectrometer.

Some calculated and measured relative counting rates due to the various processes are shown in table 2.

Table 2. Relative Counting Rates

Process in the scatterer	III	II	I
Pair production	0·05	0·05	0·01
Compton scattering	0·5	0·05	0
Photoeffect	8	1·7	0·1
Sum of above	8·6	1·8	0·1
Total observed	19	5·5	1·68
Small ^{60}Co source	2·31	1·96	1·50
Fitted value for the intruding components	17	3·5	0·2

III, Channel III, 0·95–1·10 MeV; II, channel II, 1·10–1·25 MeV; I, Channel I, 1·25–1·40 MeV.

Table 2 shows that the observed counting rate due to the total scattered radiation increased by a large factor from channel I to III. This increase was even more pronounced for the calculated counting rate due to the bremsstrahlung. On the other hand, the counting rate due to the primary gamma rays from a small ^{60}Co source, placed on the scatterer, increased very slowly from channel I to III. The counts produced in channel III by the scattered radiation were, therefore, chiefly due to bremsstrahlung. The decrease from channel III to channel I found by calculation was assumed to be qualitatively correct, and then the small correction to be applied in channel I due to the disturbing components could be found by fitting calculated and observed rates in channel III. This gave in channel I a total reduction of about 10% of the observed counting rate to get the

counting rate due to elastic scattered rays. When multiplied by 10^{-28} cm^2, the figure so obtained gives the corresponding scattering cross section. Thus, the true cross section for elastic scattering of 1·33 MeV gamma rays by lead should be about $1{\cdot}5 \times 10^{-28}$ cm^2 sterad^{-1} at an angle of 90°.

In channel II the intruding components had roughly the same intensity as the elastically scattered ray. Therefore, nothing can be said about the elastic scattering of 1·17 MeV rays, except that the counting rate indicated an elastic scattering cross section which is lower than the value predicted by the theory of Franz.

The present measurement at 90° gives a lower value than previous experiments for the elastic scattering cross section, and does not agree with the theoretical values for Rayleigh and Thomson scattering. At an angle of 90° the theory of Franz gives an elastic cross section of $5{\cdot}2 \times 10^{-28}$ cm^2 sterad^{-1} for 1·33 MeV, according to Wilson (1953) the calculation of Bethe predicts a cross section of 3×10^{-28} cm^2 sterad^{-1}, while the present result is $1{\cdot}5 \times 10^{-28}$ cm^2 sterad^{-1}. At 120° our uncorrected results of $1{\cdot}6 \times 10^{-28}$ cm^2 sterad^{-1} is in agreement with the curve of Bethe given in Wilson's paper. The experimental error in the measurement at 120° was higher than the one at 90°.

Wilson also found values which were lower than theoretically predicted ones. While earlier experiments always gave far higher cross sections than the theory, the situation now seems to be the opposite. The reason for this is that all the intruding components tend to make the measured cross section too high, and an increase in resolving power reduces their relative importance. This was experienced in the present measurements as various improvements of the spectrometer always resulted in a lower cross section.

If one adopts the present experimental result, there are two possibilities: (i) the theory of Bethe gives too large values for the Rayleigh scattering, but is more correct than the theory of Franz, (ii) in addition to the Rayleigh and Thomson scattering there is an additional elastic scattering which interferes destructively with the former.

The measurement by Strickler (1953) at 135° showed a rather good agreement with the theory of Bethe for the Rayleigh scattering. An additional destructive component, therefore, has to be assumed negligible at large angles. This is just the case for the postulated potential (Delbrück) scattering. The best explanation of the low value found in the present experiment, therefore, seems to be that the amplitude for the potential scattering at 90° of 1·33 MeV gamma rays by lead is so large that it has a measurable influence on the total scattered wave. The proper cross section for pure potential scattering to fit the present experiment with the curve of Bethe would be $2{\cdot}5 \times 10^{-29}$ cm^2 sterad^{-1}. But one must remember that errors in experiment and theory may cause relatively bigger variations in the above value for the cross section for the potential scattering. The statistical error for the experiment is rather small, but the probable error is, of course, difficult to estimate due to the many other uncertainties.

Acknowledgments

The authors are indebted to siv. ing. J. Sandstad for building the electronic equipment. The work was supported by the Royal Norwegian Council for Scientific and Industrial Research.

References

Bethe, H. A., 1935, *Proc. Roy. Soc.* A, **150,** 129.

Bethe, H. A., and Heitler, W., 1934, *Proc. Roy. Soc.* A, **146,** 83.

Bethe, H. A., and Rohrlich, F., 1952, *Phys. Rev.*, **86,** 10.

Davey, W. G., 1953, *Proc. Phys. Soc.* A, **66,** 1059.

Dayton, J. E., 1953, *Phys. Rev.*, **89,** 544.

Franz, W., 1935, *Z. Phys.*, **98,** 314.

Gray, J. H., and Tarrant, G. T. P., 1934, *Proc. Roy. Soc.* A, **143,** 706.

Guth, E., 1941, *Phys. Rev.*, **59,** 325.

Heitler, W., 1949, *Quantum Theory of Radiation*, 2nd edn (Oxford : Clarendon Press).

Jaeger, J. C., 1937, *Nature, Lond.*, **140,** 108.

Ketelaar, H., 1936, *J. Phys. Radium*, **7,** 243.

Meitner, L., and Kösters, H., 1933, *Z. Phys.*, **84,** 137.

Moon, P. B., 1950, *Proc. Phys. Soc.* A, **63,** 1189.

Pollard, E., and Alburger, D. E., 1948, *Phys. Rev.*, **74,** 926.

Rohrlich, F., and Gluckstern, R. L., 1952, *Phys. Rev.*, **86,** 1.

Storruste, A., 1950, *Proc. Phys. Soc.* A, **63,** 1197; 1951, *Thesis*, University of Oslo.

Strickler, T. D., 1953, *Phys. Rev.*, **92,** 923.

Wilson, R. R., 1953, *Phys. Rev.*, **90,** 720. See also Levinger, J. S., 1952, *Phys. Rev.*, **87,** 656, and Brown, G. E., and Woodward, J. B., 1952, *Proc. Phys. Soc.* A, **65,** 977.

The Augmented Plane Wave and related methods for Crystal Eigenvalue Problems

By R. S. LEIGH
Atomic Energy Research Establishment, Harwell, Berks.

Communicated by B. H. Flowers; MS. received 21st November 1955

Abstract. In the augmented plane wave method, and in an earlier related method, both due to Slater, the wave functions in a crystal are expressed in terms of spherical harmonics and radial functions around each atom, and of plane waves between the atoms. Convergence in these two methods with respect to the addition of l values near the atoms is discussed in the light of a variation principle which involves an arbitrary parameter. It is shown that this convergence is likely to be improved by calculating the matrix elements in a way slightly different from that given by Slater. This is illustrated by a simple example. A new method, of the same general kind, is suggested, which has some advantages over the other two methods.

§ 1. Introduction

The problem we shall be concerned with in this paper is that of finding the one-electron energy levels and wave functions for a given electrostatic potential which has the periodicity of a crystal lattice. We shall confine ourselves to the case of a single atom in the unit cell. The generalization of the discussion to the case where there is more than one atom in the unit cell, or to the case of an ordered alloy, is straightforward. Slater (1937, 1953) and Saffren and Slater (1953) have introduced methods for the solution of this problem which are designed to combine the advantages of the plane wave expansion and cellular methods. Crystal space is regarded as being partitioned by non-overlapping translationally equivalent spheres, each of which has a nucleus at its centre, and within which the potential is assumed spherically symmetrical. In the region between the spheres, each basis function for the expansion of the wave function is taken to be a single plane wave, as in the plane wave expansion method. Inside a sphere, it is taken to be a solution of the wave equation for some value of the energy, expressed as a series of products of radial wave functions and spherical harmonics as in the cellular method. It is supposed that infinitely many terms of this series are taken, and the coefficients are chosen to make the sum continuous with the plane wave everywhere on the surface of the sphere. The gradient of each basis function is, however, discontinuous over this surface. The eigenvalue problem may be solved by applying the usual variation principle for the energy to an arbitrary linear combination of these basis functions, provided the contribution to the kinetic energy from the discontinuity in gradient is taken into account. This contribution may be evaluated by a limiting process.

In practice, it is possible to take into account only a finite number of values of l, the azimuthal quantum number. In Slater's treatment this appears only as

a truncation of summations over l in the elements of the secular determinant. In this paper, the standpoint is adopted of using basis functions which contain explicitly only a finite number of terms in the spherical harmonic series. Such functions are discontinuous on the surface of the sphere as well as having a discontinuous gradient. The evaluation of the kinetic energy by a limiting process then fails, and a new variation principle is required. This is set up in § 2, and, as might be expected, found to be not unique. Arbitrariness in the variation principle leads to arbitrariness in the eigenvalue found using a given finite set of basis functions. Particular attention is given to the effect of the choice of variation principle on the convergence of the eigenvalue as more values of l are taken into account. A simple numerical example of the points discussed is given in an appendix.

Slater's two methods are particular cases of a general type of method, in which each basis function consists of a single plane wave in the region between the spheres, and of a series of products of spherical harmonics and radial functions inside a sphere. One other method of this type is suggested, which has some advantages over Slater's methods.

§ 2. A Variation Principle

In this section we set up a variation principle appropriate to trial functions $\psi(\mathbf{r})$ which may be discontinuous and have a discontinuous gradient on the surfaces of the spheres of Slater's methods, but are otherwise smooth and satisfy the Bloch condition

$$\psi(\mathbf{r}+\mathbf{R})=e^{i\mathbf{k}.\mathbf{R}}\psi(\mathbf{r}) \qquad \ldots\ldots(1)$$

for some value of $\mathbf{k}$, where $\mathbf{R}$ denotes any translation vector of the crystal. For the purposes of this section the potential need not be spherically symmetrical inside a sphere, but we do assume that it is symmetric with respect to inversion in a nucleus. This is usually but not necessarily so when there is only one atom in the unit cell. As shown in Appendix I, it is then always possible to choose the eigenfunctions so that their real parts are even and their imaginary parts odd with respect to inversion in a nucleus. We may therefore restrict ourselves to trial functions of this form, and this considerably simplifies the form of the variation principle.

Since the trial functions satisfy the Bloch condition, it is necessary to consider their values only within a single atomic cell. A variation principle may be derived in a way exactly parallel to that followed by Kohn (1952) in setting up a variation principle for the cellular method. The surface of the atomic cell is replaced by the inner and outer surfaces of the sphere. We find that the first variation of the functional $K[\psi]$, defined by the equation

$$K[\psi]=\int_{\text{cell}}\psi^*(\mathbf{r})[-\nabla^2+V(\mathbf{r})-\epsilon]\psi(\mathbf{r})d\mathbf{r} + \int_{\text{sphere}}\left[\psi^*(\mathbf{r}'')\frac{\partial}{\partial r}\psi(\mathbf{r}')-\psi(\mathbf{r}')\frac{\partial}{\partial r}\psi^*(\mathbf{r}'')\right]dS, \qquad \ldots\ldots(2)$$

vanishes if ϵ and $\psi(\mathbf{r})$ are equal to an associated eigenvalue and eigenfunction for some value of $\mathbf{k}$. The value of K itself in that case is also zero. The first term on the right-hand side of equation (2) denotes a volume integral extending over the atomic cell. Points on the surface of the sphere, where the integrand is not

defined, are excluded from the integration. $V(\mathbf{r})$ denotes the potential. The second term denotes a surface integral taken over the surface of the sphere. $\partial/\partial r$ denotes differentiation radially outwards on this surface, and the appearance of $\mathbf{r}'$ or $\mathbf{r}''$ as the argument of a function denotes that the limiting value of the function as $\mathbf{r}$ approaches the surface on its inner or outer side respectively is to be taken. The units of length and energy in equation (2), and throughout this paper, are the radius of the first Bohr orbit and the rydberg respectively. The parity properties of the trial functions enter into the derivation of this variation principle, and into what follows, by ensuring the reality of all the integrals.

We now notice that we can set up other variation principles for our problem by adding to the functional K any integral over the surface of the sphere whose first variation vanishes for variations of $\psi(\mathbf{r})$ from a smooth function. Examples of such integrals are

$$\int_{\text{sphere}} f(\mathbf{r})[\psi^*(\mathbf{r}')-\psi^*(\mathbf{r}'')]\left[\frac{\partial}{\partial r}\psi(\mathbf{r}')-\frac{\partial}{\partial r}\psi(\mathbf{r}'')\right]dS,$$

$$\int_{\text{sphere}} g(\mathbf{r})\,|\psi(\mathbf{r}')-\psi(\mathbf{r}'')|^2\,dS$$

and

$$\int_{\text{sphere}} h(\mathbf{r})\left|\frac{\partial}{\partial r}\psi(\mathbf{r}')-\frac{\partial}{\partial r}\psi(\mathbf{r}'')\right|^2 dS,$$

where $f(\mathbf{r})$ denotes an arbitrary function having the same parity properties as the trial functions on the surface of the sphere, and $g(\mathbf{r})$ and $h(\mathbf{r})$ denote arbitrary real functions, symmetric with respect to inversion in the nucleus. These three integrals are zero if $\psi(\mathbf{r})$ is a smooth function. The vanishing of the first variation of the sum of K and such integrals, for all possible variations of $\psi(\mathbf{r})$ of the prescribed type, is sufficient to ensure that $\psi(\mathbf{r})$ satisfies the wave equation for energy ϵ and is smooth at the surface of the sphere. The variation principle reduces to that set up by Slater, in which a limiting process was used to evaluate the kinetic energy, only if the surface integrals added to K vanish for $\psi(\mathbf{r}')=\psi(\mathbf{r}'')$.

Arbitrariness in the variation principle implies arbitrariness in the value of ϵ derived from a given trial function by equating the functional to zero. Differences between the values of ϵ so obtained are of the second order in differences between the trial function and the corresponding eigenfunction, but may be large for a bad trial function. The application of different variation principles will also lead to different values of any disposable parameters in a trial function. As the flexibility of the trial function is increased, the variation principle ensures that all wave functions and energies converge to eigenfunctions and eigenvalues. The choice of the arbitrary functions in the variation principle affects only the rate of this convergence. Different choices correspond to assigning different importance to the continuity of the wave function or its gradient at various parts of the surface of the sphere.

For the remainder of this paper we shall discuss only the particular functional $K'[\psi]$ defined by

$$K'[\psi]=K[\psi]+\alpha\int_{\text{sphere}}[\psi^*(\mathbf{r}')-\psi^*(\mathbf{r}'')]\left[\frac{\partial}{\partial r}\psi(\mathbf{r}')-\frac{\partial}{\partial r}\psi(\mathbf{r}'')\right]dS, \qquad \ldots\ldots(3)$$

which contains the single arbitrary real constant α. We now examine how the choice of α affects the weighting of the boundary conditions on the surface

of the sphere. The first variation of K' for variations of $\psi(\mathbf{r})$ from any function, not necessarily an eigenfunction, and for any value of ϵ, is given by the equation

$$\delta K' = 2\int_{\text{cell}} [\delta\psi^*(\mathbf{r})][-\nabla^2 + V(\mathbf{r}) - \epsilon]\psi(\mathbf{r})d\mathbf{r}$$
$$- \int_{\text{sphere}} [\psi(\mathbf{r}') - \psi(\mathbf{r}'')]\left[(1-\alpha)\frac{\partial}{\partial r}\{\delta\psi^*(\mathbf{r}')\} + (1+\alpha)\frac{\partial}{\partial r}\{\delta\psi^*(\mathbf{r}'')\}\right] dS$$
$$+ \int_{\text{sphere}} [(1+\alpha)\delta\psi^*(\mathbf{r}') + (1-\alpha)\delta\psi^*(\mathbf{r}'')]\left[\frac{\partial}{\partial r}\psi(\mathbf{r}') - \frac{\partial}{\partial r}\psi(\mathbf{r}'')\right] dS. \quad \ldots\ldots(4)$$

We are interested in the case when the trial function $\psi(\mathbf{r})$ is an arbitrary linear combination of basis functions of the general type described at the end of § 1. Suppose that inside the sphere each basis function includes all spherical harmonics of order up to and including L, but none of order greater than L. Suppose further that the coefficients of the terms included are chosen so that there is continuity on the surface of the sphere with the corresponding terms in the expansion of the plane wave in spherical harmonics. Let $\psi^{(1)}(\mathbf{r})$ denote the sum of the terms corresponding to values of l less than or equal to L in the infinite expansion of $\psi(\mathbf{r})$ in spherical harmonics in the region outside the sphere, and let $\psi^{(2)}(\mathbf{r})$ denote the sum of the remaining terms. Using the orthogonality property of spherical harmonics, we find that the surface terms in $\delta K'$ reduce to

$$2\int_{\text{sphere}} [\delta\psi^*(\mathbf{r}')]\left[\frac{\partial}{\partial r}\psi(\mathbf{r}') - \frac{\partial}{\partial r}\psi^{(1)}(\mathbf{r}'')\right] dS$$
$$+ (1+\alpha)\int_{\text{sphere}} \psi^{(2)}(\mathbf{r}'')\frac{\partial}{\partial r}[\delta\psi^{(2)*}(\mathbf{r}'')]dS$$
$$- (1-\alpha)\int_{\text{sphere}} [\delta\psi^{(2)*}(\mathbf{r}'')]\frac{\partial}{\partial r}\psi^{(2)}(\mathbf{r}'')dS.$$

The first of these terms tends to secure continuity in the contribution to the normal gradient of $\psi(\mathbf{r})$ from terms in its expansion in spherical harmonics for which $l \leqslant L$. The second and third terms tend to secure continuity of the contributions to $\psi(\mathbf{r})$ and its normal gradient respectively from terms for which $l > L$. In § 4 we shall see that the omission of terms for which $l > L$, in summations over l in the elements of the secular determinants given by Slater, is equivalent to a choice of α equal to -1. This choice removes altogether from $\delta K'$ the second of the above terms. In § 4 it is shown that choosing α equal to zero, which includes both the second and third terms with comparable weight, may be expected to lead to better convergence with respect to increasing L.

§ 3. Basis Functions

In this section and the next we consider only the case in which the potential is spherically symmetrical inside a sphere. The removal of this restriction is discussed briefly in § 5. We now introduce, for a given value of $\mathbf{k}$, three alternative sets of basis functions which have the following features in common. The functions are labelled by the reciprocal lattice points, and in the region between the spheres the one belonging to the reciprocal lattice vector $\mathbf{h}_n$ is identical with the plane wave $\exp(i\mathbf{k}_n.\mathbf{r})$, $\mathbf{k}_n$ denoting the vector $\mathbf{k}+\mathbf{h}_n$. Inside a sphere each function consists of a series of products of spherical harmonics and radial functions,

all harmonics for which $l \leqslant L$ being included, but none for which $l > L$. The coefficients in this series are chosen to give continuity with the corresponding terms in the expansion of the plane wave. Each function thus has the parity properties specified for trial functions in § 2, and so coefficients of all basis functions are to be taken real.

In the first set of basis functions, which we denote by $\phi(\mathbf{k}_n, \epsilon, \mathbf{r})$, the energy in the radial wave equations is made equal to the energy ϵ which appears explicitly in the variation principle. It is thus left as a variable parameter, as in the cellular method. This set is the same as that used by Slater (1937), except for the explicit omission of harmonics of order higher than L inside the sphere. Let the radial wave functions be denoted by $R_l(\epsilon, r)$, and let $j_l(x)$ denote regular spherical Bessel functions normalized so that they behave as $x^l/1.3.5 \ldots (2l+1)$ for small x. Let ω denote the direction of $\mathbf{r}$, and $Y_{lm}(\omega)$ complex spherical harmonics normalized to 4π over the surface of a unit sphere. Inside the sphere $\phi(\mathbf{k}_n, \epsilon, \mathbf{r})$ is then equal to

$$\sum_{l=0}^{L} i^l \frac{j_l(k_n r_0)}{R_l(\epsilon, r_0)} R_l(\epsilon, r) \sum_{m=-l}^{+l} Y_{lm}^*(\omega_n) Y_{lm}(\omega),$$

where k_n and ω_n denote respectively the magnitude and direction of $\mathbf{k}_n$, and r_0 denotes the radius of the sphere.

In the second set of basis functions, radial functions belonging to fixed energy values $E(\mathbf{k}_n)$ are used. These values, which vary from function to function but are the same for all values of l in a given function, are chosen by applying the variation principle to each $\phi(\mathbf{k}_n, E(\mathbf{k}_n), \mathbf{r})$ alone, with $E(\mathbf{k}_n)$ as a variable parameter. This procedure gives an infinite set of $E(\mathbf{k}_n)$ for each $\mathbf{k}_n$. The $\phi(\mathbf{k}_n, E(\mathbf{k}_n), \mathbf{r})$ are the same as the augmented plane waves of Saffren and Slater (1953), except for the explicit limitation on the number of l values inside the sphere.

The method of choosing the coefficients of the terms inside the sphere in each basis function may, in both sets of functions so far described, lead to unduly large or small amplitudes for some of these terms in certain cases. If $j_l(k_n r_0)$ vanishes for any l and $\mathbf{n}$, all terms for that value of l are omitted altogether inside the sphere in the corresponding function. The occurrence of such an anomaly for a low value of l in a leading term in the expansion of the wave function is likely to have an adverse effect on convergence.

The third set of basis functions seeks to avoid this by associating with each spherical harmonic inside the sphere in a given basis function two radial functions of different energy and different logarithmic derivative at $r = r_0$, the coefficients being chosen to give at $r = r_0$ a smooth join with continuous slope to the corresponding term in the expansion of the plane wave. Let $E_l^{(1)}(\mathbf{k}_n)$ and $E_l^{(2)}(\mathbf{k}_n)$ denote the energies of the two radial functions used with the lth harmonic in the basis function associated with $\mathbf{k}_n$. The $E_l^{(i)}(\mathbf{k}_n)$ may take different values for different l and the same $\mathbf{k}_n$. As with the second set of functions, any number of functions may be built up for one value of $\mathbf{k}_n$. A limiting form of this method is to use those values of $E_l^{(i)}(\mathbf{k}_n)$ for which the radial functions have the same logarithmic derivative at $r = r_0$ as $j_l(k_n r)$. Only one radial function need then be associated with each spherical harmonic. This set of radial functions is discussed by Slater (1953).

It is of interest, in principle, to enquire whether the above sets of functions provide, in the limit of infinite L, a complete basis for the representation of a wave function belonging to the given value of $\mathbf{k}$. It is possible to establish this

easily for the first set of functions, but not for the other two. However, effective convergence after a few terms is the only property of practical value, and in the case of the second and third sets of functions this may depend on the judicious choice of the $E(\mathbf{k}_n)$ or the $E_l^{(0)}(\mathbf{k}_n)$, having regard to such matters as the numbers of nodes inside the sphere.

§ 4. Application of the Variation Principle

Use of the variation principle of § 2, with any of the sets of basis functions of § 3, follows through in the usual way as regards variation of the coefficients of the basis functions. K' is a quadratic form in these coefficients, which are real, and a set of linear homogeneous equations for them is obtained, the eliminant of which, set equal to zero, gives a secular equation for ϵ. By an application of Green's theorem to the region lying between the surfaces of the atomic cell and of the sphere, it is possible to throw K' into a form in which, in the notation of § 2, values of $\psi^{(2)}(\mathbf{r})$ and its gradient on the surface of the sphere do not appear. We find that

$$\begin{aligned} K' = &\int_{\text{sphere}} \psi^*(\mathbf{r})[-\nabla^2 + V(\mathbf{r}) - \epsilon]\psi(\mathbf{r})d\mathbf{r} \\ &+ \int_{\text{cell-sphere}} \psi^*(\mathbf{r})[-(1+\alpha)\nabla^2 + V(\mathbf{r}) - \epsilon]\psi(\mathbf{r})d\mathbf{r} \\ &- \alpha \int_{\text{cell-sphere}} \operatorname{grad}\psi^*(\mathbf{r}) \,.\, \operatorname{grad}\psi(\mathbf{r})d\mathbf{r} \\ &+ \int_{\text{sphere}} \psi^{(1)*}(\mathbf{r}'')\left[\frac{\partial}{\partial r}\psi(\mathbf{r}') - (1+\alpha)\frac{\partial}{\partial r}\psi^{(1)}(\mathbf{r}'')\right] dS. \end{aligned}$$

Let $A(\mathbf{h})$ denote the integral of $\exp(i\mathbf{h}\,.\,\mathbf{r})$, where $\mathbf{h}$ is a reciprocal lattice vector, over that part of the atomic cell which lies outside the sphere, and $v(\mathbf{h})$ denote the integral of $V(\mathbf{r})\exp(i\mathbf{h}\,.\,\mathbf{r})$ over the same region, then

$$A(\mathbf{h}) = \Omega\delta_{\mathbf{h}} - \frac{4\pi r_0^2}{h}\mathrm{j}_1(hr_0),$$

where Ω denotes the atomic volume, and $\delta_{\mathbf{h}}$ takes the value unity if $\mathbf{h} = (000)$ and is zero otherwise. Let the symbol $B_l(\mathbf{k}_n, \mathbf{k}_{n'})$ be defined by

$$B_l(\mathbf{k}_n, \mathbf{k}_{n'}) = 4\pi r_0^2 \mathrm{j}_l(k_n r_0)\mathrm{j}_l(k_{n'} r_0) \sum_{m=-l}^{+l} \mathrm{Y}_{lm}{}^*(\omega_n)\mathrm{Y}_{lm}(\omega_{n'}).$$

Finally, let $F_l(\epsilon)$ denote the value of $[1/\mathrm{R}_l(\epsilon, r)]d\mathrm{R}_l(\epsilon, r)/dr$ for $r = r_0$, and $G_l(k^2)$ the value of $[k/\mathrm{j}_l(x)]d\mathrm{j}_l(x)/dx$ for $x = kr_0$. We then have that the general element $M(\mathbf{k}_n, \mathbf{k}_{n'})$ of the matrix of the set of linear equations is, for the first set of basis functions, equal to

$$\begin{aligned} &A(\mathbf{k}_n - \mathbf{k}_{n'})[\tfrac{1}{2}(1+\alpha)(k_n{}^2 + k_{n'}{}^2) - \alpha\mathbf{k}_n \,.\, \mathbf{k}_{n'} - \epsilon] + v(\mathbf{k}_n - \mathbf{k}_{n'}) \\ &\qquad + \sum_{l=0}^{L} B_l(\mathbf{k}_n, \mathbf{k}_{n'})\{F_l(\epsilon) - \tfrac{1}{2}(1+\alpha)[G_l(k_n{}^2) + G_l(k_{n'}{}^2)]\}. \end{aligned}$$

There is no term here from inside the sphere, because with this set of functions the wave equation is satisfied there for energy ϵ. Whatever the value of α, if L is taken indefinitely large, $M(\mathbf{k}_n, \mathbf{k}_{n'})$ becomes equal to the matrix element given by Slater (1937), except for the presence of $v(\mathbf{k}_n - \mathbf{k}_{n'})$. This term does not appear, because Slater takes $V(\mathbf{r})$ to be zero outside the sphere. The choice of the value of α affects the rate of convergence of $M(\mathbf{k}_n, \mathbf{k}_{n'})$ with increasing

L to its value for infinite L. A choice of α equal to -1 corresponds to using Slater's matrix element with the summation over l carried only as far as L. Because of the dominating effect of the term $l(l+1)/r^2$ in the radial wave equation, the values of logarithmic derivatives of radial wave functions at a given value of r, although becoming larger as l increases, become, for sufficiently large l, increasingly insensitive to differences of potential or energy. This suggests that a value of α which is likely to lead to good convergence of the $M(\mathbf{k}_n, \mathbf{k}_{n'})$, and thus of ϵ and $\psi(\mathbf{r})$, with respect to L, is zero. Some results are given in Appendix II for a potential which is a negative delta function at each lattice point, and zero everywhere else. α is taken equal to both -1 and zero, and it is found, in this simplified case, that the latter choice does give considerably better convergence.

In the case of the second set of basis functions, the $E(\mathbf{k}_n)$ have first to be determined. Putting $\psi(\mathbf{r})$ equal to the single function $\phi(\mathbf{k}_n, E, \mathbf{r})$, where the radial wave function energy E is independent of ϵ, and using expression (4) for $\delta K'$ together with the reduced form of the surface terms, we find that

$$\frac{\partial K'}{\partial E} = (E-\epsilon)\frac{\partial}{\partial E}\int_{\text{sphere}} |\phi(\mathbf{k}_n, E, \mathbf{r})|^2 \, d\mathbf{r}.$$

The vanishing of $\partial K'/\partial E$ is thus achieved by taking E equal to ϵ. The $E(\mathbf{k}_n)$ are then given by the vanishing of K', which, with E equal to ϵ, is just the diagonal matrix element $M(\mathbf{k}_n, \mathbf{k}_n)$ for the first set of functions. With $\alpha = -1$ we obtain the equation of Saffren and Slater (1953) for $E(\mathbf{k}_n)$, with the summation over l taken only as far as L. Additional values of E for which $\partial K'/\partial E$ vanishes are those for which the normalization integral over the sphere is stationary. There is no necessity, however, to make use of these values of E. Once the $E(\mathbf{k}_n)$ are determined the matrix elements between the $\phi(\mathbf{k}_n, E(\mathbf{k}_n), \mathbf{r})$ may be set up. We shall not give these here; they are given by Howarth (1955) in a form corresponding to $\alpha = -1$. Comments made previously on the choice of α apply equally here, of course, both to these matrix elements and to the $M(\mathbf{k}_n, \mathbf{k}_n)$ in determining the $E(\mathbf{k}_n)$. The possibility of using $M(\mathbf{k}_n, \mathbf{k}_n)$ in the form corresponding to $\alpha = 0$ is indicated by Saffren and Slater, but not discussed.

We give now the matrix elements for K' with the third set of basis functions. Let

$$\rho_l(\mathbf{k}) = F_l(E_l^{(1)}(\mathbf{k})) - F_l(E_l^{(2)}(\mathbf{k})),$$

$$\sigma_l^{(1)}(\mathbf{k}) = G_l(k^2) - F_l(E_l^{(2)}(\mathbf{k})),$$

$$\sigma_l^{(2)}(\mathbf{k}) = F_l(E_l^{(1)}(\mathbf{k})) - G_l(k^2),$$

$$\gamma_l(\mathbf{k}, \mathbf{k}') = \tfrac{1}{2}\sum_{i=1}^{2}\sum_{j=1}^{2} \sigma_l^{(i)}(\mathbf{k}) \mathrm{J}_l(E_l^{(i)}(\mathbf{k}), E_l^{(j)}(\mathbf{k}'))\sigma_l^{(j)}(\mathbf{k}')[E_l^{(i)}(\mathbf{k}) + E_l^{(j)}(\mathbf{k}')],$$

$$\delta_l(\mathbf{k}, \mathbf{k}') = \sum_{i=1}^{2}\sum_{j=1}^{2} \sigma_l^{(i)}(\mathbf{k}) \mathrm{J}_l(E_l^{(i)}(\mathbf{k}), E_l^{(j)}(\mathbf{k}'))\sigma_l^{(j)}(\mathbf{k}'),$$

and

$$\mathrm{J}_l(E, E') = \frac{\int_0^{r_0} r^2 \mathrm{R}_l(E, r)\mathrm{R}_l(E', r)dr}{r_0^2 \mathrm{R}_l(E, r_0)\mathrm{R}_l(E', r_0)}.$$

If $E \neq E'$,

$$\mathrm{J}_l(E, E') = -\frac{F_l(E) - F_l(E')}{E - E'}.$$

If the typical matrix element is equal to

$$\Gamma(\mathbf{k}_n, \mathbf{k}_{n'}) - \epsilon\Delta(\mathbf{k}_n, \mathbf{k}_{n'}),$$

then

$$\Gamma(\mathbf{k}_n, \mathbf{k}_{n'}) = A(\mathbf{k}_n - \mathbf{k}_{n'})[\tfrac{1}{2}(1+\alpha)(k_n^2 + k_{n'}^2) - \alpha\mathbf{k}_n \cdot \mathbf{k}_{n'}] + v(\mathbf{k}_n - \mathbf{k}_{n'}) + \sum_{l=0}^{L} B_l(\mathbf{k}_n, \mathbf{k}_{n'}) \left\{ \frac{\gamma_l(\mathbf{k}_n, \mathbf{k}_{n'})}{\rho_l(\mathbf{k}_n)\rho_l(\mathbf{k}_{n'})} - \tfrac{1}{2}\alpha[G_l(k_n^2) + G_l(k_{n'}^2)] \right\},$$

and

$$\Delta(\mathbf{k}_n, \mathbf{k}_{n'}) = A(\mathbf{k}_n - \mathbf{k}_{n'}) + \sum_{l=0}^{L} B_l(\mathbf{k}_n, \mathbf{k}_{n'}) \frac{\delta_l(\mathbf{k}_n, \mathbf{k}_{n'})}{\rho_l(\mathbf{k}_n)\rho_l(\mathbf{k}_{n'})}.$$

In this case, no term is required to allow for discontinuity of the normal gradient of $\psi(\mathbf{r})$ on the surface of the sphere for values of $l \leqslant L$ in its spherical harmonic expansion. There is, however, as with the $\phi(\mathbf{k}_n, E(\mathbf{k}_n), \mathbf{r})$, a contribution due to the fact that the wave equation is not satisfied by the basis functions inside the sphere. The terms with $\gamma_l(\mathbf{k}_n, \mathbf{k}_{n'})$ and $\delta_l(\mathbf{k}_n, \mathbf{k}_{n'})$ arise from this cause. A choice of $\alpha = 0$ may again be expected to favour convergence.

§ 5. Discussion

Arbitrariness in a variation principle, such as is discussed in § 2, is not peculiar to the present problem. For example, Kohn's variation principle for the cellular method admits of a similar generalization, as does any variation principle for an eigenvalue problem where trial functions are allowed which are discontinuous or have discontinuous gradient over some surface, or do not satisfy the appropriate boundary conditions. The existence of several different variation principles for scattering problems is well known. These are compared by, for example, Kohn (1948), Kato (1950) and Turner and Makinson (1953). The arbitrary generalization of variation principles for boundary value problems in partial differential equations, such as that of potential theory, is discussed by Courant (1922, 1943) in connection with the convergence of higher derivatives of the solutions obtained. In the present paper we have been interested in arbitrariness in a variation principle as it affects convergence of eigenvalues and eigenfunctions.

In § 3 and § 4 we assumed for simplicity that the potential is spherically symmetrical inside the sphere. Slater (1953) has pointed out that, though this restriction is necessary if the determination of the $E(\mathbf{k}_n)$ of augmented plane waves by the preliminary application of the variation principle to each one separately is to be done simply, it need not be retained when evaluating matrix elements between these functions. Similarly, the third set of basis functions of § 3 may be used with a potential which is not spherically symmetrical inside the sphere, but some spherically symmetrical potential is necessary, of course, to generate the radial functions. This latter potential, and that used in setting up the second set of functions, may or may not be identical with the first term in the expansion of the full potential in spherical harmonics. To secure rapid convergence, however, it must presumably be nearly so in the region where the latter is varying rapidly. The radial functions in the third set of basis functions could, for example, be those for the free atom in some stage of ionization, if these had previously been obtained for some other purpose. The first set of functions can, of course, be used only with a spherically symmetrical potential inside the sphere.

We have not so far discussed the value to be given to r_0, the radius of the spheres. In the general case evisaged in the preceding paragraph, or if the potential is

spherically symmetrical inside the inscribed sphere of the atomic polyhedron, the value of r_0 no longer implies an assumption about the potential. If the variation principle were generalized so as to take account of discontinuities over any surface within the atomic polyhedron, r_0 could be regarded as an additional parameter in the trial function. However, since there is no correct value of r_0 for a true eigenfunction, no variation principle could possibly determine the 'best' value of r_0 for a given finite set of basis functions and a given value of L. In practice, the value of r_0 may be chosen so as to balance the value of L against the size of the secular determinant. The value of L necessary to achieve adequate convergence may be decreased by making r_0 smaller, but this may increase the number of basis functions required. The most suitable value of r_0 depends on the state being considered, and, if it is desired to avoid high values of L, may be expected to decrease as the eigenvalue increases.

The second and third sets of basis functions, together with any other similar sets which use radial functions of fixed energy, have the advantage over the first set that matrix elements do not depend implicitly on ϵ through the $F_l(\epsilon)$. The second set of functions attempts in addition to make off-diagonal matrix elements smaller through the solution of a preliminary variation problem for each basis function separately. The additional labour involved would seem to be justified only if adequate convergence is achieved with a smaller number of basis functions. Howarth (1955) has applied the augmented plane wave method to copper. It is proposed to employ the third set of functions in an investigation of states in the conduction band of copper, using the same two potentials as are used by Howarth, and compare convergence in the two methods.

It is proposed also to duplicate the copper calculations, using the first set of basis functions of § 3. Very good convergence has been obtained with this set in the calculations with a δ-function potential quoted in Appendix II. If, in the application to a real metal, the convergence is found to be at least as good as in the other two methods, it may be, for potentials which are spherically symmetrical inside the sphere, that the first set of functions has something to commend it on the grounds of simplicity. An application of Slater's 1937 method to copper has in fact been made by Chodorow (1939), though unfortunately very few details have been published. Slater (1953) has referred to difficulties in his earlier method, arising from the occurrence of large secular determinants the elements of which depend implicitly on the energy, as one reason for setting up the augmented plane wave method. In connection with the occurrence of large secular determinants, it is interesting to notice that in the δ-function potential example it has been found that misleadingly low convergence with respect to the addition of basis functions may result from including too few l values. The number of l values necessary to avoid this is decreased in some cases if the 1937 method is modified as suggested in this paper. In his application of the augmented plane wave method, Howarth has apparently worked throughout with sufficient l values to achieve adequate convergence of the matrix elements.

The ultimate aim in the solution of crystal eigenvalue problems is to obtain not only accurate energies but also accurate wave functions. The great advantage of methods of the augmented plane wave type is that they offer the hope of being able to secure an accurate representation of a wave function with a number of basis functions which is much smaller than the number of plane waves which would be required, and with fewer values of l than would be needed in the cellular

method. Judicious choice of variation principle may cause the matrix elements, and so the approximate eigenvalue and basis function coefficients for a given finite set of basis functions, to converge adequately with even fewer values of l, but is unlikely to affect the number necessary for a good wave function. Rapid convergence of the matrix elements with increasing l is still, however, of great practical use.

ACKNOWLEDGMENTS

The author is indebted to Dr. B. H. Flowers, Dr. W. M. Lomer, Dr. D. F. Johnston and Dr. D. J. Howarth for valuable discussions, and to Dr. P. N. Butcher for drawing his attention to the papers by Courant and by Turner and Makinson.

REFERENCES

CHODOROW, M. I., 1939, *Phys. Rev.*, **55**, 675.
COURANT, R., 1922, *Goett. Nach.*, 144; 1943, *Bull. Amer. Math. Soc.*, **49**, 1.
HOWARTH, D. J., 1953, *Proc. Roy. Soc.* A, **220**, 513; 1955, *Phys. Rev.*, **99**, 469.
KATO, T., 1950, *Phys. Rev.*, **80**, 475.
KOHN, W., 1948, *Phys. Rev.*, **74**, 1763; 1952, *Ibid.*, **87**, 472.
SAFFREN, M. M., and SLATER, J. C., 1953, *Phys. Rev.*, **92**, 1126.
SLATER, J. C., 1937, *Phys. Rev.*, **51**, 846; 1953, *Ibid*, **92**, 603.
TURNER, J. S., and MAKINSON, R. E. B., 1953, *Proc. Phys. Soc.* A, **66**, 866.

APPENDIX I

PARITY PROPERTIES OF THE WAVE FUNCTIONS

The one-electron eigenfunctions for a crystal with one atom in the unit cell, and with a periodic electrostatic potential which is symmetric with respect to inversion in a nucleus, may always be chosen so that their real parts are even and their imaginary parts odd with respect to this inversion. This may be shown as follows.

Let J denote the operation of inversion in a nucleus, and ψ an eigenfunction belonging to some value of $\mathbf{k}$. Since the Hamiltonian is real and commutes with the operation J, it follows that $J\psi^*$ is an eigenfunction with the same energy as ψ. It is also easy to show that $J\psi^*$ belongs to the same value of $\mathbf{k}$ as ψ. If ψ is not degenerate with any other eigenfunction belonging to the same value of $\mathbf{k}$, then $J\psi^*$ must be equal to ψ multiplied by some complex constant. Since $J(J\psi^*)^* = \psi$, the modulus of this constant must be unity. If $J\psi^* = e^{i\theta}\psi$, then the function $\psi' = e^{i\theta/2}\psi$ has the desired parity properties, since $J\psi'^* = \psi'$.

If, by virtue of rotation symmetries of the potential, ψ is degenerate with one or more other eigenfunctions belonging to the same value of $\mathbf{k}$, it is necessary to show only that one eigenfunction with the desired parity properties may be constructed. Other eigenfunctions of the multiplet, generated from this one by operations in the group of $\mathbf{k}$, automatically have the same parity properties because, for this simple type of crystal, J commutes with all such operations. If $J\psi^*$ is linearly dependent on ψ, we may proceed as before. If it is not, then the function $\psi + J\psi^*$ is a suitable one.

It is easy to show that these results are not affected by the occurrence of accidental degeneracy between eigenfunctions belonging to the same value of $\mathbf{k}$ but to different symmetry types.

APPENDIX II

Some Results for a δ-function Potential

The first set of basis functions of § 3 has been used in an investigation of two states of high symmetry in a face-centred cubic lattice with a potential which is a negative δ-function at each lattice point and zero everywhere else. In this case $F_l(\epsilon) = G_l(\epsilon)$ for $l \neq 0$, and

$$F_0(\epsilon) = \frac{\gamma - \sqrt{\epsilon}\tan(r_0\sqrt{\epsilon})}{1 + (\gamma/\sqrt{\epsilon})\tan(r_0\sqrt{\epsilon})} - \frac{1}{r_0},$$

where γ is equal to the limiting value of $[1/rR_0(\epsilon, r)]d[rR_0(\epsilon, r)]/dr$ in the zero potential region as r tends to zero, and is independent of ϵ. As γ ranges from $+\infty$ to $-\infty$, each eigenvalue changes continuously from one value of k_n^2 to the next lowest value, or to $-\infty$ if there is no lower value. The only exception to this is if an eigenfunction belongs to a symmetry type which has one or more nodal planes passing through a nucleus, in which case, of course, the eigenvalue remains fixed at a free electron value whatever the value of γ.

The two states investigated are those denoted Γ_s and X_s by Howarth (1953), and correspond to $\mathbf{k} = (000)$ and $\mathbf{k} = (0, 0, 2\pi/a)$ respectively, where a denotes the lattice constant. They are the states which have the full symmetry of the appropriate group of $\mathbf{k}$ in each case, and are the only states for these values of $\mathbf{k}$ whose energy depends on γ. From each group of basis functions with the same value of k_n^2, one linear combination may be constructed which has the required symmetry. Let these latter be labelled by $\nu = 0, 1, 2, \ldots$ in order of increasing k_n^2. All combinations with $\nu \leqslant \nu_{\max}$ have been included in the trial function. For both Γ_s and X_s, only even values of l occur, and in addition $l = 2$ does not occur for Γ_s.

Table 1 shows a selection of the results obtained with r_0 equal to the radius of the inscribed sphere of the atomic polyhedron. Results are given for the two lowest states of Γ_s type and the lowest state of X_s type, for two values of γ, and for two values of the parameter α in the variation principle. The unit of energy is $(2\pi/a)^2$, which is of the order of 10 ev for typical values of a. The values of k_n^2 in the same units are 0, 3, 4, 8 for $\nu = 0, 1, 2, 3$ respectively in the case of Γ_s, and 1, 2, 5 for $\nu = 0, 1, 2$ in the case of X_s. The eigenvalues for the Γ_s states with $\nu_{\max} = 0$ and $L = 4$ are necessarily identical with those obtained with $\nu_{\max} = 0$ and $L = 0$, because there is no term with l greater then zero in the matrix element. For the same reason, this matrix element, and eigenvalues obtained from it, are independent of α.

If the true eigenvalues were of interest, it would be necessary to include higher values of ν and of l than has been done here. The present results serve, however, to illustrate the effect of using the two different values of α. In the case of the lowest Γ_s state for $\gamma a = +20$, continuity of the wave functions with $L = 0$ must be so good that the value of α is immaterial, for the number of figures quoted. In all other cases, the convergence with respect to L is better with $\alpha = 0$ than with $\alpha = -1$. Convergence of the matrix elements with respect to L is better with $\alpha = 0$ than with $\alpha = -1$ in the great majority of cases. To quote a typical example, in the case of the state X_s, and with $\gamma a = +2$ and $\epsilon = 0{\cdot}480\ (2\pi/a)^2$, the diagonal matrix elements corresponding to $\nu = 0$ are proportional to $-0{\cdot}0292$, $+0{\cdot}0681$, $+0{\cdot}0689$ for $L = 0, 2, 4$ respectively with $\alpha = 0$, and $-0{\cdot}3289$, $+0{\cdot}0560$, $+0{\cdot}0689$

Table 1. Eigenvalues obtained with r_0 equal to the Radius of the Inscribed Sphere of the Atomic Polyhedron.

$\gamma a = +20$			$\alpha = 0$				$\alpha = -1$			
	ν_{max}	0	1	2	3	0	1	2	3
	L								
Γ_8	0	−0·051	−0·051	−0·051	−0·051	(−0·051)	−0·051	−0·051	−0·051
	4	(−0·051)	−0·051	−0·051	−0·051	(−0·051)	−0·051	−0·051	−0·051
X_8	0	0·859	0·847	0·391		0·472	0·409	0·369	
	2	0·881	0·877	0·876		0·871	0·859	0·858	
	4	0·881	0·877	0·877		0·881	0·877	0·877	
Γ_8	0	2·667	2·500	2·500	2·500	(2·667)	2·226	2·099	2·057
	4	(2·667)	2·512	2·506	2·505	(2·667)	2·505	2·483	2·482

$\gamma a = +2$			$\alpha = 0$				$\alpha = -1$			
	ν_{max}	0	1	2	3	0	1	2	3
	L								
Γ_8	0	−0·178	−0·178	−0·178	−0·178	(−0·178)	−0·178	−0·179	−0·179
	4	(−0·178)	−0·178	−0·178	−0·178	(−0·178)	−0·178	−0·178	−0·178
X_8	0	0·467	0·466	0·241		0·259	0·247	0·213	
	2	0·504	0·480	0·480		0·500	0·461	0·460	
	4	0·505	0·483	0·482		0·505	0·483	0·482	
Γ_8	0	1·577	1·536	1·534	1·534	(1·577)	1·496	1·495	1·491
	4	(1·577)	1·541	1·534	1·534	(1·577)	1·540	1·527	1·527

with $\alpha = -1$. It should be said that it is possible that the good convergence with respect to L obtained with $\alpha = 0$ in the δ-function potential results may be due in part to the fact that there is no phase shift for l greater than zero.

Table 2 gives one set of results obtained with r_0 equal to half the radius of the inscribed sphere of the atomic polyhedron. These results show the expected increase in the number of basis functions required, due to the larger volume over which the wave function has to be built up from plane waves.

Table 2. Eigenvalues obtained with r_0 equal to half the value used in table 1

$\gamma a = +20$			$\alpha = 0$			
	ν_{max}	0	1	2	3
	L				
Γ_8	0	−0·048	−0·050	−0·051	−0·051
	4	(−0·048)	−0·050	−0·051	−0·051

The Intensity of Emission of Characteristic X-Radiation

By C. R. WORTHINGTON and S. G. TOMLIN
Physics Department, University of Adelaide

MS. received 31*st October* 1955 *and in final form* 23*rd January* 1956

Abstract. A method for calculating the x-ray emission intensity from thick targets as a function of the target atomic number, accelerating voltage and angle of emission has been devised, and applied to the emission of the radiation from Ag, Cu, Cr and Al. These calculations have involved a discussion of the penetration of electrons into metals and a convenient expression for the range of low energy electrons has been obtained. The theoretical emission of Cu Kα radiation has been compared with some experimental observations on emission at small angles to the target surface, with results which are satisfactory within certain limits. The bearing of these results on the design of x-ray sources, particularly for low-angle diffraction apparatus is discussed.

§ 1. Introduction

The only known relation between the intensity of emission of characteristic x-radiation from a thick target and the energy of the incident electrons is the empirical formula $I \propto (V - V_K)^{1.6}$ where V is the electron accelerating voltage, V_K the critical voltage for excitation of the characteristic radiation and I the intensity of emission. This formula is valid only if V does not exceed $4V_K$ and it was shown experimentally by Webster *et al.* (1933 b) that in the case of silver radiation the law was correct only for emission at large angles to the target surface. At small angles the intensities fell well below those calculated from the empirical formula and showed maxima for optimum voltages depending upon the angle of emission.

In general the intensity of characteristic x-ray emission is a function of the electron acceleration voltage V, the atomic number Z of the target material, and the angle ϕ between the direction of emission and the anode surface. Apart from the intrinsic interest of the problem of determining this function, a knowledge of the dependence of x-ray intensities upon the factors mentioned is of great importance in the design of x-ray diffraction apparatus, particularly in the case of low-angle diffraction equipment where very long exposure times may be involved. Although it has not been possible to obtain an explicit expression for the intensity of emission a method has been devised for the numerical calculation of intensities. These calculations are easily carried out and yield all the necessary information concerning the dependence of intensities on voltages, angles and target materials.

§ 2. Theoretical

2.1. *Introductory*

The problem to be considered is that of calculating the number of quanta of Kα x-rays emitted in a direction making an angle ϕ with the surface of a target of atomic number Z bombarded with electrons accelerated by a potential V_0.

Consider a layer of the target between x and $x+\delta x$ below the surface (figure 1) in which the number of K-shell ionizations produced per electron is δn.

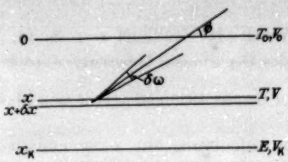

Figure 1.

If, for the moment, it is assumed that each ionization results in the emission of one quantum of radiation, the number of quanta radiated into the small solid angle $\delta\omega$ in the direction making an angle ϕ with the anode surface is $(\delta\omega/4\pi)\delta n$. This radiation traverses a path of length $x\,\mathrm{cosec}\,\phi$ in a material of density ρ and mass absorption coefficient μ and therefore the number of quanta produced between x and $x+\delta x$ emerging in the solid angle $\delta\omega$ is

$$\delta\nu_\phi = \frac{\delta\omega}{4\pi}\delta n \exp\left(-\mu\rho x\,\mathrm{cosec}\,\phi\right).$$

If x_K is the depth of penetration at which the electron energy is reduced to the K-shell excitation energy, then the total number of quanta emerging per electron is

$$\nu_\phi = \frac{\delta\omega}{4\pi}\int_0^{x_K} \exp\left(-\mu\rho x\,\mathrm{cosec}\,\phi\right)\frac{\partial n}{\partial x}\,dx.$$

However, this expression requires modification because the observed intensity of emission of Kα radiation is related to the number of primary ionizations produced, by a factor k which allows for the effects of (*a*) indirect production of Kα quanta by photo-excitation of K-shells by the continuous radiation, (*b*) fluorescence yield, (*c*) ratio of the number of Kα quanta to the total number of K quanta produced, (*d*) electron rediffusion. These effects and the factor k were discussed by Compton and Allison (1935) and more recently by Kirkpatrick and Baez (1947) who gave numerical values for k.

Thus the number of Kα quanta emitted from the target in the direction ϕ for each incident electron is correctly given by

$$\nu_\phi = \frac{\delta\omega}{4\pi}N_\phi \qquad \ldots\ldots(1)$$

where

$$N_\phi = k\int_0^{x_K} \exp\left(-\mu\rho x\,\mathrm{cosec}\,\phi\right)\frac{\partial n}{\partial x}\,dx. \qquad \ldots\ldots(2)$$

Now $\partial n/\partial x = NQ$ where N is the number of atoms per unit volume in the target and Q is the total cross section for K-shell ionization. Q will be discussed in some detail below. Here it is sufficient to note that Q is a function of electron kinetic energy and consequently the evaluation of the integral (2) requires a relation between kinetic energy T and depth of penetration x. This problem is closely connected with the calculation of the range of electrons in the target and this is now taken up.

2.2. *The Penetration of Electrons into the Target*

This discussion is based on Bethe's (1930) non-relativistic expression for electron stopping power which may be written (Mott and Massey 1949)

$$-\frac{\partial T}{\partial x} = \frac{2\pi e^4 NZ}{T} \ln \frac{2T}{J}$$

in which T is the electron kinetic energy at depth x, e the electronic charge, N the number of atoms per unit volume, Z the atomic number of the target, J the mean excitation energy of the target atoms. According to Wilson (1941) $J = 18{\cdot}4 \times 10^{-12} Z$ ergs $= 11{\cdot}5Z$ ev.

This formula was considered adequate for the range of electron energies up to about 80 kev commonly used for the generation of x-rays, and has the advantage that it can be integrated without difficulty.

If T_0 is the kinetic energy of the electrons incident on the target then the relation between kinetic energy and depth of penetration is given by

$$x = \int_{T_*}^{T} \frac{\partial x}{\partial T} dT. \qquad \ldots\ldots(3)$$

This integral may be readily evaluated to give

$$x = \frac{J^2}{8\pi e^4 NZ} [\mathrm{Ei}(2\alpha_0) - \mathrm{Ei}(2\alpha)] \qquad \ldots\ldots(4)$$

where $\alpha_0 = \ln 2T_0/J$, $\alpha = \ln 2T/J$.

If in equation (3) the range of integration is extended from T_0 to zero, x becomes the range R of the electrons in the target. However, this is not permissible, for the expression for stopping power is clearly not valid if $2T < J$, and the function $\mathrm{Ei}(\alpha) \to -\infty$ as $\alpha \to 0$. It is therefore necessary to fix the upper limit of integration in some arbitrary manner. If this is chosen as the value of T for which $\mathrm{Ei}(2\alpha) = 0$ then $T = 0{\cdot}6J$ and the electrons may then be considered to be effectively at the end of their range which is therefore given by

$$R = \frac{J^2}{8\pi e^4 NZ} \mathrm{Ei}(2\alpha_0). \qquad \ldots\ldots(5)$$

Using this formula the ranges of electrons in aluminium and copper have been calculated and compared (figure 2) with the experimental data of Schonland (1925). The theoretical curve follows very closely the trend of the experimental curve but lies above it. This is to be attributed to the measurement of an effective range necessarily slightly less than the true range (Massey 1952), and allowing for this consideration the formula (5) may be said to be very satisfactory for low energy electrons. As a further check of the formula it was used to calculate the ranges of electrons in a photographic emulsion as was done by Zajac and Ross (1949) who integrated numerically the relativistic expression for stopping power. These results are compared in figure 3 and show excellent agreement up to 60 kv beyond which point relativistic effects begin to be apparent.

These considerations make it clear that within the energy range up to 80 kv or so the formula (4) may be used with confidence in the further discussion of our problem.

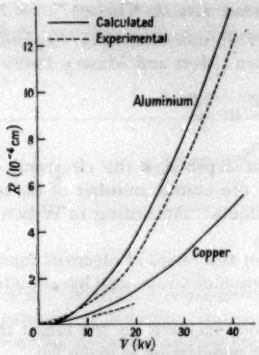

Figure 2. Variation of range R of electrons with voltage for aluminium and copper targets.

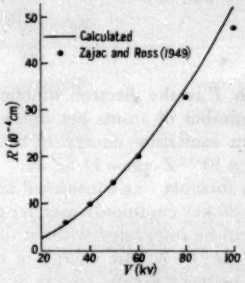

Figure 3. Range R of electrons in Kodak NT4 photographic emulsion.

2.3. *The Cross Section for K-ionization*

Mott and Massey (1949) give a discussion of Bethe's (1930) non-relativistic formula for total ionization cross section. For K-shell ionization this may be written

$$Q = \frac{2\pi e^4}{T|E|} b \ln \frac{4T}{B}$$

where T is the kinetic energy of the incident electron and E the ionization energy of the K shell. b and B are constants which, from comparison with Burhop's (1940) detailed calculations, Mott and Massey conclude should be 0·35 and $1{\cdot}65E$ respectively for K ionization. Using these values and introducing V and V_K the electron accelerating potential and the K-ionization potential respectively, and putting $V/V_K = U$ we find

$$QV_K^2 = 0{\cdot}7\pi e^2 \frac{1}{U} \ln \frac{4U}{1{\cdot}65}.$$

Thus QV_K^2 is the same function of U for all atoms. However, this formula is valid only provided U is sufficiently large, and is seriously in error for the values of U involved in our x-ray emission problem. In particular Q must be zero for $U = 1$, which would be the case if B were taken equal to $4E$. The measured values of Q (Webster *et al.* 1933 a) do in fact agree well with Bethe's formula in the range $U = 1$ to 2 if one puts $B = 4E$. It is therefore proposed to modify the Bethe formula by writing

$$B = [1{\cdot}65 + 2{\cdot}35 \exp(1 - U)]\, E$$

so that $B \to 4E$ as $U \to 1$ while, for large U, $B = 1{\cdot}65E$ as suggested by Mott and Massey. The expression leaves QV_K^2 as the same function of U for all atoms.

In figure 4 the curve shows the values of QV_K^2 calculated from this modified formula compared with the experimental points for silver (dots) and nickel (circles) as given by Kirkpatrick and Baez (1947) and Pockman *et al.* (1947)

respectively. For large U there is a considerable discrepancy between the experimental and theoretical points which is to some extent to be attributed to relativistic effects (Mott and Massey 1949). Thus in the case of silver for which $V_K = 25{\cdot}5$ kv at $U = 4$ an appreciable relativistic effect would be expected. On the other hand

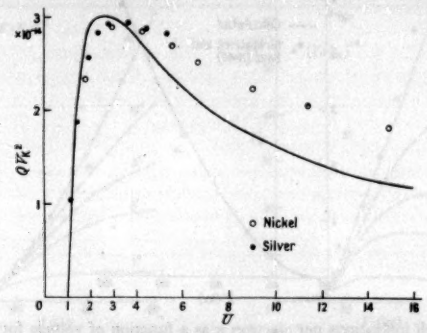

Figure 4. Comparison of the modified formula for the total cross section Q with the experimental values for nickel and silver.

for aluminium $V_K = 1{\cdot}56$ kv so that even for $U = 25$ the electron energy is such that relativistic effects must be small and the theoretical curve should be much more reliable than for elements with larger V_K values.

It was therefore decided that for the evaluation of integrals such as (2), which must necessarily be done numerically, experimental values of Q should be used for heavier elements and the theoretical curve for aluminium. For silver the experimental data are available. Copper and chromium have $V_K = 8{\cdot}98$ and $5{\cdot}99$ kv respectively and, as it was necessary to consider voltages corresponding to values of U up to 8 or so, it was decided to use the experimental values of Q for nickel ($V_K = 8{\cdot}34$ kv) assuming that these would be very close to the figures for copper and chromium. Although there must be some error in adopting this procedure it is believed that it could not be so large as materially to alter the conclusions to be drawn from the calculations.

2.4. *Total Number of K shell Ionizations*

The total number of ionizations produced per electron in a thick target has been calculated by Kirkpatrick and Baez (1947) who evaluated numerically

$$n = -\int_0^{\beta_0} \frac{\partial n}{\partial x}\frac{\partial x}{\partial T}\frac{\partial T}{\partial \beta}\, d\beta$$

in which $\beta = v/\mathbf{c}$, v being the electron velocity, and $\mathbf{c}$ the velocity of light.

These authors used the experimental values of Webster *et al.* (1933 a) and Clark (1935) for $\partial n/\partial x$ and Bethe's stopping power formulae including relativistic corrections for $\partial T/\partial x$. They found very close agreement between their calculated values of total Kα energy radiated per electron and the observed values for silver.

We have calculated the total number of ionizations produced in silver for each incident electron by numerical evaluation of

$$n = \int_0^{x_K} \frac{\partial n}{\partial x}\, dx$$

also using the experimental values for $\partial n/\partial x$, but using our non-relativistic equation (4) to give the relation between x and V. The results of these computations are shown in figure 5 in comparison with those of Kirkpatrick and Baez.

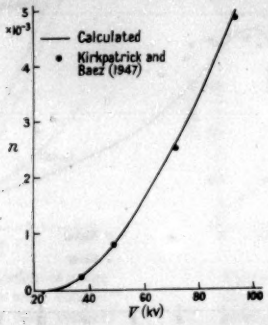

Figure 5. K-shell ionizations per electron n as a function of voltage for a silver target.

Very good agreement between these two calculations up to about 70 kv is apparent, beyond which point the relativistic effects become appreciable. This again gives confidence in the use of equation (4) for electron energies up to about 70 kv.

It may be remarked in passing that if one uses Bethe's non-relativistic expression for Q with $B=4E$, which, as has already been observed, gives reasonable agreement with experimental values of cross section at low energies, the integral

$$n=\int_{T_0}^{E}\frac{\partial n}{\partial x}\frac{\partial x}{\partial T}\,dT$$

can be evaluated in a similar way to that used for the integral of equation (3). The result of this calculation is

$$n=\frac{b}{Z}\left\{U-1+\frac{J}{4E}\ln\frac{2J}{B}\,[Ei(\alpha_0)-Ei(\alpha)]\right\} \qquad \ldots\ldots(6)$$

wherein α is as defined above (equation (4)) and b is chosen to make the experimental and calculated values of Q coincide at $U=3$. This formula could be expected to give reasonable results only for small U (not greater than 4 say) and in the case of silver for U up to 3 the values calculated from this expression agreed very well with those from the more correct numerical integration.

2.5. *The Intensity of Emission of X-Rays*

Returning now to equation (2) the numerical evaluation of the integral for N_ϕ may be considered. This has been carried out for silver, copper, chromium and aluminium targets, in each case for a range of voltages and angles of emission. The values of $\partial n/\partial x$ were taken from experimental results, and in the case of aluminium from a theoretical curve, as has already been discussed. These data give $\partial n/\partial x$ in terms of electron accelerating voltage and for the purposes of evaluating the integral the relation (4) between depth of penetration and electron kinetic energy was used.

The results of these calculations of N_ϕ are shown in figures 6, 7, 8, 9 and will be discussed later.

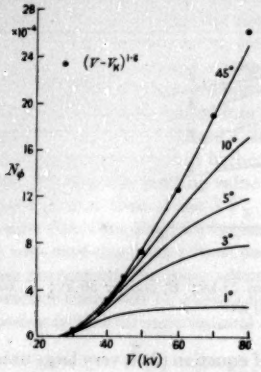

Figure 6. Theoretical x-ray emission for silver.

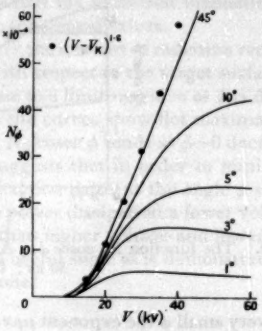

Figure 7. Theoretical x-ray emission for copper.

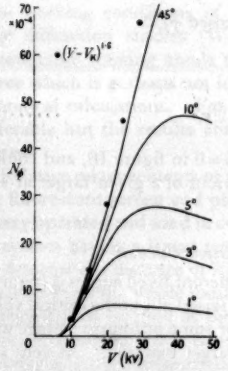

Figure 8. Theoretical x-ray emission for chromium.

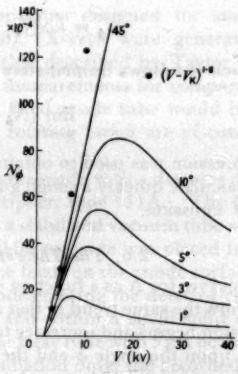

Figure 9. Theoretical x-ray emission for aluminium.

From the practical point of view of using an x-ray source with a collimating system of small angular divergence, it is necessary to take into account that variation of the angle of emission ϕ alters the effective radiating area of the target. Provided that the actual area of the focal spot on the target is always greater than the effective area, as seen by the collimator, and assuming a uniform current density in the electron beam, then the number of quanta radiated into a given collimator

is proportional to N_ϕ cosec ϕ, and this is the significant quantity in the design of diffraction apparatus. This function is shown graphically in figure 10. The limiting value to which it tends as $\phi \to 0$ may be obtained as follows.

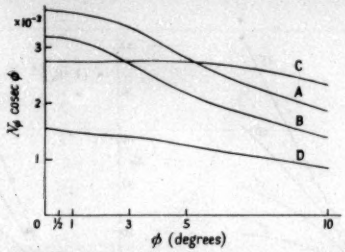

Figure 10. The function N_ϕ cosec ϕ. A, chromium 25 kv; B, copper 30 kv; C, copper 50 kv; D, silver 70 kv.

For very small ϕ the exponent $\mu\rho x$ cosec ϕ of equation (2) is very large unless x is very small. Consequently, under these conditions only a very thin surface layer of the target is effective as a radiator, and within this very small range δx, $\partial n/\partial x$ may be considered to be constant and to have the value NQ_{V_0} corresponding to the incident electron energy. Then,

$$N_\phi = kNQ_{V_0}\int_0^{\delta x} \exp(-\mu\rho x \text{ cosec } \phi)\,dx$$

from which it follows immediately that

$$\lim_{\phi \to 0} (N_\phi \text{ cosec } \phi) = k\frac{N}{\mu\rho}Q_{V_0} \qquad \ldots\ldots(7)$$

This expression was used to obtain the points at $\phi = 0$ in figure 10, and could be used to calculate quickly a rough guide to the behaviour of a given target at small angles of emission.

2.6. *The Theoretical X-Ray Emission Curves*

The curves for N as a function of voltage for different fixed angles ϕ (figures 6, 7, 8, 9) show the same trend in that as the voltage is raised above the critical voltage V_K emission begins and increases to a maximum for some optimum voltage which depends upon the angle ϕ and the nature of the target material. At very small angles this optimum voltage is low, and it increases as the angle increases. At larger angles the emission follows to some extent a $(V - V_K)^{1\cdot6}$ law as is shown in figures 6, 7, 8, 9 where the 45° curves are compared with points calculated from $I \propto (V - V_K)^{1\cdot6}$, the constant of proportionality having been chosen to fit the two curves at 50, 20, 15 and 5 kv in the cases of silver, copper, chromium and aluminium respectively. The agreement between the theoretical and empirical points is good up to about $V = 4V_K$ beyond which the theoretical points fall more and more below those calculated from the empirical equation. At a sufficiently high voltage, whatever the angle, a maximum in the emission curve is to be expected because higher energy electrons produce more x-ray

quanta at greater depths in the target and the loss from self-absorption in the target increases rapidly.

In general, the (N_ϕ, V) curves for silver are in qualitative agreement with the measurements of Webster *et al.* (1933 b) on silver Kα emission. Detailed comparison is difficult because the experimental data are mostly for voltages beyond the range of the above theory, but it seems that the measured intensities fall off less rapidly with increasing voltage than the theoretical values.

The function N_ϕ cosec ϕ which determines the amount of radiation received by a given collimating system as it is rotated with respect to the target surface is one which shows at lower voltages a slow increase to a limiting value as ϕ is decreased to zero (figure 10), while at higher voltages the curves show flat maxima at small angles. Further the limiting value to which N_ϕ cosec ϕ tends as $\phi \to 0$ decreases for voltages greater than about $3\,V_K$. This suggests that in order to minimize the exposure times required for registering diffraction patterns the angle ϕ should be near zero, and that with a fixed permissible power dissipation a lower voltage and higher current may be more advantageous than higher voltage and lower current. In practice there may be a lower limit to the useful angle as is demonstrated in the following section on experimental observations.

§ 3. Experimental

3.1.

The observations on the emission of copper Kα radiation at small angles and for voltages up to 50 kv reported here were made primarily to ascertain the optimum working conditions of a particular apparatus designed for small-angle x-ray diffraction studies (Worthington 1956). X-rays were generated by a demountable rotating anode tube similar to that described by Taylor (1949), a source which is perhaps not ideal for making measurements for comparison with theoretical calculations. For this purpose, a fixed anode tube would have been preferable but the results obtained with the rotating target are of considerable interest.

Relative measurements of x-ray intensity were made with a detector consisting of a fluorescent screen and photoelectric multiplier, type 931A. The latter was battery operated and used in conjunction with a stabilized vacuum tube voltmeter, the system having a linear response. A slit 0·03 cm wide was placed in front of the detector at a distance of 70 cm from the line focus on the anode surface. The radiation from the whole focal area on the anode entering the detector could then be regarded as emitted at the same angle ϕ and within a small solid angle $\delta\omega$. Sufficient intensity was obtained by running the x-ray tube with 5 mA beam current. In order to ensure measurement of the Kα radiation only, the recorded detector reading M was the difference between the two readings obtained with balanced nickel and iron filters respectively. In these circumstances M was proportional to N_ϕ. Intensity readings were obtained for ϕ at 0·5° intervals between 0 and 5° and with voltages in the range from 10 to 50 kv. The mean of a set of five readings was obtained for each set of conditions.

An attempt to estimate the absolute value of the quantity N for Cu Kα radiation was made as follows. Using the small-angle diffraction camera (Worthington 1956) with its axis at 2° to the anode surface, and with the central beam stop removed, the exposure time required to produce a density $D = 1{\cdot}0$

above background on an X-ray film was measured. At 30 kv the required exposure was 0·67 mA seconds using Ilford Industrial G film. Using the known camera dimensions and Seemann's (1950) figures for the number of incident Cu Kα quanta required to produce a similar density on Kodak K film (unfortunately this was not available to us), and assuming that the two kinds of film were equally sensitive, an experimental value for $N(\phi=2°)$ was obtained.

3.2. *Results*

The variation of emission with voltage at various angles is shown in figure 11 in which $M \propto N_\phi$ is plotted as a function of V the accelerating voltage, for values of ϕ of 1°, 3° and 5°. The dotted curve in this figure represents an $I \propto (V - V_K)^{1\cdot6}$ relation with the scale adjusted to match the $\phi = 5°$ experimental curve at a suitable point. In both figures 11 and 12 the emission is plotted on an arbitrary scale.

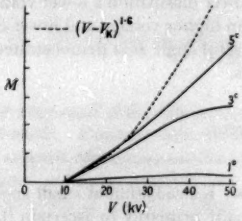

Figure 11. Experimental X-ray emission from copper.

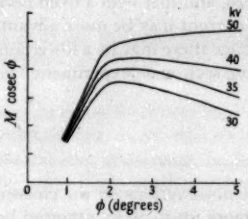

Figure 12. Radiation M cosec ϕ received by the collimator from the copper anode as a function of angle ϕ.

With $\phi = 1°$ there is a pronounced optimum voltage. At $\phi = 3°$ this is less marked, while at $\phi = 5°$ the curve shows a steady increase of emission up to 50 kv, the highest voltage used.

Figure 12 shows the variation of M cosec $\phi \propto N_\phi$ cosec ϕ with ϕ for several fixed voltages. Except in the case of the curve for 50 kv the radiation entering the collimator increases as ϕ decreases until at about 2° the curves turn over sharply and drop away to zero, thus making $\phi = 2°$ the optimum angle of emission for this particular apparatus.

As to the absolute values of emission, the experimental value of N_ϕ for $\phi = 2°$ was 5×10^{-4} quanta per electron and the calculated value 10×10^{-4} quanta per electron. The agreement here is probably as good as could reasonably be expected in view of the nature of the measurement.

3.3. *Comparison of Theoretical and Experimental Results*

It has already been remarked that the experimental data of Webster *et al.* (1933 b) for Kα radiation are in good qualitative agreement with the theoretical calculations of this paper. Very much the same sort of relation exists between the experimental data for Cu Kα radiation and the theoretical results. Thus the experimental curves for copper follow a similar trend to the theoretical curves but as the voltage is increased the experimental values for emission continue to rise

after the theoretical curves have reached maxima and turned over towards the V axis. This effect is more pronounced at larger angles ϕ. For $\phi = 1°$ the experimental curve has just reached a very flat maximum at 50 kv, while for $\phi = 3$ and 5°, no maxima appeared within the range of voltages investigated, whereas theoretically an optimum voltage of less than 60 kv occurs up to $\phi = 5°$, this optimum being only about 28 kv at $\phi = 1°$. The experimental optimum voltages were apparently considerably higher than the theoretical and were outside the range of our measurements.

The experimental values of M cosec ϕ of figure 12 which are to be compared with the theoretical curves for N_ϕ cosec ϕ of figure 10 also show qualitative agreement at larger angles than $\phi = 2°$. The rapid drop in the experimental values below this point must be attributed to imperfections of the anode surface, which although it was well polished, must have had irregularities comparable with the depths of penetration of the electrons. At lower voltages decrease in ϕ results in a steady increase of emission while at higher voltages maxima appear in the theoretical curves as in the 50 kv curve for copper (figure 10). The experimental curve for 50 kv shows an increase of emission as ϕ is increased above 2° indicating an optimum angle ϕ greater than 5° in accord with the fact that the observed values for N_ϕ continue to rise after the theoretical curves have reached a maximum.

Bear and Bolduan (1949) have reported some measurements of a quantity B equivalent to our N_ϕ cosec ϕ. Using a copper target, but unspecified voltage, they found B to increase as ϕ decreased to about 0·5° at which point a maximum appeared in the curve. They concluded that for ϕ greater than 1°, B was proportional to cosec ϕ, i.e. that the target radiated uniformly in all directions. While they conceded that this statement could not be rigorously true, it is clear from our theoretical calculations and experimental measurements that the variation of N_ϕ with ϕ is much more rapid than the results of Bear and Bolduan suggested.

§ 4. Conclusions

Although experimental data with which to compare our theoretical calculations are meagre it seems clear that the theoretical approach adopted here leads to qualitatively satisfactory results. The theoretical curves appear to be of the correct form, but the optimum voltages are much less than those found experimentally. This suggests that more x-ray quanta are emitted closer to the surface of the target than the calculations allow. In the first instance the (x, V) relation (equation (4)) might be suspect and thought to overestimate x, but recalculation of the copper N_ϕ curves with the x's reduced arbitrarily by 15% resulted in changes of only a few per cent in the values of N_ϕ. It is therefore more likely that the discrepancy arises through the assumption that the electrons follow straight line paths in the metal undeviated from the direction of incidence. Electron scattering within the metal must of course occur and is apparently an important factor in determining the intensity of x-ray emission.

In spite of the lack of complete agreement between the theoretical and experimental findings the former are nevertheless of some value in considering the choice of an x-ray source for use with diffraction equipment, especially for low-angle diffraction apparatus. Thus it is clear that x-ray tubes should be constructed so that emission at very small angles to the target surface can be used, a point already made by Bear and Bolduan (1949). However, it appears that the optimum angle ϕ also depends upon voltage and may be larger at higher voltages. The

best operating voltage may, in turn, be determined by consideration of permissible power dissipation. Thus both the experimental and theoretical curves for copper (figures 10 and 12) indicate that with $\phi = 2°$ operation at 30 kv is more efficient than at 50 kv and moderate voltages are to be preferred. A final point concerns the choice of target material for low-angle diffraction purposes. Practical experience has shown that there is little to choose between copper and chromium targets in studying the low-angle diffraction patterns of collagen, but attention may be drawn to the relatively high emission from aluminium, which with the much longer wavelength of Al Kα radiation suggests that this may offer considerable advantages as a source for use with a suitably designed diffraction camera.

Acknowledgments

One of us (C.R.W.) wishes to acknowledge the award of a University of Adelaide Post-graduate Studentship, and later of a Commonwealth Scientific and Industrial Research Organisation Australian Studentship 1953–1954.

References

Bear, R. S., and Bolduan, O. E. A., 1949, *J. Appl. Phys.*, **20**, 983.
Bethe, H. A., 1940, *Ann. Phys., Lpz.*, **5**, 325.
Burhop, E. H. S., 1940, *Proc. Camb. Phil. Soc.*, **36**, 43.
Clark, J. C., 1935, *Phys. Rev.*, **48**, 30.
Compton, A. H., and Allison, S. K., 1935, *X-Rays in Theory and Experiment* (New York: Van Nostrand).
Kirkpatrick, P., and Baez, A. V., 1947, *Phys. Rev.*, **71**, 521.
Massey, H. S. W., 1952, *Advanc. Electron.*, **4**, 56.
Mott, N. F., and Massey, H. S. W., 1949, *The Theory of Atomic Collisions* (Oxford: Clarendon Press).
Pockman, L. T., Webster, D. L., Kirkpatrick, P., and Harworth, K., 1947, *Phys. Rev.*, **71**, 330.
Schonland, B. F. J., 1925, *Proc. Roy. Soc.* A, **108**, 187.
Seemann, H. E., 1950, *Rev. Sci. Instrum.*, **21**, 314.
Taylor, A., 1949, *J. Sci. Instrum.*, **26**, 226.
Webster, D. L., Hansen, W. W., and Duveneck, F. B., 1933 a, *Phys. Rev.*, **43**, 839; 1933 b, *Ibid.*, **44**, 258.
Wilson, R., 1941, *Phys. Rev.*, **60**, 749.
Worthington, C. R., 1956, *J. Sci. Instrum.*, **33**, 66.
Zajac, B., and Ross, M., 1949, *Nature, Lond.*, **164**, 311.

RESEARCH NOTES

Time Delays in Boron Trifluoride Proportional Counters

By K. P. NICHOLSON
Atomic Energy Research Establishment, Harwell, Berks.

MS. received 17*th January* 1956

In applying boron trifluoride proportional counters to neutron time-of-flight measurements, attention should be paid to the delay between neutron capture and the production of an electrical pulse by the counter. This delay represents the drift time of the ionization electrons, formed by the products of the $^{10}B(n, \alpha)^{7}Li$ reaction, from the region of the disintegration to the anode wire of the counter.

For a counter of cylindrical geometry the magnitude of the delay will be a function of the radial position of neutron capture in the sensitive volume. It may be assumed in most practical cases that the number of capture processes per unit volume is constant and that the α-particle track length is small compared with the outside diameter of the counter. Then if the mobility of electrons in BF_3 is constant over the range of electric field existing in the counter, it follows that the predicted frequency distribution of counter pulses as a function of delay is rectangular and has a full width T given by

$$T = \frac{Pb^2 \ln (b/a)}{2kV}.$$

In this expression T is in seconds when a is the anode (wire) radius in cm, b the outside radius in cm, P the BF_3 pressure in cm Hg, V the applied potential in volts and k the mobility of electrons in BF_3 in units of $cm^2 sec^{-1} v^{-1}$ (cm Hg).

An experiment was performed using a number of different BF_3 counters to check the validity of these simplified conclusions. The time of neutron capture was fixed by the 0·478 Mev capture gamma ray which is emitted almost instantaneously for 93·5% of the $^{10}B(n, \alpha)^{7}Li$ reactions (Duren and Rosenwasser 1954). The gamma was detected with a NaI(Tl) scintillation counter, in which there is no appreciable delay. The electron drift times were then measured by a delayed coincidence method, details of which may be obtained elsewhere (Nicholson 1955). The frequency distribution of counter pulses as a function of delay for a proportional counter of outside diameter 2 in., wire diameter 0·004 in., BF_3 pressure 70 cm Hg operated at 4000 volts is shown as a full line in figure 1. The resolution function of the coincidence unit was rectangular and 0·4 μsec wide. Other timing errors were principally random and were estimated to total $\pm 0{\cdot}1$ μsec, so that the overall resolution function will have a base width of approximately 0·6 μsec. The finite resolution width means that some coincidences will be observed when the delays are reversed, i.e. the BF_3 counter delayed with respect to the scintillation detector. This is interpreted in the figure as a negative delay. At either end of the distribution the coincidence rate drops to a minimum value corresponding to the random coincidence rate of the equipment. The observed

shape corresponds closely to that calculated from the overall resolution function and a rectangular delay distribution of full width 2·8 μsec and is thus in agreement with the predictions made above. In neutron timing measurements this particular counter will introduce a zero shift of 1·4 μsec together with an uncertainty of $\pm$ 1·4 μsec.

An additional seven BF_3 counters were selected and tested in order to vary all the parameters in the expression for T at least once. These data were then used to derive a value of k for each test. It was found that values of k from all the tests agreed within the experimental errors and gave a mean value of $(1{\cdot}19 \pm 0{\cdot}06) \times 10^5\,\mathrm{cm^2\,sec^{-1}\,v^{-1}}$ (cm Hg). This value is in good agreement with the ionization chamber results of Bistline (1948) and of Bracci and Zimmer (1953). This mean value includes measurements on 1 in. diameter counters of 40 and 70 cm pressure during which the width of the resolution function was reduced to 0·2 μsec. For this diameter the assumption concerning α-particle track length can hardly be justified and in practice the delay distributions lost their pronounced rectangular shape. However, the values of the mobility k based on the full width at half height of the distribution were in good agreement with those obtained from the larger counters.

The effect of BF_3 purity on the delay distribution can be deduced from the work of Bracci and Zimmer (1953). They found no significant change in the mobility of electrons in a sample of BF_3 which had been purified once, twice and three times, so that the width of the distribution should be independent of small amounts of impurities. On the other hand an impure filling will result in reduced electron survival probabilities causing a loss in output pulse amplitude, particularly for those pulses corresponding to the longer drift times. A rectangular delay distribution will be obtained only when these attenuated pulses are included.

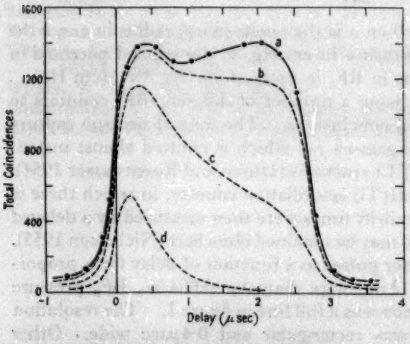

Figure 1. Experimental delay distribution for a 2 in. diameter counter of wire diameter 0·004 in., BF_3 pressure 70 cm, operated at 4000 volts.

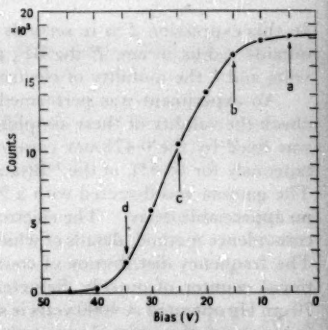

Figure 2. Bias curve of counter used in figure 1 showing discriminator levels used for the series of delay distributions.

For high pressure counters, even with a pure gas, the electron survival probabilities are again small, making it desirable in practice to reject the small neutron pulses in order to discriminate against gamma background. The broken

lines of figure 1 show the change in the delay distribution produced by increasing the discriminator level to the values indicated on the counter bias curve in figure 2. It is evident that the distribution becomes narrower with increase in discriminator level due to exclusion of events from the outer regions of the sensitive volume.

ACKNOWLEDGMENTS

In conclusion the author wishes to thank Mr. P. G. Salmon for providing the counters used in this experiment and Dr. P. A. Egelstaff for his valuable advice and encouragement.

REFERENCES

BISTLINE, J. A., 1948, *Rev. Sci. Instrum.*, **19**, 842.
BRACCI, A., and ZIMMER, E. L., 1953, *Nuovo Cim.*, **10**, 103.
DUREN, J. A., and ROSENWASSER, H., 1954, *Phys. Rev.*, **93**, 831.
NICHOLSON, K. P., 1955, *Atomic Energy Research Establishment Report* N/R. 1639.

Precision Wavelength and Energy Measurements of Gamma Rays from ^{152}Eu, ^{154}Eu, ^{153}Sm and ^{165}Dy

BY B. ANDERSSON

Department of Physics, Chalmers University of Technology, Göteborg, Sweden

MS. received 9th December 1955

§ 1. INTRODUCTION

A RECENT paper by Ryde and Andersson (1955) describes a precision curved crystal gamma-ray spectrometer constructed at the Chalmers University of Technology in Göteborg. This instrument has now been used to study the gamma radiation from europium, samarium and dysprosium. The γ-ray spectrum was studied by moving the source along the focal circle with a precision screw and plotting the γ-ray intensity reflected by the (310)-planes of the quartz crystal ($d = 1177{\cdot}63$ X.U. at 18°C) as a function of the screw settings. The γ-ray intensity was measured with a scintillation counter with a NaI (Tl activated) crystal. With the spectrometer in zero position the differential pulse-height spectrum for different samples was investigated. The spectrometer range has been enlarged so as to make measurements possible down to 0·04 MEV. The new screw is 70 cm long with a pitch of 0·5 mm. The angle arms have been made longer.

§ 2. MEASUREMENTS

Gold ^{198}Au

The 0·412 MEV radiation from ^{198}Au was used as reference line. Five runs were made for the line profiles of the first order on each side of zero wavelength position with the new arrangement. The difference between the spectrometer settings for the ^{198}Au MEV line on opposite sides of the zero wavelength position was found to be $6{\cdot}1925 \pm 0{\cdot}0012$ cm. The gold sample was activated in the BEPO pile at Harwell.

Europium ^{152}Eu *and* ^{154}Eu

Natural europium has two isotopes, ^{151}Eu (47·77%) and ^{153}Eu (52·23%), which transform to ^{152}Eu and ^{154}Eu by means of an (n, γ) reaction, when activated

in a pile. ^{152}Eu has one half-life of 12 years and another of 9·2 hours, and ^{154}Eu has a half-life of 13 years.

The source, Eu_2O_3, activated in the BEPO pile, had a weight of 0·173 g and filled up two sections of the source holder, having an initial activity of 188 mC, when the 9·2 hours activity had disappeared. The three strongest γ-ray lines from ^{152}Eu and one from ^{154}Eu were measured. We made five runs for the 0·122 MeV line, three runs for the 0·244 MeV line, four runs for the 0·344 MeV line from ^{152}Eu and six runs for the 0·123 MeV line from ^{154}Eu. It was not possible to separate the 0·122 MeV and 0·123 MeV lines in the differential pulse-height spectrum of gamma radiation from europium (figure 1). Figure 2 shows the

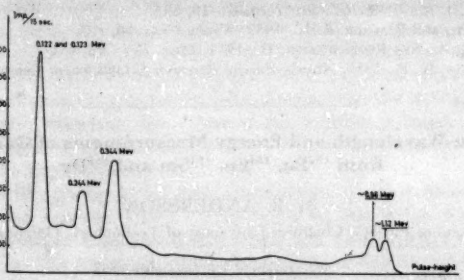

Figure 1. Differential pulse-height spectrum of gamma radiation from europium.

profiles of 0·122 MeV and 0·123 MeV γ-ray lines of the first order by selective reflection to the right from the (310)-planes of quartz. The intensity of the 0·122 MeV line is about five times greater than that of the 0·123 line. The results of the measurements are given in table 1 together with some earlier measurements. The errors are the maximum deviations from the mean values.

Table 1

	Present Measurements		Earlier Measurements of Energy (MeV)		
Isotope	Wavelength (mÅ)	Energy (MeV)	LK	CG	C
^{152}Eu	101·35 ±0·03	0·12231±0·00004	0·1212±0·0003	0·1218	0·1220
	50·672±0·017	0·24464±0·00008	0·2436±0·0007	0·2443	0·2443
	36·000±0·023	0·34434±0·00023	0·3442±0·0010		0·3438
^{154}Eu	100·34 ±0·07	0·12354±0·00009	0·1224±0·0003	0·1234	0·1232

LK = Lee and Katz 1954; CG = Church and Goldhaber 1954; C = Cork *et al.* 1950.

Samarium ^{153}Sm

The gamma radiation from 47-hour ^{153}Sm has been investigated with a sample, containing 0·562 g Sm_2O_3. The sample was activated in the pile in Stockholm, where the spectrometer is placed now. Sm_2O_3 was enclosed in three sections of the source holder. Figure 3 shows the differential pulse-height spectrum of gamma radiation from samarium. The 0·04 MeV peak has its origin from the Eu Kα lines of energies 0·0416 and 0·0410 MeV. The 0·103 MeV γ-ray line is the strongest one; the 0·07 MeV γ-ray line is much weaker. The intensity ratio is about 10:1. Precision wavelength and energy measurements

could only be performed for the 0·103 MeV line. The mean of four runs for the strong ^{153}Sm γ-ray line gave the wavelength 120·039 ± 0·023 mÅ and the energy 0·10327 ± 0·00002 MeV. In table 2 the present and some earlier measurements are given.

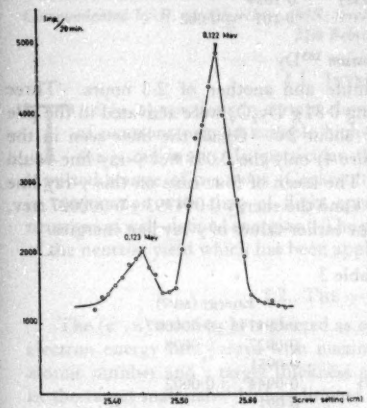

Figure 2. The profiles of 0·122 MeV and 0·123 MeV lines by reflection to right from the (310)-planes of quartz.

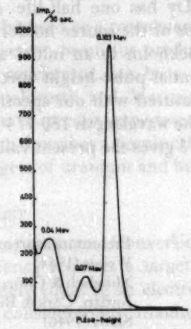

Figure 3. Differential pulse-height spectrum of gamma radiation from samarium.

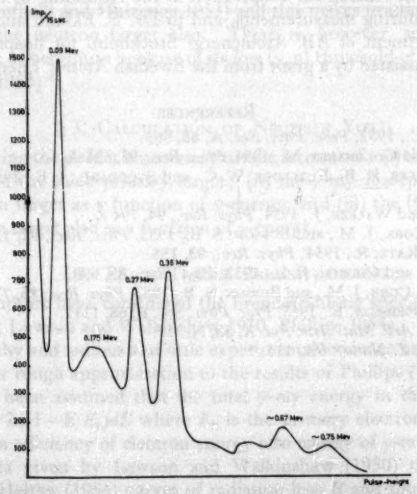

Figure 4. Differential pulse-height spectrum of gamma radiation from dysprosium.

Table 2

	Energy (MeV)
Present measurement	0·10327±0·00002
Graham & Walker (1954)	0·1025 ±0·0005
Lee & Katz (1954)	0·1027 ±0·0003
Rutledge, Cork & Burson (1952)	0·1034
Bannerman (1952)	0·101 ±0·002

Dysprosium ^{165}Dy

^{165}Dy has one half-life of 1·2 minute and another of 2·3 hours. Three sections of the source holder, containing 0·81 g Dy_2O_3 were activated in the pile in Stockholm to an initial activity of about 2 c. Of all the lines seen in the differential pulse-height spectrum (figure 4) only the 0·095 MeV γ-ray line could be measured with our spectrometer. The mean of four runs on this γ-ray line gave the wavelength 130·774 ± 0·010 m Å and the energy 0·094793 ± 0·000007 MeV. Table 3 gives the present value and some earlier values of γ-ray line energies.

Table 3

	Energy (MeV)
Present measurement	0·094793±0·000007
Weber (1954)	0·0927 ±0·0008
Mihelich & Church (1952)	0·0951
Jordan, Cork & Burson (1953)	0·0944 ±0·0002
Slätis (1946)	0·091

ACKNOWLEDGMENTS

It is a pleasure to express my gratitude to Professor N. Ryde for help and advice, to Mr. S. Nilsson for cooperation in the rebuilding of the spectrometer and assistance during measurements, and to Dr. S. Eklund and his staff at the Physical Department of AB. Atomenergi Stockholm for hospitality and help. The work was assisted by a grant from the Swedish Atomic Energy Commission.

REFERENCES

BANNERMAN, R. C., 1952, *Proc. Phys. Soc.* A, **65,** 565.
CHURCH, E. L., and GOLDHABER, M., 1954, *Phys. Rev.*, **95,** 626 A.
CORK, J. M., KELLER, H. B., RUTLEDGE, W. C., and STODDARD, A. E., 1950, *Phys. Rev.*, **77** 848.
GRAHAM, R. L., and WALKER, J., 1954, *Phys. Rev.*, **94,** 794 A.
JORDAN, W. C., CORK, J. M., and BURSON, S. B., 1953, *Phys. Rev.*, **92,** 1218.
LEE, M. R., and KATZ, R., 1954, *Phys. Rev.*, **93,** 155.
MIHELICH, J. W., and CHURCH, E. L., 1952, *Phys. Rev.*, **85,** 690.
RUTLEDGE, W. C., CORK, J. M., and BURSON, S. B., 1952, *Phys. Rev.*, **86,** 775.
RYDE, N., and ANDERSSON, B., 1955, *Proc. Phys. Soc.* B, **68,** 1117.
SLÄTIS, H., 1946, *Ark. Mat. Astr. Fys.* A, **33,** Nr. 17.
WEBER, G., 1954, *Z. Naturf.* **9A,** 115.

Neutron Production by Electrons in Uranium and Uranium–Beryllium

By A. W. AIKIN
Research Department, Metropolitan-Vickers Electrical Co. Ltd., Manchester

Communicated by B. G. Churcher; MS. received 15th November 1955, and in revised form 21st February 1956

§ 1. Introduction

The (γ, n) reactions in certain elements may be used as a convenient source of neutrons using a suitable high-energy electron beam for production of the γ-radiation. In particular the linear accelerator has been used as a pulsed source of neutrons (Cockcroft 1949, Duckworth and Merrison 1949) in conjunction with time of flight spectrometers to permit experiments with neutrons of well-defined energies. The present note describes a simple calculation of the neutron yield which has been applied to targets of uranium and beryllium.

§ 2. The γ-ray Target

The (e^-, n) reaction is neglected as of minor importance. Conversion of the electron energy into γ-rays with maximum efficiency requires a target of high atomic number and a target thickness approximately equal to an electron range in the target material. Unless limited by other considerations, uranium is the best material for this purpose.

Except for elements of low atomic number, the (γ, n) cross section increases rapidly (Price and Kerst 1950) and the (γ, n) threshold decreases, with increasing A. In addition, for uranium the $(\gamma, \text{fission})$ yield becomes comparable with the (γ, n) yield (Duffield and Huizenga 1953) and this makes uranium a very suitable material for the neutron target also. There is, however, some interest in a neutron target of beryllium because of its low (γ, n) threshold of 1·6 MeV (Nathans and Halpern 1953).

§ 3. Calculation of Neutron Yield

In calculating the yield it is necessary to take account of: (i) the bremsstrahlung spectrum from the thick primary target; (ii) the γ-ray absorption cross section in the neutron target as a function of γ-energy, and (iii) the $(\gamma$–n) cross section in the neutron target also as a function of γ-energy.

§ 4. Thick Target Bremsstrahlung

Various authors have considered the bremsstrahlung spectra of thick targets (Wilson 1953, Lawson and Walkinshaw 1950, Phillips 1954). Accurate calculations are lengthy and tedious and little experimental evidence has been published.

As a rather rough approximation to the results of Phillips (1954) and Wilson (1953) it has been assumed that the total γ-ray energy in the energy interval $(E, E+dE)$ is $2\eta(1-E/E_0)dE$ where E_0 is the primary electron energy and η is the conversion efficiency of electron energy into energy of γ-radiation.

Using data given by Lawson and Walkinshaw (1950) the Z-dependence indicated by Heitler (1954) curves of radiation loss R and total loss T (by both radiation and collision) were derived as a function of electron energy for a uranium

target. The conversion efficiency was then derived by numerical integration (figure 1) using the formula

$$\eta = \frac{1}{E_0}\int_0^{E_0} \frac{R}{T}\, dE.$$

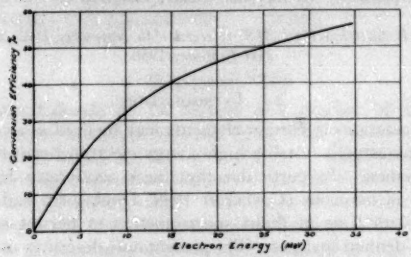

Figure 1. γ-ray conversion efficiency η for uranium.

§ 5. Neutron Yield

Allowance must be made for the differential absorption of γ-rays of different energies in the neutron target. Disregarding any contribution from scattered photons, the probability that absorption of a γ-ray in the energy range $(E, E+dE)$ results in the production of a neutron is $N\sigma(E)/\mu(E)$ where N is the number of atoms per unit cube, $\sigma(E)$ the cross section for neutron production by γ-rays of energy E and $\mu(E)$ the corresponding absorption coefficient. Since there are $(2\eta/E)(1-E/E_0)dE$ quanta in the range $(E, E+dE)$, and assuming complete γ-ray absorption, the total number of neutrons produced per incident electron is

$$\int_0^{E_0} \frac{2\eta}{E}\,\frac{(1-E/E_0)N\sigma(E)dE}{\mu(E)}. \qquad \ldots\ldots(1)$$

§ 6. The γ-Absorption Cross Section μ(E)

The processes by which a γ-ray loses energy are well known (Heitler 1954). The known formulae of Z-dependence of the Compton effect and pair production cross sections enable accurate calculation of $\mu(E)$ in the region above 5 MeV, i.e. above the threshold for neutron production. The analysis takes no account of degraded γ-rays produced by Compton scattering, but in the energy region considered the Compton cross section is small compared with that for pair production and in any case the majority of scattered quanta are of relatively low energy, below the (γ, n) threshold. Also neglected are any neutrons produced by bremsstrahlung of pair electrons or positrons, since these will also be of rather low energy.

For beryllium the major process is Compton scattering and there will be some contribution from scattered quanta not given by the treatment used. However, the majority of scattered quanta are of low energy. For example, only 25% of scattered 25 MeV quanta have energies above 8 MeV and the proportion at lower energies is much smaller. Since in any case the number of high energy quanta is small, and in view of the shape of the (γ, n) cross section curve it seems unlikely that the secondary quanta will contribute more than an additional few per cent of neutrons.

§ 7. Cross Sections for Neutron Production $\sigma(E)$

Cross sections for neutron production by γ-rays in uranium have been measured by various authors (Price and Kerst 1950, Montalbetti *et al.* 1953, Duffield and Huizenga 1953, Nathans and Halpern 1954, Goward *et al.* 1951, Terwilliger 1952). Although there are differences in derivation, the integrated cross sections are in reasonable agreement, except for that given by Goward *et al.* (1951).

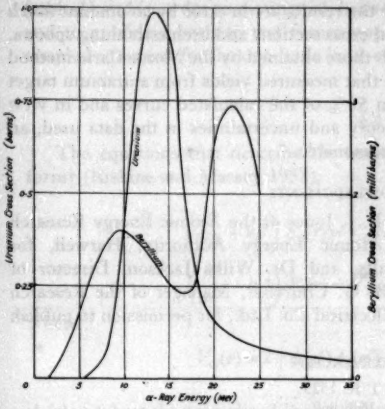

Figure 2. (γ, n) cross sections for uranium and beryllium.
(Note—α-ray in abscissa should read γ-ray)

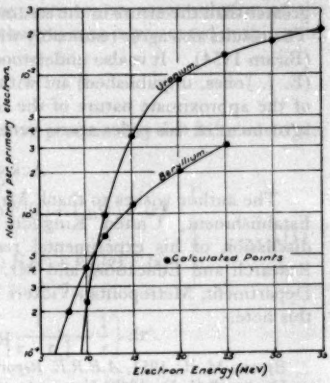

Figure 3. Neutron yields from uranium and beryllium (theoretical 100% γ-absorption).

Fortunately the total yield is not very sensitive to the shape of the yield curve provided that the integrated cross section is not in error. We have therefore taken the curve of Nathans and Halpern (1954), but have modified and extended the high energy tail in the light of other work (Terwilliger 1952) since it now seems well established that the cross section does not in fact drop to zero at about 24 Mev. The cross section curve used for beryllium is that derived by Nathans and Halpern (1953). Figure 2 shows the curves used in the calculations.

§ 8. Calculation of Neutron Yield

The yield given by equation (1) has been calculated by numerical integration for electron energies in the range 10–35 Mev for a uranium target and 5–25 Mev for a beryllium neutron target following a uranium γ target (figure 3). It is seen that for energies up to 11·5 Mev a beryllium (γ, n) target is preferred. At higher energies a uranium target is better and yields of the order of one neutron per 100 primary electrons are possible with electron energies about 20 Mev. Although higher yields are possible at higher energies, above 25 Mev no great advantage is gained since the yield for a given beam power rises very slowly above this energy.

§ 9. Conclusions

It should be emphasized that these calculations are based on rather simplified assumptions of the processes involved. The formula for thick target bremsstrahlung inevitably represents a compromise erring on the side of simplicity. It has been assumed that all the γ-rays are absorbed in the target and no allowance is made for neutrons absorbed in the target or for neutrons produced by fast fission. The form of the yield curve should be substantially correct however, and there is no reason to believe that the results are in error by an amount much greater than the errors in the assumed cross sections and bremsstrahlung spectra. The results also agree reasonably with those obtained by the Monte Carlo method (Biram 1954). It is also understood that measured yields from a uranium target (E. J. Jones, unpublished) are within 50% of the calculated curves and in view of the approximate nature of the theory and uncertainties in the data used, an agreement of this order seems very reasonable.

Acknowledgments

The author wishes to thank Mr. E. J. Jones of the Atomic Energy Research Establishment, United Kingdom Atomic Energy Authority, Harwell, for discussion of his experimental results, and Dr. Willis Jackson, Director of Research and Education, and Mr. B. G. Churcher, Manager of the Research Department, Metropolitan-Vickers Electrical Co. Ltd., for permission to publish this note.

References

Biram, M. B., 1954, *A.E.R.E. Report* T/R. 1523.
Cockroft, J. D., 1949, *Nature, Lond.*, **163,** 869.
Duckworth, J. C., and Merrison, A. W., 1949, *Nature, Lond.*, **163,** 869.
Duffield, R. B., and Huizenga, J. R., 1953, *Phys. Rev.*, **89,** 1042.
Goward, F. K., *et al.*, 1951, *Proc. Phys. Soc.* A, **64,** 95.
Heitler, W., 1954, *The Quantum Theory of Radiation* (Oxford : University Press).
Lawson, J. D., and Walkinshaw, W., 1950, *A.E.R.E. Report* G/M. 60.
Montalbetti, R., Katz, L., and Goldenberg, J., 1953, *Phys. Rev.*, **89,** 659.
Nathans, R., and Halpern, J., 1953, *Phys. Rev.*, **92,** 940; 1954, *Ibid.*, **93,** 437.
Phillips, K., 1954, *Proc. Phys. Soc.* A, **67,** 669.
Price, G. A., and Kerst, D. W., 1950, *Phys. Rev.*, **77,** 806.
Terwilliger, K. M., 1952, University of California, *U.C.R.L.* 1917.
Wilson, R., 1953, *Proc. Phys. Soc.* A, **66,** 638.

The 1s–2s Excitation of Hydrogen by Electron Impact

By B. H. Bransden† and J. S. C. McKee‡
†University of Glasgow. ‡Queen's University of Belfast

MS. received 3rd February 1956

§ 1

The calculation of cross sections for the excitation of atoms by electron impact, at incident energies close to the threshold, is complicated by the failure of Born's approximation (Bates, Fundaminsky, Leach and Massey 1950), and in the case of 1s–2s excitation of atomic hydrogen Erskine and Massey (1952) have obtained improved zero angular momentum partial cross sections by

the distorted wave (DW) method, making full allowance for exchange. For this approximation to be applicable, it is necessary for the reaction of the inelastically scattered waves on the elastically scattered waves to be small. Massey and Moiseiwitsch (1953) have obtained approximate solutions to the problem including reactive effects, employing a variational method (Moiseiwitsch 1951), which suggest that this condition is not satisfied. The considerable differences between the DW and variational solutions persist even when exchange is neglected (table 1) and in order to distinguish between the predictions of the two methods and to provide a basis to test future approximations, an exact solution of the coupled equations for the one-body (non-exchange) case is presented in this note.

§2

The equations that describe the excitation process may be reduced to the form† (Erskine and Massey 1952),

$$\left.\begin{aligned}\left(\frac{d^2}{dr^2}+k_0^2\right)F_0(r)&=V_{00}(r)\,F_0(r)+V_{01}(r)\,F_1(r)\\ \left(\frac{d^2}{dr^2}+k_1^2\right)F_1(r)&=V_{10}(r)\,F_0(r)+V_{11}(r)\,F_1(r)\end{aligned}\right\}\quad\ldots\ldots(1)$$

where

$$V_{ij}(r)=2\int\phi_i(r')\,\phi_j(r')\left\{\frac{1}{|\mathbf{r}-\mathbf{r}'|}-\frac{1}{r}\right\}d\mathbf{r}'$$

$\phi_0(r)$, $\phi_1(r)$ are the normalized 1s and 2s hydrogen wave functions, k_0^2 is the kinetic energy of the incident electron and k_1^2 that of the inelastically scattered electron. In the variational method of Moiseiwitsch (1951) all terms in equations (1) are retained but the DW method neglects V_{01} and Born's approximation also neglects V_{00} and V_{11}.

In obtaining numerical solutions of (1) it is desirable to work with real functions, so that two independent solutions ($F_0^i(r)$, $F_1^i(r)$; $i=1,\ 2$) are chosen satisfying boundary conditions

$$F_0^i(0)=F_1^i(0)=0,$$

$$F_0^i(r)\sim A^i\sin k_0r+B^i\cos k_0r,\qquad F_1^i(r)\sim C^i\sin k_1r+D^i\cos k_1r.\quad\ldots(2)$$

The coupled equations (1) are conveniently integrated using an extension of a method proposed by Fox and Goodwin (1949) for solutions of equations of the type $y''=f(x)y$, and by choosing a suitable interval the need for iteration can be generally removed. To start the integration a few values of $F_j^i(r)$ are calculated from a series expansion, independent solutions being specified by fixing the values of $F_j^{i\prime}(0)$, (a satisfactory choice proved to be $F_0^{1\prime}(0)=F_0^{2\prime}(0)=F_1^{1\prime}(0)=1$, $F_1^{2\prime}(0)=2$).

To describe the 1s–2s excitation process solutions are required with boundary conditions

$$\left.\begin{aligned}F_0^3(r)&\sim\sin k_0r+a\cos k_0r\\ F_1^3(r)&\sim d\exp(ik_1r)\end{aligned}\right\}\quad\ldots\ldots(3)$$

† Atomic units are employed throughout.

in which case the partial cross sections for zero angular momentum for elastic scattering by the ground state Q_{1s-1s} and excitation Q_{1s-2s} are (in units of πa_0^2)

$$\left.\begin{aligned} Q_{1s-1s} &= \frac{4}{k_0^2}\left|\frac{a}{1-ia}\right|^2 \\ Q_{1s-2s} &= \frac{4k_1}{k_0^3}\left|\frac{d}{1-ia}\right|^2. \end{aligned}\right\} \qquad \ldots\ldots(4)$$

To find a, d a suitable linear combination of the independent solutions must be formed, giving

$$\lambda \begin{bmatrix} A^1 \\ B^1 \\ C^1 \\ D^1 \end{bmatrix} + \mu \begin{bmatrix} A^2 \\ B^2 \\ C^2 \\ D^2 \end{bmatrix} = \begin{bmatrix} 1 \\ a \\ id \\ d \end{bmatrix}$$

Similarly by forming a solution $F_0^4(r)$, $F_1^4(r)$, so that $F_0^4(r) \sim g\exp(ik_0 r)$, $F_1^4(r) \sim \sin k_1 r + h\cos k_1 r$, Q_{2s-2s} the elastic scattering cross section by the 2s state and Q_{2s-1s} the de-excitation cross section may be found.

As the solutions are exact they should obey both reciprocity and particle conservation theorems (cf. Mott and Massey 1949): these imply that

$$k_0^2 Q_{1s-2s} = k_1^2 Q_{2s-1s}$$

and that if $a = x + iy$, $h = u + iv$ then $k_0 y = k_1 |d|^2$ and $k_1 v = k_0 |g|^2$. These relations provide a sensitive test of errors in numerical solutions but in addition it has been verified that the integral equations

$$k_0 A^i = F_0^{i\prime}(0) + \int_0^\infty \cos k_0 r \,[V_{00}(r)\, F_0^i(r) + V_{01}(r)\, F_1^i(r)]\, dr$$

$$k_0 B^i = \qquad -\int_0^\infty \sin k_0 r \,[V_{00}(r)\, F_0^i(r) + V_{01}(r)\, F_1^i(r)]\, dr$$

(with a corresponding pair for C^i, D^i) are satisfied. The final cross sections should be as accurate as the number of figures given.

§3

The calculated cross section Q_{1s-2s} is compared with those given by the DW and variational methods for a number of incident energies up to 54 ev, in table 1. It is seen that the exact cross sections are quite close to those given by the DW method, although there are signs that the DW cross section may become too large very close to the threshold; on the other hand the variational cross sections are unsatisfactory, being considerably too small. Massey and Moiseiwitsch (1953) had predicted that this might be the case as the trial junctions they employed had to be of simple form in view of the complexity of the calculations.

The DW method predicts a scattering amplitude of form $\beta \exp i(\delta_0 + \delta_1)$ where β is real number and where δ_0, δ_1 are the zero order phase shifts for elastic scattering of electrons by the 1s and 2s states of hydrogen respectively. The corresponding phase θ, of the exact scattering amplitude $[d/k_0(1-ia)] \equiv \alpha \exp i\theta$ has been evaluated and it is found that $\pi + \theta$ is quite close to $\delta_0 + \delta_1$ (table 1).

As reactive effects are included in the exact solution, the elastic scattering cross sections Q_{1s-1s}, Q_{2s-2s} will be altered from the values given by the uncoupled equations, but this effect is, in the present case, quite small and is illustrated in table 2.

Table 1. Zero-Order Partial Cross Sections for the 1s–2s Excitation of Hydrogen by Electron Impact (without exchange)

Energy of Incident Electron (ev)	Q_{1s-2s} (units of πa^2)			Phase of Scattering Amplitude (radians)	
	DW	V	E	$\pi+\theta$	$\delta_0+\delta_1$
10·2	0	0	0	—	—
11·5	—	—	0·286	3·947	—
13·5	0·198	0·076	0·204	3·643	3·66
19·4	0·127	0·041	0·102	3·060	3·08
30·4	0·058(5)	0·020	0·0450	2·636	2·61
54·0	0·019(4)	0·008	0·0155	2·124	2·10

DW : distorted wave method (from Erskine and Massey 1952) ; V : variational method (from Massey and Moiseiwitsch 1953) ; E : from numerical solution of equations (1) ; θ, δ_0, δ_1 for definition see text (δ_0 from Massey and Moiseiwitsch 1950, δ_1 from Erskine and Massey 1952).

Table 2. Zero-Order Partial Cross Sections for Elastic Scattering of Electrons by Hydrogen

Energy of Incident Electron (ev)	Q_{1s-1s} (units of πa_0^2)		Energy of Incident Electron (ev)	Q_{2s-2s} (units of πa_0^2)	
	(*a*)	(*b*)		(*a*)	(*b*)
11·5	—	2·52	1·35	—	2·05
13·5	2·47	2·12	3·38	2·21	1·97
19·4	1·57	1·42	9·32	3·62	3·40
30·4	0·885	0·828	20·3	2·49	2·39
54	0·411	0·394	43·9	1·20	1·17

From (a) uncoupled equations and (b) coupled equations.

References

Bates, D. R., Fundaminsky, A., Leech, J. W., and Massey, H. S. W., 1950, *Phil. Trans. Roy. Soc.* A, **243,** 93.

Erskine, G. A., and Massey, H. S. W., 1952, *Proc. Roy. Soc.* A, **212,** 521.

Fox, L., and Goodwin, E. T., 1949, *Proc. Camb. Phil. Soc.*, **45,** 373.

Massey, H. S. W., and Moiseiwitsch, B. L., 1950, *Proc. Roy. Soc.* A, **205,** 483 ; 1953, *Proc. Phys. Soc.* A, **66,** 406.

Moiseiwitsch, B. L., 1951, *Phys. Rev.* **82,** 753.

Mott, N. F., and Massey, H. S. W., 1949, Theory of Atomic Collisions (Oxford : Clarendon Press), 2nd ed., Chapter VIII.

LETTERS TO THE EDITOR

Raman Spectrum of Magnesium Oxide

Magnesium oxide crystallizes in the cubic system, and as Sir C. V. Raman has pointed out (1948), it should prove a perfect choice to demonstrate by its spectral behaviour, the monochromatic character of the atomic vibration frequencies in crystals. According to him the Raman spectrum of MgO should appear like that of NaCl. Extending Montroll's work to Coulomb forces, Smollett (1952) has evaluated two logarithmic infinities for a two-dimensional ionic lattice, the masses of particles in the lattice being equal. The peaks have approximately a frequency ratio of 4 to 5·9. He concludes from Blackman's work on lattices that the frequency spectrum of three-dimensional crystals should be similar to the spectrum of two-dimensional ' crystals '. Menzies, in his article (1953) on *Raman Effect in Solids*, also points out the importance of the Raman spectrum of MgO.

On the assumption that a highly refractory substance like magnesium oxide was likely to give results if used in thin flakes with long wavelengths as exciters, the experiment was tried with 4047 Å and 4358 Å of mercury and thin crystal deposits. Two lines corresponding to the Raman frequencies 617 cm^{-1} and 355 cm^{-1} were successfully photographed.

MgO was crystallized from ammonia as follows : A large quantity of MgO powder (B.P. Standard) was put in a flask and washed with repeated changes of distilled water for several days to remove soluble impurities. After washing, the powder was covered with ammonia liquor, and after three or four days the filtrate was put in a vacuum desiccator. After about a week, when the crystals had formed, they were heated for several hours on a water bath. Magnesium oxide dissolves in ammonia, forming a co-ordinate magnesium–ammonium complex. As co-ordinated valencies are not strong and easily ruptured, both the processes, vacuum crystallization and heating, help to break the co-ordinated bond and small crystals of MgO are obtained.

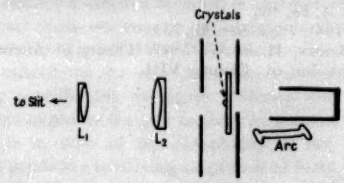

The final experiments were carried out with crystal deposits prepared as follows : The solution of MgO in ammonia was concentrated by boiling before putting it in the vacuum desiccator. It was allowed to evaporate completely and the deposit thus obtained was kept in an oven for an hour and a half at an average temperature of 125°C. One sample of this deposit was chemically tested for purity, and the plates, from which the spectra were photographed, were critically examined in polarized light.

In the beginning the experiments were performed with small crystals. The crystals were collected on a glass plate and heaped to form a line about one centimetre long, and lightly pressed down. The plate was supported vertically and illuminated as shown in the figure. This eliminated the use of the cover glass in front of the crystals. The condenser lenses L_1 and L_2 were both achromatic and formed a sharp image of the crystals on the slit of the spectrograph. The collimating lens was a Zeiss 155 mm anastigmat working at f/5, and the camera lens was a Schneider Xenar 210 mm at f/4·5. Knowing the magnification of the instrument, it was possible to determine the corresponding points on the object and the focal plane of the spectrograph.

Twenty-one spectra were photographed and both 4047 Å and 4358 Å lines of mercury were used as exciters. The time of exposure was varied from half an hour to about five hours. Eight exposures showed the effect with 4047 Å line only, four with both the exciters, one with 4358 Å line, and eight plates showed no detectable effect. The Raman shift lines were very faint, and there was considerable darkening due to parasitic light. The difficulty of repeating the experiments was realized and the final experiments were carried out with crystal-film deposits prepared as outlined above.

Fifteen exposures were made with 4358 Å as the exciter with different thicknesses of the crystal film. With such film the background darkening was considerably reduced and it was found that 0·016 mm deposit readily gave 617 cm^{-1} shift line, with exposures of one hour on Kodak P 1200 plates. The arc was at an average distance of twelve centimetres and was run at 3·5 amperes and sixty volts. To obtain 355 cm^{-1} shift line, films 0·02 mm thick were more effective and slightly longer exposures were necessary. The line was fainter and more diffused. Being closer to the exciter, it was clouded by its halation. Its frequency shift of 355 cm^{-1} was the weighted mean. The maximum thickness that could be used was 0·025 mm. There was indication that with increasing thickness of crystals, the Raman lines became broader and diffused.

The arc was directly photographed to see that lines similar to the observed shifts were neither given by the arc, nor were the ghosts formed by the apparatus.

I must thank the Reverend Father R. Rafael, S.J., head of the Department of Physics for the facilities given to me to carry out the experiments and Professor S. K. Chhapgar, Department of Chemistry, for suggesting the crystallization of MgO from ammonia.

References

Menzies, A. C., 1953, *Rep. Progr. Phys.*, **16**, 83 (London : Physical Society).
Raman, C. V., 1948, *Proc. Ind. Acad. Sci.* A, **26**, 392.
Smollett, M., 1952, *Proc. Phys. Soc.* A, **65**, 109.

Department of Physics,
St. Xavier's College,
Bombay.
22nd September 1955.

S. J. Khambáta.

On Star Production by μ-Mesons Underground

Nuclear evaporation stars produced by μ-mesons underground were first observed by George and Evans (1950) and attributed by them to the action of the virtual photons into which the electromagnetic field of a fast charged particle can be resolved, following Williams and von Weizsäcker. In fact, using the usual formula for the number of virtual quanta of energy greater than ϵ:

$$N(>\epsilon) \simeq \frac{\alpha}{\pi}\left\{\log\frac{E_0}{\epsilon}\right\}^2$$

where E_0 is the energy of the fast μ-mesons, and multiplying this by the experimentally determined photo-nuclear cross section (McMillan, Peterson and White 1949) good agreement was obtained between the calculated cross section and the value 5×10^{-30} cm^2 nucleon^{-1} observed experimentally.

In a recent paper Fowler (1955) has re-calculated the theoretical cross section, obtaining the much smaller value of $1{\cdot}6 \times 10^{-31}$ cm^2 nucleon^{-1}. Since this is lower than the observed cross section by a factor of order thirty, Fowler concludes that there exists some anomalous μ-meson–nucleon interaction of sufficient strength to explain the observed frequency of star production. The basis for such an important conclusion must be carefully examined, and it is the purpose of this letter to point out that after making such a careful examination Fowler's conclusions become invalidated.

This may be seen by considering the physical significance of the operator which Fowler uses, namely

$$\langle f|\mathbf{E}.e\mathbf{r}|i\rangle. \qquad \ldots\ldots(1)$$

This is the ordinary dipole interaction arising from the Coulomb forces between the incident particle and the protons in the target nucleus. It has been used, among others, by Levinger and Bethe (1952) and accounts in a satisfactory way for photo-nuclear reactions below the threshold for meson production. Using operator (1) the photo-nuclear cross section varies as shown in the full line in the figure. The well-known 'giant resonance' occurs around 20 Mev after the theoretical cross section decreases monotonically indefinitely.

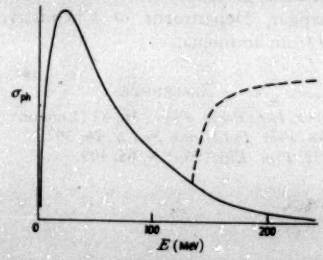

In practice, the photo nuclear cross section increases by a large amount at the meson threshold energy as indicated in the dotted line (Kikuchi 1952). This increase which is due to the coupling between the electromagnetic field and the

nucleon meson cloud is ignored by Fowler. Since most of the stars in question (having three or more prongs) correspond to excitation energies above meson threshold, it is seen that the theoretical cross section calculated by Fowler does not really have any bearing on the experimental results with which he compares his calculations.

It is of interest to recall that George and Evans (1950) calculated the approximate value of the cross section due to purely Coulomb forces and obtained the value 4×10^{-31} cm^2 nucleon^{-1}. It is gratifying that the more detailed treatment of Fowler gives an answer so close to this value.

An exact calculation, including photo-mesic effects has yet to be done. George and Evans had recourse to the Williams–Weizsäcker method in order to obtain an approximate theoretical answer. Fowler correctly points out that this is only valid provided

$$qR \ll \hbar \qquad \ldots\ldots(2)$$

where q is momentum transfer and R the dimension of the perturbed system.

The question here is: what is the perturbed system? Fowler takes it to be the whole nucleus whereas from the argument given above it is clear that it is a single nucleon. Using equation (2) this means that the Williams and von Weizsäcker method gives a reasonable approximation for energy transfers up to approximately 400 Mev, and that Fowler's conclusion that the Williams and von Weizsäcker method is not applicable to the present case is also incorrect.

The F.B.S. Falkiner Nuclear Research and Adolph Basser Computing Laboratories, School of Physics, The University of Sydney, Sydney, New South Wales, Australia.

E. P. George.

27th September 1955.

Fowler, G. N., 1955, *Proc. Phys. Soc.* A, **68**, 482.
George, E. P., and Evans, J., 1950, *Proc. Phys. Soc.* A, **63**, 1248.
Kikuchi, S., 1952, *Phys. Rev.*, **86**, 41.
Levinger, J. S., and Bethe, H. A., 1952, *Phys. Rev.*, **85**, 577.
McMillan, E. M., Peterson, J. M., and White, R. D., 1949, *Science*, **110**, 579.

REVIEWS OF BOOKS

Les épreuves sur echantillon, by M. DUMAS. Pp. 170. (Paris: Centre National de la Recherche Scientifique (Monograph A III) 1955.) 1000 *fr.*

Monsieur Dumas sets out to provide what, in France, might be called "*la cuisine de la statistique*", for the benefit of such people as physicists and engineers, who want to use statistical techniques "*sans avoir à s'initier d'abord aux méthodes générales de la statistique*", as M. Fréchet explains in his preface. On this strictly utilitarian level, the book deals with some of the techniques for estimation of parameters, acceptance sampling, significance testing and control charts.

M. Dumas starts from considerations of common sense, stressing the extent to which interpretation of statistics depends on other than statistical considerations. He then gives his collection of recipes *pro tempora diversa* as the liturgists would say, with rubrics stating the situations in which they could be used. The treatment is not incompetent; but, certainly for workers here and in America, it must be regarded as both inadequate and inferior to many books in wide use. Having nothing they would find new either in material or presentation, it has nothing but curiosity to recommend it to English readers.

The book is indeed curious. We should defer to M. Dumas and his advisers in their judgment of French needs; but, in so doing, we are impressed by the strange psychological difference between Frenchmen and ourselves in the approach to statistics of a practical nature. We are closer to America than France, it seems, being less academic in our attempts to be utilitarian.

To judge by the bibliography, a Frenchman can also be more insular than an Englishman. Only two references to other books on this subject are used explicitly: one a book of which M. Dumas is himself co-author, the other a book of which only Volume I is yet published. Both books are French.

The past ten years have seen a dramatic improvement in the supply of books on statistics written in English, and quality has improved with the quantity. There is need for statistics books in French—still. M. J. MORONEY.

Luminescence and the Scintillation Counter, by S. C. CURRAN. Pp. x+219. (London: Butterworths Scientific Publications, 1953.) 32*s.* 6*d.*

Perhaps in sympathy with the teacher's aphorism 'those that can, do', a readier ear is accorded the creator–expositor; for a subject in the hot surge of advance, there is no better guide. This little book, in twelve short chapters, is the work of one such: for the scintillation counter in its modern form was first developed by Dr. Curran but ten years ago. Already it has proved itself, thanks to its speed, sensitivity, flexibility, and discriminating power (in conjunction with associated circuitry and accessories) as one of the chief tools in the quantitative analysis of particles and radiations of all types, particularly those of nuclear origin. The present account, more specialized than the cognate *Counting Tubes* and designed for serious workers aiming to develop or use the technique, is the first integrated summary of all aspects.

Following a brief introduction, two chapters indicate the essentials of radiation–matter interaction, with special emphasis on secondary emission,

Mesons and neutrinos are included. A direct lead to multipliers is given in consideration of high secondaries yield, lattice potential and energy factors favouring the higher alkali halide complexes. Practical detail follows in the next two chapters describing general principles of the electron multiplier and characteristics of some commercial types, chiefly the 'venetian blind' and shaped dynode models, the former, though less subject to magnetic disturbance, being slower in response and with less powerfully defined field control. Features necessary in the photosensitive surfaces are fully explained and practical materials given. Figures of merit are based on spectral sensitivity, dark current, noise–temperature relation, amplification, intensity range, stages, shielding, collection efficiency, and time and amplitude resolution. Difficulties such as satellite pulses are not ignored.

A similar treatment of luminescence follows, two chapters sketching current views on fluorescence and phosphorescence, followed by two more on the preparation and properties of practical scintillants. Clearly the author has critical reservations here on established concepts and general notions, but indicates the importance of ring and bond resonance, high melting points and absence of chromophores in scintillants, of matching spectral sensitivities of scintillant and multiplier, and indicates how modern excitation methods have weeded out theories of energy transport, if only on the basis of decay times. The practical chapters detail chemical range, purification processes, phases (including plastic matrices and polymerization *in situ*) and give ample coverage to nature and properties with a natural bias to the organic crystal and solution scintillants whose extreme speed of response serves in analysis and applications.

The two streams reunite in the final three chapters, the first and last of which are especially valuable for critical assessment of suitable applications and an excellent summary of circuitry for purposes including time resolution, fast scaling, display, discrimination, pulse-sorting, or coincidence work, with frequent illustration from the Glasgow and other laboratories.

Designed for use, first rather than last words, a bench handbook rather than a sofa volume, for Ramsays rather than Rayleighs, in style compact, terse, staccato, selective, the book is suggestive and compelling with few irrelevancies, though an occasional 'salute to adventurers' gleams tribute to solid or deft analysis or technical virtuosity. Though coverage is very full and the 340 references, international in scope, include some books and reviews, in the inevitable revision further developments in medical and low-energy x-ray applications might find a place. There are a few omissions, particularly in the subject index. It must be a publisher's irony that a scientific research book's scintillating success helps to decrease its decay time ; but already it seems a far cry to those Royal Institution lectures where Rutherford, with the aid of Crowe, Green and Wynn-Williams, described the then latest 'lazy methods'.

I. MACARTHUR.

Isotopic Tracers, by G. E. FRANCIS, W. MULLIGAN and A. WORMALL. Pp.xvi + 306. (London : Athlone Press, 1954.) 37*s.* 6*d.*

Although it bears a very general title, this book deals only with the applications of radioactive and stable isotopic tracers to biology. It is based on a course presented at the Medical College of St. Bartholomew's Hospital, and the three authors are all biochemists. Naturally, such a book contains very

much which is unfamiliar to a physicist and which he is not really competent to criticize ; it will not be necessary, in these *Proceedings*, to apologize for reviewing the book mainly from a physical standpoint.

The most important and valuable portion of the work is a course of experiments which occupies the last fifty pages. There are introductory experiments on the measurement of radioactivity with Geiger–Müller counters (other detectors, including scintillators, are only briefly mentioned), and one experiment on the estimation of nitrogen with a mass spectrometer. These are followed by some interesting, well-described and apparently quite simple biological experiments, including, for instance, the introduction of ^{32}P into hens' eggs during their development, and investigation of its distribution, the measurement of red cell volume and blood volume in the rabbit, and the preparation of ^{131}I-labelled proteins and their use in a number of serological experiments.

The descriptions of the laboratory procedures are so clear that a physicist might well be tempted to try the experiments himself. There are however two general criticisms to be made. First, only a minority of the experiments make use of truly isotopic tracers. In the others, for instance when labelling proteins with ^{131}I, foreign atoms are introduced into the molecule, which could, in principle, be estimated chemically. It is asserted that the properties of the protein are not materially changed by this addition. This may well be correct, but the student is not told how to prove it. Here, as in other parts of the book, the distinction between genuine isotopic tracers and chemically dissimilar labels is blurred. The second general criticism concerns the sketchy treatment of statistics both in the text and in an appendix. Since so much biological work requires statistical methods one might have expected this subject to be more rather than less thoroughly treated than in a textbook for physicists.

The eleven introductory chapters, both biological and physical, will probably not be very useful to readers of this journal. The biological chapters presuppose a considerable amount of specialized knowledge. The matter in the physical chapters has been better presented elsewhere, and is not entirely free from errors. Nevertheless, the book will almost certainly be valuable to the biological students and research workers to whom it is addressed.

W. J. WHITEHOUSE.

Nuclear Radiation Detectors, by J. SHARPE. Pp. 179. (London : Methuen, 1955.) 11*s*. 6*d*.

The series of Methuen Monographs is claimed by the publishers to " supply science students at University level " and " workers in other branches of physics " with a " compact statement of the modern position in each subject " and this, in general, they do very well, especially when one considers the low price compared with other scientific books. It is doubtful, however, whether the volume under review quite falls into the above class. So much data and information has been compressed into its one hundred and eighty pages that it has become somewhat un-readable. In fact, in the writer's opinion, this book will be found of value mainly as a work of reference. The unfortunate omission of the index in earlier printings, including the reviewer's copy, reduced its usefulness for this purpose, but it is understood that in copies now on sale, this has been rectified.

In the preface, the author states that his endeavour was to present basic information needed by those interested in the design and use of detectors for nuclear radiations. Following a short introduction, the author discusses the interaction of nuclear radiations with matter. This is followed by a chapter on detection media (phosphors and gases) and by another on the various factors influencing detector efficiency. These chapters include a great deal of useful data in graphical and in tabular form. It was felt that some of the tabulated data might, with advantage, have been presented in graphical form, but no doubt considerations of cost precluded this. Also may the writer at this point advocate more general use of a superimposed grid on graphs in books such as this. This would enhance their usefulness very considerably and, if thin lines are employed, it need not affect the clarity appreciably. The last two chapters deal respectively with scintillation counting and with what are called ' ionization devices '. The latter deals with ionization chambers, proportional and Geiger counters. A few misprints and errors, none serious, were noted as the book was read.

The price of the book, though a little higher than others of the series, represents good value for the number of pages, and its low cost will make it a useful addition to other books in the field. H. W. WILSON.

Niels Bohr and the Development of Physics, edited by W. PAULI. Pp. vii + 195. (London : Pergamon Press, 1955.) 30*s*.

This little book has been prepared as a tribute to Professor Bohr on his seventieth birthday. The authors of its ten chapters are distinguished physicists who have collaborated with Professor Bohr in the many branches of physics in which he has played such a central role. In a book of this kind, one hopes to read of things which will endear the great man to those who have not had the privilege and inspiration of working with him in person. Such articles there are ; but some there are too which seem hardly appropriate to the occasion. Nevertheless, after reading this collection of papers one is left primarily with a feeling of wonder that one man should have done so much.

B. H. FLOWERS.

Nuclear Magnetic Resonance, by E. R. ANDREW. Pp. xi + 265. (Cambridge : University Press, 1955.) 35*s*.

Although it is now a little over ten years since the birth of nuclear magnetic resonance, no treatise on the subject has appeared apart from the valuable thesis of Bloembergen (1948), which was rapidly sold out and has since been out of print. An authoritative treatise is still lacking, but this volume by Professor E. R. Andrew, the latest in the series of Cambridge Monographs on Physics, gives as comprehensive a review as its size permits. The basic theory cannot be developed in full on such a scale, and the author has rightly relegated some of the more tedious mathematics to appendices, or given useful order of magnitude arguments, for example, in the subject of spin–lattice relaxation times. These make for easy reading for the beginner, who can thus concentrate on the physics; but it seems a pity that more use is not made of rotating coordinate systems, which are very valuable in forming a physical picture of the phenomena, particularly when dealing with transient effects.

After a brief introduction follow chapters on the basic theory and experimental methods, the latter including references to methods of optical detection and nuclear alignment. The measurement of nuclear moments and applications to some experiments in fundamental physics are then discussed, followed by three chapters on the information which nuclear magnetic resonance has given on effects in bulk material arising from the interaction of the nuclear moments with their surroundings. These will be of particular value to the applied physicist. The book ends with a short chapter on electric quadrupole effects, together with a valuable bibliography and useful tables of substances investigated, including references. A singular omission is of any table of nuclear spins and magnetic moments; the latter is excused on the grounds that moments are not of great value unless details of corrections are given. But surely, now that the spins of practically all stable isotopes have been determined, and their moments are known with fair accuracy, these could have been included in a handy table together with the references to the original experiments.

B. BLEANEY.

Quantum Theory of Solids, by R. E. PEIERLS. Pp. viii+229. (Oxford: Clarendon Press, 1955.) 30*s*.

The theory of the solid state has developed most remarkably during the past thirty years. Apart from its intrinsic interest the practical significance of the theory for technology attracts a large and active body of scientists to this field. It is, therefore, a happy and significant event when one of the principal originators of the subject takes the time and the trouble to expound the fundamentals of the theory as Professor Peierls has done in this book.

By no means all modern work in solid state physics involves the use of quantum theory, though many parts of it do, and it is with these only that the book under review deals. The object of the book is stated by the author in the preface: it is to stress the fundamental aspects of the theory rather than to concentrate on detailed applications and practical matters. As the fundamentals of both crystal dynamics and electron theory were firmly laid by the middle thirties, with one or two exceptions, one does not expect to find, and does not in fact find, much relating to post-war developments in this book. There is however, a final chapter dealing with recent work on the theory of superconductivity, and in the chapter on ferromagnetism there is a discussion of neutron scattering in magnetic materials, and a short section dealing with anti-ferromagnetics. The great strength and value of this book lies in the insight which the author displays, and conveys to his readers, into the basic ideas of both lattice dynamics and electron theory.

The book opens with three chapters on atomic vibrations in crystals in which the theory of specific heat and the theory of thermal conductivity are developed. Thermal expansion, and the effects of anharmonic vibrations on the specific heat at high temperatures are also dealt with. Lattice thermal conductivity is a subject which has presented serious difficulties to many students in the past, therefore the account given in this book, which is the clearest and most complete in the literature, will be greatly appreciated.

Chapters four to eleven are taken up with one or other of the various aspects of the electron theory of metals. Most of the well-known topics are

dealt with: band theory, cohesion, transport phenomena, para- and diamagnetism and the interaction of light with electrons in solids. Although this book was published in 1955 it is, according to the author's preface, the substance of a lecture course given in 1953. Perhaps this accounts for the most striking omission: no mention is made of the theory of plasma oscillations in metals, even though, as now seems likely, this phenomenon plays an essential part, through the introduction of a screened interaction, in the whole conception of the free electron gas.

In a notice of a book of such great value it would be ungracious to dwell on the omission of interesting topics (and there are other omissions); it is more appropriate to express appreciation of the masterly presentation of so much which is of general interest. This book can be unreservedly recommended both to those approaching the subject for the first time, and also to those who, after years of study, still find its problems difficult but fascinating.

H. JONES.

CONTENTS OF SECTION B

PAGE

Prof. L. F. Bates and Dr. A. Hart. Magnetization Curves and Domain Structure 497

Mr. C. Hilsum. The Absorption Edge of Amorphous Selenium and its change with Temperature 506

Dr. R. Stratton. Surface Barriers at Semiconductor Contacts 513

Dr. B. Donovan and Dr. N. H. March. High Frequency Conductivity in Semiconductors 528

Mr. A. R. F. Plummer. Observations on the Growth of Excess Current in Germanium p–n Junctions 539

Dr. Mary D. Waller. On Powder Striations produced by Electric Sparks . 548

Dr. R. Barrie. Electronic Conduction in Solids with Spherically Symmetric Band Structure 553

Dr. H. H. Hopkins. The Frequency Response of Optical Systems 562

Mr. J. T. Jefferies. Radiative Transfer with Central Sources of Non-Uniform Directional Intensity 577

Research Note:

Dr. A. Goswami. Disorientation of Single Crystal Substrate due to Epitaxial Stress 583

Reviews of Books 585

Corrigendum: J. Ewles and J. C. Stead 591

Contents of Section A 592

Electron Excitation Functions of the First Negative Bands of N_2^+

By D. T. STEWART
Physics Department, The Queen's University of Belfast

Communicated by K. G. Emeléus; MS. received 23rd January 1956

Abstract. A photoelectric spectrophotometer has been developed for studying the feeble light emitted from a gas at low pressure excited by an electron beam of known energy in an equipotential box. The probabilities of excitation of the (0, 0), (0, 1) and (0, 2) negative bands of the nitrogen molecular ion have been measured. The maximum cross section for formation of the $v=0$ level of the upper state involved, $B^2\Sigma$, from the ground state of the neutral molecule $X^1\Sigma_g^+$ was found to be $(9{\cdot}5 \pm 1{\cdot}0) \times 10^{-18}$ cm^2 and occurs for electrons of approximately 100 ev energy.

§ 1. Introduction

In a previous communication (Stewart 1955) some measurements of the relative excitation functions of infra-red nitrogen spectra by photographic photometry have been described. This technique was found unsuitable for the determination of absolute cross sections, and hence a photoelectric spectrophotometer has been developed for this purpose. This has to be capable of recording, in whatever region of the spectrum is of interest, the low intensities of light from an electron beam source operating at sufficiently small gas-pressures and electron currents for secondary mechanisms of excitation to be unimportant.

The bands chosen for the preliminary investigation described in the present paper were the (0, 2), (0, 1) and (0, 0) first negative bands of $N_2^+(B^2\Sigma - X^2\Sigma)$ with heads near 4709 Å, 4278 Å, and 3914 Å respectively. This choice was made chiefly on account of their importance in auroral phenomena. Measurement of the absolute intensity of a molecular band j–k emitted under known conditions of excitation, will give directly the cross section Q_{jk} for excitation of the band (Massey and Burhop 1952). In the case of the $B^2\Sigma - X^2\Sigma$ transitions, population of the $B^2\Sigma$ level by cascade from higher levels can almost certainly be ignored. Furthermore, the relative transition probabilities $A_{jk}/\Sigma A_{jk}$ of these transitions can be calculated (Bates 1952), and it is thus possible to calculate the electron collision cross section of the $v=0$ level of the $B^2\Sigma$ state from the expression $Q_{jk}=A_{jk}Q_j/\Sigma A_{jk}$, where Q_j is the cross section of the upper level.

§ 2. Experimental Procedure

The radiation to be studied was produced by an electron beam source, similar in dimensions to the one described previously (Stewart 1955). This consisted of a Pierce type electron gun firing a beam of electrons through a field-free collision box into a collector. The final anode, the collision box and the collector were all held at the same potential in order to avoid field penetration into the box.

Errors in current measurements due to secondary emission from the collector were avoided by placing a shield at cathode potential between the collector and collision box.

The source was operated at pressures of the order of 3×10^{-3} mm Hg, with electron currents of $2\text{–}5 \times 10^{-4}$ amp. Nitrogen was continuously streamed through the tube and no lines or bands, other than those from nitrogen, were observed.

The electron energy distribution in the beam was measured over a range of operating conditions by applying retarding voltages between the collector and collision box. It was found that 95% of the electrons in the beam had energies within a 3 v range of the applied accelerating potential. Furthermore, the number of slow electrons arising from secondary emission from the defining slits of the electron gun was negligible.

§ 3. Measurement of Intensities

A block diagram of the apparatus first used is shown in figure 1. An f.9 Hilger constant deviation spectroscope C was aligned at right angles to an optical bench AA and the electron beam source S. Light from a tungsten filament lamp L, calibrated for luminous intensity and colour temperature at the National

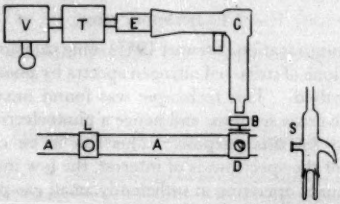

Figure 1. Basic arrangement of spectrophotometer. T is the tuned amplifier, V the valve voltmeter. For key to other symbols see text.

Physical Laboratory, or from S, could be presented to the spectroscope slit by means of a quartz prism D, mounted on a turntable. The light entering the spectroscope was chopped at 200 cycles per second by a rotating shutter B. The spectrum was formed on the photo-cathode of an E.M.I. type 6256 photo-multiplier tube E, from which the resulting modulated current was amplified by a circuit which included a narrow band filter set at the frequency of chopping. Sharp tuning was obtained by negative feedback from a late stage of the amplifier to the first stage, and by the insertion of a twin T network in the feedback loop.

In the second method of detection, which has proved more sensitive, individual pulses arising from emission of electrons from the photo-cathode were counted. These pulses were amplified and fed into an EKCO type 552 ratemeter. By discriminating against the smaller pulses due to thermionic emission from the dynodes, light fluxes of the order of 100 photons per second in the visible region could be recorded.

With both methods the optical bench was used to check the linearity of response of the spectrophotometer by means of the inverse square law. All the absolute measurements were made with the pulse-counting method, as this method had the widest range of linearity of response.

A possible criticism of the arrangement shown in figure 1 is that light from the electron beam or calibrating lamp might be polarized (Skinner and Appleyard 1928), and hence spurious results be obtained since the quartz prism and spectroscope have polarizing properties. Direct tests with polaroid screens showed, however, no observable polarization with either the beam or lamp, except possibly for the beam within a few volts of the excitation potential of the bands where the intensity measurements in any case are not exact. However, as a further check, absolute measurements were also made with the collimator directly aligned with the electron beam source, the calibrated lamp L being mounted on a pivot so that it could be placed in front of the beam source. The results obtained were not significantly different from those obtained using the prism.

§ 4. Results

The intensities of all three bands were found to be directly proportional to both pressure and current, indicating that single electron impact with an N_2 molecule in the $X^1\Sigma$ ground state was the most important mechanism for populating the $B^2\Sigma$ state of N_2^+. The relative excitation functions of all three bands were identical. There was a sharp rise from an onset potential of approximately 20 v to a broad maximum at 95 v, followed by a gradual decrease with increasing electron energy.

The intensities in absolute units (number of photons per second from the beam) of the bands for an electron energy of 100 ev and known values of gas pressure and electron current were determined by comparison with the calibrated lamp.

After determining the optimum operating conditions, four separate measurements were made for each band, using different pressures and currents, and different colour temperatures of the standard lamp. The average cross sections for excitation of these bands were then calculated directly from these measurements, and together with the observed relative excitation functions gave the curves shown in figure 2 for the variation of Q_{ik} of the bands with electron

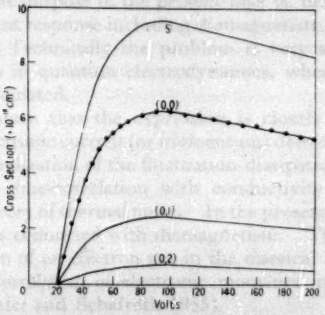

Figure 2. Excitation functions for (0, 0), (0, 1) and (0, 2) first negative bands. The top curve, marked S, gives the integrated cross sections for the $v=0$ level of the $B^2\Sigma$ state of N_2^+. Alternate experimental points only are shown on the (0, 0) curves. All experimental points lay equally closely on the other curves.

energy. The mean deviation from the average values of 6·2, 2·4 and $0{\cdot}65 \times 10^{-18}$ cm² at the maximum was for each band less than 10%.

The experimental ratio of intensities of the (0, 0), (0, 1) and (0, 2) first negative bands is 1·0 : 0·39 : 0·10, while the ratio calculated from tables of overlap integrals (Bates 1952) is 1·0 : 0·31 : 0·072. By extrapolation of the experimental results and from the calculated relative transition probabilities it appears that these bands almost certainly accounted for more than 95% of the total intensity of the $v' = 0$ progression. Allowing $0{\cdot}2 \times 10^{-18}$ cm² for the remainder of the bands in the $v' = 0$ progression, this results in a total cross section Q_j for the $v = 0$ level of the $B^2\Sigma$ state of $9{\cdot}45 \times 10^{-18}$ cm² at the maximum. The variation of Q_j with electron energy is shown in the upper curve of figure 2. It is hoped to extend these measurements into the ultra-violet region so as to record further first negative bands.

Acknowledgments

The author wishes to thank Professor K. G. Emeléus for suggesting and supervising this work, Dr. R. H. Sloane for advice, and Dr. E. B. Armstrong for discussion on our related fields of work.

References

Bates, D. R., 1952, *Mon. Not. R. Astr. Soc.*, **112**, 614.

Massey, H. S. W., and Burhop, E. H. S., 1952, *Electronic and Ionic Impact Phenomena* (Oxford : Clarendon Press).

Skinner, H. W. B., and Appleyard, E. T. S., 1928, *Proc. Roy. Soc.* A, **117**, 224.

Stewart, D. T., 1955, *Proc. Phys. Soc.* A, **68**, 404.

A Note on Momentum Correlation and Diamagnetism

By S. NAKAJIMA†
Department of Theoretical Physics, University of Liverpool

Communicated by H. Fröhlich; MS. received 19th March 1956, and in final form 1st May 1956

Abstract. Quantum statistical mechanics is applied to derive the expression for the current response of electrons in metals, caused by an electromagnetic disturbance.

The expression is closely connected with the space–time correlation of electronic momenta. Examples are given to show that diamagnetism is essentially determined by spatial correlation.

§ 1. Introduction

Recently the quantum theory of relaxation phenomena has been developed by various authors (Callan and Welton 1951, Kubo and Tomita 1954, Kubo 1955). From this point of view, Ohm's law of metallic conduction, for example, is given as the current response of conduction electrons caused by an electric disturbance, and the conductivity is expressed directly in terms of quantum mechanical operators (see equations (11) and (12) below). This way of approach to the theory of conductivity was first noticed by Nakano (1955 a) and Feynman‡, and Grüneisen's formula has been derived by making a damping theoretical approximation (Nakajima 1955 a, Nakano 1955 b). The correspondence to the usual Bloch theory has also been clarified (Kubo 1955).

The same idea can be applied to diamagnetism, which is characterized by the current response caused by a stationary external current (Schafroth 1951, Nakajima 1955 b). The purpose of the present note is, first, to derive a unified expression for the current response including diamagnetism, ohmic and dielectric polarization currents. Technically the problem is very similar to the theory of vacuum polarization in quantum electrodynamics, where the 'susceptibility of vacuum' is to be calculated.

Then it will be shown that the expression is closely connected with the correlation between electronic current (or momentum) densities at two space–time points. This is a generalization of the fluctuation-dissipation theorem (see Band 1955) which connects time-correlation with conductivity and has played an important role in the theory of thermal noise. In the present note, it will be found that space correlation is connected with diamagnetism. Thus, for instance, the vanishing diamagnetism of an electron gas in the classical limit is equivalent to the absence of space-correlation of electronic momenta in the same limit (for the latter see Blatt, Butler and Schafroth 1955).

Finally, the present unified formalism can cover superconductivity. Although the microscopic theory of superconductivity has not yet been established, the

†On leave of absence from the Physical Institute, Nagoya University, Nagoya, Japan.
‡ Lectures given in Japan, 1955.

present formalism can be used to see what sort of space–time correlation a particular phenomenological theory implies. Thus, for instance, London's theory leads, in fact, to a long-distance correlation as anticipated by London himself.

§ 2. Diamagnetic and Ohmic Currents

Suppose that the electromagnetic field

$$\mathbf{E}=-\frac{1}{c}\frac{\partial \mathbf{A}}{\partial t}-\nabla\Phi, \qquad \mathbf{B}=\operatorname{curl}\mathbf{A} \qquad \ldots\ldots(1)$$

is established by a certain source placed inside an infinite metal. Our purpose is to find the current response of the conduction electrons, caused by the field. Let $\psi(\mathbf{x})$ and $\psi^*(\mathbf{x})$ be the anti-commuting operators describing the electron wave (Schiff 1949). The current operator is then expressed as (Wentzel 1949)

$$\mathfrak{J}_\mu(\mathbf{x},t)=j_\mu(\mathbf{x})-\left(\frac{e}{mc}\right)\rho(\mathbf{x})A_\mu(\mathbf{x},t)$$

$$\mu=x,\ y,\ z,$$

where

$$\rho=e\psi^*\psi, \qquad j_\mu=\left(\frac{\hbar e}{2mi}\right)\left(\psi^*\frac{\partial\psi}{\partial x_\mu}-\text{c.c.}\right).$$

In quantum theory, the statistical distribution of the electron–phonon system is described by means of the density matrix $R(t)$ (ter Haar 1954) which satisfies

$$i\hbar\frac{dR(t)}{dt}=[H+H',\ R(t)]. \qquad \ldots\ldots(2)$$

Here H is the Hamiltonian of the electron–phonon system and H' is its interaction with the field (Wentzel 1949),

$$H'=-\frac{1}{c}\int dx j_\nu A_\nu+\int dx\rho\left(\Phi+\frac{e^2}{2mc^2}A^2\right). \qquad \ldots\ldots(3)$$

The average current is given by

$$J_\mu(\mathbf{x},t)=\operatorname{Tr}[R(t)\mathfrak{J}_\mu(\mathbf{x},t)]. \qquad \ldots\ldots(4)$$

Assume that the electron–phonon system at $t=-\infty$ is in thermal equilibrium without the field, the latter being then switched on adiabatically. Thus the density matrix at $t=-\infty$ is given by the canonical distribution†

$$R(-\infty)=R_c\equiv\exp[-\beta H]/\operatorname{Tr}(\exp[-\beta H]) \qquad \ldots\ldots(5)$$

with $\beta^{-1}=\kappa T$ and, under the gauge $\Phi(-\infty)=0$, $\mathbf{A}(-\infty)=0$. Applying perturbation theory with respect to H', the Schrödinger equation (2) with the initial condition (5) can be integrated and the average current is obtained from (4). Up to the first order of the field amplitude, the average current is thus given by

$$\begin{aligned}J_\mu(\mathbf{x},t)=&\left(\frac{Ne^2}{mc}\right)A_\mu(\mathbf{x},t)\\&+\frac{i}{\hbar c}\int_{-\infty}^{t}dt'\int dx'\langle[j_\mu(\mathbf{x},t-t'),\ j_\nu(\mathbf{x}')]\rangle A_\nu(\mathbf{x}',t')\\&-\frac{i}{\hbar}\int_{-\infty}^{t}dt'\int dx'\langle[j_\mu(\mathbf{x},t-t'),\ \rho(\mathbf{x}')]\rangle\Phi(\mathbf{x}',t') \qquad \ldots\ldots(6)\end{aligned}$$

† This initial condition can be applied as far as linear effects are concerned, because these are determined by the response of the system to an impulse, $\delta(t)$, type disturbance.

where $\langle Q\rangle \equiv \mathrm{Tr}(R_c Q)$ is the average of Q in thermal equilibrium and

$$Q(t)=\exp\left[\frac{i}{\hbar}Ht\right]Q\exp\left[\frac{-i}{\hbar}Ht\right]$$

is its Heisenberg operator. In deriving (6) it was assumed that $\langle\rho\rangle = Ne$, $\langle j\rangle = 0$. By partial integration and use of the continuity equation and of the operator identity

$$[\rho, e^{-\beta H}] = e^{-\beta H}\int_0^\beta d\lambda\, e^{\lambda H}[H,\rho]e^{-\lambda H},$$

equation (6) can be written as

$$J_\mu(\mathbf{x},t)=\int dx' K_{\mu\nu}(\mathbf{x}-\mathbf{x}')A_\nu(\mathbf{x}',t)+\int_{-\infty}^{t}dt'\int dx' L_{\mu\nu}(\mathbf{x}-\mathbf{x}',t-t')E_\nu(\mathbf{x}',t') \quad \ldots\ldots(7)$$

where the system is assumed to be homogeneous. The integral kernels are given by

$$L_{\mu\nu}(\mathbf{x},t)=\int_0^\beta d\lambda\phi_{\mu\nu}(\mathbf{x},t+i\hbar\lambda), \quad \ldots\ldots(8)$$

$$K_{\mu\nu}(\mathbf{x})=-\left(\frac{Ne^2}{mc}\right)\delta_{\mu\nu}\delta(\mathbf{x})+\frac{1}{c}L_{\mu\nu}(\mathbf{x},0), \quad \ldots\ldots(9)$$

$$\phi_{\mu\nu}(\mathbf{x}-\mathbf{x}',t)=\langle j_\nu(\mathbf{x}')j_\mu(\mathbf{x},t)\rangle. \quad \ldots\ldots(10)$$

As far as linear effects are concerned, diamagnetism, electric conductivity and dielectric polarization of the metal are generally expressed by the single integral relation (7), which, in special cases, reduces to the usual relations expressed in terms of susceptibility, conductivity and dielectric constant. For example, Landau's diamagnetism has been obtained from (9) (Schafroth 1951) and Grüneisen's conductivity from (8) (Nakajima 1955 a).

From (7) one can also draw some general conclusions. First, the electromagnetic properties are closely connected with the space–time correlation of electronic momenta, since the latter is essentially given by (10). More precisely, the operator product in (10) must be symmetrized as usual. This will be done in § 3.

The first term in (7), which is proportional to the vector potential, describes the diamagnetic current. Since the kernel is independent of time, there is no diamagnetic time-relaxation. From (9) and (10) it can already be seen that diamagnetism is essentially determined by the space-correlation of electronic momenta. A more detailed discussion will be given in § 3.

The second term in (7), which is proportional to the electric field, describes the ohmic current including the dielectric polarization, provided that the kernel (8) converges quickly to zero as $t\to\infty$ (this does not apply, of course, to superconductivity—see § 3). In particular, if the uniform electric impulse $\mathbf{E}\propto\delta(t)\boldsymbol{u}_\nu$ is applied, then (7) reduces to ($\mathbf{u}$ is a unit vector)

$$J_\mu(t)\propto\begin{cases}0 & (t<0)\\ G_{\mu\nu}(t)u_\nu & (t>0),\end{cases}$$

where $G(t)$ is given by integrating L over $\mathbf{x}$. Making use of the total electronic momentum

$$P_\mu=\int dx\psi^*(-i\hbar)\frac{\partial\psi}{\partial x_\mu}$$

and introducing the (large) normalization volume V, G can be written as

$$G_{\mu\nu}(t)=\frac{1}{V}\left(\frac{e}{m}\right)^2\int_0^\beta d\lambda\langle P_\nu P_\mu(t+i\hbar\lambda)\rangle. \qquad \ldots\ldots(11)$$

Similarly, applying a uniform electric field proportional to $\exp(-i\omega t)$, one obtains the complex dielectric constant ϵ given by

$$\left(\frac{-i\omega}{4\pi}\right)\epsilon(\omega)=\int_0^\infty dtG(t)\exp(i\omega t). \qquad \ldots\ldots(12)$$

The real part of ϵ is the usual dielectric constant and the imaginary part is connected with the conductivity σ by

$$\mathcal{I}\epsilon=(4\pi/\omega)\sigma(\omega).$$

Since G is real

$$\epsilon(\omega)=-\epsilon^*(-\omega). \qquad \ldots\ldots(13)$$

From (12), by means of Titchmarsh's theorem, one can at once obtain the Kramers–Kronig dispersion relation (Jauch and Rohrlich 1955)

$$\epsilon(\omega)=\left(\frac{-i}{\pi}\right)\mathrm{P}\int_{-\infty}^{\infty}d\omega'\frac{\epsilon(\omega')}{\omega-\omega'}, \qquad \ldots\ldots(14)$$

where P indicates taking the principal value at $\omega=\omega'$. When the system was assumed to be in thermal equilibrium at $t=-\infty$, causality was introduced and this is why (14) has been obtained almost automatically.

§ 3. The Space-Correlation and Diamagnetism

As mentioned in § 2, the correlation function is properly defined by

$$C_{\mu\nu}(\mathbf{x}-\mathbf{x}',t-t')=\tfrac{1}{2}\langle j_\mu(\mathbf{x},t)j_\nu(\mathbf{x}',t')+j_\nu(\mathbf{x}',t')j_\mu(\mathbf{x},t)\rangle. \qquad \ldots\ldots(15)$$

Introducing the Fourier expansion of the operator

$$j_\mu(\mathbf{x},t)=(2\pi)^{-1}\int_{-\infty}^{\infty}d\omega j_\mu(\mathbf{x},\omega)e^{-i\omega t}$$

the integration over λ in (8) can be formally carried out. Comparing the result with the Fourier transform of (15), one can easily find the relation

$$C_{\mu\nu}(\mathbf{x},t)=\int_{-\infty}^{\infty}dt'\Delta(t-t')L_{\mu\nu}(\mathbf{x},t') \qquad \ldots\ldots(16)$$

with

$$\Delta(t)=\frac{1}{2\pi}\int_{-\infty}^{\infty}d\omega e^{-i\omega t}\left\{\frac{\hbar\omega}{2}+\frac{\hbar\omega}{\exp(\beta\hbar\omega)-1}\right\}. \qquad \ldots\ldots(17)$$

When integrated over $\mathbf{x}$ (16) gives the connection between the time-correlation and the relaxation function G introduced by (12). This connection has been thoroughly studied by Kubo (1955), so that the following discussion will be concerned mainly with the other new aspect, i.e. the connection between the space-correlation and diamagnetism. Thus (16) will be applied successively to the classical limit, Landau's diamagnetism and superconductivity.

The well-known fact that there is no diamagnetism in the classical limit is equivalent to the absence of the space-correlation of electronic momenta in the same limit. To see the equivalence, first note that

$$\Delta(t)\to\beta^{-1}\delta(t) \qquad (\hbar\to 0). \qquad \ldots\ldots(18)$$

Thus C and L are identical in this limit, apart from the factor β. Applying classical statistical mechanics, it will be found that

$$C_{\mu\nu}(\mathbf{x}, 0) \to \left(\frac{Ne^2}{m\beta}\right)\delta_{\mu\nu}\delta(\mathbf{x}) \qquad (\hbar \to 0). \qquad \ldots\ldots(19)$$

From (9), (16), (18) and (19) one gets

$$K_{\mu\nu} \to 0 \qquad (\hbar \to 0). \qquad \ldots\ldots(20)$$

Obviously the argument can be reversed and thus (19) and (20) are equivalent to each other.

The effect of the electron–phonon interaction on the diamagnetism of the electron gas is negligible if

$$\tau \gg \hbar\beta \qquad \ldots\ldots(21)$$

where τ is the (average) relaxation time of the function L (Peierls 1933, Dingle 1952). The diamagnetic susceptibility is then given by Landau's formula. Neglecting the electron–phonon interaction in (9), the Fourier transform of K can easily be evaluated (Schafroth 1951)

$$\begin{aligned} K_{\mu\nu}(\mathbf{k}) &= (k^2\delta_{\mu\nu} - k_\mu k_\nu)(\gamma - \gamma_1 k^2 + \ldots) \\ &\simeq (k^2\delta_{\mu\nu} - k_\mu k_\nu)\exp\left[-(\gamma_1/\gamma)k^2\right] \qquad (k \to 0), \qquad \ldots\ldots(22) \end{aligned}$$

with

$$\gamma = \frac{2\pi}{3}\left(\frac{e^2}{mc}\right)k_0, \qquad \gamma_1 = \frac{4\pi}{3}\left(\frac{e^2}{mc}\right)k_0^{-1}.$$

Here k_0 is the Fermi maximum wave number and γ/c is Landau's susceptibility (Nakajima 1955 b). Under the condition (21), the approximation (18) still holds, so that

$$C_{\mu\nu}(\mathbf{x}, 0) = \left(\frac{Ne^2}{m\beta}\right)\delta_{\mu\nu}\delta(\mathbf{x}) + cK_{\mu\nu}(\mathbf{x}). \qquad \ldots\ldots(23)$$

Transforming (22) into $\mathbf{x}$-space, one can see that the space-correlation (23) decreases exponentially with the correlation distance

$$\Delta x = (\gamma_1/\gamma)^{1/2} \sim k_0^{-1}$$

which is an intrinsic quantity of the system.

One advantage of the present unified formalism is that it can cover superconductivity, where electric and magnetic properties are inseparable from each other. Of course here the microscopic theory has not yet been established, so that one cannot evaluate either L or C by means of quantum theory, as has been done above. Nevertheless, by making a phenomenological assumption on L which leads to a set of electromagnetic equations of superconductivity, use can be made of (16) to see what sort of correlation the phenomenological theory does imply. London's theory will be discussed in this manner. The theory is equivalent to the assumption (Schafroth 1951) that

$$\begin{aligned} L_{\mu\nu}(\mathbf{x}, t) &= (2\pi)^{-3}\int dk \exp\left[i\mathbf{k}\cdot\mathbf{x}\right] \\ &\times \left\{\left(\frac{N_s e^2}{m}\right)\frac{k_\mu k_\nu}{k^2} + \left(\frac{N_n e^2}{m}\right)\delta_{\mu\nu}\exp\left[-t/\tau\right]\right\}, \qquad \ldots\ldots(25) \end{aligned}$$

where N_s is the number of superconducting electrons and $N_n = N - N_s$. Inserting (25) into (7), the current is composed of two parts

$$\mathbf{J} = \mathbf{J}^s + \mathbf{J}^n.$$

In terms of the Fourier transforms

$$\mathbf{J}(\mathbf{x}, t) = (2\pi)^{-4}\int_{-\infty}^{\infty} d\omega \int dk \exp\left[i(\mathbf{k}\cdot\mathbf{x} - \omega t)\right]\mathbf{J}(\mathbf{k}, \omega) \text{ etc.},$$

the two parts are given by

$$\mathbf{J}^{n}=\left(\frac{N_n e^2}{m}\right)\left(\frac{\tau}{1-i\omega\tau}\right)\mathbf{E}, \qquad \ldots\ldots(26)$$

and

$$J_\mu^{s}=\left(\frac{N_s e^2}{mc}\right)\left(\frac{k_\mu k_\nu}{k^2}-k^2\delta_{\mu\nu}\right)A_\nu+\left(\frac{N_n e^2}{m}\right)\left(\pi\delta(\omega)+\frac{i\mathrm{P}}{\omega}\right)\frac{k_\mu k_\nu}{k^2}E_\nu \qquad \ldots\ldots(27)$$

respectively. Thus $\mathbf{J}^n$ is the normal ohmic current, whereas $\mathbf{J}^s$ satisfies London's equations,

$$\operatorname{curl}\mathbf{J}^s=-\left(\frac{N_s e^2}{mc}\right)\mathbf{B}, \qquad \frac{\partial\mathbf{J}^s}{\partial t}=\left(\frac{N_s e^2}{m}\right)\mathbf{E}.$$

Now, inserting (25) into (16), the correlation function in this case has the asymptotic behaviour

$$C_{\mu\nu}(\mathbf{x},t)\propto r^{-3}(\delta_{\mu\nu}-(x_\mu x_\nu)r^{-2}) \qquad (r=|\mathbf{x}|\to\infty,\ t\to\infty). \qquad \ldots\ldots(28)$$

There is no definite correlation distance in contrast to (24). Such a long distance correlation has been anticipated by London and discussed recently by Schafroth (1955) with reference to the charged Bose gas.

In general, because of the continuity equation and gauge invariance, the Fourier transform of K must have the form

$$K_{\mu\nu}(\mathbf{k})=(k^2\delta_{\mu\nu}-k_\mu k_\nu)K(k).$$

Combining this with Ampère's law, one obtains the vector potential in the Coulomb gauge as

$$\mathbf{A}(\mathbf{k})=\left[k^2\left\{1-\frac{4\pi}{c}K(k)\right\}\right]^{-1}\mathbf{J}_e(\mathbf{k}) \qquad \ldots\ldots(29)$$

where $\mathbf{J}_e$ is a stationary external current. In order to obtain the Meissner effect (i.e. almost perfect shielding of $\mathbf{J}_e$), $K(k)$ should be singular at $k=0$. If such a singularity is to result from the electron–phonon interaction, the interaction must be so strong that it cannot be treated as perturbation (Schafroth 1951). The long-range correlation due to the singularity depends upon the type of the latter and, at the present stage of the theory, can only be studied in the phenomenological way as shown above.

Acknowledgment

The writer expresses his thanks to Professor H. Fröhlich for stimulating discussions.

References

Band, W., 1955, *An Introduction to Quantum Statistics* (Princeton : van Nostrand), p. 322.
Blatt, J. M., Butler, S.T., and Schafroth, M. R., 1955, *Phys. Rev.*, **100**, 481.
Callen, H. B., and Welton, T. A., 1951, *Phys. Rev.*, **83**, 34.
Dingle, R. B., 1952, *Proc. Roy. Soc.* A, **211**, 517.
ter Haar, D., 1954, *Elements of Statistical Mechanics* (New York : Rinehart), p. 147.
Jauch, J. M., and Rohrlich, F., 1955, *The Theory of Photons and Electrons* (Cambridge, Mass. : Addison–Wesley), p. 469.
Kubo, R., and Tomita, K., 1954 *J. Phys. Soc. Japan*, **9**, 888.
Kubo, R., 1955, *Busseiron Kenkyu*, **88**, 72, 79.
Nakajima, S., 1955 a, *Busseiron Kenkyu*, **88**, 45; 1955 b, *Advanc. Phys.* (*Phil. Mag. Suppl.*), **4**, 313.
Nakano, H., 1955 a, *Busseiron Kenkyu*, **84**, 25; 1955 b, *Ibid.*, **88**, 53.
Peierls, R. E., 1933, *Z. Phys.*, **80**, 763.
Schafroth, M. R., 1951, *Helv. Phys. Acta*, **24**, 645; 1955, *Phys. Rev.*, **100**, 502.
Schiff, L. I., 1949, *Quantum Mechanics* (New York : McGraw-Hill), p. 344.
Wentzel, G., 1949, *Quantum Theory of Fields* (New York : Interscience), p. 66.

The Yield and Angular Distribution of Neutrons from the Reaction ^{63}Cu (p, n)^{63}Zn at 18 MeV

By D. M. THOMSON

Department of Physics, Makerere College, Kampala, Uganda, East Africa

Communicated by J. P. Andrews; MS. received 30th November 1955 *and in revised form* 10*th February* 1956

Abstract. The yield of neutrons from the reaction $^{63}Cu(p, n)^{63}Zn$ at 18 MeV has been measured at five angles to the incident proton direction, using nuclear emulsions to detect the neutrons. The anisotropic angular distributions, which show some preference for the forward direction, and the shape of the neutron energy spectrum, provide some further evidence that the statistical compound nucleus model does not completely account for reactions of this type. The total (p, n) cross section was estimated to be 2×10^{-25} cm^2, in agreement with the value found by Ghoshal at this energy.

§ 1. Introduction

One of the principal methods of investigating the interaction between nuclear matter and nucleons with energies between 10 and 40 MeV is the experimental study of nuclear reactions resulting from the bombardment of medium-heavy nuclei with nucleons in this energy range. Recent measurements (Gugelot 1951, 1954, Cohen 1953, 1955, Cohen *et al.* 1954, 1955, Eisberg and Igo 1954) cast some doubt on the adequacy of the statistical theory (Weisskopf 1937, Weisskopf and Blatt 1952, Hauser and Feshbach 1952), a doubt which can only be resolved by further experimental studies. This paper describes one such study carried out as part of a programme of investigation at Princeton University.

§ 2. Experimental Method

A foil of natural copper (70% ^{63}Cu) with a stopping power of 400 kev for 18 MeV protons was exposed, by A. Emann of Princeton University, to the external beam of the Princeton cyclotron. The energy of the incident protons was taken as 18·2 MeV. The foil was mounted at the centre of a 12 in. diameter scattering chamber, described by Ajzenberg and Franzen (1954), and Ilford C2 nuclear plates (emulsion thickness 400 microns) were supported round the chamber at 30°, 60°, 90°, 120° and 150° to the incident proton direction. The proton beam passed through the foil and was collected in an insulated carbon Faraday cup which was connected to a current integrating circuit.

After exposure the nuclear plates were processed by A. G. Rubin of Boston University, and later examined at Makerere College under a Cooke M 4000 microscope. A 45× oil immersion objective was used with 10× eyepieces.

§ 3. Treatment of Observations

Proton recoil tracks were accepted up to angles corresponding to 15° in azimuth, and 15° in dip from the neutron direction in the unprocessed emulsion. Corrections for obliquity were made individually to the small number of recoil tracks produced by neutrons with energies greater than 8 Mev, and an average correction was applied to the more numerous tracks arising from particles of lower energy. Neutron energies were obtained from the range–energy relations due to Rotblat (1951) and Gibson *et al.* (1954). The energy distributions of neutrons from the target were found by correcting the distributions in the plates for the effect of the escape of some recoil tracks from the emulsion, and for the variation of the neutron–proton scattering cross section with energy. No correction was made for neutrons from sources other than the target. Other experiments using the same apparatus and technique have shown that this background is small (Ajzenberg and Franzen 1954).

Finally differential cross sections for neutron production in the target were worked out at each angle in the centre-of-mass coordinate system. For this purpose the neutrons were divided into three groups, each group containing particles within a particular range of energy E:

1. $1{\cdot}50 < E < 4{\cdot}00$ Mev
2. $E > 4{\cdot}00$ Mev
3. $E > 8{\cdot}00$ Mev

It is not easy to divide up the continuous energy distributions of neutrons in this way into well-defined energy groups, since the number of particles per unit energy interval decreases more or less exponentially with increasing energy, and the range–energy relation is affected by the rather uncertain water content of the emulsion. The difficulties are particularly great at the lower energy limits of the groups and it is estimated that errors of up to 30% may be introduced into the absolute values of the differential cross sections from these causes.

Errors due to inaccurate alignment of the scattering chamber and the possible migration of the beam from the centre of the target during the bombardment are hard to compute; they may be as great as 10%.

It is well known that the efficiency of the observer is an important factor in all work with nuclear emulsions. An attempt has been made to check efficiency by recounting some of the data, particularly at the low energy end of the spectrum, where tracks are confined to a single field of the microscope and are therefore more likely to be missed. In the worst case a recount increased the total by 20%, but this particular count was already suspected of being low. In other cases no differences were found greater than 10%.

The standard errors shown on the graphs in figures 1 and 2 are derived simply from the counting statistics. Between 180 and 400 tracks were counted at each angle in energy groups 1 and 2, and between 25 and 60 in group 3. Though the experimental errors which have been mentioned may introduce errors of between 30 and 40% into the absolute values of the cross sections, the relative values at the various angles should be considerably more reliable. This is because all the data were recorded at the same time, and all the plates were examined by the same observer. Most of the sources of error affect the data at each angle in a similar way.

§ 4. Results

The main results are presented in figures 1 and 2. In figure 1 the energy distribution of neutrons at 30° is given in a form which is often used for comparisons with the statistical compound nucleus theory. The ordinate Y, plotted on a logarithmic scale, is $(1/ES)\ (\partial^2\sigma/\partial\Omega\partial E)$. E is the energy of the outgoing

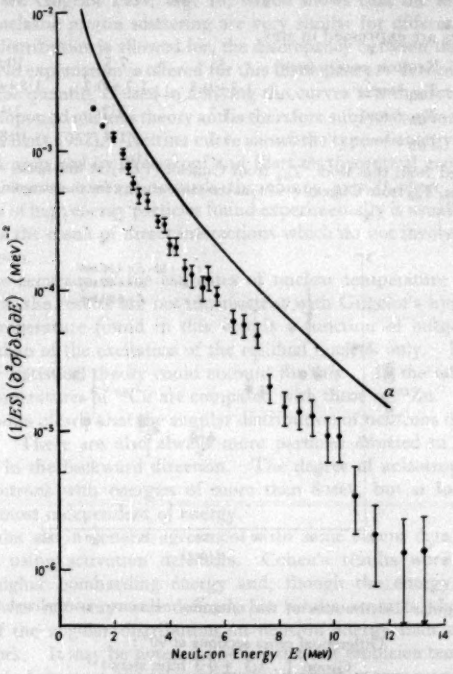

Figure 1. $(1/ES)(\partial^2\sigma/\partial\Omega\partial E)$ plotted against neutron energy at 30° for ^{63}Cu (p, n) ^{63}Zn at 18·2 Mev. Curve *a* taken from Gugelot (1954) for the reaction ^{63}Cu (p, p′) ^{63}Cu. Equal abscissae on the two curves indicate equal excitations of the residual nucleus.

particle in Mev; $\partial^2\sigma/\partial\Omega\partial E$ is the differential cross section for the emission of a particle of energy between E and $E+dE$ into unit solid angle. $\delta\Omega$ is the element of solid angle. S is the cross section, including the effects of barrier penetration, for the formation of the compound nucleus in the same state of excitation, by the reverse reaction, in which particles of energy E strike the excited residual nucleus. This last quantity cannot be measured experimentally and must be estimated. Curve *a* on figure 1 was derived from the spectrum of inelastically scattered protons found by Gugelot (1954) when a copper foil was bombarded by 18 Mev protons. It is taken from figure 10 of Gugelot's paper, and is plotted in the same absolute units as the new data. According to statistical theory both curves show the dependence of the density of levels of a nucleus of mass 63 on its energy of excitation, and should be expected to correspond closely.

In addition to comparing the densities of levels given by the two curves, nuclear 'temperatures' have been calculated from them at various energies, and the results are tabulated for comparison. The nuclear temperature T is defined by the relation (Weisskopf and Blatt 1952):

$$\frac{1}{T} = -\frac{\partial(\ln Y)}{\partial E}$$

Temperatures are expressed in MeV.

Neutron energy (MeV)	5	7·5	10·0
T_{exp} (MeV)	1·5 ± 0·3	1·7 ± 0·2	1·8 ± 0·3
T_{GA} (MeV)	1·7	2·2	2·4
T_{GB} (MeV)	1·3	1·4	1·8

T_{exp} derived from this work, T_{GA} from Gugelot (1954) at the same excitation of the residual nucleus, T_{GB} from Gugelot (1954) at the same energy for the outgoing particle.

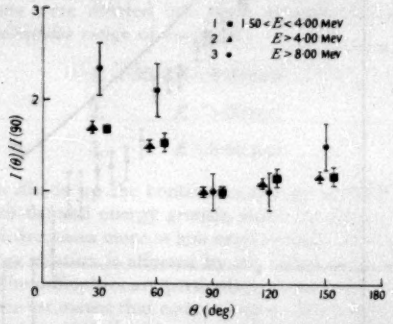

Figure 2. Angular distributions of the outgoing neutrons, normalized to unity at 90°.

Differential cross sections at 90°:

Group 1 5·3 ± 0·3 mbn sterad^{-1}
Group 2 2·41 ± 0·13 mbn sterad^{-1}
Group 3 0·21 ± 0·04 mbn sterad^{-1}

Figure 2 shows the angular distributions of the three energy groups of neutrons from the reaction $^{63}Cu(p, n)^{63}Zn$. The intensities at each angle have been divided by the intensity of the same group at 90°. The absolute values of the differential cross sections for the production of the various groups at 90° are given in the caption.

From the angular distribution data an estimate was made of the total cross section for the (p, n) reaction on copper at 18 MeV. To do this the energy spectrum was extrapolated to lower energies assuming that it followed the Maxwellian form predicted by the statistical theory (Weisskopf and Blatt 1952). The value obtained was

$$\sigma_{pn} \sim (2 \pm 0{\cdot}6) \times 10^{-25} \text{ cm}^2.$$

§ 5. Discussion of Results

The densities of levels given by the two curves in figure 1 differ by a factor of two (approximately) over the whole range of energy. This seems more than can be accounted for by the experimental errors mentioned above, or by the additional fact that Gugelot's curve refers to ^{63}Cu and 150° and the new data to ^{63}Zn and 30° (see Gugelot 1954, Fig. 10, which shows that the level densities derived from inelastic proton scattering are very similar for different elements). If the angular distribution is allowed for, the discrepancy between the two curves is increased. No explanation is offered for this discrepancy. It should be noted, however, that the quantity S used in deriving the curves is a theoretical estimate based on the compound nucleus theory and is therefore subject to some uncertainty (Weisskopf and Blatt 1952). Neither curve shows the type of energy dependence of level density proposed by Weisskopf and Blatt on theoretical grounds, which would lead to curves concave towards the energy axis (Cohen 1953). The apparent excess of high energy particles found experimentally is usually explained, qualitatively, as the result of direct interactions which do not involve compound nucleus formation.

Though the accuracy of the estimates of nuclear temperature in the table is not very high, the results are not inconsistent with Gugelot's hypothesis that the nuclear temperature found in this way is a function of outgoing particle energy rather than of the excitation of the residual nucleus only. It is not easy to see how the statistical theory could account for this. In the table of course the nuclear temperatures of ^{63}Cu are compared with those of ^{63}Zn.

Figure 2 shows clearly that the angular distribution of neutrons of all energies is anisotropic. There are also always more particles emitted in the forward direction than in the backward direction. The degree of anisotropy is slightly greater for neutrons with energies of more than 8 MeV, but at lower energies seems to be almost independent of energy.

These results are in general agreement with some recent data obtained by Cohen (1955) using activation detectors. Cohen's results were obtained at a somewhat higher bombarding energy and, though the energy response of his detectors was not very well defined, his results seem to show a greater dependence of the angular distribution on neutron energy than was found in the present work. It may be noted, however, that the emulsion technique made it difficult to get adequate statistical accuracy for the high energy neutrons, because the reduced neutron–proton scattering cross section in the emulsion, at high energies, limits the detected fraction of the already small number of high energy neutrons emitted by the target.

From the theoretical point of view the angular distribution data conflict with the statistical theory as developed by Hauser and Feshbach (1952). According to this theory the angular distributions of particles from reactions of this type should be either isotropic or symmetrical about 90°.

The value of $(2 \pm 0{\cdot}6) \times 10^{-25}$ cm^2 for the total (p, n) cross section is to be compared with the values for Cu(p, n), Cu(p, pn) and Cu(p, 2n) cross sections at various energies measured by Ghoshal (1950), using the stacked foil technique. At 18 MeV he found a total (p, n) cross section of about 2×10^{-25} cm^2, a (p, pn) cross section of 4×10^{-25} cm^2, and a negligible (p, 2n) cross section. The present result is consistent with these values if it is assumed that very few neutrons from the (p, pn) reaction have been detected.

This assumption can be made plausible by considering the effect of the Coulomb barrier on the protons emitted after a (p, pn) reaction. In the case of copper the threshold for the (p, pn) reaction is at 13 MeV, any protons emitted from a compound nucleus formed by incident protons at 18 MeV must therefore have energies considerably below the Coulomb barrier energy, which in this case is about 8 MeV. One therefore expects that most of the protons will have energies close to the theoretical maximum and that, in consequence, the associated neutrons will be mainly of very low energy. If this is so it is not surprising that they have not been detected here.

§ 6. Conclusions

These studies of the Cu(p,n)Zn reaction provide further evidence of the inadequacy of the simple statistical model of nuclear reactions, which is able to explain neither the detailed form of the energy spectrum of the outgoing particles nor the asymmetrical angular distributions. Other types of interaction between the incident particle and the target nucleus, such as those suggested by the theories of Austern, Butler and McManus (1953) and Bohr and Mottelson (1953), which do not involve compound nucleus formation, could give rise to modified energy distributions and to angular distributions in which the forward direction is preferred, but the data do not at present allow one to draw any quantitative conclusions about their importance in the Cu(p, n) process. The position may be clarified as a result of studies of the inelastic scattering of alpha particles, and of the (p, γ) process in medium-heavy nuclei where it appears that very few transitions take place via a compound nucleus (Gugelot, private communication).

Acknowledgments

The author would like to express his very sincere thanks to Professor P. C. Gugelot and to Professor F. Ajzenberg who suggested the work, arranged for the nuclear plates to be exposed at Princeton, and made them available for examination; also to Professor M. G. White for allowing the cyclotron to be used for these exposures. He would also like to thank Messrs. A. Emann of Princeton University and A. G. Rubin of Boston University for carrying out the exposures and for processing the plates, and the Physics Department of Makerere College for providing the facilities for their measurement.

References

Ajzenberg, F., and Franzen, W., 1954, *Phys. Rev.*, **94,** 409.
Austern, N., Butler, S. T., and McManus, H., 1953, *Phys. Rev.*, **92,** 350.
Bohr, A., and Mottelson, B., 1953, *K. Danske. Vid. Selsk. Mat-fys medd.*, **27,** 16.
Cohen, B. L. 1953, *Phys. Rev.*, **92,** 1245; 1955, *Ibid.*, **98,** 49.
Cohen, B. L., and Newman E., 1955, *Phys. Rev.*, **99,** 718.
Cohen, B. L., Newman, E., Charpie, R. A., and Handley, T. H., 1954, *Phys. Rev.*, **94,** 620.
Eisberg, R. M., and Igo, G., 1954, *Phys. Rev.*, **93,** 1039.
Ghoshal, S. N., 1950, *Phys. Rev.*, **80,** 939.
Gibson, W. M., Prowse, D. J., and Rotblat, J., 1954, *Nature, Lond.*, **173,** 1180.
Gugelot, P. C., 1951, *Phys. Rev.*, **81,** 51; 1954, *Ibid.*, **93,** 425.
Hauser, W., and Feshbach, H., 1952, *Phys. Rev.*, **87,** 366.
Rotblat, J., 1951, *Nature, Lond.*, **167,** 550.
Weisskopf, V. F., 1937, *Phys. Rev.*, **52,** 295.
Weisskopf, V. F., and Blatt, J. M., 1952, *Theoretical Nuclear Physics* (New York: John Wiley).

Angular Correlations between Successive Conversion Electrons in ^{80}Br

By E. BREITENBERGER†
Cavendish Laboratory, Cambridge

MS. received 10*th October* 1955

Abstract. The angular correlation between the successive K-conversion electrons from the de-excitation of 4·4-hour ^{80}Br has been investigated, using anthracene scintillation spectrometers in conjunction with coincidence single-channel kicksorters. Disturbing side effects were kept under control by a special procedure of taking data. The correlation function contains only a second-order term with $a_2 \simeq +0{\cdot}30$. This is consistent with the assignment M3/E1, and excludes M3/(M1 + E2). Shell theory then makes the intermediate and ground levels of the cascade $f_{5/2}g_{9/2}$ and $p_{3/2}p_{1/2}$, respectively, but cannot account for the isomeric level (which must be 5^-). The experimental method used in this work can be applied to other e–e cascades.

§ 1. General Introduction

During the last five years, measurements of the correlations between the directions of emission of successive nuclear radiations have become increasingly useful for the spectroscopy of short-lived nuclear states (see the recent review by Frauenfelder 1955). Most results, in form of spin assignments, values of magnetic moments and mixing ratios, were obtained from gamma-ray cascades. Cascades involving conversion electrons have received less attention. They offer many interesting possibilities, quite apart from the obvious cases in which an electromagnetic transition is so strongly converted that one can only observe the electrons. Above all, the pertaining correlation functions depend on the (relative) parities of the involved nuclear levels (e.g. Biedenharn and Rose 1953) so that one has here a means of distinguishing between electric and magnetic transitions. With mixed transitions, on the other hand, it can be helpful to investigate the angular correlations of both the unconverted and the converted cascades; this will provide a check on the results, and may serve to remove ambiguities of interpretation arising from the two possible signs of the interference term. Some other points are discussed by Rose (1953).

These attractive features are balanced by experimental complications. First of all, the interesting cases are those of reasonably large conversion coefficients. More often than not, this means low electron energies. Serious scattering effects can then occur and require the use of laborious precautions (Breitenberger 1954c). Secondly, explicit correlation functions being available for K-shell conversion only (Biedenharn and Rose 1953), the K-electrons must be singled out by a spectrometric technique.

† Now at Department of Physics, University of Malaya, Cluny Road, Singapore 10.

The first experiments did not go so far, and remained inconclusive. By means of Geiger–Müller counters and fairly thick sources, e–e correlations were observed by Russinov and Chuykin (1949) in ^{80}Br, by Ward and Walker (1949) in ^{181}Ta, and by the Zürich group (Frauenfelder, Walter and Zünti 1950, Walter, Huber and Zünti 1950) in ^{197}Hg. Lundby (1949) searched for a β–e correlation in the decay ^{181}Hf$\rightarrow$ ^{181}Ta, Stevenson and Deutsch (1951) mention a γ–e correlation in ^{86}Rb, and Roy and Goes (1953) observed an α–e correlation in the decay Io$\rightarrow$ Ra with a cloud-chamber method.

Successful measurements of e–γ and γ–e correlations have recently been made by McGowan (1953) in ^{207}Pb, using a scintillation spectrometer, by Goldberg and Frankel (1954) in ^{121}Te and ^{123}Te, and by Golden and Frankel (1954) in ^{117}Sn, using a lens spectrometer, and by the Zürich group (Gerber *et al.* 1954, Gimmi, Heer and Scherrer 1954) in ^{111}Cd, using a small 180° magnet. Golden and Frankel (1954) also paid special attention to the scattering problem.

Accurate experiments with two successive conversion electrons have not yet been done. The most obvious method to achieve the required separation of the conversion lines is to use two β-spectrometers. Arrangements of this kind have been designed for various purposes (Klemperer 1935, Feather 1940, Feather, Kyles and Pringle 1948, Fowler and Shreffler 1950, Siegbahn 1952, Bell and Graham 1952; on post-acceleration see Butt 1950, Schneider 1952 and Mayne 1952), but apart from questions of bulk and expense there is the disturbing magnetic interference between the two spectrometers which becomes quite serious if, as in all correlation work, their relative position is varied during the experiment (see especially Siegbahn 1952). One could also think of employing proportional counters with thin entrance windows. However, a simple discussion in terms of window thickness, gas pressure, etc., shows that such detectors attain unmanageable dimensions unless all relevant pulse groups happen to lie within a relatively narrow range, e.g. from 200 to 250 kev. Finally, one may consider scintillation counters. Their energy resolution can be assessed theoretically (Breitenberger 1955) and is readily found to suffice for correlation work with a good many, though not with all, e–e cascades.

The present paper describes an attempt, briefly reported earlier (Breitenberger 1954 b), to investigate e–e correlations by means of anthracene scintillation spectrometers in conjunction with coincidence single-channel kicksorters of a special design (Breitenberger 1953 a). To test the method fully the somewhat unfavourable case of ^{80}Br was chosen. Another experiment will be described later.

§ 2. The Case of ^{80}Br

The well-known 4·4-hour isomeric state of ^{80}Br de-excites through a completely converted transition of energy 48·1 kev which is followed by a partially converted γ-ray of 36·3 kev. The pertaining conversion lines are, in obvious notation,

$$\begin{array}{llll} 1_K \ldots 34{\cdot}6 & & 2_K \ldots 22{\cdot}8 & \\ 1_L \quad 46{\cdot}5 & & 2_L \quad 34{\cdot}7; & \end{array}$$

it is seen that 1_K and 2_L accidentally coincide.

Berthelot (1944), to whom the decay scheme is due, concluded that the two transitions were M3 and M1, respectively. Segrè and Helmholz (1949) later put forward that this M3/M1 cascade should permit a competitive E4 cross-over;

since no radiation of corresponding energy is observed the second transition should be E1 rather than M1, thus making the cross-over a slower M4. In fact, West and Rothwell (1950) measured a K-conversion coefficient of 1·2 for the second transition, in good agreement with the theoretical value 1·33 (from Hebb and Uhlenbeck 1938) for E1. A similar result was briefly reported by Lidofsky, Macklin and Wu (1950).

In the light of empirical lifetime–energy data (Goldhaber and Sunyar 1951) the absence of the cross-over is, however, not particularly significant, both E4 and M4 transitions being much slower than indicated by older theoretical estimates. Hence there is no strong reason why the second transition in ^{80}Br should be E1. The theoretical K-conversion coefficients are 0·61 for M1 (extrapolated according to Goldhaber and Sunyar 1951, p. 908) and 23 for E2 (from Hebb and Uhlenbeck 1938); thus the experimental value 1·2 can also be interpreted to mean mixing between M1 and E2 in a ratio of very nearly 1 : 1 (i.e. 1 : 0·025 for the unconverted γ-rays). This alternative is not excluded by the fact that the half-life of the 36 kev state is shorter than 4 mμsec (Wright and Deutsch 1951). According to the empirical data the half-life expected for pure M1 is 2 mμsec (conversion correction included), and even with an appreciable admixture of E2 it need not be larger than 4 mμsec. Thus the whole evidence, although entirely compatible with the assignment E1, does not exclude the alternative assignment M1 + E2.

The angular correlation of the successive K-conversion electrons should allow one to decide clearly between the two possibilities. The theoretical correlation coefficients are best obtained by graphical interpolation and extrapolation based on the numerical tables of Biedenharn and Rose (1953). For the M3/E1 cascade one finds

$$a_2 = +0{\cdot}293 \pm 0{\cdot}015. \qquad \ldots\ldots(1)$$

If the second transition is pure M1 the correlation is practically isotropic; in the case of mixing it becomes necessary to take into account that the spin of the ground state of ^{80}Br is 1, and one obtains for the cascade 5(M3)2(M1 + E2)1 with a mixing ratio of 1·0

$$a_2 = +0{\cdot}075 \pm 0{\cdot}015 \quad \text{or} \quad +0{\cdot}133 \pm 0{\cdot}015, \qquad \ldots\ldots(2)$$

depending on the relative phase of the matrix elements, together with an additional $a_4 = -0{\cdot}007 \pm 0{\cdot}002$ in either case. The indicated errors have been compounded from the estimated extremal uncertainties of the graphical evaluation, and represent safe upper limits for the standard deviations in a roughly gaussian sampling distribution. The alternative values (1) and (2) differ so strongly that a correlation experiment seems promising despite the embarrassingly low electron energies.

§ 3. The Apparatus

Apart from the electronic equipment which has been described elsewhere (Breitenberger 1953 a), the correlation apparatus consisted of two scintillation spectrometers mounted inside a steel vacuum bell of 31 cm internal diameter. The movable spectrometer was supported by an arm fixed to a rotating vacuum seal in the centre of the base plate of the steel bell, and could be put into all positions between 40° and 180° with respect to the fixed spectrometer; the angle of position, denoted hereafter by δ, could be adjusted from the outside to better than one-tenth of a degree. The photomultipliers (selected EMI 6262 tubes

of high sensitivity) were held vertically with the cathodes facing downwards; hollow mirrors were used to deflect the light from the vertical crystals through 90° on to the cathodes.

Anthracene was chosen as a scintillator because of its high luminescence yield, the low backscatter and the small sensitivity to γ-rays. The required crystal thickness was determined with the aid of the curves in figure 1. The ground

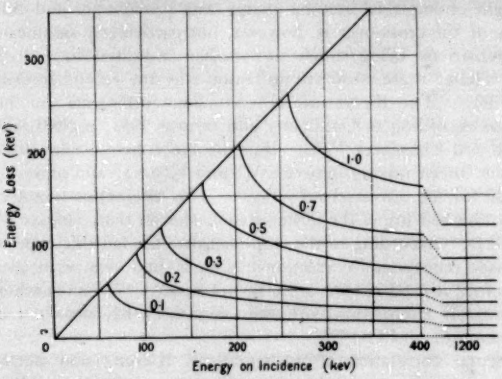

Figure 1. Energy loss suffered by monoergic electrons on passage through anthracene layers of 0·1 to 1·0 mm thickness; calculated from range–energy curves given by Glendenin (1948) for aluminium, assuming equal stopping power for all atomic electrons.

state of ^{80}Br emits β-particles with energies up to 2 MeV; it is seen that a thickness of a little more than 0·5 mm limits the pulse height so as to prevent unnecessary overloading of the amplifiers, yet not so much that the β-pulses pile right on top of the conversion electron pulses. The crystals used, of 0·6 mm thickness and 23 mm diameter, had been cemented to a supporting base of Perspex by the makers, Messrs. Nash and Thompson. An aluminium layer of about 3000 Å was evaporated on top of the anthracene to serve as reflector. This thickness stops all electrons of less than 7 kev (e.g. the L→MM Auger electrons of Br) but causes only a negligible energy loss to harder electrons (less than 1·5 kev to electrons of more than 20 kev).

Sources could be introduced into the apparatus through a vacuum lock in the side wall of the steel tank. The lock chamber was cylindrical and contained a removable sliding piston which carried the source holder; the accuracy of assembly was such that the axis of the chamber, if produced, met the axis of revolution of the movable spectrometer to within 0·3 mm. Thus the relative uncertainty of source position was very small, the source-to-crystal distance being 87 mm (cf. Breitenberger 1954 a).

The inside of the tank was covered with a layer of white wax to reduce backscatter, and the spectrometers were shielded against the source by waxed screens. During the experiments the apparatus was being continuously pumped; a 50 litre diffusion pump was required to maintain the pressure below 0·1 μ Hg against the large flow of gases from the wax.

§ 4. Preparation of the Sources

The best choice for the source backings seemed to be beryllium. It is obviously most suitable as far as electron scattering effects are concerned; being a metal, it also provides enough conduction electrons for the rapid neutralization of the Br ions left behind by the first conversion transition, so that no serious hyperfine structure perturbation of the intermediate state need be feared. Moreover, a metallic source cannot cause any troubles by charging up under the continuous loss of electrons (cf. Braden *et al.* 1948, Douglass 1949, Gross 1951).

Thin beryllium films were produced according to a technique developed in this laboratory by R. H. M. Lamb. The metal was evaporated on to microscope slides which had previously been covered, also by evaporation, with a thin layer of rock salt. The beryllium films could then be floated off on a clean water surface in the usual way, and were picked up on little wire frames of $\frac{1}{2}$ inch square. Only faultless fresh films of about 3000 Å thickness were used in the experiments.

The activity was obtained carrier-free by Szilard–Chalmers process in ethylene dibromide subsequent to neutron capture in stable ^{79}Br. About 75 cm³ of technical $C_2H_2Br_2$ were first washed twice, each time with 5 cm³ of distilled water, then twice with 5 cm³ of ammonia (20%, *pro analysi*), again twice with 5 cm³ of water, then left to clear completely, separated from water drops, and finally irradiated for one hour with slow neutrons from the Cavendish cyclotron. The bulk of the active matter could be washed out by shaking twice, each time for 5 minutes with 0·5 cm³ of distilled water.

The two portions of active solution were combined, made alkaline with ammonia in order to bind the activity in non-volatile form (NH_4BrO and NH_4Br), and concentrated to a few drops in the vacuum of a water-jet pump. The concentrate was diluted 1:1 with ethyl alcohol (96%, *p.a.*) to reduce surface tension; a drop of this mixture could safely be applied to a beryllium film and dried under a 60-watt lamp. After drying the active spot, of about 6 mm diameter, was barely visible. On a clean glass surface the mixture left no visible residue at all, provided reactive impurities were removed from the raw material by the operations outlined above, and a high standard of cleanliness was observed throughout.

Immediately after the irradiation the 18-minute ground state of ^{80}Br was present in considerable excess; equilibrium with the 4·4-hour metastable state was attained two and a half hours later. No source was used before this interval had elapsed. The sources also contained an appreciable amount of ^{82}Br, formed by neutron capture in the other stable isotope ^{81}Br; the background of β-rays and hard γ-rays from this nuclide was not further troublesome.

§ 5. The Pulse Spectrum

The observed pulse spectrum of ^{80}Br is shown by the heavy contour in figure 2. The broad hump on the right was much higher in the spectrum of a fresh source, and shrank with a half-life of 18 minutes to the relative size shown in the figure; it is thus due to the β-particles emitted by the ground state. Its long tail is compressed by amplifier overload into the sharp spike on the extreme right. The shape of the hump is easily understood from figure 1. The rise towards zero pulse height is due, according to a spectrometer calibration which was obtained from the observation of test sources, to the x-rays and K→LL Auger

electrons accompanying the internal conversion, and to the Compton edge at 4·5 kev of the unconverted 36 kev γ-rays. The high peak of the spectrum thus must be due to the three conversion lines at 23, 35 and 47 kev. The widths of these lines can be predicted (Breitenberger 1955) from the known spectrometer efficiency, and should be approximately $\eta = 0{\cdot}58$, 0·48 and 0·41, respectively; their intensities can be estimated from the K/L ratios and conversion coefficients measured by Berthelot (1944) and West and Rothwell (1950), and should be roughly in the ratio 0·5 : 1 : 0·15 (for later application, we note that the middle line contains less than 15% 2_L). With the help of these data the peak can be decomposed by trial and error into the three equidistant gaussian curves indicated in the figure.

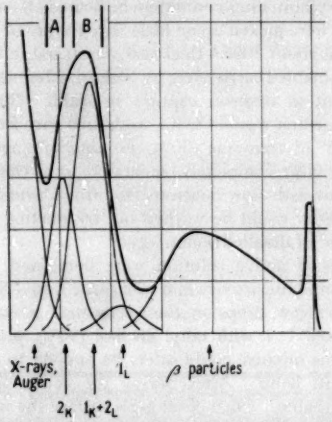

Figure 2. Pulse spectrum of ^{80}Br, as observed in anthracene crystal of 0·6 mm thickness. Ground state in equilibrium with metastable state, background from ^{82}Br subtracted.

Independent proof of this decomposition was afforded by scanning the spectrum for coincidences with the aid of the single-channel kicksorters. The two spectrometers were backed, respectively, by the channels marked A and B in figure 2; then one of the channels was swept over the spectrum while the other was kept fixed. The observed distribution of coincidences is shown in figure 3.

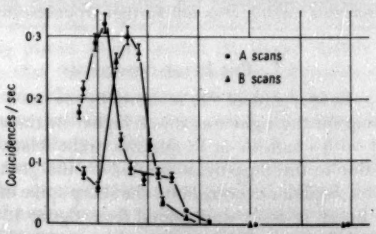

Figure 3. Distribution of coincidences in the pulse spectrum of ^{80}Br. The scale of abscissae is the same as in figure 2.

It agrees very well with the hypothetical decomposition; the slight upward shift of the 1_L line is presumably due to non-linearity of the crystal response. For this measurement the movable spectrometer was put at 54·5°; at this angle $P_2(\cos\delta)$ vanishes, so that the coincidence counts were not affected by differences in the angular correlations of the various pairs of conversion electrons.

§ 6. Manner of Taking Data

As the separation of the three conversion lines was incomplete, the correlation experiment had to be done with the two channels in such positions that the admixture of other coincidences to 1_K–2_K became as small as possible. The channels marked A and B in figure 2 were considered to be most suitable. They contain mainly 2_K and 1_K electrons, respectively, and the impurities do not amount to more than 30% 1_K and 5% 2_L in A, and 5% 1_L, 10% 2_K and 15% 2_L in B. From these figures one readily calculates that at least 80% of the total coincidence count between A and B is due to 1_K–2_K coincidences, the background being almost wholly 1_K–2_L coincidences.

In the interest of accumulating enough coincidences despite the short half-life, of making random the effects of source scattering (Breitenberger 1954 c), and of minimizing decentring errors (Breitenberger 1954 a), the correlation measurement was made on eight sources. Each source was centred as accurately as possible in a vertical plane of azimuth ϵ; the eight azimuths were chosen at 20° intervals from 20° to 160° with respect to the fixed spectrometer. It seemed convenient also to take data at eight angular positions; for a reason to be explained presently, the order of the eight counting angles δ_μ was permuted from one source to the next according to the following scheme:

ϵ \ δ	40	60	80	100	120	140	160	180
20	6	3	4	1	5	7	2	8
40	—	4	7	2	6	1	3	5
60	2	—	5	4	3	6	7	1
80	3	7	—	5	4	2	1	6
100	7	5	1	—	2	4	6	3
120	1	2	6	3	—	5	4	7
140	4	1	3	6	7	—	5	2
160	5	6	2	7	1	3	—	4

This is a sort of 'latin square' and has been constructed with the help of a table of random numbers in such a way that each of the numbers 1 . . . 7 occurs just once in each column and in each row.

Channel A was attached to the fixed spectrometer because it had to deal with softer electrons than B. The counting time per source amounted to about four hours; about 25 000 coincidences were collected in all.

The ratio of ^{80}Br to ^{82}Br was computed for each source from the observed decrease with time of the single counting rate through channel A. The contribution by ^{82}Br to each single count through A was then calculated, and subtracted. This correction was smaller than 40% throughout.

For each angle δ_μ the sum of the coincidence counts was divided by the sum of the corrected single counts through A, to give the relative coincidence rate k_μ. Apart from its bearing on the effects of scattering and decentring this procedure corrects automatically for the decay of ^{80}Br, for counting time, and for all effects

which are equivalent to fluctuations of the sensitivity of the fixed detector. The latter were presumably present in the form of apparent common channel boundary drift due to random changes in the gain of the multiplier, and are serious in as much as channel A sits on a rather steep flank of the spectrum (cf. Breitenberger 1953 a).

Since the counting rates changed appreciably during each of the eight runs the ever-present effects of pile-up of pulses and of loss of charge on coupling condensers were time-dependent, and would have imposed a trend on the k_μ if the counts of every run had been taken in the same regular sequence, for instance beginning at 40° and ending at 180°. The correction for the background from ^{82}Br, with its unavoidable inaccuracy, seemed also capable of producing such systematic deviations. Permutation of the counting angles in accordance with the scheme mentioned above destroyed all these trends, transforming them into an effectively random, and therefore harmless, error.

Finally, the standard deviations s_μ of the k_μ were estimated in the usual way from the sampling errors of the primary data, without accounting for any variability due to causes other than the randomness of radioactive decay. However, such causes of extra variability were given by the randomized trends, by the somewhat unequal activities and thicknesses of the eight sources which obviously prevented the scattering effects from balancing exactly, and also by those channel boundary drifts which affected the admixture of background correlations to the one under investigation. Consequently the s_μ had to be regarded as under-estimates.

§ 7. Reduction of Data

The data were reduced by the method outlined in an accompanying note (Breitenberger 1956). Graphical inspection showed that the experimental points were fairly well represented by the function $K'(\delta) = 1{\cdot}20 + 0{\cdot}34 P_2(\cos\delta)$. The full normal equations were then set up, but solved first for two unknowns only; i.e. the third equation was dropped, and Δ_4 was omitted from the other two. The result was:

$$\Delta = -0{\cdot}01276, \qquad \Delta_2 = +0{\cdot}00268, \qquad \ldots\ldots(3)$$

$$[pvv] = 0{\cdot}01189. \qquad \ldots\ldots(4)$$

The values (3) are so small that no second approximation is necessary.

Dividing (4) by the adopted weighting constant gives

$$[pvv]/p_0 = 13{\cdot}30. \qquad \ldots\ldots(5)$$

As a χ^2 of 6 degrees of freedom this value is significant on the 3% level, that is, the odds against its being due to pure chance are 33 to 1. Hence the fit is rather bad. In the first line, we may attribute this fact to the presence of a small P_4-term in the correlation function, which should indeed be there if the second transition is M1 + E2: see § 2. Solution of the full normal equations now results in a $[pvv]$ of 0·01007, so that

$$[pvv]/p_0 = 11{\cdot}26. \qquad \ldots\ldots(6)$$

As a χ^2 of 5 degrees of freedom this value is significant on the 5% level. Thus the fit is a little better, but it remains to be seen whether the improvement itself is significant. This question is easily settled by means of a variance ratio test. We can write $13{\cdot}30 = 11{\cdot}26 + 2{\cdot}04$. If it is possible to split a χ^2 of 6 degrees of freedom into a χ^2 of 5 degrees of freedom and a further member, the latter must

behave statistically like a χ^2 of one degree of freedom according to the definition of χ^2. Hence the quotient $2{\cdot}04/[11{\cdot}26/5]=0{\cdot}906$ is sampled in a variance ratio distribution of one degree of freedom in the numerator and 5 degrees of freedom in the denominator. The 20% point of this distribution lies at 2·18; thus the sampled value 0·906 is seen to be due to mere chance with a probability of more than 0·2. The improvement of (6) over (5) is therefore entirely insignificant, and the hypothesis of a fourth-order term must be discarded.

Since the possibility of a spurious trend in the data could be ruled out through a graphical discussion the apparently bad scatter of the points had to be attributed to a significant underrating of the counting errors. Of course, this sort of argument could always be conjured up to account for a bad fit. However, in the present case the χ^2-test allows one to show that the required provision for inadequacies of design and execution of the experiment is kept within plausible bounds. It seems indeed not unreasonable to allow for additional errors of one, or perhaps 1·5, per cent in every count. We are thus led to suspect that the s_n, which lay between 2·5 and 3%, are low by a factor of about 1·2. This will not alter the calculations, except that we now obtain instead of (5)

$$[pvv]/1{\cdot}44p_0=9{\cdot}24,$$

and this raises the goodness of fit above the 10% level, a result which may be considered satisfactory. Note that the variance ratio test remains unaffected by any change of the weighting constant.

The solutions (3) can therefore be adopted. They lead to $c_2=0{\cdot}2860$; calculating the standard error of Δ_2, and correcting for angular resolution (Breitenberger 1953 b), the apparent angular correlation coefficient becomes

$$a_2'=+0{\cdot}292\pm0{\cdot}024. \qquad \ldots\ldots(7)$$

The significance of this figure conforms to a t-distribution of 6 degrees of freedom; for example we have the 95% confidence interval

$$0{\cdot}232<\text{true value}<0{\cdot}351. \qquad \ldots\ldots(8)$$

§ 8. Discussion

Although (7) agrees excellently with the theoretical prediction (1) it does not follow straight away that the second transition is E1. Indeed, the possible influence of background correlations has yet to be assessed.

It follows from (8) that the observed mixture of correlations has a_2' greater than 0·232 with a significance of 97·5%. If this value is corrected for scattering by means of the factor given elsewhere (Breitenberger 1954 c) it becomes 0·246. If the second transition is mixed the theoretical correlation coefficient is practically certain to be smaller than 0·162 (upper limit of the 95% confidence interval for the larger of the two possible coefficients (2)), and if this value is to be increased beyond 0·246 by an admixture of at most 20% of parasitic correlations these must have a correlation coefficient of at least 0·565.

It could readily be shown in a subsidiary experiment that the background correlation was most unlikely to have such a large anisotropy. Channel A was shifted so as to lie symmetrically over channel B. It is clear from figures 2 and 3 that in this position mainly 1_K–2_L coincidences will be counted, with an admixture of less than 33% 1_K–2_K; thus what was background in the main experiment was now very prominent. One single source was then used, in the same eight

orientations as above, to take counts at 180° and 54·5° only, and from the data the expression $k(180)/k(54{\cdot}5)-1=c_2$ was calculated. Corrected for angular resolution the result became $0{\cdot}324\pm0{\cdot}036$ (gaussian sampling distribution, standard error estimated allowing for 1·5% extra variability). Here the upper limit of the 95% confidence interval, corrected for scattering, is 0·416; if this value should be due to at least 67% of background admixed to the 1_K–2_K correlation with $a_2=0{\cdot}162$ the background cannot have a correlation coefficient of more than 0·541, again with a significance of 97·5%.

This argument is easily seen to be quite insensitive to small changes in the scattering correction. Furthermore, all other influences on the correlation can safely be neglected. The β–γ and γ–γ coincidences from the decay of ^{80}Br and ^{82}Br should occur mainly in the upper part of the spectrum, and even there they were found to be negligible. In the main, but not in the subsidiary, experiment channel A also contained some Auger electrons and x-rays. The correlations between these and the conversion electrons are isotropic because such cascades proceed through an intermediate state of spin 1/2; any isotropic contribution to (7) would, however, strengthen the above argument, and not weaken it. The combined evidence therefore excludes the assignment M1+E2, and is fully consistent with the assignment E1, on a high level of significance.

It is interesting to consider this result in the light of shell theory. The ground state of ^{80}Br is known to be 1^+ (Fultz and Pool 1952) and thus must have the configuration $p_{3/2}p_{1/2}$. The 36 kev-transition being E1, the intermediate state is 2^- and therefore $f_{5/2}g_{9/2}$. Incidentally, the latter configuration is found for the ground states of ^{74}As, ^{76}As and ^{86}Rb (Nordheim 1951, Scott 1951) so that it may well be expected to compete for the ground state of ^{80}Br; this explains the low energy of the second transition. There is, however, no simple way to account for the metastable state with its spin of 5 and negative parity. On Nordheim rules the only possibility is the configuration $p_{3/2}g_{9/2}$ with a resultant spin of 5, but this would permit a one-proton transition $p_{3/2}\rightarrow f_{5/2}$, of character M1, to the intermediate state. A three-particle transition can be ruled out because parity considerations are found to require two like ones of the three excited particles to be in the same orbit, and a four-particle transition seems altogether unlikely because of the low energy involved. This problem may deserve theoretical study.

Acknowledgments

It is a pleasure to record the successful development work at the Techniques Department of this laboratory of Mr. R. H. M. Lamb, who spared no efforts to improve on the quality of the beryllium films.

This work was carried out under a British Council Scholarship.

References

Bell, R. E., and Graham, R. L., 1952, *Phys. Rev.*, **86**, 212.

Berthelot, A., 1944, *Ann. Phys., Paris*, **19**, 219.

Biedenharn, L. C., and Rose, M. E., 1953, *Rev. Mod. Phys.*, **25**, 729.

Braden, C. H., Owen, G. E., Townsend, J., Cook, C. S., and Shull, F. B., 1948, *Phys. Rev.*, **74**, 1539.

Breitenberger, E., 1953 a, *Phil. Mag.*, **44**, 987; 1953 b, *Proc. Phys. Soc.* A, **66**, 846; 1954 a, *Phil. Mag.*, **45**, 497; 1954 b, *Nature, Lond.*, **173**, 737; 1954 c, *Proc. Phys. Soc.* A, **67**, 1108; 1955, *Progr. Nucl. Phys.*, **4**, 56; 1956, *Proc. Phys. Soc.* A, **69**, 489.

BUTT, D. K., 1950, *Proc. Phys. Soc.* A, **63,** 986.
DOUGLASS, D. G., 1949, *Phys. Rev.*, **75,** 1960.
FEATHER, N., 1940, *Proc. Camb. Phil. Soc.*, **36,** 224.
FEATHER, N., KYLES, J., and PRINGLE, R. W., 1948, *Proc. Phys. Soc.* A, **61,** 466.
FOWLER, C. M., and SHREFFLER, R. G., 1950, *Rev. Sci. Instrum.*, **21,** 740.
FRAUENFELDER, H., 1955, *Beta- and Gamma-Ray Spectroscopy*, ed. K. Siegbahn (Amsterdam: North-Holland Publishing Co.), pp. 531–599.
FRAUENFELDER, H., WALTER, M., and ZÜNTI, W., 1950, *Phys. Rev.*, **77,** 557.
FULTZ, S. C., and POOL, M. L., 1952, *Phys. Rev.*, **86,** 347.
GERBER, H. J., GIMMI, F., HEER, E., and SCHERRER, P., 1954, *Helv. Phys. Acta*, **27,** 180.
GIMMI, F., HEER, E., and SCHERRER, P., 1954, *Z. Phys.*, **138,** 394.
GLENDENIN, L. E., 1948, *Nucleonics*, **2,** No. 1, 12.
GOLDBERG, N., and FRANKEL, S., 1954, *Phys. Rev.*, **93,** 1425.
GOLDEN, R. K., and FRANKEL, S., 1954, *Phys. Rev.*, **94,** 613(A).
GOLDHABER, M., and SUNYAR, A. W., 1951, *Phys. Rev.*, **83,** 906.
GROSS, L., 1951, *Phys. Rev.*, **82,** 319(A).
HEBB, M. H., and UHLENBECK, G. E., 1938, *Physica*, **5,** 605.
KLEMPERER, O., 1935, *Phil. Mag.*, **20,** 545.
LIDOFSKY, J. J., MACKLIN, P. A., and WU, C. S., 1950, *Phys. Rev.*, **78,** 318(A).
LUNDBY, A., 1949, *Phys. Rev.*, **76,** 993.
MAYNE, K. I., 1952, *Rep. Progr. Phys.* (London : Physical Society), **15,** 24.
MCGOWAN, F. K., 1953, *Phys. Rev.*, **92,** 524.
NORDHEIM, L. W., 1951, *Rev. Mod. Phys.*, **23,** 322.
ROSE, M. E., 1953, Oak Ridge National Laboratory, ORNL-1555.
ROY, R. R., and GOES, M. L., 1953, *Nature, Lond.*, **172,** 360.
RUSSINOV, L. I., and CHUYKIN, E. I., 1949, *Doklady Akad. Nauk U.S.S.R.*, **68,** 1029.
SCHNEIDER, H., 1952, *Helv. Phys. Acta*, **25,** 259.
SCOTT, J. M. C., 1951, *The Spins of Odd Nuclei with Even Mass Number* (Cavendish Laboratory, privately circulated).
SEGRÈ, E., and HELMHOLZ, A. C., 1949, *Rev. Mod. Phys.*, **21,** 271.
SIEGBAHN, K., 1952, *Ark. Fys.*, **4,** 223.
STEVENSON, D. T., and DEUTSCH, M., 1951, *Phys. Rev.*, **83,** 1202.
WALTER, M., HUBER, O., and ZÜNTI, W., 1950, *Helv. Phys. Acta*, **23,** 697.
WARD, A. H., and WALKER, D., 1949, *Nature, Lond.*, **163,** 168.
WEST, D., and ROTHWELL, P., 1950, *Phil. Mag.*, **41,** 873.
WRIGHT, W. E., and DEUTSCH, M., 1951, *Phys. Rev.*, **82,** 277.

The Capture Cross Section of Neutrons by Boron

By C. H. COLLIE†, R. E. MEADS† and E. E. LOCKETT‡

†The Clarendon Laboratory, Oxford

‡ Atomic Energy Research Establishment, Harwell, Berks.

MS. received 13*th September* 1955, *and in revised form* 24*th February* 1956

Abstract. The capture cross section of natural boron for slow neutrons has been measured by a dynamic method, in which the decay constant of neutrons in a water tank was plotted against the concentration of added borax. Samples were compared with a standard boron oxide in GLEEP at the Atomic Energy Research Establishment, Harwell. The result is quoted as $\sigma_B = 760 \pm 3$ barns for the A.E.R.E. sample of natural boron oxide.

§ 1. Introduction

The capture cross section of thermal neutrons by boron $^{10}B(n, \alpha)^7Li$ is an important constant in the practice of low energy nuclear physics. As has been pointed out recently (Green *et al.* 1954) there is a discrepancy of about 20 barns between the best American and European values of this constant which significantly exceeds the estimated error of about 5 barns which the various groups assign to their measurements.

It was therefore thought to be worth while to use the apparatus which we had set up for measuring the absolute n–p capture cross section (Meads *et al.* 1956) to make yet another precise measurement of the constant.

§ 2. Experimental Method

If a cloud of neutrons is released in a tank of water it will disappear by capture, and the total number present will decay exponentially, because the capture cross section is inversely proportional to the relative velocity of the neutron and proton.

If some borax is dissolved in the water the decay will still be exponential because the cross section of the $^{10}B(n, \alpha)^7Li$ reaction also obeys the $1/v$ law, but the average life will be less because of the large ^{10}B capture cross section. Thus one would expect a plot of the true decay constant λ against the boron concentration to be linear, with a slope determined by the ^{10}B capture cross section only.

The true decay constant can be determined by laborious integration of the neutron density throughout the tank, but this is not necessary. It is found experimentally (Meads *et al.* 1956), that the observed decay of the capture γ-rays at any point in the tank is exponential within the limits of measurement. The observed decay of counts in a scintillation detector can therefore be expressed by the product of an exponential term representing the effect of capture, and another, representing the effect of diffusion of the neutrons into or away from the region near the detector. This result is confirmed by the analysis, given in the appendix, based on simple diffusion theory.

The decay constant λ_x of the γ-ray counts at distance x from the pulsed source of neutrons (Meads *et al.* 1956) can be expressed, therefore, as follows

$$\lambda_x = (N_H{}'\sigma_H + N_B\sigma_B)\bar{v} + F(x)$$

for a borax solution containing N_B boron nuclei per cm³ of cross section σ_B. N_H' is the number of protons per cm³ of solution and σ_H the proton cross section; $\bar{v} = 2200$ m sec^{-1} and $F(x)$ represents the effect of diffusion, which is assumed to be the same in the borax solution as in the water. The validity of this assumption depends upon two subsidiary assumptions, namely, that the initial thermal neutron distribution set up as a result of slowing down fast neutrons from the source, is independent of concentration; and that the subsequent rate of diffusion is also independent of concentration. Since the diffusion effect never exceeds 10% of the measured decay, and the maximum borax concentration was about 4%, these assumptions are likely to be justified.

If N_H = number of protons per cm³ of water, we may rewrite the above equation in the form $\lambda_x = A + N_B'\bar{v}\sigma_B$ where $A = N_H\sigma_H\bar{v} + F(x)$ is independent of boron concentration and

$$N_B' = N_B\left[1 + \frac{\sigma_H}{\sigma_B}\frac{N_H' - N_H}{N_B}\right].$$

N_B' is the number of boron atoms per cm³, with a correction (0·1%) for the change in concentration of protons in the solution on addition of borax. The ratio σ_H/σ_B need not be known at all accurately. The correction can easily be calculated from the known density of borax solutions.

The experimental procedure was, therefore, to measure the γ-ray lifetimes as a function of concentration of borax for several distances of the scintillation counter from the source, and to plot λ_x as a function of N_B'. The validity of the assumptions could be tested by the internal agreement of the results; i.e. the plots should be linear, and have equal slopes at the different positions.

§ 3. Introduction of the Borax

The total weight of borax in the tank varied from 0–11·5 kg. The source of supply was 15 kg of 'Analar' borax which had been carefully mixed. A sample of this, together with samples of solution at each concentration were retained for subsequent analysis.

The iron tank (600 gallons capacity) was lined with paraffin wax and filled with demineralized water. Successive weighed quantities of borax were added after each set of decay time measurements and the solution carefully stirred after each addition. The level of liquid in the tank was kept fixed by occasional addition of distilled water to compensate for loss by evaporation.

§ 4. Volume of the Tank

The volume of the liquid in the tank was required for calculation of the concentration, and was measured in three ways: (i) using a calibrated water flow-meter, (ii) by direct weighing of the contents in 100 kg samples, (iii) by adding a known weight of potassium sulphate to fresh water in the tank, taking a sample of the solution after stirring, and determining the weight of potassium sulphate in the sample by evaporation. These gave $2{\cdot}567 \times 10^6$, $2{\cdot}569 \times 10^6$, $2{\cdot}568 \times 10^6$ cm³ respectively for the volume of the tank.

The mean temperature was about 18°C and the result of (ii) was calculated using values for the density of borax solutions quoted in the *International Critical Tables* (1928).

§ 5. Results

The γ-ray decay was measured at zero and 5 other concentrations of borax at distances of 20, 30 and 40 cm from the target. In all, 72 sets of measurements were made.

Using a value of Avogadro's number $6{\cdot}023 \times 10^{23}$, the known weights of borax in the tank were converted into values of N_B'. The figure shows the result of

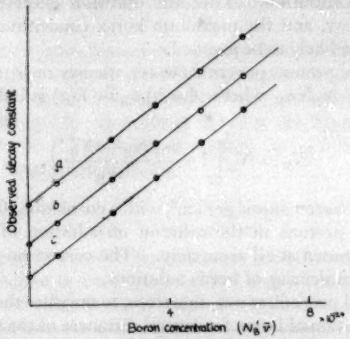

Decay constant as a function of boron concentration. *a*, 20 cm, *b*, 30 cm, *c*, 40 cm from target. Arbitrary amounts have been added to the measured decay constants so that the three graphs should be separated in the diagram.

plotting λ_z against N_B'. The constancy of the slope indicates that all points lie within the range of validity of the assumptions previously discussed. The statistics were sufficiently good to warrant a gaussian analysis, and the slope and probable error in the slope, of the lines of best fit to the experimental points were determined by the method of least squares (cf. Margenau and Murphy 1943). The results were as follows:

Distance from target	σ_B (barns)
20 cm	$758{\cdot}1 \pm 1{\cdot}6$
30 cm	$761{\cdot}6 \pm 2{\cdot}5$
40 cm	$762{\cdot}9 \pm 1{\cdot}7$

It will be seen that the values of σ_B obtained have a spread not incompatible with statistics so that a mean value of $\sigma_B = 761 \pm 2$ barns can be accepted with confidence (subject to the possible correction discussed below) as the mean thermal cross section of boron in our sample.

§ 6. Analysis of the Borax

The 'Analar' borax used had not been kept in a stabilized atmosphere (Vogel 1948) so that its composition could depart slightly from the formula $Na_2B_4O_7\,10H_2O$.

Ignition in a platinum crucible gave an anhydrous yield 0·3% higher than expected from the formula. This could be accounted for by assuming that there was originally present 0·3% less water than the formula indicates, or that the final

sample was not quite anhydrous. A similar experiment with a new specimen which had been kept in a stabilized atmosphere also gave the same result, so that it was assumed that the latter alternative was correct.

§ 7. Comparison of Cross Section of Borax Sample with the Harwell Standard

Whitehouse (see Thode *et al.* 1948) first pointed out the possibility of differences in the isotopic composition of boron from different sources, so, to be of any practical use, the cross section of our boron had to be compared with that of a standard sample.

For this purpose, a known weight of our borax was dehydrated, dissolved in heavy water, and compared by the pile oscillator method (Hughes 1953) in GLEEP with the A.E.R.E. standard boric oxide sample. The experiment was then repeated with independently prepared solutions of our borax in light water.

There is evidence that the A.E.R.E. boric oxide also contains about 0·3% by weight of water. In calculating the ratio of cross section per molecule of $Na_2B_4O_7$ to B_2O_3 the effects (initially very small) of the residual water cancel out, so that no correction is necessary.

The results of the above measurements expressed as the ratio of cross sections of Oxford to Harwell boron give

Heavy water sample	$1{\cdot}000 \pm 0{\cdot}004$
Ordinary water sample	$1{\cdot}002 \pm 0{\cdot}002$

This result which can be looked upon as an absolute calibration of the standard A.E.R.E. sample, therefore yields 760 ± 3 barns for the A.E.R.E. sample.

The following table, taken partly from Green *et al.* (1954), and partly from information supplied by Dr. P. A. Egelstaff, shows the present state of the boron measurements.

Sample	Harwell	Argonne–Brookhaven	Swedish	Oxford
Harwell	771 ± 5	759 ± 5	775 ± 5	760 ± 3
Swedish	759 ± 6	745 ± 5	763 ± 3	—
Argonne–Brookhaven	760 ± 4	752 ± 3	764 ± 3	—
Oxford	—	—	—	761 ± 2

It seems clear from these results that somewhere in the chain of intercomparisons there lurks a systematic error, but it is still not clear in which measurement it occurs, and further work is in progress.

Acknowledgments

We have to thank Dr. Handel Davies for help with the mathematics of the diffusion correction and Mr. E. Bowell of the Chemical Inspectorate, Chatham, for carrying out the analyses of the borax and the preparation of the heavy water samples. He have to thank Dr. W. D. Allen for very helpful discussions and Lord Cherwell and Sir John Cockroft for their interest in the work and the latter for permission to publish.

APPENDIX

Exponential Decay of the Observed γ-ray Intensity due to Neutron Capture

Consider the counting rate $N(x, t)$ observed with a small scintillator situated x cm from the neutron source.

Then
$$N(x,t) = A \int_{\tau} \lambda n(\mathbf{r}, t) \frac{\exp(-s/l)}{s^2} d\tau$$

in which A is a constant depending upon the efficiency of the counter, l is the mean free path of the capture γ-rays, λ is the decay constant of the neutrons due to capture alone.

The function $n(\mathbf{r}, t)$ is the neutron density at the element of volume $d\tau$, whose vector distance from the source of neutrons is $\mathbf{r}$. The density $n(\mathbf{r}, t)$ need not be symmetrical about the source, but is subject to the diffusion capture equation $\partial n/\partial t = -\lambda n + D\nabla^2 n$. Now define $q(\mathbf{r}, t)$, so that $n = qe^{-\lambda t}$; then by substitution $\partial q/\partial t = D\nabla^2 q$. To a first approximation

$$q(\mathbf{r}, t) = q(\mathbf{r}, 0) + \left[\frac{\partial q(\mathbf{r}, t)}{\partial t}\right]_0 t = q(\mathbf{r}, 0) + D\nabla^2 q(\mathbf{r}, 0)\, t$$

so that we may write

$$N(x, t) = N(x, 0)\, e^{-\lambda t}(1 + \mu t)$$

in which

$$\mu = D\frac{\int_\tau [\{\nabla^2 n(\mathbf{r}, 0) \exp(-s/l)\}/s^2]\, d\tau}{\int_\tau [\{n(\mathbf{r}, 0) \exp(-s/l)\}/s^2]\, d\tau}$$

since when $t = 0$, $q(\mathbf{r}, 0) = n(\mathbf{r}, 0)$. For sufficiently small t, $N(x, t)$ will behave as $N(x, 0) \exp\{-(\lambda - \mu)t\}$, so that $\lambda_x = \lambda - \mu$ where μ is a function only of the position x of the scintillator in the tank.

A simple logarithmic plot shows that for the variation of average life encountered in these experiments ($\sim 10\%$) the deviation of the approximate expression from a straight line would hardly be detected.

The numerical value of the correction factor μ can be determined by numerical integration from the measured values of the initial neutron distribution $n(\mathbf{r}, 0)$ and was found to have approximately the correct value. It was also possible to verify by numerical integration of the measured value of $n(\mathbf{r}, t)$ that the integral expression for $N(x, t)$ did in fact decay exponentially, within the limits of the accuracy of the numerical integration ($\sim 0{\cdot}1\%$). The conclusion reached from the rather detailed numerical work (Meads 1955) was that as well as the general exponential decay predicted in first approximation for any distribution of neutrons, the actual distribution used in this experiment was one for which the approximation was probably valid to the second order as well.

References

Green, A., Littler, D. J., Lockett, E. E., Small, V. G., Spurway, A. H., and Bowell, E., 1954, *J. Nuclear Energy*, **1**, 144.

Hughes, D. J., 1955, *Pile Neutron Research* (Cambridge, Mass.: Addison-Wesley Co.), p. 201.

International Critical Tables, 1928, Vol. 3 (York, Pa.: Maple Press).

Margenau, H., and Murphy, G. M., 1943, *Mathematics of Physics and Chemistry* (New York: Van Nostrand) p. 500.

Meads, R. E., 1955, *D.Phil. Thesis*, University of Oxford.

Meads, R. E., England, C. J., Collie, C. H., and Weeks, G. C., 1956, *Proc. Phys. Soc.* A, **69**, 469.

Thode, H. G., Macnamara, J., Lossing, F. R., and Collins, C. B., 1948, *J. Amer. Chem. Soc.*, **70**, 3008.

Vogel, I., 1948, *A Textbook of Quantitative Analysis* (London: Longmans Green and Co.), p. 204.

The Capture Cross Section of Thermal Neutrons in Water

By R. E. MEADS, C. J. ENGLAND, C. H. COLLIE and G. C. WEEKS
The Clarendon Laboratory, Oxford

MS. received 13*th September* 1955 *and in revised form* 24*th February* 1956

Abstract. The capture cross section of slow neutrons by protons has been measured by following the decay of neutrons from a pulsed source in water.

The decay was measured by detecting the capture γ-rays with a liquid scintillator.

The observed average life in water was $203{\cdot}3 \pm 2{\cdot}6$ μsec corresponding to a capture cross section of $0{\cdot}335 \pm 0{\cdot}004$ barns at a velocity of 2200 metres/sec.

§ 1. Introduction

The cross section for the photo disintegration of the deuteron, $d(\gamma, n)p$ near the threshold is an important constant in nuclear theory. An exact value is of particular interest because, near threshold, the disintegration is entirely due to the photomagnetic transition in which the angular momentum is conserved by spin flipping; it also provides the most direct measure of the difference between the singlet and triplet effective ranges. A full account of the theoretical aspects of the problem has been given by Squires (1952). A direct measurement near threshold of the photo disintegration process is not possible, but as was early pointed out by Bethe (1947) the cross section σ_{cap} of the inverse capture process can be measured directly, and is related by the theory of detailed balancing to the cross section σ_{mag} for disintegration by a quantum of energy $\hbar\omega$ by the following relationship.

$$\frac{\sigma_{cap}}{\sigma_{mag}} = 6\left(\frac{\hbar\omega}{mcv}\right)^2.$$

The capture cross section varies inversely as the relative velocity v, so that, if neutrons are released in an infinite hydrogenous medium, the total number present will decrease exponentially with time, by capture, and a measurement of the average life $T = 1/\lambda$ will enable the capture cross section to be measured in terms of the composition of the medium. The capture cross section of oxygen (U.S.A.E.C. 1952) is so small that water is a very convenient hydrogenous medium to employ.

Two methods have been used to measure the average life of neutrons in a water tank:

(*a*) The measurement of the total number of neutrons N in the water tank at a single instant of time, when they are introduced at a steady rate n neutrons per second. Clearly the average life $1/\lambda = n/N$. Owing to the difficulty of making absolute neutron measurements the method cannot be used to make absolute measurements of T. It can, however, be used to give a comparison of the capture cross section of neutrons by protons and of neutrons by another nucleus of large capture cross section which also obeys the $1/v$ law, e.g. boron.

As was first pointed out by Whitehouse (Thode *et al.* 1948) the isotopic composition of the particular boron sample must also be measured. Apart from the disadvantage of not giving an absolute value, the static method runs into other difficulties and after careful consideration we decided that we were unlikely to be able to improve on the measurements of Whitehouse and Graham (1947). However, if the initial constant source of neutrons has no fast neutrons in it which have to be slowed down, these difficulties are more easily overcome, and measurements have been made (Hamermesh, Ringo and Wexler 1953) using thermal neutrons from the Argonne pile. Although precise, their results are tied to the still uncertain capture cross section of natural boron (Green *et al.* 1954). (*b*) Direct measurement of the decay from a pulsed neutron source. This was first tried by Manley, Haworth, and Luebke (1941, 1942) and more recently by Von Dardel and Waltner (1953) and Von Dardel and Sjöstrand (1954). The dynamic method suffers from several fundamental difficulties: Firstly, the motion of the neutrons during their life must be allowed for since the local neutron concentration changes both by capture and diffusion. Secondly, if neutron detectors are used to follow the decay it is not easy to arrange that they actually measure what is required, namely the concentration of neutrons which would have been present at the position occupied by the detector had the medium not been disturbed by the presence of the detector. Thirdly, it is difficult to obtain a sufficient neutron flux to obtain good statistical accuracy.

Since it seems impossible to make the measurements without having to make corrections, we attempted to ensure that any correction should not exceed 10% of the quantity measured and could be measured experimentally in a subsidiary experiment to an accuracy of at least 10%. Working in this way, we did not have to rely entirely upon theoretical calculations in applying the correction, and hoped to arrive at a result which could be relied upon to $\pm 1\%$.

§ 2. The Experimental Method

An outline of the apparatus used in the final measurements is shown in figure 1. The source of neutrons is a heavy ice target on which falls a pulsed beam of 450 kev deuterons. In spite of the complication of liquid air cooling,

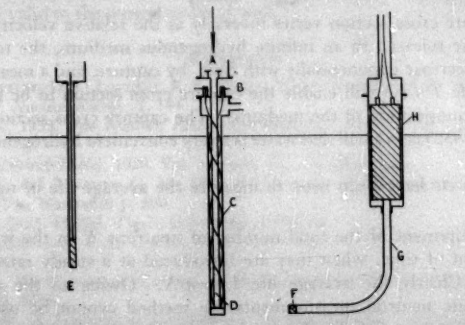

Figure 1. Heavy ice target and detector. A. Diaphragm to define the deuteron beam; B. liquid air inlet; C. vacuum jacket; D. heavy ice target; E. BF_3 neutron monitor; F. scintillator; G. Perspex light guide; H. photomultiplier.

the heavy ice target was used to get enough neutrons in each pulse (10^5 neutrons per pulse). Preliminary experiments showed that a simpler occluded target did not yield enough neutrons. While equally good or better neutron yields could be obtained with a DT source using a zirconium tritide target the large range of 14 MeV neutrons in water prevented the use of this otherwise very convenient source. Using the DD source it was possible to use a 600 gallon tank, whose dimensions were 120 cm × 120 cm × 180 cm. The neutron decay was followed by detecting the 2·2 MeV capture γ-rays with a liquid scintillator (terphenyl in cyclohexane with diphenyl hexatriene as frequency shifter) mounted on the end of a long light guide. The photomultiplier was more than 40 cm from the scintillator and the preamplifier was outside the water tank altogether. This method of detection has several advantages. It is sensitive; the cross section of the scintillator and light guide both for neutron capture and neutron scattering is so close to that of water that the disturbance of the neutron field due to the detector is negligible. Moreover, owing to the large range of γ-rays in water (~25 cm) the detector effectively integrates over a large volume, so that the effect of any small disturbance in the neutron density due to the detector is greatly reduced. This behaviour is in marked contrast to that of a conventional BF_3 neutron detector which can only with difficulty be adjusted to have the same capture cross section as that of the water it displaces, and must always have a quite different scattering cross section.

The main disadvantage of this type of detector is that it does not give the same pulse height for each γ-ray detected, and so its sensitivity depends critically on the stability of the associated electronic equipment.

This difficulty was overcome in two ways. All equipment (amplifier type 201 H.T. to photomultiplier type 1007C and scaler type 1009B) was electronically stabilized and fed from a stabilized (± 1 volt) mains supply. Measurement of the changes of sensitivity over long periods showed that the stability was just sufficient for our purpose. Small fluctuations about the mean sensitivity do not affect the measured lifetime; any long term drift could be detected and allowed for by suitable design in the delay sorter and in fact no errors due to electronic instability could be detected.

§ 3. The Delay Sorter

The neutron decay was followed by counting the γ-rays produced from an initial 100 μsec pulse of neutrons, in successive 50 μsec intervals, the whole cycle being repeated every 1600 μsec. A series of accurately spaced pulses controlled the following series of events. The radio-frequency oscillator running the ion source switched on for 100 μsec giving a pulse of neutrons from the heavy ice target. The subsequent γ-ray pulses produced by the capture of this group of neutrons were counted by a group of four gated scalers. The gates were arranged so that counts were made in the three intervals 200–400 μsec (group B) 400–600 μsec (group C) 600–800 μsec (group D) as determined by a manually controlled selector switch.

The individual scalers were gated so as to record pulses in four successive 50 μsec channels. It would have been possible to count in all twelve channels using twelve scalers, but these were not easily available and it was found quite satisfactory to follow the decay in successive 200 μsec periods.

The gating pulses were obtained from a 20 kc/s blocking oscillator feeding two scale of four ring circuits. Accuracy of timing was ensured by locking the oscillator on to a 100 kc/s crystal controlled master oscillator. Owing to the use of double triodes (CV858) the gating pulses had a 1 μsec rise time. This was allowed for by calibrating the channels with random pulses from a radioactive source. This calibration was made frequently during the course of the measurements. A very small correction was made for differences in the decay in the channels of unequal length.

§ 4. The Ion Source

A conventional radio-frequency ion source (Thonemann 1948) was driven from a pulsed radio-frequency supply; in order to obtain regular striking the instantaneous radio-frequency power input was raised to 1·5 kilowatts. As the duty cycle was only 1/16, the mean dissipation was less than the usual 200–300 watts and no troubles due to over-running were experienced. However, the large wall absorption at the beginning of each pulse sufficiently reduced the instantaneous pressure to cause unsteady running. This trouble was overcome by replacing the dome of the discharge tube with a spherical volume of from 1 to 2 litres capacity.†

The maximum beam current used was about 1 mA corresponding to about 70 μA mean current. The liquid air cooling was just adequate to maintain the heavy ice target under this heavy bombardment. Since the slowing down time of the neutrons in the water is only a few microseconds, and no measurements were made for 100 μsec, it is not very important that the beam should end sharply. It is, however, important that there should be no neutron production during the time the decay is being measured. This was verified by displaying the amplified beam current on a cathode-ray tube. Incipient deterioration of the discharge conditions was readily detected by the appearance of large current spikes in the dead time which disappeared when the conditions in the radio-frequency arc were changed. It is clear that any failure in this respect would increase the measured value of the half-life of the neutrons.

§ 5. Measurement of Decay Time

When all the equipment was working satisfactorily the actual measurement of the neutron decay presented little difficulty. The neutrons were monitored by a fixed BF_3 counter placed in the tank 25 cm from the target and diametrically opposite the scintillator. A separate scaler was also used to count all the γ-ray pulses from the scintillator which entered channel group D(600–800 μsec) irrespective of which group was being operated. The background correction offered some difficulty since the metal cell containing the scintillator liquid became slightly radioactive owing to the neutron bombardment. The original cell was made from aluminium, but a change to a stainless steel cell very much reduced this unwelcome effect. The residual error due to this cause was eliminated by investigating the rise and fall of the activity empirically at various positions in the tank. A correction curve was then constructed based on a particular schedule of measurements which was carefully adhered to.

† We have to thank Dr. Thonemann for suggesting this remedy.

At the beginning of each run measurements were first made in channel group D, so that the smallest γ-ray count also had the smallest correction for neutron induced activity.

Correction for induced activity was only necessary when the scintillator was less than 40 cm from the target.

§ 6. Normalization of Counts

All measurements were normalized to a constant number of counts in the BF_3 chamber used as a neutron monitor. This was frequently calibrated with a 20 mc Ra–Be source but no significant changes in its sensitivity were found. Small changes in the gain of the amplifier do not affect the decay time observed in one group of channels but must be avoided if the measurements in the three groups of channels at one place in the tank are to be combined into a single decay curve covering the whole 600 μsec decay period. This was done by measuring the total counts in group D independently. Only those runs were accepted in which the group D counts bore a constant ratio to the neutrons counted by the monitor, thus showing that the amplifier gain had not changed.

§ 7. Correction for the Target Tube

The tube through which the deuterons reach the target is an unavoidable part of the apparatus, whose presence must be allowed for. It affects the observed results in two ways.

Firstly, owing to its presence the initial neutron distribution is less symmetrical than the ideal distribution which would have been obtained from a source entirely surrounded by water.

Secondly, some slow neutrons will leave the tank during the period of measurement by diffusion up the target tube which would otherwise have been captured and contributed to the γ-ray count. The effect of the target tube was estimated experimentally by introducing a dummy vertically below it. The thickness of the walls of the dummy was chosen so as to have the same capture cross section for slow neutrons as that of the actual target tube. Measurements with and without the dummy tube in position enabled an estimate founded on experiment to be made of the effect of the target tube on the results.

§ 8. Experimental Results

Four independent sets of measurements were made, namely: measurements with the γ-ray detector along the horizontal and vertical axes through the target; measurements with a BF_3 neutron detector along the horizontal and vertical axes.

The following subsidiary measurements were also made with the object of placing the corrections upon a sound experimental basis: measurements with the γ-ray detector along the horizontal axis in the presence of the dummy target; measurements with the BF_3 chamber of the angular distribution of the neutron density about the target.

The variations of the neutron density in time and space are shown in figure 2. The outward diffusion of the neutrons during the capture process is clearly shown in these curves by the outward migration of the maxima. The difference

between the measurements along the horizontal and vertical axis is nearly all due to the asymmetry in the angular distribution of the neutrons from the DD reaction.

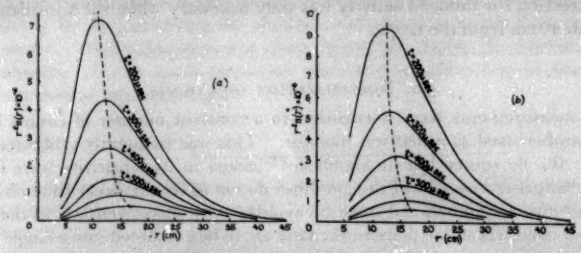

Figure 2. Distribution of thermal neutrons about the target : (*a*) in the horizontal plane; (*b*) vertically below the target.

Slight deviations from strict exponential decay were observed in neutron measurements at a given position. The logarithmic plots of count against time were convex downwards for distances less than 10 cm from the target and convex upwards for greater distances. This effect was, however, only just discernible and did not prevent the assignment of a lifetime to each measurement. The variation with distance is shown in table 1.

Table 1

(1)	(2)	(3)	(4)	(5)	(6)
10	174·0 ± 0·6	171·7 ± 0·7	178·1	171·5	164·6
15	194·6 ± 0·4	192·6 ± 0·7	—	202·5	187·4
20	204·0 ± 0·2	201·7 ± 0·4	203·5	232·3	212·9
25	208·0 ± 0·84	—	—	261·0	236·0
30	211·1 ± 0·7	206·2 ± 0·85	211·8	278·0	249·3
35	207·4 ± 1·5	—	—	287·7	258·2
40	206·9 ± 0·8	205·3 ± 1·4	210·2	289·5	258·5
45	204·2 ± 0·7	202·2 ± 1·9	—	—	—
50	204·7 ± 0·5	201·9 ± 0·5	207·1		
55	203·1 ± 1·5	202·3 ± 1·8			
60	200·5 ± 0·85	197·6 ± 0·4			
65	201·5 ± 1·4	—			
70	203·7 ± 0·5	197·0 ± 0·8			
75	201·1 ± 1				
80	199·0 ± 1·4				

(1) Distance in cm of detector from target ; (2) average life in μsec measured with γ counter in horizontal plane through target; (3) average life measured with γ-ray counter in horizontal plane through target with dummy target in position below target; (4) average life measured with γ counter vertically below target; (5) approximate average life measured with neutron counter in horizontal plane; (6) approximate average life measured with neutron counter vertically below the target.

The errors quoted are the probable errors derived from the statistics. The neutron measurements have a negligible statistical error.

The decay of the γ-ray scintillations was strictly exponential at all points in the tank at which it was measured. This result, which is rather surprising in view of the appreciable change in the neutron distribution caused by diffusion,

was carefully verified. It is derived on simple diffusion theory by Collie, Meads and Lockett (1956). Typical decay curves are shown in figure 3. The result of all measurements can therefore be expressed graphically as the variation of average lifetime with position in the tank, and also the variation of counting rate in one channel with position. The effect of the dummy target was to reduce the average life by a few microseconds as shown in table 1.

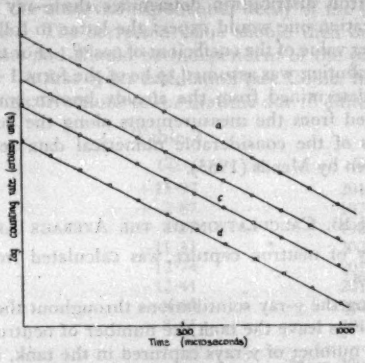

Figure 3. Exponential decay curves.

a. γ-ray decay curve at 15 cm from the target in the presence of the dummy target $T=192{\cdot}6$ μsec;
b. β-ray decay curve at 25 cm from the target $T=203{\cdot}3$ μsec;
c. Integrated neutron curve $T=201{\cdot}9$ μsec;
d. Integrated γ-ray curve $T=203{\cdot}3$ μsec.

§ 9. The Angular Distribution of the Radiation

The neutrons emitted from the target are known to have a far from isotropic distribution even in the centre-of-gravity system; other factors causing a departure from symmetry are the presence of the target tube and the momentum of the incoming deuterons.

The initial lack of symmetry in the distribution of neutrons is of course greatly reduced by the random collisions of the fast neutrons in the slowing down process. The angular distribution was investigated mainly with a neutron counter. The results showed a peak in the backward direction near the target tube, but otherwise the neutron densities are well represented by a simple formula of the type $1+a\cos^2\theta$. The existence of this backward peak is due to fast neutrons which have travelled up the target tube for some distance before entering the water. In this way a measurable concentration of neutrons is obtained near the target tube at distances from the target otherwise quite incompatible with the known stopping power of water for fast neutrons.

This appearance of neutrons near the free surface of the tank accounts for another puzzling feature of the experimental results, namely the rather large change in decay time ($\sim$5 μsec) introduced by the dummy target. It is possible to calculate from the measured neutron distribution how many neutrons leave the tank by diffusion up the target tube. It is quite small and corresponds to a target correction of $\frac{1}{3}$ μsec. The neutrons near the surface of the water tank

will, however, be able to leave the tank by diffusion and so account for the larger dummy target effect. This explanation is confirmed by the observation that the dummy target correction is greater for large distances r from the target than for a small r, since the region near the point of entry of the beam into the tank subtends a proportionately larger solid angle as one proceeds outward from the target along a horizontal axis.

Since the neutron distribution determines the γ-ray distribution through a process of integration one would expect the latter to follow the same law but with a much smaller value of the coefficient of $\cos^2\theta$. For the purpose of calculation the γ-ray distribution was assumed to be of the form $1+a\cos^2\theta$ in which the coefficient a was determined from the already known counting rates at $\theta=0°$ and $\theta=90°$ obtained from the measurements along the vertical and horizontal axes. An analysis of the considerable numerical data recorded by the delay sorter has been given by Meads (1955).

§ 10. Calculation of the Average Life

The probability of neutron capture was calculated from the experimental results in three ways:

(i) By integrating the γ-ray scintillations throughout the tank. Provided no neutrons and no γ-rays leave the tank the number of neutrons present is strictly proportional to the number of γ-rays captured in the tank, i.e. to the number of scintillations recorded, integrated over all positions with respect to the target. This integrated figure was obtained for each channel in each group, i.e. for 12 successive periods of 50 μsec from the experimental results in the following way.

The measurements beyond 35 cm from the target at a given time were accurately represented by the semi-empirical relationship $I_r=(I_0/r^2)e^{-kr}$ in which I_0 and k were determined experimentally.

This formula was used to extrapolate the results beyond the last point at which measurements were feasible. Any error introduced by this extrapolation was very small since it contributed only a few per cent of scintillations which all decayed with very nearly the correct average life. The effect of the target tube was allowed for by assuming that the difference between the ideal distribution with no target tube and the observed distribution would have been the same as the observed difference introduced by the dummy target. These are the only two corrections necessary to convert the observed measurements into the results of an ideal experiment in which a pulse of neutrons is released in an infinite volume of water. The integrated values for the various channels should show exponential decay. That this is so is shown in figure 3. The average life is found to be $203{\cdot}3\pm2{\cdot}6$ μsec. The estimated probable error is based on the following assumed errors: statistical error of the measurements 1 μsec; uncertainty in the target correction (maximum correction is 6 μsec) 2 μsec; an estimated uncertainty of 1–2 mm in the target–scintillator distance which would give an error of 1 μsec in the numerical integration.

(ii) The integration method can be applied to the neutron density as measured with the BF_3 chamber. This shows an excellent exponential decay (figure 3) with an average life of $201{\cdot}9\pm0{\cdot}13$ μsec. The error assigned is the statistical error of the measurements. There is also a systematic error due to the finite

size of the counter and the difference between its capture cross section and that of the displaced water. Since the copper walled counters used have a higher absorption for neutrons than the displaced water one can expect (von Dardel and Waltner 1953) that the true value of the average life is greater than the observed 202 μsec.

(iii) The observed neutron distribution can be used to calculate the part played by diffusion in the observed exponential decay of the γ-ray scintillations in any part of the tank. The corrected value should then be the true average life due to capture alone and should be independent of the part in the tank for which it is calculated. A first order calculation (see Collie, Meads and Lockett 1956) gave the following corrections to the lifetime due to diffusion (table 2).

Table 2

(1)	(2)	(3)
12	+15·97	201·5
15	+ 2·87	197·8
20	− 8·27	198·5
25	−11·31	202·3
30	−12·74	201·7
35	−12·41	201·1
40	− 8·50	202·6
45	− 8·15	201·5
		Mean 200·7 μsec

(1) Distances from target (cm); (2) calculated correction (μsec); (3) corrected value of average life (μsec).

The diffusion correction behaves as was to be expected, being positive for small r when most of the neutrons are diffusing away from the detector and negative at large values of r when the neutrons are nearly all diffusing outwards towards the detector. A similar calculation, using the vertical data, was not carried out in full, since it became clear during the course of the above calculation, that tangential diffusion due to the asymmetry of the neutron distribution was not negligible. The calculation, which was very laborious, was unlikely to add much to the accuracy of the result as obtained by the first method. A value of the position in the tank of zero diffusion correction was, however, obtained from the vertical data. This was 18·3 cm, corresponding to a mean life of 204·0 μsec. It is likely, therefore, that a complete computation, taking the angular distribution of the neutrons into account, would yield a value not very different from 202 μsec.

We consider the first method (in which the total correction for angular distribution only amounts to a few microseconds) to be soundly based and the best way of treating the observational data.

The second and third methods give results which agree with the first method within their rather larger limits of error. This agreement while adding little to accuracy of the results is useful confirmation that the general picture of the behaviour of the expanding neutron cloud is correct.

§ 11. Comparison with Other Results

As has been seen the results of the measurements can be expressed in terms of a cross section for capture at a standard velocity (2200 m sec^{-1}) or as the average life in μsec of a neutron in water.

A summary of recent results expressed in barns is shown in table 3 which also indicates the method used to overcome the fundamental difficulties referred to in the introduction.

Table 3

Experimenters	Method	Results (barns) at 2200 m sec^{-1}
Whitehouse and Graham (1947)	Static, boron ratio using small counters	Originally $0{\cdot}310 \pm 0{\cdot}025$. With revised boron value (760 barns) $0{\cdot}332 \pm 0{\cdot}025$
Scott, Thomson and Wright (1954)	Dynamic, in small tank. Escape correction measured by extrapolation	$0{\cdot}323 \pm 0{\cdot}008$
von Dardel and Waltner (1953)	Dynamic, in large tank using special BF_3 counters	$0{\cdot}321 \pm 0{\cdot}005$ (This result was discussed in the paper of von Dardel and Sjöstrand (1954))
Hamermesh, Ringo and Wexler (1953)	Static. Boron ratio using thermal neutrons and integrating tank. Boron comp. with standard	$0{\cdot}329 \pm 0{\cdot}004$
Harris *et al.* (1953)	Direct comparison with standard boron by pile oscillator method	$0{\cdot}332 \pm 0{\cdot}007$
von Dardel and Sjöstrand (1954)	Dynamic, in small tank. Escape correction obtained by extrapolation	$0{\cdot}333 \pm 0{\cdot}003$
Present Authors	Dynamic, in large tank, measuring the capture γ-rays	$0{\cdot}335 \pm 0{\cdot}004$

The present measurement is of the same order of accuracy as that of von Dardel and Sjöstrand (1954), who rely on the elimination of higher harmonic modes than the fundamental of the diffusion neutrons in a small tank of water. The correction for 'buckling' in such a measurement involves extrapolation of measured lifetimes over a wide range of values.

This possible source of error is avoided by the present method of integration of the capture γ-rays, which has the further advantage (previously discussed) of avoiding the problem of the perturbing effect of BF_3 counters which arose in the static method and the work of von Dardel and Waltner (1953).

Acknowledgments

Two of us wish to thank the Department of Scientific and Industrial Research for maintenance grants (R. E. M. and G. C. W.).

We have to thank Dr. Handel Davies for help with the diffusion calculations, and Lord Cherwell for his unfailing interest in the work.

References

Bethe, H. A., 1947, *Elementary Nuclear Theory* (New York : John Wiley).

Collie, C. H., Meads, R. E., and Lockett, E. E., 1956, *Proc. Phys. Soc.* A, **69**, 464.

von Dardel, G., and Waltner, A. W., 1953, *Phys. Rev.*, **91**, 1284.

von Dardel, G., and Sjöstrand, N. G., 1954, *Phys. Rev.*, **96**, 1245.

Green, A., Littler, D. J., Lockett, E. E., Small, V. G., Spurway, A. H., and Bowell, E., 1954, *J. Nuclear Energy*, 1, 144.

Hamermesh, B., Ringo, G. R., and Wexler, S., 1953, *Phys. Rev.*, **90**, 603.

HARRIS, S. P., MUEHLHAUSE, C. O., ROSE, D., SCHROEDER, H. P., THOMAS, G. E., and WEXLER, S., 1953, *Phys. Rev.*, **91**, 125.

MANLEY, J. H., HAWORTH, L. J., and LUEBKE, E. A., 1941, *Rev. Sci. Instrum.*, **12**, 587, 591; 1942, *Phys. Rev.*, **61**, 152.

MEADS, R. E., 1955, *D. Phil. Thesis*, University of Oxford.

SCOTT, F. R., THOMSON, D. B., WRIGHT, W., 1954, *Phys. Rev.*, **95**, 582.

SQUIRES, G. L., 1952, *Progress in Nuclear Physics*, Vol. II. (London : Pergamon Press).

THODE, H. G., MACNAMARA, J., LOSSING, F. R., and COLLINS, C. B., 1948, *J. Amer. Chem. Soc.*, **70**, 3008.

THONEMANN, P. C., 1948, *Proc. Phys. Soc.*, **61**, 483.

United States Atomic Energy Commission Report, 1952, A.E.C.U. 2040.

WHITEHOUSE, W. J., and GRAHAM, G. A. R., 1947, *Canad. J. Res.*, A, **25**, 261.

Approximate Molecular Orbitals

V: The 1sσ and 2pπ states of HeH^{2+}

By B. L. MOISEIWITSCH† and A. L. STEWART‡

† Department of Applied Mathematics, The Queen's University of Belfast
‡ Department of Physics, The Queen's University of Belfast

Communicated by D. R. Bates; MS. received 30th January 1956

Abstract. Approximate wave functions for the 1sσ and 2pπ states of the HeH^{2+} molecular ion are obtained by the variational method. The values of the electronic total energies, potential energies, dipole moments and quadrupole moments computed using the approximate wave functions are compared with the exact values of these quantities.

§ 1. Introduction

In the previous papers of this series (Dalgarno and Poots 1954, Moiseiwitsch and Stewart 1954, Carson and Dalgarno 1955, Dalgarno and Lewis 1956), analytic approximations to the wave functions of a number of states of H_2^+ have been obtained with the aid of the variational method. The present paper is concerned with similar work on the 1sσ and 2pπ states of HeH^{2+}. These states can be treated comparatively easily since they are the lowest which have zero and unit angular momentum respectively about the internuclear axis.

The accuracy achieved is assessed by comparing the values obtained for the electronic energies and for other quantities with the corresponding values based on the exact two centre wave functions which have recently become available (Bates and Carson 1956). One of the aims of the investigation is to find if the accuracy achieved using certain types of approximate wave function is affected by the lack of nuclear symmetry. This lack does not alter the general form of the customary united atom approximation but it naturally renders much simpler the customary separated atoms approximation.

§ 2. Choice of Wave Functions

In the cases of the 1sσ and 2pπ states of HeH^{2+} the dissociation products are a H^+ ion and a He^+ ion in the 1s and $2p_z$ states respectively. Simple approximations which take account of this behaviour at large internuclear distances are

$$\Psi(1s\sigma) = \exp(-2r_a) \qquad \ldots\ldots(1a)$$

and

$$\Psi(2p\pi) = r_a \sin\theta_a \cos\phi_a \exp(-r_a) \qquad \ldots\ldots(1b)$$

where $\mathbf{r}_a$ is the position vector of the electron relative to the helium nucleus A and θ_a and ϕ_a are the usual polar angles. These approximations may be improved by the introduction of a screening parameter:

$$\Psi(1s\sigma) = \exp(-2\beta r_a) \qquad \ldots\ldots(2a)$$

and

$$\Psi(2p\pi) = r_a \sin\theta_a \cos\phi_a \exp(-\beta r_a) \qquad \ldots\ldots(2b)$$

β being varied to minimize the energy.

In the limit of small nuclear separations the wave functions tend to those of the Li^{2+} ion and we may therefore write

$$\Psi(1s\sigma)=\exp\{-\alpha(2r_a+r_b)\} \qquad \ldots\ldots(3a)$$

and

$$\Psi(2p\pi)=r_a\sin\theta_a\cos\phi_a\exp\{-\tfrac{1}{2}\alpha(2r_a+r_b)\} \qquad \ldots\ldots(3b)$$

where $\mathbf{r}_b$ is a vector directed from the hydrogen nucleus B to the electron and α is a variable parameter. To first order in the nuclear separation these approximations are equivalent to

$$\Psi(1s\sigma)=\exp(-3\alpha r) \qquad \ldots\ldots(4a)$$

and

$$\Psi(2p\pi)=r\sin\theta\cos\phi\exp(-3\alpha r/2) \qquad \ldots\ldots(4b)$$

$\mathbf{r}$ being the position vector of the electron relative to the centre of charge of the constituent nuclei. This type of approximation has been used by Streetman and Matsen (1954) but it involves the evaluation of some rather troublesome integrals when used in conjunction with the separated atom approximation and has no compensating advantage.

It is clearly desirable to use a trial wave function which has the proper behaviour at both large and small nuclear separations R. This may be achieved by writing

$$\Psi(1s\sigma)=\frac{1}{S_1}\left\{\frac{27\alpha^3}{\pi}\right\}^{1/2}\exp\{-\alpha(2r_a+r_b)\}+p\left\{\frac{8\beta^3}{\pi}\right\}^{1/2}\exp(-2\beta r_a) \qquad \ldots\ldots(5a)$$

and

$$\Psi(2p\pi)=\frac{1}{S_2}\left\{\frac{243\alpha^5}{32\pi}\right\}^{1/2}\exp\{-\tfrac{1}{2}\alpha(2r_a+r_b)\}r_a\sin\theta_a\cos\phi_a + p\left\{\frac{\beta^5}{\pi}\right\}^{1/2}\exp(-\beta r_a)r_a\sin\theta_a\cos\phi_a \qquad \ldots\ldots(5b)$$

in which

$$S_1^2=\frac{1}{\alpha R}[(6\alpha R-4)\exp(-2\alpha R)+(3\alpha R+4)\exp(-4\alpha R)]$$

and

$$S_2^2=\frac{96}{(\alpha R)^3}[\{1+\alpha R-\tfrac{3}{4}(\alpha R)^2+\tfrac{3}{16}(\alpha R)^3\}\exp(-\alpha R) - \{1+2\alpha R+\tfrac{3}{4}(\alpha R)^2+\tfrac{3}{32}(\alpha R)^3\}\exp(-2\alpha R)].$$

§ 3. Description of Calculations

The values of the parameters α, β and p have been determined over a wide range of R by minimization of the electronic energy of the system

$$E=-\int\Psi^*\left(\nabla^2+\frac{4}{r_a}+\frac{2}{r_b}\right)\Psi d\mathbf{r} \qquad \ldots\ldots(6)$$

where Ψ is the normalized wave function. The functions considered were of the type (5*a*) and (5*b*) with

(i) $p=\infty$, $\beta=1$.
(ii) $p=\infty$, β variable.
(iii) $p=0$, $\alpha=1$.
(iv) $p=0$, α variable.
(v) $\alpha=1$, $\beta=1$, p variable.
(vi) α as determined by (iv) and β by (ii), p variable.

Exact values of E have already been calculated by Bates and Carson (1956). To test further the approximate wave functions, both they and the exact wave functions of Bates and Carson have been used for the computation of the potential energies

$$V = -\int \Psi^* \left(\frac{4}{r_a} + \frac{2}{r_b} \right) \Psi \, d\boldsymbol{r}$$

the quadrupole moment integrals,

$$\overline{X^2} = \int \Psi^* x_a^2 \Psi \, d\boldsymbol{r}, \quad \overline{Z^2} = \int \Psi^* z_a^2 \Psi \, d\boldsymbol{r}$$

and the dipole moment integral,

$$\bar{Z} = \int \Psi^* z_a \Psi \, d\boldsymbol{r}$$

(x_a, y_a, z_a) being the cartesian coordinates of the electron in a system with its origin on the helium nucleus, its z-axis directed towards the hydrogen nucleus and (in the case of the $2p\pi$ state) its x-axis perpendicular to the nodal plane.

§ 4. Results

The values of α, β and p obtained for the functions (ii), (iv), (v) and (vi) are given in table 1 for the $1s\sigma$ state and in table 2 for the $2p\pi$ state. In tables 3 and 4 are compared the approximate electronic energies, derived using the functions (i) to (vi), with the exact electronic energies. Similar comparisons for the potential energies and for $\overline{X^2}$, $\overline{Z^2}$ and $\bar{Z}$ are made in tables 5 to 12.

All quantities are measured in Hartree units (a_0 for length, $e^2/2a_0$ for energy).

§ 5. Discussion

As would be expected function (i) is unsatisfactory for small values of the nuclear separation. Function (ii), which has the correct asymptotic form at both limits, is naturally much superior. Like function (i), however, it gives the dipole moment integral to be identically zero and thus fails completely to represent an essential property of the ion.

Though functions (iii) and (iv) are accurate at small separations they are rather poor at large separations. Due to the lower orbital quantum number of the $1s\sigma$ state they are worse for this state than for the $2p\pi$ state.

The energies computed using functions (v) and (vi) are never in error by more than 0·7% and 0·4% respectively in the case of the $1s\sigma$ state, nor by more than 0·5% and 0·2% respectively in the case of the $2p\pi$ state. Further, these two functions represent the potential energy, the quadrupole moment and the dipole moment integrals quite well.

In tables 13 and 14 the percentage errors in the energies of HeH^{2+} and H_2^+ associated with corresponding types of approximate wave functions are compared. It may be seen that the united atom approximations, (iii) and (iv), are less satisfactory for HeH^{2+} than for H_2^+, but that for the separated atom approximations, (i) and (ii), and for the combined united–separated approximations, (v) and (vi), the reverse is true.

The variation with R of the potential energy $V' = V + 4/R$, the kinetic energy T, and the total energy $E' = E + 4/R$ of the $1s\sigma$ and $2p\pi$ states, is illustrated in

Table 1. Parameters of the 1sσ Wave Functions

R		0·0	0·25	0·5	0·75	1·0	1·5	2·0	2·5	3·0	3·5	4·0	5·0
Function													
(ii)	β	1·5000	1·3114	1·0826	1·0403	1·0083	1·0015	1·0003	1·0001	1·0000	1·0000	1·0000	1·0000
(iv)	α	1·0000	0·9352	0·8653	0·8164	0·7842	0·7549	0·7583	0·7825	0·8153	0·8465	0·8719	0·9064
(v)	p	0·0000	0·213	0·573	1·009	1·560	3·238	5·994	10·04	15·40	22·03	29·84	48·88
(vi)	p	0·0000	0·063	0·211	0·455	0·836	2·227	4·803	8·812	14·27	21·06	29·05	48·42

Table 2. Parameters of the 2pπ Wave Functions

R		0·0	0·25	0·50	0·75	1·0	1·5	2·0	2·5	3·0	3·5	4·0	5·0
Function													
(ii)	β	1·5000	1·4747	1·4188	1·3573	1·3009	1·2113	1·1485	1·1050	1·0748	1·0539	1·0394	1·0221
(iv)	α	1·0000	0·9923	0·9738	0·9508	0·9271	0·8834	0·8472	0·8185	0·7961	0·7792	0·7669	0·7539
(v)	p	0·0000	0·0198	0·0724	0·1485	0·2416	0·4660	0·7353	1·054	1·434	1·886	2·423	3·787
(vi)	p	0·0000	0·0064	0·0245	0·0518	0·0880	0·1874	0·3282	0·5201	0·7759	1·110	1·537	2·722

Table 3. Total Electronic Energies $-E$ of the 1sσ State

R	0·0	0·25	0·5	0·75	1·0	1·5	2·0	2·5	3·0	3·5	4·0	5·0
Function												
(i)	8·0000	7·5854	6·9173	6·3348	5·8901	5·3201	4·9983	4·7998	4·6666	4·5714	4·5000	4·4000
(ii)	9·0000	8·0432	7·0485	6·3675	5·8975	5·3204	4·9983	4·7998	4·6666	4·5714	4·5000	4·4000
(iii)	9·0000	8·2287	7·1771	6·3307	5·6939	4·8547	4·3590	4·0486	3·8435	3·7013	3·5984	3·4613
(iv)	9·0000	8·2642	7·3094	6·5401	5·9420	5·0986	4·5515	4·1855	3·9370	3·7654	3·6435	3·4861
(v)	9·0000	8·2592	7·3038	6·5630	6·0268	5·3692	5·0166	4·8073	4·6701	4·5732	4·5010	4·4004
(vi)	9·0000	8·2651	7·3215	6·5853	6·0457	5·3764	5·0186	4·8078	4·6702	4·5732	4·5010	4·4004
Exact	9·0000	8·2673	7·3311	6·6027	6·0667	5·3909	5·0244	4·8098	4·6710	4·5736	4·5012	4·4005

Table 4. Total Electronic Energies $-E$ of the $2p\pi$ State

R / Function	0·0	0·25	0·50	0·75	1·0	1·5	2·0	2·5	3·0	3·5	4·0	5·0
(i)	2·00000	1·99204	1·96913	1·93547	1·89469	1·80402	1·71429	1·63328	1·56327	1·50392	1·45394	1·37609
(ii)	2·25000	2·22381	2·16043	2·08248	2·00315	1·85944	1·74157	1·64660	1·56983	1·50723	1·45566	1·37661
(iii)	2·25000	2·23204	2·18459	2·11895	2·04441	1·89114	1·74984	1·62727	1·52334	1·43585	1·36220	1·24724
(iv)	2·25000	2·23217	2·18612	2·12424	2·05567	1·91769	1·79134	1·68044	1·58425	1·50092	1·42853	1·31013
(v)	2·25000	2·23213	2·18573	2·12309	2·05369	1·91530	1·79169	1·68729	1·60111	1·53055	1·47277	1·38575
(vi)	2·25000	2·23217	2·18614	2·12435	2·05608	1·91981	1·79735	1·69300	1·60607	1·53442	1·47556	1·38698
Exact	2·25000	2·23218	2·18623	2·12463	2·05663	1·92105	1·79929	1·69543	1·60868	1·53691	1·47775	1·38844

Table 5. Electronic Potential Energies $-V$ of the $1s\sigma$ State

R / Function	0·0	0·25	0·5	0·75	1·0	1·5	2·0	2·5	3·0	3·5	4·0	5·0
(i)	12·00	11·56	10·92	10·34	9·89	9·32	9·00	8·80	8·67	8·57	8·50	8·40
(ii)	18·00	14·92	12·46	11·06	10·23	9·39	9·01	8·80	8·67	8·57	8·50	8·40
(iii)	18·00	16·46	14·35	12·66	11·39	9·71	8·72	8·10	7·69	7·40	7·20	6·92
(iv)	18·00	15·52	12·88	11·05	9·78	8·19	7·33	6·88	6·65	6·53	6·46	6·38
(v)	18·00	15·66	13·19	11·60	10·58	9·51	9·04	8·80	8·66	8·56	8·49	8·39
(vi)	18·00	15·49	12·82	11·07	10·01	9·06	8·78	8·66	8·58	8·52	8·46	8·38
Exact	18·00		12·99		10·25		8·96		8·66		8·50	8·40

Table 6. Electronic Potential Energies $-V$ of the $2p\pi$ State

R / Function	0·0	0·25	0·50	0·75	1·0	1·5	2·0	2·5	3·0	3·5	4·0	5·0
(i)	3·000	2·992	2·969	2·935	2·895	2·804	2·714	2·633	2·563	2·504	2·454	2·376
(ii)	4·500	4·399	4·173	3·925	3·695	3·327	3·061	2·868	2·725	2·618	2·536	2·421
(iii)	4·500	4·464	4·369	4·238	4·089	3·782	3·500	3·255	3·047	2·872	2·724	2·494
(iv)	4·500	4·430	4·261	4·049	3·832	3·435	3·108	2·845	2·632	2·444	2·317	2·103
(v)	4·500	4·438	4·283	4·084	3·876	3·496	3·194	2·963	2·788	2·657	2·558	2·424
(vi)	4·500	4·430	4·259	4·043	3·821	3·420	3·099	2·857	2·679	2·547	2·459	2·349
Exact	4·500	4·430	4·261	4·051	3·837	3·452	3·147	2·916	2·744	2·618	2·526	2·408

Table 7. $\overline{X^2}$ for 1sσ State

R	0·0	0·25	0·5	0·75	1·0	1·5	2·0	2·5	3·0	3·5	4·0	5·0
Function												
(i)	0·250	0·250	0·250	0·250	0·250	0·250	0·250	0·250	0·250	0·250	0·250	0·250
(ii)	0·111	0·145	0·185	0·213	0·231	0·246	0·249	0·250	0·250	0·250	0·250	0·250
(iii)	0·111	0·114	0·122	0·132	0·143	0·164	0·184	0·200	0·215	0·227	0·237	0·253
(iv)	0·111	0·130	0·160	0·190	0·217	0·261	0·287	0·297	0·299	0·299	0·298	0·300
(v)	0·111	0·132	0·160	0·184	0·203	0·227	0·239	0·245	0·247	0·248	0·249	0·250
(vi)	0·111	0·131	0·164	0·198	0·224	0·252	0·256	0·254	0·252	0·251	0·251	0·251
Exact	0·111	—	0·156	—	0·203	—	0·243	—	0·248	—	0·249	0·249

Table 8. $\overline{X^2}$ for 2pπ State

R	0·0	0·25	0·50	0·75	1·00	1·5	2·0	2·5	3·0	3·5	4·0	5·0
Function												
(i)	4·50	4·50	4·50	4·50	4·50	4·50	4·50	4·50	4·50	4·50	4·50	4·50
(ii)	2·00	2·07	2·24	2·44	2·66	3·07	3·41	3·69	3·90	4·05	4·17	4·31
(iii)	2·00	2·01	2·03	2·06	2·10	2·21	2·33	2·46	2·60	2·73	2·87	3·12
(iv)	2·00	2·04	2·14	2·27	2·43	2·78	3·14	3·49	3·83	4·15	4·44	4·93
(v)	2·00	2·04	2·14	2·28	2·44	2·78	3·10	3·38	3·62	3·81	3·97	4·18
(vi)	2·00	2·04	2·14	2·28	2·45	2·82	3·21	3·57	3·88	4·12	4·29	4·48
Exact	2·00	—	2·12	—	2·39	—	3·04	—	3·61	—	4·00	4·22

Table 9. $\overline{Z^2}$ for 1sσ State

R	0·0	0·25	0·5	0·75	1·0	1·5	2·0	2·5	3·0	3·5	4·0	5·0
Function												
(i)	0·250	0·250	0·250	0·250	0·250	0·250	0·250	0·250	0·250	0·250	0·250	0·250
(ii)	0·111	0·145	0·185	0·213	0·231	0·246	0·249	0·250	0·250	0·250	0·250	0·250
(iii)	0·111	0·124	0·158	0·206	0·262	0·381	0·493	0·587	0·663	0·721	0·767	0·828
(iv)	0·111	0·140	0·196	0·267	0·347	0·514	0·670	0·790	0·869	0·918	0·947	0·978
(v)	0·111	0·134	0·182	0·217	0·242	0·264	0·266	0·263	0·260	0·258	0·256	0·254
(vi)	0·111	0·140	0·193	0·245	0·283	0·304	0·290	0·275	0·266	0·261	0·258	0·255
Exact	0·111	—	0·193	—	0·292	—	0·299	—	0·263	—	0·255	0·251

Table 10. $\overline{Z^2}$ for $2p\pi$ State

R	0·0	0·25	0·50	0·75	1·00	1·5	2·0	2·5	3·0	3·5	4·0	5·0
Function												
(i)	1·50	1·50	1·50	1·50	1·50	1·50	1·50	1·50	1·50	1·50	1·50	1·50
(ii)	0·67	0·69	0·75	0·81	0·89	1·02	1·14	1·23	1·30	1·35	1·39	1·44
(iii)	0·67	0·68	0·71	0·76	0·84	1·03	1·27	1·54	1·82	2·12	2·42	2·99
(iv)	0·67	0·69	0·75	0·84	0·95	1·22	1·55	1·92	2·32	2·74	3·17	4·01
(v)	0·67	0·69	0·75	0·83	0·92	1·12	1·30	1·44	1·54	1·60	1·64	1·66
(vi)	0·67	0·69	0·75	0·83	0·94	1·18	1·42	1·62	1·77	1·86	1·89	1·86
Exact	0·67	—	0·75	—	0·94	—	1·45	—	1·81	—	1·91	1·83

Table 11. $\overline{Z}$ for $1s\sigma$ State

R	0·0	0·25	0·50	0·75	1·0	1·5	2·0	2·5	3·0	3·5	4·0	5·0
Function												
(i)	0·000	0·000	0·000	0·000	0·000	0·000	0·000	0·000	0·000	0·000	0·000	0·000
(ii)	0·000	0·000	0·000	0·000	0·000	0·000	0·000	0·000	0·000	0·000	0·000	0·000
(iii)	0·000	0·082	0·158	0·226	0·286	0·381	0·449	0·498	0·533	0·558	0·576	0·600
(iv)	0·000	0·082	0·160	0·233	0·300	0·416	0·506	0·568	0·606	0·627	0·640	0·652
(v)	0·000	0·070	0·107	0·120	0·117	0·088	0·059	0·039	0·027	0·019	0·014	0·009
(vi)	0·000	0·078	0·133	0·160	0·159	0·115	0·070	0·043	0·028	0·020	0·015	0·009
Exact	0·000	—	0·137	—	0·180	—	0·088	—	0·035	—	0·018	0·012

Table 12. $\overline{Z}$ for $2p\pi$ State

R	0·0	0·25	0·50	0·75	1·0	1·5	2·0	2·5	3·0	3·5	4·0	5·0
Function												
(i)	0·000	0·000	0·000	0·000	0·000	0·000	0·000	0·000	0·000	0·000	0·000	0·000
(ii)	0·000	0·000	0·000	0·000	0·000	0·000	0·000	0·000	0·000	0·000	0·000	0·000
(iii)	0·000	0·083	0·166	0·246	0·325	0·474	0·612	0·737	0·851	0·953	1·045	1·200
(iv)	0·000	0·083	0·166	0·247	0·326	0·479	0·625	0·762	0·892	1·015	1·129	1·332
(v)	0·000	0·082	0·157	0·221	0·274	0·343	0·375	0·379	0·364	0·336	0·303	0·235
(vi)	0·000	0·083	0·162	0·235	0·300	0·405	0·470	0·497	0·489	0·456	0·408	0·302
Exact	0·000	—	0·162	—	0·304	—	0·493	—	0·528	—	0·455	0·346

figures 1 and 2. Slater (1933) has shown that an initial decrease in the kinetic energy as two nuclei approach is in general necessary for the formation of a one-electron bond. The previous papers on H_2^+ gave several examples all in agreement with this result. The figures show that, for HeH^{2+}, T passes through a minimum in the case of the $1s\sigma$ state but that, in the R range covered in the present paper, it does not do so in the case of the $2p\pi$ state. Though both states are repulsive both are bonding in the sense that the electronic energy becomes increasingly negative as the internuclear separation is decreased. Minima in T are therefore to be expected from the work of Slater (1933), for it may readily be seen from the virial theorem that the Coulomb repulsion between the nuclei gives no contribution to dT/dR.

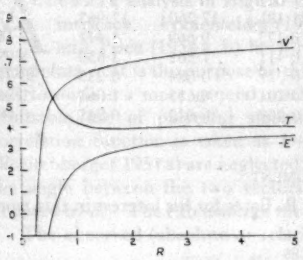

Figure 1. $-V'$, T, $-E'$ as functions of R for the $1s\sigma$ state.

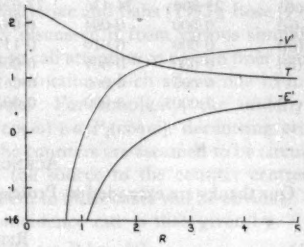

Figure 2. $-V'$, T, $-E'$ as functions of R for the $2p\pi$ state.

Table 13. Percentage Error in Total Electronic Energy of HeH^{2+}

				$1s\sigma$ State			
R	0·0	0·5	1·0	2·0	3·0	4·0	5·0
Function							
(i)	11·111	5·644	2·911	0·520	0·094	0·027	0·011
(ii)	0·000	3·855	2·789	0·520	0·094	0·027	0·011
(iii)	0·000	2·101	6·145	13·243	17·716	20·057	21·343
(iv)	0·000	0·296	2·055	9·412	15·714	19·055	20·780
(v)	0·000	0·372	0·658	0·155	0·019	0·004	0·002
(vi)	0·000	0·131	0·346	0·115	0·017	0·004	0·002
				$2p\pi$ State			
(i)	11·111	9·930	7·874	4·724	2·823	1·611	0·890
(ii)	0·000	1·180	2·600	3·208	2·415	1·495	0·852
(iii)	0·000	0·075	0·594	2·748	5·305	7·819	10·170
(iv)	0·000	0·005	0·047	0·442	1·519	3·331	5·640
(v)	0·000	0·023	0·143	0·422	0·471	0·337	0·194
(vi)	0·000	0·004	0·027	0·108	0·162	0·148	0·105

Table 14. Percentage Error in Total Electronic Energy of H_2^+

R	0·0	0·4	0·8	1·2	2·0	3·0	4·0
Function							
				1sσ State			
(i)	25·000	19·752	13·643	9·289	4·433	2·031	1·159
(ii)	0·000	0·108	0·510	0·958	1·452	1·437	1·097
(iii)	0·000	0·705	3·131	6·174	12·232	19·107	25·460
(iv)	0·000	0·044	0·246	0·657	2·075	4·868	8·690
(v)	0·000	0·241	0·729	0·999	0·902	0·504	0·293
(vi)	0·000	0·019	0·027	0·063	0·193	0·356	0·393
				2pπ State			
(i)	25·000	24·436	23·022	21·181	17·260	12·963	9·676
(ii)	0·000	0·004	0·048	0·173	0·669	1·471	2·166
(iii)	0·000	0·010	0·117	0·411	1·561	3·650	5·997
(iv)	0·000	0·001	0·006	0·021	0·084	0·233	0·475
(v)	0·000	0·006	0·063	0·201	0·613	1·061	1·264
(vi)	0·000	0·000	0·003	0·009	0·022	0·045	0·087

Acknowledgment

Our thanks are extended to Professor D. R. Bates for his interest in this work.

References

Bates, D. R., and Carson, T. R., 1956, *Proc. Roy. Soc.*, A, **234**, 207.
Carson, T. R., and Dalgarno, A., 1955, *Proc. Phys. Soc.* A, **68**, 569.
Dalgarno, A., and Lewis, J. T., 1956, *Proc. Phys. Soc.* A, **69**, 57.
Dalgarno, A., and Poots, G., 1954, *Proc. Phys. Soc.* A, **67**, 343.
Moiseiwitsch, B. L., and Stewart, A. L., 1954, *Proc. Phys. Soc.* A, **67**, 457.
Slater, J. C., 1933, *J. Chem. Phys.*, **1**, 687.
Streetman, J. R., and Matsen, F. A., 1954, *J. Chem. Phys.*, **22**, 1366.

RESEARCH NOTES

Remarks on the Least-Squares Reduction of Angular Correlation Data

By E. BREITENBERGER†
Cavendish Laboratory, Cambridge

MS. received 19*th October* 1955, *and in final form* 13*th March* 1956

ACCURATE analysis of angular correlation data is a statistical matter of some intricacy. Frauenfelder (1952), Chatterjee and Saha (1953), Rose (1953) and Price (1954 a, b) have recently discussed it from various simplified viewpoints. It is the purpose of this note to call attention to certain finer details and to outline a more general method of reduction which allows one to make profitable use of powerful statistical tools. For simplicity, the underlying correlation function is taken as $1+a_2P_2(\cos\omega)+a_4P_4(\cos\omega)$, decentring errors (Breitenberger 1954 a) are neglected, and the counters are assumed to be circular; the angle between the two vectors from the source to the counter centres is denoted by δ. The extension of the argument to other cases will be obvious.

The observed (absolute or relative) coincidence rate is then given by

$$K(\delta)=A[1+c_2P_2(\cos\delta)+c_4P_4(\cos\delta)], \qquad \ldots\ldots(1)$$

where A is a scale factor, whereas c_2 and c_4 are products of the unknown correlation coefficients a_2 and a_4 with known angular resolution factors (the $C_n(\alpha)C_n(\beta)/C_0(\alpha)C_0(\beta)$ in the notation of Breitenberger (1953)), scattering factors (Frankel 1951, Breitenberger 1954 b) and attenuation factors (e.g. Abragam and Pound 1953). In the experiment one makes

$$\left.\begin{array}{r} m \text{ measurements } k_1,\ldots,k_m \\ \text{with estimated standard errors } s_1,\ldots,s_m \\ \text{at the angles } \delta_1,\ldots,\delta_m \end{array}\right\} \qquad \ldots\ldots(2)$$

and then wants to infer the 'most probable' values of c_2 and c_4, viz. those values of the constants in (1), assumed as the correct formal description of the process, which are most likely as predicting the given counting data (2). Usually all coincidence counts are so large (greater than 1000) that the k_μ can be supposed to have normal parent populations; under this condition the 'postulate of maximum likelihood' takes the analytical form of the 'principle of least squares', thus permitting the use of familiar statistical methods.‡

At first one would be inclined to adopt the following procedure: having assigned relative weights $p_\mu=p_0/s_\mu^2$ to the measurements k_μ, with p_0 a suitable constant, one abbreviates $A=x_0$, $Ac_2=x_2$ and $Ac_4=x_4$, sets up the normal equations for a regression curve $x_0+x_2P_2+x_4P_4$, and calculates from their solutions

† Now at Department of Physics, University of Malaya, Cluny Road, Singapore 10.

‡ Provided, however, that the angles δ_μ are known without significant uncertainty; if this is not so the analysis of the data becomes most difficult. Lindley (1947) reviews the underlying problem.

$c_2 = x_2/x_0$ and $c_4 = x_4/x_0$. Except in one special case this method is, however, incorrect. The solutions x_i of a regression problem are *correlated*; the sampling covariance of x_i and x_j is proportional to the element z_{ij} of the inverse matrix of the normal equations (the 'covariance matrix'). Hence, unless all z_{i0} happen to vanish, the quotients x_i/x_0 do not represent the *most probable* values of the c's. For the same reason one cannot in general calculate the sampling errors of the c's from the estimated standard errors of the x_i by means of the usual formula

$$\epsilon(x/y)^2 = (x/y)^2[\epsilon(x)^2/x^2 + \epsilon(y)^2/y^2]. \qquad \ldots\ldots(3)$$

The error involved in setting $c_i = x_i/x_0$ depends very much on the given data, especially on the way in which the angles δ_μ are chosen, and can be larger than the sampling error of c_i; the sampling errors calculated from (3) can be wrong by 20%.

It should be mentioned that even if the z_{i0} vanish the procedure is not always practical. The sampling distribution of the quotient of two uncorrelated regression coefficients is of a type which has not been tabulated but differs markedly from a gaussian unless the number of degrees of freedom is large; therefore the full meaning of the errors calculated from (3) remains unknown unless there are many degrees of freedom. This should be borne in mind when using an orthogonalization method (e.g. Price 1954a).

The difficulty is readily seen to arise from the non-linearity of (1) in the unknowns A, c_2 and c_4. A simple remedy consists in a method of successive approximations applied to a linearized regression function. Suppose we have found that the function

$$K'(\delta) = A'[1 + c_2' P_2(\cos\delta) + c_4' P_4(\cos\delta)] \qquad \ldots\ldots(4)$$

fits the data fairly well. The exact values of the unknowns will be

$$\left.\begin{aligned} A &= A' + \Delta \\ c_2 &= c_2' + \Delta_2 \\ c_4 &= c_4' + \Delta_4. \end{aligned}\right\} \qquad \ldots\ldots(5)$$

Inserting these into (1), and neglecting terms containing the products $\Delta\Delta_2$ and $\Delta\Delta_4$, we find that

$$K(\delta) = K'(\delta) + \Delta\frac{K'(\delta)}{A'} + \Delta_2 A' P_2 + \Delta_4 A' P_4. \qquad \ldots\ldots(6)$$

Using this approximation we set $v_\mu = K(\delta_\mu) - k_\mu$, and obtain from the least-squares condition $[pvv] \to$ min. the normal equations for the required corrections:

$$\begin{aligned} A'^{-2}[pK'K']\Delta + [pK'P_2]\Delta_2 + [pK'P_4]\Delta_4 &= -A'^{-1}[p(K'-k)K'] \\ [pK'P_2]\Delta + A'^2[pP_2P_2]\Delta_2 + A'^2[pP_2P_4]\Delta_4 &= -A'[p(K'-k)P_2] \\ [pK'P_4]\Delta + A'^2[pP_4P_2]\Delta_2 + A'^2[pP_4P_4]\Delta_4 &= -A'[p(K'-k)P_4] \end{aligned} \qquad \ldots\ldots(7)$$

where pvv stands for $p_\mu v_\mu v_\mu$, $pK'P_2$ for $p_\mu K'(\delta_\mu)P_2(\cos\delta_\mu)$ etc., and $[\ldots]$ denotes summation over μ from 1 to m. In addition we have the relation

$$\begin{aligned} [pvv] = \frac{1}{A'}[p(K'-k)K']\Delta + A'[p(K'-k)P_2]\Delta_2 \\ + A'[p(K'-k)P_4]\Delta_4 + [p(K'-k)(K'-k)] \end{aligned}$$

which is very useful because $[pvv]/p_0$ is sampled in a χ^2-distribution of $m-q$ degrees of freedom, where q denotes the number of unknowns (here 3); an accompanying paper (Breitenberger 1956) contains illustrative examples of tests

of significance and goodness of fit based on this property. Note that any such test can wield its full power only if there are enough degrees of freedom.

For the sampling errors of the solutions of (7) we have the unbiased asymptotically efficient estimates

$$\left(\frac{[pvv]}{m-q}z_{ii}\right)^{1/2} \qquad \ldots\ldots(8)$$

where z_{ii} is the appropriate diagonal element in the covariance matrix of (7); they are identical with the sampling errors of the unknowns (5). The significance of an observed regression coefficient x_i with respect to some hypothetical value ξ_i can be assessed through the fact that $x_i - \xi_i$ divided by the estimated standard error (8) is distributed like a t of $m-q$ degrees of freedom. If narrow confidence intervals for the measured x_i are required the number of degrees of freedom must not be too small. The occurrence of the t-distribution also makes it impossible to check the reliability of one's apparatus by repeating the experiment, and comparing the results in an elementary χ^2-test; a complete analysis of variance is required instead.

The approximation (6) is readily seen to converge towards the true $K(\delta)$ if Δ/A', $\Delta_2 A'$ and $\Delta_4 A'$ are much smaller than 1 in magnitude. If the first approximation (4) has been well chosen, e.g. from a careful graphical inspection of the data, one least-squares step (7) will suffice to yield results of the desired accuracy. The normal equations should be computed and solved to at least five places of decimals in order to avoid serious rounding-off errors; $[pvv]$ should be computed to at least three safe figures if the rather sensitive variance ratio test is used.

For a full account of the statistical notions touched in this discussion see the standard treatise by Cramér (1946). A suitable presentation of the essentials is given, for example, by Weatherburn (1949), a brief survey of the theory of estimation by Arley and Buch (1950). Many numerical examples on regression analysis and testing procedures are contained in elementary books by Quenouille (1950, 1952). For extensive tables of the χ^2, variance ratio and t distributions see Fisher and Yates (1953); six-figure tables of Legendre polynomials have been computed by Tallqvist (1938).

References

Abragam, A., and Pound, R. V., 1953, *Phys. Rev.*, **92,** 943.

Arley, N., and Buch, K. R., 1950, *Introduction to the Theory of Probability and Statistics* (New York: McGraw-Hill).

Breitenberger, E., 1953, *Proc. Phys. Soc.* A, **66,** 846; 1954 a, *Phil. Mag.*, **45,** 497; 1954 b, *Proc. Phys. Soc.* A, **67,** 1108; 1956, *Ibid.*, **69,** 453.

Chatterjee, S., and Saha, A. K., 1953, *Z. Phys.*, **135,** 141.

Cramér, H., 1946, *Mathematical Methods of Statistics* (Princeton: University Press).

Fisher, R.A., and Yates, F., 1953, *Statistical Tables*, 4th Edn (Edinburgh: Oliver and Boyd).

Frankel, S., 1951, *Phys. Rev.*, **83,** 673.

Frauenfelder, H., 1952, *Annu. Rev. Nucl. Sci.*, **2,** 129.

Lindley, D. V., 1947, *Suppl. J. R. Statist. Soc.*, **9,** 218.

Price, P. C., 1954 a, *Phil. Mag.*, **45,** 237; 1954 b, *Proc. Camb. Phil. Soc.*, **50,** 491.

Quenouille, M. H., 1950, *Introductory Statistics* (London: Butterworth); 1952, *Associated Measurements* (London: Butterworth).

Rose, M. E., 1953, *Phys. Rev.*, **91,** 610.

Tallqvist, H. J., 1938, *Acta Soc. Sci. Fenn.*, **A2,** no. 11.

Weatherburn, C. E., 1949, *A First Course in Mathematical Statistics*, 2nd Edn (Cambridge: University Press).

On the Bohm–Pines Theory of a Quantum-Mechanical Electron Plasma

By C. G. KUPER
Department of Theoretical Physics, University of Liverpool

MS. received 27th January 1956

In the theory of metals, it is usual to neglect the Coulomb interaction between electrons. Bohm and Pines (1953) have attempted to take this interaction into account, using the longitudinal 'plasma' oscillations of an electron gas (e.g. Pines and Bohm 1952, Bohm and Pines 1953, Appendix 1) to define a set of collective coordinates. They find the residual 'individual particle' motion to be influenced only by a *screened* interaction of short range.

In their description of an electron gas, Bohm and Pines introduce a set of superabundant variables, and a subsidiary condition for each canonical pair of these extra variables. These superabundant variables, after transformation, appear as coordinates and momenta of the plasma oscillators. Other terms in the (transformed) Hamiltonian function include the kinetic energy of the individual electronic motions and the screened inter-electronic potential energy. The selection of the set of plasma oscillators is made variationally—a trial wave function is introduced whose form is a product of oscillator ground-state functions and a Slater determinant (for free electrons in their ground state). The subsidiary conditions are ignored, and the set of oscillators is chosen so as to minimize the expectation value of the energy. However, the wave function of Bohm and Pines does *not* satisfy the subsidiary conditions (Adams 1955). The present paper will show that, in a slightly more general framework, the neglect of these conditions can lead to absurd results.† The notation will be that of Bohm and Pines, except that the oscillator momenta will be denoted $\pi_{\mathbf{k}}$. The Hamiltonian of the system is

$$H=\sum_i \tfrac{1}{2}p_i'^2/m+2\pi e^2\sum_{i,j,\mathbf{k}\neq 0} k^{-2}\exp i\mathbf{k}.(\mathbf{x}_i'-\mathbf{x}_j')-2\pi ne^2\sum_{\mathbf{k}\neq 0}k^{-2} \qquad \ldots\ldots(1)$$

where $\mathbf{x}_i'$ and $\mathbf{p}_i'$ are the position and momentum operators of the ith electron and n is the number density of electrons. There is assumed to be a uniform background of positive charge, to ensure electrical neutrality of the system as a whole. This is expressed by excluding $\mathbf{k}=0$ from the summation. Periodic boundary conditions are imposed, in a box of unit volume.

The extra set of variables $q_{\mathbf{k}}'$, $\pi_{\mathbf{k}}'$, satisfying

$$\left.\begin{aligned} q_{\mathbf{k}}{}^{*\prime} &= -q_{-\mathbf{k}}' \\ \pi_{\mathbf{k}}{}^{*\prime} &= -\pi_{-\mathbf{k}}' \end{aligned}\right\} \qquad \ldots\ldots(2)$$

and

$$\left.\begin{aligned} [q_{\mathbf{k}}', \pi_{\mathbf{l}}'] &= \tfrac{1}{2}i\hbar\{\delta_{\mathbf{k},\mathbf{l}}+\delta_{\mathbf{k},-\mathbf{l}}\} \\ [q_{\mathbf{k}}', q_{\mathbf{l}}'] &= [\pi_{\mathbf{k}}', \pi_{\mathbf{l}}'] = 0 \end{aligned}\right\} \qquad \ldots\ldots(3)$$

† Adams (1955) has criticized the neglect of the subsidiary conditions from a different point of view. He shows that a wave function which satisfies the subsidiary conditions is incompatible with the oscillators being in their ground states—in fact the expectation value of the oscillator energies diverges.

are introduced. If H_1 is defined by

$$H_1 = -\tfrac{1}{2}\sum_{\mathbf{k}\neq 0} \pi_{\mathbf{k}}'\pi_{-\mathbf{k}}' - i\sum_{i,\mathbf{k}\neq 0} (4\pi e^2/k^2)^{1/2}\gamma_k \pi_{\mathbf{k}}' \exp(-i\mathbf{k}\cdot\mathbf{x}_i'), \quad \ldots\ldots(4)$$

then the Hamiltonian $H+H_1$, with the subsidiary conditions

$$\pi_{\mathbf{k}}'\Psi = 0 \quad \ldots\ldots(5)$$

is clearly equivalent to the original form (1). In (4) γ_k is unspecified. Bohm and Pines choose the particular form

$$\left.\begin{aligned} \gamma_k &= 1, \quad k<k_c \\ \gamma_k &= 0, \quad k>k_c \end{aligned}\right\} \quad \ldots\ldots(6)$$

The significance of γ_k will appear presently. In fact $1-\gamma_k{}^2$ is a measure of the 'screening' of the Coulomb interaction.

With the unitary transformation

$$S = \exp\left\{\sum_{i,\mathbf{k}\neq 0} -\hbar^{-1}(4\pi e^2/k^2)^{1/2}\gamma_k q_{\mathbf{k}}' \exp(i\mathbf{k}\cdot\mathbf{x}_i')\right\} \quad \ldots\ldots(7)$$

the variables transform as follows:

$$\left.\begin{aligned} \mathbf{p}_i &= S^{-1}\mathbf{p}_i' S = \mathbf{p}_i' - (4\pi e^2)^{1/2}\sum_{\mathbf{k}\neq 0}\gamma_k q_{\mathbf{k}}' \boldsymbol{\epsilon}_{\mathbf{k}} \exp(i\mathbf{k}\cdot\mathbf{x}_i') \\ \mathbf{x}_i &= S^{-1}\mathbf{x}_i' S = \mathbf{x}_i' \\ \pi_{\mathbf{k}} &= S^{-1}\pi_{\mathbf{k}}' S = \pi_{\mathbf{k}}' + i\gamma_k(4\pi e^2/k^2)^{1/2}\sum_i \exp(i\mathbf{k}\cdot\mathbf{x}_i') \\ q_{\mathbf{k}} &= S^{-1}q_{\mathbf{k}}' S = q_{\mathbf{k}}' \end{aligned}\right\} \quad \ldots\ldots(8)$$

where $\boldsymbol{\epsilon}_{\mathbf{k}} = \mathbf{k}/k$. In terms of the new variables, (5) becomes

$$\Omega_{\mathbf{k}}\Psi = \left\{\pi_{\mathbf{k}} - i\gamma_k(4\pi e^2/k^2)^{1/2}\sum_i \exp(i\mathbf{k}\cdot\mathbf{x}_i)\right\}\Psi = 0 \quad \ldots\ldots(9)$$

and the Hamiltonian $H+H_1$ (equations (1) and (4)) is

$$\begin{aligned} &H+H_1 \\ &= \sum_i \tfrac{1}{2}\left\{\mathbf{p}_i + (4\pi e^2)^{1/2}\sum_{\mathbf{k}\neq 0}\gamma_k q_{\mathbf{k}}\boldsymbol{\epsilon}_{\mathbf{k}}\exp(i\mathbf{k}\cdot\mathbf{x}_i)\right\}^2 \Big/ m + 2\pi e^2 \sum_{i,j,\mathbf{k}\neq 0} k^{-2}\exp\{i\mathbf{k}\cdot(\mathbf{x}-\mathbf{x}_j)\} \\ &\quad - 2\pi n e^2 \sum_{\mathbf{k}\neq 0} k^{-2} - \tfrac{1}{2}\sum_{\mathbf{k}\neq 0}\left\{\pi_{\mathbf{k}} - i\gamma_k(4\pi e^2/k^2)^{1/2}\sum_i \exp(i\mathbf{k}\cdot\mathbf{x}_i)\right\} \\ &\quad \times \left\{\pi_{-\mathbf{k}} - i\gamma_k(4\pi e^2/k^2)^{1/2}\sum_i \exp(-i\mathbf{k}\cdot\mathbf{x}_i)\right\} - i\sum_{i,\mathbf{k}\neq 0}(4\pi e^2/k^2)^{1/2}\gamma_k \\ &\quad \times \left\{\pi_{\mathbf{k}} - i\gamma_k(4\pi e^2/k^2)^{1/2}\sum_j \exp(i\mathbf{k}\cdot\mathbf{x}_j)\right\}\exp(i\mathbf{k}\cdot\mathbf{x}_i) \\ &= \sum_i \tfrac{1}{2}p_i{}^2/m \quad \ldots\ldots(10a) \\ &\quad + \sum_{i\neq j,\mathbf{k}\neq 0}(1-\gamma_k{}^2)k^{-2}(2\pi e^2)\exp\{i\mathbf{k}\cdot(\mathbf{x}_i-\mathbf{x}_j)\} \quad \ldots\ldots(10b) \\ &\quad - \tfrac{1}{2}\sum_{\mathbf{k}\neq 0}\pi_{\mathbf{k}}\pi_{-\mathbf{k}} - \tfrac{1}{2}\sum_{\mathbf{k}\neq 0}(4\pi n e^2/m)\gamma_k{}^2 q_{\mathbf{k}}q_{-\mathbf{k}} - 2\pi n e^2\sum_{\mathbf{k}\neq 0}\gamma_k{}^2 k^{-2} \quad \ldots\ldots(10c) \\ &\quad + \sum_{i,\mathbf{k}\neq 0}(4\pi e^2)^{1/2}m^{-1}\gamma_k \exp(i\mathbf{k}\cdot\mathbf{x}_i)q_{\mathbf{k}}\boldsymbol{\epsilon}_{\mathbf{k}}\cdot(\mathbf{p}_i + \tfrac{1}{2}\hbar\mathbf{k}) \quad \ldots\ldots(10d) \\ &\quad + \sum_{i,\mathbf{k}\neq\mathbf{l}\neq 0}(2\pi e^2/m)\gamma_k\gamma_l q_{\mathbf{k}}q_{\mathbf{l}}\boldsymbol{\epsilon}_{\mathbf{k}}\cdot\boldsymbol{\epsilon}_{\mathbf{l}}\exp\{i(\mathbf{k}-\mathbf{l})\cdot\mathbf{x}_i\}, \quad \ldots\ldots(10e) \end{aligned}$$

where (10 *a*, *b*, *c*, *d*, *e*) are respectively a free particle Hamiltonian, a modified interaction potential energy between particles, a set of harmonic ('plasma') oscillators, an oscillator–particle interaction and the 'random phase' term of

Bohm and Pines. If γ_k is chosen according to (6), then (10 *b*) is Bohm and Pines' screened potential. With the introduction of the set of canonical creation and destruction operators a_k^*, a_k,

$$\left.\begin{aligned} q_k &= (\hbar/2\omega_k)^{1/2}(a_k - a_{-k}^*) \\ \pi_k &= i(\hbar\omega_k/2)^{1/2}(a_k^* + a_{-k}), \end{aligned}\right\} \qquad \ldots\ldots(11)$$

(10 *c*) takes the form

$$\sum_{k\neq 0}\{\tfrac{1}{2}\hbar\omega_k(a_k^* a_k + a_k a_k^*) - 2\pi ne^2\gamma_k^2 k^{-2}\} = \sum_{k\neq 0}\{\hbar\omega_k(a_k^* a_k + \tfrac{1}{2}) - 2\pi ne^2\gamma_k^2 k^{-2}\}. \qquad \ldots\ldots(12)$$

Here

$$\omega_k = \gamma_k\omega_p = \gamma_k(4\pi ne^2/m)^{1/2} \qquad \ldots\ldots(13)$$

where ω_p is the macroscopic plasma frequency.

With the (normalized) trial wave function

$$\Psi = \left\{\prod_{k\neq 0}|\,0_k\rangle\right\}\det\{\exp(i\mathbf{k}\cdot\mathbf{x}_j)\} \qquad \ldots\ldots(14)$$

the expectation value of the Hamiltonian (10) is

$$\begin{aligned} E(\gamma) = \langle H + H_1\rangle = &\sum_i \tfrac{1}{2}\langle p_i^2\rangle/m \\ &+ \sum_{i\neq j,\,k\neq 0}\langle(1-\gamma_k^2)2\pi e^2 k^{-2}\exp\{i\mathbf{k}\cdot(\mathbf{x}_i - \mathbf{x}_j)\}\rangle \\ &+ \sum_{k\neq 0}(\tfrac{1}{2}\hbar\omega_k - \gamma_k^2 2\pi ne^2/k^2) \qquad \ldots\ldots(15) \end{aligned}$$

exactly. (The interaction terms (10 *d*) and the random phase terms (10 *e*) both have vanishing expectations, since

$$\langle 0_k\,|\,q_k\,|\,0_k\rangle = \langle 0_k\,|\,\langle 0_1\,|\,q_k q_1\,|\,0_k\rangle\,|\,0_1\rangle = 0.)$$

The correct statement of the variational principle, *with* the subsidiary conditions, is

$$\delta\left\{E(\gamma) - \sum_{k\neq 0}\langle\Lambda_k\Omega_k\rangle\right\} = 0 \qquad \ldots\ldots(16)$$

where the Lagrangian undetermined multipliers Λ_k are operators. It has not so far proved possible to make any progress using this expression. Bohm and Pines' method is equivalent to assuming that the Λ_k are *c*-numbers.† If this approximation were valid, then (15) should be an upper bound to the energy of the lowest eigenstate, for *any* choice of the function γ_k. However, it is obvious that a variation with respect to γ_k will allow $E(\gamma)$ to become negatively infinite. Thus the neglect of (9) cannot be justified.

Bohm and Pines do not find this divergence, since by (6) they never allow γ_k to exceed unity. Indeed if the *ad hoc* restriction $0 \leqslant \gamma_k \leqslant 1$ is imposed, then $H + H_1$ is positive definite, and the variation of (15) with respect to γ_k then leads precisely to the results of Bohm and Pines. A choice $\gamma_k > 1$ means that the 'short-range' part of the Coulomb interaction is chosen to be attractive. Since

† Since $\langle\Omega_k\rangle = \int\Psi^*\Omega_k\Psi\,dq_k\ldots dx_j\ldots = 0$ for all $\mathbf{k}$, the state (14) does actually satisfy the subsidiary conditions on the *average*. Varying $E(\gamma) + \sum_{k\neq 0}\Lambda_k\langle\Omega_k\rangle$ is equivalent to varying $E(\gamma)$ itself, as Bohm and Pines do. A better approximation might be to vary $E(\gamma) + \sum_{k\neq 0}\Lambda_k\langle\Omega_k^2\rangle$.

this choice of γ_k is physically unreasonable, it should be expected to raise the energy; in fact it has been shown that the energy is lowered without limit. While I believe that the physical idea of Bohm and Pines is essentially correct, it thus appears that their formulation is not satisfactory.

I wish to thank Professor H. Fröhlich and Mr. S. Doniach for valuable discussions.

REFERENCES

ADAMS, E. N., 1955, *Phys. Rev.*, **98**, 1130.
BOHM, D., and PINES, D., 1953, *Phys. Rev.*, **92**, 609.
PINES, D., and BOHM, D., 1952, *Phys. Rev.*, **85**, 338.

Proton–Proton Scattering at 147 MeV

BY J. M. CASSELS†
Atomic Energy Research Establishment, Harwell, Berks.

Communicated by D. W. Fry; MS. received 7th March 1956

SEVERAL early p–p scattering experiments (Birge, Kruse and Ramsey 1951, Towler 1951, Cassels, Pickavance and Stafford 1952, Oxley and Schamberger 1952) indicated values for the cross section between 100 and 250 MeV which were substantially higher than those reported by Chamberlain, Segrè and Wiegand (1951). Later work (Marshall, Marshall and Nedzel 1953, Kruse, Teem and Ramsey 1954, Chamberlain and Garrison 1954) suggested strongly that the high values were incorrect, and in fact one source of error has recently been uncovered by Birnbaum, Crandall, Millburn and Pyle (1954). They have shown that the $^{12}C(p, pn)^{11}C$ cross sections published by Aamodt, Peterson and Phillips (1952) were too high by some 20–30%. The cross sections for this reaction were used as a standard in all four experiments. Some other error must also have been present in the experiment of Cassels *et al.*, because an independent calibration of the beam was made by a photographic plate method. This error has not been traced, although it has been shown that the track density in the plates was accurately determined.

The purpose of this note is to report the result of a remeasurement, with improved apparatus, of the 90° differential cross section at 147 MeV. The scattered and recoil protons from polyethylene and carbon targets were detected by two scintillation counters in coincidence. The scattering geometry was defined by the dimensions of a thin plastic scintillator in one counter, while the scintillator in the other counter subtended a large solid angle at the targets. The proton beam was monitored by an ionization chamber through which the proton beam passed before striking the targets or other apparatus. The ion chamber was calibrated by counting the primary beam, at low intensity, by means of a double coincidence scintillation counter telescope. The linear dependence of the ionization chamber current on the primary beam current was checked at intensities up to the maximum used in the experiment. The calibration of the

† Now at Nuclear Physics Research Laboratory, University of Liverpool.

ion chamber by this method was within 1% of that obtained by Dr. Dorothy Skyrme of this establishment, using the photographic plate method and an improved camera.

The result obtained for the 90° differential cross section was $4{\cdot}05 \pm 0{\cdot}28$ mbn sterad^{-1}, where the standard deviation is intended to allow for possible systematic errors. This value, which was reported at the Glasgow Conference in July 1954, is reasonably consistent with most others, particularly the result of the transmission experiment described by Taylor and Wood (1956).

References

Aamodt, R., Peterson, V., and Phillips, R., 1925, *Phys. Rev.*, **88,** 739.
Birge, R. W., Kruse, U. E., and Ramsey, N. F., 1951, *Phys. Rev.*, **83,** 274.
Birnbaum, W., Crandall, W. E., Millburn, G. P., and Pyle, R. V., 1954, *University of California* UCRL-2756.
Cassels, J. M., Pickavance, T. G., and Stafford, G. H., 1952, *Proc. Roy. Soc.* A, **214,** 262.
Chamberlain, O., and Garrison, J. D., 1954, *Phys. Rev.*, **95,** 1349.
Chamberlain, O., Segrè, E., and Wiegand, C., 1951, *Phys. Rev.*, **83,** 923.
Kruse, U. E., Teem, J. M., and Ramsey, N. F., 1954, *Phys. Rev.*, **94,** 1795.
Marshall, J., Marshall, L., and Nedzel, V. A., 1953, *Phys. Rev.*, **92,** 834.
Oxley, C. L., and Schamberger, R. D., 1952, *Phys. Rev.*, **85,** 416.
Taylor, A. E., and Wood, E., 1956, *Proc. Phys. Soc.* A, **69,** in the press.
Towler, O. A., 1951, *Phys. Rev.*, **84,** 1262.

The Nuclear Scattering of 0.4 and 0.5 MeV Electrons in Composite Aluminium–Uranium Foils

By B. Brown, E. Matsukawa and E. A. Stewardson

Physics Department, University College of Leicester

MS. received 1*st February* 1956

In a recent note by Chapman, Matsukawa, Rose and Stewardson (1955) a brief account was given of a method for the absolute measurement of the differential cross sections for the nuclear scattering of electrons, and results of such measurements in the case of high angle scattering by ^{13}Al were given. Greater interest is attached however to the high angle (90° and greater) scattering in heavy elements, as Paul and Reich (1952), Kinzinger and Bothe (1952), and Kinzinger (1953) have all found the measured differential cross sections to fall below the quantum theoretical values for Coulomb scattering by an amount which increases with atomic number and with angle of scattering. The present note describes the results of some experiments on the scattering of 0·4 and 0·5 MeV electrons at 90° and 105° by ^{92}U, carried out by the method described previously. The heaviest scatterer used by Kinzinger and Bothe was ^{79}Au and for this element they found a discrepancy between theory and experiment of the order of 13% at 90° and of 22% at 110° for 245 kev electrons, while later Kinzinger found a discrepancy for the same element at 120° of about 25%, this being independent of energy over the range 150 to 400 kev. The heaviest element used by Paul and Reich was ^{78}Pt and they found a discrepancy in this case of approximately

18% at 90° for 2·2 Mev electrons. A rough extrapolation of the results of Kinzinger and Bothe indicates that the discrepancies for ^{92}U should be of the order of 20% at 90° and 30% at 110°.

In our experiments, owing to the difficulty of preparing uranium foils sufficiently thin to give predominantly single scattering and to be at the same time self-supporting, the uranium metal was sputtered on to thin aluminium foil and the scattering produced by the composite foil was measured. The foils were weighed before and after sputtering on a quartz micro-balance. The aluminium foils had densities of the order of 0·25 mg cm^{-2} the uranium deposits ranging from the 0·061 to 0·127 mg cm^{-2}. The foils were used at an angle of 45° to the electron beam and measurements were made on the transmission side as it seems that the scattering on this side is likely to be affected less by plural scattering. The foils were orientated so that the beam was incident first on the aluminium (Al–U position) and then reversed so that it was incident first on the uranium (U–Al position). In measuring the intensity of scattering the beam current I_0 was varied over a range of the order of 3 to 1 and the scattered current I_s measured simultaneously. The ratio I_s/I_0 was found in general to show extreme deviations from the mean only of the order of $\pm 2\%$. The overall accuracy however is probably poorer than this, due mainly to uncertainty in the weights of the uranium deposits and to the likelihood of the uranium layers not being perfectly uniform. The overall accuracy in the cross section measurements is therefore likely to be little closer than $\pm 4\%$. In order to provide a control and general check on adjustments and calibrations, the composite foils were replaced by pure aluminium foils twice during the course of the experiments, and the aluminium cross sections measured over the complete high angle range 90°–150°. In all cases very good agreement with theory (closer than 2%) was obtained. These results incidentally confirm those previously published.

Theoretical values for the cross sections for aluminium were calculated from the α^4 expansion of McKinley and Feshbach (1948), and for uranium from the α^8 expansion of Curr (1955). From these the intensities of single scattering (I_s/I_0) per unit solid angle were computed for the actual aluminium and uranium foils used. The single scattering calculated for the aluminium varied from 5% to 10% of that due to the uranium. It was found that the sums of the two calculated intensities differed from the measured intensities of scattering per unit solid angle from the composite foils by amounts only of the order of the experimental error. While it is obviously possible to interpret this result in other ways, it does seem reasonable to infer (1) that by far the greater number of electrons scattered by the composite foil are singly scattered either in the aluminium or the uranium but rarely in both and (2) that it is unlikely that the differential cross sections for uranium fall appreciably below their theoretical values. The principal uncertainty in making this inference is the extent to which double scattering (i.e. successive single scatters in the two metals) occurs. That it does occur to some extent is indicated by the fact that, while changing from the U–Al position to the Al–U produces a change in the intensity of scattering only of the order of magnitude of the experimental error, it is nevertheless a systematic change in that the Al–U results invariably lie below the U–Al results. The effect however is small, and it does not seem likely that such double scattering could be sufficient to give a 20% or 30% discrepancy in the uranium cross sections. Assuming this to be the case, subtraction of the calculated single scattering due

to the aluminium from the measured scattering produced by the composite foil should give a close approximation to the uranium scattering. Some typical results derived in this way for the two uranium layers (0·062 and 0·127 mg cm^{-2}—the lightest and heaviest used) are shown in the figure. This shows the relation

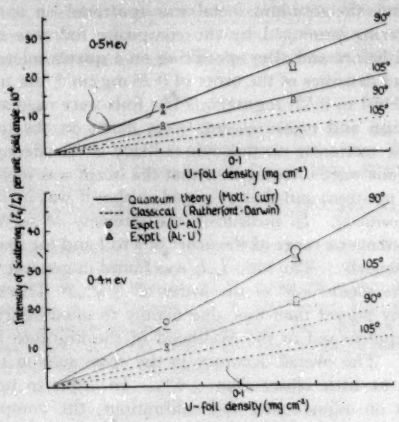

between scattering intensity (I_s/I_0) per unit solid angle and density (in mg cm^{-2}) of the uranium scattering layer. The full lines are the theoretical curves calculated from Curr's tables, and the points the measured scattering intensities per unit solid angle for uranium derived by the subtraction method described, the circles being those for the U–Al orientations, and the triangles those for the reverse orientation. The vertical dimensions of circles and triangles represent the approximate range of estimated experimental error. The broken lines are the curves calculated for Rutherford scattering and are included as a matter of general interest. No corrections have been applied for multiple scattering and for electron screening, as an estimate shows that at these angles they are only of the order of magnitude of the experimental error and of course the two corrections operate in opposite directions. The mean values of the uranium cross sections yielded by the results plotted on these curves are given in the table.

Energy (Mev)	0·4	0·4	0·5	0·5
θ (deg)	90	105	90	105
$\sigma \times 10^{24}$ (cm^2) (exp.)	1039	659	707	437
$\sigma \times 10^{24}$ (cm^2) (theor.)	1043	653	731	447

Several measurements have also been made on the reflection side of the foils. Here, as is usually the case, the measured scattering is in excess of the theoretical amount, but it has not been found possible to obtain consistent results showing systematic variation with the uranium thickness. In one case a reflection–transmission excess of as much as 30% was obtained for 90° scattering. On general grounds one would expect contributions from plural scattering to be

much greater on the reflection side and to be much more influenced by foil irregularities arising either from non-uniformity or from slight wrinkling. It is hoped to make the reflection–transmission effect the subject of further study.

Since the experiments described in this note were commenced, Bayard and Yntema (1955) have published the results of measurements of the scattering of electrons of energies of the order of 1 MeV in aluminium and gold over the angular range 30°–150°. Owing to uncertainty in the density of the very thin gold foil used by them, the accuracy in the absolute cross section measurement for this metal is only about 20% but their results, when normalized at 90°, agree so well with the theoretical values that, in accord with the uranium results described here, there seems little likelihood of large deviations from theory in the high angle scattering.

ACKNOWLEDGMENTS

We would like to express our thanks to Dr. R. M. Curr for communicating a copy of his tables for the calculation of Mott cross sections prior to their publication.

REFERENCES

BAYARD, R. T., and YNTEMA, J. L., 1955, *Phys. Rev.*, **97**, 372.
CHAPMAN, K. R., MATSUKAWA, E., ROSE, P. H., and STEWARDSON, E. A., 1955, *Proc. Phys. Soc.* A, **69**, 928.
CURR, R. M., 1955, *Proc. Phys. Soc.* A, **68**, 155.
KINZINGER, E., 1953, *Z. Naturf.*, **89**, 312.
KINZINGER, E., and BOTHE, M., 1952, *Z. Naturf.*, **79**, 390.
MCKINLEY, W. A., and FESHBACH, H., 1948, *Phys. Rev.*, **74**, 1759.
PAUL, W., and REICH, H., 1952, *Z. Phys.* **131**, 326.

REVIEWS OF BOOKS

Fundamentals of Radiobiology, by Z. M. Bacq and P. Alexander. Pp. xii+389. (London: Butterworths Scientific Publications, 1955.) 40*s*.

This is a fascinating and readable volume by two acknowledged experts. It comprises a series of comprehensive reviews of individual topics, selected by the authors as being, in their view, the most signficant aspects of radiobiology at the present time. The authors point out that the book is not written for specialists, and in many ways this is its particular virtue. Although the individual chapters covering the various topics are complete in themselves, the book forms a broad coherent survey of the fundamentals of radiobiology. In view of recent developments in this field it is particularly valuable to have the subject reviewed from the standpoint of physiology and chemistry rather than physics. In an interesting foreword, Dr. L. H. Gray points out the extreme difficulty of the task which the authors have set themselves, not only on account of the amount of material covered (960 original papers are quoted in the bibliographies), but because of the variety of the disciplines involved. The book comprises 17 chapters covering the effects of ionizing radiations on matter, radiation chemistry, pathological biochemistry, cytology and genetics, chemical radiomimetics, radiation sickness, chemical protection against x- and gamma rays and the value of injections of tissue homogenates, whilst the final chapter is entitled "Observations in Human Beings". The chapters are very well documented and the book is a mine of information.

The introductory chapter on the effects of ionizing radiations on matter provides a useful general account for the non-physicist, although the physicist would perhaps find it somewhat rough in places. For instance, it is disconcerting to find reference to radon as emitting beta rays as well as alpha rays. The selection of isotopes in Table I is also somewhat curious, for instance, ^{24}Na which is an important isotope in physiological investigations is omitted whereas the rare 25-day isotope ^{33}P is included as well as the much-used ^{32}P. In suggesting the mode of formation of the isotopes in the atomic pile there is no reference to fission or to (n, p) reactions which are of such great importance in the preparation of isotopes of high specific activity (e.g. for ^{32}P and ^{14}C). The book does not include any discussion of the metabolism of radioactive materials nor of the carcinogenic action of such materials lodged in the bone; but this could hardly be expected under the title of fundamental radiobiology.

Several chapters deal with the irradiation of the living organisms and one of the most interesting is on the pathological biochemistry of irradiated living organisms. Other chapters deal with the processes of restoration after irradiation and the study of radiation sickness, the physiopathology and treatment. A final chapter on observations in human beings covers work on cancer patients treated by local irradiation, the effects of atomic explosions and the studies made in two instances of overexposure at the Los Alamos Scientific Laboratory in the U.S.A. The remainder of this chapter is devoted to the radiation hazards of the population. In some ways this is the least satisfactory part of the book and much of this section is devoted to the exposure of occupationally

exposed groups. The statement in this section that arrangements are made to bury the radioactive wastes in a concentrated and water-soluble form is, of course, erroneous, but perhaps is a translation error. The references to biological concentration in human food are also rather superficial. It is noted, for instance, that certain isotopes scattered on pastures may become concentrated in animals used by man as food: the paragraph goes on to refer to one of the most dangerous isotopes in this respect being ^{14}C, but there is no doubt that the isotopes of ^{89}Sr and ^{90}Sr and ^{131}I are far more important on account of their metabolic properties and the fact that they will be produced in enormous quantities in nuclear power systems.

In a short postscript the writers summarize in about two pages the outlook in radiobiology at the present time. They refer to the current concepts of the biological effects of radiation and to four applications of chemotherapy in the domain of human radiobiology which can be predicted or have to some extent already been achieved. They conclude that the application of radiobiological research to the solution of many important practical problems seems hopeful and the future is full of promise.

The descriptions of some of the complex biochemical and physiological aspects of this subject may be read by physicists with very great profit. The book is essentially one for the non-specialist in this complex field and in this field which embraces so many disciplines a book of this type is invaluable. The book is well illustrated with an excellent selection of photographs, and graphs specifically drawn to summarize the data in the text are well presented: a word of credit should also be allowed for the translator whose work is, on the whole, very well done. There is an excellent index extending over 30 pages which, together with the large bibliography of the various chapters, makes the book not only a readable account of the subject but a useful work of reference.

W. G. MARLEY.

An Introduction to Quantum Statistics, by W. BAND. Pp. xiii + 342. (Princeton: van Nostrand; London: Macmillan, 1955.) 42*s*.

This text is intended as "a first course in statistical mechanics for postgraduate students in physics and physical chemistry" and its aim is primarily "to train the young postgraduate in the actual handling of statistical mechanics as a tool for himself, rather than to describe to him what more mathematically expert theoretical physicists have been able to do". The book is admirably suited for this purpose as it treats a few problems in quantum statistics in full detail and any student who has worked through both the detailed presentation of the material and the exercises and problems at the end of each chapter should have an excellent working knowledge of statistical methods.

The author confines himself mainly to a discussion of Fermi–Dirac and Bose–Einstein systems, ringing the changes and discussing in turn the ideal gas, mobile monolayers, multilayer adsorption, imperfect gases, clustering phenomena and liquids. Among the solid state problems which are briefly discussed are the crystalline solid, ferromagnetism, substitutional alloys, electrical and thermal conductivity and superconductivity.

Dr. Band has himself made many contributions to the problems he discusses and as a result the book is very much alive and is very stimulating to all those

who are interested in the field. A result of this is, however, that it makes the impression of being a monograph rather than a textbook. It should be used by the same group of scientists who are now using Mayer and Mayer's text—it covers practically the same ground from a more modern point of view—that is, chemical physicists and physical chemists.

I was very disappointed in the selection of references for further study. With but seven exceptions (1 Canadian, 3 Japanese and 3 Dutch references) the student is referred only to American or British books and journals, the vast majority of the references being to papers in the *Journal of Chemical Physics* and the *Physical Review*. This gives a completely false picture of the present state of statistical mechanics research and also underestimates in my opinion both the excellence of the average American college library and the ability of the average American postgraduate to read at least one foreign language.

D. TER HAAR.

Annual Review of Nuclear Science, Vol 5, edited by J. G. BECKERLEY, M. D. KAMEN and L. I. SCHIFF. Pp. ix+448. (Stanford: Annual Reviews Inc., 1955) $7.50.

In the Preface to this volume the Editorial Committee comments on the problems with which it is faced in choosing subjects for successive issues in this well-known review series. The main questions relate to the type of reader, the scope of Nuclear Science, and the timing of the reviews. The committee feels that there is no simple answer to any of these questions and has therefore sought in general to appeal to a wide range of readers, and at a variety of levels of specialization. The average reader will probably find about one third of a volume such as this to be directly his concern, about one third to be not in his own field but still interesting and useful and the remainder to be perhaps almost unintelligible.

The chapters on Electromagnetic Transitions in Nuclei (M. Goldhaber and J. Weneser) and on Nuclear Reactions of Intermediate Energy Particles (D. C. Peaslee) are timely and expert accounts of subjects of which understanding is rapidly increasing. Both are concerned to show how experimental information is interpreted by nuclear models; the former relating particularly to models predicting the properties of low lying excited states (single particle model, independent particle model and collective model) and the latter giving a most useful analysis of the inter-relation between models describing more highly excited states (optical model, statistical model). The article 'The Distribution of Charge in the Nucleus' (K. W. Ford and D. L. Hill) is less specialized; it treats the many different methods of estimating a nuclear radius and correlates the information so obtained in terms of the radial shape and angular shape of the nuclear potential. The interesting and readable article by W. B. Fretter on 'Nuclear Particle Detection' describes the evolution and experimental application of the expansion chamber, the diffusion cloud chamber and the bubble chamber. This article gains much from the inclusion of a short historical introduction, a feature which might well have been adopted by some other contributors. The article concludes with a note on the Russian luminescent chamber.

Two reviews deal with nuclear reactors. The availability of enriched material has made it possible for industrial firms and universities to contemplate the installation of reactors for research purposes, and a helpful comparison of several designs is given by L. B. Borst. He estimates costs and discusses some of the problems likely to be encountered in the construction, start up and operation of a reactor in a relatively public environment. The shielding of such reactors is a major concern, and the present status of the economical design of massive radiation shields is reviewed by E. P. Blizard ('Nuclear Radiation Shielding'). It is unfortunate that so much of the empirical knowledge of this important subject is available only in Progress Reports of interested institutions.

Radiation chemistry, which depends on the production of free radicals in collision processes, is well reviewed by F. S. Dainton in an article which will be found interesting by physicists in general. The production of particular ionic species by the impact of low energy electrons is a closely related subject and is dealt with at length, with particular reference to mass spectrometry, by M. Krauss, A. L. Wahrhaftig and H. Eyring. The application of mass spectrometry in industrial analysis is briefly treated by C. E. Berry and J. K. Walker. The nuclear physicist who is coming more and more to rely on chemical assistance will find the article on 'Radiochemical Separation Techniques' (H. L. Finston and J. Miskel) very valuable. There are useful tables of precipitation, solvent extraction, volatilization and chromatographic procedures and references to more detailed reviews are given.

The dividing line between radiation chemistry and radiobiology is not well defined and the present volume illustrates this in four reviews wholly or mainly of a biological nature. In 'The Fundamentals of Radio-autography' W. P. Norris and L. A. Woodruff describe both the mechanism of the photographic process and the preparation of biological specimens. They use a new word 'quantitation' which, it is to be hoped, will not be widely adopted. R. K. Mortimer and C. A. Beam have written a very comprehensive review of 'Cellular Radiobiology', to judge by the 11 pages of unclassified references which accompany it. It is detailed, technical and difficult to read for one not acquainted with the field, but it leaves the impression that some form of chemical protection against radiation damage may become possible. This is also emphasized in an article on 'Vertebrate Radiobiology: Physiology' by A. Edelmann. J. Schubert contributes a review of some practical interest entitled 'Removal of Radioelements from the Mammalian Body', in which he discusses particularly methods of elimination of metallic poisons. This article is enlivened by a number of case histories.

Although most of the chapters of this volume cover only material originating in the two years ending early in 1955, the amount of information presented is very large. It would aid in the assimilation of this wealth of detail if the Editors insisted on a system of classified references.

W. E. BURCHAM.

CONTENTS OF SECTION B

PAGE

Dr. S. G. Cohen and Mr. A. Weinreb. Energy Transfer from Solvent to Solute in Liquid Organic Solutions under Ultra-Violet Excitation 593

Dr. L. Ainsworth. Single Crystal Bismuth Telluride 606

Mr. C. Wood. Some Observations on the Theory of Photoconductivity in the Lead Sulphide Group of Compounds 613

Mrs. M. A. E. Nutkins. The Density of Electronic States in Body-Centred Cubic Crystals 619

Dr. J. H. Andreae, Mr. E. L. Heasell and Dr. J. Lamb. Ultrasonic Relaxation and the Vibrational Specific Heat of Carbon Disulphide 625

Dr. J. M. Baker. Paramagnetic Resonance in Chromic Methylamine Alum . 633

Dr. J. H. Coupland. Variation of Contrast in Electron Microscope Images with size of Objective Aperture 642

Mr. D. J. Craik. A Study of Bitter Figures using the Electron Microscope . 647

Dr. W. J. R. Calvert (the late). Pre-Breakdown Current and Vacuum Breakdown 651

Mr. P. T. Landsberg and Dr. T. S. Moss. Recombination Theory for Indium Antimonide 661

Mr. J. Ewles and Mr. D. S. Barmby. Optical and Electrical Properties of some Oxygen Activated Alkali Halides 670

Research Notes :

Prof. R. S. Krishnan and Mr. R. Srinivasan. Thermal Expansion of Caesium Bromide 679

Mr. R. Thorburn and Prof. J. D. Craggs. Electron Impact Studies of the Dissociation Energies of N_2 and H_2 682

Dr. J. J. O'Dwyer. A Note on the Electron Distribution Function in Insulators at High Field Strength 685

Mr. R. A. Hyman. Epitaxial Growth of Crystals of Hexagonal Selenium . 687

Letters to the Editor :

Mr. C. A. F. T. Spray. A Simple Etching Technique for revealing Dislocations in Silicon 689

Dr. D. W. Goodwin and Mr. T. P. McLean. Radiative Recombination in InSb 689

Dr. A. J. Manuel. The Magnetic Properties of MnAs and MnBi . . 691

Mr. H. M. Ashton and Prof. E. A. Guggenheim. A New Method for Determining the Second Virial Coefficient of a Gas 693

Reviews of Books : 695

Contents of Section A 696

The de Haas–van Alphen Effect in Alloys

By V. HEINE
Royal Society Mond Laboratory, Cambridge

Communicated by N. F. Mott; MS. received 10th February 1956

Abstract. The theory of primary solid solutions is applied to the de Haas–van Alphen effect in dilute alloys. The experimental results are largely in agreement with the theory, except where there is the possibility of the existence of a bound state round the solute atoms. The de Haas–van Alphen effect appears to be well suited for studying this phenomenon as well as the effect of solutes from different rows of the periodic table.

§ 1. Introduction

In the de Haas–van Alphen effect (Shoenberg 1952) the susceptibility of metal crystals at low temperatures shows oscillations of which the period and amplitude are of interest. The period P, measured in units of $1/H$ (β/E_0 in Shoenberg's notation), is related to the electronic structure of the metal by the formula $P=eh/cS_m$. Here S_m is the area in momentum space of a section of that part of the Fermi distribution to which the observed effect is due by a plane perpendicular to the magnetic field and so chosen as to make the area a maximum (Onsager 1952, Pippard 1954, Lifshitz and Kosevitch 1954). S_m may thus be considered a function of E_M, the energy at the surface of the Fermi distribution in the pure metal.

As shown in the papers quoted above, we may deduce from the variation with temperature of the amplitude of the oscillations a quantity which we call the effective mass m_1, and which is related to the variation of S_m with E_M and hence to the band structure by the formula

$$\frac{m_1}{m}=\frac{1}{2\pi m}\frac{\partial S_m}{\partial E_M}. \qquad \ldots\ldots(1)$$

In what follows we shall assume, following Friedel (1954), that the effect of alloying is to displace each energy level by an amount E_0, which in general is not the same for every energy level. Let the energy at the Fermi level in the alloy be $E_M+\Delta E_M$. Then the energy levels are displaced by an amount $-\delta E$ relative to the Fermi level, where $-\delta E=E_0-\Delta E_M$. Thus the net effect of alloying on the surface of the Fermi distribution is as if the band structure of the pure metal had been filled up with electrons to a new level $E_M+\delta E_M$, where δE_M is the value of δE at the Fermi level.

The corresponding change in the period P which results from alloying can be calculated from (1), since m_1 is known from experiment. It is convenient to express the change δP in P in terms of the quantity R defined by

$$R=\delta P/PZC', \qquad \ldots\ldots(2)$$

where Z is the valence of the solute relative to the solvent atom, and C' is the concentration of solute atoms per atom of solvent. Thus we obtain

$$R = \mp 2\pi m P \frac{\delta E_M}{ZC'}\left(\frac{m_1}{m}\right). \qquad \ldots\ldots(3)$$

The sign of R indicates whether the band responsible for the de Haas–van Alphen effect consists of electrons or positive holes. In what follows, we will calculate R from (3) by calculating δE_M and using experimental values for P and m_1/m. Thus although the de Haas–van Alphen effect is usually very anisotropic, the data we require for comparing the experimental results with the theory are the effective mass of the pure metal, the period, and the change in period on alloying, all for a single direction of the magnetic field. We do not need any knowledge about their variation with orientation.

On the rigid band model of an alloy, δE_M is simply the shift calculated from the change δN in the number of conduction electrons per unit volume and from the density of states $n_0(E_M)$ defined by $n_0(E_M) = \partial N/\partial E_M$. Thus the value of R, calculated from (3) with the rigid band model, is

$$R_{rb} = \mp 8{\cdot}66 \times 10^7 \left(\frac{m_1}{m}\right)\frac{P}{n_0'(E_M)},$$

where $n_0'(E_M)$ is the density of states, now expressed as per atom per electron volt. In the table R_{rb} is compared with the experimentally observed changes in period, expressed using (2) as the quantity R_{obs}. $n_0'(E_M)$ was obtained from the observed values of the electronic specific heat, except for bismuth as discussed in §2. No effect was observed in the periods of the first four entries in the table, and the limits shown for R_{obs} are set by the experimental errors. The values of R_{obs} and R_{rb} are seen to agree as to order of magnitude. The non-zero results will now be discussed in terms of the more detailed theory of alloys as presented by Friedel (1954), following his notation and working in atomic units. We will take into account in §2 the signs of Z and of the screening charges, exchange, and the non-validity of the modified Thomas–Fermi approximation near the band edge, in §3 the effect of solutes from different rows of the periodic table, and in §4 the possibility of bound states.

§2. The Screening Radius and the Band Shift

The calculation of R proceeds in two stages; first we determine the screening radius $1/q_1$ of the potential round the solute atoms, and then the change in energy of the band giving the de Haas–van Alphen effect and hence from (3) the corresponding value of R, which we shall refer to as R_{calc}. Experimentally the alloys used have a low concentration (less than 1%) of solute, so that we have effectively infinite dilution and zero absolute shift ΔE_M of the Fermi energy (Friedel 1954, pp. 457, 462).

In the first order of approximation (Friedel 1954, p. 460) the screening radius is $1/q$ where

$$q^2 = 4\pi n_0(E_M). \qquad \ldots\ldots(4)$$

The perturbing potential

$$V_P = (-Z/r)\exp(-qr)$$

shifts the energy of every state in the band by

$$(-\delta E) = \frac{1}{\overline{v}_i}\int V_p\, dv = \frac{-4\pi Z}{\overline{v}_i q^2} = \frac{-ZC}{n_0(E_M)} \qquad \ldots\ldots(5)$$

in the approximation of the first order perturbation theory, where $\overline{v}_i$ is the mean volume per solute atom, and $C = 1/\overline{v}_i$ is the volume concentration of solute. Friedel (1954, pp. 464–5) has shown how the present statistical approach in this first order of approximation leads to the rigid band model. In particular, we obtain from (3) and (5) the result $R = R_{rb}$.

(1)	(2)	(3)	(4)	(5)	(6)	(7)	(8)	(9)
Sn In	−1	$\lvert R\rvert \leqslant 10$	a					
Sn Hg	−2			?	$\lvert R\rvert = 9$	f		
Sn Sb	+1	$\lvert R\rvert < 25$	b					
Al Mg high freq.	−1	$\lvert R\rvert \leqslant 4$	c	holes	+5	g		
Al Mg low freq.	−1	-9 ± 4	c	electrons	−40	g	0·63	−25
Zn Cu	−1	$+156 \pm 15$					>1·07	>+145
			d	holes	+145	h		
Zn Al	+1	$\lvert R\rvert \leqslant 4$					<1·07	<+145
Bi Te	+1	−15000					12	−18000
Bi Sn	−1	−3000	e	electrons	−3400	see	>2·5	$-R > 1000$
Bi Pb	−1	−1000				text	2·5	−1000
Bi Sb	0	rel. v. small effect			zero effect			

(1) Alloy; (2) Z; (3) R_{obs}; (4) references† (experimental data); (5) nature of carriers responsible for de Haas–van Alphen effect; (6) R_{rb}; (7) references† ($n_0'(E_M)$); (8) screening radius $1/q_1$ (Bohr units); (9) R_{calc}.

† The key to the letters in the references columns is contained in the list of references at the end.

In a higher order of approximation the screening radius $1/q_1$ is not simply given by (4) and it depends on the sign of Z and on whether the screening electrons at the Fermi level behave as negative electrons or as positive holes (Friedel 1954, p. 484). To obtain the values of $1/q_1$ shown in the table, we first calculate q from (4) using the density of states determined from low temperature specific heat measurements, except for bismuth as explained below. As we do not know experimentally the value of $\partial n_0(E_M)/\partial E_M$ we cannot calculate q_1 from q by formula (52) of Friedel (1954, p. 484). Instead we will assume that for screening purposes the electrons in the metal may be taken to behave in the same way as a gas of some appropriate number of free electrons or positive holes having the observed density of states at the Fermi level, so that we can use the relationship between q_1 and q for the free electron gas (Friedel 1954, pp. 486–8). In aluminium the Fermi surface corresponds very closely to a sphere containing three electrons per atom (Heine, to be published), and we can take the carriers as electrons, in agreement with the observed Hall effect (Seitz 1940, p. 183). In zinc, we assume the existence of equal numbers of positive holes and electrons, the holes having the smaller effective mass and thus giving rise to the positive Hall coefficient

(Wilson 1953, pp. 213, 218), and the electrons having the greater effective mass and giving the main contribution to the density of states. Thus for screening purposes, the effect of the electrons predominates over that of the holes, but because the effective masses are not very different (Wilson 1953) the simple model of a gas of electrons is not good. Thus for zinc we will only assume that $\partial n_0(E_M)/\partial E_M$ is positive but probably small, this then determining the sign of the correction $q_1 - q$, whose magnitude is then also small (Friedel 1954, p. 484, eqn 52). The density of states in bismuth was taken as 0·016 electron (counting both spins) per atom per electron volt mainly due to a band containing about $1{\cdot}5 \times 10^{-4}$ hole per atom to give good agreement between R_{obs} and the final calculated values. This figure for the density of states is about half that deduced from the low temperature specific heat measurements of Keesom and Pearlman (1954). The exchange effect (Friedel 1954, p. 471, eqn 33) was also taken into account for **Al** Mg, which is the only case approximating to the free electron model for this purpose.

In calculating the effect of the screened coulomb potential on the states of the band giving the de Haas–van Alphen effect, it is quite unsatisfactory to use the modified Thomas–Fermi approximation (Friedel 1954, p. 455) which leads to almost zero or infinite values for R because the difference between the energies of the Fermi surface and the lowest (or highest) state of the band is so small. Instead, the shift in energy of the lowest (or highest) state of this band relative to the Fermi energy was calculated using perturbation theory, the second order term being relatively small (1% to 20%) because of the low effective mass in this band. We assume that the wave functions of the band can be written in the form $u_0(\mathbf{r})\exp(i\mathbf{k}\,.\,\mathbf{r})$, where $\mathbf{k}$ is measured from the point of the Brillouin zone which has the lowest (or highest) energy in the band, and that the nodes and maxima of $u_0^* u_0$ effectively average out so that we can regard it as a constant. We also assume that the energy in the band has the form $E(\mathbf{k}) = E_M \pm \mathbf{k}^2/2\mu$ with μ of the order of m_1/m. Here and elsewhere, the upper sign refers to a band of electrons, and the lower one to positive holes. We then apply the perturbing potential $(-Z/r)\exp(-q_1 r)$ to the second order, neglect matrix elements connecting states in different bands, and obtain

$$(-\delta E_M) = \frac{-4\pi ZC}{q_1^2}\left(1 \pm \frac{2\mu Z}{q_1}\right). \qquad \ldots\ldots(6)$$

Comparison with (5) gives

$$R_{calc} = R_{rb}\frac{q^2}{q_1^2}\left(1 \pm \frac{2\mu Z}{q_1}\right), \qquad \ldots\ldots(7)$$

from which we obtain the values in the table, subject to the discussion of the next section. We see that the different screening of solute atoms with positive and negative Z can account for the large difference between R_{obs} for **Bi** Te and **Bi** Pb, and incidentally that the density of states in bismuth must be principally due to a band containing positive holes.

The particle densities $\psi^*\psi$ are not the same for the electrons responsible for the de Haas–van Alphen effect and the other electrons at the Fermi surface as assumed so far. Only the difference is important, and we could take it into account if the wave functions were known. Since the states concerned are likely to be near points in the Brillouin zone having special symmetry in the wave function, this effect may be important and may account for the discrepancy between R_{obs}

and R_{calc} for **Al** Mg and for the difference between P for bismuth and P for **Bi** Sb alloys. However, it should not seriously affect comparison between different alloys of one solvent.

§ 3. Different Rows of the Periodic Table

Solutes not from the same row of the periodic table as the solvent are not adequately treated by the preceding theory, which may be extended by introducing a local density of states $n_0(E, \mathbf{r})$ not constant in space, which is defined by

$$n_0(E, \mathbf{r}) = n_0(E)\overline{\psi^*(\mathbf{r})\psi(\mathbf{r})}.$$

Here $\psi(\mathbf{r})$ is the wave function of a state with energy E and with an amplitude of one electron per unit volume, and the bar denotes an average over all states with energy E. Comparing for instance **Zn** Al and **Zn** Ga, the solute ions in the former are smaller and the conduction electrons come closer in to the nucleus, so that they provide better screening but are also more affected by the perturbation potential. The following theorem, which we state in a general form applicable also to finite concentrations, shows that these two effects cancel one another in the first order of approximation. Consider the alloy **Zn** Mg, and take the local density of states $n_0(E, \mathbf{r})$ as referring to it. Although the local density of states $n_0(E, \mathbf{r})$ in **Zn** Mg differs from that in pure zinc near the sites of the magnesium atoms, we may assume (cf. § 4) that the net density of states $n_0(E)$ in the conduction-band is the same in **Zn** Mg as in pure zinc. We then consider the magnesium to be replaced by aluminium, retain the modified Thomas–Fermi approximation and assume the perturbing potential V_P to be small, so that the Poisson's equation which determines V_P becomes (Friedel 1954, pp. 455, 459)

$$\nabla^2 V_P = 4\pi(V_P - \Delta E_M)n_0(E_M, \mathbf{r}) + O(V_P^2), \qquad \ldots\ldots(8)$$

with the boundary conditions $V_P \sim -Z/|\mathbf{r}-\mathbf{r}_i|$ near each solute atom $\mathbf{r}_i$, and that $\partial V_P/\partial \mathbf{n}$ vanishes over some surface S enclosing a volume v containing a large number of solute atoms. We assume that the radial charge density round a magnesium atom in **Zn** Mg of a state with energy near the Fermi energy, is the same for the electrons involved in the de Haas–van Alphen effect as those in the density of states. Then considering a state in **Zn** Mg in the band to which the de Haas–van Alphen effect is due and with energy E_M, the shift $-\delta E_M$ in its energy relative to the Fermi level as we pass to **Zn** Al becomes

$$\begin{aligned}(-\delta E_M) &= \frac{\int_v V_P(\mathbf{r})n_0(E_M, \mathbf{r})\,dv}{\int_v n_0(E_M, \mathbf{r})dv} - \Delta E_M, \\ &= \frac{(1/4\pi)\int_{S'} \nabla V_P \,.\, d\mathbf{S}}{v n_0(E_M)} \quad \text{from (8)}, \\ &= \frac{-ZC}{n_0(E_M)}.\end{aligned}$$

Here the surface S' is S plus an infinitesimal spherical surface round each solute nucleus. The result is identical with that obtained in the usual first order approximation (5) not taking the variation of $n_0(E_M, \mathbf{r})$ with $\mathbf{r}$ into account. Since

in zinc the effect of the second order of approximation is small (q_1 is nearly the same for $Z = \pm 1$), we would expect on the basis of this analysis that R_{calc} for **Zn** Al differs by only a few per cent from the value shown in the table which really refers to **Zn** Ga. Thus these considerations do not explain the very small value of R_{obs} for **Zn** Al.

We cannot base a discussion of the difference between **Bi** Sn and **Bi** Pb on (8) since in this case the series expansion $O(V_P^2)$ does not converge, due to the low density of states in bismuth. Higher order effects are dominant, giving rise for instance to values of q_1 depending markedly on Z as shown in the table. However, we can argue qualitatively as follows. The smaller atomic and ionic radii of tin as compared with lead would indicate that the valence electrons in the tin can penetrate closer to the nucleus. Thus the attraction of the nucleus and the exchange repulsion of the ion core electrons balance in such a way that the valence electrons in tin are acted on by an additional net attractive potential using the modified Thomas- Fermi point of view. Since in bismuth alloys the screening charges act as positive holes, the local density of states around the solute atoms in **Bi** Sn is lowered by the additional attractive potential (attractive as seen by negatively charged electrons) so that the screening is reduced and $|R|$ is increased, in agreement with experiment. We would expect the corresponding effect in **Bi** Te with Z positive to be very small, because with such a large screening radius, the holes do not penetrate to near the repulsive tellurium centres.

§ 4. Bound States

Among the alloys listed in the table, **Bi** Te and **Zn** Al have positive values of Z, so that the possibility arises that one or two electrons are held in localized bound states round the solute ion cores in these alloys. We will now discuss to what extent the existence of bound states affects the calculations of the previous sections, and in particular whether their existence could explain the discrepancy between R_{obs} and R_{calc} for **Zn** Al. Such bound states are simply subtracted from the bottom of the conduction band as described by Friedel (1952) but the change in the de Haas–van Alphen effect period depends on how the states remaining in the band are affected by the perturbation. More precisely, we wish to determine to what level compared with the pure solvent the band is filled by the available number of electrons. As we cannot do this in general, we shall only discuss two extreme types of situation, which we may reasonably expect to correspond approximately to **Bi** Te and **Zn** Al respectively.

Consider first the alloy **Cu** Ag. In this alloy, the attractive perturbing potential due to the higher atomic number of silver is sufficient to subtract 18 states from the conduction band to form the 4s, 4p and 4d shells of silver, and an equal number of states are added to the conduction band by subtracting them from unfilled higher bands. Thus it is usually assumed (Friedel 1952, p. 171) that the distribution of states in the conduction band remains unaltered, while each wave function is changed from a 4s one into a 5s one round each silver atom. The reverse situation would apply to **Ag** Cu and also **Bi** Sb. Thus on this model, we would expect **Bi** Sb to have the same de Haas–van Alphen period as pure bismuth apart from the effect mentioned at the end of § 2, in approximate agreement with experiment (Shoenberg and Uddin 1936).

Similarly we may assume that **Bi** Te behaves in essentially the same way as **Bi** Po, to which we restrict the following discussion. In a bismuth alloy, particularly one with positive Z, the large screening radius calculated by the modified Thomas–Fermi method above (cf. the values in the table) would lead us to expect a bound state according to the criterion $Z/q_1 \geqslant 0{\cdot}7$ (Friedel 1954, p. 491), and with such a slowly decreasing potential the localized wave function would extend over several atoms. In this case, if we expand the wave function of the bound state in terms of the wave functions of states in the pure solvent, only the states with energies near the lowest energy of the conduction band enter into the expansion with large coefficients, as in the theory of donor states in semiconductors (Kittel and Mitchell 1954). If we also expand the perturbed wave functions of the conduction band in terms of the unperturbed wave functions, we can regard this transformation from the unperturbed to the perturbed states as a unitary transformation, affecting mainly the states in the conduction band with energies well below the Fermi energy. This has two consequences. Firstly, the total charge density due to these occupied states with low energies (including the bound state in the perturbed case) remains unaltered by the transformation, so that they can provide no net screening of the perturbing potential. The actual screening is again due to electrons at the Fermi level. Secondly the density of states in the actual conduction band is reduced, so that the total number of states, including the bound one, below some level in the band which is well above the lowest energy in the band, remains unchanged by the transformation. These two conclusions show that the existence of a bound state round each solute atom in **Bi** Po or **Bi** Te should not invalidate the calculation of R_{calc} in the previous sections. The argument is unaffected if we have a doubly occupied bound orbital instead of a single bound state.

In **Zn** Mg, the situation is similar to that in **Ag** Cu and **Bi** Sb. We assume again that the perturbing potential due to 18 less nuclear charges and 18 less electrons modifies all wave functions in such a way that the distribution of states in the conduction band is the same in **Zn** Mg as in pure zinc, in which case the alloy and the pure metal would also have the same de Haas–van Alphen effect period. If we assume further that in **Zn** Al one electron is held in a bound 3s state round the aluminium ion core, the difference between the potentials near solute atoms in **Zn** Mg and **Zn** Al is not very large, and the distribution of states in the conduction band of **Zn** Al may again be the same as in pure zinc. In this case **Zn** Al and zinc would also have the same de Haas–van Alphen effect period, because the extra electron in **Zn** Al is in the bound state, and R for **Zn** Al would be zero. This argument could only hold if the occupied part of the conduction band of zinc has less than 50% s-like symmetry near the atomic nuclei, as otherwise the bound state would seriously affect the conduction band because of the exclusion principle, but this could well be true.

In an alloy with one bound electron round the ion core of each solute atom, the bound electron should give rise to a paramagnetism, as appears to be observed in some cases (Friedel 1952). At low temperatures, it may be possible to saturate this paramagnetism using magnetic fields of the order of ten kilogauss. Then due to the exchange effect, electrons with spins parallel and antiparallel to the magnetic field would move in different effective potential fields near the solute atoms, and would thus give rise to different de Haas–van Alphen effect periods. The difference might be observable in some cases.

In conclusion, the de Haas–van Alphen effect is seen to give information that can readily be related to the theory of primary solid solution alloys. It would appear to be very suitable for studying further experimentally the nature of bound states and the effect of solutes from different rows of the periodic table.

ACKNOWLEDGMENT

The author is indebted to the Royal Dutch/Shell Group for the award of a Postgraduate Scholarship.

REFERENCES

b CROFT, G. T., LOVE, W. F., and NIX, F. C., 1954, *Phys. Rev.*, **95,** 1403.
FRIEDEL, J., 1952, *Phil. Mag.*, **43,** 153; 1954, *Advanc. Phys.* (*Phil. Mag.* Suppl.), **3,** 446.
c GUNNERSEN, E. M., 1955, *Thesis*, University of Cambridge.
g HOWLING, D. H., MENDOZA, E., and ZIMMERMAN, J. E., 1955, *Proc. Roy. Soc.* A, **229,** 86.
KEESOM, P. H., and PEARLMAN, N., 1954, *Phys. Rev.*, **96,** 897.
KITTEL, C., and MITCHELL, A. H., 1954, *Phys. Rev.*, **96,** 1488.
LIFSHITZ, I. M., and KOSEVITCH, A. M., 1954, *Doklady Akad. Nauk*, **96,** 963.
d MARCUS, J. A., 1950 a, *Report of the International Conference on Very Low Temperature Physics* (Cambridge, Mass.: Massachusetts Institute of Technology); 1950 b, *Phys. Rev.*, **77,** 750.
ONSAGER, L., 1952, *Phil. Mag.*, **43,** 1006.
PIPPARD, A. B., 1954, *Solvay Congress Report*, 1.
SEITZ, F., 1940, *Modern Theory of Solids* (London and New York: McGraw-Hill).
a SHOENBERG, D., 1952, *Phil. Trans. Roy. Soc.* A, **245,** 1; and private communication.
e SHOENBERG, D., and UDDIN, M. Z., 1936, *Proc. Roy. Soc.* A, **156,** 701.
h SILVIDI, A. A., and DAUNT, J. G., 1950, *Phys. Rev.*, **77,** 125.
f WILSON, A. H., 1953, *The Theory of Metals* (Cambridge: University Press).

The code letters on the left refer to the entries in the table.

The Band Structure of Bismuth

By V. HEINE
The Royal Society Mond Laboratory, Cambridge

Communicated by N. F. Mott; MS. received 10th February 1956

Abstract. The properties of bismuth and its alloys are considered, with a view to deciding whether or not the band structure is such that there are only $1{\cdot}5 \times 10^{-5}$ free electrons per atom with the same number of holes. It is shown that there is considerable evidence that such is the case. There appear to be no facts that directly contradict this view, but not all the properties of bismuth can be accounted for in detail. The inadequacy of the Landau–Peierls formula for the diamagnetism of conduction electrons appears to be well demonstrated, but this does not affect the usual interpretation of the de Haas–van Alphen effect in terms of the shape of the Fermi surface.

§ 1. Introduction

In bismuth, the existence of a particular band of electrons appears to be well established by the de Haas–van Alphen effect (Shoenberg 1939, Shoenberg and Uddin 1936, p. 717) the galvanomagnetic effects (Abelès and Meiboom, unpublished), and cyclotron resonance (Tinkham 1956). The number N_1 of electrons in this band is $1{\cdot}5 \times 10^{-5}$ per atom. The observations show that they are distributed in momentum space inside three equivalent ellipsoidal Fermi surfaces related to one another by the crystal symmetry, and have a small very anisotropic effective mass (approximately $m_1/m = 0{\cdot}0024$, $m_2/m = 2{\cdot}53$, $m_3/m = 0{\cdot}025$ referred to the principal axes of the ellipsoids), the Fermi level being 0·012 electron volt (equivalent to 205°K, Dhillon and Shoenberg 1955) above the lowest energy in the band. The question to be discussed here is whether there is in addition another incompletely filled band (or bands) containing a considerably larger number N_2 of electrons per atom. In any case there must be a band (or bands) containing N_3 holes per atom, where $N_3 = N_1 + N_2$, say with an effective mass assumed isotropic μ_3 times the free electron mass. We shall refer to these bands of electrons and holes as bands I, II and III respectively.

The purpose of this paper is to test the hypothesis that band II of electrons does not exist and thus that $N_3 = N_1 = 1{\cdot}5 \times 10^{-5}$. We will show in §§ 2 and 3 that the properties of bismuth and its alloys can be roughly explained on the basis of this hypothesis, but they are not at present understood in detail so that in general we cannot say they are inconsistent with any other model of the band structure of bismuth. However, in § 4 we will discuss four particular aspects of the observed magnetic properties that make the hypothesis appear very plausible, and which set in any case an upper limit of about 10^{-4} to N_2 and N_3.

§ 2. The General Properties of Bismuth and its Alloys

The observed galvanomagnetic effects (Abelès and Meiboom 1956), and mean free path effects (Chambers 1953, Wilson 1953, pp. 230–1) are shown by these authors to be consistent with our hypothesis that band II does not exist, so that we will not discuss these effects further.

Let the density of states at the Fermi level E_M be $n_0'(E_M)$ per atom per electron volt for both spin directions together. The value of $n_0'(E_M)$ may be deduced from measurement of the low temperature specific heat (Mott and Jones 1936, p. 179, eqn 11, Keesom and Pearlman 1954, Ramanathan and Srinivasan 1955), and from the change on alloying of the period of the de Haas–van Alphen effect (the periodic variation of the magnetic susceptibility at low temperatures when plotted against $1/H$, where H is the applied magnetic field: Heine 1956). The values of $n_0'(E_M)$ deduced in these two ways differ only by a factor of two, and for the sake of definiteness we adopt the value

$$n_0'(E_M) = 1{\cdot}65 \times 10^{-2} \qquad \ldots\ldots(1)$$

deduced from the de Haas–van Alphen effect. The measurements of this effect indicate that the density of states is principally due to a band containing positive holes, so that we deduce from (1) that μ_3 and N_3 are related by the formula

$$\mu_3^3 N_3 = 5{\cdot}4 \times 10^{-5}. \qquad \ldots\ldots(2)$$

On the basis of our hypothesis about the band structure, we deduce from (2) that $\mu_3 = 1{\cdot}5$. Then if we add donor atoms (e.g. tellurium) to bismuth, the extra electrons almost all go to fill up the band of holes, because of the high effective mass μ_3 there, until at a concentration c_1 of donors slightly greater than $N_1 (= 0{\cdot}0015\%$ per atom), there are no holes left and all further electrons go into band I. On the other hand, a much larger concentration c_2 of acceptors (tin or lead) is required to empty band I of electrons, because the effective mass in band III is so much larger than that in band I. A simple calculation assuming a rigid band structure unaffected by alloying gives $c_2 = 0{\cdot}08\%$. With all the physical properties that have been studied, the effects of alloying bismuth with tin and lead respectively are nearly identical, except that about one third or one quarter as much tin is required to produce the same effect as a certain concentration of lead. A possible explanation of this fact is given by Heine (1956), and this explanation also leads one to expect that lead is behaving normally and contributing one hole per atom. Thus all comparisons with experimental data will refer to lead alloys.

At a concentration of acceptors greater than c_2 but still of this order of magnitude, band I is completely empty at absolute zero and a finite activation energy of a few hundred degrees absolute is required to excite an electron from band III to band I where it has a higher mobility due to the lower effective mass. This leads to a maximum in the variation of the resistance with temperature as shown experimentally and theoretically by Thompson (1936). This effect only occurs at a concentration of lead greater than about $0{\cdot}1\%$, in good agreement with our calculated value of c_2 above. Thus contrary to a statement made by Wilson (1953, p. 228), these experimental facts are consistent with our hypothesis and do not indicate that N_2 is of the order of 10^{-3}. A similar maximum occurs in the temperature variation of the magnetic susceptibility $\chi_\perp$ (Shoenberg and Uddin 1936, p. 694: their χ_1 and χ_3 are $\chi_\perp$ and $\chi_\parallel$ respectively).

The variation of $\chi_\perp$ with concentration of lead shows a maximum, which will also be associated with the emptying of band I in §3. At 75°K, this maximum occurs at a concentration of $0{\cdot}3\%$ lead (Shoenberg and Uddin 1936, p. 698), but inspection of the variation of $\chi_\perp$ with temperature (Shoenberg and Uddin 1936, p. 694) indicates that at very low temperature this maximum would occur at about $0{\cdot}13\%$ lead, in good agreement with our calculated value of c_2.

§ 3. The Diamagnetic Susceptibility

The usual Landau–Peierls theory of diamagnetism in metals is quite inadequate to explain the observed variation of the susceptibility on alloying bismuth with donors and acceptors (Shoenberg and Uddin 1936, p. 698). This can be seen without reference to any particular model of the band structure of bismuth.

The Landau–Peierls formula (Mott and Jones 1936, p. 209, eqn 56, Wilson 1953, p. 175, eqn 6.8.1) predicts that a full Brillouin zone by itself has zero susceptibility, that some holes inside the zone (in band III in our nomenclature) give a diamagnetic susceptibility varying as $(N_3)^{1/3}$, and that some additional electrons in band I and II do likewise. Now it is observed that the diamagnetic susceptibility $-\chi_\perp$ decreases with increasing concentration of tellurium. On the Landau–Peierls theory, this could only be due to some band of holes filling up, in which case the contribution from this band to the susceptibility would vary as $(N_3')^{1/3}$ where N_3' is the number of holes per atom left in it. This contribution would have an infinite gradient at some finite concentration of donors when N_3' becomes zero. However, the observed variation of $-\chi_\perp$ has quite a different shape, which is thus at variance with the Landau–Peierls theory. Similar remarks apply to the variation of $-\chi_\perp$ and $-\chi_\parallel$ with the addition of donors. Incidentally, the density of states in bismuth is so low that the Pauli spin paramagnetism (Mott and Jones 1936, p. 184) is negligible.

Let us therefore abandon the Landau–Peierls theory and study the experimental variations of $\chi_\parallel$ and $\chi_\perp$ as functions of donor and acceptor concentrations. These indicate that if the Brillouin zone were completely filled and there were no electrons outside it, it would have a large diamagnetic susceptibility, which is continuously decreased by an increasing concentration of donors or acceptors (i.e. by the presence of additional electrons outside the zone or holes inside it) if we disregard in the meantime the more complicated behaviour at the low concentrations. This general conclusion is independent of any particular assumptions about bands I, II and III. We will first give a qualitative explanation of it, and then show how the more complicated variations of the susceptibility at low concentrations of donors and acceptors can be accounted for on the basis of our particular hypothesis about the band structure.

Adams (1953) has shown that when we have a band with a very low effective mass such as band I in bismuth, various correction terms that are omitted in the Landau–Peierls theory become important, and give a contribution to the susceptibility of the same order as the usual Landau–Peierls diamagnetic susceptibility. This additional contribution cannot be estimated quantitatively at present. Let us first consider the susceptibility that the Brillouin zone would have if there were no holes inside it and no additional electrons outside it, and then the modifying influence of the electrons and holes in bands I, II and III. Adams (1953) has shown that the zone by itself would have a diamagnetic susceptibility due to the filled states near the boundary of the zone and to the presence of unfilled states outside the zone with only slightly higher energy, both having a small effective mass say μ times the free electron mass. This susceptibility should be of the order of $1/\mu$ times the Landau diamagnetism of a free electron gas (Mott and Jones 1936, p. 210, eqn 59) with a density of five electrons per atom, so that we obtain agreement with experiment with μ of the order of 0·02, a not unreasonable figure in view of the effective mass in band I. This diamagnetism would then be

reduced by electrons filling the states in bands I and II, and by holes removing the electrons inside the zone near the zone boundaries.

Thus on the basis of our hypothesis, we would interpret the variation of $\chi_\perp$ and χ_{II} with donor and acceptor concentrations (Shoenberg and Uddin 1936, p. 698) as follows. The presence of electrons in band I has a very strong paramagnetic effect (i.e. decreases the magnitude of the diamagnetism) on $\chi_\perp$ and a very weak one on χ_{II}. In each case the magnitude of the effect is of the order of the corresponding susceptibility calculated from the Landau–Peierls formula, but of opposite sign as already discussed. The presence of holes in band III has paramagnetic effects of intermediate magnitude on both $\chi_\perp$ and χ_{II}. Thus $-\chi_\perp$ increases with the addition of acceptors due to the predominating effect of the emptying of band I, until it is completely empty at a concentration $c_2 \simeq 0{\cdot}1\%$, after which the effect of the holes in band III becomes evident. Similarly the sudden increase in $-\chi_{II}$ on adding donors is due to band III becoming filled at a concentration $c_1 \simeq 0{\cdot}0015\%$: the corresponding effect in $\chi_\perp$ is not observed owing to the predominating effect of band I.

§ 4. Four Observations which favour our Hypothesis

We can now discuss the four effects which suggest particularly that our hypothesis is correct. Firstly, the sudden increase in $-\chi_{II}$ on addition of some concentration of donors less than 10^{-4} per atom (Shoenberg and Uddin 1936, p. 698) is very difficult to explain except by assuming that some band containing fewer than this number of holes has been filled with electrons. Although this is not necessarily the only band of holes, the variation of $\chi_\perp$ and χ_{II} with donor concentration gives no indication that other bands with a larger number of holes are also filling up.

Secondly, there is the observation that no de Haas–van Alphen oscillations have been observed in bismuth besides those due to the electrons in band I (Dhillon and Shoenberg 1955, Shoenberg 1953). This fact, together with a consideration of the amplitude of the expected oscillations due to the holes in band III, will allow us to set a limit on the value of N_3. The observation is for instance quite consistent with our hypothesis, because with $N_3 = 1{\cdot}5 \times 10^{-5}$ and $\mu_3 = 1{\cdot}5$ (cf. § 2) the temperature-dependent factor in the amplitude of the oscillations due to the holes is extremely small (Wilson 1953, p. 171). More generally, if we assume that N_2 is not zero, N_3 and μ_3 are related by (2), μ_3 being reduced as N_3 increases. Both these factors increase the amplitude which detailed considerations show should be observable if $N_3 > 10^{-4}$.

The third and fourth points below depend essentially on the usual interpretation of the period of the de Haas–van Alphen oscillations. For these arguments to be valid, we have to show that the usual interpretation of the period remains unaffected by the large corrections that are necessary in the usual Landau–Peierls theory of the steady susceptibility (Adams 1953), although the latter is based on the same fundamental approximation (cf. Harper 1955, p. 878, Adams 1953, p. 638). This is proved in the Appendix.

Thirdly, we consider the de Haas–van Alphen effect period of the **Bi** Te alloys (Shoenberg and Uddin 1936, p. 712). As in § 2, we would expect on the basis of our hypothesis that all the electrons from donors appear in band I when the donor concentration is greater than about 0·0015%. The period of the oscillations in the usual interpretation of the de Haas–van Alphen effect is inversely

proportional to the area of cross section of the Fermi distribution in momentum space (Onsager 1952, Pippard 1954), and thus varies as $(N_1')^{-2/3}$, where N_1' is the total number of electrons in band I. From the value of N_1 we can thus calculate for any donor concentration the expected value of λ, which we define as the ratio of the period for the alloy to the period for pure bismuth. Reasonable agreement with experiment is obtained, as shown in table 1, for a donor concentration from 0·002% up to the highest measured (0·009%). It is very difficult

Table 1.

Donor concentration (%)	0·002	0·004	0·008	0·009
Observed λ	0·75	0·58	0·40	0·38
Calculated λ	0·83	0·52	0·33	0·30

to see how this result could occur by chance if a partially filled band II and some holes in band III are present as well. The shift in energy on alloying of states in these two bands would have to be of opposite signs or zero, which would be inexplicable on the present theory of alloys (Friedel 1954, Heine 1956, eqn 6).

Fourthly, we consider the difference between the effects of introducing donors and acceptors on the de Haas–van Alphen period (Shoenberg and Uddin 1936, p. 712). It is convenient to work in terms of the quantity R defined by Heine (1956) which is proportional to the magnitude of the effect, R_d and R_a referring to alloys with donors and acceptors respectively. Although the calculated order of magnitude of R_d and R_a is determined by $n_0'(E_M)$ their precise value and in particular the ratio R_d/R_a depend on the density of the carriers responsible for screening the solute atoms, which in our case is N_3. Table 2 shows values of

Table 2.

N_3	$1{\cdot}5\times10^{-3}$	$1{\cdot}5\times10^{-3}$	$1{\cdot}5\times10^{-4}$	$1{\cdot}5\times10^{-5}$
R_d/R_a	1·7	5·1	17	†

† Statistical theory not applicable.

R_d/R_a calculated by a modified Thomas–Fermi method (Friedel 1954) in the manner of Heine (1956) for various values of N_3. The observed ratio is 15, so that we deduce from table 2 that N_3 is of the order of 10^{-4} or less. The values of R_d/R_a in table 2 are probably over-estimates, because with the large screening radii in bismuth dielectric polarization will help to reduce the perturbing potential round the solute atoms as in semiconductors (Mott and Gurney 1940, chap. 3). Although the condition for the validity of the statistical calculation is not really fulfilled, namely that the number of holes should be large inside a volume over which the perturbing potential does not vary appreciably, we would expect it to give answers of the right order of magnitude except for the lowest value of N_3 that corresponds to our hypothesis that $N_3 = N_1$. In this case the concentration of introduced atoms becomes much larger than N_3, and we have to consider R_d and R_a separately. We have already shown that the period of the de Haas–van Alphen effect of **Bi** Te alloys supports our hypothesis; as regards R_a we can only say at present that it is not inconsistent with the hypothesis.

Summarizing, we have found that the properties of bismuth and its alloys are consistent with our hypothesis that there are only $1{\cdot}5\times10^{-5}$ free electrons and the same number of holes present in bismuth. There do not appear to be any observations that contradict this view, and there are four that particularly support it, although in the present vague state of our knowledge none of the

evidence provided by them is by itself entirely unassailable. Accurate determinations of the de Haas–van Alphen period and of χ_{II} at very small donor concentrations would be expected to give more decisive evidence for the filling up of a band containing such a small number of holes.

A study of **Bi** Sb alloys may also be helpful. The de Haas–van Alphen period of bismuth is increased by the addition of antimony, which means that N_1 is decreased. Presumably N_3 is decreased equally because both metals have the same number of valence electrons per atom. Rather uncertain extrapolation of the observed data would indicate that N_1 may decrease to zero at a concentration of about 4% antimony. At higher concentrations the material would then be a typical semiconductor, which may make band III more accessible to direct study. The observed variations of the steady susceptibility with antimony concentration and with temperature (Shoenberg and Uddin 1936), and the variation of resistance with temperature (Thompson 1936), are not inconsistent with this view but the data are very meagre.

ACKNOWLEDGMENT

The author is indebted to the Royal Dutch/Shell Group for a postgraduate scholarship.

APPENDIX

Consider a single band containing N electrons per atom, and an applied magnetic field H. The highly degenerate energy levels of the electrons with zero component of momentum along the magnetic field are

$$E_n=(n+\gamma)2\beta_0 H/\mu \qquad \ldots\ldots(3)$$

relative to the lowest energy of the band, where n is an integer, β_0 the Bohr magneton, γ some constant less than one, and μ the ratio of the effective mass to the free electron mass. If the Fermi level in the band is E_M relative to the lowest energy of the band, the maxima of the susceptibility in the de Haas–van Alphen effect occur according to the usual theory (Pippard 1954) at fields given by the relation

$$\frac{1}{H_n}=(n+\gamma')\frac{2\beta_0}{\mu E_M}, \qquad \ldots\ldots(4)$$

where γ' differs from γ by some constant such as $\frac{1}{8}$ or $\frac{3}{8}$. The Landau–Peierls susceptibility per atom (Mott and Jones 1936, p. 209) may be written in the form

$$-\chi_{LP} = N\beta_0^2/2E_M\mu^2,$$

where in the case of ellipsoidal energy surfaces μ is the same combination of the principal effective masses as μ in (3). Adams' (1953) additional terms in the susceptibility are of the order of χ_{LP}, and thus correspond to an average additional energy per electron of the order of

$$\frac{\beta_0^2H^2}{4E_M\mu^2}=\frac{2\beta_0 H/\mu}{8(n+\gamma)} \text{ from (3).} \qquad \ldots.(5)$$

Thus we must correct the energy levels (3) by something of this order of magnitude, and then the relation determining H_n becomes

$$\frac{1}{H_n}=\frac{2\beta_0}{\mu E_M}\left(n+\gamma'+\frac{\gamma''}{8(n+\gamma)}\right), \qquad \ldots\ldots(6)$$

where γ'' is some constant. Thus comparing (6) and (4) we would only expect the first few oscillations at high magnetic fields to be affected appreciably, but not the period as determined at lower fields.

There still remains the possibility that energy correction terms larger than (5) by an order of magnitude, i.e. linear in H, do exist but, being sometimes positive and other times negative, average to zero over all the electrons. Such terms do exist and broaden each energy level (3) into a little band (Harper 1955). In a single band that does not overlap other bands these terms cannot affect the mean energy of each broadened level to the same order of magnitude, as this would lead to a term linear in H in the energy of the whole electron gas. However, when two bands overlap in energy, the levels in them may be affected oppositely by an amount of the order $\beta_0 H/\mu$. This may seriously upset the periodicity of the energy levels (3) in each band, but we would expect to see a de Haas–van Alphen effect with an approximate period equal to the lowest common multiple of the individual periods of the bands (Harper 1955, p. 890). This is unlikely to be the situation in bismuth because the variation of period with orientation and the temperature dependence of the amplitude all fit the ellipsoidal model so well, and because successive maxima and minima come with great regularity without any irregular subsidiary maxima in between (Shoenberg 1939, Dhillon and Shoenberg 1955).

References

Abelès, B., and Meiboom, S., 1956, *Phys. Rev.*, **101,** 544.

Adams, E. N., II, 1953, *Phys. Rev.*, **89,** 633.

Chambers, R. G., 1953, *Physica*, **19,** 365; and private communication.

Dhillon, J. S., and Shoenberg, D., 1955, *Phil. Trans. Roy. Soc.* A, **248,** 1.

Friedel, J., 1954, *Advanc. Phys.* (*Phil. Mag.* Suppl.), **3,** 446.

Harper, P. G., 1955, *Proc. Phys. Soc.* A, **68,** 874, 879.

Heine, V., 1956, *Proc. Phys. Soc.* A, **69,** 505.

Keesom, P. H., and Pearlman, N., 1954, *Phys. Rev.*, **96,** 897.

Mott, N. F., and Gurney, R. W., 1940, *Electronic Processes in Ionic Crystals* (Oxford : University Press).

Mott, N. F., and Jones, H., 1936, *The Theory of Metals and Alloys* (Oxford : University Press).

Onsager, L., 1952, *Phil. Mag.*, **43,** 1006.

Pippard, A. B., 1954, *Solvay Congress Report*, 1.

Ramanathan, K. G., and Srinivasan, T. M., 1955, *Phys. Rev.*, **99,** 442.

Shoenberg, D., 1939, *Proc. Roy. Soc.* A, **170,** 341; 1953, *Physica*, **19,** 791; and private communication.

Shoenberg, D., and Uddin, M. Z., 1936, *Proc. Roy. Soc.* A, **156,** 687, 701.

Thompson, N., 1936, *Proc. Roy. Soc.* A. **155.** 111.

Tinkham, M., 1956, *Phys. Rev.*, **101,** 902.

Wilson, A. H., 1953, *The Theory of Metals* (Cambridge : University Press).

Band Spectra Emitted by Strontium and Barium in Arcs and Flames

By MONIQUE CHARTON† and A. G. GAYDON
Chemical Engineering Department, Imperial College, London

MS. received 15*th November* 1955, *and in final form* 7*th March* 1956

Abstract. Studies have been made of the spectra given by strontium and barium in an oxy-hydrogen flame, in a ' vacuum arc ' in water vapour, in a ' vacuum arc ' in heavy-water vapour (D_2O), and in an arc in air at atmospheric pressure. For strontium, a band with some structure at 6050 Å and diffuse bands with maxima at 6460, 6590, 6675 and 6820 Å are attributed to SrOH, in agreement with James and Sugden's suggestion, the assignment being supported by small isotopic displacements with SrOD. Bands at 5950, 6050 and the far red, obtained best in the arc at 1 atmosphere, have a very complex structure suggesting a polyatomic emitter and variation of strength with concentration when strontium nitrate solution is sprayed into a flame supports assignment to the dimer of the oxide, Sr_2O_2. For barium, bands in the green and photographic infra-red are attributed to BaOH, the assignment again being supported by the isotopic shift. Diffuse complex bands near 4800, 5020 and 5500 Å in the arc in air may be due to the corresponding oxide dimer, Ba_2O_2.

§ 1. Introduction

The bright red and green colours obtained when strontium and barium salts are introduced into a flame are well known, and for strontium visual observations on the band spectrum apparently go back as far as 1823, when it was described by Herschel. Salts of strontium and barium are the basis of many coloured flares and fireworks (Barrow and Caldin 1949). It has been generally assumed that the bands (other than those due to halides) are emitted by the diatomic metal oxides, but for the strongest flame bands no analyses have been made. Thus, for barium, an extensive system of bands of simple structure, extending from the far red to the blue, has been analysed (Mahanti 1934) and definitely attributed to BaO, but the strong flame bands in the green have not been studied in detail. For strontium, relatively weak systems in the photographic infra-red, the blue and the near ultra-violet are observed in arcs and these have been analysed and assigned to SrO (for summarized data see Pearse and Gaydon 1950), but the much stronger systems in the yellow-orange and in the far red have not been analysed; flames containing strontium also show bands in the yellow-orange and far red. Similarly, for calcium, bands due to CaO are known in the infra-red and in the blue, but the very strong orange and green systems have not been studied in detail until very recently (Gaydon 1955).

James and Sudgen (1955) suggested as the result of quantitative flame studies that the flame bands of these alkaline earth metals were due to triatomic hydroxide molecules, CaOH, SrOH and BaOH. Following this valuable suggestion, the

† Usual address : Laboratoire de Chimie Générale, 1, Rue Victor Cousin, Paris V.

bands of calcium were studied (Gaydon 1955) in a flame, in an ordinary arc in air at atmospheric pressure, and in ' vacuum ' arcs in ordinary water vapour (H_2O) and heavy-water vapour (D_2O). An isotope shift was observed, and the assignment to CaOH was confirmed. It was also rather surprisingly found that the green and orange bands obtained from an arc in air at 1 atmosphere were not the same as the flame bands, although in such a closely similar spectral region. These arc bands are apparently due to an oxide, but their structure is extremely complex; they cannot be due to transitions between singlet electronic states of CaO, and while they could conceivably be due to transitions between triplet states of CaO, it was suggested that they also might be due to a polyatomic emitter, and the dimer of the oxide $(CaO)_2$ appears most likely. For the yellow-orange band of strontium in a flame, it has also recently and independently been shown by Lagerqvist and Huldt (1955) that there is an isotopic change in the structure on replacing hydrogen by deuterium, confirming the assignment of this band to SrOH. They did not study the arc spectra, but sprayed strontium nitrate dissolved in ordinary water and dissolved in heavy water into a flame.

The bands now assigned to SrOH occur readily in a flame or a vacuum arc in water vapour, while the arc in air shows different bands in a similar region. For Ba, strong bands of BaOH occur in the flame in the green (4870 and 5120 Å) and infra-red (7100–8400 Å) but these are more difficult to obtain in a vacuum arc. The arc in air shows mainly Mahanti's system of BaO, but also some complex structure near 4800 and 5020 Å. The assignment of these various bands is important for determinations of dissociation energies, and is also of astrophysical interest.

§ 2. Experimental

Three main types of source were used to excite the various band systems, an arc in air, a vacuum arc and an oxy-hydrogen flame.

The arc in air was of the usual form, between graphite poles 1 cm in diameter. The arc was maintained by a 220 volts d.c. supply at a current of 6 to 8 amps. The salts (strontium carbonate, strontium nitrate, barium nitrate) were packed into a small hole drilled in the graphite.

The vacuum arc has been described previously (Gaydon 1955). Graphite electrodes were again used, and the arc was run in an atmosphere of ordinary water vapour or heavy-water vapour at a few mm Hg pressure, slow continuous pumping serving to sweep out hydrogen and other decomposition products. The arc was struck with the aid of a Tesla coil.

For most of the work the oxy-hydrogen flame was run on a commercial welding burner and the salt was introduced by holding a rolled-up filter paper soaked in strong salt solution in the edge of the flame. In some cases crushed salt crystals were rolled up in the filter paper. For the work with a spray of strontium nitrate solution, a special burner was used. This was a burner specially developed for quantitative spectrochemical analysis kindly lent by Mr R. L. Warren of the Courtauld's Institute for Biochemistry. It was water-cooled and consisted essentially of a central spray nozzle surrounded by a ring of fine holes. Pre-mixed hydrogen and oxygen passed through the ring of holes and formed the main flame, while the spray of salt solution was carried into the centre of the flame by a stream of oxygen. It gave a very intense steady flame. The solution could be changed without altering any of the adjustments of the flame or spray nozzle.

For the spectroscopic observations a medium glass spectrograph (Hilger E 495) and a two-prism glass Littrow-type instrument, giving a dispersion of about 6 Å mm^{-1} in the orange, were used. For the strontium arc in air, some plates were also taken with the 21 ft concave grating spectrograph in the Physics Department ; a grating with 30 000 lines per inch was used, this giving a dispersion of 1·23 Å mm^{-1}. Iron arc comparison spectra were used. Ilford Astra III and Ilford Long Range spectrum plates were employed; the latter were sensitive to 8500 Å.

§ 3. Bands of SrOH and SrOD

The bands of SrOH, as obtained from the flame, have been photographed with the medium glass and the Littrow spectrographs. The yellow-orange band, centred at about 6050 Å, is very similar in general appearance to the green band of CaOH which has been studied in detail (Gaydon 1955). On the short-wave side the band is diffuse, but on the longer wavelength side there are a number of heads, apparently shaded to the violet. Towards the centre of the bands the structure, although strong, is largely masked by the continuous emission ; towards longer wavelengths the structure becomes weaker but clearer because there is less background. Lagerqvist and Huldt (1955) studied this band under large dispersion (0·8 Å mm^{-1}) and record heads at 6114·2, 6111·8, 6109·8, 6107·9, 6107·5 and 6105·2 Å. With our plates, on smaller dispersion, the most prominent features are at rather shorter wavelengths. The heads occur in pairs, and the following are our measurements, with rough visual estimates of intensity.

λ	I	λ	I
6109·6 ± 0·3	1	6089·9	6
6106·7		6088·1	
6101·1	3	6084·7	10
6099·6		6082·5	
6095·9	4	6076·6	8
6094·7		6075·0	

These wavelengths agree moderately well with those given by Barrow (see Pearse and Gaydon 1950) and attributed to SrO.

Using the vacuum arc in H_2O and D_2O, there is no large isotopic displacement of this band at 6050 Å, but there does appear to be a slight shift towards the red with deuterium. We have only compared these bands of SrOH and SrOD under small dispersion. Some change in the detailed structure is observed, and this has also been reported by Lagerqvist and Huldt.

The far red bands of SrOH are shown in strip *c* of the plate. The bands are wide and diffuse, showing intensity maxima at about 6460, 6590, 6675 and 6820 Å. Strip *d* of the plate shows the first three of these bands, with the larger dispersion of the Littrow spectrograph; the bands are quite diffuse and structureless apart from a trace of superposed oxide (?Sr_2O_2) bands. They appear to be analogous to the diffuse orange-red bands of CaOH. In the vacuum arc the corresponding bands of SrOD have been obtained (see strip *b*). Although there is no large isotopic shift, slight displacements are observed. Thus for SrOH the 6460 band lies symmetrically between the Sr lines 6408 and 6504 Å, but the corresponding band of SrOD lies definitely nearer to the 6504 line. The SrOH band at 6820 is displaced definitely to longer wavelengths with SrOD. It is

therefore clear that the emitter of these diffuse bands contains a hydrogen atom, and in view of the previous work on the analogous system of CaOH and the flame studies of James and Sugden there is no reason to doubt the assignment to SrOH.

§ 4. The Complex Bands of Strontium Oxide (? Sr_2O_2)

These bands occur best in the arc in air at atmospheric pressure, using strontium carbonate or strontium nitrate on graphite poles. They appear weakly in some of our plates of the vacuum arc in water vapour and when strontium nitrate is introduced in high concentration into the oxy-hydrogen flame. In the yellow-orange the strong band at about 5950 lies in a region clear of SrOH (see strips *a* and *c* of the plate), and the weaker band at 6050 has a different fine structure from the SrOH. In the far red region the general intensity distribution is very similar to that of SrOH, but with the larger dispersion of the Littrow spectrograph (strips *d* and *e*) the oxide bands show definite structure and are clearly not the same as the flame bands.

For the calcium arc (Gaydon 1955) it was pointed out that the corresponding bands were much too complex to be due to transitions between singlet electronic states of CaO. It was considered possible that the bands might be due to transitions between triplet electronic states, but more probable that the emitter was polyatomic, possibly Ca_2O_2. With strontium, we have studied the 5950 Å arc band with the 21 ft grating (strip *f*). The structure is extremely complex, with no sign of regular rotational branches. It is known that under this dispersion the various triplet systems of ZrO and TiO (molecules with comparable rotational and vibrational constants to SrO) show fairly well resolved rotational fine structure, with definite branches. There can be little doubt, therefore, that the emitter of this band is polyatomic.

Using the special burner for spraying, we have studied the effect of concentration on the absolute and relative intensities of the 5950 and 6050 bands. Spectra were taken with the Littrow spectrograph, using a wide slit. We found that the strength of the SrOH band at 6050 was roughly proportional to the concentration of strontium sprayed into the flame, but that the 5950 band varied as some higher power of the concentration.

These results are illustrated in strips *g* and *h* of the plate. Strip *g* shows the spectrum of a saturated solution of strontium nitrate sprayed into the flame, with an exposure time of $\frac{1}{2}$ minute. Strip *h* shows a $\frac{1}{8}$ saturated solution, with the exposure time increased to 3 minutes. Processing of plates and prints have been kept the same, apart from an accidental minor change in the enlargement size, and the flame was held the same for the two exposures. It will be seen that the 5950 band is obviously very much weaker with the weaker solution, despite the longer exposure time. The main band of SrOH is too heavily exposed to be seen well in the reproduction but from negatives it is clear that its strength is roughly proportional to the product of concentration and exposure time. Precise quantitative measurements do not appear possible. Apart from the error in using exposure times instead of intensities for photographic work, there is some overlapping of the bands so that the strong SrOH contributes some background in the region of 5950, and also the oxy-hydrogen flame itself gives some weak continuous emission which will be stronger in the longer exposure. It is not possible to say that the strength of the 5950 band varies as the square of the strontium concentration, but it clearly varies more rapidly than the first power.

These results indicate that the emitter of the 5950 Å band contains more than one Sr atom. Although it is not certain with present information that it actually does contain two atoms of Sr, the results appear consistent with the emitter being Sr_2O_2. Although, with low concentrations, the strength of Sr lines and SrOH bands should tend to be proportional, in first approximation, to the first power of the concentration, and the Sr_2O_2 band to the square of the concentration, this will not be strictly so in higher approximation. Obviously as the amount of Sr_2O_2 increases at high concentrations it will reduce the amount of Sr available for formation of the hydroxide, so that the true rate of variation of strength of the bands with concentration will depend on the set of equilibria between Sr, SrOH, Sr_2O_2 and the flame gases; other species such as Sr^+ may also be involved.

Under small dispersion the 5950 band appears to be shaded to the red with diffuse heads at about 5938 and 5969 Å. The 6050 arc band also appears shaded to the red with two diffuse heads. With the larger dispersion of the grating, however, the structure is found to be very complex with a number of weak heads, many of them degraded in the other direction, i.e. towards the violet. There is a strong feature at 5969·8 Å; it is not certain whether this is a band head degraded to the red or a diffuse atomic line. We have measured heads degraded to the violet at λλ 5945·4, 5950·7, 5952·8, 5954·2, 5955·4, 5957·6, 5962·4, 5963·1, 5965·1, 5972·5, 5976·3, 5977·0, 5980·6, and 5986·2. A head at 5974·8 appears to be degraded to the red and there are broader maxima at 5967·4, 5966·3 and 5965·6 Å. This type of structure, with a general shading to the red and most individual heads shading to the violet, supports the assignment to a polyatomic rather than a diatomic emitter.

The red bands in the arc show a lot of structure but few prominent features. Weak heads have been measured (to ± 1 Å) at 6447·3, 6451·1, 6454·4, 6466·1, 6507·8, 6511·6, 6515·8, 6521·4, 6585·8, 6600·6, 6634·3, 6637·4, and 6672·4; these are degraded to the violet. A head at 6620·7 may be degraded to the red and there is broader structure at 6455·7–6458·6. There appears to be no prospect of making any analysis of these bands.

§5. Bands of BaOH and BaOD

The green bands at 4870 and 5120 appear readily in the flame. These bands (see strip *l*) are rather wide and diffuse, and unlike the corresponding short-wave bands of CaOH and SrOH do not show any fine structure when examined with the Littrow spectrograph. There is also emission in the infra-red;† this is divided into two strong regions, 7120–7580 and 7830–8390, but the apparent distribution of intensity is determined more by variation of plate sensitivity with wavelength (Long-Range Spectrum plates were used) than by the actual band structure.

The green BaOH bands have also been obtained from the vacuum arc in H_2O vapour, but do not appear as readily or cleanly as the systems of CaOH and SrOH. In the case of barium there is a very strong line spectrum of Ba, a general continuous background and on most plates some of the arc bands as well. We have had most success using barium metal on the arc poles, rather than the nitrate. Strip *j* of the plate shows the vacuum arc in H_2O, and the BaOH bands are visible. With the arc in D_2O we have had difficulty in getting clear plates

† Kleman and Liljeqvist (1955) have recently observed band structure in the region 0·8 to 1·0 μ in a flame; this is attributed by them to BaO.

(e.g. strip *k*) but it appears that there is an appreciable isotopic shift, the 5120 band of BaOH being displaced appreciably to the red in BaOD; the bands of the complex oxide ($?Ba_2O_2$) confuse the appearance of this plate. However, the evidence for an isotopic shift appears fairly definite and supports James and Sugden's assignment of these bands to BaOH.

§ 6. Arc Bands of Barium Oxide

The arc in air at atmospheric pressure, using barium nitrate on graphite poles, shows Mahanti's system of BaO together with more complex bands near 4800, 5020 and 5500 Å. The bands at 4800 and 5020 are rather wide; we have examined them with the Littrow spectrograph, and their structure is again complex, and overlapping by the resolved rotational fine structure of the BaO bands makes location of weak heads difficult.

The band near 5020 does show one good group of heads, degraded to the red, commencing at 5007 Å. The following are the first five heads in this sequence: 5007·0, 5009·6, 5012·6, 5015·1, 5017·6 Å. The appearance of this sequence is very similar to one of BaF (see Datta 1921) and the region is quite close, the first head of BaF being at 5000·6, but the other stronger sequence of BaF at 4950 is quite absent from our plates.

In the 4800 Å region, the plates on the Littrow spectrograph show heads, degraded to the red, at λλ 4729·9, 4739·6, 4789·1, 4830·5, 4844·5, 4846·4, and 4855·1; there are maxima at 4821 and 4827 Å. Although the heads are in this case quite sharp, there again appears little prospect of analysis. The fairly strong emission in the 5500 region comprises two main bands, 5445–5452 and 5482–5488 and is shown in strip *i* of the plate; strong Ba lines confuse the appearance a little.

The barium arc in air also shows some emission in the infra-red. Some small dispersion plates on a small glass prism instrument, using Kodak 144 Q plates, show two strong bands with heads at about 8176 and 8652 ± 5 Å; these are degraded to longer wavelengths, and although there are known bands of CaO at these wavelengths these are degraded the other way. From the small dispersion spectra it is not possible to say much about their structure or whether they are due to BaO or a polyatomic emitter.†

§ 7. Conclusions and Discussions

These studies, showing an isotope shift on replacing H by D, have supported James and Sugden's assignment of flame bands to SrOH and BaOH, and it has been shown, as with calcium, that the bands in the spectrum of the ordinary arc are not the same. The arc bands are provisionally assigned to a dimer of the oxide, this being strongly supported by the variation of intensity with concentration for Sr. The close correspondence in spectral region of the hydroxide bands, the complex oxide bands and also (as pointed out by James and Sugden) of the fluoride bands is remarkable. The table illustrates this for calcium, strontium and barium.

For all these emitters, as we pass from calcium through strontium to barium, the separation between the two systems increases, the longer-wave system moving

† Very recently Inghram and Chupka (1955) have found Ba_2O_2, Ba_2O and Ba_2O_3 with a mass spectrometer.

into the infra-red. The other halides of Ca, Sr and Ba also show spectra in the visible and near infra-red. All these systems are only weakly degraded, suggesting that the electron responsible for the transitions may not be one of the bonding electrons. The similarity in spectral regions between the fluorides and the isoelectronic hydroxides is perhaps not surprising, but the similarity to the complex oxide is more difficult to explain. These results pose some interesting problems on the electronic configurations of this type of molecule.

Comparison of Spectral Regions of Band Spectra

Metal	Hydroxide	Complex oxide	Fluoride
M	MOH	? M_2O_2	MF
Ca	Green 5540	Green 5490–5520	Green 5291, 5145
	Orange-red 6230	Orange 6040–6170	Orange 6037, 6064
Sr	Orange 6050	Orange 5950, 6050	Yellow 5772
	Far red 6400–6800	Far red 6400–6800	Red 6512, 6633
Ba	Green 4870, 5120	Green 4800, 5020, 5500	Green 4950, 5000
	Red & infra-red	(Infra-red)	Red & infra-red
	7120–7580	(8176)	7119
	7830–8390	(8650)	8151, 8571

The existence of these hydroxides and complex oxide spectra greatly complicates the determination of the dissociation energies of the simple oxides CaO, SrO and BaO. Results by Huldt and Lagerqvist's flame method are untenable and any method based on chemical equilibria will be difficult. It is unlikely that the very strong arc bands of these metals, now attributed to the complex oxide, will be found in stellar sources; the very low pressure in such sources favours the simpler diatomic emitters.

Acknowledgments

We are indebted to the British Council for a bursary (M.C.) and to the Royal Society for a Warren Fellowship (A.G.G.). We should also like to express our thanks to Mr. R. L. Warren for loan of the spray burner.

References

Barrow, R. F., and Caldin, E. F., 1949, *Proc. Phys. Soc.* B, **62,** 32.
Datta, S., 1921, *Proc. Roy. Soc.* A, **99,** 437.
Gaydon, A. G., 1955, *Proc. Roy. Soc.* A, **231,** 437.
Inghram, M. O., and Chupka, W. A., 1955, *J. Chem. Phys*, **23,** 2159.
James, C. G., and Sugden, T. M., 1955, *Nature, Lond.*, **175,** 333.
Kleman, B., and Liljeqvist,.B., 1955, *Ark. Fys.*, **9,** 377.
Lagerqvist, A., and Huldt, L., 1955, *Naturwissenschaften*, **42,** 365.
Mahanti, P. C., 1934, *Proc. Phys. Soc.*, **46,** 51.
Pearse, R. W. B., and Gaydon, A. G., 1950, *The Identification of Molecular Spectra* (London : Chapman and Hall).

Isotopic Spin Changes in τ and θ Decay†

By R. H. DALITZ
Department of Mathematical Physics, University of Birmingham

Communicated by R. E. Peierls; MS. received 16th February 1956

Abstract. The decay of τ and θ particles is discussed on the hypothesis that the amplitude for an isotopic spin change of ΔT in τ and θ decay to pions should decrease with increasing ΔT, the transition $\Delta T = \frac{1}{2}$ being dominant. Assuming zero spin for τ and θ, the large difference between θ^0 and θ^+ lifetimes and the τ'/τ branching ratio (predicted as 0·32) both agree well with this hypothesis.

§ 1. Introduction

In the decay of τ and θ particles, the final pion system may be described in terms of states of definite isotopic spin T. In general the final pion state will not be an eigenstate ϕ_T of T but will be a superposition of ϕ_T for the various possible T. It is now believed that the initial particle may also be described in terms of isotopic spin, both τ and θ particles being considered to be a member of a $T = \frac{1}{2}$ doublet. Clearly isotopic spin cannot be conserved in such a decay process since this leads from a state of half-integral isotopic spin to a state of integral isotopic spin; a half-integral change ΔT in the total isotopic spin is effective.

It has been noted by Pais (1955) that in all of the weak decay processes observed, both for K-particles and hyperons, which lead to final states which may be described in terms of isotopic spin, there is a change $\Delta T_3 = \pm\frac{1}{2}$ in the isotopic spin component. For the τ^+ and θ^+ decay, $\Delta T_3 = +\frac{1}{2}$ whereas $\Delta T_3 = -\frac{1}{2}$ for hyperon decay or for anti-K-particle decay (τ^- or θ^-). Further, the cross-over transition $\Xi^- \to N + \pi^-$ which is energetically very favourable and for which $\Delta T_3 = -1$ would be necessary has not been observed to compete with $\Xi^- \to \Lambda_0 + \pi^-$, for which $\Delta T_3 = -\frac{1}{2}$. Gell-Mann (1955) has remarked that this rule could be a consequence of a more restrictive rule requiring that the total isotopic change by $\frac{1}{2}$ in such decay processes. This rule $\Delta T = \frac{1}{2}$ would then limit the isotopic spin states ϕ_T present in the final configuration.

Our purpose in this note is to consider the interpretation of the experimental evidence on the states ϕ_T in the final configuration of τ and θ decay in terms of the less restrictive hypothesis that the matrix elements $M(\Delta T)$ for isotopic spin change ΔT should decrease with increasing ΔT. In particular it will be found that the difference in the θ^0, θ^+ lifetimes and the τ'/τ branching ratio have a natural interpretation‡ on the basis of this hypothesis.

† The work described here was carried out whilst the author was Visiting Associate Physicist at the Brookhaven National Laboratory.

‡ Whilst the manuscript was being prepared, pre-publication copies of papers which discuss the application of the strict $\Delta T = \frac{1}{2}$ rule to hyperon and K-particle have been received by the author from Dr. R. Gatto and from Professor Wentzel.

§ 2. The Decay of the θ-Mesons

Consider first the partial lifetimes of θ^0, θ^+ mesons for their decay to two pions. Since the θ-mesons are assigned $T=\frac{1}{2}$ in the Gell-Mann (1953) scheme, a transition $\Delta T=\frac{1}{2}$ may then lead to a final pion state with $T=0$ or $T=1$; a final state $T=2$ may be reached by the weaker transition $\Delta T=\frac{3}{2}$ or even $\Delta T=\frac{5}{2}$. We will denote the operator effective in this decay transition by

$$O_t=O_t(\tfrac{1}{2})+O_t(\tfrac{3}{2})+O_t(\tfrac{5}{2}), \qquad \ldots\ldots(2.1)$$

where $O_t(\Delta T)$ denotes the operator for isotopic spin change ΔT, the change ΔT_3 being $\Delta T_3=t=+\frac{1}{2}$.

Since the two pions are Bose particles, their total isotopic spin must be odd or even according as their total angular momentum (equal to the θ-meson spin j) is odd or even. For odd j, only $T=1$ is possible for the final state both in θ^0 and θ^+ decays. For even j, the final state in θ^+-decay can only be a $T=2$ state, whilst the θ^0-decay can proceed through a more favourable channel to a final $T=0$ state.

Now, in the Gell-Mann scheme, the θ^0 and its antiparticle $\bar{\theta}^0$ have different T_3 and are therefore distinct. On the basis of the natural assumption that all interactions are invariant under charge conjugation (interchange of particles with antiparticles), Gell-Mann and Pais (1955) have pointed out that the neutral θ-particles which have definite masses and lifetimes are not θ^0, $\bar{\theta}^0$, but the θ_1^0, θ_2^0 particles with definite charge conjugation parities c. At a given time, the θ_1^0, θ_2^0 fields are related to the θ^0, $\bar{\theta}^0$ fields by

$$|\theta^0\rangle=\sqrt{\tfrac{1}{2}}(|\theta_1^0\rangle+i|\theta_2^0\rangle), \qquad |\bar{\theta}^0\rangle=\sqrt{\tfrac{1}{2}}(|\theta_1^0\rangle-i|\theta_2^0\rangle). \qquad \ldots\ldots(2.2)$$

Statements concerning charge independence apply only to the particle mixtures θ^0 and $\bar{\theta}^0$; the particles θ_1^0, θ_2^0 do not even have a definite T_3 value. By definition, it is the θ_1^0 particle which decays to $\pi^++\pi^-$ and has charge conjugation parity $c=(-1)^j$. For the θ_2^0 particle, $c=(-1)^{j+1}$ and a 2π-decay is forbidden; its modes of decay are not yet known experimentally.

Consider first odd spin j. The decay amplitude for θ^0, θ^+ mesons is given by

$$\langle 1, m+t|O_t|\tfrac{1}{2}, m\rangle, \qquad \ldots\ldots(2.3)$$

the matrix element of (2.1) from the initial $T=\frac{1}{2}$ state ($m=\pm\frac{1}{2}$ for θ^0, θ^+ mesons respectively) to the final state $T=1$, $T_3=m+t$. This may be evaluated by use of the general result

$$\langle JM|O_t(T)|Im\rangle=c(ITJ, mtM)\langle J\|O(T)\|I\rangle, \qquad \ldots\ldots(2.4)$$

where $c(ITJ, mtM)$ denotes the Clebsch–Gordan coefficient and the reduced matrix element $\langle J\|O(T)\|I\rangle$ is independent of the m-values. For the θ_1^0 particle, the matrix element for 2π-decay is related to (2.3) by

$$\langle 2\pi|O_t|\theta_1^0\rangle=\sqrt{2}\langle 2\pi|O_t|\theta^0\rangle \qquad \ldots\ldots(2.5)$$

in consequence of (2.2), since the transformation of a θ_2^0 particle to two pions is forbidden. Finally the matrix elements for θ_1^0 and θ^+ decay for odd spin j are

$$\left.\begin{aligned} M(\theta_1^0)&=\langle 1\|O(\tfrac{1}{2})\|\tfrac{1}{2}\rangle-\langle 1\|O(\tfrac{3}{2})\|\tfrac{1}{2}\rangle,\\ M(\theta^+)&=\langle 1\|O(\tfrac{1}{2})\|\tfrac{1}{2}\rangle+\tfrac{1}{2}\langle 1\|O(\tfrac{3}{2})\|\tfrac{1}{2}\rangle.\end{aligned}\right\} \qquad \ldots\ldots(2.6)$$

The ratio of the two reduced matrix-elements in (2.6) is real, since they lead to the same final scattering-state. The ratio $|M(\theta_1^0)/M(\theta^+)|^2$ may therefore have

any value, in general. However, with the hypothesis that $O(\frac{1}{2})$ matrix elements are large relative to $O(\frac{3}{2})$, it would follow that θ_1^0 and θ^+ lifetimes would be equal.

For odd j, then, the hypothesis that $O(\frac{1}{2})$ is dominant appears to be excluded by the data. Direct measurement of the θ^+ lifetime by Fitch and Motley (1956) and also by Alvarez *et al.* (1956) has given a value $1{\cdot}2 \pm 0{\cdot}1 \times 10^{-8}$ sec, whereas the θ_1^0 lifetime is known (Gaythier 1955) to be $1{\cdot}7^{+0{\cdot}7}_{-0{\cdot}4} \times 10^{-10}$ sec. It should be added here that observation of a $2\pi^0$-decay mode for the θ_1^0 meson would exclude odd spin values.

Next consider even spin j. In this case the matrix element from θ_0 to $T=0$ state has amplitude $-\langle 0 \| O(\frac{1}{2}) \| \frac{1}{2} \rangle = -a_1/\sqrt{2}$, that from θ_0 to $T=2$ state has amplitude

$$\langle 2 \| O(\tfrac{3}{2}) \| \tfrac{1}{2} \rangle - \langle 2 \| O(\tfrac{5}{2}) \| \tfrac{1}{2} \rangle = (a_3 - a_5)/\sqrt{2}. \qquad \ldots\ldots(2.7)$$

It has recently been pointed out by Takeda (1956) that the phase of a_1, a_3 or a_5 is not arbitrarily assignable, but is given by the phase shift δ_T of the pion–pion scattering state of isotopic spin T and angular momentum j. In terms of these amplitudes the branching ratio in θ_1^0 decay is

$$\frac{P(\theta_1^0 \to 2\pi^0)}{P(\theta_1^0 \to \pi^+ + \pi^-)} = \left| \frac{a_1 + \sqrt{2}(a_3 - a_5)}{\sqrt{2}a_1 - (a_3 - a_5)} \right|^2. \qquad \ldots\ldots(2.8)$$

For the θ^+ particle, a strict $\Delta T = \frac{1}{2}$ rule would forbid the $K_{\pi 2}$ decay, since the only allowed final state ($T=2$) cannot be directly reached. However, the $T=2$ state can be reached with a $\Delta T = \frac{1}{2}$ rule by appeal to the electromagnetic interactions, which violate the isotopic spin selection rules.† This state could then be reached by emission and absorption of a virtual photon, giving a matrix element of order $\alpha O(\frac{1}{2})$ where α is the fine structure constant 1/137. The partial lifetime for $\theta^+ \to \pi^+ + \pi^0$ would then be of order $\alpha^2 \sim 10^{-4}$ times that for θ_1^0 decay. Of course the θ^+ decay element may contain numerical factors to increase this ratio but it seems rather unlikely that these should be so large as to give the observed ratio $\sim 10^{-2}$.

For this reason it seems necessary to allow direct transitions through the $\Delta T = \frac{3}{2}$ and $\frac{5}{2}$ channels to a final $T=2$. The matrix element is $(\sqrt{\frac{3}{4}}a_3 + \sqrt{\frac{1}{3}}a_5)$, so that

$$\frac{P(\theta^+ \to \pi^+ + \pi^0)}{P(\theta_1^0 \to 2\pi)} = \frac{3}{4} \frac{|a_3 + 2a_5/3|^2}{a_1^2 + (a_3 - a_5)^2}. \qquad \ldots\ldots(2.9)$$

Assuming $a_5 \ll a_3 \ll a_1$, it will be seen that the observed lifetime ratio may be obtained with

$$\left| \frac{a_3}{a_1} \right| = \left| \frac{\langle 2 \| O(\frac{3}{2}) \| \frac{1}{2} \rangle}{\langle 0 \| O(\frac{1}{2}) \| \frac{1}{2} \rangle} \right| \simeq 0{\cdot}13. \qquad \ldots\ldots(2.10)$$

It should be noted that this $T=2$ admixture implies a considerable deviation from the θ_1^0 branching ratio of $\frac{1}{2}$ as given by the $\Delta T = \frac{1}{2}$ rule. With the above value of $|a_3/a_1|$, this branching ratio becomes, to a sufficient approximation,

$$0{\cdot}5[1 \pm 3\sqrt{2}\,|a_3/a_1| \cos(\delta_2 - \delta_0) \ldots], \qquad \ldots\ldots(2.11)$$

which lies between about 0·2 and about 0·8, depending on the value of the phase shifts δ_2, δ_0.

† Violation of the strict $\Delta T = \frac{1}{2}$ rule could also arise from the $\pi^\pm$, π^0 and N, P mass differences (which probably arise from virtual electromagnetic interactions). The pion mass difference is the larger effect and may be considered as a perturbation $\delta(\mu^2)\, T_3^2$ which can change the isotopic spin of the system by $\Delta T = 2$. The amplitude of this $\Delta T = 2$ violation will be of order $\delta(\mu^2)R^2 \sim (\mu R)^2/15$ relative to $O(\frac{1}{2})$, the allowed θ_1^0 amplitude. With $R \sim \hbar/M_\tau c$, this θ^+ matrix element is again of order α relative to the θ_1^0 amplitude.

It is now important to discuss the possibility of alternate decay processes for which the mechanism slowing down the $K_{\pi 2}^+$ decay is not effective and which might therefore compete successfully with $K_{\pi 2}^+$ decay. For example, the decay process

$$\theta^+ \to \pi^+ + \pi^0 + \gamma \qquad \ldots\ldots (2.12)$$

is permitted through the $\Delta T = \frac{1}{2}$ interaction $O(\frac{1}{2})$ since the pions may now carry odd angular momentum and have $T = 1$. This process is of course possible as an internal bremsstrahlung from the $K_{\pi 2}$ mode but this would have probability at most of the order of α relative to $K_{\pi 2}$ decay and therefore be unimportant. However, a direct emission process is also possible and would, in general, have matrix element of order e relative to the $O(\frac{1}{2})$ amplitude which gives rise to θ_1^0 decay.

For a scalar θ particle, process (2.12) could proceed by emission of an electric dipole photon leaving the pions with unit angular momentum. The amplitude for this process would be

$$\sim \eta e g R[\mathbf{p} \cdot \mathbf{E}(\mathbf{k}) R^2], \qquad \ldots\ldots (2.13)$$

where $g \simeq {}^{\text{w}}\langle \| O(\frac{1}{2}) \| \frac{1}{2} \rangle$, $\mathbf{E}(\mathbf{k}) = k\boldsymbol{\epsilon}$ is the electric field of the emitted photon, $\mathbf{p}$ is the relative momentum of the two pions and R is the effective θ-particle radius. In (2.13) the last factor represents the centrifugal barrier amplitudes for the outgoing particles and η is a constant of order unity. The phase space estimate for (2.12), obtained by taking matrix element $eg\eta R$, is

$$\frac{P(\theta^+ \to \pi^+ + \pi^0 + \gamma)}{P(\theta^0 \to 2\pi)} = 0{\cdot}83\eta^2 \frac{\alpha}{2\pi} (\mu R)^2. \qquad \ldots\ldots (2.14)$$

Already this gives $P(\theta^+ \to \pi^+ + \pi^0 + \gamma)/P(\theta^+ \to \pi^+ + \pi^0) \sim \eta^2(\mu R)^2/10$, where μ is the pion mass. The barrier penetration amplitudes of (2.12) reduce this by a further factor $0{\cdot}10\ (\mu R)^4$. With $R \sim \hbar/M_\theta c$, the branching ratio for the radiative decay (2.12) becomes quite negligible, of order $\sim 10^{-5}$.

For spin 2^+, the direct emission of an electric dipole photon again leaves the pions in a $T = 1$, $j = 1$ state. In this case the barriers faced in radiative decay are quite similar to those faced in the $K_{\pi 2}$ decay and the phase space estimate (2.14) gives an adequate indication of the branching ratio. This value is $\sim \eta^2(\mu R)^2/10 \sim 10^{-2}$, as above, being small in virtue of the smallness of phase space for three-particle decay. This result is typical of higher spin values for the θ particle.

It is of interest to mention also the radiative decay process

$$\theta^+ \to \pi^+ + \gamma \qquad \ldots\ldots (2.15)$$

which the $\Delta T = \frac{1}{2}$ interaction would allow for a non-zero θ-spin. For spin 2^+, the emission is of an M2 photon: the matrix element is about e times the θ^0 decay amplitude (since the barrier penetration amplitudes are nearly equal), so that $P(\theta^+ \to \pi^+ + \gamma)/P(\theta^+ \to \pi^+ + \pi^0) \sim 100\alpha \simeq 1$. No such decay process (2.15) has been observed, although the resultant π-meson would have significantly longer range than for normal $K_{\pi 2}$ decay and about 40–50 $K_{\pi 2}$ secondary ranges have now been measured.† Similarly the internal conversion process associated with (2.15)

$$\theta^+ \to \pi^+ + e^+ + e^- \qquad \ldots\ldots (2.16)$$

† Secondary ranges from $K_{\pi 2}$ decay have been measured by many groups, for example the G-stack collaboration (1955), Ritson *et al.* (1956), Crussard *et al.* (1956) and Whitehead *et al.* (1956).

would have a branching ratio of order 10^{-2} relative to the $K_{\pi 2}$ decay, for a non-zero θ-spin. Such a decay process, giving a coplanar pion and electron pair would be readily identified in emulsion work, but the only events (about six in number now) giving a pion and electron pair† have been non-coplanar and interpreted as $K_{\pi 2}$ decay followed by the alternate mode of π^0 decay $\pi^0 \to \gamma + e^+ + e^-$. It is of interest to note that process (2.16) is forbidden in first order in α for a scalar θ-meson since (2.16) is then a zero–zero transition with parity change; (2.16) is, however, possible in order α^2 but its probability is then negligible (branching ratio less than α^4).

§ 3. The Decay of Charged τ-Mesons

In addition to the well-established decay mode

$$\tau^{\pm} \to \pi^{\pm} + \pi^{+} + \pi^{-}, \qquad \ldots\ldots(3.1)$$

the τ-meson is now considered to have an alternate pion decay process, the τ' decay,

$$\tau^{\pm} \to \pi^{\pm} + \pi^{0} + \pi^{0}. \qquad \ldots\ldots(3.2)$$

The final state of three pions of unit total charge may be written generally as a superposition of states of total isotopic spin $T=1$, 2 or 3 with appropriate coefficients. Consider now the configuration in which three pions have been emitted with momenta **P**, **Q**, **R**, where $P \geqslant Q \geqslant R$. Functions with total isotopic spin T may now be formed by adding the isotopic spins of the pions P and Q to give a sum $t=0$, 1 or 2, and then adding the third isotopic spin to this to give the total T. In this way six isotopic spin functions χ_t^T may be formed. For example,

$$\left.\begin{aligned} \chi_0^1 &= u_3(u_1w_2 + u_2w_1 - v_1v_2)/\sqrt{3}, \\ \chi_2^1 &= \{u_3(u_1w_2 + u_2w_1 + 2v_1v_2) - 3v_3(u_1v_2 + u_2v_1) + 6w_3u_1u_2\}/\sqrt{60}, \end{aligned}\right\} \ldots\ldots(3.3)$$

where u, v, w are the isotopic spin functions with $m = +1$, 0, -1 for a single pion and the suffices 1, 2, 3 refer to the pions with momenta **P**, **Q**, **R** respectively.

The coefficient associated with each of these isotopic spin functions in the wave function for the final state will be denoted by F_t, G_t and H_t according as $T=1$, 2 or 3. These coefficients are then functions of the momenta (P, Q, R). The final wave function must then be symmetrized, the pions being Bose particles irrespective of charge in the isotopic spin formalism, with the result

$$\tfrac{1}{6}\textstyle\sum_P (F_0\chi_0^1 + F_1\chi_1^1 + F_2\chi_2^1 + G_1\chi_1^2 + G_2\chi_2^2 + H_2\chi_2^3). \qquad \ldots\ldots(3.4)$$

Here Σ_P denotes summation over all permutations of the suffices (123) referring to the three pions in χ_t^T and in the coefficients F, G, H. Since the isotopic spin states χ_t^T are mutually orthogonal, the total probability for this configuration **P**, **Q**, **R** of pions, irrespective of the distribution of charges between the three pions, is given by

$$(F_0^2 + F_1^2 + F_2^2 + G_1^2 + G_2^2 + H_2^2). \qquad \ldots\ldots(3.5)$$

Now a function of three variables, suffices 1, 2, 3, can generally have one of three types of symmetry. It may be completely symmetrical (symmetry type [3]) or completely antisymmetrical (symmetry type [111]). There is also a third type of symmetry denoted by the symbol [21], giving a two-dimensional representation of the symmetry operations. For a given function $f(123)$, the totally

† Events of this type have been observed by Anderson, Lawlor and Nevin (1955), by Birge *et al.* (1956), and by other groups.

symmetric part may be picked out by use of the symmetrization operator, with result $\frac{1}{6}\Sigma_P f(123)$. The totally antisymmetric part may be picked out as $\frac{1}{6}\Sigma_P(-1)^P f(123)$ by use of the antisymmetrization operator, $(-1)^P$ being $+1$ or -1 according as the permutation P is even or odd. After these two parts are subtracted from $f(123)$, what remains must belong to the [21] representation.

Now it is clear that none of these functions χ_t^T can contain a totally antisymmetric part, since the final pion system necessarily contains two identical pions. The type of symmetry contained in each of these functions χ_t^T may therefore be determined simply by applying the symmetrization operator. Thus χ_1^1, χ_1^2 and χ_2^2 belong to the [21] symmetry class, since the symmetrization operator gives zero when operating on these functions. Similarly it is readily shown that χ_2^3 is totally symmetric. Finally, for the functions χ_0^1, χ_2^1,

$$\left.\begin{aligned}\tfrac{1}{6}\textstyle\sum_P \chi_0^1 &= \tfrac{5}{9}\chi_0^1 + \tfrac{2\sqrt{5}}{9}\chi_2^1,\\ \tfrac{1}{6}\textstyle\sum_P \chi_2^1 &= \tfrac{2\sqrt{5}}{9}\chi_0^1 + \tfrac{4}{9}\chi_2^1,\end{aligned}\right\} \qquad \ldots\ldots(3.6)$$

from which it follows at once that $(\sqrt{5}\chi_0^1+2\chi_2^1)/3$ is totally symmetric and $(2\chi_0^1-\sqrt{5}\chi_2^1)/3$ belongs to the class [21]. It is therefore convenient to define new amplitudes

$$\left.\begin{aligned}I &= (\sqrt{5}/3)F_0 + (2/3)F_2,\\ J &= (\sqrt{5}/3)F_2 - (2/3)F_0,\end{aligned}\right\} \qquad \ldots\ldots(3.7)$$

appropriate to these functions. The amplitudes I and H are now symmetrical functions of P, Q, R, whereas the remaining amplitudes are all of the [21] representation. J and G_2 are clearly even for interchange of P, Q whilst F_1 and G_1 are necessarily odd. These functions must occur in pairs J, F_1 and G_1, G_2 since there must be two functions to provide a basis for the two-dimensional [21] representation of the permutation group on P, Q, R, for each of the cases $T=1$ and 2 when this representation occurs (cf. Dalitz 1953). In the region $P \geqslant Q \geqslant R$, these functions J and F_1 (and similarly G_1 and G_2) are independent functions.

3.1. *The Charged Decay Mode*

We will denote by $A(\pi^-\pi^+\pi^+)$ the amplitude for decay in which the negative pion has greatest momentum P, the positive pions having momenta Q and R. In the figure we show the semi-circular plot described previously (Dalitz 1954) for the specification of τ-meson decay configurations. In this plot, the decay configuration is specified by a point X such that the perpendiculars XP, XQ and XR to the sides of the equilateral triangle LMN are proportional to the energies of the negative and of the two positive pions respectively. These points X are confined to the region internal to ABCD by the requirement that the momenta P, Q, R can sum vectorially to total momentum zero. With the non-relativistic energy-momentum relation, ABCD is the inscribed circle to the triangle LMN; with the relativistic relations, ABCD is distorted somewhat from the circular shape (Fabri 1954), especially near points B and D. The lines OC and OB always divide this allowed region into three equal parts.

A point X within the region DOC (as shown in the figure) corresponds to a situation described by $A(\pi^-\pi^+\pi^+)$, the negative pion having the greatest momentum. Consider next the points Y, the reflection of X in OC, and Z,

the reflection of Y in OB. These points again correspond to configurations with the same pion energies but with a different distribution of charges. The amplitude $A(\pi^+\pi^-\pi^+)$ refers to the point Y, where the negative pion has the intermediate momentum **Q**, and $A(\pi^+\pi^+\pi^-)$ to the point Z, where the negative pion has the least momentum **R**. If the amplitude A is totally symmetric then the value of A is the same at X, Y and Z.

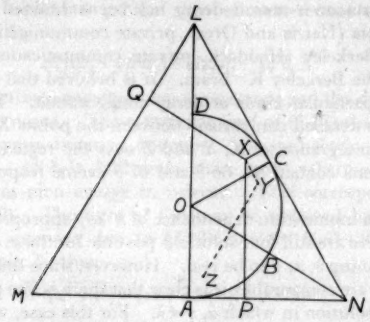

These amplitudes $A(\pi^-\pi^+\pi^+)$, $A(\pi^+\pi^-\pi^+)$ and $A(\pi^+\pi^+\pi^-)$ may now be obtained by inspection from (3.4) after writing out the various χ_t^T in full. Taking account of the replacement (3.7),

$$A(\pi^-\pi^+\pi^+)=\frac{1}{\sqrt{3}}\lambda-\frac{1}{\sqrt{6}}\alpha-\frac{1}{\sqrt{2}}\gamma, \qquad \ldots\ldots(3.8\,a)$$

$$A(\pi^+\pi^-\pi^+)=\frac{1}{\sqrt{3}}\lambda-\frac{1}{\sqrt{6}}\alpha+\frac{1}{\sqrt{2}}\gamma, \qquad \ldots\ldots(3.8\,b)$$

$$A(\pi^+\pi^+\pi^-)=\frac{1}{\sqrt{3}}\lambda+\sqrt{\frac{2}{3}}\alpha, \qquad \ldots\ldots(3.8\,c)$$

where we have used the following notation

$$\lambda=(2I+H)/\sqrt{5}, \qquad \rho=(I-2H)/\sqrt{5},$$
$$\alpha=(J+G_2)/\sqrt{2}, \qquad \beta=(J-G_2)/\sqrt{2},$$
$$\gamma=(F_1-G_1)/\sqrt{2}, \qquad \delta=(F_1+G_1)/\sqrt{2}.$$

With this notation, the sum of the squares of the amplitudes (3.8) becomes

$$\sigma(2\pi^++\pi^-)=\lambda^2+\alpha^2+\gamma^2, \qquad \ldots\ldots(3.9)$$

whilst the total decay probability (3.5), irrespective of pion charges, is

$$(\lambda^2+\alpha^2+\gamma^2)+(\rho^2+\beta^2+\delta^2). \qquad \ldots\ldots(3.10)$$

It is of interest to note that the intensity of τ decay events at X, Y or Z contains interference terms between amplitudes of different symmetry classes, whereas the sum $\sigma(2\pi^++\pi^-)$ of these intensities does not.† By a comparison of these three intensities, it may therefore be possible to obtain separately the amplitudes

† It is of interest to note here that the quantity which is plotted on the sector diagram proposed (Dalitz 1953 b) for representing τ-decay when the charge signs of the pions are unknown, is actually $\sigma(2\pi^++\pi^-)$. In this diagram, the perpendiculars PL, PN and PM refer to the momenta P, Q, R respectively.

λ, α, γ. These amplitudes are, however, generally complex quantities. Their phase arises from the interactions between the three pions after their emission. Since the interactions between pions are likely to be of short range, being transmitted through intermediate nucleon–antinucleon states, it seems reasonable to assume that the phases introduced by these pion–pion interactions are small, especially in view of the low relative pion energies of interest in τ-decay. It therefore seems reasonable to assume that λ, α, γ, etc. are real parameters.

Considerable data on τ-meson decay has been obtained systematically by groups† at Columbia (Harris and Orear, private communication), M.I.T. (Feld *et al.* 1955) and Berkeley (Haddock, private communication) from emulsion stacks exposed in the Berkeley K^+ beam. It is believed that these data contain no bias favouring particular kinds of decay configuration. These data are not sufficient to allow a detailed comparison between the points X, Y and Z and we therefore consider integration of X, Y and Z over the regions COD, BOC and BOA. These regions contain 83, 66·5 and 67·5 events respectively, for a total of 217 events.

After assuming a momentum dependence of λ, α, γ appropriate to the τ-meson spin considered, there are still four solutions possible for the averaged magnitudes of λ, α, γ, even assuming λ, α, γ to be real. However, since the number of events in the three regions are comparable, it is clear that there is one particularly simple solution, namely a solution in which $\alpha, \gamma \ll \lambda$. For this case, we may neglect the squares of α and γ in the squares of the amplitudes (3.8) and obtain the result

$$\overline{\lambda\alpha^*}/\overline{\lambda^2} = (2Z - X - Y)/2\sqrt{2}(X + Y + Z),$$
$$\overline{\lambda\gamma^*}/\overline{\lambda^2} = -\sqrt{6}(X - Y)/4(X + Y + Z).$$

The data mentioned above give

$$\overline{\lambda\alpha^*}/\overline{\lambda^2} = -0{\cdot}025 \pm 0{\cdot}022, \qquad \overline{\lambda\gamma^*}/\overline{\lambda^2} = -0{\cdot}025 \pm 0{\cdot}022. \quad \ldots\ldots(3.11)$$

The simplest interpretation of these ratios is then that the final wave function consists dominantly of a term totally symmetric in isotopic spin and space coordinates, with a very small admixture (at most 5% in amplitude) of a term of $[21] \times [21]$ symmetry.

For a pseudoscalar τ-meson, this situation would seem very reasonable. The simplest decay configuration is one in which the negative pion and the relative motion of the two positive pions are in S-states. It is reasonable to expect that this amplitude $d_{00}(p^2)$ may have some weak momentum dependence‡ of order $(pR)^2$ depending on the finite size of the τ-meson. The amplitude is completely symmetrical apart from these correction terms, and terms of order $(pR)^2$ will

† Additional data on τ-decay has recently become available from the work of groups at Göttingen (Biswas *et al.* 1956), at Berkeley (Smith *et al.* 1955) and at Padua (private communication). Together with the above data, the regions X, Y, Z now contain 207, 181·5 and 176·5 events respectively, for a total of 565 analysable events. The numbers (3.11) are obtained from the complete data now available.

‡ If the τ-decay amplitude is assumed to have momentum dependence $\{1 + B(p/M_\tau c)^2\}$, then the function λ is the constant $\sqrt{3}(1 + B\mu t_m/M_\tau^2 c^2)$ and the functions α and γ have the forms

$$\alpha = B(Q^2 - P^2)/\sqrt{2}(M_\tau c)^2, \qquad \gamma = B(2R^2 - Q^2 - P^2)/\sqrt{6}(M_\tau c)^2.$$

Integration of these expressions over the region DOC allows comparison with the empirical results (3.11). Comparison for α gives a value $B = 2{\cdot}0 \pm 1{\cdot}7$, whilst comparison for γ gives $B = 1{\cdot}1 \pm 1{\cdot}0$.

give [21] admixtures of the general order (3.11) for an assumed radius $R \sim \hbar/M_\tau c$. The next configuration which is appropriate for a pseudoscalar τ-meson, consists of $(l, L) = (2, 2)$, two D-states, and would be expected to occur with rather small amplitude of order $(pqR^2/15)^2$ since the centrifugal barriers are then quite considerable.

It will be of interest to discuss briefly the next spin–parity value not excluded for the τ-meson by the present data, namely spin 2^-. For this case, the decay amplitude may be estimated as the sum of two terms, corresponding to $(l, L) = (2, 0)$ and $(0, 2)$,

$$A(p_i p_j - \tfrac{1}{3}p^2\delta_{ij}) + B(q_i q_j - \tfrac{1}{3}q^2\delta_{ij}), \qquad \ldots\ldots(3.12)$$

where **p**, **q** are respectively negative pion momentum and the difference between the positive pion momenta. The symmetric part of (3.12) may be obtained by application of the symmetrization operator; the symmetric term alone gives a total intensity $5(A+3B)^2\mu^2 t_m^2/12$ times phase space, where μ is the pion mass and t_m the maximum pion energy in τ-decay. This corresponds to the term λ^2 of expression (3.9). The term $\alpha^2+\gamma^2$ may be obtained by subtracting this term from the total intensity due to (3.12), namely $5(A^2+9B^2)\mu^2 t_m^2/6$ times phase space. For spin 2^-, then

$$\overline{\lambda^2}/(\overline{\alpha^2+\gamma^2}) = |A+3B|^2/|A-3B|^2. \qquad \ldots\ldots(3.13)$$

It is useful to note that the angular correlation between **p** and **q**, averaged over the magnitudes of p and q is proportional to

$$5(A^2+9B^2) + 18\mathscr{R}(A^*B)P_2(\cos\theta). \qquad \ldots\ldots(3.14)$$

Rough isotropy in τ-decay suggests that $A \sim 3B$ and that $\mathscr{R}(A^*B)$ is small. In this case, the terms of symmetry [3] and [21] contribute about equally to the total decay rate.

3.2. *The τ' Decay Mode*

Here we will consider only the overall branching ratio between τ and τ' modes. The amplitudes $A(\pi^+\pi^0\pi^0)$, $A(\pi^0\pi^+\pi^0)$ and $A(\pi^0\pi^0\pi^+)$ can be obtained by inspection from (3.4) as before. Alternatively the sum of squares of these amplitudes may be obtained from (3.10) which gives the total probability of τ and τ' modes together; thus

$$\sigma(\pi^+ + 2\pi^0) = \rho^2 + \beta^2 + \delta^2. \qquad \ldots\ldots(3.15)$$

The ratio of $\sigma(\pi^+ + 2\pi^0)/\sigma(2\pi^+ + \pi^-)$ given by (3.9) and (3.15) agrees with the values given earlier for pure T-states. In particular, if attention be confined to $T=1$, then $\lambda = 2\rho$ and $\alpha = \beta$, so that this ratio would lie between $\frac{1}{4}$ and 1, the limiting values being attained for a state totally symmetric in P, Q, R ($\alpha = 0$), and for a state of $[21]\times[21]$ symmetry ($\lambda = \rho = 0$) respectively.

The ratio of the total probabilities for the decay processes (3.1) and (3.2) is now given by the ratio of the integrals of $\sigma(2\pi^0+\pi^+)$ and $\sigma(2\pi^+ + \pi^-)$ over all momenta P, Q, R satisfying energy and momentum conservation. For the process (3.2) this is given by (cf. Dalitz 1955)

$$\int \sigma(2\pi^0+\pi^+)(2\pi)^4\delta(\omega_P' + \omega_Q' + \omega_R - M)\delta(\mathbf{P}+\mathbf{Q}+\mathbf{R})\,\frac{d_3P}{(2\pi)^3\omega_P'}\frac{d_3Q}{(2\pi)^3\omega_Q'}\frac{d_3R}{(2\pi)^3\omega_R}, \qquad \ldots\ldots(3.16)$$

where $\omega_x' = (\mu_0^2 + x^2)^{1/2}$ is the energy of a neutral pion of momentum x. Expression (3.16) may be reduced to

$$2\int \sigma(2\pi^0+\pi^+)\left\{\frac{(\omega^2-\mu^2)(M^2-2M\omega+\mu^2-4\mu_0^2)}{M^2-2M\omega+\mu^2}\right\}^{1/2} d\omega. \qquad \ldots\ldots(3.17)$$

The corresponding expression for the τ-decay is obtained from (3.17) by replacing μ_0 by μ and $\sigma(2\pi^0+\pi^+)$ by $\sigma(2\pi^++\pi^-)$. The integrals may each be written

$$\frac{4(M\mu)^{1/2}}{M-\mu}\int_0^{t_m} \sigma\{t(t_m-t)\}^{1/2}\left\{\frac{1+t/2\mu}{1-2Mt/(M-\mu)^2}\right\}^{1/2} dt, \qquad \ldots\ldots(3.18)$$

where $t_m = (M-2\mu_0-\mu)(M+2\mu_0-\mu)/2M$ is the maximum kinetic energy for the odd pion. Neglecting any momentum dependence of σ, the phase space integral may be approximated by expanding the second square root and integrating term by term to give

$$2{\cdot}33 t_m^2\left\{1+0{\cdot}40\frac{t_m}{\mu}+0{\cdot}195\left(\frac{t_m}{\mu}\right)^2+\ldots\right\}. \qquad \ldots\ldots(3.19)$$

Since the neutral pion has mass $4{\cdot}7 \pm 0{\cdot}3$ MeV less than the charged pion, the energy release in the τ' decay is 83·7 MeV in place of the 74·3 MeV for the τ-decay. Using expression (3.19), the phase space for the τ'-decay is 1·295 times that for the τ-decay.

If the squared amplitudes σ have momentum dependence, this must be included in the integration (3.17). For spin values greater than 0, momentum dependence of σ will arise from the variation of the amplitudes for centrifugal barrier penetration as function of energy. Since the centrifugal barriers become less effective with increasing particle momentum, this effect would increase the τ'-decay further relative to the τ-decay.

For a pseudoscalar meson, we have seen that it is expected that the final state wave function will consist mostly of a completely symmetrical term. The admixture of [21] symmetry was found to be of relative amplitude $(\alpha, \gamma)/\lambda \lesssim 0{\cdot}05$. Since the τ'/τ ratio depends only on the square of the [21] admixture, this admixture will have a negligible effect on the branching ratio. We therefore consider only completely symmetric final states.

The application of the selection rule $\Delta T = \frac{1}{2}$ would allow only $T=1$ for the final pion state, since $T=\frac{1}{2}$ is assumed for the τ-meson. For the symmetrical $T=1$ state (all amplitudes zero except I) the ratio $\sigma(2\pi^0+\pi^+)/\sigma(2\pi^++\pi^-)$ is $\frac{1}{4}$ according to (3.9) and (3.15) and the τ'/τ branching ratio is predicted to be

$$\tau'/\tau = \tfrac{1}{4} \times 1{\cdot}295 = 0{\cdot}325 \qquad \ldots\ldots(3.20)$$

The most reliable experimental numbers on the τ'/τ ratio are those of Birge *et al.* (1955), obtained by following K-meson tracks to their ending. These workers found ten τ' events compared with 41 τ events, giving a ratio $0{\cdot}24 \pm 0{\cdot}09$. From an area scan of emulsions exposed to the Berkeley K^+ beam, Ritson *et al.* (1956), give a ratio $0{\cdot}22 \pm 0{\cdot}07$, after making corrections for the relative scanning efficiency for τ and τ'. In the G-stack collaboration (1955), the ratio 6/30 found was considered to be an overestimate, since not all possible τ events were examined. Finally, Crussard *et al.* (1956) have recently found a relative frequency 4·5/30 for τ-mesons produced in an emulsion by the passage of 6 GeV protons. Although these individual values are not incompatible with the ratio 0·325, each of these

values does lie low by about a standard deviation. It is clear that a more accurate value for this ratio, obtained under unbiased conditions, is now very desirable.†

Let us consider next how deviations from the value (3.20) given by the $\Delta T=\frac{1}{2}$ rule may be interpreted. For a symmetrical pion state, $T=3$ is allowed as well as $T=1$, although an isotopic spin change of $\Delta T=\frac{5}{2}$ is needed in the decay. Including this state, the τ'/τ ratio becomes

$$\frac{\tau'}{\tau}=1{\cdot}295\left(\frac{I-2H}{2I+H}\right)^2\simeq 0{\cdot}325\left(1-5\frac{H}{I}\right). \qquad \ldots\ldots(3.21)$$

Generally a given ratio τ'/τ may be obtained for two different values of the ratio H/I. However, the observed ratio is quite close to the value obtained for $H=0$, so the simplest interpretation of the ratio is obtained with the assumption $H/I\ll 1$. The τ'/τ ratio is quite sensitive to small admixtures of $T=3$ state; an admixture of only $H/I\simeq 0{\cdot}06$ is necessary to bring the ratio down to the observed mean value.‡ This ratio may then give an indication of the relative magnitude of the amplitude for isotopic spin change $\Delta T=\frac{5}{2}$ relative to that for $\Delta T=\frac{1}{2}$.

Finally, it should be pointed out that such a simple interpretation of the τ'/τ ratio, based on a $\Delta T=\frac{1}{2}$ rule, does not generally go through for higher spin values. For a final $T=1$ state, $\lambda=2\rho$, $\alpha=\beta$ and $\gamma=\delta=0$, so that the τ'/τ ratio may be expressed in terms of the ratio (3.13). For spin 2^-, the τ'/τ ratio is then

$$\frac{\tau'}{\tau}=1{\cdot}63\left\{\frac{5}{8}-\frac{9}{4}\frac{\mathscr{R}(A^*B)}{A^2+9B^2}\right\}, \qquad \ldots\ldots(3.22)$$

where the first factor represents the ratio of the phase space integrals for this case. It will be seen that the angular correlation (3.14) is closely related to the τ'/τ ratio. To give a τ'/τ value as low as the observed mean value would imply an angular correlation far stronger than the present data on τ-decay permit.

§ 4. The τ^0-Mesons

If the Gell-Mann assignment $T=\frac{1}{2}$ to the τ-meson is correct, then there must exist also a neutral τ-meson. This would be expected to have the decay modes

$$\tau^0 \nearrow \pi^0+\pi^0+\pi^0 \qquad \ldots\ldots(4.1\,a)$$

$$\tau^0 \searrow \pi^++\pi^-+\pi^0. \qquad \ldots\ldots(4.1\,b)$$

Although some 'anomalous θ-particle' events which have been reported (e.g. Arnold *et al.* 1955) would be consistent with interpretation as the τ^0-decay (4.1 *b*), there are many other anomalous θ-events which cannot be interpreted in this way, so that there is no compelling evidence for the existence of the τ^0

† *Note added in Proof.* Drs R. W. Birge and D. H. Stork have kindly infomed me that a more recent Berkeley investigation based on 50 τ' events leads to a ratio $0{\cdot}39\pm 0{\cdot}096$. Taking this together with the data mentioned above, they obtain a current τ'/τ value of $0{\cdot}332\pm 0{\cdot}067$, in good agreement with equation (3.20).

‡ Some modification of the τ'/τ ratio will result from the Coulomb interactions between the pions in the τ-decay. These interactions can produce a $\Delta T=2$ isotopic spin change to a final $T=3$ state. To a good approximation the Coulomb interaction between pions i and j increases the intensity of τ-decay by a factor $(1-\pi e_i e_j/v_{ij})$ where v_{ij} is the relative velocity between the pions. Taking this into account for each pion pair, the τ-decay probability is increased by $2{\cdot}6\%$, the average value of $1/v_{ij}$ being $1{\cdot}2$. This effect depresses the τ'/τ ratio (3·20) only to 0·316. The virtual effects of the $\pi^\pm$, π^0 mass difference can also lead to a final $T=3$ state and produce further changes (of unknown sign) in τ'/τ of comparable order of magnitude to this.

particle at the present time. However, it is of some interest to discuss briefly the characteristics of the decay modes (4.1).

First, it will be apparent that, just as for the θ-particles, it is the τ^0 states of definite charge conjugation parity c which have definite masses and lifetimes. The τ^0 particle with $c=+1$ will be referred to as the τ_1^0 particle, the τ_2^0 particle having $c=-1$. At a given time the τ_1^0, τ_2^0 wave functions are related to the τ^0, $\bar{\tau}^0$ wave functions by the expressions

$$|\tau_1^0\rangle = \frac{1}{\sqrt{2}}(|\tau^0\rangle + |\bar{\tau}^0\rangle), \qquad |\tau_2^0\rangle = \frac{1}{i\sqrt{2}}(|\tau^0\rangle - |\bar{\tau}^0\rangle).$$

Now, for the decay mode (4.1 *b*), denote by L the angular momentum carried off by the neutral pion and by l the angular momentum of the relative motion of the $\pi^+\pi^-$ pair. The vector sum of l, L must equal the τ-meson spin, $\mathbf{j}=\mathbf{l}+\mathbf{L}$. The space parity of the final system is then $w=(-1)^{j+L+l}$, and the charge conjugation parity $c=(-1)^l$. Thus, for the τ_1^0 decay, l must be even, and the configurations (l, L) allowable for a given spin (j, w) are just those allowed for the τ^+ decay. For the τ_2^0 decay, l must be odd and a different set of configurations apply. For spin 0^-, $(l, L)=(1, 1)$ is now the allowed configuration with the least barriers; the partial lifetime of the τ_2^0 decay to pions would then be expected to be long (by a factor $\sim(\mu R)^4/324$) compared with τ_1^0 decay. For spin 2^-, the least (L, l) is again (1, 1) for τ_2^0 decay compared with (2, 0) and (0, 2) for τ_1^0 decay; for this case the partial lifetimes would be comparable.

The final isotopic-spin state in τ^0-decay may be discussed as in § 3.2. There is now an additional state $T=0$ possible, whose amplitude we denote by E; this state is totally antisymmetric. The states χ_t^T, now with $m_T=0$, may be written down as before. The intensity of the $3\pi^0$ decay is given by $(\sqrt{2}H-\sqrt{3}I)^2/5$; it may be noted that $3\pi^0$ decay occurs only in symmetrical isotopic-spin states. The total intensity for decay modes (4.1) is given by $(E^2+I^2+H^2+J^2+G_1^2+F_1^2+G_2^2)$.

Here we consider only the case of a pseudoscalar τ^0-meson. The application of the $\Delta T=\frac{1}{2}$ rule now allows both $T=0$ and $T=1$ final states. However, the $T=0$ state, totally antisymmetric in the space coordinates of all three pions, is difficult to form for total spin–parity 0^-. The simplest amplitude for this state has the form $(p_1^2-p_2^2)(p_2^2-p_3^2)(p_3^2-p_1^2)R^6$ and will give a contribution to the final state which is negligible in comparison with that of the totally symmetric $T=1$ state. With the $\Delta T=\frac{1}{2}$ rule, generally

$$\frac{P(\tau_1^0\to 3\pi^0)}{P(\tau_1^0\to\pi^+ + \pi^- + \pi^0)} = \frac{\frac{3}{5}I^2}{E^2+\frac{2}{5}I^2+F_1^2+J^2}.$$

With the symmetrical state dominant, as expected for a pseudoscalar τ-meson, this branching ratio will have the value 1·5. If the amplitude for pion decay of τ_2^0 may be neglected relative to τ_1^0 decay, then the dominance of the $\Delta T=\frac{1}{2}$ transition would imply equal partial lifetimes for τ_1^0 and τ^+, as far as pion decay is concerned.

For a pseudoscalar τ_2^0-meson, the configuration $(l, L)=(1, 1)$ is dominant. The simplest estimate of this amplitude, $(\mathbf{p}.\mathbf{q}R^2)$ has [21] symmetry so that $3\pi^0$ decay would be unimportant. The partial lifetime for pion decay of the τ_2^0 would be longer than that of the τ^+ by a factor $\sim 10^3/(\mu R)^4$; it seems likely that decay processes involving neutrinos (e.g. $\mu^+ + \nu + \pi^-$) might be rather more probable.

§ 5. Conclusion

It has been seen that two outstanding features of τ and θ decay, the τ'/τ branching ratio and the θ^0, θ^+ lifetime difference, may be simply understood if an isotopic spin change $\Delta T=\frac{1}{2}$ is dominant in the pion decay processes. However, in each case, an admixture of higher isotopic spin changes has been found necessary to fit the available data in detail; for θ decay, a $\Delta T=\frac{3}{2}$ admixture of amplitude of order 13% was necessary, and for τ decay a $\Delta T=\frac{5}{2}$ admixture of amplitude of order 6%.

At this point it should be emphasized that, if an electromagnetic transition from τ to θ is responsible for the observed decay properties (this is one of the possibilities suggested by Lee and Orear (1956)), then the lifetime of the daughter θ particle would be unknown empirically and the interpretation discussed here may have no relevance to the true situation for the θ particle. If the τ particle is the parent of the θ, the difference in the apparent θ^0, θ^+ lifetimes may simply reflect the difference between the (τ^+, θ^+) and (τ^0, θ^0) mass separations, since the lifetime for this electromagnetic parent–daughter transition may be expected to depend sensitively on the mass-difference.† Such a situation could in fact account for the absence of evidence for the τ^0 particles—for example, the characteristic decay modes of the $\tau_1{}^0$ would be in unfavourable competition compared with an electromagnetic $\tau_1{}^0 \to \theta_1{}^0$ transition with a lifetime of order 10^{-10} sec, the observed over-all $\theta_1{}^0$ lifetime. However, the absence of evidence for τ^0-decay may simply reflect the difficulty of observation of neutral unstable particles of lifetime long compared with 10^{-9}–10^{-10} sec.

Acknowledgments

I am very pleased to acknowledge stimulating discussions with Professor M. Gell-Mann and with Professor A. Pais, particularly concerning § 2.

References

Alvarez, L. W., Crawford, F. S., Good, M. L., and Stevenson, M. L., 1956, *Phys. Rev.*, **101**, 503.

Anderson, P., Lawlor, G., and Nevin, T. E., 1955, *Nuovo Cim.*, **2**, 608.

Arnold, W. H., Martin, W., and Wyld, H. W., 1955, *Phys. Rev.*, **100**, 1545.

Birge, R. W., Haddock, R. P., Kerth, L. T., Peterson, J. R., Sandweiss, J., Stork, D. H., and Whitehead, M. N., 1956, *Proceedings of the International Conference on Elementary Particles, Pisa*, 1955; Suppl. to *Nuovo Cim.* (in the press).

Biswas, N., Ceccarelli-Fabrichesi, L., Ceccarelli, M., Gottstein, K., Varshneya, N., and Waloschek, P., 1956, *Nuovo Cim.*, **3**, 825.

Crussard, J., Fouche, V., Hennessy, J., Kayas, G., Leprince-Ringuet, L., Morellet, D., and Renard, F., 1956, *Nuovo Cim.*, in the press.

† If τ and θ each have spin 0, the $\tau \to \theta$ electromagnetic transition must be a two-photon process, involving emission of an M1 and an E1 photon. For this process, the matrix-element may be written

$$\eta e^3[\mathbf{E}(\mathbf{k}_1) \cdot \mathbf{H}(\mathbf{k}_2)+\mathbf{E}(\mathbf{k}_2) \cdot \mathbf{H}(\mathbf{k}_1)]R^2$$

where η is a numerical constant. The probability for this transition per unit time is then

$$\frac{128\pi}{3}\frac{\alpha^3}{140}(\mu R)^4\left(\frac{\mu}{M}\right)^3\left(\frac{\Delta}{\mu}\right)^7\mu.$$

If Δ is measured in Mev, this gives a lifetime of about $1{\cdot}3\times10^{-3}/\eta^3(\mu R)^4\Delta^7$ sec. With $\eta\sim1$ and $(\mu R)\sim1$, a partial lifetime of order 2×10^{-9} sec requires $\Delta\sim5$ Mev, a mass difference of the order of 10 electron masses.

DALITZ, R. H., 1953 a, *Proc. Phys. Soc.* A, **66,** 710; 1953 b, *Phil. Mag.*, **44,** 1068; 1954, *Phys. Rev.*, **94,** 1046; 1955, *Ibid.*, **99,** 915.

FABRI, E., 1954, *Nuovo Cim.*, **11,** 479.

FELD, B. T., ODIAN, A. C., RITSON, D. M., and WATTENBURG, A., 1955, *Phys. Rev.*, **100,** 1539.

FITCH, V., and MOTLEY, R., 1956, *Phys. Rev.*, **101,** 496.

G-STACK COLLABORATION, 1955, *Nuovo Cim.*, **2,** 1063.

GAYTHER, B. D., 1955, *Phil. Mag*, **46,** 1362.

GELL-MANN, M., 1953, *Phys. Rev.*, **92,** 833; 1955, *Proceedings of the Fifth Rochester Conference on High Energy Physics* (New York : Interscience Publishers).

GELL-MANN, M., and PAIS, A., 1955, *Phys. Rev.*, **97,** 1387.

HADDOCK, R. P., 1956, University of California, UCRL—3284.

LEE, T. D., and OREAR, J., 1956, *Phys. Rev.*, **100,** 932.

OREAR, J., HARRIS, G., and TAYLOR, S., 1956, *Phys. Rev.*, in the press.

PAIS, A., 1955, *Proceedings of the Fifth Rochester Conference on High Energy Physics* (New York : Interscience Publishers).

RITSON, D. M., PEVSNER, A., FUNG, S. C., WIDGOFF, M., ZORN, G. T., GOLDHABER, G., and GOLDHABER, S., 1956, *Phys. Rev.*, **101,** 1085.

SMITH, F. M., HECKMAN, H. H., and BARKAS, W. H., 1955, *Phys. Rev.*, **100,** 1802.

TAKEDA, G., 1956, *Phys. Rev.*, **101,** 1547.

WHITEHEAD, M. N., STORK, D. H., PETERSON, J. R., PERKINS, D. H., and BIRGE, R. W., 1956, University of California, UCRL—3295.

The Decay of the Isomeric State of ^{198}Tl

By P. S. FISHER and V. KNAPP
Department of Physics, University of Birmingham

Communicated by W. E. Burcham; MS. received 16th December 1955, and in revised form 2nd March 1956

Abstract. The gamma rays from ^{198}Tl and ^{198m}Tl have been examined with a sodium iodide spectrometer singly and in coincidence. Radiation at 637, 588 and 411 kev, decaying with a period of 1·8 hours, is associated with transitions in ^{198}Hg following a 60% K capture branch from the isomeric state ^{198m}Tl. Tentative spins and parities are assigned.

§ 1. Introduction

The decay schemes so far proposed for the radioactive nuclei of mass 198 are shown in figure 1 (Orth *et al.* 1949, Bergström *et al.* 1953, Passell *et al.* 1954). For ^{198}Tl the spin assignments are only tentative and many gamma-ray energies not included in this scheme have been observed with the

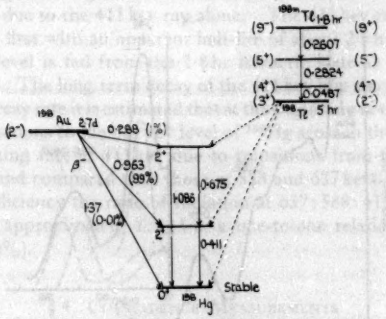

Figure 1. Decay scheme previously proposed for ^{198}Tl and ^{198m}Tl (The 2⁻ assignment for ^{198}Au is from Elliott, Preston and Wolfson 1954, 1955).

half-life of the ground state (5 hr) and more recently with the period of the excited state (1·8 hr) (Knight and Baker 1955). Consequently the complete decay scheme must be considerably more complicated than is shown in figure 1. By contrast the decay of ^{198}Au is relatively simple: it proceeds mainly by the well-known 411 kev gamma ray that was used to demonstrate nuclear resonant scattering in ^{198}Hg (Moon and Storruste 1953, Davey and Moon 1953). The present work arose from an attempt to see whether the 411 kev radiation from the decay of ^{198}Tl could also be used for resonant scattering. For this purpose higher energy gamma radiation present was examined with a sodium iodide

scintillation spectrometer to find its contribution to radiation scattered with energy in the region of 411 kev. A new mode of decay of the isomeric state of ^{198}Tl, giving gamma radiation of about 610 kev was found.

§ 2. Preparation of Source

Gold targets approximately 0·001 in. thick were prepared by electroplating on a polished copper cylinder 0·6 in. in diameter. These targets were bombarded with the internal beam of He^{2+} ions in the 60 in. Nuffield cyclotron of this laboratory. The bombarding energy was always greater than 37 Mev and with beams of about 10 μA bombardments of 10 minutes gave a strongly active sample. The thin targets ensured that the bombarding energy was above threshold for the ^{197}Au $(\alpha, 3n)^{198m}$Tl reaction throughout the target depth and reduced to a minimum the competing $(\alpha, 2n)$ and (α, n) reactions. After bombardment the target material was dissolved from the surface of the copper cylinder with *aqua regia* and freed chemically from copper, gold and traces of mercury, and the active thallium was precipitated on carrier as thallous iodide. The method followed *Chemical Procedures used in Bombardment Work at Berkeley* (Meinke 1949), with the addition of an extraction into ether in the early stages.

§ 3. Energy Spectra

The gamma-ray spectrum was studied with sodium iodide (Tl) crystal spectrometers singly and in coincidence. Figure 2 shows the appearance of the spectrum taken on such a spectrometer, covering the energy range 0–1100 kev.

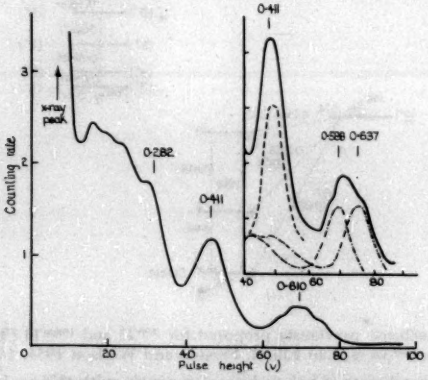

Figure 2. Single count scintillation spectrum.

This spectrum shows four principal features—a very strong peak corresponding to K x-rays of thallium or mercury, a general hump covering the region 0–350 kev, where the rays of the cascade reported by Bergström *et al.* would be found, the clearly defined peak at 411 kev corresponding to the decay of an excited level in mercury, and a weaker peak at about 610 kev. There is also a significant counting rate at higher energies but no peaks are resolved.

The region 0–350 kev is troublesome to investigate with a sodium iodide spectrometer, mainly because of the presence of the Compton distribution from the higher energy lines. In order to resolve the peaks in this region a series of spectra was taken at widely separated time intervals. The spectra were scaled to a common value for the 411 kev peak and the later curves were subtracted from the earlier ones. This procedure emphasizes components due to the decay of the isomeric state, and a peak at 282 kev corresponding to one of the transitions reported by Bergström *et al.* was found. The 261 kev component of the cascade from the isomeric state did not appear because it is strongly internally converted.

The range 350–700 kev contains the two well-defined peaks at 411 and about 610 kev. The latter is so broad (cf. figure 2) and of such an irregular shape that it is certainly due to at least two gamma rays close in energy. Conversion electrons have been observed corresponding to gamma-rays of 637 and 588 kev and Knight and Baker (1955) associate these with ^{198}Tl.

The inset to figure 2 shows how two radiations of this energy could be responsible for the 610 kev peak if they were present in approximately equal intensity. The shape of the pulse height distribution does not vary with time, so the two components must decay with the same period. The decay of the peak as a whole was followed over a period of ten half-lives with a sodium iodide scintillation spectrometer and gave a half-life of 1·90 hr. In order to follow the decay of the 411 kev line, the composite structure proposed above was used to estimate the counting rate in this region due to the Compton distribution from 588 and 637 kev gamma rays. Subtracted from the observed counting rate, this gave the rate due to the 411 kev ray alone. The 411 kev radiation was thus found to decay at first with an apparent half-life of about 2·5 hr, which suggests that the 411 kev level is fed from the 1·8 hr isomeric state as well as from the 5 hr ground state. The long-term decay of the 411 kev line showed a 5 hr period. From the initial decay rate it is estimated that at the beginning of this set of observations 60% of transitions to the 411 kev level of ^{198}Hg arose in the ^{198m}Tl, and this enables the counting rate at 411 kev due to transitions from the isomeric state to be calculated, and compared with those at 588 and 637 kev. When corrected for variation of efficiency the ratio of radiation at 637 : 588 : 411 kev from ^{198m}Tl was found to be approximately 1 : 1 : 1·3, a one-to-one relationship within the limits of error (20%).

§ 4. Coincidence Measurements

In order to clarify the inter-relation of these lines, a series of coincidence spectra was taken using circuits with a resolving time of about 5×10^{-7} sec. Since a number of the rays present are in cascades with highly converted gamma rays or follow K capture, nearly all give strong coincidence with K x-rays, and consequently measurements of spectra in coincidence with these rays are little more helpful than the single count measurements. The Berkeley group (Passel *et al.* 1954) report measurements of coincidence between K x-rays and the 282·4 kev rays. We also observe x-gamma coincidences which could be attributed to the 282·4 kev gamma rays, but with the channel settings used these coincidences could also have been due to the Compton distributions of higher energy gamma rays following K-capture in ^{198m}Tl.

Spectra taken in coincidence with the 610 kev lines do, however, give clear and useful spectra. Figure 3 shows the lines at roughly 610 kev (which have been taken as 588 and 637 kev) to be in coincidence with each other, and also with

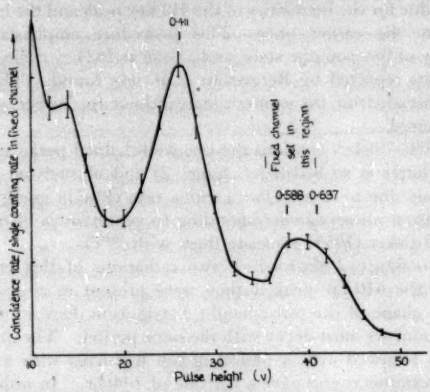

Figure 3. Spectrum in coincidence with radiation at about 610 kev.

the 411 kev rays. The difference in shape between the coincidence and single count spectra of the higher energy peak is consistent with a composite peak having its components in coincidence, since the fixed channel was set to receive a higher proportion of the lower energy component. A triple coincidence measurement showed gamma rays in the region of 588, 637 and 411 kev to be in triple coincidence. The coincidence spectrum at low energy shows a very strong coincidence of 610 kev radiation with K x-rays, and suggests the association of the 610 kev lines with K capture.

§ 5. Conclusion

The measurements of the radiations from ^{198m}Tl and ^{198}Tl in the energy range 350–700 kev thus suggest lines at energies of 588 and 637 kev which decay with the period of the isomeric state and are in coincidence. They are also in triple coincidence with the 411 kev radiation, which decays with a composite period, and with radiations in the K x-ray region. These observations may be explained by the decay scheme shown in figure 4, which postulates a K capture mode of decay from ^{198m}Tl in competition with the isomeric transition. The K capture is then followed by a triple cascade of 637, 588 and 411 kev gamma rays. The order of the two higher energy components is not settled. Such a scheme is supported by the observation of Knight and Baker (1955) that conversion lines at 637 and 588 kev are produced by conversion in mercury, and also by the present scintillation spectra which indicate that all three gamma rays are produced in about equal intensity.

Comparison of the intensities of the 282 kev and 637 kev gamma rays showed that ^{198m}Tl decays roughly 60% by K capture, thus giving a half-life for this process of $1{\cdot}1 \times 10^4$ sec. Now the energy released by K capture from the isomeric

level of ^{198}Tl to the suggested 1636 kev level in mercury is approximately the same as that from the ground state to the 1086 kev level. This second process was found by Bergström to have a half-life probably more than ten times that estimated above for the isomeric state, and consequently it is possible that capture from the isomeric state of ^{198}Tl is allowed, whilst that from the ground state to the 1086 and 411 kev levels (both 2^+) and ground state (0^+) of ^{198}Hg is first forbidden. Calculations on this basis, using an extrapolation of the information collected by Hoff and Thompson (1954) for elements in the region $Z=89$–97 and the half-life of $1{\cdot}1\times10^4$ sec, would give an energy release of about 650 kev for allowed K capture from the isomeric state. This estimate, and calculations based on it, must be regarded as extremely crude in view of the large spread in K capture transition probabilities in the compilations of both Hoff and Thompson and of Major and Biedenharn (1954). However, from this value for the energy release, the energy difference between the ground states of ^{198}Tl and ^{198}Hg can be estimated as about 1·7 MeV, which compares with 2·2 MeV predicted from the semi-empirical mass formula (Metropolis and Reitweisner 1950). Again using the classification of Hoff and Thompson, a first forbidden K capture, from the ground state of ^{198}Tl to 1086 kev and 411 kev levels and the ground state of ^{198}Hg, would give a resultant half-life of about 140 minutes (or roughly half the observed value) and a partition ratio between the 1086 : 411 kev levels of about 1 : 15 which compares with the experimental value of about 1 : 10. If K capture is first forbidden from the ground state, and allowed from the isomeric state, the spin change must be 0 or 1 with no change of parity for the capture from the isomeric state, and 0, 1 or 2 with a parity change for the ground state transitions.

In considering the decay of the ground state of ^{198}Tl, we have assumed that the probabilities of K capture to the ground state and the 411 and 1086 kev excited levels of ^{198}Hg would be equal, apart from the dependence on energy. The relative abundance observed for K x-rays to 411 kev gamma radiation, shows that the two processes are probably of about equal importance, and that there is certainly not a preponderance of the decay taking place between the ground states.

A satisfactory assignment of spins and parities must reconcile the requirements of K capture transitions with the changes associated with the emission of the gamma rays. The fact that strong coincidences have been observed between all the components of the cascade following K capture, using resolving times of about 10^{-6} sec, indicates that the lifetime of any one of the components is not likely to be much greater than this. On the basis of the Weisskopf lifetime–energy relation, this would exclude radiation of multipolarity higher than E2 or M2. Since the spin change appears to be large the proposed scheme (figure 4) shows both 637 and 588 kev gamma rays as quadrupoles, which would give a maximum spin of 6 for the level in ^{198}Hg to which electron capture takes place. Passel's assignment gives a spin of 9 for the isomeric state (see figure 1), hence an allowed K capture process would be impossible between these levels. This difficulty may be removed either by assuming that the spin assigned to ^{198m}Tl is too high, or that a further component of the gamma cascade following K capture has been overlooked. This second possibility is unlikely, since none of the other conversion lines associated with the isomeric state have been found to be associated with gamma rays of sufficient intensity when examined with a sodium iodide spectrometer. We accordingly believe that the spin of the isomeric state should be not greater than 7.

A 0^- assignment for the ground state of ^{198}Tl would be in accord with the expectations of the shell model if the odd proton in a $3s_{1/2}$ state is coupled to the odd neutron in a $4p_{1/2}$ state with spins opposed. Such a spin would place K

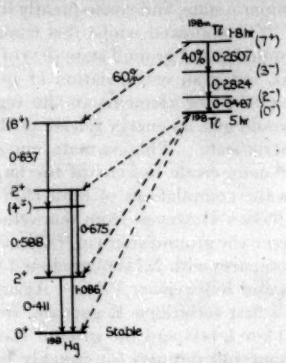

Figure 4. Decay scheme proposed here for ^{198}Tl and ^{198m}Tl.

capture from the ground state of ^{198}Tl to the 1086, 411 kev and ground state levels of ^{198}Hg on an equal basis because if the transition between ground states is a $0^- \rightarrow 0^+$ transition each would be first forbidden according to Gamow–Teller selection rules, and third forbidden for Fermi rules. The assignment of 0^- to the ground state of ^{198}Tl is thus in accord with expectations from the shell model, and also with our estimation that about half of electron capture in ^{198}Tl takes place directly to the ground state of ^{198}Hg. A 2^- ground state for ^{198}Tl would favour capture to the 2^+ excited levels at 411 and 1086 kev. This reduction in ground state spin would similarly decrease the spin assigned to the isomeric state by two units to 7^+, which is consistent with allowed K capture to a 6^+ level in mercury.

The spins and parities proposed in figure 4 result from these considerations, and they appear to be consistent with observation, although now that an approximately 50% competing mode of decay has been found the association of the 48·4 kev transition with the isomeric gamma cascade may have to be reconsidered.

Acknlowledgments

It is a pleasure to thank Professor W. E. Burcham for the help and advice which he has given during the course of this work. We would also like to thank Mr. W. Hardy and the cyclotron operators for providing the bombardments. One of us (P.S.F.) is indebted to the Department of Scientific and Industrial Research for a maintenance grant.

References

Bergström, I., Hill, R. D., and DePasquali, G., 1953, *Phys. Rev.*, **92**, 918.
Davey, W. G., and Moon, P. B., 1953, *Proc. Phys. Soc.* A, **66**, 956.
Elliott, L. G., Preston, M. A., and Wolfson, J. L., 1954, *Canad. J. Phys.*, **32**, 153 ; 1955, *Ibid.*, **33**, 607.

HOFF, R. W., and THOMPSON, S. G., 1954, *Phys. Rev.*, **96,** 1350.

KNIGHT, J. D., and BAKER, E. W., 1955, *Bull. Amer. Phys. Soc.*, **30,** 20 (see also 1955, *Phys. Rev.*, **100,** 1334, a fuller account).

MAJOR, J. K., and BIEDENHARN, L. C., 1954, *Rev. Mod. Phys.*, **26,** 321.

MEINKE, W. W., (Ed.) 1949, *Chemical Procedures used in Bombardment Work at Berkeley.* UCRL-432.

METROPOLIS, N., and REITWEISNER, G., 1950, U.S.A.E.C. Report 1980 (table of atomic masses).

MOON, P. B., and STORRUSTE, A., 1953, *Proc. Phys. Soc.* A, **66,** 585.

ORTH, D. A., MARQUEZ, L., HEIMAN, W. J., and TEMPLETON, D. H., 1949, *Phys. Rev.*, **75,** 1100.

PASSELL, T. O., MICHEL, M. C., and BERGSTRÖM, I., 1954, *Phys. Rev.*, **95,** 999.

Calculations on the Band Structure of Silicon

By D. P. JENKINS
Radar Research Establishment, Malvern, Worcs.

MS. received 16*th September* 1955, *and in final form* 14*th March* 1956

Abstract. The electronic band structure of silicon has been calculated along two axes of momentum space. The results agree qualitatively with experiment, but quantitative values are distorted by uncertainties in the potential used. The variational cellular method used is not too laborious in application, but appears to suffer from unexpected disadvantages at low-symmetry points in momentum space.

§ 1. Introduction

The experimental interest in the electronic properties of many crystals, especially those of the Group IV elements and the so-called III–V compounds, makes it very desirable that the electronic properties of these crystals should be studied theoretically. Now that several methods are available for such investigation (Howarth and Jones 1952, Slater and Saffren 1953, Herman 1954 a) it becomes necessary to make comparisons not only of the results they give, but of the ease with which such results are obtained. The calculations reported here were carried out partly to study the band structure of silicon and partly to assist an evaluation of what we shall call the variational cellular method (Jenkins and Pincherle 1954). Some preliminary results of these calculations have already been published (Bell *et al.* 1954, Jenkins 1954).

Silicon was chosen for study as a crystal on which much experimental work bearing on the band structure was in progress so that there was hope of a close comparison of theory and experiment. Previous theoretical calculations on silicon (Mullaney 1944, Holmes 1952, Yamaka and Sugita 1953) have been confined to the origin of $\mathbf{k}$ space and give conflicting results. The present calculations cover the two main axes of $\mathbf{k}$ space, the 1,0,0 and 1,1,1, as it seemed likely that $\mathbf{k} = 0$ might not be the most important point in the band structure. The results have confirmed this since the lowest point of the conduction band proved to be in the 1,0,0 direction in agreement with experimental observations.

Similar theoretical calculations have shown that the results obtained may be sensitive to the potential chosen to represent the effect of the crystal on the motion of an individual electron (Herman 1954 b). The present calculations for the 1,0,0 direction have been carried out with two different potentials to investigate this possibility, and although there are quantitative differences these do not affect the general conclusions on the shapes of the bands.

§ 2. Physical Description

Silicon forms a diamond-type crystal with two atoms in the primitive unit cell. These two atoms are on different face-centred lattices for each of which a typical unit vector is $(0, a, a)$. It is convenient to use coordinate axes which are the inverse of each other for the two types of atom, so that the four nearest (unlike)

neighbours of any atom are situated at points such as $\frac{1}{2}a$ (1,1,1). The first Brillouin zone is a truncated octahedron, with unit vectors like (π/a) (1,1,1), two of the principal endpoints of the first zone being (π/a) (1,0,0) and $(\pi/2a)$ (1,1,1). For silicon $a = 5{\cdot}13$ atomic units, and this value was used throughout the calculation.

The electronic energy levels forming the valence and conduction bands of the crystal are derived mainly from the 3s and 3p atomic levels of silicon, the K and L shells being too tightly bound to broaden appreciably into bands. Since there are two atoms in the unit cell each cell will give rise to eight energy levels which, by analogy with molecular theory, may be divided into four bonding levels forming the valence band, and four anti-bonding levels forming the conduction band. The eight M shell electrons in each unit cell just fill the valence band. This is the band picture for the more chemical description of silicon in which each atom is joined to its four nearest neighbours by tetrahedrally directed bonds. These bonds are represented by s–p hybrid orbitals joining atoms in pairs and each occupied by two electrons, one from each atom. The orbital picture and the band picture are, of course, related by a suitable transformation.

§ 3. Mathematical Formulation and Method of Solution

Following the usual simplification, the energy levels $E(\mathbf{k})$ of electrons having wave vector $\mathbf{k}$ and wave function $\psi(\mathbf{k}, \mathbf{r})$ are given by solutions of equation (1) in which atomic units are used.

$$[-\tfrac{1}{2}\nabla^2 + V(\mathbf{r}) - E(\mathbf{k})]\psi(\mathbf{k}, \mathbf{r}) = 0. \qquad \ldots\ldots(1)$$

This equation implies the Hartree approximation of writing the total electronic wave function as a product of one-electron functions and assuming a potential $V(\mathbf{r})$ which neglects the effect of exchange. To solve this equation with the condition that $\psi(\mathbf{k}, \mathbf{r})$ is a Bloch function,

$$\psi(\mathbf{k}, \mathbf{r}) = u(\mathbf{k}, \mathbf{r}) \exp(i\mathbf{k} \cdot \mathbf{r}), \qquad \ldots\ldots(2)$$

$u(\mathbf{k}, \mathbf{r})$ having the periodicity of the lattice, we adopt the cellular method. In this the crystal is divided into polyhedra each having an atomic nucleus at its centre, and the wave function inside each polyhedron is approximated by an expansion in terms of suitable basis functions. The energy levels are determined by the condition that these approximate expansions must join smoothly from cell to cell.

To obtain suitable basis functions a further approximation is required; the potential inside each cell must have spherical symmetry. With this assumption the wave function inside cell a can be approximated by

$$\psi(\mathbf{k}, \mathbf{r}) = \sum_s A_s(\mathbf{k}) \phi_s(\mathbf{r}_a, \lambda) \qquad \ldots\ldots(3)$$

where ϕ_s are solutions of

$$\{-\tfrac{1}{2}\nabla^2 + V(|\mathbf{r}_a|) - \lambda\}\phi_s(\mathbf{r}_a, \lambda) = 0 \qquad \ldots\ldots(4)$$

and λ and the coefficients A_s have to be chosen to satisfy the continuity condition on the wave functions. Various techniques for doing this have been proposed (Howarth and Jones 1952, Bell *et al.* 1953), but the results reported here were all obtained using the variation principle discussed by Jenkins and Pincherle (1954). For the particular case of silicon the basic equation of this method can be simplified, since the two atoms in the unit cell are physically identical. As a result, the electron distributions in the two types of polyhedra must be the same, and it can be shown

by group theory, or from the form of the variation functional, that corresponding coefficients in the two cellular expansions of the wave function (the A_s of equation (3)) must be complex conjugates of each other.

The cellular polyhedra in silicon are truncated tetrahedra with three small triangular faces forming a pyramid on each of the four corners. This gives four large hexagonal faces separating nearest neighbour atoms in different face-centred lattices, and twelve small triangular faces separating atoms in the same lattice. To carry out the matching technique, surface integrals over all these faces must be evaluated, but fortunately they can be obtained from the values over one hexagonal and three triangular faces only.

The energy levels are obtained by the condition that the functional

$$J(A_s,\lambda) = \left[\lambda - E(\mathbf{k})\right]\sum_s \bar{A}_s A_s + \sum_{su}\left[\sum_{|2T|} \bar{A}_s A_u T_{su}(\mathbf{k},\lambda) + \sum_{|H|} \bar{A}_s \bar{A}_u H_{su}(\mathbf{k},\lambda)\right] \quad \ldots\ldots(5)$$

shall be stationary for variation of λ and the A_s.

$$T_{su} = \tfrac{1}{4}\exp(i\mathbf{k}\,.\,\mathbf{t})\int_T \frac{\partial}{\partial n}\left[\phi_s(\mathbf{r},\lambda)\,.\,\phi_u(\mathbf{t}-\mathbf{r},\lambda)\right] dS \quad \ldots\ldots(6)$$

$\mathbf{t}$ being the vector between atoms separated by the triangular surface T, with a similar expression for the hexagonal face H. The condition on the A_s leads to an expression which determines $\lambda - E(\mathbf{k})$ as the latent roots of a matrix whose elements are sums and differences of the T_{su} and H_{su}. Each latent root gives an estimate, $E_\lambda(\mathbf{k})$, of $E(\mathbf{k})$, and it can be shown that the best estimate of $E(\mathbf{k})$ is obtained when $E_\lambda(\mathbf{k})$ is stationary for variations of λ. This latent root method and a simpler determinantal technique for obtaining the energies are discussed by Jenkins and Pincherle (1954). As explained there the latter introduces spurious solutions for crystals like silicon, and for this reason the latent root method has been used in the present calculations.

§ 4. Potential

To complete the transition from physics to mathematics the potential acting on the electrons in the crystal must be defined. Strictly speaking, this potential is determined by the electrons themselves so that a self-consistent method should be used to obtain it. However, it seems (Bell *et al.* 1953) that it would be very tedious to obtain a completely self-consistent field, while anything less than this is probably no better than much simpler approximations. The potential actually assumed in each cellular polyhedron was that derived from an atomic self-consistent field by Mullaney (1944). He added three fourths of the field of a 3s and three 3p electrons to the core field of a Si^{4+} ion, neglecting the effect of exchange, and hence obtained a spherically symmetrical potential. The same potential was assumed for electrons in both the valence and conduction bands to simplify the calculation, but it would be a better approximation to use a neutral atom field when calculating the conduction band energy levels (Hall 1954). To see how sensitive the band shapes were to changes of potential some calculations were also carried out using a modification of Mullaney's potential. This followed Mullaney's value to the surface of the inscribed sphere (roughly one third of the volume of the cell) but outside the sphere a constant value equal to that on the sphere was taken. Since a neutral atom potential would be approximately constant over this outer volume, the modified potential might be taken as a better approximation to the conduction band

potential apart from differences in energy zero caused by the different values of the constant potential. Unfortunately it is difficult to estimate this correction.

It will be realized that much uncertainty is attached even to a spherically symmetrical potential. The fact that the true cellular potential will have additional terms with an angular dependence like xyz/r^3 causes even more uncertainty, and such terms have been completely neglected though they could in principle be included to a limited extent. Calculations by March (1954) suggest that that these non-spherical terms are only appreciable near the extreme corners of the tetrahedron so that over most of the cell the spherical approximation is justified.

§ 5. Cellular Wave Functions

The basis functions ϕ_s used in the expansion of the wave function were linear combinations of solutions of equation (4) for the same value of the angular quantum number l which transformed according to the irreducible representations of the tetrahedral group (Bell 1954). They were normalized inside the equal volume sphere, and are orthogonal to each other inside this sphere. Strictly, the variation function (5) assumes that the basis functions are orthonormal inside the cellular polyhedron; when this condition is not satisfied terms like $[\lambda - E(\mathbf{k})]\, \bar{A}_s A_u$ appear and their neglect produces errors in the latent roots which are of the order of the error in the orthonormalization condition. It was felt that such errors are probably so small that the computational effort required to remove them was not worth while.

The symmetry properties of a wave function expanded about a silicon atom are determined by the tetrahedral geometry of the lattice and by the form of the vector $\mathbf{k}$ associated with the function. Because of this symmetry the matrix of the surface integrals for a given value of $\mathbf{k}$ can be factorized into smaller parts each containing functions which transform according to one of the irreducible representations of a sub-group of the tetrahedral group. This enables us to name the energy bands systematically from their symmetry properties, and we shall follow the nomenclature of Bell (1954) in doing this. For some points in $\mathbf{k}$ space the wave function has additional symmetry by virtue of the point of inversion in the lattice mid-way between nearest neighbour atoms; functions invariant under this operation will be characterized by prefix g and those which change sign by prefix u.

The cellular expansions used included all functions of the correct symmetry up to and including the g-type atomic functions. The only exception was for the O_p band in the 1,0,0 direction (this band is degenerate with the O_p' band because of the point of inversion) where the g-function $xy(x^2-y^2)$ was omitted. After allowing for symmetry this meant that nine real coefficients had to be determined for the O_s bands and five complex coefficients for the O_p band (1,0,0 direction), while in the (1,1,1) direction both the I_s and the I_p bands had seven complex coefficients. The convergence of these expansions was checked in the 1,0,0 direction and appeared to be quite good, expansions up to d functions only often giving substantially the same energy levels as the complete expansions.

§ 6. Computational Aspects

Since one aim of this investigation was to study the utility of the variational cellular method, the computational details will be gone into rather fully.

The principal stages of the calculation, once the potential has been fixed, are: (*a*) Integrate the radial Schrödinger equation for all required l values at selected values of λ, the energy parameter; this is a standard process and need not be discussed further. (*b*) Calculate the values of the surface integrals between all required functions. (*c*) Set up the compatibility matrices and find their latent roots. (*d*) From the behaviour of the latent roots as a function of λ at constant wave vector determine the energy for that wave vector.

It is convenient to consider stage (*d*) first as this determines the range of λ values required. This range should span the energies expected since the best value of λ for any wave function should be approximately equal to the corresponding energy level. To reduce the labour required on radial functions most of our results were obtained using λ at 0·1 atomic unit intervals, though these were supplemented by some calculations using interpolated surface integrals. The energy levels for a given value of $\mathbf{k}$ are obtained by plotting the values of $E_\lambda(\mathbf{k})$ given by the latent roots as a function of λ. In fortunate cases these curves show horizontal portions where $E_\lambda(\mathbf{k})$ is nearly independent of λ, and hence gives the value of $E(\mathbf{k})$. Usually however, there are many curves arising from the different latent roots of each matrix, and the horizontal portions are obscured by the fact that these curves cannot cross. The best value of $E_\lambda(\mathbf{k})$ may then correspond to a different latent root for different values of λ, and the interpretation of the data becomes rather doubtful.

The crux of the method is the evaluation of the surface integrals in T_{su} and H_{su}. There is a large number of these (we evaluated about 200 for each value of λ used) and since they can only be obtained by numerical quadrature they must be calculated very systematically. Fortunately each integration can conveniently be divided into two parts, one over angle and the other over radius vector, since the basis functions are expressed as the product of an angular function (the lattice harmonic) independent of λ, and a radial function.

The major integration, over angle for the products of pairs of lattice harmonics, can be carried out once for all, and if suitable scaling factors are chosen the results can be used directly in calculations on all crystals having the zinc blende structure, the Group IV and the III–V semiconductors in particular. These standard values are then combined with products of radial functions corresponding to each value of λ to obtain the final surface integrals. A useful property of the surface integrals is that they seem to be smooth functions of λ, and 4 point interpolation in a table at 0·1 atomic unit intervals gives quite accurate results, and considerably reduces the computation required.

In these days of high speed digital computers, any large scale calculation must be considered in relation to such a machine. No such assistance was available when the work on silicon was started, but practically all the final results have been obtained on the Radar Research Establishment parallel computer. Given the values of the surface integrals, programmes have been constructed which will carry out stage (*c*) and give the latent roots for any point in the 1,0,0 or 1,1,1 directions. It has been found that these programmes can deal with one band in less than a day and from their results the (E, $\mathbf{k}$) curves are quickly drawn. To assist work on the modified potential a preliminary programme was drawn up which constructed the surface integrals from radial-function products and the standard lattice-harmonic products. By using this and other programmes being developed at the Radar Research Establishment it would be quite feasible, once a

potential has been chosen, to run the complete calculation on the computer, the output from each stage becoming the input to the next. This piecemeal running of the problem is at present forced by the small memory (512 words) of the computer.

§ 7. The Energy Levels

The energy levels at seven points in each of the two directions of **k** space were obtained by calculation and used to draw the $E(\mathbf{k})$ curves shown in the figures. The standard Mullaney potential gave the results for the 1,0,0 and 1,1,1 directions shown in figure 1, while figure 2 shows the bands obtained in the 1,0,0 direction using the modified potential (constant outside the inscribed sphere). No attempt has been made to allow for any spin–orbit interaction which may affect the details of the degeneracy of various energy levels (Elliott 1954, Herman 1954 b), but not the picture as a whole since the effect in silicon is quite small.

The most striking feature of the figures is that what are expected to be the conduction bands, shown dotted, in fact overlap the valence bands by about 2 ev. This is obviously incorrect since silicon is not a metal, and the error arises from the potential chosen for conduction band electrons. As mentioned earlier this was

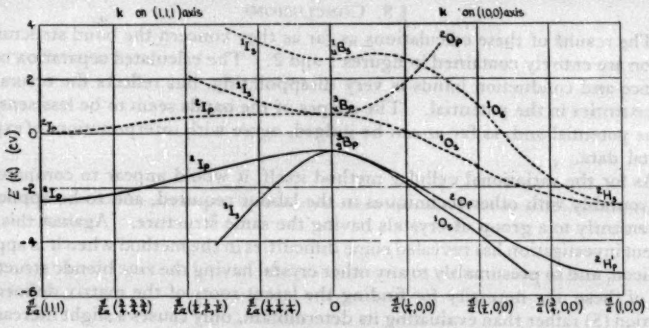

Figure 1. $E(\mathbf{k})$ curves for silicon.

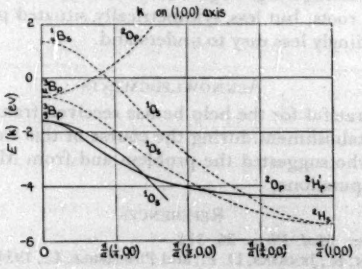

Figure 2. $E(\mathbf{k})$ curves for silicon, modified potential.

too attractive, and a more correct potential would raise the energy of the whole of the conduction bands. However, not much alteration in shape would be expected since the modified potential (which tends towards the true conduction band potential apart from its zero) gives rise to bands very similar to the original ones. With this modification it is seen that the calculations predict that the top of the valence band should be at the origin of **k** space, but place the lowest energy in the conduction band near the end point of the 1,0,0, direction, (π/a) (1,0,0). This agrees with estimates made by Herman (1954b) from perturbations to the band structure he calculates for germanium. The experimental evidence on the shapes of the bands in silicon confirms these theoretical calculations rather well. Cyclotron resonance experiments on n-type silicon indicate that the lowest points of the conduction band are in the 1,0,0 direction (Dexter *et al.* 1954), and this is supported by measurements of the magneto-resistance (Pearson and Herring 1954) and piezo-resistance (Smith 1954) effects. From the shape of the absorption edge in silicon and a theory of the intensity of 'forbidden transitions' Macfarlane and Roberts (1955) have estimated that the 1,0,0 minimum must be near the point (π/a) (0·8,0,0). The calculated width of the valence bands is about 13 electron volts compared with the experimental value of 19 ev (O'Bryan and Skinner 1934).

§ 8. Conclusions

The results of these calculations as far as they concern the band structure of silicon are entirely contained in figures 1 and 2. The calculated separation of the valence and conduction bands is very disappointing, but reflects the errors and uncertainties in the potential. The shapes of the bands seem to be less sensitive to the potential and, as far as can be judged, agree with interpretations of experimental data.

As for the variational cellular method itself, it would appear to compare not unfavourably with other techniques in the labour required, and to be applicable conveniently to a group of crystals having the same structure. Against this, the present investigation has revealed some difficulties in the method when it is applied to silicon, and so presumably to any other crystal having the zinc blende structure. One of these, the necessity for finding the latent roots of the matrix defined by equation (5) rather than evaluating its determinant, only causes a slight increase in time when a high speed electronic computer is used. More serious is the problem of determining which of many latent roots is associated with a given energy level. For wave functions having a high degree of symmetry this is not difficult since there are then few latent roots, but less symmetrically situated points in the Brillouin zone are correspondingly less easy to understand.

Acknowledgments

The author is grateful for the help he has received from his colleagues at the Radar Research Establishment during the course of this work, particularly from Dr. L. Pincherle who suggested the problem and from Miss R. Hensman who assisted in the computations.

References

Bell, D. G., 1954, *Rev. Mod. Phys.*, **26**, 311.

Bell, D. G., Hensman, R., Jenkins, D. P., and Pincherle, L., 1954, *Proc. Phys. Soc.* A, **67**, 562.

Bell, D. G., Hum, D. M., Pincherle, L., Sciama, D. W., and Woodward, P. M., 1953, *Proc. Roy. Soc.* A, **217**, 71.

DEXTER, R. N., LAX, B., KIP, A. F., and DRESSELHAUS, G., 1954, *Phys. Rev.*, **96**, 222.
ELLIOTT, R. J., 1954, *Phys. Rev.*, **96**, 266.
HALL, G. G., 1954, *Symposium on Band Structure*, R.R.E., Malvern, p. 5.
HERMAN, F., 1954 a, *Phys. Rev.*, **93**, 1214 ; 1954 b, *Physica*, **20**, 801.
HOLMES, D. K., 1952, *Phys. Rev.*, **87**, 782.
HOWARTH, D. J., and JONES, H., 1952, *Proc. Phys. Soc.* A, **65**, 355.
JENKINS, D. P., 1954, *Physica*, **20**, 967.
JENKINS, D. P., and PINCHERLE, L., 1954, *Phil. Mag.*, **45**, 93.
MACFARLANE, G. G., and ROBERTS, V., 1955, *Phys. Rev.*, **98**, 1865.
MARCH, N., 1954, *Symposium on Band Structure*, R.R.E., Malvern, p. 24.
MULLANEY, J. F., 1944, *Phys. Rev.*, **66**, 326.
O'BRYAN, H. M., and SKINNER, H. W. B., 1934, *Phys. Rev.*, **45**, 370.
PEARSON, G. L., and HERRING, C., 1954, *Physica*, **20**, 975.
SLATER, J. C., and SAFFREN, M. M., 1953, *Phys. Rev.*, **92**, 1126.
SMITH, C. S., 1954, *Phys. Rev.*, **94**, 42.
YAMAKA, E., and SUGITA, T., 1953, *Phys. Rev.*, **90**, 992.

Paramagnetic Resonance Spectra of the Alkali Superoxides and Chlorine Dioxide

By J. E. BENNETT †, D. J. E. INGRAM † and D. SCHONLAND ‡
† Department of Electronics, University of Southampton
‡ Department of Mathematics, University of Southampton

MS. received 16*th February* 1956, *and in revised form* 5*th April* 1956

Abstract. The paramagnetic resonance absorption spectra of chlorine dioxide and the alkali superoxides are described in detail and a theoretical analysis is made of the results in terms of molecular orbital theory. The unpaired electron is associated with the binding orbitals in each case and the variation of g values and hyperfine splitting are used to calculate the details of the energy levels. Variation of the spectra with temperature has also been studied and has revealed an averaging effect on the chlorine hyperfine structure due to the 'tumbling' motion of the solvent molecules.

§ 1. Introduction

Although most of the initial work on paramagnetic resonance was confined to compounds of the transition group elements the technique is now being used in an increasing measure to investigate other systems containing unpaired electrons. In most cases of chemical binding the spins of the valence electrons are balanced, either in the outer shell of ions or in the shared pairs of covalent bonds, and thus the vast majority of compounds are diamagnetic. There are certain exceptions to this, however, in which the normal chemical binding is modified and an unpaired electron is present in the system. Apart from the relatively large number of such organic derivatives, usually termed 'free radicals', there are also several inorganic compounds which possess unpaired electrons and are thus paramagnetic. The magnetic properties of these compounds are somewhat different from those of the transition group elements, since the unpaired electron is not now associated strongly with the one paramagnetic atom, but with the chemical binding of the molecule as a whole. Its behaviour is thus characterized by molecular orbitals rather than atomic orbitals, and the unpaired electron may well interact quite strongly with more than one atom. Such compounds can be studied by paramagnetic resonance and considerable information obtained concerning the molecular orbitals involved in the binding. The detailed measurements of Beringer and Castle (1950, 1951) on oxygen, nitric oxide and nitrogen peroxide are a good example of such a study, and the interaction of the electron with the nitrogen nuclei was found to produce a marked hyperfine structure.

There is one other common gas which also possesses an unpaired electron in its bonding, namely, chlorine dioxide. A similar situation also occurs in the superoxides of the alkali metals, although in this case the unpaired electron is confined to the O_2^- ion which exists as a separate entity in the crystalline lattice. In this paper measurements are reported on both the alkali superoxides and

chlorine dioxide, together with an analysis of the observed spectra in terms of the molecular orbitals associated with the O_2^- ion and the ClO_2 molecule. The chlorine dioxide was not studied as a gas, but in the liquid and solid phases, and also in solutions in water and various organic solvents. One of the most striking results of these experiments is the sudden change in spectrum when the solvent is cooled through its freezing point, which is attributed to the removal of the effective 'averaging out' process produced by the mobile solvent molecules.

§ 2. Experimental

The paramagnetic resonance spectrometers used for these measurements were of the standard crystal–video detection type, and low temperature resonators which incorporate nickel–silver waveguide feed to the cylindrical cavities were employed (Ingram 1955). Since the compounds studied were either in solution or of a polycrystalline form, the resulting spectra were always an average of all possible orientations and thus usually in the form of broad asymmetrical absorption lines. In order to check whether the shape of the lines was due to a g-value variation or to electronic or hyperfine splitting, measurements were made at wavelengths of 3 cm, 1·25 cm and 8 mm. In this way it was possible to show that the absorption curve of the superoxides corresponded to a true g-value variation, whereas the spectra from the chlorine dioxide were mainly determined by the hyperfine interaction with the chlorine nuclei.

The superoxide samples studied were mainly in a magnetically diluted form, and were an intimate mixture with the corresponding peroxides. Chemical and physical tests (George 1942) on commercially available sodium peroxide have shown that this contains about 10% of the superoxide NaO_2, and it can thus be used directly as a magnetically dilute sample of the O_2^- ion. The superoxide can also be prepared by passing oxygen over the heated distilled metal, and the samples of potassium superoxide were obtained in this way. In every case the paramagnetic absorption was found to disappear when the samples were treated with water, confirming that the signal was due to the O_2^- ions, as the latter are decomposed by water.

The chlorine dioxide was generated by the action of oxalic acid on potassium chlorate and the resulting gas either passed into a container at about $-80°$C when samples of the pure liquid or solid were required, or bubbled through the appropriate solvent when the solutions were being studied. The samples were always freshly prepared before each series of experiments.

In most cases the samples were placed in a small distrene cup, which was attached centrally to the bottom of an H_{111} resonator, but at wavelengths of 3 cm and sometimes 1·25 cm, small tubes held along the axis of an H_{101} resonator were employed. The magnetic field was measured with a proton resonance meter and both the proton and microwave signals were displayed simultaneously on the oscilloscope screen. The most accurate determinations of g values were made by comparison with the field position of the absorption line from a small amount of hydrazyl which was used as a standard marker.

§ 3. Results on the Superoxides

Photographs of the absorption lines obtained from sodium superoxide are shown in figure 1, for the wavelengths 3 cm and 1·25 cm. In each case an asymmetrical line is observed with a marked shoulder on the low field side,

the splitting between the low-field shoulder and the main peak being accurately proportional to the frequency of measurement. This fact is confirmed by the measurements at 8 mm where the field separation of 1100 gauss is too large for a photograph to be taken. This dependence on frequency of measurement

Figure 1. Absorption from sodium superoxide. Wavelength: (*a*) 1·25 cm, (*b*) 3 cm. Unit of field sweep at bottom represents 500 gauss.

shows that the line shape is determined by a *g*-value variation. The *g* value corresponding to the main peak can be measured accurately by comparison with the hydrazyl signal, and its values, together with those corresponding to the shoulder, are shown in table 1 for the three wavelengths used.

Table 1

Wavelength	$g_{\parallel}$	$g_{\perp}$
3 cm	2·165 ± 0·01	2·00 ± 0·01
1·25 cm	2·175 ± 0·005	2·000 ± 0·005
0·8 cm	2·179 ± 0·005	2·000 ± 0·005

The parallel and perpendicular suffixes are used to indicate that $g_{\parallel}$ is associated with the smaller absorption, since a *g*-value variation with axial symmetry will have an integrated intensity from directions nearly perpendicular to the axis twice as great as from those nearly parallel. The shape of the absorption line suggests that such axial symmetry is in fact present to an appreciable extent, although the direction of the axis cannot be identified from the polycrystalline specimens used. Most of the spectra were obtained at 90°K; the only difference apparent in samples cooled to 20°K was that the width of the lines in the wings was reduced considerably showing that a certain amount of spin–lattice broadening is present at liquid oxygen temperatures.

The *g*-value variation can be explained satisfactorily by considering the molecular orbitals of the O_2^- ion. This theory has been given in some detail by Stanley Griffith (Bennett *et al.* 1955), and can be summarized as follows.

The free ion would be in a $^2\Pi$ state, which is split by the spin–orbit coupling into $^2\Pi_{1/2}$ and $^2\Pi_{3/2}$ states. In O_3^- the latter state will lie lowest. If, however, the symmetry about the molecular axis is partially removed, as x-ray measurements at low temperatures suggest (Zhdanov and Zvonkova 1952), one of the π_g 2p orbitals will have a higher energy than the other. The expected g values will then depend on the ratio between the splitting of these two levels and the spin–orbit coupling coefficient. Zero splitting of the levels would give $g_{\parallel}=4$ and $g_{\perp}=0$, and for infinite splitting, with complete orbital quenching, $g_{\parallel}=g_{\perp}=2$. It therefore follows that for intermediate values of splitting $2<g_{\parallel}<4$ with $0<g_{\perp}<2$, and detailed calculation gives $g_{\perp}=1{\cdot}99$ when $g_{\parallel}=2{\cdot}175$, in good agreement with the experimental results.

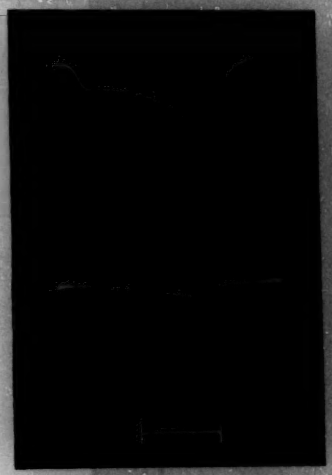

Figure 2. Comparison of superoxide and ozonate absorptions. (*a*) Superoxide, (*b*) ozonate. Both at 1·25 cm and same field sweep. Unit of field sweep = 500 gauss.

Figure 3. Ozonate absorption at low field sweep. Unit of field sweep at bottom is 100 gauss.

In contrast to this relatively wide g-value variation of the superoxide ions, the absorption line obtained from the higher oxide, the ozonate, is much more symmetrical, and the g-value variation very much smaller. This is illustrated in figure 2 where the spectrum of the ozonate is shown directly under that of the superoxide, both being taken with the same magnetic field sweep and at 1·25 cm wavelength. The ozonate absorption line is also shown in figure 3, but with a much smaller magnetic field sweep, so that the slight asymmetry of the line shape can be seen. This asymmetry is of the opposite form to that of the superoxide, the shoulder now being on the high field side of the peak. Measurements at different wavelengths again confirm that the shape is due to a true g-value variation, and thus for the O_3^- ion $g_{\parallel}=2{\cdot}003\pm0{\cdot}003$ and $g_{\perp}=2{\cdot}015\pm0{\cdot}004$.

§ 4. Results for Chlorine Dioxide

The paramagnetic absorption spectrum obtained from solutions of chlorine dioxide varies considerably with the physical state of the solvent. The simplest type of spectrum is that observed when the solvent is in the liquid phase, and is shown in figure 4. The three spectra shown are all for solutions in ethyl alcohol at 193°K, and for the three different wavelengths of 3 cm, 1·25 cm and 8 mm. In each case four well-resolved lines are obtained and, since their separation is independent of wavelength (in marked contrast to the spectra of the superoxides), they can be identified as hyperfine components due to the interaction between the magnetic moment of the unpaired electron and the magnetic moments of

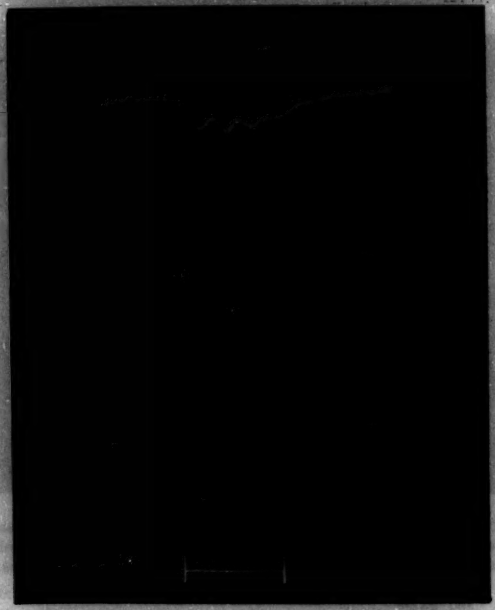

Figure 4. Chlorine dioxide solution in liquid phase. (*a*) 8 mm wavelength, (*b*) 1·25 cm wavelength, (*c*) 3 cm wavelength. Unit of field sweep at bottom = 100 gauss.

the ^{35}Cl and ^{37}Cl nuclei. Although the separation of the hyperfine pattern remains constant the position of the centre of the pattern relative to a hydrazyl signal moves quite appreciably as the wavelength is decreased. From the shift of the pattern with frequency the g value corresponding to the centre of the four lines can be determined as $2{\cdot}010 \pm 0{\cdot}003$. The width of the individual hyperfine components is 8 gauss, and the separation between them is 17 gauss so that $A = B = 16 \times 10^{-4}\text{cm}^{-1}$.

The width of the individual lines is affected by both spin–spin and spin–lattice broadening. Thus, as the solution becomes more concentrated the lines widen

and eventually merge to form one single broad peak. Such a single peak is also observed from pure chlorine dioxide in either the liquid or solid phase, a single line with total half width of 150 gauss being obtained. The fact that this width is considerably larger than the overall hyperfine splitting shows that in the pure chlorine dioxide the spin–spin interaction is the dominant effect. There is no noticeable change in this width as the temperature of the undiluted chlorine dioxide is raised through its melting point, indicating the same random orientation of the molecules in both the solid and liquid phase. The spin–lattice interaction can be demonstrated by observing the change in width of the individual hyperfine components as the temperature of a single sample is raised slowly from 193° to 273°K. The broadening of the individual lines as the temperature increases can be clearly seen, and the lines finally merge to form one broad line at room temperature.

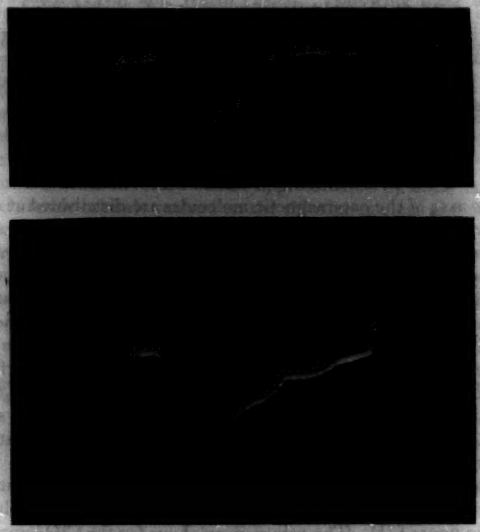

Figure 5. Spectra from an alcoholic solution of chlorine dioxide. (*a*) In liquid state at 193°K, (*b*) frozen at 90°K. An approximate analysis of extreme hyperfine splittings is shown with (i) $A=55$ gauss, (ii) $B=22$ gauss.

The fact that such an isotropic and well-resolved hyperfine pattern can be obtained from the solutions in a liquid phase can be attributed to the mobility of the solvent molecules and their effect in 'averaging out' the orbital contribution which produces the anisotropy associated with a single molecule of chlorine dioxide. The same spectrum has been observed from solutions in several different solvents, including water, acetone, alcohol and benzene, indicating that there is no noticeable interaction of the unpaired electron with the solvent molecules.

A very marked change in the spectrum is observed, however, when any of the solutions are cooled below their freezing points. This is shown in figure 5, in which the spectrum from the same alcoholic solution at 1·25 cm wavelength is shown (*a*) in the liquid phase (193°K) and (*b*) in the solid phase (90°K). It is seen that the pattern obtained from the solid phase is much wider and far less resolved. This suggests that the absorption curve is due to the averaging over all orientations of an anisotropic hyperfine structure and g variation. The sudden change to this type of spectrum is observed in all the different solutions studied, and always occurs at the freezing point of the solvent concerned. The spectrum is again independent of the particular solvent used. This sudden change of the spectrum on freezing can be explained by assuming that in the solid phase the solvent molecules are no longer mobile and cannot exert their 'tumbling' or 'averaging' effect (Pake 1955) on the chlorine dioxide molecules, so that the anisotropy associated with the different orientations of the molecule is obtained. The analysis of the observed absorptions on this basis is carried out in the next section, and from the measurements at 1·25 cm and 8 mm wavelength the normal spin Hamiltonian coefficients can be quoted as $g_{\parallel}=2{\cdot}01\pm0{\cdot}005$, $g_{\perp}=2{\cdot}02\pm0{\cdot}005$, $A=55\pm5\times10^{-4}\,\mathrm{cm}^{-1}$, $B=20\pm7\times10^{-4}\,\mathrm{cm}^{-1}$, where axial symmetry has been assumed as a first approximation.

§ 5. Theoretical Analysis of Results

5.1. *Resolution of the Spectrum*

When the axes of the paramagnetic molecules are distributed at random about the direction of the applied field, and there is no hyperfine structure, the absorption curve is of the form shown in figure 1 (for the O_2^- system) and has a peak associated with the perpendicular direction and a smaller shoulder associated with the parallel direction. When there is a hyperfine structure then, for a random distribution of the molecular axes, each component line will broaden out into a similar shaped curve; for the line characterized by m ($m=I$, $I-1$, ..., $-I$, where I is the spin of the nucleus responsible for the hyperfine structure) the peak occurs at field $h\nu/g_{\perp}\beta+mB$ and the shoulder at field $h\nu/g_{\parallel}\beta+mA$. The total absorption curve is a superposition of curves of this type and so will exhibit a pattern of $2I+1$ peaks, centred on $g_{\perp}$ with separation B, and a pattern of $2I+1$ shoulders, centred on $g_{\parallel}$ with separation A (Sands 1955).

These patterns will be obscured by the line broadening, but they can be plausibly recognized in the absorption curve for the frozen ClO_2 solution ($I=3/2$) as indicated in figure 5 (*b*). The values given above for the ClO_2 spin Hamiltonian constants were estimated from the general appearance of the curve and from the spacing of the isolated peak and shoulder occurring at the low field end of the spectrum which can be identified with the absorption curve arising from $m=-3/2$.

If the hyperfine structure has only approximate axial symmetry one must introduce two constants B_1 and B_2 to describe it in the perpendicular plane. The signs of these constants do not affect the absorption curve so that the value of $|B|$ given above is the mean of $|B_1|$ and $|B_2|$.

Another relation between A, B_1 and B_2 is given by the isotropic hyperfine structure obtained from the ClO_2 solution in the liquid phase, when the rapid 'tumbling' motion of the molecules averages out the anisotropy associated with the different molecular axes. Since the g values are so nearly isotropic the

averaged separation of the hyperfine lines is given to a fair approximation by $\frac{1}{3}|A+B_1+B_2|$.

From the numerical values given for these quantities in the preceding paragraph one can find two possible sets of values for A, B_1 and B_2: $A=\pm 55\times 10^{-4}$ cm^{-1}, $B_1=\pm 16{\cdot}5\times 10^{-4}$ cm^{-1}, $B_2=\mp 23{\cdot}5\times 10^{-4}$ cm^{-1}.

5.2. *Theory*

ClO_2 is a bent molecule and has the group of symmetry C_{2v}. The irreducible representations of this group, used to classify the molecular orbitals, are all one-dimensional and are referred to by the symbols A_1, A_2, B_1, B_2 (Mulliken 1933). The molecular axes used below have their origin at the chlorine nucleus, with the x axis perpendicular to the plane of the molecule and the z axis bisecting the O–Cl–O angle.

The electronic structure of ClO_2 has been discussed, in terms of molecular orbitals, by Mulliken (1942) and Walsh (1953). Following these authors, the ground state arises from the configuration $\ldots(a_2)^2(a_1)^2(b_2)^2(b_1)$ with a wave function transforming under the representation B_1. The lowest lying excited levels arise from the excitation of an inner electron to fill the outer b_1 shell. The first three excited states then have wave functions transforming under the representations B_2, A_1 and A_2, and if only this group of excited levels is considered with the ground state the system may be pictured as a hole placed in one or other of the four shells.

The molecular orbitals involved can be approximated by linear combinations of 3s, 3p and 3d atomic orbitals centred on the chlorine nucleus and of 2p orbitals centred on the oxygen nuclei. The appropriate forms for these are (Moffitt 1950), neglecting overlap,

$$\begin{aligned}\psi(b_1)&=b\phi_{Cl}(b_1)-(1-b^2)^{1/2}\phi_0(2pb_1)\\ \psi(a_2)&=a\phi_{Cl}(a_2)+(1-a^2)^{1/2}\phi_0(2pa_2)\\ \psi(a_1)&=\phi_{Cl}(a_1)\\ \psi(b_2)&=\phi_0(2pb_2)'\end{aligned}\qquad\ldots\ldots(1)$$

where the oxygen-centred orbitals are given by Moffitt, and the chlorine orbitals are

$$\begin{aligned}\phi_{Cl}(b_1)&=\cos\beta\phi(3p_x)-\sin\beta\phi(3d_{xz})\\ \phi_{Cl}(a_1)&=\cos\alpha\phi(3p_z)-\sin\alpha\phi(3s)\\ \phi_{Cl}(a_2)&=\phi(3d_{xy})\end{aligned}\qquad\ldots\ldots(2)$$

Spin–orbit coupling admixes a certain amount of the excited state wave functions into the ground state, and the departure of the measured g values from the free spin value shows that the admixture is not negligible in spite of the very wide spacing between the excited states and the ground state. (The first optical absorption for ClO_2 in solution occurs at an energy of some 27 000 cm^{-1} (Buser and Honisch 1952).) For the orbitals specified by (1) and (2) spin–orbit type coupling in second-order perturbation theory gives rise to ground doublet state vectors of the form

$$\begin{aligned}|+\rangle&=N|B_1,\tfrac{1}{2}\rangle+i\mu|B_2,\tfrac{1}{2}\rangle-\nu|A_1,-\tfrac{1}{2}\rangle-i\sigma|A_2,-\tfrac{1}{2}\rangle\\ |-\rangle&=N|B_1,-\tfrac{1}{2}\rangle-i\mu|B_2,-\tfrac{1}{2}\rangle+\nu|A_1,\tfrac{1}{2}\rangle-i\sigma|A_2,\tfrac{1}{2}\rangle\end{aligned}\qquad\ldots\ldots(3)$$

where $N=1-\frac{1}{2}(\mu^2+\nu^2+\sigma^2)$, and μ, ν, σ are small. In (3) the spin has been quantized along the molecular z axis and the symbols $\frac{1}{2}$, $-\frac{1}{2}$ refer to the two possible spin states of the hole.

If the interactions with the applied magnetic field and with the chlorine magnetic moment are treated as first-order perturbations on (3) in the usual way (Abragam and Pryce 1951) one arrives at the spin Hamiltonian

$$\mathscr{H}=\beta(g_xS_xH_x+g_yS_yH_y+g_zS_zH_z)+(A_xS_xI_x+A_yS_yI_y+A_zS_zI_z)$$

where

$$g_x=2(1+r)\,;\qquad g_y=2(1+s)\,;\qquad g_z=2(1+t) \qquad \ldots\ldots(4)$$

$$A_x=P\{b^2(\tfrac{4}{7}\cos^2\beta+\tfrac{2}{7}f\sin^2\beta)-\tfrac{3}{7}s+2fr-k\}\ldots \qquad \ldots\ldots(5a)$$

$$A_y=P\{-b^2(\tfrac{2}{7}\cos^2\beta+\tfrac{1}{7}f\sin^2\beta)+2s+\tfrac{6}{7}fr+k\}\ldots \qquad \ldots\ldots(5b)$$

$$A_z=P\{-b^2(\tfrac{2}{7}\cos^2\beta-\tfrac{2}{7}f\sin^2\beta)+\tfrac{3}{7}s-\tfrac{3}{7}fr-k\}\ldots. \qquad \ldots\ldots(5c)$$

In these expressions, r, s and t are proportional to σ, ν and μ respectively, and the reason for the non-occurrence of t in (5) is that the molecular orbital $\psi(b_2)$ of (1), associated with the parameter μ, is centred on the oxygen nuclei and so does not contribute to the hyperfine structure. The quantity $P=2g_N\beta\beta_N\langle r^{-3}\rangle_p$, where $\langle r^{-3}\rangle_p$ is the mean value of r^{-3} for the Cl 3p wave functions and g_N is the g value of the Cl nucleus expressed in terms of the nuclear magneton β_N; f is such that $f\langle r^{-3}\rangle_p$ is the mean value of r^{-3} for the Cl 3d orbitals; the parameter k arises from the coupling of the 3s part of the orbital $\psi(a_1)$ with itself by the δ function term in the interaction responsible for the hyperfine structure; and b and β define the properties of the orbital $\psi(b_1)$ in which the unpaired electron is placed.

5.3. *Comparison of Theory with Experiment*

Of the parameters occurring in (5), P depends only on the nature of the Cl atomic orbitals from which the molecular orbitals (1) are constructed, and can be estimated from measurements on free Cl atoms. The hyperfine structure of the $^2P_{3/2}$ ground state of Cl (Davies *et al.* 1949) gives $P=128{\cdot}4\times10^{-4}$ cm^{-1} for ^{35}Cl and $P=106{\cdot}8\times10^{-4}$ cm^{-1} for ^{37}Cl; the mean of these two values, weighted with the relative abundances of these two isotopes, is $123{\cdot}0\times10^{-4}$ cm^{-1}. The remaining parameters in (4) and (5) have to be estimated from the measurements reported in this paper.

A comparison of the form of the expressions (5) with the two possible sets of numerical values for the hyperfine structure constants suggests that the constant A should be taken as negative and identified with A_z; then the z axis is the 'parallel' axis and $g_z\simeq g_y=2{\cdot}02$. If this identification is made, equations (4) give $r=s=0{\cdot}01$ and equations (5) have to be solved with this value for r and s, and with $A_z=-55\times10^{-4}$ cm^{-1}, $A_x=-16{\cdot}6\times10^{-4}$ cm^{-1}, and $A_y=23{\cdot}5\times10^{-4}$ cm^{-1}.

With the value given above for P there are four unknown parameters b, β, k and f and these conditions are not sufficient to determine them uniquely. If the results are expressed in terms of f as the free parameter, one finds

$$k=0{\cdot}41+0{\cdot}02f$$

$$b^2=(0{\cdot}229/f)+0{\cdot}328-0{\cdot}020f$$

$$\tan^2\beta=(0{\cdot}229+0{\cdot}057f)/f(0{\cdot}271-0{\cdot}020f).$$

The condition $b^2 \leqslant 1$ is then only satisfied if $f \geqslant 0{\cdot}34$. If the Cl 3p and 3d orbitals had a pure hydrogen-like radial dependence the value of f would be 0·2 so that it is not unreasonable to assume that the value of f appropriate for the actual Cl orbitals will lie close to its lower limit of 0·34. If this is the case, then $b^2 \simeq 1$ and $\tan^2\beta \simeq 2{\cdot}7$ which leads to the conclusion that the orbital $\psi(b_1)$ in which the unpaired electron moves is almost entirely centred on the Cl nucleus and has approximately 70% 3d character and 30% 3p character.

Acknowledgments

We would like to express our thanks to Professor Philip George for initially suggesting the experiments with the alkali superoxides and to Dr. M. C. R. Symons for making the ozonate samples. We are also much indebted to the Royal Society for a grant towards the cost of the apparatus and one of us (J. E. B.) to the Department of Scientific and Industrial Research for a maintenance grant.

References

Abragam, A., and Pryce, M. H. L., 1951, *Proc. Roy. Soc.* A, **205,** 135.
Bennett, J. E., Ingram, D. J. E., Symons, M. C. R., George, P., and Stanley Griffith, J., 1955, *Phil. Mag.*, **46,** 443.
Beringer, R., and Castle, J. G., 1950, *Phys. Rev.*, **78,** 581; **80,** 114; 1951, *Ibid.*, **81,** 82.
Buser, W., and Honisch, H., 1952, *Helv. Chem. Acta*, **35,** 2547.
Davis, L., Feld, B. T., Zabel, C. W., and Zacharias, J. R., 1949, *Phys. Rev.*, **76,** 1096.
George, P., 1942, *Disc. Faraday Soc.*, No. 2, 203, 218.
Ingram, D. J. E., 1955, *Spectroscopy at Radio and Microwave Frequencies* (London : Butterworths Scientific Publications) p. 66.
Moffitt, W., 1950, *Proc. Roy. Soc.* A, **200,** 409.
Mulliken, R. S., 1933, *Phys. Rev.*, **43,** 279; 1942, *Rev. Mod. Phys.*, **14,** 204.
Pake, G. E., 1955, *Disc. Faraday Soc.*, No. 19, 185.
Sands, R. H., 1955, *Phys. Rev.*, **99,** 1222.
Walsh, A. D., 1953, *J. Chem. Soc.*, Pt. 3, 2266
Zhdanov, G. S., and Zvonkova, Z. V., 1952, *Doklady Acad. Nauk. S.S.S.R.*, **82,** 743.

Attenuated Angular Correlations between K-conversion Electrons in ^{197}Hg

By E. BREITENBERGER†
Cavendish Laboratory, Cambridge

MS. received 22*nd November* 1955, *and in final form* 13*th March* 1956

Abstract. The angular correlation between the successive K-conversion electrons from the de-excitation of 23-hr ^{197}Hg has been investigated in an attempt to determine the limitations of correlation work with conversion electrons in cases of cascades with a long-lived intermediate state. Sources prepared by embedding the activity carrier-free in thin aluminium films exhibited consistent behaviour; the second-order term of the correlation function was attenuated $18 \pm 5\%$ below the theoretical value. It is concluded that in cases of this type the necessity of using very thin sources, the limited choice of source backing materials, and the nuclear recoil accompanying the first conversion transition do not generally allow one to avoid all perturbative effects.

An oxidized source exhibited complete 'loss of correlation memory'. An explanation of this phenomenon in terms of non-stationary hyperfine-structure interaction is proposed. If the highly charged ions left behind by the first conversion transition have a lifetime similar to that of the intermediate nuclear state, as can happen in a badly conducting course, the progressing neutralization affects the nuclear precession in a random way and thus leads to isotropy.

In contrast to a previous paper on e–e correlations in ^{80}Br (Breitenberger 1956, hereafter referred to as I) the present one describes an experiment undertaken to explore the limitations of angular correlation work with conversion electrons in cases of cascades with a long-lived intermediate state. The well-known nuclide ^{197}Hg seemed best suited for this purpose; the apparatus and experimental method were the same as in I.

§ 1. The Isomerism of ^{197}Hg

Isomerism and decay of ^{197}Hg have been elucidated by Frauenfelder *et al.* (1950), Huber *et al.* (1951) and Mihelich and de Shalit (1953). The isomeric transition, of energy 165·3 kev and half-life 23 hours, is fully converted and is followed by a strongly converted transition of 134·0 kev; the intermediate state has a half-life of 7 or 8 mμ sec (McGowan 1950, Deutsch and Wright 1950). From conversion, K/L ratio and lifetime–energy considerations the two transitions have been classified as M4 and E2 respectively, in perfect agreement with shell theory which predicts the level sequence $i_{13/2}$–$f_{5/2}$–$p_{1/2}$ (Goldhaber and Hill 1952, de Shalit, Huber and Schneider 1952). The ground state decays by K-capture with a half-life of 65 hours to an excited level of ^{197}Au; the subsequent transition to the ground

† Now at Department of Physics, University of Malaya, Cluny Road, Singapore 10.

state of ^{197}Au, of energy 77·4 kev, is strongly converted in the L-, M- and N-shells but not in the K-shell, the K binding energy of gold being 80·7 kev.

The main conversion lines of the ^{197}Hg cascade are :

1_K. . .	82·2	2_K. . .	50·9
1_L. . .	~151	2_L. . .	~120

The electron spectrum from $^{197}Hg + ^{197}Au$ (see Mihelich and de Shalit (1953) for a complete spectrogram) also contains the conversion lines of the 77 kev transition, of energies 63·1–77·0 kev, and some weak lines beyond 110 kev which are due to feeble branching of the K-capture to high-lying levels of ^{197}Au.

Evidently ^{197}Hg is very well suited for an e–e correlation experiment; the 1_K and 2_K lines can be singled out by one broad channel without serious admixture of other coincident radiations. The theoretical coefficients of the K-conversion electron correlation function are found to be

$$a_2 = +0{\cdot}450 \pm 0{\cdot}025, \quad a_4 = +0{\cdot}0320 \pm 0{\cdot}0045 \qquad \ldots\ldots(1)$$

(evaluation method and errors as in I).

§ 2. The Sources

With a long-lived intermediate state such as this it becomes necessary to embed the activity in a cubic, diamagnetic metal in order to avoid quadrupole and hyperfine-structure perturbations. Hence beryllium, with its hexagonal close-packed structure, is here unsuitable. On the other hand, cubic metals of higher Z like copper or silver must be ruled out because of the danger of excessive electron scattering effects. Aluminium remains as the sole practical choice; it is only faintly paramagnetic (atomic susceptibility $+16{\cdot}2 \times 10^{-6}$) and has a cubic face-centred lattice with an interatomic distance of 2·86 Å. Unfortunately, mercury atoms cannot be expected to match this lattice very well. Solid mercury has the A10 structure with interatomic distances of 3·00 and 3·46 Å. These bonds are appreciably longer than those of aluminium; it is therefore not certain that mercury atoms can occupy regular sites in an aluminium host lattice. Moreover, it is well known that the structure of thin metal films always exhibits a certain amount of disorder and strain : see, for instance, Pinsker (1953, chap. 9) and the preliminary reports of a group at the Georgia Institute of Technology (Raudebaugh and Belser 1953, 1954, and accompanying abstracts). Thus there is no guarantee that mercury nuclei contained in an aluminium film are not exposed to any magnetic fields or electric field gradients caused by lattice irregularities.

The activity was produced by (p, n) process in ^{197}Au. The target, a stripe of 'assay' gold (99·998% pure), was bombarded in the Harwell synchro-cyclotron with protons of about 50 Mev. At this energy the barrier penetrability is high enough for the (p, n) process to have a fairly high yield, whereas other reactions like (p, pn), (p, α) etc. do not yet compete too seriously. To the extent that such competing reactions occurred they led to isotopes of gold and the platinum metals, so that the irradiated material contained ^{197}Hg as the only volatile component.

The aluminium base films were prepared in the usual way by evaporation of the metal on to microscope slides which had been covered with a fine layer of yellow soap, floating off on a clean water surface and lifting up on wire frames of ½ in. square. One such film, not more than 1000 Å thick, was mounted in the vaporizer. Filings from the target were put into a little steel oven of 1 cm^3 volume, which had

an exit funnel of 25 mm in length and 1·5 mm in diameter, and could be heated electrically to 1000°C. The filled oven was installed under a radiation shield with the funnel aiming at the centre of the base film, the funnel orifice being kept about 2 cm below the film. After evacuation of the vaporizer the oven was outgassed by slight heating, and a fresh layer of aluminium, a few hundred ångströms thick, was evaporated on to the base film from a nearby tungsten filament. The oven was then heated for 5 minutes to about 100° below the melting point of gold (1063°), and left to cool for 10 minutes. Finally another layer of aluminium, about 1000 Å thick, was evaporated on to the film.

The sources had the appearance of pure aluminium and did not oxidize in air. One of them was later autoradiographed; the active spot appeared as a circle of 3 mm diameter with a sharp boundary.

§ 3. The Pulse Spectrum

The pulse spectrum of a fresh source is shown by the heavy contour in figure 1. The upper part of the spectrum, including the spike on the extreme right caused by amplifier overload, shrinks with a half-life of 23 hours and is therefore due to the isomeric transition. The high peak in the middle could be identified from its decay as being due mainly to the conversion lines of the 77 kev transition in ^{197}Au. Assuming that the maximum of the peak occurs at 70 kev, and that the response of anthracene is linear between 50 and 120 kev, the four conversion lines of ^{197}Hg should occur at the abscissae marked in the figure by arrows. Corresponding

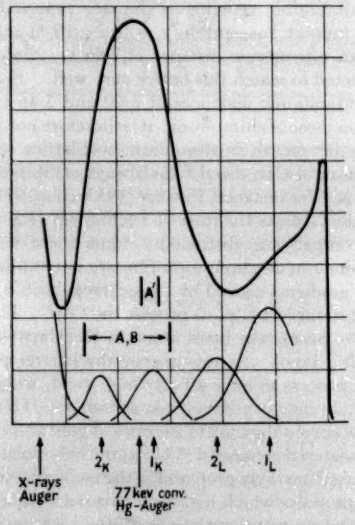

Figure 1. Pulse spectrum of ^{197}Hg+^{197}Au, as observed in an anthracene crystal of 0·6 mm thickness about seven hours after target bombardment.

gaussian pulse height distributions, with the widths calculated from the known spectrometer efficiency and with *relative* heights calculated from the experimental conversion data of Huber *et al.* (1951), can then be drawn in provisionally.

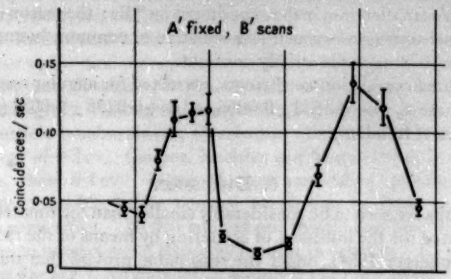

Figure 2. Distribution of coincidences in the pulse spectrum. The scale of abscissae is divided as in figure 1.

The location of these lines was verified by scanning the spectrum for coincidences (cf. I). One of the spectrometers was backed by the channel marked A′ in the figure, and the other by an equally wide channel B′ which was swept over the spectrum. Figure 2 shows the observed distribution of coincidences. Except for some non-linearity in the energy scale the result agrees with figure 1. Accordingly, the best arrangement for the correlation experiment was to set two congruent, wide channels over the interval marked A, B in figure 1.

§ 4. The Anisotropy of the Cascade

On each of three sources the anisotropy $A = W(180)/W(90) - 1$ was measured several times during 48 hours. The sources were inserted at $\epsilon = 135°$; the data taken at $\delta = 90°$ and 180° were corrected for angular resolution under the simplifying assumption that the correlation function contained only a second-order term, and A was then calculated without allowance for scattering effects.

Eleven observations yielded the mean $A = +0{\cdot}651 \pm 0{\cdot}011$. An analysis of variance showed that there was no statistical correlation between the age of a source and its anisotropy, and a χ^2-test showed that the scatter of the eleven values about the mean was consistent, on the 10% level, with their estimated sampling errors. According to (1) the theoretical value of A is about 0·88. Thus perturbations were present, but the observations clearly indicate that these perturbations were the same in all three sources and did not depend on source age.

§ 5. The Full Correlation

The strongest of the three sources was used to measure the complete correlation function. The methods of taking data and of evaluating results were the same as in I, the only difference being that one single source was employed instead of eight. Large decentring errors were not to be expected because the source was so small and homogeneous that it could be centred to within 0·5 mm. About 65 000 coincidences were counted in 38 hours. Afterwards the source was weighed and found to be 60 μg cm^{-2} (2200 Å) thick, with an estimated uncertainty of $\pm$ 10%.

The correlation function exhibited a small fourth-order term which was found by the variance ratio test to be significant on the 2% level. The χ^2-test of goodness of fit indicated a significance of 75%; thus the fit was excellent but not yet *suspiciously* good. The quality of the fit shows that the various extra errors were here appreciably smaller than in the experiment on ^{80}Br; the reason is, presumably, that the channel setting was much less sensitive to common boundary drift, and that the source thickness was strictly constant.

The measured correlation coefficients, corrected for angular resolution but not for scattering, are $a_2' = +0{\cdot}3533 \pm 0{\cdot}0066$, $a_4' = +0{\cdot}0258 \pm 0{\cdot}0081$ (significance of a t of 5 degrees of freedom).

§ 6. Discussion

These results are seen to be considerably smaller than the theoretical values (1). If a_2' is corrected for the influence of scattering by means of the factor given elsewhere (Breitenberger 1954), under the reasonable proviso that this correction is uncertain in a gaussian distribution with standard deviation 0·015, the attenuation factor of the second-order term becomes

$$G_2 = 0{\cdot}822 \pm 0{\cdot}049 \qquad \ldots\ldots (2)$$

(upper limit for the standard error in a nearly gaussian sampling distribution, hence the departure of G_2 from unity is significant on the 0·01% level or better).

Experimental errors alone could not have falsified the correlation so strongly. Coincidences involving the unconverted 134 kev γ-rays can be neglected because these γ-rays are absorbed to only 4% in 0·6 mm anthracene; moreover the relevant Compton distribution, with its edge at 46 kev, lay partly outside the channels. Coincidences involving K x-rays of Hg or Au cannot have been observed at all, the Compton electrons having energies below 20 kev (Hg Kγ lies at 81 kev); likewise all L x-rays were barred from detection by their low energy (Hg Lγ lies at 14 kev). The K$\rightarrow$LL Auger electrons of Hg have energies between 51·9 and 56·6 kev (Mihelich 1952) and thus lay right inside the channels, but they are emitted so seldom that they cannot have caused a significant number of coincidences. Lastly, it is clear from figures 1 and 2 that the admixture of 1_K–2_L coincidences was very small.

Thus the observed attenuation must be ascribed, at least partly, to perturbations of the intermediate state. The absence from the correlation function of terms other than P_2 and P_4 shows that the perturbing fields were oriented randomly (cf. Abragam and Pound 1953), as would be expected for a microcrystalline source. If the attenuation factor (2) is interpreted as resulting from pure quadrupole interaction in randomly oriented, axially symmetric fields of equal strength, the quadrupole frequency $\Delta\nu_Q = (eQ/h)(\partial^2 V/\partial z^2)$ is found from Abragam and Pound's equation (29) to be 3 Mc/s. Of course it cannot be affirmed that the perturbing fields were axially symmetrical and of the same strength for every atom, nor that they were purely electric; weak magnetic perturbation due to deformations of the valency orbitals may well have been present. Only strong hyperfine-structure interaction due to atomic paramagnetism seems altogether implausible.

Lattice irregularities causing perturbing fields presumably existed in the source from the beginning, as mentioned above. However, as a result of the nuclear recoil accompanying the ejection of the first conversion electron these irregularities may have been accentuated, and some new ones created. The recoil energy is

readily calculated to be 0·246 ev. Though small, this amount is by no means insignificant. Seitz (1949) has estimated at 25 ev the energy required to make a Frenkel defect in a faultless lattice, but near dislocations or grain boundaries the irreversible displacement of an atom should be possible with an expenditure of only 5 ev or so; an *impurity* atom, under such circumstances, is still easier to displace from a substitutional to an interstitial position, the required energy being perhaps 1 ev (for up-to-date surveys of the whole subject see Lintner and Schmid (1955), or Seitz and Koehler (1955)). Some experiments reveal even lower displacement energies. Among the many annealing effects which are observed in metals after particle bombardment, Overhauser (1953) found one which had an activation energy of 0·2 ev; Cooper, Koehler and Marx (1954), in a similar case, suspected less than 0·1 ev. Some of these annealing phenomena possibly indicate highly reversible lattice damage which can be done or undone with practically the same effort. In this context one should also bear in mind that the energy required to break a metal lattice by melting is very low; for aluminium the heat of fusion is 85 cal g^{-1}, corresponding to only 0·11 ev per atom. Summing the evidence, it appears not unlikely that a recoil of $\frac{1}{4}$ ev as in the present experiment can produce some lattice damage.

Thus the result of the experiment is rather a negative one. In angular correlation work with conversion electrons the necessity of using very thin sources, the limited choice of cubic metals of low Z for the source backings, and the unavoidable nuclear recoil accompanying the first conversion transition are circumstances under which it is not generally possible to avoid all perturbative effects if the intermediate state has a long lifetime. The conclusion assumes a wider significance if it is regarded in the light of the consistency among three sources : quite generally, consistent behaviour of the sources prepared according to some technique does *not* guarantee the absence of all perturbations.

§ 7. A Case of Attenuation to Isotropy

A fourth source was inadvertently prepared in bad vacuum. This source had a greyish, oxidized appearance and exhibited practically no correlation, its anisotropy being $0{\cdot}023 \pm 0{\cdot}045$.

The phenomenon of 'loss of correlation memory' is not yet understood although it has been extensively discussed (see Frauenfelder 1955, Steffen 1955). Abragam and Pound (1953) have shown that no stationary interaction can altogether destroy the correlation. The reason is, essentially, that steady nuclear precession represents a periodic, but not a random, perturbation of the intermediate state so that the nuclei can never completely lose their information about the direction of the first radiation. Even if the precession periods are much shorter than the lifetime τ_N of the intermediate state a 'hard core' of the correlation remains. With time-dependent interactions the situation is different. A typical example is the quadrupole perturbation caused in a liquid source by the irregular configuration of inactive atoms around every emitting atom. The random relaxation of these instantaneous configurations continually alters the electric field gradients, and thereby interrupts the periodicity of the perturbation in a random way. If the relaxation time is appreciably smaller than τ_N, and if the nuclei precess rapidly enough, the correlation will be wiped out entirely.

It has been noted that in all observed cases of attenuation below the hard core the first radiation was preceded by strong ionization, and the activity was embedded

in a badly conducting medium (see Steffen (1955) and further references given there). Similarly in the present experiment the chain of x-ray, Auger and Coster–Kronig transitions initiated by the expulsion of the first K-conversion electron resulted in a severe depletion of the atomic shell. Calculations on this very complex process of atomic de-excitation have been made by Cooper in 1942; he found that in bromine ($Z=35$) one K-shell vacancy leads on the average to 4·7 vacancies in the outermost shell. In heavy elements such as mercury ($Z=80$) still greater ionization will occur because, although the Auger cross section decreases with rising Z (e.g. Mott and Sneddon 1948, p. 344), the number of possible Auger transitions increases strongly.

When ^{197}Hg is embedded in oxidized, badly conducting aluminium the intense ionization accompanying the first conversion electron cannot be repaired immediately. Thus the life of the intermediate state is spent in a heavily damaged atomic shell. Strong hyperfine-structure interaction will then attenuate the correlation, leaving only the hard core if every ion has a sufficiently strong magnetic moment. However, the shell may not remain in its original state of depletion for any length of time of the order τ_N, and beginning neutralization of the ion would destroy the periodicity of the hyperfine-structure perturbation. Indeed, every recapture of an electron will in general alter both the magnitude and the orientation of the magnetic moment of the atomic shell. The analogy with the relaxation mechanism in liquids is obvious. In order to account for the observed isotropy we only have to assume that the mean lifetime of an ion was comparable with τ_N, that is, roughly 10 mμ sec, and that the average nuclear precession period was one order of magnitude shorter, that is 1 mμ sec, or perhaps less. Such conditions appear to be quite reasonable. The argument still holds good if a small quadrupole perturbation is present at the same time (cf. Abragam and Pound 1953, §VI(A)), and suggests equally reasonable conditions when it is applied to other known cases. Of course, if the initial ions are not as heavily charged as in the present case, or if the neutralization proceeds rather slowly compared with the nuclear de-excitation, one cannot expect the correlation to be destroyed entirely; perhaps one or both of these reasons explain why small residual anisotropies have often been observed with the familiar ^{111}In–^{111}Cd embedded in non-conductors, whereas complete isotropy resulted with ^{197}Hg embedded in a partly oxidized metal.

Acknowledgments

Thanks are due to the Director, Atomic Energy Research Establishment, Harwell, for the permission to make use of the Harwell synchro-cyclotron, and to the cyclotron crew for their efficient collaboration.

Mr. R. H. M. Lamb gave valuable assistance in the preparation of the sources.

This work was begun under a British Council Scholarship, and supported towards its end by grants from the Cavendish Laboratory and from Gonville and Caius College, Cambridge.

References

Abragam, A., and Pound, R. V., 1953, *Phys. Rev.*, **92**, 943.
Breitenberger, E., 1954, *Proc. Phys. Soc.* A, **67**, 1108; 1956, *Ibid.*, **69**, 453.
Cooper, H. G., Koehler, J. S., and Marx, J. W., 1954, *Phys. Rev.*, **94**, 496.
Cooper, J. C., 1942, *Phys. Rev.* **61**, 1.

DEUTSCH, M., and WRIGHT, W. E., 1950, *Phys. Rev.*, **77,** 139.
FRAUENFELDER, H., 1955, *Beta- and Gamma-Ray Spectroscopy*, ed. K. Siegbahn, (Amsterdam : North-Holland), p. 531.
FRAUENFELDER, H., HUBER, O., DE SHALIT, A., and ZÜNTI, W., 1950, *Phys. Rev.*, **79,** 1029.
GOLDHABER, M., and HILL, R. D., 1952, *Rev. Mod. Phys.*, **24,** 179.
HUBER, O., HUMBEL, F., SCHNEIDER, H., DE SHALIT, A., and ZÜNTI, W., 1951, *Helv. Phys. Acta*, **24,** 127.
LINTNER, K., and SCHMID, E., 1955, *Ergebn. exakt. Naturw.*, **28,** in the press.
MCGOWAN, F. K., 1950, *Phys. Rev.*, **77,** 138.
MIHELICH, J. W., 1952, *Phys. Rev.*, **88,** 415.
MIHELICH, J. W., and DE SHALIT, A., 1953, *Phys. Rev.*, **91,** 78.
MOTT, N. F., and SNEDDON, I., 1948, *Wave Mechanics and its Applications*, (Oxford : University Press).
OVERHAUSER, A. O., 1953, *Phys. Rev.*, **90,** 393.
PINSKER, Z. G., 1953, *Electron Diffraction*, (London : Butterworth's Scientific Publications).
RAUDEBAUGH, R. J., and BELSER, R. B., 1953, *Phys. Rev.*, **91,** 449 (A) ; 1954, *Ibid.*, **93,** 930 (A).
SEITZ, F., 1949, *Disc. Faraday Soc.*, **5,** 271.
SEITZ, F., and KOEHLER, J. S., 1955, *Int. Conf. on the Peaceful Uses of Atomic Energy*, Geneva, paper P/749.
DE SHALIT, A., HUBER, O., and SCHNEIDER, H., 1952, *Helv. Phys. Acta.*, **25,** 279.
STEFFEN, R. M., 1955, *Advanc. Phys.*, **4,** 294.

RESEARCH NOTE

Intensities of Bands in the System $b^3\Sigma^+$–$a^3\Pi$ of Carbon Monoxide

By R. F. BARROW, W. B. GRATZER and J. F. MALHERBE
Physical Chemistry Laboratory, University of Oxford

MS. received 31*st January* 1956

§ 1. Introduction

The starting point of this work was the observation of Gaydon (1953) that there appears to be no record of bands with $v' \geqslant 2$ in the $b^3\Sigma^+$–$a^3\Pi$ system of carbon monoxide: if the absence of these bands is due to predissociation, then one would be forced to accept a limit below 10·95 v for the dissociation energy of carbon monoxide.

In fact although it is difficult to prove that a progression of bands is not excited at all, it may be possible, from a study of the intensities of bands within a system, to state that a band is unexpectedly weak. We have therefore examined the intensity distribution among some of the bands of the $b^3\Sigma^+$–$a^3\Pi$ system of carbon monoxide.

§ 2. Intensity Calculation

The intensity of an emission band v', v'' may be written

$$I_{v',v''} = KN_{v'}\nu_{v',v''}{}^4 \left| \int \psi_{v'} R(r) \psi_{v''}\, dr \right|^2$$

where $N_{v'}$ is the number of molecules in the initial state v', $\nu_{v',v''}$ is the energy separation between states v' and v'', $R(r)$ is the electronic transition moment, and K is a constant depending upon the geometry of the system. It is commonly assumed that the electronic transition moment may be taken as constant, so that the intensity becomes proportional to the square of the vibrational overlap integral, $\left| \int \psi_{v'} \psi_{v''}\, dr \right|^2 \equiv p(v', v'')$.

The overlap integrals may be estimated in several ways. We have assumed that the two electronic states in question can adequately be represented by Morse functions, and have evaluated wave functions by numerical integration (details of the procedure are given by Jarmain and Nicholls 1952). The results agree satisfactorily with those obtained by the approximate analytical method of Fraser and Jarmain (1953) in spite of the rather big difference in the magnitudes of the constants for the two states. Values of the molecular constants used are given in table 1, and the results of the calculations in table 2.

Table 1. Molecular Constants

State	$b^3\Sigma^+$	$a^3\Pi$
r_e (Å)	1·088	1·2093
w_e (cm^{-1})	2263·5	1739·5
$x_e w_e$ (cm^{-1})	32·7	14·47

Note. The values of the constants have been taken from Herzberg (1950). Estimates of w_e and $x_e w_e$ for $b^3\Sigma^+$ have been calculated from $\Delta G_{1/2} = 2198$ cm^{-1} and $\alpha = 0{\cdot}033$, using the Pekeris relation (see Herzberg 1950, p. 108 : this relation does not always give very reliable results, but quite a rough estimate of $x_e w_e$ for $b^3\Sigma^+$ suffices for our present purpose).

Table 2. Values of $p(v', v'')$ relative to $p(0, 0)$

v' \ v''	0	1	2	3
2	5·44	0·48	0·66	1·89
1	3·63	3·39	1·23	0·19
	(3·77)			
0	1·00	2·39	3·27	3·35
		(2·32)	(3·14)	(3·26)

Notes : (1) The values in parentheses were obtained by the analytical method.
(2) The actual value of $p(0, 0)$ is 0·058, by numerical integration.

§ 3. Experimental

The $b^3\Sigma^+$–$a^3\Pi$ bands may be excited conveniently in a tube containing a pressure of several millimetres of carbon monoxide, which is surrounded by a coil forming part of a tuned circuit fed with radio-frequency power. Integrated intensities of several bands were determined, using the conventional method of spectrophotometry. Three plates, taken on Hilger small, medium and large quartz spectrographs respectively, were measured. The results (table 3) agree about as closely as would be expected, indicating that there is no serious error arising from the finite resolving power employed.

Table 3. Integrated Band Intensities, relative to 0, 0 Band

Band	Spectrograph		
v', v''	Small Quartz	Medium Quartz	Large Quartz
0, 0	1·00	1·00	1·00
0, 1	1·57	2·00	2·00
0, 2	2·42	2·42	
0, 3		2·67	2·21
1, 0		0·31	
1, 1			0·085
1, 2			0·059
1, 4			0·15

It may be remarked first that the intensities in the $v' = 0$ progression increase more slowly with increasing value of v'' than do the corresponding theoretical probabilities (table 2). This effect may be genuine, and arise from a real variation in the electronic transition moment (see, for example, Poots 1953, Turner and Nicholls 1954).

In order to estimate the intensity of the (unobserved) 2, 0 band with respect to that of the 0, 0 band, we may proceed to determine an effective vibrational temperature from the results for the pairs of bands 1, 0 and 0, 0; 1, 1 and 0, 1; 1, 2 and 0, 2. We obtain 1167°, 829° and 1176°K, respectively, with a mean value of 1060°K. Using this vibrational temperature and the value of $p(2, 0)/p(0, 0)$ given in table 2, it is estimated that the intensity of the 2, 0 band in this particular discharge should be about 0·023 of that of the 0, 0 band; i.e. it should be about forty times weaker.

The system was photographed in a first order of a 2·4 m grating in an Eagle mounting, giving a dispersion of about 7·4 Å mm^{-1} on the plate. The

0, 0 band was distinctly observable after an exposure of 1 minute and the 1, 0 band (which should be about three times weaker than the 0, 0 band) appeared with roughly the same intensity as the 0, 0 band after an exposure of 5 minutes. However, after an exposure of 60 minutes there was no trace of a band in the position expected for a 2, 0 band (the strongest band of the 2, v'' progression). Even on an exposure of 3000 minutes there is found to be little evidence for a violet-degraded band at the correct wavelength: it is however impossible to affirm categorically that there is no trace of emission which could arise from a 2, 0 band, since there is structure both from the 4th Positive system and from a weak feature which may be one of the Kaplan bands (Kaplan 1930).

§ 4. Conclusions

It is concluded that bands with $v'=2$ in $b^3\Sigma^+$–$a^3\Pi$ are, if not absent, definitely weaker than expected. If this effect arises from a predissociation, then, by extrapolating to the expected position of $v'=2$ in $b^3\Sigma^+$, $D_0(CO)\leqslant 88262\,cm^{-1}$ or $\leqslant 10{\cdot}94$ ev.

It is not easy to reconcile this with the interpretation of the well-established predissociations in the state $B^1\Sigma^+$ (Douglas and Møller 1955), which give a dissociation limit at 89595 cm^{-1}.

If the limit from $B^1\Sigma^+$ is correct, it has to be assumed that the non-appearance of bands with $v'=2$ in $b^3\Sigma^+$ arises from the effects of perturbations, known already in $v'=0$ and 1 (Dieke and Mauchley 1933, Beer 1937). It is, however, difficult to see how such perturbations would lead to the total suppression of the 2, 0 band, and it seems therefore that there is a real anomaly here. A further study of the levels in $b^3\Sigma^+$, both from the $b^3\Sigma^+$–$a^3\Pi$ system, and perhaps from the $b^3\Sigma^+$–$x^1\Sigma^+$ system, with ^{12}CO and ^{13}CO, seems desirable.

References

Beer, B. S., 1937, *Z. Phys.*, **107**, 73.

Dieke, G. H., and Mauchley, J. W., 1933, *Phys. Rev.* **43**, 12.

Douglas, A. E., and Møller, C. K., 1955, *Canad. J. Phys.*, **33**, 125.

Fraser, P. A., and Jarmain, W. R., 1953, *Proc. Phys. Soc.* A, **66**, 1145.

Gaydon, A. G., 1953, *Dissociation Energies* (London : Chapman and Hall).

Herzberg, G., 1950, *Spectra of Diatomic Molecules* (New York : Van Nostrand).

Jarmain, W. R., and Nicholls, R. W., 1952, *University of Western Ontario Science Report*, No. 4. Contract No. AF 19(122)-470.

Kaplan, J., 1930, *Phys. Rev.*, **35**, 1298.

Poots, G., 1953, *Proc. Phys. Soc.* A, **66**, 1181.

Turner, R. G., and Nicholls, R. W., 1954, *Canad. J. Phys.*, **32**, 469, 475.

REVIEWS OF BOOKS

Methods of Mathematical Physics, 3rd Edn, by SIR HAROLD JEFFREYS and BERTHA SWIRLES (LADY JEFFREYS). Pp. xii + 714. (Cambridge: University Press, 1956). 84*s*.

When the first edition of this monumental work was issued in 1946 it was fully reviewed in these *Proceedings*, 1947, **59**, 512. Since then a second edition in 1950 corrected a few minor errors, and added some 50 pages of new material. The fact that a third edition is now called for is a tribute to the uniqueness of this book, and the fact that hardly any changes are now required is a tribute to its excellence. The first reviewer said of it that " it is a book of quite exceptional importance ". The present reviewer can merely echo these words. For this account of the methods of mathematical physics is still magnificent in its scope and architecture. There must be very few major techniques in theoretical physics which are not explained here, and illustrated by some genuine example. It remains, and is likely to continue for many years, an almost indispensable work of reference for anyone attempting research in theoretical physics. Even its price, which seems pretty high, is not altogether unreasonable. There will not be many of the people for whom this book is intended who would not save themselves four guineas' worth of time by possessing it.

C. A. COULSON.

Nuclear Stability Rules, by N. FEATHER. Pp. ix + 162. (Cambridge: University Press, 1952.) 20*s*.

This book was written just at the time when the nuclear shell model was invented; too late to influence that dramatic break-through, too early to take it into account. But precisely for that reason it is less likely to be out-dated soon than if it had been written at any other time. For, as the author points out, theories change while facts remain. The value of this immensely thorough compilation lies precisely in that it presents the facts uncoloured by theory, or at least by any of the more transitory forms of theory. The book is not concerned much with the excited states of nuclei, of which our knowledge has grown greatly during the last years; of the ground state of nuclei it still is, and will be for some time, a valid and most valuable presentation. The style may appear laboured in places, but the precision of expression achieved may well set an example to some who write a more readable but less accurate language.

O. R. FRISCH.

Introductory Nuclear Physics, by D. HALLIDAY. 2nd Edn. Pp. x + 493. (New York: John Wiley; London: Chapman and Hall, 1955.) 60*s*.

This, the second edition of a well-known textbook, will be examined with interest by every teacher of nuclear physics.

About half of the book is devoted to classical nuclear physics—basic ideas about nuclei, radioactive decay, the passage of radiation through matter, and the

detection of radiation. The second half discusses the more vital topics—nuclear structure, reactions, fission, spin, magnetic moment, cosmic rays, and so on.

Several important changes have been made in this new edition. Very many quite recent developments have been included so that the book is really up to date. Thus there are references to the ' cloudy crystal ball ' and the collective models, to Coulomb excitation experiments, to stripping reactions, and to recent studies of the time dependence of cosmic rays. A chapter has been added on elementary quantum mechanics; this seems hardly necessary.

The treatment of nuclear reactions rightly avoids complications due to spin, though this has led the author into a misleading definition of scattering (p. 313). The " conservation of statistics theorem " is introduced as if it were an accident (p. 381) and not a logical consequence of quantum mechanics. Many proofs are quite properly relegated to an appendix, while others are just quoted without full development; there is sometimes a certain inconsistency in what is chosen to be proved and what is quoted which is hardly conducive to clarity in a teaching text. It is, moreover, surprising to find that there are 43 pages about the experimental measurement of nuclear spins and magnetic moments, and very little reference to the theoretical interpretation of these results.

The book is in plan essentially an undergraduate text, though in many parts it is useful for a research student. It will surely appeal to both classes of readers though the English undergraduate may find some sections too advanced, and the research student would be advised to remember the first word of the book's title.

A. V. COHEN.

Annual Review of Nuclear Science, Vol. 3, 1953. Pp. ix + 412. Edited by J. G. BECKERLEY, M. D. KAMEN, D. F. MASTICK and L. I. SCHIFF. (Stanford : Annual Reviews, 1953.) $7.00.

A review article should serve two main purposes; it should provide the specialist with an organized account of recent advances in his own subject and it should offer the specialist in another subject an opportunity of interesting himself in a new field. Most of the topics covered by the *Annual Reviews of Nuclear Science* are rapidly developing and the expert may find that the reviews which most closely interest him depreciate sharply in value after a few years. This is not necessarily true for the more general reader, particularly if the articles give broad comment as well as detailed information. Most of the chapters of the present volume were completed early in 1953 and some of the subjects have already been treated again (Vols. 4 and 5).

Rather less than half the book is concerned with nuclear physics and the remainder with related subjects. E. M. Henley, M. A. Ruderman and J. Steinberger discuss the ' Reactions of π-mesons with Nuclei '; they give a good account of the theory of isotopic spin and a clear treatment of π-nucleon scattering, but they were not able to include the important results now available from the Brookhaven Cosmotron. Similarly the report by L. Leprince-Ringuet on ' Mesons and Heavy Unstable Particles in Cosmic Rays ' although able to present details of the Bagnères Congress of 1953, was written before the operation of the Berkeley Bevatron had revealed properties of K-particles. D. R. Corson and A. O. Hanson write on the ' Extranuclear Interactions of

Electrons and Gamma Rays', from an experimental point of view and show how accurate experiments have verified the details of the theory particularly in respect of ionization loss, pair production and bremsstrahlung. A very readable article by D. J. Hughes surveys the general methods and application of neutron optics. The standardization of measurements of energy and intensity of neutrons of all velocities is an important matter and is fully discussed in an article by A. Wattenberg. Another mainly technical article which will still be widely found useful is that by Y. Goldschmidt-Clermont on nuclear emulsions; it deals with processing, range–energy relations, multiple scattering and improvements in microscope techniques.

Four chapters are primarily chemical. J. L. Magee describes the elementary processes of radiation chemistry and J. E. Willard the chemical effects of nuclear transformations, of which the Szilard–Chalmers' process is the best known example. P. C. Stevenson and H. G. Hicks contribute a short chapter on 'Separation Techniques used in Radiochemistry' in which the methods of ion exchange and paper chromatography are perhaps too briefly treated. Isotopic substitution, using both stable and active nuclei, is an important method of chemical investigation and recent applications of the H, C, O, S and Hg isotopes are described by P. E. Yankwich (Isotope Effects in Chemical Reactions).

The remaining chapters are concerned directly or indirectly with the biological effects of radiation. In 'Radiation Dosimetry and Protection', L. D. Marinelli discusses the physical methods of dosage estimation for neutrons and photons. R. Hugh (Vertebrate Radiobiology; Embryology) gives evidence from studies with fowl, fish and mammal that the embryo is more radiosensitive than the adult animal. The effect of radiation on various organs of the body is described by J. Furth and A. C. Upton (Vertebrate Radiobiology; Histopathology and Carcinogenesis) while the physico-chemical processes leading to cell damage are treated by A. H. Sparrow and F. Forro, Jr. (Cellular Radiobiology) in an article which also discusses possible means of modifying the radiosensitivity of cells. Finally, in a chapter entitled 'Practical Aspects of Radiation Injury', L. H. Hempelmann and J. G. Hoffman give a graphic description of the progress of acute radiation sickness based on actual case histories.

This volume, like its predecessors, has been carefully produced and includes very full lists of references.

W. E. BURCHAM.

CONTENTS OF SECTION B

PAGE

Mr. J. B. Arthur, Dr. A. F. Gibson and Mr. J. B. Gunn. Carrier Accumulation in Germanium 697

Mr. J. B. Arthur, Dr. A. F. Gibson and Mr. J. B. Gunn. Current Gain at L–H Junctions in Germanium 705

Mr. D. Haneman. Current Gain in Formed Point Contact n-type Germanium Transistors 712

Dr. J. B. Birks and Mr. F. D. Brooks. Scintillation Response of Anthracene to 6–30 kev Photoelectrons 721

The late Prof. N. A. V. Piercy, Dr. E. G. Richardson and Dr. H. F. Winny. On the Convection of Heat from a Wire moving through Air close to a Cooling Surface 731

Dr. R. A. Hyman. The Electrical Conductivity of Hexagonal Selenium . . 743

Dr. P. T. G. Flynn. The Discharge Mechanism in the High-Vacuum Cold-Cathode Pulsed X-ray Tube 748

Research Notes:

Dr. P. T. Landsberg. Note on turnover in Germanium Contacts . . 763

Mr. B. V. Paranjape. Polarization of the Continuous Spectrum in a Gas Discharge 765

Letters to the Editor:

Prof. L. G. H. Huxley. Electronic Motion in Gases and the Method of Free Paths 769

Dr. R. A. Hyman. Bending of Single Crystals of Selenium 771

Reviews of Books 773

Contents of Section A 780

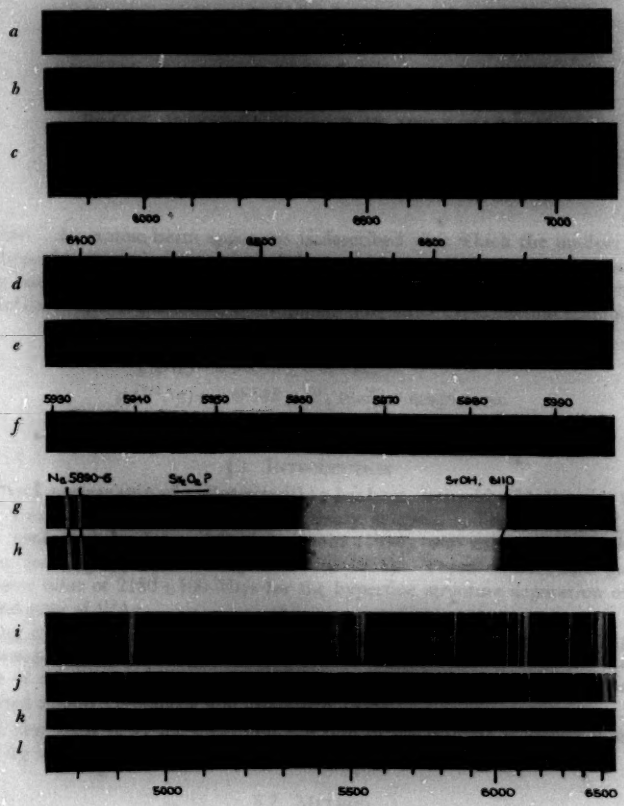

Spectra *d*, *e*, *g* and *h* were taken with the glass Littrow spectrograph, and spectrum *f* on the 21-ft concave grating ; the remainder were taken with the medium glass instrument. Spectra *a*, *b*, *c* and *f* were taken on Ilford Long Range Spectrum plates, and the remainder on Ilford Astra III.

a. Strontium carbonate in arc in air (graphite poles).
b. Strontium carbonate in vacuum arc in heavy-water vapour (D_2O).
c. Strontium carbonate in vacuum arc in water vapour (H_2O). Fe arc below.
d. Strontium nitrate (on moistened filter paper) in oxy-hydrogen flame. Fe arc above.
e. Strontium carbonate in arc in air. Fe arc above.
f. Strontium nitrate in arc in air. Grating spectrograph.
g. Saturated solution of strontium nitrate sprayed into oxy-hydrogen flame. Exposure $\frac{1}{2}$ min. Wide slit, 0·1 mm.
h. Dilute solution (1/6 saturated) of strontium nitrate sprayed into same flame. Exposure 3 min.
i Barium nitrate in arc in air.
j Barium metal on carbon poles in vacuum arc in water vapour (H_2O).
k Barium metal in vacuum arc in heavy-water vapour (D_2O).
l Barium nitrate in oxy-hydrogen flame. Fe arc below.

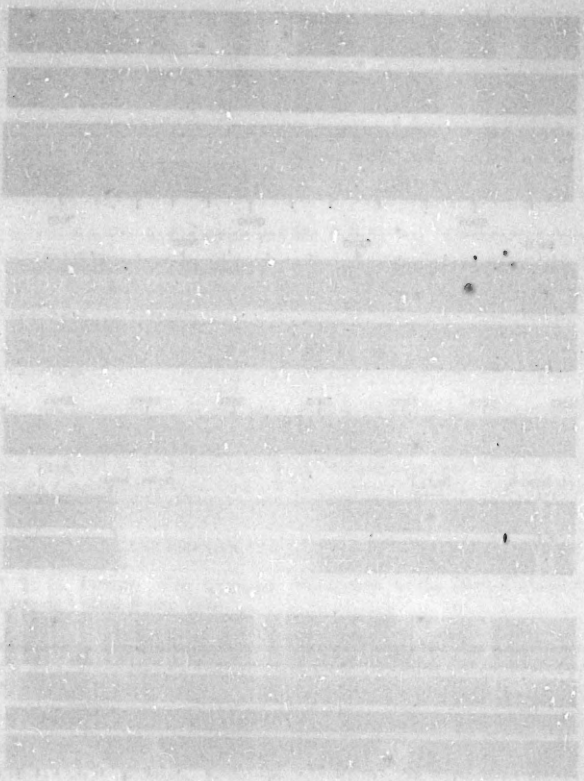

Hyperfine Structure of Radioactive Silver $^{111}_{47}Ag$

By G. K. WOODGATE and R. W. HELLWARTH†
Clarendon Laboratory, Oxford

Communicated by H. G. Kuhn; MS. received 9th March 1956

Abstract. An atomic-beam apparatus is described with which the nuclear spin and hyperfine structure separation of the ground state of the radioactive isotope $^{111}_{47}Ag$ have been found. The nuclear spin is $I=\frac{1}{2}$, in agreement with the result of McGinnis and of Lemonick and Pipkin. The other experimental results are:

$$\Delta\nu(^{111}Ag)=2204{\cdot}54\pm0{\cdot}05 \text{ Mc/s},$$
$$g_J(Ag)=2{\cdot}00235\pm0{\cdot}00012,$$
$$\mu_I(^{111}Ag)=-0{\cdot}145\pm1\% \text{ nuclear magnetons.}$$

§ 1. Introduction

The nuclear spin of radioactive $^{111}_{47}Ag$ has been derived by McGinnis (1948) from an analysis of the nuclear decay scheme. The value $I=\frac{1}{2}$ was confirmed by Lemonick and Pipkin (1954), who used an atomic beam of the focusing type (Friedburg and Paul 1951). These authors also gave a tentative value of 2180 ± 100 Mc/s for the hyperfine structure separation of the ground state of $^{111}_{47}Ag$.

Our experiment was begun concurrently with that of Lemonick and Pipkin, but was pursued, after the publication of their tentative result, until an accurate value of the hyperfine structure was obtained. The results have been briefly reported already (Woodgate and Hellwarth 1955).

A new value of g_J for silver and the sign of the nuclear magnetic moment of $^{111}_{47}Ag$ were also derived from this experiment.

§ 2. Method

The magnetic resonance method of atomic beams developed by Rabi and his collaborators has been fully described in the literature (Kusch, Millman and Rabi 1940, Zacharias 1942). Our apparatus has been built with the purpose of measuring nuclear spins and hyperfine structures of the ground states of radioactive isotopes.

The method for measuring the nuclear spin I and the hyperfine structure separation $\Delta\nu$ of $^{111}_{47}Ag$ is the same as that described by Bellamy and Smith (1952). We shall use the notation of these authors in this paper, but shall not repeat the formulae because the method is now so widely used.

The apparatus is arranged in a conventional 'flop-in' manner, in which the gradients of A and B fields are in the same direction. For a $^2S_{1/2}$ ground state, atoms which have undergone a transition designated by $m_J=+\frac{1}{2}\longleftrightarrow m_J=-\frac{1}{2}$ are 'refocused' at a detector located on the axis of the beam; these atoms

† Now at Hughes Research Laboratories, Culver City, California.

contribute to a maximum of beam intensity superimposed on the minimum of the Stern–Gerlach pattern formed by unperturbed atoms.

The value of the C field, H (or rather the parameter $y=\mu_0 H/h$ Mc/s), in this experiment was measured with a beam of $^{39}_{19}$K, for which $I=3/2$ and μ_I is positive. The transition used for this purpose was $F=2$, $m=-1\longleftrightarrow-2$, which is a field-dependent π line. Since silver and potassium are both in a $^2S_{1/2}$ ground state, the behaviour of the energy levels in a magnetic field is described by the Breit–Rabi formula (Breit and Rabi 1931). The following values of the constants associated with $^{39}_{19}$K were used in evaluating y: $\Delta\nu=461{\cdot}723\pm0{\cdot}010$ Mc/s (Kusch and Taub 1949); $g_J=2{\cdot}00228\pm0{\cdot}00002$ (Franken and Koenig 1952); $g_I=-1{\cdot}419\times10^{-4}$ (Brun *et al.* 1954).

The frequency of the π line ($F=1$; $m=1\longleftrightarrow0$) of $^{111}_{47}$Ag was measured at low and intermediate fields (ν_1 in figure 1); this labelling of m assumes a

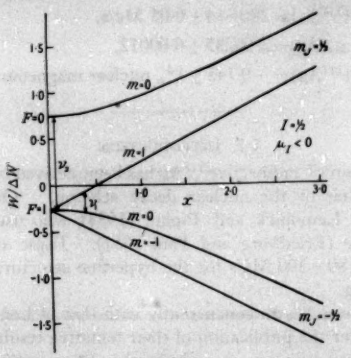

Figure 1.

negative sign for the nuclear magnetic moment of $^{111}_{47}$Ag. From the results the nuclear spin was confirmed, and an estimate of $\Delta\nu$ was made in the usual way. An accurate value of $\Delta\nu$ was found by measuring the frequency of the σ line ($F=0\longleftrightarrow F=1$; $m=0$) near zero field, where the frequency is independent of field to first order (ν_2 in figure 1).

§ 3. Apparatus and Experimental Procedure

We include in this section, not a full account, but only certain details of experimental procedure which we have found useful.

The vacuum envelope which is a brass cylinder ten inches in diameter is divided into three chambers, separately pumped, containing the ovens, the magnets and the detectors. The wall separating magnet- and detector-chambers is provided with a gate-valve so that the latter chamber may be opened to atmospheric pressure without affecting the vacuum in the rest of the system. The customary separating chamber, independently pumped, between ovens and magnets is omitted in order to shorten the path of the beam between oven and detector, which is about 40 cm. However, the opening which connects the oven- and magnet-chambers is in the form of a narrow rectangular tube which allows free passage of the beam but impedes the residual gas molecules in their path between the two chambers.

The oven for evaporating silver was made of tantalum. It had a channel $\frac{1}{2}$ in. long and 0·010 in. wide to conserve material, and was heated by electron bombardment. The operating temperature was in the region of 1000°c, and was kept steady during a run by manual adjustment. The oven was loaded with about 5 millicuries of $^{111}_{47}Ag$ mixed with about 10 mg of stable silver. It could be removed from the apparatus and replaced quickly and safely without disturbing the heating element. The $^{111}_{47}Ag$, which is a β-emitter with a half-life of 7·5 days, was obtained by irradiation of $^{110}_{46}Pd$ with neutrons in the Harwell pile. This was mixed with stable silver, separated chemically from the palladium and its other products, and electroplated on a thin platinum foil which was inserted in the well of the oven. It is probable that a good deal of the silver was lost in the oven by alloying with the tantalum.

Before each run the apparatus was lined up with a potassium beam. After removing all slits from the path of the beam, one could observe the image of the slit of the potassium oven through a telescope fitted with crosswires and mounted on the axis of the beam at the detector end of the apparatus. The slit of the silver oven, nearly at its operating temperature, could then be brought into the same position while it was being observed through the telescope.

The collimator slit was 0·010 in. wide. Another slit 0·008 in. wide was situated immediately in front of the target, on which the beam of silver was deposited, in order to exclude from the target the side peaks of the Stern–Gerlach pattern. These side peaks occurred about 0·012 in. from the axis of the beam. The detector slit was lined up by means of a potassium beam with all magnets off. We noticed that a refocused potassium resonance peak was of no use for this purpose because the peak was 0·003 in. off axis. The effect was attributed to a second derivative of the magnetic field across the gaps of the deflecting magnets. The 'flop-in' deflecting system was therefore not symmetrical, and caused different trajectories of the potassium beam to be refocused at different positions in the plane of the detector. Because the trajectories of silver atoms were less expanded than those of potassium atoms, the effect produced a resonance peak for silver less than 0·001 in. off axis.

The target for silver was a strip of aluminium foil 0·001 in. thick wrapped round a cylindrical liquid-air trap. The strip was divided into 26 marked sections each of which could be exposed in turn to the beam by rotating the liquid-air trap. A whole resonance curve was scanned before the targets were removed, cut up into sections, and counted in a 4π Geiger counter. A counting rate of between 200 and 300 counts per minute was typical for an undeflected beam of silver deposited for two minutes. With the same time of deposition a resonance peak was often 30 counts per minute above the background caused by fast atoms in the Stern–Gerlach pattern. During a run deposits were made with the radio frequency on and off alternately. A stop-wire was provided for preventing fast atoms on the axis of the beam from reaching the detector, and so contributing to the background. However, it was not used in this experiment because the difference in counting rate with radio frequency on and off was relatively large; also, the counting rate with radio frequency off gave a useful indication of the constancy of vapour pressure in the oven during a run.

The deflecting magnets, which were of the usual design with soft-iron pole pieces, gave a ratio of gradient to field of 3:1 per cm. The windings were insulated with coating Araldite. All three magnets were excited from a 2 v 10 000 ampere-hour submarine battery. The C field drifted linearly with time

during a run, and corrections were made to frequency readings by interpolation.

A coaxial radio-frequency loop of rectangular cross section was used to excite σ transitions. This loop gave a double-peaked resonance curve as described by Woodgate and Hellwarth (1956). For exciting π transitions an unshielded radio-frequency loop $\frac{1}{8}$ in. long was used. With this loop the theoretical half-intensity width at optimum radio-frequency power is about 130 kc/s for both potassium and silver. The line width observed with silver was about 240 kc/s and over 300 kc/s with potassium. The large widths can be attributed to the effect of a field gradient in the vertical direction in the C magnet. This gradient was measured with the aid of a narrow horizontal slit which limited the height of a potassium beam to one-tenth of its usual height, which was 5 mm. When this slit was moved up and down under vacuum to select different vertical sections of the beam, the peak frequency of a narrow symmetrical line obtained with a small double loop (Ramsey 1949) shifted by the expected amount. It was possible almost to eliminate the effect of longitudinal field inhomogeneities by adjusting the A and B fields which strayed into the C magnet, and by moving the radio-frequency loop into a direction parallel to the beam.

Power oscillators made in the laboratory were used to excite the radio-frequency field. Low frequencies were measured with a BC 221 wavemeter. High frequencies were measured with a Marconi T.F. 723A crystal calibrator in conjunction with a Hallicrafters SX 28 communications receiver. These instruments were calibrated from a frequency standard, and the precision of frequency measurement was about ± 2 kc/s.

§ 4. Results

In the table are given the resonance frequencies ν_1 observed in the line $F=1$, $m=1\longleftrightarrow 0$ of $^{111}_{47}$Ag at a magnetic field corresponding to the frequencies of the line $F=2$, $m=-2\longleftrightarrow -1$ of $^{39}_{19}$K.

ν (^{39}K) (Mc/s)	$7{\cdot}50\pm 0{\cdot}05$	$460{\cdot}000\pm 0{\cdot}00$	$460{\cdot}000\pm 0{\cdot}00$
ν_1 (^{111}Ag) (Mc/s)	$14{\cdot}38\pm 0{\cdot}050$	$428{\cdot}390\pm 0{\cdot}025$	$428{\cdot}415\pm 0{\cdot}025$

The first measurement confirmed that for $^{111}_{47}$Ag $I=\frac{1}{2}$, since $\nu_1(^{111}\text{Ag})=2\nu(^{39}\text{K})$ except for a small discrepancy introduced by second-order terms in the field. A search was made for resonances at frequencies corresponding to other half-integral values of $I(^{111}\text{Ag})$ but none was found. Several intermediate field measurements not shown in the table led to better and better estimates of $\Delta\nu(^{111}\text{Ag})$ as the field was increased.

The pair of measurements at $\nu(^{39}\text{K})=460$ Mc/s were made as accurately as possible. They are quoted in the table in a form corrected for drift of the C field, and normalized to a value of exactly 460 Mc/s for $\nu(^{39}\text{K})$, the experimental limits of error being lumped together and appended to the value of $\nu_1(^{111}\text{Ag})$.

The resonance curve of $\nu_1(^{111}\text{Ag})=428{\cdot}39$ Mc/s is plotted in figure 2. The vertical bars on each point represent statistical errors of counting after the counting rate of the background (with radio frequency off) has been subtracted from that with radio frequency on. The horizontal bars represent equivalent errors generated by the experimental uncertainty in $\nu(^{39}\text{K})$ when this frequency is taken to be exactly 460 Mc/s. In the absence of reasons for assigning unequal weights to the last two values of $\nu_1(^{111}\text{Ag})$ in the table, the mean value of $\nu_1(^{111}\text{Ag})$ is taken to be $428{\cdot}403\pm 0{\cdot}025$ Mc/s when $\nu(^{39}\text{K})=460$ Mc/s exactly. The

quoted limits of error are arbitrarily chosen owing to the lack of a large body of data; they correspond to the possibility of finding the peak of a resonance line to within about one-tenth of the half-intensity width. This value of $\nu_1(^{111}\mathrm{Ag})$ led to an estimated value of $\Delta\nu(^{111}\mathrm{Ag})$ of about 2203 Mc/s.

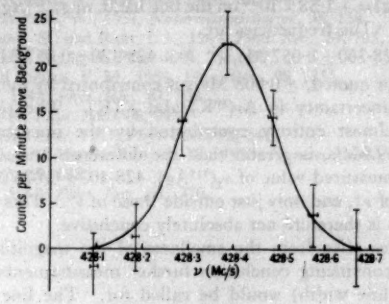

Figure 2.

The frequency of the σ line $F=1\longleftrightarrow 0$, $m=0$ which is independent of field to first order was measured at a magnetic field of 2·3 oersteds. The measured frequency $\nu_2=2204{\cdot}55\pm 0{\cdot}05$ Mc/s gives a value for the hyperfine structure separation of $^{111}_{47}\mathrm{Ag}$:

$$|\Delta\nu(^{111}\mathrm{Ag})|=2204{\cdot}54\pm 0{\cdot}05\ \text{Mc/s}.$$

The quantities

$$\Delta\nu(^{111}\mathrm{Ag})=2204{\cdot}54\pm 0{\cdot}05\ \text{Mc/s},\quad \nu_1(^{111}\mathrm{Ag})=428{\cdot}403\pm 0{\cdot}025\ \text{Mc/s}$$

and

$$y=367{\cdot}992\pm 0{\cdot}006\ \text{Mc/s}$$

(corresponding to $\nu(^{39}\mathrm{K})=460{\cdot}000$ Mc/s) were substituted in the Breit–Rabi formula. Two unknown quantities remain, namely $g_J(\mathrm{Ag})$ and $g_I(^{111}\mathrm{Ag})$. From the ratio of the hyperfine structure splittings of $^{111}_{47}\mathrm{Ag}$ and $^{109}_{47}\mathrm{Ag}$ and from the nuclear magnetic moment of the latter, the magnitude of $g_I(^{111}\mathrm{Ag})$ can be found if the hyperfine structure anomaly (Bohr and Weisskopf 1950) is ignored. $\Delta\nu(^{109}\mathrm{Ag})$ and $g_I(^{109}\mathrm{Ag})$ are known from the work of Wessel and Lew (1953) and Brun *et al.* (1954) respectively. The magnitude of $g_I(^{111}\mathrm{Ag})$ is $1{\cdot}58\times 10^{-4}$. Substitution of $g_I=\pm 1{\cdot}58\times 10^{-4}$ leads to two values of $g_J(\mathrm{Ag})$: for $g_I>0$, $g_J(\mathrm{Ag})^+=2{\cdot}00242\pm 0{\cdot}00014$, for $g_I<0$, $g_J(\mathrm{Ag})^-=2{\cdot}00258\pm 0{\cdot}00014$. These are to be compared with the value given by Wessel and Lew:

$$g_J(\mathrm{Ag})=2{\cdot}00224\pm 0{\cdot}00020.$$

We conclude therefore that $g_I(^{111}\mathrm{Ag})$ is positive, leading to a value

$$\mu_I(^{111}\mathrm{Ag})=-0{\cdot}145\ \text{nuclear magnetons},$$

accurate to about 1% if a hyperfine structure anomaly is not ignored. As an indication of the size of the anomaly to be expected, that for the stable isotopes of silver is $-0{\cdot}416\pm 0{\cdot}008\%$ (Wessel and Lew 1953).

A new value of $g_J(\mathrm{Ag})$ is taken to be the weighted mean of our $g_J(\mathrm{Ag})^+$ and the value given by Wessel and Lew. It is $g_J(\mathrm{Ag})=2{\cdot}00235\pm 0{\cdot}00012$. This value is slightly different from that quoted in our previous publication (Woodgate and Hellwarth 1955).

§ 5. Discussion of Results

The problem of determining the sign of g_I may be reformulated as follows: assuming that $g_J(\mathrm{Ag}) = 2{\cdot}00224 \pm 0{\cdot}00020$ as given by Wessel and Lew, we need to know what values of $\nu_1(^{111}\mathrm{Ag})$ at a value of $y = 367{\cdot}992 \pm 0{\cdot}006$ Mc/s would be consistent with $g_I(^{111}\mathrm{Ag}) = +1{\cdot}58 \times 10^{-4}$ on the one hand, or $g_I(^{111}\mathrm{Ag}) = -1{\cdot}58 \times 10^{-4}$ on the other hand. The frequencies are

$$\nu^+ = 428{\cdot}360 \pm 0{\cdot}057 \text{ Mc/s}, \quad \nu^- = 428{\cdot}320 \pm 0{\cdot}057 \text{ Mc/s}.$$

In the limits of error quoted, $\pm 0{\cdot}008$ Mc/s is contributed by the uncertainty in y arising from the uncertainty in $\Delta\nu(^{39}\mathrm{K})$ and $g_J(\mathrm{K})$. The remaining figure, $\pm 0{\cdot}049$ Mc/s, is almost entirely contributed by the uncertainty in $g_J(\mathrm{Ag})$. This number, 0·049 Mc/s, is greater than the difference $\nu^+ - \nu^-$, which is only 0·040 Mc/s. Our measured value of $\nu_1(^{111}\mathrm{Ag})$, $428{\cdot}403 \pm 0{\cdot}025$ Mc/s, lies within the limits of error of ν^+, and only just outside those of ν^-. This evidence for the choice of sign of g_I is therefore not absolutely conclusive.

These difficulties arise from the smallness of the magnitude of $g_I(^{111}\mathrm{Ag})$. To reach a more convincing conclusion further measurements with increased precision (narrow line width) would be called for. The line width in these experiments was limited by magnetic field inhomogeneities in the interaction region, as described in § 3.

In spite of the large line widths, the resonance curves were symmetrical and it was possible to find the peak frequencies to the accuracy quoted. If the curves are shifted bodily by the field inhomogeneity, one would expect both potassium and silver lines to be shifted in the same direction. A relatively large shift would have to be postulated to reconcile the measured values with $\mu_I(^{111}\mathrm{Ag}) > 0$ because only second-order field dependence would affect the calculated result.

The negative sign of the nuclear magnetic moment of $^{111}_{47}\mathrm{Ag}$ agrees with the theory of nuclear shell structure, which would not predict this sign to differ from that of the moments of the two stable silver isotopes. For reference we tabulate here the results for the three isotopes of silver so far investigated.

Isotope	I	$\Delta\nu$(Mc/s)	μ_I(n.m.)	h.f.s. anomaly (%)
$^{107}_{47}\mathrm{Ag}$	$\frac{1}{2}$	$-1712{\cdot}56 \pm 0{\cdot}04$	$-0{\cdot}113014 \pm 0{\cdot}000004$	$-0{\cdot}416 \pm 0{\cdot}008$
$^{109}_{47}\mathrm{Ag}$	$\frac{1}{2}$	$-1976{\cdot}94 \pm 0{\cdot}04$	$-0{\cdot}129924 \pm 0{\cdot}000004$	
$^{111}_{47}\mathrm{Ag}$	$\frac{1}{2}$	$-2204{\cdot}54 \pm 0{\cdot}05$	$-0{\cdot}145 \pm 1\%$	—

Our value for the hyperfine structure separation of $^{111}_{47}\mathrm{Ag}$ is sufficiently accurate for a determination of the hyperfine structure anomaly when $\mu_I(^{111}\mathrm{Ag})$ can be measured accurately by some other method.

Acknowledgments

One of us (G. K. W.) is indebted to Imperial Chemical Industries for a Research Fellowship and the other (R. W. H.) to the Rhodes Trust for the grant of a scholarship. We should also like to thank the Royal Society for a grant from the Paul Instrument Fund towards the cost of the apparatus, Dr. P. F. D. Shaw for instruction and assistance in the chemical separation of radioactive isotopes, and Mr. W. Sandford for his skill in machining the parts for the apparatus.

References

Bellamy, E. H, and Smith, K. F., 1952, *Phil. Mag.*, **44**, 33.
Bohr, A., and Weisskopf, V. F., 1950, *Phys. Rev.*, **77**, 94.
Breit, G., and Rabi, I. I., 1931, *Phys. Rev.* **38**, 2082.
Brun, E., Staub, H. H., Oeser, J., and Telschow, C. G., 1954, *Phys. Rev.*, **93**, 172.
Franken, P., and Koenig, S., 1952, *Phys. Rev.*, **88**, 199.
Friedburg, H., and Paul, W., 1951, *Naturwissenschaften*, **38**, 159.
Kusch, P., Millman, S., and Rabi, I. I., 1940, *Phys. Rev.*, **57**, 765.
Kusch, P., and Taub, H., 1949, *Phys. Rev.*, **75**, 1477.
Lemonick, A., and Pipkin, F. M., 1954, *Phys. Rev.*, **95**, 1356.
McGinnis, C. L., 1948, *Phys. Rev.*, **81**, 734.
Ramsey, N. F., 1949, *Phys. Rev.*, **76**, 996.
Wessel, G., and Hin Lew, 1953, *Phys. Rev.*, **92**, 641.
Woodgate, G. K., and Hellwarth, R. W., 1955, *Nature, Lond.*, **176**, 395; 1956, *Proc. Phys. Soc.* A, **69**, 588.
Zacharias, J. R., 1942, *Phys. Rev.*, **61**, 270.

Shape of Resonance Curves in Atomic Beam Experiments

By G. K. Woodgate and R. W. Hellwarth
Clarendon Laboratory, Oxford

Communicated by H. G. Kuhn; MS. received 9th March 1956

Abstract. In magnetic resonance experiments with atomic beams an atom is often exposed to a radio-frequency field whose amplitude varies along the path of the beam. To obtain an estimate of the shape of the resonance line to be expected with various radio-frequency loops, the Fourier transform of a function resembling the amplitude of the radio-frequency field has been taken in each case. These transforms are compared with experimental curves, and qualitative agreement is found.

§ 1. Introduction

In the course of a magnetic resonance experiment with an atomic beam (Woodgate and Hellwarth 1955) we have had occasion to use various forms of radio-frequency loop for exciting σ transitions ($\Delta m = 0$). The resulting resonance curves are not of the usual bell-shaped form, but are often double-peaked. From informal discussions we understand that other workers have observed these effects, but very little on this subject appears to have been published. Exceptions are the well-known Millman effect (Millman 1939) and the resonance curves peculiar to a Ramsey double loop (Ramsey 1949).

Three of the radio-frequency loops we have used are sketched in the insets of figures 1 and 2. The purpose of this note is to draw attention to some of the characteristics of these loops. Because our main interest was directed elsewhere at the time, we present only a few experimental results in support of our conclusions.

§ 2. Method

The interaction region, in which an atom experiences a perturbation as it passes through an atomic-beam apparatus, is defined by a radio-frequency magnetic field superimposed on a steady magnetic field H_0. The length of this region is determined by the length l of the loop which supplies the radio-frequency field. Rabi (1937, also Torrey 1941) has given an expression for the probability of transition from the state p to the state q:

$$P(\omega) = \frac{(2b)^2 \sin^2 \tfrac{1}{2}\tau \left[(2b)^2 + (\omega - \omega_0)^2\right]^{1/2}}{(2b)^2 + (\omega - \omega_0)^2} \qquad \ldots\ldots(1)$$

in which τ is the time spent in the interaction region by an atom of velocity V, and b is given by the matrix elements of the perturbation $\langle \mathrm{p}|V|\mathrm{q}\rangle = \hbar b e^{i\omega t}$ and $\langle \mathrm{q}|V|\mathrm{p}\rangle = \hbar b e^{-i\omega t}$. b is proportional to the radio-frequency amplitude H_1. It is assumed that no states other than q and p are involved, and that the interaction region is an ideal one in which an atom is exposed for a time τ to a radio-frequency field of amplitude H_1, which is constant for the duration τ but is otherwise zero. In practice, a radio-frequency loop for inducing π transitions (magnetic dipole transitions in which $\Delta m = \pm 1$) usually consists of a pair of parallel current sheets of width l and separation a; the beam passes centrally between these sheets in a direction parallel to the dimension l. The ideal case is approached if the ratio l/a

is large and the loop is closely shielded (Kusch 1956). When the expression $P(\omega)$ of equation (1) is averaged over the distribution of atomic velocities, the resonance line shape is obtained.

If the radio-frequency amplitude does not change suddenly from zero to a constant value at the entrance and exit of a radio-frequency loop, a rigorous derivation of $P(\omega)$ is difficult. In attempting to find the line shapes for various loops, we have adopted the following procedure to obtain approximate solutions.

1. For each loop, we have calculated the amplitude of radio-frequency field in the plane of the beam on the assumption that the loop consists of a pair of thin uniform current sheets, infinitely long in a direction perpendicular to the beam and to the steady magnetic field. This amplitude is plotted as curve *a* in each figure. The abscissa is $t=x/\alpha$ where x is the position in the loop of an atom travelling with velocity α, the most probable velocity in the oven.

2. A simple function $h(t)$ is chosen as an approximation to the radio-frequency amplitude, of frequency ω_0, as a function of t. This is curve *b* in the figures.

3. We have then taken the Fourier transform $g(\omega)$ of $h(t)\cos\omega_0 t$, and put the transition probability proportional to $E(\omega)=(2/\pi)g(\omega)g^*(\omega)$. This is plotted against $(\omega-\omega_0)\tau$, curve *c* in the figures. In each case $\tau=l/\alpha$ where l is the length of the radio-frequency loop in the direction of the beam.

Terms containing $\omega+\omega_0$ are neglected since these shift the resonance peak by an amount which is negligible for all but the lowest frequencies (Bloch and Siegert 1940). We have not averaged over the velocity distribution, and have taken no account of the variation of line shape with radio-frequency power (Kusch 1956).

The function

$$\begin{aligned} h(t)&=A, \text{ constant}, \quad |t|\leqslant\tfrac{1}{2}\tau, \\ &=0 \qquad\qquad\quad |t|>\tfrac{1}{2}\tau, \end{aligned} \qquad \ldots\ldots(2)$$

describes the radio-frequency amplitude for an ideal π loop mentioned above. The square of the Fourier transform $E(\omega)$ of $h(t)\cos\omega_0 t$ is given by

$$\frac{E(\omega)}{A^2\tau^2/4\pi^2}=\left\{\frac{\sin\frac{1}{2}(\omega-\omega_0)\tau}{\frac{1}{2}(\omega-\omega_0)\tau}\right\}^2. \qquad \ldots\ldots(3)$$

This is a bell-shaped curve, with subsidiary maxima, which has a half-intensity full width of $\delta\nu=\delta\omega/2\pi=0{\cdot}88/\tau$ in frequency units. For comparison the half-width of the rigorous function $P(\omega)$ in equation (1), in which $2b=\pi/\tau$, is $0{\cdot}8/\tau$. The difference between these two curves is small enough to make our procedure appear reasonable for the estimates about to be made. For this field distribution, $(2b)^2(\pi^2/A^2)E(\omega)$ is the transition probability derived from the solution of the time-dependent Schrödinger equation by first-order perturbation theory, whereas $P(\omega)$ of equation (1) is derived from an exact solution. This is the justification for using Fourier transforms in this treatment.

As a further test, the radio-frequency amplitude along the axis of an unshielded π loop in which the length l is about twice the separation a of the current sheets can be represented fairly well by the function

$$\begin{aligned} h(t)&=\tfrac{1}{2}A(1+\cos qt) \qquad |t|\leqslant\tfrac{1}{2}\tau \\ &=0 \qquad\qquad\qquad\quad |t|>\tfrac{1}{2}\tau, \end{aligned} \qquad \ldots\ldots(4)$$

where $q=2\pi/2\tau$. The transform of $h(t)\cos\omega_0 t$ gives another bell-shaped curve with a half-width $\delta\nu=0{\cdot}73/\tau$. This is slightly narrower than that for the ideal

case. The spreading of the radio-frequency field beyond the physical dimensions of the loop corresponds to a larger effective τ. As stated before, the ideal case is approached the larger the ratio l/a becomes.

§ 3. Results with σ Loops

The analysis of the previous section is applied to the shape of a field-independent σ line ($F=2 \leftrightarrow F=1, m_F=0 \leftrightarrow 0$) in the hyperfine structure of ^{39}K, and is compared with experimental results. Magnetic field inhomogeneities are expected to have no influence on the shape of this particular line.

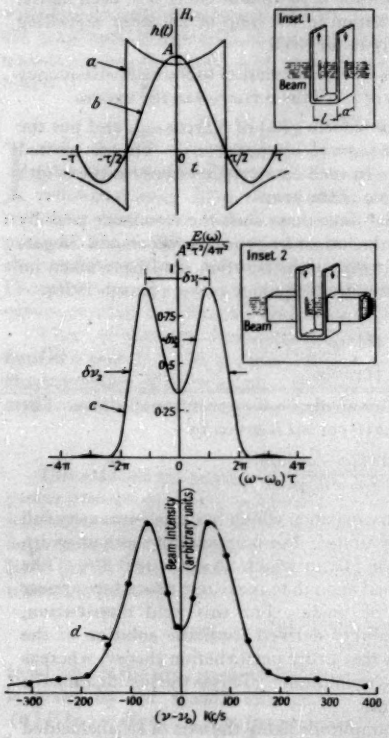

Figure 1

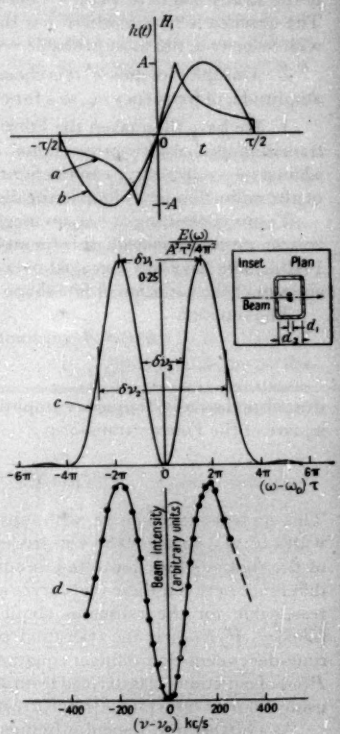

Figure 2

Curve a of figure 1 shows the radio-frequency amplitude parallel to the steady magnetic field and perpendicular to the beam for a σ loop (inset 1) in which the dimensions are $l=a=0{\cdot}3$ cm. The slits which allow passage of the beam are assumed to have no effect on the radio-frequency field.

Since in practice the curve *a* is rounded off, the function

$$h(t)=\tfrac{1}{2}A(1+2\cos pt) \qquad -\tau\leqslant t\leqslant\tau$$
$$=0 \qquad\qquad t<-\tau,\ t>\tau, \qquad\qquad \ldots\ldots(5)$$

is taken to represent the radio-frequency field. Here $p=2\pi/1{\cdot}5\tau$. The transform (curve *c*) has two peaks. If $\alpha=4\times10^4$ cm sec^{-1} for ^{39}K in this experiment, $1/\tau$ becomes 133 kc/s. The peak-to-peak separation in frequency units is $\delta\nu_1=135$ kc/s. The outside width at half peak intensity is $\delta\nu_2=220$ kc/s. The inside width at the mean of peak and trough intensities is $\delta\nu_3=80$ kc/s. The ratio of intensities, peak to trough, is 2·5. These values are to be compared with the experimental results (curve *d*): $\delta\nu_1=128$ kc/s, $\delta\nu_2=236$ kc/s, $\delta\nu_3=72$ kc/s. The peak-to-trough intensity ratio was difficult to measure, but fell between 2 and 3 in various runs.

One might try to improve the correspondence between curves *b* and *a* by adding more terms to $h(t)$. As the curve *b* is made less rounded, so the subsidiary maximum (between 2π and 4π) in curve *c* is accentuated. This might account for the 'tails', which are quite pronounced, in the experimental curve *d*. In view of the simplifications made we have not thought it worth going into great detail.

When tubular shields 1 cm long were fitted to the outside of this loop (figure 1, inset 2), the peak-to-peak separation became very small as expected. Its value was about 40 kc/s, and the central dip fell only about 2% below the peak intensity. This curve is not shown.

A coaxial loop of rectangular cross section (figure 2, inset), with its inner and outer conductors short-circuited at the end below the beam, was used to induce σ transitions in an experiment on ^{111}Ag at about 2200 Mc/s. This was done to reduce radiation losses at this high frequency at which the power available from the oscillator was low, but the loop was also used with a beam of ^{39}K near 461 Mc/s.

If a circular cross section is taken as an approximation to the shape of the coaxial loop, curve *a* shows the amplitude of radio-frequency field, where the diameters of the inner and outer conductors are $d_1=0{\cdot}05$ cm and $d_2=0{\cdot}24$ cm. Curve *b* is the function chosen to correspond to the radio-frequency amplitude. It is

$$h(t)=A\sin rt \qquad -\tfrac{1}{2}\tau\leqslant t\leqslant\tfrac{1}{2}\tau$$
$$=0 \qquad\qquad t<-\tfrac{1}{2}\tau,\ t>\tfrac{1}{2}\tau, \qquad\qquad \ldots\ldots(6)$$

where $r=2\pi/\tau$ and $\tau=d_2/\alpha$. The transform again has two peaks (curve *c*), with zero intensity at the frequency ω_0. The latter feature would be expected with any odd function $h(t)$.

With the notation of figure 1, $\delta\nu_1=364$ kc/s, $\delta\nu_2=557$ kc/s and $\delta\nu_3=175$ kc/s. Here we have taken $1/\tau=214$ kc/s corresponding to $d_2=0{\cdot}19$ cm, and not 0·24 cm, in order to fit $\delta\nu_1$ to the experimental result. From the experimental curve *d*, $\delta\nu_1=364$ kc/s, $\delta\nu_2=670$ kc/s and $\delta\nu_3=170$ kc/s. The central minimum of intensity is very close to zero.

Finally, an unshielded π loop, mentioned in § 2, was rotated by about 20° about a vertical axis through its centre. The plane of the beam contained this axis, but was at an angle to the current sheets. With this arrangement both π and σ transitions are excited. The π lines should retain their previous shape, but should have a slightly smaller half width. The σ component of radio-frequency field amplitude is similar in form to curve *b* of figure 1. The experimental result for the

σ line ($m=0 \leftrightarrow m=0$) is similar to curve *d* of figure 1. If the radio-frequency loop were to be translated perpendicular to the beam as well as rotated, one would expect the resonance curves for both π and σ lines to be asymmetrical, but we have no experimental results to illustrate this case.

§ 4. Conclusion

In spite of the approximations and simplifications made here, the method gives qualitative and, to some extent, quantitative agreement with experiment. The special effects described above are prominent largely because the dimensions *l* and *a* of a loop are nearly equal. This is in contrast with high-precision measurements with a single radio-frequency loop in which *l*/*a* may be quite large, say 25. Short loops, giving a large half width, are useful in experiments with radioactive atoms which are detected by counting the radioactivity of a beam deposited on a target, because this method of detection with its long time constant makes searching for a line very tedious. We suggest that in such experiments the coaxial loop of figure 2 is convenient in that it provides a large outside half width for ease in searching, and at the same time an inside half width only about a quarter as great for a relatively precise determination of the centre of the pattern. The Ramsey double loop has this same feature together with other more important properties; indeed, the coaxial loop may be regarded as a species of Ramsey loop.

It should be pointed out that with the low oven temperatures used in these experiments, about 10% of the low-velocity potassium atoms are lost in our apparatus. This modification of the velocity distribution in the beam should not affect our qualitative conclusions (cf. Hughes *et al.* 1953, King and Jaccarino 1954).

Acknowledgments

One of the authors (G.K.W.) would like to thank Imperial Chemical Industries for a Research Fellowship; the other (R.W.H.) is indebted to the Rhodes Trust for the grant of a scholarship.

References

Bloch, F., and Siegert, A., 1940, *Phys. Rev.*, **57**, 522.
Hughes, V., Tucker, G., Rhoderick, E., and Weinreich, G., 1953, *Phys. Rev.*, **91**, 828.
King, J. G., and Jaccarino, V., 1954, *Phys. Rev.*, **94**, 1610.
Kusch, P., 1956, *Phys. Rev.*, **101**, 627.
Millman, S., 1939, *Phys. Rev.*, **55**, 628.
Rabi, I. I., 1937, *Phys. Rev.*, **51**, 652.
Ramsey, N. F., 1949, *Phys. Rev.*, **76**, 996.
Torrey, H. C., 1941, *Phys. Rev.*, **59**, 293.
Woodgate, G. K., and Hellwarth, R. W., 1955, *Nature, Lond.*, **176**, 395.

α-Particle Counting Behaviour of Diamond Conduction Counters at Field Strengths up to 200 kV cm^{-1}.

By K. W. TAYLOR

Wheatstone Physics Laboratory, King's College, London

Communicated by J. T. Randall ; MS. received 12th October 1955, and in revised form 8th March 1956

Abstract. The general behaviour of a set of eighteen diamonds of size about 1 mm^3 was examined, particularly at applied field strengths from 10 kv cm^{-1} up to 200 kv cm^{-1}. The set includes all those high resistance types usually found in a sample of gem-quality diamonds. All the specimens were found to give conduction pulses and several type 1 specimens which were hitherto classed as non-counters for field strengths below 10 kv cm^{-1}, were found to give small conduction pulses for higher field strengths. The general counting behaviour was similar for all diamonds, although the magnitudes of the various effects varied over wide ranges from specimen to specimen and within each specimen. At higher applied field strengths two additional phenomena were apparent : the appearance of large pulses after a short period of counting and, on removing the applied field after a period of counting, the presence of depolarization pulses which were in the same direction as the normal counting pulses.

The observed behaviour of all these specimens can be explained by assuming the presence of continuous spatial variations in trap density on a microscopic scale within each specimen. The mean of these microscopic variations varies over macroscopic distances within each specimen and, also, from specimen to specimen.

§ 1. Introduction

The ability of diamonds of gem quality to act as conduction counters under α, β and γ-irradiation has been widely investigated and reported and has been reviewed by Hofstadter (1949) and Champion (1953a). However, most of the investigations have been carried out at applied electric fields of the order of 10 kv cm^{-1} and less. Consequently diamonds as a whole have been classed as counters or non-counters according to their behaviour at these fields.

An account is given here of the behaviour of a wide range of specimens as counters of 5·3 Mev α-particles, particularly at higher applied fields up to about 200 kv cm^{-1}. A set of eighteen diamonds has been investigated, the ultra-violet transmission limits varying from one specimen to another in the range 2250 Å to 3150 Å.

A brief account is first given of the experimental method of investigation, followed by a general account of the results obtained and, finally, a short discussion.

§ 2. Experimental

The electrode arrangement used in the investigation was as shown in figure 1. Two phosphor-bronze electrodes were mounted with edges parallel on a flat surface, usually the {111} face, of a diamond. The gap between the edges was

generally about 0·2 mm and α-particles were incident on the diamond surface in a direction perpendicular to the surface. Potentials of up to 4 kv could be applied to one of the electrodes giving a theoretical maximum available field of about 200 kv cm^{-1}. Owing to the electrode disposition and to the penetration of the α-particles to a depth of about 15μ, this field will be to some extent non-uniform in the region in which the counting occurs. However, the use of this electrode arrangement was shown to give very similar results to those obtained with electrodes placed on either side of a diamond with plane parallel faces, α-bombardment taking place on a surface between the electrodes. Furthermore, changing the electrode shape and nature did not alter the readings appreciably, so that reliable qualitative results are obtained by this method and quantitative results are significant.

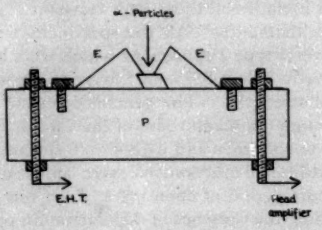

Figure 1. Electrode arrangement employed in this investigation. P was a polythene or polystyrene block of dimensions $2 \times \frac{1}{4} \times \frac{3}{8}$ in. and the electrodes E were of phosphor-bronze.

The charge pulses induced on the electrode system by the movement of the carriers released in the diamond were amplified by an A.E.R.E. Type 201 linear amplifier and discriminator. A low frequency head amplifier together with differentiation and integration time constants of 8μsec were used in order to obtain the maximum sensitivity of which the amplifying system was capable. The high voltage was obtained from an A.E.R.E. Type 200 power unit and was applied to one electrode through a 10 MΩ resistor. The electrode system was mounted in a chamber evacuated to a pressure below 1μ of mercury in order to prevent breakdown of the atmosphere between the electrodes at the higher fields. The amplified pulses were counted by an A.E.R.E. Type 200 scaler and were presented visually on the screen of a Cossor Type 1049 oscilloscope. Pulse spectra were obtained by photographing the pulses with a camera attachment and then counting the pulses on the projected image. α-particles of homogeneous energy at 5·3 Mev were obtained from a polonium source placed at a distance of about 2 cm vertically above the gap in the electrode system, a swinging shutter being used to block the α-irradiation when necessary.

§ 3. Results

3.1. *Initial Counting Behaviour*

In the following results, unless otherwise stated, the pulse height referred to is the maximum pulse height observed over a short period of time, usually three or four seconds, from the time of commencement of α-irradiation. The largest

number of counts above 5000 ion pairs during this interval was about 500. The observations are regarded as those for the unpolarized condition of the counting volume.

The eighteen diamonds examined have been found to count with a wide range of pulse height–field strength curves and of saturation pulse heights. The curves for four representative specimens are shown in figure 2, the range of saturation pulse heights extending from 270 000 ion pairs down to at least 5000 ion pairs. The noise level of the amplifier was equivalent to a pulse height of 3000 ion pairs

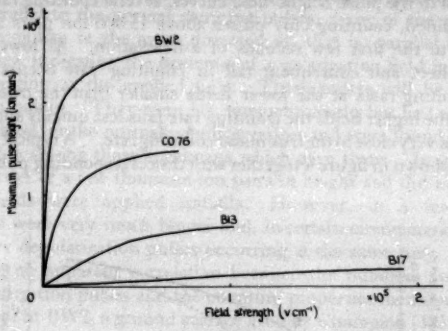

Figure 2. Typical curves showing the variation of pulse height with field strength in four diamonds.

but because of the occurrence of many discharge pulses, which distorted the noise level, counting could not definitely be discerned below 5000 ion pairs at higher fields. The range of the slopes of the pulse height–field curves is from 83 ion pairs per v cm^{-1} to less than 1 ion pair per v cm^{-1}, the better counters having the greater slopes.

Each diamond exhibited a saturation pulse height which varied according to the disposition of the electrodes on its surfaces but for the specimens examined

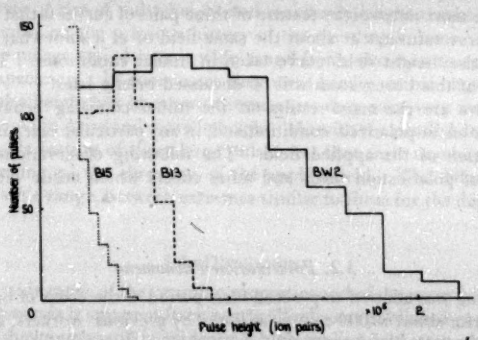

Figure 3. Typical pulse height spectra for three diamonds.

the variation was generally only by a factor of five or less whereas the variation between good and poor counters was by a factor of fifty or more. The saturation pulse heights quoted above are the maxima observed for each specimen and the slopes are the corresponding values.

Each diamond and electrode disposition gave a spectrum of pulses in which there were generally many more small pulses than large ones and no diamond so far examined has given a monochromatic pulse height in any condition. Three typical pulse height spectra taken at saturation fields are shown in figure 3.

In addition to the pulse height–field curves, several counting rate–field curves were also obtained, counting only pulses above 15 000 ion pairs and restricting the counting to the first few seconds of α-irradiation. At lower fields, some polarization effect and consequent fall in counting rate occurs which makes measured counting rates at the lower fields smaller than the true initial values. However, for the higher fields the counting rate falls less quickly and the measured counting rate is very close to the true initial counting rate. A typical counting rate–field curve is shown in figure 4 together with the corresponding pulse height–field

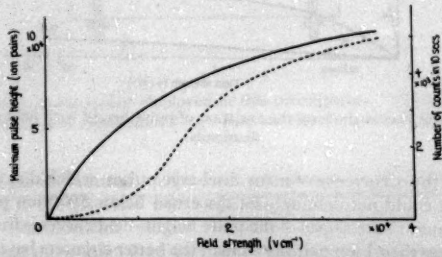

Figure 4. Typical curves showing variation of counting rate with field strength (broken line) and corresponding variation of pulse height with field strength (full line).

curve. The most noteworthy feature of these pairs of curves is that the counting rate–field curve saturates at about the same field or at a somewhat greater field than the pulse height–field curve taken in similar conditions. The probable significance of this observation will be discussed briefly later.

The above are the main results on the initial counting behaviour of the diamonds in an unpolarized condition and, in any particular case, are similar for either direction of the applied field. The following observations are on the production of polarization fields and other effects which occur with prolonged counting.

3.2. *Polarization Phenomena*

If counting was allowed to proceed for a period of the order of one minute or more, that is for about 10 000 counts, as found by previous workers, a polarization field was built up in the counting volume by the trapping of the moving carriers. If the applied field was then removed an internal field remained in the crystal in

the opposite direction to the initially applied field. Counting then occurred with pulses in the opposite direction to the normal counting pulses. These pulses will be called depolarization pulses in order to differentiate them from the normal counting pulses. The depolarization pulses are of a similar magnitude to the normal counting pulses and reach saturation at similar applied fields, indicating that the polarization field is very similar in magnitude to the applied field, provided counting with the field applied proceeds for a time sufficient for the polarization field to reach saturation.

However, in addition to the ordinary depolarization pulses, which are of course antiparallel to the normal counting pulses, many of the specimens gave depolarization pulses in the same direction as, that is, parallel to, the normal counting pulses, indicating the presence of a polarization field in the crystal in the same direction as the applied field. These pulses will be called parallel depolarization pulses. They were not monochromatic but had spectra not dissimilar from those for the normal counting pulses and were found to have a wide range of heights among those specimens which gave them. In most cases they were of the order of a few thousand ion pairs in height and did not appear until quite high fields were applied initially. However, in a few cases these parallel pulses were very much bigger and, in certain circumstances, even as big as the ordinary depolarization pulses occurring at the same time.

There was no apparent correlation between the numbers and sizes of the parallel depolarization pulses and the counting properties mentioned above. In fact, one surface of BW2, a ground surface used by Champion (1953b), itself gave a wide range of parallel depolarization pulse behaviour according to the electrode disposition, although the corresponding initial counting properties varied only slightly. An additional feature of these pulses was that their number and height differed according to the direction of the applied field, the differences varying over a wide range from specimen to specimen and within specimens. In the extreme cases the pulses were either similar in size and number or were very prominent for one direction of the field and absent for the other.

A second phenomena apparent at higher fields was the occurrence of large pulses during normal counting. These pulses were not present immediately counting commenced but grew in number and magnitude as polarization proceeded, the rate of rise of pulse height and maximum height reached depending very considerably on the previous history of the counting volume. The height of these large pulses varied over a wide range from specimen to specimen and within each specimen. In some cases they were hardly visible above the initial maximum pulse height but in other extreme cases they were very numerous and up to 10 million ion pairs and more in height. As with the parallel depolarization pulses, a notable feature of these large pulses was that their number and height differed according to the direction of the applied field. The differences again varied over a wide range, between extremes similar to those for the depolarization pulses.

§ 4. Discussion

The very wide range of the counting properties and of the many other physical features of diamonds is apparent from nearly all relevant published papers. This wide range is shown to be still in evidence at high applied field strengths. In fact, several additional phenomena occurring at the higher fields show wide variations

which are independent of the normal counting properties, as exemplified by the values of the initial pulse height. However, although there are wide variations in the magnitude of certain effects, these effects are common to most specimens and, no doubt, would be observed in all specimens if greater sensitivity were available in the amplifying system.

It seems evident that the wide range of pulse height–field curves is brought about by corresponding variations in trap density from diamond to diamond and within each diamond. The pulse height spectra again indicate a varying trap density but in this case on a microscopic scale within each specimen. In one particular case, that of the best available counter, the spectrum contains pulses of all sizes from 3000 ion pairs to 270 000 ion pairs, this requiring a variation in trap density by a factor of at least 100 in a distance of the order of 1 mm.

The counting rate–field curves show that the small pulses are still increasing in height until the maximum pulse height reaches saturation and, in some cases, even after that. This indicates that a large proportion of the smaller pulses are being formed in the poorer counting regions of the counting volume. It is of interest to note that, for the case of a crystal having a homogeneous distribution of traps broken only by narrow impenetrable barriers at random separations, the smaller pulses should saturate at a proportionately lower field than the large pulses, which is contrary to the experimental observation.

The polarization phenomena are now explicable in terms of these variations in trap density. Carriers will be trapped on the slopes of the density variations in such a way as to increase the field in regions of higher trap density and decrease the field in regions of lower trap density. The actual distribution of the trapped charges will depend on the strength of the applied field, the mean position of the trapped charge moving further up the slopes of the trap density variations as the field is raised. The decrease of field in the regions of lower trap density produces the normal polarization effects associated with counting. The increase of field in the regions of higher trap density produces the additional phenomena noted at higher field strengths where saturation of pulse height occurs. Three possibilities are apparent. Firstly, the movement of carriers in the regions of high trap density will now make a more significant contribution to any given pulse height. Secondly, the field will now probably be in the pre-breakdown region in some places, where carrier multiplication might be expected. Finally, in the extreme case, the field may actually reach breakdown value and a discharge will occur across a narrow region of very high trap density. These three possibilities, or any combination of them, will account for the large pulses which appear after some seconds of counting when the polarization fields have had time to build up. On subsequent removal of the applied field, the field remaining in the regions of high trap density will be in the same direction as that applied and will account for the parallel depolarization pulses noted for many specimens.

The wide range of behaviour found within each of these general phenomena indicates that widely different variations in trap density are present within different specimens. Furthermore, the asymmetric nature of the phenomena would seem to show that the density variations are themselves asymmetric, or that the two carriers have different sets of variations. Owing to the fact that the trap density variations are present on a microscopic scale, it seems likely that an α-particle will produce its ionization in several regions of different trap density. Thus, the detailed analysis of the production of the pulses will be very complicated.

These results are in general agreement with observations of previous workers (Jentschke 1948, Ahearn 1948, 1951) and various suggestions have been made to account for the phenomena (Freeman and van der Velden 1950, Ahearn 1951, Champion 1953b). Klemens (1952) and Berman, Simon and Ziman (1953) have suggested that the results from observations on the thermal conductivity of diamond at low temperatures indicate the presence of clusters of defects or impurities in the diamond structure. Furthermore, the number of such clusters would have to be about 10^5 per cm^3 to account for the magnitude of the thermal resistance. The counting behaviour requires there to be, for a medium type of counter, of the order of one prominent peak of density in a distance of 0·1 mm in all three dimensions, that is, approximately 10^6 peaks of density per cm^3. Thus, there would seem to be general agreement between this result and that from the thermal conductivity measurements.

§ 5. Conclusion

The results indicate that the wide range of counting behaviour of gem-quality diamonds is due to continuous variations of trap density from specimen to specimen and within each specimen, on both macroscopic and microscopic scales. The general phenomena are observed in all types of diamonds, type 1, type 2 and the intermediate types. It seems likely that these variations must be considered when measuring the electrical conductivity properties of diamonds, such as, for example, in measurement of carrier mobilities, ionization energies, trap densities and even trap depths, when a counting method is employed.

Acknowledgments

The author wishes to thank Dr. F. C. Champion for his helpful criticism and advice during the course of this work and in the preparation of this paper.

During the course of this work the author was in receipt of a maintenance grant from the Department of Scientific and Industrial Research.

References

Ahearn, A. J., 1948, *Phys. Rev.*, **73**, 1113 ; 1951, *Ibid.*, **84**, 798.
Berman, R., Simon, F. E., and Ziman, J. M., 1953, *Proc. Roy. Soc.* A, **220**, 171.
Champion, F. C., 1953 a, *Progress in Nuclear Physics*, **3**, 159 ; 1953b, *Proc. Roy. Soc.* A, **220**, 485.
Freeman, G. P., and van der Velden, H. A., 1950, *Physica*, **16**, 486.
Hofstadter, R., 1949, *Nucleonics*, **4**, 2, **5**, 29.
Jentschke, W., 1948, *Phys. Rev.*, **73**, 77.
Klemens, P. G., 1952, *Phys. Rev.*, **86**, 1055.

The Alpha-Particle and Shell Models of the Nucleus

By J. K. PERRING and T. H. R. SKYRME
Atomic Energy Research Establishment, Harwell, Berks.

Communicated by B. H. Flowers ; MS. received 23rd February 1956

Abstract. It is shown that it is possible to write down α-particle wave functions for the ground states of ^{8}Be, ^{12}C and ^{16}O, which become, when antisymmetrized, identical with shell-model wave functions. The α-particle functions are used to obtain potentials which can then be used to derive wave functions and energies of excited states. Most of the low-lying states of ^{16}O are obtained in this way, qualitative agreement with experiment being found. The shell structure of the 0^+ level at 6·06 Mev is analysed, and is found to consist largely of single-particle excitations. The lifetime for pair-production is calculated, and found to be comparable with the experimental value. The validity of the method is discussed, and comparison made with shell-model calculations.

§ 1. Introduction

It has been known for some time that the shell-model wave function for a light 4n-type nucleus will automatically give something of an α-particle structure. This is purely a consequence of the exclusion principle and the symmetry properties of the individual orbitals, and holds quite independently of inter-nucleon forces. A similar result holds in atomic structure; for example, it is well known that the sp^3 configuration of carbon can be described by tetrahedrally directed orbitals. The shell-model in its simplest form does not allow for correlation between nucleons of differing spin and isotopic spin, and we might expect an α-particle model, which emphasizes the positive correlations between nucleons, to be a better representation of the structure of the nucleus.

The α-particle model does, indeed, seem to work fairly well in certain ways, for instance in accounting for the binding energies of the 4n nuclei; and Dennison (1954) has recently been able to interpret most of the low-lying levels of ^{16}O on this basis. An advantage of such a model is that it requires us to solve a problem with only one quarter of the number of degrees of freedom of the individual-particle model, using, in general, methods that are well known from the theory of molecular spectra. If such a simplification can be achieved it will be very desirable, since the algebraic and numerical manipulations of the shell model become complex very quickly.

In this paper we shall use a method which will enable us to predict energy levels for α-particle nuclei, and which will also allow us to derive shell-model wave functions for excited states. Our aim is to compare our conclusions with those of the shell-model, and to see to what extent these are independent of particular assumptions about inter-nucleon forces; then, perhaps, we may be able to use the method as a guide to the structure of more complex systems. Our approach is based on a simple but surprising mathematical identity. This enables us to write down a simple and reasonable α-particle wave function which turns out to be identical with a shell-model function.

§ 2. General Method

The transformations we shall make depend on the simple and convenient properties of harmonic-oscillator wave functions. In the individual-particle model we suppose that we can take the nucleon wave functions to be the solutions of the equation

$$\sum_{i=1}^{N} [-(\hbar^2/2m)\nabla_i^2 + \tfrac{1}{2}k(\mathbf{r}_i - \mathbf{S})^2]\Psi = E\Psi \qquad \ldots\ldots(1)$$

where $\mathbf{S}$ is the centre-of-mass coordinate.

If we measure lengths in units of $(\hbar^2/km)^{1/4}$ and energies in units of $(k\hbar^2/m)^{1/2}$ this becomes

$$\tfrac{1}{2}\sum_{i=1}^{N} [-\nabla_i^2 + (\mathbf{r}_i - \mathbf{S})^2]\Psi = E\Psi. \qquad \ldots\ldots(2)$$

The wave functions of the individual particles are then of the form (polynomial) $\times \exp\{-(\mathbf{r}-\mathbf{S})^2/2\}$ and their energy levels are spaced by single units. Many-particle wave functions are built up of products of these, and therefore contain the factor $\exp[-\frac{1}{2}\sum(\mathbf{r}_i - \mathbf{S})^2]$. A general shell-model wave function can thus be written

$$\sum \pm P(\mathbf{r}_i - \mathbf{S}, \ldots, \mathbf{r}_N - \mathbf{S}) \exp[-\tfrac{1}{2}\sum(\mathbf{r}_i - \mathbf{S})^2] F(1, \ldots, N), \quad \ldots\ldots(3)$$

where P is a polynomial in the $3N$ variables $(\mathbf{r}_i - \mathbf{S})$, $F(1, \ldots, N)$ is a spin–charge function, and the product is antisymmetrized with respect to all the variables.

Now let us consider an α-particle nucleus consisting of $4N$ nucleons. We may split the coordinates $\mathbf{r}_i$ into groups of four, with centres $\mathbf{R}_j$, say, to correspond to α-particles,

$$\mathbf{R}_j = \tfrac{1}{4}\sum_{i=4j-3}^{4j} \mathbf{r}_i, \qquad \ldots\ldots(4)$$

and it is easily shown that

$$\sum_{i=1}^{4N} (\mathbf{r}_i - \mathbf{S})^2 = \sum_{j=1}^{N} \sum_{i=4j-3}^{4j} (\mathbf{r}_i - \mathbf{R}_j)^2 + 4\sum_{j=1}^{N} (\mathbf{R}_j - \mathbf{S})^2. \qquad \ldots\ldots(5)$$

In the expression (3) the exponential factor is completely symmetric and can therefore be taken outside the antisymmetrization. Then for certain types of polynomial P it is possible to express the anti-symmetrized expression $\Sigma \pm PF$ as the result of antisymmetrizing an expression

$$Q(\mathbf{R}_1, \ldots, \mathbf{R}_N) \prod_{j=1}^{N} F_\alpha(4j-3, \ldots, 4j) \qquad \ldots\ldots(6)$$

where Q is a symmetric polynomial and F_α is the α-particle spin charge function. When this condition holds we may re-write the wave function (3) as

$$\sum \pm Q(\mathbf{R}_1, \ldots, \mathbf{R}_N) \exp\{-2\sum(\mathbf{R}_j - \mathbf{S})^2\} \prod_{j=1}^{N} [\exp\{-\tfrac{1}{2}\sum(\mathbf{r}_i - \mathbf{R}_j)^2\} F_\alpha(4j-3, \ldots, 4j)] \qquad \ldots\ldots(7)$$

each term of which may be thought of as the product of an α-particle wave function with the internal wave functions of its constitutents.

These ideas allow us to construct a shell-model wave function, corresponding to any α-particle wave function of the form

$$\psi_\alpha = Q(\mathbf{R}_1, \ldots \mathbf{R}_N) \exp\{-2\sum(\mathbf{R} - \mathbf{S})^2\}. \qquad \ldots\ldots(8)$$

The converse is not true in general. To any such wave function (8) there is a corresponding α-particle potential $U(\mathbf{R}_1, \ldots \mathbf{R}_N)$, such that

$$\{(-\tfrac{1}{8})\sum_j \nabla_j^2 + U(\mathbf{R}_1, \ldots \mathbf{R}_N)\}\psi_\alpha = E\psi_\alpha. \qquad \ldots\ldots(9)$$

We can take this potential to represent the combined effects of the central potential and the exclusion principle. The forms of ψ_α and U derived are not unique, and it is necessary to impose a further condition on them. If we start from a shell-model wave function (3) representing the ground state of the system it is reasonable to demand that ψ_α and U shall be such that ψ_α is the lowest eigenfunction of U; this excludes some choices, but still leaves a range of functions U.

Once we have fixed U we can consider other states of the system. There is no guarantee that this effective potential U is the same for excited states as for the ground state, but in order to make progress we shall assume that it is. With this assumption we can solve the Schrodinger equation (9) to obtain wave functions for the excited states, which we can interpret in terms of the rotations and vibrations of the system of α-particles. From each new function we can construct the corresponding shell-model function, by antisymmetrizing, and thus find the fractions of the various configurations which it comprises.

This procedure is a way of choosing particular configurations so as to keep together the α-particle groups. Physically, this is effected by predominantly Majorana inter-nucleon forces. The relation between these and our effective potential U is rather obscure; the origin of the excitation energy seems to be entirely different in the two models.

We shall now consider in more detail the three simplest α-particle nuclei: ^{8}Be, ^{12}C, ^{16}O. We have been most interested in the last because of the possibility of comparing our results with the shell-model calculations recently made by Elliott (to be published).

§ 3. Beryllium 8

We may expect the ground state of ^{8}Be on the shell model to be composed principally of the most symmetric state of the configuration s^4p^4. This we may write in the form (3) with

$$\left.\begin{aligned} P &= (\mathbf{r}_5 \cdot \mathbf{r}_6)(\mathbf{r}_7 \cdot \mathbf{r}_8) + (\mathbf{r}_5 \cdot \mathbf{r}_7)(\mathbf{r}_6 \cdot \mathbf{r}_8) + (\mathbf{r}_5 \cdot \mathbf{r}_8)(\mathbf{r}_6 \cdot \mathbf{r}_7) \\ F &= F_\alpha(1, \ldots, 4) F_\alpha(5, \ldots, 8) \end{aligned}\right\} \qquad \ldots\ldots(10)$$

The polynomial P is equivalent under antisymmetrization to the α-particle expression $Q = (\mathbf{R}_1 - \mathbf{R}_2)^4$. This may be verified directly by antisymmetrizing each expression in the pairs 1 and 5, 2 and 6, 3 and 7, 4 and 8, when each gives

$$[(\mathbf{r}_1 - \mathbf{r}_5) \cdot (\mathbf{r}_2 - \mathbf{r}_6)][(\mathbf{r}_3 - \mathbf{r}_7) \cdot (\mathbf{r}_4 - \mathbf{r}_8)] + [(\mathbf{r}_1 - \mathbf{r}_5) \cdot (\mathbf{r}_3 - \mathbf{r}_7)][(\mathbf{r}_2 - \mathbf{r}_6) \cdot (\mathbf{r}_4 - \mathbf{r}_8)] + [(\mathbf{r}_1 - \mathbf{r}_5) \cdot (\mathbf{r}_4 - \mathbf{r}_8)][(\mathbf{r}_2 - \mathbf{r}_6) \cdot (\mathbf{r}_3 - \mathbf{r}_7)].$$

It seems to be true in general that it is only necessary to antisymmetrize with respect to particles with the same spin–charge function, which is a fortunate simplification. We can now write ψ_α as $\psi_\alpha = R^4 \exp(-R^2)$ where

$$\mathbf{R} = \mathbf{R}_1 - \mathbf{R}_2. \qquad \ldots\ldots(11)$$

This ψ_α satisfies the Schrödinger equation with $U(\mathbf{R}) = R^2 + 5/R^2$ in which we may regard the second term as a manifestation of the exclusion principle. We could have taken for Q any polynomial in $\mathbf{R}$ of the fourth degree and obtained the same equivalent shell-model wave function (terms of lower degree than the

fourth disappear on antisymmetrization). We should then have obtained a different U, and ψ_α might no longer have been the ground state of U. The present choice is, however, the simplest.

The first excited state of this potential has angular momentum $J=2$. (Only even angular momenta and even parity states are allowed, since the α-particles obey Bose statistics.) The wave function is

$$R^n \exp(-R^2) Y_2(\theta,\phi) \quad \text{with} \quad n=\tfrac{1}{2}(\sqrt{105}-1)\simeq 4{\cdot}62 \qquad \ldots\ldots(12)$$

and the energy of excitation is 0·62 unit. It can be seen that there is a certain amount of rotation–vibration interaction; a pure rotational wave functon would have $n=4$ in (12).

In order to obtain the shell-model wave functions we must put (12) into a rational form. The minimum of the potential $U(R)$ is at $R=5^{1/4}$. Hence we write $R^{4{\cdot}62}=R^4\{5^{1/2}+(R^2-5^{1/2})\}^{0{\cdot}31}$ and expand by the binomial theorem. The leading term gives just the ^{1}D state of the configuration $1s^4 1p^4$; further terms are equivalent to higher configurations.

The first pure vibrational state is $(R^2-11/4)R^4\exp(-R^2)$ with an energy of excitation of 2 units. The resulting shell-model configurations are those in which one particle is doubly excited, e.g. $1s^3 1p^4 2s$. No configurations occur for which two particles are singly excited (e.g. $1s^2 1p^6$). The reason for this is that the present form of the α-particle model implies the exclusive use of configurations of the maximum spatial symmetry [44]. There are five such states involving single excitation of two particles, but all of these are spurious states which describe motion of the centre of mass (Elliott and Skyrme 1955; we are indebted to Dr. Elliott for discussions on this point).

§ 4. Carbon 12

If we take the ground-state of ^{12}C to be that complementary to ^{8}Be, so that the four holes have P given by (10), we can carry out a similar analysis. The α-particle wave function may be taken as

$$\psi_\alpha = |N|^4 \exp\{-2\textstyle\sum(\mathbf{r}_i-\mathbf{S})^2\} \qquad \ldots\ldots(13)$$

where

$$N=(\mathbf{R}_1\times\mathbf{R}_2+\mathbf{R}_2\times\mathbf{R}_3+\mathbf{R}_3\times\mathbf{R}_1) \qquad \ldots\ldots(14)$$

which is twice the vector area of the triangle formed by the three α-particles. The corresponding potential is

$$U(\mathbf{R}_1,\mathbf{R}_2,\mathbf{R}_3)=2\textstyle\sum_i(\mathbf{R}_i-\mathbf{S})^2+2\sum_i(\mathbf{R}_i-\mathbf{S})^2/N^2 \qquad \ldots\ldots(15)$$

which has a minimum when $\mathbf{R}_1, \mathbf{R}_2, \mathbf{R}_3$ lie at the vertices of an equilateral triangle of side $(4/3)^{1/4}$.

Excited states may be dealt with in much the same way as for ^{8}Be, except that it is not always possible to write down exact wave functions. The analysis may be simplified somewhat by eliminating the centre-of-mass motion. Introducing the internal coordinates

$$\left.\begin{aligned}\mathbf{G}&=\tfrac{1}{3}(\mathbf{R}_1+\omega\mathbf{R}_2+\omega^2\mathbf{R}_3)\\ \mathbf{H}&=\tfrac{1}{3}(\mathbf{R}_1+\omega^2\mathbf{R}_2+\omega\mathbf{R}_3)\\ \omega&=\exp 2\pi i/3\end{aligned}\right\} \qquad \ldots\ldots(16)$$

(13) then becomes

$$\psi_\alpha = 3^6|\mathbf{G}\times\mathbf{H}|^4\exp(-12\mathbf{G}.\mathbf{H}) \qquad \ldots\ldots(17)$$

with the corresponding Schrödinger equation

$$\left\{-\frac{1}{12}\nabla_G\cdot\nabla_H+12\mathbf{G}\cdot\mathbf{H}-\frac{4}{9}\frac{\mathbf{G}\cdot\mathbf{H}}{|\mathbf{G}\times\mathbf{H}|^2}\right\}\psi_\alpha=E\psi_\alpha. \quad \ldots\ldots(18)$$

Although the coordinates are complex, all quantities appearing in (17) and (18) are real.

§ 5. Oxygen 16

We shall treat the oxygen 16 nucleus in rather more detail. The ground state is the closed shell $1s^41p^{12}$, and the corresponding α-particle wave function is

$$\psi_\alpha = V^4\exp -2\sum(\mathbf{R}_i-\mathbf{S})^2 \quad \ldots\ldots(19)$$

where V is six times the volume of the tetrahedron formed by $\mathbf{R}_1, \mathbf{R}_2, \mathbf{R}_3, \mathbf{R}_4$. Analytically, V is given by the determinant whose rows are $(1, X_i, Y_i, Z_i)$ where X_i, Y_i, Z_i, are the components of the vector $\mathbf{R}_i$.

The corresponding potential is

$$U(\mathbf{R}_1,\ldots\mathbf{R}_4)=2\sum_i(\mathbf{R}_i-\mathbf{S})^2+\frac{3}{2}\sum_i|N_i|^2/V^2 \quad \ldots\ldots(20)$$

in which the $\mathbf{N}_i$ are twice the vector areas of the faces of the tetrahedron, and are given by expressions similar to (14). U has a minimum for a regular tetrahedral configuration of side $(108)^{1/4}=3{\cdot}2$.

The analysis can be considerably simplified by eliminating the centre-of-mass motion, introducing internal coordinates analogous to (11) and (16):

$$\left.\begin{aligned}\mathbf{F}&=\tfrac{1}{4}(\mathbf{R}_1+\mathbf{R}_2-\mathbf{R}_3-\mathbf{R}_4)\\ \mathbf{G}&=\tfrac{1}{4}(\mathbf{R}_1-\mathbf{R}_2+\mathbf{R}_3-\mathbf{R}_4)\\ \mathbf{H}&=\tfrac{1}{4}(\mathbf{R}_1-\mathbf{R}_2-\mathbf{R}_3+\mathbf{R}_4)\end{aligned}\right\} \quad \ldots\ldots(21)$$

Then V is proportional to the triple scalar product $\mathbf{F}.(\mathbf{G}\times\mathbf{H})=(\mathbf{FGH})$, and $\Sigma_i(\mathbf{R}_i-\mathbf{S})^2=4(F^2+G^2+H^2)$; so that $\psi_\alpha=(\mathbf{FGH})^4\exp\{-8(F^2+G^2+H^2)\}$ and

$$\{-\tfrac{1}{32}(\nabla_F{}^2+\nabla_G{}^2+\nabla_H{}^2)+8(F^2+G^2+H^2)+\tfrac{3}{8}[(\mathbf{F}\times\mathbf{G})^2+(\mathbf{G}\times\mathbf{H})^2 +(\mathbf{H}\times\mathbf{F})^2]/(\mathbf{FGH})^2\}\psi_\alpha=E\psi_\alpha. \quad \ldots\ldots(22)$$

We can now look for excited states, by analogy with the case of ^{8}Be, with wave functions of the form $\psi=P\psi_0$ where $P(\mathbf{F},\mathbf{G},\mathbf{H})$ must satisfy

$$\sum_{F,G,H}[\nabla_F{}^2+8\{(\mathbf{G}\times\mathbf{H})(\mathbf{FGH})^{-1}-4\mathbf{F}\}.\nabla_F]P=-32(E-E_0)P,$$

which has elementary solutions $(F^2-11/32)$, $\mathbf{F}.\mathbf{G}$, $(F_iF_j-\frac{1}{3}F^2\delta_{ij})$, etc. with excitation energy of two units. Now α-particles obey Bose statistics, so we must take combinations of these solutions with the correct symmetry. The effect of a permutation of α-particles is to permute **F**, **G** and **H**, either with no change of sign, or with the signs of two coordinates changed simultaneously. Thus allowed forms of P are

$$(F^2+G^2+H^2-33/32) \quad \ldots\ldots(23)$$

$$\sum_{F,G,H}(F_iF_j-\tfrac{1}{3}F^2\delta_{ij}). \quad \ldots\ldots(24)$$

The first expression (23) is the wave function for the symmetrical 'breathing' mode of vibration (ω_1 in the language of molecular spectroscopy), and (24) is a combined vibrational–rotational mode with angular momentum $J=2$ and even parity. The other vibrational modes, which would, if allowed, be degenerate with ω_1, are ω_2: (F^2-G^2), $(2H^2-F^2-G^2)$; ω_3: $\mathbf{F}.\mathbf{G}$, $\mathbf{G}.\mathbf{H}$, $\mathbf{H}.\mathbf{F}$.

We may identify (23) with the 0^+ pair-emitting level at 6·06 Mev and (24) with the 2^+ level at 6·91 Mev. The remaining low-lying levels known are a 3^- at 6·14 Mev a 1^- at 7·12 Mev (Ajzenberg and Lauritsen 1955) and a 2^- at 8·85 Mev (Wilkinson 1955). It does not seem possible to obtain exact solutions of (22) with odd parity, and we have been forced to use approximate forms, and to seek the aid of the variation principle. Expressions for P with the correct symmetry requirements are

$$1^-: \sum_{F,G,H} (\mathbf{F}.\mathbf{G})(\mathbf{F}\times\mathbf{G})(\mathbf{FGH})^{-1}, \sum_{F,G,H} (\mathbf{F}.\mathbf{G})\mathbf{H} \qquad \text{.....(25)}$$

$$2^-: \sum_{F,G,H} (F^2G_iG_j - G^2F_iF_j)(\mathbf{FGH})^{-1} \qquad \text{.....(26)}$$

$$\left.\begin{aligned} 3^-: &\sum_{F,G,H} (F_iG_j - \tfrac{1}{3}\mathbf{F}.\mathbf{G}\delta_{ij})(\mathbf{F}\times\mathbf{G})_k(\mathbf{FGH})^{-1} \\ &\sum_{F,G,H} [F_iG_jH_k - \tfrac{1}{5}(F_i\delta_{jk} + F_j\delta_{ki} + F_k\delta_{ij})\mathbf{G}.\mathbf{H}] \end{aligned}\right\} \qquad \text{.....(27)}$$

It should be noted that whereas there are two simple tensors of 1^- and 3^- symmetry, there is only one of 2^-.

If we now work out $(\psi|H|\psi)/(\psi|\psi)$ for each of these expressions, we shall obtain estimates of the energy. Better estimates can be obtained for the 1^- and 3^- levels by allowing mixtures of the two types of expressions in (25) and (27). The levels obtained, after some complicated and laborious algebra, are shown in table 1.

It so happens that the two functions taken for the 3^- state overlap very considerably, the integral of the normalized functions being 0·92; this explains the very high energy obtained for the higher level. If we take our unit of energy to be about 3 Mev, to give reasonable agreement for the 0^+ and 2^+ states, we find the 1^- level in good agreement with experiment, but the 2^- and 3^- levels completely wrong (see table 1). It should be noted that the second form of P for the 1^- and 3^- states is the more important, the coefficients being in the ratio 0.63 : 1 for the 1^- state and 0.18 : 1 for the 3^-. This implies that the main constituents of these states should correspond to triple rather than single, shell-model excitations, i.e. to configurations such as $p^{-3}\,d^3$ rather than $p^{-1}\,d$.

It is possible to obtain some exact results for the states in which P is a quartic expression. These have excitation energies of 4 units. Three 0^+ states are obtained, for which the P's are orthogonal combinations of

$$\left.\begin{aligned} &(F^2+G^2+H^2)^2 - (35/16)(F^2+G^2+H^2) + 1155/1024 \\ &(F^2G^2+G^2H^2+H^2F^2) - (11/16)(F^2+G^2+H^2) + 363/1024 \\ &[(\mathbf{F}.\mathbf{G})^2+(\mathbf{G}.\mathbf{H})^2+(\mathbf{H}.\mathbf{F})^2] - (1/16)(F^2+G^2+H^2) + 33/1024 \end{aligned}\right\} \qquad \text{.....(28)}$$

together with one 2^+ state

$$\sum (F_iF_j - \tfrac{1}{3}F^2\delta_{ij})(F^2+G^2+H^2-37/32) \qquad \text{.....(29)}$$

and one 4^+ state

$$\sum (F_iF_j - \tfrac{1}{3}F^2\delta_{ij})\{\sum (F_iF_j - \tfrac{1}{3}F^2\delta_{ij}) - (4/35)(F^2+G^2+H^2)\}, \qquad \text{.....(30)}$$

It seems likely that there are also neighbouring 2^+ and 4^+ states, the wave functions of which can be approximated by such expressions as

$$P = \sum \mathbf{F}.\mathbf{G}(F_iG_j + F_jG_i - \tfrac{2}{3}\mathbf{F}.\mathbf{G}\delta_{ij}) \qquad (2^+),$$

$$P = \sum F^2(G_iG_j - \tfrac{1}{3}G^2\delta_{ij}) \qquad (2^+),$$

$$P = \sum (F_iG_j + F_jG_i - \tfrac{2}{3}\mathbf{F}.\mathbf{G}\delta_{ij})^2 \qquad (4^+), \text{ etc.}$$

Energies for these functions could be estimated by the variation principle. This has not been done, as the algebra involved would be extremely complex.

Energies for the states given in (28), (29) and (30), are shown together with the others in table 1. It is apparent that no precise correspondence with experiment can be established. The experimental level scheme becomes complicated, and is not definitely complete, above 11 MeV excitation.

Table 1.

State	Experimental Energy (MeV)	Calculated Energy (units of $(k\hbar^2/m)^{1/2}$)	Calculated Energy ($(k\hbar^2/m)^{1/2}$=3 MeV)
0^+	6·06	2	6·0
2^+	6·91	2	6·0
1^-	7·12	2·22	6·7
1^-	9·58	4·33	13·0
2^-	8·85	4·32	13·0
3^-	6·14	0·97	2·9
3^-	11·62	14·9	45
0^+ (3 states)	11·25, etc.	4	12·0
2^+	9·84	4	12·0
4^+	10·36	4	12·0

Experimental data, with one exception, are taken from the compilation of Ajzenberg and Lauritsen (1955). The value for the energy of the 2^- state is due to Wilkinson (1955).

§ 6. Shell-Model Wave Functions

We shall now reverse our initial procedure, and find to what shell-model wave functions the 0^+ excited-state wave function (23) corresponds. The method is simplified by using instead of the individual-particle coordinate $\mathbf{r}_i$, certain combinations of them

$$\boldsymbol{\rho}_i = \tfrac{1}{4}(\mathbf{r}_i + \mathbf{r}_{i+4} - \mathbf{r}_{i+8} - \mathbf{r}_{i+12}),$$
$$\boldsymbol{\sigma}_i = \tfrac{1}{4}(\mathbf{r}_i - \mathbf{r}_{i+4} + \mathbf{r}_{i+8} - \mathbf{r}_{i+12}),$$
$$\boldsymbol{\tau}_i = \tfrac{1}{4}(\mathbf{r}_i - \mathbf{r}_{i+4} - \mathbf{r}_{i+8} + \mathbf{r}_{i+12}),$$

so that $\mathbf{F} = \frac{1}{4}\Sigma\boldsymbol{\rho}_i$, $\mathbf{G} = \frac{1}{4}\Sigma\boldsymbol{\sigma}_i$, $\mathbf{H} = \frac{1}{4}\Sigma\boldsymbol{\tau}_i$. Then P of (23) is proportional to

$$\sum_i(\boldsymbol{\rho}_i^2 + \boldsymbol{\sigma}_i^2 + \boldsymbol{\tau}_i^2) + 2\sum_{i>j}(\boldsymbol{\rho}_i\cdot\boldsymbol{\rho}_j + \boldsymbol{\sigma}_i\cdot\boldsymbol{\sigma}_j + \boldsymbol{\tau}_i\cdot\boldsymbol{\tau}_j) - 33/2. \quad \ldots\ldots(31)$$

We take the spin–charge functions in the form

$$(\alpha_1\beta_2\gamma_3\delta_4)\,(\alpha_5\beta_6\gamma_7\delta_8)\ldots$$

Then we need to antisymmetrize within the four sets (1, 5, 9, 13), (2, 6, 10, 14), ... Under a permutation of one of these sets the variables $\boldsymbol{\rho}_i$, $\boldsymbol{\sigma}_i$, $\boldsymbol{\tau}_i$ are permuted among themselves, with either no sign changes, or two simultaneous changes. In particular the triple product $(\boldsymbol{\rho}_i\boldsymbol{\sigma}_i\boldsymbol{\tau}_i)$ is completely antisymmetric, and is the expression of lowest degree which is so. Hence the factor $(FGH)^4$ must reduce to a multiple of

$$(\boldsymbol{\rho}_1\boldsymbol{\sigma}_1\boldsymbol{\tau}_1)(\boldsymbol{\rho}_2\boldsymbol{\sigma}_2\boldsymbol{\tau}_2)(\boldsymbol{\rho}_3\boldsymbol{\sigma}_3\boldsymbol{\tau}_3)(\boldsymbol{\rho}_4\boldsymbol{\sigma}_4\boldsymbol{\tau}_4). \quad \ldots\ldots(32)$$

The remaining terms in (31) contribute two steps of excitation to the wave function; either a single particle can be doubly excited, or a pair of particles can

each be singly excited. For the moment we need consider only single or double excitation of sets. Double excitation of a set gives a contribution.

$$(\rho_i^2+\sigma_i^2+\tau_i^2)(\rho_i\sigma_i\tau_i) \qquad \ldots\ldots(33)$$

to the wave function, and single excitation expressions of the type

$$Q(a,b;\,c,d)=\begin{vmatrix} \rho_a\rho_b & \rho_c\rho_d & 1 \\ \sigma_a\sigma_b & \sigma_c\sigma_d & 1 \\ \tau_a\tau_b & \tau_c\tau_d & 1 \end{vmatrix} \qquad \ldots\ldots(34)$$

where a, b, c, d, are coordinate indices. The extraction of the correct constants to multiply the expressions (32), (33), and (34) is extremely laborious and will not be given in full here.

If we antisymmetrize with respect to the sets 3 and 4, keeping only the parts corresponding to excitations of sets 1 and 2, the wave function reduces to a multiple of

$$[(\rho_1+\rho_2)^2+(\sigma_1+\sigma_2)^2+(\tau_1+\tau_2)^2-K](\rho_1+\rho_2,\sigma_1+\sigma_2,\tau_1+\tau_2)^2(\rho_3\sigma_3\tau_3)(\rho_4\sigma_4\tau_4) \qquad \ldots\ldots(35)$$

where $K=495/56$. Antisymmetrizing the part of this which depends on sets 1 and 2, we find that

$$(\rho_1+\rho_2,\sigma_1+\sigma_2,\tau_1+\tau_2)^2\to 4(\rho_1\sigma_1\tau_1)(\rho_2\sigma_2\tau_2)$$

which must be multiplied by

$$\sum_{i=1,2}(\rho_i^2+\sigma_i^2+\tau_i^2)-K$$

to give the contribution to (35), and

$$(\rho_1\cdot\rho_2+\sigma_1\cdot\sigma_2+\tau_1\cdot\tau_2)(\rho_1+\rho_2,\sigma_1+\sigma_2,\tau_1+\tau_2)^2$$
$$\to\sum_{i=1,2}(\rho_i^2+\sigma_i^2+\tau_i^2)(\rho_1\sigma_1\tau_1)(\rho_2\sigma_2\tau_2)-\tfrac{1}{3}\sum\epsilon_{abc}\epsilon_{uvw}Q_1(d,a;b,v)Q_2(d,u;c,w)$$

in which the second summation is over all repeated indices. In this way the total wave function is reduced to

$$[6\sum_{i=1}^{4}(\rho_i^2+\sigma_i^2+\tau_i^2)-4K](\rho_1\sigma_1\tau_1)(\rho_2\sigma_2\tau_2)(\rho_3\sigma_3\tau_3)(\rho_4\sigma_4\tau_4)$$
$$-2\sum\sum\epsilon_{abc}\epsilon_{uvw}Q_1(d,a;\,b,v)Q_1(d,u;\,c,w)(\rho_k\sigma_k\tau_k)(\rho_i\sigma_i\tau_i).$$

The summations in the second term are over $i<j<k<l$, and repeated indices.

It is now necessary to transform back to the original coordinates. Using the relations

$$(\rho_1\sigma_1\tau_1)=-\frac{1}{16}\begin{vmatrix} 1 & x_1 & y_1 & z_1 \\ 1 & x_5 & y_5 & z_5 \\ 1 & x_9 & y_9 & z_9 \\ 1 & x_{13} & y_{13} & z_{13} \end{vmatrix}$$

$$Q(a,b;\,c,d)=-\frac{1}{64}[(1,r_a,r_c,r_br_d)+(1,r_a,r_d,r_br_c)+(1,r_b,r_c,r_ar_d)$$
$$+(1,r_b,r_d,r_ar_c)]$$

this is readily accomplished, and it only remains to transform the elements of the determinants into the orthogonal polynomials of the single-particle wave functions.

When this is done, and identical terms are collected, the intensities (amplitudes squared) of the different configurations found in the wave functions are as shown in table 2.

Table 2.

Configuration	$1s^{-1}\,2s$	$1p^{-1}\,2p$	$1p^{-2}1d^2$	$1p^{-2}1d2s$	$1p^{-2}\,2s^2$
Intensity (%)	29	52	17	1·9	0·15

Strictly, we should include the ground state $1s^4 1p^{12}$, which would amount to about 20%. This arises because the method is not self-consistent. However, it would not be possible to attach any firm significance to the resulting wave function, and we have therefore omitted the ground state.

A noteworthy feature of these figures is the large proportion of single-particle excitation, which is in agreement with the lifetime for pair emission. The matrix element for this transition is

$$\int \psi_0^* \sum r_p^2 \psi_{ex}\, dT,$$

the mean square radius of the proton distribution, to which only single-particle excitations contribute. If we take the excited state to be at 6 MeV, the unit of length is $3{\cdot}7 \times 10^{-13}$ cm. The matrix element is then 11×10^{-26} cm^2, which is comparable with the experimental value of $3{\cdot}8 \times 10^{-26}$ cm^2 (Devons, Goldring and Lindsey 1954). Alternatively, we can take this result to define our unit of length, and hence find our unit of energy to be 8·4 MeV. The energy of the 3^- state then becomes 8·2 MeV, which is too high; however, the change is in the right direction.

This brings out a point of interest: a different unit of length seems to be required for properties which depend on the nuclear size—the energy of the pure rotational state and the value of the matrix element above—from that required for the vibrations, which involve the inter-particle forces. The latter makes the nucleus far too large.

§ 7. Conclusions

Considering the crudity of the approximations we have made, the agreement, though qualitative, is surprisingly good. Starting from a shell-model wave function, we have been able to deduce, qualitatively, the ^{16}O spectrum. In particular, the order of the lowest odd-parity levels, 3^-, 1^-, 2^-, is that found experimentally and the ratio of their separations is of the right order. However, Elliott (to be published), in a shell-model calculation, has been able to fit these levels considering only single excitations, whereas our model predicts large amounts of triple excitation in the 1^- and 3^- states.

The quantitative agreement of the 0^+, 2^+, and 1^- levels with experiment seems to be largely coincidental. If we are to obtain quantitative agreement for all the lower levels, we must be able to find vibration and rotation constants of the order of Dennison's empirical values. In our model the three vibration frequencies are equal, whereas Dennison's are $\omega_1 = 6{\cdot}05, \omega_2 = 6{\cdot}77, \omega_3 = 4{\cdot}7$ MeV, for his scheme (*a*), and our rotation parameter $R = \hbar^2/I$ is far too small. Now according to Dennison's scheme (*a*) $E(0^+) = \omega_1$, $E(1^-) = E(2^+) = \omega_3 + 9R/4$; since we have found $\omega_1 = \omega_3$ and R to be small, we do find that the three levels lie close together. However, we cannot fit the remaining low-lying levels satisfactorily. Similar reasoning applies to Dennison's scheme (*b*).

There is a further experimental feature which finds no place in either our model or Dennison's. This is that the threshold for the dissociation $^{16}O \rightarrow {}^{12}C + \alpha$ lies at an excitation of 7·15 Mev (Ajzenberg and Lauritsen 1955) just above the first excited states. We should therefore expect the potential for any motion which separates one α-particle from the other three to differ considerably from the harmonic approximation and to be much more like a Morse function with a rather shallow well. The vibration ω_3 is such a motion; we therefore cannot expect to find any good agreement between a harmonic-oscillator analysis and experiment for the 1^- and 2^+ levels. Similar considerations will also hold for the interpretation of higher levels.

It seems difficult to devise any satisfactory way of improving the present model. To begin with, one has no guide to the validity of the fundamental approximation, in which the potential is assumed to be independent of the state considered. In order to obtain any better agreement with experiment it would be necessary to alter this potential, which would certainly complicate the solution of the wave equation. A further problem which would have to be solved is that of finding the shell-model wave functions. The method used in § 6 is extremely complex, and it would be impracticable to apply it to a large number of states, or to larger nuclei, such as ^{20}Ne or ^{24}Mg.

References

Ajzenberg, F., and Lauritsen, T., 1955, *Rev. Mod. Phys.*, **27**, 77.

Dennison, D. M., 1954, *Phys. Rev.*, **96**, 378.

Devons, S., Goldring, G., and Lindsey, G. R., 1954, *Proc. Phys. Soc.* A, **67**, 134.

Elliott, J. P., and Skyrme, T. H. R., 1955, *Proc. Roy. Soc.* A, **232**, 561.

Wilkinson, D. H., 1955, *Phys. Rev.*, **99**, 631.

The Oscillator Strengths of the 1sσ–2sσ, 1sσ–3dσ and 2sσ–3dσ Transitions of HeH^{2+}

By A. DALGARNO, N. LYNN and E. J. A. WILLIAMS
Department of Applied Mathematics, The Queen's University of Belfast

Communicated by D. R. Bates ; MS. received 29th March 1956

Abstract. The oscillator strengths of the 1sσ–2sσ, 1sσ–3dσ and 2sσ–3dσ transitions of HeH^{2+} are calculated from the exact two-centre wave functions. A comparison is made with results obtained from the LCAO approximation with and without mixing, both the dipole length and dipole velocity formulae being used in each case.

§ 1. Introduction

In recent years, Bates and his collaborators have calculated many properties of H_2^+ from the exact two-centre wave functions of Bates, Ledsham and Stewart (1953). Besides giving precise information (which cannot as yet be obtained experimentally) on the fundamental properties of homonuclear molecules, this work provided exact comparison data with which the accuracy of approximate methods could be reliably assessed. There are, however, fundamental differences between homonuclear and heteronuclear molecules and it is desirable to extend the calculations to a molecule of the latter type. Bates and Carson (1956) have tabulated the exact two-centre electronic wave functions of a number of states of HeH^{2+} so that calculation of their properties is now practicable.

§ 2. Calculations

2.1. If the nuclei are regarded as held fixed at a distance R apart, the oscillator strength associated with the transition from a lower state A to an upper state B is given by

$$f(\mathrm{A–B}|R) = \tfrac{2}{3}E(\mathrm{A–B}|R)G(\mathrm{A–B})|Q(\mathrm{A–B}|R)|^2 \qquad \ldots\ldots(1)$$

where $E(\mathrm{A–B}|R)$ is the vertical energy difference in rydbergs, $G(\mathrm{A–B})$ is the orbital degeneracy factor and $Q(\mathrm{A–B}|R)$ is the dipole transition integral in atomic units (Mulliken 1939). The transition integral is given by

$$Q^{\mathrm{L}}(\mathrm{A–B}|R)\mathfrak{t} = \int \chi_{\mathrm{A}}^*(\mathbf{r}|R)\mathbf{r}\chi_{\mathrm{B}}(\mathbf{r}|R)d\mathbf{r} \qquad \ldots\ldots(2)$$

in the dipole length formulation and by

$$Q^{\mathrm{V}}(\mathrm{A–B}|R)\mathfrak{t} = -\frac{2}{E(\mathrm{A–B}/R)}\int \chi_{\mathrm{A}}^*(\mathbf{r}|R)\nabla\chi_{\mathrm{B}}(\mathbf{r}|R)d\mathbf{r} \qquad \ldots\ldots(3)$$

in the dipole velocity formulation (Chandrasekhar 1945), χ_{A} and χ_{B} being the electronic wave functions in atomic units. The two integrals are equal when exact wave functions are used.

2.2. The exact two-centre wave functions of HeH^{2+} can be written in the form

$$\chi(\mathbf{r}|R) = \Lambda(\lambda|R)\mathrm{M}(\mu|R)\Phi(\phi) \qquad \ldots\ldots(4)$$

where λ and μ are the usual confocal elliptic coordinates and ϕ is the azimuthal angle. Λ and M can be obtained from tables published by Bates and Carson (1956) and Φ is unity for the σ states considered here. Substituting (4) into (2), it follows that for σ–σ transitions

$$Q(\mathrm{A}\text{–}\mathrm{B}|R) = 2\pi\left(\frac{R}{2}\right)^4\left\{\int_1^\infty \lambda^3\Lambda_\mathrm{A}\Lambda_\mathrm{B}d\lambda\int_{-1}^{+1}\mu\mathrm{M}_\mathrm{A}\mathrm{M}_\mathrm{B}d\mu - \int_1^\infty \lambda\Lambda_\mathrm{A}\Lambda_\mathrm{B}d\lambda\int_{-1}^{+1}\mu^3\mathrm{M}_\mathrm{A}\mathrm{M}_\mathrm{B}d\mu\right\} \qquad \ldots\ldots(5)$$

the wave functions being normalized according to

$$2\pi\left(\frac{R}{2}\right)^3\left\{\int_1^\infty \lambda^3\Lambda^2 d\lambda\int_{-1}^{+1}\mathrm{M}^2 d\mu - \int_1^\infty \Lambda^2 d\lambda\int_{-1}^{+1}\mu^2\mathrm{M}^2 d\mu\right\} = 1 \qquad \ldots\ldots(6)$$

Although it is possible to carry out the integrations over λ and μ analytically, it is less laborious to perform them numerically.

2.3. The LCAO approximations to the wave functions of the $1s\sigma$, $2s\sigma$ and $3d\sigma$ states of HeH^{2+} have the form

$$\chi(1s\sigma) = \left(\frac{8}{\pi}\right)^{1/2}\exp(-2r_1) \qquad \ldots\ldots(7)$$

$$\chi(2s\sigma) = \left(\frac{1}{\pi}\right)^{1/2}\left\{l(R)(1-r_1)+m(R)r_1\cos\theta_1\right\}\exp(-r_1) \qquad \ldots\ldots(8)$$

$$\chi(3d\sigma) = \left(\frac{1}{\pi}\right)^{1/2}\left\{m(R)(1-r_1)-l(R)r_1\cos\theta_1\right\}\exp(-r_1) \qquad \ldots\ldots(9)$$

where r_1 is the distance of the electron from the helium nucleus, θ_1 is its polar angle measured from the internuclear axis, $l^2+m^2 = 1$ and the ratio $l(R):m(R)$ is determined by minimizing the electronic energy, given in rydbergs by

$$E = -\int \chi^*\left(\nabla^2 + \frac{4}{r_1} + \frac{2}{r_2}\right)\chi d\tau, \qquad \ldots\ldots(10)$$

r_2 being the distance of the electron from the proton.

Substituting (7), (8), and (9) into (2) and (3) we find

$$\left.\begin{aligned} Q^\mathrm{L}(1s\sigma\text{–}2s\sigma) &= 0{\cdot}3724_7 m(R)\\ Q^\mathrm{L}(1s\sigma\text{–}3d\sigma) &= -0{\cdot}3724_7 l(R)\\ Q^\mathrm{L}(2s\sigma\text{–}3d\sigma) &= \tfrac{3}{2}\{l^2(R)-m^2(R)\}\end{aligned}\right\} \qquad \ldots\ldots(11)$$

$$\left.\begin{aligned} Q^\mathrm{V}(1s\sigma\text{–}2s\sigma) &= \frac{1{\cdot}1174_0}{E(1s\sigma\text{–}2s\sigma)}\,m(R)\\ Q^\mathrm{V}(1s\sigma\text{–}3d\sigma) &= \frac{-1{\cdot}1174_0}{E(1s\sigma\text{–}3d\sigma)}\,l(R)\\ Q^\mathrm{V}(2s\sigma\text{–}3d\sigma) &= 0\end{aligned}\right\} \qquad \ldots\ldots(12)$$

2.4. The choice of the LCAO approximation for the $2s\sigma$ and $3d\sigma$ states can be criticized on the grounds that for infinite separation these states have the same energy as the $2p\sigma$ state, so that considerable mixing with this state is to be anticipated. The LCAO approximation to the $2p\sigma$ state is

$$\chi(2p\sigma) = \left(\frac{1}{\pi}\right)^{1/2} \exp(-r_2) \qquad \ldots\ldots(13)$$

and as a refinement of (8) and (9), we introduce

$$\chi(2s\sigma) = \left(\frac{1}{\pi}\right)^{1/2} \left\{ l_1(R)(1-r_1)\exp(-r_1) + m_1(R) r_1 \cos\theta_1 \exp(-r_1) + n_1(R)\exp(-r_2) \right\} \qquad \ldots\ldots(14)$$

and similarly for $\chi(3d\sigma)$ with l_2, m_2 and n_2 in place of l_1, m_1 and n_1 respectively. The three possible values of the ratio $l:m:n$ (the third set $l_3:m_3:n_3$ corresponding to the $2p\sigma$ state) are determined by minimizing (10).

The choice of wave function (14) demonstrates a difficulty in the calculation of dipole transition integrals; the approximate wave function of the $1s\sigma$ state is no longer orthogonal to the approximate wave functions of the $2s\sigma$ and $3d\sigma$ states so that the dipole length integrals corresponding to the $1s\sigma$–$2s\sigma$ and to the $1s\sigma$–$3d\sigma$ transitions depend upon the location of the origin to which the electron position vector $\mathbf{r}$ is referred. The analytical expressions for Q^{L} and Q^{V} become rather cumbersome when the mixed wave functions are used and will not be reproduced here.

§ 3. Results and Discussion

3.1 Figures 1, 2 and 3 show the calculated values of the $1s\sigma$–$2s\sigma$, $1s\sigma$–$3d\sigma$ and $2s\sigma$–$3d\sigma$ transition integrals, Q being obtained from the exact wave functions and Q^{L} and Q^{V} from the LCAO approximations, the exact energies being used in the evaluation of Q^{V}. The integrals Q^{L} and Q^{V} are in good agreement with each other and with Q for the $1s\sigma$–$2s\sigma$ transition, Q^{L} being superior to Q^{V} except at small values of R. For the $1s\sigma$–$3d\sigma$ transition, Q^{V} agrees well with Q for R greater than 3 but overestimates considerably for smaller R. It is superior to Q^{L} which, though in fair agreement with the magnitude of Q for large R, has the wrong shape. The values of Q^{L} and Q^{V} for the $2s\sigma$–$3d\sigma$ transition are grossly in error both as regards magnitude and shape at small R, whilst for larger values of R, Q^{L} is quite accurate but not Q^{V} which vanishes everywhere.

When mixing is taken into account, the crossing of the exact $2s\sigma$ and $3d\sigma$ energy curves exercises a profound influence on the mixing parameters (see also Coulson and Lester 1955), and the values of Q^{L} and Q^{V} derived using these approximate orbitals vary in an apparently irregular way. It does not seem worth while to reproduce the values obtained, for in the $1s\sigma$–$2s\sigma$ and $1s\sigma$–$3d\sigma$ transitions, Q^{L} is so sensitive to the location of the origin that no meaningful prediction can be made and even in those cases independent of the origin, agreement with Q is very poor.

Because of the near crossing of the approximate $2s\sigma$ and $3d\sigma$ energy curves it is difficult to draw any general conclusions from these comparisons. It is clear, however, that it is essential to use orthogonal wave functions and that considerable caution must be used before accepting any value of Q derived from variational

wave functions, especially if the energy of either of the states involved lies near to that of some other state at some value of the nuclear separation; it should perhaps be stressed that equality of Q^L and Q^V is in itself no guarantee of accuracy.

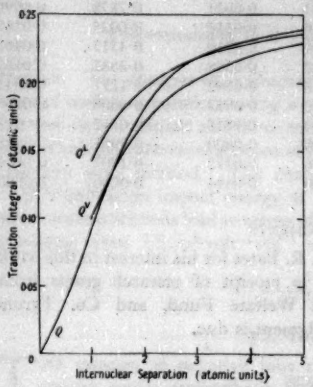

Figure 1. 1sσ–2sσ transition integral.

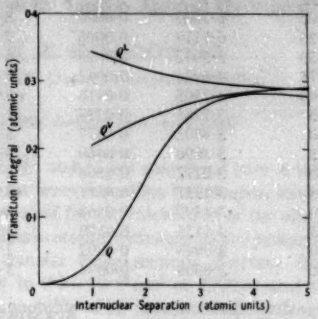

Figure 2. 1sσ–3dσ transition integral

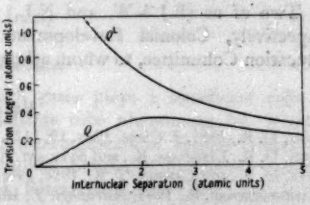

Figure 3. 2sσ–3dσ transition integral.

Q refers to the exact values and Q^L and Q^V to the LCAO approximation.

All the values of Q vanish at the united-atom limit and Q (2sσ–3dσ) at the separated-atoms limit also, so that high sensitivity of the transition integrals to the detailed nature of the wave functions is to be anticipated. The variation of Q with internuclear distance at large values of R is very slow for all three transitions and suggests that a more hopeful procedure for the prediction of transition integrals may be to employ a direct perturbation calculation rather than to use variationally determined approximate wave functions (cf. Dalgarno and Stewart 1956).

3.2. The oscillator strengths obtained by substituting Q into (1) are given in the table. As would be expected since the transition is of the *sub-Rydberg* type (Herzberg 1950) $f(2s\sigma–3d\sigma/R)$ is very small and varies rapidly with nuclear separation; the change in sign is due to the crossing of the 2sσ and 3dσ energy curves. The 1sσ–2sσ and 1sσ–3dσ transitions are not of the *sub-Rydberg* type and the oscillator strengths are considerably larger than $f(2s\sigma–3d\sigma)$ although smaller than those of the *charge-transfer* type which occur in homonuclear molecules (cf. Bates 1951).

Of particular interest is the 1sσ–2pσ transition and calculations of its oscillator strengths and other properties of HeH^{2+} are in progress.

Table. Photon Energies and Oscillator Strengths of some Transitions of HeH^{2+}

	$1s\sigma$–$2s\sigma$		$1s\sigma$–$3d\sigma$		$2s\sigma$–$3d\sigma$	
R	E	f	E	f	E	f
0·00	6·7500	0·0000	8·0000	0·00000	1·2500	0·0000
0·25	6·1119	0·0006	7·2657	0·00002	1·1538	0·0006
0·50	5·3072	0·0025	6·3246	0·00017	1·0174	0·0025
0·75	4·6926	0·0062	5·5875	0·00068	0·8949	0·0056
1·00	4·2505	0·0116	5·0383	0·0021	0·7878	0·0096
1·5	3·7165	0·0253	4·3190	0·0112	0·6025	0·0167
2·0	3·4502	0·0377	3·8819	0·0319	0·4317	0·0169
2·5	3·3096	0·0460	3·5782	0·0540	0·2687	0·0107
3·0	3·2272	0·0508	3·3548	0·0742	0·1277	0·0044
3·5	3·1751	0·0541	3·1960	0·0812	0·0208	0·0006
4·0	3·1392	0·0562	3·0875	0·0818	−0·0517	−0·0012
4·5	3·1135	0·0579	3·0170	0·0800	−0·0965	−0·0018
5·0	3·0943	0·0592	2·9736	0·0772	−0·1207	−0·0019
∞	3·0000	0·0694	3·0000	0·0694	0·0000	0·0000

Acknowledgments

The authors wish to thank Professor D. R. Bates for his interest in this work.

Two of us (E.J.A.W. and N.L.) are in receipt of research grants from, respectively, Colonial Development and Welfare Fund, and Co. Tyrone Education Committee, to whom acknowledgment is due.

References

Bates, D. R., 1951, *J. Chem. Phys.* **19**, 1122.
Bates, D. R., Ledsham, K., and Stewart, A. L., 1953, *Phil. Trans. Roy. Soc.* A, **246**, 215.
Bates, D. R., and Carson, T. R., 1956, *Proc. Roy. Soc.* A, **234**, 207.
Chandrasekhar, S., 1945, *Astrophys. J.*, **102**, 223.
Coulson, C. A., 1952, *Valence* (Oxford : Clarendon Press).
Coulson, C. A., and Lester, G. R., 1955, *Trans. Faraday Soc.*, **51**, 1605.
Dalgarno, A., and Stewart, A. L., 1956, *Proc. Roy. Soc.* A, in the press.
Herzberg, G., 1950, *Spectra of Diatomic Molecules* 2nd Edn. (London : Macmillan).
Mulliken, R. S., 1939, *J. Chem. Phys.*, **7**, 14.

Charge Transfer and the Mobility of H^- Ions in Atomic Hydrogen

By A. DALGARNO and M. R. C. McDOWELL
Department of Applied Mathematics, The Queen's University of Belfast

Communicated by D. R. Bates ; MS. received 24th April 1956

Abstract. The energies of interaction of H^- and H are calculated over a wide range of nuclear separations using molecular wave functions based upon various forms of atomic orbitals and these energies used for the calculation of the charge transfer and diffusion cross sections of H^- ions in atomic hydrogen by the perturbed stationary state method. The charge transfer cross sections decrease from 2×10^{-14} cm^2 at an impact energy of 1 ev to $0{\cdot}3\times10^{-14}$ cm^2 at 1000 ev and the diffusion cross sections lead to values of the mobility of H^- ions in atomic hydrogen decreasing from $3{\cdot}5$ cm^2 volt^{-1} sec^{-1} at 100°K to $1{\cdot}8$ cm^2 volt^{-1} sec^{-1} at 600°K.

§ 1. Introduction

The passage of negative ions through gases plays a significant role in various upper atmospheric and discharge tube phenomena (cf. Massey 1950) but apart from the laboratory measurements of Hasted (1954), of Hasted and Stedeford (1955) and of Hasted and Smith (1956) and the quantal investigations of Bates and Massey (1943), Bates and Lewis (1955) and Bates and Boyd (1956) on some special recombination processes, little precise information on low energy impacts involving negative ions is available (cf. Bates and Dalgarno 1956). It is generally very difficult to study slow heavy particle collisions theoretically but in addition to the curve-crossing cases treated by Bates and his collaborators, slow *resonance* collisions can be treated by the perturbed stationary state method (Massey and Smith 1933, Bates, Massey and Stewart 1953) provided the energies of interaction of the colliding species are known. This method has been applied successfully in one form or another by a number of authors since the original work of Massey and Smith (cf. Massey and Burhop 1952).

§ 2. Theory

The theory of inelastic heavy particle collisions at low impact energies has been discussed in detail by Bates, Massey and Stewart (1953, to be referred to as BMS) and only a brief description is necessary here. Essentially the whole system is supposed in equilibrium with the colliding particles at rest and the relative motion is introduced as a perturbation. Then if $u^{+,-}(R)$ are the effective interaction energies in the g and u modes (BMS eqn 41), R being the nuclear separation, and $g_l^{+,-}$ are the solutions, which vanish at the origin, of the equation

$$\left\{\frac{d^2}{dR^2}+k^2-u^{+,-}-\frac{l(l+1)}{R^2}\right\}g_l^{+,-}=0 \qquad \ldots\ldots(1)$$

such that asymptotically (BMS eqn 103)

$$g_l^{+,-} \sim k^{-1} \sin(kR - \tfrac{1}{2}l\pi + \eta_l^{+,-}) \qquad \ldots\ldots(2)$$

where k is the wave number of the initial relative motion, it may be shown that (BMS eqn 101) the cross section for charge transfer is

$$Q_t(k) = \frac{\pi}{k^2} \sum_l (2l+1) \sin^2(\eta_l^+ - \eta_l^-). \qquad \ldots\ldots(3)$$

The cross section effective in diffusion (cf. Chapman and Cowling 1941) is

$$Q_d(k) = \frac{4\pi}{k^2} \sum_l (l+1) \sin^2(\delta_l - \delta_{l+1}) \qquad \ldots\ldots(4)$$

where $\delta_{2r} = \eta_{2r}^+$ and $\delta_{2r+1} = \eta_{2r+1}^-$ and the diffusion coefficient D is

$$D \sim \frac{3\pi^{1/2}}{16} \left\{ \frac{2(M_1+M_2)}{M_1 M_2} kT \right\}^{7/2} \frac{1}{(n_1+n_2)P_{12}} \qquad \ldots\ldots(5)$$

where

$$P_{12} = \int_0^\infty v^5 Q_d(v) \exp\{-M_1 M_2 v^2/2kT(M_1+M_2)\}\, dv, \qquad \ldots\ldots(6)$$

M_1 and M_2 are the masses of the atoms, n_1 and n_2 are their number densities, k is Boltzmann's constant, T is the absolute temperature and v is the relative velocity. The mobility κ is then given by

$$\kappa = eD/kT, \qquad \ldots\ldots(7)$$

e being the charge of the ion.

§ 3. Approximate Expressions for the Cross Sections

By using Jeffreys' approximation to the phases (cf. Mott and Massey 1949), (3) can be written as (BMS eqn 135)

$$Q_t = 2\pi \int_0^\infty P \sin^2\{\zeta(P)\}\, dP \qquad \ldots\ldots(8)$$

where

$$\zeta(P) = \frac{1}{\hbar} \int_{R_c}^\infty \frac{\Delta E(R)}{v(R)} \left\{ 1 - \frac{v(\infty)^2}{v(R)^2} \frac{P^2}{R^2} \right\}^{-1/2} dR \qquad \ldots\ldots(9)$$

(BMS eqn 134) in which

$$\Delta E(R) = \frac{\hbar^2(M_1+M_2)}{M_1 M_2} (u^+ - u^-), \qquad \ldots\ldots(10)$$

$v(R)$ is the velocity of relative motion when the nuclei are a distance R apart and R_c is the outermost zero of the integrand. It is usually possible to replace $v(R)$ by $v(\infty)$ without serious loss of accuracy (cf. Jackson 1954) so that (9) simplifies to

$$\zeta(P) \sim \frac{1}{\hbar v(\infty)} \int_P^\infty \frac{R\Delta E(R)}{(R^2 - P^2)^{1/2}}\, dR. \qquad \ldots\ldots(11)$$

For small values of P, $\sin^2\{\zeta(P)\}$ oscillates rapidly and may be replaced by its average value of $\frac{1}{2}$. Thus if P^* is the largest value of P for which $\zeta(P)$ equals $\pi/2$,† (8) may be written

$$Q_t = \frac{\pi P^{*2}}{2} + 2\pi \int_{P^*}^\infty P \sin^2\{\zeta(P)\}\, dP. \qquad \ldots\ldots(12)$$

† The choice of P^* is rather arbitrary and this introduces a small uncertainty into the calculated cross sections (cf. Geltman 1953, and §5 of this paper).

The integral from P^* to infinity may be computed from numerical integration of (11) and this procedure is then analogous to that adopted in the phase shift method (cf. Buckingham and Dalgarno 1952). However (11) shows that the major contribution to $\zeta(P)$ comes from the neighbourhood of P and if $\Delta E(R)$ is fitted in this region of R by an exponential $A\exp(-\alpha R)$ where A and α are functions of P, we may write

$$\zeta(P)\sim\frac{A}{\hbar v}\int_P^\infty\frac{R\exp(-\alpha R)}{(R^2-P^2)^{1/2}}\,dR \qquad \ldots\ldots(13)$$

$$=\frac{A}{\hbar v}PK_1(\alpha P) \qquad \ldots\ldots(14)$$

(Erdelyi and Cossar 1944) where $K_1(x)$ is the modified Bessel function of the second kind (Watson 1944) of which adequate tables are available (Bickley 1950, 1952). A very simple approximation to Q_t providing a rapid estimate of its order of magnitude, may be developed by breaking (8) into two parts, from 0 to $\bar{P}$ and from $\bar{P}$ to ∞ where $\bar{P}$ is such that $\zeta(P)=\pi/4$ and supposing that when $\sin^2\{\zeta(P)\}<\frac{1}{2}$, it may be replaced by $\{\zeta(P)\}^2$. Then (8) becomes

$$Q_t\sim\frac{\pi\bar{P}^2}{2}+\frac{2\pi A^2}{\hbar^2v^2}\int_{\bar{P}}^\infty P^3\{K_1(\alpha P)\}^2\,dP. \qquad \ldots\ldots(15)$$

and if A and α are assumed independent of P and αP is assumed large so that

$$K_1(\alpha P)\sim\sqrt{\frac{\pi}{2\alpha P}}\exp(-\alpha P) \qquad \ldots\ldots(16)$$

(15) simplifies to

$$Q_t\sim\frac{\pi\bar{P}^2}{2}+\frac{\pi^3}{16\alpha^2}\left(\alpha\bar{P}+1+\frac{1}{2\alpha\bar{P}}\right)\dagger \qquad \ldots\ldots(17)$$

where $\bar{P}$ is such that

$$\bar{P}\exp(-2\alpha\bar{P})=\frac{\pi}{8}\frac{\hbar^2v^2}{A^2}\alpha. \qquad \ldots\ldots(18)$$

In order to obtain a simple formula for Q_d in terms of the impact parameter P, certain assumptions can be made depending upon the value of R at which the integrand appearing in Jeffreys' approximation to the phase (BMS eqn 111) vanishes. For small values of R, it usually occurs that

$$\delta_s-\delta_{s+1}\sim\pm\zeta(P) \qquad \ldots\ldots(19)$$

whilst at large values of R, $u^+(R)=u^-(R)=-C/R^4$ and $\zeta(P)=0$. Massey and Mohr (1934) have shown that the phases corresponding to this interaction are given approximately by

$$\delta_s\sim\pi Ck^2/8(s+\tfrac{1}{2})^3 \qquad \ldots\ldots(20)$$

from which we estimate $\delta_s-\delta_{s+1}$ according to

$$\delta_s-\delta_{s+1}\sim-\frac{\partial\delta_s}{\partial s}\sim 3\pi C/8k^2P^4. \qquad \ldots\ldots(21)$$

Thus a rough approximation to Q_d is

$$Q_d=2(Q_t+Q_p) \qquad \ldots\ldots(22)$$

† This expression is similar to those obtained by Holstein (1952) and Demkov (1952) using a different approach.

where Q_p is derived from (21) and may be evaluated in a similar way to (17) to give

$$Q_p \sim 2\pi \int_{\bar{P}}^{\infty} P \sin^2 \left\{ \frac{3C\pi}{8k^2P^4} \right\} dP. \qquad \ldots\ldots(23)$$

In §5 the cross sections will be evaluated with and without these various approximations.

§ 4. The Evaluation of the Interaction Energies

Before the calculation of the cross sections can be completed, a knowledge of the interaction energies of H^- and H over a wide range of nuclear separations is required. Since we are interested primarily in the energies at large separations we select molecular wave functions based upon their form at infinity. If $\bar{\psi}_a(1)$ is the wave function of a hydrogen atom with nucleus A and $\bar{\phi}_b(2,3)$ is the wave function of a hydrogen negative ion with nucleus B, 1, 2 and 3 representing the coordinates (including spin) of the three electrons, approximate molecular wave functions corresponding to the two possible modes of interaction and antisymmetrical in all the electrons are given by

$$X_g(1,2,3) = \frac{1}{\sqrt{2}}(\Psi_{ab} + \Psi_{ba}) \qquad \ldots\ldots(24)$$

$$X_u(1,2,3) = \frac{1}{\sqrt{2}}(\Psi_{ab} - \Psi_{ba}) \qquad \ldots\ldots(25)$$

where

$$\Psi_{ab} = \frac{1}{\sqrt{3}}\{\bar{\psi}_a(1)\bar{\phi}_b(2,3) + \bar{\psi}_a(2)\bar{\phi}_b(3,1) + \bar{\psi}_a(3)\bar{\phi}_b(1,2)\}. \qquad \ldots\ldots(26)$$

A difficulty arises from the fact that the space part $\phi_b(\mathbf{r}_2, \mathbf{r}_3)$, $\mathbf{r}_2$ and $\mathbf{r}_3$ being position vectors of the electrons, of $\bar{\phi}_b(2,3)$ is not known exactly. We adopt three different forms for ϕ_b which, in order of increasing accuracy, are

$$\phi_b'(\mathbf{r}_2, \mathbf{r}_3) = \frac{1}{\pi} \exp[-(r_{2b} + r_{3b})] \qquad \ldots\ldots(27)$$

$$\phi_b''(\mathbf{r}_2, \mathbf{r}_3) = \frac{x^3}{\pi} \exp[-x(r_{2b} + r_{3b})] \qquad \ldots\ldots(28)$$

$$\phi_b'''(\mathbf{r}_2, \mathbf{r}_3) = \frac{1}{\pi}\left(\frac{y^3z^3}{2}\right)^{1/2} \{\exp[-(yr_{2b} + zr_{3b})] + \exp[-(zr_{2b} + yr_{3b})]\} \qquad \ldots\ldots(29)$$

where r_{2b} and r_{3b} denote the distances of electrons 2 and 3 from the nucleus B and the parameters are determined from variational calculations of the energy of H^- (Eckart 1930, Chandrasekhar 1944). The space part of the wave function of atomic hydrogen is accurately

$$\psi_a(\mathbf{r}_1) = \frac{1}{(\pi)^{1/2}} \exp(-r_{1a}). \qquad \ldots\ldots(30)$$

The energies are given by

$$\mathscr{E}^+(R) = \int X_g^* \mathscr{H} X_g \, d\boldsymbol{\tau} \Big/ \int X_g^* X_g \, d\boldsymbol{\tau} \qquad \ldots\ldots(31)$$

$$\mathscr{E}^-(R) = \int X_u^* \mathscr{H} X_u \, d\boldsymbol{\tau} \Big/ \int X_u^* X_u \, d\boldsymbol{\tau} \qquad \ldots\ldots(32)$$

where $\mathscr{H}$ is the Hamiltonian of the entire system, and may readily be evaluated once the molecular integrals have been computed. The procedure is well known and details of the calculation have been relegated to an appendix. Depending upon whether the interaction energies are calculated including in $\mathscr{H}$ only the interaction terms or by using the complete Hamiltonian and subtracting the energies computed at infinite separation, different values result (cf. Margenau and Rosen 1953) and a comparison of results $\mathscr{E}_1^{+,-}(R)$ and $\mathscr{E}_2^{+,-}(R)$, respectively, obtained by the two methods using all three functions (27), (28) and (29) in (31) and (32) is given in figures 1 and 2. The discrepancies between $\mathscr{E}_1^{+,-}$ and

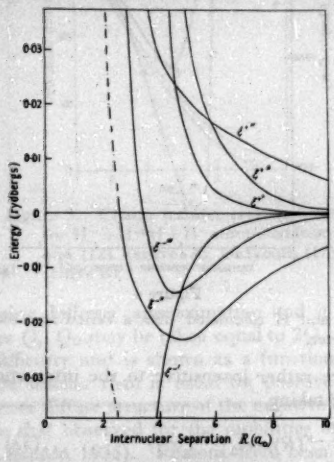

Figure 1. Interaction energies of H^- and H calculated assuming that the atomic orbitals are exact.

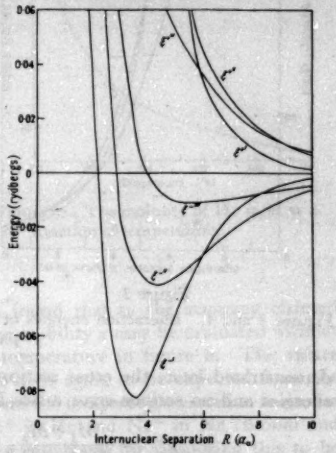

Figure 2. Interaction energies of H^- and H calculated without assuming that the atomi corbitals are exact.

$\mathscr{E}_2^{+,-}$ become smaller as improved forms of ϕ_b are used but are still quite large even for the best of the H^- wave functions. Theoretically $\mathscr{E}_2^{+,-}(R)$ would seem preferable to $\mathscr{E}_1^{+,-}(R)$ and certainly it is much less sensitive to the form of the wave function.

The molecular wave functions (24) and (25) may be improved by the introduction of a scale factor ξ with respect to which the energy may be varied. This has been done previously for the u state of H_2^- using ϕ_b' by Eyring, Hirschfelder and Taylor (1936) and their results (somewhat extended) are reproduced in figure 4, which shows also the values of $\mathscr{E}_2^-(R)$ resulting from the use of ϕ_b'' and ϕ_b''' whilst figure 3 shows the values of $\mathscr{E}_2^+(R)$ resulting from ϕ_b', ϕ_b'' and ϕ_b''. Since these energies are derived from a variational wave function containing a scale factor, they satisfy the quantal virial theorem (Coulson and Bell 1945) but no great accuracy can be claimed even for the best values $\mathscr{E}_2^{+,-''}(R)$ for it has been demonstrated by Hirschfelder and Linnett (1950) and stressed recently by Dalgarno and Lynn (1956) that to obtain accurate energies at large

separations it is necessary to use trial wave functions which take account explicitly of the mutual polarization of one species by the other. However, as will be

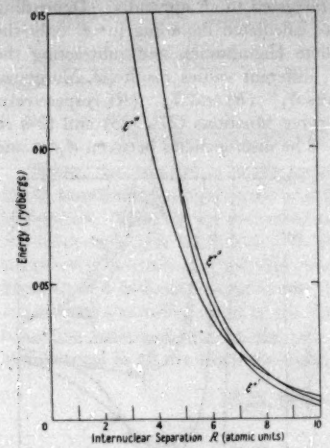

Figure 3

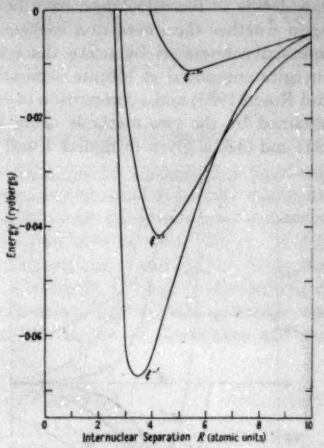

Figure 4

Figures 3 and 4. Interaction energies of H^- and H calculated with a varied screening parameter.

demonstrated later, the cross sections are rather insensitive to the interaction energies and no serious error arises from taking

$$u^{+,-} = \frac{M_1+M_2}{\hbar^2(M_1+M_2)}\{\mathscr{E}_2^{+,-'}(R)-\mathscr{E}_2^{+,-'}(\infty)\} \qquad \ldots\ldots(33)$$

in (2).

§ 5. Charge Transfer Cross Sections and Mobility

It has been checked that (11) is a very accurate representation of (9) for P greater than P^* and charge transfer cross sections over a wide range of impact energies have been evaluated by numerical integration of (12) using the expression for $\zeta(P)$ given by (14). It should be stressed that no loss of accuracy occurs from the use of (14) in place of (11) in that some curve fitting approximation to to $\Delta E(R)$ must be used to overcome the inevitable limitation that $\Delta E(R)$ is known only at discrete values of R. The results are illustrated in figure 5 together with values obtained using the approximate formula (17). As is to be expected from the much more diffuse structure of the negative ion the magnitude of Q_t is rather greater than those of the cross sections for similar reactions involving positive ions, whilst the variation with energy is typical of a resonance reaction. The simple approximation (17) is seen to be remarkably accurate except at high energies of impact where in any event the perturbed stationary state method is inadequate since it ignores transfer of momentum (cf. Dalgarno and Yadav 1953). The success of (17) allows an estimate of the sensitivity of Q_t to $\Delta E(R)$

to be easily made, and a comparison of Q_t derived from it using $\mathscr{E}_2^{+,-''}$ and $\mathscr{E}_2^{+,-'''}$ reveals a difference of at most 10% in the two curves of Q_t. It seems not unreasonable to claim that Q_t as given in figure 5 is accurate to within a possible error of 10%. The phase differences required for Q_d were calculated

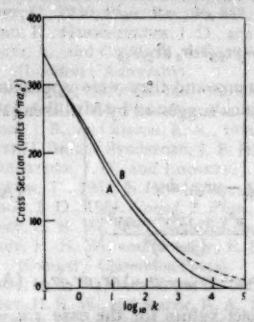

Figure 5. Charge transfer cross sections for $H^- + H \rightarrow H + H^-$ computed from eqn (12) (curve A) and eqn (17) (curve B).

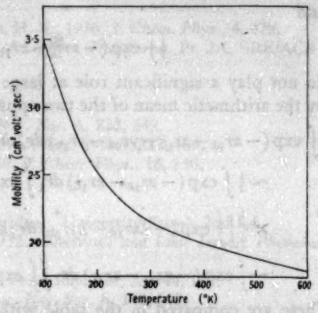

Figure 6. The mobility of H^- in H as a function of temperature.

using Jeffreys' approximation and it was found that to the accuracy claimed for Q_t, Q_d may be taken equal to $2Q_t$. The mobility κ may be evaluated without difficulty and is shown as a function of temperature in figure 6. The values are smaller than is usual for positive ions as is again to be expected from the more diffuse structure of the negative ion and the temperature variation is similar to that observed for the mobilities of He^+ in He and Ne^+ in Ne (Biondi and Channin 1955). Reasons have been given elsewhere for supposing this to be typical of the mobility of ions in their parent gases (Dalgarno 1956).

Acknowledgments

Apart from the exchange type, all the integrals were computed by one of us (A. D.) whilst a guest at the Massachusetts Institute of Technology. He wishes to record his appreciation of the hospitality accorded to him by Professor P. M. Morse and by Professor J. C. Slater and is particularly indebted to Dr. F. C. Corbató without whose expert advice the programming of the Whirlwind would not have been completed in the limited time available.

APPENDIX

The Evaluation of $\mathscr{E}^+(R)$ and $\mathscr{E}^-(R)$

The expressions for $\mathscr{E}^+(R)$ and $\mathscr{E}^-(R)$ can be broken down into combinations of one or two electron two-centre integrals, and it is the evaluation of these and their combination that provides the major computational burden.

The techniques of their evaluation are well known (cf. Dalgarno 1954) and apart from two of the exchange integrals all were calculated on the Whirlwind

electronic computer at the Massachusetts Institute of Technology, the programmes being based upon certain auxiliary routines due to Corbató (1956). The integrals

$$\iint \exp(-r_{1a}-r_{1b}-zr_{2a}-zr_{2b})\,d\mathbf{r}_1\,d\mathbf{r}_2/r_{12}$$

and

$$\iint \exp(-z\overline{r_{1a}}-zr_{1b}-yr_{2a}-yr_{2b})\,d\mathbf{r}_1\,d\mathbf{r}_2/r_{12}$$

do not play a significant role at large separations and they were approximated by the arithmetic mean of the two approximations suggested by Mulliken (1949):

$$\left.\begin{aligned}\iint \exp(-zr_{1a}-zr_{1b}-yr_{2a}-yr_{2b})\,d\mathbf{r}_1\,d\mathbf{r}_2/r_{12}\\ \sim \tfrac{1}{2}\int \exp(-zr_{1a}-zr_{1b})\,d\mathbf{r}_1 \int \exp(-yr_{2a}-yr_{2b})\,d\mathbf{r}_2\\ \times\left\{\iint \exp(-2zr_{1a}-2yr_{2b})\,d\mathbf{r}_1\,d\mathbf{r}_2/r_{12}+\frac{z^3y+3z^2y^2+zy^3}{(y+z)^3}\right\}\end{aligned}\right\} \quad (A.1)$$

$$\sim \int \exp(-zr_{1a}-zr_{1b})\,d\mathbf{r}_1 \iint \exp(-2zr_{1a}-yr_{2a}-yr_{2b})\,d\mathbf{r}_1\,d\mathbf{r}_2/r_{12}. \quad (A.2)$$

These are compared in the table with the exact values for the case $z/a_0=1{\cdot}0$, $y/a_0=1{\cdot}04$, the error being only 6% even at an internuclear separation of $10a_0$.

Neither the values of the screening parameter ξ appropriate to the three wave functions used nor the values of the integrals will be tabulated here, but they are available on request.

Mulliken's Approximations to $\iint \exp(-r_{1a}-r_{1b}-1{\cdot}04r_{2a}-1{\cdot}04r_{2b})\,d\mathbf{r}_1d\mathbf{r}_2/r_{12}$

$R\,(A_0)$	eqn (A1)	eqn (A2)	Arithmetic Mean	Exact
1	0·437043	0·441515	0·439279	0·438689
2	0·178690	0·177776	0·178233	0·180167
3	0·542915 (1)	0·531990 (1)	0·537452 (1)	0·556643 (1)
4	0·142851 (1)	0·138246 (1)	0·140549 (1)	0·142528 (1)
5	0·339138 (2)	0·297040 (2)	0·318089 (2)	0·326568 (2)
6	0·746236 (3)	0·610246 (3)	0·678240 (3)	0·688396 (3)
7	0·154754 (3)	0·118033 (3)	0·136394 (3)	0·136363 (3)
8	0·306014 (4)	0·217969 (4)	0·261992 (4)	0·257425 (4)
9	0·581973 (5)	0·388031 (5)	0·485002 (5)	0·467692 (5)
10	0·107139 (5)	0·670541 (6)	0·870967 (6)	0·823574 (6)

The figure in brackets indicate the power of ten by which the preceding number is to be divided.

References

Bates, D. R., and Boyd, T. J. M., 1956, *Proc. Phys. Soc.* A, **69**, in the press.

Bates, D. R., and Dalgarno, A., 1956, *The Aurora and Airglow*, Ed. E. B. Armstrong and A. Dalgarno (London : Pergamon Press).

Bates, D. R., and Lewis, J. T., 1955, *Proc. Phys. Soc.* A, **68**, 173.

Bates, D. R., and Massey, H. S. W., 1943, *Phil. Trans. Roy. Soc.* A, **239**, 269.

Bates, D. R., Massey, H. S. W., and Stewart, A. L., 1953, *Proc. Roy. Soc.* A, **216**, 437.

Bickley, W. G. (Ed.), 1950, *B.A. Tables of Bessel Functions* Pt. I (Cambridge : University Press) ; 1952, *Ibid.*, Pt. II.

Biondi, M. A., and Channin, L. M., 1955, *Phys. Rev.*, **99**, 1658, (A).

Buckingham, R. A., and Dalgarno, A., 1952, *Proc. Roy. Soc.* A, **213**, 506.

Chandrasekhar, S., 1944, *Astrophys. J.*, **100**, 176.

Chapman, S., and Cowling, T. G., 1941, *Mathematical Theory of Non-Uniform Gases* (Cambridge : University Press), 2nd Ed.

Corbató, F. J., 1956, *J. Chem. Phys.*, **24**, 452.

COULSON, C. A., and BELL, R. P., 1945, *Trans. Faraday Soc.*, **41**, 141.
DALGARNO, A, 1954, *Math. Tab. Wash.*, **8**, 203.
DALGARNO, A., and LYNN, N., 1956, *Proc. Phys. Soc.* A, **69**, in the press.
DALGARNO, A., 1956, U.S.A.F. Cambridge Conf. on Chemical Aeronomy, in the press.
DALGARNO, A., and YADAV, H. N., 1953, *Proc. Phys. Soc.* A, **66**, 173.
DEMKOV, U. H., 1952, *Ann. Leningr. Univ.*, **146**, 74.
ECKART, C., 1930, *Phys. Rev.*, **36**, 882.
EYRING, H., HIRSCHFELDER, J. O., and TAYLOR, H. S., 1936, *J. Chem. Phys.*, **4**, 479.
ERDELYI, A., and COSSAR, J., 1944, *Dictionary of Laplace Transforms*, Pt. 2A, SRE/ACS 68 (London : Admiralty).
GELTMAN, S., 1953, *Phys. Rev.*, **90**, 808.
HASTED, J. B., 1954, *Proc. Roy. Soc.* A, **222**, 74.
HASTED, J. B., and SMITH, R. A., 1956, *Proc. Roy. Soc.* A, **235**, 349.
HASTED, J. B., and STEDEFORD, J. B. H., 1955, *Proc. Roy. Soc.* A, **227**, 466.
HIRSCHFELDER, J. O., and LINNETT, J. W., 1950, *J. Chem. Phys.*, **18**, 130.
HOLSTEIN, T., 1952, *J. Phys. Chem.*, **56**, 832.
JACKSON, J. D., 1954, *Canad. J. Phys.*, **32**, 60.
MASSEY, H. S. W., 1950, *Negative Ions* (Cambridge : University Press), 2nd Ed.
MASSEY, H. S. W., and BURHOP, E. H. S., 1952, *Electronic and Ionic Impact Phenomena* (Oxford : Clarendon Press).
MASSEY, H. S. W., and MOHR, C. B. O., 1934, *Proc. Roy. Soc.* A, **144**, 188.
MASSEY, H. S. W., and SMITH, R. A., 1933, *Proc. Roy. Soc.* A, **142**, 142.
MARGENAU, H., and ROSEN, P., 1953, *J. Chem. Phys.*, **21**, 394.
MOTT, N. F., and MASSEY, H. S. W., 1949, *Theory of Atomic Collisions* (Oxford : Clarendon Press), 2nd Edn.
MULLIKEN, R. S., 1949, *J. Chim. Phys.*, **46**, 487, 675.
WATSON, G. N., 1944, *Theory of Bessel Functions* (Cambridge: University Press) 2nd Edn.

An Investigation of the γ-Rays from the Reactions $^{24}Mg(p, \gamma)^{25}Al$ and $^{12}C(p, \gamma)^{13}N$, with a Note on the Positron Disintegration of ^{25}Al

By D. R. CHICK, W. W. EVANS, D. A. HANCOCK, S. E. HUNT and R. A. POPE

Research Laboratory, Associated Electrical Industries Ltd., Aldermaston, Berks.

MS. received 7th March and in final form 22nd May 1956

Abstract. ^{12}C and ^{24}Mg targets were irradiated by protons of energy 456·8 kev and 225·5 kev corresponding to the formation of excited levels in ^{13}N and ^{25}Al of energy 2·37 and 2·50 Mev respectively. The gamma-ray spectra were investigated using a 20 mm cube sodium iodide crystal and photomultiplier feeding into a Hutchinson–Scarrott type pulse height analyser.

A single gamma ray was observed from the 2·37 Mev state in ^{13}N. Peaks observed from ^{25}Al could best be explained in terms of excited levels at 0·46, 1·54 and 2·5 Mev.

A search was made for γ-radiation accompanying the positron decay of ^{25}Al to ^{25}Mg. The only peak observed was one at 0·51 Mev corresponding to annihilation radiation. It therefore seems probable that a simple positron transition between the ^{25}Al and ^{25}Mg ground state takes place.

§ 1. Experimental Procedure

Thick natural magnesium and carbon targets were irradiated by proton beams of energy 230 kev and 460 kev respectively from an air insulated electrostatic generator.

Beam energy measurement and stability was obtained by using an absolute electrostatic analyser, followed by a deflecting magnet for mass analysis (Hunt 1952). ^{25}Al was produced by resonant capture in the $^{24}Mg(p, \gamma)^{25}Al$ reaction at 225·5 kev, the yield from other magnesium isotopes at this energy being negligible (Hunt, Jones, Churchill and Hancock 1954) and ^{13}N was produced by resonant capture in the $^{12}C(p, \gamma)^{13}N$ resonance at 456·8 kev (Hunt and Jones 1953).

The γ-ray spectrometer consisted of a 20 mm × 20 mm cubic crystal of thallium-activated sodium iodide and a 14 stage photomultiplier tube type EMI 6262A. Pulses from the photomultiplier were amplified and fed into a 120-channel pulse-height analyser of the Hutchinson–Scarrott type (1951) made by Sunvic Controls Limited. This instrument accepted pulses of from 0 to 100 volts and the channel width could be varied from 0·83 to 0·042 volt.

The response of the detecting apparatus was continuously checked and calibrated by using gamma rays of known energy from ^{137}Cs, ^{124}Sb, ^{60}Co, ^{22}Na. No effort was made to collimate the γ-rays from the target, since the yield from the reactions was low and maximum detection efficiency was desirable. The resolution was consequently limited to 12% at 0·667 Mev and 7% at 2·3 Mev.

§ 2. Results

A diagram of the γ-ray spectrum obtained from the carbon target is shown in figure 1. A photoelectric peak was observed at 2·37 Mev with the Compton edge

at 2·13 MeV and pair peak at 1·35 MeV. A peak at 1·9 MeV is interpreted as a pair peak with the escape of one quantum only.

The positron decay of ^{25}Al was investigated by irradiating ^{24}Mg for one minute and then observing the yield for 20 seconds immediately after irradiation. The process was repeated until sufficiently high statistical accuracy was obtained. A

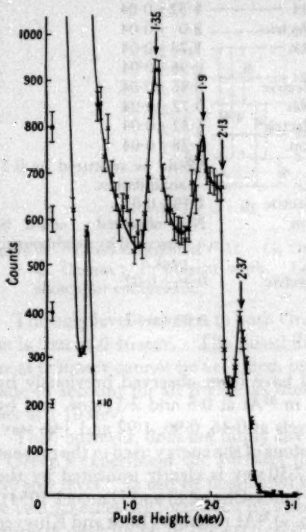

Figure 1. ^{13}N spectrum.

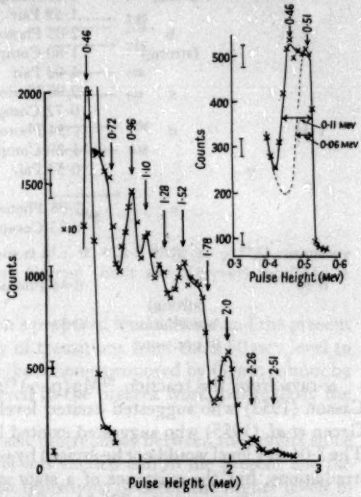

Figure 2. γ-ray spectrum of ^{25}Al. Region 0·2 to 0·65 MeV for Al.

peak at 0·51 MeV corresponding to the annihilation of the positrons was observed but there was no indication of the presence of higher energy γ-rays.

The γ-ray spectrum observed during the irradiation of ^{24}Mg is shown in figure 2, for which a channel width corresponding to 0·04 MeV was used. The results are analysed in the table. The region between 0·2 MeV and 0·65 MeV was investigated in more detail using a channel width corresponding to 0·01 MeV. It will be seen from the spectrum obtained (figure 2) that a peak at 0·46 MeV is incompletely resolved from the annihilation peak at 0·51 MeV. This was confirmed by comparing the half-width of the composite peak with that of the simple annihilation peak from ^{22}Na. The half-widths were found to be in the ratio 11 : 6.

§ 3. Discussion of Results

The results obtained with the carbon target indicate the existence of a single γ-ray of energy $2{\cdot}37 \pm 0{\cdot}03$ MeV. This would be produced by the de-excitation of a level at 2·37 MeV direct to the ground state in agreement with the level scheme proposed by Jackson and Galonsky (1952).

In agreement with the work of Elbek *et al.* (1955) it was found that the positron decay of ^{25}Al was not accompanied by a γ-ray, a possibility which had been suggested by one of us from an analysis of the positron absorption curve

(Hunt, Jones and Churchill 1954). A simple positron transition between the ^{25}Al and ^{25}Mg ground states is therefore indicated.

Energy Level	Transition	Expected Peaks (MeV)	Observed Peaks (MeV)
2·51	a	2·50 Photoelectric	2·5
	(weak)	2·25 Compton	2·26 ± 0·04
		1·49 Pair	1·52 ± 0·04
	b	2·05 Photoelectric	2·0 ± 0·04
	(strong)	1·80 Compton	1·78 ± 0·04
		1·03 Pair	0·96 ± 0·04
	c	0·96 Photoelectric	0·96 ± 0·04
		0·72 Compton	0·72 ± 0·04
1·54	d	1·54 Photoelectric	1·52 ± 0·04
		1·29 Compton	1·28 ± 0·04
		0·54 Pair	Could be obscured by 0·51 annihilation.
	e	1·08 Photoelectric	1·10 ± 0·03
		0·83 Compton	Not observed: could be obscured by neighbouring peak.
0·46	f (strong)	0·46 Photoelectric	0·46 ± 0·02
	Annihilation of positrons	0·51	0·51 ± 0·02

γ-rays from the reaction ^{24}Mg(p, γ)^{25}Al have been observed previously by Casson (1953) who suggested excited levels in ^{25}Al at 0·5 and 2·51 MeV, and by Green *et al.* (1955) who suggested excited levels at 0·46, 0·96, 1·92 and 3·04 MeV. The 3·04 MeV level would not be excited by protons of the energy used in the present irradiations, but the existence of a state at 2·50 MeV is clearly indicated by the proton capture resonance at 225·5 kev (Hunt, Jones, Churchill and Hancock 1954), assuming a Q value of 2·29 MeV for the ^{24}Mg(p, γ)^{25}Al reaction (Endt and Kluyver 1954). Peaks at 2·26 and 1·49 can be interpreted as the Compton and pair peaks of the γ-ray from this level to the ground state. The photoelectric peak would be expected at 2·5 MeV and in some runs a slight increase in yield was noted at this energy but it was not sufficient to be statistically significant. A falling off in the height of the photoelectric peak from a small crystal at this energy was, however, to be expected. The presence of a gamma ray of energy 0·46 and intensity comparable with that from the annihilation of the positrons, is in agreement with the result of Green *et al.* (1955).

All the peaks observed in the present work could be explained in terms of the level diagram shown in figure 3. This differs from that proposed by Casson in that a 1·54 MeV excited level has been introduced. Peaks expected from this scheme are compared with observed peaks in the table. In two instances observed peaks could be composite. A peak at 1·52 ± 0·04 could be produced by a combination of the pair peak from transition a at 1·49 MeV and the photoelectric peak of transition d at 1·54 MeV ; and a peak at 0·96 ± 0·04 MeV to the photoelectric peak from transition c plus the pair peak from transition b. Two expected peaks were not observed, a pair from the 1·54 MeV γ-ray and a Compton from the 1·08 MeV γ-ray, but these were expected to be weak and were in the neighbourhood of much stronger peaks.

It was not possible to obtain a quantitative measure of the relative intensities

of the γ-rays involved in the transitions, but it was obvious that the direct transition from the 2·50 MeV state to the ground state was much weaker than the competing transition b via the 0·46 MeV level. Transitions via the 1·54 MeV state appeared to be of intermediate strength.

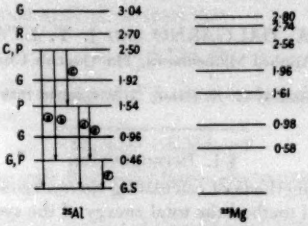

Figure 3. Level diagram of ^{25}Al. G, Green *et al.*; R, 418·5 ^{24}Mg (p. γ) ^{25}Al resonance C, Casson ; P, present work. Level diagram (Endt and Kluyver) for ^{25}Mg is shown for comparison.

The only level common to both Green's proposed level scheme and the present one is that at 0·46 MeV. The possibility of transitions from the 2·50 MeV level to one at 0·96 MeV cannot be excluded, but the scheme proposed by Green cannot be made to account for all the peaks observed in the present work, particularly the peak at 1·10 MeV.

This, however, does not imply any basic discrepancy between the results since in Green's experiment the 3·04 MeV level was excited and in the present one the 2·50 MeV level. It can be postulated that transitions between the higher levels in the two schemes are forbidden by selection rules so that in order to obtain a more complete description of the excited states of ^{25}Al the two schemes must be combined. A level of 2·70 MeV due to the ^{24}Mg(p, γ)^{25}Al resonance at 418·5 keV (Hunt and Jones 1953) must also be added. When this is done the level scheme obtained is closely analogous to that for the mirror nucleus ^{25}Mg (Endt and Kluyver 1954).

Acknowledgments

The authors would like to acknowledge the assistance of Mr. F. Verdaguer who collaborated in the earlier part of this work, and of Mr. R. Rowe who assisted in the experiments.

Thanks are also due to Dr. T. E. Allibone, for permission to publish this work.

References

Casson, H., 1953, *Phys. Rev.*, **89**, 809.
Elbek, B., Madsen, B.S., and Nathan, O., 1955, *Phil. Mag.*, **46**, 663.
Endt, P. M., and Kluyver, J. C., 1954, *Rev. Mod. Phys.*, **23**, 95.
Green, L. L., Singh, J. J., and Willmott, J., 1955, *Phil. Mag.*, **46**, 982.
Hunt, S. E., 1952, *Proc. Phys. Soc.* A, **65**, 982.
Hunt, S. E., and Jones, W. M., 1953, *Phys. Rev.*, **89**, 1283.
Hunt, S. E., Jones, W. M., and Churchill, J. L. W., 1954, *Proc. Phys. Soc.* A, **67**, 479.
Hunt, S. E., Jones, W. M., Churchill, J. L. W., and Hancock, D. A., 1954, *Proc. Phys. Soc.* A, **67**, 443.
Hutchinson, G. W., and Scarrott, G. G., 1951, *Phil. Mag.*, **42**, 792.
Jackson, H. L., and Galonsky, A. I., 1952, *Phys. Rev.*, **84**, 401.

RESEARCH NOTES

The Equivalence of Variational and Perturbation Calculations of Small Disturbances

By A. DALGARNO and J. T. LEWIS †
Department of Applied Mathematics, The Queen's University of Belfast

Communicated by D. R. Bates; MS. received 16th April 1956

§ 1. Introduction

There are three methods of calculating the energies of small disturbances: in the variational method the total energy of the system is minimized with respect to a selected trial wave function and the perturbation energy obtained by subtracting the energy of the undisturbed system (Hassé 1930), in the method proposed by Slater and Kirkwood (1931) (see also Lennard-Jones 1930) the energy of the undisturbed system is subtracted immediately and the perturbation energy obtained as an integral involving the solution of a certain differential equation, and in the perturbation method (Schrödinger 1926) the perturbation energy is expressed as an infinite sum of products of matrix elements of the perturbing potential.

§ 2. Theory of Small Disturbances

Let H be the Hamiltonian of the undisturbed system and let ψ_0 be its (normalized) wave function satisfying the equation

$$(H-E_0)\psi_0=0. \qquad \ldots\ldots(1)$$

Suppose that ψ_p represents any other possible stationary state of the system with eigenvalue E_p so that

$$(H-E_p)\psi_p=0. \qquad \ldots\ldots(2)$$

If a small perturbation, described by an operator h, is applied, the wave function Ψ of the disturbed system is the solution of the equation

$$\mathscr{H}\Psi\equiv(H+h)\Psi=E\Psi \qquad \ldots\ldots(3)$$

which may be written alternatively as

$$\delta E=0 \qquad \ldots\ldots(4)$$

where

$$E=\int\Psi^*\mathscr{H}\Psi\,d\mathbf{r}\Big/\int\Psi^*\Psi\,d\mathbf{r}. \qquad \ldots\ldots(5)$$

We wish to calculate the perturbation energy

$$\mathscr{E}=E-E_0. \qquad \ldots\ldots(6)$$

Substituting

$$\Psi=\psi_0+\phi\psi_0 \qquad \ldots\ldots(7)$$

into (3) and using (1) and (6), it follows that

$$(h-\mathscr{E})\psi_0+(H-E_0+h-\mathscr{E})\phi\psi_0=0 \qquad \ldots\ldots(8)$$

† Now at the Mathematical Institute, University of Oxford.

which on multiplication by ψ_0^* and integration over all space yields

$$\mathscr{E} = \frac{\int \psi_0^* h \psi_0 \, d\mathbf{r} + \int \psi_0^* h(\phi\psi_0) \, d\mathbf{r}}{1 + \int \psi_0^* \phi \psi_0 \, d\mathbf{r}}. \qquad \ldots\ldots(9)$$

2.1. *The Slater–Kirkwood Method*

The Slater–Kirkwood method assumes that

$$\mathscr{E}_1 = \int \psi_0^* h \psi_0 \, d\mathbf{r} \qquad \ldots\ldots(10)$$

is zero (as is usually the case) and $\mathscr{E}$ is then evaluated by taking ϕ to be the solution of the equation

$$h\psi_0 + (H - E_0)\phi\psi_0 = 0 \qquad \ldots\ldots(11)$$

obtained from (8) when only first-order terms are retained. Thus to the second order

$$\mathscr{E} = \mathscr{E}_2 = \int \psi_0^* h(\phi\psi_0) \, d\mathbf{r}. \qquad \ldots\ldots(12)$$

The method may readily be generalized to cases for which $\mathscr{E}_1 \neq 0$; to the second order of small quantities

$$\mathscr{E} = \mathscr{E}_1 + \mathscr{E}_2' - \mathscr{E}_1 \int \psi_0^* \phi_1 \psi_0 \, d\mathbf{r} \qquad \ldots\ldots(13)$$

where ϕ_1 is a solution of

$$(h - \mathscr{E}_1)\psi_0 + (H - E_0)\phi_1\psi_0 = 0. \qquad \ldots\ldots(14)$$

2.2. *The Perturbation Method*

Writing

$$(p \mid L \mid q) = \int \psi_p^* L \psi_q \, d\mathbf{r} \qquad \ldots\ldots(15)$$

the well-known second order perturbation formula for $\mathscr{E}$ is

$$\mathscr{E} = \mathscr{E}_1 + \sum_p{}' \frac{(0 \mid h \mid p)(p \mid h \mid 0)}{E_0 - E_p} \qquad \ldots\ldots(16)$$

where the prime indicates that the term $p = 0$ is excluded and the summation includes an integration over the continuum. Dalgarno and Lewis (1955) (and also Dalgarno and Stewart, in preparation), have recently made use of a sum rule technique to evaluate the infinite summation in (16) with the result that

$$\sum_p{}' \frac{(0 \mid h \mid p)(p \mid h \mid 0)}{E_0 - E_p} = \int \psi_0^* h(\phi_1\psi_0) \, d\mathbf{r} - \mathscr{E}_1 \int \psi_0^* \phi_1 \psi_0 \, d\mathbf{r} \qquad \ldots\ldots(17)$$

where ϕ_1 is a solution of (14).

The equivalence of (16) to (13) is immediately recognized. It may be demonstrated also by expanding $\phi_1\psi_0$ according to

$$\phi_1\psi_0 = \sum_s a_s \psi_s, \qquad \ldots\ldots(18)$$

substituting in (14) and multiplying throughout by ψ_p^*. After integration one obtains

$$a_p = \frac{(p \mid h \mid 0)}{E_0 - E_p}, \quad p \neq 0 \qquad \ldots\ldots(19)$$

and substituting (18) into (13) using (19), equation (16) is recovered.

2.3. *Variational Method*

In the variational method of calculating small disturbances, the trial function (7) is substituted into (5) and quantities of the third and higher orders of smallness are ignored. Thus

$$E = E_0 + \frac{\mathscr{E}_1 + 2\int \psi_0^* h(\phi\psi_0)\,d\tau + \int(\phi\psi_0)^*(H-E_0)\phi\psi_0\,d\tau}{1+2\int\psi_0^*\phi\psi_0\,d\tau}. \qquad \ldots\ldots(20)$$

Now for arbitrary variation of the *function* ϕ (cf. Hartree 1947) the condition that (20) be stationary requires that ϕ be a solution of

$$(h-\mathscr{E}_1)\psi_0 + (H-E_0)\phi\psi_0 = 0 \qquad \ldots\ldots(21)$$

in which case

$$\mathrm{E} = \frac{\mathscr{E}_1 + \mathscr{E}_1\int\psi_0^*\phi\psi_0\,d\tau + \int\psi_0^* h\phi\psi_0\,d\tau}{1+2\int\psi_0^*\phi\psi_0\,d\tau} \qquad \ldots\ldots(22)$$

which to the second order of small quantities is

$$\mathscr{E} = \mathscr{E}_1 + \int\psi_0^* h\phi\psi_0\,d\tau - \mathscr{E}_1\int\psi_0^*\phi\psi_0\,d\tau. \qquad \ldots\ldots(23)$$

Equation (23) is equivalent to (13) and (16).

Thus for any calculation of small disturbances the choice of method rests upon the accuracy with which it may be applied, the three methods when applied exactly yielding identical results. This conclusion is perhaps not unexpected but a direct demonstration seemed desirable. Its importance in *approximate* applications of perturbation theory has been emphasized recently by Dalgarno and Stewart (in preparation).

References

Dalgarno, A., and Lewis, J. T., 1955, *Proc. Roy. Soc.* A, **233**, 70.
Hartree, D. R., 1947, *Rep. Progr. Phys.*, **11**, 113 (London : Physical Society).
Hassé, H. R., 1931, *Proc. Camb. Phil. Soc.*, **27**, 66.
Lennard-Jones, J. E., 1930, *Proc. Roy. Soc.* A, **129**, 598.
Slater, J. C., and Kirkwood, J. E., 1931, *Phys. Rev.*, **37**, 682.
Schrödinger, E., 1926, *Ann. Phys., Lpz.*, **80**, 437.

New Evidence about the Nature of the Liquid Helium Transition

By H. N. V. Temperley

Atomic Weapons Research Association, Aldermaston, Berks.

MS. received 2nd March 1956

§ 1. Presentation and Discussion of Evidence

Goldstein and Reekie (1955) and Goldstein (1955) have succeeded in determining from x-ray data the separate variations with temperature of the kinetic and potential energies of liquid helium. According to them the 'kinetic specific heat' shows a typical λ-anomaly even more violent than that of the total specific heat. This they interpret as quite definite evidence that the transition is related to the momentum space properties of the liquid partition function. They interpret the accompanying anomaly in the 'potential specific

heat', of *inverted* λ-form, as implying some consequential effect of the transition on the liquid structure (cf. F. London 1943). It is the purpose of this note to show that these ideas can be made more precise.

The main difference between Landau (1941, 1947) and Temperley's models of HeII (1952 a, b, 1953) can be stated very simply. According to Landau, HeII is to be represented by a Debye-like model which becomes unstable above the λ-point. According to Temperley, this situation is just reversed and it is HeI that is to be represented by the Debye-like model, which becomes unstable *below* the λ-point. In this note, we shall show that Temperley's model gives a simple interpretation of Goldstein and Reekie's result. Unfortunately, the theory involves a small energy difference which cannot yet be calculated *a priori*, so no convincing quantitative treatment can yet be given. It is certainly possible (Temperley 1952 a) for a simple Debye lattice to become unstable below a certain temperature (in comparison with an assembly of free atoms of small energy) as a result of the entropy of the lattice passing through a maximum if expressed, at fixed energy and volume, as a function of the total number of atoms contained in it. This represents a generalization of the Bose–Einstein condensation when interactions are strong. The picture has been developed further (Temperley 1953) by postulating equilibrium between a Debye lattice, representing the 'large' aggregates of atoms present in any liquid, each of which has more than one bound level, and therefore some internal degrees of freedom, and 'small' aggregates, each of which consists of enough atoms to have a bound level, and yet has no excited levels. ('Small' aggregates are possible only with weak interaction, otherwise even an isolated pair would have more than one bound level.) The condition of equilibrium is, as usual,

$$g_c = g_1 \simeq \frac{\partial}{\partial N_1}\left(E_1^0 - \frac{3\pi^4}{5}\frac{N_1 \boldsymbol{k} T^4}{\Theta^3}\right) \qquad \ldots\ldots(1)$$

where the suffix c refers to 'small' aggregates, 1 to 'large' ones, represented as portions of a Debye lattice, E_1^0 is the total lattice energy at $T=0$ and N_1 the total number of atoms in them. E_1^0 is, as many writers have stressed, the algebraic sum of the (numerically nearly equal) interatomic interaction and the zero-point kinetic energies. E_1^0 is, however, large compared with the temperature term describing the intrinsic specific heat of a Debye-like lattice. It is not easy to give a satisfactory expression for g_c, the partial potential of the 'small' aggregates. To a first approximation, we could write simply

$$g_c = \epsilon_c^0 \qquad \ldots\ldots(2)$$

where ϵ_c^0 represents the mean energy per atom in a 'small' aggregate at $T=0$. Like E_1^0 this represents the algebraic sum of the potential energy and the zero-point kinetic energy. Although we are supposing that the 'small' aggregates have no excited levels and, therefore, no 'internal' entropy, we ought really to correct (2) to allow for the fact that each 'small' aggregate has some energy of translation as a whole. If we suppose that, near the transition temperature, their number is small, we could probably treat them, from the translational energy point of view, as a nearly perfect gas. This would give, instead of (2),

$$g_c = \epsilon_c^0 = \boldsymbol{k} T\left[\log\left(qV_c/N_c\right) + \tfrac{3}{2}\log\left(2\pi \boldsymbol{m} q \boldsymbol{k} T/\boldsymbol{h}^2\right)\right] \qquad \ldots\ldots(3)$$

where N_c is the total number of atoms in the small aggregates, each containing q atoms on the average. Equating (1) and (3) we have, in principle, our transition

curve. If we neglected altogether the variation of such quantities as $\partial E_1^0/\partial N_1$, Θ and ϵ_c^0 with N_1 and N_c, the numbers of atoms in the 'large' and 'small' aggregates respectively (with $N_c + N_1$ kept constant) we should simply obtain an equation for the transition temperature at which 'large' aggregates were first becoming unstable. If we could take these variations into account, we should get an implicit equation relating N_1 (or N_c) with T. Some of the above quantities are probably fairly sensitive to N_1 so we cannot calculate the variation of $\partial E_1^0/\partial N_1$ with ϵ_c^0 *a priori*, nor can we compute the expected anomaly in the specific heat which arises as a consequence of (1) and (3), since the free energy of the whole assembly depends on N_1 and thus has an 'extra' dependence on T. Extra terms involving the differential coefficients of N_c with respect to T now appear in the specific heat, which would drop out as soon as N_c became zero, this being analogous to a Weiss type model. (We now know of more realistic models of co-operative phenomena, which permit the 'key' parameter, here N_c, to remain finite on the high-temperature side of the anomaly.)

We can, however, say that Goldstein and Reekie's results (1955) are consistent with a steady increase of N_c at the expense of N_1 as we drop further below the λ-point. They find that the rate of decrease of mean kinetic energy with falling temperature increases abruptly at the λ-point and then diminishes slowly. Now it seems certain that the zero-point *kinetic* energy per atom in a 'small' aggregate is significantly less than it is in a 'large' one. This follows very simply from the fact that the potential energy per atom must certainly be numerically smaller in the 'small' aggregates, since each atom has fewer others to interact with, and so the ground-level kinetic energy per atom must be smaller also, since an atom acquires more kinetic energy if it is more strongly confined. (It is very much more difficult to make predictions about the *total* energies of aggregates in their ground-levels.) Nothing about this model requires that N_c/N approaches unity as $T \to 0$, and it is more likely that it approaches a fraction. When the variation of N_c with T becomes small the anomalous part of the specific heat becomes negligible, and the model again behaves like a Debye lattice. If the 'small' aggregates are just pairs, their zero-point kinetic energy must agree roughly with the depth of the potential well, that is it must correspond to 3°–5°K per atom, compared with Goldstein's (1955) best estimates for the liquid of 16·2°K per atom near the λ-point and 13·0°K per atom near $T = 0$. This would imply that, as $T \to 0$, the fraction of atoms in 'small' aggregates is of the order of 0·2–0·3 which seems not unreasonable, though we have no independent check on this figure at present.

We have seen that a small, but definite, anomaly occurs in the 'potential' specific heat, in a sense opposed to the much larger anomaly in the 'kinetic' specific heat. Goldstein and Reekie (1955) couple the former effect with the anomaly in the expansion coefficient, attributing both to a 'defence mechanism'. If we take account of the translational energy of the 'small' aggregates, it seems possible to give a reasonable physical interpretation of this 'defence mechanism'. Consider what we may expect if some of the 'large' aggregates partly break down into 'small' ones. The latter make a contribution to the pressure as the result of their translational motion. (We recall that, in a classical assembly treated by the Mayer theory, the pressure is strictly proportional to the total number of clusters.) Put in another way, at constant total volume, the volume V_c 'available' to the 'small' aggregates must adjust itself, at constant total volume, until the

free energy of the whole assembly is a minimum. If, as is to be expected, the mean spacing between atoms in 'small' aggregates is greater than in 'large' ones, the necessary 'elbow room' can only be obtained by the 'larger' aggregates becoming denser. Thus, we get an increase in total pressure as we go below the transition temperature at constant volume, that is a negative expansion coefficient. As the temperature falls further, this extra pressure will vary roughly like $N_c T$, and should, with the expected variation of N_c with T, thus pass through a maximum and fall to zero. At very low temperatures we shall be left with the coefficient of expansion of the Debye-like lattice alone, which should be positive, as found by Atkins and Edwards (1954). (In fact, if the estimated contribution of the Debye lattice is 'subtracted out', the remaining contribution to the density was found to be roughly proportional to ρ_n.) Thus, the 'defence mechanism', with the initial rise in potential energy as we recede from the λ-point, is interpreted simply as the compression of the 'large' aggregates as a result of the extra pressure contributed by the translations of the small ones.

We have mentioned that the 'anomalous' part of the change of density is roughly proportional to ρ_n and we know empirically that above $1°\text{K}$ ρ_n follows the specific heat curve fairly accurately, whereas the ρ_n for a Debye lattice does not do so. It is therefore tempting to split ρ_n into a 'Debye' contribution and an 'anomalous' contribution, the latter arising from the presence of the 'small' aggregates, and probably also as the result of a shift in the ratio N_c/N when the assembly is set into motion. (Temperley (1952 a, Appendix) has shown that the calculation of the 'Landau effective mass' can be generalized in principle to any assembly, it being only necessary to take account of the fact that, if an assembly is known to be sharing a certain total momentum among its individual atoms, the probabilities of occupation of its various levels do differ slightly from those appropriate when the total momentum is known to be zero.) In view of our uncertainty about the variations with N_c of some of the quantities occurring in (1) and (3), we cannot yet compute the expected variation of ρ_n with T in the neighbourhood of the λ-point, though we can still use Landau's (1941) calculation for the Debye lattice when T is small. It seems not unreasonable that the anomalous parts of ρ_n, of the specific heat, and of the coefficient of expansion should vary in roughly the same way with temperature, since, according to this model, they are all consequences of N_c being finite and varying with T, while, according to Landau (1947), they are consequences of the presence of 'rotons'. By 'anomalous' we mean, in all three cases, what is left when the Debye-like contribution is subtracted, the Debye Θ being approximately $25°$–$30°\text{K}$, which gives a reasonable fit both for HeI and for the low temperature part of the HeII region, besides agreeing with the observed velocity of ordinary sound.

There is other evidence, hard to interpret solely on the basis of a Debye-like model and mean free paths, that does seem to show that the structure of HeII is unexpectedly sensitive to quite small motions of the boundary, as the above ideas require. Heikkila and Hollis Hallett (1955) find that boundary velocities have to be very slow to permit proper viscosity measurements, and other complex effects (which might be explained on the basis that 'small' and 'large' aggregates attain relative equilibrium only slowly (Temperley 1953)) are being discovered (see, for example Hall and Vinen 1955, Winkel, van Groenou and Gorter 1955). Hurst and Henshaw (1955) find, by neutron diffraction, that the shifts in the first peak of their liquid distribution function as the temperature changes are less

than would be expected on the basis of changes in the observed density. This seems consistent with a finite value of N_c/N. They say: "A possible model to explain the remaining density change is the existence of unoccupied sites in an array with separations that are little, if at all, temperature dependent. Increased density would then be largely due to increased occupation of these sites, i.e. the filling of 'holes'."

§ 2. Conclusion

The above evidence lends further support to the hypothesis of the physical existence of 'small' aggregates in HeII. It is certain theoretically that any correct treatment of an assembly of helium atoms would have to take account of the formation and dissociation of bound pairs, triplets, etc., at *some* range of densities. An *a priori* prediction of the range of densities concerned awaits a better handling of the many-body problem, meanwhile it is a satisfactory working hypothesis that these effects are still important in HeII, even though they may not be so in other liquids where interactions are stronger and zero-point effects less significant.

Note added in proof.—Since writing the above, I have seen various attempts to derive 'individual' and 'collective' excitation spectra directly from the many-body Hamiltonian rather than via quantum hydrodynamics. See, for example, Tomonaga (1955), Zubarev (1953), Brenig (1956). A number of points of detail arise, which I hope to deal with in another paper. Although it cannot yet be made fully quantitative, Brenig's (1956) approach seems to give quite natural interpretations of the λ-point and the variation of ρ_n with T in terms of the properties of the individual spectrum, which seem to be very similar to the interpretations suggested above. In addition, Zubarev's (1953) work on the Fermi model seems to be quite consistent with either of the two semi-empirical models proposed by Temperley, (1954, 1955) for He_3.

Acknowledgment

I wish to thank the Director, Atomic Weapons Research Establishment, for permission to publish this note.

References

Atkins, K. R., and Edwards, M. H., 1954, *Phys. Rev.*, **93**, 1416.
Brenig, W., 1956, *Z. Phys.*, **144**, 488.
Goldstein, L., 1955, *Phys. Rev.*, **100**, 981.
Goldstein, L., and Reekie, J., 1955, *Phys. Rev.*, **98**, 857.
Hall, H. E., and Vinen, W. F., 1955, *Phil. Mag.*, **46**, 546.
Heikkila, W. J., and Hollis-Hallett, A. C., 1955, *Canad. J. Phys.*, **33**, 420.
Hurst, D. G., and Henshaw, D. G., 1955, *Phys. Rev.*, **100**, 994.
Landau, L. D., 1941, *J. Phys. U.S.S.R.*, **5**, 71 ; 1947, *Ibid.*, **11**, 91.
London, F., 1943, *J. Chem. Phys.*, **11**, 203.
Temperley, H. N. V., 1952 a, *Proc. Phys. Soc.* A, **65**, 490 ; 1952 b, *Ibid.*, **65**, 619 ; 1953, *Ibid.*, **66**, 995 ; 1954, *Ibid.*, **67**, 495 ; 1955, *Ibid.*, **68**, 1136.
Tomonaga, S., 1955, *Progr. Theor. Phys.*, **13**, 467, 482.
Winkel, P., van Groenou, A. B., and Gorter, C. J., 1955, *Physica*, **21**, 345.
Zubarev, D. N., 1953, *J. Exp. Theor. Phys.*, **25**, 548.

The Magnetic Moments of Odd–Odd Nuclei

By C. A. CAINE

The Clarendon Laboratory, Oxford

MS. received 26th April 1956

§ 1. Introduction

It has been shown by Blin-Stoyle and Perks (1954, to be referred to as I; see also Arima and Horie 1954) that the deviations of the magnetic moments of most odd A nuclei from the Schmidt lines can be explained in terms of simple interconfigurational mixing. In the present work an attempt has been made to apply the same methods to calculate the magnetic moments of odd–odd nuclei and, in particular, to justify the empirical rule for calculating such moments (Schwartz 1953). In this it is assumed that each separate odd-group of nucleons retains those properties which it displays when associated with an even-group, and that the g factors of the separate odd-groups are given by those of the neighbouring odd A nuclei. We assume that the results and interpretations of I are essentially correct and that the empirical g factors of the odd-groups in odd A nuclei may be found from them. From this we show that the magnetic moments of most odd–odd nuclei will be given by the values calculated using the empirical rule together with certain other terms which, in general, are seen to be small.

§ 2. The Empirical Rule

Consider an odd–odd nucleus of total angular momentum I which, on the j–j coupling shell model, consists of an odd-group of protons and an odd-group of neutrons outside closed shells. The magnetic moment operator $\boldsymbol{\mu}$ of the nucleus is assumed to have the form:

$$\boldsymbol{\mu} = g\mathbf{j} + g'\mathbf{j}' \qquad \ldots\ldots(1)$$

where $\mathbf{j}$, $\mathbf{j}'$ are the angular momenta of the separate odd-groups and g, g' are their g factors measured from the magnetic moments of the neighbouring odd–even and even–odd nuclei. This gives

$$\mu = \tfrac{1}{2}(g+g')I + (g-g')\frac{j(j+1)-j'(j'+1)}{2(I+1)}. \qquad \ldots\ldots(2)$$

We take first the neighbouring odd–even nucleus in which the second group has now an even number of nucleons and is assumed to have zero angular momentum. Let ϕ_j be the shell model wave function (ignoring the even group of nucleons) and let $\chi_{\gamma,J}$ be any other configuration of the odd nucleons where J is the angular momentum and γ any other variables needed to specify the state completely. As in I, we neglect second-order corrections to the amplitude of ϕ_j, and take as our true wave function

$$\psi_j = \phi_j + \sum_{\gamma} \alpha_\gamma \chi_{\gamma,j}. \qquad \ldots\ldots(3)$$

To the first order in the α's we obtain:

$$g=\frac{1}{j}\left\{\langle\phi_j|\mu|\phi_j\rangle+2\sum_\nu\alpha_\nu\langle\phi_j|\mu|\chi_{\nu j}\rangle\right\} \qquad \ldots\ldots(4)$$

where μ is the magnetic moment operator of the odd group of particles, i.e. the sum of the single particle operators taken over all the nucleons of the odd-group. If we let V be the sum of the interactions between the nucleons in the odd-group, the α's are given by perturbation theory:

$$\alpha_\nu=-\langle\phi_j|V|\chi_{\nu j}\rangle/\Delta E_{\nu j} \qquad \ldots\ldots(5)$$

where $\Delta E_{\nu j}$ is the energy difference between the states $\chi_{\nu j}$ and ϕ_j.

Similarly, considering the neighbouring even–odd nucleus and defining $\phi'_{j'}$, $\chi'_{\nu' J'}$, μ', V', and $\Delta E'_{\nu' J'}$ in exactly the same way, we have

$$g'=\frac{1}{j'}\left\{\langle\phi'_{j'}|\mu'|\phi'_{j'}\rangle+2\sum_{\nu'}\alpha'_{\nu'}\langle\phi'_{j'}|\mu'|\chi'_{\nu' j'}\rangle\right\} \qquad \ldots\ldots(6)$$

where

$$\alpha'_{\nu'}=-\langle\phi'_{j'}|V'|\chi'_{\nu' j'}\rangle/\Delta E'_{\nu' j'}. \qquad \ldots\ldots(7)$$

Now we consider the odd–odd nucleus. The shell model wave function is $\Phi_I\sim\{\phi_j\phi'_{j'}\}_I$, and since the magnetic moment operator is the sum of single particle operators, the only admixtures contributing linearly in their amplitudes to the magnetic moment are of the forms

$$\Phi_I(\nu J)\sim\{\chi_{\nu J}\phi'_{j'}\}_I \quad \text{and} \quad \Phi'_I(\nu' J')\sim\{\phi_j\chi'_{\nu' J'}\}_I$$

where J can take all half-integral values satisfying $I+j'\geqslant J\geqslant|I-j'|$ and similarly for J'. The coefficient of the admixture $\Phi_I(\nu J)$ is again given by perturbation theory to be

$$-\langle\Phi_I|V+V_{12}|\Phi_I(\nu J)\rangle/\Delta E_{\nu J}=\alpha_\nu\delta_{Jj}+\beta_{\nu J} \qquad \ldots\ldots(8)$$

where V_{12} is the sum of the interactions between all dissimilar nucleons, and

$$\beta_{\nu J}=-\langle\Phi_I|V_{12}|\Phi_I(\nu J)\rangle/\Delta E_{\nu J}. \qquad \ldots\ldots(9)$$

Similarly the coefficient of $\Phi'_I(\nu' J')$ is $\alpha'_{\nu'}\delta_{J' j'}+\beta'_{\nu' J'}$ where

$$\beta'_{\nu' J'}=-\langle\Phi_I|V_{12}|\Phi'_I(\nu' J')\rangle/\Delta E'_{\nu' J'}. \qquad \ldots\ldots(10)$$

Hence for our true wave function we take

$$\Psi_I=\Phi_I+\sum_\nu\alpha_\nu\Phi_I(\nu j)+\sum_{\nu'}\alpha'_{\nu'}\Phi'_I(\nu' j')+\sum_{\nu J}\beta_{\nu J}\Phi_I(\nu J)+\sum_{\nu' J'}\beta'_{\nu' J'}\Phi'_I(\nu' J'), \ldots(11)$$

which, neglecting terms in α^2, β^2, can be written symbolically as

$$\Psi_I\sim\{(\psi_j+\sum_{\nu J}\beta_{\nu J}\chi_{\nu J})(\psi'_{j'}+\sum_{\nu' J'}\beta'_{\nu' J'}\chi'_{\nu' J'})\}_I \qquad \ldots\ldots(12)$$

and to the first order in the α's and β's the magnetic moment is

$$\begin{aligned}\mu=&\langle\Phi_I|\mu+\mu'|\Phi_I\rangle+2\sum_\nu\alpha_\nu\langle\Phi_I|\mu|\Phi_I(\nu j)\rangle+2\sum_{\nu'}\alpha'_{\nu'}\langle\Phi_I|\mu'|\Phi'_I(\nu' j')\rangle\\&+2\sum_{\nu J}\beta_{\nu J}\langle\Phi_I|\mu|\Phi_I(\nu J)\rangle+2\sum_{\nu' J'}\beta'_{\nu' J'}\langle\Phi_I|\mu'|\Phi'_I(\nu' J')\rangle.\end{aligned} \qquad \ldots\ldots(13)$$

Provided that the α_ν's and $\alpha'_{\nu'}$'s are such that the empirical g factors are given correctly by (4) and (6), we see that the first three terms in (13) correspond to the value of μ given by (2), i.e. by the empirical rule. The correction to this value is given by

$$\delta\mu=2\sum_{\nu J}\beta_{\nu J}\langle\Phi_I|\mu|\Phi_I(\nu J)\rangle+2\sum_{\nu' J'}\beta'_{\nu' J'}\langle\Phi_I|\mu'|\Phi'_I(\nu' J')\rangle. \qquad \ldots\ldots(14)$$

In the odd A case we have neglected admixtures corresponding to type (iii) of I, i.e. excitation of a nucleon from the even-group, but it is shown in I that the effects of such admixtures are generally small compared with those of admixtures in which an odd nucleon is excited. In the odd–odd case these correspond to the contributions

$$2\sum_{\gamma}\beta_{\gamma j}\langle\Phi_I|\mu|\Phi_I(\gamma j)\rangle \quad \text{and} \quad 2\sum_{\gamma'}\beta'_{\gamma' j'}\langle\Phi_I|\mu'|\Phi'_I(\gamma' j')\rangle.$$

The case where only this type of admixture is allowed in the odd A nucleus is considered in § 4.

§ 3. Inter-configurational Mixing

In order to simplify the calculations and to enable us to use the results of I, each odd-group is considered to consist of three nucleons only. Only admixtures giving first-order contributions to the magnetic moment are considered, and throughout $j=l-\frac{1}{2}$, $k=l+\frac{1}{2}$ refer to one group, and $j'=l'-\frac{1}{2}$, $k'=l'+\frac{1}{2}$ to the other. If we write

$$\phi_j\sim[(l_k)_0{}^2 l_j]_j, \qquad \chi_{KJ}\sim[(l_k l_j)_K l_j]_J$$
$$\phi_k\sim[(l_k)_0{}^2 l_k]_k, \qquad \bar{\chi}_{KJ}\sim[(l_k l_j)_K l_k]_J \qquad \ldots\ldots(15)$$

and similarly for the primed functions, we need only consider three cases:

Type (i). The basic state is $\Phi_I\sim\{\phi_j\phi'_{j'}\}_I$ and we consider admixtures of the forms

$$\Phi_I(KJ)\sim\{\chi_{KJ}\phi'_{j'}\}_I \quad \text{and} \quad \Phi'_I(K'J')\sim\{\phi_j\chi'_{K'J'}\}_I.$$

Type (ii). Basic state : $\Phi_I\sim\{\phi_k\phi'_{k'}\}_I$, with admixtures

$$\Phi_I(KJ)\sim\{\bar{\chi}_{KJ}\phi'_{k'}\}_I \quad \text{and} \quad \Phi'_I(K'J')\sim\{\phi_k\bar{\chi}'_{K'J'}\}_I.$$

Type (iii). Basic state : $\Phi_I\sim\{\phi_j\phi'_{k'}\}_I$, with admixtures

$$\Phi_I(KJ)\sim\{\chi_{KJ}\phi'_{k'}\}_I \quad \text{and} \quad \Phi'_I(K'J')\sim\{\phi_j\bar{\chi}'_{k'j'}\}_I.$$

The internucleon interaction is taken to be of zero range,

$$V(\mathbf{r}_{ij})=A\delta(\mathbf{r}_{ij}) \qquad \ldots\ldots(16)$$

and the value $\epsilon_t/\epsilon_s\sim 1{\cdot}5$ where ϵ_t, ϵ_s are the triplet and singlet interaction energies (Pryce 1952). In calculating the coefficients of the admixtures, ΔE_{KJ} is now the spin–orbit splitting between j and k, and the values of the parameters $\xi_l=(\epsilon_s/\Delta E)_l$ are taken from the appropriate tables in I. The g factors of the separate odd-groups (4), (6), now correspond to the results of I and hence to their empirical values, and corresponding to (14) the correction to the empirical value of the magnetic moment is

$$\delta\mu=2\sum_{KJ}\beta_{KJ}\mu_{KJ}+2\sum_{K'J'}\beta'_{K'J'}\mu'_{K'J'} \qquad \ldots\ldots(17)$$

where

$$\mu_{KJ}=\langle\Phi_I|\mu|\Phi_I(KJ)\rangle, \quad \beta_{KJ}=-\langle\Phi_I|\Sigma V(\mathbf{r}_{np})|\Phi_I(KJ)\rangle/\Delta E_{KJ} \qquad \ldots\ldots(18)$$

and similarly for the primed quantities.

The calculations proceed exactly as in I, but the final result for $\delta\mu$ is too lengthy to be reproduced here. In each case it is found that $\delta\mu$ is given by the sum of terms, each of which is of an order of magnitude smaller than the terms occurring in the summation for $\Delta\mu$ (where $\Delta\mu$ is the empirical correction to the single particle model value, i.e. the second and third term in (13)) primarily

because each involves the square of a Racah coefficient whereas in $\Delta\mu$ only first-order terms occur. Moreover, in the summation for $\delta\mu$ the signs of the terms are roughly alternating and hence we may expect $\delta\mu$ to be appreciably smaller than $\Delta\mu$. In the cases where a full numerical calculation has been carried out $|\delta\mu| \sim 0{\cdot}05$.

§ 4. Exceptions to the Empirical Rule

There are, however, certain odd–odd nuclei for which the foregoing description cannot be applied, namely when either (or both) of the odd-groups consists of one particle in a $k=l+\frac{1}{2}$ state, or one 'hole' in a $j=l-\frac{1}{2}$ state. For the single particle in a $k=l+\frac{1}{2}$ state, there will be a first-order contribution to the magnetic moment from the state in which this particle is excited to the $j=l-\frac{1}{2}$ level. Similarly for an odd-group consisting of one 'hole' in a $j=l-\frac{1}{2}$ level there will be a contribution from the state in which a nucleon is excited from the closed $k=l+\frac{1}{2}$ subshell to fill the $j=l-\frac{1}{2}$ subshell. Neither of these admixtures is allowed in the corresponding odd A nuclei (type (iii) of I) since the angular momentum of the odd-group has to be conserved if there is to be a first-order contribution to μ. Consequently we may now expect deviations from the values of the magnetic moments calculated from the empirical g factors. Unfortunately, it is difficult to state with any certainty that a particular subshell has only one 'hole' or only one nucleon except in the case of $s_{1/2}$ groups where there is no spin–orbit doublet, and $p_{1/2}$ odd-groups of which the only example is ^{14}N for which both the j–j coupling model and the zero-range interaction are expected to be poor approximations (Lane 1953). Only in the case of a doubly closed L–S shell nucleus in which both the even-groups are plus or minus an odd nucleon can such an assignment be made with reasonable accuracy. In this case the corresponding odd A nuclei are correctly predicted to show little deviation from the Schmidt lines (see I). However, as we have pointed out, for the odd–odd nucleus it is clear that there may be some deviation. The only stable odd–odd nucleus of this type, other than ^{14}N and ^{6}Li for which our method is not suitable (Lane 1955), is ^{40}K. For the values of the neutron and proton spin–orbit splittings we take $\Delta E_n \sim 2$ Mev (Ford and Levinson 1955) and $\Delta E_p \sim 9$ Mev (Elliott and Lane 1954). The calculation is again straightforward and gives to the first order

$$\mu = \mu_0 - \epsilon_s \left\{ \frac{0{\cdot}47}{\Delta E_n} - \frac{0{\cdot}37}{\Delta E_p} \right\}$$

i.e.

$$\mu = \mu_0 - 0{\cdot}194\epsilon_s \qquad \ldots\ldots(19)$$

where μ_0 is the single particle model value of $-1{\cdot}68$. Thus to obtain the measured value $\mu = -1{\cdot}29$ we must take $\epsilon_s \sim -2$ Mev. If we take into account the second-order corrections to μ the experimental value may be reproduced using a slightly smaller value for the magnitude of ϵ_s: $\epsilon_s \sim -1{\cdot}7$ Mev. Such values for ϵ_s are not unreasonable. This result agrees qualitatively with those of Tauber and Wu (1954) who show that the observed magnetic moment may be obtained using intermediate coupling approached from the L–S extreme and for a variety of more realistic (finite range) forces.

Thus we may expect deviations from the empirical rule for odd–odd nuclei whose corresponding odd A nuclei show little deviation from the Schmidt lines.

ACKNOWLEDGMENTS

I would like to thank Dr. R. J. Blin-Stoyle for his help and encouragement during the course of this work and also for suggesting changes in the manuscript. I am indebted to the Department of Scientific and Industrial Research for a maintenance grant.

REFERENCES

ARIMA, H., and HORIE, H., 1954, *Progr. Theor. Phys., Japan*, **11**, 509.
BLIN-STOYLE, R. J., and PERKS, M. A., 1954, *Proc. Phys. Soc.* A, **67**, 885.
ELLIOTT, J. P., and LANE, A. M., 1954, *Phys. Rev.*, **96**, 1160.
FORD, K. W., and LEVINSON, C., 1955, *Phys. Rev.*, **100**, 1.
LANE, A. M., 1953, *Proc. Phys. Soc.* A, **66**, 977; 1955, *Ibid.*, **68**, 189.
PRYCE, M. H. L., 1952, *Proc. Phys. Soc.* A, **65**, 773.
SCHWARTZ, H. M., 1953, *Phys. Rev.*, **89**, 1293.
TAUBER, G. E., and WU, T., *Phys. Rev.*, **94**, 1307.

The Quadrupole Moment of a Hydrogen Atom in a Uniform Field

BY A. D. BUCKINGHAM†, C. A. COULSON‡ AND J. T. LEWIS‡
†Physical Chemistry Laboratory, Oxford ‡Mathematical Institute, Oxford

MS. received 26*th March* 1956

WHEN a uniform field of strength F is applied to an atom in an S state a quadrupole moment Θ is induced. Provided that F is not too large Θ may be expressed as a series in F:

$$\Theta = \alpha_q F^2 + \gamma_q F^4 + \ldots\ldots \qquad \ldots\ldots(1)$$

where α_q is termed the quadrupole polarizability§ and γ_q the quadrupole hyperpolarizability, by analogy with the well-known dipole polarizability and hyperpolarizability. These quantities may be calculated exactly for the hydrogen atom; while it is unlikely that it will be possible to compare them with experimental values they are nevertheless of some interest since few quantities can at present be calculated exactly and those that can provide a test of approximate methods.

Sewell (1949) used a method devised by Coulson (1941) to obtain the wavefunction Ψ and energy E of a hydrogen atom in a uniform field of strength F in the form of a power series in F:

$$E = E_0 + E_1 F + E_2 F^2 + \ldots\ldots \qquad \ldots\ldots(2)$$

$$\Psi = \Psi_0 + \Psi_1 F + \Psi_2 F^2 + \ldots\ldots \qquad \ldots\ldots(3)$$

It may be shown that expressed in polar coordinates, and atomic units

$$\left.\begin{aligned} \psi_0 &= e^{-r} \\ \psi_1 &= A(r)P_1(\cos\theta) \\ \psi_2 &= B(r)P_2(\cos\theta) + C(r)P_0(\cos\theta) \\ \psi_3 &= D(r)P_3(\cos\theta) + G(r)P_1(\cos\theta) \end{aligned}\right\} \qquad \ldots\ldots(4)$$

§ This should not be confused with the quantity which was introduced by Mayer and Mayer (1933) in connection with the interpretation of the spectral term defects of the alkali metals, and called the quadrupole polarizability by Sternheimer (1954), but which might be described more accurately as the field-gradient quadrupole polarizability.

where

$$\left.\begin{aligned} A(r) &= e^{-r}\{r^2+2r\}/2 \\ B(r) &= e^{-r}\{2r^4+10r^3+15r^2\}/24 \\ C(r) &= e^{-r}\{r^4+6r^3+18r^2\}/24 \\ D(r) &= e^{-r}\{2r^6+18r^5+63r^4+84r^3\}/240 \\ G(r) &= e^{-r}\{6r^6+64r^5+344r^4+852r^3+1590r^2+3180r\}/480 \end{aligned}\right\} \quad \ldots\ldots(5)$$

when the field is in a direction parallel to the polar axis.

Using (3), (4) and (5) we may express the quadrupole moment

$$\Theta = \frac{\int \Psi^* r^2 P_2(\cos\theta)\Psi d\tau}{\int \Psi^*\Psi d\tau} \quad \ldots\ldots(6)$$

as a power series in F. Then by comparing coefficients with (1) we may determine α_q and γ_q. It is found that

$$\begin{aligned} \alpha_q &= 213/4 \qquad = 0{\cdot}244\times10^{-38}\ \text{e.s.u.} \\ \gamma_q &= 174{,}081/32 = 0{\cdot}846\times10^{-51}\ \text{e.s.u.} \end{aligned} \quad \ldots\ldots(7)$$

using $a_0 = 0{\cdot}5292$ Å where a_0 is the first Bohr radius.

Similarly the octupole moment Ω induced by a uniform field may be expressed as

$$\Omega = \alpha_r F^3 + \ldots\ldots \quad \ldots\ldots(8)$$

or as

$$\Omega = \frac{\int \Psi^* r^3 P_3(\cos\theta)\Psi d\tau}{\int \Psi^*\Psi d\tau} \quad \ldots\ldots(9)$$

which yields $\alpha_r = 4905/4$ atomic units. $\ldots\ldots(10)$

An alternative method of calculating these quantities leads to an interesting physical interpretation of the coefficients of the series development of the energy of interaction of a proton and a hydrogen atom in inverse powers of R, the nuclear separation. We illustrate this by calculating α_q.

Ψ defined above may be expressed in terms of the wave functions ϕ_i and energies E_i^0 of the unperturbed hydrogen atom by means of Rayleigh–Schrödinger perturbation theory (see, for example, Condon and Shortley 1953):

$$\begin{aligned} \Psi = \phi_0 &+ F\sum_i{}'\phi_i \frac{(i|rP_1|0)}{(E_0^0-E_i^0)} \\ &+ F^2\sum_i{}'\left\{ \sum_j{}'\phi_i \frac{(i|rP_1|j)\,(j|rP_1|0)}{(E_0^0-E_i^0)\,(E_0^0-E_j^0)} - \phi_i\frac{(i|rP_1|0)^2}{(E_0^0-E_i^0)^2}\right\} + \ldots \end{aligned} \quad \ldots\ldots(11)$$

where $(i|rP_1|j) = \int \phi_i^* r P_1(\cos\theta)\,\phi_j d\tau$ and $\sum_i{}'$ denote ssummation over all discrete levels other than $i = 0$ and integration over the continuum. Use of (11) in place of (3) yields

$$\alpha_q = \sum_{i,j}{}' \frac{2(0|r^2P_2|i)\,(i|rP_1|j)\,(j|rP_1|0) + (0|rP_1|i)\,(i|r^2P_2|j)\,(j|rP_1|0)}{(E_0^0-E_i^0)\,(E_0^0-E_j^0)} \quad \ldots(12)$$

which may be evaluated directly by the method of Dalgarno and Lewis (1955). Alternatively we may note that the term in R^{-7} in the energy of interaction of a proton and a hydrogen atom when calculated using the perturbation

$$V = -\sum_{n=1}^{\infty}(r^n/R^{n+1})P_n(\cos\theta) \quad \ldots\ldots(13)$$

involves precisely the same expression (12). Comparing it with the exact value of the coefficient obtained by Coulson (1941), we find that $\alpha_q = 213/4$ in agreement with (7).

In a similar way it is possible to interpret the other coefficients of the series development. The term in R^{-4}, as is well known, is related to the dipole polarizability; the term in R^{-6} to the field-gradient quadrupole polarizability, and that in R^{-8} to the dipole hyperpolarizability and the octupole moment induced by the second derivative of the field. The octupole polarizability and the quadrupole hyperpolarizability occur in the coefficients of the R^{-10} and R^{-11} terms respectively.

References

Condon, E. U., and Shortley, G. H., 1953, *The Theory of Atomic Spectra* (Cambridge : University Press).

Coulson, C. A., 1941, *Proc. Roy. Soc. Edinb.* A, **61**, 20.

Dalgarno, A., and Lewis, J. T., 1955, *Proc. Roy. Soc.* A, **233**, 70.

Mayer, J. E., and Mayer, M. G., 1933, *Phys. Rev.*, **43**, 605.

Sewell, G. S., 1949, *Proc. Camb. Phil. Soc.*, **45**, 678.

Sternheimer, R. M., 1954, *Phys. Rev.*, **96**, 951.

The Reaction $^{24}Mg(p, \gamma)^{25}Al$

By J. VARMA

Department of Natural Philosophy, University of Glasgow

Communicated by P. I. Dee; MS. received 14*th October* 1955, *and in revised form* 13*th April* 1956.

§ 1. Introduction

The levels of ^{25}Al have been studied by several workers employing different techniques and reactions (Endt and Kluyver 1954). The energies of the lower excited states of ^{25}Al are reported to be 0·48, 0·95, 1·81, 1·94, 2·51 and 2·71 Mev. From the reaction $^{24}Mg(d, n)^{25}Al$ Goldberg (1953) has found the spin values for the ground and first excited states to be $5/2^+$ and $1/2^+$ respectively with a possible spin of $5/2^+$ or $3/2^+$ for the 0·95 Mev level. From the study of the reaction $^{24}Mg(p, \gamma)^{25}Al$ at $E_p = 222$ kev Casson (1953) has reported the presence of gamma-rays of energies $0{\cdot}48 \pm 0{\cdot}005$, $1{\cdot}95 \pm 0{\cdot}06$ and $2{\cdot}35 \pm 0{\cdot}1$ Mev.

Since the present work was started Craig *et al.* (1954) have suggested that the 222 kev proton resonance level in ^{25}Al could have a spin value 1/2 or 3/2. The spin value of the 2·71 Mev and the 0·95 Mev level is suggested to be $3/2^+$ (Bartholomew *et al.* 1954).

In the investigation of the reaction at proton energy of 222 kev presented here, gamma-ray spectra, angular distributions and angular correlation of gamma rays were studied with the aim of determining the spins and parities of some of the lower excited states of ^{25}Al.

§ 2. Experimental Procedure

The apparatus consisted of two NaI(Tl) scintillation counters. The sodium iodide crystals, each 2 inches thick and 1·75 inches in diameter, were mounted on DuMont 6292 photomultiplier tubes. The output pulses, after amplification in

Isotope Development Wide Band Amplifiers type 652, were fed to a 80 channel pulse height analyser (Hutchinson and Scarrott 1951). To avoid the low energy pulses choking the analyser the input spectrum was gated with itself above a desired pulse height. When observing the coincidence spectrum the input to the analyser was gated by the output of the coincidence circuit ($2\tau = 0{\cdot}25\,\mu$sec). In most of the measurements the distance between the target and the sodium iodide crystal was two inches.

§ 3. Measurements

A thick natural magnesium target was bombarded with a proton beam of about 30 μA at 230 kev. Figure 1 shows the pulse spectrum observed in the scintillation counter due to the emitted gamma rays. The spectrogram indicates the presence of gamma rays of energies 2·51, 2·06, 1·57 and 0·94 Mev. The asymmetry of the

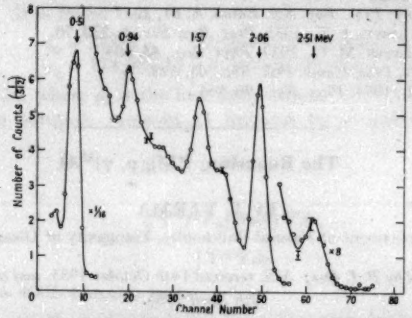

Figure 1. Pulse-height spectrum in a NaI(Tl) counter due to the gamma-rays from proton capture in ^{24}Mg as observed with a 80 channel pulse-height analyser.

annihilation radiation peak at 0·51 Mev suggests the presence of a gamma ray of energy less than 0·5 Mev. The fact that the first and second annihilation radiation escape peaks for the 2·06 Mev gamma ray fall approximately at the same positions as the full energy peaks for the 1·57 and 0·94 Mev radiations makes it difficult to obtain from figure 1 the intensities of the 1·57 and 0·94 Mev gamma rays with any accuracy. However, knowing the contribution due to the 2·06 Mev gamma ray in the full energy peaks of the 1·57 and 0·94 Mev radiations, the relative intensities of the three transitions can be estimated approximately. The calibration curves giving the relative areas of the full energy peak, the first and second escape peaks and the Compton contribution as a function of gamma-ray energy were obtained by measuring the pulse spectra for known monoenergetic gamma rays. These curves are independent of the energy resolution of the scintillation spectrometer and, therefore, are preferred to those in terms of peak heights. If the Compton contribution and the areas of the first and second escape peaks due to the 2·06 Mev gamma ray are subtracted and the proper corrections for the interaction cross section are applied, the areas of the full energy peaks due to the 0·94, 1·57 and 2·06 Mev gamma rays give the relative intensities of the radiations to be 1·0 : 1·4 : 10. The intensity of the 2·51 Mev transition was found to be 3% of the 2·06 Mev gamma ray. To avoid contribution to the intensity of the 2·51 Mev gamma ray, due to the simultaneous detection of the 2·06 Mev gamma ray and the soft radiations

in coincidence with it, a lead absorber 11 g cm^{-2} thick was placed between the target and the counter.

The energy and intensity of the soft gamma ray was measured by observing coincidences between pulses from the two scintillation counters. The spectrum was biased at 0·6 Mev in one counter and at 0·3 Mev in the other. In this way the coincidences due to the annihilation radiations were practically eliminated. The coincidence spectrum as observed in the pulse height analyser and the single spectrum are plotted in figure 2, where the calibration peaks due to the gamma rays from ^{137}Cs and due to annihilation radiation coincidences are also shown. The

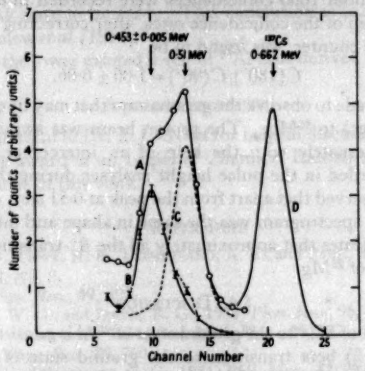

Figure 2. Coincidence spectrum in the vicinity of 0·5 Mev. The curves A and B represent the single and coincidence spectrum respectively. The calibration peaks C and D are from annihilation radiation coincidences and the gamma-rays from ^{137}Cs respectively.

energy of the soft gamma ray from the reaction is 0·453 ± 0·005 Mev. From the coincidence rate and the geometry of the counters the intensity of the 0·453 Mev radiations was estimated to be approximately the same as that of the 2·06 Mev transitions. These measurements suggest that the 2·06 and 0·453 Mev radiations are emitted in immediate cascade, and that the 2·51 Mev gamma ray represents the cross-over transition. As previous measurements (Goldberg 1953) indicate the first excited state to be in the vincinity of 0·45 Mev, it is reasonable to assume that the 0·453 Mev gamma ray is emitted from this level.

To obtain the spin values of the levels of ^{25}Al the angular distribution of the gamma rays was measured. To eliminate the errors due to change in pulse height with the position of the counter, and also to study the distribution of all the gamma rays simultaneously, series of pulse spectra were obtained for each angle. The spectra were recorded for a predetermined number of monitor counts in another NaI(Tl) counter biased at about 0·8 Mev. The target current ($\simeq 30\,\mu$A) and, therefore, the time of observation was kept fairly constant to minimize the variations in the background in the monitor counter. For the calculation of the angular distributions the counts in the full energy peaks of the gamma rays were obtained. The angular distribution of the 2·06 Mev gamma ray was found to be given by

$$W(\theta) = 1 - (0{\cdot}001 \pm 0{\cdot}014)\cos^2\theta.$$

Evidently the distribution is isotropic as was also the whole gamma ray spectrum.

The angular correlation of the 2·06–0·453 MeV gamma ray cascade was studied, employing two NaI(Tl) counters each subtending a half angle of about 18° at the target. One of the counters was biased at 0·66 MeV and the other, which was shielded in a lead cylinder, at 0·35 MeV. The coincidence and single counts in the two counters were recorded for positions of the movable counter at 90° and 180° alternately to the other counter which was placed at 90° to the incident proton beam. When the target was bombarded with a beam of 50 μA the coincidence rate was 16 counts per minute, of which about one count was background. The random coincidence rate was calculated to be about 0·02 counts per minute and was therefore neglected. About 1000 coincidences were recorded in each position of the counter and the ratio of the coincidence rates, after correcting for single counting rate in the movable counter, was found to be

$$C(180°)/C(90°) = 1{\cdot}00 \pm 0{\cdot}06.$$

An effort was made to observe the gamma rays that may be emitted in the decay of ^{25}Al ($T_{1/2} = 7{\cdot}6$ sec) to ^{25}Mg. The proton beam was switched 'on' and 'off' for 15 seconds alternately with the help of an interceptor. The gamma-ray spectrum was recorded in the pulse height analyser during the periods of beam cut-off. It was observed that apart from the peak at 0·51 MeV, due to the annihilation radiations, the spectrogram was the same in shape and intensity as the background. This indicates that approximately all the β^+-transitions in ^{25}Al proceed to the ground state of ^{25}Mg.

§ 4. Discussion

The assignment of $5/2^+$ to the ground state of ^{25}Al is consistent with the superallowed (log $ft = 3{\cdot}5$) beta transition to the ground state of ^{25}Mg having spin $5/2^+$. The assignment of $1/2^+$ to the 0·453 MeV state is in agreement with the isotropic angular correlation of the 2·06–0·453 MeV cascade as reported here. The

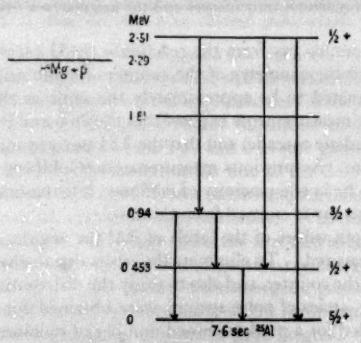

Figure 3. The levels of ^{25}Al.

angular distribution measurements show conclusively the spin of the 2·51 MeV state to be 1/2. As this spin value could be obtained by both s- and p-wave proton capture the angular distribution measurements do not predict the parity of the state, which in this case can be deduced from the intensities of the gamma-ray transitions. If the parity of this level were odd the 2·06 and 2·51 MeV transitions

would be E1 and M2 respectively, which from the consideration of the intensities is very unlikely. If, on the other hand, the parity of this level is even, the two transitions would be M1 and E2 which, as in the case of heavier nuclei, could easily compete to the extent they do in the present case. This leads to the conclusion that the parity of the 2·51 MeV state of ^{25}Al is even.

The relative intensities of the 0·94 and 1·57 MeV transitions suggest that the level at 0·94 MeV is fed by the 1·57 MeV gamma ray and that it decays in part to the 0·453 MeV state. The branching in the decay of the 2·51 and 0·94 MeV states could be explained if all the transitions involved are magnetic dipole, thus giving the spin of the 0·94 MeV state to be $3/2^+$. This conclusion is in agreement with the results of Bartholomew *et al.* (1954).

The scheme of the lower excited levels of ^{25}Al thus derived is shown in figure 3.

ACKNOWLEDGMENTS

The author is grateful to Dr. P. J. Grant for helpful discussions and also wishes to acknowledge the award of an Imperial Chemical Industries Research Fellowship during the course of this work.

REFERENCES

BARTHOLOMEW, G. A., GOVE, H. E., LITHERLAND, A. E., and PAUL, E. B., 1954, *Bull. Amer. Phys. Soc.*, **30**, No. 3.
CASSON, H., 1953, *Phys. Rev.*, **89**, 809.
CRAIG, W. S., CROSS, W. G., and JARVIS, R. G., 1954, *Phys. Rev.*, **96**, 825 (A).
ENDT, P. M., and KLUYVER, J. C., 1954, *Rev. Mod. Phys.*, **26**, 95.
GOLDBERG, E., 1953, *Phys. Rev.*, **89**, 760.
HUTCHINSON, G. W., and SCARROTT, G. G., 1951, *Phil. Mag.*, **42**, 792.

Proton–Proton Scattering at 134 MeV

BY A. E. TAYLOR AND E. WOOD
Atomic Energy Research Establishment, Harwell, Berks.

Communicated by D. W. Fry; *MS. received 7th March* 1956

§ 1. INTRODUCTION

DETERMINATIONS of the differential cross section for p–p scattering at 90° centre of mass by various authors in the region of 150 MeV have shown, until recently, some measure of disagreement (Cassels 1956). The present note describes the determination of the total cross section of hydrogen for 134 MeV protons from which a value for the differential cross section at 90° centre of mass can be obtained. Similar determinations by this method have been reported by Chamberlain, Pettengill, Segrè and Wiegand (1954 b) at 225 and 330 MeV and by Marshall, Marshall and Nedzel (1954) at 408 MeV.

§ 2. APPARATUS AND METHOD

The integrated cross section for the scattering of protons by hydrogen through angles greater than θ was determined by measuring the absorption in a liquid hydrogen target. Several measurements were made for centre-of-mass values

of θ between 8·4° and 20·9°. Two small scintillation counters C_1 and C_2, 1 cm diameter, operated in double coincidence defined and monitored the external unpolarized proton beam of the 110-in. synchrocyclotron. A third, large area, scintillation counter, C_3, 17 cm diameter, operated in triple coincidence measured the transmission of the target (figure 1). By altering the axial position L of the third counter measurements were made for the different scattering angles θ. The sensitivity of the large area counter was carefully checked and found to be constant over the whole surface. The liquid hydrogen target employed expanded polystyrene and a liquid nitrogen jacket as thermal shields, but had only 0·004 in. of copper and 2 in. of expanded polystyrene of density 0·07 g cm^{-3} in the direct beam.

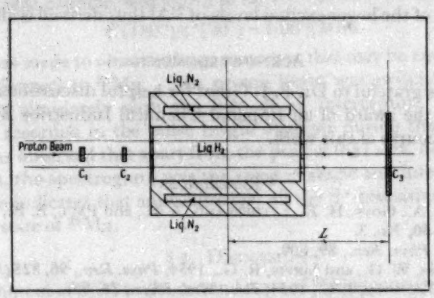

Figure 1. Counter telescope arrangement.

A surface density of liquid hydrogen of 2·06 g cm^{-2} was chosen as giving the largest attenuation without producing undue energy loss or multiple coulomb scattering. This meant that the nuclear attenuation was only about 0·03 and that therefore particular attention had to be paid to counting losses and the stability of the apparatus. With this amount of liquid hydrogen the mean energy of the experiment was 134 MeV.

The short resolving time of the coincidence circuit together with the long flight path used gave some energy selection and ensured that low energy charged particles in the beam were not detected if their energy was less than 40 MeV. Range measurements had shown that the high energy spread in the beam amounted to about 1%. There was therefore little distortion of the result to be expected from inhomogeneities in the beam.

§ 3. Experimental Details and Corrections

Without the liquid hydrogen in the target the ratio of triple coincidence counts to double coincidence counts was 0·9788 for θ equal to 10·4° and a double rate of 6 counts per second. This ratio, which measures the transmission of the container, varied slightly with the beam intensity and the position of the third counter. The greater part of the difference between the double and triple coincidence counts could be accounted for by nuclear and coulomb scattering in the hydrogen container, counters and air path and by counting losses. Since the protons lost energy in going through the liquid hydrogen, the nuclear and coulomb scattering in the container, counters and air path would be greater than without the liquid hydrogen. Using values of the cross sections of light

elements determined in a separate experiment and estimates of the multiple coulomb scattering, the transmission of the empty target at the 10·4° position was calculated to be $0{\cdot}9832 \pm 0{\cdot}0015$ as against the measured value, corrected for counting losses, of $0{\cdot}9814 \pm 0{\cdot}0010$. The estimated transmission at the reduced energy was 0·0020 smaller. In view of the agreement between the calculated and measured transmissions it was thought justified to correct the measured transmissions by 0·0020 in order to take account of the reduction in energy. The error in this correction arises from the change in energy and is therefore small and has been taken as 0·0002. A further small correction was applied for the air displaced by the liquid hydrogen.

Tests were made to find the variation of the ratio of triple to double coincidences with beam intensity. The double rate was held in the experiment within the limits 5–7 double counts per second and the appropriate corrections for fluctuations in the beam intensity applied. These corrections changed the cross section by 0·1%.

A further correction was considered since the boiling of the liquid hydrogen would produce bubbles in the beam path and reduce the surface density of hydrogen. The extent of the reduction depends upon the evaporation rate, the size and rate of growth of the bubbles and whether the bubbles are uniformly distributed throughout the volume of the liquid. The largest correction is required for relatively large bubbles travelling slowly through the liquid and growing in size slowly.

The correction for uniform bubbling was estimated to be of the order of 0·1%. However, since the main bubbling occurs at the edges and surfaces of the container rather than in the main volume the correction was considered to be negligible. The density of the liquid hydrogen was therefore taken as the normal value at atmospheric pressure, namely $0{\cdot}0709\ \mathrm{g\,cm^{-3}}$.

§ 4. Results and Errors

The integrated cross sections $\sigma_t(\theta)$ for the different values of θ are tabulated below, where θ is the centre-of-mass scattering angle measured from the centre of the target. The errors are standard deviations based on total counts.

θ (deg)	20·9	15·94	12·94	10·35	8·38
$\sigma_t(\theta)$ (mbn)	21·03 ± 1·5	24·09 ± 1·5	24·17 ± 1·7	22·72 ± 1·6	23·29 ± 1·7

The largest systematic errors arise from the measurement of the length of the liquid hydrogen and from the correction to the transmission of the target. These produce errors of 1% and 0·7% respectively in the integrated cross section. Counting loss corrections only changed the value of σ_t by 0·1% and therefore the error associated with this correction will be negligible. Since the other corrections were very small, the errors associated with them were also taken to be negligible. The possible systematic error was therefore thought to be less than 2·0%.

§ 5. Discussion

Early measurements of the angular distribution in p–p scattering had shown the scattering to be isotropic within the errors of the measurements at 75 and 105 Mev (Birge, Kruse and Ramsey 1951), at 118, 164, 250 and 345 Mev (Chamberlain, Segrè and Wiegand 1951), at 147 Mev (Cassels, Pickavance and Stafford 1952) and at 240 Mev (Oxley and Schamberger 1952, Towler 1951).

Recent measurements at small angles (Chamberlain and Garrison 1954, Garrison 1954, Fischer and Goldhaber 1954, Chamberlain, Pettengill, Segrè and Wiegand 1954a, Taylor and Wood, to be published) have suggested that the isotropy is maintained down to the angles covered by this experiment. The integrated cross section $\sigma_t(\theta)$ is then related to the differential cross section for isotropic scattering $d\sigma/d\omega$ by the relation $\sigma_t(\theta)=2\pi\cos\theta(d\sigma/d\omega)$. The results in the table would give a value of $d\sigma/d\omega$ of $3{\cdot}79\pm0{\cdot}13$ mbn sterad^{-1}.

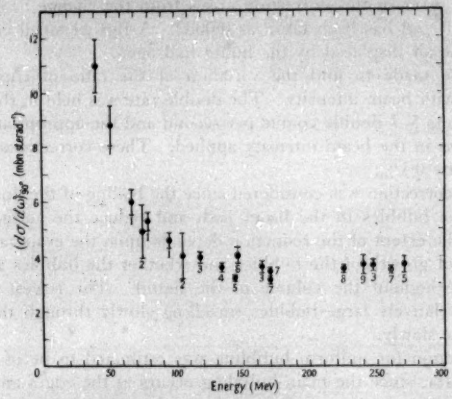

Figure 2. Variation of the p–p differential cross section with energy.

LEGEND

1. Kruse, Teem and Ramsey 1954.
2. Birge, Kruse and Ramsey 1951. Corrected for the change in the $^{12}C(p, pn)^{11}C$ cross section.
3. Chamberlain, Segrè and Weigand 1951.
4. Taylor and Wood (present results).
5. Marshall, Marshall and Nedzel 1954.
6. Cassels 1956.
7. Garrison 1954.
8. Chamberlain *et al.* 1954 b.
9. Oxley and Schamberger 1952. Corrected for change in the $^{12}C(p, pn)^{11}C$ cross section.

However, recent measurements at 95 MeV (Kruse, Teem and Ramsey 1954) have shown that for θ between 40° and 90° $d\sigma/d\omega$ may vary as much as 8%. A similar variation is suggested by the work at 170 and 260 MeV (Chamberlain and Garrison 1954, Garrison 1954) and indeed the results at 147 MeV (Cassels *et al.* 1952) are not inconsistent with such a variation. If we fit the relation

$$\left(\frac{d\sigma}{d\omega}\right)_{\theta}=\left(\frac{d\sigma}{d\omega}\right)_{90°}(1+a\cos^2\theta)$$

to these measurements outside the region where coulomb scattering is important, we find the mean value of a to be $0{\cdot}14\pm0{\cdot}02$. With this variation, $\sigma_t(\theta)$ is now related to $(d\sigma/d\omega)_{90°}$ by the relation

$$\sigma_t(\theta)=2\pi\left(\frac{d\sigma}{d\omega}\right)_{90°}\cos\theta\left(1+\frac{a}{3}\cos^2\theta\right)$$

which gives from the values of $\sigma_t(\theta)$ in the table a value for $(d\sigma/d\omega)_{90°}$ of $3{\cdot}63 \pm 0{\cdot}15$ mbn sterad^{-1}. The error has been increased to allow for the error in *a*. Both these values are in excellent agreement with other determinations as is illustrated in figure 2.

ACKNOWLEDGMENTS

We would like to thank Dr. K. Mendelssohn of the Clarendon Laboratory, Oxford, for the supply of liquid hydrogen and also to thank many colleagues for useful help and discussions.

REFERENCES

BIRGE, R. W., KRUSE, U. E., and RAMSEY, N. F., 1951, *Phys. Rev.*, **83,** 274.
CASSELS, J. M., 1956, *Proc. Phys. Soc.* A, **69,** 495.
CASSELS, J. M., PICKAVANCE, T. G., and STAFFORD, G. H., 1952, *Proc. Phys. Soc.* A, **214,** 262.
CHAMBERLAIN, O., and GARRISON, J. D., 1954, *Phys. Rev.*, **95,** 1349.
CHAMBERLAIN, O., PETTENGILL, SEGRÈ, E., and WIEGAND, C., 1954 a, *Phys. Rev.*, **95,** 1348; 1954 b, *Ibid.*, **93,** 1424.
CHAMBERLAIN, O., SEGRÈ, E., and WIEGAND, C., 1951, *Phys. Rev.*, **83,** 923.
FISCHER, D., and GOLDHABER, G., 1954, *Phys. Rev.*, **95,** 1350.
GARRISON, J. D., 1954, *Thesis*, University of California UCRL-2659.
KRUSE, U. E., TEEM, J. M., and RAMSEY, N. F., 1954, *Phys. Rev.*, **94,** 1795.
MARSHALL, J., MARSHALL, L., and NEDZEL, V. A., 1954, *Phys. Rev.*, **92,** 834.
OXLEY, C. L., and SCHAMBERGER, R. D., 1952, *Phys. Rev.*, **85,** 416.
TOWLER, O. A., 1951, *Phys. Rev.*, **84,** 1262.

LETTERS TO THE EDITOR

Nuclear Charge Density Distributions

Experimental observations on the nuclear scattering of 183 MeV electrons have been recently made (Hahn, Ravenhall and Hofstadter 1956) for several middle and heavy elements. In the case of those nuclei for which asphericity may be assumed negligible, these experimental data have been correlated on the basis of spherically symmetric nuclear charge density distributions with a constant charge density in the central region and a smoothed-out surface. These calculations have been carried out on the basis of an exact partial wave analysis for the nuclear scattering of a Dirac electron. It has been established, from an analysis of the experimental data on Au, that the functional forms of the surface are not important, but that essentially two parameters, one c related to the nuclear radius and the other t related to the surface thickness are significant.

Out of the various nuclear charge density distributions considered only the Fermi distribution $\rho_F(r)$ and the modified gaussian distribution $\rho_G(r)$ may be regarded as physically interesting.

These are given by

$$\rho_F(r)=\bar{\rho}_F/[1+\exp\{4\cdot4(r-c)/t\}] \qquad \ldots\ldots(1)$$

$$\rho_G(r)=\bar{\rho}_G/[1+\exp\{2\cdot2(r^2-c^2)/ct\}] \qquad \ldots\ldots(2)$$

where $\bar{\rho}_F$ and $\bar{\rho}_G$ are normalization constants. The parameters c and t are found to be the same for both these distributions in the case of Au. Further, it has been established that for the Fermi distributions appropriate for different elements, c is proportional to $A^{1/3}$ while t is independent of A. Presumably, the parameters c and t for the modified gaussian distribution behave similarly. These parameters have the values $c=(1\cdot07\pm0\cdot02)\,A^{1/3}10^{-13}$ cm and $t=(2\cdot4\pm0\cdot3)\times10^{-13}$ cm.

The above nuclear charge density distributions, when evaluated for Au, are found to be practically identical. Therefore, it has been suggested that experimental data at a higher energy would be necessary to distinguish between them. However, it may be expected that the distribution at the nuclear surface would significantly affect the central density and consequently the theoretical differential cross section in the case of a light element. The only experimental data suitable for the purpose consist of the absolute differential scattering cross sections at various angles for the nuclear scattering of 187 MeV electrons by carbon (Fregeau and Hofstadter 1955). Nuclear asphericity can be regarded as negligible for this element also. Neglecting the probable errors on the parameters, one has $c=2\cdot45\times10^{-13}$ cm, $t=2\cdot4\times10^{-13}$ cm for carbon, which on graphical normalization to unity give $\bar{\rho}_F=0\cdot011\times10^{39}\,\mathrm{cm}^{-3}$ and $\bar{\rho}_G=0\cdot013\times10^{39}\,\mathrm{cm}^{-3}$.

It is quite reasonable to assume the validity of the first Born approximation for the nuclear scattering of such high energy electrons by such a light element. The differential scattering cross section $\sigma(s)$ for such density distributions (Mathur and Gatha 1953) can be written as

$$\sigma(s)=\left(\frac{4\pi z}{137}\right)^2\frac{4k^2-s^2}{s^6}\left[\int_0^\infty \rho(r)\sin(sr)r\,dr\right]^2 \qquad \ldots\ldots(3)$$

where $s = 2k \sin(\phi/2)$ with $k = E/\hbar c$. Substituting in equation (3) for $\rho(r)$ from equations (1) and (2), with the parameters appropriate for carbon, $\sigma_F(s)$ and $\sigma_G(s)$ have been calculated for various values of s by numerical integration for the Fermi and the modified gaussian density distributions respectively. These theoretical $\sigma_F(s)$ and $\sigma_G(s)$, together with the experimental values, are shown in the figure.

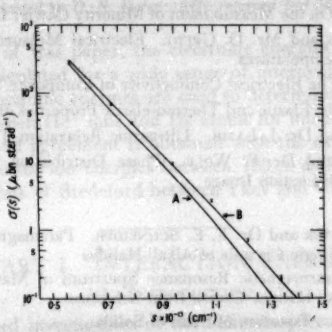

Differential scattering cross sections for carbon. Theoretical curves A and B are based on the Fermi and the modified gaussian nuclear charge density distributions. The points represent the experimental data.

A comparison of the theoretical and the experimental values of the differential scattering cross sections indicates that the modified gaussian density distribution may be regarded as superior to the Fermi density distribution for correlating the experimental data on the nuclear scattering of high-energy electrons. Consequently, the modified gaussian nuclear charge density distribution deserves further investigation with other elements.

Physics Department,
Institute of Science,
Bombay.

M. K. Advani.
P. Harihar.
K. M. Gatha.

12th May 1956.

Fregeau, J. H., and Hofstadter, R., 1955, *Phys. Rev.*, **99**, 1503.
Hahn, B., Ravenhall, D. G., and Hofstadter, R., 1956, *Phys. Rev.*, **101**, 1131.
Mathur, A. L., and Gatha, K. M., 1953, *Proc. Phys. Soc.* A, **66**, 773.

CONTENTS OF SECTION B

PAGE

Mr. J. B. Gunn. Avalanche Injection in Semiconductors 781

Dr. C. A. Hogarth. On the Measurement of Minority Carrier Lifetimes in Silicon 791

Dr. D. M. Finlayson and Mr. D. Greig. Electrical Measurements on Natural Galena at Low Temperatures 796

Dr. E. H. Kerner. The Electrical Conductivity of Composite Media . . 802

Dr. E. H. Kerner. The Elastic and Thermo-elastic Properties of Composite Media 808

Dr. J. H. Andreae and Dr. J. Lamb. Ultrasonic Relaxation Theory for Liquids 814

Dr. E. H. Linfoot and Dr. E. Wolf. Phase Distribution near Focus in an Aberration-free Diffraction Image 823

Research Notes:

Mr. P. A. Forrester and Dr. E. E. Schneider. Paramagnetic Resonance of Manganese in Single Crystals of Alkali Halides 833

Dr. W. Low. Paarmagnetic Resonance Spectrum of Manganese in Single Crystals of Alkali Halides Grown from Solutions 837

Dr. R. S. Sharma. Equation of State of Solids 838

Mr. R. U. Ayres and Dr. R. H. Tredgold. On the Crystal Structure of the Rare Gases 840

Prof. H. Fröhlich, Mr. B. V. Paranjape, Mr. C. G. Kuper and Mr. S. Nakajima. The Influence of Interelectronic Collisions and of Surfaces on Electronic Conductivity 842

Dr. D. M. Evans. The Temperature Dependence of the Mobility of Electrons in Germanium 845

Letters to the Editor:

Dr. E. Matsukawa and Dr. A. N. Hunter. The Variation of Sound Velocity with Stress in Sand 847

Mr. W. A. Smith. The Electric Strength and Surface Condition of the Alkali Halides 848

Dr. D. P. Morris and Mr. R. P. Preston. Structural Transition and Antiferromagnetism in the Alloy AuMn 849

Dr. P. J. Price. Anomalous Lorenz Numbers in Mixed Semiconductors . 851

Mr. B. Richards and Dr. E Wolf. The Airy Pattern in Systems of High Angular Aperture 854

Mr. M. R. Piggott. The Relation between Wear and Distance Run, for Steel and Coated Steel Surfaces 857

Dr. B. Bleaney, Dr. P. M. Llewellyn and Dr. D. A. Jones. Paramagnetic Resonance of Uranium Ions 858

Dr. D. M. Finlayson, Mr. D. Greig, Mr. J. P. Llewellyn and Mr. T. Smith. Some Electrical Characteristics of Single Crystal Iron Monotelluride . 860

Dr. R. Mansfield. The Hall Effect in Semiconductors 864

Dr. W. P. Doyle. The Absorption Spectrum of Solid Arsenic Trisulphide 865

Corrigenda (Fröhlich and Paranjape) 866

Reviews of Books 867

Contents of Section A 867

Interaction Energy and Charge Exchange between Helium Atoms and Ions

By B. L. MOISEIWITSCH

Department of Applied Mathematics, Queen's University of Belfast

Communicated by D. R. Bates; MS. received 2nd May 1956

Abstract. In Part I of this paper, the electronic energies for the $^2\Sigma_u$ and $^2\Sigma_g$ states of He_2^+ are calculated for a wide range of internuclear distances.

In Part II, the electronic energies are used to determine the cross section for charge exchange between He^+ ions and He atoms for ion energies ranging from $\frac{1}{10}$ ev to 100 kev. Good agreement is obtained with the experimental results of Wolf and of Rostagni for ion energies between 100 ev and 1 kev, and also with the experimental results of Stedeford between 1 kev and 40 kev.

PART I. INTERACTION ENERGY

§ 1. Introduction

The first detailed investigation of the helium molecular ion was made by Pauling (1933) using the variational method for bound states. Further work was later carried out by Weinbaum (1935) using a more involved type of trial wave function. The work of both Pauling and Weinbaum was confined to the region of the equilibrium internuclear distance as they were mainly interested in determining a value for the dissociation energy. Pauling gives interaction energies corresponding to the lowest states of u and g symmetry for internuclear separations less than $4a_0$, whereas Weinbaum gives only the dissociation energy.

The first part of this paper is concerned with extending the study of the He_2^+ ion to much larger internuclear separations than were considered previously, the extension being required for an adequate investigation of charge exchange between He^+ ions in He gas.

§ 2. Theoretical Discussion

The wave equation for the helium molecular ion is

$$(H-E)\Psi=0 \qquad \ldots\ldots(1)$$

where the Hamiltonian is given in Hartree units by the expression

$$H\equiv -\nabla_1^2-\nabla_2^2-\nabla_3^2-\frac{4}{r_{A1}}-\frac{4}{r_{B1}}-\frac{4}{r_{A2}}-\frac{4}{r_{B2}}-\frac{4}{r_{A3}}-\frac{4}{r_{B3}}+\frac{2}{r_{12}}+\frac{2}{r_{23}}+\frac{2}{r_{13}}+\frac{8}{r_{AB}} \qquad \ldots\ldots(2)$$

and E is the electronic energy. The helium nuclei are denoted by A and B, and the electrons by 1, 2, 3.

If $\Psi_t(1, 2, 3)$ is the trial function used in the variational method, then an upper limit for the electronic energy is given by

$$E\leqslant \int \Psi_t^* H\Psi_t\, d\tau \Big/ \int \Psi_t^*\Psi_t\, d\tau. \qquad \ldots\ldots(3)$$

In the limit of infinite nuclear separation the helium molecular ion in the $^2\Sigma_u$ and $^2\Sigma_g$ states dissociates into a He^+ ion and a He atom in their ground states. This behaviour can be allowed for by choosing a trial function of the form

$$\Psi_t(1,2,3)=\sum_{1,2,3}[\phi(\mathbf{r}_{A1},\mathbf{r}_{A2})\psi(\mathbf{r}_{B3})\pm\phi(\mathbf{r}_{B1},\mathbf{r}_{B2})\psi(\mathbf{r}_{A3})]\chi^-(1,2;3) \quad \ldots\ldots(4)$$

where

$$\chi^-(1,2;3)=\frac{1}{\sqrt{2}}(\alpha_1\beta_2-\beta_1\alpha_2)\alpha_3 \quad \ldots\ldots(5)$$

is a doublet spin function antisymmetrical in the interchange of electrons 1 and 2. The summation in function (4) is cyclical, and the + sign corresponds to the g state while the − sign corresponds to the u state. Also ϕ and ψ are given by the expressions

$$\phi(\mathbf{r}_1,\mathbf{r}_2)=\frac{1}{\sqrt{2}}\{u(\alpha;\mathbf{r}_1)u(\beta;\mathbf{r}_2)+u(\beta;\mathbf{r}_1)u(\alpha;\mathbf{r}_2)\}, \quad \ldots\ldots(6)$$

$$\psi(\mathbf{r})=u(\gamma;\mathbf{r}), \quad \ldots\ldots(7)$$

where

$$u(Z;\mathbf{r})=\left(\frac{Z^3}{\pi}\right)^{1/2}e^{-Zr}. \quad \ldots\ldots(8)$$

In the investigation carried out by Pauling, it was assumed that $\alpha=\beta=\gamma$, whereas Weinbaum supposed that $\alpha=\beta$ only and varied α and γ independently. They obtained dissociation energies of 2·47 ev and 2·22 ev, and equilibrium internuclear separations of $2\cdot05a_0$ and $2\cdot07a_0$ respectively.

The primary aim of the first part of this paper is to obtain fairly accurate potential energy curves for large internuclear distances. In the dissociation limit $\phi(\mathbf{r}_1,\mathbf{r}_2)$ is the wave function of a normal helium atom and $\psi(\mathbf{r})$ is the wave function of a normal singly charged helium ion. For the purpose of this paper it is adequate to take α, β and γ fixed at their appropriate values in the separated atom–ion limit since the variation of these parameters makes only negligible changes to the electronic energies at large internuclear distances. Three cases were considered :

$$\left.\begin{array}{ll}\text{(i)} & \alpha=\beta=\gamma=2;\\ \text{(ii)} & \alpha=\beta=1\cdot6875,\quad \gamma=2;\\ \text{(iii)} & \alpha=2\cdot19,\quad \beta=1\cdot18,\quad \gamma=2.\end{array}\right\} \quad \ldots\ldots(9)$$

In case (i) it is assumed that the two electrons of the helium atom do not screen each other. This is a rather crude approximation and the results obtained with this trial function should be rather poor. The function $\phi(\mathbf{r}_1,\mathbf{r}_2)$ of case (ii) is the simplest Hylleraas wave function for a helium atom. It has been used widely in collision problems involving helium atoms and has proved very satisfactory. Case (iii) corresponds to a two-parameter helium atom wave function which gives a somewhat better value for the binding energy than does the simplest Hylleraas wave function (Hylleraas 1929, 1930, Chandrasekhar 1944, Moiseiwitsch 1954). One would expect this function to yield the most satisfactory results for the electronic energies of the helium molecular ion at large internuclear separations.

§ 3. Discussion of Results

The values of the electronic energies E_u and E_g obtained for the attractive $^2\Sigma_u$ and repulsive $^2\Sigma_g$ states of He_2^+ using functions (i), (ii) and (iii) are given

in the table. The effect of the polarization of the helium atom by the helium ion has not been taken into account. The values of the dissociation energy D for the He_2^+ molecular ion given by the three functions are 3·1 ev, 2·0 ev, and 1·5 ev respectively, while the values of the equilibrium internuclear distance are $2{\cdot}1a_0$, $2{\cdot}2a_0$ and $2{\cdot}5a_0$ respectively. Pauling (1933) has also carried out calculations with function (i) and quotes a value for the dissociation energy of 2·9 ev but this appears to be a misprint. The dissociation energy given by (ii) is only 0·2 ev less than the value obtained by Weinbaum. It thus seems that in this case the effect of varying the parameters is slight, even for quite small internuclear separations.

Electronic Energies (in units of $e^2/2a_0$) for the $^2\Sigma_u$ and $^2\Sigma_g$ states of He_2^+

	$^2\Sigma_u$ state			$^2\Sigma_g$ state		
R	(i)	(ii)	(iii)	(i)	(ii)	(iii)
0·5	7·73	8·19	8·58	14·5	10·2	8·10
1·0	1·01	1·37	1·58	4·24	3·90	3·64
1·5	−0·108	0·084	0·188	1·53	1·51	1·52
2·0	−0·228	−0·147	−0·090	0·607	0·630	0·642
2·5	−0·163	−0·142	−0·112	0·258	0·283	0·291
3	−0·0919	−0·0951	−0·0823	0·114	0·135	0·141
4	−0·0221	−0·0308	−0·0312	0·0231	0·0336	0·0374
5	−0·00451	−0·00837	−0·0101	0·00455	0·00855	0·0107
6	−0·000853	−0·00211	−0·00304	0·000854	0·00212	0·00313
7	−0·000154	−0·000507	−0·000886	0·000154	0·000508	0·000893
8	−0·000027	−0·000119	−0·000248	0·000026	0·000118	0·000246
9	−0·000004	−0·000027	−0·000066	0·000004	0·000027	0·000065
10	−0·000001	−0·000006	−0·000016	0·000001	0·000006	0·000016

(i), (ii) and (iii) refer to the three wave functions defined in the text.

Herzberg (1950) gives 3·1 ev for the dissociation energy of He_2^+ but remarks that this value is uncertain. This makes it rather difficult to decide which theoretical value for the dissociation energy is most reliable. The most involved calculation which has been done so far is that by Weinbaum, and his value for D of 2·2 ev is usually quoted as being correct. However, it is not certain that this is so, and it could be that some of the less detailed calculations have fortuitously given a value of D which is closer to the true value.

At large internuclear separations it seems likely that function (iii) gives the most reliable values for the electronic energy. It can be seen from the table that the electronic energy falls off more slowly with increasing internuclear distance for function (iii) than for either (ii) or (i). Also, the equilibrium internuclear separation given by function (iii) is somewhat larger than those given by the other two functions.

Part II. Charge Exchange

§ 1. Introduction

Theoretical investigations of charge exchange between He^+ ions and He atoms have been made by Massey and Smith (1933), Dallaporta and Bonfiglioli (1943) and more recently by Firsov (1951), Demkov (1952) and Jackson (1954).

Massey and Smith used the electronic energies for He_2^+ calculated by Pauling which they extended to larger internuclear distances by means of crude wave functions. They employed the method of perturbed stationary states and covered the range of energies from 500 ev to 12 kev. The most recent calculations are those of Jackson. He also used Pauling's electronic energies for He_2^+ but did not take into account the tail of the potential curve corresponding to internuclear distances greater than about $4a_0$. He used the impact parameter method (Mott 1931, Firsov 1951, Demkov 1952, Bates, Massey and Stewart 1953) and covered the range of energies from 200 ev to 100 kev.

In the present paper, the electronic energies calculated with functions (i), (ii) and (iii) are used in conjunction with the impact parameter method to obtain cross sections for charge exchange between He^+ ions and He atoms. The use of reasonably accurate electronic energies for He_2^+ extending out to large internuclear separations has made it possible to cover the wide range of energies from $\frac{1}{10}$ ev to 100 kev.

§ 2. Theoretical Discussion

The impact parameter method of Mott has been used by Bates, Massey and Stewart (1953) to obtain an expression for the cross section for elastic scattering with charge exchange. They show that the cross section is given by

$$Q = 2\pi \int_0^\infty P \sin^2 \zeta \, dP \qquad \ldots\ldots(10)$$

where

$$\zeta(P) = \frac{1}{\hbar v(\infty)} \int_P^\infty \frac{R(E_g - E_u)}{(R^2 - P^2)^{1/2}} \, dR, \qquad \ldots\ldots(11)$$

$v(\infty)$ being the initial velocity of relative motion, R the internuclear distance and E_u, E_g the electronic energies for the lowest states of u, g symmetry respectively.

The integral (10) can be split up into two parts corresponding to $0 \leqslant P \leqslant P_0$ and $P_0 \leqslant P < \infty$. P_0 is so chosen that in the first region $\sin \zeta$ oscillates sufficiently rapidly for it to be possible to replace $\sin^2 \zeta$ by its average value $\frac{1}{2}$. Then we have

$$Q = \frac{\pi P_0^2}{2} + \pi \int_{P_0}^\infty P \sin^2 \zeta \, dP. \qquad \ldots\ldots(12)$$

The cross section Q for resonance charge exchange is essentially determined by the difference ΔE between the electronic energies for the lowest states of u and g symmetry. Thus the effect of polarization can be neglected in obtaining E_u and E_g as it cancels to good approximation.

The expression for $\zeta(P)$ given by (11) is valid provided the relative velocity $v(R)$ of the particles never changes significantly from the initial velocity of relative motion $v(\infty)$. This condition should hold down to very small values of $v(\infty)$ as at low energies P_0 is large and consequently ΔE is small for R greater than P_0.

For large values of $v(\infty)$ the impact parameter method breaks down as then the collision can no longer be regarded as adiabatic. The method is applicable provided momentum transfer is unimportant and provided $a \Delta E / \hbar v(\infty) \gg 1$, where a is the effective range of interaction, which gives an upper limit for the energy of the incident ion of the order of 10 to 100 kev.

§ 3. Discussion of Results

Displayed in figure 1 is a comparison between the values of the cross section for resonance charge transfer between He^+ ions and He atoms calculated in this paper with the values of the same cross section calculated by previous investigators.

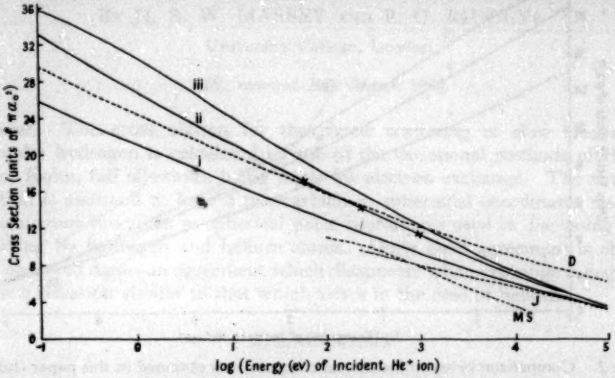

Figure 1. Comparison between theoretical cross sections. Full lines correspond to present and broken lines to previous calculations. (i), (ii) and (iii) refer to the different wave functions defined in the text. D, Demkov; J, Jackson; MS, Massey and Smith. The crosses show values given by Firsov.

The cross section curve obtained by Jackson should coincide with the cross section curve obtained by using function (i). That it does not do so is probably due mainly to the neglect by Jackson of the effect of the interaction energy for internuclear distances greater than $4a_0$.

Firsov (1951) and Demkov (1952) have also used the impact parameter method to obtain the cross section for charge transfer between He^+ ions and He atoms. It can be seen from figure 1 that Firsov's results lie close to curve (ii). The cross section curve obtained by Demkov is parallel to (i) but is displaced upwards.

In figure 2, the cross sections calculated in this paper are compared with experiment. Between 100 ev and 1 kev the agreement between curves (ii) and (iii) and the data of Wolf (1935) and Rostagni (1935) is seen to be very good, though for energies below 100 ev the results of Wolf tend to fall below these curves and the results of Rostagni rise above them. However, at such low energies the experiments are rather difficult and are not very reliable. The experimental results of Hasted (Stedeford and Hasted 1955) in the same energy range lie close to curve (i) but it does not seem likely that this curve can be correct in view of the rather crude He_2^+ wave functions on which it is based.

Between 1 kev and 100 kev the theoretical curves (i), (ii) and (iii) lie close together. The experimental data of Stedeford in this energy range are in excellent agreement with theory, particularly with curve (ii). Experimental work has also been done by Smith (1934) and by Keene (1949). Their results lie respectively somewhat below and above the cross section curves obtained in this paper.

Owing to the uncertainty in the experimental data, it does not seem possible at this stage to decide whether the cross section curve (iii) is superior to (ii) or not. More experimental investigation is still required.

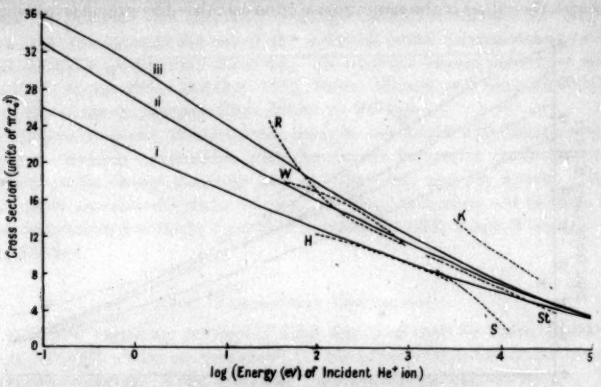

Figure 2. Comparison between theoretical cross sections obtained in this paper (full lines) and experimental cross sections (broken lines). (i), (ii) and (iii) refer to the different wave functions defined in the text. H, Hasted; K, Keene; R, Rostagni; S, Smith; St, Stedeford; W, Wolf.

Acknowledgments

It is a pleasure to thank Professors P. M. Morse and J. C. Slater for the hospitality of their departments at the Massachusetts Institute of Technology where the calculations involved in Part I of this paper were carried out, and to thank Dr. F. J. Corbató for his invaluable assistance in connection with the use of the Whirlwind electronic computing machine. The molecular integrals required for the evaluation of the electronic energies of He_2^+ were calculated using programmes due to Dr. F. J. Corbató (1956), Dr. A. Dalgarno and Dr. P. Merryman.

References

Bates, D. R., Massey, H. S. W., and Stewart, A. L., 1953, *Proc. Roy. Soc.* A, **216**, 437.
Chandrasekhar, S., 1944, *Astrophys. J.*, **100**, 176.
Corbató, F. J., 1956, *J. Chem. Phys.* **24**, 452.
Dallaporta, N., and Bonfiglioli, P., 1943, *Comment. Pontif. Acad. Sci.*, **7**, 141.
Demkov, U. H., 1952, *Uchen. Zap. Leningr. Univ. Seria Phiz. Nauk*, **146**, 74.
Firsov, O. B., 1951, *J. Exp. Theor. Phys.*, **21**, 1001.
Herzberg, G., 1950, *Spectra of Diatomic Molecules*, 2nd Edn. (London : MacMillan).
Hylleraas, E. A., 1929, *Z. Phys.*, **54**, 347; 1930, *Ibid.*, **60**, 624.
Jackson, J. D., 1954, *Canad. J. Phys.*, **32**, 60.
Keene, J. P., 1949, *Phil. Mag.*, **40**, 369.
Massey, H. S. W., and Smith, R. A., 1933, *Proc. Roy. Soc.* A, **142**, 142.
Moiseiwitsch, B. L., 1954, *Proc. Phys. Soc.* A, **67**, 25.
Mott, N. F., 1931, *Proc. Camb. Phil. Soc.*, **27**, 553.
Pauling, L. J., 1933, *J. Chem. Phys.*, **1**, 56.
Rostagni, A., 1935, *Nuovo Cim.*, **12**, 134.
Smith, R. A., 1934, *Proc. Camb. Phil. Soc.*, **30**, 514.
Stedeford, J. B. H., and Hasted, J. B., 1955, *Proc. Roy. Soc.* A, **227**, 466.
Weinbaum, S., 1935, *J. Chem. Phys.*, **3**, 547.
Wolf, F., 1935, *Ann. Phys., Lpz.*, **23**, 285.

Application of Variational Methods to the Theory of the Scattering of Slow Electrons by Hydrogen Molecules

By H. S. W. Massey and R. O. Ridley†
University College, London

MS. received 26*th March* 1956

Abstract. The cross section for the elastic scattering of slow electrons by molecular hydrogen is calculated by use of the variational methods of Hulthén and of Kohn, full allowance being made for electron exchange. The trial wave function is assumed to have a form which in spheroidal coordinates resembles the analogous functions in spherical polar coordinates used in discussing elastic scattering by hydrogen and helium atoms. Quite good agreement is obtained with observed data—an agreement which disappears when exchange is neglected; this is a situation similar to that which arises in the case of helium.

§ 1. Introduction

Detailed applications of variational methods have already been made to the theory of the scattering of electrons by hydrogen and helium atoms. The most extensive work of this kind has been carried out using the variational methods of Hulthén (1944) and of Kohn (1948) with trial functions of a similar quite simple form. The results obtained have been encouraging. Thus if the elastic scattering is treated on the assumption that polarization effects are ignored but full allowance is made for exchange as well as direct potential interaction, so that the problem is reduced to one of solving an appropriate integro-differential equation, it was found that the variational method gave results for both atomic hydrogen (Massey and Moiseiwitsch 1950) and helium (Moiseiwitsch 1953) which differed only slightly from those obtained by accurate solution of the equation (Allis and Morse 1933). Because of the relative simplicity of the method it seemed desirable to apply it to the simplest axially symmetrical molecular scattering problem—the electron scattering of slow electrons by molecular hydrogen.

Comparatively little work has been done on the theory of the scattering of slow electrons by diatomic molecules. Stier (1932) showed that the observed scattering by N_2 could be fitted on the assumption of a certain empirical scattering potential. This approach was developed by Fisk (1936) who showed that observations, not only for N_2 but for a number of other molecules including H_2, could also be fitted reasonably well in this way. The only attempt, however, to calculate the scattering from a molecular potential derived from the quantum theory of the molecule is that of Nagahara (1953, 1954). Even in his work, however, no allowance was made for exchange effects. Since these are well known to be of major importance for the scattering of slow electrons by the

† Now at the Atomic Energy Research Establishment, Harwell.

nearest two-electron atom of helium and are also quite large for atomic hydrogen, it is unlikely that they are unimportant for molecular hydrogen. It has proved possible, because of the relative simplicity of the variational method, to treat exchange scattering on the same basis as direct scattering and in this paper an account is given of the detailed application of the method and of the results obtained. These results show that exchange is indeed important, at least for electron energies below 15 ev. Furthermore, they agree with observed data to an extent which is probably closer than warranted when allowance is made for the various approximations which have to be made in treating a molecular scattering problem.

§ 2. General Account of the Method

The only appreciable contribution to the scattering of sufficiently slow electrons by atoms comes from those electrons with zero angular momentum about the nucleus. The scattering is therefore determined by the distortion of the wave function of these electrons by the atomic field. If k is the wave number of the incident electron this wave function $F(r)$ will then have the asymptotic form

$$F(r) \sim r^{-1} \sin(kr + \delta_0) \qquad \ldots\ldots(1)$$

or alternatively

$$\sim (1+a^2)^{-1/2} (\sin kr + a \cos kr) r^{-1} \qquad \ldots\ldots(2)$$

where $\delta_0 = \arctan a$, is the zero order phase shift due to the atomic field. The zero order scattering cross section is then $4\pi \sin^2 \delta_0 / k^2$.

The determination of the phase shift δ_0, allowing for exchange, may be carried out approximately by a variational method as follows.

We consider from the outset a three-electron problem, that of elastic scattering of electrons by helium atoms (Moiseiwitsch 1953). The three electrons are distinguished by the suffixes 1, 2, 3, and the corresponding spin functions for electron i by α_i, β_i according as the z component of spin is $\pm \frac{1}{2}\hbar$. If $\psi_0(r_1, r_2)$ is the wave function of the ground state of helium, electrons 1 and 2 being the atomic electrons, then the wave function representing the scattering is taken to have the form

$$\Psi = \frac{1}{\sqrt{3}} \sum_{i=1}^{3} \psi(r_j, r_k) F(r_i) \alpha_i \chi_{jk} \qquad \ldots\ldots(3)$$

where

$$\chi_{jk} = \frac{1}{\sqrt{2}} (\alpha_j \beta_k - \alpha_k \beta_j). \qquad \ldots\ldots(4)$$

This wave function is antisymmetric in each pair of electrons and each term is an eigenfunction for total z component of spin $\frac{1}{2}\hbar$. To determine δ_0 approximately we consider the integral

$$L = \int \Psi (H - E) \Psi \, d\tau_1 \, d\tau_2 \, d\tau_3, \qquad \ldots\ldots(5)$$

where H is the Hamiltonian of the three-electron system and E is the total energy $E_0 + k^2$, E_0 being that of the ground state of helium and k the electron wave number in atomic units. The integration is supposed to include summation over the spin coordinates.

If Ψ were an exact solution of the three-electron problem with F having the asymptotic form (2) then L must vanish, but if instead a trial form for $F(r)$ is

used which is everywhere bounded and has the same asymptotic form (2) except that the exact a is replaced by a varied form $a+\delta a$, it is easy to show that

$$\delta L = k\delta a. \qquad \ldots\ldots(6)$$

Variational methods for determining a and hence δ_0 approximately are based on the assumption of a trial form $F_t(r)$ involving arbitrary parameters $c_1, c_2, \ldots, c_n$, and with asymptotic form (2). In Hulthén's procedure the n parameters and a are determined from the equations

$$\frac{\partial L}{\partial c_r}(c_1, \ldots, c_n, a) = 0, \quad r = 1, \ldots, n; \qquad L(c_1, \ldots, c_n, a) = 0. \qquad \ldots\ldots(7)$$

An alternative is to work from

$$\frac{\partial L}{\partial c_r} = 0, \quad r = 1, \ldots, n, \qquad \frac{\partial L}{\partial a} = 0, \qquad \delta_0 = \arctan\left(a - \frac{L}{k}\right). \qquad \ldots\ldots(8)$$

This has the advantage that, if the parameters $c_1, \ldots, c_n, a$ appear linearly in the trial function, the equations (8) are all linear, whereas the last one of (7) is quadratic. On the other hand there is some empirical evidence that Hulthén's equations give slightly better results in practice. To distinguish which is to be taken of the two roots for a which they give, resort may be made to the integral equation for the phase shift or to the choice of that solution which is closest to the one given by Kohn's equations.

Moiseiwitsch (1953) applied this procedure to scattering by helium using as trial function a form suggested by Huang (1949) and used by Massey and Moiseiwitsch (1950) for electron scattering by atomic hydrogen:

$$F_t(r) = r^{-1}\{\sin kr + (a + b\,e^{-r})\cos kr\}. \qquad \ldots\ldots(9)$$

This gave quite good results as may be seen by reference to their paper.

This method may be extended to apply to scattering by a molecule provided appropriate modification of the trial function F_t is made. Thus in (3) $\psi(r_1, r_2)$ now becomes the space wave function of the ground state of molecular hydrogen and the spin functions are unchanged. The function representing the relative motion of electron and molecule will, however, depend not only on the distance R_i of the electron from the centre of the molecule, but also on its angular coordinates θ_i, ϕ_i and the angle of orientation λ, μ of the molecular axis. Previous calculations for scattering of molecules have worked in terms of spheroidal coordinates ξ, η, ϕ where

$$\xi = \frac{r+p}{d}, \qquad \eta = \frac{r \sim p}{d} \qquad \ldots\ldots(10)$$

r and p being the distances of the electron from the respective nuclei, and d the nuclear separation. In terms of these coordinates a plane wave propagating in the direction (θ_0, ϕ_0) relative to the nuclear axis and azimuthal reference plane may be expanded in the form (Morse 1935, Stratton *et al.* 1941)

$$e^{ikz} = 2\sum_{m,n} \cos m(\phi - \phi_0) i^{m+n} \frac{2 - \delta_{0,m}}{2^m m!} A_{mn} S^{(1)}_{m,n}(c, \cos\theta) S^{(1)}_{m,n}(c, \cos\theta_0) R^{(1)}_{m,n}(\xi) \qquad \ldots\ldots(11)$$

where $\eta = \cos\theta$, $c = \frac{1}{2}kd$. The functions $S^{(1)}_{m,n}$ are spheroidal harmonics. They may be expanded in terms of spherical harmonics in the form

$$S^{(1)}_{m,n}(c, \cos\theta) = \sum_s{}' d^n_s(c) P_{m+s}^{m}(\cos\theta), \qquad \ldots\ldots(12)$$

where the prime indicates that the summation is over even values of s if n is even and over odd values if n is odd. For values of c much less than 1 all values of d_s^n are very small except that for which $s=n$. In the limit $d\to 0$, $S_{m,n}\to P_{m+n}^m(\cos\theta)$.

The functions $R^{(1)}_{m,n}(\xi)$ may similarly be expanded in the form

$$R^{(1)}_{m,n}(\xi)=\frac{(\xi^2-1)^{m/2}}{\xi^m\sum_{s=0}^{\infty}{}' d_s^n\frac{(s+2m)!}{s!}}\sum_s{}' i^{m-s}d_s^n\frac{(s+2m)!}{s!}\mathrm{j}_{m+s}(c\xi) \quad \ldots\ldots(13)$$

where j_{m+s} is the usual Bessel function

$$\mathrm{j}_n(z)=(\pi/2z)^{1/2}\mathrm{J}_{n+\frac{1}{2}}(z). \quad \ldots\ldots(14)$$

The normalization is adjusted so that, for large ξ,

$$R^{(1)}_{m,n}(\xi)\sim\frac{1}{c\xi}\sin\{c\xi-\tfrac{1}{2}(m+n)\pi\}, \quad \ldots\ldots(15)$$

and this ensures that when $d\to 0$, $R^{(1)}_{m,n}(\xi)$ tends to the usual solution in spherical polar coordinates.

A_{mn} is a constant whose value need not concern us at the moment.

If the wave equation, including the scattering potential, is separable with the η equation unchanged, the scattering may be described in terms of phase shifts ζ_{mn} which are such that the solution of the ξ equation, with scattering potential included, has the asymptotic form for large ξ

$$\frac{1}{c\xi}\sin\{c\xi-\tfrac{1}{2}(m+n)\pi+\zeta_{mn}\}. \quad \ldots\ldots(16)$$

For impact velocities which are so small that $uc\ll 1$ where u is the ratio of the effective range of interaction to the nuclear separation, the only important phase shift is ζ_{00}. Hence if the equations are approximately separable, the scattering at these velocities will be described to a good approximation in terms of a function

$$F(\xi,\eta)=S_{00}(c,\eta)\mathscr{R}(c,\xi) \quad \ldots\ldots(17)$$

where $\mathscr{R}(c,\xi)$ has the asymptotic form (16) with $m=n=0$. Furthermore, if $c\ll 1$, S_{00} does not differ very much from unity (the zonal harmonic P_{00}). Thus even for $c=1$ in (12) $d_0^0=0{\cdot}948$, $d_0^2=-0{\cdot}102$, $d_0^4=0{\cdot}0017$. Since for a light molecule such as hydrogen u will not be much greater than 1, it seems that, for velocities for which $c\ll 1$, suitable trial functions could be taken of the form

$$F(\xi)=\mathscr{R}_{\mathrm{t}}(c,\xi) \quad \ldots\ldots(18)$$

with no dependence on η introduced. A simple improvement would be to take

$$F(\xi,\eta)=\mathscr{R}_{\mathrm{t}}(c,\xi)[1+g\eta^2] \quad \ldots\ldots(19)$$

where g is an additional adjustable parameter. However, in this paper the simplest form was first assumed. As unexpectedly good results were obtained, it was not considered worth while, because of the additional labour involved, to extend the calculations with the function (19).

By an obvious analogy to the atomic cases (see (9)), $\mathscr{R}_{\mathrm{t}}(c,\xi)$ was taken of the form

$$\mathscr{R}_{\mathrm{t}}(c,\xi)=(1+a^2)^{-1/2}\frac{1}{c(\xi-1)}[\sin\{c(\xi-1)\}+\{a+be^{-\gamma(\xi-1)}\}\{1-e^{-\gamma(\xi-1)}\}\cos c(\xi-1)]. \quad \ldots\ldots(20)$$

This has the asymptotic form

$$\mathscr{R}_t(c,\xi) \sim \frac{1}{c\xi}\sin(c\xi+\zeta_{00}^t), \qquad \ldots\ldots(21)$$

where

$$\zeta_{00}^t = (\arctan a) - c. \qquad \ldots\ldots(22)$$

Hulthén's and Kohn's formulae apply immediately for the determination of a and hence of ζ_{00}^t. The scattering cross section to this approximation is given by

$$\frac{4\pi}{k^2}\sin^2\zeta_{00}^t. \qquad \ldots\ldots(23)$$

§ 3. Details of the Calculation

We require to evaluate

$$L = \iiint \Psi(H-E)\Psi\, d\tau_1\, d\tau_2\, d\tau_3 \qquad \ldots\ldots(24)$$

where

$$H = -\sum_1^3\left\{-\nabla_i^2 + 2\left(\frac{1}{r_i}+\frac{1}{p_i}\right)\right\} - 2\sum_{ij}\frac{1}{r_{ij}},$$

$$E = E_0 + k^2,$$

E_0 being the energy of the ground state of H_2.

The integration is assumed to include also summation over the spin coordinates of the three electrons. Substituting (3) for Ψ with F given by (18) and (20) and carrying out this summation we find $L = L_D - L_E$ where

$$L_D = -\int \{\psi(\mathbf{r}_1,\mathbf{r}_2)\}^2 F(\xi_3)\left[\nabla_3^2 + \frac{2}{r_3} + \frac{2}{p_3} + k^2 - \frac{2}{r_{13}} - \frac{2}{r_{23}}\right] F(\xi_3)\, d\tau_1\, d\tau_2\, d\tau_3 \qquad \ldots\ldots(25)$$

$$L_E = -\int \psi(\mathbf{r}_1,\mathbf{r}_2)F(\xi_3)\left[\nabla_1^2 + \frac{2}{r_1} + \frac{2}{p_1} + k^2 - \frac{2}{r_{12}} - \frac{2}{r_{13}}\right] F(\xi_1)\psi(\mathbf{r}_3,\mathbf{r}_2)\, d\tau_1\, d\tau_2\, d\tau_3 \qquad \ldots\ldots(26)$$

L_E being the contribution from exchange.

If $V(\mathbf{r}_3)$ is the mean potential interaction of an electron with the molecule so that

$$V(\mathbf{r}_3) = \int \{\psi(\mathbf{r}_1,\mathbf{r}_2)\}^2\left\{-\frac{2}{r_3} - \frac{2}{p_3} + \frac{2}{r_{13}} + \frac{2}{r_{23}}\right\} d\tau_1\, d\tau_2 \qquad \ldots\ldots(27)$$

we have

$$L_D = -\int F(\xi_3)[\nabla_3^2 + k^2 - V(r_3)]F(\xi_3)\, d\tau_3. \qquad \ldots\ldots(28)$$

$V(\mathbf{r}_3)$ may be written in the form

$$V(\mathbf{r}_3) = -\frac{8\xi_3}{d(\xi_3^2-\eta_3^2)} + 2f(\xi_3,\eta_3) \qquad \ldots\ldots(29)$$

where the first term represents the Coulomb field of the nuclei.

A choice is available of many approximate forms for $\psi(\mathbf{r}_1,\mathbf{r}_2)$. It was found that considerable simplification of the rather extensive analysis could be made if the self-consistent function given by Coulson (1938) is used. This is given by

$$\psi(\mathbf{r}_1,\mathbf{r}_2) = \phi(\mathbf{r}_1)\phi(\mathbf{r}_2), \qquad \ldots\ldots(30)$$

where

$$\left[\nabla_1^2+\epsilon+\frac{2}{r_1}+\frac{2}{p_1}-2\int\frac{\phi^2(\mathbf{r}_2)}{r_{12}}d\tau_2\right]\phi(\mathbf{r}_1)=0. \qquad \ldots\ldots(31)$$

On substitution in (26), using (31), we find that

$$L_E=-(J_1+J_2). \qquad \ldots\ldots(32)$$

where

$$J_1=(k^2-\epsilon)\{\int\phi(\mathbf{r})F(\xi)\,d\tau\}^2, \qquad \ldots\ldots(33)$$

$$J_2=-\frac{2}{\pi}\int\int\frac{\phi(\mathbf{r}_2)\phi(\mathbf{r}_1)F(\xi_2)F(\xi_1)}{r_{12}}d\tau_1\,d\tau_2. \qquad \ldots\ldots(34)$$

Coulson (1938) gives

$$\phi(\mathbf{r})=Ne^{-\gamma\xi}(1+\alpha\eta^2+\beta\xi), \qquad \ldots\ldots(35)$$

where $\alpha=0{\cdot}2195$, $\beta=0{\cdot}07957_5$, $\gamma=0{\cdot}75$, $N=0{\cdot}693$. This does not satisfy (31) exactly but is a sufficiently good approximation for (33) and (34) to be assumed correct. There is no difficulty in evaluating the integrals involved in the calculation of L_D and L_E if (35) is assumed for ϕ and (20) for F, with γ as in (35).

It is of interest to note the form obtained for the mean molecular potential interaction. To quite a close approximation it can be written in the form

$$V(\mathbf{r}_3)=-\frac{8\xi}{d(\xi^2-\eta^2)}+2u(\xi), \qquad \ldots\ldots(36)$$

where $u(\xi)$ is tabulated in table 1.

Table 1. Function $u(\xi)$ appearing in expression (36) for Mean Potential Interaction of an Electron with a Hydrogen Molecule

ξ	$u(\xi)$	ξ	$u(\xi)$	ξ	$u(\xi)$
1·0	1·9022	2·6	1·0869	4·0	0·7243
1·2	1·7775	2·8	1·0183	4·2	0·6898
1·4	1·6595	3·0	0·9563	4·4	0·6583
1·6	1·5454	3·2	0·9003	4·6	0·6294
1·8	1·4377	3·4	0·8497	4·8	0·6029
2·0	1·3378	3·6	0·8038	5·0	0·5784
2·2	1·2461	3·8	0·7622	6·0	0·4805
2·4	1·1626				

§ 4. Results

The phase shifts ζ_0 obtained are given in table 2.

Table 2. Phase Shifts ζ_0 obtained by use of Hulthén and Kohn Variational Methods

kd	k (A.U.)	(Volts) $^{1/2}$	ζ_0 (radians) Exchange ignored		Exchange included	
			H	K	H	K
0·1	0·143	0·52	2·103	2·095	2·941	3·001
0·2	0·286	1·05	1·778	1·722		
0·3	0·429	1·58	1·514	1·457	2·352	2·785
0·5	0·714	2·63	1·228	1·234	1·830	1·749
1·0	1·429	5·25	0·748	(1·644)	1·056	1·027

Apart from the case $kd=1{\cdot}0$, the Hulthén and Kohn methods both give closely similar results when exchange is ignored, i.e. when $L=L_D$. This suggests that the trial function assumed is quite good under these circumstances. On the other hand when exchange is included the two methods do not agree so well, so that the trial function must be deemed less satisfactory. Nevertheless comparison with the observed data shows that the phases given by the Hulthén method are not far from correct.

The figure gives a comparison of observed and calculated cross sections. The observed results fall into two groups which are only very roughly consistent. Curve I gives the total cross section measured by the Ramsauer method as a function of electron velocity in $(\text{volts})^{1/2}$, while curve II refers to the mean cross

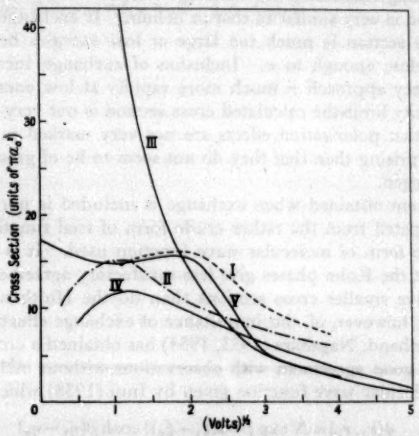

Comparison of observed and calculated cross sections for scattering of electrons by molecular hydrogen : I, observed by Ramsauer method ; II, observed by swarm diffusion methods (in this case the ordinate is the mean cross section and the abscissa the mean electron velocity in $(\text{volts})^{1/2}$); III, calculated by the method of the present paper, ignoring exchange ; IV, calculated by the method of the present paper, including exchange ; V, calculated by Fisk using an empirical molecular scattering potential with adjustable constants.

section as a function of mean electron velocity measured by swarm methods. These measurements include the recent extension to very low mean electron energies by Crompton and Sutton (1952). Even allowing for the somewhat different significance of the coordinates for the two types of observation it is clear that they do not agree very well. This must be borne in mind when considering the relation to the calculated values.

The cross sections obtained from the Hulthén phases ζ_0 in table 2, ignoring exchange, are much too large at low electron energies (curve III of the figure). On the other hand when exchange is included the departure from the observed

curve II is not greater than the discrepancy between the two sets of observed curves, while the shape of the cross section velocity curve is given correctly. The calculated cross section can be expected to fall below the observed at the higher electron energies, for two reasons. The observed cross sections include inelastic collisions and in any case contributions to the elastic scattering from partial cross sections other than the (0, 0) which we have considered are becoming important. Our simple trial function becomes less satisfactory as the energy increases for reasons already indicated in the preceding section.

For comparison the cross section calculated by Fisk (1936) using his empirical molecular scattering potential is also given. At the higher energies it agrees quite closely with that calculated from our phases ignoring exchange. The fact that Fisk adjusts the interaction to fit the data at low energies means he is essentially allowing empirically for exchange effects.

The situation is very similar to that in helium. If exchange is neglected the calculated cross section is much too large at low energies because the phase shifts are not close enough to π. Inclusion of exchange increases the phase shifts so that they approach π much more rapidly at low energies; thus even in the low velocity limit the calculated cross section is not very seriously wrong. This indicates that polarization effects are not very marked in this case. It is perhaps not surprising then that they do not seem to be of great importance for molecular hydrogen.

The agreement obtained when exchange is included is perhaps closer than might be anticipated from the rather crude form of trial function assumed and from the simple form of molecular wave function used. It is of some interest to note also that the Kohn phases give less satisfactory agreement with observations as they give smaller cross sections than do the Hulthén phases. There seems no doubt, however, of the importance of exchange effects at low energies

On the other hand, Nagahara (1953, 1954) has obtained a cross section which is in reasonably good agreement with observations without including exchange. He uses the molecular wave function given by Inui (1938) which takes the form

$$\psi(\mathbf{r}_1, \mathbf{r}_2) = N \exp\{-\alpha(\xi_1 + \xi_2)\} \cosh \beta(\eta_1 - \eta_2)$$

where $\alpha = 1{\cdot}75$, $\beta = 1{\cdot}375$, and calculates the scattering by the corresponding mean molecular potential (27) by a method of expansion in spheroidal wave functions which does not assume separability. It is not clear from the small amount of detail given in his second paper (Nagahara 1954) how the coupled differential equations involved in his method were actually solved. There is obviously room both for further theoretical and experimental work on the subject. Thus it would be of interest to approach the problem using spherical instead of spheroidal harmonic analysis. When spheroidal coordinates do not introduce separability it is likely that any 'naturalness' they possess for the particular problem is more than offset by the comparative complexity attendant on their use.

Acknowledgments

We are indebted to Miss Fosgate, Mrs. Sida and Mrs. Gillis for assistance with the numerical calculations and to Professor L. G. H. Huxley for informing us of his experimental results in advance of publication.

References

ALLIS, W. P., and MORSE, P. M., 1933, *Phys. Rev.*, **44**, 269.
COULSON, C. A., 1938, *Proc. Camb. Phil. Soc.*, **34**, 204.
CROMPTON, R. W., and SUTTON, D. J., 1952, *Proc. Roy. Soc.* A, **215**, 467.
FISK, J. B., 1936, *Phys. Rev.*, **49**, 951.
HUANG, S. S., 1949, *Phys. Rev.*, **76**, 477.
HULTHÉN, L., 1944, *K. Fysiogr. Sällsk. Lund. Förh.*, **14**, no. 21.
INUI, T., 1938, *Proc. Phys.-Math. Soc. Japan*, **20**, 790.
KOHN, W., 1948, *Phys. Rev.*, **74**, 1763.
MASSEY, H. S. W., and MOISEIWITSCH, B. L., 1950, *Proc. Roy. Soc.* A, **205**, 483.
MOISEIWITSCH, B. L., 1953, *Proc. Roy. Soc.* A, **219**, 102.
MORSE, P. M., 1935, *Proc. Nat. Acad. Sci.*, **21**, 56.
NAGAHARA, S., 1953, *J. Phys. Soc. Japan* **8**, 165 ; 1954, *Ibid.*, **9**, 52.
STIER, H., 1932, *Z. Phys.*, **76**, 439.
STRATTON, J. M., MORSE, P. N., CHU, L. J., and HUTNER, R. A., 1941, *Elliptic Cylinder and Spheroidal Wave Functions* (New York : John Wiley).

The Inelastic Scattering of Nucleons by the Surface Interaction

By S. YOSHIDA

Department of Mathematical Physics, University of Birmingham†

Communicated by R. E. Peierls ; MS. received 14*th March* 1956, *and in revised form* 14*th May* 1956

Abstract. The effect of the surface interaction, based on A. Bohr's collective model, on the inelastic scattering of nucleons by a nucleus at medium energy is discussed. The wave function is expressed as a sum of amplitudes, which correspond to various states of target nucleus and incident nucleon. From the Schrödinger equation one can derive a set of coupled equations for the amplitudes, which correspond to a state of the surface excitation while the effect of the other amplitudes is replaced by distorting potentials. The interaction between the states considered explicitly is assumed as the surface interaction proposed by A. Bohr, and taken to have a δ-function type radial dependence. The coupled equations are solved without further approximation. The distorting potential is chosen so as to give the right result for the elastic scattering in the presence of the surface interaction. If that interaction is strong enough, the distorting potential differs considerably from the usual optical potential, which would give a good result for the elastic scattering in the absence of surface interaction. The theory is applied to proton scattering by ^{24}Mg at 10 Mev, and the result shows that the strong angular dependence of the inelastic scattering is due to the surface interaction while the main contribution comes from the compound nucleus.

§ 1. Introduction

The elastic scattering of a nucleon by nuclei has been investigated by many authors, and it has been found that the cloudy crystal ball or optical model gives fairly good agreement with experiments. On the other hand, for inelastic scattering or for reactions we have only succeeded in obtaining a qualitative explanation by the so-called statistical model, and there remain many serious quantitative discrepancies between the theory and the experiments. Among them the angular distribution of inelastically scattered protons shows a strong angular dependence at medium energy, which is far from being explained by the conventional statistical model and, in fact, the angular distribution is sometimes asymmetric about 90° (see for example Saxon *et al.* 1955). Most published work on this subject assumes that the direct process is more important than that involving formation of a compound nucleus. These problems were treated by the Born approximation as well as the method of the distorted waves. Hayakawa and Yoshida (1955) and Brink (1955) also discussed the importance of the surface interaction, based on the collective model of A. Bohr and Mottelson (1952, 1953) in terms of the latter method.

When we use the distorted wave, the most important problem is how to choose a distorting potential. As the method for obtaining the distorting potential for the

† On leave from the Research Institute for Fundamental Physics, Kyoto, Japan.

inelastic scattering has not yet been thoroughly investigated, we were obliged in our previous paper to use the optical potential, which was adjusted so as to give the correct elastic scattering. This choice of the optical potential will give a good approximation, if the surface interaction is weak. But if the surface interaction is strong, it also affects the elastic scattering in second and higher orders, and the optical potential must therefore be readjusted to fit the elastic scattering†.

To take into account the higher order processes which are involved in the strong interaction, we start from a wave function composed of a sum of various amplitudes corresponding to various excited states of the target nucleus. If we put this wave function into the Schrödinger equation and use the orthogonality of different eigenfunctions of the target nucleus, we obtain a set of coupled equations for the amplitudes, the coupling term being the matrix element of the interaction between the incident nucleon and the target nucleus, evaluated between the ground and the excited states of the target nucleus. It is convenient to classify the states into two groups, strongly coupled and weakly coupled states, according to the magnitude of the matrix element, which connects each state with the ground state‡. We can eliminate the weakly coupled amplitudes in an approximate way. We then obtain coupled equations in terms of the strongly coupled amplitudes, in which the diagonal matrix element of the interaction together with the terms corresponding to the second order processes in weak interactions may be replaced by optical potentials (we shall call these distorting potentials hereafter). In the case of strong coupling these may be quite different from the usual optical potential which fits the elastic scattering without allowing for the coupling. The resulting equations should be solved without using a perturbation method. It is still difficult to solve them in the general cases, but we shall see that they can be easily solved exactly in the case of the δ-function type surface interaction used in our previous paper. Our next problem is to evaluate the distorting potential. It is clear that if we eliminate amplitudes other than those corresponding to the ground state of the target nucleus, we get the effective potential for elastic scattering, i.e. the usual optical potential. This has been investigated thoroughly phenomenologically and we can make use of this knowledge to evaluate the distorting potential in our equations.

We can evaluate the contribution to the cross section from the direct interaction by the method outlined above, but the contribution which comes through the weakly coupled states is also important. This may be treated by the conventional statistical model by calculating the cross section of compound nucleus formation and using detailed balancing, neglecting the interference terms. The angular dependence of this contribution is probably weak, but its magnitude may be large compared with the direct contribution.

A numerical result will be given for the case of the scattering of protons by ^{24}Mg. The parameters which come into our theory may be determined by other experiments such as the elastic scattering and the quadrupole moment of neighbouring nuclei or the lifetime of γ-transition in this nucleus.

† The author is indebted to Dr. A. Bohr and Mr. A. M. Lane, who drew his attention to the work of C. F. Wandel (*Thesis*, Copenhagen 1954, unpublished).

‡ The strongly coupled state is not necessarily connected to the ground state directly. For example we may treat the spin 4 and 6 states as the strongly coupled state in the rotational spectra of even–even nuclei.

§ 2. Elimination of the Weakly Coupled States

The solution to our problem can be stated in terms of the S-matrix. In this section we shall discuss the method for simplifying our equation by eliminating the weakly coupled states and shall introduce the distorting potentials. First we write the wave function of the whole system, which has a definite total angular momentum J, its Z component M and parity and consider only one incident channel specified by the quantum numbers of the target nucleus α, the channel spin s and the orbital angular momentum l of the incident nucleon. The wave function is given by

$$\Psi_{\alpha sl}^{JM} = \frac{1}{r}[u_{J\alpha sl}(r)\,\phi_{J\alpha sl}^{M} + \sum_{\alpha' s' l'} v_{J\alpha' s' l'}(r)\,\phi_{J\alpha' s' l'}^{M} + \sum_{\beta s' l'} w_{J\beta' s' l'}(r)\,\phi_{J\beta' s' l'}^{M}] \quad \ldots(2.1)$$

where the first term of the right-hand side corresponds to the entrance channel; the second represents the strongly coupled amplitudes which correspond to a few excited states as well as some channels, other than the entrance channel, with the target nucleus in the ground state. The third term represents the weakly coupled states, which we want to eliminate. r is the radial coordinate of the incident nucleon and u, v, w are its radial wave function whose asymptotic form must be chosen as follows: u is an outgoing plus an incoming wave, v and w are outgoing waves only, or exponentially decaying if the incident energy is not enough to emit nucleons. $\phi_{J\alpha sl}^{M}$ represents the spin-angular wave functions which form an orthonormal complete set and may be written as

$$\phi_{J\alpha sl}^{M} = \sum_{m} (slM-mm\,|\,slJM)\, i^{l} Y_{lm}(\theta\varphi)\, \chi_{\alpha sM-m} \quad \ldots\ldots(2.2)$$

where $(slM-mm\,|\,slJM)$ is the usual Clebsch–Gordan coefficient, $Y_{lm}(\theta\varphi)$ are spherical harmonics whose arguments θ, φ are the angular coordinates of the incident nucleon. The phase factor i^{l} is introduced in order to give the right phase change for the time reversal according to Huby (1954). $\chi_{\alpha sM-m}$ is the wave function of the channel spin and the target nucleus and has the following form :

$$\chi_{\alpha sM} = \sum_{\nu} (\sigma I \nu M-\nu\,|\,\sigma ISM)\, \chi_{\sigma\nu}\, \psi_{\alpha IM-\nu}. \quad \ldots\ldots(2.3)$$

In this equation $\chi_{\sigma\nu}$ is the spin wave function of the incident nucleon and $\psi_{\alpha IM}$ is the target nucleus wave function whose spin is I, its z-component M, energy state α and satisfies the following equation,

$$(H_{t}-\epsilon_{\alpha})\,\psi_{\alpha IM-\nu}=0. \quad \ldots\ldots(2.4)$$

H_{t} is the Hamiltonian of the target nucleus and ϵ_{α} is its eigenvalue. The wave function defined above does not satisfy the Pauli principle. As it is difficult in practice to make the functions antisymmetric, we shall neglect this requirement throughout this work.

The total Hamiltonian H of our system is expressed as a sum of the kinetic energy T of the incident particle, the Hamiltonian of the target nucleus H_{t}, and the interaction between the incident particle and the target nucleus V:

$$H=T+H_{t}+V. \quad \ldots\ldots(2.5)$$

Then the Schrödinger equation is

$$(H-E)\,\Psi_{\alpha sl}^{JM}=0 \quad \ldots\ldots(2.6)$$

where E is the energy of the total system. Putting the equations (2.1) and (2.5) into the Schrödinger equation (2.6), we get the following coupled equations

$$(T_l+\epsilon_\alpha-E)u_{J\alpha sl}(r)+V_{\alpha sl,\,\alpha sl}^{J}u_{J\alpha sl}(r)+\sum_{\alpha's'l'}V_{\alpha sl,\,\alpha's'l'}^{J}v_{J\alpha's'l'}(r)+\sum_{\beta s'l'}V_{\alpha sl,\,\beta s'l'}^{J}w_{J\beta s'l'}(r)=0 \quad \ldots\ldots(2.7a)$$

$$(T_{l'}+\epsilon_\alpha-E)v_{J\alpha's'l'}(r)+V_{\alpha's'l',\,\alpha sl}^{J}u_{J\alpha sl}(r)+\sum_{\alpha''s''l''}V_{\alpha's'l',\,\alpha''s''l''}^{J}v_{J\alpha''s''l''}(r)+\sum_{\beta s''l''}V_{\alpha's'l',\,\beta s''l''}^{J}w_{J\beta s''l''}(r)=0 \quad \ldots\ldots(2.7b)$$

$$(T_{l'}+\epsilon_\beta-E)w_{J\beta's'l'}(r)+V_{\beta's'l',\,\alpha sl}^{J}u_{J\alpha sl}(r)+\sum_{\alpha''s''l''}V_{\beta's'l',\,\alpha''s''l''}^{J}v_{J\alpha''s''l''}(r)+\sum_{\beta''s''l''}V_{\beta's'l',\,\beta''s''l''}^{J}w_{J\beta''s''l''}(r)=0. \quad \ldots\ldots(2.7c)$$

where

$$T_l=-\frac{\hbar^2}{2M}\frac{d^2}{dr^2}+\frac{\hbar^2l(l+1)}{2Mr^2}$$

and $V_{\alpha sl,\,\alpha's'l'}^{J}$ is the matrix element of V evaluated between the states $_{J\alpha sl}$ and $_{J\alpha's'l'}$ and is a function of r.

We now eliminate the weakly coupled amplitudes w from our equation by solving equation (2.7c) in terms of u and v. As the weakly coupled amplitudes are probably small compared with the strongly coupled ones u and v, it seems to be a good approximation to neglect the non-diagonal matrix element $V_{\beta's'l',\,\beta''s''l''}^{J}$ in the last equation (2.7c). Then we can solve that equation in a formal way as

$$w_{J\beta sl}(r)=a_{J\beta sl}^{-1}\left[V_{\beta sl,\,\alpha sl}^{J}u_{J\alpha sl}(r)+\sum_{\alpha's'l'}V_{\beta sl,\,\alpha's'l'}^{J}v_{J\alpha's'l'}(r)\right] \quad \ldots\ldots(2.8)$$

where

$$a_{J\beta sl}^{-1}=[E+i\eta_\beta-T_l-\epsilon_\beta-V_{\beta sl,\,\beta sl}^{J}]^{-1} \quad \ldots\ldots(2.9)$$

is an integral operator and η_β is the notation to specify the asymptotic boundary conditions. Next we put (2.8) into equations (2.7a) and (2.7b) and get the following simplified coupled equations

$$(T_l+U_{\alpha sl}^{J}+\epsilon_\alpha-E)u_{J\alpha sl}(r)+\sum_{\alpha's'l'}V_{\alpha sl,\,\alpha's'l'}^{J}v_{J\alpha's'l'}(r)=0. \quad \ldots\ldots(2.10a)$$

$$(T_{l'}+U_{\alpha's'l'}^{J}+\epsilon_{\alpha'}-E)v_{J\alpha's'l'}(r)+V_{\alpha's'l',\,\alpha sl}^{J}u_{J\alpha sl}(r)+\sum_{\alpha''s''l''}V_{\alpha's'l',\,\alpha''s''l''}^{J}v_{J\alpha''s''l''}(r)=0. \quad \ldots\ldots(2.10b)$$

$$U_{\alpha sl}^{J}u_{J\alpha sl}(r)=V_{\alpha sl,\,\alpha sl}^{J}u_{J\alpha sl}(r)+\sum_{\beta s'l'}V_{\alpha sl,\,\beta s'l'}^{J}a_{J\beta s'l'}^{-1}V_{\beta s'l',\,\alpha sl}^{J}u_{J\alpha sl}(r)+\sum_{\beta s'l'}V_{\alpha sl,\,\beta s'l'}^{J}a_{J\beta s'l'}^{-1}V_{\beta s'l',\,\alpha's'l'}^{J}v_{J\alpha's'l'}(r). \quad \ldots\ldots(2.10c)$$

$$U_{\alpha's'l'}^{J}v_{J\alpha's'l'}(r)=V_{\alpha's'l',\,\alpha's'l'}^{J}v_{J\alpha's'l'}(r)+\sum_{\beta s'l'}V_{\alpha's'l',\,\beta s'l'}^{J}a_{J\beta s'l'}^{-1}V_{\beta s'l',\,\alpha sl}^{J}u_{J\alpha sl}(r)+\sum_{\beta s'l'}V_{\alpha's'l',\,\beta s'l'}^{J}a_{J\beta s'l'}^{-1}V_{\beta s'l',\,\alpha's'l'}^{J}v_{J\alpha's'l'}(r). \quad \ldots\ldots(2.10d)$$

In the first two equations the weakly coupled channels are eliminated, and instead of them we have introduced the distorting potentials U to take into account the effect of these eliminated weakly coupled channels. Now our equations are reduced to coupled equations for u, v, U, and they should be solved in a self-consistent way. This method is a natural extension of the method of Brueckner and Levinson (1955) and of Cini and Fubini (1955) in calculating the optical potential for elastic scattering.

§ 3. Calculation of the S-Matrix

It is still difficult to solve the equations (2.10) in the general case. However, if the strong interaction is approximated by a surface interaction, which has a radial dependence of δ-function type, the equation can be solved without further approximation. The distorting potential U will be assumed to be a complex square well for convenience in the practical calculation. However, in our previous paper we had not given a method for finding the distorting potential. In this section the S-matrix will be derived without further approximation when the distorting potentials are given, and a later section will describe a method for finding the magnitude of the distorting potential. According to the assumption, we express the interaction as

$$V_{\alpha sl,\,\alpha' s' l'}^{J}=\delta(r-R_0)\frac{\hbar^2}{2MR_0}W_{\alpha sl,\,\alpha' s' l'}^{J}. \qquad \text{.....(3.1}a\text{)}$$

$$U_{\alpha sl}^{J}(r)=V_{\alpha sl}^{J}(r)+\delta(r-R_0)\frac{\hbar^2}{2MR_0}W_{\alpha sl,\,\alpha sl}^{J}. \qquad \text{.....(3.1}b\text{)}$$

$$\begin{aligned} V_{\alpha sl}^{J}(r)&=-V_{\alpha sl}^{J} && r<R_0\\ &=0 && r>R_0 \end{aligned} \qquad \text{.....(3.1}c\text{)}$$

where R_0 is the nuclear radius†. If we put these potentials into the coupled equations (2.10 a, b) the coupling interaction vanishes except at the nuclear surface ($r=R_0$), and we get the following uncoupled equation

$$(T_l+V_{\alpha sl}^{J}(r)+\epsilon_\alpha-E)u_{J\alpha sl}(r)=0. \qquad \text{.....(3.2}a\text{)}$$

$$(T_{l'}+V_{\alpha' s' l'}^{J}(r)+\epsilon_{\alpha'}-E)v_{J\alpha' s' l'}(r)=0. \qquad \text{.....(3.2}b\text{)}$$

The solution of the above equation for both sides of the nuclear surface should be connected to satisfy the original coupled equations (2.10 a, b) and the given boundary condition. To carry out this step we define the following logarithmic derivatives

$$f_{J\alpha sl}^{(+)}=R_0\left[\frac{du_{J\alpha sl}/dr}{u_{J\alpha sl}}\right]_{r=R_0^+} \qquad \text{.....(3.3}a\text{)}$$

$$g_{\alpha' l'}^{(+)}=R_0\left[\frac{dv_{J\alpha' s' l'}/dr}{v_{J\alpha' s' l'}}\right]_{r=R_0^+} \qquad \text{.....(3.3}b\text{)}$$

$$g_{J\alpha sl}^{(-)}=R_0\left[\frac{du_{J\alpha sl}/dr}{u_{J\alpha sl}}\right]_{r=R_0^-} \qquad \text{.....(3.3}c\text{)}$$

$$g_{J\alpha' s' l'}^{(-)}=R_0\left[\frac{dv_{J\alpha' s' l'}/dr}{v_{J\alpha' s' l'}}\right]_{r=R_0^-} \qquad \text{.....(3.3}d\text{)}$$

The first two logarithmic derivatives are evaluated just outside the nuclear surface; the last two are evaluated just inside the nuclear surface and may be evaluated from the solutions of equation (3.2). As the boundary condition at infinity for the wave function other than the entrance channel is an outgoing wave, we can easily evaluate $g_{\alpha' l'}^{(+)}$. The only unknown quantity is $f_{J\alpha sl}^{(+)}$ which will be determined by the conditions at the nuclear surface. In the presence of the δ-type interaction at the nuclear surface, the following relations must be satisfied at $r=R_0$:

$$(g_{J\alpha sl}^{(-)}-f_{J\alpha sl}^{(+)}+W_{\alpha sl,\,\alpha sl}^{J})u_{J\alpha sl}+\sum_{\alpha' s' l'}W_{\alpha sl,\,\alpha' s' l'}^{J}v_{J\alpha' s' l'}=0. \qquad \text{.....(3.4}a\text{)}$$

$$(g_{J\alpha' s' l'}^{(-)}-g_{\alpha' l'}^{(+)}+W_{\alpha' s' l',\,\alpha' s' l'}^{J})v_{J\alpha' s' l'}+W_{\alpha' s' l',\,\alpha sl}^{J}u_{J\alpha sl}+\sum_{\alpha'' s'' l''\neq\alpha' s' l'}W_{\alpha' s' l',\,\alpha'' s'' l''}^{J}v_{J\alpha'' s'' l''}=0. \qquad \text{.....(3.4}b\text{)}$$

† The δ-type interaction in equation (3.1b) may be dropped, if we change V so as to include the effect of it, but this V must be allowed to depend on energy and angular momentum.

The quantities u and v without arguments represent the values at the nuclear surface. Here we define the S-matrix by the following equations

$$u_{J\alpha sl}(r)=u_{\alpha l}^{(-)}(r)-S_{\alpha sl,\,\alpha' s' l'}^{J}u_{\alpha' l'}^{(+)}(r) \qquad \text{.....(3.5}a\text{)}$$

$$v_{J\alpha' s' l'}(r)=-(k_\alpha/k_{\alpha'})^{1/2}S_{\alpha' s' l',\,\alpha sl}^{J}u_{\alpha' l'}^{(+)}(r) \qquad \text{.....(3.5}b\text{)}$$

where $u_{\alpha l}^{(\pm)}(r)$ is the outgoing (incoming) wave defined by Blatt and Weisskopf (1952) and have the following asymptotic form

$$u_{\alpha l}^{(\pm)}(r)\sim\exp\left[\pm i(k_\alpha r-\tfrac{1}{2}l\pi-\gamma_\alpha\ln(2k_\alpha r))\right] \quad \text{for} \quad k_\alpha r\gg l. \qquad \text{.....(3.5}c\text{)}$$

The quantity k_α is the wave number of the particle in channel α, and $\gamma_\alpha=Zze^2/(\hbar v_\alpha)$ where Ze and ze are the electric charge of the target nucleus and incident nucleon respectively, and v_α is the velocity of the particle in the channel α. To simplify the equations (3.4) we introduce the following matrix Q

$$S_{\alpha' s' l',\,\alpha sl}^{J}=\left[\delta_{\alpha'\alpha}\delta_{s's}\delta_{l'l}+\left(\frac{k_{\alpha'}}{k_\alpha}\right)^{1/2}2is_{\alpha l}Q_{\alpha' s' l',\,\alpha sl}^{J}\right]\frac{u_{\alpha l}^{(-)}}{u_{\alpha' l'}^{(+)}} \qquad \text{.....(3.6)}$$

where $s_{\alpha l}=k_\alpha R_0/|u_{\alpha l}^{(+)}|^2$ is the penetrability. Then the amplitude of the wave functions and the unknown logarithmic derivative at the nuclear surface are expressed simply by

$$u_{J\alpha sl}=-2is_{\alpha l}Q_{\alpha sl,\,\alpha sl}^{J}u_{\alpha l}^{(-)}. \qquad \text{.....(3.7}a\text{)}$$

$$v_{J\alpha' s' l'}=-2is_{\alpha l}Q_{\alpha' s' l',\,\alpha sl}^{J}u_{\alpha l}^{(-)}. \qquad \text{.....(3.7}b\text{)}$$

$$f_{J\alpha sl}^{(+)}=g_{\alpha l}^{(+)}+(Q_{\alpha sl,\,\alpha sl}^{J})^{-1}. \qquad \text{.....(3.7}c\text{)}$$

By using equation (3.7) equation (3.4) reduces to

$$(g_{J\alpha sl}^{(-)}-g_{\alpha l}^{(+)}+W_{\alpha sl,\,\alpha sl}^{J})Q_{\alpha sl,\,\alpha sl}^{J}+\sum_{\alpha' s' l'}W_{\alpha sl,\,\alpha' s' l'}^{J}Q_{\alpha' s' l',\,\alpha sl}^{J}=1. \qquad \text{.....(3.8}a\text{)}$$

$$(g_{J\alpha' s' l'}^{(-)}-g_{\alpha' l'}^{(+)}+W_{\alpha' s' l',\,\alpha' s' l'}^{J})Q_{\alpha' s' l',\,\alpha' s' l'}^{J}+W_{\alpha' s' l',\,\alpha sl}^{J}Q_{\alpha sl,\,\alpha sl}^{J}+\sum_{\alpha'' s'' l''\neq\alpha' s' l'}W_{\alpha' s' l',\,\alpha'' s'' l''}^{J}Q_{\alpha'' s'' l'',\,\alpha sl}^{J}=0. \qquad \text{.....(3.8}b\text{)}$$

If we define the matrix H by

$$(H)_{\alpha sl,\,\alpha' s' l'}^{J}=\delta_{\alpha\alpha'}\delta_{ss'}\delta_{ll'}(g_{J\alpha sl}^{(-)}-g_{\alpha l}^{(+)})+W_{\alpha sl,\,\alpha' s' l'}^{J},$$

equation (3.8) is written as

$$HQ=\mathrm{I} \qquad \text{.....(3.9)}$$

where I is the unit matrix.

Further, by definining the following diagonal matrices

$$\left.\begin{aligned}(P)_{\alpha sl,\,\alpha' s' l'}&=\delta_{\alpha\alpha'}\delta_{ss'}\delta_{ll'}s_{\alpha l},\\(e^{-i\phi})_{\alpha sl,\,\alpha' s' l'}&=\delta_{\alpha\alpha'}\delta_{ss'}\delta_{ll'}u_{\alpha l}^{(-)}(s_{\alpha l}/k_\alpha R_0)^{1/2},\end{aligned}\right\} \qquad \text{.....(3.10)}$$

the S-matrix is given by

$$S=e^{-i\phi}[1+2i\sqrt{P}H^{-1}\sqrt{P}]e^{-i\phi}. \qquad \text{.....(3.11)}$$

Here we note that the resulting S-matrix is symmetric for the exchange of suffices $S_{\alpha' s' l',\,\alpha sl}^{J}=S_{\alpha sl,\,\alpha' s' l'}^{J}$. This character follows from the fact that the off-diagonal matrix element of H (i.e. W) is symmetric, because of the right choice of the phase of the wave function for the time reversal and Hermitian character of interaction V.

§ 4. Calculation of the Matrix Element and the Cross Section

In order to evaluate the matrix element it is necessary to assume a concrete form of the interaction, for which we use the interaction proposed by A. Bohr (1952) in his collective model,

$$V=-V_0R_0\delta(r-R_0)\sum Y_{\lambda\mu}(\theta\varphi)(-)^\mu\alpha_{\lambda-\mu}^{*} \qquad \text{.....(4.1)}$$

where r, θ, φ are the polar coordinates of the incident particle, R_0 the average nuclear radius and $\alpha_{\lambda\mu}$ is the parameter which determines the shape of the nuclear core. We shall treat only the case of $\lambda=2$. This is the same interaction as in our previous paper, and accordingly we shall not repeat the calculation, but give the results only. The matrix element defined by (3.1) are

$$W_{\alpha sl,\,\alpha' s' l'}^{J} = \left(-\frac{2MR_0^2}{\hbar^2}\right) V_0 (-)^{\sigma-I+\lambda+l-J} (2s+1)^{1/2} (2s'+1)^{1/2} W(lsl's';\ J\lambda) \times W(IsI's';\ \sigma\lambda)(l\|Y_\lambda\|l')(I\|\alpha_\lambda\|I') \qquad \ldots\ldots(4.2)$$

where $W(abcd;\ ef)$ is the Racah coefficient (Racah 1942). The reduced matrix elements are given by

$$(l\|Y_\lambda\|l') = i^{l'-l}\left[\frac{(2\lambda+1)(2l'+1)}{4\pi}\right]^{1/2} (l'\lambda 00\,|\,l'\lambda l 0) \qquad \ldots\ldots(4.3)$$

and

$$(KI\|\alpha_\lambda\|KI') = (2I'+1)^{1/2}(-)^{\lambda+I'-I}\left(\frac{\pi}{5}\right)^{1/2}\frac{4}{3}\epsilon\,(\lambda I'0K\,|\,\lambda I'IK) \qquad \ldots\ldots(4.4)$$

if we take the strong coupling approximation of A. Bohr (1952). The formula for the other approximations will not be given here; the detailed account was given in our previous paper. In equation (4.4), K is the component of spin I along the nuclear symmetry axis and ϵ is the ratio of the difference of the major and minor axes of the nuclear core to the average nuclear radius, and is expressed in terms of the intrinsic quadrupole moment Q_0 and charge number Z by

$$\epsilon \equiv \frac{\Delta R}{R_0} = \frac{5Q_0}{4ZR_0^2}. \qquad \ldots\ldots(4.5)$$

From the formula for the matrix element, we can calculate the S-matrix by the equation given in the previous section. The differential cross section may be obtained from the S-matrix by using the formula of Blatt and Biedenharn (1952),

$$\frac{d\sigma_{\alpha'\alpha}}{d\Omega} = \sum_{ss'} \frac{k_\alpha^{-2}}{(2I+1)(2\sigma+1)} \sum_L B_L(\alpha' s', \alpha s)\, P_L(\cos\theta). \qquad \ldots\ldots(4.6a)$$

$$B_L(\alpha' s', \alpha s) = \sum_{\substack{J_1 J_2 l_1 l_2 \\ J_1' J_2' l_1' l_2'}} \frac{(-)^{s'-s}}{4} Z(l_1 J_1 l_2 J_2; sL) Z(l_1' J_1 l_2' J_2; s' L) \times \mathscr{R}\left[(\delta_{\alpha'\alpha}\delta_{s's}\delta_{l_1 l_1'} - S^{J_1}_{\alpha' s' l_1',\,\alpha s l_1})^* (\delta_{\alpha'\alpha}\delta_{s's}\delta_{l_2' l_2} - S^{J_2}_{\alpha' s' l_2',\,\alpha s l_2})\right]. \qquad \ldots\ldots(4.6b)$$

In this equation P_L is the Legendre polynomial of order L and Z is the revised Z-coefficient defined by Huby (1954). In general, we must use the revised Z instead of the original Z defined by Biedenharn, Blatt and Rose (1952), because of the choice of the phase factor in the wave function; however, in our case, both Z's give the same results since the interaction (4.1) ($\lambda=2$) does not change the parity of the incident particle.

So far, we have worked out the general case by using the channel spin coupling scheme. But for some special cases it may prove more convenient to use another coupling scheme. First, we consider the case when the distorting potential includes a spin–orbit interaction. In this case it is convenient to use the coupling scheme in which first the spin σ of the nucleon and the orbital angular momentum l are coupled to make the total nucleon angular momentum j. The wave function (2.1) should be written as

$$\Psi_{J\alpha jl}^{M} = \frac{1}{r}\left[u_{J\alpha jl}(r)\,\phi_{J\alpha jl}^{M} + \sum_{\alpha' j' l'} v_{J\alpha' j' l'}(r)\,\phi_{J\alpha' j' l'}^{M} + \sum_{\beta j' l'} w_{J\beta j' l'}(r)\,\phi_{J\beta j' l'}^{M}\right]$$

and all the formulae must be changed. But the change is only replacement of the suffix s by j and the matrix element is given by

$$W_{\alpha jl,\,\alpha' j' l'}^{J} = -\frac{2MR_0^2}{\hbar^2} V_0 (-)^{j+l'-J-l'-\sigma-\lambda+j} (2j+1)^{1/2}(2j'+1)^{1/2} W(ljl'j';\ \sigma\lambda)$$
$$\times W(jIj'I';\ J\lambda) \times (l \,||\, Y_\lambda \,||\, l')(I \,||\, \alpha_\lambda \,||\, I'). \qquad \ldots\ldots(4.7)$$

The S-matrix in this coupling scheme will be transformed into the channel spin coupling scheme by

$$S_{\alpha' s' l',\,\alpha s l}^{J} = \sum_{jj'} \langle \sigma I'(s') l' J \,|\, \sigma l'(j') I' J \rangle S_{\alpha' j' l',\,\alpha j l}^{J} \langle l\sigma(j) lJ \,|\, \sigma I(s) lJ \rangle \quad \ldots\ldots(4.8)$$

where transformation function is expressed by the Racah coefficient

$$\langle \sigma I(s) lJ \,|\, \sigma l(j) IJ \rangle = [(2s+1)(2j+1)]^{1/2} W(Isjl, \sigma J). \qquad \ldots\ldots(4.9)$$

Next we consider the case when the distorting potential is spin-independent. In this case we should first couple the spin I of the target nucleus and the orbital angular momentum l of the incident nucleon. By a similar procedure to that used in the first case, we can show that the correct result is obtained in this case by neglecting the spin of the incident nucleon throughout the calculation.

§ 5. Perturbation Approximation

We have chosen a few excited states which are connected to the ground state by the strong interaction and treated them without approximations. A strong interaction means one which is not small compared with the effect of the distorting potential. If all matrix elements W appearing in equation (3.8) are small compared with the discontinuity of the logarithmic derivatives $g_{J\alpha sl}^{(-)} - g_{\alpha l}^{(+)}$, then we can apply the perturbation approximation. In fact we encounter such a case when at a certain incident energy a group of partial waves, say even parity waves, are far from resonance. In this case the perturbation approximation should be used for calculations relating to even parity, because it makes the calculation less involved.

We now separate the matrix H, appearing in equation (3.9) into two parts:

$$H = G + W \qquad \ldots\ldots(5.1)$$

$$(G)_{\alpha sl,\,\alpha' s' l'}^{J} = \delta_{\alpha\alpha'}\delta_{ss'}\delta_{ll'}(g_{J\alpha sl}^{(-)} - g_{\alpha l}^{(+)}) \qquad \ldots\ldots(5.1a)$$

where W has been defined by (3.1). Then we assume that the matrix elements of W are small compared with those of G. The matrix Q can be expanded in terms of W, and if we stop at the linear term we get from equations (3.9) and (5.1)

$$Q = (G+W)^{-1} = G^{-1} - G^{-1}WG^{-1} + \ldots \qquad \ldots\ldots(5.2)$$

Since the matrix G is diagonal, the S-matrix can easily be calculated as

$$S_{\alpha' s' l',\,\alpha s l}^{J} = \frac{u_{\alpha l}^{(-)}}{u_{\alpha l}^{(+)}} \frac{g_{J\alpha sl}^{(-)} - g_{\alpha l}^{(+)*}}{g_{J\alpha sl}^{(-)} - g_{\alpha l}^{(+)}} \delta_{\alpha\alpha'}\delta_{ll'}\delta_{ss'} + \frac{i}{2R_0(k_\alpha k_{\alpha'})^{1/2}} u_{J\alpha' s' l'}^{(0)} W_{\alpha' s' l',\,\alpha s l}^{J} u_{J\alpha sl}^{(0)}$$
$$\ldots\ldots(5.3)$$

where

$$u_{J\alpha sl}^{(0)} = \frac{-2is_{\alpha l}u_{\alpha l}^{(-)}}{g_{J\alpha sl}^{(-)} - g_{\alpha l}^{(+)*}} \qquad \ldots\ldots(5.3a)$$

First we consider the elastic scattering. The first term of the right-hand side of equation (5.3) gives the same result as the usual optical model, provided the distorting potential (3.1b) is independent of the angular momentum. The second term is the contribution from the surface interaction. This term vanishes if the

spin of the target nucleus is 0 or $\frac{1}{2}$, otherwise we can make it vanish by changing the distorting potential to take into account the effect of surface interaction, although the distorting potential then becomes dependent on angular momentum and energy. Therefore the same result will be obtained for the elastic scattering if we allow the optical potential to be angular momentum and energy dependent. For the inelastic scattering, (5.3) gives the same result as was given in our previous paper (Hayakawa and Yoshida 1955) and by Brink (1955), since $u^{(0)}_{\alpha sl}$ is the wave amplitude which is distorted by the optical potential, evaluated at the nuclear surface. Now we see that the previous calculations by Hayakawa and Yoshida and by Brink can be used only when the direct interaction is not strong, provided the distorting potential is assumed to be the usual optical potential adjusted to give the correct results for elastic scattering.

Although when $G \ll W$, it is possible to expand Q in powers of G, we can hardly expect such a case to be realized because all the partial waves appearing in G must be at resonance simultaneously.

§ 6. Contribution of the Compound Nucleus in the Statistical Model

In the previous section we have considered only the effect of the strong interaction, but the contribution from the particles which are absorbed in the weakly coupled channel is important at a medium incident energy. In this section the effect of the absorbed particles will be estimated on the basis of the statistical model. Since we used a complex potential as the distorting potential, the resulting S-matrix is not unitary. Therefore if we calculate the net flux which comes into the nuclear surface we may obtain the cross section for the formation of the compound states.

$$\sigma^{(c)}_{\alpha J} = \frac{\pi}{k_\alpha{}^2} \sum_{sl} \frac{2J+1}{2s+1} T^J_{\alpha sl} \qquad \ldots\ldots(6.1)$$

$$T^J_{\alpha sl} = 1 - \sum_{\alpha' s' l'} |S_{\alpha' s' l', \alpha sl}{}^J|^2. \qquad \ldots\ldots(6.2)$$

This expression is slightly different from the one in the usual statistical model because in the usual model all channels except the ground state are regarded as compound states. In our case the compound states are the channels other than the strongly coupled ones.

The compound states decay into various excited states of the residual nucleus by emitting particles. The branching ratio may be calculated from the cross sections of the reverse processes, the formation of the compound states by the reciprocity theorem. Here the effect of the interference between different channels is neglected according to the statistical assumption. The differential cross section was given by Wolfenstein (1951) and by Hauser and Feshbach (1952):

$$\frac{d\sigma^{(c)}_{\alpha'\alpha}}{d\Omega} = \sum_{ss'} \frac{1}{k_\alpha{}^2 (2s+1)} \sum B^{(c)}_L(\alpha' s', \alpha s)\, P_L(\cos\theta) \qquad \ldots\ldots(6.3)$$

$$B^{(c)}_L(\alpha' s', \alpha s) = \tfrac{1}{4} \sum_{JJ'} \frac{T^J_{\alpha' s' l'}\, T^{J'}_{\alpha sl}}{\sum_{\alpha'' s'' l''} T^J_{\alpha'' s'' l''}} Z(lJlJ; sL)\, Z(l'Jl'J; s'L). \qquad \ldots\ldots(6.4)$$

The sums over $\alpha'' s'' l''$ should be carried out for all possible channels into which the compound state with spin J and certain parity can decay, that is to say the possible strongly coupled channels as well as the weakly coupled channels. When we calculate $T^J_{\alpha sl}$ for the weakly coupled state the usual optical potential may be used.

In this way we can calculate the contribution from the compound states not only for the strongly coupled channels but also for the weakly coupled ones. These cross sections should be added to the one from the direct interaction for the strongly coupled channel.

§ 7. Evaluation of the Distorting Potential

In our calculation we assumed the complex square well potentials take into account the effects of the weakly coupled states, but the values of their parameters have not yet been estimated. Many elastic scattering data have been analysed by the complex square well potential and it has been shown that the agreement between theory and experiment is fairly good, at least below 10 Mev for light and medium nuclei. Nevertheless, it will be shown that we cannot use these optical potentials as the distorting potentials in our theory when the surface interaction is strong.

From equation (3.7*c*) we can obtain the value of the logarithmic derivative for the elastic scattering just outside the nuclear surface in terms of Q. This matrix Q is a function of the assumed distorting potentials $V_{\alpha sl}^{J}$ and $V_{\alpha' s' l'}^{J}$, because of equations (3.8) or (3.4) which contain $g^{(-)}$. Therefore we get the logarithmic derivative as a function of the distorting potentials

$$f_{J\alpha sl}^{(+)}(V_{\alpha sl}^{J},\ V_{\alpha' s' l'}^{J}) = g_{sl}^{(+)} + [Q_{\alpha sl,\,\alpha sl}^{J}(V_{\alpha sl}^{J},\ V_{\alpha' s' l'}^{J})]^{-1}.$$

As the diagonal matrix element of Q or $f_{J\alpha sl}^{(+)}$ determines the elastic cross section, we can obtain a complex square well potential $V_{J\alpha sl}^{\text{eff}}$ (we call this effective potential) which gives the same elastic scattering when there is no surface interaction. If we use the notation $f_{J\alpha sl}^{\text{eff}}(V_{J\alpha sl}^{\text{eff}})$ for the logarithmic derivative at the nuclear surface in the usual optical model, the following equation must be satisfied

$$f_{J\alpha sl}^{\text{eff}}(V_{J\alpha sl}^{\text{eff}}) = f_{J\alpha sl}^{(+)}(V_{\alpha sl}^{J},\ V_{\alpha' s' l'}^{J}) = g_{sl}^{(+)} + [Q_{\alpha sl,\,\alpha sl}^{J}(V_{\alpha sl}^{J},\ V_{\alpha' s' l'}^{J})]^{-1}.$$

From the above equation we can get the effective potential, $V_{J\alpha sl}^{\text{eff}}$, when the distorting potentials $V_{J\alpha sl}^{J}$ and $V_{\alpha' s' l'}^{J}$ are given, and conversely the distorting potentials may be obtained if the effective potentials are given.

It is easily seen that $V_{\alpha sl}^{J}$ is very different from $V_{J\alpha sl}^{\text{eff}}$ when the surface interaction is strong, and that the $V_{\alpha sl}^{J}$ is not independent of α, s, l and J even if $V_{\alpha sl}^{J\text{eff}}$ is assumed to be independent of them. The energy dependence of $V_{\alpha sl}^{J}$ is different from that of $V_{J\alpha sl}^{\text{eff}}$.

§ 8. Numerical Examples

In this section our theory will be applied to the inelastic scattering of protons by ^{24}Mg at 10 Mev. The reasons for choosing ^{24}Mg as an example are the following. Firstly, measurements of the differential cross section are available both for the elastic and inelastic scattering. Also we have the necessary knowledge about spins, parities and energies of the excited states of the nuclei. Secondly, ^{24}Mg is supposed to be a strongly deformed nucleus. Therefore we are dealing with strong coupling in this reaction, and the surface interaction becomes important.

The level scheme of ^{24}Mg is shown in figure 1. The spin assignment is taken from papers by Endt and Kluyver (1954), by Newton (1954) and by Grant *et al.* (1955). The first and second excited levels are considered as rotational levels, because they have spins and parities 2^+ and 4^+, and the ratio of the excitation energy is 3·0 which is very close to that of the rotational spectra, 10/3. In fact,

^{24}Mg is one of the nuclei whose first excitation energy satisfies the criterion for the rotational state by Bohr and Mottelson (1955). As the strongly coupled states we ought to take the excited states up to the second in this nucleus. But for simplicity we shall take only the ground state and the first excited state in the actual calculation. The neglect of the second excited state may not be justified, but at any rate it is not connected directly to the ground state and its effect will be taken into account as a weakly coupled state.

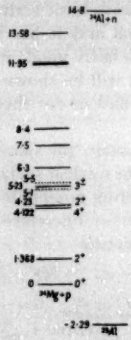

Figure 1. Energy scheme for ^{24}Mg.

The figures on the left of the energy levels show the excitation energies in MeV measured from the ground state of ^{24}Mg with a zero energy proton. The figures on the right of the levels show spins and parities of the excited state of ^{24}Mg. The data are taken from Endt *et al.* (1954) except the 5·23 MeV level of ^{24}Mg which is taken from Newton (1954) and Grant *et al.* (1955) and used as the fourth excited state of ^{24}Mg in our calculation.

To make a numerical calculation it is necessary to fix the values of parameters. The ratio of the difference between major and minor axes of the nuclear core to the average nuclear radius ϵ is determined from the quadrupole moment of the neighbouring nuclei. The data of the quadrupole moment of ^{23}Na and ^{27}Al are taken from the papers by Sagalyn (1954) and Klinkenberg (1952); $\epsilon = 0{\cdot}33 \pm 0{\cdot}20$ for ^{23}Na and $0{\cdot}20 \pm 0{\cdot}04$ for ^{27}Al. From them we choose the value

$$\epsilon = 0{\cdot}3 \qquad \ldots\ldots(8.1)$$

for ^{24}Mg. If we calculate ϵ from the moment of inertia for the rotational motion on the basis of the irrotational liquid drop model, we get $\epsilon = 0{\cdot}74$. But the ϵ calculated from the moment of inertia is always about twice as large as that calculated from the quadrupole moment and the lifetime of the quadrupole γ-transition for heavy nuclei, because of the deviation from irrotational flow of the nuclear matter (cf. Ford 1954, Sunyar 1945 and Bohr and Mottelson 1955). Provided that this is true also for ^{24}Mg we obtain $\epsilon = 0{\cdot}37$. There is another way to determine ϵ; this is by the lifetime of the γ-transition from the first excited state to the ground state. This lifetime was measured by Coleman (1955) and gives the value $\epsilon = 0{\cdot}08 \pm 0{\cdot}04$, which is quite small compared with the other two data. We shall

use the value (8.1) in our calculation because the cross section based on the smaller value 0·08 seems to be similar to the result calculated by the perturbation approximation.

Next we must evaluate the distorting potential. If we know all the diagonal elements of the S-matrix for the strongly coupled channel, the distorting potential for each channel may be uniquely determined. However, as it is impossible to obtain from experiments the diagonal element of the S-matrix, we are forced to make some assumptions about the angular momentum dependence of the potential to obtain the distorting potential from the experiments on elastic scattering. For simplicity we consider the following two cases : the distorting potential is the usual complex square well independent of the angular momentum ; or alternatively the effective potential for the elastic scattering is independent of angular momentum. The former assumption seems to be less unreasonable than the latter because the distorting potential is a sum of contributions from many weakly coupled states and seems to be less angular momentum dependent than the effective elastic potential. On the other hand the effective potential for the elastic scattering is composed of contributions from the weakly coupled as well as strongly coupled states and seems to be rather angular momentum dependent. Nevertheless, to avoid laborious numerical calculations, we shall make the assumption that the distorting potential is dependent only on the total angular momentum J, while the effective potential is the usual complex square well potential independent of the angular momentum. Then we can neglect the spin of the incident nucleus throughout the numerical calculation as discussed in § 4.

The angular distribution of the elastically scattered proton at 9·8 Mev is calculated by using the following two effective potentials.

$$V^{\text{eff}}=(35+5i)\,\text{Mev} \qquad R_0=1{\cdot}45\times10^{-13}A^{1/3}\,\text{cm.} \qquad \ldots\ldots(8.2a)$$

$$V^{\text{eff}}=(30+5i)\,\text{Mev} \qquad R_0=1{\cdot}45\times10^{-13}A^{1/3}\,\text{cm.} \qquad \ldots\ldots(8.2b)$$

The results are shown in figure 2, together with the experimental result by Fisher (1955), and Greenlees and Souch (1956). From these curves it is difficult to decide which potential is better. The difference of the two potentials is that the former gives a p-wave resonance while the latter an f-wave resonance. Since the experimental angular distribution for the inelastic scattering for the first excited state has a large component of fourth order spherical harmonic (see figure 3), it seems likely that the latter potential is better than the former for the inelastic scattering. The even parity waves are far from the resonance for both potentials, so the perturbation approximation may be used for them. If we estimate the distorting potential by the method of § 7, we get the results shown in table 1. The imaginary part of the distorting potential is smaller than that of the effective potential. This is reasonable since the effective potential must include the effect of the absorption into the first excited state.

Table 1. The Parameters for the Distorting Potentials for $^{24}\text{Mg}(\text{p},\text{p}')^{24}\text{Mg}$ at 9·8 Mev

Effective potential for elastic scattering (Mev)		$35+5i$	$30+5i$
Distorting potential (Mev)	$J=1$	$37{\cdot}80+2{\cdot}02i$	$33{\cdot}09+2{\cdot}00i$
	$J=3$	$35{\cdot}42+3{\cdot}09i$	$27{\cdot}53+3{\cdot}36i$

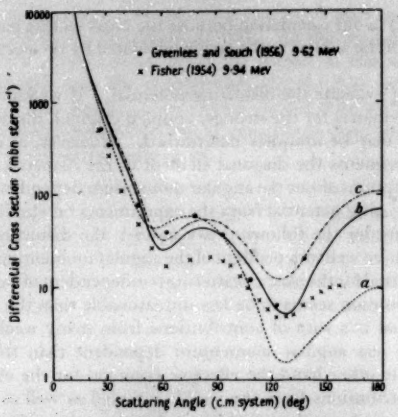

Figure 2. The elastic scattering of protons by ^{24}Mg.
The curve a is the theoretical result for the optical potential $V=(35+5i)$ MeV and the curve b for $V=(30+5i)$ MeV both without the surface interaction (for 9·8 MeV protons). The curve c is also the theoretical result for the effective elastic scattering potential $V^{\text{eff}}=(30+5i)$ MeV. The contribution from the compound nucleus is included and the 5·23 MeV level is assumed to be 3^-.

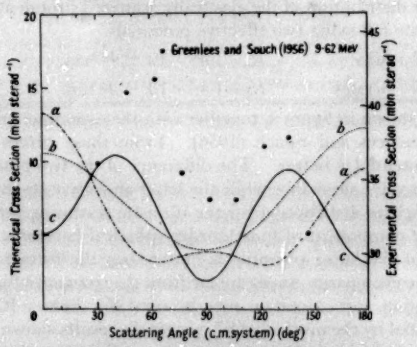

Figure 3. The inelastic scattering of protons by ^{24}Mg for the first excited state.
The curve a is the theoretical result by the perturbation approximation assuming the distorting potential $V=(30+5i)$ MeV and the curves b and c are results assuming the effective elastic potential. ($V^{\text{eff}}=(35+5i)$ MeV and $V^{\text{eff}}=(30+5i)$ MeV respectively). These theoretical curves are calculated for the 9·8 MeV proton energy.

The differential cross section for the inelastic scattering which leaves the residual nucleus in the first excited state is shown in figure 3. Although the contributions from the weakly coupled channels, which are supposed to have an almost isotropic distribution, must be added to the cross section in figure 3, it is clear that the potential (8.2*b*) gives a much better agreement with experiment than the potential (8.2*a*) as we expected.

The contribution from the weakly coupled channels is calculated on the basis of the statistical theory by the method of § 6. As shown in figure 1, the threshold energy of the (p, n) reaction is very high, so it is enough to consider only proton emission from the compound states. We shall take into account excited states up to the fourth in our calculation.

The optical potentials used for the higher excited states are given in table 2. They are chosen on the following basis. It is assumed that the imaginary part of the optical potential for the excited state is the same as that for the ground state bombarded by a proton whose energy is smaller than the original energy by the excitation energy of the excited state. The imaginary part for the ground state is fixed by interpolating between the potentials used in this work for 10 Mev protons and by Feshbach *et al.* for 1 Mev neutrons. The energy variation of the real part

Table 2. Optical Potentials for the Higher Excited States of $^{24}Mg(p, p')^{24}Mg$ at 9·8 Mev

Excited states	2nd and 3rd	4th
V (Mev)	$30+3i$	$30+2{\cdot}5i$

owing to the small effective mass of the nucleon (Brueckner and Levinson 1955) should be considered, but we neglect it because the difference is small for energies below 10 Mev. For the ground and first excited states we use the S-matrix calculated before by assuming the effective potential (8.2*b*) for the elastic scattering. The calculation has been done assuming the parity of the fourth excited state as even or odd. However, the result for the elastic scattering is shown in figure 2 only for odd parity. The other choice of parity gives almost the same cross section for the elastic scattering. In figure 4 the resultant cross section for the first excited state is shown with the surface and compound state contributions included. We see from this figure that the contribution of the compound states

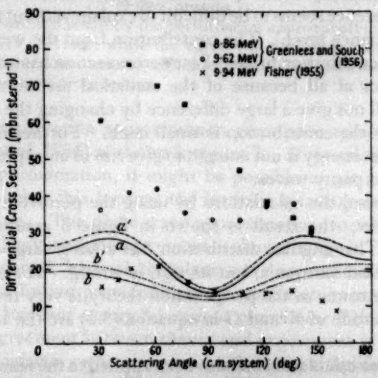

Figure 4. The inelastic scattering of protons by ^{24}Mg for the first excited state. The curves a and a' are the theoretical cross sections which include both the surface and compound contribution, while b and b' are the contribution from the compound state only. The fourth excited state is assumed 3^- for a and b, on the other hand 3^+ for a' and b'. All theoretical curves are calculated assuming that the incident proton energy 9·8 Mev and the effective elastic scattering potential $V^{\text{eff}}=(30+5i)$ Mev.

is twice as large as that of the surface interaction, but the angular dependence is mainly due to the surface contribution. Figure 5 shows the results for the doublet of the second and third excited states and for the fourth excited state.

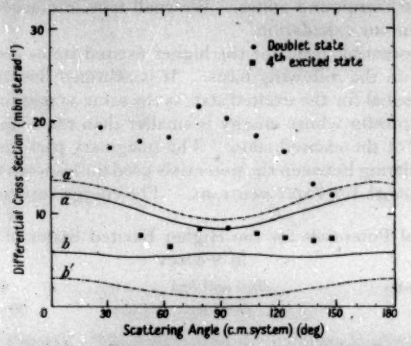

Figure 5. The inelastic scattering of protons by ^{24}Mg for the higher excited levels. The curves a and a' are the theoretical results for the doublet of the second and third excited states while b and b' are for the fourth excited states. The parameters used are the same as those in figure 4. The fourth excited state is assumed to be odd parity for a and b and even parity for a' and b'. The experimental values are by Greenlees and Souch (1956) (9·62 MeV protons).

There exist also measurements by Greenlees and Souch (1956) for the inelastic scattering at 8·86 MeV for the first excited state; these are shown in figure 4. It is surprising that the component of the first-order spherical harmonic in the angular distribution increases very much with a change of less than 1 MeV in the incident energy. This difference seems to be difficult to explain without taking into account the effect of a resonance level. The contribution from the weakly coupled states which is the main contribution to the 9·8 MeV cross section has no component of odd spherical harmonics at all because of the statistical assumption. The surface interaction also will not give a large difference by changing the incident energy by only 1 MeV because the contribution is small itself. Furthermore, the change of 1 MeV in the incident energy is not enough to give rise to an appreciable interference of the even and odd parity waves.

We also performed the calculations by using the perturbation approximation for all partial waves; the result is shown in figure 3 assuming the distorting potential (8.2*b*). This angular distribution has a fairly large component of the fourth order spherical harmonic, but its sign is wrong. It shows that the effect of the higher order terms in the perturbation theory is very important. In fact, the orders of magnitude of W and G in equation (5.2) are the same for odd parity states.

The perturbation calculation has also been applied to the reactions ^{12}C(p, p')^{12}C and ^{20}Ne(p, p')^{20}Ne for 9 MeV protons and for the first excited state. In both cases the optical potential $(35 + 5i)$ MeV gives a good fit for the elastic scattering, therefore we used it for the distorting potential. The result for ^{12}C is shown in figure 6 together with the experimental result by Burcham *et al.* (1954). The agreement between the calculation and the experiment is not good; the signs of the coefficients

of the fourth order spherical harmonics are opposite. We therefore introduce the spin–orbit interaction $V_{so} = a\delta(r - R_0)(\boldsymbol{\sigma} \cdot \mathbf{l})$, $a = 3 \times 10^{-13}$ Mev cm. The value of a was chosen to give the correct energy separation between the $d_{3/2}$ and $d_{5/2}$ states of ^{17}O. The result with the spin–orbit interaction included in the calculation is shown in figure 6. Both theoretical curves in the figure are normalized to give the same total cross section as the experiment.

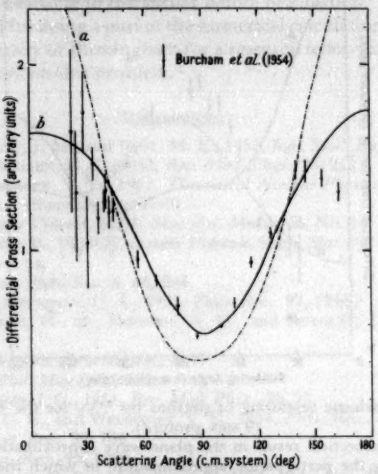

Figure 6. The inelastic scattering of protons by ^{18}C for the first excited state (9 Mev protons.)

The curve a is the theoretical result by the perturbation approximation using the distorting potential $V = (35 + 5i)$ Mev, while the curve b is the result assuming the distorting potential which includes the spin–orbit interaction. All cross sections are normalized to give the same total cross section.

For ^{20}Ne the perturbation approximation gives poor agreement with experiment (Freemantle *et al.* 1954) as shown in figure 7. If we calculate without using the perturbation approximation, it might be possible to get a better result, but we have not tried doing this because the intrinsic quadrupole moment, or ϵ, is difficult to determine. The plane wave approximation, in which the distorting potential is not used, gives a good agreement as shown in figure 7. This is curious, but it may be accidental, because the plane wave approximation always gives a similar angular distribution provided that the excitation energy is not very large compared with the incident energy for various nuclei near ^{20}Ne.

Although the agreement between theory and experiment is not excellent, it is not altogether unsatisfactory when we consider the many simplifications which were made during our calculation. The potential was assumed as a square well; however, we may improve our calculation by using the smoothed square well potential (Saxon *et al.* 1955) which is known to give a better result for the elastic scattering. If we use the smoothed square well potential, it seems reasonable to replace the δ-function type surface interaction by some smoother surface

interaction. If the second excited state is taken into account as a strongly coupled state instead of weakly coupled state, it might also improve agreement between the theory and experiment, especially for the doublet state of the second and third excited states.

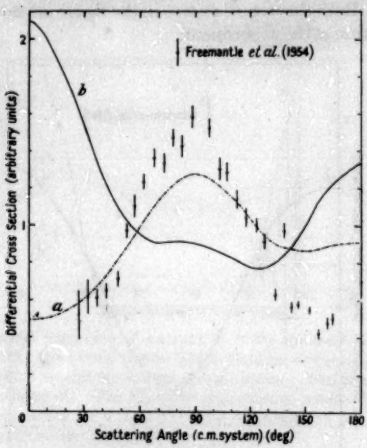

Figure 7. The inelastic scattering of protons by ^{20}Ne for the first excited state (9 MeV protons).

The curve a is the theoretical result in the plane wave approximation while the curve b is the result by the perturbation approximation, in which the distorting potential assumed $V=(35+5i)$ MeV without the spin–orbit interaction. All cross sections are normalized to give the same total cross section.

§ 9. Conclusions

The main conclusions may be summarized as follows. The surface interaction which is considered in this work plays a very important role in the angular distribution of the inelastic scattering of nucleons even if the bulk of the contribution comes from the compound state, provided the surface coupling is strong. The angular distribution is very sensitive to the choice of the distorting potential and the particular approximation adopted. When the surface interaction is strong, the distorting potential should not be taken to be the same as the optical potential, which gives the best fit for the elastic scattering, but should be determined so as to give the best fit to the elastic scattering data by solving a coupled equation. For such a strong surface interaction the perturbation approximation is very poor. The contribution from the compound states seems to be important irrespective of their widths. If the widths are large enough compared with the level spacing, or if we take an average of the cross section over energy, the statistical theory gives a large cross section in the intermediate energy region although the angular dependence is weak. If, on the other hand, the widths are small, the effect of individual resonance levels seems to be important.

We have investigated a simple example of the direct interaction which can be solved easily, but the above conclusions and the method of calculation are considered to be just as applicable to the general interaction. As it is difficult to solve the equation in the general case, we shall be obliged to use further approximations.

ACKNOWLEDGMENTS

The author is very grateful to Professor R. E. Peierls for valuable discussions and suggestions during the course of this work. He would also like to thank members of the Department of Mathematical Physics, and Professor E. W. Burcham and Dr. G. W. Greenlees in the Department of Physics for their stimulating discussions. By the kindness of Dr. G. W. Greenlees the experimental data on ^{24}Mg became available to the author before publication. Thanks are due also to Mr. J. Stuttard for doing a part of the numerical calculation. The author is indebted to the University of Birmingham for a research fellowship, which made it possible for him to work on this problem.

REFERENCES

BIEDENHARN, L. C., BLATT, J. M., and ROSE, M. E., 1952, *Rev. Mod. Phys.*, **24**, 249.

BLATT, J. M., and BIEDENHARN, L. C., 1952, *Rev. Mod. Phys.*, **24**, 258.

BLATT, J. M., and WEISSKOPF, V. F., 1952, *Theoretical Nuclear Physics* (New York : John Wiley ; London : Chapman and Hall).

BOHR, A., 1952, *K. Danske Vidensk. Selsk. Mat.-fys. Medd.*, **26**, No. 14.

BOHR, A., and MOTTELSON, B., 1953, *K. Danske Vidensk. Selsk. Mat.-fys. Medd.*, **27**, No. 16 ; 1955, *Ibid.*, **30**, No. 1.

BRINK, D. M., 1955, *Proc. Phys. Soc.* A, **68**, 994.

BRUECKNER, K. A., and LEVINSON, C. A., 1955, *Phys. Rev.*, **97**, 1344.

BURCHAM, W. E., GIBSON, W. M., HOSSAIN, A. H., and ROTBLAT, J., 1954, *Phys. Rev.*, **92**, 1266.

CINI, M., and FUBINI, S., 1955, *Nuovo Cim.*, **2**, 75.

COLEMAN, C. F., 1955, *Phil. Mag.*, **46**, 1135.

ENDT, P. M., and KLUYVER, J. C., 1954, *Rev. Mod. Phys.*, **26**, 95.

FESHBACH, H., PORTER, C. E., and WEISSKOPF, V. F., 1954, *Phys. Rev.*, **96**, 448.

FISHER, G. E., 1954, *Phys. Rev.*, **96**, 704.

FORD, K. W., 1954, *Phys. Rev.*, **95**, 1250.

FREEMANTLE, R. G., PROWSE, D. J., and ROTBLAT, J., 1954, *Phys. Rev.*, **96**, 1268.

GRANT, P. J., RUTHERGLEN, J. G., FLACK, F. C., and HUTCHISON, G. W., 1955, *Proc. Phys. Soc.* A, **68**, 369.

GREENLEES, G. W., and SOUCH, A. E., 1956, *Proc. Phys. Soc.*, A **69**, 686.

HAUSER, H., and FESHBACH, H., 1952, *Phys. Rev.*, **87**, 366.

HAYAKAWA, S., and YOSHIDA, S., 1955, *Proc. Phys. Soc.* A, **68**, 656, *Progr. Theor. Phys.*, Japan, **14**, 1.

HUBY, R., 1954, *Proc. Phys. Soc.* A, **67**, 1103.

KLINKENBERG, P. F. A., 1952, *Rev. Mod. Phys.*, **24**, 63.

NEWTON, J. O., 1954, *Phys. Rev.*, **96**, 241.

RACAH, G., 1942, *Phys. Rev.*, **62**, 438.

SAGALYN, P. L., 1954, *Phys. Rev.*, **94**, 885.

SAXON, D. S., FESHBACH, H., and MCMANUS, H., 1955, *Statistical Aspects of the Nucleus*, Report of Conference held at Brookhaven National Laboratory.

SUNYAR, A. W., 1955, *Phys. Rev.*, **98**, 653.

WOLFENSTEIN, L., 1951, *Phys. Rev.*, **82**, 690.

The Scattering of 9·6 MeV Protons by Mg

By G. W. GREENLEES and A. E. SOUCH†

Department of Physics, University of Birmingham

MS. received 14*th March* 1956

Abstract. Absolute differential cross sections are given for the elastic and inelastic scattering of 9·62 MeV protons by Mg for an angular range of 25°–145° (laboratory coordinates). For scattering by the 1·37 MeV level of ^{24}Mg, the angular distribution is also given for an incident energy of 8·86 MeV. A marked difference in angular distribution at the two energies is noted.

§ 1. Introduction

The scattering of protons by Mg at incident energies in the region 9·5–10 MeV has been studied by Baker *et al.* (1952) and by Fischer (1954) using, respectively, 9·6 MeV and 9·94 MeV protons. The two sets of results for elastic scattering show good agreement in their general form as regards angular distribution and absolute cross section. The angular distributions for inelastic scattering by the 1·37 MeV level of ^{24}Mg show a marked difference, though neither distribution is symmetric about 90°. Fischer suggests that the asymmetry is due to the presence of a direct collision effect between the ingoing proton and a surface nucleon.

It was decided to investigate these reactions further to confirm the asymmetry of the inelastic angular distribution and to decide whether the differences between the two sets of results were due to the different incident energy, or to an error in one set of measurements.

§ 2. Apparatus

The Nuffield 60 inch cyclotron was used to provide a beam of approximately 20 MeV H_2^+ ions. Such ions split into two protons of 10 MeV on striking a target. The extracted beam was focused in a horizontal plane, by means of a subsidiary magnet, into a scattering chamber located in a radiation screened room. A beam intensity of 1·5–2 μA cm^{-2} was available.

The scattering chamber was a modified version of that described by Westcott *et al.* (1954). In this chamber the detector is *in vacuo* and can be set at any angle between $\pm 145°$ to the line of the incident beam. The beam was measured by collection in a Faraday cup and, because of interference in the beam collection by the detector, the effective minimum forward angle was 25°.

The detector was a triple proportional counter with common cathode and total depth about 11 mg cm^{-2} Al. A gas gain of about 50 was used. The pulses from the three counters were separately amplified and passed through three two-level discriminators and thence to a coincidence circuit. By suitable choice of

† Now at the Atomic Weapons Research Establishment, Aldermaston.

level settings of the three discriminators it could be arranged that only protons at the end of their range gave a coincidence output. Varying thicknesses of Al absorber could be placed in front of the counter in steps of about 1·5 mg cm^{-2} and hence a differential range spectrum obtained at any angle.

The defining telescope was 20 cm long with slits 6 mm × 2 mm, the 6 mm side being perpendicular to the scattering plane. The angular definition was $\pm 1°$. Provision was made for introducing Al foils in front of the defining telescope in order to obtain reduced energy beams of the same angular definition. The consequent reduction of beam intensity limited the amount of absorber which could be used and hence the range of energies avaiable.

§ 3. Procedure

With the bias levels adjusted to record only protons entering the counter at the end of their range, counts were taken for a given integrated beam at various absorber settings. In this way differential range spectra were obtained at a number of angles and the groups observed assigned to known energy levels. It can easily be shown that the optimum resolution is obtained in such a system when the normal to the scattering foil bisects the angle of scattering. In the present arrangement the foil angle could be adjusted independently of the counter setting. To determine the angular distributions it was considered desirable not to reset the foil for optimum resolution at each angle since this might introduce errors due to uncertainty in the effective thickness. The foil was therefore left at a fixed setting and a particular group counted at a number of angles. Because of loss of resolution there is a limit to the range of angles which can be used at any one foil setting. The angular distribution was therefore measured in four parts with an overlap between successive angular ranges. The ranges used were: 25°–60° with foil setting 20°, 45°–90° (foil 35°), 75°–120° (foil 50°) and 105°–145° (foil 70°).

The differential cross section for any observed peak will be proportional to the area of that peak. A plot of peak area mg^{-1} cm^{-2} of scattering foil against angle was found to give consistent results with good fitting between the sections of the curve in the region of overlap of angles. The constant of proportionality needed to convert these relative cross sections into absolute values is uncertain because of difficulties in estimating the fraction of particles detected by the system for any given setting. Absolute values were therefore obtained by measuring the elastic scattering from gold at forward angles and assuming that this obeyed a Rutherford law. The gold scattering showed a Rutherford angular dependence in the range 25°–45° and it was felt that this assumption was reasonable at the energies used (~10 MeV).

§ 4. Experimental Results

The target used in these experiments was a piece of pure Mg foil weighing 3·25 mg cm^{-2}. A typical range spectrum is shown in figure 1. This curve was taken at 60° with an incident energy of 9·83 MeV. Several well resolved groups are apparent. The table gives average Q values, found from a number of such curves, together with their probable assignment to isotopes. Angular distribution measurements were made for the four groups $Q = 0$ (elastic), $Q = -1{\cdot}37$ MeV, $Q = -4{\cdot}22$ MeV and $Q = -5{\cdot}24$ MeV (inelastic ^{24}Mg) at full

energy which corresponded to an energy of 9·62 Mev at the foil centre. In the case of the ^{24}Mg inelastic group $Q = -1{\cdot}37$ Mev, the angular distribution was also measured at a reduced incident energy (8·86 Mev at foil centre).

Mg (pp′) Mg Q values using 9·62 Mev protons, together with probable isotopic assignment and comparison with other data (Endt and Kluyver 1954, Grant *et al.* 1955).

$-Q$(Mev) $\pm$ 0·05 Mev present data)	0·55	0·98	1·37	4·22	4·77	5·24	6·00	6·42	6·90
Isotopic assignment	^{25}Mg	^{25}Mg	^{24}Mg	^{24}Mg	^{25}Mg or ^{26}Mg	^{24}Mg	^{25}Mg or ^{26}Mg	^{25}Mg	^{25}Mg
Other data (Mev)	0·58	0·98	1·368	4·122 4·23	4·62 ; 4·86 4·84 ; 4·92	5·26	5·94 ; 6·15	6·40	6·98

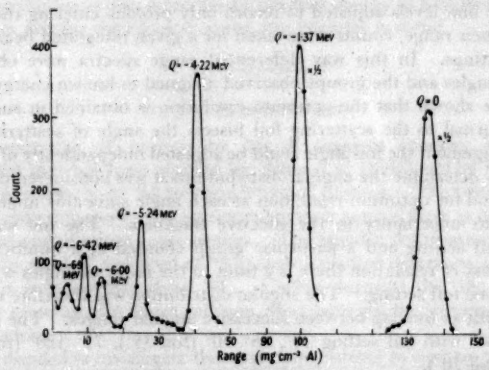

Figure 1. Differential range spectrum for the scattering of 9·83 Mev protons by Mg at 60°.

The angular distribution for elastic scattering is given in figure 2, that for $Q = -1{\cdot}37$ Mev inelastic scattering at two energies in figure 3, and that for $Q = -4{\cdot}22$ Mev and $Q = -5{\cdot}24$ Mev inelastic scattering in figure 4. The relative values for the cross sections are thought to be accurate to 3% but the absolute values may be in error by 10%. The angular distribution obtained by Fischer (1954) is also plotted in figure 3.

The angular distribution for the $Q = -1{\cdot}37$ Mev inelastic group, obtained in the present experiment (9·62 Mev) is very similar in shape to that obtained by Fischer (9·94 Mev) though the present cross sections are about twice those of Fischer. Since the cross section increases considerably at forward angles, in the present experiments, with a reduction of incident energy to 8·86 Mev, this difference between the 9·62 Mev and 9·94 Mev results might be real and not instrumental. However, the 8·86 Mev and 9·62 Mev cross sections at large angles are approximately equal but twice those of Fischer (9·94 Mev); this is suggestive of some systematic difference in absolute values.†

† *Note added in proof.* This experiment has recently been repeated, and the results obtained show that the differential cross sections given by curves 2 and 3 in figure 3 are too high by a factor or two.

§ 5. Discussion

From these results an estimate of the total proton inelastic scattering cross section for ^{24}Mg at 9·62 MeV can be made. The value obtained is 782 ± 100 mbn.

The results for elastic scattering (figure 2) show a characteristic form and this type of angular distribution is well represented on the basis of scattering by a complex potential (cf. Burge *et al.* 1956).

The most noticeable feature of all the inelastic scattering results for $Q = -1{\cdot}37$ MeV (figure 3) is the asymmetry about 90° of the angular distribution. The marked forward peaking and increase of cross section of the angular distribution at the reduced energy (8·86 MeV) is suggestive of some type of resonance

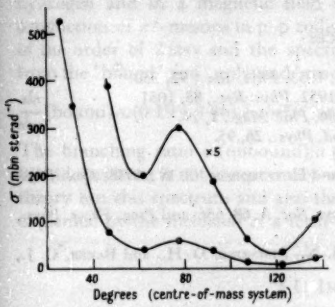

Figure 2. Angular distribution for the elastic scattering of 9·63 MeV protons by Mg.

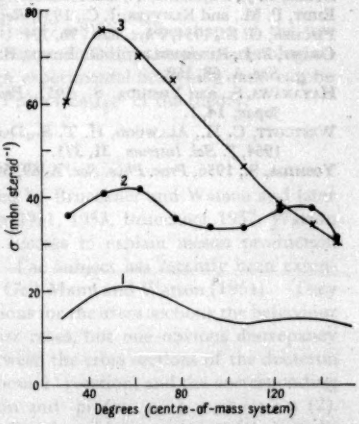

Figure 3. Angular distributions for the inelastic scattering ($Q = -1{\cdot}37$ MeV) of protons by ^{24}Mg. Curve 1, Fisher, 9·94 MeV; curve 2, present results, 9·62 MeV; curve 3, present results, 8·86 MeV.

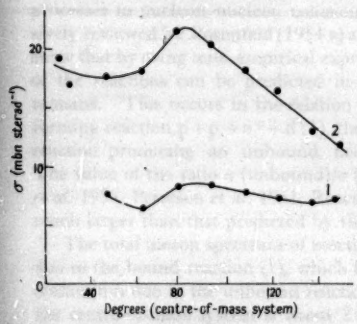

Figure 4. Angular distributions for the inelastic scattering of 9·63 MeV protons by ^{24}Mg. Curve 1, $Q = -5{\cdot}24$ MeV; curve 2, $Q = -4{\cdot}22$ MeV.

effect. It is difficult to see how this can be explained on the basis of a compound nucleus with an excitation energy of 12 MeV as in the present case. Two alternative suggestions have been made. Fischer (1954) suggested the presence of a direct collision effect between the ingoing proton and a surface nucleon (Austern

et al. 1953). Such an interaction produces forward peaks in the angular distribution. Hayakawa and Yoshida (1955) and Yoshida (1956) have discussed the problem on the basis of scattering by a complex potential combined with an effect due to the surface oscillations expected on the basis of the collective model. This treatment predicts an asymmetry about 90° but not of sufficient magnitude to fit the present data.

Acknowledgments

The authors wish to thank Messrs M. Petravic and B. C. Haywood for assistance in recording the results. They are also grateful to Dr. Yoshida for many helpful discussions.

References

Austern, N., Butler, S. T., and McManus, H., 1953, *Phys. Rev.*, **92**, 350.
Baker, C. J., Dodd, J. N., and Simmons, D. H., 1952, *Phys. Rev.*, **85**, 1051.
Burge, E. J., Fujimoto, Y., and Hossain, A., 1956, *Phil. Mag.*, **1**, 19.
Endt, P. M., and Kluyver, J. C., 1954, *Rev. Mod. Phys.*, **26**, 95.
Fischer, G. E., 1954, *Phys. Rev.*, **96**, 704.
Grant, P. J., Rutherglen, J. G., Flack, F. C., and Hutchinson, G. W., 1955, *Proc. Phys. Soc.* A, **68**, 369.
Hayakawa, S., and Yoshida, S., 1955, *Proc. Phys. Soc.* A, **68**, 656, and *Prog. Theor. Phys., Japan*, **14**, 1.
Westcott, C. H., Allwood, H. T. S., Dodd, J. N., Simmons, D. H., and Baker, C. J., 1954, *J. Sci. Instrum.*, **31**, 371.
Yoshida, S., 1956, *Proc. Phys. Soc.* A, **69**, 668.

A Study of Positive Pion Production in p–p Collisions at 383 MeV

By MARGARET H. ALSTON, A. V. CREWE†, W. H. EVANS and G. von GIERKE‡

Nuclear Physics Research Laboratory, University of Liverpool

Communicated by H. W. B. Skinner ; MS. received 2nd February 1956, and in final form 8th May 1956

Abstract. An 18 in. diffusion cloud chamber filled with 28 atmospheres of hydrogen and in a magnetic field of 11 200 gauss is used to investigate the production of π^+-mesons in p–p collisions at 383 MeV. The energy resolution is of the order of 2 MeV and the spectrum obtained can be divided into mesons from the 'bound' and 'unbound' reactions. The angular distributions found are

$$\frac{d\sigma}{d\omega}(\text{bound}) \propto (0{\cdot}19 \pm 0{\cdot}06) + \cos^2\theta' \quad \text{and} \quad \frac{d\sigma}{d\omega}(\text{unbound}) \propto (0{\cdot}21 \pm 0{\cdot}07) + \cos^2\theta'.$$

The branching ratio σ (unbound)/σ (total) $= (47 \pm 8)\%$. The shape of the unbound spectrum is not in agreement with that predicted by the phenomenological theory but this spectrum and also the high experimental branching ratio can be explained by the inclusion of a term $\sigma_{10}''(\text{Pp}) \simeq 1{\cdot}2\eta_{\max}^8$ in the theory.

§ 1. Introduction

A phenomenological theory proposed by Brueckner and Watson and later extended (Brueckner and Watson 1951, 1953, Brueckner 1952, Watson 1952) has been used with great success to explain meson production processes in nucleon–nucleon collisions. The subject has recently been extensively reviewed by Rosenfeld (1954 a) and Gell-Mann and Watson (1954). They show that by using semi-empirical expressions for the cross sections the behaviour of the reactions can be predicted in most cases, but one obvious discrepancy remains. This occurs in the relation between the cross sections of the deuteron forming reaction $\text{p} + \text{p} \rightarrow \pi^+ + \text{d}$ (1), the 'bound' reaction, and the corresponding reaction producing an unbound neutron and proton $\text{p} + \text{p} \rightarrow \pi^+ + \text{n} + \text{p}$ (2). The value of the ratio σ (unbound)/σ (total) is found by experiment (Cartwright *et al.* 1953, Peterson *et al.* 1951, Rosenfeld 1954b, de Carvalho *et al.* 1954) to be much larger than that predicted by the theory.

The total meson spectrum of reactions (1) and (2) consists of a line spectrum, due to the bound reaction (1), which lies just above the high energy cut-off of a continuum due to the unbound reaction (2). The separation of these spectra in the centre-of-mass system is about 2 MeV; the binding energy of the deuteron corrected for relativistic effects. The energy resolution in most experiments is poor, making the division of the spectra unreliable and a detailed study of the unbound reaction impossible. Further errors are often introduced by neglecting low energy mesons and also, since measurements are usually only made at a few fixed angles in the laboratory system, the conversion of the spectrum to the centre-of-mass system is inaccurate.

† Now at the Institute for Nuclear Studies, University of Chicago.
‡ Now at C.E.R.N., Geneva with the Synchrocyclotron Group.

The present experiment is a study of the reactions

(1) $p+p \rightarrow \pi^+ + d$ Bound reaction

(2) $p+p \rightarrow \pi^+ + n + p$ Unbound reaction.

The high intensity external proton beam from the synchrocyclotron is well collimated and observations are made on the production angle and momentum of the pions using a hydrogen-filled diffusion cloud chamber in conjunction with a pulsed magnetic field. This method has the advantage that all production angles and meson energies can be observed accurately in one experiment and the accuracy of the momentum measurement is closer than 2%. The 'bound' and 'unbound' spectra can be separated, and a detailed study of the unbound spectrum and angular distribution can be made. The results show that there is a definite discrepancy between the experimental and predicted values of both the ratio σ (unbound) / σ (total) and the unbound spectrum. However, this discrepancy can be explained by an extension of the theory.

§ 2. Apparatus and Technique

2.1. *The Diffusion Cloud Chamber*

Figure 1 (*a*) is a schematic diagram of the 18 in. diameter diffusion cloud chamber. The bottom section is of non-magnetic stainless steel with total height 7 in. The lower part of the walls are 5/16 in. thick and the base 1 in. thick. The two illumination windows are of 1 in. thick Perspex and are placed on the ends of short extension ports which are rectangular in shape, 10 in. wide and 4 in. high. The incident particles enter the chamber through a rectangular beam entry port placed midway between the illumination ports and with its centre 1½ in. above the base.

The top section of the chamber embodies the vapour tray which contains about 200 cm^3 of liquid. It is made of cast phosphor bronze and is electrically insulated from the rest of the chamber for the application of a clearing field. Above the tray is a 15 in. diameter armour plate glass 1½ in. thick. It is clamped in position by a cast phosphor bronze ring, which leaves an aperture of 13 in. diameter. With pressure in the chamber the glass is pushed against the top ring and the seal is of the Bridgman type. All the seals are made with rubber gaskets. The chamber can withstand 600 lb $in.^{-2}$ and is used with hydrogen gas fillings of between 300 and 450 lb $in.^{-2}$.

A good photographic background is obtained by having 'nigrosine', a black dye, dissolved in the pool of alcohol at the bottom of the chamber and by covering the walls with black velvet to prevent reflection. A 70 mm stereoscopic camera is placed 20 in. above the top glass window on a light-tight mounting. Two Mullard LSD 17 quartz flash tubes are mounted in light-tight boxes at the ends of the illumination ports, and illumination of the tracks is provided by discharging 400 μF at 2000 volts through each tube.

The base of the chamber is cooled to $-60°$C by passing cold acetone through copper pipes soft-soldered to the base (Alston, Crewe and Evans 1954). Heat is applied to the top part of the chamber by a heating tape wrapped round the top ring and heating wires passing through a tube soldered to the side walls just above the ports. The wire is in four sections because less heat is required above the side ports than between them since the thermal paths are different and a uniform temperature around the wall must be maintained at any height above the

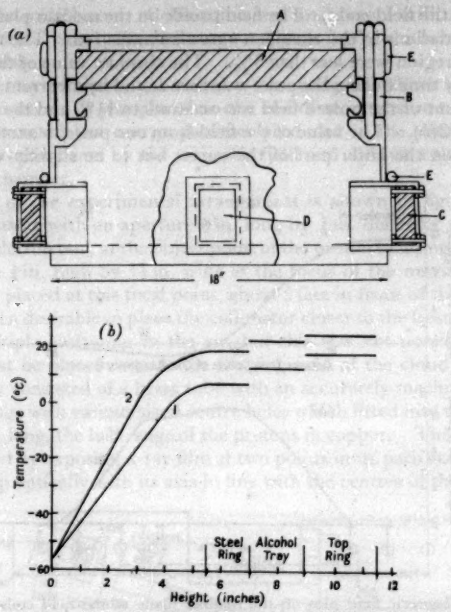

Figure 1. (*a*) Schematic drawing of the 18 in. diffusion cloud chamber : A, armour-plate glass window ; B, insulated alcohol tray ; C, rectangular Perspex window ; D, beam entry port ; E, heaters.
(*b*) Operational temperature distributions : 1, hydrogen at 20–28 atmospheres; the gradient in the sensitive region is 5 deg cm^{-1} ; 2, air at 1 atmosphere ; the gradient in the sensitive region is 7·5 deg cm^{-1}.

base. The top glass is kept just above room temperature by a stream of hot air. The best operational temperature distributions, as measured on the outside of the chamber wall, for operation with 1 atmosphere of air or 20–28 atmospheres of hydrogen, exposed to cosmic-ray background, are shown in figure 1 (*b*). With these temperatures a sensitive depth of 2½ in.–3 in. is maintained. It can be seen that the temperature gradient for hydrogen is only 5 deg cm^{-1}, a much lower value than that quoted by other authors (Fowler *et al.* 1953, Sargent *et al.* 1955). For the experiment the chamber was filled with 28 atmospheres of hydrogen and the temperature gradient was increased to 5·5 deg cm^{-1} to cope with the larger ionization level.

2.2 *Magnetic Field and Timing Sequence*

A uniform magnetic field was produced in the sensitive region of the chamber by passing a large pulsed current through a pair of air-cored water-cooled coils mounted as a Helmholtz pair with their axes vertical. The exciting current of the generator was controlled by a metadyne and the output was extremely stable. For calibration a low steady field was compared with a known field to obtain the

coil constant of the field coils. The field profile on the median plane (figure 2 (*a*)) and the field variations in the chamber were also measured. The field variations in the sensitive region were less than 3%. The absolute value of the pulsed magnetic field at any time during the pulse was then found by a current measurement. The measurement of the pulsed field was accurate to 1½% and the pulse shape is shown in figure 2 (*b*). The value of the field from one pulse to another was found to be constant on the latter part of the curve, but to be slightly variable at the beginning.

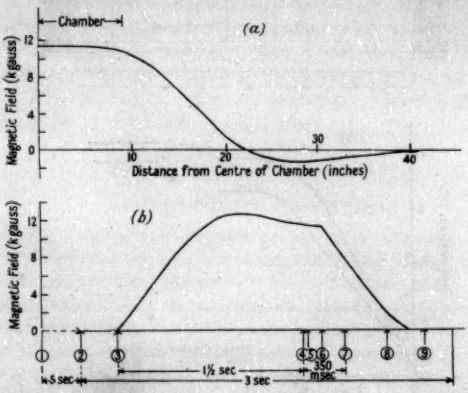

Figure 2. (*a*) Magnetic field plot on the median plane of the field coils. (*b*) Magnetic field pulse shape and timing sequence. 1, Clearing field off 5 seconds before the beginning of the main sequence ; 2, start of sequence ; 3, magnetic field on ; 4, pulse to synchrocyclotron indicating that particles are required ; 5, magnetic field measured ; 6, magnetic field off ; 7, lights flash ; 8, clearing field on ; 9, film wound on.

Since several consecutive pulses of particles were accepted from the synchrocyclotron for one cloud chamber picture, the particles were admitted to the chamber about 1½ seconds after the magnetic field pulse began, so that the field was as constant as possible for about 100 msec and was also the same from one pulse to another. The timing of the control sequence was not required to great accuracy and so a mechanical control system was used because of its simplicity and reliability. The timing sequence is shown in figure 2 (*b*). The value of the magnetic field when the particles entered the chamber was 11 200 ± 200 gauss.

2.3. *Experimental Arrangement*

A very high intensity proton beam of flux 4×10^{10} protons cm^{-2} sec^{-1} is produced by the Liverpool 156 in. synchrocyclotron (Crewe and Gregory 1955). The absolute value of the energy of this beam has been measured as 383 ± 3 Mev by a range method and the beam energy spread is negligible. The synchrocyclotron produces beam pulses as 10 msec intervals and a selected number of consecutive pulses can be obtained from the machine when the cloud chamber magnetic field has reached a steady value. For the experiment very good collimation of the proton beam was required to prevent background from obscuring the tracks

coming from the main beam. Collimation was made more difficult by the large fringing field of the cloud chamber magnet (figure 2 (*a*)) which bent the proton beam considerably.

The beam entry window of the chamber was made of 0·006 in. thick Dural and was $\frac{3}{4}$ in. in diameter. It was placed on the end of an extension tube 10 in. long, so that any unwanted low energy particles produced in the window were bent away from the main beam by the magnetic field and did not enter the sensitive region of the chamber.

A diagram of the experimental arrangement is shown in figure 3. A preliminary collimator with an aperture 6 in. long by $\frac{1}{4}$ in. diameter was placed just outside the cyclotron tank at the object point of the proton bending magnet, giving a beam profile $\frac{1}{4}$ in. high by $1\frac{1}{2}$ in. wide at the focus of the magnet. The main collimator was placed at this focal point, about 5 feet in front of the chamber. It would have been desirable to place the collimator closer to the beam entry window to reduce multiple scattering in the air, but this was not possible because the collimator must be placed outside the fringing field of the cloud chamber coils. The collimator consisted of a brass tube with an accurately machined centre hole and copper plugs with various sized centre holes which fitted into the tube. Each plug was $2\frac{1}{2}$ in. long, the half range of the protons in copper. The beam direction was determined by exposing x-ray film at two points in its path and the collimator was then set up optically with its axis in line with the centres of the beam profiles.

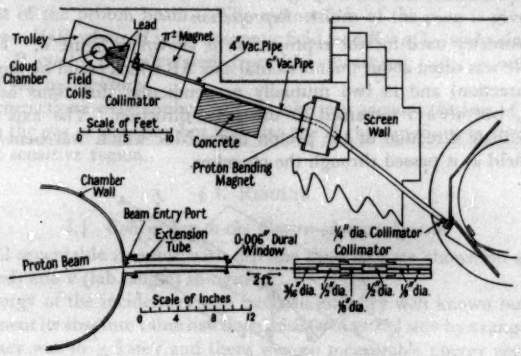

Figure 3. Experimental arrangement.

The chamber was then placed behind the collimator so that the beam passed symmetrically through it when no magnetic field was applied. The best combination of collimator plugs and the final position of the collimator was found by making visual observations of the proton beam as it passed through the chamber. The final arrangement was: 5 in. × $\frac{1}{8}$ in. dia. + $2\frac{1}{2}$ in. × $\frac{1}{2}$ in. dia. + $2\frac{1}{2}$ in. × $\frac{1}{8}$ in. dia. + $2\frac{1}{2}$ in. × $\frac{1}{2}$ in. dia. + $2\frac{1}{2}$ in. × $\frac{3}{16}$ in. dia. (figure 3.) The actual collimation was produced by the first 5 in. × $\frac{1}{8}$ in. dia. hole and the other apertures removed slit scattered protons as much as possible. In order to find the trajectory of the beam when the pulsed magnetic field was applied to the chamber an x-ray film was exposed at the approximate position of the beam entry window. To obtain a sufficiently dense image about 100 beam pulses were required. The cloud

chamber was then moved so that the beam entered the chamber through the beam entry window and passed through the extension tube, when the magnetic field was at its correct value. Final adjustments were made by observing the collimated beam in the chamber. Protons scattered by the main collimator produced a low energy 'fan' in the chamber. These were removed by placing a wall of lead blocks in front of the chamber, the position of the aperture in the wall being found by trial and error. The intensity of the low energy 'fan' of protons provided a sensitive method of judging the efficiency of the collimation and the intensity of the main beam could be estimated from the number of p–p elastic collisions observed in the chamber.

The beam profile obtained at the beam entry window of the chamber is shown in figure 4 (Plate). The beam appeared in the chamber as a very intense core about $\frac{1}{4}$ in. wide surrounded by a 'fan' of scattered protons. A typical picture is shown in figure 5 (Plate). The beam intensity was reduced to give about 2×10^4 protons per picture. This yielded one acceptable meson (dip angle $< 20°$) per 7 pictures, and was the maximum number for easy reprojection as found from a preliminary experiment. With this intensity the repetition rate was 2 minutes and the chamber was completely recovered. An argon-filled ionization chamber placed behind the cloud chamber was used as a crude monitor. 1300 stereoscopic pairs of pictures were taken on 70 mm Ilford 5G91 film, giving 182 acceptable mesons.

2.4. *Reprojection*

The geometry used for the reprojection is shown in figure 6. The reprojection table was tilted about the horizontal axis AB which could be moved vertically (y direction) and in two mutually perpendicular directions horizontally (x and z), but always remained in the same direction. The axis AB gave the approximate direction of the proton beam MN which was bent 7° by the magnetic field as it passed through the chamber.

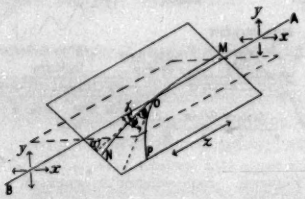

Figure 6. The geometry used in reprojection. AB, axis of rotation of the table ; MON, incident proton beam ; OP, π-meson track ; α, dip angle ; ϕ, measured angle ; θ, production angle, γ, correction angle. AB is horizontal and can be moved in the x, y or z directions but always remains in the same direction in space.

The camera and a glass plate, identical with the one used as the top window of the chamber during the experiment, were placed above the reprojection table so that the geometry of the experiment was reproduced. The film was replaced accurately in the camera and the images of the tracks were projected on to a piece of white paper placed on the reprojection table. The pictures were carefully scanned for mesons which could be recognized by their curvature and their specific ionization. This was particularly useful in distinguishing between a

proton and a π^+ meson near 90° in the laboratory system and a π^+ meson and a positron at large scattering angles.

A pion track OP was measured if its dip was less than 20°. It was impossible to see the origin of the track and the track was assumed to start in the middle of the proton beam; if there was any possibility that it did not start in the chamber gas, it was rejected. Measurements were made of the radius of curvature of the track ρ by comparison with curves of known radius drawn in ink on pieces of white paper, the angle ϕ between the tangent to the beginning of the meson track and the axis AB, and the dip angle α. The coordinates x, y, and z and the direction of the track (i.e. left or right) were also noted. The measurements were made by three observers independently and the results were always within $\pm 2\%$ and usually $\pm 1\%$. Scanning was obviously inefficient in the forward and backward directions because the π-meson track was masked by the incident proton beam and there was also considerable uncertainty in the origin of the pion track. At intermediate angles scanning efficiency approached 100% with no bias between mesons from the bound and unbound reactions.

Measurements were also made on a few p–p elastic scattering events to make sure that the distribution in the centre-of-mass system was isotropic, showing that the geometry of the experiment was correct.

The angle γ between the proton beam and AB was also measured for various values of z so that the production angle θ could be obtained from the measured angle ϕ. Then $\theta = \phi \pm \gamma$, the sign depending upon whether the track was to the left or right of the proton beam. The momentum of the pion is given by the expression $p = HeR$, where H is the magnetic field, and $R = \rho(1 - \sin^2\alpha \sin^2\phi)/\cos\alpha$. The value R could be calculated from the measured value ρ and gave a measure of the momentum.

Small corrections were applied to R to take into account the loss of energy of the pion in the gas of the chamber and also the slight variations in the magnetic field in the sensitive region.

§ 3. Results

3.1. *Conversion to the Centre-of-mass System*

The 182 acceptable mesons, with dip less than 20°, are shown on a graph of R (corrected) and θ (lab. angle) in figure 7.

The energy of the incident proton beam is not very well known but prior to our experiment its absolute value had been measured as 383 MeV by a range method. The accuracy was to ± 3 MeV and there was no measurable energy spread. An energy of 383 MeV is assumed and calculations to relate θ, R, θ' (the centre-of-mass angle), and T(the kinetic energy in the centre-of-mass system) are based on this figure. The energy T_D of the pion from the 'bound' reaction is then 40·5 MeV and the high energy cut-off T_0 of the 'unbound' spectrum is 38·5 MeV. Values of R and θ are then calculated for a pion emitted at an angle θ' in the centre-of-mass system with kinetic energy T. Curves of equal angle θ' at 20° intervals, and equal energy T at intervals of 4 MeV between 8 and 36 MeV, and 2 MeV between 36 and 44 MeV, are shown in figure 7.

3.2. *The Total Spectrum and Angular Distribution*

Mesons at angles θ' below 40° and above 160° are neglected because of the inefficiency in scanning already discussed. A total spectrum of the remaining

161 mesons between 40° and 160° is similar to that shown in figure 9 (*a*). The energy of the peak indicates that either the choice of incident proton energy is not correct or the magnetic field measurement is inaccurate. Since an error of 3 MeV in the proton energy makes more error in the meson energy than an error of 1½% in the magnetic field measurement, the momentum measured in the experiment is considered to be correct and all subsequent calculations are based on this value. The inaccurate choice of proton energy makes no appreciable error in the curves already drawn in figure 7.

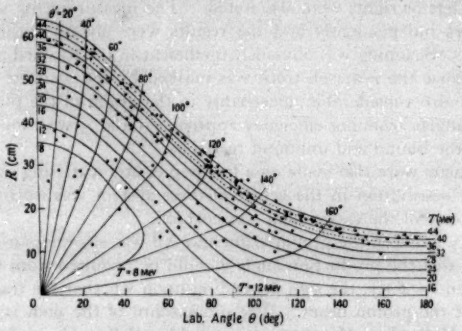

Figure 7. A plot of the acceptable mesons on a graph of R (the corrected radius of curvature) and θ (the laboratory angle). Lines of equal angle θ' in the centre-of-mass system are drawn at 20° intervals. Lines of equal kinetic energy T in the centre-of-mass system are drawn at 4 MeV intervals from 8 to 36 MeV and 2 MeV intervals from 36 to 44 MeV.

The accurate separation of the 'bound' and 'unbound' spectra is difficult because they overlap. Since the peak energy of the line spectrum is 41–42 MeV the upper limit of the unbound spectrum, ignoring the experimental spread, is 39–40 MeV and its maximum should be at 37–38 MeV. The spectrum (40° to 160°) is divided at 38 MeV to ensure that the number of mesons from the unbound spectrum is not over-estimated. Our experimental angular distributions will not be affected by a possible error of 2 MeV in the point of division, since they are found to be similar.

The angular distributions in the centre-of-mass system are plotted in 20° intervals (figure 8). The distribution for the bound reaction shows that there is a decrease in scanning efficiency below 80° ($<45°$ in the laboratory system) since this distribution should be $A+\cos^2\theta'$, i.e. symmetrical about 90°. The decrease in efficiency is not surprising as some mesons at low angles are certain to be lost in the 'fan' round the proton beam.

A least squares fit of $A+\cos^2\theta'$ to the 'bound' distribution between 80° and 160° gives:

$$\frac{d\sigma}{d\omega}(\text{bound}) = \frac{d\sigma'}{d\omega} \propto (0{\cdot}19 \pm 0{\cdot}06) + \cos^2\theta'. \qquad \ldots\ldots(1)$$

The semi-empirical formulae of Rosenfeld (1954 a) give $A = 0{\cdot}1 + 0{\cdot}6\eta_D^{-2}$, where η_D is the momentum of the pion in the centre-of-mass system in units of μc.

From our spectrum (see later), $T_D = 41{\cdot}8$ MeV, and $\eta_D = 0{\cdot}83$; this gives $A = 0{\cdot}19$, in agreement with the experimental value.

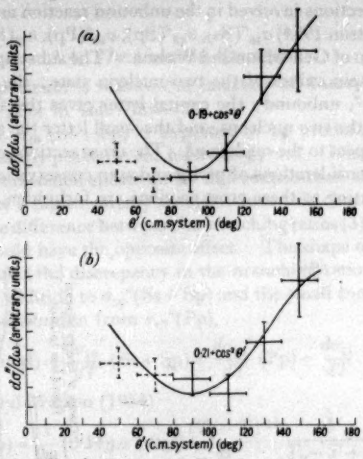

Figure 8. The angular distributions. (*a*) The bound reaction. A least squares fit gives $0{\cdot}19 \pm 0{\cdot}06 + \cos^2\theta'$. (*b*) The unbound reaction. A least squares fit gives $0{\cdot}21 \pm 0{\cdot}07 + \cos^2\theta'$.

The angular distribution of the unbound reaction should be $B + \cos^2\theta'$ since all contributions are either isotropic or of the form $C + \cos^2\theta'$, where C is a constant, and there is no asymmetric interference between the contributions. A least squares fit to the experimental distribution between 80° and 160° gives:

$$\frac{d\sigma}{d\omega}(\text{unbound}) = \frac{d\sigma''}{d\omega} \propto (0{\cdot}21 \pm 0{\cdot}07) + \cos^2\theta'. \qquad \ldots\ldots(2)$$

3.3. *The Branching Ratio, σ (unbound)/σ (total)*

The total spectrum of the 109 mesons lying between 80° and 160° in the centre-of-mass system is plotted in figure 9. A gaussian is fitted to the mesons above 38 MeV giving a maximum at 41·8 MeV, $\eta_D = 0{\cdot}83$, and an experimental standard deviation of 2 MeV. With this choice of energy the upper limit of the unbound spectrum is $T_0 = 39{\cdot}8$ MeV and $\eta_{max} = 0{\cdot}807$, where η_{max} is the maximum possible momentum of a pion from the unbound reaction in the centre-of-mass system in units of μc. A calculated standard deviation of 2 MeV is obtained by considering the uncertainties in the curvature measurements, angle measurements, magnetic field, and the spread in energy of the incident protons.

If it is assumed that the experimental error of 2 MeV remains constant in the energy range 32–48 MeV the unbound distribution can be folded into this error (figure 9) and shows that the initial division of the spectrum at 38 MeV underestimates the number of mesons from the unbound reaction by one meson. Mesons in the energy range 36–42 MeV are shared between the bound and unbound reactions in the ratio of the areas under the two curves.

$$\text{Then } \frac{\sigma\,(\text{unbound})}{\sigma\,(\text{total})}\,(80°\text{–}160°) = \frac{51 \pm 7}{109 \pm 11} = (47 \pm 8)\%. \qquad \ldots\ldots(3)$$

Since the angular distributions of the mesons from the two reactions are so similar the branching ratio from 0° to 180° is the same as (3).

Possible cross sections involved in the unbound reaction are (Rosenfeld 1954a, Gell-Mann and Watson 1954) $\sigma_{10}''(\mathrm{Ss})$, $\sigma_{10}''(\mathrm{Sp})$, $\sigma_{10}''(\mathrm{Pp})$, $\sigma_{11}(\mathrm{Ss})$, $\sigma_{11}(\mathrm{Pp})$, $\sigma_{11}(\mathrm{Ps})$. [We use the notation of Gell-Mann and Watson. The subscripts denote the initial and final isotopic spin values of the two-nucleon state; the primes denote the reaction: ', bound; ", unbound; the capital letter gives the angular momentum of the final state of the two nucleons, and the small letter the angular momentum of the pion with respect to the nucleons.] The cross sections $\sigma_{11}(\mathrm{Sp})$ and $\sigma_{10}''(\mathrm{Ps})$ are missing since considerations of parity and spin conservation show that all the transitions contributing to these cross sections are forbidden.

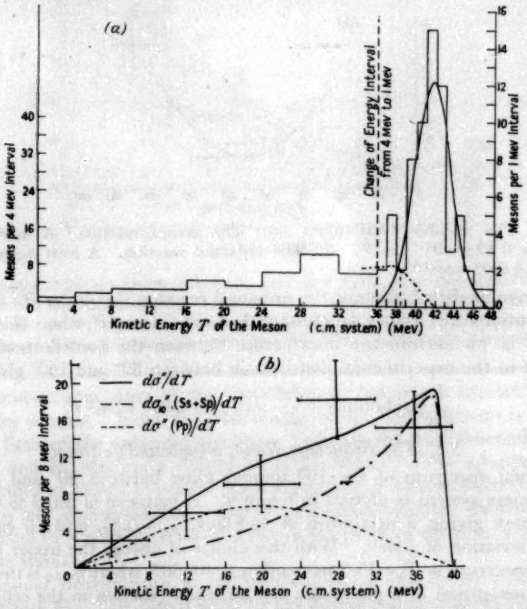
(a)
Mesons per 4 Mev Interval
Change of Energy Interval from 4 Mev to 1 Mev
Mesons per 1 Mev Interval
Kinetic Energy T of the Meson (c.m. system) (Mev)
(b)
dσ''/dT
dσ''₁₀ (Ss+Sp)/dT
dσ'' (Pp)/dT
Mesons per 8 Mev Interval
Kinetic Energy T of the Meson (c.m. system) (Mev)

Figure 9. (*a*) Total spectrum of mesons between 80° and 160° in centre-of-mass system. *Note.* Change of energy interval at 36 Mev. (The gaussian has a maximum at 41·8 Mev and a standard deviation of 2 Mev.)

(*b*) Unbound spectrum of mesons between 80° and 160° in centre-of-mass system, showing the contributions from σ_{10}'' (Ss+Sp) and σ'' (Pp).

The experimental ratio can be compared with a 'predicted' branching ratio R_1 obtained by Rosenfeld (1954a) and Gell-Mann and Watson (1954) by assuming that $\sigma_{10}''(\mathrm{Pp})$ and σ_{11} are negligible:

$$R_1 = \frac{\sigma\,(\text{unbound})}{\sigma\,(\text{total})} = \frac{\sigma_{10}''(\mathrm{Ss}+\mathrm{Sp})}{\sigma_{10}''(\mathrm{Ss}+\mathrm{Sp})+\sigma_{10}'} = 30\% \text{ at our energy.} \quad \ldots\ldots(4)$$

This strongly suggests a discrepancy between the predicted ratio and the experimental ratio and indicates that a contribution of appreciable size has been neglected in expression (4).

3.4. *The Unbound Spectrum*

The unbound spectrum is redrawn in intervals of 8 MeV, figure 9, because the statistics are too poor in 4 MeV intervals.

The contribution $\sigma_{10}''(\mathrm{Ss}+\mathrm{Sp})$ is expected to be predominant but gives a spectrum which is sharply peaked at the high energy end. It is difficult to explain the shape of our experimental spectrum by this contribution alone. Division of the total spectrum at a higher energy would reduce this discrepancy but would, however, increase the difference between the branching ratios (3) and (4). Division at a lower energy would have the opposite effect. The shape of the experimental unbound spectrum and the discrepancy in the branching ratios can be explained by assuming that in addition to $\sigma_{10}''(\mathrm{Ss}+\mathrm{Sp})$ and the small contribution σ_{11} there is an appreciable contribution from $\sigma_{10}''(\mathrm{Pp})$,

$$\text{i.e.}\quad \frac{d\sigma}{dT}(\text{unbound}) = \frac{d\sigma_{10}''}{dT}(\mathrm{Ss}+\mathrm{Sp}) + \frac{d\sigma_{10}''}{dT}(\mathrm{Pp}) + \frac{d\sigma_{11}}{dT}. \qquad \ldots\ldots(5)$$

From Gell-Mann and Watson (1954)

$$\frac{d\sigma_{10}''}{dT}(\mathrm{Ss}+\mathrm{Sp}) = \frac{1}{2\pi}(0{\cdot}14\eta + 1{\cdot}0\eta^3)\frac{(T_0-T)^{1/2}}{B}\frac{1}{T_0-T+B}\ \text{millibarns} \qquad \ldots\ldots(6)$$

where B = deuteron binding energy = 2·23 MeV, T_0 = maximum energy of pion in centre-of-mass system = 39·8 MeV. The shape of the spectrum of σ_{11} is uncertain because the predominant transition could be (Pp) (Rosenfeld 1954 a) or (Ps) (Rosenfeld, private communication). However, since this cross section is small and the shape of the spectrum will have little effect upon the value of σ_{10}'' (Pp) required to fit our experimental spectrum, we assume that σ_{11} is composed entirely of (Pp) transitions.

Then

$$\frac{d\sigma''}{dT}(\mathrm{Pp}) = \frac{d\sigma_{10}''}{dT}(\mathrm{Pp}) + \frac{d\sigma_{11}}{dT}(\mathrm{Pp}) = K\eta^3(T_0-T)^{3/2} \qquad \ldots\ldots(7)$$

where K is an unknown constant. No correction is applied to the experimental spectrum 80°–160° to obtain the spectrum 0°–180° since comparison of the 'bound' and 'unbound' angular distributions indicates that the angular distributions of the possible $\sigma_{10}''(\mathrm{Pp})$ contribution is similar to that of $\sigma_{10}''(\mathrm{Ss}+\mathrm{Sp})$. Any errors introduced by this procedure would be comparatively small.

A least squares fit of the spectra (6) and (7) to the experimental spectrum, figure 9 (*b*), gives a ratio

$$\frac{\sigma''(\mathrm{Pp})}{\sigma(\text{unbound})} = \frac{\sigma''(\mathrm{Pp})}{\sigma''(\mathrm{Pp})+\sigma_{10}''(\mathrm{Ss}+\mathrm{Sp})} = 0{\cdot}38 \pm 0{\cdot}30 \qquad \ldots\ldots(8)$$

where 0·30 is the mean error.

The contribution $\sigma''(\mathrm{Pp})$ has an η^8 dependence. By normalizing to the calculated value of $\sigma_{10}''(\mathrm{Ss}+\mathrm{Sp})$ a value of $\sigma''(\mathrm{Pp})$ is obtained from the shape of the unbound spectrum:

$$\sigma''(\mathrm{Pp}) = (1{\cdot}0 \pm 0{\cdot}9)\eta_{\max}{}^8. \qquad \ldots\ldots(9)$$

An independent value of $\sigma''(\mathrm{Pp})$ is obtained from the measured branching ratio alone since

$$\frac{\sigma\,(\text{unbound})}{\sigma\,(\text{total})}\,\text{expt.} = \frac{\sigma_{10}''(\mathrm{Ss}+\mathrm{Sp})+\sigma''(\mathrm{Pp})}{\sigma_{10}''(\mathrm{Ss}+\mathrm{Sp})+\sigma''(\mathrm{Pp})+\sigma_{10}'}. \qquad \ldots\ldots(10)$$

Then

$$\sigma''(\mathrm{Pp}) = (1{\cdot}8 \pm 0{\cdot}8)\eta_{\max}{}^8. \qquad \ldots\ldots(11)$$

These two values of $\sigma''(\mathrm{Pp})$ agree within the large statistical errors and the weighted mean is

$$\sigma''(\mathrm{Pp}) = (1{\cdot}4 \pm 0{\cdot}6)\eta_{\max}{}^8 \qquad \ldots\ldots(12)$$

Experiments on the reaction $\mathrm{p}+\mathrm{p}\rightarrow\pi^0+\mathrm{p}+\mathrm{p}$ give a value for σ_{11} but the results are rather inconsistent. A value $\sigma_{11}\simeq 0{\cdot}2\eta_{\max}{}^8$ is in fair agreement with the experimental cross sections for incident energies between 340 and 450 MeV (Rosenfeld 1954 a and private communications from Rosenfeld and Squire). If this value is assumed then $\sigma_{10}''(\mathrm{Pp})\simeq 1{\cdot}2\eta_{\max}{}^8$.

§ 4. Comparison with other Experimental Results and Conclusions

The results of our experiment show that the discrepancy between the observed and 'predicted' branching ratio can be explained by taking into account the (Pp) transitions in σ_{10}'', which have been neglected in all previous papers. The absolute value of the cross section is rather unreliable.

Comparison of Experimental and Calculated Branching Ratios

$$R_1 = \text{Old predicted ratio } \frac{\sigma\,(\text{unbound})}{\sigma\,(\text{total})} = \frac{\sigma_{10}''(\mathrm{Ss}+\mathrm{Sp})}{\sigma_{10}'+\sigma_{10}''(\mathrm{Ss}+\mathrm{Sp})}$$

$$R_2 = \text{New predicted ratio } \frac{\sigma\,(\text{unbound})}{\sigma\,(\text{total})} = \frac{\sigma_{10}''(\mathrm{Ss}+\mathrm{Sp})+\sigma''(\mathrm{Pp})}{\sigma_{10}'+\sigma_{10}''(\mathrm{Ss}+\mathrm{Sp})+\sigma''(\mathrm{Pp})}$$

Values Used

$$\sigma_{10}''(\mathrm{Ss}+\mathrm{Sp}) = \int_0^{T_0} (0{\cdot}14\eta + 1{\cdot}0\eta^3)\left(\frac{T_0-T}{B}\right)^{1/2}\frac{1}{T_0-T+B}\,\text{mbn}$$

$$\left.\begin{aligned}\sigma_{10}''(\mathrm{Pp}) &= 1{\cdot}2\eta_{\max}{}^8\,\text{mbn}\\ \sigma_{11}(\mathrm{Pp}) &= 0{\cdot}2\eta_{\max}{}^8\,\text{mbn}\end{aligned}\right\}\sigma''(\mathrm{Pp}) = 1{\cdot}4\eta_{\max}{}^8\,\text{mbn}$$

$$\sigma_{10}' = (0{\cdot}14\eta_{\mathrm{D}} + 1{\cdot}0\eta_{\mathrm{D}}{}^3)\ \text{mbn}$$

Author	Incident Energy (MeV)	η_{D}	Exptl Ratio (%)	R_2 (%)	R_1 (%)
Cartwright	340	0·59	35 ± 10	25·5	20
Peterson	340	0·59	45 ± 10	25·5	20
Our result	384	0·83	47 ± 8	44	30
Hildebrand	400	0·95	60 ± 15	55	33
Rosenfeld	440	1·07	53 ± 16	67	36

Experimental results for the total reaction $\mathrm{p}+\mathrm{p}\rightarrow\pi^+ +$ nucleons have been found by other authors (Cartwright *et al.* 1953, Peterson *et al.* 1951, Rosenfeld 1954 b, Passman *et al.* 1952) using nuclear emulsions. Counter techniques have been used by de Carvalho *et al.* (1954) and Dzhelepov *et al.* (1955). Total cross

sections for the reaction $n+p\rightarrow\pi^0+$nucleons have been measured by Rosenfeld (private communication) and Pontecorvo and Selivanov (1955) and a branching ratio has been obtained by Hildebrand (1955, p.245).

The experimental results for incident energies from 340 to 460 MeV are compared with the values given by the theory including a term $\sigma''(\mathrm{Pp})=1{\cdot}4\,\eta_{\max}{}^8$. For this comparison the cross sections obtained from the reaction

$$n+p\rightarrow\pi^0+\text{ nucleons}$$

should be corrected for the different cross sections involved (σ_{01} instead of σ_{11}) and multiplied by the statistical factor 2. The first correction is small and very uncertain and a direct comparison of

$$2\sigma(n+p\rightarrow\pi^0+\text{nucleons})$$

with

$$\sigma(p+p\rightarrow\pi^++\text{nucleons})$$

is made. The table shows the experimental branching ratios and the values predicted by the theory when a term $\sigma''(\mathrm{Pp})$ is included (R_2) and also when this term is neglected (R_1). A comparison of the total cross sections is made in figure 10. No accurate results on the unbound spectrum have been obtained and comparison is not possible. A preliminary result by Stork (1955) showed disagreement between the spectrum and the old theory which neglected $\sigma''(\mathrm{Pp})$.

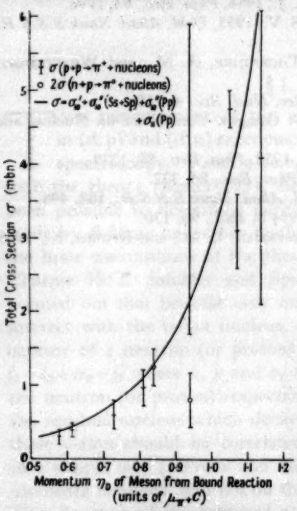

	Ref.	η_D	σ (tot) meas. (mbn)
$p+p\rightarrow\pi^+$ +nucleons, $\sigma_{10}+\sigma_{11}$	C	0·58	0·28 ± 0·10
	Pa	0·615	0·39 ± 0·10
		0·73	0·59 ± 0·18
		0·81	0·96 ± 0·25
	D	0·94	3·8 ± 2·1
		1·14	4·1 ± 2·0
	de C	1·05	4·75 ± 0·24
	R	1·07	3·1 ± 0·51
$n+p\rightarrow\pi^0$ +nucleons, $\frac{1}{2}(\sigma_{10}+\sigma_{01})$	R, H	0·84	0·62 ± 0·12
	Po	0·94	0·40 ± 0·20

C, Cartright; Pa, Passmann; D, Dzhelepov; de C, de Carvalho; R, Rosenfeld; H, Hildebrand; Po, Pontecorvo. The values of Passmann *et al.* have been corrected because the excitation function of the reaction $^{12}C(p,pn)^{11}C$, which was used for monitoring in the experiment, has been redetermined recently (Rosenfeld, private communication).

Figure 10. A comparison of the experimental total cross sections of the reactions $p+p\rightarrow\pi^++$nucleons and $n+p\rightarrow\pi^0+$nucleons with cross sections calculated assuming the values given in the table.

The results of these comparisons show that better agreement can be obtained between the phenomenological theory and the experimental results if the (Pp) transitions in $\sigma_{10}{}''$ are included in addition to σ_{11} and a value $\sigma_{10}{}''(\mathrm{Pp})=1{\cdot}2\eta_{\max}{}^8$ is used. The large value of the cross section is surprising and seems to indicate

that the interaction between two nucleons in a P-state may be larger than anticipated although the presence of a meson may very possibly influence this interaction.

ACKNOWLEDGMENTS

The authors would like to thank Professor H. W. B. Skinner for his encouragement and advice, Mr. P. R. Williams and the cyclotron crew under Mr. B. Halliday for their cooperation during the cyclotron run, Messrs. A. Cave, H. Price and R. Thompson for building some of the apparatus and Mr. J. W. G. Gregory for designing and installing the radio frequency pulser.

Dr. G. von Gierke wishes to thank Professor Skinner for the hospitality received during his stay in Liverpool.

REFERENCES

ALSTON, M. H., CREWE, A. V., and EVANS, W. H., 1954, *Rev. Sci. Instrum.*, **25**, 547.
BRUECKNER, K. A., 1952, *Phys. Rev.*, **86**, 106, 1952.
BRUECKNER, K. A., and WATSON, K., 1951, *Phys. Rev.*, **83**, 1 ; 1953, *Ibid.*, **92**, 1023.
CARTWRIGHT, W. F., RICHMAN, C., WHITEHEAD, M. N., and WILCOX, H. A., 1953, *Phys. Rev.*, **91**, 677.
CREWE, A. V., and GREGORY, J. W. G., 1955, *Proc. Roy. Soc.* A, **232**, 242.
DE CARVALHO, H. G., MARSHALL, L., and MARSHALL, J., 1954, *Phys. Rev.*, **94**, 1796.
DZHELEPOV, V. P., MOSKALEV, V. I., and MEDVED, S. V., 1955, *Dokl. Akad. Nauk S.S.S.R.*, **104**, 380.
FOWLER, E. C., FOWLER, W. B., SHUTT, R. P., THORNDIKE, A. M., and WHITTEMORE, W. L., 1953, *Phys. Rev.*, **91**, 135.
GELL-MANN, M., and WATSON, K., 1954, *Annu. Rev. Nucl. Sci.*, **4**, 219.
HILDEBRAND, R. H., 1955, Proceedings of the 1954 Glasgow Conference on Nuclear and Meson Physics (London : Pergamon Press).
PASSMANN, S., BLOCK, M. M., and HAVENS, W. W., 1952, *Phys. Rev.*, **88**, 1239.
PETERSON, V., ILOFF, E., and SHERMAN, D., 1951, *Phys. Rev.*, **84**, 372.
PONTECORVO, B., and SELIVANOV, G. I., 1955, *Dokl. Akad. Nauk S.S.S.R.*, **102**, 495.
ROSENFELD, A. H., 1954 a, *Phys. Rev.*, **96**, 139 ; 1954 b, *Ibid.*, **96**, 130.
SARGENT, C. P., CORNELIUS, R., RINEHART, M., LEDERMAN, L. M., and ROGERS, K., 1955, *Phys. Rev.*, **98**, 1349.
STORK, D., 1955, *Phys. Rev.*, **99**, 641 (A).
WATSON, K., 1952, *Phys. Rev.*, **85**, 852.

The Proton Gamma Angular Correlations in the $^{28}Si(d, p\gamma)^{29}Si$ Stripping Reaction

By K. W. ALLEN †, B. COLLINGE, B. HIRD, B. C. MAGLIĆ ‡ AND P. R. ORMAN §

Nuclear Physics Research Laboratory, University of Liverpool

Communicated by H. W. B. Skinner; MS. received 16th January 1956

Abstract. The angular correlation between the protons and γ-rays from the reaction $^{28}Si(d,p\gamma)^{29}Si$ has been measured. Protons were selected which correspond to the excitation of the 1·28 Mev level in ^{29}Si, the proton counter being set on the maximum of the stripping angular distribution at 30° to the deuteron beam direction. The angular correlation in the plane of scattering was found to be in agreement with the simple stripping hypothesis, but measurements in a plane perpendicular to the direction of the absorbed neutron, which according to the simple theory is an axis of symmetry, showed significant anisotropy.

§ 1. Introduction

The measurement of the angular distribution of protons and neutrons in (d, p) and (d, n) reactions has proved to be a useful technique in nuclear spectroscopy. From a comparison of the measured angular distributions with the theory (Butler 1951, Bhatia, Huang, Huby and Newns 1952) it has been possible to determine parities of states which agree with determinations made by β-decay and other methods so that some confidence can be placed in the basic assumptions of the theory. Several authors (Biedenharn, Boyer and Charpie 1952, Satchler and Spiers 1952, Gallaher and Cheston 1952) have pointed out that because only one particle within the deuteron is assumed to interact with the target nucleus, the process is formally analogous to resonant capture of a neutron (or proton) with orbital angular momentum l_n satisfying $j_i + l_n + \sigma_n = j_f$ where j_i, j_f and σ_n are the spins of the initial state, final state and the neutron (or proton) respectively. If the capture leads to a bound state of the residual nucleus which decays to the ground state by γ-ray emission, then these γ-rays should be correlated with the direction of the captured neutron in a simple way (Devons and Hine 1949) which depends only on the angular momenta involved, and not on the detailed mechanism of the stripping process. The direction of the captured neutron, which we shall refer to as the neutron axis, is given by $k_n = k_d - k_p$, where k_d and k_p are the wave vectors of the deuteron and proton respectively. If, on the other hand, the simple stripping hypothesis is not valid and the outgoing particle does interact with the target nucleus, Horowitz and Messiah (1954) have shown that the symmetries about the direction of the captured particle are modified. Thus a study of the (d, pγ)

† Now at Atomic Weapons Research Establishment, Aldermaston, Berks.

‡ Now at the Massachusetts Institute of Technology.

§ Now at Atomic Energy Research Establishment, Harwell, Berks.

angular correlations would be expected to throw some light on the mechanism of the stripping process.

Recent investigations by Williamson and Cox which include such angular measurements have been briefly reported (1955). They find qualitative agreement with simple stripping theory for ^{9}Be ^{10}Be and ^{24}Mg(d, p,$^{\gamma}$) angular correlations.

The experimental work described in this paper was begun by Allen, Collinge and Orman, who studied, in the plane containing the proton and deuteron, the angular distribution of the γ-rays emitted in the decay of the 1·28 MeV excited state of ^{29}Si formed in the reaction ^{28}Si(d, p)^{29}Si at a deuteron bombarding energy of 9·02 MeV. Partly due to faulty operation of the cyclotron, the experiment proved to be difficult. The distribution appeared to show the expected symmetry about the neutron axis ($k_d - k_p$) and was of the form $1 - 0{\cdot}30 \pm 0{\cdot}10 \cos^2\theta$ referred to this axis but the results were not sufficiently consistent for certainty. After two of the authors had left Liverpool, these preliminary measurements were repeated with improved apparatus and technique by Hird and Maglić, who also studied the angular correlation in the plane perpendicular to the neutron axis. It is only these later results, which had much improved statistical accuracy, which will be discussed in detail in this paper.

^{28}Si was chosen as a target nucleus for a preliminary study of the (d, pγ) correlation for three reasons:

(i) The angular distribution of the proton group leading to the first excited state of ^{29}Si has been measured, figure 1, and shows that $l_n = 2$ for this state (Holt and Marsham 1953).

(ii) The spin–parity assignment of the 1·28 MeV state is known to be 3/2, even, from the β-decay of ^{29}Al and ^{29}P (Endt and Kluyver 1954).

(iii) The spin of ^{28}Si is zero, so there is no channel spin ambiguity.

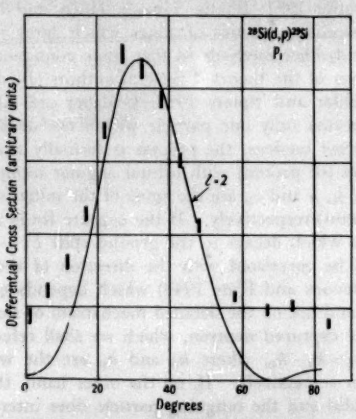

Figure 1. Angular distribution of the proton group leading to the first excited state of ^{29}Si. Taken from Holt and Marsham (1953).

A disadvantage of this choice of γ-ray transition 3/2, even, $\rightarrow$3/2, even, is the possibility that E2 radiation will compete with M1, leading to an uncertainty

in the coefficient A in the correlation function $1+A\cos^2\theta$ depending on the amount of mixing. In the event that the E2 admixture should prove to be negligible, as was hoped (Blatt and Weisskopf 1952), the correlation function would be of the very anisotropic form $1-0{\cdot}6\cos^2\theta$.

§ 2. Experimental Arrangement

The extracted deuteron beam from the Liverpool 37 in. cyclotron was focused at an external point about ten feet from the exit port of the tank. A heavy concrete wall two feet thick separated the apparatus from the cyclotron, and background was further reduced by the use of gold slits to define the beam. Self-supporting targets were made by breaking off suitable flakes from bubbles blown in fused silica. The targets used varied in thickness from 3 to 7 mg cm^{-2}, and were carried by a wire frame. A gold beam stop, sufficiently thick to absorb the deuteron beam completely, was mounted behind the target. It was possible to rotate the target frame, so that the target could be removed from the path of the beam. In this way, the effective background in the γ-ray detector was determined.

The beam energy of 9·02 Mev was determined from the measured range in a nuclear emulsion of deuterons elastically scattered from a piece of gold leaf.

Disintegration protons were detected by means of an anthracene flake approximately 13 mg cm^{-2} thick. This was mounted on a short light pipe so that the γ-ray counter could pass behind it. Provision was made for mounting aluminium absorbers in front of the scintillator, and it was found possible to choose an absorber and discriminator bias level to select the proton group leading to the 1·28 Mev level with very good discrimination against γ-ray background.

The γ-ray detector was a 1 in. cube of NaI(Tl) viewed by an EMI 6260 photomultiplier. There was a considerable background of γ-rays from (d, p) and (d, n) reactions in silicon and oxygen, from the gold beam stop and defining apertures, and also from induced activity in iodine produced by room scattered slow neutrons. It was found that most of the γ-rays came from the gold beam stop and defining apertures, and not from the target. The direct γ-ray flux from the cyclotron was quite small. Some improvement was obtained by rejecting, with an anticoincidence circuit, pulses from the counter larger than those corresponding to 1·28 Mev, the energy of the first excited state of ^{29}Si.

The general design of the electronic circuits followed that of Bell, Graham and Petch (1951). These authors combined a fast coincidence circuit using amplitude limited pulses with a conventional microsecond coincidence unit operated from pulse height discriminators at the output of slow amplifiers, thus obtaining pulse height discrimination with millimicrosecond resolving times. Two systems of this type were used: one recorded the total coincidence rate, while the other, by interposing a suitable delay between the channels, recorded simultaneously the random coincidence rate. As a cyclotron beam is naturally bunched at the radio frequency applied to the dees, it was necessary to make the delay one radio-frequency cycle (80 mμsec). The resolving times of the order of 40 mμsec, while less than the interval between beam pulses, were considerably greater than the expected duration of each burst ($\sim 10^{-8}$ sec) so that the random coincidence rate was not very dependent on small differences in the resolving time.

The resolving times of the circuits were measured using a ^{60}Co source and decreasing the anthracene scintillator bias so that γ–γ coincidences were counted.

A geometry was chosen with both counters subtending large solid angles so that the proportion of random counts was small. The coincidence count was then plotted against input delay for each counter in turn. The circuit not being investigated was used as a monitor to normalize the count of the other. The delay curves are shown in figure 2. The slow rise time of NaI(Tl) is responsible for the displacement of the centre of the curves from zero delay. In the experiment this was compensated by delaying the proton pulses 8·5 mμsec.

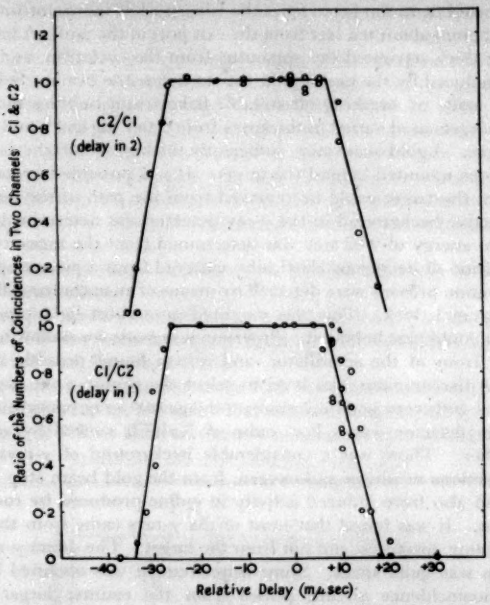

Figure 2. Delay curves showing the resolving times of the coincidence circuits.

To check the correct functioning of the circuits, both units were arranged at intervals during the experiments to count either the total coincidence rate or the random rate. Several hundred counts were then observed to see that the two units behaved identically.

§ 3. Results

3.1. *Angular Correlation in the Plane of the Reaction*

The arrangement of target chamber and detectors is shown in figure 3. The proton counter was set at the maximum of the stripping angular distribution (30° to the deuteron beam). The neutron axis is then almost exactly at 60° to the deuteron direction and is rather insensitive to the exact proton direction. The proton counter was therefore allowed to subtend a large solid angle (0·03 steradian) with negligible loss of definition in the direction of the neutron axis.

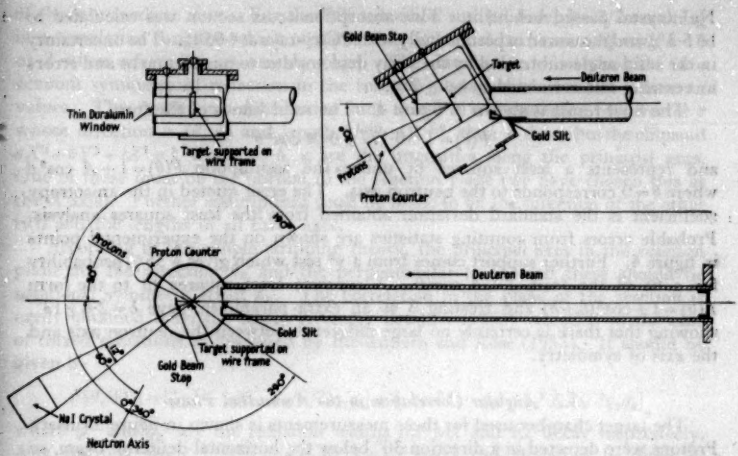

Figure 3. Target chamber used to measure the correlation in the plane of scattering (θ plane).
Inset: Target chamber used to measure the correlation in the plane perpendicular to the neutron axis (azimuthal plane).

Throughout the experiments the deuteron beam current was adjusted so that true and random coincidence rates were approximately equal. The magnitude of the current was 0·01 μA. Even with this small current the random rate equalled the true coincidence rate, both being approximately 100 counts per hour. Measurements were made at 26 angles in the region $0° < \theta < 190°$ and $290° < \theta < 360°$ where θ is the angle between the γ-ray counter and the neutron axis. At least two counts were taken at each position. There was no evidence for any systematic drifts. All measurements were normalized to the proton counting rate.

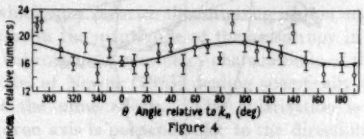

Figure 4

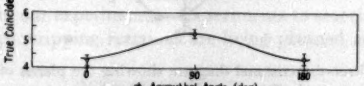

Figure 5

Figure 4. Experimental angular correlation and least squares fit in the plane of scattering.
Figure 5. Experimental angular correlation and least squares fit in the azimuthal plane.

Corrections were made to allow for the finite angular resolution of the proton detector (<1%) and for the absorption due to the proton detector when the

NaI crystal passed behind it. This absorption cross section was calculated to be 5·3% and measured experimentally with ^{60}Co γ-rays at 4·95%. The uncertainty in the solid angle subtended by the γ-ray detector due to misalignment and errors in centring was estimated to be $\pm 2\%$.

The final result is shown in figure 4. The solid line is of the form

$$F(\theta) = 1 - 0{\cdot}177 \pm 0{\cdot}04 \cos^2\theta$$

and represents a least squares fit under the assumption $F(\theta) = 1 + A \cos^2\theta$ where $\theta = 0$ corresponds to the neutron axis. The error quoted in the anisotropy coefficient is the standard deviation obtained from the least squares analysis. Probable errors from counting statistics are shown on the experimental points in figure 4. Further support comes from a χ^2 test which gives a 55% probability for a fit of the form $1 + A \cos^2\theta$. A separate least squares fit to the form $F(\theta) = 1 + \cos^2(\theta + \delta)$ and treating δ as an extra parameter, gave $\delta = 2{\cdot}6 \pm 13°$, showing that there is certainly no large difference between the neutron axis and the axis of symmetry.

3.2. *Angular Correlation in the Azimuthal Plane*

The target chamber used for these measurements is shown in figure 3 (inset). Protons were detected in a direction 30° below the horizontal deuteron beam, so that the neutron axis coincided with the axis of the target chamber. The turntable carrying the counters was then inclined so that the axis of rotation coincided with the neutron axis and counting was carried out as before, at the three angles $\phi = 0°$, 180° and 90°. The directions represented by these angles are shown in the three-dimensional diagram, figure 6. The correlation was found to be anisotropic and of the form $1 - 0{\cdot}171 \pm 0{\cdot}044 \cos^2\phi$ if a distribution of the form $1 + A \cos^2\phi$ was assumed, figure 5.

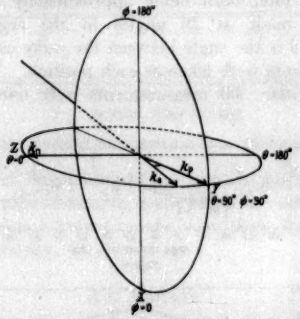

Figure 6. Three-dimensional diagram showing the planes of measurement. (Direction k_a should read k_d.)

§ 4. Discussion

Certain symmetries must occur in the three-dimensional (d,pγ) correlation $F(\theta, \phi)$ on any theory. In the general theory of angular correlations (Biedenharn and Rose 1953) the degree of complexity is limited by the angular momentum of the particle captured, the multipolarity of the radiation emitted, or the spin

of the intermediate state. For the ^{29}Si transition studied here, $j_f = 3/2$ resulting in a correlation function which contains only spherical harmonics P_k^q with $k = 0$ or 2 when referred to an axis $k_d - k_p$.† The distribution must also take into account symmetry of reflection in the reaction plane, which restricts q to even values. This results in a distribution such that if it is represented by a vector $\mathbf{r}$ whose direction is (θ, ϕ) and length $[F(\theta, \phi)]^{-1/2}$, then $\mathbf{r}$ describes the ellipsoid $aX^2 + bY^2 + cZ^2 = 1$ where a, b, c are the intensities along the principal axes. One of these must be the normal to the reaction plane (we have chosen this as the X axis). Further assumptions must be made to fix the direction of the other two and the lengths of all three axes.

According to the simple stripping theory, the principal axes in the reaction plane are the direction k_n and the perpendicular to k_n, and there should be rotational symmetry about k_n. The correlation in the plane of the reaction is easily obtained from the tables given by Satchler (1953) extended to the case of mixed radiations as discussed by Biedenharn and Rose (1953). It should be given by

$$F(\theta, 90^\circ) = [\tfrac{5}{4}q_1^2 + \tfrac{3}{4}q_2^2 - (\sqrt{3}/2)q_1q_2] + \tfrac{3}{4}\cos^2\theta[-q_1^2 + q_2^2 + 2\sqrt{3}q_1q_2]$$

where q_1^2 and q_2^2 are the radiation widths for M1 and E2 decay respectively. Any isotropy from $1 - 0{\cdot}6\cos^2\theta$ to $1 + 1{\cdot}2\cos^2\theta$ can therefore be fitted by assuming the appropriate mixture of radiations. Our experimental value of $1 - 0{\cdot}177\cos^2\theta$ may therefore, on the simple theory, be accounted for by an E2/M1 radiation width ratio of 0·04 which is not unreasonable for this transition.

The anisotropy in the azimuthal plane represents a definite departure from the simple theory. This may be due to the inadequacy of the simple theory or to the influence of a compound nucleus type of interaction. It seems unlikely however that a compound nucleus reaction amplitude could disturb the distribution in the azimuthal plane without destroying the symmetry about the neutron axis in the plane of the reaction.

It is possible that our results may be interpreted on the lines of a more general theory such as that of Horowitz and Messiah (1954). This allows for certain types of interaction of the outgoing proton with the nucleus. Unfortunately, for our purpose, their analysis is confined to reactions where $l_n \leqslant 1$. Their interaction allows for processes which may polarize the outgoing proton and they show that this results in a decrease in the magnitude of the anisotropy in the plane of the reaction and destroys the rotational symmetry characteristic of the simple theory. The semi-classical model of Newns (1953) dealing specifically with polarization of the protons shows the same effects. The polarization is expected to be greatest when the neutron axis is perpendicular to the direction of the outgoing proton which is true in our experiments. Experiments to search for polarization of the protons in (d, p) stripping reactions are being planned at Liverpool.

ACKNOWLEDGMENTS

We are indebted to Dr. A. E. Litherland, now at the Chalk River Laboratory, for many valuable discussions in the early stages of this work. We also wish to thank Dr. R. Huby and Dr. H. Newns of Liverpool and Dr. J. A. Spiers and

† It is usual to refer to the captured particle direction as the axis, but in this case some specific assumptions as to the type of interaction would be required to define this direction. The above choice avoids this difficulty.

Dr. G. R. Satchler of the Clarendon Laboratory, Oxford, for their interest and clarification of theoretical points. One of us (B. C. M.) is indebted to The Institute of Nuclear Sciences "Boris Kidrič", Belgrade, for financial support. We are very grateful to Professor H. W. B. Skinner for his support and interest throughout these experiments.

References

Bell, R. E., Graham, R. L., and Petch, H. E., 1951, *Canad. J. Phys.*, **30**, 35.
Bhatia, A. B., Huang, K., Huby, R., and Newns, H. C., 1952, *Phil. Mag.*, **43**, 485.
Blatt, J. M., and Weisskopf, V. F., 1952, *Theoretical Nuclear Physics* (New York and London : Wiley), p. 628.
Butler, S. T., 1951, *Proc. Roy. Soc.* A, **208**, 559.
Biedenharn, L. C., Boyer, K., and Charpie, R. A., 1952, *Phys. Rev.*, **88**, 517.
Biedenharn, L. C., and Rose, M. E., 1953, *Rev. Mod. Phys.*, **25**, 729.
Devons, S., and Hine, M. G. N., 1949, *Proc. Roy. Soc.* A, **199**, 73.
Endt, P. M., and Kluyver, J. C., 1954, *Rev. Mod. Phys.*, **26**, 124.
Gallaher, L. J., and Cheston, W. B., 1952, *Phys. Rev.*, **88**, 684.
Holt, J. R., and Marsham, T. N., 1953, *Proc. Phys. Soc.* A, **66**, 467.
Horowitz, J., and Messiah, A. M. L., 1954, *J. Phys. Radium*, **15**, 142.
Newns, H. C., 1953, *Proc. Phys. Soc.* A, **66**, 477.
Satchler, G. R., 1953, *Proc. Phys. Soc.* A, **66**, 1081.
Satchler, G. R., and Spiers, J. A., 1952, *Proc. Phys. Soc.* A, **65**, 980.
Williamson, R. M., and Cox, S. A., 1955, *Phys. Rev.*, **99**, 631 (A), 644 (A).

RESEARCH NOTES

r-Centroids for the O_2^+ Second Negative, N_2 Lyman–Birge–Hopfield, and N_2 Vegard–Kaplan Band Systems

By R. W. NICHOLLS, D. ROBINSON, W. PARKINSON and W. R. JARMAIN

Department of Physics, University of Western Ontario, London, Canada

MS. received 26th April 1956

In a previous paper (Nicholls and Jarmain 1956, to be referred to as I) the r-centroid $\bar{r}_{v'v''}$ of the $(v' \rightarrow v'')$ molecular band has been defined as

$$\bar{r}_{v'v''} = \int \psi_{v'} r \psi_{v''} \, dr \Big/ \int \psi_{v'} \psi_{v''} \, dr \qquad \ldots\ldots(1)$$

and its properties have been discussed. $\psi_{v'}$ and $\psi_{v''}$ are vibrational wave functions and r is internuclear separation. One application of the r-centroid concept has been made in another paper (Nicholls 1956 a, to be referred to as II) in which the behaviour of the electronic transition moment with internuclear separation was inferred from a knowledge of band intensities, r-centroids and Franck–Condon factors for a number of band systems.

Arrays of r-centroids were given in I for ten important band systems. It is the purpose of this note to present arrays for three more important systems, namely, the O_2^+ Second Negative, the N_2 Lyman–Birge–Hopfield and the N_2 Vegard–Kaplan band systems.

It will be recalled from I that one useful property of an r-centroid array was the fact that approximately constant differences $\Delta\bar{r}$, $(\Delta\bar{r} = \bar{r}_{v'+1,\, v''+1} - \bar{r}_{v'v''})$, existed between neighbouring r-centroids in sequences $v' - v'' = \text{constant}$. Complete arrays of r-centroids may therefore be built up from a knowledge of the leading observed members (usually, but not necessarily always, $\bar{r}_{v',0}$ or $\bar{r}_{0,v''}$) of sequences and of the constant difference appropriate to the sequence.

In tables 1, 2 and 3, r-centroids of the leading members of sequences together with the appropriate constant differences and wavelengths are presented for the O_2^+ Second Negative, N_2 Lyman–Birge–Hopfield and N_2 Vegard–Kaplan systems. From these tables the reader may construct the complete arrays quite simply. In each case the r-centroids were determined by the graphical method described in I and the basic molecular constants needed were taken from the compilation of Herzberg (1950) and the leading bands of sequences have been taken from the compilation of Pearse and Gaydon (1950).

In each of the three band systems studied here, the equilibrium internuclear separation $r_{e'}$ of the upper state is greater than $r_{e''}$ that of the lower state and it will be observed that in each case $\bar{r}_{v'v''}$ therefore increases smoothly with increase of $\lambda_{v'v''}$ in accordance with the discussion of I.

A study of the Franck–Condon factor surfaces formed when $q_{v'v''}$ is treated as a function of v' and v'' has been found useful (Nicholls 1956 b). It is therefore natural to inquire what may similarly be learned of the surfaces which are formed when $\bar{r}_{v'v''}$ is treated as a function of v' and v''. Unlike the $q_{v'v''}$-surfaces, which are in general undulatory, the $\bar{r}$-surfaces exhibit slopes which do not change sign. The two general forms of surface may be inferred from the form of the $\lambda_{v'v''}$-surface and the two possible forms of relationship which can exist between $\bar{r}_{v'v''}$ and $\lambda_{v'v''}$. The $\lambda_{v'v''}$-surface for a band system is a sheet which rises steeply as v'' increases and v' remains small, and which falls as v' increases and v'' remains small. For band systems where $r_{v'} > r_{v''}$ (and thus where $\bar{r}_{v'v''}$ rises with $\lambda_{v'v''}$), the $\bar{r}_{v'v''}$ surface will follow the above general form of the $\lambda_{v'v''}$ surface. For band systems where $r_{v'} < r_{v''}$ (and thus where $\bar{r}_{v'v''}$ falls as $\lambda_{v'v''}$ increases) the $\bar{r}_{v'v''}$-surface will be a smooth sheet which rises steeply when v' increases and v'' remains small and which falls when v'' increases while v' remains small. Because $\Delta\bar{r}$ is a constant for each sequence ($\Delta v = \text{const.}$), the surface profile at the line $\Delta v = \text{const.}$ will in each case be a straight line whose slope is $\Delta\bar{r}/\sqrt{2}$.

Table 1. r-Centroids and Wavelengths: O_2^+, Second Negative System

Band	$\lambda_{v'v''}$(Å)	$\bar{r}_{v'v''}$(Å)	$\Delta\bar{r}$(Å)
0, 12	5443	1·472	0·009
0, 11	5035·1	1·449	0·009
0, 10	4678·5	1·426	0·009
0, 9	4363·1	1·405	0·009
0, 8	4082·4	1·384	0·009
0, 7	3830·5	1·365	0·009
0, 6	3603·7	1·346	0·009
0, 5	3397·8	1·328	0·009
1, 5	3300·3	1·319	0·009
1, 4	3123·1	1·301	0·009
2, 4	3043·6	1·293	0·009
2, 3	2890·3	1·277	0·009
3, 3	2823·7	1·269	0·009
3, 2	2688·5	1·254	0·009
4, 2	2632·7	1·248	0·009
4, 1	2512·9	1·233	0·009
5, 1	2465·8	1·227	0·009
6, 1	2421·8	1·221	0·009
6, 0	2317·9	1·207	0·009
7, 0	2281·3	1·201	0·009
8, 0	2246·9	1·196	0·009
9, 0	2213·8	1·192	0·009
10, 0	2183·9	1·187	0·009
11, 0	2155·3	1·183	0·009
12, 0	2128·4	1·179	0·009

$\lambda_{v'v''}$(Å) = wavelength of head of R_1 branch; $\bar{r}_{v'v''}$ = r-centroid of first observed leading member of sequence; $\Delta\bar{r}$(Å) = constant difference $(\bar{r}_{v'+1,\, v''+1} - \bar{r}_{v'v''})$ down sequence.

Table 2. r-Centroids and Wavelengths: N_2, Lyman–Birge–Hopfield System

Band	$\lambda_{v'v''}$(Å)	$\bar{r}_{v'v''}$(Å)	$\Delta\bar{r}$(Å)
0, 6	1273·7	1·308	0·007
0, 5	1299·0	1·279	0·007
0, 4	1325·8	1·251	0·007
0, 3	1354·2	1·225	0·007
0, 2	1384·4	1·200	0·007
0, 1	1416·5	1·176	0·007
0, 0	1450·7	1·152	0·007
1, 0	1501·3	1·135	0·007
2, 0	1554·9	1·119	0·007
3, 0	1611·9	1·103	0·007
4, 0	1672·3	1·088	0·007
5, 0	1736·8	1·074	0·007
6, 0	1805·2	1·06	0·007

$\lambda_{v'v''}$(Å) = wavelength of band-head ; $\bar{r}_{v'v''}$(Å) = r-centroid of first observed leading member of sequence ; $\Delta\bar{r}$(Å) = constant difference $(\bar{r}_{v'+1,\ v''+1} - \bar{r}_{v',\ v''})$ down sequence.

Table 3. r-Centroids and Wavelengths: N_2 Vegard–Kaplan System

Band	$\lambda_{v'v''}$(Å)	$\bar{r}_{v'v''}$(Å)	$\Delta\bar{r}$(Å)
0, 14	5060·1	1·471	0·008
2, 15	4837·1	1·459	0·007
1, 13	4319·8	1·427	0·007
0, 11	3889·2	1·397	0·006
0, 10	3603·0	1·372	0·007
(0, 9)		1·352	0·007
(0, 8)		1·331	0·007
0, 7	2935·7	1·310	0·007
0, 6	2760·6	1·291	0·007
0, 5	2603·8	1·271	0·007
0, 4	2461·6	1·252	0·007
0, 3	2332·8	1·234	0·007
(0, 2)		1·217	0·006
(0, 1)		1·202	0·006
(0, 0)		1·186	0·006
(1, 0)		1·176	0·006
(2, 0)		1·166	0·007

$\lambda_{v'v''}$(Å) = wavelength of band head ; $\bar{r}_{v'v''}$(Å) = r-centroid of leading observed member of sequence ; note bands in parentheses ( ) head unobserved sequences ; $\Delta\bar{r}$(Å) = constant difference $(\bar{r}_{v'+1,\ v''+1} - \bar{r}_{v'v''})$ down sequence.

Following the comparable study of Franck–Condon factors (Nicholls 1956 b) the way in which these surfaces are influenced by the character of the transition, and the possibility of using an interpolation process to find preliminary values of $\bar{r}_{v'v''}$ for new systems is being investigated.

Acknowledgment

This work was supported by the Air Force Cambridge Research Centre through Contract AF 19(604)–1718.

References

Herzberg, G., 1950, *The Spectra of Diatomic Molecules* (New York : Van Nostrand).

Nicholls, R. W., 1956 a, *Proc. Phys. Soc.* A (in the press) ; 1956 b, *J. Chem. Phys.* **24**, 1104.

Nicholls, R. W., and Jarmain, W. R., 1956, *Proc. Phys. Soc.* A, **69**, 253.

Pearse, R. W. B., and Gaydon, A. G., 1950, *The Identification of Molecular Spectra*, 2nd ed. (London : Chapman and Hall).

REVIEWS OF BOOKS

Darstellungen von Gruppen (*mit Berücksichtigung der Bedürfnisse der modernen Physik*) (Group Representation Theory), by H. BOERNER. Pp. xi+287. (Berlin : Springer, 1955). (Die Grundlehren der Mathematischen Wissenschaften. Bd. LXXIV.)

This book presents in a self-contained and elegant form the mathematical theory of the irreducible matrix representations of the permutation groups and of the continuous groups of non-singular linear transformations in n-dimensional space (including the unitary, rotation and generalized Lorentz groups but not the symplectic groups). Only in the introductory chapter on matrices are theorems stated without proof, otherwise proofs are everywhere complete. The treatment specifically avoids abstract mathematical generalizations and concentrates on the main classical problems. Specific applications to physics are brought only in one or two isolated instances (Kemmer, de Broglie algebra). The theoretical physicist wishing to apply group theory will find however that there is little in this book which he does not need to know (but much that he will still have to learn !).

The representation theory of the permutation group follows the Young treatment (it is a pity that only the Young ' natural ' representation and not the orthogonal one is treated, as the latter is the one which is most used in physics). The representation theory of the full linear group follows the Weyl treatment with bisymmetric transformations. It is known of course that Weyl came to this method by considering the problems of quantum mechanics and it seems to the reviewer a pity that a physicist wishing to apply this is left to translate the pure mathematics back into the original quantum physics form from which it originated. Detailed instructions are given for the construction of the matrices of representations of continuous groups and the reader is left here with the words " the rest is numerical calculation ". The mathematician might here again follow Weyl's example and look at what the physicist is doing. In the hands of Racah, by means of a subclassification through subgroups, a tensor operator form for infinitesimal operators and the use and generalization of Casimir operators, considerable progress has been made here in recent years and it is not all just numerical work.

The relation between the characters of the linear and permutation groups is treated as in Weyl. For the permutation group a useful formula of Gamba generalizing work of Murnaghan is derived. The reduction of product representations of the linear group is treated by means of character formulae : a reference here to Littlewood's simple recipe would have been welcome.

The rotational group in n-dimensional space receives a very detailed treatment, whilst the symplectic groups and the Cartan exceptional simple groups (which have found application in Racah's hands to atomic and nuclear spectroscopy) are mentioned only in a footnote. The detailed treatment of the rotation groups makes much use of two recent papers of Stiefel (1942, 1945); it might be mentioned that the Stiefel diagram occurs in an earlier paper by Cartan (1927); the symmetry group of the diagram was of course considered by Weyl and plays an important part in the work of Racah referred to above. The treatment of the spin representations of the rotation groups follows Brauer and Weyl and

again of course there is much 'stealing' from quantum physics. The book closes with a valuable chapter on the representations of the Lorentz group, although with no reference to Wigner's contribution to this subject.

In conclusion we might comment on the well-known reluctance of theoretical physicists to use openly group theoretical language in their work, and the converse which one seems to detect in the present book: the mathematician's dislike of physical concepts. Both tendencies are of course regrettable, as it is where the two disciplines of pure mathematics and theoretical physics meet that the most fruitful ideas of both are to be found and both would become sterile if there were no meeting at all. Unfamiliarity with each other's language and literature is the cause and there still seems need of a book which would weld together the mathematical theory and its physical application in a common language agreed to on both sides and with balanced literature references. The present book should make the writing of that second book an easier task.

H. A. JAHN.

Proceedings of the International Conference of Theoretical Physics, 1953, *Kyoto and Tokyo*, edited by I. IMAI. Pp. xxviii + 942. (Tokyo: Science Council of Japan, 1954).

The published proceedings of the International Conference on theoretical physics, held in Kyoto and Tokyo in September 1953, form an enormous volume of some nine hundred and forty-two large pages. The contents cover most aspects of modern physics. Three hundred pages are devoted to Field Theory and Elementary Particles, Nuclear Physics takes up another seventy pages, Statistical Mechanics one hundred and eighty, Molecules and Solids three hundred and ten, and Liquid Helium and Superconductivity the remaining space. The name index of those taking part in the conference contains one hundred and sixty names, and includes many of the world's leading authorities in each of the above-mentioned fields. In addition to the printed version of the lectures there are many pages devoted to reporting the discussions which took place at each session. Both the lectures and the discussions were tape-recorded, and the reports have been constructed from these records with the minimum of modification.

Facts such as these ensure that the volume under review is an important addition to the literature of theoretical physics. Perhaps its most valuable aspect, to those not privileged to attend the meetings, is the opportunity which it gives to the reader of learning the views of the experts on unsettled and still controversial topics. Apart from this and the valuable synoptic view which the collection of articles provide, many readers may feel disappointment at their inability to understand quite a large fraction of the whole work. Many of the lectures are summaries, or reviews, of matter published in greater detail elsewhere and are readily intelligible only to those already well acquainted with such work. Nevertheless much of value may be gleaned by the diligent reader, and the organizers of the conference are to be congratulated on the production of this report.

As this was a truly international conference it is, perhaps, necessary to mention that, with only one exception, all papers are in English, or at least in that very nice international language for scientists: broken English. Even the

articles by authors for whom English is the mother tongue are refreshingly colloquial in style as a result of the direct transcription from the tape-recordings.

H. JONES.

Spectroscopy at Radio and Microwave Frequencies, by D. J. E. INGRAM. Pp. xii + 332. (London: Butterworths Scientific Publications, 1955.) 45*s*.

This book is a useful survey of the experimental techniques and applications of microwave and radio-frequency spectroscopy. In view of the wide field to be covered, it is not surprising that many topics are treated very briefly, particularly gaseous spectroscopy and nuclear magnetic resonance. On the whole however, the most important experiments in each branch of the subject are clearly emphasized, and are supplemented by an admirable set of references.

After a short introduction, the first 90 pages are devoted to the experimental techniques of microwave spectroscopy. These are described in some detail with many diagrams of apparatus and electronic circuits, and give a useful idea of the requirements for setting up a microwave spectroscope. There follows an account of microwave spectra in gases (30 pages) and in liquids and solids (80 pages). Much of the latter consists of a rather detailed discussion of the spectra from transition group ions in crystals, and the balance of the book might have been improved, with no loss of clarity, if this discussion were reduced and more space allocated to other topics such as nuclear magnetic resonance.

The very short section of the book on radio-frequency spectroscopy deals with atomic and molecular beam experiments (12 pages), and nuclear resonance techniques and experiments (25 pages). The discussion of the nuclear resonance results might profitably have been enlarged by a greater reference to specific examples. The book ends with an interesting summary of the applications of high-frequency spectroscopy to various physical and chemical problems, ranging from the determination of nuclear spins and chemical parameters to the establishment of frequency standards.

The book can be recommended for its extensive survey of the literature over the whole field, for making clear the many useful applications of high-frequency spectroscopy and for outlining the kind of experiments that are performed. On the other hand, with so condensed a treatment, it is difficult for the non-specialist to obtain any real understanding of many of the topics discussed without recourse to references.

J. OWEN.

Descriptive College Physics, by H. E. WHITE. Pp. x + 485. (New York: Van Nostrand; London: Macmillan, 1955.) 42*s*.

This well-written book is a survey of Physics based on a course given by the author at the University of California for " students not majoring in any of the physical or life sciences ". The text is consequently largely non-mathematical, demanding only a knowledge of simple algebra.

It is an attractive book to read. Beginning with the simple fundamental concepts of mechanics, the text includes clearly written accounts of the properties of matter, heat, sound, light, electricity and magnetism and, finally, atomic and nuclear physics. Perhaps the outstanding merit of the work is that it shows how a very considerable knowledge of physics can be gained with little mathematical equipment.

Much of the material included can be found in the usual physics textbooks for schools, though the author often illuminates aspects of the subject with comments and examples not found in the average text. On the whole, the author displays excellent insight into the difficulties of a beginner and avoids many of the *faux pas* often taken by those writers who write popular expositions of science. Many escellent diagrams assist the reader, but lapses occur occasionally. For example, a diagram of three basins containing water and labelled 'cold', 'warm', and 'hot' seems unnecessary to a reader who is going to persist until he encounters diagrams and a description of the bevatron!

Is this book likely to be of interest to students and teachers in Britain? Much is said now-a-days about the necessity for a liberal education of scientists and technologists. Less is said about the need for educating the student of arts and commerce in science, though this would appear to be just as desirable and might even be profitable! If courses for this latter purpose existed to any significant extent in Britain, this book would serve admirably to give an outline of physics. It lacks, indeed does not pretend to possess, the more rigorous approach necessary in school and university teaching for the science student. At the same time, it could well be read with profit by physics masters since they would be sure to find new ideas, illustrations and examples in this text which would be helpful in compiling lectures. J. YARWOOD.

Relativity: The Special Theory, by J. L. SYNGE. Pp. xv+450. (Amsterdam: North-Holland Publishing Company, 1956.) 76*s*.

The reader who is familiar with the numerous papers which Professor Synge has written will expect the subject matter of any book of which he is the author to be treated in a novel and interesting manner and will hope to gain a fresh outlook on old problems. These readers will not be disappointed with the book under review and will look forward to the appearance of a second volume on General Theory. The student who is learning the subject is advised to read one of the more elementary text-books before attempting to digest Professor Synge's work as some of the ideas and algebra are quite intricate and occasionally a result is mentioned which is obtained further on in the book. It must also be mentioned that the reader is expected to be equipped with some knowledge of the tensor calculus and matrix algebra.

The book, written in a delightful manner, is never dull. In fact, here and there, in the middle of a complicated argument the reader comes across a witty and amusing phrase—a rare event in mathematical literature.

The book is divided into ten chapters, each of which is subdivided into a number of paragraphs. These subdivisions, some 145 in all, are listed in a Table of Contents, which together with a full Index, enables the reader to find any particular topic without difficulty. All the most important practical applications of the special theory are dealt with and on this account the book is extremely useful as a work of reference. Its chief value, however, lies in the manner in which the fundamental ideas are discussed. The most important of these are listed on the jacket cover.

In the first three chapters the Space–Time Continuum is described in some detail. Chapter IV is devoted to the Lorentz Transformation and Chapter V to its applications. The reviewer found these two chapters, which form about a quarter of the book, most absorbing. The transformation is regarded as a

rotation in space–time and the part played by invariant null-lines is emphasized. The optical applications of the Transformation are discussed thoroughly—the topics including the expanding universe in Special Relativity.

The mechanics of a single particle is described in Chapter VI, and several collision problems are considered. The mechanics of a system of particles (Chapter VII) is based on the assumption that momentum and energy are conveyed from particle to particle by elementary impulses travelling with the speed of light. By representing angular momentum by a skew-symmetric tensor a number of collision problems involving particles possessing intrinsic angular momentum are solved.

In Chapter VIII the transition is made from a discrete system to a continuum by means of a statistical argument and the concept of incompressibility is discussed in some detail.

The Electromagnetic Field *in vacuo* is treated in Chapter IX by means of skew-symmetric tensors. In the final chapter the fields due to and the influence of fields on electric charges are considered.

Five useful subsidiary calculations are presented in an Appendix.

G. L. C.

Errors of Observation and their Treatment, by J. TOPPING. Pp. 119. (London : Institute of Physics (Monographs for Students), 1955.) 5*s*.

Dr. Topping's monograph is compact and competent within the limits aimed at and should help academic students who want to acquire a knowledge of the simpler methods of treating observational data. No attempt is made to go beyond the needs of the kind of laboratory work that students of the physical sciences normally encounter. The contents will appear thin to the professional statistician, but I suspect that Dr. Topping takes a very realistic view of what students, already burdened with the learning of basic science, are likely to be able to manage. It would be something achieved if all students of science did have an acquaintance with the simple theory of errors, least squares regression, and the common distributions.

Dr. Topping's book will be a real help to both students and teachers, both for its clear explanations and for the many numerical examples. Some teachers who are not themselves familiar with statistical methods and may suffer from lack of confidence will regret that no answers are given. The references for further reading struck me as a rather odd assortment. They vary considerably in scope and standard of treatment. It is a pity Dr. Topping does not help the student by indicating (a) parallel and (b) next step reading. Some of the references given are moderately advanced in style and the impression gained is that the bibliography as a whole is something of a random sample. M. J. MORONEY

Les fonctions orthogonales dans les problèmes aux limites de la physique mathématique, by T. VOGEL. Pp. iv + 191. (Paris : Editions du Centre National de la Recherche Scientifique, 1953.) 1200 *fr*.

This monograph is written for physicists and engineers who have occasion to deal with the solution of what are loosely known as 'the equations of mathematical physics'.

The first chapter gives an account of the general theory of orthogonal functions. It begins with an account of the basic properties of functional

spaces and of the concept of orthogonality in such spaces, goes on to discussions of the theory of systems of linear differential equations (ordinary and partial), of the closure of certain sequences of functions and concludes with a brief discussion of classical perturbation theory.

The second chapter is devoted to the study of the properties of those sets of orthogonal functions which occur most frequently in applications to physics—trigonometric functions and Fourier series, Bessel functions, Legendre functions, Mathieu functions and the polynomials of Jacobi, Tchebycheff, Laguerre, Hermite and Charlier.

The application of these functions (and their associated series expansions) to the solution of boundary value problems in classical and quantum physics is considered in the final chapter. The problems considered are taken from wave mechanics, potential theory, diffusion theory, elasticity and the theory of wave propagation.

There is a sufficiently full bibliography at the end of each chapter to enable the reader to continue his study of the topics raised, and (at the end of the monograph) a very useful table giving the sums of certain Fourier series with simple coefficients. This monograph will make difficult reading for a physicist who has not also studied mathematics extensively. It is beautifully written but it assumes on the part of the reader a high degree of maturity and an acquaintance with such abstract topics as Lebesque integration. (The brevity of the exposition can be judged by the fact that the theory of Bessel functions is dealt with in less than ten pages.) It should prove a valuable textbook for students of applied mathematics or theoretical physics.

I. N. SNEDDON.

Numerical Analysis, by Z. KOPAL. Pp. xiv + 556. (London: Chapman and Hall, 1955.) 63*s*.

With the development of the subject of numerical analysis, and with the prospects of considerable further developments in view of the particular facilities and limitations of automatic calculating machines, there has come to be room for two kinds of books on the subject, one concerned with the algebraical and analytical theory which may lie behind practical procedures for carrying out numerical calculations, either by hand or with an automatic machine, and the other concerned with those procedures themselves. This book is of the first kind, and its main value, which is considerable, will be to those concerned with the development of practical numerical procedures rather than to the users of those procedures; it will not be of much help to the physicist or engineer who has a specific numerical problem and wants some practical advice, as brief as possible, on how to set about finding a solution. Nor is it a suitable book for a beginner: it is too comprehensive and too general. For example, the beginner is likely to be confused rather than helped by being presented with a whole array of interpolation formulae, those of Newton, Gauss, Stirling, Bessel, Everett, Steffensen, Chebycheff–Bessel, Chebycheff–Everett and the modified forms of the two last, all with their algebraic derivations; what he wants is one or two formulae which are easy to use in practice and will give the results he wants; and, if he is a physicist or engineer, these results are likely to be numbers of five figures or fewer, rather than numbers of ten figures

or more which may be the main field for some of the more sophisticated formulae.

Some of the treatment seems rather unrealistic from the point of view of the reader who really does want to carry out a practical numerical calculation. For example, concerning the Picard method for integration of a differential equation the author gives a formal proof, and emphasizes by printing in italics, that " the maximum error of the nth approximation can be made less than any preassigned quantity provided only that n has been taken large enough ". To anyone who has really considered what would be involved in evaluating, say, e^{-50} by Picard's method applied as a numerical process to the equation $y' = -y$, the word ' only ' here might seem to be meant ironically ! The emphasis here, and similar wording elsewhere, suggests the outlook of the pure mathematician rather than an appreciation of the realities of practical numerical work. To generalize a statement of Jeffreys, " in order that a series should be useful for numerical computation, it is neither necessary nor sufficient that it should converge "; and this should never be far out of mind for a writer on numerical analysis. Another example of unreality is the dismissal of the subject of integration of a first-order linear equation by a footnote stating that such an equation " would be integrable in terms of quadratures "; so it would, but it does not follow that this would be the best practical way of dealing numerically with such an equation. However, the possibility that other methods may be needed in practice is not even mentioned.

For a book of this size there are some surprising omissions besides that just mentioned. Almost two whole chapters—about 100 pages—are devoted to boundary-value problems, in the restricted sense of characteristic-value problems of homogeneous linear differential equations with homogeneous boundary conditions. However, other problems of differential equations with ' jury ' conditions (to use L. F. Richardson's term) are dismissed in a single sentence, " non-linear systems would call for an essentially different method of approach "; so they would, indeed, but this bare statement is not much help to a reader faced with such a problem and needing some advice about how to deal with it. And even for linear equations there is no mention of the method, which may be more useful in practice than any mentioned in the text, of integrating from both ends of the range and matching at some intermediate value of x. Nor would the reader get any hint of the scope of the relaxation process applied to ordinary differential equations with two-point boundary conditions, or of the application in this context of Choleski's matrix factorization procedure, as developed by Thomas and by Fox. Some of the detailed algebra of Chapter V could well be spared to give space for consideration of these procedures.

However, the reader with some previous knowledge of the subject, and with practical experience of the realities of numerical work, will find much of value in this book. Topics which may be selected as being of particular interest are the optimum size of interval in numerical differentiation, a thorough treatment of quadrature formulae of Gauss type, the use of Chebycheff polynomials in approximate representation of functions by polynomials and in interpolation, an original study of methods for replacing a differential equation by a difference equation of higher order without introducing a dominant spurious ' solution ', and the numerical treatment of integral and integro-differential equations.

And not the least merit of the book is that it provokes thought and discussion on many of the topics with which it is concerned. D. R. HARTREE.

The Theory of Games and Linear Programming, by S. VAJDA. Pp. 106. (London: Methuen's Monographs on Physical Subjects, 1956.) 8*s.* 6*d.*

The present vogue for the theory of games dates only from 1944 when a monumental original work on the subject was published by von Neumann and Morgenstern. The subject is by no means as frivolous as the title may suggest since many situations arising in economics and in warfare are illuminated by it. Linear programming is a related but quite distinct subject. Here the object is to maximize or minimize a linear function of a given number of variables subject to constraints expressed as linear inequalities. An example of a practical problem which can be solved by linear programming is that facing a housewife who is able to buy a variety of foodstuffs each containing a different proportion of protein, carbohydrate, etc. and who wishes to provide her family with a balanced diet at minimum cost.

Both the theory of games and linear programming are subjects which may prove to have applications in unexpected places and Dr. Vajda has presented their essentials in an admirable manner. His book can be highly recommended, not only to the general scientific reader who has heard of the subjects and who wishes to know what they are about, but also to the student who is embarking on a serious study. M. V. WILKES.

Champs de vecteurs et de tenseurs. Introduction à l'électromagnétisme, by E. BAUER. Pp. vii + 204. (Paris: Masson et Cie, 1955.) 2200 *fr.*

In the preface to this beautifully written account of the vector and tensor calculus, the author says: "J'ai toujours pensé que, pour bien comprendre la physique, pour distinguer nettement les lois données par l'experience, ou les hypothèses théoriques, de ce qui est simple identité mathématique, il est nécessaire de préciser d'abord le langage mathématique, d'en faire un cadre abstrait, général, dans lequel pourra venir s'insérer ensuite notre connaissance des faits. Une fois achevé ce travail préliminaire, le terrain est déblayé, les réalités physiques fondamentales se dégagent de la gangue de calculs dans laquelle elles sont trop souvent noyées."

Professor Bauer has succeeded admirably in his aim of showing that an elegant abstract mathematical scheme provides the natural setting for the description of the physical world. His book includes a detailed account of the theory of vector and tensor fields in three dimensions, a chapter on general tensor theory and an excellent brief modern introduction to electromagnetic theory. The lucid simple style of the book should commend it particularly to readers (such as the reviewer) whose command of the French language is limited, and its treatment of the subject should serve as an example both to those who still regard 'applied mathematics' primarily as a parade ground for the exercise of pure mathematical tricks, and to those extremists of the opposite camp (if any still exist) who remain to be convinced of the need for precise mathematical language in the description of nature. E. H. SONDHEIMER.

CONTENTS OF SECTION B

PAGE

Mr. E. L. Heasell and Dr. J. Lamb. The Absorption of Ultrasonic Waves in a Number of Pure Liquids over the Frequency Range 100 to 200 Mc/s . . 869

Dr. D. A. Jones and Dr. T. Smith. An X-ray Study of the Structure of a Sodium Chloride Crystal Grown by the Kyropoulos Method 878

Mr. J. J. Benbow. The Determination of Dynamic Moduli and Internal Friction of High Polymers from Creep Measurements 885

Mr. R. B. Robinson and Dr. R. H. Buchanan. Undamped Free Pulsations of an Ideal Bubble 893

Dr. I. C. Browne, Mr. J. V. Evans, Mr. J. K. Hargreaves and Dr. W. A. S. Murray. Radio Echoes from the Moon 901

Mr. C. Rubenstein. A General Theory of the Surface Friction of Solids . . 921

Mr. J. W. Elder. Halide Activated Halide Phosphors 934

Dr. F. Berz. On the Theory of Plasma Waves 939

Research Notes:

Mr. J. V. Evans. The Measurement of the Electron Content of the Ionosphere by the Lunar Radio Echo Method 953

Dr. P. Crosby. Tables for Quick Calculation of Optical Constants and Variation of the Ellipse of Vibration with Angle of Incidence . . 955

Dr. D. T. Stewart. Spectroscopic Evidence for Presence of Atoms in Active Nitrogen 956

Prof. M. Anastassiades and Mr. D. Ilias. On the Anomalous Rectification of Cuprous Sulphide Detectors 958

Letters to the Editor:

Prof. H. Fröhlich and Mr. S. Doniach. Plasma Interaction and Conduction in Semiconductors 961

Reviews of Books 962

Contents of Section A 964

Figure 4. Beam profile (actual size) obtained when x-ray film was exposed at the beam entry window of the chamber. The lead blocks in front of the chamber were moved slightly after this picture was taken so that the lead did not obstruct the beam on the left-hand side.

Figure 5. A typical cloud chamber picture taken during the experiment. A well collimated beam of 383 MeV protons of intensity $\sim 2 \times 10^4$ enters the chamber at the top of the picture. A π-meson of radius of curvature 11 cm is produced to the left of the beam at an angle of 135° in the laboratory system. This π-meson can be seen decaying in the chamber gas into a μ-meson.

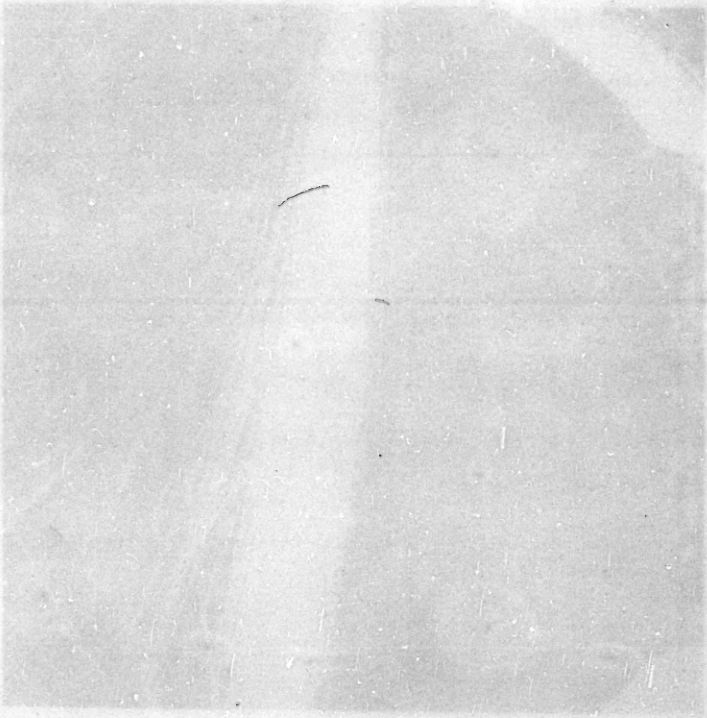

The Momentum Spectrum of μ-Mesons at a Depth of 40 Metres Water Equivalent

By W. F. NASH and A. J. POINTON

Physics Department, University of Nottingham

Communicated by L. F. Bates: MS. received 22nd March 1956

Abstract. Scattering distributions, obtained in two lead plates, each 2 cm thick, placed in a cloud chamber situated at a depth of 40 metres water equivalent, have been used to determine the momentum spectrum of μ-mesons in the range 0·22–1·0 Gev c^{-1}. The spectrum is in good agreement with the spectrum derived from the sea level data of Holmes and co-workers.

§ 1. Introduction

In the past few years a number of experiments have been performed underground or under thick absorbers at sea level to investigate the properties of the μ-mesons present in cosmic radiation. George, Redding and Trent (1953), Leontic and Wolfendale (1953) and MacDiarmid (1955) investigated the large angle scattering of μ-mesons in absorbers contained in a cloud chamber. Leontic and Wolfendale used a form of analysis to give results independent of the momentum spectrum of the μ-mesons, but in the other experiments the analysis was performed using an assumed form for the underground spectrum to enable the experimental results to be compared with those obtained theoretically. Similarly, Kannangara and Zivkovic (1953), working on the large angle scattering of μ-mesons in photographic emulsions, required a knowledge of this spectrum. In all these experiments and others (see Lloyd and Wolfendale (1955) for summary) there was found to be 'anomalous' large angle scattering which apparently could not be accounted for by ordinary Coulomb scattering theories. In all but the experiments of Leontic and Wolfendale the evidence for the existence of anomalous scattering depends on the form of the spectrum assumed.

George and Shrikantia took for the momentum spectrum the form $N(p)dp=(p+p_0)^{-2\cdot7}dp$, where p_0 is the momentum loss due to ionization in the earth above the apparatus and the exponent $-2\cdot7$ is based on the data of Barrett *et al.* (1952). A similar spectrum was assumed by Kannangara and Zivkovic. This form has since been shown to be inaccurate (Rochester and Wolfendale 1954).

MacDiarmid obtained a more accurate form than the 'power law' spectrum of George and Shrikantia by applying an ionization cut-off to the sea-level spectrum found experimentally by Holmes *et al.* (private communication). An attempt was made to estimate the low-momentum part of the spectrum by applying a statistical analysis to the scattering distribution obtained in the experiment. The method was not rigorous and the final result depended on the form of the spectrum assumed, since the high momentum part of the spectrum was found by subtracting the estimated low momentum part from the assumed spectrum which, in the low momentum region, may have been in error.

It is possible that the derived forms of the underground spectrum of the μ-mesons are in error due to neglect of the effect of the scattering of the μ-mesons in the earth above the apparatus and the differences in path lengths of particles which are not incident vertically. If such errors existed the results of some of the above experiments would be affected.

It was therefore decided to measure the underground momentum spectrum and compare it with the forms derived from the 'power-law' spectrum and the experimental spectrum of Holmes *et al.* The method consisted of analysing the scattering of μ-mesons in the lead plates of a cloud chamber and applying a statistical method to obtain the form of the momentum spectrum in the apparatus consistent with the observed scattering.

§ 2. Experimental Arrangement

The experiment was performed in a cave situated beneath 19·85 metres of sandstone rock equivalent to 39·7 metres of water. The upper surface of the rock was flat over that part covered by the solid angle of the counter telescope used. The rock ensured that the incident flux of penetrating particles was sensibly free from any nuclear interacting component.

The apparatus consisted of a cylindrical cloud chamber, of diameter 28 cm and illuminated depth 8 cm, containing two 2 cm lead plates and triggered by a three-fold coincidence counter telescope shown in figure 1. Between the second and third trays of the counter system was placed a thickness of lead Σ which gave a low momentum cut-off to the momentum spectrum of the particles observed in the cloud chamber. The counter system introduces a bias in the momentum spectrum of the observed particles since they may be scattered out of or into the counter system by the lead plates of the cloud chamber. This effect must be taken into account when a comparison is made between the experimental results and the derived spectrum.

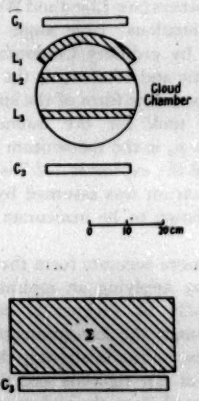

Figure 1. Experimental Arrangement.
C_1, C_2, C_3 counter trays, L_1, L_2, L_3 and Σ lead absorbers.

The tracks produced by the μ-mesons were photographed stereoscopically by a camera with two lenses situated 7 cm apart and 50 cm from the front plate of the cloud chamber. The projected angles of scatter of the μ-mesons in the lead plates were measured by projecting these photographs on to a circular protractor as described by MacDiarmid (1954). The angles could be read to 0·1°.

To check whether any systematic errors existed in the measured angle of scattering, a frequency plot of the positive and negative deflections of some 250 particles (i.e. some 500 angles) was made for each set of readings. From the symmetry of the histograms obtained it was found that if any systematic errors occurred they were certainly less than 0·2°.

The effect of random errors or 'noise level' scattering, which is much larger than that of the systematic errors, will be discussed in the next section. The 3 cm of lead was placed above the chamber to enable events occurring therein to be examined inside the chamber. Its only effect in this experiment was to modify slightly the momentum spectrum of the particles observed.

§ 3. Estimation of the Momentum Spectrum

From previous measurements on the scattering of μ-mesons (Whittemore and Shutt 1952, MacDiarmid 1955, Lloyd and Wolfendale 1955) it has been shown that the angular distribution follows closely the gaussian form as given by Rossi and Greisen (1941) and others, at least up to energies of the order 10 Gev. Thus a probability distribution for the momentum of a slow particle, penetrating a small number of plates, can be obtained. The method follows Annis *et al.* (1953) and Lloyd and Wolfendale (private communication). Instead of the momentum p the independent variable $p\beta$ was used, where βc is the velocity of the particle considered.

If $\langle\phi\rangle$ is the measured r.m.s. angle of scatter for a particle traversing n plates in a cloud chamber and σ is the value of this angle for an infinite number of traversals (ignoring momentum loss) then the probability that $\langle\phi\rangle$ lies between $\langle\phi\rangle$ and $\langle\phi\rangle+d\langle\phi\rangle$ is

$$P(\langle\phi\rangle;\sigma)d\langle\phi\rangle=f_1(n)\frac{\langle\phi\rangle^{n-1}}{\sigma^n}\exp\left(-\frac{n}{2}\frac{\langle\phi\rangle^2}{\sigma^2}\right)d\langle\phi\rangle \quad \ldots\ldots(1)$$

where $f_1(n)$ is a normalizing constant.

Now, if $p_0\beta_0$ is the value of $p\beta$ obtained from the measured value of $\langle\phi\rangle$, the probability that the true value lies between $p\beta$ and $p\beta+d(p\beta)$ is, from (1)

$$P_1(p\beta;p_0\beta_0)d(p\beta)=f_2(n)\left(\frac{p\beta}{p_0\beta_0}\right)^n\exp\left[-\frac{n}{2}\left(\frac{p\beta}{p_0\beta_0}\right)^2\right]d\left(\frac{p\beta}{p_0\beta_0}\right) \quad \ldots(2)$$

since $p_0\beta_0\langle\phi\rangle=$ constant (Rossi and Greisen 1941); $f_2(n)$ is a normalizing constant. The form of this distribution has been checked by Lloyd and Wolfendale by experiment. The distribution given in (2) is applicable only if there is no 'noise' or random scattering and there is a 'flat' incident momentum spectrum. Since neither of these conditions is satisfied in practice these effects must be taken into account.

If the 'noise level' scattering is represented by an r.m.s. angle σ_1 and the ratio of the measured angle of scattering $\langle\phi\rangle$ to σ_1 by m, then the momentum distribution for a given particle is given in terms of $p_1\beta_1/p_0\beta_0$ instead of $p\beta/p_0\beta_0$ where

$$\frac{p_1\beta_1}{p_0\beta_0}=\left\{\left(\frac{p_0\beta_0}{p\beta}\right)^2+\frac{1}{m^2-1}\right\}^{-1/2}. \quad \ldots\ldots(3)$$

This new distribution is obtained by replotting at any particular value of $p\beta/p_0\beta_0$ the ordinate found at $p_1\beta_1/p_0\beta_0$ on the curve given by (2). The effect of the 'noise' is to introduce an asymmetry into the distribution and an asymptotic value equal to the ordinate at $p\beta/p_0\beta_0=(m^2-1)^{1/2}$ on the original curve given by (2). Figure 2 shows the distributions for the present experiment (i.e. $n=2$) for m equal to 2, 4 and infinity, the latter corresponding to the form given by (2).

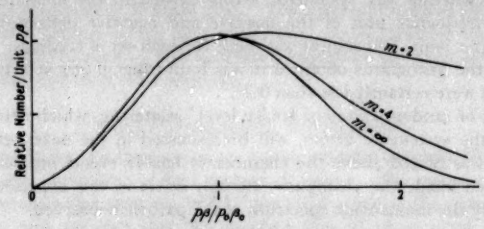

Figure 2. Momentum distribution functions for $n=2$.

MacDiarmid (1954) showed that the value of σ_1 may be found from the distribution of the measured r.m.s. angles of scattering. When the values of $p\beta$ tend to infinity the measured scattering will be mainly that due to 'noise' and if a frequency plot of the measured r.m.s. angles is made there will be a peak value $\langle\phi\rangle_p$ at small angles, given by

$$\langle\phi\rangle_p^2=\frac{n-1}{n}\sigma_1^2 \qquad \ldots\ldots(4)$$

where n is the number of plates in the chamber. Hence the value of σ_1 may be obtained. The results of (4) were checked by Lloyd and Wolfendale (1955) using a more rigorous method.

Since the momentum spectrum is not 'flat' there is another probability distribution introduced into the $p\beta$ distribution for a given particle. Therefore, to obtain the final form of the $p\beta$ distribution, the theoretical form must be multiplied at any given point by the corresponding value of the $p\beta$ spectrum. The form of the spectrum at large values of $p\beta$ is well known and can certainly be used, but at small values of $p\beta$ an assumed form must be taken. It is the determination of the true form of this spectrum at low values of $p\beta$ that is the object of the present experiment.

The resulting distributions are then normalized to the observed number of particles corresponding to the $p_0\beta_0$ and m values considered. These normalized distributions are then summed and a form of the spectrum results. If the resulting spectrum is different from the assumed form then the procedure is repeated using the derived form of the spectrum until a self-consistent spectrum is obtained. Since the method is one of successive approximation the initially assumed form of the spectrum is not critical. The lead Σ between the second and third counter trays gives a low-momentum cut-off to the assumed, and hence to the resulting, form of the spectrum.

Only the spectrum below 1·0 Gev c^{-1} is considered in this experiment, since above this value the derived spectrum is uncertain because of the effect of 'noise level' scattering which renders angles smaller than about 1·0° unusable.

In the present case the $p_0\beta_0$ and m values were taken as the means for groups of particles with r.m.s. angles within a range of 0·2°.

§ 4. Experimental Results

Two series of photographs, referred to as Series I and Series II, were obtained with different values of Σ, the thickness of lead beneath the chamber. Series I was taken with Σ at 9·5 cm and Series II with Σ at 19 cm giving low-momentum cut-off at $p\beta$ equal to 0·22 Gev c^{-1} and 0·35 Gev c^{-1} respectively. In each series some two thousand photographs (corresponding to some four thousand angles of scatter) were measured, and the angles of scatter of the tracks found as described above. Only tracks satisfying the following conditions were accepted: (*a*) there must be little obvious distortion in the track, (*b*) the particle must be unaccompanied: otherwise it might be part of a secondary penetrating shower and therefore may not be a μ-meson.

In Series I, 993 tracks were used in the determination of the 'noise level' scattering angle σ_1, the value of which was found to be 0·7°. Another 845 tracks (having $\langle\phi\rangle > 1°$) were used in the estimation of the $p\beta$ spectrum. In Series II, 851 and 818 tracks were used respectively, and the value of σ_1 was found to be 0·53°. The difference in the values of σ_1 is because better thermal conditions obtained for Series II than for Series I. The self-consistent form of the spectra found after three successive approximations are shown in figure 3 for the two series.

§ 5. Conclusions and Discussion

It will be seen from figure 3 that the peaks of the spectra, Series I and Series II, are for $p\beta$ equal to 0·6 Gev c^{-1} and 0·68 Gev c^{-1} respectively, but that otherwise the curves are similar. A calculation of the difference produced by the scattering of the particles in the lead Σ beneath the chamber showed that the effect was sufficient to account for the difference in the peaks, but would not otherwise affect the spectrum to any great extent. To give a direct comparison between the spectra, the estimated percentage of particles with values of $p\beta$ in the range

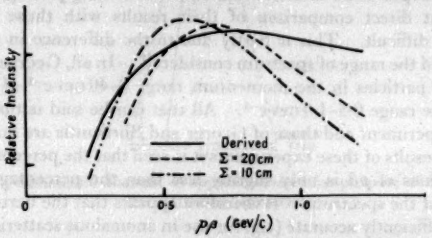

Figure 3. Measured spectra compared with the form derived from the sea level data of Holmes *et al.*

0·5–1·0 Gev c^{-1} for each series was found. The values were 6·22 ± 0·53% and 6·18 ± 0·55%, which are in close agreement. The curves of figure 3 have been normalized to give corresponding areas for that section of the spectrum in the range 0·5–1·0 Gev c^{-1}. The errors stated are purely statistical.

The experimental spectra were compared with the spectra derived from the sea-level spectrum of Holmes *et al.* and from the 'power law' form $N(p)dp = p^{-\gamma}dp$,

with γ equal to 2·7. These spectra were adjusted for the ionization loss in the rock above the apparatus and for the scattering of the particles inside the apparatus. The scattering correction, calculated on the assumption that all the particles are incident vertically (MacDiarmid 1954 and others), gave spectra with a peak at about 1·6 Gev c^{-1} and the number of particles in the $p\beta$ range 0·5–1·0 Gev c^{-1} much less than the percentage found experimentally. When, however, a refined calculation was performed taking into account the variation of incident angle (see Appendix) the agreement between the experimental forms and the derived forms of the spectrum was good. For comparison the form derived from the more accurate spectrum of Holmes *et al.* is shown in figure 3 normalized in a similar manner to the experimental curves. The peak of the spectrum is at $p\beta$ equal to 0·72 Gev c^{-1} and the number of particles in the $p\beta$ range 0·5–1·0 Gev c^{-1} is 6·42%: for the 'power law' spectrum the peak was found at 0·61 Gev c^{-1} and the percentage of particles 7·9%.

It will be seen that above about 1·0 Gev c^{-1} the experimental forms of the spectrum fall off more rapidly than the spectrum derived from the result of Holmes *et al.* This effect is caused by the 'noise level' scattering which excludes from the analysis particles which would have contributed to this part of the spectrum. Since the 'power law' form of the spectrum is empirical, it is only to be expected that the percentages found for the given range should not agree very well.

If there were any anomalous scattering as suggested by the work of Leontic and Wolfendale (1953) and others, it would be apparent in the part of the spectrum considered here, since it is the larger angles which are considered in this analysis. However, while such scattering might have an appreciable effect on the shape of the spectrum at low values of $p\beta$, due to the large normalization factors, there would be a negligible effect on the percentages involved since the experiments mentioned above have shown the number of anomalous scatters to be only a small fraction of the total number.

Recently George and Shrikantia (1956) have obtained a form of the μ-meson spectrum at a depth of 56 metres water equivalent using photographic emulsion techniques but direct comparison of their results with those of the present experiment is difficult. This is partly due to the difference in the techniques, the location and the range of spectrum considered. In all, George and Shrikantia measured 317 particles in the momentum range 0–40 Gev c^{-1} of which only 13 occurred in the range 0·5–1·0 Gev c^{-1}. All that can be said is that the results of the present experiment and those of George and Shrikantia are not incompatible.

From the results of these experiments it is seen that the percentage of particles with small values of $p\beta$ is only slightly less than the percentage given by the derived form of the spectrum. It therefore appears that the derived form of the spectrum is sufficiently accurate (e.g. for use in anomalous scattering experiments (cf. § 1)).

Acknowledgments

We are glad to record our indebtedness to Professor L. F. Bates for his interest in these experiments, to Dr. A. W. Wolfendale and Mr. J. L. Lloyd for making available the results of their work prior to publication, and for many helpful and illuminating discussions. We also thank the Nottingham Corporation for permission to work in the cave. One of us (A. J. P.) is indebted to the Department

of Scientific and Industrial Research for the provision of a maintenance grant.

The apparatus used in this work was built in part with a grant from the Government Grant Committee of the Royal Society.

APPENDIX

Correction to the Derived Spectrum due to Scattering in the Apparatus

It is required to calculate the probability that a particle incident on the top counter tray with a given value of $p\beta$ will also cross the bottom counter tray.

For the purpose of calculation the Coulomb scattering distribution given by Rossi and Greisen (1941) is assumed. This assumption is justified by the experiments of Whittemore and Shutt (1952) and others who found that the scattering of μ-mesons, at the values of $p\beta$ considered here, follows a gaussian form. It is also assumed that the three lead plates act as one lead plate situated at their centre of gravity. Further, the front view, or x direction, and the side view, or y direction, are considered to be independent since, to a good approximation, the projected angles of scattering in planes at right angles are independent. Thus only the x direction is considered in detail as the results for the y direction will be formally analogous. The system for the x direction is shown in figure 4.

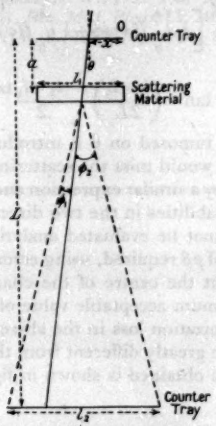

Figure 4. Schematic diagram of apparatus, used for purpose of calculating the scattering correction.

It is assumed that the particle is incident on the top tray in a distance x to $x+dx$ from O with a projected angle θ to $\theta+d\theta$ in this plane. The probability that the particle is incident on the top tray in the interval dx is dx/l_1, and that it is incident in the interval $d\theta$ is $K_1\cos^2\theta d\theta$ where K_1 is a constant. The assumption of a $\cos^2\theta$ distribution is not critical. The probability that the particle crosses the bottom tray is given by

$$P(\theta, x) = \tfrac{1}{2}\int_0^{\phi_1} f(\phi)d\phi + \tfrac{1}{2}\int^{\phi_2} f(\phi)d\phi \qquad \ldots\ldots(A\,1)$$

where $f(\phi)d\phi$ is the probability of the particle being scattered by the lead block through a projected angle ϕ to $\phi+d\phi$, and ϕ_1 and ϕ_2 are given by

$$\phi_1=\tan^{-1}\left[\frac{\frac{1}{2}(l_2+l_1)-x-a\tan\theta}{L-a}\right]-\theta$$

$$\phi_2=\tan^{-1}\left[\frac{\frac{1}{2}(l_2-l_1)+x+a\tan\theta}{L-a}\right]+\theta.$$

Rossi and Greisen (1941) give

$$f(\phi)d\phi=\frac{1}{\sqrt{\pi}}\frac{p\beta}{E_s t^{1/2}}\exp\left[-\left(\frac{p\beta\phi}{E_s t^{1/2}}\right)^2\right]d\phi$$

where $E_s=21\times10^6$ ev and t is the thickness of the absorber in radiation lengths.

When ϕ_1 becomes negative the probability given by (A 1) becomes

$$P(\theta,x)=\tfrac{1}{2}\int_0^{\phi_2}f(\phi)d\phi-\tfrac{1}{2}\int_0^{\phi_1}f(\phi)d\phi.$$

The probability of observing a particle with a given value of $p\beta$ (i.e. that it will pass through the top and bottom counter trays) is obtained by averaging $P(\theta,x)$ over all values of θ and x, and is given by

$$K_2\int_0^{l_1}\int_0^{\tan^{-1}\frac{l_1-x}{a}}\left[\tfrac{1}{2}\int_0^{\phi_1}f(\phi)d\phi+\tfrac{1}{2}\int_0^{\phi_2}f(\phi)d\phi\right]\cos^2\theta\,d\theta\,dx \qquad \ldots(\text{A 2})$$

where

$$K_2=2\left[\left(\frac{l_2+l_1}{2}\right)\tan^{-1}\left(\frac{l_2+l_1}{2L}\right)-\frac{l_2-l_1}{2}\tan^{-1}\frac{l_2-l_1}{2(L-a)}\right]^{-1}.$$

The limit $\tan^{-1}\{(l_1-x)/a\}$, imposed on θ is introduced, since for angles greater than this value the particle would miss the scattering material. The probability for the y direction is given by a similar expression and the total probability is given by the product of the probabilities in the two directions.

The integrals (A 2) cannot be evaluated analytically but must be calculated numerically for each value of $p\beta$ required, using error function tables. The value taken for $p\beta$ is the value at the centre of the chamber. Since in the present experiment there is a minimum acceptable value of $p\beta$ defined by the thickness of lead Σ the maximum ionization loss in the absrober is about 4%. Hence the value of $p\beta$ used will not be greatly different from the incident value.

The correction function obtained is shown in figure 5.

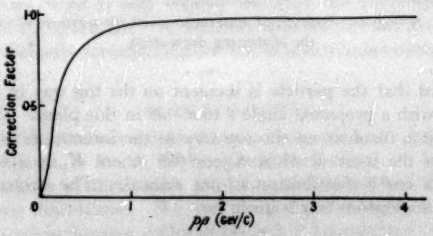

Figure 5. Calculated correction function.

It should be noted that, in general, in experiments on μ-mesons underground no account has been taken of the angular variation of incident direction and that in the present experiment the correction function, calculated assuming all the particles to be incident vertically and assuming a variation of incident angle, differ by as much as a factor two at the lower values of $p\beta$. This is due to the fact that, while the incident intensity is not greatly affected by a small variation of incident angle, the probability of loss of a particle is affected, since at small values of $p\beta$ the particle, while missing the bottom counter tray in its original path, may be scattered in such a way that it will pass through this tray.

References

Annis, M., Bridge, H. S., and Olbert, S., 1953, *Phys. Rev.*, **89**, 1216.

Barrett, P. M., Bollinger, L. M., Cocconi, G., Eisenberg, Y., and Greisen, K., 1952, *Rev. Mod. Phys.*, **24**, 133.

George, E. P., Redding, J. L., and Trent, P. T., 1953, *Proc. Phys. Soc.* A, **66**, 533.

George, E. P., and Shrikantia, G. S., 1956, *Nuclear Phys.*, **1**, 54.

Kannangara, M. L. T., and Zivkovic, M., 1953, *Phil. Mag.*, **44**, 797.

Leontic, B., and Wolfendale, A. W., 1953, *Phil. Mag.*, **44**, 1101.

Lloyd, J. L., and Wolfendale, A. W., 1955, *Proc. Phys. Soc.* A, **68**, 1045.

MacDiarmid, I. B., 1954, *Phil. Mag.*, **45**, 933; 1955, *Ibid.*, **46**, 177.

Rochester, G. D., and Wolfendale, A. W., 1954, *Phil. Mag.*, **45**, 980.

Rossi, B., and Greisen, K., 1941, *Rev. Mod. Phys.*, **13**, 240.

Whittemore, W. L., and Shutt, R. P., 1952, *Phys. Rev.*, **88**, 1312.

The Fermi, or Exchange, Hole in Atoms

By V. W. MASLEN

Mathematical Institute, Oxford

Communicated by C. A. Coulson; MS. received 22nd March 1956

Abstract. Slater has recently introduced the concept of an averaged exchange hole as a basis for an approximation to the exchange potential, which arises in the Hartree–Fock equations. Use of the density matrix leads to a natural definition of the exchange hole which is identical with that obtained in a different manner by Slater. The distribution, size and shape of the exchange hole have been studied for neon and argon, using Slater wave functions, and the results give further information concerning the nature of the hole. The Slater approximation of a spherical exchange charge, centred at the electron, is discussed.

§ 1. Introduction

In recent papers, Huntington (1942) and Slater (1951) have shown that the normal form (1) of the Hartree–Fock equations,

$$H_1\psi_i(1)+\left[\sum_{k=1}^{N}\int \psi_k^*(2)\psi_k(2)\,d\tau_2/r_{12}\right]\psi_i(1) - \left[\sum_{k=1}^{N}\int \psi_k^*(2)\psi_i(2)\,d\tau_2/r_{12}\right]\psi_k(1)=E_i\psi_i(1) \quad \ldots\ldots(1)$$

may be alternatively written

$$H_1\psi_i(1)+\left[\sum_{k=1}^{N}\int \psi_k^*(2)\psi_k(2)\,d\tau_2/r_{12}\right]\psi_i(1) - \left[\sum_{k=1}^{N}\int \psi_i^*(1)\psi_k^*(2)\psi_k(1)\psi_i(2)\,d\tau_2/\{\psi_i^*(1)\psi_i(1)r_{12}\}\right]\psi_i(1)=E_i\psi_i(1). \quad \ldots\ldots(2)$$

H_1 is the one-electron part of the Hamiltonian for electron 1, ψ_m, ψ_n, ... are the orthonormal set of one-electron wave functions and (1), (2), ..., (N) indicate the coordinates, both space and spin, of electrons 1, 2, ..., N. Integrations over $d\tau_2$ include summation over spins and therefore the exchange terms vanish unless ψ_i, ψ_k have their spins parallel.

In equation (2), the exchange term has the standard form of a potential energy term in a one-electron Schrödinger equation. Slater has interpreted it to be the potential, at the position of the first electron, of an exchange charge density

$$-\sum_{k=1}^{N}{}_{\|\text{ spins}}\ \psi_i^*(1)\psi_k^*(2)\psi_k(1)\psi_i(2)/[\psi_i^*(1)\psi_i(1)]. \quad \ldots\ldots(3)$$

This exchange charge density, he points out, integrates to minus one over the space of electron 2. Being mainly negative, it has the nature of a hole within the total charge distribution and accounts for the fact that no other electron of

the same spin can occupy the same position as electron 1 and is unlikely even to be near it. In form (3), however, the exchange charge differs for each solution ψ_i of the Hartree–Fock equations. To make the problem tractable Slater forms a weighted average over all occupied orbitals of the same spin, thereby obtaining, for the average exchange hole, the expression

$$-\left[\sum_{j,\,k=1}^{N}{}'\psi_j^*(1)\psi_k^*(2)\psi_k(1)\psi_j(2)\right]\Big/\left[\sum_{j=1}^{N}{}'\psi_j^*(1)\psi_j(1)\right]. \qquad \ldots\ldots(4)$$

$\|$ spins

Unfortunately, even calculation of the potential due to (4) is too difficult for many purposes and so Slater has approximated to it with a spherical distribution, centred at the electron.

With this approximation of a spherical exchange charge, Pratt (1952) has solved the Hartree–Fock equations for Cu^+. The energy values in this instance showed little improvement over the Hartree values, but the wave functions obtained are generally an accurate approximation to the Hartree–Fock solution. Gaspar (1954) claims that an exchange potential equal to two-thirds of the Slater value gives better results in the case of Cu, but this claim deserves further investigation.

Whether or not the exchange potential due to an averaged exchange charge (4) is in good approximation to that due to the correct distribution (3) has already been discussed by Herman, Callaway and Acton (1954) and will not be pursued further here.

In the present paper it is shown that use of density matrices yields a definition of the exchange hole which is identical with Slater's average exchange hole (cf. also Löwdin 1955). The distribution of exchange charge density is examined for neon and argon, using Slater orbitals, and the Slater approximation of a spherical distribution of exchange charge is discussed.

§ 2. Density Matrix Formulation of the Fermi Hole

For a system of N interacting particles in the state $\Psi(1, 2, \ldots, N)$ we define the density matrix to be

$$\rho_N(1, 2, \ldots, N\,;\, 1', 2', \ldots, N') = N!\,\Psi(1, 2, \ldots, N)\Psi^*(1', 2', \ldots, N'). \qquad \ldots\ldots(5)$$

The diagonal element $\rho_N(1, 2, \ldots, N\,;\, 1, 2, \ldots, N)$ is the probability density for one particle to be at point 1, another at point 2, etc., simultaneously. The factor $N!$ accounts for the $N!$ possible permutations of the electrons among these positions. (It is to be noted that the convention of using the factor $N!$ is not universal. We follow here the definition given by McWeeny (1955).) To find the probability of $N-1$ electrons having coordinates 1, 2, 3, …, $N-1$, simultaneously, we integrate $\rho_N(1, 2, \ldots, N\,;\, 1, 2, \ldots, N)$ over all values of the coordinate N. With suitable normalization, we may therefore define a 'reduced density matrix'

$$\rho_{N-1}(1, 2, \ldots, N-1\,;\, 1', 2', \ldots, (N-1)')$$

$$= N(N-1)\ldots.3.2\int \Psi(1, 2, \ldots, N-1, N)\,\Psi^*(1', 2', \ldots, (N-1)', N)\,d\tau_N$$

and, by continued integration,

$$\rho_2(1, 2 ; 1', 2') = N(N-1) \int \Psi(1, 2, \ldots, N)\Psi^*(1', 2', 3, \ldots, N)\, d\tau_3 \ldots d\tau_N$$

and

$$\rho_1(1 ; 1') = N \int \Psi(1, 2, \ldots, N)\Psi^*(1', 2, \ldots, N)\, d\tau_2 \ldots d\tau_N.$$

Dirac (1931) has shown that, when $\Psi(1, 2, \ldots, N)$ may be approximated as a single determinant of one-electron functions,

$$\Psi(1, 2, \ldots, N) = (N!)^{-1/2} \det |\psi_1(1)\psi_2(2) \ldots \psi_N(N)|$$

then

$$\rho_1(1 ; 1') = \sum_{r=1}^{N} \psi_r(1)\psi_r^*(1') \qquad \ldots\ldots(6)$$

and all higher order density matrices may be expressed in terms of $\rho_1(1; 1')$. In particular,

$$\rho_2(1, 2 ; 1', 2') = \rho_1(1 ; 1')\rho_1(2 ; 2') - \rho_1(1 ; 2')\rho_1(2 ; 1').$$

When the space and spin variables are separable, we may divide ρ_1 into two parts. Thus

$$\rho_1(1 ; 1') = \rho_1^{\alpha}(1 ; 1')\alpha(1)\bar{\alpha}(1') + \rho_1^{\beta}(1 ; 1')\beta(1)\bar{\beta}(1') \qquad \ldots\ldots(7)$$

and

$$\rho_2(1, 2 ; 1', 2') = \rho_2^{\alpha\alpha}(1, 2 ; 1', 2')\alpha(1)\alpha(2)\bar{\alpha}(1')\bar{\alpha}(2') + \rho_2^{\alpha\beta}(1, 2 ; 1', 2')\alpha(1)\beta(2)\bar{\alpha}(1')\bar{\beta}(2') + \text{similar terms.} \qquad \ldots\ldots(8)$$

If, further, we integrate equations (7), (8) over the spin variables to obtain the 'spinless density matrices' $P_1(1 ; 1')$, $P_2(1, 2 ; 1', 2')$, then

$$P_1(1 ; 1') = P_1^{\alpha}(1 ; 1') + P_1^{\beta}(1 ; 1')$$

and

$$P_2(1, 2 ; 1', 2') = P_2^{\alpha\alpha}(1, 2 ; 1', 2') + P_2^{\alpha\beta}(1, 2 ; 1', 2') + P_2^{\beta\alpha}(1, 2 ; 1', 2') + P_2^{\beta\beta}(1, 2 ; 1', 2')$$

where

$$P_2^{\alpha\beta}(1, 2 ; 1', 2') = P_1^{\alpha}(1 ; 1')P_1^{\beta}(2 ; 2') \qquad \ldots\ldots(9)$$

and

$$P_2^{\alpha\alpha}(1, 2 ; 1', 2') = P_1^{\alpha}(1 ; 1')P_1^{\alpha}(2 ; 2') - P_1^{\alpha}(1 ; 2')P_1^{\alpha}(2 ; 1') \qquad \ldots\ldots(10)$$

with similar expressions for $P_2^{\beta\alpha}$ and $P_2^{\beta\beta}$. 1, 1', 2, 2' refer now only to space coordinates and P_1, P_2 to spatial distributions. The diagonal element of (9) gives the well-known result that, in the one-electron approximation, there is no spatial correlation between electrons of opposite spin. From (10),

$$P_2^{\alpha\alpha}(1, 2 ; 1, 2) = P_1^{\alpha}(1 ; 1)[P_1^{\alpha}(2 ; 2) - P_1^{\alpha}(1 ; 2)P_1^{\alpha}(2 ; 1)/P_1^{\alpha}(1 ; 1)]. \qquad \ldots\ldots(11)$$

Expressed in this form, $P_2^{\alpha\alpha}(1, 2 ; 1, 2)$ is interpreted as follows. The first factor on the right-hand side is the probability of an electron being at 1. The second factor is the probability that another will have position 2, subject to there being an electron at 1. The second term within this factor is dependent upon the coordinates 1 and is therefore a correlation term. Being mainly negative, it has the nature of a hole within $P_1^{\alpha}(2 ; 2)$ and we adopt it as a definition of the Fermi hole, $F^{\alpha}(1 ; 2)$. Thus

$$F^{\alpha}(1 ; 2) = -P_1^{\alpha}(1 ; 2)P_1^{\alpha}(2 ; 1)/P_1^{\alpha}(1 ; 1). \qquad \ldots\ldots(12)$$

If we substitute (6) into equation (12) then this definition is seen to be equivalent to (4), obtained by Slater.

In the next section the form of (12) in simple cases is examined.

§ 3. Exchange Charge Distributions for Neon and Argon

The wave function of a closed shell atom may be approximately expressed as a single determinant of one-electron functions and the exchange charge distribution is examined for two such atoms, neon and argon.

For neon, the normalized Slater wave functions, in atomic units, are

$$\left.\begin{aligned} \psi(1s) &= 17{\cdot}04e^{-9{\cdot}7r}, \qquad \psi(2s) = 4{\cdot}67re^{-2{\cdot}9r}, \\ \psi(2p_x) &= 8{\cdot}08xe^{-2{\cdot}9r} \end{aligned}\right\} \quad \ldots\ldots(13)$$

yielding an exchange charge density, for electrons of the same spin, of

$$\begin{aligned} F^x(1\,;\,2) &= F^\beta(1\,;\,2) \\ &= [290{\cdot}4\exp\{-9{\cdot}7(r_1+r_2)\} + 21{\cdot}75r_1r_2(1+3\cos\gamma)\exp\{-2{\cdot}9(r_1+r_2)\}]^2 \\ &\quad \div [290{\cdot}4\exp(-19{\cdot}4r_1) + 87{\cdot}0r_1^2\exp(-5{\cdot}8r_1)] \qquad \ldots\ldots(14) \end{aligned}$$

where γ is the angle between $\mathbf{r}_1$ and $\mathbf{r}_2$. Contours of constant $F^x(1\,;\,2)$ are shown in figure 1 for four values of r_1, the distance of the electron from the nucleus. Both from the figure and from (14) it is evident that, for r_1 small, (and, consequently, electron 1 most probably in a 1s state), $F(1\,;\,2)$ approximates to a

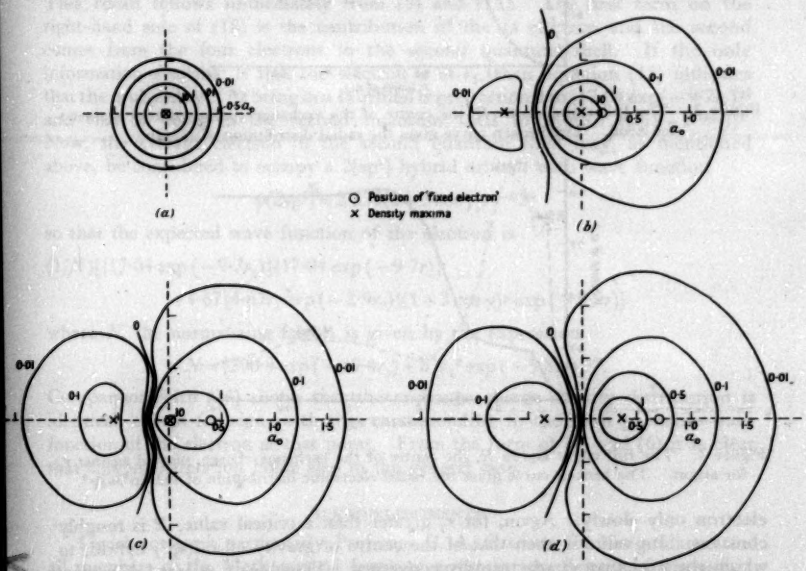

Figure 1. Contours of constant exchange charge density in neon, for various values of r_1. (*a*) $r_1=0$, (*b*) $r_1=0{\cdot}2a_0$, (*c*) $r_1=0{\cdot}4a_0$, (*d*) $r_1=0{\cdot}7a_0$. (The figure gives charge in units of $+e$).

1s distribution. Similarly, for r_1 large, with the electron most probably in the second quantum shell, $F(1\,;\,2)$ tends to a $2(sp^3)$ distribution. That it does approximate to a $2(sp^3)$ distribution for large r_1 is due to the use of the same exponent in the 2s and 2p functions so that their energies are the same and the average electron in the second quantum shell may be assumed to occupy a $2(sp^3)$ orbital.

In Slater's spherical charge approximation, the exchange charge is centred at the electron. The distributions plotted in figure 1 indicate that this is, as expected, not strictly correct. In figure 2 is plotted the variation in R, the distance of the centre of gravity of the exchange charge from the nucleus, against r_1. Due to the spherical symmetry of the atom, $\mathbf{R}$ and $\mathbf{r}_1$ lie in the same direction. The nature of this variation of R is particularly interesting at its extremities. For r_1 small, $R \simeq 0$ and the exchange charge 'follows' the

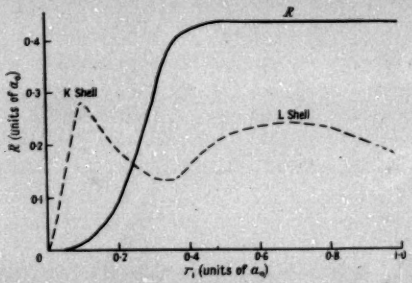

Figure 2. The full curve shows R, the centre of the exchange charge, plotted against r_1 for neon. The broken curve gives the radial distribution of $1s2s2p^3$.

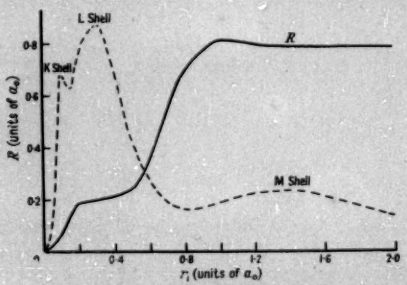

Figure 3. The full curve shows R, the centre of the exchange charge, plotted against r_1 for argon. The broken curve gives the radial electronic distribution of $1s2s2p^33s3p^3$.

electron only slowly. Again, for r_1 greater than a critical value, R is roughly constant. Its value is then that of the centre of gravity of a $2(sp^3)$ hybrid, to which the exchange charge rapidly converges. Thus, again at large distances, the exchange hole ceases to 'follow' the electron radially.

The exchange hole in argon is very similar to that in neon. The exchange charge distribution alters, as r_1 increases, from that of a predominantly 1s orbital

to a $2(sp^3)$ hybrid and, for very large r_1, to a $3(sp^3)$ hybrid. In figure 3 is shown the variation of the centre of gravity R of the exchange charge with the distance of the electron from the nucleus. This exhibits, for r_1 small and r_1 large, those features which were observed for neon.

§ 4. Discussion

Slater has stated that the exchange charge density for, say, α spins is equal to $P_1^{\alpha}(1\,;\,1)$ at the position of the electron, gradually falling off as we go away from this point. This observation is used as the basis of an argument both for the averaged exchange charge approximation and for the further approximation of a spherical exchange charge. We see, however, that although the exchange charge density does have the value $P_1^{\alpha}(1\,;\,1)$ at the position of the electron, as it must in order to satisfy the Pauli exclusion principle, this is not necessarily its maximum value. Nor does the density always fall off as we go away from the electron. And, as we noted above, in the outer parts of the atom the exchange charge no longer 'follows' the change in r_1. It rapidly converges to a constant distribution.

The nature of the exchange hole for neon leads to an interesting interpretation of its general form. The one-electron density distribution for neon is

$$P_1^{\alpha}(1\,;\,1)=\{17{\cdot}04\exp(-9{\cdot}7r_1)\}^2+4\{4{\cdot}67r_1\exp(-2{\cdot}9r_1)\}^2 \quad \ldots\ldots(15)$$

This result follows immediately from (6) and (13). The first term on the right-hand side of (15) is the contribution of the 1s electron and the second comes from the four electrons in the second quantum shell. If the only information available is that the electron is at r_1, then equation (15) indicates that the probability of its being in a 1s orbital is proportional to $\{17{\cdot}04\exp(-9{\cdot}7r_1)\}^2$ and that of being in the second quantum shell to $4\{4{\cdot}67r_1\exp(-2{\cdot}9r_1)\}^2$. Now, the average electron in the second quantum shell may, as mentioned above, be considered to occupy a $2(sp^3)$ hybrid orbital, with wave function

$$\psi(2sp^3)=2{\cdot}335(1+3\cos\gamma)re^{-2{\cdot}9r}$$

so that the expected wave function of the electron is

$$(1/N)[\{17{\cdot}04\exp(-9{\cdot}7r_1)\}\{17{\cdot}04\exp(-9{\cdot}7r)\}$$
$$+4{\cdot}67\{4{\cdot}67r_1\exp(-2{\cdot}9r_1)\}(1+3\cos\gamma)r\exp(-2{\cdot}9r)]$$

where N, the normalizing factor, is given by the expression

$$N=\{290{\cdot}4\exp(-19{\cdot}4r_1)+87r_1^2\exp(-5{\cdot}8r_1)\}^{1/2}.$$

Comparison with (14) shows that the exchange charge density distribution is identical, except for sign, with that corresponding to the most probable wave function of the electron at that point. From the form of (4) and (6) it is clear that this interpretation holds also in the general case.

Acknowledgments

I wish to thank particularly Professor C. A. Coulson for his guidance and all members of the Mathematical Institute group for the benefit of discussion. The work was made possible by the grant of a Hackett Research Studentship by the University of Western Australia.

References

Dirac, P. A. M., 1931, *Proc. Camb. Phil. Soc.*, **27**, 240.
Gaspar, R., 1954, *Acta Phys. Hung.*, **3**, 263.
Herman, F., Callaway, J., and Acton, F. S., 1954, *Phys. Rev.*, **95**, 371
Huntington, H. B., 1942, *Phys. Rev.*, **61**, 325.
Löwdin, Per-Olov, 1955, *Phys. Rev.*, **97**, 1490.
McWeeny, R., 1955, *Proc. Roy. Soc.* A, **232**, 114.
Pratt, G. W., Jr., 1952, *Phys. Rev.*, **88**, 1217.
Slater, J. C., 1951, *Phys. Rev.*, **81**, 385.

The Interpretation of Intensity Distributions in the CN Violet, C_2 Swan, OH Violet and O_2 Schumann–Runge Band Systems by use of their *r*-Centroids and Franck–Condon Factors

By R. W. NICHOLLS

Department of Physics, University of Western Ontario, London, Ontario, Canada

MS. received 26th April 1956

Abstract. Intensity distributions in the CN violet, C_2 Swan, OH violet and O_2 Schumann–Runge band systems are examined to determine in each case the dependence of the electronic transition moment $R_e(r)$ upon internuclear separation r, with the aid of Franck–Condon factors $q_{v'v''}$ and r-centroids $\bar{r}_{v'v''}$. It is found that $R_e(r)=\text{const}\,(-1+2{\cdot}579r)$ for the CN violet system, that $R_e(r)=\text{const}\,(1+0{\cdot}056r)$ for the C_2 Swan system, that $R_e(r)=\text{const}\,(1-0{\cdot}756r)$ for the OH violet system and that $R_e(r)=\text{const}\,(-1+2{\cdot}416r-0{\cdot}897r^2)$ for the O_2 Schumann–Runge system. 'Smoothed' arrays of relative vibrational transition probabilities have thereby been determined for each band system.

§ 1. Introduction

A characteristic internuclear separation $\bar{r}_{v'v''}$ associated with the $v'\rightarrow v''$ band of a diatomic molecular band system and called the r-centroid of the band was discussed in a previous paper (Nicholls and Jarmain 1956, to be referred to as I).

It will be recalled from I that

$$\bar{r}_{v'v''}=\int \psi_{v'} r \psi_{v''}\,dr \Big/ \int \psi_{v'}\psi_{v''}\,dr \qquad \ldots\ldots(1)$$

$$\int \psi_{v'} r^n \psi_{v''}\,dr=(\bar{r}_{v'v''})^n \int \psi_{v'}\psi_{v''}\,dr \qquad \ldots\ldots(2)$$

$$\int \psi_{v'} f(r) \psi_{v''}\,dr=f(\bar{r}_{v'v''}) \int \psi_{v'}\psi_{v''}\,dr. \qquad \ldots\ldots(3)$$

The wide range of conditions under which it is possible to write equations (1), (2) and (3) have been established by Fraser (1954 a, b) and are stated in detail in I. In these equations $\psi_{v'}$, $\psi_{v''}$ are vibrational wave functions of the levels v' and v'' respectively, r is the internuclear separation, n is an integer less than about 10, $f(r)$ is a polynomial function of r, of degree less than about 10. Arrays of r-centroids for a variety of band systems were presented in I.

In the present paper a practical application of equation (3) to the interpretation of arrays of intensities of band systems will be discussed and illustrated for four band systems for which intensity measurements are available.

1.1. *Factors which control Band Intensities*

The integrated intensity in emission $I_{v'v''}$ of a band may be written

$$I_{v'v''}=HN_{v'}E_{v'v''}P_{v'v''} \qquad \ldots\ldots(4)$$

where H is a constant which allows for units and the geometry of the optical system, $N_{v'}$ is the population of the level v', $E_{v'v''}$ is the energy quantum of the band and $P_{v'v''}$ is the transition probability of the band. In fact

$$P_{v'v''} = \frac{64\pi^4}{3h^4c^3} E_{v'v''}^3 \left| \int \psi_{v'} R_e(r) \psi_{v''} \, dr \right|^2 \qquad \ldots\ldots(5)$$

where $R_e(r)$ is the electronic transition moment of the transition and

$$R_e(r) = \int \psi_{e'}^* M \psi_{e''} \, dr. \qquad \ldots\ldots(6)$$

Here $\psi_{e'}$, $\psi_{e''}$ are the electronic wave functions of the upper and lower states of the transition and M is the multipole moment associated with the transition.

The vibrational transition probability $p_{v'v''}$ may be defined as

$$p_{v'v''} = \left| \int \psi_{v'} R_e(r) \psi_{v''} \, dr \right|^2 \qquad \ldots\ldots(7)$$

and its variation from band to band is a measure of the distribution between the bands of the oscillator strength of the electronic transition involved.

Equation (4) may then be rewritten as

$$I_{v'v''} = K N_{v'} E_{v'v''}^4 p_{v'v''} \qquad \ldots\ldots(8)$$

where K incorporates all the constants. Thus an array of relative $p_{v'v''}$ may be determined from $I_{v'v''} N_{v'} E_{v'v''}^4$ when the integrated band intensities $I_{v'v''}$ have been measured and when information is available on the change in vibrational population $N_{v'}$ with v'. Such experimentally determined arrays of $p_{v'v''}$ have been published in a few cases (see below) and while valuable, suffer from the defect that the individual values of $p_{v'v''}$ vary in relative accuracy because the percentage error in measurement of high intensities is much less than in the measurement of low intensities. In cases where no information on $N_{v'}$ is available, $I_{v'v''} E_{v'v''}^4$ provides a relative measure along a v'' progression ($v' = \text{const}$) of the variation of $p_{v'v''}$. Suitable rescaling procedures (Turner and Nicholls 1954b) may then be employed to place all the $p_{v'v''}$ on the same scale, but the objection of possible large variation in relative accuracy from band to band still remains, however.

A superior method (Fraser 1954a, Turner and Nicholls 1954a, b) which leads to a 'smoothed' array of $p_{v'v''}$ is outlined briefly below.

The right-hand side of equation (7) is similar in form to the left-hand side of equation (3). $R_e(r)$ is expected to be a smoothly varying function of r and thus equation (7) may be rewritten as

$$p_{v'v''} = R_e^2(\bar{r}_{v'v''}) \left| \int \psi_{v'} \psi_{v''} \, dr \right|^2 = R_e^2(\bar{r}_{v'v''}) q_{v'v''} \qquad \ldots\ldots(9)$$

where

$$q_{v'v''} = \left| \int \psi_{v'} \psi_{v''} \, dr \right|^2 \qquad \ldots\ldots(10)$$

is the Franck–Condon factor of the band in question.

Tables of Franck–Condon factors have been computed for a number of important band systems (see, for example, Jarmain, Fraser and Nicholls 1953, 1955, Fraser, Jarmain and Nicholls 1954, Pillow 1951, 1953a, b, Bates 1949, 1952, and papers referred to therein).

From equations (8) and (9)

$$I_{v'v''} = K N_{v'} E_{v'v''}^4 R_e^2(\bar{r}_{v'v''}) q_{v'v''}, \qquad \ldots\ldots(11)$$

This equation may be used to determine the form of $R_e(r)$ for a band system. Equation (9) may then be employed to determine a 'smoothed' array of $p_{v'v''}$ for the band system. Finally, in some cases, the variation of $N_{v'}$ with v', from which source mechanisms may be inferred, may be found from equation (11).

1.2. *Determination of Behaviour of Electronic Transition Moment*

If the integrated band intensities $I_{v'v''}$ be measured for a system for which arrays of $\bar{r}_{v'v''}$ and $q_{v'v''}$ are available, the relation

$$(I_{v'v''}/q_{v'v''}E_{v'v''}{}^4)^{1/2}=(KN_{v'})^{1/2}R_e(\bar{r}_{v'v''}) \qquad \ldots\ldots(12)$$

which follows from equation (11), may be employed to determine the relative variation of $R_e(r)$ with r for each v'' progression by plotting the left-hand side against $\bar{r}_{v'v''}$. A rescaling procedure, described in more detail for particular cases below, may be employed to place the points for each progression on the same ordinate scale. A *smooth curve* fitted by a least squares criterion through the resulting points then shows the relative variation of $R_e(r)$ with r for the band system. Examples of the application of this procedure may be seen in the work of Turner and Nicholls (1954a, b) and Wallace and Nicholls (1955). It is important to note that *all* of the measured intensities contribute to the determination of the curve and also that application of the least squares criterion smooths out to a large extent the effect of experimental scatter. Scatter is introduced from two main sources: intensity measurements and Franck–Condon factors. The experimental error in integrated intensity measurement decreases with increasing intensity. The Franck–Condon factors are computed to 2–3 significant figures, on the basis of some assumed model of molecular potential (parabolic, Morse, etc.). Inaccuracies arise, particularly at higher quantum numbers, when the assumed model is only of limited applicability to the molecule in question. Apart from this, the larger factors are more accurate than the smaller factors.

1.3. *Determination of 'Smoothed' Array of Vibrational Transition Probabilities*

Once a smooth curve has been obtained which shows the relative variation of $R_e(r)$ with r, equation (9) may be employed to determine a *smoothed* array of $p_{v'v''}$. Values of $R_e(\bar{r}_{v'v''})$ are read from the curve at values of $\bar{r}_{v'v''}$ appropriate to each band. $R_e{}^2(\bar{r}_{v'v''})q_{v'v''}$ is then a relative measure of $p_{v'v''}$ for each band. The array of $p_{v'v''}$ thereby obtained may be normalized such that $p_{00}=1$.

§ 2. Interpretation of Intensity Distributions

Very few arrays of reliable integrated band intensities have been published, probably because of the many difficulties associated with accurate intensity measurement. It is worth while therefore to examine some of the few published arrays for evidence of variation of electronic transition moment with internuclear separation and thereby to derive 'smoothed' arrays of relative vibrational transition probabilities. In this paper band intensities of the CN violet ($B^2\Sigma^+\rightarrow X^2\Sigma^+$) (Ornstein and Brinkman 1931), C_2 Swan ($A^3\Pi_g\rightarrow X^3\Pi_u$) (King 1948), OH violet ($A^2\Sigma^+\rightarrow X^2\Pi$) (Dieke and Crosswhite 1949) and O_2 Schumann–Runge ($B^3\Sigma_u^-\rightarrow X^3\Sigma_g^-$) (Ditchburn and Heddle 1954) systems are examined.

Apart from purely instrumental difficulties, the ease by which integrated band intensities may be reliably measured greatly depends upon whether or not

individual bands are overlapped by the structure of neighbouring bands. In cases where there is no overlap or only a very small overlap between adjacent bands, e.g. N_2 First Positive ($B^3\Pi_g \rightarrow A^3\Sigma_u^+$) (Turner and Nicholls 1954a, b), N_2 Second Positive ($C^3\Pi_u \rightarrow B^3\Pi_g$), N_2^+ First Negative ($B^2\Sigma_u^+ \rightarrow X^2\Sigma_g^+$) (Wallace and Nicholls 1955), true integrated intensities may be obtained from areas beneath band profiles. However, in cases where severe overlap occurs one is forced to employ the intensity vested in unoverlapped parts of bands (e.g. band heads), as indicative of the intensity of the whole band. Such 'fractional band intensities' should be most useful when the fraction of the band chosen is known with accuracy. As indicated in §§ 2.1 and 2.2, the fraction of intensity associated with a well-developed band head will depend upon v' and may therefore be expected to be roughly constant in v'' progressions. When sufficient dispersion is available, individual band lines may be used as indicative of the intensity of the whole band (see §§ 2.3, 2.4). In the following $I_{h v' v''}$ denotes band head intensity.

2.1. *The CN Violet* ($B^2\Sigma^+ \rightarrow X^2\Sigma^+$) *Band System*

Bands of this system are strongly overlapped within the sequences $\Delta v = -2$, -1, 0 and the sequences are fairly well separated from each other. Consequently Ornstein and Brinkman (1931) measured band head (P branch) intensities in emission by photographic photometry of the bands which lie in the wavelength range 4606–3584 Å. The bands were excited in a carbon arc in air. Each band head intensity was corrected for the effect of overlap with the tail (R branch) of the preceding band. Ornstein and Brinkman determined the vibrational temperature T from the slope of the line $[\log(\Sigma_{v''} I_{v'v''}/E_{v'v''}{}^4), v']$. They then determined $N_{v'}/N_0$ from

$$N_{v'}/N_0 = \exp(-E_{v'}/kT) \qquad \ldots\ldots(13)$$

and evaluated a set of relative vibrational transition probabilities $p_{h v' v''}$ by use of equation (8) on *each* of the measured bands. A partial list of these measured $p_{h v' v''}$ is given in table 1.

The variation of electronic transition moment with internuclear separation was obtained from the band head intensities as follows: A plot (figure 1(*a*)) was made for each v'' progression of $(I_{h v' v''}/q_{v' v''} E_{v' v''}{}^4)^{1/2}$ against $\bar{r}_{v' v''}$. The published values of $I_{h v' v''}/E_{v' v''}{}^4$ of Ornstein and Brinkman were employed for those bands ($0 < v' < 3$; $0 < v'' < 3$) for which the Franck–Condon factors computed on the basis of a Morse model were available (Fraser, Jarmain and Nicholls 1954), and also for which the r-centroids were available (see I).

It will be noticed in figure 1(*a*) that although the points for each progression evidently indicate a rise of $R_e(r)$ with r, there is a displacement in ordinate from progression to progression. The displacement is due to two causes: (*a*) the variation in $N_{v'}$ from progression to progression and (*b*) the variation with v' of the fraction of the total band intensity vested in the head. The effect of (*b*) will be discussed in more detail in the case of the C_2 Swan system below. In order to represent the behaviour of $R_e(r)$ over the complete range of r for the system, the segments, one for each progression, must be placed upon the same ordinate scale. The objective rescaling procedure which was employed has been described by Turner and Nicholls (1954b). The segment which extends over the greatest

Table 1. Basic Data for the CN Violet ($B^2\Sigma^+ \rightarrow X^2\Sigma^+$) Band System

Band	$\lambda_{v'v''}$(Å)	$I_{hv'v''}/E_{v'v''}{}^4$	$p_{hv'v''}$	$q_{v'v''}$	$\bar{r}_{v'v''}$(Å)	$p_{v'v''}$
0,0	3883·4	1000	1000	0·92	1·166	1000
0,1	4216·0	55	55	0·074	1·046	58
0,2	4606·1	3	3	0·005	0·966	3
1,0	3590·4	97	160	0·079	1·291	120
1,1	3871·4	514	870	0·787	1·176	880
1,2	4197·2	57	95	0·121	1·046	94
1,3	4578	4·1	7	0·014	0·982	9
2,1	3585	102	290	0·137	1·305	210
2,2	3861·9	271	770	0·691	1·186	790
2,3	4181·0	43	120	0·147	1·043	110
3,2	3583·9	51	240	0·180	1·320	280
3,3	3854·7	137	670	0·625	1·198	740

$\lambda_{v'v''}$(Å)=wavelength; $I_{hv'v''}/E_{v'v''}{}^4$ (arbitrary units)=reduced band head intensity (Ornstein and Brinkman 1931); $p_{hv'v''}$ (arbitrary units)=experimental relative vibrational transition probability (Ornstein and Brinkman 1931); $q_{v'v''}$=Franck–Condon factor (Fraser, Jarmain and Nicholls 1954); $\bar{r}_{v'v''}$(Å)=r-centroid (Nicholls and Jarmain 1956); $p_{v'v''}$=smoothed relative vibrational transition probability: from equation (9), arbitrary units adjusted to make p_{00}=1000, third significant figure ' indicative of trends ' only.

range of r was adopted as standard ($v'=1$ segment in this case) and the other segments are plotted on the same ordinate scale by use of a scaling factor for each segment. The factor is derived from the quotient of the areas under the two segments in the region of overlap.

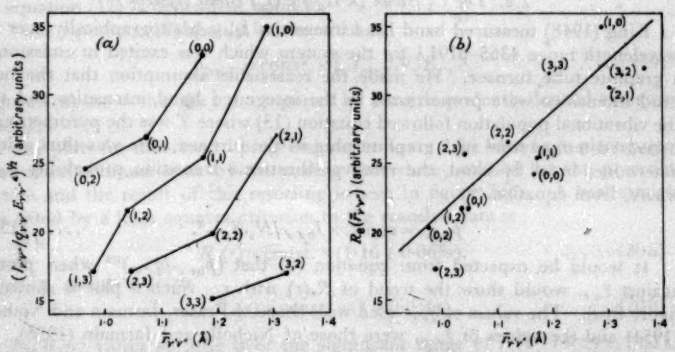

Figure 1. Variation of the electronic transition moment with internuclear separation for the CN violet band system; (*a*), plots for individual v''-progressions; (*b*), plot, after rescaling data of individual progressions, for the whole system.

The apparent rise of $R_e(r)$ with r here was most simply represented by an empirical linear relationship. By applying the least squares method the best

straight line was found to be

$$R_e(r) = \text{const.} \times (35{\cdot}38r - 13{\cdot}72), \qquad \ldots\ldots(14a)$$

or, in 'standard form'

$$R_e(r) = \text{const.} \times (-1 + 2{\cdot}579r). \qquad \ldots\ldots(14b)$$

These equations adequately represent the behaviour of the electronic transition moment for the CN violet system over the range of $0{\cdot}95\,\text{Å} < r < 1{\cdot}32\,\text{Å}$. Equation (14*a*) and rescaled points are represented graphically in figure 1(*b*). For the purposes of comparison with other band systems equation (14*a*) has also been recast, by virtue of the arbitrary multiplicative constant, into the 'standard form' of equation (14*b*). Here the magnitude of the constant term in the polynomial in r (linear in this case) has been adjusted to unity. The scatter of points in figure 1(*b*) about the line is due to varying errors both in measured band intensities and also in the Franck–Condon factors. The errors in intensity measurement have been referred to in §1. Errors in Franck–Condon factors may arise from inadequacy of model of molecular potential adopted. A set of 'smoothed' values of $R_e^2(\bar{r}_{v'v''})$ was obtained from equation (14*a*) and multiplied by the appropriate Franck–Condon factors $q_{v'v''}$ to give a 'smoothed' set of $p_{v'v''}$ for the system. The resulting $p_{v'v''}$ are expressed in table 1 on a scale where $p_{00} = 1000$.

Table 1 contains the basic data used for the system and compares the 'smoothed' values of $p_{v'v''}$ with the values $p_{hv'v''}$ originally published by Ornstein and Brinkman. Agreement between the two is fairly good: this may be due in part to the fact that Ornstein and Brinkman used a smoothing procedure (which involved all of their measurements) to determine $N_{v'}$.

2.2. *The C_2 Swan ($A^3\Pi_g \rightarrow X^3\Pi_u$) Band System*

King (1948) measured band head intensities $I_{hv'v''}$ photographically over the wavelength range 4365–6191 Å for the system which was excited in emission in a graphite tube furnace. He made the reasonable assumption that the band head intensities were proportional to the integrated band intensities and that the vibrational population followed equation (13) where T was the pyrometrically measured temperature of a graphite plug in the furnace. He was thus able to determine, band by band, the relative vibrational transition probability $p_{hv'v''}$ where, from equation (8)

$$p_{hv'v''} = \text{const.} \times I_{hv'v''}/N_{v'}E_{v'v''}^4. \qquad \ldots\ldots(15)$$

It would be expected from equation (9) that $(p_{hv'v''}/q_{v'v''})^{1/2}$ when plotted against $\bar{r}_{v'v''}$ would show the trend of $R_e(r)$ with r. Such a plot is shown in figure 2(*a*). The values of $q_{v'v''}$ used were those of Fraser, Jarmain and Nicholls (1954) and the values of $\bar{r}_{v'v''}$, were those of Nicholls and Jarmain (1956).

It will be observed in figure 2(*a*) that approximate constancy of $R_e(r)$ is obtained in each v'' progression, but that there is a regular displacement in ordinate from one v'' progression to the next. The displacement seems to be due almost entirely to a dependence upon v' of the fraction of total band intensity vested in the band head, as in this case allowance has been made by King for the variation of $N_{v'}$ with v'. The effect of variation with v' in fraction of band intensity located in the band head may be seen as follows:

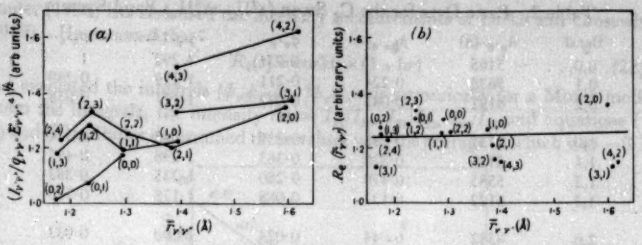

Figure 2. Variation of the electronic transition moment with internuclear separation for the C_2 Swan band system; (*a*), plots for individual v''-progressions; (*b*), plot, after rescaling data of individual progressions, for the whole system.

The intensity I_J of the Jth band line may be written as

$$I_J = \text{const.} \times E_J^4 S_J \exp(-B_{v'}J(J+1)/kT_R) \qquad \ldots\ldots(16)$$

where S_J is the line strength factor and depends upon the character of the electronic transition and upon J. E_J is the energy quantum associated with the line, and (Phillips 1948) the rotational constant $B_{v'}$ of the $A^3\Pi$ state of C_2 is

$$B_{v'} = 1{\cdot}7527 - 0{\cdot}01608(v'+\tfrac{1}{2}) - 0{\cdot}001274(v'+\tfrac{1}{2})^2\,\text{cm}^{-1}. \qquad \ldots\ldots(17)$$

The fraction $f_{v'}$ of the band vested in the head will be

$$f_{v'} = \sum_{\text{Head}} I_J / \sum_{\text{Band}} I_J. \qquad \ldots\ldots(18)$$

The exponential term in equation (16) is dominant in determining $f_{v'}$, which by equation (17) is dependent upon v'.

Thus equation (15) should be rewritten as

$$p_{h\,v'v''} = \text{const.} \times f_{v'} I_{v'v''} / N_{v'} E_{v'v''}^4. \qquad \ldots\ldots(19)$$

Figure 2(*a*) shows that the $p_{h\,v'v''}$ reported by King do evidently depend somewhat upon $f_{v'}$.

The plots for different v'' progressions on figure 2(*a*) have been placed upon a common ordinate scale by the scaling procedure outlined for the preceding system and the result of this rescaling is seen in figure 2(*b*). A best straight line fitted by a least squares criterion to the rescaled data is

$$R_e(r) = \text{const.} \times (1{\cdot}16 + 0{\cdot}065r). \qquad \ldots\ldots(20a)$$

Thus in 'standard form'

$$R_e(r) = \text{const.} \times (1 + 0{\cdot}056r). \qquad \ldots\ldots(20b)$$

As $R_e(r)$ varies so little over the significant range of r ($1{\cdot}17\,\text{Å} < r < 1{\cdot}62\,\text{Å}$), it may be considered constant and it is therefore safe to conclude that for this system the Franck–Condon factors are a relatively reliable measure of the vibrational transition probability.

Table 2 contains the basic data. $\bar{r}_{20}$, which is not included in I, was obtained by the graphical method described therein. $\bar{r}_{31}$ and $\bar{r}_{42}$ were then determined by a small extrapolation on a curve of $\bar{r}_{v'v''}$ against $\lambda_{v'v''}$.

Table 2. Basic Data for the C_2 Swan ($A^3\Pi_g \rightarrow X^3\Pi_u$) Band System

Band	$\lambda_{v'v''}$(Å)	$p_{hv'v''}$	$q_{v'v''}$	$\bar{r}_{v'v''}$(Å)	$p_{v'v''}$
0,0	5165	1	0·731	1·292	1
0,1	5635	0·224	0·211	1·229	0·289
0,2	6191	0·043	0·042	1·171	0·058
1,0	4737	0·358	0·237	1·349	0·324
1,1	5129	0·520	0·363	1·298	0·497
1,2	5585	0·470	0·280	1·235	0·383
1,3	6122	0·123	0·088	1·178	0·120
2,0	4382	0·044	0·024	1·600	0·033
2,1	4715	0·525	0·356	1·385	0·487
2,2	5097	0·256	0·162	1·303	0·222
2,3	5540	0·497	0·280	1·240	0·383
2,4	6059	0·188	0·124	1·184	0·170
3,1	4371	0·111	0·060	1·610	0·082
3,2	4697	0·718	0·405	1·391	0·554
3,4	5501	0·802	0·265	1·245	0·360
4,2	4365	0·252	0·097	1·620	0·133
4,3	4684	0·952	0·427	1·397	0·584

$\lambda_{v'v''}$(Å)=wavelength; $f_{hv'v''}$ (arbitrary units)=experimental relative vibrational transition probability (King 1948); $q_{v'v''}$=Franck–Condon factor (Fraser, Jarmain and Nicholls 1954); $\bar{r}_{v'v''}$(Å)=r-centroid (Nicholls and Jarmain 1956); $p_{v'v''}$=smoothed relative vibrational transition probability from equation (9), arbitrary units adjusted to make $p_{00}=1$.

2.3. *The OH Violet* ($A^2\Sigma^+ \rightarrow X^2\Sigma^+$) *Band System*

Photographic intensity measurements of individual band lines of the system were made by Dieke and Crosswhite (1948) and reported in the well-known 'Bumblebee Report No. 87' in the form of relative vibrational transition probabilities. Improved photoelectric intensity measurements upon the P branches of bands between 2811 and 3428 Å were made by the same authors Dieke and Crosswhite (1949).† Measurements were also made upon the R branch in the case of the 0–0 band and were interpreted as measured relative vibrational transition probabilities $p_{mv'v''}$.

Figure 3 shows a plot of $(p_{mv'v''}/q_{v'v''})^{1/2}$ against $\bar{r}_{v'v''}$ for the system which, according to equation (9) is equivalent to a plot of $R_e(\bar{r})_{v'v''}$ against $\bar{r}_{v'v''}$. The $p_{mv'v''}$ were taken from the 1949 data of Dieke and Crosswhite, the $q_{v'v''}$ were evaluated upon a Morse model by Jarmain, Fraser and Nicholls (1955) and the $\bar{r}_{v'v''}$ were computed by Nicholls and Jarmain (1956).

As figure 3 appears to be linear, a least squares best straight line was fitted over the range $0{\cdot}8<r<1{\cdot}3$ Å to the points in the figure. It was

$$R_e(r)=\text{const.}\times(185-140r) \qquad \ldots\ldots(21\,a)$$

which can be recast in 'standard form' as

$$R_e(r)=\text{const.}\times(1-0{\cdot}756r). \qquad \ldots\ldots(21\,b)$$

† The author is very grateful to Dr. R. C. Herman of the Johns Hopkins University for making available a copy of the *Quarterly Report*, Oct. 1st–Dec. 31st, 1949, Contract NOrd 8036 JHB-3 Problem A, in which the improved measurements were reported, and also to Dr. G. H. Dieke for permission to use these unpublished results.

Shuler (1950) has also used the intensity measurements of Dieke and Crosswhite (1949). He *assumed* that

$$R_e(r) = \text{const.} \times (1 + ar) \qquad \ldots\ldots(22)$$

and evaluated the integrals $\int \psi_{v'} \psi_{v''} dr$, $\int \psi_{v'} \psi_{v''} r\, dr$ numerically for a Morse model. From the integrals, the intensity ratios I_{11}/I_{10}, I_{21}/I_{22}, I_{32}/I_{33} and equations (7), (8) and (22), Shuler determined three values of a, the average of which was $-0{\cdot}75$.

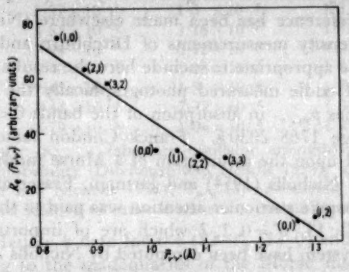

Figure 3. Variation of the electronic transition moment with internuclear separation for the OH violet band system.

It will be noted that equation (21 *b*) confirms this value and, together with figure 3, also confirms the *assumption* made by Shuler of a linear relationship between $R_e(r)$ and r for this system.

In so far as the scatter of points about the line in figure 3 is concerned, it is probably due to error not only in the intensity measurements but also in the Franck–Condon factors. Chamberlain and Roesler (1955) have shown that the ground $x^2\Pi$ state of this system is not too well represented by a Morse potential and thus except for the lowest values of v'', the $q_{v'v''}$ may be somewhat in error. However, as has been previously pointed out, the smoothing procedure reduces the effect of errors in Franck–Condon factors and intensities and allows a

Table 3. Basic Data for the OH Violet ($A^2\Sigma^+ \rightarrow X^2\Pi$) Band System

Band	$\lambda_{v'v''}$(Å)	$I_{mv'v''}$	$q_{v'v''}$	$\bar{r}_{v'v''}$(Å)	$p_{v'v''}$
0,0	3064	1000	0·907	1·010	1000
0,1	3428	5	0·089	1·270	3
1,0	2811	480	0·086	0·835	231
1,1	3122	780	0·716	1·050	600
1,2	3484	13	0·186	1·300	1
2,1	2875	680	0·169	0·885	366
2,2	3185	520	0·514	1·090	313
3,2	2945	810	0·237	0·925	423
3,3	3254	300	0·321	1·130	134

$\lambda_{v'v''}$(Å)=wavelength; $I_{mv'v''}$ (arbitrary units)=experimental relative vibrational transition probability (Dieke and Crosswhite 1949); $q_{v'v''}$=Franck–Condon factor (Jarmain, Fraser and Nicholls 1955); $\bar{r}_{v'v''}$(Å)=r-centroid (Nicholls and Jarmain 1956) $p_{v'v''}$=smoothed relative vibrational transition probability from equation (9), arbitrary units adjusted to make p_{00}=1000, third significant figure ' indicative of trends ' only.

'smoothed' array of relative vibrational transition probabilities to be derived in which *all* the data contribute to the determination of each $p_{v'v''}$.

Table 3 contains the basic data employed here together with a set of smoothed values of $p_{v'v''}$. The values of $\bar{r}_{10}$, $\bar{r}_{21}$ and $\bar{r}_{32}$ were obtained by extrapolation using the almost linear ($\bar{r}_{v'v''}$, $\lambda_{v'v''}$) relationship which exists in this case.

2.4. *The* O_2 *Schumann–Runge Band System* ($B^3\Sigma_u^- \rightarrow X^3\Sigma_g^-$)

Although brief reference has been made elsewhere (Nicholls 1956) to the treatment of the intensity measurements of Ditchburn and Heddle (1954) for this system, it will be appropriate to include here the results of this analysis.

Ditchburn and Heddle measured photographically the relative vibrational transition probabilities $p_{m v'v''}$ in absorption of the bands $0<v'<20$, $v''=0$ over the wavelength range 1768–2030 Å. Franck–Condon factors for this system have been computed upon the assumption of a Morse model by Pillow (1950), Fraser, Jarmain and Nicholls (1954) and Jarmain, Fraser and Nicholls (1955). In the last of these papers particular attention was paid to the very small factors for the bands $0<v'<15$, $v''=0, 1, 2$ which are of importance in absorption. r-centroids for this system have been computed by Nicholls and Jarmain (1956).

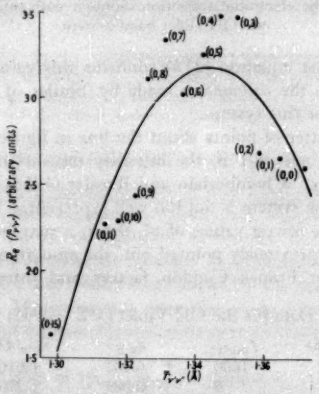

Figure 4. Variation of the electronic transition moment with internuclear separation for the O_2 Schumann–Runge band system.

To find the form of $R_e(r)$ equation (9) was employed. Values of $(p_{m v'v''}/q_{v'v''})^{1/2}$ are plotted against $\bar{r}_{v'v''}$ in figure 4. It was found that the empirical 'least squares' parabola

$$R_e(r)=(-825r^2+2220r-919) \qquad \ldots\ldots(23\,a)$$

could be fitted to the points over the range $1{\cdot}295\,\text{Å}<r<1{\cdot}375\,\text{Å}$. As the values of $p_{m v'v''}$ given by Ditchburn and Heddle are absolute oscillator strengths, no arbitrary constant is involved in equation (23 *a*). However, the standard form of equation (23 *a*) for comparison with other systems is seen in equation (23 *b*)

$$R_e(r)=\text{const.}\times(-1+2{\cdot}416r-0{\cdot}897r^2). \qquad \ldots\ldots(23\,b)$$

A relatively large variation of $R_e(r)$ with r is noted.

Smoothed relative vibrational transition probabilities $p_{v'v''}$ computed from equation (9) are included in table 4 which contains the other basic data. At the

Table 4. Basic Data for O_2 Schumann–Runge ($B^3\Sigma_u^- \rightarrow X^3\Sigma_g^-$) Band System

Band	$\lambda_{v'v''}$(Å)	$p_{mv'v''}$	$q_{v'v''}$	$\bar{r}_{v'v''}$(Å)	$p_{v'v''}$
0,0	2030	$1{\cdot}55\times10^{-8}$	$2{\cdot}31\times10^{-9}$	1·372	$2{\cdot}08\times10^{-8}$
1,0	1997·5	$1{\cdot}89\times10^{-7}$	$2{\cdot}69\times10^{-8}$	1·365	$2{\cdot}76\times10^{-7}$
2,0	1971·4	$1{\cdot}18\times10^{-6}$	$1{\cdot}64\times10^{-7}$	1·359	$1{\cdot}48\times10^{-6}$
3,0	1946·7	$8{\cdot}35\times10^{-6}$	$6{\cdot}94\times10^{-7}$	1·353	$5{\cdot}84\times10^{-6}$
4,0	1923·5	$2{\cdot}76\times10^{-5}$	$2{\cdot}28\times10^{-6}$	1·348	$2{\cdot}64\times10^{-5}$
5,0	1901·9	$6{\cdot}65\times10^{-5}$	$6{\cdot}3\times10^{-6}$	1·343	$5{\cdot}67\times10^{-5}$
6,0	1881·7	$1{\cdot}37\times10^{-4}$	$1{\cdot}5\times10^{-5}$	1·337	$1{\cdot}26\times10^{-4}$
7,0	1863	$3{\cdot}53\times10^{-4}$	$3{\cdot}18\times10^{-5}$	1·332	$3{\cdot}46\times10^{-4}$
8,0	1845·8	$5{\cdot}94\times10^{-4}$	$6{\cdot}12\times10^{-5}$	1·327	$5{\cdot}88\times10^{-4}$
9,0	1830·1	$6{\cdot}40\times10^{-4}$	$1{\cdot}08\times10^{-4}$	1·323	$1{\cdot}11\times10^{-3}$
10,0	1815·6	$9{\cdot}45\times10^{-4}$	$1{\cdot}8\times10^{-4}$	1·318	$1{\cdot}41\times10^{-3}$
11,0	1803·1	$1{\cdot}44\times10^{-3}$	$2{\cdot}77\times10^{-4}$	1·314	$1{\cdot}35\times10^{-3}$
15,0	1767·1	$2{\cdot}79\times10^{-3}$	$1{\cdot}04\times10^{-3}$	1·298	$2{\cdot}04\times10^{-3}$

$\lambda_{v'v''}$(Å)=wavelength; $p_{mv'v''}$ (absolute oscillator strength)=experimental relative vibrational transition probability (Ditchburn and Heddle 1954); $q_{v'v''}$=Franck–Condon factor (Jarmain, Fraser and Nicholls 1955); $\bar{r}_{v'v''}$(Å)=r-centroid (Nicholls and Jarmain 1956); $p_{v'v''}$=smoothed relative vibrational transition probability from equation (9).

suggestion of Dr. Heddle,† data for the (12–0), (13–0) and (14–0) bands have not been used owing to the inadequacies of the Morse model for the $v'=12$, 13, 14 levels of the upper ($B^3\Sigma_u^-$) state.

§ 3. Discussion

From the above analyses, and also those of Turner and Nicholls (1954 a, b), and of Wallace and Nicholls (1955) it is clear that for the seven band systems involved, the electronic transition moment is *not* independent of internuclear separation, except possibly in the case of the C_2 Swan system. Thus, the assumptions often made that $R_e(r)$ is independent of r, and that the Franck–Condon factors $q_{v'v''}$ control almost entirely the intensity distribution within a band system, are by no means necessarily valid. A knowledge of the variation of $R_e(r)$ with r and of the factors which determine the variation for a system is thus important.

One very crude index of the variation of $R_e(r)$ with r over the significant range of r for the system is $\Delta R_e/\bar{R}_e$. Here ΔR_e is the maximum variation of R_e encountered, and $\bar{R}_e$ is its average value, over the system. Table 5 records $\Delta R_e/\bar{R}_e$ for the seven band systems for which information is available. The relative change in $R_e(r)$ across a band system appears to vary by a factor which lies between 0·017 and 1·83 for the seven band systems.

Table 5. Relative Variation ($\Delta R_e/R_e$) of Electronic Transition Moment over Band System

Band System	$\Delta R_e/\bar{R}_e$
1. C_2 Swan ($A^3\Pi_g \rightarrow X^3\Pi_u$)	0·02
2. N_2^+ First Negative : ($B^2\Sigma_u^+ \rightarrow X^2\Sigma^+$)	0·25
3. CN Violet : ($B^2\Sigma^+ \rightarrow X^2\Sigma^+$)	0·47
4. N_2 Second Positive : ($C^3\Pi_u \rightarrow B^3\Pi_g$)	0·54
5. O_2 Schumann–Runge : ($B^3\Sigma_u^- \rightarrow X^3\Sigma_g^-$)	0·72
6. N_2 First Positive : ($B^3\Pi_g \rightarrow A^3\Sigma_u^+$)	0·86
7. OH Violet : ($A^2\Sigma^+ \rightarrow X^2\Pi$)	1·83

Note : (i) ΔR_e is the maximum variation of $R_e(r)$ over the system.
(ii) $\bar{R}_e$ is the average value of $R_e(r)$ for the system.
(iii) For 1, 3, 5, 7 see this paper; for 6 see Turner and Nicholls (1954 a, b); for 2, 4 see Wallace and Nicholls (1955)

† The author would like to acknowledge with thanks valuable correspondence with Professor Ditchburn and Dr. Heddle.

The variation of $R_e(r)$ with r is not unexpected, as the electronic wave functions and also the multipole moment which occur in equation (6) are in general dependent on r. A relatively larger variation in $R_e(r)$ over a band system would be expected when there is a large change in the configuration of the electron charge cloud between the two electronic states involved in the transition than when there is a small change in the charge cloud configuration. While no detailed conclusions can be drawn concerning the change in electron cloud configuration from the information in table 5, it is consistent with the suggestion of Bates (1949) that the variation of $R_e(r)$ with r will be larger for perpendicular band systems ($\Delta\Lambda = \pm 1$) than for parallel band systems ($\Delta\Lambda = 0$). The N_2 First Positive and OH band systems are perpendicular ($\Pi \longleftrightarrow \Sigma$) while all the others are parallel ($\Sigma \longleftrightarrow \Sigma$, $\Pi \longleftrightarrow \Pi$).

It is very desirable to perform a theoretical study of the electronic transition moment (Fraser 1954 b). A major requirement in such work is extreme accuracy in the electronic wave functions and a start has been made in this direction (Sahni 1955 a, b, c, 1956). It is also very desirable to measure the intensity distribution of further band systems in order that the behaviour of the electronic transition moment may be studied experimentally. Arrays of smoothed relative vibrational transition probabilities which are still not available for many important band systems could thereby be obtained.

For some band systems whose intensity distributions have not been measured, it has been found possible to use the published eye estimates (after application of a criterion of quantitative significance) together with Franck–Condon factors and r-centroids to derive preliminary information on the behaviour of $R_e(r)$ with r and on the source conditions (Nicholls 1954). For the N_2 First and Second Positive systems, eye estimates lead to substantially the same conclusions regarding $R_e(r)$ as do the measured band intensities. This fact increases confidence in the method for use as an interim procedure until measured band intensities are available. It is interesting to record in this connection that $R_e(r)$ appears to be almost independent of r for the NO β ($B^2\Pi \rightarrow X^2\Pi$) and NO γ ($A^2\Sigma \rightarrow X^2\Pi$) systems, while it appears to be strongly dependent on r for the O_2 Herzberg ($A^3\Sigma_u^+ \rightarrow X^3\Sigma_g^-$) system (Nicholls 1956). For NO the eye estimates were taken from *The Identification of Molecular Spectra* (Pearse and Gaydon 1950), while for O_2 the estimates of Broida and Gaydon (1954) were employed.

Acknowledgment

This work has been made possible through the support of the Air Force Cambridge Research Centre by Contract AF 19 (604)-1718.

References

Bates, D. R., 1949, *Proc. Roy. Soc.* A, **196**, 217; 1952, *Mon. Not. R. Astr. Soc.*, **112**, 614.

Broida, H. P., and Gaydon, A. G., 1954, *Proc. Roy. Soc.* A, **222**, 181.

Chamberlain, J. W., and Roesler, F. L., 1955, *Astrophys. J.*, **121**, 541.

Dieke, G. H., and Crosswhite, H. M., 1948, *The Ultra Violet Bands of OH: Fundamental Data*, Bumblebee Report No. 87, Department of Physics, The Johns Hopkins University, Contract NOrd 8036; 1949, Quarterly Report Oct. 1–Dec. 31 Contract NOrd 8036 JHB–3 Problem A.

Ditchburn, R. W., and Heddle, D. W. O., 1954, *Proc. Roy. Soc.* A, **226**, 509.

Fraser, P. A., 1954 a, *Canad. J. Phys.*, **32**, 515; 1954 b, *Approximate Calculations of Electronic Transition Moment*, Scientific Report No. 17, Department of Physics, University of Western Ontario, Contract AF 19(122)–470.

FRASER, P. A., JARMAIN, W. R., and NICHOLLS, R. W., 1954, *Astrophys. J.*, **119**, 286.

JARMAIN, W. R., FRASER, P. A., and NICHOLLS, R. W., 1953, *Astrophys. J.*, **118**, 228; 1955, *Ibid.*, **122**, 55.

KING, A. B., 1948, *Astrophys. J.*, **108**, 429.

NICHOLLS, R. W., 1954, *Canad. J. Phys.*, **32**, 722; 1956, *Airglow and Aurora Conference, Belfast* 1955, (London : Pergamon Press), in the press.

NICHOLLS, R. W., and JARMAIN, W. R., 1956, *Proc. Phys. Soc.* A, **69**, 253.

ORNSTEIN, L. S., and BRINKMAN, H., 1931, *Proc. Roy. Acad. Amsterdam*, **34**, 33.

PEARSE, R. W. B., and GAYDON, A. G., 1950, *The Identification of Molecular Spectra*, 2nd edn. (London : Chapman and Hall).

PHILLIPS, J. G., 1948, *Astrophys. J.*, **108**, 434.

PILLOW, M. E., 1950, *Proc. Phys. Soc.* A, **63**, 940; 1951, *Ibid.* **64**, 772; 1953 a; *Ibid.*, **66**, 733; 1953 b, *Ibid.*, **66**, 1064.

SAHNI, R. C., 1955 a, *Automatic Computation of Electronic Wave Functions*, Department of Physics, University of Western Ontario, Contract AF 19(122)–470, Scientific Report No. 19; 1955 b, *Automatic Computation of the Electronic Wave Functions of the* $B^2\Sigma_u^+$ *and* $X^2\Sigma_g^+$ *States of the* N_2^+ *Molecule*, Ibid., No. 21; 1955 c, *The Electronic Structure of* BH, Ibid, No. 22; 1956, *J. Chem. Phys.* **25**, 332.

SHULER, K. E., 1950, *J. Chem. Phys.* **18**, 1221.

TURNER, R. G., and NICHOLLS, R. W., 1954 a, *Canad. J. Phys.*, **32**, 468; 1954 b, *Ibid.*, **32**, 475.

WALLACE, L. V., and NICHOLLS, R. W., 1955, *J. Atmos. Terr. Phys.*, **7**, 101.

An Investigation of the Reactions: $^{10}B(d, n)^{11}C$ and $^{11}B(d, n)^{12}C$

By E. E. MASLIN, J. M. CALVERT† and A. A. JAFFE†
Nuclear Physics Research Laboratory, University of Liverpool

Communicated by H. W. B. Skinner; *MS. received 21st March* 1956

Abstract. The $^{10}B(d, n)^{11}C$ and $^{11}B(d, n)^{12}C$ reactions have been investigated by bombarding the separated isotopes of ^{10}B and ^{11}B with a beam of 9 Mev deuterons and analysing the neutron groups with a fast-neutron spectrometer. Angular distributions and cross sections for a number of neutron groups have been measured. The theory of the stripping process has been applied to assign parities to levels in ^{11}C and ^{12}C and to obtain information about the spins of these levels.

§ 1. Introduction

An investigation has been made of the angular distributions of certain neutron groups from the reactions: $^{10}B(d, n)^{11}C$ and $^{11}B(d, n)^{12}C$, initiated by the bombardment of targets of the separated isotopes ^{10}B and ^{11}B with a beam of 9 Mev deuterons from the Liverpool University 37 in. cyclotron. The ground state Q-values of the two reactions are 6·47 and 13·7 Mev respectively giving maximum neutron energies of 15·5 and 22·7 Mev.

The reaction $^{10}B(d, n)^{11}C$ has been studied previously by Paris and Endt (1954) at the low deuteron energy of 0·3 Mev. They measured the angular distributions of the three highest energy neutron groups, using the photographic plate technique. Johnson (1952) has measured the neutron spectra for both $^{10}B(d, n)^{11}C$ and $^{11}B(d, n)^{12}C$, at 3·6 Mev, with photographic plates and these measurements proved of value in identifying certain neutron groups, while Gibson (1949) using deuterons of 0·8 Mev has also measured the neutron spectra from these two reactions. Previous work on the reaction $^{11}B(d, n)^{12}C$ has been done at 0·6 Mev by Ward and Grant (1955), at 0·8 Mev by Ihsan (1955), at 0·85 Mev by Graue (1954) and at 8·1 Mev by Gibson (1953) again using the photographic plate technique.

§ 2. Experimental

The neutron spectra were analysed with a fast-neutron spectrometer using scintillation counters which has been described in a previous paper (Calvert *et al.* 1955). In the present investigation the experimental arrangement was similar to that of the previous work. The targets of the separated isotopes of ^{10}B and ^{11}B were deposited on a gold backing, and were of thicknesses 2·2 mg cm^{-2} and 2·3 mg cm^{-2} respectively. Neutrons from these targets were analysed, over an

† Now at the University of Manchester.

energy range of from 7 to 23 Mev, at various angles between 0° and 60° with respect to the direction of the incident neutron beam.

§ 3. Results

Figure 1 shows one neutron spectrum obtained from each of the reactions studied. It should be noted that the relative intensities of the neutron groups in these spectra depend upon the efficiency of the spectrometer which is a

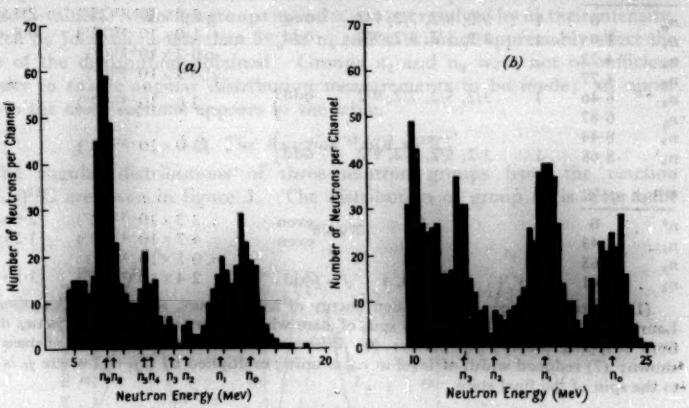

Figure 1. (*a*) Neutron energy spectrum obtained at 20° from $^{10}B(d, n)^{11}C$. (*b*) 30° spectrum from $^{11}B(d, n)^{12}C$.

function of neutron energy. Angular distributions have been plotted for those neutron groups which could be identified and resolved, and are shown in figures 2 and 3, the errors on the points being statistical probable errors. The distributions are seen to be characteristic of those expected according to stripping theory and have been compared with theoretical curves calculated by means of the theory of Butler (1951), using a value for the radius parameter of $(1{\cdot}7 + 1{\cdot}22A^{1/3}) \times 10^{-13}$ cm. In addition, the absolute cross sections for the reactions were measured and a summary of the experimental results is given in the table.

3.1. *The Reaction* $^{10}B(d,n)^{11}C$

The angular distributions of the neutron groups (n_0, n_1) corresponding to the formation of ^{11}C in its ground and first excited states are shown in figure 2. Theoretical curves, calculated by means of Butler's theory for an angular momentum transfer of $l=1$, are drawn in each case and show a good fit to the experimental points. Paris and Endt working with deuterons of 0·3 Mev suggest $l=1$ and $l=3$ for n_0 and n_1 but in view of the low deuteron energy it is not certain that the stripping process is responsible for their distribution.

On the basis of the neutron spectra obtained by Johnson we conclude that the two prominent neutron groups designated n_4, n_5 and n_8, n_9 in the spectrum of figure 1 consist of, in each case, two closely spaced levels not resolved by us. Thus we can only plot distributions for the combined levels and these are given

in figure 2. Both these distributions show the anomalous forward dip which has previously been observed in certain cases of neutron groups with negative Q and $l=1$ (Middleton *et al.* 1953). The distributions are predominantly $l=1$ and

(1)	(2)	(3)	(4)	(5)	(6)	(7)
^{10}B(d, n)^{11}C						
n_0	0	1	3/2, 5/2, 7/2, 9/2	odd	$2{\cdot}2\times10^{-27}$(22°)	$2{\cdot}1\times10^{-19}$
n_1	1·9	1	3/2, 5/2, 7/2, 9/2	odd	$1{\cdot}0\times10^{-27}$(22°)	$0{\cdot}8\times10^{-19}$
n_2	4·23				$<0{\cdot}2\times10^{-27}$(0°)	
n_3	4·77				$<0{\cdot}2\times10^{-27}$(0°)	
n_4	6·46	1	3/2, 5/2, 7/2, 9/2	odd	$2{\cdot}6\times10^{-27}$(12°)	
n_5	6·87					
n_8	8·44					
n_9	8·68	1	3/2, 5/2, 7/2, 9/2	odd	$13{\cdot}0\times10^{-27}$(12°)	
^{11}B(d, n)^{12}C						
n^0	0	1	0	even	$3{\cdot}3\times10^{-27}$(22°)	$2{\cdot}6\times10^{-19}$
n_1	4·43	1	2	even	$4{\cdot}7\times10^{-27}$(22°)	$3{\cdot}2\times10^{-19}$
n_2	7·65				$<0{\cdot}5\times10^{-27}$(0°)	
n_3	9·61	2	0, 1, 2, 3, 4	odd	$2{\cdot}4\times10^{-27}$(38°)	$3{\cdot}1\times10^{-19}$

(1) Neutron group; (2) excitation energy of level in MeV, as listed by Ajzenberg and Lauritsen (1955); (3) l-value; (4) spin of state where known or alternative values derived from stripping theory; (5) parity; (6) differential cross section at centre-of-mass angle shown; (7) reduced width of level in c.g.s. units, multiplied by $(2j_f+1)$ where j_f is equal to the spin of the final state.

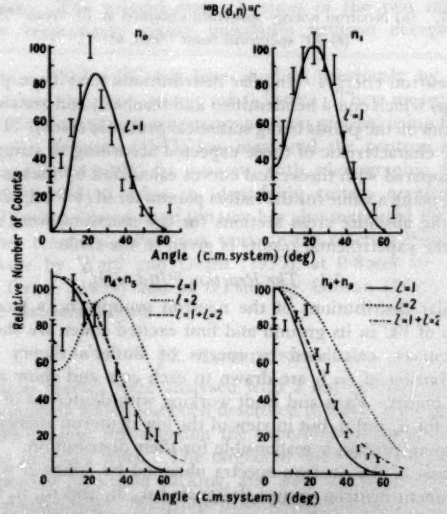

Figure 2. Angular distributions of neutron groups corresponding to the ground state of ^{11}C and states at 1·90, 6·46 and 8·68 MeV.

so, on the basis of the relative intensities of n_4, n_5 and of n_8, n_9 given by Johnson (at 0° and 3·6 MeV), we can say that the more intense member of each of the two groups, namely n_4 and n_9 are formed by capture of $l=1$ protons. It is possible to make a better fit to both the distributions with a curve that is a mixture of $l=1$ and $l=2$ and so one could interpret this as showing that the weaker members of the groups, i.e. n_5 and n_8, have an $l=2$ distribution which would agree with the smaller intensities of these groups. However, this cannot be said with certainty in view of the doubt which attaches to the shape of an $l=1$ distribution at these Q-values. Although groups n_6 and n_7 are not resolved by us their intensity, as given by Johnson, is less than 5% of n_5 and so will not appreciably affect the shape of the distribution obtained. Groups n_2 and n_3 were not of sufficient intensity to enable angular distribution measurements to be made; an upper limit to the cross sections appears in the table.

3.2. *The Reaction* $^{11}B(d,n)^{12}C$

The angular distributions of three neutron groups from the reaction $^{11}B(d,n)^{12}C$ are given in figure 3. The distribution of group n_0 is seen to be

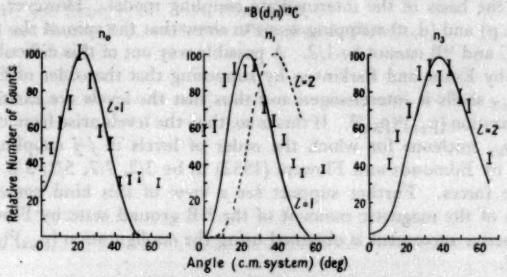

Figure 3. Angular distributions of neutron groups corresponding to the ground state of ^{12}C and states at 4·43 and 9·61 MeV.

characteristic of $l=1$ and is thus in agreement with the previous measurements at low bombarding energies of Ward and of Graue which indicated that this group has an l-value of unity. At the larger energy of 8·1 MeV, Gibson also obtained an indication of $l=1$.

Group n_1 shows the characteristic shape of an $l=1$ curve, in agreement with the work of Gibson.

We cannot resolve a group (n_2) reported by Graue and can only give an upper limit to the cross section for the formation of ^{12}C in this state. The shape of the group n_3 is that of an $l=2$ curve and confirms the indication of $l=2$ found by Graue. Points for 0° and 5° could not be obtained since at these angles the group could not be resolved from other groups of lower energy which appear to peak very strongly in the forward direction suggesting the presence of components having $l=0$.

§ 4. Discussion

The spins and parities of the ground and first excited states of ^{11}C have not been previously measured. The l-value for the corresponding neutron groups ($l=1$) shows the parities of these states to be odd while the spins are restricted

to the values given in the table. In terms of the shell model the ground state would be expected to be 3/2 corresponding to the configuration $(p_{3/2})^7$ and this is compatible with our measurements. Groups n_4 and n_9 also have odd parity since the l-value is again one and this must be regarded as superseding the tentative assignment of even parity made by Johnson. This assignment was made on the basis of intensity measurements at 0° and 80° which were interpreted as indicating $l=0$ behaviour.

It is interesting to compare the $^{10}B(d, n)^{11}C$ reaction with the corresponding (d, p) reaction, namely $^{10}B(d, p)^{11}B$ which gives information about the levels of the mirror nucleus ^{11}B and has been the subject of an investigation by Evans and Parkinson (1954). The form of the distribution for the ground state proton group in their work, being $l=1$, is in agreement with that of the neutron group observed by us. They also find $l=1$ for the transition to the first excited state in agreement with our result for ^{11}C. This is of especial interest because an angular momentum transfer of $l=1$ means that the first excited state cannot have a spin of 1/2. The first excited state of ^{11}B has previously been assigned spin 1/2 by Jones and Wilkinson (1952) and this has also been suggested by Inglis (1953) on the basis of the intermediate coupling model. However, the results of both (d, p) and (d, n) stripping seem to show that the spin of the first excited state of ^{11}C and ^{11}B cannot be 1/2. A possible way out of this difficulty has been suggested by Evans and Parkinson by supposing that the order of filling of the $p_{3/2}$ and $p_{1/2}$ shells is interchanged and thus that the levels are excited states of the configuration $(p_{1/2})^4(p_{3/2})^3$. If this is so, then the levels arise from the coupling of three $p_{3/2}$ nucleons for which the order of levels in j–j coupling has been calculated by Edmonds and Flowers (1952) to be 3/2, 7/2, 5/2, 3/2 and 1/2 for long range forces. Further support for a view of this kind comes from the calculation of the magnetic moment of the ^{11}B ground state by Flowers (1952) in which better agreement is obtained using the configuration $(p_{3/2})^5(p_{1/2})^2$ rather than $(p_{3/2})^7$.

The energy levels of ^{12}C have been tabulated by Ajzenberg and Lauritsen (1955). Spins and parities of the ground and first excited states are known to be 0^+ and 2^+ respectively and, as the present work shows both these levels to be formed by capture of $l=1$ protons, this is in agreement with the generally held view that these levels are states of the $(p)^8$ configuration.

As has been remarked, the neutron group from the formation of the second excited state of ^{12}C is too weak to be observed by us and a possible explanation for this reduced intensity is that the l-value is large, as would be the case if the level were 4^+ for which the lowest possible l-value would be three. Alternatively, if this level is 0^+ as has been suggested by Harries (1954) then angular momentum conservation alone will not explain the absence of the neutron group. In this case the reason would be that the state does not come from the $(p)^8$ configuration but from something more complex which cannot easily be formed from the ground state of ^{11}B.

Since the level at 9·6 Mev is formed by protons with $l=2$, the parity of this level is odd and so probably represents the beginning of the $(p)^7(d)$ configuration.

Acknowledgments

The authors would like to thank Professor H. W. B. Skinner for his continued interest in this work. We also wish to thank the Atomic Energy Research

Establishment, Harwell, for the supply of the separated boron isotopes. One of us (E. E. M.) is grateful to the Department of Scientific and Industrial Research for the award of a maintenance grant.

References

Ajzenberg, F., and Lauritsen, T., 1955, *Rev. Mod. Phys.*, **27**, 77.
Butler, S. T., 1951, *Proc. Roy. Soc.* A, **208**, 559.
Calvert, J. M., Jaffe, A. A., and Maslin, E. E., 1955, *Proc. Phys. Soc.* A, **68**, 1017.
Edmonds, A. R., and Flowers, B. H., 1952, *Proc. Roy. Soc.* A, **215**, 120.
Evans, N. T. S., and Parkinson, W. C., 1954, *Proc. Phys. Soc.* A, **67**, 684.
Flowers, B. H., 1952, *Phil. Mag.*, **43**, 1330.
Gibson, W. M., 1949, *Proc. Phys. Soc.* A, **62**, 586; 1953, *Phil. Mag.*, **44**, 297.
Graue, A., 1954, *Phil. Mag.*, **45**, 1205.
Harries, G., 1954, *Proc. Phys. Soc.* A, **67**, 153.
Ihsan, M. A., 1955, *Proc. Phys. Soc.* A, **68**, 393.
Inglis, D. R., 1953, *Rev. Mod. Phys.*, **25**, 390.
Johnson, V. R., 1952, *Phys. Rev.*, **86**, 302.
Jones, G. A., and Wilkinson, D. H., 1952, *Phys. Rev.*, **88**, 423.
Middleton, R., El-Bedewi, F. A., and Tai, C. T., 1953, *Proc. Phys. Soc.* A, **66**, 95.
Paris, C. H., and Endt, P. M., 1954, *Physica*, **20**, 585.
Ward, A., and Grant, P. J., 1955, *Proc. Phys. Soc.* A, **68**, 637.

The Scattering of 130 MeV Neutrons by Protons

By T. C. RANDLE, D. M. SKYRME, M. SNOWDEN, A. E. TAYLOR, F. URIDGE and E. WOOD
Atomic Energy Research Establishment, Harwell, Berks.

Communicated by D. W. Fry; MS. received 8th May 1956

Abstract. The differential cross section for the scattering of neutrons by protons has been measured at an effective neutron energy of 130 Mev using a diffusion cloud chamber.

An asymmetrical distribution with a minimum at a scattering angle of about 80° in the centre-of-mass system was obtained. This is in contrast to the near symmetry about 90° indicated by measurements at 90 Mev and with the observation of a minimum at about 100° at higher energies.

§ 1. Introduction

Extensive measurements of the differential cross section for the scattering of neutrons by protons have been made with 90 Mev neutrons (Hadley, Kelley, Leith, Segrè, Wiegand and York 1949, Brueckner, Hartsough, Hayward and Powell 1949, Fox 1950, Wallace 1951, Selove, Strauch and Titus 1953, Chamberlain and Easley, 1954, Chung Ying Chih 1954, Stahl and Ramsey 1954) and with those of much higher energies, between 300 and 400 Mev (Dzhelepov and Kazarinov 1954, Hartzler, Siegel and Optiz 1954, De Pangher 1955). In addition, Kelley, Leith, Segrè and Wiegand (1950), Guernsey, Mott and Nelson (1952) and Easley (1954) have worked at energies between 180 and 290 Mev.

Earlier measurements of n–p scattering using neutrons from the Harwell 110 in. synchrocyclotron have been reported; Randle, Taylor and Wood (1952) have used counters to detect the recoil protons over a range of angles extending from 178° to 50°, Thresher, Voss and Wilson (1955) detected scattered neutrons from 61·5° to 6·5°, while Griffith (to be published) observed recoil protons in photographic emulsions over the angular range 58·5° to 19·5°. All the angles mentioned refer to the centre-of-mass system. The effective energies of the neutrons used in these three experiments were 153, 137 and 140 Mev respectively. The present experiment, using a diffusion cloud chamber, was undertaken to supplement and to some extent to integrate these earlier observations. The cloud chamber has the advantage over counting techniques that a very wide angular range can be covered, although it is unfortunately necessary to accept a wide spread in neutron energy and the analysis of the results is extremely laborious.

§ 2. Experimental Method

2.1. *Apparatus*

Neutrons, produced from a lithium deuteride target bombarded by the internal proton beam of the cyclotron, were filtered by 22 in. of polyethylene to increase the relative number of high energy particles. After passing through a horizontal collimator 1 in. wide by $\frac{3}{8}$ in. high in the main shielding wall the neutrons entered

the 18 in. diffusion cloud chamber (Snowden 1953) which contained hydrogen at a pressure of 288 lb in^{-2}. A pair of Helmholtz coils produced a vertical magnetic field of 12 000 oersted uniform to $\pm 1{\cdot}5\%$ over the sensitive volume of the cloud chamber. Recoil proton tracks were photographed by a stereoscopic camera arranged with the optical axes of its lenses vertical and in a plane containing the incident neutron beam. Reference marks fixed to the bottom of the cloud chamber were aligned with the neutron beam and were recorded in each photograph.

Exposures were made once every 30 seconds following the sequence of event shown in table 1, the cyclotron being pulsed for about 0·06 sec to produce neutrons. After an interval of 0·2 sec, which was adequate for the growth of recoil proton tracks, a pair of photographs was taken with an exposure time of about 100 μsec, determined by the duration of the flash. The magnitude of the magnetic field, measured by a calibrated electronic fluxmeter (Snelling and Lewis 1952), was recorded for each photograph. The voltage applied to the clearing field electrode to remove background ions was restored for the remainder of the cycle.

Table 1

Period elapsing (sec)	Operation
	Warning bell
1·0	Magnetic field on
1·2	Clearing field off
0·3	Start of cyclotron pulse
	Fluxmeter read
0·2	Lights flashed
0·1	Magnetic field off
0·3	Clearing field on

The period elapsing is that between succeeding operations.

2.2. *Track Measurements and Calculations*

Measurements of the radius of curvature and the scattering angle of each recoil proton track were made on a scanning table, using the stereoscopic camera to reproject the photographs (Whitby 1953). The position in space of a proton track was found by moving the table until the stereoscopic images of the track coincided. For curvature measurements the table was adjusted to be in the plane defined by (i) the chord of the curved proton track and (ii) the horizontal line perpendicular to the start of the track. The following measurements were made on each track:

(*a*) the coordinates of the start, (*b*) the curvature ρ measured by matching the track to a series of arcs of known radii and choosing the best fit, (*c*) the length of the track, (*d*) the inclination α of the start of the track to the horizontal, (*e*) the horizontal projection θ' of the proton recoil angle. The proton recoil angle θ was calculated using the formula

$$\cos\theta = \cos\alpha \cos\theta'.$$

The proton kinetic energy E_p was usually calculated from the relation

$$100E_p(E_p + 1878) = (3H\rho\cos\alpha)^2$$

where H is the magnetic field in kilooersteds, ρ is in cm and E_p in Mev. However, for protons with an energy less than 30 Mev there was an appreciable change of curvature along the length of the track. The curvature measured by arc matching was shown experimentally to be the curvature near the mid-point of the track and

therefore, using the range–energy relation for protons in hydrogen, it was possible to apply a correction to give the initial energy of these lower energy protons. If a proton came to the end of its range within the sensitive volume of the cloud chamber the length of the track was used to determine E_p; such a proton was distinguished from one leaving the sensitive volume by the heavy ionization and abrupt end that occurred in the former case.

From the values of E_p and θ, the incident neutron kinetic energy E_n was then obtained using

$$E_n = E_p \sec^2\theta \Big/ \left(1 - \frac{E_p}{1878} \tan^2\theta\right)$$

and the scattering angle Φ in the centre-of-mass space from

$$1878 \tan^2 \tfrac{1}{2}(\pi - \Phi) = (E_n + 1878) \tan^2\theta$$

where E_p and E_n are in MeV.

2.3. *Track Acceptance Conditions*

Proton tracks were included in the angular distribution provided that, (*a*) the angle between the plane of scattering and the horizontal was 30° or less, (*b*) the start of the track was within a defined volume in the cloud chamber and (*c*) the calculated energy of the incident neutron was greater than 90 MeV.

Since a distorted angular distribution might have been obtained had any of these conditions varied with scattering angle, the results were examined for any possible sources of variation. It was shown, for all scattering angles, that there was a uniform distribution of the angles which the scattering planes made with the horizontal. It was also verified that the spatial distribution of the start of the tracks was the same for all scattering angles. Distortion caused by any variation in the accuracy of the neutron energy measurements is shown to be small (see § 2.5).

2.4. *Backgrounds*

It has already been stated that measurements were carried out on proton tracks which started within a certain volume of the cloud chamber. Part of this volume was traversed by the collimated neutron beam and part was not. Events starting in the former part were used for the angular distribution and those in the latter part gave a measure of the number of events from uncollimated neutrons. These background events were divided into the same angle groups as were used for the angular distribution and this enabled the background to be subtracted for each angle group. The largest value of this background was 2·6% of the genuine events.

Some of the tracks used in the angular distribution were from the oxygen and carbon content of the methyl alcohol vapour present in the cloud chamber. Their number was estimated by examining photographs taken with the cloud chamber filled with nitrogen. The ratio of single prong to multiprong events produced by the neutron beam in the nitrogen was measured and the ratio was assumed to apply also to oxygen and carbon. From the number of multiprong stars recorded in the n–p experiment it was estimated that not more than 1·5% of the total number of tracks used in the n–p angular distribution were from oxygen and carbon. No correction was applied for this background, but as the number of these one prong events was small and did not have a strong dependence on angle, their effect on the shape of the n–p angular distribution was negligible.

2.5. *Measurement of Neutron Energy Spectrum*

The energy spectrum of the neutrons from the lithium deuteride target was measured in a separate experiment. Recoil protons from matched carbon and polyethylene scatterers were detected at an angle of 10° to the incident neutron beam by a double coincidence scintillation counter telescope which had been calibrated in the external proton beam of the cyclotron. The second counter was thick enough to stop the recoil protons of maximum energy. Making proper allowance for the background and for the energy variation of the neutron–proton scattering cross section at 10°, a pulse height analysis of the output of the second phosphor was converted into a neutron energy distribution (Curve A, figure 1). Curve B in figure 1 is the energy spectrum of the neutrons which caused the events used in the angular distribution; it is derived from curve A by applying a cut-off at

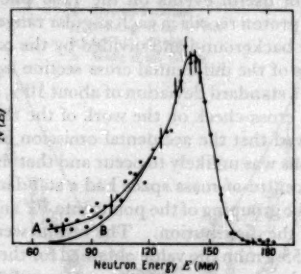

Figure 1. Energy spectrum of neutrons from the lithium deuteride target. Curve A, drawn through the experimental points, shows the distribution in energy of the neutrons entering the cloud chamber. Curve B shows the energy spectrum of neutrons used in the angular distribution measurement.

90 MEV since events caused by neutrons of lower energy were not meant to be included. The assignment of a neutron energy to each scattering event was, of course, based on measurements of the recoil proton track in the reprojected cloud chamber photographs. Errors in these measurements will lead to the inclusion of some events caused by neutrons with energy less than 90 MEV and to the rejection of others which were in fact caused by those with energy greater than 90 MEV. To allow for the effect of these errors on the effective energy of the experiment a gaussian distribution with a standard deviation of 18 MEV was used in calculating the shape of the cut-off. Since most of the neutrons were well above 90 MEV in energy small variations with scattering angle in the shape of the cut-off will not distort the results significantly.

§ 3. CALCULATION OF EFFECTIVE NEUTRON ENERGY

The effective energy $\bar{E}$ of the neutrons used in obtaining the angular distribution was calculated from the equation

$$\sigma(\bar{E})\int_0^\infty N(E)\,dE = \int_0^\infty \sigma(E)N(E)\,dE$$

which defines the mean total n–p cross section $\sigma(\bar{E})$. $N(E)$ is the number of neutrons per MEV as given by curve B, figure 1, and $\sigma(E)$ is the total n–p cross section

for neutrons of energy E obtained from the results of Taylor and Wood (1953). A value of (130 ± 2) MeV was obtained in this way for $\bar{E}$. Strictly, an effective energy for each scattering angle Φ should be defined by substituting $\sigma(\Phi, E)$, the appropriate differential cross section, in place of $\sigma(E)$ in the above equation. The variation with energy of $\sigma(\Phi, E)$ is not yet known in detail; using the published results to give the general trend, the effective neutron energies for values of Φ equal to 155°, 90° and 25° were calculated to be 131, 129 and 129 MeV respectively. Therefore, it would appear that the effective neutron energy is constant over the angular distribution within the limits of error assigned to $\bar{E}$.

§ 4. Results

The total number of useful events on the 1200 photographs examined was 1261. The number of proton recoils in each angular range of 10° in centre-of-mass space was corrected for background and divided by the corresponding solid angle to obtain relative values of the differential cross section as a function of scattering angle. Each value has a standard deviation of about 10% arising from the number of events included. A cross-check on the work of the three observers concerned with the scanning showed that the accidental omission of a track which satisfied the acceptance conditions was unlikely to occur and that the observational error on the scattering angle in centre-of-mass space had a standard deviation of about 1°. Neither this error, nor the grouping of the points into 10° angular ranges, produces a significant distortion of the distribution. The results were placed on an absolute scale by normalizing to 55·2 mbn the value obtained for the mean total cross section (see § 3). The extrapolation to 0° and 180° necessary for the normalization was such that $\sigma(0°)$ and $\sigma(180°)$ equalled 10 and 12 mbn sterad^{-1} respectively. Errors in this extrapolation together with the error in the mean cross section can affect the absolute values of the differential cross section by not more than ±4%. This error will not distort the angular distribution but only shift the results bodily up or down.

Table 2

(1)	(2)	(1)	(2)
20–30	6·55 ± 0·75	90–100	2·54 ± 0·30
30–40	5·59 ± 0·59	100–110	3·13 ± 0·34
40–50	3·86 ± 0·44	110–120	3·80 ± 0·39
50–60	3·31 ± 0·38	120–130	5·31 ± 0·48
60–70	2·45 ± 0·31	130–140	5·23 ± 0·51
70–80	2·96 ± 0·33	140–150	6·13 ± 0·62
80–90	2·64 ± 0·31	150–160	8·75 ± 0·87

(1) c.m. scattering angle (deg); (2) differential cross section (mbn sterad^{-1})

The results shown in table 2 include events with centre-of-mass scattering angles Φ from 20° to 160°. Events with Φ less than 20° were excluded because of the possibility of missing the short track of the recoil proton. The length of the shortest track used was 2·3 cm. Events with Φ greater than 160° were excluded because of the reduced stereoscopic effect for protons moving almost parallel to the line joining the two lenses of the camera. The errors quoted in table 2 are the standard deviation of the relative values of the differential cross sections.

§ 5. DISCUSSION

The results of the present experiment are shown in figure 2 together with those obtained at the neighbouring energies of 137 MEV (Thresher *et al.* 1955), 140 MEV (Griffith, to be published) and 153 MEV (Randle *et al.* 1952). Together they cover scattering angles from 6·3° to 178°. The agreement between the values of the differential cross section obtained at angles common to two or more experiments suggests that the main features of the angular distribution do not change very greatly over this range of neutron energies. The trend of the results obtained near 90 MEV and in the range 290–400 MEV is included to illustrate the effect on the angular distribution of a large change in neutron energy.

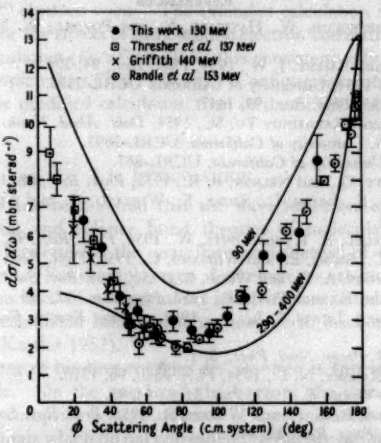
This work 130 MeV
Thresher et al. 137 MeV
Griffith 140 MeV
Randle et al. 153 MeV
90 MeV
290 - 400 MeV
dσ/dω (mbn ster⁻¹)
φ Scattering Angle (c.m. system) (deg)

Figure 2. Neutron–proton differential cross section against scattering angle in centre-of-mass space for different values of neutron energy. The 90 MEV line is based on Thresher *et al.* (1955, Fig. 5), and that representing the 290–400 MEV results on the work of Easley (1954), Hartzler *et al.* (1954), Dzhelepov and Kazarinov (1954) and De Pangher (1955).

The approximate symmetry about 90° which is shown by the 90 MEV results is not present at the highest energies. The present experiment shows that asymmetry occurs at an energy as low as 130 MEV and that the differential cross section has a minimum value at a scattering angle of about 80°. This is in agreement with the conclusion of Randle *et al.*, and contrasts with the results obtained between 290 and 400 MEV, where the minimum occurs at about 100°. At 130 MEV the cross section at scattering angles less than 90° is smaller than it is at the supplementary angle but the ratio is nearer to unity than that found at much higher energies. A χ^2-test applied to our results gave 0·1% for the probability of their being drawn from a symmetrical distribution. This lack of symmetry implies that the interaction between neutrons and protons cannot be described by a Serber force.

ACKNOWLEDGMENTS

Information supplied by the Brookhaven laboratory was used in the design of the cloud chamber. The authors are indebted to Messrs. H. Hadley, D. Kirkman, G. P. Walker, D. M. Welsh and H. C. Whitby for assistance with the cloud chamber and its associated equipment and to Misses R. Clinch and B. Harrison for assistance with the calculations. Some of the calculations were checked by members of the Atomic Energy Research Establishment computing group under Dr. J. Howlett. Our thanks are due to the cyclotron crew for their co-operation and to Dr. T. G. Pickavance and Mr. B. Rose for their interest and encouragement during the experiment.

REFERENCES

BRUECKNER, K., HARTSOUGH, W., HAYWARD, E., and POWELL, W. M., 1949, *Phys. Rev.*, **75,** 555.
CHAMBERLAIN, O., and EASLEY, J. W., 1954, *Phys. Rev.*, **94,** 208.
CHUNG YING CHIH, 1954, University of California UCRL-2575.
DE PANGHER, J., 1955, *Phys. Rev.*, **99,** 1447.
DZHELEPOV, V. P., and KAZARINOV YU. M., 1954, *Dokl. Akad. Nauk. S.S.S.R.*, **99,** 939.
EASLEY, J. W., 1954, *University of California*, UCRL-2693.
FOX, R. H., 1950, *University of California*, UCRL-867.
GUERNSEY, G., MOTT, G., and NELSON, B. K., 1952, *Phys. Rev.*, **88,** 15.
HADLEY, J., KELLY, E., LEITH, C., SEGRÈ, E., WIEGAND, C., and YORK, H., 1949, *Phys. Rev.*, **75,** 351.
HARTZLER, A. J., SIEGEL, R. T., and OPITZ, W., 1954, *Phys. Rev.*, **95,** 591.
KELLY, E., LEITH, C., SEGRÈ, E., and WIEGAND, C., 1950, *Phys. Rev.*, **79,** 96.
RANDLE, T. C., TAYLOR, A. E., and WOOD, E., 1952, *Proc. Roy. Soc.* A, **213,** 392.
SELOVE, W., STRAUCH, K., and TITUS, F., 1953, *Phys. Rev.*, **92,** 724.
SNELLING, G. F., and LEWIS, I. A. D., 1952, *Atomic Energy Research Establishment*, G/M 131.
SNOWDEN, M., 1953, *Progr. Nucl. Phys.*, **3,** 1.
STAHL, R. H., and RAMSEY, N. F., 1954, *Phys. Rev.*, **96,** 1310.
TAYLOR, A. E., and WOOD, E., 1953, *Phil. Mag.*, **44,** 95.
THRESHER, J. J., VOSS, R. G. P., and WILSON, R., 1955, *Proc. Roy. Soc.* A, **229,** 492.
WALLACE, R., 1951, *Phys. Rev.*, **81,** 493.
WHITBY, H. C., 1953, *Atomic Energy Research Establishment*, GP/R 1129.

The Bindng Energy of the Nitrogen Molecule

By A. C. HURLEY†
Department of Theoretical Chemistry, University of Cambridge

MS. received 27th March 1956

Abstract. A recent self-consistent field molecular orbital calculation on the nitrogen molecule by Scherr is extended to include configuration interaction. In this way the calculated binding energy D_e is increased from 1·19 electron volts to 3·29 electron volts. The extended calculation is then modified to make allowance for the effects of intra-atomic electron correlation. The result of this modified calculation ($D_e > 9{\cdot}18 \pm 0{\cdot}5$ ev) is consistent only with the higher of the two spectroscopic values (7·52, 9·91 ev). Configuration interaction is much less important in the modified calculation than in the orbital calculation.

§ 1. Introduction

In recent years it has been found that the wave functions employed in the molecular orbital and valence bond theories of molecular structure are not sufficiently accurate for the quantitative calculation of many important molecular parameters. For example, even if all electrons are included explicitly in the wave function and all configurations involving unexcited atomic orbitals are considered, the calculated binding energy may be so inaccurate that it is of no practical value (Kastler 1953).

If useful estimates of binding energies are required it appears that two procedures are possible. On the one hand the basis of the calculations may be greatly enlarged to comprise a large number of determinantal functions, some of which involve orbitals which do not correspond to valence or inner shell orbitals of the atoms in the molecule (Boys 1955). This, of course, involves a great increase in the labour of computation. Alternatively, the accuracy of the orbital wave functions may be increased by re-interpreting the role of atomic orbitals. In practice the latter procedure, which was first suggested by Moffitt (1951), is semi-empirical in that it involves the use of atomic spectral data, but in principle this data could be obtained by very accurate atomic calculations. In effect one uses the atomic spectral data to infer the existence of atomic wave functions which are more accurate than those appearing in the orbital calculation.

In a recent series of papers (Hurley 1955, 1956a, b) it has been shown that Moffitt's original procedure, the method of atoms in molecules, is not wholly satisfactory, but that a closely related theory employing an intra-atomic correlation correction leads to useful estimates of molecular binding energies. In this paper the intra-atomic correlation correction is applied to a recent molecular orbital calculation on the nitrogen molecule (Scherr 1955). Before the correction is applied Scherr's calculation is extended to include configuration interaction.

† On leave of absence from the Chemical Physics Section, Commonwealth Scientific and Industrial Research Organisation, Melbourne, Australia; now at the Solid State and Molecular Theory Group, Massachusetts Institute of Technology, U.S.A.

§ 2. The Orbital Calculation

The basic atomic orbitals are taken as orthogonalized Slater functions centred on the nitrogen nuclei a and b:

$$\begin{aligned}
1s_a &= \left(\frac{c^3}{\pi}\right)^{1/2} \exp(-cr_a),\\
2s_a &= N\left\{\left(\frac{\mu^5}{3\pi}\right)^{1/2} r_a \exp(-\mu r_a) - \alpha \,.\, 1s_a\right\},\\
2p\sigma_a &= \left(\frac{\mu^5}{\pi}\right)^{1/2} z_a \exp(-\mu r_a), \qquad \ldots\ldots(2.1)\\
2p\pi_a &= \left(\frac{\mu^5}{\pi}\right)^{1/2} x_a \exp(-\mu r_a),\\
2p\bar{\pi}_a &= \left(\frac{\mu^5}{\pi}\right)^{1/2} y_a \exp(-\mu r_a),
\end{aligned}$$

with a corresponding set of orbitals centred on nucleus b.

Here r_a is the distance from nucleus a; x_a, y_a and z_a are Cartesian coordinates centred on nucleus a with the z axis directed towards nucleus b; $\mu = 1{\cdot}95$ and $c = 6{\cdot}7$.

In order to keep the degree of the secular equation as small as possible, hybridization of the 2s and 2pσ orbitals is introduced at the start of the calculations. This leads to an orthonormal set of hybrid orbitals centred on nucleus a

$$\begin{aligned}
k_a &= 1s_a\\
l_a &= \cos\theta \,.\, 2s_a - \sin\theta \,.\, 2p\sigma_a,\\
h_a &= \sin\theta \,.\, 2s_a + \cos\theta \,.\, 2p\sigma_a, \qquad \ldots\ldots(2.2)\\
x_a &= 2p\pi_a,\\
y_a &= 2p\bar{\pi}_a,
\end{aligned}$$

and a corresponding set on nucleus b.

From these hybrid orbitals the following normalized symmetry orbitals are constructed:

$$\begin{aligned}
k_g &= \{2(1+s_k)\}^{-1/2}(k_a + k_b), & k_u &= \{2(1-s_k)\}^{-1/2}(k_a - k_b),\\
l_g &= \{2(1+s_l)\}^{-1/2}(l_a + l_b), & l_u &= \{2(1-s_l)\}^{-1/2}(l_a - l_b),\\
h_g &= \{2(1+s_h)\}^{-1/2}(h_a + h_b), & h_u &= \{2(1-s_h)\}^{-1/2}(h_a - h_b), \ldots(2.3)\\
x_u &= \{2(1+s_\pi)\}^{-1/2}(x_a + x_b), & x_g &= \{2(1-s_\pi)\}^{-1/2}(x_a - x_b),\\
y_u &= \{2(1+s_\pi)\}^{-1/2}(y_a + y_b), & y_g &= \{2(1-s_\pi)\}^{-1/2}(y_a - y_b),
\end{aligned}$$

where

$$s_k = \int k_a k_b dv, \quad s_l = \int l_a l_b dv, \quad s_h = \int h_a h_b dv, \quad s_\pi = \int x_a x_b dv = \int y_a y_b dv.$$

The molecular orbitals are now obtained by a Schmidt orthogonalization of those orbitals of the set (2.3) which belong to the same symmetry class.

$$\begin{aligned}
&(1)\ 1\sigma_g = k_g, && (2)\ 1\sigma_u = k_u,\\
&(3)\ 2\sigma_g = a_g l_g + b_g k_g, && (4)\ 2\sigma_u = a_u l_u + b_u k_u,\\
&(5)\ 3\sigma_g = c_g h_g + d_g l_g + e_g k_g, && (10)\ 3\sigma_u = c_u h_u + d_u l_u + e_u k_u, \quad .(2.4)\\
&(6)\ 1\pi_{ux} = x_u, && (8)\ 1\pi_{gx} = x_g,\\
&(7)\ 1\pi_{uy} = y_u, && (9)\ 1\pi_{gy} = y_g.
\end{aligned}$$

In order to simplify the expressions for the configurational functions these molecular orbitals will be designated by the numbers in parentheses in equations (2.4).

The hybridization parameter θ of equations (2.2) is now chosen so that the ratio of the coefficients of the functions $2s_a$ and $2p\sigma_a$ in the orbital $2\sigma_u$ is the same as that obtained by Scherr (1955) in his self-consistent field molecular orbital calculation. This ensures that the lowest configurational function constructed from the functions (2.4), namely

$$\tilde{\Theta}_1 = (14!)^{-1/2} \det(1, \bar{1}, 2, \bar{2}, 3, \bar{3}, 4, \bar{4}, 5, \bar{5}, 6, \bar{6}, 7, \bar{7}), \quad \ldots\ldots(2.5)$$

differs from Scherr's optimum molecular orbital function only in as much as we have omitted any contributions to the orbitals $1\sigma_g$ and $1\sigma_u$ from the two-quantum atomic orbitals.‡

Since the function (2.5) is almost an optimum molecular orbital function it will not interact appreciably with any singly excited configurational functions. We therefore confine our attention to doubly excited configurations and use just enough of these to ensure that, as the nuclear separation tends to infinity, the pairs of electrons in the bonding orbitals (5), (6) and (7) each go over on to one or other of the nitrogen nuclei. From the properties of the paired-electron orbital wave function (Hurley, Lennard-Jones and Pople 1953) it is clear that the necessary configurations are those corresponding to the double excitations $(\sigma_g)^2 \rightarrow (\sigma_u)^2$ and $(\pi_u)^2 \rightarrow (\pi_g)^2$. Thus in addition to the function (2.5) we use the following excited configurational functions:

$$\begin{aligned}
\tilde{\Theta}_2 &= (14!)^{-1/2} \det(1, \bar{1}, 2, \bar{2}, 3, \bar{3}, 4, \bar{4}, 10, \overline{10}, 6, \bar{6}, 7, \bar{7}),\\
\tilde{\Theta}_3 &= 2^{-1/2}\{(14!)^{-1/2} \det(1, \bar{1}, 2, \bar{2}, 3, \bar{3}, 4, \bar{4}, 5, \bar{5}, 6, \bar{6}, 9, \bar{9})\\
&\quad + (14!)^{-1/2} \det(1, \bar{1}, 2, \bar{2}, 3, \bar{3}, 4, \bar{4}, 5, \bar{5}, 8, \bar{8}, 7, \bar{7})\}\\
\tilde{\Theta}_4 &= 2^{-1/2}\{(14!)^{-1/2} \det(1, \bar{1}, 2, \bar{2}, 3, \bar{3}, 4, \bar{4}, 10, \overline{10}, 6, \bar{6}, 9, \bar{9})\\
&\quad + (14!)^{-1/2} \det(1, \bar{1}, 2, \bar{2}, 3, \bar{3}, 4, \bar{4}, 10, \overline{10}, 8, \bar{8}, 7, \bar{7})\}\\
\tilde{\Theta}_5 &= (14!)^{-1/2} \det(1, \bar{1}, 2, \bar{2}, 3, \bar{3}, 4, \bar{4}, 5, \bar{5}, 8, \bar{8}, 9, \bar{9}),\\
\tilde{\Theta}_6 &= (14!)^{-1/2} \det(1, \bar{1}, 2, \bar{2}, 3, \bar{3}, 4, \bar{4}, 10, \overline{10}, 8, \bar{8}, 9, \bar{9}).
\end{aligned} \quad \ldots\ldots(2.6)$$

This orthonormal set of configurational functions will be designated by the row vector $\tilde{\Theta}$.

$$\tilde{\Theta} = (\tilde{\Theta}_1, \tilde{\Theta}_2, \tilde{\Theta}_3, \tilde{\Theta}_4, \tilde{\Theta}_5, \tilde{\Theta}_6). \quad \ldots\ldots(2.7)$$

The energy matrix $\tilde{H}^0$ between the functions (2.7) may be evaluated by standard methods (Condon and Shortley 1935). The ground state wave function $\tilde{\Phi}$ and energy $\tilde{E}$ are then given by the equations

$$\tilde{\Phi} = \tilde{\Theta}\tilde{\Gamma}^0, \quad \det(\tilde{H}^0 - I\tilde{E}) = 0, \quad (\tilde{H}^0 - I\tilde{E})\tilde{\Gamma}^0 = 0, \quad \ldots\ldots(2.8)$$

where I is the 6×6 unit matrix.

In order to apply the intra-atomic correlation correction to this orbital calculation we must find the expression for the total wave function $\tilde{\Phi}$ in a valence bond representation. This expression is most easily obtained by a direct expansion of the determinants (2.5), (2.6) as sums of determinants of atomic orbitals. For example we have,

$$\begin{aligned}
\tilde{\Theta}_5 &= (14!)^{-1/2} \det(k_g, \bar{k}_g, k_u, \bar{k}_u, a_g l_g + b_g k_g, \overline{a_g l_g + b_g k_g}, a_u l_u + b_u k_u,\\
&\qquad \overline{a_u l_u + b_u k_u}, c_g h_g + d_g l_g + e_g k_g, \overline{c_g h_g + d_g l_g + e_g k_g},\\
&\qquad x_g, \bar{x}_g, y_g, \bar{y}_g)\\
&= (14!)^{-1/2} a_g^2 a_u^2 c_g^2 \det(k_g, \bar{k}_g, k_u, \bar{k}_u, l_g, \bar{l}_g, l_u, \bar{l}_u, h_g, \bar{h}_g, x_g, \bar{x}_g, y_g, \bar{y}_g),\\
&= NN_5(\tilde{\Psi}_1 + \tilde{\Psi}_2 - 2^{1/2}\tilde{\Psi}_3 - 2^{1/2}\tilde{\Psi}_4 + \tilde{\Psi}_5 + \tilde{\Psi}_6),
\end{aligned} \quad \ldots\ldots(2.9)$$

‡ The functions $2\sigma_g$ and $3\sigma_g$ differ markedly from those of Scherr, and, strictly speaking, are not molecular orbitals at all. However, since $1\sigma_g$, $2\sigma_g$, $3\sigma_g$ form a completely filled class this has no effect on the function $\tilde{\Theta}_1$ (Scherr 1955).

where $N=\dfrac{2^{-3/2}a_g^{\,2}a_u^{\,2}}{(1-s_k^{\,2})(1-s_l^{\,2})}$, $N_5=\dfrac{c^{\,2}}{(1+s_h)(1-s_n)^2}$,

$$\begin{aligned}
\tilde{\Psi}_1&=2^{-3/2}\Psi(h_a-h_b, x_a-x_b, y_a-y_b),\\
\tilde{\Psi}_2&=2^{-3/2}\{\Psi(h_a^{\,2}, x_a-x_b, y_a-y_b)+\Psi(h_b^{\,2}, x_a-x_b, y_a-y_b)\},\\
\tilde{\Psi}_3&=2^{-2}\{\Psi(h_a-h_b, x_a^{\,2}, y_a-y_b)+\Psi(h_a-h_b, x_b^{\,2}, y_a-y_b)\\
&\quad+\Psi(h_a-h_b, x_a-x_b, y_a^{\,2})+\Psi(h_a-h_b, x_a-x_b, y_b^{\,2})\},\\
\tilde{\Psi}_4&=2^{-3}\{\Psi(h_a^{\,2}, x_a^{\,2}, y_a-y_b,)+\Psi(h_b^{\,2}, x_b^{\,2}, y_a-y_b)\\
&\quad+\Psi(h_a^{\,2}, x_a-x_b, y_a^{\,2})+\Psi(h_b^{\,2}, x_a-x_b, y_b^{\,2})\\
&\quad+\Psi(h_a^{\,2}, x_b^{\,2}, y_a-y_b)+\Psi(h_b^{\,2}, x_a^{\,2}, y_a-y_b)\\
&\quad+\Psi(h_a^{\,2}, x_a-x_b, y_b^{\,2})+\Psi(h_b^{\,2}, x_a-x_b, y_a^{\,2})\},\\
\tilde{\Psi}_5&=2^{-3/2}\{\Psi(h_a-h_b, x_a^{\,2}, y_a^{\,2})+\Psi(h_a-h_b, x_b^{\,2}, y_b^{\,2})\\
&\quad+\Psi(h_a-h_b, x_a^{\,2}, y_b^{\,2})+\Psi(h_a-h_b, x_b^{\,2}, y_a^{\,2})\},\\
\tilde{\Psi}_6&=2^{-3/2}\{\Psi(h_a^{\,2}, x_a^{\,2}, y_a^{\,2})+\Psi(h_b^{\,2}, x_b^{\,2}, y_b^{\,2})+\Psi(h_a^{\,2}, x_b^{\,2}, y_b^{\,2})\\
&\quad+\Psi(h_b^{\,2}, x_a^{\,2}, y_a^{\,2})+\Psi(h_a^{\,2}, x_a^{\,2}, y_b^{\,2})+\Psi(h_b^{\,2}, x_b^{\,2}, y_a^{\,2})\\
&\quad+\Psi(h_a^{\,2}, x_b^{\,2}, y_a^{\,2})+\Psi(h_b^{\,2}, x_a^{\,2}, y_b^{\,2})\}.
\end{aligned} \qquad \ldots\ldots(2.10)$$

The Ψ's occurring on the right of equations (2.10) are bond-eigenfunctions in which the doubly occupied k and l orbitals have been suppressed. Each of these bond-eigenfunctions is constructed from 2^N determinants where N is the number of bonds (0, 1, 2 or 3) (Eyring, Walter and Kimball 1944). For example, the function $\Psi(h_a-h_b, x_a^{\,2}, y_b^{\,2})$ is defined by the equation

$$\begin{aligned}
&\Psi(h_a-h_b, x_a^{\,2}, y_b^{\,2})\\
&\quad=(14\,!)^{-1/2}\{\det(k_a, \bar{k}_a, k_b, \bar{k}_b, l_a, \bar{l}_a, l_b, \bar{l}_b, h_a, \bar{h}_b, x_a, \bar{x}_a, y_b, \bar{y}_b)\\
&\quad+\det(k_a, \bar{k}_a, k_b, \bar{k}_b, l_a, \bar{l}_a, l_b, \bar{l}_b, h_b, \bar{h}_a, x_a, \bar{x}_a, y_b, \bar{y}_b)\}.
\end{aligned}$$

The normalization factors in equation (2.10) have been so chosen that $\tilde{\Psi}_1 \ldots \tilde{\Psi}_6$ are each normalized for infinite separation of the nuclei. This (non-orthogonal) valence bond basis will be denoted by the row vector $\tilde{\Psi}$:

$$\tilde{\Psi}=(\tilde{\Psi}_1, \tilde{\Psi}_2, \tilde{\Psi}_3, \tilde{\Psi}_4, \tilde{\Psi}_5, \tilde{\Psi}_6). \qquad \ldots\ldots(2.11)$$

The transformation matrix T which relates the two bases (2.7) and (2.11) may be derived by the same methods which led to equation (2.9):

$$\tilde{\Theta}=\tilde{\Psi}T, \qquad \ldots\ldots(2.12)$$

where

$$T=N\begin{bmatrix}
N_1, & -N_2, & -2^{1/2}N_3, & 2^{1/2}N_4, & N_5, & -N_6\\
N_1, & N_2, & -2^{1/2}N_3, & -2^{1/2}N_4, & N_5, & N_6\\
2^{1/2}N_1, & -2^{1/2}N_2, & 0, & 0, & -2^{1/2}N_5, & 2^{1/2}N_6\\
2^{1/2}N_1, & 2^{1/2}N_2, & 0, & 0, & -2^{1/2}N_5, & -2^{1/2}N_6\\
N_1, & -N_2, & 2^{1/2}N_3, & -2^{1/2}N_4, & N_5, & -N_6\\
N_1, & N_2, & 2^{1/2}N_3, & 2^{1/2}N_4, & N_5, & N_6
\end{bmatrix} \qquad (2.13)$$

with

$$N=\frac{2^{-3/2}a_g^{\,2}a_u^{\,2}}{(1-s_k^{\,2})(1-s_l^{\,2})},\quad N_1=\frac{c^{\,2}}{(1+s_h)(1+s_n)^2},\quad N_2=\frac{c_u^{\,2}}{(1-s_h)(1+s_n)^2}$$

$$N_3=\frac{c_g^{\,2}}{(1+s_h)(1-s_n^{\,2})},\quad N_4=\frac{c_u^{\,2}}{(1-s_h)(1-s_n^{\,2})},\quad N_5=\frac{c_g^{\,2}}{(1+s_h)(1-s_n)^2},$$

$$N_6=\frac{c_u^{\,2}}{(1-s_h)(1-s_n)^2}.$$

The overlap matrix $\tilde{M}$ and energy matrix $\tilde{H}$ in the valence bond representation are now given by the equations

$$\tilde{M}=S^{\dagger}S,\ \tilde{H}=S^{\dagger}\tilde{H}^{0}S, \qquad \ldots\ldots(2.14)$$

where $S=T^{-1}$, and the symbol † denotes the Hermitian conjugate.

In this representation equations (2.8) may be written as follows:

$$\tilde{\Phi}=\tilde{\Psi}\tilde{\Gamma},\ \det(\tilde{H}-\tilde{M}\tilde{E})=0,\ (\tilde{H}-\tilde{M}\tilde{E})\tilde{\Gamma}=0. \qquad \ldots\ldots(2.15)$$

All the quantities appearing in the above equations are evaluated for the equilibrium nuclear separation (2·0675 atomic units) using Scherr's (1955) values for the necessary integrals over the atomic orbitals (2.1). The results obtained in this way are discussed below (§ 5).

§ 3. Valence State Energies

If the internuclear separation is made very large without altering the atomic orbitals (2.2), the wave functions (2.10) yield the following valence states:

$$\begin{aligned}
&\tilde{\Psi}_1 \rightarrow N(l^2hxy, V_3)+N(l^2hxy, V_3),\\
&\tilde{\Psi}_2 \rightarrow N^{-}(l^2h^2xy, V_2)+N^{+}(l^2xy, V_2),\\
&\tilde{\Psi}_3 \rightarrow N^{-}(l^2hx^2y, V_2)+N^{+}(l^2hx, V_2),\\
&\tilde{\Psi}_4 \rightarrow \tfrac{1}{2}[N^{2-}(l^2h^2x^2y, V_1)+N^{2+}(l^2x, V_1)]+\tfrac{1}{2}[N(l^2h^2y, V_1)+N(l^2x^2y, V_1)], \quad \ldots(3.1)\\
&\tilde{\Psi}_5 \rightarrow \tfrac{1}{2}[N^{2-}(l^2hx^2y^2, V_1)+N^{2+}(l^2h, V_1)]+\tfrac{1}{2}[N(l^2hx^2, V_1)+N(l^2hx^2, V_1)],\\
&\tilde{\Psi}_6 \rightarrow \tfrac{1}{4}[N^{3-}(l^2h^2x^2y^2, V_0)+N^{3+}(l^2, V_0)]+\tfrac{1}{2}[N^{-}(l^2h^2x^2, V_0)+N^{+}(l^2x^2, V_0)]\\
&\qquad\qquad +\tfrac{1}{4}[N^{-}(l^2x^2y^2, V_0)+N^{+}(l^2h^2, V_0)].
\end{aligned}$$

The incomplete separation of the valence states derived from $\tilde{\Psi}_4$, $\tilde{\Psi}_5$ and $\tilde{\Psi}_6$ is due to the use of a restricted basis. If the basis (2.7) were extended to ten configurational functions instead of six, each of the corresponding ten valence bond functions $\tilde{\Psi}_1 \ldots \tilde{\Psi}_{10}$ would yield unique valence states. However, since the valence states which are artificially coupled in the expressions (3.1) are all of minor importance, such an extension of the bases would produce only a small improvement in the results.

The valence states (3.1) are constructed from hybrid orbitals. Their empirical energies are estimated using the interpolation formula given by Moffitt (1950). The theoretical and empirical energies of valence states in first order hybridization which are required for this calculation are given in table 1. The theoretical values in this table are calculated using Slater's values for the atomic screening constants, namely,

	N^{3+}	N^{2+}	N^{+}	N	N^{-}	N^{2-}	N^{3-}	
c	6·7	6·7	6·7	6·7	6·7	6·7	6·7	……(3.2)
μ	2·475	2·300	2·125	1·950	1·775	1·600	1·425	

The empirical values given in table 1 are those of Pritchard and Skinner (1953), supplemented when necessary by reference to Moore's (1949) tables of atomic spectra. The origin of the energy scale is taken as the energy of a nitrogen atom in the ground state (^{4}S).

Table 1. Theoretical and Empirical Valence State Energies (ev)

State	Theoretical	Empirical	State	Theoretical	Empirical
$N^{3+}(s^2,V_0)$	90·03	91·58	N (sp^2pp,V_3)	17·24	14·23
(p^2,V_0)	111·61	116·90	(s^2p^2p,V_1)	4·48	2·92
$N^{2+}(s^2p,V_1)$	41·93	44·15	(sp^4,V_1)	20·03	17·01
(sp^2,V_1)	54·97	58·10	(p^4p,V_1)	35·65	28·88
(p^3p,V_1)	68·00	71·01	N^- (s^2p^2pp,V_2)	6·99	0·32
N^+ (s^2pp,V_3)	13·30	15·02	(sp^4p,V_2)	22·86	12·65
(sp^2p,V_2)	27·93	28·55	(s^2p^4,V_0)	9·54	1·32
(p^3pp,V_2)	42·57	41·73	(p^6,V_0)	41·35	22·42
(s^2p^2,V_0)	16·35	17·08	$N^{2-}(s^2p^4p,V_1)$	23·67	6·50±1·0
(p^4,V_0)	45·62	43·79	(sp^5,V_1)	39·25	15·50±1·0
N $(s^2p^3,^4S)$	(0·00)	(0·00)	$N^{3-}(s^2p^5,V_0)$	49·26	19·14±5
(s^2ppp,V_3)	1·68	1·18			

Most of the empirical values given in table 1 are obtained either directly from atomic spectral data or by short reliable extrapolations, with errors of about 0·2 ev or less. The empirical energies for the states of the ions N^{2-} and N^{3-} are, however, much less reliable as is indicated by the probable errors assigned to these values in the table. Fortunately, these states play a minor role in the calculation and the final results are only slightly affected by large changes in their energies.

The diagonal elements of the asymptotic energy matrix W, that is the energies of the valence states (3.1), are calculated from table 1 using Moffitt's (1950) interpolation formula. Except for a few states this formula reduces to an interpolation which is linear with respect to $\cos^2\theta$, where θ is the hybridization parameter (equation (2.2)).

The resulting values are given in table 2, together with two theoretical matrices $\widetilde{W}$ and $\widetilde{W}'$. The matrix $\widetilde{W}$, which is required for determining the atoms in molecules correction, is calculated using the values $\mu=1{\cdot}95$, $c=6{\cdot}7$ of the screening constants for all the valence states irrespective of their ionicity. The matrix $\widetilde{W}'$, which gives the intra-atomic correlation correction, is calculated using the values (3.2), which are effectively optimum values for each valence state (Hurley 1956 b).

Table 2. The Asymptotic Energy Matrix (ev)

Diagonal element (i)	$\widetilde{W}_{ii}$	From table 1 $\widetilde{W}_{ii}'$	From table 1 W_{ii}	Extrapolated $\widetilde{W}_{ii}'$	Extrapolated W_{ii}
1	7·08	7·08	5·48	(7·08)	(5·48)
2	$\widetilde{W}_{11}+J_{hh}=29{\cdot}17$	25·46	20·06	(25·46)	(20·06)
3	$\widetilde{W}_{11}+J_{xx}=27{\cdot}85$	23·94	18·43	(23·94)	(18·43)
4	$\widetilde{W}_{11}+J_{hh}+J_{xx}=49{\cdot}93$	42·31	32·96(±0·5)	42·32	33·01
5	$\widetilde{W}_{11}+2J_{xx}=48{\cdot}61$	40·85	31·30(±0·5)	40·80	31·39
6	$\widetilde{W}_{11}+2J_{xx}+J_{hh}=70{\cdot}69$	59·24	46·01(±1·2)	59·17	45·96

As shown in table 2 the matrix $\widetilde{W}$ has an especially simple structure. The differences between its diagonal elements are just integral multiples of the two coulomb integrals $J_{hh}=\int h^2(1)h^2(2)(1/r_{12})dv_1dv_2$, and $J_{xx}=\int x^2(1)x^2(2)(1/r_{12})dv_1dv_2$.

As a consequence of this simple structure the elements $\widetilde{W}_{44}$, $\widetilde{W}_{55}$, $\widetilde{W}_{66}$ may be extrapolated exactly from the values of $\widetilde{W}_{11}$, $\widetilde{W}_{22}$, $\widetilde{W}_{33}$. Indeed, the following equations are satisfied:

$$\left.\begin{aligned}\widetilde{W}_{44}&=\widetilde{W}_{22}+\widetilde{W}_{33}-\widetilde{W}_{11},\\ \widetilde{W}_{55}&=2\widetilde{W}_{33}-\widetilde{W}_{11},\\ \widetilde{W}_{66}&=\widetilde{W}_{22}+2\widetilde{W}_{33}-2\widetilde{W}_{11}.\end{aligned}\right\}\quad\ldots\ldots(3.3)$$

In table 2 the extrapolated values of the elements of $\tilde{W}'$ and W are obtained by assuming that equations of the form (3.3) are valid for these matrices also. It is clear from the table that this procedure leads to negligible error in the case of the matrix $\tilde{W}'$, and that the values obtained for W_{44}, W_{55} and W_{66} are well within the limits set by the uncertainties in the energies of the N^{2-} and N^{3-} states. This extrapolation procedure enables us to calculate the asymptotic energy matrices solely from the asymptotic energies of the covalent structure Ψ_1 and the singly ionic structures Ψ_2 and Ψ_3; the labour involved in calculating the matrix $\tilde{W}'$ is halved and it is unnecessary to estimate the empirical energies of the very inaccessible states of the ions N^{2-} and N^{3-}. For these reasons the extrapolated values of the matrices W and $\tilde{W}'$ are employed in the modified calculations rather than those derived wholly from table 1.

§ 4. The Modified Calculations

In the modified calculations the basic functions (2.10) of the orbital theory are regarded as approximations to a more accurate set of functions

$$\Psi=(\Psi_1, \Psi_2, \Psi_3, \Psi_4, \Psi_5, \Psi_6). \qquad \ldots\ldots(4.1)$$

In the atoms in molecules theory the functions (4.1) are taken as exact wave functions for the valence states (3.1). The modified energy matrix H_a is then given by the equation (Moffitt 1951)

$$H_a=H+\tfrac{1}{2}[\tilde{M}(W-\tilde{W})+(W-\tilde{W})\tilde{M}]. \qquad \ldots\ldots(4.2)$$

This procedure has been shown to be unsatisfactory (Pauncz 1954, Hurley 1955). In the present case it leads to an uncorrected binding energy of 11.85 electron volts for the N_2 molecule if only the first three states of the basis (4.1) are used. When the functions Ψ_4, Ψ_5 and Ψ_6 are included in the calculations binding energies around 15 electron volts are obtained. These values are much too high.

In a calculation employing the intra-atomic correlation correction the basic functions (4.1) are taken as the best possible (lowest energy) wave functions for the valence states (3.1) subject to the restriction that the total charge density for each valence state remains the same as that given by the functions (2.1) of the orbital calculation. The modified energy matrix H is now given by the equation (Hurley 1956 a)

$$H=\tilde{H}+\tfrac{1}{2}[\tilde{M}(W-\tilde{W}')+(W-\tilde{W}')\tilde{M}]. \qquad \ldots\ldots(4.3)$$

The ground state wave function Φ and energy E are then given by the equations

$$\Phi=\Psi\Gamma,\ \det(H-\tilde{M}E)=0,\ (H-\tilde{M}E)\Gamma=0. \qquad \ldots\ldots(4.4)$$

In the molecular orbital representation equations (4.3) and (4.4) become

$$\mathrm{H}^0=\tilde{\mathrm{H}}^0+\tfrac{1}{2}[(W-\tilde{W}')^0+(W-\tilde{W}')^{0\dagger}],$$
$$\Phi=\Theta\Gamma^0,\ \det(H^0-IE)=0,\ (H^0-IE)\Gamma^0=0, \qquad \ldots\ldots(4.5)$$

where $(W-\tilde{W}')^0=T^{-1}(W-\tilde{W}')T$.

§ 5. Numerical Results

The numerical values which result from the orbital calculations (§ 2) and from modified calculations employing the intra-atomic correlation correction (equations (4.3), (4.4) and (4.5)) are given in table 3 together with the two possible spectroscopic values (Herzberg 1950). The table includes calculations using all six

valence states (3.1) and less complete calculations involving a smaller number of functions.

Table 3. Calculated and Spectroscopic Binding Energies of N_2 (ev)

Orbital calculations		Modified calculations		Spectroscopic
Basis	D_e	Basis	D_e	D_e
SCFMO‡	1·19			7·52 or 9·91
$\tilde{\Theta}_1$	1·07	Θ_1	$>8·47(\pm 0·2)$	
$\tilde{\Psi}_1$	−2·62			
$\tilde{\Psi}_1, \tilde{\Psi}_2, \tilde{\Psi}_3$	2·74	Ψ_1, Ψ_2, Ψ_3	$>7·62$	
$\tilde{\Theta}_1 \ldots \tilde{\Theta}_6$	3·29	$\Theta_1 \ldots \Theta_6$	$>9·18(\pm 0·2)$	
$\tilde{\Psi}_1 \ldots \tilde{\Psi}_6$	3·29	$\Psi_1 \ldots \Psi_6$	$>9·18(\pm 0·2)$	

‡ From Scherr (1955).

The results of the orbital calculation show several features of interest.

The small difference between the energies for the single function $\tilde{\Theta}_1$ and Scherr's self-consistent field function shows that it is a good approximation to ignore any contributions from the valence shell orbitals to the inner shell molecular orbitals (§ 2).

The very poor binding energy obtained with the covalent function $\tilde{\Psi}_1$ is rather surprising. This function is seen to be much worse than the best single determinant molecular orbital function. In part this result is to be attributed to the choice of the hybridization parameter θ. In § 2 this parameter was chosen as optimum for the molecular orbital function Θ_1. The value obtained in this way gives $\cos\theta = 0·938$, $\sin\theta = 0·345$. This corresponds to 12% s character in the bond atomic orbitals of $\tilde{\Psi}_1$. An increase in the value of θ would probably improve the function $\tilde{\Psi}_1$ somewhat, but even with this refinement it is unlikely that $\tilde{\Psi}_1$ would lead to a positive binding energy.

Configuration interaction is seen to be quite important in the orbital calculation. The inclusion of the excited configurations $\tilde{\Theta}_2 \ldots \tilde{\Theta}_6$ lowers the total energy by more than 2 ev and almost trebles the calculated binding energy. Nevertheless, it is clear that even the full six-term orbital function is much too crude to distinguish between the two spectroscopic values of the binding energy. The six-term orbital calculation yields the following total wave function $\tilde{\Phi}$:

$$\begin{aligned}\tilde{\Phi} &= 0·9618\tilde{\Theta}_1 - 0·0508\tilde{\Theta}_2 - 0·2662\tilde{\Theta}_3 + 0·0141\tilde{\Theta}_4 \\ &\quad + 0·0361\tilde{\Theta}_5 - 0·0019\tilde{\Theta} \\ &= 0·3571\tilde{\Psi}_1 + 0·1612\tilde{\Psi}_2 + 0·2440\tilde{\Psi}_3 + 0·1107\Psi_4 \qquad \ldots\ldots(5.1) \\ &\quad + 0·0824\tilde{\Psi}_5 + 0·0375\tilde{\Psi}_6.\end{aligned}$$

The modified calculation, on the other hand, decides unequivocably in favour of the higher of the two spectroscopic values. Since the basis (4.1) of the modified calculation includes the exact* wave function for the system at infinite nuclear separation, the values obtained for the binding energy are lower limits (to within the accuracy of the approximations underlying equation (4.3)).

The errors quoted in table 3 for some of the modified calculations correspond to assumed errors of ± 1 electron volt in the energies of the N^{3-} states and ± 5 electron volts in the energy of the N^{3-} state (table 1). It is felt that this allowance for error

* Here we ignore the difference between the exact charge density of an isolated nitrogen atom in its ground state and the charge density given by the orbital functions (2.1).

in the energies of the N^{2-} and N^{3-} states is quite liberal, especially in view of the fact that the empirical estimates of the energies of these states are not used in the final calculation (§ 3). The probable errors in the energies of the other valence states of table 1 are much smaller and should not affect the calculated binding energy by more than 0·1 electron volt.

Apart from these errors arising from the uncertainties of the valence state energies, one must consider the errors introduced by the two approximations underlying equation (4.3) (Hurley 1956 a), namely (i) the correlation energy of an atom or ion is unaltered by small changes in the screening constants, (ii) the atoms-in-molecules type correction (4.3) gives accurate results provided that the orbital and accurate wave functions lead to the same charge density for each of the valence states involved in the calculation. The first of these approximations is not essential and could, if necessary, be replaced by a more accurate interpolation of correlation energies along the appropriate isoelectronic sequencies. However, such a refinement has a very small effect on the final results and is probably not justified in view of the uncertainties of approximation (ii).

For a system as complicated as the nitrogen molecule it is not possible to calculate directly the errors introduced by approximation (ii). This would require a complete molecular calculation in terms of wave functions which were sufficiently accurate to give the empirical excitation energies listed in table 1. This is out of the question at present. However, in one particular case, that of the hydrogen molecule at the equilibrium nuclear separation, such a calculation has been carried through (Pauncz 1954). Comparing Pauncz's results with those obtained from an equation of the type (4.3) (Hurley 1955) we find a difference of 0·003 atomic unit between the calculated equilibrium nuclear separations and a difference of 0·03 electron volt in the calculated binding energies. Thus in the only case in which an accurate estimate has been made the errors introduced by approximation (ii) are very small. For a system as complex as the nitrogen molecule the error introduced by approximation (ii) is probably somewhat larger than this, but it seems unlikely that it should exceed 0·3 electron volt. A very much larger error in the calculated binding energies would be required to reconcile the results of table 3 with the lower of the spectroscopic values for the binding energy. The higher spectroscopic value ($D_e = 9{\cdot}91$ ev) is therefore established. This result is in accord with recent thermochemical work (see Christian, Duff and Yarger 1955, where other references are given).

The total wave function Φ for the six-term modified calculation is given by the equations

$$\Phi = 0{\cdot}9874\Theta_1 + 0{\cdot}0318\Theta_2 - 0{\cdot}1545\Theta_3 - 0{\cdot}0050\Theta_4 + 0{\cdot}0119\Theta_5 + 0{\cdot}0004\Theta_6 \qquad (5.2)$$
$$= 0{\cdot}1614\Psi_1 + 0{\cdot}2580\Psi_2 + 0{\cdot}1532\Psi_3 + 0{\cdot}2445\Psi_4 + 0{\cdot}0724\Psi_5 + 0{\cdot}1157\Psi_6.$$

From table 3 and equations (5.1) and (5.2) we see that configuration interaction is markedly reduced by the introduction of the intra-atomic correlation correction.

§ 6. Discussion

The results obtained here for the nitrogen molecule are consistent with earlier calculations on the molecules H_2 (Hurley 1956 a) and HF (Hurley 1956 b). The binding energy of N_2 calculated using the intra-atomic correlation correction lies about 8% below the empirical value. This is to be compared with 4% for

HF and 0·5% for H_2. These percentage errors reflect quite faithfully the relative accuracy of the wave functions employed. The H_2 wave function is considerably more accurate than those for the other calculations, inasmuch as the atomic screening constants are varied to minimize the total energy of the system and inter-atomic correlation is introduced by including configurations constructed from excited atomic orbitals.

The difference in accuracy between the HF and N_2 wave functions arises mainly from the treatment of hybridization. In the case of HF hybridization was included by a complete configuration interaction treatment. This is a basically more accurate procedure than that of the present paper (Coulson 1952); furthermore it ensures that the degree of hybridization is optimum for the modified calculation as well as for the orbital calculation. A re-variation of the hybridization parameter to minimize the total energy in the modified calculation should improve the calculated dissociation energy of N_2 slightly. A larger improvement in both the HF and N_2 calculations is to be expected from a variation of the atomic screening constants to minimize the total energy. However this would involve a substantial increase in the labour of computation.

We conclude that the present method of calculation is capable of yielding the binding energies of diatomic molecules to an accuracy rather closer than 5% (about 0·5 ev). Thus, for example, the method should certainly decide between the high value and the (now generally accepted) low value for the heat of dissociation of F_2 and might well distinguish between the three most probable dissociation energies of CO(11·108, 9·605 and 9·141 ev (Herzberg 1950)).

The intra-atomic correlation correction may be applied to calculations on polyatomic molecules without any difficulty, either theoretical or computational. However, the necessary orbital calculations, involving as they must an exact treatment of inner shell electrons, are very much more difficult than for diatomic molecules.

References

Boys, S. F., 1955, *Symposium on Quantum Theory of Molecules, Svensk. Kem. Tidskr.*, **67**, 365.

Christian, R. H., Duff, R. E., and Yarger, F. L., 1955, *J. Chem. Phys.*, **23**, 2045.

Condon, E. U., and Shortley, G. H., 1935, *The Theory of Atomic Spectra* (Cambridge : University Press).

Coulson, C. A., 1952, *Valence* (Oxford : Clarendon Press).

Eyring, E., Walter, J., and Kimball, G. E., 1944, *Quantum Chemistry* (New York : Wiley).

Herzberg, G., 1950, *Spectra of Diatomic Molecules* (New York : Van Nostrand).

Hurley, A. C., Lennard-Jones, Sir John, and Pople, J. A., 1953, *Proc. Roy. Soc.* A, **220**, 446.

Hurley, A. C., 1955, *Proc. Phys. Soc.* A, **68**, 149 ; 1956 a, *Ibid.*, **69**, 49 ; 1956 b, *Ibid*, **69**, 301.

Kastler, D., 1953, *J. Chim. Phys.*, **50**, 556.

Moffitt, W., 1950, *Proc. Roy. Soc.* A, **202**, 534 ; 1951, *Ibid.*, **210**, 245.

Moore, C. M., 1949, *Atomic Energy Levels*, Circ. U.S. Bur. Stand., 467.

Pauncz, R., 1954, *Acta Phys. Hung.*, **4**, 237.

Pritchard, H. O., and Skinner, H. A., 1953, *Trans. Faraday Soc.*, **49**, 1254.

Scherr, C. W., 1955, *J. Chem. Phys.*, **23**, 569.

The Quadrupole Polarizability of the Hydrogen Atom

By C. A. COULSON and M. J. STEPHEN

Mathematical Institute, Oxford

MS. received 4th June 1956

Abstract. The quadrupole moment of a hydrogen atom in a general state induced by a uniform electric field has been evaluated to second powers of the field strength. It is also shown that a uniform magnetic field may induce an electrical quadrupole moment and this has been calculated for the lowest two states of the hydrogen atom.

When an electric field F is applied to a hydrogen atom in a general state a quadrupole moment Q is induced. If F is not too large Q may be expressed as a power series in F:

$$Q = Q_0 + FQ_1 + F^2Q_2 + \ldots \qquad \ldots\ldots (1)$$

The term Q_0 independent of the field arises because of the degeneracy of the unperturbed level. The perturbation removes this degeneracy and determines the correct linear combinations of the n^2 degenerate wave functions (n is the principal quantum number). These linear combinations are in general not spherically symmetrical, thus giving rise to the zero order term Q_0.

For the ground state the first two terms in (1) vanish, and higher powers have been determined by Buckingham, Coulson and Lewis (1956). While it is unlikely that it will be possible to compare these quantities (called the quadrupole polarizability by Buckingham, Coulson and Lewis) with experiment, they are nevertheless of interest as they may be calculated exactly. Only in the case of hydrogen-like atoms is an exact calculation possible.

The wave functions required for the evaluation of the quadrupole moment are identical with those encountered in the Stark effect. Epstein (1926) and Schrödinger (1926) have shown that great simplification results from working in parabolic coordinates $\xi = r + z$; $\eta = r - z$ and ϕ. The wave equation is separable in these coordinates and the solutions, though still degenerate from the standpoint of their energy, are already the correct linear combinations for use in the ordinary perturbation theory.

Writing the wave functions for the hydrogen atom as $\psi(\xi\eta)\,e^{im\phi}$ the wave equation in parabolic coordinates is

$$\frac{2}{\xi+\eta}\left[\frac{\partial}{\partial\xi}\xi\frac{\partial}{\partial\xi} + \frac{\partial}{\partial\eta}\eta\frac{\partial}{\partial\eta} - \frac{m^2}{4}\left(\frac{1}{\xi}+\frac{1}{\eta}\right)\right]\psi + (E-V)\psi = 0.$$

m is an exact quantum number in the presence of a uniform field owing to the axial symmetry around the field direction. In atomic units

$$E = -\frac{1}{2n^2} + \epsilon; \qquad V = -\frac{2}{\xi+\eta} + \frac{F}{2}(\xi-\eta)$$

corresponding to a uniform field in the positive z direction. The wave equation may now be written

$$L\psi + [\tfrac{1}{2}n^2(x+y)\epsilon - \tfrac{1}{4}n^3(x^2-y^2)F]\psi = 0 \qquad \ldots\ldots(2)$$

where $\xi = nx$ and $\eta = ny$ and

$$L = \frac{\partial}{\partial x}x\frac{\partial}{\partial x} + \frac{\partial}{\partial y}y\frac{\partial}{\partial y} - \frac{m^2}{4}\left(\frac{1}{x}+\frac{1}{y}\right) - \frac{x+y}{4} + n.$$

ψ and ϵ are expressed in the form of a power series in the field F

$$\psi = \psi_0 + F\psi_1 + F^2\psi_2 \ldots \qquad \ldots\ldots(3)$$

$$\epsilon = F\epsilon_1 + F^2\epsilon_2 \ldots . \qquad \ldots\ldots(4)$$

The correct zero order solutions to equation (2) are, in unnormalized form (Condon and Shortley 1953)

$$\psi_0 = f_{k_1}(x)f_{k_2}(y)$$

where

$$f_k(x) = e^{-x/2}x^{|m|/2}L^{|m|}_{k+|m|}(x)$$

$L^{|m|}_{k+|m|}(x)$ is the associated Laguerre polynomial. The parameters k_1 and k_2 are necessarily positive integers or zero, and are related to the principal and magnetic quantum numbers n and m by the relation $k_1 + k_2 + |m| + 1 = n$. Substituting the expansions (3) and (4) in (2) and equating powers of F we find the following set of equations:

$$L\psi_0 = 0 \qquad \ldots\ldots(5a)$$

$$L\psi_1 = \tfrac{1}{4}n^3(x^2-y^2)\psi_0 - \tfrac{1}{2}n^2(x+y)\epsilon_1\psi_0 \qquad \ldots\ldots(5b)$$

$$L\psi_2 = \tfrac{1}{4}n^3(x^2-y^2)\psi_1 - \tfrac{1}{2}n^2(x+y)(\epsilon_2\psi_0 + \epsilon_1\psi_1) \qquad \ldots\ldots(5c)$$

etc.

Introduce the notation $f_{k_1+r}(x)f_{k_2+s}(y) = \{r, s\}$;

$\psi_1\psi_2 \ldots$ are expressed in terms of this complete set of functions:

$$\psi_1 = \sum_{rs} a_{rs}\{r, s\} \qquad \ldots\ldots(6)$$

$$\psi_2 = \sum_{rs} b_{rs}\{r, s\} \qquad \ldots\ldots(7)$$

etc.

The coefficients a_{rs}, $b_{rs}\ldots$ are determined from equations (5) by equating coefficients of $\{r, s\}$. The following recurrence relations were used (see Coulson and Gillam 1948).

$$L\{r, s\} = -(r+s)\{r, s\} \qquad (k_1 + k_2 + |m| + 1 = n)$$

$$x^p\{r, s\} = \sum_{i=-p}^{+p} H_{r+i}\{r+i, s\}$$

where

$$H_{r+i} = \frac{(k_1+r+i)!}{(k_1+r+i+|m|)!}(p!)^2(-1)^i\sum_c \frac{(p+|m|+k_1+r-c)!}{(k_1+r-c)!\,c!\,(p-c)!\,(c+i)!\,(p-c-i)!}. \qquad \ldots\ldots(8)$$

Similarly for $y^p\{r, s\}$. The summation in (8) is over all integral values of c which make every one of the factorials non-negative. The coefficients in (6) and (7) for which $r+s=0$ are indeterminate, but may be found from a study of the wave function of order one higher than that being determined. This type of situation is discussed by Coulson and Gillam (1948).

The quadrupole moment Q may be expressed as

$$Q = \frac{\int \psi^* r^2 P_2(\cos\theta)\psi \, d\tau}{\int \psi^* \psi \, d\tau}. \qquad \ldots\ldots(9)$$

From (9), (6) and (7) the coefficients in the expansion (1) are determined to be

$$Q_0 = 3n^2(k_1 - k_2)^2 - \tfrac{1}{2}n^2(n^2-1) \qquad \ldots\ldots(10a)$$

$$Q_1 = \tfrac{3}{8}n^4[-2n(k_1^2+k_2^2)+21n(k_1+k_2)(n-1) + k_1k_2(104-38n)+6n^3+21n^2+23n](k_2-k_1) + \frac{3n^3}{2}Q_0(k_1-k_2) \qquad \ldots\ldots(10b)$$

$$Q_2 = \frac{n^5}{64}\sum_r (k_1^r + k_2^r)[n^2 A_r - 2Q_0 B_r] + \frac{3n^3}{2}Q_1(k_1-k_2). \qquad \ldots\ldots(10c)$$

The non-zero coefficients A_r and B_r in Q_2 are given in the Appendix. For the ground state Q_0 and Q_1 vanish and $Q_2 = 213/4$ in agreement with the value given by Buckingham, Coulson and Lewis. Numerical values of Q_0, Q_1 and Q_2 for some of the more important excited states are given in table 1.

Table 1

n	k_1	k_2	Q_0	Q_1	Q_2
1	0	0	0	0	$\frac{213}{4}$
2	1	0	6	−1224	103200
2	0	0	−6	0	104064
3	2	0	72	−33534	5604×3^7
3	1	0	−9	−16767	$\frac{58161}{8} \times 3^7$
3	1	1	−36	0	$\frac{31699}{4} \times 3^7$
3	0	0	−36	0	5328×3^7

Certain sum rules may be proved for the coefficients Q_0, Q_1, Q_2 ... when we consider all the degenerate set corresponding to the same unperturbed energy level. Consider a basic set of degenerate atomic orbitals ψ_i ($i = 1, 2 \ldots m$) which may be conveniently taken to be the conventional s, p, d, ... type orbitals. In the perturbation theory for degenerate levels, the ψ_i are replaced by m appropriate linear combinations, suitable as zero-order unperturbed wave functions:

$$\phi_i = \sum_{j=1}^{m} c_{ij}\psi_j.$$

It is not difficult to prove quite generally that for the coefficients of an expansion of the type (1)

$$\sum_{i=1}^{m} Q_n(\psi_i) = \sum_{i=1}^{m} Q_n(\phi_i). \qquad \ldots\ldots(11)$$

In (11) Q_n is not necessarily the quadrupole polarizability but may be any one-electron observable. In the case where the Q_n refer to the quadrupole

polarizability $\Sigma Q_0 = 0$ and $\Sigma Q_n = 0$ when n is odd. The summations here are over all the degenerate set corresponding to the same unperturbed energy level.

The above formulae are also applicable to hydrogen-like atoms of nuclear charge Ze if a change of units is made. The energy of the atom in the presence of the field is now written $-Z^2/2n^2 + Z^2\epsilon$ and the new atomic unit of field strength is defined by $F_1 = F/Z^3$.

In (1) F is replaced by F/Z^3 and $Q_0, Q_1 \ldots$ are replaced by $Q_0/Z^3, Q_1/Z^2 \ldots$.

If a uniform magnetic field $\mathscr{H}$ is applied to a hydrogen atom an expansion similar to (1) is possible:

$$Q^{(H)} = Q_0^{(H)} + HQ_1^{(H)} + H^2Q_2^{(H)} \qquad \ldots\ldots(12)$$

where H has been written for $\mathscr{H}/2c$. $\mathscr{H}$ is measured in atomic units ($c = 137$). The wave equation in atomic units is

$$\nabla^2\psi + 2(E - V)\psi = 0. \qquad \ldots\ldots(13)$$

In these units

$$E = -\frac{1}{2n^2} + \epsilon; \quad V = -\frac{1}{r} + \frac{\mathscr{H}_z}{2c}(L_z + 2S_z) + \frac{\mathscr{H}_z^2}{8c^2} r^2 \sin^2\theta$$

for a uniform magnetic field in the z direction (Condon and Shortley 1953).

L_z is the orbital angular momentum operator and S_z the corresponding operator for spin angular momentum. With the substitutions $\zeta = 2r/n$ and $H = \mathscr{H}_z/2c$ (13) becomes

$$L'\psi + \frac{n^2}{4}\left[2\epsilon - 2H(L_z + 2S_z) - \frac{n^2}{4}H^2\zeta^2\sin^2\theta\right]\psi = 0 \qquad \ldots\ldots(14)$$

where

$$L' = \frac{1}{\zeta^2}\frac{\partial}{\partial\zeta}\left(\zeta^2\frac{\partial}{\partial\zeta}\right) + \frac{1}{\zeta^2\sin^2\theta}\frac{\partial^2}{\partial\phi^2} + \frac{1}{\zeta^2\sin\theta}\frac{\partial}{\partial\theta}\left(\sin\theta\frac{\partial}{\partial\theta}\right) + \frac{n}{\zeta} - \frac{1}{4}. \qquad \ldots\ldots(15)$$

r, θ and ϕ are the usual spherical polar coordinates. With the expansions

$$\psi = \psi_0 + H\psi_1 + H^2\psi_2 \ldots$$
$$\epsilon = H\epsilon_1 + H^2\epsilon_2 \ldots$$

a set of equations similar to (5) is obtained. The zero order solutions of (14) which apply when $H = 0$ are the conventional s, p, d, ... hydrogen wave functions for the appropriate value of n (Pauling and Wilson 1935).

Difficulty is here encountered with the correct zero order wave functions for use in the perturbation theory. Only the case of field strength corresponding to a complete Paschen–Back effect is considered. The first order perturbation $L_z + 2S_z$ splits each configuration into $2l + 3$ equally spaced levels. The system is still degenerate in the azithmuthal quantum number l and the second order perturbation $\zeta^2\sin^2\theta$ connects states with l differing by ± 2. In general to obtain the correct zero order wave functions a secular determinant, which has been given by Halpern and Sexl (1929) must be solved. For n greater than 4 no explicit solutions have been found. As a result no general formula such as (10) can be provided for the polarizability coefficients in (12). However, for the states $n = 1$, 2, which are of interest here, the conventional hydrogen wave functions may be shown to be the correct zero order solutions, and we can proceed

with conventional perturbation theory. $\psi_1, \psi_2 \ldots$ are now expanded in terms of the complete set of functions

$$F_{\nu\lambda\mu}(\zeta, \theta, \phi) = \Lambda_{\nu\lambda}(\zeta)\Theta_{\lambda\mu}(\theta)\Phi_{\mu}(\phi)$$

where

$$\Lambda_{\nu\lambda}(\zeta) = \left\{\frac{(\nu-\lambda-1)\,!}{[(\nu+\lambda)\,!]^3}\right\}^{1/2} \zeta^{\lambda} e^{-\zeta/2} L_{\nu+\lambda}^{2\lambda+1}(\zeta)$$

$$\Theta_{\lambda\mu}(\theta) = \left\{\frac{(2\lambda+1)(\lambda-|\mu|)\,!}{2(\lambda+|\mu|)\,!}\right\}^{1/2} P_{\lambda}^{|\mu|}(\cos\theta)$$

$$\Phi_{\mu}(\phi) = \frac{1}{\sqrt{(2\pi)}} e^{i\mu\phi}.$$

The functions $F_{\nu\lambda\mu}$ are identical with the hydrogen wave functions for $\nu = n$ and satisfy the differential equation

$$L' F_{\nu\lambda\mu}(\zeta, \theta, \phi) = 0.$$

L' is given by (15) in which n has been replaced by ν. Recurrence relations for these functions are given in Pauling and Wilson (1935).

It is now quite straightforward to determine $\psi_1, \psi_2 \ldots$. The quadrupole moment is given by (9) and using $\psi_1, \psi_2 \ldots$ the coefficients in the expansion (12) may be found. All coefficients connected with odd powers of H vanish. This arises because the first order perturbation $L_z + 2S_z$ is diagonal with respect to all the quantum numbers and therefore there are no wave functions of odd order. Consequently the induced electric quadrupole moment is only due to the diamagnetism of the atom. Numerical values of $Q_0^{(H)}$ and $Q_2^{(H)}$ in atomic units for the two lowest energy levels of the hydrogen atom are given in table 2. No general formulae are presented as these would only be valid for $n = 1, 2$ and for some of the states of $n = 3, 4$.

These coefficients also obey the general sum rule (11) and in particular $\Sigma Q_0^{(H)} = 0$ summation extending over all the degenerate set corresponding to the same unperturbed energy.

The above results are also applicable to hydrogen-like atoms of nuclear charge Ze if H is replaced by H/Z^2 in the expansion (12). $Q_0^{(H)}$, $Q_2^{(H)}$ are replaced by $Q_0^{(H)}/Z^2$, $Q_2^{(H)}/Z^2 \ldots$.

Table 2

n	l	$\lvert m\rvert$	Q_0	Q_2
1	0	0	0	5
2	0	0	0	3280
2	1	0	12	−192
2	1	1	−6	2688

APPENDIX

$p = n - 1$

$A_6 = -6p^2 + 30p + 36$; $\quad A_5 = 12pk_1k_2 + 13p^3 + 57p^2 + 68p$

$A_4 = -12k_1^2k_2^2 - k_1k_2(294p + 352) + 6p^4 - 260p^3 - 792p^2 - 1144p - 700$

$A_3 = -42pk_1^2k_2^2 + k_1k_2(-59p^3 + 279p^2 + 128p) - 19p^5 + 64p^4 - 858p^3 - 1621p^2 - 1316p$

$$A_2 = 52k_1^3k_2^3 + k_1^3k_2^2(84p^2 + 456p + 752)$$
$$+ k_1k_2(36p^4 + 358p^3 + 4633p^2 + 7845p + 5432)$$
$$+ 6p^6 + 120p^5 + 984p^4 + 3616p^3 + 4662p^2 + 3770p + 1324$$
$$A_1 = 30pk_1^3k_2^3 + k_1^3k_2^2(34p^3 - 24p^2 - 466p)$$
$$+ k_1k_2(3p^5 - 246p^4 - 620p^3 - 96p^2 + 761p)$$
$$+ 14p^6 + 781p^5 + 2634p^4 + 4739p^3 + 4948p^2 + 2076p$$
$$A_0 = -40k_1^4k_2^4 - k_1^3k_2^3(74p^2 + 296p + 355)$$
$$- k_1^2k_2^2(24p^4 + 267p^3 + 2859p^2 + 5856p + 4441)$$
$$+ k_1k_2(9p^5 - 1080p^4 - 5378p^3 - 9137p^2 - 8718p - 3400)$$
$$+ 58p^6 + 562p^5 + 2310p^4 + 5256p^3 + 7082p^2 + 5336p + 1704$$
$$B_3 = 4p^2 - 20; \qquad B_2 = k_1k_2(-8p + 40) - 15p^3 - 6p^2 - 125p - 98$$
$$B_1 = k_1k_2(-6p^2 - 126p) + 16p^4 + 65p^3 + 352p^2 + 323p$$
$$B_0 = k_1^2k_2^2(9p + 33) + k_1k_2(14p^2 - 227p - 225) + 8p^4 + 97p^3 + 360p^2 + 521p + 250.$$

Acknowledgment

M. J. S. would like to thank the Salters Institute for the award of a Fellowship which enabled him to undertake this work.

References

Buckingham, A. D., Coulson, C. A., and Lewis, J. T., 1956, *Proc. Phys. Soc.* A, **69**, 639.
Condon, E. U., and Shortley, G. H., 1953, *The Theory of Atomic Spectra*, (Cambridge : University Press), pp. 399, 149.
Coulson, C. A., and Gillam, C. M., 1948, *Proc. Roy. Soc., Edinb.*, **62**, 360.
Epstein, P. S., 1926, *Phys. Rev.*, **28**, 695.
Halpern, O., and Sexl, T., 1929, *Ann. Phys., Lpz.*, **3**, 565.
Pauling, L., and Wilson, E. B., 1935, *Introduction to Quantum Mechanics* (New York : McGraw-Hill), p. 196.
Schrödinger, E., 1926, *Ann. Phys., Lpz.*, **80**, 457.

LETTERS TO THE EDITOR

The Infra-Red Resonance Lines of Lutetium

The arc spectrum of lutetium—the last member of the rare earths series—presents some interesting features. It has fewer lines than the other members of the series and evidence from the absorption spectra (Bovey and Garton 1954) suggests that there must be at least two low lying levels. One of these levels—the ground state, ^2D—was found in the first analysis (Meggers and Scribner 1930). Work by Bovey and Pearse (1954) and Klinkenberg (1955) showed that the second level was ^2P arising from the configuration $6p(6s)^2$ and the latter author suggested that the $^2P_{1/2}$ should be 4136 cm^{-1} above $^2D_{3/2}$. Since the ground state configuration is $5d(6s)^2$ there should be a strong infra-red multiplet arising from transitions between these two doublets.

A small Fastie–Ebert type spectrometer (f/7 aperture, 100 cm focal length mirrors) has recently been designed and is in the course of completion. It is at present equipped with an experimental N.P.L. grating (6 in. wide and 3 in. high), with 7500 lines per inch and a blaze at 3·5 μ.

It was decided to try and obtain experimental evidence for the positions of the multiplets, since the indirect evidence from the visible spectrum was not completely convincing. The small King furnace used previously for the absorption study was adapted for emission work. A mixture of Johnson, Matthey ' Specpure ' lutetium oxide and pure graphite was put in the carbon tube. One charge appeared to last for some 45 minutes at 2400°c. The spectrum was viewed simultaneously in the visible region through a constant deviation spectroscope (Hilger type D186) to see if the element was present.

Transition	Wave number (cm^{-1}) (in vacuo) Calculated	Observed	Intensity	Calibration	
$^2D_{3/2}$–$^2P_{3/2}$	7476·35	7476·2 ± 0·7	10	2·6 μ H_2O†	BP
$^2D_{5/2}$–$^2P_{3/2}$	5482·43	5482·6 ± 0·5	100	1·8 μ H_2O	N
$^2D_{3/2}$–$^2P_{1/2}$	4136·00	4136·3 ± 0·5	100	2·4 μ ^{13}CO	PBS

† Line in second order.

BP, Benedict and Plyler 1951; N, Nelson 1949; PBS, Plyler, Benedict and Silverman 1952.

The results are shown in the table. The frequencies of the lines were determined relative to water vapour and carbon monoxide (with enriched ^{13}C) absorption bands. The line at 4136 cm^{-1} should be the most accurately measured since there is no interference from atmospheric absorption. That at 5482 cm^{-1} was also relatively easy to measure. The large error of measurement of the line at 7476 cm^{-1} is caused partly by its weakness—which meant that the slit width of the instrument was considerably greater than that on which the calibration spectra were originally taken.

The close agreement between the calculated and observed results is satisfactory, and the relative positions of the two systems of levels based on ^{2}D and ^{2}P respectively are now well established. The lines are one of the first examples of ' resonance ' lines (i.e. the transitions between the two lowest levels of an element) occurring in the infra-red. Previous knowledge of these lines would have been of great value in the original work on the term analysis. We hope to continue this work and see if other lines can be found.

Atomic Energy Research Establishment,
Harwell, Berks.
25th July 1956.

L. F. H. Bovey.
E. B. M. Steers.
H. S. Wise.

Benedict, W. S., and Plyler, E. K., 1951, *J. Res. Nat. Bur. Stand.*, **46**, 246.
Bovey, L. F. H., and Garton, W. R. S., 1954, *Proc. Phys. Soc.* A, **67**, 291.
Bovey, L. F. H., and Pearse, R. W. B., 1954, *K. Fysiogr. Sällsk. Hand. N. F.* (Sweden), **65**, 82.
Klinkenberg, P. F. A., 1955, *Physica*, **21**, 53.
Meggers, W. F., and Scribner, B. F., 1930, *J. Res. Nat. Bur. Stand.*, **5**, 73.
Nelson, R. C., 1949, *Summary Report* No. 4, Contract NObs 28373 Northwestern University.
Plyler, E. K., Benedict, W. S., and Silverman, S., 1952, *J. Chem. Phys.*, **20**, 175.

Application of the Rayleigh–Schrödinger Perturbation Theory to the Hydrogen Atom

Two papers with this title have been published recently. Writing the wave equation of an electron in the field of a nucleus of charge Z as

$$\left\{\nabla^2+\frac{2Z_1}{r}+\frac{2(Z-Z_1)}{r}\right\}\Psi=\epsilon\Psi \qquad \ldots\ldots(1)$$

where $\mathbf{r}$ is the electron–nucleus separation in units of the Bohr radius a_0, ϵ is the binding energy in rydbergs and Z_1 is an arbitrary parameter, Wigner (1954) has shown that perturbation theory based upon the eigenfunctions of (1) when $Z=Z_1=0$ and a perturbation $2Z/r$ yields in the second order an eigenvalue for the ground state which though finite is incorrect numerically. More recently, Trees (1956) has shown that provided Z_1 is not taken as exactly zero "it is fairly certain" that second order perturbation theory based upon a perturbation $2(Z-Z_1)/r$ will yield the correct eigenvalue. It is the purpose of this note to demonstrate rigorously this latter assertion.

It has been demonstrated elsewhere (Dalgarno and Lewis 1955, Dalgarno and Stewart 1956), that the infinite summation in the conventional second order perturbation formula may be written $\epsilon_2=(0\,|\,Vf\,|\,0)-(0\,|\,V\,|\,0)(0\,|\,f\,|\,0)$ where V is the perturbation, $(0\,|\,\ \,|\,0)$ represents an average over the unperturbed wave function ψ_0 and f satisfies the equation

$$2\nabla\psi_0.\nabla f+\psi_0\nabla^2 f=V\psi_0-(0\,|\,V\,|\,0)\psi_0.$$

For the problem considered here, $\psi_0 = (Z_1^3/\pi)^{1/2} \exp(-Z_1 r)$ and $V = 2(Z - Z_1)/r$. Then it may easily be verified that

$$(0 \mid V \mid 0) = 2Z_1(Z - Z_1), \quad f = -(Z - Z_1)r, \quad (0 \mid f \mid 0) = -3(Z - Z_1)/2Z_1$$

and

$$\epsilon_2 = -2(Z - Z_1)^2 + \frac{3(Z - Z_1)}{2Z_1} 2(Z - Z_1)Z_1 = (Z - Z_1)^2.$$

The zero and first order perturbation energies are simply Z_1^2 and

$$(0 \mid V \mid 0) = 2Z_1(Z - Z_1)$$

respectively, so that to the second order

$$\epsilon = Z_1^2 + 2Z_1(Z - Z_1) + (Z - Z_1)^2.$$

But this is just Z^2, the correct expression for the binding energy.

Similar methods may be used to show that third and higher-order perturbation energies all vanish.

Department of Applied Mathematics, A. DALGARNO.
The Queen's University of Belfast.
27th September 1956.

DALGARNO, A., and LEWIS, J. T., 1955, *Proc. Roy. Soc.* A, **233**, 70.
DALGARNO, A., and STEWART, A. L., 1956, *Proc. Roy. Soc.* A (in the press).
TREES, R. E., 1956, *Phys. Rev.*, **102**, 1553.
WIGNER, E. P., 1954, *Phys. Rev.*, **94**, 77.

REVIEWS OF BOOKS

Meson and Fields, Volume I. Fields, by S. S. SCHWEBER, H. A. BETHE and F. DE HOFFMANN. Pp. xvi + 449. (Evanston, Ill.: Row, Peterson and Co., 1955.) $8.00.

The years since the war have seen great developments in meson physics. On the one hand, the construction of particle accelerators of sufficient energy to produce mesons artificially has lead to a mass of experimental data on their properties, and a detailed confirmation of all the qualitative predictions of the Yukawa theory. (This material, with a partial theoretical analysis, is covered in Volume II of this series.) On the other hand, the discovery and explanation of the Lamb shift greatly increased our understanding of the interaction of the electromagnetic field with electrons and positrons. Quantum electrodynamics was set up in an explicitly covariant way, the graphical representation of the *S*-matrix was developed, and the technique of renormalization showed the way round the physically meaningless infinities, which had bedevilled previous formulations. All these developments have been taken over, at least formally, into meson theory. *Mesons and Fields, Volume I*, presents meson theory from this modern point of view for the first time. It was certainly high time that such a book should be written, as it had become virtually impossible for the student to separate the wheat from the chaff in the mass of papers which have been published on this subject during the last ten years.

The book opens with a discussion of relativistic equations from the one-particle point of view. The fundamental difficulties are explained, which force one to abandon this approach in favour of the many-particle, or field theoretic, picture. A preliminary, semi-heuristic, derivation of Feynmann's graphical rules is given at this stage. The quantization of the fields is then carried out using the Hamiltonian formalism. The *S*-matrix is defined, and the Feynmann graphs are derived by way of Wick's theorem. The 'renormalizable' interactions are then renormalized. The book ends with a derivation of the Bethe–Salpeter equation, and closed forms for the one-particle propagators in terms of Heisenberg operators.

This is not a great book. It has clearly been influenced by the much publicized, but never published, lectures of Dyson at Cornell University, but it lacks their crispness and authority. It is not the fault of the authors that renormalization can, so far, only be carried out in the context of an expansion in powers of the coupling constant, which is certainly not applicable to the strong meson–nucleon interaction. The graphical formalism still has to be understood by anyone interested in this subject, and the various simplifications and complications, which arise in taking over these concepts from photons to mesons, are sufficiently complex to be worth collecting coherently in one place. This has been well done, but it is a pity that this aspect of the theory is emphasized almost to the exclusion of all else. For example, the powerful technique, exploited particularly by Schwinger, of using functional derivatives with respect to external sources is not discussed, and the invariance properties of the fields, which have proved so valuable in analysing heavy meson data are treated rather scrappily or not at all. However, the book does what it sets

out to do adequately. It will certainly be out of date immediately any real advance is made in the field theoretic explanation of strong inter-particle interactions. But this may not be for a very long time, and in the meanwhile it will be very useful to many people. P. T. MATTHEWS.

Applications of Spinor Invariants in Atomic Physics, by H. C. BRINKMAN. Pp. 72. (Amsterdam: North-Holland, 1956.)

This book is described as giving a survey of the method of spinor invariants introduced by H. A. Kramer in 1930. It consists of three chapters, on notations and unitary transformations, wave function and spinor invariants, and the application of spinor invariants to detailed calculations. The author points out that the use of spinor invariants is dispersed amongst the journals and nowhere is collected together to form a coherent presentation, and had designed this book to remedy the situation. It is a readable book and will serve as a good introduction to the subject. It is a pity, however, that it is so brief. On several occasions the discussion breaks off before a problem is concluded with a reference to the complete treatment. The combination of two angular momenta is discussed in detail, but there is no reference to the fact that the method of spinor invariants will also solve the combination of three or more angular momenta, and can be used for example to produce the Racah coefficients in a straightforward manner. Indeed, there is only one reference to original work later than 1933. The book is, however, still useful and when the reviewer recalls the need he felt in undergraduate days for a good text to explain those mysterious ξ's and η's, he feels it will be much appreciated by beginners. S. F. EDWARDS.

BOOK NOTICES

Nuclear Levels in the Neighbourhood of the IF 7/2 *State*, by R. H. NUSSBAUM. Pp. 78. (Assen: von Gorcum, 1955.) 7.90 fl.

Chimie physique nucléaire appliquée, by J. ERRERA. Pp. 226. (Paris: Masson et Cie, 1956.) 2100 *fr.*

The Relations between Scientific Research in the Universities and Industrial Research (A Report on Conditions in Great Britain), Edited by V. E. COSSLETT. Pp. vii+187. (London: International Association of University Professors and Teachers, 1955.) 15*s.*

CONTENTS OF SECTION B

PAGE

Dr. A. N. Hunter. Measurements of the Velocity and Absorption of High-Frequency Ultrasonic Waves in Supercooled Liquids 965

Dr. J. Woods. Changes in Conductivity resulting from Breakdown in Cadmium Sulphide Single Crystals 975

Dr. F. C. Roesler. Brittle Fractures near Equilibrium 981

Dr. K. J. Standley and Dr. K. W. H. Stevens. The Anisotropy Correction in Ferromagnetic Resonance 993

Prof. L. F. Bates and Dr. S. J. Leach. The Magnetic Susceptibilities of Palladium–Uranium Alloys 997

Mr. W. S. Carter and Dr. K. W. H. Stevens. The Magnetic Susceptibilities of two Polymorphic Forms of Manganese Sulphide 1006

Dr. J. D. Eshelby. Supersonic Dislocations and Dislocations in Dispersive Media 1013

Prof. R. E. Burgess. The Statistics of Charge Carrier Fluctuations in Semiconductors 1020

Mr. A. E. Carte. The Freezing of Water Droplets 1028

Dr. J. S. Hey, Mr. G. S. Stewart, Mr. J. T. Pinson and Mr. P. E. V. Prince. The Scattering of Electromagnetic Waves by Conducting Spheres and Discs . . 1038

Research Notes :

Dr. S. A. Ahern and Prof. W. Sucksmith. Saturation Magnetization in Copper–Nickel Alloys 1050

Mr. G. S. Barlow and Dr. K. J. Standley. Spectroscopic Splitting Factors for Iron and Silicon–Iron 1052

Dr. I. S. Kerr. The Origin of the Hydrated Oxide formed when Anodic Aluminium Oxide Films are ' Sealed ' in Boiling Water 1055

Dr. P. T. Landsberg. Defects with Several Trapping Levels in Semiconductors 1056

Dr. T. B. Rymer, Dr. F. J. Fayers and Dr. S. J. Hewitt. Stacking Faults in Vacuum Evaporated Crystals of Copper and Silver 1059

Reviews of Books 1062

Contents of Section A 1068

Pseudoscalar Interaction in the Decay of ^{144}Pr

By M. J. LAUBITZ†
Cavendish Laboratory, Cambridge

Communicated by E. S. Shire; MS. received 14th November 1955, and in revised form 16th May 1956

Abstract. The ground state beta transition of ^{144}Pr has been studied experimentally and the results analysed. The analysis depends upon the spin assumed for the ground state of ^{144}Pr; if that state has spin and parity 0^-, as strong evidence indicates, then pseudoscalar interaction is needed to explain the results satisfactorily. The ratio of the coupling constants of pseudoscalar to tensor interactions required is approximately 100.

§ 1. Introduction

The determination of the spin of RaE as 1 (Smith and Title, private communication), and the reinterpretation of that transition in terms of the scalar (S) and the tensor (T) interactions (Yamada 1953, Plassmann and Langer 1954), removed the only direct evidence for the existence of the pseudoscalar (P) interaction. There is some evidence, however, that P does contribute to first and second forbidden transitions (Peaslee 1953, King and Peaslee 1954). In the first forbidden transition, P can contribute only to the cases where no change of spin occurs, and of those, the $0\rightarrow 0$ type are of particular interest, for there only one other nuclear element, $\int \beta\boldsymbol{\sigma}.\mathbf{r}$ of T, can contribute. According to Rose and Osborn (1954) an investigation of a spectrum of that kind should give the ratio of the coupling constants, g_P/g_T, if P does exist. We have, therefore, studied the ground state transition of ^{144}Pr, which is believed to be of type $0^-\rightarrow 0^+$.

§ 2. Summary of Previous Results

The beta spectrum of ^{144}Pr consists of three components, and is followed by three gamma rays. The essential features of the decay scheme are shown in figure 1. The results of recent investigations are summarized in the table. These

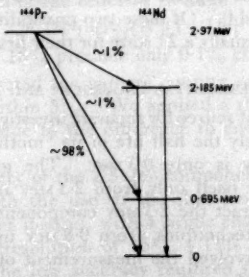

Figure 1. Decay scheme of ^{144}Pr.

† Now at the National Research Council of Canada.

results agree well in respect of beta and gamma ray energies. However, estimates of the intensities of the components of the beta transition vary considerably, and those determined from Kurie plots are larger than those from gamma ray intensities (Emmerich, Auth and Kurbaton 1954). This suggests that the Kurie plot of the ground state transition has not an allowed shape, but is slightly concave.

Summary of Results on Decay of ^{144}Pr

Reference	Beta rays			Gamma rays		
Energy (MeV)						
(1)	2·965	2·3	0·86	2·185	1·48	0·695
(2)	2·97	2·27	0·780	2·185	1·49 (?)	0·696
(3)	2·98	2·28	0·80			
(4)				2·185	1·49	0·695
(5)	3·12			2·18	1·49	0·688
Intensity of Components (%)						
(1) from Kurie Plot	~90	~5	~5			
(2) from Kurie Plot	>98	<1	<1			
(3) from Kurie Plot	95·5	1·7	2·8			
(3) from γ-rays	97·4	0·8	1·9			
(4) from γ-rays	97·3	1·44	1·26			
log *ft*						
(1)	6·6					
(2)	6·53					
(3)	6·5	8·1	6·0			

(1) Alburger and Kraushaar 1952.
(2) Porter and Cook 1952
(3) Emmerich *et al.* 1954
(4) Kreger and Cook 1954
(5) Cork *et al.* 1954

In addition to the results of the table, Porter and Cook (1952) reported a 60·3 kev internally converted gamma ray, which they assigned to ^{144}Nd. The report was confirmed by Emmerich *et al.* (1954) who also found the conversion line, but who could not find a 60 kev free gamma ray in chemically separated ^{144}Pr. Cork, Brice and Schmidt (1954) maintain, however, that there is no 60 kev line in Nd: it results from a misinterpretation of a 59 kev line in Pr.

Alburger and Kraushaar (1952) determined the angular correlation of the Nd gamma rays. Their results suggest a 1–1–0 or 1–2–0 cascade, the spin of the ground state being assumed 0. Of these two possibilities the latter is preferable, as even–even nuclei have usually a 2^+ state for their first excited level.

§ 3. Experimental Procedure and Results

^{144}Pr is a very convenient source for accurate investigation. It has an extensive energy range, and effectively the half life of its 'mother' nucleus, ^{144}Ce, whose maximum beta ray energy is only 0·3 MeV. The ground state transition of ^{144}Pr can be measured by itself only from 2·3 MeV upwards. To extend this range, we decided to subtract the 2·3 MeV component from the total spectrum by means of coincidence techniques, from 0·8 MeV upwards, giving a working range of 2·2 MeV. This involved the measurement of the total spectrum from 0·8 MeV to its end point, the measurement of the coincidence spectrum from 0·8 MeV to its end point, and then the subtraction of the coincidence from the total spectrum.

3.1. *Total Spectrum*

We measured the total spectrum in a thin lens spectrometer set at 6% resolution. The sources were prepared from high specific activity processed ^{144}Ce (obtained from the Radiochemical Centre, Amersham, England) dissolved in HCl. That solution was directly deposited on 0·2 mg cm^{-2} mica backing mounted in aluminium holders. The sources were 0·5 cm in diameter, uniform to the eye, and of average thickness of 25 μg cm^{-2}. We tested the quality of these sources by observing the conversion line of the 135 kev gamma ray of Ce. Two sources were selected from several that were prepared, both having uniform and symmetrical conversion lines. We determined the spectrum in 55 kev steps. The statistics were such that when all the results were combined, the standard deviation of each point varied from 0·3% at the edges of the spectrum to 0·15% at its centre.

3.2. *Coincidence Spectrum*

In order to obtain the pure ground state transition from 0·8 Mev upwards, we had to subtract the 2·3 Mev component. We achieved this by a coincidence technique. For in a coincidence circuit

$$N_\beta(W)=\epsilon_\beta[N_G(W)+N_1(W)] \qquad \ldots\ldots(1)$$

$$N_c(W)=N_1(W)\epsilon_\beta\epsilon_\gamma \qquad \ldots\ldots(2)$$

where $N_\beta(W)$ is the beta counting rate at energy W, $N_c(W)$ is the coincidence counting rate; $N_G(W)$, $N_1(W)$ refer to ground state and first excited transitions respectively. ϵ_β and ϵ_γ are the beta and gamma counter efficiencies inclusive of solid angle. Relation (2) holds if the resolving time is large enough to include all coincidences; this was true of our experiment. Thus

$$\frac{N_G(W)}{N_1(W)}=\left[\frac{N_\beta(W)}{N_c(W)}\epsilon_\gamma-1\right]=\gamma \qquad \ldots\ldots(3)$$

and since

$$N_G(W)+N_1(W)=N_T(W) \qquad \ldots\ldots(4)$$

where $N_T(W)$ is the total number of beta rays of energy W, then

$$N_G(W)=\frac{N_T(W)}{1+1/\gamma}. \qquad \ldots\ldots(5)$$

Previous results show that the 2·3 Mev component has an intensity of approximately 1%. γ is therefore of the order of 10^2, and

$$N_G(W)=N_T(W)[1-1/\gamma] \qquad \ldots\ldots(6)$$

Errors in γ of the order of 10% produce only 0·1% errors in $N_G(W)$.

To obtain ϵ_γ we calibrated the gamma counter on a source of ^{137}Cs, whose strength was known to within 5%. We applied a theoretical correction to the efficiency of the counter due to the difference in energy of the ^{137}Cs and ^{144}Pr gamma rays.

Due to the low intensity of the 2·3 Mev component, we could not obtain the coincidence spectrum with the use of the thin lens spectrometer. We used a scintillation spectrometer instead, with a single channel pulse height analyser. The arrangement had a resolution of 15%. This we considered to be quite satisfactory, in view of the low accuracy required for γ. Figure 2 shows the Kurie plots of the coincidence spectrum. We show the allowed Kurie plot,

and one corrected with the factor corresponding to the B_{ij} matrix element (Konopinski and Uhlenbeck 1941), giving end point energies of 2·35 MEV and 2·28 MEV respectively. The expected end point energy is 2·27 MEV (see table), and the close agreement between this and the end point of the corrected Kurie plot lends support to the spin assignment of 0^- to ^{144}Pr.

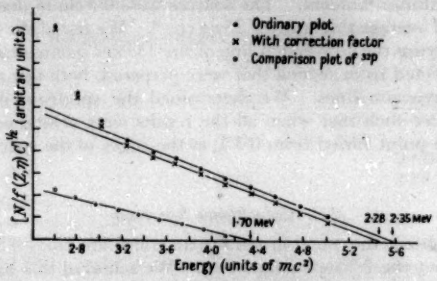

Figure 2. Kurie plots of the coincidence spectrum. Correction factor corresponds to B_{ij}.

The coincidence spectrum was used to calculate γ by means of relation (3), and then $N_G(W)$ was calculated using (6). The possible error in $N_G(W)$ is difficult to assess accurately; it will be considered here only approximately. The error in each N_G is of two kinds: the statistical error in N_T, and the error in γ. Errors in γ are not of a statistical nature, as the results have been 'smoothed' by the use of the Kurie plot. They arise mainly from a possible energy dependent error in N_β/N_c, due to the large resolution of the crystal spectrometer, and a possible constant error in ϵ_γ. Each of these errors does not exceed 5%. The standard deviation of N_T varies between 0·15% and 0·3%, so that the total error in each N_G should not exceed 0·5%.

§4. Analysis

Figure 3 shows the Kurie plot† of the total spectrum of ^{144}Pr, giving an end point of 2·99 MEV. It also shows the allowed Kurie plot for the ground state transition alone, corrected for the screening effect of atomic electrons†. This plot is not linear; there is a definite curvature concave upwards. This curvature must be genuine; the sources used were of such quality as to cause no possible distortion at the high energies considered, and calculations done by us show that the 6% resolution of the spectrometer has no effect whatsoever on the spectral shape in the range of 0·8 to 2·8 MEV. If, as we have assumed, the transition is $0^-\rightarrow 0^+$, the Kurie plot must be corrected with the first forbidden correction factor given by Rose and Osborn (1954)

$$C_1 = g_T{}^2 C_{1T} + g_T g_P C_{1TP} + g_P{}^2 C_{1P} \qquad \ldots\ldots(7)$$

where g_T and g_P are the coupling constants of the T and P interactions, C_{1T} and C_{1P} are the corresponding correction factors appropriate to $0\rightarrow 0$, yes,

† The analysis of the spectrum was carried out using the tables of the National Bureau of Standards (*Appl. Math. Series* No. 13). This reference was also used for calculating the screening effect of atomic electrons.

transitions, and C_{1TP} is an interference term. C_{1T}, C_{1P} and C_{1TP} were calculated using tables prepared by Rose, Perry and Dismuke (ORNL-1459). The calculations of C_{1P} and C_{1TP} require the estimation of the nuclear radius in evaluating the function U of Rose and Osborn (1954). We have assumed $R = 1{\cdot}45 \times 10^{-13} A^{1/3}$ cm. Figure 3 also shows the Kurie plots corrected with C_1 for $g_P = 0$ and $g_T = 0$. Both these plots are concave, showing that the interaction cannot be pure T or pure P if the transition is $0^- \rightarrow 0^+$.

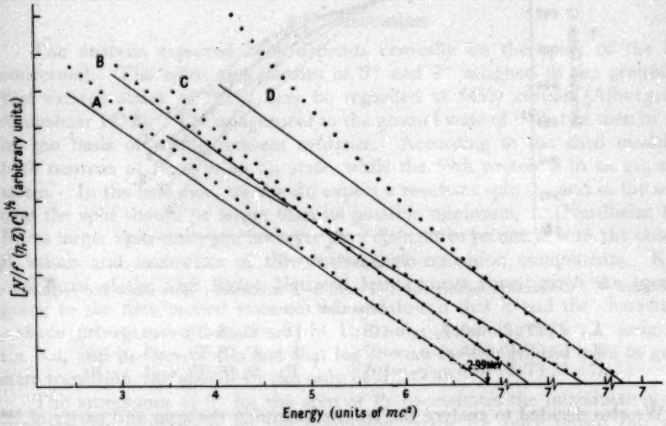

Figure 3. Kurie plots of the total spectrum and the separated ground state spectrum : A, total spectrum; B, allowed plot of ground state spectrum; C, ground state spectrum corrected with C_{1T}; D, ground state spectrum corrected with C_{1P}.

In further analysis we decided to use as test the shape of the correction factor required rather than the linearity of the Kurie plot, the former being more sensitive to deviations. The shape of the spectrum is given by

$$N(W)dW = \left(\frac{g^2}{2\pi^3}\left|\int \ldots\right|^2\right) F(Z,W)pW(W_0 - W)^2 C_1(W)dW \quad \ldots(8)$$

where $C_1(W)$ is the required correction factor. We assumed $W_0 = 2{\cdot}99$ MeV, and the correction factor obtained from (8) is shown in figure 4. To obtain the theoretical factor, (7) was changed to form

$$C_1 = g_T^2\left(C_1 + \frac{g_P}{g_T}C_{1TP} + \frac{g_P^2}{g_T^2}C_{1P}\right). \quad \ldots\ldots(9)$$

Taking the ratio of two widely separated points of the required C_1 and solving equation (9), two values for g_P/g_T were obtained, 107 and 131. $g_P/g_T = 131$ gives $C_1 \sim 0$, occasionally assuming negative values, $g_P/g_T = 107$ gives a correction factor which fits the required one very well; it is shown in figure 4, where correction factors for $g_P/g_T = 105$ and 110 are also given for purposes of comparison. The Kurie plot for the spectrum corrected with $C_1(g_P/g_T = 107)$ shows no deviation

from linearity whatsoever; small deviations were present when $C_1(g_P/g_T=105)$ and $C_1(g_P/g_T=110)$ were used. It is worth noting that g_P/g_T must be positive; any negative value makes the Kurie plot more concave than that for pure T.

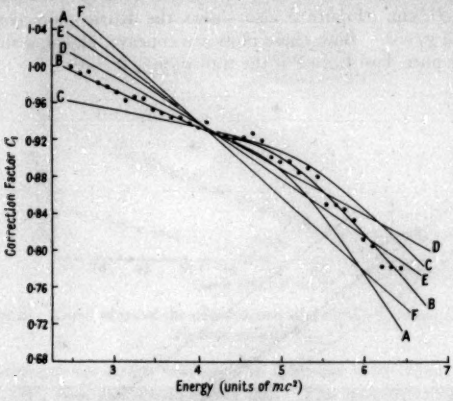

Figure 4. Correction factors for T–P and S–T mixtures; dots show the required correction factor.

A: C_1 (T–P) with $g_P/g_T=110$; D: C_1 (S–T), $\epsilon=1$, $\chi=70$
B: C_1 (T–P) with $g_P/g_T=107$; E: C_1 (S–T), $\epsilon=1$, $\chi=60$
C: C_1 (T–P) with $g_P/g_T=105$; F: C_1 (S–T), $\epsilon=1$, $\chi=50$

We also decided to analyse the results assuming the spin and parity of ^{144}Pr to be 1^- and 2^-. For the 2^- case, the only matrix element contributing is the B_{ij} of the T interaction; the shape of its correction factor makes this choice of spin unacceptable. For the 1^- case both the T and S (scalar) interactions can contribute and

$$C_1=g_S^2C_{1S}+g_Sg_TC_{1ST}+g_T^2C_{1T} \qquad \ldots\ldots(10)$$

where C_{1S} and C_{1T} are given by Konopinski and Uhlenbeck (1941) and C_{1ST} by Smith (1951).

In the notation of Konopinski and Uhlenbeck:

$$\epsilon=i\frac{g_S}{g_T}\frac{\int\beta\mathbf{r}}{\int\beta\boldsymbol{\sigma}\times\mathbf{r}}; \qquad \chi=\frac{\int\beta\mathbf{r}}{\int\beta\boldsymbol{\sigma}\times\mathbf{r}}$$

$$a=\tfrac{1}{6}K^2L_0+\tfrac{1}{2}L_1+M_0-\tfrac{2}{3}KN_0, \qquad b=L_0,$$

$$c=\tfrac{1}{3}K^2L_0+2L_1+M_0+\tfrac{2}{3}KN_0, \qquad d=2(\tfrac{1}{3}KL_0-N_0),$$

$$e=2(M_0-L_1), \qquad f=-2(N_0+\tfrac{1}{3}KL_0)$$

equation (10) becomes

$$C_1=g_T^2\left|\int\beta\boldsymbol{\sigma}\times\mathbf{r}\right|^2(a+b\chi^2+c\epsilon^2-d\chi+e\epsilon-f\epsilon\chi). \qquad \ldots\ldots(11)$$

The values of a, b, etc., were calculated from the tables by Rose, Perry and Dismuke. Then, choosing values for ϵ, different values for χ were tried in an attempt to fit the required correction factor. Values chosen for ϵ ranged from

-3 to $+3$. Some results are shown in figure 4. Agreement of the same order as that obtained with $\epsilon=+1$, $\chi=60$ (figure 4) was found for any value of ϵ selected, but a fit as good as that of the T–P mixture could not be obtained. However, from the point of view of linearity of the Kurie plot the correction factors obtained with pairs like $\epsilon=+1$, $\chi=60$ give quite acceptable results. The deviations from linearity can barely be perceived on a large scale graph. All the pairs of most acceptable values of ϵ and χ were found to lie on the straight line $\chi=41{\cdot}5\epsilon+19$; similar findings were reported by Plassmann and Langer (1954) in their analysis of RaE.

§ 5. Discussion

The analysis reported here depends critically on the spins of the levels concerned. The spins and parities of 0^+ and 2^+ assigned to the ground and first excited states of ^{144}Nd may be regarded as fairly certain (Alburger and Kraushaar 1952). The assignment to the ground state of ^{144}Pr can then be made on the basis of strong indirect evidence. According to the shell model, the 85th neutron of Pr is in an $f_{7/2}$ state, while the 59th proton is in an $g_{7/2}$ or $d_{5/2}$ states. In the first case, we should expect a resultant spin 0^-, and in the second case the spin should be larger than its possible minimum, 1^- (Nordheim 1951). Spins larger than unity are however very difficult to reconcile with the observed *ft* values and intensities of the various beta-transition components. Ketelle and Brosi of the Oak Ridge National Laboratories investigated the spectrum going to the first excited state of Nd, and found that it had the characteristic α shape (private communication by M. E. Rose). Assuming the 0^+, 2^+ assignment for Nd, and in view of the fact that $\log ft=6{\cdot}6$ for the ground state to ground state transition, the spin of Pr can only be 0^-.

The acceptance of 0^- for the spin of Pr necessitates the introduction of the pseudoscalar interaction, as the correction factor for pure tensor interaction increases the curvature of the Kurie plot to an unacceptable extent. The value of $g_P/g_T=107$ obtained in this experiment cannot be considered accurate, however. It depends heavily on the value of the nuclear radius assumed, and, of course, on the validity of the Rose and Osborn theory. This theory can be criticized on two points. Primarily, it makes no allowances for possible nuclear forces with pseudoscalar coupling. Such pseudoscalar coupled potentials would have a large effect on nuclear matrix elements (Ruderman 1953, Peaslee 1953). Secondarily the T–P correction factor with $g_P/g_T\sim100$ involves large cancellation; its numerical value is only about 4% of that for T alone. Under these conditions terms of order $1/M^2$ neglected by Rose and Osborn may become very important and change the shape of the correction factor considerably; Alaga *et al.* (1953) maintain that such terms are important even without cancellation. A further correction may arise from the finite nuclear size effect (Rose and Holmes 1951). This is not expected to affect our results much; although corrections to the quantities L_K, M_K and N_K are of the order of 30%, they are insensitive to energy variations, and occur in C_{1T}, C_{1P} and C_{1TP} in roughly the same form. They would therefore not affect the cancellation required to straighten the Kurie plot to any large extent. In view of these possible corrections, the value of g_P/g_T obtained by us is in considerable doubt, and cannot be really considered in disagreement with the results of Alaga *et al.* (1953) who obtain $g_P/g_T\leqslant100$ from

a study of the spectrum of ^{6}He, and $g_P/g_T \leqslant 50$ from ^{12}B. Our results are, however, in disagreement with those of Brysk (1954), who obtains upper limits on g_P/g_T from the study of Δl-forbidden transitions. His results are: $g_P/g_T \leqslant 20$ from ^{32}P, $g_P/g_T \leqslant 4$ from ^{14}C and $g_P/g_T \leqslant 15$ from transitions with $A \sim 30$.

There is another argument which can be used to show that P is necessary if the transition is $0^- \rightarrow 0^+$. Brysk (1954) suggests that the following is a reasonable estimate:

$$\left| \int \beta\sigma \right| = \left| R^{-1} \int \beta\sigma \,.\, \mathbf{r} \right|.$$

Using ft values for the $\Delta J = 1$, no, transitions where $\int\beta\sigma$ operates, we can then calculate the numerical value of the correction factor for the ^{144}Pr transition. Taking $\log ft = 4{\cdot}6$ for the allowed transitions with even A, and $\log ft = 6{\cdot}6$ for Pr, we get $C_1 \simeq 20$. This must be compared with $C_1 \simeq 160$ for pure T, and $C_1 \simeq 5$ for T–P mixture with $g_P/g_T = 100$. Thus a certain amount of cancellation is necessary to reduce C_1 from its value for pure T, though the cancellation required does not appear to be as large as that found by us from the shape of the correction factor.

It is interesting to note that our results can be explained quite well by the S–T mixture, assuming the spin of Pr to be 1^-. According to theory (Pursey 1951, Ahrens and Feenberg 1952) one would expect the following values for the ratios of the nuclear matrix elements: $\epsilon = +1$ if the proton state is $d_{5/2}$ and $\epsilon = +\frac{1}{3}$ if the proton state is $g_{7/2}$ (assuming $g_S/g_T = -1$). In both cases $\Lambda = (\alpha Z/2R)^{-1}X = 1$–$2$. Our results can be explained quite well with pairs of values lying on the line $\Lambda = 3{\cdot}6\epsilon + 1{\cdot}6$ in the range $\epsilon = -3$ to $+3$. Thus, for $\epsilon = +1$ and $+\frac{1}{3}$ we get $\Lambda = 5$ and 2 respectively. The second pair of values agrees well with the theoretical predictions. That the theory gives roughly the right magnitude for the ratio of the matrix elements is shown by the results of Plassmann and Langer (1954) for RaE. They found a good fit for the spectrum with $\epsilon \simeq 0{\cdot}2$ and $\Lambda \simeq 1{\cdot}7$, while the theory predicts $\epsilon = 0{\cdot}1$, $\Lambda = 1$–2, if the 1^- spin of RaE arises from an $h_{9/2}$ proton coupling with a $g_{9/2}$ neutron.

§ 6. Conclusions

The experimental results of Alburger and Kraushaar (1952) and Ketelle and Brosi leave little doubt that the ground state to ground state transition of ^{144}Pr is of type $0^- \rightarrow 0^+$. The transition then cannot be explained in terms of the tensor interaction alone; pseudoscalar interaction is necessary to account for both the shape and magnitude of the correction factor. The ratio of coupling constants required is approximately 100.

References

Alaga, G., Kofoed-Hansen, O., and Winther, A., 1953, *K. Danske Vidensk. Selsk., Mat.-fys. Medd.*, **28**, No. 3.

Ahrens, T., and Feenberg, E., 1952, *Phys. Rev.*, **86**, 64.

Alburger, D. E., and Kraushaar, J. J., 1952, *Phys. Rev.*, **87**, 448,

Brysk, H., 1954, *Phys. Rev.*, **94**, 1794.

Cork, T. M., Brice, M. K., and Schmidt, L. C., 1954, *Phys. Rev.*, **96**, 1295.

Emmerich, W. S., Auth, W. T., and Kurbaton, T. D., 1954, *Phys. Rev.*, **94**, 110.

King, R. W., and Peasler, D. C., 1954, *Phys. Rev.*, **94**, 1284.

Konopinski, E. J., and Uhlenbeck, G. E., 1941, *Phys. Rev.*, **60**, 308.

Kreger, W. E., and Cook, C. S., 1954, *Phys. Rev.*, **96**, 1276.

NORDHEIM, L. W., 1951, *Rev. Mod. Phys.*, **23**, 332.
PEASLEE, D. C., 1953, *Phys. Rev.*, **91**, 1447.
PLASSMANN, E. A., and LANGER, L. M., 1954, *Phys. Rev.*, **96**, 1593.
PORTER, F. T., and COOK, C. S., 1952, *Phys. Rev.*, **87**, 464.
PURSEY, D. L., 1951, *Phil. Mag.*, **42**, 1193.
ROSE, M. E., and HOLMES, D K., 1951, *Phys. Rev.*, **83**, 190.
ROSE, M. E., and OSBORN, R. K., 1954, *Phys. Rev.*, **93**, 1315.
RUDERMAN, M., 1953, *Phys. Rev.*, **89**, 1227.
SMITH, A. M., 1951, *Phys. Rev.*, **82**, 955.
YAMADA, M., 1953, *Progr. Theor. Phys., Japan*, **10**, 252.

π^+–p Scattering at 10–35 MeV in a Diffusion Cloud Chamber

By M. H. ALSTON, W. H. EVANS, MARIA FIDECARO,†
R. W. NEWPORT, G. VON GIERKE‡ and P. R. WILLIAMS
Nuclear Physics Research Laboratory, University of Liverpool

Communicated by H. W. B. Skinner; MS. received 18*th June* 1956
and in final form 18*th July* 1956

Abstract. An investigation has been made of π^+–p scattering at incident pion energies of $20(^{+15}_{-10})$ MeV, using a hydrogen filled diffusion cloud chamber in a magnetic field. Fifteen π^+–p scattering events were observed and the incident pion spectrum and path length were determined from measurements on π–μ decays. The results were analysed by using the values for the phase shifts $\alpha_{33} = 0{\cdot}235\eta^3$, $\alpha_{31} = 0$ and assuming that α_3 is directly proportional to η. The phase shift α_3 was then found to be $-(0{\cdot}13 \pm 0{\cdot}035)\eta$ radians, where η is the pion momentum in mass units.

§ 1. Introduction

The low energy scattering of π-mesons by protons is of great interest, since at these energies the S-wave scattering is not masked by the P-wave scattering and the small S-wave phase shifts can be found. A knowledge of these phase shifts is important and at the time when the present experiment was in progress there was a discrepancy between the values obtained from experiments on the Panofsky ratio and low energy pion–nucleon scattering. The difference between the results is now within the experimental errors and any small disagreement which may remain can possibly be explained by the failure of isotopic spin conservation at low energies (Noyes 1956).

At low energies pion–nucleon scattering experiments are difficult because the cross sections are small and the short ranges of all the particles necessitate the use of thin targets. Counter techniques have only been used above 30 MeV for elastic scattering (Angell and Perry 1953 a, b, c, Barnes *et al.* 1953, Leonard and Stork 1954, Sachs *et al.* 1955) and above 20 MeV for charge exchange scattering (Spry 1954, Tinlot and Roberts 1953, 1954). For elastic scattering experiments at 20–30 MeV nuclear emulsions have been used. Orear *et al.* (1954 a), Orear (1955 a) have observed scattering events occurring in the emulsion and Whetstone and Stork (1956) have used an emulsion stack to detect pion scattering by a liquid hydrogen target. The first method has the disadvantage that the target is not pure and in the second the actual scattering event is not observed. In both methods the identification of events is difficult and the emulsions require specialized scanning.

A study of negative pion–proton scattering at 0 to 25 MeV has been made by Rinehart *et al.* (1955) using a hydrogen filled diffusion cloud chamber in a magnetic field. The gas filling of such a chamber is almost a pure proton target and the scanning although tedious is straightforward. Scattering events can be easily

† On leave of absence from the University of Rome, Italy.
‡ Member of the Synchrocyclotron Division of C.E.R.N., now at Geneva.

identified and the measurement of π–μ decay events gives a simple and accurate method of obtaining the pion path length and spectrum. This method of obtaining scattering events is very slow since the gas density is low and the repetition rate is limited by the slow recovery of the cloud chamber. Liquid hydrogen bubble chambers would obviously be more efficient detectors for this type of experiment and they will undoubtedly be used in the future.

The values of the phase shifts obtained in the earlier experiments have been summarized by Orear (1954, 1955 b) and the later work by Whetstone and Stork (1956).

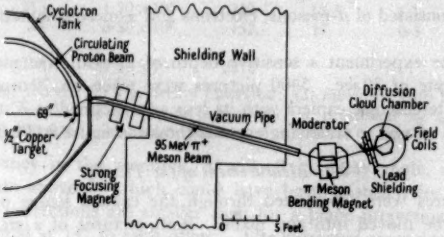

Figure 1. Experimental arrangement.

Operating conditions of the diffusion cloud chamber :

Run	Pressure (lb in^{-2})	Mean gas density (mg cm^{-3})
1	348	2·54
2	378	2·74
3	365	2·64

Mean temperature in sensitive region -35°c.

Moderator: 1st run: 1·532 in. of copper = 35 g cm^{-2};
2nd & 3rd runs: 9·75 in. of polythene = 22·6 g cm^{-2}.

§ 2. Experimental Procedure

The arrangement of the apparatus is shown in figure 1. The 18 in. diameter diffusion cloud chamber already described (Alston *et al.* 1956) was filled with approximately 25 atmospheres of hydrogen and a steady magnetic field of 2·3 kilogauss was applied. The pressure and the mean temperature of the gas in the sensitive region of the chamber were carefully monitored throughout the experiment to obtain the mean gas density. A 95 Mev beam of π^+-mesons was produced by the proton bombardment of a $\frac{1}{2}$ in. thick copper target placed in the cyclotron tank at a radius of 69 in. This beam was moderated at the focus of the π-meson magnet and entered the chamber through a phosphor bronze window 2 in. × 3 in. × 0·018 in.

It is difficult to obtain a moderated beam with the required characteristics. The track measurements would be simplified if a monoenergetic beam were available and for the reliable detection of π–μ decays the track density should be low and uniform throughout the sensitive region of the chamber. A monoenergetic beam could only be obtained by attenuating the original beam in front of the π-meson magnet and this procedure yielded a low energy beam of insufficient intensity. To obtain a beam in which the tracks are well separated

a heavy moderator would be preferable since the multiple scattering angle is large. In a preliminary run a copper moderator was used but a very diffuse pion spectrum was obtained and a polyethylene absorber was used in the two subsequent runs. This gave a moderated beam with a less diffuse spectrum which extended from 0 to 40 Mev and was peaked at 20 Mev. The synchrocyclotron produced 100 beam pulses per second and a small number of these were used per picture. Unfortunately the radio-frequency pulser was unreliable and the beam intensity was small and variable. The average number of beam pulses per picture was three and the π^+-meson intensity, in the energy range 10–35 Mev, was seven per picture for an average length of 35 cm. There was also a contamination of 30% which consisted of μ-mesons, electrons and π-mesons outside the accepted energy range.

During the experiment a sensitive depth of $2\frac{1}{2}$–3 in. was maintained with a repetition rate of 30 sec. 5400 pictures were taken on 70 mm Ilford 5G91 film using a stereoscopic camera with its lens axes inclined at 7° to the vertical. A photograph of a π^+–p scattering event is shown in figure 2 (Plate).

2.1. *Measurement of the Tracks*

The pictures were reprojected through the camera lenses on to a screen which could be moved into any plane. Both pictures of a stereo pair were scanned for π^+–p and π–μ decay events with the screen horizontal.

The true radius of curvature and dip angle of a decaying pion were measured if the projection of the decay angle on to the horizontal plane from either lens was equal to or greater than 5° and the incident energy was between 5 and 40 Mev. From these measurements and a knowledge of the gas density and π-meson life-time the π-meson spectrum and the scanned path length in g cm^{-2} could be computed (Fowler *et al.* 1953).

Scattering events were identified by kinematics and were accepted if the scattering angle in the centre-of-mass system was greater than 60° (~52° in the laboratory system) and if the incident energy was between 10 and 35 Mev. If the curvature of the incident track could not be measured it was estimated from the proton range and/or the curvature of the scattered meson track. The cut-off in angle and the lower cut-off in energy were applied so that the ranges of the proton recoils from acceptable scattering events were greater than 5 mm. This ensured that π–p events were not missed and that there was no confusion between π–μ decays with associated δ-rays and true scattering events. The high energy cut-off was imposed because there were relatively few π–μ decays above 35 Mev and also because accurate measurement of the track curvature was difficult.

All the pictures were rescanned for π–p events only and the combined scanning for scattering events was then considered to be 100% efficient. 1000 pictures were rescanned very carefully for π–μ decays to obtain the efficiency of the first scan. The π–μ decay events obtained in the two scans were compared and when they had been suitably combined it was assumed that all the decays with projected angle greater than 5° had been found. The mean efficiency for finding π–μ decay events was found to be 82% for the first scan and 94% for the second. The efficiency appeared to be uniform over the spectral range and showed no systematic variations.

2.2. *Results*

During the first scan 2841 π–μ decays in the energy range 5–40 MeV were measured. Corrections are applied to the spectrum obtained (table 1) to allow

Table 1. The Incident π^+-Meson Spectrum

(1)	(2)	(3)	(4)	(5*a*)	(5*b*)	(6)
5–10	465	$1{\cdot}20\times10^5$	317	6	6	388
10–15	601	$1{\cdot}98\times10^5$	522	8	3	657
15–20	655	$2{\cdot}58\times10^5$	677	10	2	896
20–25	559	$2{\cdot}51\times10^5$	659	12	1·5	900
25–30	262	$1{\cdot}32\times10^5$	348	13·5	1	486
30–35	215	$1{\cdot}20\times10^5$	312	15·5	1	447
35–40	84	$0{\cdot}50\times10^5$	132	17	0·5	192
Total 10–35	2292	$9{\cdot}59\times10^5$	2518			3386

(1) Incident energy (MeV); (2) π–μ decays measured; (3) measured path length L (cm); (4) measured path length x (g cm^{-2}); (5) corrections: a, projection $\alpha_p(\%)$, b, Coulomb scattering α_c; (6) corrected path length $[x/(1-\alpha_p+\alpha_c)]100/82$ (g cm^{-2}).

for the inefficiency in the scanning, 5° cut-off in decay angle, and coulomb scattering events above 5° which could have been mistaken for π–μ decays. The 5° cut-off corrections are smaller than for a plane projection because the lenses are inclined at 14° to each other. The corrected spectrum is shown in figure 3.

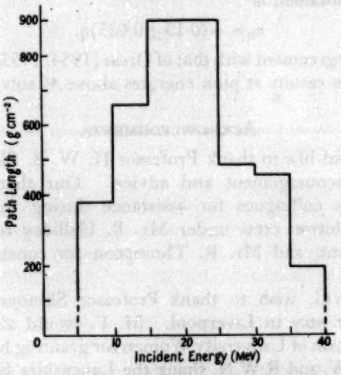

Figure 3. Corrected spectrum of incident π^+-mesons.

Fifteen π^+–p scattering events were found with incident energy in the range 10–35 MeV and with scattering angle greater than 60° in the centre-of-mass system (table 2). No events were missed due to the 5° cut-off in reprojection.

Table 2. Accepted π^+–p Scattering Events

Incident pion energy (MeV)	10–12	16	19	21	23	23	25	26
Pion scattering angle (c.m.s.) (deg.)	152	74	110	137	150	157	116	152
Incident pion energy (MeV)	26	25–27	25–27	29	31	32	31–34	
Pion scattering angle (c.m.s.) (deg.)	79	78	80	114	141	70	165	

The average total cross section over the accepted energy range for $\theta > 60°$ is found to be 7·4 millibarns.

The differential cross section for π^+–p scattering at low energies is given by

$$\frac{d\sigma^+}{d\omega} = \lambda^2 \left\{ \left[\alpha_3 + (2\alpha_{33} + \alpha_{31}) \cos\theta - \frac{\alpha}{1-\cos\theta} \right]^2 + (\alpha_{33} - \alpha_{31})^2 \sin^2\theta \right\} \quad \ldots\ldots(1)$$

(Bethe and de Hoffmann 1955). We assume (Orear 1954)

$$\alpha_{33} = 0{\cdot}235\eta^3, \qquad \alpha = 1/137\beta_\pi, \qquad \alpha_{31} = 0$$

and also

$$\alpha_3 = -q\eta \quad \ldots\ldots(2)$$

where q is a constant, η the momentum of the incident pion in the centre-of-mass system in units of μc and β_π the velocity of the pion in the laboratory system in units of c.

From equations (1) and (2) and the incident pion spectrum (figure 3), the predicted number of events for various values of q is calculated and compared with the number actually found. This calculation gives a value $q = 0{\cdot}13 + 0{\cdot}03$, where the error is the standard deviation in the number of events only.

The systematic experimental error is estimated as 5%, arising from errors in the knowledge of scanning efficiency, gas density and the corrections applied to the spectrum. A further small error may be introduced by assuming $\alpha_{31} = 0$; however, this phase shift is known to be small and a value $\alpha_{31} = 1°$ makes less than 1% difference to the predicted number of events.

The final value obtained is

$$\alpha_3 = -(0{\cdot}13 \pm 0{\cdot}035)\eta. \quad \ldots\ldots(3)$$

This value is in good agreement with that of Orear (1954, 1955 a, b), i.e. $\alpha_3 = -0{\cdot}11\eta$ deduced mainly from results at pion energies above 40 MeV.

Acknowledgments

The authors would like to thank Professor H. W. B. Skinner and Dr. J. M. Cassels for their encouragement and advice. Our thanks are also due to Dr. Cassels and his colleagues for assistance during the preliminary beam engineering, the cyclotron crew under Mr. B. Halliday for their co-operation during the experiment, and Mr. R. Thompson for constructing some of the apparatus.

M. F. and G. von G. wish to thank Professor Skinner for the hospitality received during their stay in Liverpool. M. F. would also like to thank the International Federation of University Women for granting her an Alice Hamilton Fellowship and P.R.W. and R.W.N. thank the Lancashire Education Committee and D.S.I.R. respectively for maintenance grants.

References

Alston, M. H., Crewe, A. V., Evans, W. H., and von Gierke, G., 1956, *Proc. Phys. Soc.* A, **69**, 691.

Angell, C. E., and Perry, J. P., 1953 a, *Phys. Rev.*, **91**, 468; 1953 b, *Ibid.*, **91**, 1289; 1953 c, *Ibid.*, **92**, 835.

Barnes, S. W., Angell, C. E., Perry, J. P., Miller, D., Ring, J., and Nelson, D., 1953, *Phys. Rev.*, **92**, 1327.

BETHE, H. A., and DE HOFFMANN, F., 1955, *Mesons and Fields*, Vol. 2, (New York: Row, Peterson), Sec. 33A.
FOWLER, E. C., FOWLER, W. B., SHUTT, R. P., THORNDIKE, A. M., and WITTMORE, W. L., 1953, *Phys. Rev.*, **91**, 135.
LEONARD, S., and STORK, D., 1954, *Phys. Rev.*, **93**, 568.
NOYES, H. P., 1956, *Phys. Rev.*, **101**, 320.
OREAR, J., 1954, *Phys. Rev.*, **96**, 176; 1955 a, *Ibid.*, **98**, 239; 1955 b, **100**, 288.
OREAR, J., SLATER, W., LORD, J. J., EILENBERGER, S. L., and WEAVER, A. B., 1954, *Phys. Rev.*, **96**, 175.
RINEHART, M. C., ROGERS, K. C., and LEDERMAN, L. M., 1955, *Phys. Rev.*, **100**, 883.
SACHS, A. M., WINICK, H., and WOOTEN, B. A., 1955, *Phys. Rev.*, **100**, 1255.
SPRY, W., 1954, *Phys. Rev.*, **95**, 1295.
TINLOT, J. A., and ROBERTS, A., 1953, *Phys. Rev.*, **90**, 951; 1954, *Ibid.*, **95**, 137.
WHETSTONE, S. L., and STORK, D., 1956, *Phys. Rev.*, **102**, 251.

The Energy Spectrum of Extensive Air Showers

By R. J. NORMAN
Physics Department, University of Melbourne

Communicated by L. H. Martin; MS. received 2nd February 1956 and in revised form 24th April 1956

Abstract. The integral shower density spectrum from 20–1000 particles per square metre is measured with three-fold proportional counters 60 metres above sea level, and follows a law

$$\nu(\rho) = 540\,\rho^{-1\cdot39\pm0\cdot04}\,\mathrm{h}^{-1}, \text{ for } \rho < 500 \text{ particles m}^{-2},$$

in agreement with previous Geiger counter results; an agreement which confirms energy loss measurements as a means of particle density determination. For $\rho > 500$ the exponent increases quickly, reaching 2·2 at $\rho = 1000$, which is typical of the value observed with ionization chambers.

The density spectrum is analysed, allowing for effects of shower age on structure to obtain the distribution in number

$$S(N) = 2\cdot3 \times 10^{-4}\,(N \times 10^{-6})^{-1\cdot47\pm0\cdot1}\,\mathrm{m}^{-2}\,\mathrm{h}^{-1},$$

with evidence for a rapid increase in exponent above $N = 10^6$ particles. Using cascade theory the latter is shown to be produced by a primary energy spectrum

$$V(E) = 0\cdot32\,(E \times 10^{-14})^{-1\cdot5}\,\mathrm{m}^{-2}\,\mathrm{h}^{-1}\,\mathrm{sterad}^{-1},$$

for $10^{13} < E < 10^{15}$, above which the exponent increases rapidly, reaching about -3 at $E = 10^{17}$ ev. Since shower primaries of these energies should be little affected by solar or terrestrial magnetic fields, this will be the form of the primary spectrum.

§ 1. Introduction

Molière's (1946) theory of the cascade development of air showers, and its extension by Nishimura and Kamata (1951) to include ionization losses, starts with the assumption that showers are initiated by single high energy photons or electrons. The theory is in substantial agreement with experimental determinations of shower structure at distances from the core exceeding one metre. The shower structure closer to the core has been shown to be flatter than that predicted by cascade theory, due presumably to multiple core production in the initial interaction. It is now practically certain that the primary radiation consists not of electrons or photons, but of protons, alpha particles and heavier nuclei (Bradt and Peters 1950). Since the primary interaction is a nuclear one, we can be assured of the multiple character of the meson producing act; and although there is no convincing experimental evidence for multiple core detection, none would be expected if the multiplicity is high, when neighbouring cores would tend to smooth and flatten the structure function.

From earlier shower experiments it has been concluded that individual primaries have energies exceeding 10^{17} ev, but the evidence in support of this is indirect. In particular it has been contested by Cocconi, Cocconi-Tongiorgi and Greisen

(1949), who state that what has been proved, in fact, is that counters of small area and a few metres apart or of large area hundreds of metres apart have been simultaneously discharged with appreciable frequency. The conclusions drawn from such experiments are based upon a number of assumptions: (1) that all showers are at maximum development and have the Molière (1946) structure, (2) that there are no local condensations or multiple cores in the shower and (3) that the apparatus has a uniform response regardless of the direction of arrival.

These conclusions depend, moreover, upon a detailed knowledge of the exponent of the primary energy distribution above 10^{13} ev, and especially upon the existence or absence of a high energy cut-off. The high altitude photographic plate work, which extends only as far as 10^{10} ev, gives direct evidence for an exponent of about 1·45 in the primary spectrum. But the greater part of the evidence, which is indirect, comes from the particle density distribution. For this, Geiger counter measurements indicate an exponent of 1·4–1·5, and ionization chambers, at a higher density, indicate 1·5–3·1, with no agreement between the two methods in the region of overlap. This makes the choice of exponent uncertain where an exact knowledge of the spectral form is most essential. If this spectrum does continue to infinite energies with the value of 1·5, which is usually taken as the exponent, it can be shown that primaries with energy greater than 10^{17} ev arrive at the rate of 1 per square metre every 60 years. Because of the great rarity of these events, the statistical uncertainties involved, and the questionable nature of the assumptions, conclusions drawn therefrom are possibly in error.

Measurements on the particle density distribution are made in the present experiment, in a density range produced by showers of energy 10^{13} to 10^{17} ev. Pulse heights from three proportional counters, in a triangular arrangement, are recorded photographically whenever a coincidence occurs. The integral pulse height distribution at any individual counter is identified with the particle density spectrum, and has an exponent similar to that of the Geiger counter measurements at the lower densities, and similar to the ionization chamber measurements at high densities. Starting from this particle density distribution, a simple change in shower structure with age is assumed, and the distribution in number evaluated. The primary spectrum deduced from this distribution shows a rapid increase in exponent above 10^{15} ev, which is consistent with a cut-off in the energy–nucleon spectrum.

§ 2. Apparatus

The apparatus is housed in a cement sheet hut on the roof of the Physics building, University of Melbourne, about 60 metres above sea level and at 38°S geomagnetic latitude. The particle density measurements are made with three proportional counters which are arranged radially, in a horizontal plane 1 metre below the hut roof, at the three corners of a 5-metre equilateral triangle, one side of which lies in the E–W direction. The proportional counters, which have been recently described (Norman 1955) are of the control grid type, 0·05 square metre in area, with a grid system of 24 fine wires surrounding the central wire at a 1 cm radius. Both the centre wire and grid system are mounted concentrically in a thin shell made from 0·006 in. tin-plate, which, together with the electrostatic shield (0·004 in.), constitutes the entire thickness of the counter wall. The

counters are filled with a dried mixture of 94% Arc-argon and 6% commercial methane, to a total pressure of 82 cm Hg. The gas gain is 400 when the counter supply is 5 kv, of which 3 kv is applied to the control grid, and the remainder used for electron collection. It is not feasible to test directly with shower electrons for the effect of space charge on counter linearity, but this effect is found to produce a 50% reduction in gas gain for polonium α-particles. These particles release about 2×10^5 ion pairs, to produce a total population (including the gas gain increase) of 4×10^7 positive ions clustered around a few cm of the wire length. In contrast to the α-particles a shower electron releases only 700 ion pairs, resulting in 3×10^5 ion pairs along a similar length of wire. Even at the highest observed densities there is an average of less than one shower particle per cm of wire length, so, on a proportionate basis, the decrease in gas gain is expected to be negligible, and the counter linearity unaffected.

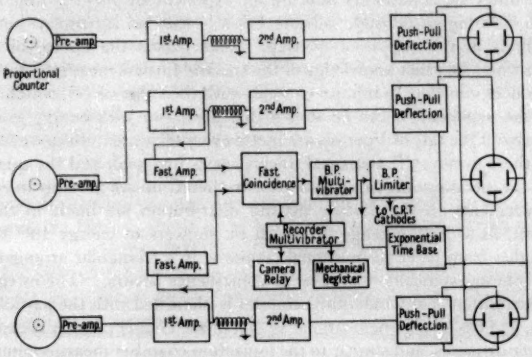

Figure 1. Block diagram of the shower recording apparatus.

A block diagram of the apparatus is shown in figure 1. The proportional counter output pulse passes to the signal amplifier which has four parts: the signal receives a voltage gain of 100 in the pre-amplifier which is built on to the proportional counter case; the first and second sections of the main amplifier have a gain of 100 and 70 respectively, while the push–pull deflection circuits have a gain of only 20 since they are required to deliver large deflecting voltages to the cathode ray tubes. With the exception of the deflection circuits, the amplifiers are basically 'model 100' design, modified to decrease the rise time to 0·2 μsec at the expense of some high frequency gain stability, the loss of which proved to be quite unimportant. The amplifier gain available is variable in fine steps from 10^4 to 10^7, with a maximum overall gain of 10^9 including counter gas amplification. The fast coincidence amplifiers have a rise time of 0·1 μsec, and, operating at the delay line input from two channels only, trigger a two-fold coincidence circuit when the pulses are time coincident to within the electronic resolving time of 1 μsec. The coincidence circuit output pulse is lengthened by a 20 μsec multivibrator circuit to produce a large and fast-rising square pulse. Three outputs are taken from this multivibrator: the first passes to the brightening pulse limiting circuit which controls the amplitude of the brightening pulse supplied to the cathodes of

all the cathode ray tubes; the second output operates the cathode ray tube exponential time base, while the third operates a 0·1 sec pulse-lengthening multivibrator for the camera and mechanical register circuits. The voltage pulse from the latter multivibrator is integrated so that after a 0·02 sec delay it reaches the firing voltage required by a small neon lamp, and the ensuing pulse injected into the pulse brightening circuit. This produces a recirculating brightening pulse and time base, which serves as a zero base reference line from which the signal pulse height may later be measured. All d.c. voltage supplies are electronically regulated, and it is necessary to supply the valve filaments from an a.c. (r.m.s.) stabilizer, mainly because the cathode followers distributed through each amplifier produce a cascaded change in gain with filament voltage variations. Stability requirements for the 5 kv proportional counter supply are exacting, since a 150 v change doubles the gas amplification. Chart recorder tests on this supply showed a maximum variation of $\pm 0{\cdot}4$ v over a 48 hour interval. Overall linearity and gain stability proved to be better than 2% over long periods.

Ilford GX film is used in a shutter-less 35 mm recording camera fitted with a Zeiss f/1·5 lens. Since the film is continuously exposed to the cathode ray tube screens, traces are recorded whenever the brightening circuit operates; and to allow for the screen persistence, a delay of 0·1 sec is incorporated before the camera relay moves the film on. Also, the cathode ray tube filament light limits the maximum standing time to 5 min, but the use of an orthochromatic film, and reduction of the filament voltage from 4·0 to 3·7, increases the standing time to about 2 hours, with no apparent reduction in writing speed.

A transmission method of x-ray calibration (Norman 1955) is employed to ensure correct counter operation. If the white radiation from an x-ray tube is allowed to fall on a thin (0·017 in.) molybdenum filter, the emerging radiation is sufficiently concentrated below the K absorption edge at 20·0 kev to permit accurate calibration. The filtered x-rays produced in this way are then allowed to penetrate the electrostatic shield and counter wall (0·010 in. Fe), beyond which some will produce photoelectrons in the counter gas. Pulse height distributions obtained by this method have a width of 12–13% at half height, and are carried out both before and after the experiment to test the counter performance. As an operational test, overall stability of gain is checked regularly by means of the 46·7 kev gamma ray line from a RaD + E + F source. When using this source, a 10 sec exposure at reduced lens aperture is taken for calibration purposes on every second film, and no significant change was recorded over the course of the experiment. The absolute calibration of shower density in terms of pulse height is obtained by reference to mesons near minimum ionization in the following way. From the known meson spectrum it is possible to calculate the most probable energy loss for those mesons passing diametrically across the counter which are also capable of penetrating 10 cm of lead. This energy loss is found to be the same as the experimentally determined value of $16{\cdot}0 \pm 0{\cdot}1$ kev obtained from a subsidiary experiment in which events are selected by a pair of small Geiger counters. The most probable energy loss is now computed for a single hit by these mesons anywhere on the counter and a value of 15·2 kev obtained. If this value is now multiplied by the ratio of energy loss suffered by shower electrons to that suffered by mesons, a value of 20·0 kev results, which is the most probable energy loss suffered by a shower electron hitting the counter anywhere. It is believed that this provides an absolute calibration accuracy of better than 10%. Finally, because

of multiplication of the shower particles in the hut roof, the shower density inside the hut or, more particularly, inside the counter, will be higher than the density in open air. Bethe (see Williams 1948) has shown that the materialization of photons is largely responsible for the increase in shower density beneath thin absorbers, and that it follows a relation of the form

$$M = 1 + 2\left(1 - \frac{7{\cdot}2}{Z}\right)\frac{t}{X_0}, \qquad \ldots\ldots (1)$$

where t = thickness of layer, Z = atomic number, X_0 = radiation unit (of cascade theory) for the material. Thus the effective shower density is increased 8% by the corrugated iron roof, 2% by the cement sheet ceiling and a further 2% by the counter wall, producing 12% multiplication in all.

§ 3. Local Particle Density Spectrum

Cocconi (1954) has estimated that the shower structure should be elliptical because of the deflection of the charged shower particles in the earth's magnetic field. Since a significant variation of structure function with direction would produce an error in the energy spectrum exponent derived from the density spectrum, a preliminary experiment has been carried out to determine the magnitude of this effect at sea level (Norman 1956). No change in structure function is found with change in orientation, within the experimental error of 4%, so it is concluded that the ellipticity is negligible.

Only two of the three counters are connected to the coincidence circuit, so pulses that are time coincident in these two channels within the resolving time of 1 μsec cause an exposure to be made. The final selection of coincidences is made visually from the photographic records, when the resolving time may be reduced to 0·1 μsec by comparison of the signal traces, because the 20 μsec exponential time base moves quickly at the beginning of its stroke. The electronic resolving time for the third channel pulse is, effectively, the full duration of the time base, and the visual resolving time 0·1 μsec also. It is concluded that no accidental coincidences are registered because of the absence of non-coincident third channel pulses. The possibility of nuclear disintegrations making a significant contribution is excluded for the following reasons: (1) the counter has a small mass and therefore a low probability for disintegrations, (2) with 5 m counter separation and radial symmetry, each counter presents a very small solid angle to the other two, (3) the use of pulse shape techniques failed to disclose the presence of any other than the typical shower pulse shape and (4) if disintegration products had been making a significant contribution, more two-fold coincidences would be produced than three-fold. Two-fold coincidences, which are observed only at low densities, can be completely accounted for in terms of statistical fluctuations in shower density and shower density gradients.

The particle density spectrum is a well established method of comparing results obtained by different observers on a common basis. Only three-fold coincidences are used in this experiment as a method of extensive shower selection. Consequently there is a very real chance of missing a three-fold coincidence at the lower densities due to statistical variations below the average particle density at any counter. If the average shower density is ρ particles m^{-2}, the probability of hitting three counters of area A with one or more particles each is

$$P(\rho, A_3) = \{1 - \exp(-\rho A)\}^3. \qquad \ldots\ldots (2)$$

The shower frequency at a density ρ must be multiplied by this correction factor to compensate for the statistical loss of counts. At a shower density of 60 particles m^{-2} this correction is only 10%, while at 25 particles m^{-2} it rises rapidly to 100%, and the accuracy of the curve at this point will be governed not by the statistical accuracy of the number of counts received, but by the uncertainty in the absolute shower density. Accordingly, the errors shown on the curve at particle densities below 60 particles m^{-2} are those incurred by an uncertainty of up to 10% in the absolute shower density. The rates corresponding to densities less than 25 particles m^{-2} are excluded because of the magnitude of the error that this uncertainty can produce.

The experimental data are analysed in two different ways—firstly, including the density gradient across the counter system, and secondly, neglecting it. Using the former classification, the pulse height distribution is taken for each counter alone, the other two being used for shower selection purposes only. This distribution, shown as curve A in figure 2, is the true particle density spectrum, and follows an inverse power law

$$\nu(\rho) = 540\,\rho^{-1\cdot39\pm0\cdot04}\,h^{-1}, \text{ for } 20<\rho<500. \qquad \ldots\ldots(3)$$

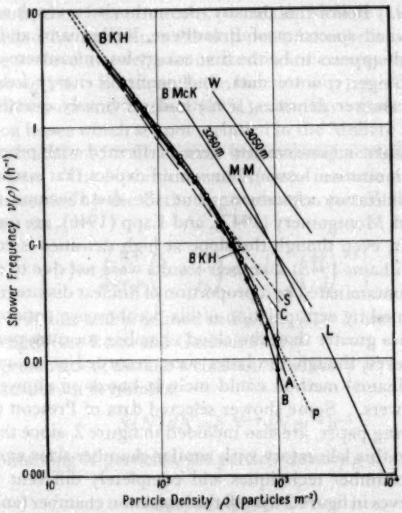

Figure 2. The integral shower density spectrum at sea level. The effect of shower density gradients over the apparatus is included in curve A, and not in B. L, Lapp (1946), M M, Montgomery and Montgomery (1947), W, Williams (1948), C, Cocconi and Cocconi-Tongiorgi (1949), B McK, Brown and McKay (1949), P, Prescott (1950), B K H, Broadbent, Kellermann and Hakeem (1950), S, Singer (1951), A, B, author.

In order to see whether these density gradients will affect the interpretation of the density spectrum, it is now assumed that the particle density is constant over the extent of the apparatus as Cocconi *et al.* (1949) and Singer (1951) have done in order to interpret their experiments. They reason that the counter separation of 4 m used by them is small compared with the lateral shower unit of 75 m, and that consequently the particle density gradient over this distance must be negligible. It is possible that density gradients have little effect on their result, nevertheless it may be calculated that the density gradient across two counters 5 m apart exceeds 0·5 in approximately half the coincidences. These density gradients have been used by Williams (1948) for core placement, and by Campbell and Prescott (1952) for evaluation of shower structure function. If the shower density is the same for all three detectors, the average pulse height is equivalent to the density. Therefore the averaged three-fold pulse height distribution is shown as curve B (figure 2) which is given by

$$\nu(\rho) = 500\,\rho^{-1\cdot39\pm0\cdot04}\,\mathrm{h}^{-1}. \qquad \ldots\ldots(4)$$

This curve is slightly lower than and, within the experimental error, parallel to curve A. It may thus be concluded that the assumption of zero density gradient over the extent of such an apparatus has only a small effect on the particle density spectrum. The counter results of Cocconi *et al.* (1949) and Singer (1951) are also shown in figure 2, from which it will be noticed that the author's curve B agrees very well with that obtained by Singer based on a similar assumption, at least up to $\rho = 500$. Below this density, the author's curves A and B straddle the precisely determined spectrum of Broadbent, Kellermann and Hakeem (1950). The present result appears to be the first energy loss measurement to reach agreement with the Geiger counter data, and confirms energy loss as a method of measurement of shower densities, a method previously questioned by Cocconi (1946).

Since the present measurements were performed with proportional counters (which measure ionization losses), one would expect that similar data would be obtained with ionization chambers; but the distributions found earlier by Montgomery and Montgomery (1947), and Lapp (1946), are quite different from the present result, even though the slope at high densities is comparable. It is now believed (Williams 1948) that their results were not due to extensive showers alone, but were contaminated by a proportion of nuclear disintegrations. Williams' own value, obtained by extrapolation of his decoherence data to zero separation, is about four times greater than the cloud chamber measurements of Brown and McKay (1949), even though the latter were recorded at a similar altitude. It appears that Williams' method could include knock-on showers in addition to extensive air showers. Some shower selected data of Prescott (1950), presented in an accompanying paper, are also included in figure 2, since they were recorded some years ago in this laboratory with similar chamber sizes and separations, but with ionization chamber techniques and completely different apparatus. It is clear from the curves in figure 2 that all the ionization chamber (and cloud chamber) evidence points to a greater exponent above 500 particles m^{-2}, but below this density the exponent remains almost constant.

The results obtained by several authors for the particle density spectrum are collected in table 1. Since a small error in the exponent will require a large compensatory change in the constant, agreement between the various results at sea level is quite good.

Table 1.

Worker	Altitude (m)	Method	k†	c†
Cocconi & Cocconi-Tongiorgi (1949)	s.l.	G–M Counters	460	1·45
Singer (1951)	s.l.	,,	560	1·40
Broadbent, Kellermann & Hakeem (1950)	s.l.	,,	620	1·425 ± 0·02
Author	s.l.	Proportional Counters	540	1·39 ± 0·04
Williams	3050	Ionization Chamber	9900	1·5
Brown and McKay (1949)	3260	Cloud Chamber	5100	1·6

† $\nu(\rho) = k\rho^{-c}\, h^{-1}$ s.l. = sea level.

§ 4. Distribution in Number and Energy

It is possible to evaluate the shower distribution in number $S(N)\,dN$ from the experimental particle density distribution $\nu(\rho)\,d\rho$, where $S(N)\,dN$ is the number of showers per hour containing in all between N and $N+dN$ particles at the point of detection, whose cores pass through a horizontal area of 1 m². Let the particle density at a radius r from the shower axis be given by the function $\phi(r)$ at the plane of the cascade maximum, for which the shower age $s = 1{\cdot}0$ (Blatt 1949), and by $\phi'(r)$ at a later stage of development, well past maximum, for which the shower age $s = 1{\cdot}4$. If a constant structure function is assumed for interpretation of sea level measurements, then it is erroneous to use the Molière (1946) function $\phi(r)$, which was evaluated for maximum development, because it is known that most showers reaching sea level are well past maximum and correspond more closely to a shower age s of about 1·4. Fortunately the function $\phi'(r)$, as well as $\phi(r)$, has been computed by Nishimura and Kamata (1951), who have made allowance for the effect of ionization losses which are not included in the Molière function. Nevertheless the two calculations for the cascade maximum agree closely out to distances of about 400 metres. The Nishimura and Kamata function $\phi(r)$ should then be equally well represented by the Bethe approximation (see Williams 1948) to the Molière function, viz.,

$$\phi(r) = \frac{2.85}{2\pi r_0 r}\left(1+\frac{4r}{r_0}\right)\exp\left\{-\left(\frac{4r}{r_0}\right)^{2\cdot3}\right\} \qquad \ldots\ldots(5)$$

where r_0 = shower radius and is defined as $E_s X_0/\epsilon$, $E_s = 21$ Mev, ϵ = critical energy, X_0 = radiation length (see Rossi and Greisen 1941).

As a first approximation, assume a constant function $\phi'(r)$ and a constant exponent τ in the distribution in number

$$S(N)\,dN = k\,N^{-\tau}\,dN\,m^{-2}\,h^{-1}. \qquad \ldots\ldots(6)$$

For a shower containing N particles, the particle density ρ at a distance r from the core is

$$\rho(r) = N\phi'(r). \qquad \ldots\ldots(7)$$

The contribution at any fixed point from showers striking within an annulus of width dr and radius r is then $2\pi r\,dr\,S(N)$, while the differential density spectrum at that point will be

$$\nu(\rho)\Delta\rho = 2\pi\int_0^\infty S(N)\Delta N r\,dr. \qquad \ldots\ldots(8)$$

Substituting from (6) and (7) we obtain

$$\nu(\rho)\,\Delta\rho = 2\pi \int_0^\infty k\,N^{-\tau}\,\Delta N\,r\,dr \qquad \ldots\ldots(9)$$

$$= 2\pi\,k\rho^{-\tau}\,\Delta\rho \int_0^\infty \phi'(r)^{\tau-1}\,r\,dr. \qquad \ldots\ldots(10)$$

Experimentally $\nu(\rho)\,d\rho = T\rho^{-\gamma-1}d\rho$ and for agreement $\gamma+1$ must equal τ, a result which is independent of the form of $\phi'(r)$. Consequently, if τ in (6) and $\phi'(r)$ remain constant, $\nu(\rho)\,d\rho$ will have the same exponent as $S(N)\,dN$. But very little is known about the behaviour of $S(N)\,dN$, particularly for large N, and the structure function does change with increase in N, becoming more peaked because the larger showers reach maximum development at lower altitudes. Therefore, equality of the exponent of $S(N)\,dN$ and $\nu(\rho)\,d\rho$ can only be regarded as a crude approximation. Nevertheless a numerical integration is carried out since it draws attention to the range of shower sizes involved in the production of a particle density spectrum. The smallest shower capable of exceeding the bias level $\rho = 20$ particles m^{-2} of the three detectors lying on a 2·5 m radius ($r' = 2{\cdot}5$ m) is clearly one whose core passes through the centre. For a typical sea level shower whose age $s = 1{\cdot}4$, $N_0 = 44\,000$ particles are required, in contrast to 11 000 particles for a young shower with $s = 1{\cdot}0$. Using the structure function $\phi'(r)$ and a trial exponent of $-1{\cdot}47$ for $S(N)$, i.e. $\tau = 2{\cdot}47$, the contribution to the count rate from showers in the number interval N to $N+dN$ is

$$Z(\rho, r')\,dN = \pi R^2\,k\,N^{-\tau}\,dN, \qquad \ldots\ldots(11)$$

where $R = r - r'$ is the maximum distance, from (7), at which a shower containing N particles may overcome the bias at the furthest detector. It is convenient to plot this contribution as a function of NdN (figure 3 (*a*)), where $\pi R^2 N^{-1{\cdot}47}\,dN$ is the

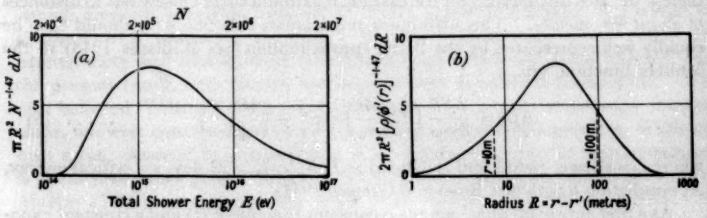

Figure 3

coincidence rate produced by a number interval NdN wide at N. The particle density spectrum thus integrates over three orders of magnitude of shower number, and the area under the curve between any two N values gives the relative contribution from that interval. When $E = 10^{15}$ ev $N = 2 \times 10^5$ at sea level. The integral counting rate

$$Z(\rho, r') = \pi R^2 k \int_{\rho/\phi'(r)}^\infty N^{-\tau}\,dN \qquad \ldots\ldots(12)$$

shown as curve A in figure 4, is a straight line as was expected from (10).

It is interesting to consider the contributions to coincidence rate made by showers striking at different distances from the detectors. From a similar

argument to that above, it can be shown that the contribution from an annulus dR wide at radius R will be

$$X(\rho, r')\,dr = 2\pi\, RdR\,\sigma\,\{\rho/\phi'(r)\}^{-\gamma}, \text{ if } S(N) = \sigma N^{-\gamma}. \quad \ldots\ldots(13)$$

The function $2\pi R^2\{\rho/\phi'(r)\}^{-1\cdot47}\,dR$ then gives the contribution from an annular interval RdR (figure 3 (*b*)), so that the area under the curve between any two R values gives the relative contribution from that radius interval. Thus, at sea level, half the coincidence rate is produced by showers striking outside 35 m, and as many coincidences are caused by showers lying outside 100 m as within 10 m, each contributing about 10%.

Compare the structure of two showers containing N particles but of different ages, say $s = 1{\cdot}0$ and $s = 1{\cdot}4$. The calculations of Nishimura and Kamata (1951) indicate $\phi(r) = \phi'(r)$ at $r = 50$ m, this value of r being the cross-over point above and below which the old or the young shower respectively have the greatest density. Different experimental arrangements will respond perferentially to showers of a particular age. Consequently, an experimental arrangement with large detector separation will select preferentially those showers with the flattest structure, i.e. the old showers. Furthermore, since the proportion of old showers decreases with increasing energy, the effective exponent in the density or energy spectrum evaluated from such an experiment will be greater than that obtained with smaller separations (unless the effect of changing shower age is taken into account). To illustrate this point, Williams (1948) obtains a higher exponent for his density spectrum with a chamber separation of 12·2 m than he does with 0·15 m, and Cranshaw and Galbraith (1954), using a 54 m counter separation, find an effective exponent as high as 1·7.

It is now necessary to find whether a variation in shower age with size will influence the exponent of $S(N)$ which is deduced from $\nu(\rho)$. In the absence of details of this variation, a change of shower age with number is assumed such that there are 100% old showers at 10^{12} ev ($N \sim 10^2$) and 100% young ones at 10^{16} ev ($N \sim 10^6$), with an age in between these limits given by

$$s = 1{\cdot}4 - 0{\cdot}1 \log (N/200). \quad \ldots\ldots(14)$$

This relation at least satisfies the fundamental requirements, viz., that a decrease in shower age from 1·4 to 1·0 occurs with increasing energy or number, and that most showers are old, or well past maximum development.

The density spectrum (curve B, figure 4) is computed with the above change in age and, as in curve C (figure 4) a constant exponent for $S(N)$ equal to $-1{\cdot}47$. Although a 6% overall decrease in slope is produced, it is clear that this age variation could not account for the increase in slope of the experimental points (also in figure 4).

Since the local particle density ρ is obtained by an integration over three orders of magnitude of N (figure 3 (*a*)), a rapid increase in exponent of $\nu(\rho)$ may be immediately explained by either a more rapid change in exponent of $S(N)$, or possibly a complete cut-off. Accordingly, particle density distributions have been computed for an exponent of $-1{\cdot}47$ in $S(N)$, a shower age from equation (14), and a number at cut-off of 2, 4 and 8×10^6 particles. The curve D in figure 4, corresponding to a cut-off at $N = 4 \times 10^6$ fits the experimental data best, and the cut-off N is sharply defined. If, instead of a complete cut-off, the exponent is increased from 1·47 to 2·0 at $N = 10^6$, the resulting density spectrum does not fit the data very well. The distribution in number is therefore best represented by

$$S(N) = 2{\cdot}3 \times 10^{-4}\,(N/10^6)^{-1{\cdot}47 \pm 0{\cdot}1}\ \text{m}^{-2}\ \text{h}^{-1}, \quad \ldots\ldots(15)$$

for $N<10^6$, with an exponent greater than 2 for higher N, (i.e. within the experimental error the exponent is between 2 and ∞). The values of $S(N)$ obtained by other workers are listed in table 2 for comparison with the present result. The higher constant found by Williams will be attributable in part to the higher altitude, e.g. when $E=10^{15}$ ev the number of particles at 3050 m is about four times the number at sea level.

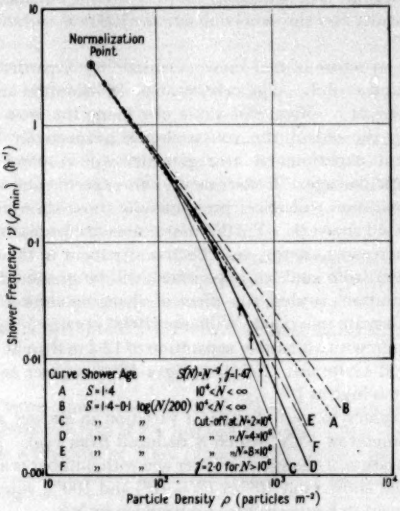

Figure 4. Synthesis of particle density distribution using various assumptions about the shower age and distribution in number. The experimental points are the rate of showers exceeding the bias level ρ in all three counters.

Table 2.

Worker	Altitude (m)	Method	σ†	γ†
Singer (1951)	s.l.	G–M Counters	$0·7\times10^{-4}$	1·4
Author	s.l.	Proportional Counters	$2·3\times10^{-4}$	$1·47\pm0·1$
Williams (1948)	3050	Ionization Chambers	$8·4–18\times10^{-4}$	1·50

†$S(N)=\sigma(N/10^6)^{-\gamma}\ m^{-2}\ h^{-1}$

From 'Approximation B' of ordinary cascade theory, the number of particles remaining in a shower of initial energy E can be found at any depth t. Using the method of Synder and Serber (see Rossi 1952), it is found that for showers arriving within small zenith angles, the number of particles at sea level is related to the primary particle energy by the relation

$$E=1·26\times10^{11}N^{0·755}, \text{ for } 10^2<N<10^8. \qquad \ldots\ldots(16)$$

If it is assumed that all showers arrive within small zenith angles, (16) may be substituted into (15) giving a primary spectrum with a slope of 1·9 between 10^{14}

and 10^{16} ev. If all showers are assumed to have the same structure, then a primary spectrum with a slope of 1·8 is required. This approximation is clearly incorrect when primary energies greater than 10^{15} ev are involved, since these can make considerable contributions at larger zenith angles.

Consequently it is necessary to integrate over showers of all energies, and all zenith and azimuth angles, to obtain $V(E)$ from $S(N)$, where

$$S(N)=\int_0^{\infty}\int_0^{\pi/2}\int_0^{2\pi}(M,\theta,\chi)\,dM\,d\theta\,d\chi \qquad \ldots\ldots(17)$$

and $M=f(E,t)$, where $t=h(\theta)$, $\theta=$ zenith angle, $\chi=$ azimuth angle, $t=$ number of standard atmospheres and $E=$ shower primary energy.

The function $S(N)$ has been calculated for constant exponents in the primary spectrum of 1·8 and 2·0, and these are shown in figure 5 together with the

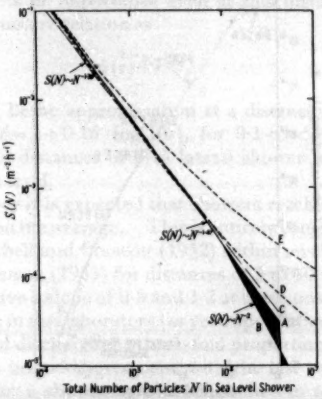

Figure 5. The distribution in number given by either curve, A or B, can produce the observed particle density spectrum, within the experimental error. Curve C is the number spectrum required in the absence of a variation of structure with shower age; while D and E are the number spectra produced at sea level by primary spectra with constant exponents of 2·0 and 1·8 respectively.

experimentally deduced $S(N)$. Instead of producing a constant exponent in $S(N)$, as results when only small zenith angles are included, the exponent shows a gradual decrease. Thus, in order to fit a distribution $S(N)$ having a constant exponent, it is necessary to have an energy spectrum with an increasing exponent.

The form of $V(E)$ required to fit satisfactorily the experimental relation for $S(N)$ in equation (15), is shown as curve A in figure 6, and extends from about 4×10^{13} to 10^{17} ev. The exponent of $V(E)$ increases rather quickly from 1·5 at 10^{14} ev, where the spectrum is of the form $V(E)=0{\cdot}32\,(E\times10^{-14})^{-1{\cdot}5}$ m^{-2} h^{-1} sterad^{-1}, to 3 at 10^{17} ev. The spectrum may be fitted very roughly by a constant exponent of 2 between these energy limits.

It has been pointed out by Peters (1952) that the extensive air showers which carry energies of 10^{17} ev or higher are possibly connected with the heavy nuclei rather than the protons in the primary cosmic radiation. It has also been shown

by Peters (1952) and Kaplon *et al.* (1952) that the primary radiation around 10^9 ev comprises nearly 10% alpha particles and heavier nuclei; and from a very limited number of observations at 10^{13} ev, that the composition there is roughly the same. If this composition continues to the highest energies, then it is possible to evaluate the spectrum for the energy–nucleon from the total energy spectrum. This is given by curve B in figure 6. It can also be shown that at this composition the total energy spectrum may not have an exponent exceeding about 3 unless there is a cut-off in the energy–nucleon spectrum. $V(E)$ has a gradient approaching 3 at about 10^{17} ev, thus, if the assumed composition is correct, this would imply a cut-off in the energy–nucleon spectrum at this energy. Under these conditions the maximum energy carried with any one shower would be, as an order of magnitude estimate, 10^{19} ev.

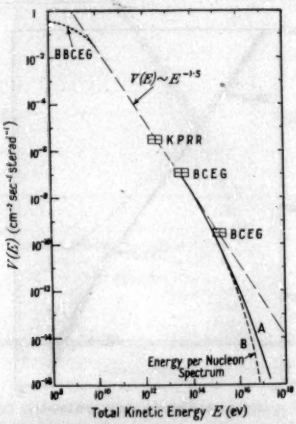

Figure 6. The primary cosmic ray spectrum. Curve A is the distribution required to produce the observed density spectrum; whilst B is the energy–nucleon spectrum assuming the primary radiation still contains roughly 10% of nuclei heavier than hydrogen. BBCEG, Barrett *et al.* 1952, KPRR, Kaplon *et al.* 1952, BCEG, Barrett *et al.* 1954.

§ 5. Discussion

It is interesting to consider what justification exists for the various assumptions used in the previous analysis. The evaluation of $S(N)$ from $\nu(\rho)$ depends upon a knowledge of both the structure function at sea level and variations in structure with shower size. The structure predicted theoretically by Molière (1946), and extended by Nishimura and Kamata (1951) to include ionization losses, is used in this analysis.

Experimental investigations of the structure function from 1 m to 250 m from the core, for showers at maximum development, have been in good agreement with the Molière theory (Cocconi *et al.* 1949, Hazen *et al.* 1952, Vavilov *et al.* 1953 and Dovzhenko *et al.* 1955). These workers find that the structure within 1 m from the core is flatter than predicted by the theory, although dissentient results are reported by Sitte *et al.* (1954), who find a flatter structure from 2 m to 8 m. The

explanation of this disagreement could possibly be found in terms of inaccuracy in core placement (Dovzhenko *et al.* 1955). These inconsistencies with the theory near the core are presumed to be due to multiple core production in the initial interaction and the combined characteristics of a nucleon + cascade shower. In a review of Russian work, Wataghin (1952) reports an experimentally determined structure function slope of $3{\cdot}1 \pm 0{\cdot}3$ at 60 m from the core, which agrees well with the Nishimura (1951) slope of 3·3.

The solutions for the structure function obtained by Nichimura and Kamata (1951) give the number of electrons of all energies at a distance r from the axis at a depth t, which close to the shower core are of the form $\phi(r) \sim r^{s-2}$ for $s<2$. It must be emphasized, however, that this form is applicable only *very close* to the core, for the same reason that the Molière function, which approximates to r^{-1} 'near' to the core, already at 1 metre (sea level) is actually $r^{-1{\cdot}15}$, viz. the exponential factor in the formula is of importance even at this distance. It is possible to reconstruct the age-structure relation as

$$\phi(r) \sim r^{s-\xi}, \qquad \ldots\ldots(18)$$

where $\xi = 1 +$ slope of Bethe approximation at a distance r from the core. To a first approximation, $\xi = 2 + 0{\cdot}16 \log(10r)$, for $0{\cdot}1 < r < 10$ m (sea level). This form holds well out to distances of 0·15 lateral shower units from the core, i.e. about 10 metres at sea level.

From shower theory it is expected that showers reaching sea level will have an age parameter $s = 1{\cdot}4$ on the average. This is entirely consistent with the measurements made by Campbell and Prescott (1952) within several metres from the core and Haddara and Jakeman (1953) for distances of 5 to 50 metres. The structure function is found to have a slope of 0·8 and 1·2 at these positions respectively. In a current investigation in this laboratory (as yet unpublished), the average structure of all showers capable of discharging a three-fold proportional counter arrangement has been found to be in good agreement with the last two results and with the Nishimura function for a shower age $s \simeq 1{\cdot}4$, from 1 m to 300 m from the core. Because of these and the previous results, it is considered justifiable to make some correction for variation of shower structure with age. The function $S(N)$ has been calculated from the experimental density distribution both with and without this correction, and the difference between the two distributions (A and C in figure 5) is possibly no more than that from the experimental error in $\nu(\rho)$. The final form of $S(N)$ has an exponent of 1·47 below $N = 10^6$ and, within the experimental error, some value between 2 and infinity above $N = 10^6$. This is supported by Blatt (1949) who analysed the ionization chamber results of Williams (1948), and suggested as a first approximation a discontinuity in $S(N)$ at $N = 10^6$ particles, with an exponent of 1·5 below and 1·9 above it. A discontinuity of this sort would be expected from ordinary cascade theory even in the presence of a constant primary spectrum exponent. It should occur, not at $N = 10^6$, but at $N = 10^8$, where the whole atmospheric depth is required for the full development of the shower; and those showers of still higher energy would be unable to reach maximum development except for some small contribution from higher zenith angles. Since any particular N value at sea level is produced by one or more orders of shower energy E, the simplest cause of a discontinuity in $S(N)$ is a more rapid one in $V(E)$.

It has been shown that if all showers arrive within small zenith angles—that portion of $S(N)$ which has a constant exponent 1·47 can be produced by an energy spectrum $V(E)$ with a constant exponent 1·9—that when the further complication of showers arriving at different zenith angles is included, $S(N)$ may be roughly fitted by a constant exponent of 2 in $V(E)$. Two points require special emphasis; the first is that the exponent of $V(E)$ must increase slowly to produce that portion of $S(N)$ with a constant exponent, and the second is that the exponent of $V(E)$ must increase more quickly than the increasing exponent of $S(N)$. When these two requirements are superimposed, the resulting $V(E)$ will have an exponent which increases slowly at first and then more quickly at the higher energies.

The main limitation of the present analysis is that it depends upon the accuracy with which ordinary cascade theory relates the primary energy to the number of particles at a depth t in the atmosphere. The development of air showers is far from being fully understood, being far more complex than was originally thought; thus the relation between E and N given by cascade theory may be in error by a factor of 2 or 3 (Rossi 1955). Therefore, it may be necessary to slide that portion of the energy spectrum deduced from air shower observations up or down the energy scale by this factor. On the other hand, the deduced energy spectrum is in substantial agreement at 4×10^{18} ev with the value estimated by Barrett, Cocconi, Eisenberg and Greisen (1952) to be the minimum energy of protons necessary to produce a given frequency of mesons capable of penetrating 1600 m water equivalent.

The evidence for very large showers using counters with large separations must be interpreted with great caution. As mentioned earlier by Cocconi and Cocconi-Tongiorgi (1949) and more recently by Rossi (1955), the possibility must not be overlooked that, through some extreme fluctuation, a shower may exhibit abnormally high concentrations at the places where the detectors are placed, and thus appear to have a higher energy than it actually possesses. It is only by making density measurements at many different places that this difficulty can be reduced. Experiments of the n-fold coincidence type have been carried out, notably by Cranshaw and Galbraith (1954) who record 10·1 three-folds per hour in a detector square of 162 m side. Their calculations of the most probable number of particles involved gives $N = 7 \times 10^5$. If the rate of such showers from figure 5 is multiplied by the detector area, a value of 10 per hour is obtained. Similarly, their other rates may be reproduced, and, although the absolute agreement may well be fortuitous because of the uncertainties in establishing the most probable N, the relative agreement is most significant and their experimental results may be taken to be in entire agreement with the present ones. Since the exponent of their energy distribution is based upon a simple proportionality between E and N, no comparison with the present spectrum may be made. A brief report of later work from the Harwell group (1955), indicates energies as high as 10^{19} ev. In view of the tentative prediction made earlier that if the primary radiation still contained roughly ten per cent of nuclei heavier than hydrogen, no individual shower should possess a total energy exceeding roughly 10^{19} ev, this report is particularly interesting. If the present analysis is correct, the presence of showers carrying energy of roughly 10^{20} ev is evidence for a change in chemical composition of the primary radiation at the highest energies.

It is interesting to consider the relationship of this result to the acceleration of the cosmic ray primaries. It has been suggested by Morrison, Olbert and Rossi

(1954) that part or all of this acceleration process takes place in the galaxy, and that the termination of the process is escape from the galaxy. The mean life of cosmic ray particles in the galaxy must, at some energy, be a decreasing function of energy, since particles of higher energy are deflected less by magnetic fields, and will therefore escape more easily. Depending upon the structure of the galactic magnetic fields, the theory allows the mean life to decrease gradually or suddenly. The existence of extensive magnetic fields of the order 6×10^{-5} gauss has been demonstrated by a number of independent arguments, the most important of which is the partial polarization of light from distant stars (Hiltner 1951, Fick 1955). Further argument by Fermi (see Rossi 1955), based upon energy density considerations, support the view that the whole galactic field has a fairly regular structure. If this is correct, and if the cosmic rays do gain energy stepwise, by collisions with moving gas clouds during their motion through space (Fermi 1949), then the mean life before escape and fractional energy gain per unit time should remain constant up to energies of the order of 10^{15} ev, (Morrison *et al.*). At some energy above this, the mean life suddenly decreases and one would expect a sharp cut-off in the energy spectrum. The intensity would then drop to an unobservable low value before any appreciable asymmetry develops. It has already been shown that, under these conditions, the observed power spectrum with constant exponent is obtainable from the theory (Rossi 1955).

Considered from another point of view, it is known that the radiation around 10^{10} ev is isotropic to within 1/1000. A measurable anisotropy at some high energy indicates that the mean life before escape gradually decreases with energy (the fractional energy gain per unit time must then increase to off-set the decrease in mean life, in order to produce the observed spectrum). But a remarkable degree of isotropy has been observed by Cranshaw and Galbraith (1954) up to energies estimated by them to be about 10^{17} ev; and this is incompatible with the idea of a gradual decrease in mean life. The hypothesis of gradual acceleration of the cosmic ray primaries and constant mean life up to some critical energy, suggested here to be of the order 10^{17} ev nucleon^{-1}, would seem then to satisfy both the theory and the experimental data.

Additional Note

At the recent Cosmic Ray Conference at Mexico, the Harwell Group (1955) presented a paper in which they have deduced the high energy portion of the primary spectrum up to 10^{18} ev, on the assumption that the factor relating E to N at sea level is constant, and equal to 10^{10}. The author is indebted to Drs. Cranshaw and Galbraith for communicating a copy of this paper, and also for reporting a suggestion made by Olbert (M.I.T.) at the Conference: that the factor relating E to N is not constant, but is about 3×10^9 at $E = 10^{18}$ ev. If this is correct, the Harwell group's energy spectrum can be moved down the energy scale by a factor of 3 at 10^{18} ev, where it is in close agreement with the present total energy spectrum.

Acknowledgments

The author gratefully acknowledges the advice and support of Professor L. H. Martin, valuable discussion with Associate Professor C. B. O. Mohr, and also thanks Dr. J. R. Prescott for providing pre-publication ionization chamber data.

References

Barrett, P. H., Bollinger, L. M., Cocconi, G., Eisenberg, Y., and Greisen, K., 1952, *Rev. Mod. Phys.*, **24,** 133.

Barrett, P. H., Cocconi, G., Eisenberg, Y., and Greisen, K., 1954, *Phys. Rev.*, **95,** 1571.

Blatt, J. M., 1949, *Phys. Rev.*, **75,** 1584.

Bradt, H. L., and Peters, B., 1950, *Phys. Rev.*, **77,** 54.

Broadbent, D., Kellermann, E. W., and Hakeem, M. A., 1950, *Proc. Phys. Soc.* A, **63,** 864.

Brown, W. W., and McKay, A. S., 1949, *Phys. Rev.*, **76,** 1034.

Campbell, I. D., and Prescott, J. R., 1952, *Proc. Phys. Soc.* A, **65,** 258.

Cocconi, G., 1946, *Phys. Rev.*, **70,** 975; 1954, *Ibid.*, **95,** 1705.

Cocconi, G., Cocconi-Tongiorgi, V., 1949, *Phys. Rev.*, **75,** 1058.

Cocconi, G., Cocconi-Tongiorgi, V., and Greisen, K., 1949, *Phys. Rev.*, **76,** 1020.

Cranshaw, T. E., and Galbraith, W., 1954, *Phil. Mag.*, **45,** 1109.

Dovzhenko, O. I., and Nikolski, S. I., 1955, *Doklady Akad. Nauk, S.S.S.R.*, **102,** 241.

Fermi, E., 1949, *Nuovo Cim.*, Suppl. No. 3, **6,** Ser. 9, 317.

Fick, E., 1955, *Z. Phys.*, **140,** 308.

Haddara, S. R , and Jakeman, D., 1953, *Proc. Phys. Soc.* A, **66,** 549.

Harwell Group, 1955, *Nature, Lond.*, **176,** 1105.

Hazen, W. E., 1952, *Phys. Rev.*, **85,** 455.

Hiltner, W. A., 1951, *Astrophys. J.*, **114,** 241.

Kaplon, M. F., Peters, B., Reynolds, H. L., and Ritson, D. M., 1952, *Phys. Rev.*, **85,** 295.

Lapp, R. E., 1946, *Phys. Rev.*, **69,** 321.

Molière, G., 1946, *Cosmic Radiation*, Ch. 3, ed. Heisenberg, W. (New York : Dover).

Montgomery, C. G., and Montgomery, D. D., 1947, *Phys. Rev.*, **72,** 131.

Morrison, P., Olbert, S., and Rossi, B., 1954, *Phys. Rev.*, **94,** 440.

Nishimura, J., and Kamata, K., 1951, *Progr. Theor. Phys., Japan*, **6,** 628.

Norman, R. J., 1955, *Aust. J. Phys.*, **8,** 419 ; 1956, *Phys. Rev.*, **101,** 1405.

Peters, B., 1952, *Progress in Cosmic Ray Physics*, **1,** Ch. 4 (Amsterdam: North-Holland).

Prescott, J. R., 1950, *Ph.D., Thesis*, University of Melbourne.

Rossi, B., 1952, *High Energy Particles*, Ch. 5 (New York : Prentice-Hall); 1955, *Nuovo Cim.*, Suppl. 1, **2,** Ser. 10, 275.

Rossi, B., and Greisen, K., 1941, *Rev. Mod. Phys.*, **13,** 240.

Singer, S. F., 1951, *Phys. Rev.*, **81,** 579.

Sitte, K., Stierwalt, D. L., and Kofsky, I. L., 1954, *Phys. Rev.*, **94,** 977, 988.

Vavilov, Yu. N., Nikolski, S. I., and Tukish, Ye. I., 1953, *Doklady Akad. Nauk, S.S.S.R.*, **93,** No. 2.

Wataghin, G., 1953, *Nuovo Cim.* Suppl. 1–4, **10,** Ser. 9, 489.

Williams, R. W., 1948, *Phys. Rev.*, **74,** 1689.

Resonance Forces at Large Separations

By A. DALGARNO and N. LYNN

Department of Applied Mathematics, The Queen's University of Belfast

Communicated by D. R. Bates; MS. received 5th July 1956

Abstract. A simple perturbation method is suggested for the calculation of energies of the states of homonuclear molecules at large internuclear distances R for which the identity of the nuclear fields must be taken into account, a comparison with exact data on the $1s\sigma_g$ and $2p\sigma_u$ states of H_2^+ showing that results of high accuracy can be obtained without undue labour. The method is also applied to the $^1\Sigma_g$ and $^3\Sigma_u$ states of H_2 and reasons are advanced for supposing that the results are, at least for R greater than $4a_0$, more accurate than those of any previous calculation.

§ 1. Introduction

The importance of obtaining methods of calculating accurately the forces arising between atoms which are at large separations from one another has been emphasized recently by applications of the curve-crossing method (Zener 1932, Landau 1932, Stueckelberg 1932) to predictions of reaction rates (Bates and Massey 1954, Bates and Moiseiwitsch 1954, Dalgarno 1954, Bates and Lewis 1955, Bates and Boyd 1956).

Apart from the work of Eisenschitz and London (1930), of Margenau (1939 a) and of Hirschfelder and Linnett (1950), all calculations of forces at large separations between similar atoms have ignored the degeneracy arising from the identity of the nuclear fields. It was stressed recently (Dalgarno and Lewis 1956 a) that frequently the major factor limiting the accuracy of the calculations is neglect of this degeneracy.

§ 2. Perturbation Method

For simplicity we restrict our description of the perturbation method to that for the case of a proton interacting with a hydrogen atom in the ground state. If $\psi_0(\mathbf{r}_a)$ is the wave function of the atom, $\mathbf{r}_a$ being the position vector of the electron relative to the nucleus A, then when nucleus B is an infinite distance away, $\psi_0(\mathbf{r}_a)$ satisfies the equation

$$H_a\psi_0(\mathbf{r}_a) \equiv (\nabla^2 + 2/r_a)\psi_0(\mathbf{r}_a) = E_0\psi_0(\mathbf{r}_a) \qquad \ldots\ldots(1)$$

where E_0 is the binding energy of the electron in rydbergs and length is measured in units of a_0 ($a_0 = 5{\cdot}29 \times 10^{-9}$ cm). The wave equation for the interacting system is

$$\mathscr{H}\Psi(\mathbf{r}) \equiv \left(\nabla^2 + \frac{2}{r_a} + \frac{2}{r_b} - \frac{2}{R}\right)\Psi(\mathbf{r}) = E\Psi(\mathbf{r}) \qquad \ldots\ldots(2)$$

where R is the distance between nuclei A and B and E is the system energy we wish to calculate. It follows immediately from (1) that

$$\mathscr{H}\psi_0(\mathbf{r}_a) = (E_0 + V_a)\psi_0(\mathbf{r}_a) \qquad \ldots\ldots(3)$$

where

$$V_a = \frac{2}{r_b} - \frac{2}{R}. \qquad \ldots\ldots(4)$$

It is convenient here to introduce a permutation operator P which interchanges a and b : thus

$$V_b = PV_a = \frac{2}{r_a} - \frac{2}{R}\,; \qquad \ldots\ldots(5)$$

and we further define

$$(p\,|\,L\,|\,q) = \int \psi_p^{*} L \psi_q \, d\mathbf{r} \qquad \ldots\ldots(6)$$

where ψ_p is the wave function of the pth excited state of hydrogen with corresponding eigenvalue E_p and L is any operator.

If we ignore the identity of the nuclei, Brillouin's formal expansion (1932) for the eigenvalue taken to the second order leads to the formula

$$E = (0\,|\,\mathscr{H}\,|\,0) + \sum_p{}' \frac{\{(0\,|\,\mathscr{H}\,|\,p) - E(0\,|\,1\,|\,p)\}\{(p\,|\,\mathscr{H}\,|\,0) - E(p\,|\,1\,|\,0)\}}{E - (p\,|\,\mathscr{H}\,|\,p)} \qquad \ldots\ldots(7)$$

where the prime indicates that the term $p = 0$ is excluded from the summation. Using (3), (7) is easily simplified to

$$E - E_0 = (0\,|\,V_a\,|\,0) + \sum_p{}' \frac{(0\,|\,V_a\,|\,p)(p\,|\,V_a\,|\,0)}{E - E_p - (p\,|\,V_a\,|\,p)} \qquad \ldots\ldots(8)$$

which becomes identical to conventional second order perturbation theory when $E - (p\,|\,V_a\,|\,p)$ is replaced by E_0:

$$E - E_0 = (0\,|\,V_a\,|\,0) + \sum_p{}' \frac{(0\,|\,V_a\,|\,p)(p\,|\,V_a\,|\,0)}{E_0 - E_p} \qquad \ldots\ldots(9)$$

Although (9) can be evaluated exactly for large R for the case considered here (Dalgarno and Lewis 1955), this is not in general possible and it is usual to make Unsöld's approximation (1927) by which $E_0 - E_p$ is replaced by a constant ϵ and to use the sum rule

$$\sum_m (0\,|\,L\,|\,m)(m\,|\,M\,|\,n) = (0\,|\,LM\,|\,n) \qquad \ldots\ldots(10)$$

yielding the approximate formula

$$E - E_0 = (0\,|\,V_a\,|\,0) + \epsilon^{-1}\{(0\,|\,V_a^2\,|\,0) - (0\,|\,V_a\,|\,0)^2\}. \qquad \ldots\ldots(11)$$

It has been demonstrated by Dalgarno and Lewis (1956a), (see also Dalgarno and Stewart 1956) that if ϵ is chosen equal to 8/9, (11) is an extremely accurate representation of the direct forces at large separations and is exact in the limit of infinite R.

To take account of the identity of the nuclear fields, we introduce a set of symmetric and antisymmetric functions

$$\chi_p^{\pm}(\mathbf{r}) = [2\{1 \pm (p\,|\,P\,|\,p)\}]^{-1/2}(1 \pm P)\psi_p(\mathbf{r}_a) \qquad \ldots\ldots(12)$$

and define

$$\overline{(p\,|\,L\,|\,q)}^{\pm} = \int \chi_p^{\pm *} L \chi_q^{\pm} \, d\mathbf{r}. \qquad \ldots\ldots(13)$$

In future, where there is no danger of confusion we shall omit the superscripts. An equation identical with (7) results when Brillouin's expansion is used with the set (12) as basis except that the matrix elements are altered according to

$$(p\,|\,L\,|\,q) \longrightarrow \overline{(p\,|\,L\,|\,q)}. \qquad \ldots\ldots(14)$$

Applying Unsöld's approximation, we then obtain after some manipulation

$$E^{\pm} - E_0 = \mathscr{L} + \mathscr{M} - \mathscr{N} \qquad \ldots\ldots(15)$$

where

$$\begin{aligned} \mathscr{L} &= (1 \pm \delta)^{-1}\{(0 \mid V_a \mid 0) \pm (0 \mid V_a P \mid 0)\} \\ \mathscr{M} &= \epsilon^{-1}(1 \pm \delta)^{-1}\{(0 \mid V_a^2 \mid 0) \pm (0 \mid V_a P V_a \mid 0)\} \\ \mathscr{N} &= \epsilon^{-1}(1 \pm \delta)^{-2}\{(0 \mid V_a \mid 0) \pm (0 \mid V_a P \mid 0)\}^2 \end{aligned} \qquad \ldots\ldots(16)$$

with

$$\delta = (0 \mid P \mid 0). \qquad \ldots\ldots(17)$$

The expression $\mathscr{L}$ is the familiar LCAO approximation to the $1s\sigma_g$ and $2p\sigma_u$ states of H_2^+ whilst $\epsilon^{-1}(0 \mid V_a^2 \mid 0)$ is the usual expression for the attractive van der Waals force and is the dominant term at very large values of R. For calculations ignoring degeneracy it is customary to expand according to

$$V_a \sim \frac{2}{R} \sum_{n=1}^{\infty} \left(\frac{r_a}{R}\right)^n P_n(\cos\theta_a) \qquad \ldots\ldots(18)$$

and, if overlap is ignored, (15) reduces to

$$E^{\pm} - E_0 = \pm(0 \mid V_a P \mid 0) + \epsilon^{-1}\{(0 \mid V_a^2 \mid 0) \pm (0 \mid V_a P V_a \mid 0)\} - \epsilon^{-1}(0 \mid V_a P \mid 0)^2. \qquad \ldots\ldots(19)$$

Attention is drawn to the fact that taking into account the identity of the nuclear fields introduces a term $\epsilon^{-1}(0 \mid V_a P \mid 0)^2$ which has the nature of a *direct* force. It decreases rapidly with increasing R and (19) then becomes

$$E^{\pm} - E_0 = \pm(0 \mid V_a P \mid 0) + \epsilon^{-1}\{(0 \mid V_a^2 \mid 0) \pm (0 \mid V_a P V_a \mid 0)\}. \qquad \ldots\ldots(20)$$

§ 3. Variational Methods

Margenau (1939) has described a variational method of calculating resonance forces. He selects a trial wave function

$$\Psi^{\pm}(\mathbf{r}) = \{1 + \lambda[\mathscr{H} - E_0]\}(1 \pm P)\psi_0(\mathbf{r}_a) \qquad \ldots\ldots(21)$$

and formally minimizes $E^{\pm}$. With certain assumptions valid at large R, he shows that the resulting expression for $E^{\pm}$ is given approximately by

$$E^{\pm} - E_0 = \frac{\mathscr{L} + \lambda\epsilon\mathscr{M}}{1 + 2\lambda\mathscr{L} + \lambda^2\epsilon\mathscr{M}} \qquad \ldots\ldots(22)$$

which he further approximates by

$$E^{\pm} - E_0 = \mathscr{L} + \lambda\epsilon\mathscr{M}. \qquad \ldots\ldots(23)$$

The parameter λ is now chosen so that (23) is correct in the limit of infinite R. If ϵ is chosen so that the perturbation expression (20) is correct at infinite R, then (20) and (23) are identical. A similar but more precise relationship holds when degeneracy is ignored (Dalgarno and Lewis 1956 b).

Amongst the many conventional variational calculations of $E^{\pm}$, that of Hirschfelder and Linnett (1950, to be referred to as HL) is the only one with any claims to high accuracy over a wide range of R.† Their trial wave function for

† This ignores a paper by Teller (1930). However, his method is not easily generalized to more complex systems.

the $^1\Sigma_g$ state of H_2 is given by

$$\Psi^{\pm}_{HL}(\mathbf{r}_1, \mathbf{r}_2) = (1+P)\{[1+(\alpha z^2)(x_{a1}x_{b2}+y_{a1}y_{b2}) + (\beta z^2)z_{a1}z_{b2}]a(1)b(2)+\gamma a(1)a(2)\} \quad \ldots\ldots(24)$$

where $a(1)=(z^3/\pi)^{1/2}\exp(-zr_{a1})$ and (x_{a1}, y_{a1}, z_{a1}) are the cartesian coordinates of electron 1 relative to the nucleus A as origin, the z axis lying along AB. For the $^3\Sigma_u$ state, Hirschfelder and Linnett chose a trial function similar to (24) but with $\gamma=0$. The labour involved in varying the four parameters α, β, γ and z is of course very considerable. For purposes of comparison we shall make use later of a modification of (24) for the $1s\sigma_g$ and $2p\sigma_u$ states of H_2^+ given by

$$\Psi^{\pm}_{HL}(\mathbf{r}) = (1\pm P)\{1+(\alpha z_a)\}a(1). \quad \ldots\ldots(25)$$

§ 4. Results and Discussion for H_2^+

The energies of the $1s\sigma_g$ and $2p\sigma_u$ states of H_2^+ have been calculated by substituting the exact form (4) of V_a into the usual perturbation formula (11) which neglects degeneracy and into the perturbation formula (15) and the variational formula (22) which take account of it, the parameter ϵ being taken as a constant such that (11), (15) and (22) are correct in the limit of infinite R, where it is known that $E^{\pm}-E_0 \sim \alpha/R^4$, α being the polarizability of the hydrogen atom in atomic units (a_0^3). All the integrals required have been listed by Eisenschitz and London (1930) and by Coulson (1942). To help in assessing the accuracy of the calculations by Hirschfelder and Linnett (1950) for H_2, the energies have also been computed by the variational method using the trial function (25) with $z=1$† and all the results are collected in tables 1 and 2 which reproduce also the exact data of Bates, Ledsham and Stewart (1953).

The accuracy achieved by the perturbation and variational methods when degeneracy is taken into account is very good and even at R as small as 3 in the $1s\sigma_g$ case and 4 in the $2p\sigma_u$ case, the energies are more accurate than those obtained using the LCAO approximation with a variable screening parameter (cf. Dalgarno and Poots 1954). The Hirschfelder–Linnett function also yields results of high accuracy even when z is not varied but although they are superior to the perturbation results at small R, they tend asymptotically to $8\alpha/9R^4$ and not to α/R^4 whereas the essential merit of the perturbation formula is that it behaves correctly at infinite separation. However, the importance of taking into account the identity of the nuclear fields is clearly demonstrated by all the results and it is not until R increases to a value of about 15 that (11) provides an adequate representation of $E^{\pm}$.

In general the evaluation of $(0\,|\,V_aPV_a\,|\,0)$ will be a very considerable computational task and it is desirable to find an accurate approximate expression for it. We assume that

$$(0\,|\,V_aPV_a\,|\,0) \sim \frac{(0\,|\,(2z_a/R^2)PV_a\,|\,0)(0\,|\,PV_a\,|\,0)}{(0\,|\,P(2z_a/R^2)\,|\,0)}, \quad \ldots\ldots(26)$$

$2z_a/R^2$ being the first term of the expression (18); using (26) in (16) we obtain the results in the sixth rows of tables 1 and 2. The loss in accuracy is slight, as comparison with the third row reveals, except at small separations where the perturbation method is, in any event, itself unsatisfactory.

† For $R>3$ the variation of z has a negligible effect on the energies.

The inaccuracy of the perturbation method at smaller separations can be overcome by a simple semi-empirical modification, whose success is based upon the observation that the values of ϵ required to give the exact energies vary only slowly with R, and whose utility is based upon the observation that in general there will be available accurate experimental data on the energies at one particular separation. Thus assuming that ϵ, considered as a function of R, can be represented by

$$\epsilon(R)=\epsilon(\infty)+C\delta, \qquad \ldots\ldots(27)$$

δ being the overlap integral (17), and calculating the constant C from the known value of ϵ (chosen here to be at $R=2$, the equilibrium separation of the $1s\sigma_g$ state), improved values of ϵ can be obtained. When they are used in (15) with the approximation (26), the energies in the last rows of tables 1 and 2 result. The accuracy is extremely high at all separations even for the $2p\sigma_u$ state for which cancellation is severe. It may be noted that some of the error involved in (26) is removed by this semi-empirical method of choosing ϵ.

§ 5. Results and Discussion for H_2

The application of the perturbation method to H_2 introduces no further points of principle and need be described but briefly. An approximation similar to (26) was used to evaluate $(0\,|\,V_a PV_a\,|\,0)$, $2z_a/R^2$ being replaced by the first term $2(x_{a1}x_{b2}+y_{a1}y_{b2}+2z_{a1}z_{b2})/R^3$ of the expansion of V_a (Margenau 1939 b), and ϵ was chosen initially so that the asymptotic form of (15) was identical to the very accurate result $E^{\pm}-E_0\sim 12{\cdot}998/R^6$ calculated by Pauling and Beach (1935). Many of the integrals required have been tabulated by Hirschfelder and Linnett (1950), and the analysis for those remaining has been given by Eisenschitz and London (1930) and by Margenau (1939 a). The calculations of Eisenschitz and London and of Margenau make use of an inadequate approximation to $(0\,|\,V_a PV_a\,|\,0)$ so that their results though valuable have only a qualitative significance, but those of Hirschfelder and Linnett, who used the complicated trial function (24), provide the most accurate energies at large separations hitherto known. Their results are reproduced in tables 3 and 4 and illustrated over a limited range in figures 1 and 2. Included also in the figures are the experimental data for the $^1\Sigma_g$ state and three values for the $^3\Sigma_u$ state computed by James, Coolidge and Present 1936) using a highly flexible trial wave function. Values of ϵ have been calculated assuming the form (27), the constant C being evaluated by requiring that (16) yields the observed energy at $R=2$ for the $^1\Sigma_g$ state and the energy at $R=2$ obtained by a short extrapolation of the calculations of James, Coolidge and Present for the $^3\Sigma_u$ state. Results computed from (15) using constant and varied values of ϵ are given in tables 3 and 4 and in figures 1 and 2.

The variation of ϵ is not significant for R greater than about 4, but for small R it effects a marked improvement in the predicted energies. For the $^1\Sigma_g$ state, the perturbation results when ϵ is varied are in essentially complete agreement with available experimental data down to $R=1{\cdot}75$ and represent a considerable improvement in accuracy over the HL values. Their values must be too great since they use the variational method and it is noteworthy that at all values of R, both for the $^1\Sigma_g$ and $^3\Sigma_u$ states, the perturbation results lie below the HL values. Further, the asymptotic form of the HL energies is $12/R^6$ whereas the correct form is $12{\cdot}998/R^6$ so that at large R the HL energies are too small by 7·7%. It

Table 1. $E-E_0$ for the $1s\sigma_g$ State of H_2^+ in rydbergs

$R(a_0)$	2	3	4	5	6	7	8	9	10	15
Exact	0·20525	0·15511	0·09216	0·04884	0·02393	0·01119	0·00514	0·00239	0·00116	0·000098
Eqn. (11)	0·26635	0·07753	0·02464	0·00924	0·00411	0·00210	0·00119	0·00073	0·00047	0·000091
Eqn. (15)	0·33119	0·18335	0·09915	0·05006	0·02378	0·01090	0·00496	0·00230	0·00112	0·000097
Eqn. (22)	0·22822	0·14670	0·08762	0·04696	0·02305	0·01075	0·00493	0·00229	0·00111	0·000097
Eqn. (25)	0·13182	0·13092	0·08786	0·04736	0·02302	0·01059	0·00479	0·00219	0·00105	0·000086
Eqn. (15) using (26) with ϵ constant	0·28690	0·16928	0·10120	0·05212	0·02493	0·01144	0·00519	0·00240	0·00115	0·000098
Eqn. (15) using (26) with ϵ varied	0·20525	0·15232	0·09536	0·05046	0·02450	0·01134	0·00517	0·00239	0·00115	0·000098

Table 2. $E-E_0$ for the $2p\sigma_u$ State of H_2^+ in rydbergs

$R(a_0)$	2	3	4	5	6	7	8	9	10	15
Exact	0·66493	0·26382	0·10890	0·04542	0·01871	0·00745	0·00279	0·00091	0·00020	−0·000084
Eqn. (11)	−0·26635	−0·07752	−0·02464	−0·00923	−0·00411	−0·00210	−0·00119	−0·00073	−0·00047	−0·000091
Eqn. (15)	0·53346	0·25280	0·10729	0·04480	0·01835	0·00725	0·00268	0·00086	0·00017	−0·000085
Eqn. (22)	0·07243	0·34335	0·12148	0·04706	0·01870	0·00730	0·00269	0·00086	0·00017	−0·000085
Eqn. (25)	0·66923	0·26051	0·10918	0·04560	0·01884	0·00755	0·00286	0·00097	0·00024	−0·000073
Eqn. (15) using (26) with ϵ constant	0·36354	0·22369	0·11030	0·04730	0·01962	0·00781	0·00292	0·00096	0·00021	−0·000084
Eqn. (15) using (26) with ϵ varied	0·66493	0·26202	0·11023	0·04695	0·01984	0·00810	0·00309	0·00103	0·00024	−0·000084

Table 3.† $E-E_0$ for the $^1\Sigma_g$ State of H_2 in rydbergs

$R(a_0)$	4	5	6	7	8	10	12
W	0·02269	0·005051	0·001014	0·000191	0·000035	0·000002	$0{\cdot}0000000_3$
$W+P$	0·02353	0·005408	0·001201	0·000283	0·000079	$0{\cdot}000014_0$	$0{\cdot}0000040_4$
$W+P+I$	0·02662	0·005924	0·001274	0·000293	0·000080	$0{\cdot}000014_0$	$0{\cdot}0000040_4$
Eqn. (15) (ϵ constant)	0·03405	0·007975	0·001813	0·000437	0·000123	$0{\cdot}000018_5$	$0{\cdot}0000052_8$
Eqn. (15) (ϵ varied)	0·03306	0·007904	0·001809	0·000437	0·000123	$0{\cdot}000018_5$	$0{\cdot}0000052_8$

† See also figure 1.

Table 4.‡ $-(E-E_0)$ for the $^3\Sigma_u^+$ State of H_2 in rydbergs

$R(a_0)$	4	5	6	7	8	10	12
$W+P$	+0·01371	+0·00289	+0·000497	+0·000044	−0·000019	−0·000012	$-0{\cdot}0000039_9$
Eqn. (15) (ϵ constant)	+0·00462	+0·00072	−0·000047	−0·000102	−0·000062	−0·000017	$-0{\cdot}0000052_8$
Eqn. (15) (ϵ varied)	+0·00758	+0·00094	−0·000032	−0·000101	−0·000062	−0·000017	$-0{\cdot}0000052_8$

‡ See also figure 2.

seems a legitimate claim that the perturbation results are superior to the HL results, at least for R greater than 4, where the variation of ϵ is insignificant, although a final decision must await experimental evidence.

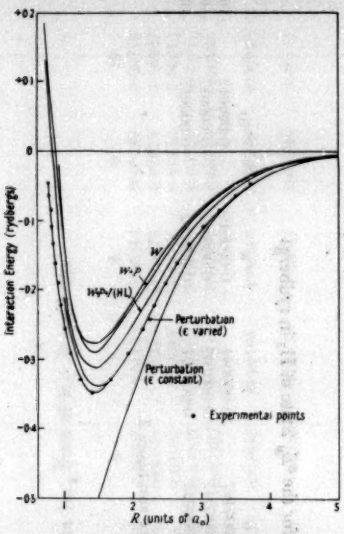

Figure 1. Interaction energy of the $^1\Sigma_g$ state of H_2. W, $W+P$ and $W+P+I$ refer to energies calculated using (24) with $\alpha=\beta=\gamma=0$, $\gamma=0$ and all parameters varied respectively.

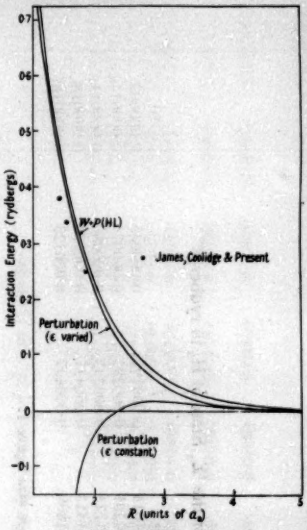

Figure 2. Interaction energy of the $^3\Sigma_u$ state of H_2. $W+P$ refers to energies calculated using (24) with $\gamma=0$.

The differences between HL and the perturbation energies are quite striking in the $^3\Sigma_u$ case where severe cancellation occurs. The equilibrium distances found by the two methods differ by more than unity and the depths of the minimum by a factor of about five.

The methods described in this paper carry calculations of interaction energies to the second order yet require not much greater computational labour than is involved in a first order LCAO calculation.

Acknowledgments

We are indebted to Professor D. R. Bates and Dr. J. T. Lewis for their interest in this work. One of us (N. L.) is grateful to the County Tyrone Education Committee for a research grant.

References

Bates, D. R., and Boyd, T. J. M., 1956, *Proc. Phys. Soc.* A, **69** in the press.
Bates, D. R., Ledsham, K., and Stewart, A. L., 1953, *Phil. Trans. Roy. Soc.* A, **246**, 215.
Bates, D. R., and Lewis, J. T., 1955, *Proc. Phys. Soc.* A, **68**, 173.
Bates, D. R., and Massey, H. S. W., 1954, *Phil. Mag.*, **45**, 111.

BATES, D. R., and MOISEIWITSCH, B. L., 1954, *Proc. Phys. Soc.* A, **67,** 805.
BRILLOUIN, L., 1932, *J. Phys. Radium*, S.7, **3,** 373.
COULSON, C. A., 1942, *Proc. Camb. Phil. Soc.*, **38,** 210.
DALGARNO, A., 1954, *Proc. Phys. Soc.* A, **67,** 1010.
DALGARNO, A., and LEWIS, J. T., 1955, *Proc. Roy. Soc.* A, **233,** 70; 1956 a, *Proc. Phys. Soc.* A, **69,** 57; 1956 b, *Ibid.*, **69,** 628.
DALGARNO, A., and POOTS, G., 1954, *Proc. Phys. Soc.* A, **67,** 343.
DALGARNO, A., and STEWART, A. L., 1956, *Proc. Roy. Soc.* A, **238, 269, 276.**
EISENSCHITZ, R., and LONDON, F., 1930, *Z. Phys.*, **60,** 491.
HIRSCHFELDER, J. O., and LINNETT, J. W., 1950, *J. Chem. Phys.*, **18,** 130.
JAMES, H. M., COOLIDGE, A. S., and PRESENT, R. D., 1936, *J. Chem. Phys.*, **4,** 187.
LANDAU, L., 1932, *Z. Phys. Sowjet*, **2,** 46.
MARGENAU, H., 1939 a, *Phys. Rev.*, **56,** 1000; 1939 b, *Rev. Mod. Phys.*, **11,** 1.
PAULING, L., and BEACH, J. Y., 1935, *Phys. Rev.*, **47,** 686.
STUECKELBERG, E. C. G., 1932, *Helv. Phys. Acta*, **5,** 370.
TELLER, E., 1930, *Z. Phys.*, **61,** 458.
UNSÖLD, A., 1927, *Z. Phys.*, **43,** 563.
ZENER, C., 1932, *Proc. Roy. Soc.* A, **137,** 696.

On the Reaction $^{13}C(\alpha, n)^{16}O$

By M. G. RUSBRIDGE
Cavendish Laboratory, Cambridge

Communicated by E. S. Shire; MS. received 19th June 1956

Abstract. The reaction $^{13}C(\alpha, n)^{16}O$ has been examined from 1·0 to 2·5 Mev bombarding energy. The positions and widths of seven resonances have been measured. Angular distributions have been obtained in five cases, and some tentative spin and parity assignments made. Measurements of the absolute cross section are given and values of reduced neutron and alpha-particle widths have been calculated for three levels in ^{17}O.

§ 1. Introduction

This reaction was first observed by Jones and Wilkinson (1953) who found two narrow resonances superimposed upon a rising background. Since then many further resonances have been found, and some spin assignments given, by Trumble (1954), Walton *et al.* (1955), Walton and Clement (1956), Schiffer, Bonner, Kraus and Marion (1956) and Schiffer, Kraus and Risser (1956), mainly for the region of bombarding energies above 2 Mev.

In this paper I describe measurements of yield curves and of absolute cross sections for bombarding energies between 1·0 and 2·5 Mev and also of angular distributions at five resonances. I have made spin and parity assignments for certain levels in the compound nucleus ^{17}O.

§ 2. Experimental Arrangements

I used a beam of singly charged helium ions from the Cavendish Laboratory Electrostatic Generator to bombard both natural carbon targets and targets of carbon enriched in ^{13}C supplied by the Atomic Energy Research Establishment, Harwell. All the targets used were deposited on a backing of 0·01 in. thick molybdenum and were 10–20 $\mu g\ cm^{-2}$ thick. To detect the neutrons I used Hornyak counters (Hornyak 1952) which have the advantages of being insensitive to γ-radiation and of giving very low background counting rate. This makes it possible to use them, in spite of their relatively low efficiency (of the order of 0·5%), in the study of reactions that give a low yield. They were however too insensitive for me to use in measuring the angular distribution at the lowest resonance and for this purpose I used a liquid scintillator. This consisted of a saturated solution of terphenyl in xylene with 0·1% diphenyl hexatriene and was used in conjunction with two EMI 6262 photomultiplier tubes in coincidence. It had an efficiency of about 50% for neutrons, but as it was also sensitive to γ-rays care had to be taken to reduce background from the electrostatic generator.

To measure angular distributions I used three Hornyak counters. One in a fixed position served as a monitor; the other two had Hornyak buttons of the same size and composition. Their efficiencies were compared at frequent intervals by a return to standard positions. One of the movable counters was designed for use at angles of up to 167° to the incident beam.

Since large angular momenta, and consequently high order Legendre polynomials, might have been involved at some resonances, the counters were arranged to subtend a small solid angle at the target. The solid angle used, 0·043 steradian, is small enough to reduce the coefficient of P_6 by less than 10% (Breitenberger 1953).

I assumed that the efficiency of the Hornyak counter was directly proportional to neutron energy, as indicated by the data given by Hornyak (1952). The efficiency of the counters was calibrated with a polonium–beryllium neutron source whose activity was known to 10%. I assumed that the efficiency of the liquid scintillator was also proportional to neutron energy; this is consistent with the results of a measurement of the angular distribution at 1·34 MeV. The conclusions drawn from the angular distributions are not critically dependent on these assumptions.

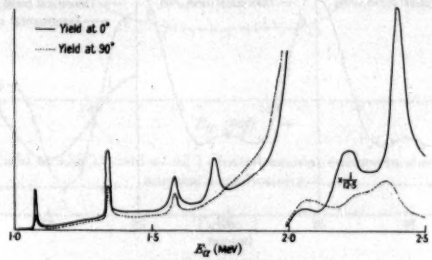

Figure 1. Yield curves at 0° and 90°.

Table 1

E_α (MeV)	Γ (kev) in lab. space	Γ_α	Angular distributions in c.m. space (only statistically significant terms included)
1·065 ± 0·01	3·5 ± 1	16 ± 3 ev	$P_0+(0{\cdot}1\pm0{\cdot}03)P_1+(0{\cdot}77\pm0{\cdot}04)P_2$ $+(0{\cdot}46\pm0{\cdot}05)P_4$
1·340 ± 0·01	⩽2	38 ± 6 ev	$P_0-(0{\cdot}12\pm0{\cdot}02)P_1+(0{\cdot}78\pm0{\cdot}02)P_2$ $-(0{\cdot}19\pm0{\cdot}03)P_3+(0{\cdot}58\pm0{\cdot}03)P_4$ $+(0{\cdot}15\pm0{\cdot}04)P_5$
1·575 ± 0·01	7 ± 3		$P_0+(0{\cdot}42\pm0{\cdot}02)P_1+(0{\cdot}08\pm0{\cdot}03)P_2$ $-(0{\cdot}50\pm0{\cdot}04)P_3$
1·735 ± 0·015	20 ± 10		$P_0+(0{\cdot}14\pm0{\cdot}02)P_1-(0{\cdot}18\pm0{\cdot}04)P_2$ $-(0{\cdot}16\pm0{\cdot}05)P_3$
2·05 ± 0·03	~100		
2·22 ± 0·03	~80		
2·40 ± 0·03	60 ± 15	10 ± 4 kev or 36 ± 9 kev	$P_0-(0{\cdot}18\pm0{\cdot}01)P_1+(0{\cdot}67\pm0{\cdot}02)P_2$ $+(1{\cdot}03\pm0{\cdot}03)P_3-(0{\cdot}20\pm0{\cdot}03)P_4$

The voltmeter of the electrostatic generator was calibrated using the known resonance energies in the reactions $^{27}Al(p, \gamma)^{28}Si$ and $^{27}Al(p, \alpha\gamma)^{24}Mg$.

§ 3. Experimental Results

Figure 1 shows yield curves (not corrected to centre-of-mass space or for variation of counter efficiency) for the forward direction and at 90° to the incident beam. Table 1 shows the seven resonances observed and their total widths

together with partial widths and angular distributions where they were measured. I obtained the total widths of the three lowest energy resonances from the profiles of the low energy sides of the peaks; the others I estimated from the yield curve and the known thickness of the natural carbon target. My value of the width of the 1·07 MeV resonance agrees well with the value of 3 kev given by Jones and Wilkinson.

I used Price's method (1954) for the angular distributions, observing at eleven angles in all cases, except at 1·735 MeV where I used seven angles. Figure 2 shows the results for three resonances for which comparison with theoretical predictions is possible.

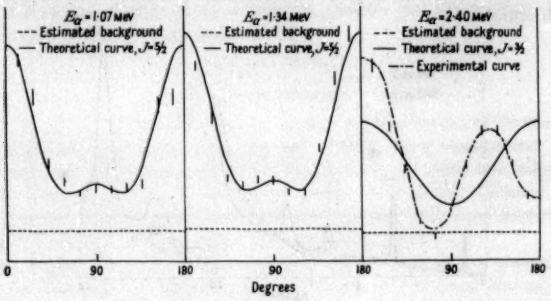

Figure 2. Angular distributions at 1·07 MeV, 1·34 MeV and 2·40 MeV compared with theoretical predictions.

I made absolute measurements of differential cross sections in the forward direction with a natural carbon target whose thickness was found to be 22 ± 5 kev from the apparent width of the 1·34 MeV resonance. Values obtained are: at the 2·40 MeV resonance, 36 ± 10 mbn sterad^{-1}; for the non-resonant background at 1·40 MeV, $0{\cdot}3 \pm 0{\cdot}1$ mbn sterad^{-1}, and at 1·0 MeV, $0{\cdot}03 \pm 0{\cdot}01$ mbn sterad^{-1}. These values are in agreement with those of Walton *et al.* (1955) and Schiffer, Bonner, Kraus and Marion (1956).

The α-particle widths at the 1·34 and 1·07 MeV resonances were obtained from the integrated cross sections at these resonances. Since the widths of these resonances are much less than the thickness of the target, the height of the observed peak gives the integrated cross section across the resonance. Assuming the α-particle width Γ_α to be much smaller than the neutron width, we have $G_\alpha = 2\Sigma/\lambda_\alpha{}^2$ where Σ is the integrated cross section across the resonance, λ_α the α-particle wavelength, and G_α is equal to Γ_α multiplied by a statistical factor.

Figure 3 shows the results of a determination of the ratio of the yields at 138° to that at 42° to the incident beam, in the centre-of-mass system, as a function of energy between 1·3 MeV and 1·9 MeV. I attempted to measure the variation with energy of the angular distributions around the 1·58 and 1·735 MeV levels, but could not obtain sufficient accuracy to interpret the results in terms of theoretical angular distributions. It was clear however that such variation is very marked.

§ 4. Discussion

Table 2 shows the possible theoretical angular distribution for this reaction, calculated by the method of Blatt and Biedenharn (1952), using the tables of Sharp *et al.* (1953) for the necessary coefficients. In this reaction both the incident and emergent channel spins are $\frac{1}{2}$, consequently both incident and emergent l-values are unique for a compound state of given J, π. The theoretical angular distributions are unambiguous; deviations from them must be attributed to interference between levels.

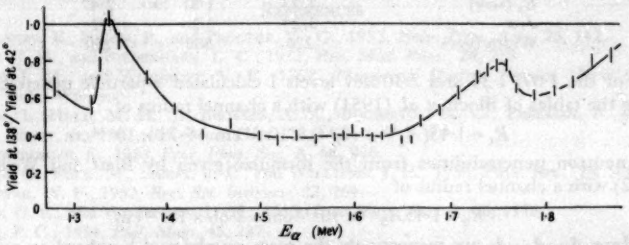

Figure 3. (Yield at 138°)/(yield at 42°) plotted against energy to show asymmetry of angular distributions.

Table 2

J	Angular distribution
1/2	Isotropic
3/2	P_0+P_2
5/2	$P_0+8P_2/7+6P_4/7$
7/2	$P_0+25P_2/21+81P_4/77+25P_6/33$

Comparison of these distributions with those given in table 1 allows the assignment of $J=5/2$ to the 1·07 MeV and 1·34 MeV levels. The experimental points and theoretical curves are compared in figure 2; to obtain the best fit one third of the total cross section has been assumed to be due to background. This is consistent with the yield curves from the targets used. In other cases the interference amplitudes are so large that the measured distributions are ambiguous. These are apparently due to the broad levels found in the reaction $^{16}O(n, n)^{16}O$ which form the continuous background in this reaction. Table 3 shows the levels of importance in this region of excitation (Freier *et al.* 1950, Baldinger *et al.* 1952). Here E_α is the bombarding energy at which the level would be centred if it were visible in the $^{13}C(\alpha, n)$ reaction. A strong asymmetry representing the interference between the $3/2^+$ and $3/2^-$ levels would be expected between 1·2 and 1·8 MeV, and this is in fact observed (figure 3). This figure shows that the approximate symmetry of the angular distribution at 1·34 MeV is accidental, i.e. due to the near cancellation of asymmetric interference amplitudes of opposite sign. This suggests negative parity for this level since the nearest broad level has positive parity. This assignment is supported by the values of the reduced neutron widths presented below.

No assignments can be made on the basis of the angular distributions at 1·58 and 1·735 MeV. I did not measure angular distributions at 2·05 or 2·22 MeV, as the resonances are very weak compared with the background and I did not expect that any interpretation would be possible. The 2·40 MeV resonance is strong in the forward direction though absent at 90°; the angular distribution indicates $J<5/2$, with $J=3/2$ as the more probable value.

Table 3

Excitation (MeV)	7·28	7·72	8·23
E_α (MeV)	1·23	1·81	2·47
J, π	$3/2^+$	$3/2^-$	$1/2^-$
Width (kev)	220	800	280

For the 1·07, 1·34 and 2·40 MeV levels I calculated α-particle penetrabilities using the tables of Bloch *et al.* (1951) with a channel radius of

$$R_1 = 1{\cdot}45(A_1^{1/3}+A_2^{1/3})\times 10^{-13}\,\text{cm} = 5{\cdot}71\times 10^{-13}\,\text{cm}$$

and neutron penetrabilities from the formulae given by Blatt and Weisskopf (1952) with a channel radius of

$$R_2 = 1{\cdot}45A_3^{1/3}\times 10^{-13}\,\text{cm} = 3{\cdot}66\times 10^{-13}\,\text{cm}.$$

Here A_1, A_2, A_3 are respectively the mass numbers of bombarding particle, target nucleus and residual nucleus. I used the calculated penetrabilities to obtain reduced widths from the measured partial widths. Table 4 shows the values obtained with the corresponding spin and parity assignments. The values of the neutron reduced widths for the 1·07 and 1·34 MeV levels are unusually small; the assignment of negative parity, which in each case gives the larger value of the reduced width, is therefore more plausible than that of positive parity.

Table 4

E_α (MeV)	E_x (MeV)	J, π	l_α	$\frac{\gamma_\alpha^2}{3\hbar^2/2mR_1^2}$	l_n	$\frac{\gamma_n^2}{3\hbar^2/2mR_2^2}$
1·07	7·16	$5/2^+$	3	$1{\cdot}6\pm 0{\cdot}3$	2	$(1{\cdot}1\pm 0{\cdot}4)\times 10^{-3}$
		$5/2^-$	2	$0{\cdot}23\pm 0{\cdot}04$	3	$(1{\cdot}1\pm 0{\cdot}4)\times 10^{-2}$
1·34	7·37	$5/2^+$	3	$0{\cdot}35\pm 0{\cdot}08$	2	$\leqslant 5\times 10^{-4}$
		$5/2^-$	2	$0{\cdot}05\pm 0{\cdot}01$	3	$\leqslant 5\times 10^{-3}$
2·40	8·18	$3/2^-$	2	$0{\cdot}11\pm 0{\cdot}04$	1	$(3{\cdot}3\pm 0{\cdot}8)\times 10^{-3}$
				or $0{\cdot}40\pm 0{\cdot}09$		or $(0{\cdot}9\pm 0{\cdot}3)\times 10^{-3}$
		$3/2^+$	1	$0{\cdot}04\pm 0{\cdot}01$	2	$(9\pm 2)\times 10^{-3}$
				or $0{\cdot}14\pm 0{\cdot}03$		or $(2{\cdot}5\pm 0{\cdot}6)\times 10^{-3}$

The two partial widths of the 2·40 MeV level are of the same order of magnitude and it is not possible to distinguish between them; hence two values of each reduced width must be given in this case. In the other cases the partial widths differ by a factor of the order of 100, and the smaller is then taken as the alpha-particle width. For the upper level there is insufficient difference between the various values for any parity assignment to be made.

The levels observed in this reaction have not so far been observed in the reaction $^{16}O(n, n)^{16}O$: I suggest, however, that the broad level at 8·23 MeV excitation (see table 3) may consist of an unresolved group of the three levels between 2·07 and 2·40 MeV bombarding energy observed in this reaction. The data of Freier *et al.* (1950) and Baldinger *et al.* (1952) appear to be consistent with this suggestion if we assume that one of the three has $J, \pi = 1/2^-$.

ACKNOWLEDGMENTS

I wish to express my thanks to Mr. E. S. Shire for suggesting the study of this reaction and for much valuable advice and encouragement during the experiment, to Mr. N. W. Tanner for the use of the liquid scintillator, to Mr. J. V. Simao for providing me with the results of his calibration of the electrostatic generator, to Mr. R. Lamb for the natural carbon targets, to the Department of Scientific and Industrial Research for a maintenance grant, and to Trinity Hall for a Research Studentship.

REFERENCES

BALDINGER, E., HUBER, P., and PROCTOR, W. G., 1952, *Helv. Phys. Acta*, **25,** 142.

BLATT, J. M., and BIEDENHARN, L. C., 1952, *Rev. Mod. Phys.*, **24,** 258.

BLATT, J. M., and WEISSKOPF, V. F., 1952, *Theoretical Nuclear Physics* (New York: John Wiley).

BLOCH, I., HULL, M. H., Jr, BROYLES, A. A., BOURICIUS, W. G., FREEMAN, B. E., and BREIT, G., 1951, *Rev. Mod. Phys.*, **23,** 147.

BREITENBERGER, E., 1953, *Proc. Phys. Soc.* A, **66,** 846.

FREIER, G., FULK, M., LAMPI, E. E., and WILLIAMS, J. H., 1950, *Phys. Rev.*, **78,** 508.

HORNYAK, W. F., 1952, *Rev. Sci. Instrum.*, **23,** 264.

JONES, G. A., and WILKINSON, D. H., 1953, *Proc. Phys. Soc.* A, **66,** 1176.

PRICE, P. C., 1954, *Phil. Mag.*, **45,** 237.

SCHIFFER, J. P., BONNER, T. W., KRAUS, A. A., Jr, and MARION, J. B., 1956, *Bull. Amer. Phys. Soc.* II, **1,** 20.

SCHIFFER, J. P., KRAUS, A. A., Jr, and RISSER, J. R., 1956, *Bull. Amer. Phys. Soc.* II, **1,** 211.

SHARP, W. T., KENNEDY, J. M., SEARS, B. J., and HOYLE, M. G., 1953, *Tables of Coefficients for Angular Distribution Analysis*, CRT-556 (Atomic Energy of Canada, Ltd., Chalk River, Ontario).

TRUMBLE, R. E., Jr, 1954, *Phys. Rev.*, **94,** 748.

WALTON, R. B., BECKER, R. L., CLEMENT, J. D., and ZUCKER, M. S., 1955, *Phys. Rev.*, **99,** 1649.

WALTON, R. B., and CLEMENT, J. D., 1956, *Bull. Amer. Phys. Soc.* II, **1,** 211.

The β-disintegration of RaD

By W. STANNERS and M. A. S. ROSS
Department of Natural Philosophy, University of Edinburgh

Communicated by N. Feather; MS. received 23rd July 1956

Abstract. Electron-sensitive nuclear emulsion impregnated with RaD citrate was used. RaD events associated with β-particles of RaE were studied to determine the total number of developed grains produced in each RaD event. An analysis of the resulting grain-count distribution provides evidence of the occurrence of a ground-state to ground-state β-process in RaD with an intensity of $15{\cdot}5 \pm 3{\cdot}5\%$ of all disintegrations. The total intensity of excitation of the 46·5 kev state of RaE is thus $84{\cdot}5 \pm 3{\cdot}5\%$ and the intensity of conversion electrons from this state is $81 \pm 4\%$. The last of these values is consistent with the results previously published by Wu, Boehm and Nagel and by Cranberg.

§ 1. Introduction

It has been established that the nucleus of RaD normally disintegrates by β-emission to form an excited state of RaE. The maximum energy of the β-particle has been reported as follows:

15 kev	(Richardson and Leigh-Smith 1937)
$15{\cdot}2 \pm 1$ kev	(Jaffe and Cohen 1953)
$18 \pm 2{\cdot}5$ kev	(Insch *et al.* 1952)
$23{\cdot}0 \pm 2{\cdot}5$ kev	(Huster 1953).

The excited state of RaE emits a γ-ray having an energy of $46{\cdot}52 \pm 0{\cdot}02$ kev (Ewan and Ross 1952). The total intensity of this mode of disintegration is the sum of the intensities of the γ-ray and the corresponding conversion electrons. These intensities have been reported as follows :

Number of γ-ray quanta per hundred disintegrations

somewhat less than 4	(Gray 1932)
$3{\cdot}1 \pm 1{\cdot}2$	(Bramson 1930)
3·6	(von Droste 1933)
7 ± 2	(Wu *et al.* 1953)
$3{\cdot}8 \pm 0{\cdot}6$	(Damon and Edwards 1954)

Number of conversion electrons per hundred disintegrations

74 ± 5	(Cranberg 1950)
$\geqslant 59 \pm 5$	(Butt and Brodie 1951)
58 ± 3	(Bashilov *et al.* 1953)
85 ± 5	(Wu *et al.* 1953).

These results suggest that the total intensity of this mode of disintegration is less than 100%. It will be noted, however, that Wu, Boehm and Nagel estimate the deficiency as only $8 \pm 5\%$.

The most recent work on RaD by γ- and β-spectroscopy (Ewan and Ross 1952, Wu *et al.*, 1953) makes it appear unlikely that the 46·5 kev state of RaE is de-excited to any significant extent by a cascade of transitions. Previous reports of γ-rays and conversion electrons of appropriate energies have not been confirmed. The possibility remains, however, that a ground-state to ground-state β-transition occurs, with a maximum energy of 62 to 70 kev. The present work was undertaken with the object of setting intensity limits to this mode of β-decay. We shall refer to this possible mode as the β_0 mode to distinguish it from the well established, or β_{46} mode.

§ 2. Experimental Method

A nuclear emulsion method was chosen for the investigation since it was known from the work of Bisgård (1952) that the technique of grain counting applied to measure the total energy in low-energy electron tracks gives good energy resolution. The total energy carried by low-energy electrons would register in the emulsion and the difficulties encountered with source backings in magnetic spectrometers and with wall effect in proportional gas counters would not arise. It was clear however, that on account of the small total energy of disintegration of RaD, (i) isolated RaD events could not be distinguished from low-energy events produced in the plate by cosmic rays, (ii) the point at which a disintegration electron originated (which we shall call the origin) would not usually be identifiable, and (iii) in about 3% of all RaD events the β_{46} particle would be the only electron emitted and a certain proportion of these would produce no grains.

To overcome these difficulties it was decided to make the time between the impregnation and the development of the plate sufficiently long to allow many of the RaE nuclei formed in the plate by the disintegration of RaD to disintegrate in turn into Po. The half-lives of RaE and Po are respectively 5 days and 140 days. The β-particles of RaE constitute a single spectrum with an endpoint of 1·16 Mev and the only other electrons released in this disintegration are those produced by inner bremsstrahlung in an intensity (about 1 in 10^4 β-particles) quite negligible for the present work (Novey 1953, Bolgiano *et al.* 1953). From unpublished work of Spurgin in this laboratory on 'electron stars' from $MsTh_2$ it was known that, if the β-particle of RaE had an energy of 200 kev or more, the high-energy end of the RaE β-particle track could be identified with certainty and the associated RaD tracks could not then be misinterpreted as branches at the low-energy end of an electron track. Thus the association of a RaD event with a relatively energetic RaE track would differentiate the RaD tracks from background tracks and, if the source were initially pure RaD, would indicate the origins of a random sample of RaD events—including those events in which no visible grains were produced.

The source of RaD was cleared of daughter products and used in the form of a neutral solution of RaD citrate to impregnate an Ilford G5 plate, 200 μ in thickness. The plate was dried and stored together with a blank plate for 19 days, a time sufficient to ensure that about two thirds of the RaD events would be found at the origin of a RaE β-particle track. After processing, the plates were examined under a $\frac{1}{12}$-inch objective of numerical aperture 1·28, giving good grain resolution. A photograph of a typical event with a RaD cluster of grains is shown in figure 1 (Plate).

Two difficulties presented themselves in the early stages of the work: (i) even when the origin of the RaD cluster of tracks was indicated it was not possible to

enumerate and distinguish the individual tracks in the cluster because of the high frequency of branching and large angle scattering in low-energy electron tracks; (ii) there was a sampling problem: the larger RaD clusters were easily recognized while events with few grains were more difficult to detect. The following procedure was therefore adopted: Long but 'well-defined' electron tracks were selected at random and followed to discover whether they originated in the emulsion. If they did so they were assumed to be RaE tracks, and at their origins a RaD disintegration was assumed to have occurred. Tracks were regarded as 'well defined' if they did not become entangled with other electron tracks and if their grain density was sufficient to make them easy to follow. Such tracks have a grain density about twice that of a minimum ionization track, correspond to an initial energy of about 300 to 600 kev, and show appreciable deviations from straightness. The following observations were made on each event: (i) The total number of grains in the RaD cluster (or first blob of the RaE track) was counted. (ii) the first 20 to 25 blobs of the RaE track were used to determine the mean grain density g, and the frequency of occurrence of one-grain blobs, two-grain blobs, etc. (iii) A length d was measured: that length, in line with the high-energy end of the RaE track, which lay within the projected area of the RaD cluster.

In following this procedure it was recognized that some of the long electron tracks might possibly be background tracks produced by cosmic rays, or tracks of β-particles from atoms of RaE originally present in the impregnating solution (either because of incomplete separation of daughter products, or through disintegration of RaD atoms after chemical separation but before completion of the impregnation process). The limits of error from these causes were estimated. The contribution from background tracks was obtained from the blank plate. Out of 200 long electron tracks which were examined in this plate, three, with rather low grain density, were found which might (but probably would not all) have been accepted as 'well-defined tracks' originating in the emulsion. The density of tracks in the impregnated plate was about twice that in the blank plate. It was, therefore, concluded that the intensity of background tracks was certainly not greater than $1\frac{1}{2}\%$ of all observed events.

No measurements were made of the amount of RaE present in the solution actually used for impregnation, but the residual RaE content was measured for a series of similar source preparations. The observations showed that $(2{\cdot}5 \pm 2{\cdot}0)\%$ of the initial (equilibrium) content of RaE remained with the RaD. The impregnation process was complete two hours after the time of the separation. Under these conditions $(2{\cdot}0 \pm 1{\cdot}6)\%$ of the RaE tracks in the plate would not be associated with RaD disintegrations.

§ 3. Analysis of the Observations

The impregnated plate was studied during two periods separated by an interval of three months. 400 events were recorded in the first period and 401 in the second. The histograms of the grain counts obtained in the two periods are compared in figure 2 and show no systematic difference in the estimation of grain numbers. The combined histogram is shown in figure 3. It indicates two distinct groups of events. The main group, consisting of events having from 6 to 30 grains, must include all events involving conversion electrons. The other group (events having from 1 to 5 grains) must include all the spurious events, numbering at most

28 ± 14 (of which $12 \pm 3{\cdot}5$ are attributed to background tracks, and 16 ± 13 to RaE tracks unassociated with RaD disintegrations). Deducting these spurious events, there remain 773 ± 14 RaD events in the combined histogram.

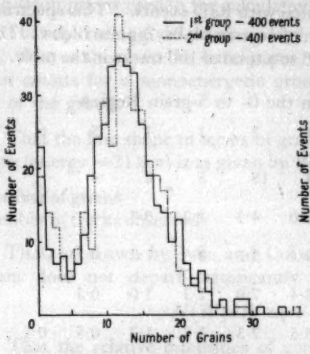

Figure 2. Comparison of grain-count histograms obtained in two periods of study showing no change in the estimation of grain numbers.

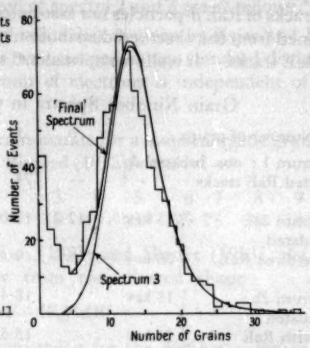

Figure 3. Grain-count histogram of all observed events and calculated spectra.

Before discussing the RaD events in detail, it is necessary to consider the effect on the grain-count histogram of the inclusion in the RaD clusters of grains belonging to the RaE tracks. Among the events recorded in figure 3 as having N observed grains, let the mth event have a RaE track with a grain-density g_m and an intercept (as previously defined) d_m. Let dx be the length of a small element of the intercept d_m at distance x from the point at which the RaE track emerges from the RaD cluster. We shall assume that the probability that the origin lies in the element dx is dx/d_m. The total probability that n grains of the cluster belong to the RaE track is then

$$ {}^{m}_{n}\mathrm{p}(N) = (d_m n\,!)^{-1} \int_0^{d_m} (g_m x)^n \exp(-g_m x)\, dx $$

and this is the probability that the true count of the event is $N-n$. This probability was evaluated for each track, for a sufficient range of n. On this basis, in a corrected histogram, there is a contribution

$$ {}_{n}\mathrm{p}(N) = \sum_{m} {}^{m}_{n}\mathrm{p}(N) $$

from column N to the column $N-n$. Hence the total height of the Nth column in the corrected histogram is

$$ \mathrm{P}(N) = {}_{0}\mathrm{p}(N) + {}_{1}\mathrm{p}(N+1) + {}_{2}\mathrm{p}(N+2) + \ldots . $$

The application of this correction made no appreciable alteration to the shape of the histogram, but it reduced the mean grain-count in the region of 6 to 30 grains, by 0·5 grain.

In order to analyse the uncorrected histogram, calculated grain-count spectra were evaluated for the three known types of event contributing to the total histogram.

Spectrum 1. Distribution of first-blob grain-counts on background tracks and tracks of RaE β-particles not associated with RaD events. This spectrum was obtained from the observed distribution of 1-grain blobs, 2-grain blobs . . . etc. on the RaE tracks. It is shown normalized to a total of 100 tracks in the table.

Grain Number Spectra in the 0- to 5-grain Region

Number of grains		0	1	2	3	4	5	6	Total
Spectrum 1 : obs. backgrd & isolated RaE tracks		—	74	18	5	2	1	—	100
Spectrum 2a : calculated β_{46} without RaE	15 kev	12·2	11·0	4·3	1·2	0·3	—	—	29
	20 kev	9·6	9·9	5·2	2·6	1·2	0·3	—	29
Spectrum 2b : calculated β_{46} with RaE	15 kev		18·4	7·0	2·3	1·0	0·3		29
	20 kev		15·5	7·3	3·8	1·7	0·5	0·1	29
Spectrum 1 + 2b : calculated	15 kev		39·1	12·0	3·7	1·6	0·6		57
	20 kev		36·2	12·3	5·2	2·3	0·8	0·1	57
Observed spectrum			42	23	19	13	11		108
Excess of observed over calculated	15 kev		2·9	11·0	15·3	11·4	10·4		51
	20 kev		5·8	10·7	13·8	10·7	10·2		51

Spectrum 2. The β_{46} continuum of RaD observed in disintegrations in which the γ-ray is emitted. The calculated spectrum 2a in the table is obtained by converting the energy distribution for an allowed β-spectrum to a grain-count distribution, making allowance for the grain-count line shape. Spectrum 2b, also shown in the table, is obtained from spectrum 2a by calculating, for each grain-count represented in 2a, the probability that 0, 1, 2 etc. grains from the RaE track are included in the RaD cluster. Spectra 2a and 2b are each calculated for end-points of 15 and 20 kev and are normalized to 29 events. This intensity corresponds to the intensity of the γ-ray as measured by Damon and Edwards (1954), their value, $3{\cdot}8 \pm 0{\cdot}6\%$, being regarded as the highest of the acceptable measurements.†

Spectrum 3. RaD events in which the β_{46} continuum is accompanied by conversion electrons and the subsequent atomic de-excitation. The calculation was carried out by the method used for spectrum 2a and an addition of 0·5 grain was made to allow for grains contributed by the RaE electrons. The spectrum was

† Since the γ-ray of RaD is known to be of very pure M1 character, an absolute upper limit to its intensity may be calculated assuming 100% excitation of the 46 kev level in RaE. Taking the L-shell internal conversion coefficient in Bi to be 18 (Rose *et al.*, private communication) and the ratio of L-conversion to conversion in higher shells as 3 (Wu *et al.* 1953, Cranberg 1950), this maximum intensity is 4·0%.

normalized to a total of 657 events corresponding to an absolute intensity of 85%. This intensity, observed by Wu *et al.*, is the highest of the experimental values. Spectrum 3, which is of negligible intensity within the range covered by the table, is shown in figure 3.

The assumptions used in the calculation of spectra 2 and 3 are as follows:

(*a*) That the mean grain-count–energy relation is as given by Zajac and Ross (1949); also, as shown in the same paper, that the percentage standard deviation of grain counts for a monoenergetic group of electrons is independent of the energy of the group.

(*b*) That the line shape in terms of grain-counts for a monoenergetic group of electrons (energy ~21 kev) is as given by Bisgård (1952), namely:

Number of grains	3	4	5	6	7	8	9
Number of tracks observed	16	55	83	129	75	36	14

(*c*) That, as shown by Jaffe and Cohen (1953) and Huster (1953), the β_{46} spectrum does not depart significantly from the allowed shape

$$N(W)dW \propto (W-W_0)^2 dW.$$

(*d*) That the relative intensities of conversion for the 46·5 kev γ-ray in the different atomic shells of Bi are as given by Cranberg (1950) and that the Auger yields are as given by Ross *et al.* (1955).

In the following analysis we examine first the total numbers of events in the two regions of the histogram and subsequently compare the observed and calculated spectra. The total number of events in the 1- to 5-grain region is 108, while the number expected in this region is not more than 57 ± 14. There is, therefore, an excess in this region of at least 51 ± 14 events.

Out of the total of 773 ± 14 events attributed to RaD, 693 have six or more grains. In the absence of a ground-state to ground-state transition, these must all be interpreted as events involving conversion electrons. This implies an intensity of $(89{\cdot}7 \pm 2{\cdot}0)\%$ for the conversion electrons, a value at least as high as the previous highest experimental value of $(85 \pm 5)\%$, obtained by Wu *et al.* (1953). Even supposing no events were spurious, the conversion group would still represent 86·5% of the total. It therefore appears likely that there is an excess of a few events per hundred in this group.

Turning to the spectrum of the 1- to 5-grain region as shown in the table, the combined spectrum of the known components is obtained by adding spectrum 1, normalized to 28 events, to spectrum 2b. The observed spectrum of 108 events is also shown in the table and, in the last line, the excess of the observed over the calculated spectrum. This excess is most marked in the region of 2, 3 and 4 grains, and it is clear that no increase in the intensities assigned to spectra 1 and 2b could remove this excess.

Lastly, for the spectrum of the 6- to 30-grain region, the histogram and spectrum 3 are compared in figure 3. It is evident that the two spectra agree closely in the region between 18 and 30 grains. This agreement substantially verifies the grain-count–energy relation employed for the calculated spectrum. On the other hand, the agreement is not so good over the peak of the spectrum from 10 to 17 grains. The events contributing to this region, however, include the most complicated which the RaD disintegration produces. These involve a

β_{46} particle, an L-conversion electron, an L- and up to 3 M-Auger electrons. In such cases more than one electron may pass through one or more of the grains. In the larger clusters, also, one or occasionally two grains might be masked by a group of grains lying higher in the emulsion. The distortion over the peak of the curve is therefore not unexpected. Both causes of distortion should disappear in the region of 6 to 9 grains, but here a considerable excess is evident above the calculated curve. It seems fair to conclude that the excess already suspected in the 6- to 30-grain group occurs predominantly in this lower energy portion of the group.

It might be argued that such an excess could be accounted for by postulating that the assumed line shape is too sharp on the low-energy side of the line. This would imply that all the measured intensities of conversion quoted in § 1 are too low. Such an implication is not itself untenable, but there are two objections to the postulate. First, there is good evidence from recent unpublished work by Peat in this laboratory, that the grain-count line shape on the low-energy side is not broader than the shape given by Bisgård (1952). Peat finds that on the low-energy side of a monoenergetic line, the profile height at twice the half-width from the peak is less than 3% of the peak height. This rule cannot be applied directly to the main peak of the RaD histogram since the latter has a complex spectrum, but it certainly implies that the intensity of the conversion spectrum should be very small at 5 grains. The second objection is that no broadening of the main peak can remove the excess events between 2 and 4 grains. In fact, if a smooth curve is drawn to represent the histogram above 5 grains and extended smoothly downwards to pass through the origin, this curve would include only half the excess in the low-energy region.

Having, therefore, established an 'inexplicable' excess in the 2- to 5-grain region and found strong reasons to believe that there is also an excess in the region from 6 to 9 grains, we are forced to conclude that there is a fourth component in the spectrum, which comes from an alternative mode of disintegration of RaD. This conclusion is intelligible only if the end-point of this spectrum is sufficiently high to permit appreciable contribtions at the low-energy end of the conversion spectrum. The simplest assumption is that this fourth component derives from a ground-state to ground-state transition.

§ 4. Intensity of the β_0 Transition

To estimate the intensity of the β_0 transition we fit a calculated grain-count spectrum for the β_0 continuum to that portion of the observed spectrum of excess events, in which the number of these events can be determined with best accuracy. This portion of the spectrum is the 3-, 4- and 5-grain region. As shown in the table, the total number of observed events in this region is 43. From this total we deduct three events belonging to the conversion group (see spectrum 3, figure 3) and 5·9 or 8·3 events (depending on the end-point energy of the β_{46} spectrum) for the known low-energy components (see table). Taking account of the statistical errors and of the 25% error in the total intensity of the known low-energy components, the number of excess events in this region is found to be 34 ± 7 for a β_0 end-point of 62 kev, or 32 ± 7 for an end-point of 67 kev.

The nucleus of RaD has zero spin and even parity, while that of RaE has spin 1 and odd parity. The β_0 transition must therefore be 0^+ to 1^-. The terms in the matrix element for this transition are presumably not very different from those for

the RaE 1^- to 0^+ transition, although the large difference in end-point energy may affect the relative importance of the energy-dependent terms. Also the cancellation of first-order terms may be less in evidence. On the basis of these considerations the shape factor of the β_0 spectrum is likely to be somewhere between unity and the shape factor of the RaE spectrum. A grain-count spectrum was, therefore computed both for the allowed shape and for the RaE shape:

$$N(W)dW = C(Z, W)\,F(Z, W)pW(W - W_0)^2\,dW.$$

Tabulated values of $F(Z, W)$ were taken from the tables of Rose *et al.* (1953) and the correction factor $C(Z, W)$ was computed using the best fit parameters $x = 2{\cdot}2$, $\xi_1 = 0{\cdot}2$ (Plassmann and Langer 1954). Calculations for an end-point of 62 kev showed that 43·7% of the RaE-type spectrum, or 39·3% of the allowed-shape spectrum, should have 6 or more grains and that 25·0% and 25·6% respectively should have 3, 4 or 5 grains. Equating the latter figures to 34 ± 7 events, we obtain 136 and 133 (± 28) events respectively in the total β_0 spectrum. (Calculations were also performed for an end-point of 67 kev using 32 ± 7 events as the value to be fitted. The resulting total intensities in the β_0 spectrum were essentially the same as in the first calculation.)

On this basis, 59 (or, using the allowed shape, 52) β_0 events with six or more grains would be expected in our sample. This is not an unreasonable figure for the experimental 'excess' in the main peak of figure 3. Similarly, in the 1- and 2-grain region, 43 (or alternatively 47) ± 8 events would be expected while 13 to 17 ± 15 are given by the observations. Here the difference between calculated and observed intensities is relatively large, but this is not altogether unexpected. It should be remembered that, for the 1- and 2-grain events, a maximum deduction has been made in our analysis for the known low-energy components, that other workers have found a deficiency of β particles at the low-energy end of the β_{46} continuum (Jaffe and Cohen 1953, Huster 1953) which has not been taken into consideration here, and moreover, that, if this deficiency exists in the β_{46} spectrum, a similar deficiency should exist in the β_0 spectrum. We therefore consider that the observations are probably reliable. We balance out these various factors by striking a mean between the calculated and observed intensities in the 1- and 2-grain region, attributing half the deficiency (15 events) to the β_0 spectrum and half to the other causes of deficiency and finally give as the intensity of the β_0 spectrum about 120 events or $15{\cdot}5 \pm 3{\cdot}5\%$ of all disintegrations.

It follows that the intensity of the β_{46} spectrum is $84{\cdot}5 \pm 3{\cdot}5\%$ and the total intensity of the conversion spectrum is then $81 \pm 4\%$. This intensity is in agreement, within the error limits, with the values $85 \pm 5\%$ and $74 \pm 5\%$ given respectively by Wu *et al.* (1953) and Cranberg (1950) for the intensity of conversion electrons, but is not in agreement with the values given by Butt and Brodie (1951) and Bashilov *et al.* (1953) who find intensities slightly below 60% of all disintegrations. An intensity as low as this is inconsistent with the grain-count distribution shown in figure 3.

Having determined the relative intensities of the β_0 and β_{46} spectra, and taking the half-life of RaD as 22 years, it is possible to calculate $\log_{10} f_0 t$ for both spectra provided the end-points are known. Assuming an end-point energy of 15 kev for the β_{46} spectrum, values of 5·2 and $7{\cdot}84 \pm 0{\cdot}09$ are obtained respectively for β_{46} and β_0. Raising the end-point energy for the β_{46} spectrum to 20 kev increases the value of $\log f_0 t$ for this spectrum to about 5·7 but makes relatively little change in the

value for β_0. Following Wu (1955), the β_{46} process in RaD may be compared with another 0^+ to 0^- transition in a nucleus of similar atomic number, $^{212}Pb \rightarrow ^{212}Bi^*$ having $\log f_0 t = 5{\cdot}17$, or with the 0^- to 0^+ transition $^{206}Tl \rightarrow ^{206}Pb$ having $\log f_0 t = 5{\cdot}18$. Some parity-forbidden transitions not $0 \rightarrow 0$ give rather higher values, but present evidence favours 5·2 rather than about 5·7 for β_{46}. Hence an end-point energy around 15 kev appears more likely than one about 20 kev. The β_0 spectrum may be compared with the spectra of RaE and of the 1^- to 0^+ transition $^{212}Bi \rightarrow ^{212}Po$. Log $f_0 t$ for the former is 8·0 and for the latter 7·22 (Horton 1956). It, therefore, appears that the shape factor for β_0 of RaD may not be very different from that for RaE.

As a check on the present analysis of the electron spectrum of RaD, a curve has been calculated assuming a β_0/β_{46} branching ratio of 15·5/84·5 and a RaE shape factor for the β_0 spectrum. The agreement between this 'final' calculated curve, as shown in figure 3, and the observed histogram is considered to be satisfactory, taking account of the comments previously made regarding the fit at the peak of the spectrum.

Acknowledgments

The RaD sources were prepared by Dr. N. Miller of this department. Professor Feather has assisted the investigation in various ways. The work was supported by the award of a Carnegie Scholarship to one of the Authors (W.S.).

References

Bashilov, A. A., Dzhelepov, B. S., and Chervinskaya, L. S., 1953, *Izv. Akad. Nauk. S.S.S.R., Ser. Fiz.*, **17**, 428.

Bisgård, K. M., 1952, *Proc. Phys. Soc.* A, **65**, 677.

Bolgiano, P., Mandansky, L., and Rasetti, F., 1953, *Phys. Rev.*, **89**, 679.

Bramson, S., 1930, *Z. Phys.*, **66**, 721.

Butt, D. K., and Brodie, W. D., 1951, *Proc. Phys. Soc.* A, **64**, 791.

Cranberg, L., 1950, *Phys. Rev.*, **77**, 155.

Damon, P. E., and Edwards, R. R., 1954, *Phys. Rev.*, **95**, 1698.

von Droste, G., 1933, *Z. Phys.*, **84**, 17.

Ewan, G. T., and Ross, M. A. S., 1952, *Nature, Lond.*, **170**, 760.

Gray, J. A., 1932, *Nature, Lond.*, **130**, 738.

Horton, J. W., 1956, *Phys. Rev.*, **101**, 717.

Huster, E., 1953, *Phys. Rev.*, **92**, 1076, *Z. Phys.*, **136**, 303.

Insch, G. M., Balfour, J. G., and Curran, S. C., 1952, *Phys. Rev.*, **85**, 805.

Jaffe, A. A., and Cohen, S. G., 1953, *Phys. Rev.*, **89**, 454.

Novey, T. B., 1953, *Phys. Rev.*, **89**, 672.

Plassmann, E. A., and Langer, L. M., 1954, *Phys. Rev.*, **96**, 1593.

Richardson, H. O. W., and Leigh-Smith, A., 1937, *Proc. Roy. Soc.* A, **160**, 454.

Rose, M. E., Perry, C, L., and Dismuke, N. M., 1953, *Oak Ridge National Laboratory Report No.* 1459.

Ross, M. A. S., Cochran, A. J., Hughes, J., and Feather, N., 1955, *Proc. Phys. Soc.* A, **68**, 612, 942.

Wu, C. S., Boehm, F., and Nagel, E., 1953, *Phys. Rev.*, **91**, 319.

Wu, C. S., 1955, *Beta and Gamma Ray Spectroscopy*, edited by K. Siegbahn, (Amsterdam: North-Holland), p. 343.

Zajac, B., and Ross, M. A. S., 1949, *Nature, Lond.*, **164**, 411.

A Liquid Scintillator Investigation of the Second Maximum in the Cosmic Ray Transition Curve

By P. D. McCORMACK
Dublin Institute for Advanced Studies

MS. received 28*th June* 1956

Abstract. A liquid scintillator, designed to detect stars produced in the phosphor by the cosmic radiation at sea level, has been used to investigate the star transition curve at depths of lead absorber in the region of twenty centimetres. The anomalous maximum at a depth of twenty centimetres, first reported by Schopper, Höcker and Rössle, has been confirmed. It appears that low energy μ-mesons are the most likely primaries, the stars being produced by neutrons released in the slow μ-meson nuclear absorption process.

§ 1. Introduction

Schopper, Höcker and Rössle (1951) have carried out an extensive absorption analysis of the star producing component of the cosmic radiation at an altitude of 2950 metres, using photographic plates. They detected an anomalous transition effect at a depth of 20 cm lead absorber, subsequent investigation showing that the events constituting the effect were mostly low energy stars, the number of evaporation products (prong number) per star was less than or equal to ten, with most stars having a value round three. Thus, the particle number spectrum alone tended to exclude photon or nucleon primaries. Moreover, the sharpness, position and magnitude of the maximum served to eliminate the nucleon cascade as a possible origin. In 1954, Schopper and Kuhn repeated this work using a crystal scintillator star detector and confirmed the presence of this maximum.

It must be noted that Perkins (1947) and George and Evans (1948), using photographic plates, and George and Michaelis (1951), using a crystal scintillator, carried out similar absorption experiments up to large depths of lead (greater than 20 cm), and failed to observe such an anomaly. However, their points of observation were spaced too far apart to detect it efficiently.

This investigation was designed to investigate the absorption in lead of the star producing component of the cosmic radiation at sea level as thoroughly as possible, and thus to confirm or contradict the existence of the effect which Schöpper, Höcker and Rossle have observed with their apparatus.

§ 2. Apparatus

This consisted of a Perspex box, 15 cm × 5 cm × 5 cm, filled with a solution of p-terphenyl in phenylcyclohexane (3 g $l.^{-1}$). A minute amount of diphenylhexatriene was added to the solution to change the emission spectrum from the ultra-violet to the blue, thus reducing self-absorption in the liquid, and allowing a much better matching to the spectral sensitivity characteristic of the photomultiplier. In six months' working this liquid showed no sign of deterioration.

The interior of the box was lined with polished aluminium to increase the light collection efficiency. Two end-window type EMI 6260 photomultipliers viewed the liquid, their photo-cathodes being in optical contact with the end-window of the box. The photomultiplier resistor chains were soldered directly to the high voltage insulator bases. This unit was placed inside a light tight steel box, cathode follower valves being mounted on the box itself so that the output leads from the photo-tubes to them were as short as possible. Valve stabilized voltages were fed to the photo-tubes and cathode followers, decoupling condensers being also put in the box.

The output pulses were taken to two identical negative feedback linear pulse amplifiers, which at the frequencies involved (in the region of 100 Mc/s) gave an amplification of about 80. Having passed through valve discriminators, they entered a fast Rossi coincidence circuit, the coincident pulses operating a mechanical register via a monostable multivibrator and power valve. The use of two tubes in coincidence reduces the rate of spurious pulses caused by photo-tube background and electronic peculiarities. The rate of spurious counts was determined by putting black paper shields between the scintillator end-windows and the photo-cathodes. Under the most adverse conditions of high e.h.t. and low discriminator bias, the rate was always less than 1 in 24 hours, which is very satisfactory. A block diagram of the system is shown in figure 1.

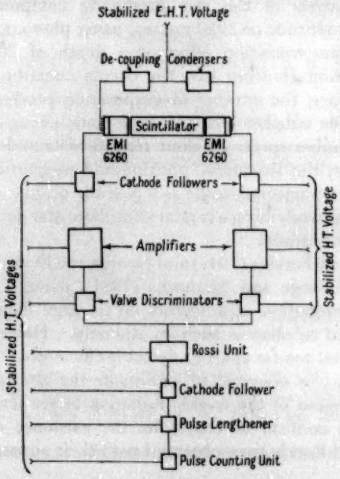

Figure 1. Schematic diagram of scintillator layout and associated electronics.

By keeping the e.h.t. voltage constant and varying the discriminator bias, and with no lead over the box, the integral pulse height distribution was obtained both for the two tubes in coincidence and for a single tube. These curves are shown in figures 2 and 3. From the bias characteristic of figure 3, one can separate two main components:

(*a*) In the region from 36–43 volts the points lie on a straight line: the rate of events in this region (45/minute at 38v) is what one would expect from the flux of single particles at sea level, viz. the total flux at sea level is approximately

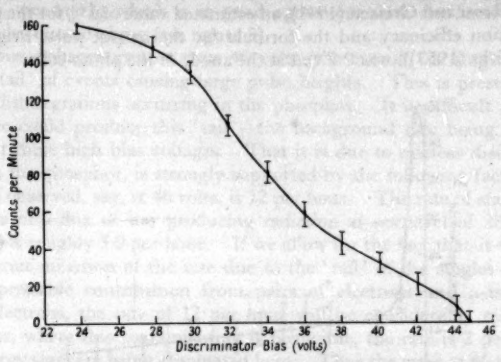

Figure 2. Discriminator bias characteristic; single phototube, no lead absorber.

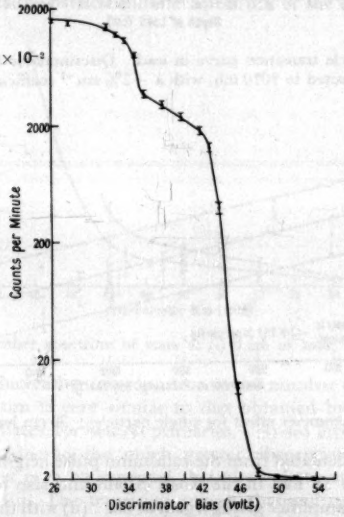

Figure 3. Discriminator bias characteristic; two phototubes in coincidence, no lead absorber.

0·8 cm^{-1} $sterad^{-1}$ (see Rossi 1948) and with a phosphor area of 75 cm^2, one expects roughly 56 per minute. The spread in pulse heights is due to particles passing through the liquid at angles to the vertical and thus dissipating more energy due

to increased path in the liquid. Further evidence that this component consists, in fact, of single particles may be summarized as follows: (i) the estimated pulse height due to a single particle crossing the liquid vertically, using the energy formula of Rossi and Greisen (1941), an estimated value of 5% for the geometrical light collection efficiency and the formula for the output pulse height in volts (given by Birks (1953)), was 0·7 volt at the anode of the photo-tube. This agrees

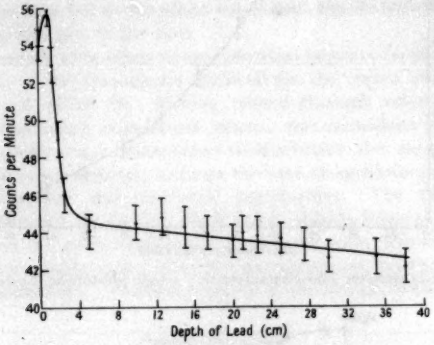

Figure 4. Single particle transition curve in lead. Discriminator bias at 38 v. All rates corrected to 1010 mb, with a -2% cm^{-1} coefficient.

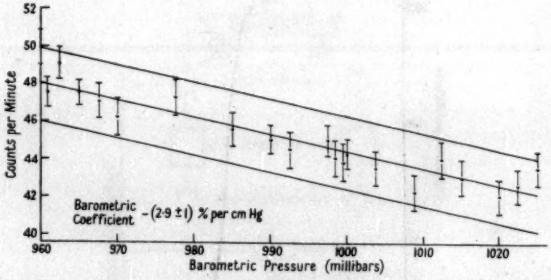

Figure 5. Barometer effect for single particles; 20 cm lead absorber.

very well with that calculated from the minimum pulse height of this component, 40 volts, allowing for 5v loss in the Rossi circuit and also for slight loss in the cathode follower, the amplifier giving a gain of 80. (ii) with the bias set at 38 volts, that is, in the single-particle region, a transition curve in lead was carried out up to a depth of 40 cm. This showed the usual soft cascade maximum at about 1 cm of lead, and the characteristic slow absorption of the penetrating component (mostly μ-mesons) at greater depths (figure 4). (iii) with the bias set at 38 volts and with 20 cm of lead over the scintillator (this eliminates the soft component,

leaving the hard component with its known barometer coefficient of -2% per cm Hg) the rate over a 30 minute period was taken each day. These rates were plotted against the pressure. The plot of these values yielded a value of $(-2{\cdot}9 \pm 1)\%$ per cm Hg which is in good agreement with the known value for single particles quoted above (see figure 5).

(*b*) At bias voltages greater than 46 volts (the cut-off for single particles), there is a 'tail' of events causing large pulse heights. This is presumably due to nuclear disintegrations occurring in the phosphor. It is difficult to see what other source could produce this 'tail'—the background rate being completely negligible at these high bias voltages. That it is due to nuclear disintegrations (or stars) in the phosphor, is strongly supported by the following facts: (i) The rate of stars observed, say, at 46 volts, is 12 per hour. The rate of stars expected on the basis of a flux of star producing radiation at sea level of $28\,cm^{-2}\,day^{-1}$ (Page 1950) is roughly 5·0 per hour. If we allow for the fact that at 46 volts one still has a contamination of the rate due to the 'tail' of the singles component and an appreciable contribution from pairs of electrons and μ-mesons plus knock-on electrons, the rate of 12 per hour will be considerably reduced. At 48 volts bias, where this contamination is negligible, the rate is 2 per hour, but the low energy stars are being eliminated here. Thus the rates at 46 and 48 volts bracket the expected star rate. (ii) The integral pulse height distribution shown in figure 6 is in effect the particle number spectrum of the stars, the photo-tube

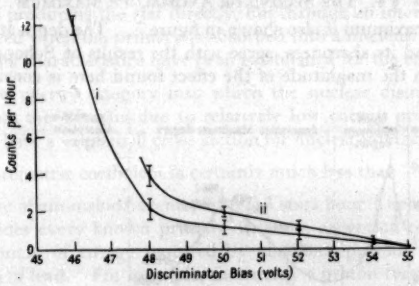

Figure 6. Particle number spectrum of stars at (i) 0 cm of lead, (ii) 20 cm of lead.

output pulse height increasing in proportion to the number of prongs of the star. This number spectrum is very similar to that obtained by Brown *et al.* (1949) using photographic plates, for neutral primaries. At sea level there is a predominance of neutrons (due to the much greater absorption of protons in the atmosphere) and so it is to be expected that most of the stars are produced by neutral primaries. (iii) The transition curves obtained under lead and water absorbers for this component agree with those found by other workers.

§ 3. Reliability of the Apparatus

Besides the points mentioned previously, the following two measurements served to demonstrate the reliability and efficiency of the apparatus used for star detection.

3.1. *Integral Photo-nuclear Cross Section for Photons of Energy greater than* 10^7 ev

At a depth of 1·5 cm of lead, the now well established first or Rossi maximum in the star transition curve (see figure 7) was detected. Using the fact that this is a photo-nuclear effect arising from an electron photon cascade produced by incident photons (see Heitler and Powell 1940, Bernardini *et al.* 1949, and Schopper, Höcker and Rössle 1951) from the observed rate of events, and the known flux of incident photons of energy greater than 10^7 ev (only high energy photons can produce stars) (Rossi 1948) one can compute a value for the integral photo-nuclear cross section for photons of energy greater than 10^7 ev. The value obtained was $\sigma = (3{\cdot}8 \pm 0{\cdot}4) \times 10^{-27}$ cm^2 nucleon^{-1}. This agrees well with the result of Kikuchi (1951) for stars produced by photons of less than 200 Mev, most of the photons at sea level having energies in this region.

3.2. *Absorption Length of the Star producing N-Radiation*

Finally, from the region of the transition curve at depths of lead greater than 30 cm, where the transition effects have died out and the absorption is closely exponential, a value of the absorption length for the incident nucleon component was deduced. It was $\lambda_A = 280 \pm 20$ g sec^{-2}, which also agrees well with the results of previous measurements (Bernardini *et al.* 1949, George and Jason 1949).

Thus, in confirming such well established results, the reliability, efficiency and correct working of the apparatus was demonstrated.

§ 4. The Second or Anomalous Maximum

The second maximum is also shown in figure 7. The depth at which it occurs, 20 cm of lead, and its sharpness, agree with the results of Schopper, Höcker and Rössle, although the magnitude of the effect found here is considerably greater,

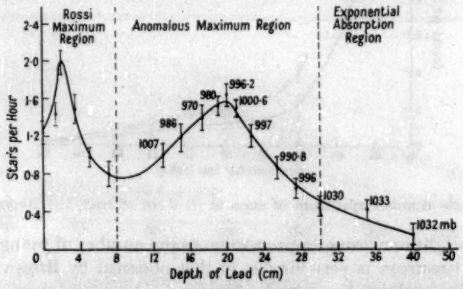

Figure 7. Star transition curve as a function of lead absorber depth.

viz. 60–70% compared with 30%. One would expect this, as the photo-multipliers 'scan' the liquid for stars produced in it much more efficiently than human observers can scan photographic plates, especially as this effect (see below) is caused mainly by low energy stars. Moreover, in photographic emulsions there is a large percentage of heavy nuclei (Ag and Br) which require more energy to produce stars, whereas in the liquid phosphor only the light nuclei O, C and N are present, with smaller binding energies. The liquid phosphor, for this reason also, is more efficient than the NaI scintillator used in the more recent work of Schopper and Kuhn (1954).

The origin of this maximum being unknown, it was not possible to normalize the rates to the same pressure. However, the average pressures over the various observation periods at each depth are noted, and it can be seen that even the use of a barometric coefficient of $-10\%\,\text{cm}^{-1}$ will only decrease the maximum slightly.

Although insufficient observations at each depth have been made to establish a barometric coefficient, there is an indication that, while at 20 cm of lead absorber a small value is operative, in fact much smaller than 10%, at depths of 15 and 25 cm a coefficient of 10% applies. This point is of interest in connection with a discussion of possible origins of the effect (see § 5).

The particle number spectrum at 20 cm of lead is shown in figure 6, and also that for 0 cm with which it may be compared. It is seen that at 20 cm there is a relatively higher percentage of stars with a small number of prongs (1 to 3). This was also found by Schopper, Höcker and Rössle. It suggests that the second maximum is caused mainly by events consisting of one or two heavily ionizing evaporation products.

§ 5. Conclusions

The existence of a pronounced second maximum in the absorption curve of the star producing component of the cosmic radiation at sea level at a depth of 20 cm of lead absorber, has been confirmed.

The sharpness of the maximum indicates that a two-particle process is involved, the primary not producing the star directly, but through an intermediate particle which is produced when the primary is absorbed into a nucleus.

The following characteristics have been established for the effect:

(i) The low energy category into which the nuclear disintegrations (star) fall, indicate that the effect is due to relatively low energy primaries. These, therefore, must have a very small cross section for nuclear interaction.

(ii) The barometric coefficient is certainly much less than -10% per cm Hg.

(iii) The rate of anomalous events, $0{\cdot}9 \pm 0{\cdot}3$ stars hour^{-1} over a detector area of 75 cm^2 excludes every known primary with the exception of μ-mesons, due to the large amount of energy required by neutrons, protons and electrons to penetrate 20 cm of lead. For example, the energy a proton requires to penetrate 20 cm is roughly 1 Gev. The flux of protons of this energy at sea level would be far too small to account for such a rate of events as observed, even with a geometric interaction cross section.†

The only known particle which could fill the role of a primary for these anomalous events appears to be the μ-meson. Making this assumption, I have made an estimate of the nuclear cross section required to explain the rate of events observed. This was, $\sigma = (1{\cdot}5 \pm 0{\cdot}5) \times 10^{-29}$ cm^2 nucleon^{-1}, and agrees with the values of $3\text{–}4 \times 10^{-29}$ cm^2 nucleon^{-1} obtained by Annis, Wilkins and Miller (1954) and Althaus and Sard (1948) for μ-meson interactions in which at least one evaporation neutron was produced. The lower value observed here would be expected, as in this case only events in which the neutrons produced a star in the phosphor are detected.

A possible mechanism lies in the negative μ-meson charge exchange reaction,

† Neutrons are eliminated, as Schopper *et al.* have demonstrated that charged primaries are involved.

in which the meson interacts with a proton in the nucleus through which it is passing, charge exchange occurring and a neutron plus another neutral particle of very small rest mass being produced. The reaction is

$$\mu^- + \mathrm{P} \rightarrow \mathrm{N} + \mathrm{V}.$$

This neutron will have an energy in the region of 10 Mev and has an interaction length in lead of roughly 12·5 cm. Consider an incident μ-meson with energy of 150 Mev. Due to energy loss by ionization in the lead (roughly 2 Mev g^{-1} cm^{-2}) it will have lost most of its energy after penetrating a depth of 90 g cm^{-2} (8 cm of lead) and have a high probability for nuclear absorption. As mentioned above, if the produced neutron has a most probable interaction length of 12·5 cm, one would expect a star to be produced at a total depth of 20·5 cm below the surface of the lead absorber.

As it has been shown that there is a maximum in the incident μ-meson spectrum at sea level in the region of 200 Mev energy (Wilson 1946, Heyland and Duncanson 1953), a similar increase in the star rate due to this cause might be expected round a depth of 20 cm of lead absorber. Finally, in support of this hypothesis, it must be noted that Hogrebe (1952) has detected an excess of neutron production by the cosmic radiation at depths of 20 cm and more of lead absorber, above that predicted by the normal exponential absorption theory.

Thus, it appears that a fairly statisfactory explanation for the anomalous second maximum observed in the star transition curve of the cosmic radiation at sea level, under large depths of lead absorber, can be found in low energy μ-meson nuclear absorption.

Acknowledgments

I am indepted to the Board of the Dublin Institute for Advanced Studies for a scholarship granted to me for two years while carrying out this work.

References

Althaus, E. J., and Sard, R., 1948, *Phys. Rev.*, **74,** 1364.
Annis, M., Wilkins, H. C., and Miller, I. D., 1954, *Phys. Rev.*, **94,** 1038.
Bernardini, G., Cortini, G., and Manfredini, A., 1949, *Phys. Rev.*, **76,** 1792.
Birks, J. B., 1953, *Scintillation Counters* (London : Pergamon Press).
Brown, R. H., Camerini, V., Fowler, P., Heitler, W., King, D., and Powell, C., 1949, *Phil. Mag.*, **40,** 862.
George, E. P., and Evans, J., 1948, *Nature, Lond.*, **162,** 333; 1949, *Proc. Phys. Soc.* A, **62,** 243; 1950, *Ibid.*, **63,** 1248; 1951, *Ibid.*, **64,** 193.
George, E. P., and Jason, A. C., 1949, *Proc. Phys. Soc.* A, **62,** 243.
George, E. P., and Michaelis, M., 1951, *Proc. Phys. Soc.* A, **64,** 662.
Heitler, W., and Powell, C., 1940, *Nature, Lond.*, **144,** 283.
Heyland, G. R., and Duncanson, W. E., 1953, *Proc. Phys. Soc.* A, **66,** 40.
Hogrebe, K., 1952, *Z. Naturf.*, **7a,** 772.
Kikuchi, S., 1951, *Phys. Rev.*, **81,** 1060.
Page, N., 1950, *Proc. Phys. Soc.* A, **63,** 250.
Perkins, D., 1947, *Phys. Rev.*, **79,** 925.
Rossi, B., 1948, *Rev. Mod. Phys.*, **20,** 537.
Rossi, B., and Greisen, K., 1941, *Rev. Mod. Phys.*, **13,** 240.
Schopper, E., Höcker, K. H., and Rössle, E., 1951, *Z. Phys.*, **6a,** 603.
Schopper, E., and Kuhn, G., 1954, *Z. Naturf.*, **9a,** 851.
Schopper, E., and Rössle, E., 1954, *Z. Naturf.*, **9a,** 836.
Wilson, J. G., 1946, *Nature, Lond.*, **158,** 415.

The Angular Distribution of Neutrons from High Energy Fission

By G. N. HARDING and F. J. M. FARLEY†
Atomic Energy Research Establishment, Harwell, Berks.

MS. received 13*th July* 1956

Abstract. A measurement has been made of the ratio of the numbers of neutrons emitted in directions parallel and perpendicular to the motion of the fission fragments, when fission is induced in natural uranium by 147 MeV protons. The value obtained, $1{\cdot}27 \pm 0{\cdot}11$, is consistent with the greater part of the neutron emission occurring before fission, the remainder ($2{\cdot}5 \pm 1$ neutrons) being emitted from the moving fragments, as in thermal fission.

§ 1. Introduction

When fission of heavy nuclei is induced by charged particles with energies of the order of 100 MeV, two main features distinguish the process from thermal-neutron-induced fission: (i) the fission is accompanied by emission of large numbers of neutrons (Harding 1956); (ii) the distributions of mass, energy and range of the fission fragments indicate that the most probable mode of fission is symmetrical (Goeckermann and Perlman 1949, Jungerman and Wright 1949, Ivanova, Perfilov and Shamov 1955). To explain these observations, two alternative hypotheses have been suggested: the first, put forward by Goeckermann and Perlman to explain their results on the fission of bismuth with 190 MeV deuterons, supposes that after the incident fast particle has reacted with the target nucleus in the manner described by Serber (1947) resulting in the emission of 'prompt' particles and thermal excitation of the nucleus, neutrons are evaporated from the nucleus, causing an increase of the fission parameter Z^2/A until fission becomes more probable than neutron emission. This hypothesis is supported by Yamaguchi (1950), who calculates that the fission probability will not exceed the neutron emission probability until 10 neutrons have been evaporated, and also by the measurements of Douthett and Templeton (1954) on the ranges in aluminium of fragments from high energy fission of uranium. A similar conclusion is reached by Goldansky, Tarumov and Penkina (1955) from a detailed consideration of fission cross sections. The predominantly symmetrical character of the fission is tentatively explained by Goeckermann and Perlman with the argument that the actual process of fission occurs so rapidly that it is not necessary, as in thermal fission, for the fission mode in which most energy is released to be the most probable.

In the second hypothesis, proposed by Marquez (1954), fission occurs as a result of excitation of the nucleus before any neutrons have been evaporated, and the neutron emission takes place from the moving fragments.

In the present state of our knowledge of the mechanism of fission, it is difficult to say with certainty which of these proposals is correct, and a direct experimental proof is required. This would require the measurement of time intervals considerably shorter than 10^{-13} sec, which is not possible at present. However, an

† On leave from Auckland University College, Auckland, New Zealand.

approach to the problem may be made by measuring the angular distribution of the neutrons with respect to the fission fragments: if they are emitted from the excited target nucleus before fission, the distribution will be isotropic apart from a small effect due to recoil of uranium nuclei; if emitted from the moving fragments after fission, the neutrons, emitted isotropically in the frame of reference of the fragments, will appear in the laboratory system to be more numerous along the line of motion of the fission fragments.

§ 2. Measurements

The present experiment was made with natural uranium and 147 MeV protons; a measurement with bismuth was not practicable with this apparatus because of its small fission cross section. The uranium was deposited on the electrodes of an ionization chamber and exposed to the external proton beam of the Harwell 110 in. synchrocyclotron. Neutrons arising from fission were detected in a proportional counter, and were recorded only when in coincidence with the detection of a fission fragment in the ionization chamber. The fission fragments were collimated inside the ionization chamber, and the neutron detector was placed alternately in positions such that it received neutrons emitted in line with, and perpendicular to, the direction of emission of the fission fragments. To eliminate the effects of the above-mentioned anisotropy of neutron emission due to recoil of the uranium nuclei in the direction of the proton beam, the measurements were all made in a plane perpendicular to the beam. Figure 1 is a diagrammatic cross section of the apparatus in this plane.

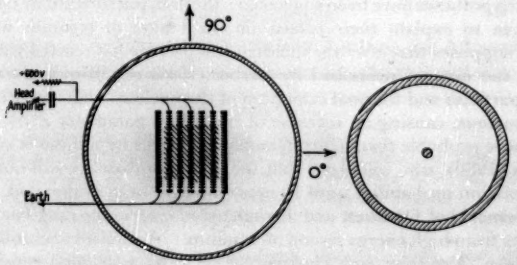

Figure 1. Section through collimated fission chamber and methane proportional counter in a plane perpendicular to the proton beam. The approximate area covered by the beam is shaded.

The design of the experiment was a compromise between obtaining sufficiently high angular resolution and a workable counting rate without an excessive accidental coincidence rate. The neutron counter was placed so that it subtended an angle of 17° on either side of the chosen direction. This would result in an apparent reduction in anisotropy, for which a correction has been applied in the calculated values given below.

The accidental coincidence rate was measured concurrently by delaying the pulses from the neutron counter by 2·4 μsec and feeding them and the fission pulses into a second coincidence unit having the same resolving time as the main unit ($2\tau = 1\,\mu$sec).

§ 3. The Fission Chamber

This was an electron-collection chamber with seven parallel-plate electrodes spaced 2 mm apart. The electrodes carried a total of 170 mg of uranium oxide in twelve deposits 3 cm in diameter and 2 mg cm^{-1} thick, over which were placed collimators consisting of plates of duralumin 0·9 mm thick each drilled with a hexagonal array of 469 holes 0·9 mm in diameter. The mean angular emission of the fission fragments was thus $\pm 18°$ from the normal. The proton beam entered and left the chamber through thin duralumin windows. Its direction was parallel to the planes containing the electrodes.

The chamber was filled to atmospheric pressure with a mixture of 95% argon and 5% CO_2. The collection time was less than 5×10^{-7} sec. The collector electrodes were connected to a potential of +600 volts, and to the head amplifier through a 50 pF condenser. The pulses were amplified by a wide-band linear amplifier having a time constant of $3{\cdot}2 \times 10^{-8}$ second, to prevent 'build-up' of pulses due to the beam protons. A discriminator following the amplifier was set so that only fission fragments were detected.

§ 4. The Neutron Detector

This has been fully described by Farley (1956). It is a proportional counter of diameter 2 inches and effective length 8 inches, filled to a pressure of 40 atmospheres with very pure methane so that electron collection is obtained. A potential of 12·5 kv was applied to the collecting electrode, and connection to the head amplifier was through a high voltage condenser of 50 pF. A collection time of about 1 μsec was obtained. Because of the large stopping power of the gas for electrons, it was necessary to set the discriminator to a high level to ensure that no fission γ-rays were recorded. The threshold for neutron detection was then 1·8 Mev, and the calculations which follow refer to that part of the neutron spectrum which is above this energy.

4.1. *Preliminary Measurements with Thermal Neutron Fission*

As a general check of the correct functioning of the equipment, it was first set up near the Harwell pile so that a beam of thermal neutrons induced fission in the ^{235}U present on the electrodes of the fission chamber. The ratio of numbers of fission neutrons detected at 0° and 90° was $4{\cdot}17 \pm 0{\cdot}15$. The value of this ratio, calculated by the method described by Fraser (1952) and using the primary neutron energy spectrum given by him, is 4·46. The 6% discrepancy is probably due to an error in correcting for angular resolution, since no account was taken of the extension of the neutron counter parallel to the beam.

§ 5. Measurements with 147 Mev Protons: Results

In table 1 are given the counting rates obtained with 147 Mev protons, averaged over a large number of separate measurements made in the two positions. The errors shown are statistical.

Table 1

Position	Time (min)	Fission Rate (min^{-1})	Neutron Rate (min^{-1})	Coincidence Rate genuine	accidental
0°	784	165	12690	$1{\cdot}32 \pm 0{\cdot}08$	1·75
90°	1186	168	12500	$1{\cdot}06 \pm 0{\cdot}06$	1·75

The relative numbers of neutrons are obtained by dividing the genuine coincidence rates by the fission rates. The ratio of the numbers at 0° and 90° is

$$N_0/N_{90} = 1{\cdot}27 \pm 0{\cdot}11.$$

§ 6. Discussion

In order to calculate the relative numbers of neutrons at 0° and 90° expected in the case where the neutrons are supposed to be evaporated from the moving fragments after fission, we first need to know the primary energy spectrum of these neutrons in the reference frame of the fragment. This was calculated by the method described by Le Couteur (1950) assuming that fission is symmetrical and the average mass number of the fragments therefore 119. The mean excitation energy was taken to be 20 Mev and the energy level constant 34 Mev^{-1}. This neutron spectrum is shown in figure 2. Experimental confirmation of the spectrum is lacking, but it probably errs on the side of having too many high energy neutrons. Since the neutron counter is biased in favour of the high energy end of the neutron spectrum, this would result in the calculated anisotropy being too low, and the quoted value should, therefore, be taken as a lower limit. Using the spectrum of

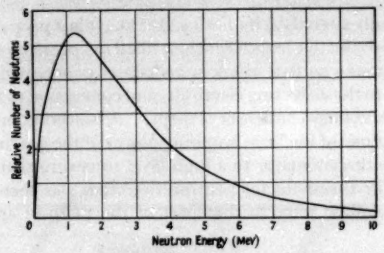

Figure 2. Calculated neutron energy spectrum for case where neutron emission follows fission.

figure 2, the ratio of expected numbers of neutrons at 0° and 90° was calculated by the method described by Fraser but with slightly different assumptions: (1) only symmetrical fission is considered; (2) in every case the fragment velocity is taken to be $1{\cdot}2 \times 10^9$ cm sec^{-1}, which is the mean fragment velocity deduced from the kinetic energy measurements of Jungerman and Wright, corrected for ionization defect from the data of Leachman (1952); (3) the neutrons are assumed to be evaporated isotropically in the frame of reference of the moving fragment. A correction was then applied for the angular resolution of the apparatus and for absorption of neutrons in the collimators, which is calculated to be 1% more in the 90° position. The value for the ratio so obtained is given in table 2, together with that expected if the emission is isotropic, again corrected for neutron absorption.

Table 2. Calculated Ratios of Numbers of Neutrons detected at 0° and 90°

Assumption	Ratio
All neutrons evaporated after fission	$\geqslant 2{\cdot}25$
All neutrons evaporated before fission	$1{\cdot}01$
1·5 neutrons evaporated after fission, the remainder before	$1{\cdot}17 \pm 0{\cdot}02$
2·5 ,, ,, ,, ,, ,,	$1{\cdot}29 \pm 0{\cdot}05$
3·5 ,, ,, ,, ,, ,,	$1{\cdot}42 \pm 0{\cdot}07$

In the last three lines of table 2 are given three further calculated values, included because the experimental value does not agree with either of those obtained with the two assumptions so far considered. For these it is assumed that 1·5, 2·5 and 3·5 neutrons per fission respectively are evaporated from the fragments, and the remainder before fission. The total number of neutrons per fission from uranium under the conditions of this experiment is $13{\cdot}1 \pm 1{\cdot}6$ (Harding 1956). For these calculations the primary neutron spectrum used was that calculated by Fraser for the thermal fission case, the other assumptions being the same as above. The errors shown are due to the uncertainty in the total number of neutrons per fission.

The experimental value is thus seen to be consistent with the evaporation of most of the neutrons before fission, a number of the order of $2{\cdot}5 \pm 1$ per fission being emitted from the fragments.

Acknowledgments

The authors wish to thank Mr. W. J. Whitehouse for suggesting this measurement and for discussion, Dr. E. Bretscher, Head of Nuclear Physics Division, Atomic Energy Research Establishment, Harwell, Dr. G. H. Stafford and members of the Harwell cyclotron team, Dr. T. H. R. Skyrme for assistance with the calculation of the neutron spectrum, and Mr. Ralph Jackson for the construction of the apparatus.

References

Douthett, E. M., and Templeton, D. H., 1954, *Phys. Rev.*, **94,** 128.
Farley, F. J. M., 1956, *J. Sci. Instrum.*, **33,** 276.
Fraser, J. S., 1952, *Phys. Rev.*, **88,** 536.
Goeckermann, R. H., and Perlman, I., 1949, *Phys. Rev.*, **76,** 628.
Goldansky, V. I., Tarumov, E. Z., and Penkina, V. S., 1955, *Doklady Akad. Nauk., S.S.S.R.*, **101,** 1027.
Harding, G. N., 1956, *Proc. Phys. Soc.* A, **69,** 330.
Ivanova, N. S., Perfilov, N. A., and Shamov, V. P., 1955, *Doklady Akad. Nauk, S.S.S.R.*, **103,** 573.
Jungerman, J., and Wright, S. C., 1949, *Phys. Rev.*, **76,** 1112.
Leachman, R. B., 1952, *Phys. Rev.*, **87,** 444.
Le Couteur, K. J., 1950, *Proc. Phys. Soc.* A, **63,** 259.
Marquez, L., 1954, *Nuovo Cim.*, **12,** 288.
Serber, R., 1947, *Phys. Rev.*, **72,** 1114.
Yamaguchi, Y., 1950, *Progr. Theor. Phys., Japan*, **5,** 143.

RESEARCH NOTES

The 440 keV Transition in ^{23}Na

By R. BERENBAUM†, J. H. TOWLE‡ and J. H. MATTHEWS†
Physics Department, Imperial College of Science, London

MS. received 16*th May* 1956

§ 1. Introduction

The ground state of ^{23}Na is known to have spin 3/2 and even parity. On the basis of the shell model, the configuration of the three protons outside the closed 1p shell is expected to be $(d_{5/2})^3 3/2$ in abnormal coupling (Mayer and Jensen 1955). The first excited state at 440 kev might be expected to be of configuration $(d_{5/2})^3 5/2$ or $[(d_{5/2})^2 s_{1/2}]1/2$, while the collective model would predict a level of spin 5/2. It is of interest, therefore, to determine the spin of the 440 kev level and to investigate the nature of the gamma-ray transition to the ground state.

This note describes measurements of the K shell internal conversion coefficient of the transition and of the angular distribution of gamma rays following the reaction $^{23}Na(p, p')^{23}Na^*$. Taken together, these measurements show that the 440 kev level most probably has spin 5/2 and decays mainly by M1 radiation.

§ 2. Experimental Procedure

2.1. The internal conversion coefficient was measured, using a beta-ray spectrometer, by comparing the number of internal conversion electrons with the number of photoelectrons produced by the gamma radiation from a thin gold radiator.

The beta spectrometer, designed by one of us (R. B.), was an annular focusing, medium lens type having a resolution of 2% with a transmission of 2% of 4π. The electron detector consisted of a Pamelon plastic scintillator, a Perspex light pipe and an E.M.I. photomultiplier. The latter was situated on the axis of the spectrometer coil inside a long steel cylinder for magnetic shielding: the presence of the steel did not impair the resolving power or linearity of the spectrometer (see figure 1). The pulses from the electron counter were fed to a single channel kicksorter which was adjusted to accept only pulses of the appropriate energy.

The 440 kev level was excited by the reaction $^{23}Na(p, p')^{23}Na^*$ at the 1·46 Mev resonance (Stelson and Preston 1954). The targets consisted of thin evaporated layers of NaCl on a gold backing. For internal conversion measurements, the thickness of the backing was about 1 mg cm^{-2}; for observations of the photoelectrons the backing served also as radiator and its thickness ($\sim$17 mg cm^{-2}) was then chosen so as to make the straggling of the photoelectrons comparable with the spectrometer resolution. This optimized the yield and overall resolution. In fact several radiators cut from the same foil were used and the average photoyield was taken, to allow for variations of thickness over the foil.

† Now at the Physical Laboratories, University of Manchester.
‡ Now at the Atomic Weapons Research Establishment, Aldermaston, Berks.

The yields of internally and externally converted electrons were measured relative to a monitoring Geiger counter which was well shielded from stray radiation. To reduce any error arising from drifts in the detector efficiencies, a series of measurements of the internal conversion yield was taken, interspersed among measurements of the photoelectron yield from the gold radiator. The

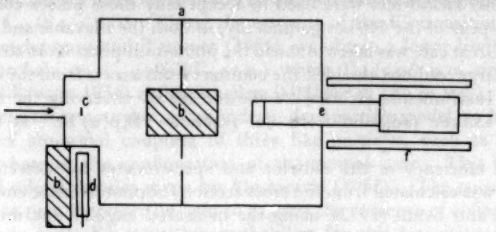

Figure 1. General Arrangement of Apparatus :
a, spectrometer (schematic); b, lead shielding; c, target; d, Geiger counter; e, electron detector; f, steel tube.

relative counting efficiency of the spectrometer and its associated electronic channels for electrons at the two energies concerned was determined by comparison with the well-known shape of the ^{137}Cs beta spectrum (e.g. Langer and Moffat 1951).

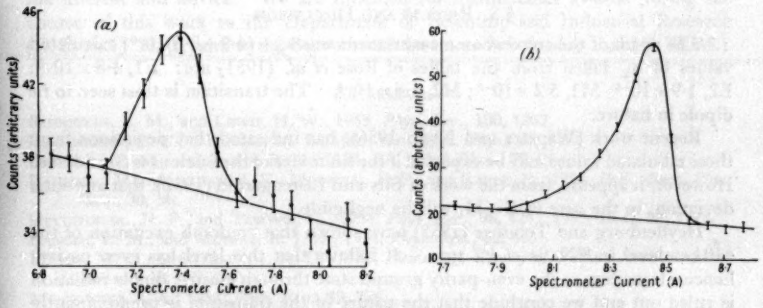

Figure 2. Spectra of electrons from 440 kev transition in ^{23}Na.
(*a*) Internal conversion electron spectrum.
(*b*) Spectrum of photoelectrons produced from gold radiator.

The results of the measurements on internal conversion electrons and the photoelectrons from the radiator are shown in figure 2; calculation of the internal conversion coefficient from these measurements involves also a knowledge of the angular distributions of both the electrons and the gamma rays from the reaction.

2.2. The angular distribution of the 440 kev gamma rays in the reaction $^{23}Na(p, p')^{23}Na^*$ was measured at the 1·29 and 1·46 Mev resonances (Stelson 1954)

using sodium iodide crystals and photomultipliers as detectors. One counter was attached to the target box and could be moved, in a plane containing the beam, about an axis through the target. The distance of this crystal from the target was about four inches.

The target used here was a thin ($\sim 50\,\mu g\,cm^{-2}$) evaporated layer of NaCl. Single channel kicksorters were used to accept only those pulses corresponding to the photo-peak of the 440 kev gamma ray, in both the movable and monitoring counters. Great care was taken to shield the photomultipliers from stray magnetic fields and a large lead box shielded the counters from x-rays from the electrostatic generator. Instrumental errors were allowed for by observing the isotropically distributed 430 kev radiation from the reaction $^{10}B(p,\alpha)^{7}Be^{*}$ at the 1·5 Mev resonance.

2.3. The efficiency of the radiator and spectrometer for detecting 440 kev gamma rays was calculated from the cross section for photoelectric emission given by Davisson and Evans (1952), using the measured angular distribution of the gamma radiation together with the acceptance parameters of the spectrometer and the angular distribution of photoelectrons from the radiator (Sauter 1931). The reliability of this type of calculation has been confirmed by a measurement, made in this way, of the internal conversion coefficient of the 660 kev transition in ^{137}Cs.

The small correction for the angular distribution of the internally converted electrons was found from the measured distribution of the gamma radiation at the resonance concerned (1·46 Mev) using the tables of Biedenharn and Rose (1953).

§ 3. Results and Discussion

The result of the conversion measurement was $\alpha_K = (4{\cdot}9 \pm 0{\cdot}6)10^{-5}$; calculated values of α_K taken from the tables of Rose *et al.* (1951) are: E1, $4{\cdot}8 \times 10^{-5}$; E2, $1{\cdot}9 \times 10^{-4}$; M1, $5{\cdot}2 \times 10^{-5}$; M2, $1{\cdot}8 \times 10^{-4}$. The transition is thus seen to be dipole in nature.

Recent work (Wapstra and Nijgh 1956), has indicated that deviations from these tabulated values may be expected if the finite size of the nucleus is considered. However, it appears, from the work of Sliv and Listengarten (1952), that any such deviation, in the case of $Z = 11$, will be negligible.

Heydenburg and Temmer (1955) have shown that coulomb excitation of the 440 kev level in ^{23}Na is of E2 type. It follows that this level has even parity; hence a transition to the even-parity ground state through electric dipole radiation is ruled out and we conclude that the nature of the transition is predominantly M1. This could arise if the 440 kev level had a spin of $\frac{1}{2}$, 3/2 or 5/2.

The results of the angular distribution measurements for the gamma rays are: 1·29 Mev resonance: $W(\theta) = 1 - 0{\cdot}18(\pm 0{\cdot}02)\cos^2\theta$, 1·46 Mev resonance: $W(\theta) = 1 - 0{\cdot}12(\pm 0{\cdot}01)\cos^2\theta$. It is not possible to determine uniquely the spin of the excited state from these measurements, but from the anisotropic distribution of the gamma rays, spin 1/2 is, of course, ruled out.

The 1·29 Mev resonance leading to the compound nucleus ^{24}Mg has been shown to be most probably 1^- (Stelson 1954) and formed mainly in channel spin 2 with appreciable interference between p and f waves. The angular distribution of 440 kev gamma rays which we obtain is consistent with this assignment and with a spin of 5/2 for the 440 kev level. As it is unlikely that the

first excited state of ^{23}Na has the same spin as the ground state, we conclude that the former most probably has the assignment 5/2. This is supported by a measurement of the cross section of the ^{23}Na(n, n')^{23}Na reaction, which is consistent with a spin of 5/2 for this level (Hausman *et al.* 1956).

It is seen from the measurement of the conversion coefficient, and the calculated values of Rose, that a limit on the ratio of the M1 and E2 transition probabilities is given by $\Gamma_{E2}/\Gamma_{M1} \leqslant 0{\cdot}05$. Using the estimate of the E2 transition probability given by Heydenburg and Temmer (1954), we obtain a lower limit for the M1 transition probability $\Gamma_{M1} \geqslant 0{\cdot}06\Gamma_{M1}$(s.p.) where Γ_{M1}(s.p.) is a single particle estimate (Wilkinson 1956) and is equal to $0{\cdot}021E\gamma^3$ ev ($E\gamma$ in Mev).

It is of interest to note that, on an independent particle model, an M1 transition to a state of abnormal coupling of three like particles, such as $(d_{5/2})^3 3/2$, is forbidden whatever the configuration of the excited state. This follows from two general selection rules given by Moskowski (1953). The occurrence of an M1 transition may therefore be held to suggest the presence of collective motion. The relatively large E2 transition probability for this transition, obtained by Heydenburg and Temmer, which is 70 times the single particle value, lends further support to this suggestion.

A similar example of a predominantly M1 transition to a ground state, which, on the basis of the shell model, has abnormal coupling, occurs in ^{55}Mn (Bernstein and Lewis 1955).

Acknowledgments

We would like to thank Professor S. Devons for suggesting this work and for his interest and advice. We are indebted for maintenance awards during the course of this work to the Department of Scientific and Industrial Research (R. B. and J. H. T.) and to the Beaverbrook Overseas Scholarship Fund (J. H. M.).

References

Bernstein, E. M., and Lewis, H. W., 1955, *Phys. Rev.*, **100,** 1367.
Biedenharn, L. C., and Rose, M. E., 1953, *Rev. Mod. Phys.*, **25,** 729.
Davisson, C. M., and Evans, R. D., 1952, *Rev. Mod. Phys.*, **79,** 24.
Hausman, H., Monahan, J. E., Mooring, F. P., and Raboy, S., 1956, *Bull. Amer. Phys. Soc.*, **30,** 56.
Heydenburg, N. P., and Temmer, G., 1954, *Phys. Rev.*, **96,** 426; 1955, *Ibid.*, **98,** 1198.
Langer, L. M., and Moffat, R. J. D., 1951, *Phys. Rev.*, **82,** 635.
Mayer, M. G., and Jensen, J. H. D., 1955, *Elementary Theory of Nuclear Shell Structure* (New York : Wiley).
Moskowski, S. A., 1953, *Phys. Rev.*, **89,** 474.
Rose, M. E., Goertzel, G. H., and Perry, C. L., 1951, *U.S. Atomic Energy Commission, ORNL Report*, 1023.
Sauter, F., 1931, *Ann. Phys., Lpz.*, **11,** 454.
Sliv, L. A., and Listengarten, M. A., 1952, *Zh. Exper. Teor. Fiz.*, **22,** 29.
Stelson, P. H., 1954, *Phys. Rev.*, **96,** 1584.
Stelson, P. H., and Preston, W. M., 1954, *Phys. Rev.*, **95,** 974.
Wapstra, A. H., and Nijgh, G. J., 1956, *Nuclear Phys.*, **1,** 245.
Wilkinson, D. H., 1956, *Phil. Mag.*, **1,** 127.

The Alpha Activity Induced in Platinum by Bombardment with Nitrogen Ions

By W. E. BURCHAM and B. C. HAYWOOD
Department of Physics, University of Birmingham

MS. received 17*th August* 1956

§ 1. Introduction

The reactions observed between accelerated nitrogen ions and heavy nuclei include capture followed by emission of neutrons (Ghiorso *et al.* 1954, Burcham 1954 a). The distribution in mass of radioactive products of atomic number $Z+7$ resulting from the bombardment of a nucleus of atomic number Z by nitrogen ions of energy greater than 100 Mev is qualitatively consistent with the predictions of the familiar evaporation theory (Blatt and Weisskopf 1952). If target nuclei which lead to alpha-emitting capture products are used it is relatively easy to identify and measure the relative yields of residual nuclei formed by the (^{14}N, xn) reactions. This has already been done for gold (Burcham 1954 a) and in this paper similar work with platinum, leading to neutron-deficient isotopes of astatine, is reported.

§ 2. Experimental Method

Platinum foils of thickness 0·0006 in. (Johnson Matthey 99·99% purity) were bombarded in the internal nitrogen ion beam of the 60 in. Nuffield cyclotron. The beam current was collected, after passage through the foil, by a screened electrode. In this way only ions of energy above 50 Mev were recorded; the upper limit of the continuous distribution of ion energies was about 110 Mev. Beam currents of 10^{-8}–10^{-9} ampere were used.

Astatine isotopes were extracted by heating the irradiated foils to redness near a silver foil as collector. This procedure also transferred up to about 25% of any polonium isotopes present in the platinum. The silver foils were mounted in the parallel plate ionization chamber used in earlier work (Burcham 1954 a, b) and pulse height distributions were recorded at intervals using a 60-channel analyser. The ionization chamber and recording system were calibrated by using a source of ^{210}Po ($E_\alpha = 5{\cdot}298$ Mev), and by assuming an energy of 6·10 Mev for the 7-minute activity attributed to ^{203}At (§ 3). This energy was checked, in terms of the alpha-particle group from ^{210}Po, by means of a signal generator. The resolution of the apparatus was to 2% for alpha-particle energies of about 6 Mev. The time required for mounting the foils and filling the chamber was about five minutes, and activities with periods much shorter than this would not have been detected. Gross decay curves of irradiated platinum foils were also taken with the ionization chamber.

The identification of the alpha-emitting products evaporated from the platinum foils was based on the energy and lifetime measurements.

§ 3. Results

The gross alpha decay curve of the irradiated platinum (figure 1) showed periods of 6·8 minutes, 23 minutes, 80 minutes and 4·2 hours. Pulse analysis of the activity

evaporated to the silver foils enabled these periods to be identified as shown in the table, using the values of lifetime and energy given by Asaro and Perlman (1954). Figure 2 gives a typical pulse size distribution.

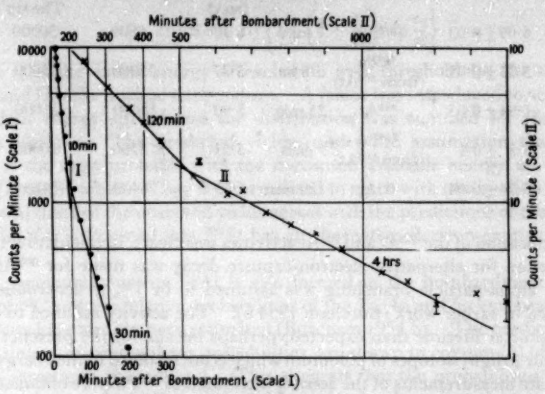

Figure 1. Gross decay of alpha activity from platinum bombarded by nitrogen ions. Bombardment 6×10^{-9} ampere for 30 minutes. Solid angle of ionization chamber $= 2\pi$. The lifetimes shown are approximate values for the main activities present.

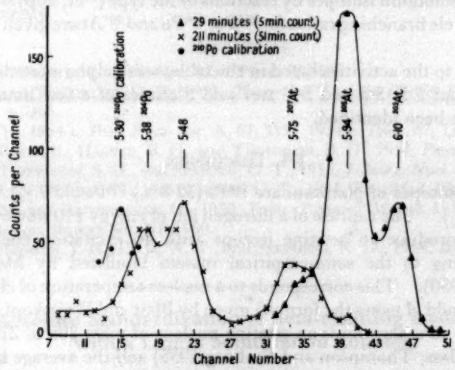

Figure 2. Pulse size distribution observed on silver foils at given time after end of bombardment.

The tabulated lifetimes are the averages of those obtained from the gross decay curve and from the pulse analyser experiments; the energies given are also the averages of several determinations. The reaction yields in column (6) of the table were obtained from the gross decay curve and give approximately the saturation activity in disintegrations per minute for a bombarding current of 10^{-9} ampere of nitrogen ions with the particular energy distribution used.

Alpha Emitters observed in the Reaction Pt + ^{14}N

Observed		Accepted Values			Reaction Yield		
Lifetime	Energy (MeV)	Assignment	Lifetime	Energy (MeV)	Observed	Predicted	
						Theory	Au + ^{12}C
7·1 ± 1·5 min	6·09 ± 0·03	^{203}At	7 min	6·10	6800	50000	15000
3·5 ± 0·6 hr	5·35 ± 0·05	^{204}Po (from ^{204}At)	3·8 hr	5·37	25000	25000	25000
22·7 ± 4 min	5·94 ± 0·03	^{205}At	25 min	5·90	58000	21000	26000
—	5·3 ± 0·1	^{206}Po (from ^{206}At)	9 days	5·21	⩽ 5700	10000	11000
83 ± 8 min	5·76 ± 0·04	^{207}At	120 min	5·75	6400	4800	5500

Identification of the ^{203}At and ^{205}At activities was clear; in calculating the yields no correction for alternative electron-capture decay was made for ^{203}At but for ^{205}At the alpha-particle branching was assumed to be 7% in accordance with a figure used in earlier work (Burcham 1954 b). The activity ascribed to ^{207}At has a rather shorter lifetime than expected, perhaps because of the presence of some activity due to light isotopes of polonium which is not resolved in the energy spectra. No accurate measurements of the activity attributed to ^{206}Po were obtained and the reaction yield is based on a small residual activity found on the irradiated platinum and on some of the silver foils. The activities assigned to ^{204}Po and ^{206}Po were assumed to arise from electron-capturing astatine parents ^{204}At and ^{206}At although production of polonium isotopes by reactions of the type (^{14}N, $x$np) is also possible. The alpha particle branching ratios for ^{204}Po, ^{206}Po and ^{207}At are given by Hollander *et al.* (1953).

In addition to the activities listed in the table, weak alpha-particle groups with energies of about 5·5, 5·3 and 5·1 MeV and lifetimes of a few hours were seen. These have not been identified.

§ 4. Discussion

The main isotopes of platinum are ^{194}Pt (32·8%) ^{195}Pt (33·7%) ^{196}Pt (25·4%) and ^{198}Pt (7·2%). The capture of a nitrogen ion of energy 110 MeV by any of these nuclei would produce an astatine isotope with an excitation energy of about 80 MeV according to the semi-empirical masses tabulated by Metropolis and Reitwiesner (1950). This corresponds to a nuclear temperature of about 2·65 MeV in a nucleus of odd A using the formula given by Blatt and Weisskopf (1952). The binding energy of a neutron is an astatine nucleus of mass 205 to 210 is probably about 8 MeV (Glass, Thompson and Seaborg 1955) and the average kinetic energy removed by the evaporation of a neutron is twice the nuclear temperature. Allowing for decrease in nuclear temperature as evaporation proceeds it seems likely that up to seven neutrons could be emitted. The probability of emission of a large number of neutrons of small energy is high because successive nuclei are then formed with high excitation energies, at which the level density is large. In the present case, for a homogeneous incident beam, the (^{14}N, 7n) reaction would be considerably more likely than the (^{14}N, 6n, 5n, 4n) and other reactions. The incident beam however has a continuous distribution of ion energies from 110 MeV downwards (Walker *et al.* 1954) and this increases the predicted yield of the 6n and 5n reactions with respect to the 7n evaporation.

The relative probabilities of production of the astatine isotopes by (xn) reactions were calculated roughly by successive applications of the formula for secondary reactions given by Blatt and Weisskopf (1952). This is

$$\sigma(\mathrm{a},\ 2\mathrm{n}) \simeq \sigma(\mathrm{a},\ \mathrm{n}) \left\{ 1 - \left(1 + \frac{\epsilon_c}{\Theta} \right) \exp \frac{\epsilon_c}{\Theta} \right\}$$

in which ϵ_c is the excess energy of excitation over threshold for the secondary reaction and Θ is the nuclear temperature. A factor was introduced to account for the incident energy spread and the distribution was summed for the various platinum isotopes. The predicted yields, under the assumption that the 7n reaction is the most probable with the maximum available energy, are shown in column (7) of the table. They are normalized to agree with observation for ^{204}At. The general trend of the observed yields agrees with the predictions of the evaporation model if it is assumed that ^{203}At has an alternative electron-capture mode of decay.

The compound nucleus ^{210}At is also formed in the bombardment of ^{197}Au by ions of ^{13}C and the relative probabilities of the 3n, 4n and 5n evaporation from this nucleus have already been estimated (Burcham 1954 b). The predicted yields from platinum, assuming these probabilities, are shown in column (8) of the table and also agree with those found. This suggests that the probabilities of the 6n and 7n reactions are lower than expected from the simple evaporation model.

ACKNOWLEDGMENTS

We are grateful to Messrs. G. Queen and P. G. Mitchell for assistance with these experiments.

REFERENCES

ASARO, F., and PERLMAN, I., 1954, *Rev. Mod. Phys.*, **26**, 456.
BLATT, J. B., and WEISSKOPF, V. F., 1952, *Theoretical Nuclear Physics* (New York: John Wiley), p. 365.
BURCHAM, W. E., 1954 a, *Proc. Phys. Soc.* A, **67**, 555; 1954 b, *Ibid.*, **67**, 733.
GHIORSO, A., ROSSI, B., HARVEY, B. G., and THOMPSON, S. G., 1954, *Phys. Rev.*, **93**, 257.
GLASS, R. A., THOMPSON, S. G., and SEABORG, G. T., 1955, *J. Inorg. Nucl. Chem.*, **1**, 3.
HOLLANDER, J. M., PERLMAN, I., and SEABORG, G. T., 1953, *Rev. Mod. Phys.*, **25**, 469.
METROPOLIS, N., and REITWIESNER, G., 1950, *Table of Atomic Masses*, U.S. Atomic Energy Commission, Report No. NP 1980.
WALKER, D., FREMLIN, J. H., LINK, W. T., and STEPHENS, K. G., 1954, *Brit. J. Appl. Phys.*, **5**, 157.

Absolute Standardization of Beta-emitting Isotopes with a Liquid Scintillation Counter

BY J. STEYN

Nuclear Physics Division, National Physical Laboratory, Pretoria, South Africa

MS. received 6th July 1956

THE most general way of standardizing aqueous solutions of beta emitters is by absolute counting of the beta particles by means of 4π-counters (Putman 1955). With this method it is necessary to be very careful when preparing sources in order to reduce absorption and self-absorption of beta particles as much as possible. This makes source preparation time-consuming and tedious.

The liquid scintillation counter, where the radioactive substance is dissolved in the scintillator, offers the big advantage that almost no source preparation is necessary. In the case of alpha emitters, this method has been shown to yield absolute disintegration rates (Basson and Steyn 1954). It has since been found that absolute standardization of beta emitters in aqueous solution is also possible by this means.

The experimental setup consisted of a DuMont 6292 photomultiplier mounted vertically inside a refrigerator, a Chase–Higenbotham non-overloading amplifier (Chase and Higenbotham 1952), a single channel pulse height analyser and a scaler. The temperature inside the refrigerator was kept at $-20°$C by thermostatic control. A sample cell containing 10 ml. of scintillator could be placed directly on top of the multiplier tube and covered with a hemispherical mirror.

With a sample of the radioactive solution dissolved in the scintillator, the photomultiplier voltage and electronic amplification were adjusted so that usually more than 50% of the pulses from the counter saturated the non-overloading amplifier. It was then found that the differential distribution of the remainder of the pulses was essentially constant and the integral distribution curve was a straight line which could be extrapolated accurately to zero pulse height to give the true disintegration rate of the sample. The figure shows that in the case of ^{60}Co

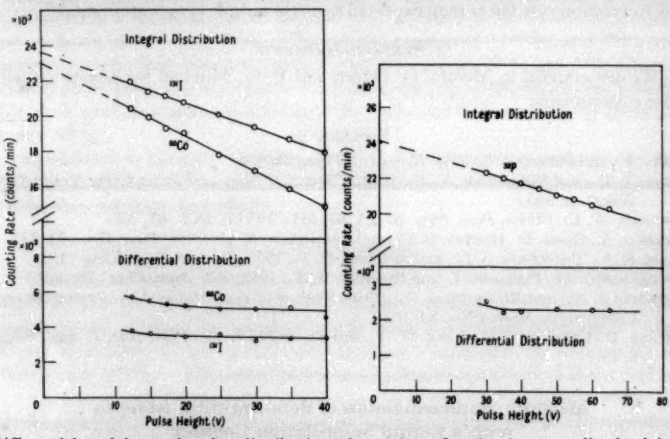

Differential and integral pulse distributions for various β-active isotopes dissolved in a liquid scintillator. The integral curve extrapolated to zero pulse height gives the absolute disintegration rate.

the extrapolation amounts to a correction of about 10%; for ^{131}I it is about 7% while in the case of ^{32}P at room temperature (20°c) the correction is 8%.

Results are given in the table for the isotopes ^{32}P, ^{131}I and ^{60}Co. A National Physical Laboratory (Teddington) standard was available in the case of ^{131}I. The ^{32}P solution was standardized by means of a 4π proportional counter whilst the ^{60}Co solution was standardized with a 4π Geiger–Müller counter and by the coincidence method. Good reproducibility is obtained and the agreement with other methods is very satisfactory.

Comparison of Standardizations

^{131}I ($\mu c\ g^{-1}$).						
Liquid scintillation counter :	25·00,	25·15,	25·39,	25·37,	25·05	(Mean : 25·19)
N.P.L. standardization :		25·0 ± 5% (Ampoule no. 33, April 1956).				
^{32}P ($\mu c\ g^{-1}$).						
Liquid scintillation counter :	23·52,	23·48,	23·30,	23·71		(Mean : 23·50)
4π-proportional counter :				23·60 ± 1%		
^{60}Co ($\mu c\ g^{-1}$).						
Liquid scintillation counter :	10·49,	10·40,	10·49,	10·32		(Mean : 10·42)
4π G–M counter :				10·40 ± 3%		
Coincidence method :				10·74 ± 2%		

It was required that the liquid scintillator would be able to mix with water to a certain extent, would keep the radioisotope in solution and would not freeze at the low temperature. This could be achieved by using a mixture of suitable solvents (Hayes *et al.* 1955). The scintillator employed consisted of a mixture of toluene and ethyl alcohol in the ratio 82 :18, the solute being 2, 5, diphenyl oxazole (P.P.O.) at a concentration of 4 g $l.^{-1}$. Aliquot parts of the radioactive solution, weighing between 0·03 and 0·04 g, could readily and rapidly be mixed with 10 ml. of this scintillator. Since it was necessary to ensure that the radioactivity did not precipitate from solution or adsorb on to the walls of the sample cell, the radioisotope had to be in a chemical form soluble in either alcohol or toluene. This meant that a suitable carrier substance had to be added to both the radioactive solution and the scintillator. For instance, H_3PO_4, being soluble in ethyl alcohol, was used as carrier material in the case of ^{32}P. In the case of ^{60}Co, $CoCl_2$ was added to the scintillator to give a concentration of 40 mg $l.^{-1}$. For ^{131}I and ^{32}P, NaI and H_3PO_4 were used respectively at a concentration of 10 mg $l.^{-1}$.

The presence of gamma radiation following the beta decay within the resolving time of the counter does not complicate the interpretation of the extrapolation as giving the true disintegration rate. The efficiency of the 10 ml. liquid scintillator is small for gamma radiation. Furthermore, the interaction is mainly by the Compton process, which also gives a more or less constant intensity pulse spectrum in the range of pulse sizes considered here. The 'wall effect' will cause a lowering of scintillation intensity for those particles that are stopped by the walls of the sample cell before dissipating all their energy in the scintillator, but the extrapolation will automatically compensate for pulses lost in this way.

The liquid scintillator, it seems, offers a simple, fast and reliable way for the absolute counting of beta particles.

Acknowledgments

This communication is published by permission of the South African Council for Scientific and Industrial Research.

References

Basson, J. K., and Steyn, J., 1954, *Proc. Phys. Soc.* A, **67**, 297.
Chase, R. L., and Higenbotham, W. A., 1952, *Rev. Sci. Instrum.*, **23**, 34.
Hayes, F. N., *et al.*, 1955, *Nucleonics*, **13**, (1), 46.
Putman, J. L., 1955, *Beta- and Gamma-Ray Spectroscopy*, Editor K. Siegbahn (Amsterdam: North-Holland Publishing Company), p. 823.

On the Binding Energy of the Helium Hydride Ion

By A. C. HURLEY†
Department of Theoretical Chemistry, University of Cambridge

MS. received 18*th June* 1956

A new technique for calculating the binding energies of molecules has recently been developed and applied to the molecules H_2, HF and N_2 (Hurley 1956 a, b, c). For these systems it is found that the new method, which embodies an intra-atomic correlation correction derived from atomic spectral data, leads to a larger value for the binding energy than does the usual procedure of subtracting the total molecular energy from the energy of the separated atoms calculated using the same wave function. Nevertheless, the binding energies obtained by the intra-atomic correlation correction method are lower limits‡ to the accurate values, while those calculated by the usual method are not. This important advantage of the new technique is well illustrated in the case of the helium hydride ion.

Coulson and Duncanson (1938) have carried out extensive calculations on the system HeH^+. The most general wave function considered by these authors may be written in the form

$$\tilde{\Psi} = \tilde{\Gamma}_I \tilde{\Psi}_I + \tilde{\Gamma}_c \tilde{\Psi}_c + \tilde{\Gamma}_p \tilde{\Psi}_p, \qquad \ldots\ldots(1)$$

where

$$\begin{aligned} \tilde{\Psi}_I &= \psi_a(1)\psi_a(2), \\ \tilde{\Psi}_c &= 2^{-1/2}\{\psi_a(1)\psi_b(2) + \psi_a(2)\psi_b(1)\}, \\ \tilde{\Psi}_p &= 2^{-1/2}\{\psi_a(1)\phi_a(2) + \psi_a(2)\phi_a(1)\}, \end{aligned} \qquad \ldots\ldots(2)$$

with

$$\begin{aligned} \psi_a &= \left(\frac{c^3}{\pi}\right)^{1/2} \exp(-cr_a), \\ \psi_b &= \left(\frac{\alpha^3 c^3}{\pi}\right)^{1/2} \exp(-\alpha c r_b), \\ \phi_a &= \left(\frac{\alpha^5 c^5}{\pi}\right)^{1/2} r_a \cos\theta_a \exp(-\alpha c r_a). \end{aligned}$$

Here (r_a, θ_a) are polar coordinates centred on the He nucleus, with the internuclear axis chosen as the line $\theta_a = 0$, and r_b is the distance from the H nucleus. Coulson and Duncanson minimized the total molecular energy given by the wave function (1) with respect to variations of the parameters α and c, the ratios $\tilde{\Gamma}_I : \tilde{\Gamma}_c : \tilde{\Gamma}_p$ and the nuclear separation ρ. An uncorrected dissociation energy $D_e = 2{\cdot}31$ electron volts was then obtained by subtraction from the energy which the wave function (1) yielded for the ground state dissociation products $(He(1s)^2\,{}^1S + H^+)$. Coulson and Duncanson pointed out that the value of D_e obtained in this way was

† On leave of absence from Chemical Physics Section, C.S.I.R.O., Melbourne, Australia; now at Solid State and Molecular Theory Group, M.I.T., Cambridge, Mass., U.S.A.

‡ To within the accuracy of the approximations employed (Hurley 1956 c).

probably too large, since the wave function (1) is better suited to the system HeH^+ than to an isolated He atom for which only the first term survives. This view has been confirmed by the recent calculation of Evett (1956), who obtains the value $D_e = 1{\cdot}90$ electron volts, using a 23-term wave function of the James–Coolidge type. From Evett's results it is almost certain that the true value lies in the range $1{\cdot}9 < D_e < 2{\cdot}0$ electron volts.

Let us consider the effect of applying the intra-atomic correlation correction to Coulson and Duncanson's calculation. The wave functions (2) are now regarded as approximations to a more accurate set of wave functions

$$\Psi_I, \Psi_c\,(\equiv\tilde{\Psi}_c), \Psi_p, \qquad \ldots\ldots(3)$$

which make allowance for intra-atomic correlation. The energy matrix H with respect to the functions (3) is calculated from the formula (Hurley 1956 a)

$$H = \tilde{H} + \tfrac{1}{2}[\tilde{M}(W - \tilde{W}') + (W - \tilde{W}')\tilde{M}], \qquad \ldots\ldots(4)$$

where $\tilde{H}$ and $\tilde{M}$ are the energy and overlap matrices with respect to the orbital wave functions (2) and $W - \tilde{W}'$ is the diagonal matrix

$$W - \tilde{W}' = \text{diag}\,\{W_I - W_I', W_c - \tilde{W}_c', W_p - \tilde{W}_p'\}. \qquad \ldots\ldots(5)$$

Here W_I, W_c, W_p are the accurate (experimental) energies of the states $He(1s)^2\,{}^1S + H^+$, $He(1s) + H(1s)$, $He(1s)(2p)\,{}^1P + H^+$, respectively, and $\tilde{W}_I'$, $\tilde{W}_c'$, $\tilde{W}_p'$ are the values obtained for these energies from the wave functions (2) using optimum values of the parameters α and c for each state. If we use values for W_I and W_p given by Moore (1949), we find after a simple calculation

$$W - \tilde{W}' = \text{diag}\,\{-0{\cdot}0558, 0, -0{\cdot}0015\}\ \text{(atomic units)}. \qquad \ldots\ldots(6)$$

It is clear from equations (4) and (6) that for HeH^+ the calculation using the intra-atomic correlation correction will yield a smaller value for D_e than the unmodified calculation of Coulson and Duncanson. This arises from the fact that the correlation correction for the lowest energy state of the dissociation products Ψ_I is considerably greater than that for either of the other states Ψ_c and Ψ_p. Consequently the application of the correction leads to an *increase* in the energy separations between Ψ_I and Ψ_c, Ψ_p. This results in a decrease in the interaction between the states and a reduction in the calculated binding energy. For most systems the result of applying the correction is the reverse change where the energy gap between the ground state (covalent) and excited states (ionic) is decreased by the large correlation corrections for the negative ions (Hurley 1956 a, b, c).

Detailed numerical calculations were carried out for the parameter values $\rho = 1{\cdot}432$, $c = 1{\cdot}9252$ and $\alpha = 0{\cdot}7567$. These are the optimum values obtained by Coulson and Duncanson using the first two terms in the wave function (1). The value of ρ is equal, fortuitously, to the value obtained by Evett (1956).

The results of the calculations are given in tables 1 and 2. In table 2 two values of the dissociation energy are given for each unmodified wave function. The bracketed value is obtained by subtraction from the experimental energy of $He\,(1s)^2$, $-2{\cdot}9035$ A.U., instead of from the theoretical energy, $-2{\cdot}8477$ A.U., given by wave function (1). These bracketed values are, of course, strict lower limits to the true value of D_e in virtue of the variational principle.

Table 1. Calculated Total Energies for HeH^+ (A.U.)

Wave functions	Orbital calculation	I.C.C.	Evett
Ψ_I, Ψ_c	−2·9285*	−2·9635	−2·9733
Ψ_I, Ψ_c, Ψ_p	−2·9325‡	−2·9684	

Table 2. Uncorrected Dissociation Energies D_e, for HeH^+ (ev).

Wave functions	Orbital calculation	I.C.C.	Evett
Ψ_I, Ψ_c	2·20*(>0·68)	>1·63	>1·90
Ψ_I, Ψ_c, Ψ_p	2·31‡(>0·79)	>1·77	

* Coulson and Duncanson (1938).

‡ These values are slightly inferior to the best values of Coulson and Duncanson who obtained a slightly lower total energy (−2·9332 A.U.) by re-varying the parameters α, c and ρ for the three-term wave function.

It is clear from table 2 that the unsatisfactory features of the orbital calculation are removed by applying the intra-atomic correlation correction. The resulting binding energies are now lower limits to the true value. If we compare them with the bracketed values for the orbital calculation, which are the only *certain* information given by such a calculation, we see that the intra-atomic correlation correction has led to an improvement of about 1 ev in the lower limit to the binding energy. The three-term intra-atomic correlation correction calculation yields a result which is only slightly inferior to that of Evett.

References

Coulson, C. A., and Duncanson, W. E., 1938, *Proc. Roy. Soc.* A, **165**, 90.

Evett, A. A., 1956, *J. Chem. Phys.*, **24**, 150.

Hurley, A. C., 1956 a, *Proc. Phys. Soc.* A, **69**, 49; 1956 b, *Ibid.*, **69**, 301; 1956 c, *Ibid.*, **69**, 767.

Moore, C. M., 1949, " Atomic Energy Levels ", *Nat. Bur. Stand., Wash., Circular* 467.

The Density Distribution of Extensive Showers

By J. R. PRESCOTT

Australian Atomic Energy Commission, Physics Department, University of Melbourne

MS. received 9th February 1956

§ 1. Introduction

In an accompanying paper, Norman (1956) discusses the relationship between the primary cosmic-ray spectrum and the density distribution of bursts due to extensive showers in ionization chambers and proportional counters.

In his discussion, Norman makes use of burst size distributions obtained in this laboratory in a previous experiment (Campbell and Prescott 1952, Prescott 1952) but not hitherto published. It now seems appropriate to publish this data,

The apparatus has been described previously (Prescott and Mohr 1949, Campbell and Prescott 1952). It consisted of complementary ionization chamber and Geiger counter systems. The two ionization chambers were cylindrical, 57·6 cm long and 8·8 cm in diameter, filled to 39 atmospheres with nitrogen. A burst of $2{\cdot}8 \times 10^5$ ion pairs corresponded to a shower density of 400 particles m^{-2} which is the minimum burst size used in this analysis. In making this correspondence between ion pairs and shower densities, an effective specific ionization of 53·5 ion pair cm^{-1} atm^{-1} was assumed; this figure includes corrections for secondary ionization, recombination and multiplication in the chamber walls and roof. Coincidences were recorded between the two chambers. Three Geiger counters in coincidence were located immediately above one chamber (chamber A): these acted as a 'master group'. Counters located at 3 and 5 m from the master group allowed bursts due to extensive showers to be identified. The efficiency of the whole counter system for identifying bursts due to extensive showers of greater than a given density at chamber A was: 400 particles m^{-2}, 88%; 500 particles m^{-2}, 96%; 600 particles m^{-2}, 99%. The observations were carried out at sea level.

§ 2. The Density Distributions

In the figure, curve A, is shown the integral density response curve for coincident bursts greater than a given size in both chambers at a separation of 5 m. The data represent 70 coincidences in 725·8 hours. The curve joins smoothly on to data of Norman (1956) (curve N) for lower densities, obtained with proportional counters of almost identical dimensions at the same separation and the same location. Norman has shown that his results at lower density are in good agreement in both absolute rate and exponent with the Geiger counter measurements of the density spectrum (Cocconi and Cocconi-Tongiorgi 1949, Broadbent *et al.* 1950, Singer 1951) which give an exponent of about $-1{\cdot}45$ in the density range 10–1000 particles m^{-2}. The spectrum of Broadbent *et al.* is shown in curve C as representative of these data. The observations at higher density presented here suggest that the exponent of the density distribution increases at large densities, particularly above 1000 particles m^{-2}.

Since the number of coincidences is relatively small, it is important to establish that the change in slope is, in fact, significant. This may be done on an objective basis by a statistical analysis using the 'method of maximum likelihood' (Annis *et al.* 1953). This shows that there is a probability 0·07 that the observations represent a line of slope $-1{\cdot}45$, which is the value obtained with Geiger counter measurements at lower densities. This probability is not by itself significant at the common accepted level of 0·05.

However, we now consider the data of curve B in the figure, which is the integral distribution of burst sizes in a *single* ionization chamber, the bursts being identified as due to extensive showers by the simultaneous discharge of the Geiger counter system. Curve B represents 115 bursts obtained in 627·9 hours; the data overlap those of curve A in time to the extent of 250 hours. At the low density end, curve B can be joined smoothly to a line of slope $-1{\cdot}45$, representing the Geiger counter data.

The probability that the observations of curve B as a whole represent a line of slope $-1{\cdot}45$ is 0·04. Taking curves A and B together, the probability that *both* sets of observations are consistent with lines of slope $-1{\cdot}45$ is only 0·003, which is

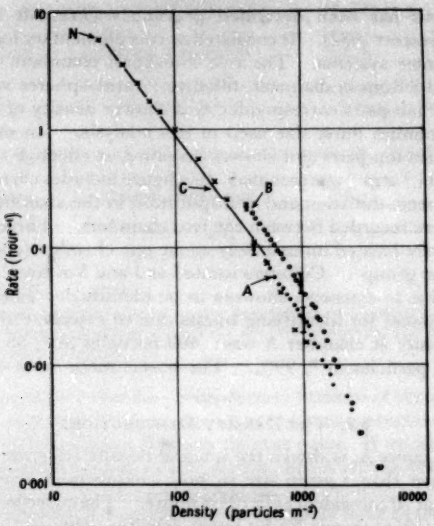

Integral density spectra for extensive showers.

Curve A (solid circles); coincidence rate for bursts greater than a given size in two ionization chambers at 5 m separation. Curve B (open circles); rate for bursts due to showers in a single ionization chamber. Curve N (crosses) proportional counter data of Norman. Curve C Geiger counter data of Broadbent *et al.* Representative probable errors are shown on curves A and B.

certainly insignificant. It is also possible to establish that the slope of curve B changes significantly with density. Thus, the slope of curve B in the region 500–1000 particles m^{-2} is $1{\cdot}54 \pm 0{\cdot}14$ and for densities greater than 1000 particles m^{-2} it is $2{\cdot}4 \pm 0{\cdot}4$. The probability that the slope does not change above 1000 particles m^{-2} is then 0·04.

We can therefore say that the slope of the density distribution increases with increasing density particularly above 1000 particles m^{-2}.

Observations in the high density region at sea level have been reported by Montgomery and Montgomery (1947), Lapp (1946) and recently by Carmichael and Steljes (1955). Of these observations, Montgomery and Montgomery did not employ any method for the specific selection of bursts due to extensive showers and relied on an empirical method involving an analysis of the effect of shielding to eliminate the contribution of disintegrations from their burst-size distribution; this may well be misleading (see, for example, Prescott 1952). Lapp employed counter selection to identify shower bursts but apart from indicating that about 85% of his bursts were due to showers, did not give a burst-size distribution for such bursts. However, the slope for his largest bursts (say, greater than 2500 particles m^{-2}), which he states are predominantly due to showers, is about $-2{\cdot}4$, which supports the conclusion of an increased exponent for large densities. Carmichael and Steljes employed ionization chambers in coincidence

to identify extensive showers and obtained an exponent $-1{\cdot}73 \pm 0{\cdot}01$ which, however, they find to be valid over the whole density range from 40 to about 7000 particles m^{-2}.

§ 3. Absolute Rates for Shower Densities

Finally it is perhaps worth while to comment on the absolute rates obtained in the present experiments. The rate obtained with a single chamber is higher by a factor of two than that obtained with Geiger counter techniques in a comparable density range. It is customary in the interpretation of Geiger counter experiments to neglect the effect of shower structure and to assume a constant density over the apparatus. Ise and Fretter (1949) and Broadbent *et al.* (1950) have shown that this assumption can lead to erroneous values for the density *exponent* although the errors involved are relatively small (rather less than 10%). The neglect of the density gradient does not in any case affect the value of the exponent obtained by the method of variation of counter area and it appears that the assumption of constant density is not unreasonable where the value of the exponent only is in question.

This is no longer true where the absolute counting rate is concerned. If the density were, in fact, strictly constant over the apparatus, then the coincidence rate for bursts greater than a given size in two (or more) ionization chambers should be the same as that for a single chamber. This is not so, as the figure shows : the single chamber rate is greater than the coincidence rate for two chambers at 5 m separation by a factor of two. Moreover, calculation shows (Blatt 1949, Campbell and Prescott 1952) that whereas the coincidence rate for a system of ionization chambers varies but slowly with separation distances greater than, say, 3 m, the coincidence rate rises rather sharply at small chamber separations. This rise is due to the density gradient in the showers. An unpublished calculation by I. D. Campbell similar to those described by Ise and Fretter (1949) and Singer (1951) for the counter system used in the present experiments shows a completely analogous effect, namely, a rather small variation in counting rate from 1 to 10 m but a sharp increase at small separations giving, in fact, a counting rate for effectively zero separation greater by a factor of two than at 5 m. Blatt (1949) reports a similar calculation but gives no details.

This throws some doubt on the practice of equating or extrapolating extensive shower rates obtained at separations of some metres to the equivalent rate for an infinitesimal detector and suggests that the reason for the discrepancies noted between the density spectra obtained by Geiger counters and single ionization chambers is due not to uncertainty, say, in the effective specific ionization of shower particles (Cocconi 1946, Carmichael 1948) but to the neglect of the variation in density over the apparatus.

If the density gradient effect *is* significant, we should expect to obtain harmonious agreement between counting rates obtained with chambers and counters in coincidence only at similar separations. The agreement shown in the figure between curve A and the proportional counter data of Norman (1956) on the one hand and the Geiger counter data on the other appears to confirm this.

One reservation is necessary : the observed density spectrum depends directly on the distribution-in-number of the total number of particles in a shower. If this distribution does not have a constant exponent, as suggested by Blatt (1949) and Norman (1956), then different density spectra may be observed with different sets of apparatus, and good agreement will be obtained only when such apparatus responds predominantly to showers in the same range of particle numbers.

ACKNOWLEDGMENTS

Mr. I. D. Campbell was associated with the author in obtaining the data reported here. Thanks are due to Mr. R. J. Norman for permission to make use of his results in advance of publication and to Professor L. H. Martin for making available the facilities of the laboratory.

REFERENCES

ANNIS, M., CHESTON, W., and PRIMAKOFF, H., 1953, *Rev. Mod. Phys.*, **25**, 818.
BLATT, J. M., 1949, *Phys. Rev.*, **75**, 1584.
BROADBENT, D., KELLERMANN, E. W., and HAKEEM, M. A., 1950, *Proc. Phys. Soc.* A, **63**, 864.
CAMPBELL, I. D., and PRESCOTT, J. R., 1952, *Proc. Phys. Soc.* A, **65**, 258.
CARMICHAEL, H., 1948, *Phys. Rev.*, **74**, 1667.
CARMICHAEL, H., and STELJES, J. F., 1955, *Phys. Rev.*, **99**, 1542.
COCCONI, G., 1946, *Phys. Rev.*, **70**, 975.
COCCONI, G., and COCCONI-TONGIORGI, V., 1949, *Phys. Rev.*, **75**, 1058.
ISE, J., and FRETTER, W. B., 1949, *Phys. Rev.*, **76**, 933.
LAPP, R. E., 1946, *Phys. Rev.*, **69**, 321.
MONTGOMERY, C. G., and MONTGOMERY, D. D., 1947, *Phys. Rev.*, **72**, 131.
NORMAN, R. J., 1956, *Proc. Phys. Soc.* A, **69**, 804.
PRESCOTT, J. R., 1952, *Proc. Phys. Soc.* A, **65**, 925.
PRESCOTT, J. R., and MOHR, C. B. O., 1949, *Aust. J. Sci. Res.* A, **2**, 184.
SINGER, S. F., 1951, *Phys. Rev.*, **81**, 579.

REVIEWS OF BOOKS

Electromagnetically Enriched Isotopes and Mass Spectrometry. Proceedings of the Conference held in the Cockcroft Hall, Atomic Energy Research Establishment, Harwell, 13–16 September 1955. Edited by M. L. SMITH, (London: Butterworth's Scientific Publications; New York: Academic Press, 1956.) 45*s*.

The large scale separation of isotopes by electromagnetic means was first undertaken for military purposes. Since 1945 several 'calutrons' have been devoted to the separation of the isotopes of most of the elements of the Periodic System, and these are now available in tens of milligrammes or more for general use. In addition to this high intensity work many University laboratories, particularly in Scandinavia, have installed small electromagnetic machines of high resolution for the preparation of targets for nuclear reaction studies and for the analysis of the products, both stable and radioactive, of nuclear transmutations. The present Conference report gives a valuable and up-to-date survey of progress and prospects in this field.

The papers presented group naturally into those devoted to techniques and those describing specific applications of separated isotopes or of mass spectrometers. There are detailed discussions of ion source and collector problems and M. L. Smith stresses the importance of suitable target preparation from enriched materials. Targets of gaseous elements are often made by bombarding metal foils with ions accelerated by a voltage of about 50 kev; a theoretical and experimental study of the range of slow atomic particles in matter is presented by K. O. Nielsen.

The application of stable isotopes in nuclear physics is well surveyed in general by W. D. Allen, and in some detail in other papers on particular (pγ) reactions. H. G. Kuhn reports briefly on the application of electromagnetically enriched isotopes in spectroscopy and solid state physics; more might perhaps have been said about the low temperature experiments. The analysis of isotopic abundance by mass spectrometry, and in particular the method of isotopic dilution, is discussed in several papers; it is clear that the sensitivity of the method approaches that of radioactive measurements. An interesting result on the half life of rhenium obtained by this method is reported by H. Hintenberger.

The final sessions of the conference were devoted to the general design of electromagnetic separators for all purposes and to the separation of active materials. An ingenious high frequency mass spectrometer using fields which resemble those now applied in 'strong focusing' accelerators is described by O. Osberghaus, but there is no report on the more familiar time-of-flight separators. Electromagnetic analysis of the products of fission and spallation reactions is briefly discussed by G. Andersson, who also reports on the use of the method in preparing thin sources for beta-spectroscopy.

Although a conference report can hardly be expected to give a complete or balanced account of a wide field the present report gives an excellent appraisal of many of the more interesting developments of the electromagnetic method. Full reports of the discussions are included and there is an adequate index.

W. E. BURCHAM.

CONTENTS OF SECTION B

PAGE

Dr. J. S. Greenhow and Mr. E. L. Neufeld. Phase Changes and Resonance Effects in Radio Echoes from Meteor Trails 1069

Dr. R. G. Giovanelli and Mr. J. T. Jefferies. Radiative Transfer with Distributed Sources 1077

Dr. R. A. Hyman. Optical Absorption in Liquid Sulphur–Selenium Co-polymers 1085

Dr. Sampooran Singh. Spatial Distribution of Fragments of Explosively Loaded Thin-Walled Steel Cylinders. 1089

Dr. P. G. Harper. Effect of the Electron–Lattice Interaction on Phonon Frequencies 1095

Dr. J. R. Drabble and Dr. R. Wolfe. Anisotropic Galvanomagnetic Effects in Semiconductors 1101

Prof. L. F. Bates and Mr. P. F. Davis. 'Lozenge' and 'Tadpole' Domain Structures on Silicon–Iron Crystals 1109

Mr. D. C. Champeney. The Flow of Liquid Helium I through Narrow Channels 1112

Dr. S. M. Bhagat. The Specific Heat and Entropy of Liquid Helium Three . 1117

Dr. G. G. Hall. The Form of the Effective Electronic Potential in a Crystal . 1124

Dr. A. D. Buckingham and Dr. J. A. Pople. A Theory of Magnetic Double Refraction 1133

Dr. W. E. Spear. Volume Generated Currents and Secondary Effects in Amorphous Selenium Films 1139

Mr. J. F. Strachan and Mr. N. L. Harris. Bombardment of Various Elements by Hg^+ and A^+ Ions 1148

Research Notes:

Dr. L. E. Lyons and Mr. G. C. Morris. Photo- and Semi-Conduction of Aromatic Hydrocarbon Crystals 1162

Letters to the Editor:

Prof. R. W. Ditchburn, Dr. D. H. Fender, Dr. S. Mayne, Mr. R. M. Pritchard. A Stabilized Retinal Image of the Iris 1165

Dr. B. Bleaney, Prof. C. A. Hutchison, Dr. P. M. Llewellyn and Mr. D. F. D. Pope. Paramagnetic Resonance Absorption in $^{235}UCl_3$, and the Nuclear Electric Quadrupole Moment of ^{235}U . . . 1167

Dr. W. Low. The Paramagnetic Resonance Spectrum of Fe^{3+} in the Cubic Field of MgO 1169

Reviews of Books 1171

Corrigendum: Mr. E. L. Heasell and Dr. J. Lamb 1171

Contents of Section A 1172

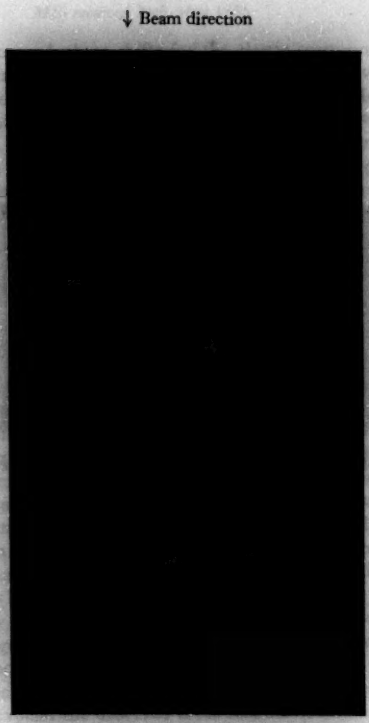

Figure 2. A picture of a π^+–p scattering event. Incident energy = 23 MeV, pion scattering angle (lab) = 152°, proton recoil angle (lab) = 12°, pion scattering angle (c.m.s.) = 157°. The picture also shows two π–μ decay events.

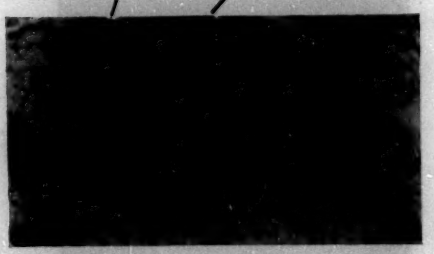

Figure 1. A photograph of a typical event produced by the successive disintegrations of RaD and RaE.

The Elastic Scattering of Neutrons by Tritons and ^{3}He

By B. H. BRANSDEN,† H. H. ROBERTSON‡¶ and P. SWAN§

† Department of Natural Philosophy, The University, Glasgow

‡ The National Physical Laboratory, Teddington, Middlesex

§ Department of Physics, The University, Melbourne

MS. received 24th May 1956

Abstract. Cross sections and phase shifts for the elastic scattering of neutrons by tritons and ^{3}He are calculated over the energy range 1 to 14 MeV using central forces. Resonating group wave functions are employed to derive integro-differential equations for which accurate solutions are obtained with the aid of an electronic computer. The two-body interaction has exchange properties of either the Serber or the symmetrical type and a gaussian radial dependence with constants consistent with the binding energies of the alpha particle and the deuteron.

The calculated angular distributions are found to depend sensitively on the exchange nature of the interaction, although the available experimental data are insufficient to distinguish between the interactions considered.

§ 1. Introduction

The properties of a two-nucleon system, at low energies, can be described in terms of short range phenomenological interactions, having various exchange properties. It is of great importance to find whether such interactions are sufficient to determine the properties of many nucleon systems or whether it is necessary to invoke more complicated many-body interactions. The study of the scattering of nucleons by the lightest nuclei may be expected to provide such information and in addition evidence as to the exchange nature of the two-body interaction, which is not determined from the study of the bound systems. The collision of neutrons with deuterons has been investigated extensively, and the information obtained has been summarized and discussed by de Borde and Massey (1955). It has been found that while the comparison of observation with theory suffices to distinguish between potentials of the ordinary and those of the exchange type, at present it is difficult to decide between the merits of different exchange potentials. The scattering of neutrons by alpha particles has also received attention, and again it is found that exchange rather than ordinary forces are required to explain the observed cross sections (Hochberg *et al.* 1954, 1955, Bransden and McKee 1954). It is, therefore, of great interest to extend calculations to the scattering of nucleons with the nuclei of mass three to provide another source of information which may help to distinguish between different exchange forces.

In the present paper the elastic scattering of neutrons by tritons and ^{3}He is calculated for incident neutron energies of up to 14 MeV, using interactions of both the Serber and symmetrical type. The potential is assumed to be purely central and of a form consistent with the binding energies of the deuteron and alpha particle. Such an interaction does not provide the best equivalent central

¶ Now at CERN, European Organisation for Nuclear Research, Geneva.

potential for the two-body problem, but, as pointed out by de Borde and Massey (1955), it is reasonable to suppose that the best equivalent central potential for a n-body scattering problem is that which gives the n-body binding energy correctly. As in an earlier calculation of the scattering of neutrons by tritons and of protons by ^{3}He (Swan 1953 a, b), the integro-differential equations describing the collision are obtained with the help of a resonating group wave function (Wheeler 1937). The present work differs from that of Swan (1953 a, b), in that these equations are written in a form that is more consistent with the approximate triton and ^{3}He wave functions employed, and also in that exact solutions have been obtained, with the aid of the pilot ACE electronic computer of the National Physical Laboratory, whereas the earlier calculations were based on approximate variational solutions.

§ 2. General Theory

2.1. *The Neutron–^{3}He Collision*

The wave function $\Psi(1234)$ of the four-nucleon system is a solution of the Schrödinger equation, in the centre-of-mass system,

$$\left(T+\sum_{\text{all pairs}}\mathscr{V}(ij)-E_{\mathrm{H}}-E_{\mathrm{n}}\right)\Psi(1234)=0, \qquad \ldots\ldots(1)$$

where E_{H} is the ^{3}He binding energy, E_{n} is the incident neutron energy in the centre-of-mass system ($E_{\mathrm{n}}=\frac{3}{4}E_{\mathrm{lab}}$), and T is the kinetic energy operator.

$$T=-(\hbar^2/2m)(2\nabla_{23}{}^2+\tfrac{3}{2}\nabla_{23-1}{}^2+\tfrac{4}{3}\nabla_{123-4}{}^2), \qquad \ldots\ldots(2)$$

where m is the neutron or proton mass. The interaction $\mathscr{V}(ij)$ may be written

$$\mathscr{V}(ij)=(w+mM+hH+bMH)V(ij)+\epsilon_{ij}V_{\mathrm{c}}(ij), \qquad \ldots\ldots(3)$$

where V_{c} is the coulomb interaction and $\epsilon_{ij}=1$ if i, j are both protons and zero otherwise. M and H are the Majorana and Heisenberg exchange operators and w, m, h, b, are constants so that

$$\left.\begin{aligned} w+m+h+b&=1\\ w+m-h-b&=x\end{aligned}\right\} \qquad \ldots\ldots(4)$$

where x is the ratio of the singlet and triplet interaction between neutron and proton in an even state.

The wave function Ψ assumes a different form for the two systems considered. For the neutron–^{3}He collision a resonating group wave function of correct symmetry may be written (i.e. 1, 2 refer to protons, 3, 4 to neutrons)

$$\Psi(1234)=\tfrac{1}{2}(1-P_{34})\psi_{\mathrm{H}}(123)F(4)\chi(1234) \qquad \ldots\ldots(5)$$

where ψ_{H} is the ground state wave function of ^{3}He, χ is an appropriate spin wave function, $F(4)$ is the spatial wave function of neutron 4 relative to the centre of mass of the ^{3}He nucleus and P_{34} is the operator which interchanges all coordinates of 3 and 4.

The total spin of the system is either $S=1$ for the triplet or $S=0$ for the singlet state in which case, if ψ_{H} is assumed to be totally symmetric in the coordinates of 1, 2 and 3, χ is given by

$$S=1,\ {}^3\chi_1(1234)=\frac{1}{\sqrt{2}}\{\alpha(1)\beta(2)-\beta(1)\alpha(2)\}\alpha(3)\alpha(4)$$

$${}^3\chi_0(1234)=\tfrac{1}{2}\{\alpha(1)\beta(2)-\beta(1)\alpha(2)\}\{\alpha(3)\beta(4)+\beta(3)\alpha(4)\}$$

$${}^3\chi_{-1}(1234)=\frac{1}{\sqrt{2}}\{\alpha(1)\beta(2)-\beta(1)\alpha(2)\}\beta(3)\beta(4)$$

$$S=0,\ {}^1\chi_0(1234)=\tfrac{1}{2}\{\alpha(1)\beta(2)-\beta(1)\alpha(2)\}\{\alpha(3)\beta(4)-\beta(3)\alpha(4)\}. \quad \ldots\ldots(6)$$

Both an exact and a variationally determined ^{3}He wave function satisfy

$$\int \psi_{\mathrm{H}}(123)\left[-\frac{\hbar^2}{M}\nabla_{23}{}^2-\frac{3\hbar^2}{4M}\nabla_{23-1}{}^2+V_{\mathrm{c}}(12)+V(12)+V(23)+V(13)-E_{\mathrm{H}}\right]\psi_{\mathrm{H}}(123)d\tau_{123}=0. \quad \ldots\ldots(7)$$

Substituting the wave function (5) into (1), multiplying by $\psi_{\mathrm{H}}(123)^{3,1}\chi(1234)$, integrating over the coordinates of 1, 2, 3, summing over spins and using relation (7), an integro-differential equation is obtained for $F(4)$, in the form

$$(\nabla^2+k^2)F(\mathbf{r})=V(r)F(\mathbf{r})+\int K(\mathbf{r},\mathbf{r}')F(\mathbf{r}')d\mathbf{r}', \quad \ldots\ldots(8)$$

where coordinates $\mathbf{r}=\mathbf{r}_4-\frac{1}{3}(\mathbf{r}_1+\mathbf{r}_2+\mathbf{r}_3)$, $\mathbf{r}'=P_{34}\mathbf{r}$, $\mathbf{R}=\mathbf{r}_1-\mathbf{r}_2$ have been introduced, $k^2=3mE_{\mathrm{n}}/2\hbar^2$ and $V(r)=\alpha U(r)$.

$$K(\mathbf{r},\mathbf{r}')=\beta\{Q(\mathbf{r},\mathbf{r}')+S(\mathbf{r},\mathbf{r}')\}+\gamma T(\mathbf{r},\mathbf{r}')+\delta R(\mathbf{r},\mathbf{r}')+\epsilon L(\mathbf{r},\mathbf{r}')+\eta\left\{\left(\frac{E_{\mathrm{n}}}{E_{\mathrm{H}}}+1\right)N(\mathbf{r},\mathbf{r}')+P(\mathbf{r},\mathbf{r}')\right\}. \quad \ldots\ldots(9)$$

α, β, γ, δ, ϵ, η are constants which depend on the total spin and on the values of w, m, b and h, as shown in table 1 (*a*).

Table 1. Constants for (*a*) Neutron–^{3}He and (*b*) Neutron–Triton Scattering

Total	(*a*)		(*b*)	
spin	1	0	1	0
α	$\frac{3}{2}(3w+2b-m-h)$	$\frac{3}{2}(3w+m-h)$	$-\frac{3}{2}(3w+2b-m-2h)$	$\frac{3}{2}(3w-m-2h)$
β	$-\frac{3}{4}(2w+2m+b+h)$	$+\frac{3}{4}(2m+2w+b+h)$	$-3(w+m)$	$3(b+h-w-m)$
γ	$\frac{3}{4}(3m+2h-w-b)$	$\frac{3}{4}(3m+w-b)$	$\frac{3}{4}(3m+2h-w-2b)$	$\frac{3}{4}(3m-w-2b)$
δ	$-\frac{3}{4}(w+m-b-h)$	$+\frac{3}{4}(w+m-b-h)$	$-\frac{3}{4}(w+m)$	$-\frac{3}{4}(w+m+2b+2h)$
ϵ	$-\frac{3}{2}$	$+\frac{3}{2}$	0	0
η	$+1$	-1	$+1$	$+1$

The potential function U and the kernels Q, S, etc. are

$$U(r)=\left(\frac{9}{8}\right)^3\frac{M}{\hbar^2}\int\int d\mathbf{R}\,d\mathbf{r}'\{\psi_{\mathrm{H}}(123)\}^2V(14). \quad \ldots\ldots(10)$$

$$\begin{Bmatrix}Q(\mathbf{r},\mathbf{r}')\\S(\mathbf{r},\mathbf{r}')\\T(\mathbf{r},\mathbf{r}')\\R(\mathbf{r},\mathbf{r}')\\L(\mathbf{r},\mathbf{r}')\\N(\mathbf{r},\mathbf{r}')\end{Bmatrix}=\left(\frac{9}{8}\right)^3\frac{M}{\hbar^2}\int d\mathbf{R}\,.\,\psi_{\mathrm{H}}(123)\psi_{\mathrm{H}}(124)\begin{Bmatrix}V(14)\\V(13)\\V(34)\\V(12)\\V_{\mathrm{c}}(12)\\\frac{3}{2}E_{\mathrm{H}}\end{Bmatrix} \quad \ldots\ldots(11)$$

$$P(\mathbf{r},\mathbf{r}')=\frac{3}{8}\left(\frac{9}{8}\right)^3\int d\mathbf{R}\psi_{\mathrm{H}}(123)\psi_{\mathrm{H}}(124)\left[\frac{27\nabla_{3-12}\psi_{\mathrm{H}}(123)\nabla_{4-12}\psi_{\mathrm{H}}(124)}{32\psi_{\mathrm{H}}(123)\psi_{\mathrm{H}}(124)}+\left(\frac{9}{8}\right)^2\left\{\frac{\nabla_{3-12}{}^2\psi_{\mathrm{H}}(123)}{\psi_{\mathrm{H}}(123)}+\frac{\nabla_{4-12}{}^2\psi_{\mathrm{H}}(124)}{\psi_{\mathrm{H}}(124)}\right\}+\frac{3}{2}\frac{\nabla_{\mathrm{R}}{}^2\psi_{\mathrm{H}}(124)}{\psi_{\mathrm{H}}(124)}\right].$$

Expanding $F(\mathbf{r})$ and $Q(\mathbf{r},\mathbf{r}')$ so that

$$F(\mathbf{r})=\sum_n r^{-1}f_n(r)\mathrm{P}_n(\cos\theta), \quad \ldots\ldots(12)$$

$$Q(\mathbf{r},\mathbf{r}')=\sum_n\frac{(2n+1)}{4\pi rr'}\mathrm{P}_n(\cos\Theta)q_n(r,r');\quad rr'\cos\Theta=\mathbf{r}.\mathbf{r}'$$

with similar expansions of S, T, R, L, N and P in terms of s_n, t_n, r_n, l_n, n_n and p_n, the equation (8) may be reduced to radial form:

$$\left(\frac{d^2}{dr^2}+k^2-\frac{n(n+1)}{r^2}\right)f_n(r)=V(r)f_n(r)+\int_0^\infty k_n(r,r')f_n(r')dr',$$

where

$$k_n=\beta(q_n+s_n)+\gamma t_n+\delta r_n+\epsilon l_n+\eta\left\{\left(\frac{E_n}{E_H}+1\right)n_n+p_n\right\}. \quad \ldots\ldots(13)$$

The scattering phases ${}^{3,1}\delta_n$ are defined for the triplet and singlet states by the boundary conditions

$${}^{3,1}f_n(0)=0; \qquad {}^{3,1}f_n(r)\sim\sin(kr-\tfrac{1}{2}n\pi+{}^{3,1}\delta_n) \quad \ldots\ldots(14)$$

and the differential cross section $I(\theta)$ is expressed as

$$I(\theta)=\tfrac{3}{4}|{}^3g(\theta)|^2+\tfrac{1}{4}|{}^1g(\theta)|^2, \quad \ldots\ldots(15)$$

where

$${}^{3,1}g(\theta)=\frac{1}{2ik}\sum_n(2n+1)\{\exp(2i{}^{3,1}\delta_n)-1\}P_n(\cos\theta).$$

The total cross section for elastic scattering Q is obtained by integrating (15) over all solid angles:

$$Q=2\pi\int_0^\pi I(\theta)\sin\theta\,d\theta. \quad \ldots\ldots(16)$$

2.2. *The Neutron–Triton Collision*

The wave function $\Psi(1234)$ may be expressed in a form analogous to (5):

$$\Psi(1234)=\frac{1}{\sqrt{3}}(1-P_{34}-P_{24})\psi_T(123)F(4)\chi(1234) \quad \ldots\ldots(17)$$

where $\psi_T(123)$ is the triton ground state wave function and where the spin functions $\chi(1234)$ are defined by (6). An integro-differential equation of the form (8) can be obtained where the constants α, β, γ, δ, ϵ, η are now given by table 1 (*b*) and where the kernels are defined by (10) and (11) with the replacement of ψ_H and E_H by ψ_T and E_T everywhere. The scattering phases and cross sections are again given by the solution of (13) with boundary conditions (14).

In the previous formulation of the problem by Swan (1953 a, b) use was made of the relation

$$\int\psi_T(124)\left\{-\frac{\hbar^2}{M}\nabla_{23}{}^2-\frac{3\hbar^2}{4M}\nabla_{23-1}{}^2+V(12)+V(23)+V(13)-E_T\right\}\psi_T(123)d\tau_{123}=0, \quad \ldots\ldots(18)$$

which is satisfied by the exact triton ground state wave function $\psi_T(123)$, to reduce the kernel $K(\mathbf{r},\mathbf{r}')$ to the form $K'(\mathbf{r},\mathbf{r}')$, where

$$K'(\mathbf{r},\mathbf{r}')=\beta'\{Q+S\}+\gamma' T+\delta' R+\eta'\left\{\left(\frac{E_n}{E_T}-\frac{5}{4}\right)N+P'\right\} \quad \ldots\ldots(19)$$

where the definitions of Q, S, T, R, N are unchanged but

$$P'=\frac{3}{8}\left(\frac{9}{8}\right)^3\int d\mathbf{R}\psi_T(123)\psi_T(124)\left[\frac{9}{4}\frac{\nabla_{3-12}\psi_T(123).\nabla_{4-12}\psi_T(124)}{\psi_T(123)\psi_T(124)}-\frac{5\nabla_R{}^2\psi_T(123)}{\psi_T(123)}\right].$$

In general $K(\mathbf{r},\mathbf{r}')$ can be written in a number of different forms by application of relation (18) to the function ψ_T occurring in the kernel definitions. However, as was noted by Hochberg, Massey and Underhill (1954) in connection with the corresponding problem in neutron alpha particle scattering, the relation (18)

is only satisfied by exact triton wave functions, but not by the approximate wave functions used, and therefore it is inconsistent to employ the reduced form of kernel $K'(\mathbf{r}, \mathbf{r}')$. The equation (18) satisfied by $F(r)$ may be obtained by requiring

$$\delta \int \Psi^*(H-E)\Psi \, d\tau = 0$$

when $F \to F + \delta F$, so that F as determined from (18) represents the best wave function Ψ of the form (5), whether ψ_T is an exact triton wave function or not. On these grounds it is clearly preferable to use $K(\mathbf{r}, \mathbf{r}')$ in its original form.

§ 3. Interactions and Wave Functions

Two special cases of the interaction (3) are investigated, namely the symmetrical exchange force $m = 2b = \frac{1}{3}(1+3x)$, $h = 2w = \frac{1}{3}(1-3x)$, and the Serber exchange force $m = w = \frac{1}{4}(1+x)$, $h = b = \frac{1}{4}(1-x)$.

The potential well $V(r)$ is chosen to be of gaussian form in order that the kernels k_n may be evaluated analytically:

$$V(r) = V_0 \exp(-\mu r^2) \qquad \ldots\ldots(20)$$

and for the same reason gaussian wave functions for the ^{3}He nucleons and the triton are employed:

$$\psi_H = N_H \exp\left(-\frac{\nu}{2}\sum_{ij} r_{ij}^2\right), \qquad \psi_T = N_T \exp\left(-\frac{\lambda}{2}\sum_{ij} r_{ij}^2\right). \qquad \ldots\ldots(21)$$

The parameters $V_0 = -45$ Mev, $\mu = 0{\cdot}2669 \times 10^{26}\,\mathrm{cm}^{-2}$, $x = 0{\cdot}6$ represent a potential of longer range than that now suggested by the two-body scattering data, but, as explained above, this potential is consistent with the four-body bound state ($E_\alpha = -27$ Mev compared with the experimental value of -28 Mev) and also with the binding energy of the deuteron. The wave function constants ν, λ are found by minimizing the energies E_H, E_T given by relation (7), which is, therefore, automatically satisfied. The constants are found to be $\lambda = 0{\cdot}1436 \times 10^{26}\,\mathrm{cm}^{-2}$, $\nu = 0{\cdot}1404 \times 10^{26}\,\mathrm{cm}^{-2}$, giving

$$E_T = -5{\cdot}49\ \text{Mev}, \qquad E_H = -4{\cdot}74\ \text{Mev}. \qquad \ldots\ldots(22)$$

The values of E_T, E_H are somewhat lower than those observed, $-8{\cdot}3$ and $-7{\cdot}55$ Mev, but scattering cross sections are generally insensitive to binding energy values, provided the theoretical values (22) are used when evaluating $k_n(r, r')$.

With these forms for the potentials and wave functions the potential function U and the kernels q_n, s_n etc. assume the form

$$U(r) = A_U \exp(-\gamma_U r^2), \qquad \ldots\ldots(23)$$

$$q_n(r, r') = A_q \exp(-\gamma_q r^2 - \Gamma_q r'^2)\mathscr{I}_{n+1/2}(\kappa_q rr')$$

with similar expressions for s_n, t_n, l_n, r_n and n_n in terms of A_s, A_t etc. and

$$P_n(r, r') = A_p \exp\{-\gamma_p(r^2+r'^2)\}\left[\left\{18(r^2+r'^2) - \frac{608}{27\nu}\right\}\mathscr{I}_{n+1/2}(\kappa_p rr') - 28rr'\mathscr{I}'_{n+1/2}(\kappa_p rr')\right]. \qquad \ldots\ldots(24)$$

$\mathscr{I}_{n+1/2}(x)$ is defined as $\mathscr{I}_{n+1/2}(x)=(-1)^n\sqrt{(\frac{1}{2}\pi x)}I_{n+1/2}(x)$ and

$$A_u=27\left(\frac{mV_0}{\hbar^2}\right)\frac{\nu^{3/2}}{(9\nu+2\mu)^{3/2}}, \qquad \gamma_U=\frac{9\mu\nu}{9\nu+2\mu},$$

$$A_q=\left(\frac{mV_0}{\hbar^2}\right)\sqrt{\left(\frac{3}{\pi}\right)\left(\frac{81}{2}\right)}\frac{\nu^2}{(6\nu+\mu)^{1/2}(3\nu+2\mu)}, \qquad \gamma_q=\frac{9}{16}\frac{\nu(15\nu+16\mu)}{(6\nu+\mu)},$$

$$\Gamma_q=\frac{9}{16}\frac{\nu(15\nu+4\mu)}{(6\nu+\mu)}, \qquad \kappa_q=\frac{27}{8}\frac{\nu(3\nu+2\mu)}{(6\nu+\mu)},$$

$$A_s=A_q, \quad \gamma_s=\Gamma_q, \qquad \Gamma_s=\gamma_q, \quad \kappa_s=\kappa_q,$$

$$A_t=\left(\frac{mV_0}{\hbar^2}\right)\frac{81}{\sqrt{(2\pi)}}\frac{\nu^{3/2}}{(6\nu-4\mu)}, \qquad \gamma_t=\Gamma_t=\frac{9}{64}(10\nu+4\mu),$$

$$\kappa_t=\frac{9}{32}(6\nu-4\mu),$$

$$A_l=\left(\frac{me^2}{\hbar^2}\right)\left(\frac{\nu}{\pi}\right)\left(\frac{27}{2}\right)\sqrt{3}, \qquad \gamma_l=\Gamma_l=\frac{45}{32}\nu, \quad \kappa_l=\frac{27\nu}{16},$$

$$A_r=81\sqrt{\left(\frac{3}{\pi}\right)\left(\frac{mV_0}{\hbar^2}\right)}\frac{\nu^2}{(6\nu+4\mu)^{3/2}}, \qquad \gamma_r=\Gamma_r=\gamma_l, \quad \kappa_r=\kappa_l,$$

$$A_n=\left(\frac{3m}{2\hbar^2}\right)\left(\frac{27}{2}\right)\sqrt{\left(\frac{\nu}{2\pi}\right)}, \qquad \gamma_n=\Gamma_n=\gamma_l, \quad \kappa_n=\kappa_l,$$

$$A_p=\left(\frac{9}{8}\right)^4\sqrt{\left(\frac{8\nu^5}{\pi}\right)}, \qquad \gamma_p=\Gamma_p=\gamma_l, \quad \kappa_p=\kappa_l.$$

§ 4. Numerical Calculations and Results

Accurate solutions of equations (13) with boundary conditions (14) have been obtained with the pilot ACE electronic computer of the National Physical Laboratory using a programme constructed by one of us (H. H. R.) and described elsewhere (Robertson 1956). The phases ${}^{3,1}\delta_n$ have been found for all significant n (up to $n=4$) for both the Serber and symmetrical potentials for incident neutron energies in the laboratory system of $E_{\text{lab}}=1{\cdot}0$, $2{\cdot}5$, $5{\cdot}0$, $8{\cdot}0$ and $14{\cdot}0$ MeV. The computed phases are displayed in table 2, where the normalization is such that $\delta\pm\pi$ is recorded if $|\delta|$ exceeds $\pi/2$. Swan (1955) has shown that the absolute normalization of the zero order phases for both neutron–triton and neutron–^{3}He scattering is such that ${}^{3,1}\delta_0\to\pi$ at zero incident energy.

Table 2. Calculated Phases

Phases are given in degrees and decimals, and normalized so that $\delta\pm\pi$ is recorded if $|\delta|$ exceeds $\pi/2$. The energy E is in MeV (lab).

1. Neutron–^{3}He Collisions

(*a*) *Serber interaction—total spin* 1.

E	$n=$ 0	1	2	3	4
1·0	−28·967	+9·707	−0·026		
2·5	−44·998	+38·096	−0·199		
5·0	−61·807	+63·577	−0·734		
8·0	−75·558	+67·735	−1·386	+0·416	
14·0	+86·271	+62·945	−1·515	+1·620	−0·016

Table 2 *continued*

(*b*) *Serber interaction—total spin* 0.

E	$n=$ 0	1	2	3	4
1·0	−10·277	−0·740	+0·076		
2·5	−18·506	−1·822	+0·664		
5·0	−29·748	−1·267	+3·091		
8·0	−41·001	+4·420	+7·920		
14·0	−58·739	+26·338	+19·427	+0·252	+0·213

(*c*) *Symmetrical interaction—total spin* 1.

1·0	−30·707	+3·777	−0·042		
2·5	−47·899	+13·080	−0·336		
5·0	−66·254	+25·505	−1·374		
8·0	−81·676	+31·285	−3·076		
14·0	+77·054	+30·739	−6·413	+0·804	−0·097

(*d*) *Symmetrical interaction—total spin* 0.

1·0	−16·285	−1·583	+0·059		
2·5	−26·755	−4·921	+0·500		
5·0	−39·540	−9·846	+2·220		
8·0	−51·681	−13·676	+5·374		
14·0	−70·471	−14·901	+12·113	−0·311	+0·154

2. Neutron–Triton Collisions

(*a*) *Serber interaction—total spin* 1.

1·0	−29·360	+7·945	−0·028		
2·5	−45·664	+30·282	−0·217		
5·0	−62·845	+53·747	−0·821		
8·0	−76·982	+59·231	−1·619	+0·400	
14·0	+84·226	+55·604	−2·141	+1·546	−0·025

(*b*) *Serber interaction—total spin* 0.

1·0	−30·567	+6·162	−0·035		
2·5	−47·607	+22·097	−0·274		
5·0	−65·656	+40·232	−1·060		
8·0	−80·602	+45·523	−2·175	+0·397	
14·0	+79·402	+42·268	−3·403	+1·474	−0·052

(*c*) *Symmetrical interaction—total spin* 1.

1·0	−30·454	+4·453	−0·038	+0·001	
2·5	−47·491	+15·688	−0·306	+0·010	
5·0	−65·651	+30·292	−1·240		
8·0	−80·856	+36·396	−2·732	+0·293	
14·0	+78·332	+35·186	−5·412	+1·021	−0·078

(*d*) *Symmetrical interaction—total spin* 0.

1·0	−32·263	+2·423	−0·054		
2·5	−50·432	+7·688	−0·440		
5·0	−69·992	+13·710	−1·826		
8·0	−86·596	+15·349	−4·168		
14·0	+70·198	+11·094	−9·097	+0·461	−0·160

Examination of table 2 shows that the neutron–triton phases are nearly independent of the total spin of the system. The zero order phases are also insensitive to the exchange nature of the interaction, but the Serber force is effective in producing phases which are considerably in excess of those given by the symmetrical interaction. The corresponding calculated angular distributions (figures 1 to 5) show in general that the Serber potential gives rise to greater

maxima at 0° and 180° than does the symmetrical potential and also the Serber total cross sections (table 3) are considerably larger than those derived from the symmetrical potential.

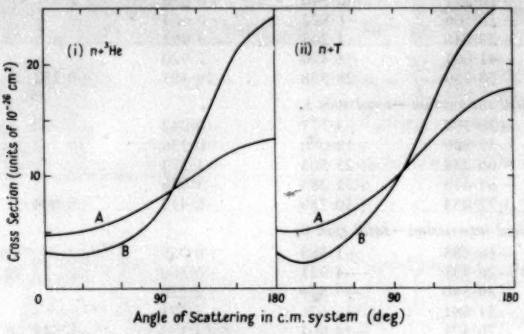

Figure 1.

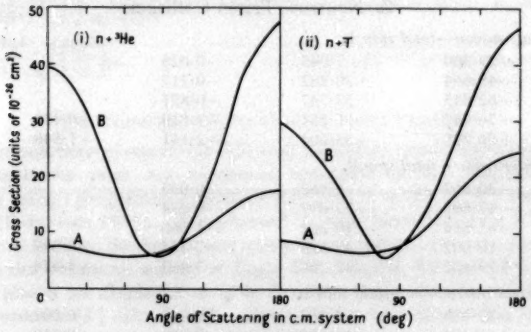

Figure 2.

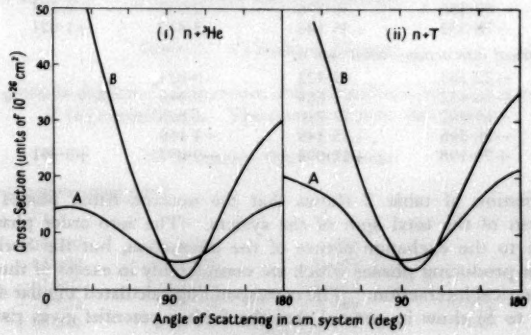

Figure 3.

(For captions see below figure 5.)

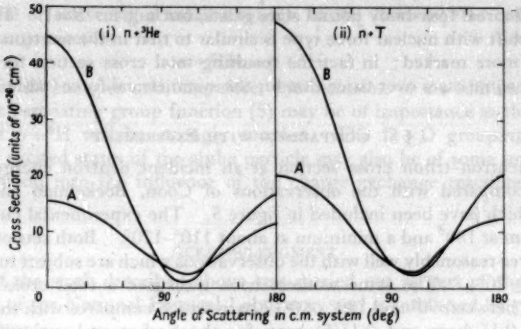

Figure 4.

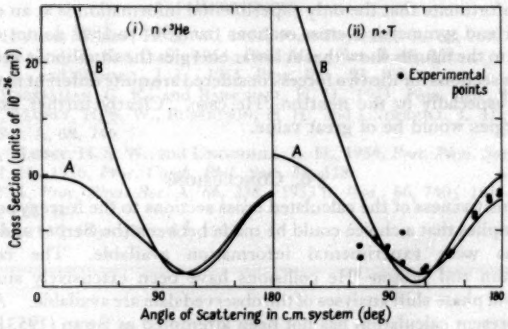

Figure 5.

Figures 1 to 5: Angular distributions for the elastic scattering of neutrons by ^3He and tritons at incident neutron energies of 1·0, 2·5, 5·0, 8·0, 14·0 MeV respectively.

A, Symmetrical interaction. B, Serber interaction.

Table 3. Calculated Total Cross Sections

1. *Neutron–^3He Collisions*

Force type	E (MeV)	1·0	2·5	5·0	8·0	14·0
Serber		1·15	2·33	2·27	1·60	0·993
Symmetrical		1·04	1·08	1·08	0·901	0·554

2. *Neutron–Triton Collisions*

Force type	E (MeV)	1·0	2·5	5·0	8·0	14·0
Serber		1·37	2·22	2·38	1·74	0·947
Symmetrical		1·29	1·36	1·35	1·06	0·589

Cross sections are in units of 10^{-24} cm².

In contrast to the neutron–triton system, the neutron–^3He phases depend markedly on the total spin of the system. This is not unexpected, as for total

spin $S=0$ a real four-body bound state exists, but not for $S=1$. The variation of phase shift with nuclear force type is similar to that in the neutron–triton case, but even more marked; in fact the resulting total cross section for the Serber force is in some cases over twice that for the symmetrical force (table 3).

§ 5. Comparison with Experiment

The neutron–triton cross section at an incident neutron energy of 14 Mev may be compared with the observations of Coon, Bockelman and Barschall (1951), which have been included in figure 5. The experimental curve exhibits a maximum at 180° and a minimum at about 110°–120°. Both sets of theoretical curves agree reasonably well with the observations which are subject to an absolute error of $\pm 20\%$. The same workers have measured a total cross section for scattering between 90° and 180° of 0·17 barn which compares with the calculated values of 0·15 barn and 0·15(5) barn for the Serber and symmetrical forces respectively.

It is unfortunate that the only experimental information is at an energy where the Serber and symmetrical cross sections from 90° to 180° do not differ widely. Reference to the figures show that at lower energies the situation is very favourable as the cross sections for the two forces considered are quite different in the backward direction, especially in the neutron–^{3}He case. Clearly further experiments at lower energies would be of great value.

§ 6. Conclusions

The sensitiveness of the calculated cross sections to the force type at the lower energies implies that a choice could be made between the Serber and symmetrical interactions were experimental information available. The corresponding proton–triton and proton–^{3}He collisions have been extensively studied experimentally and phase shift analyses of the observed data are available. A comparison with the present calculation has not been attempted as Swan (1953 b) has shown that the coulomb interaction introduces important modifications of the phase shifts at these energies, but an extension of the calculations to these systems is at an advanced stage, and will be published shortly.

Comparison of the present results with those of Swan (1953 a, b) for the neutron–triton collision reveals important differences. While the phases δ_0 are comparable, the present δ_1 phases are larger than and of opposite sign to those of the previous calculation. As discussed above, this difference is probably due to the different form of kernel K employed. As in addition Swan solved his equations by a variational method, it would be useful to estimate the accuracy of such methods applied to nuclear scattering problems, and it is intended to investigate this point in the proton–^{3}He case.

The present formulation of the four-body scattering problem is subject to a number of errors whose importance it is difficult to assess. Polarization of the target nucleus by the incoming neutron is neglected, but this effect has been found to be small for energies above 2 Mev in the scattering of neutrons by deuterons (Christian and Gammel 1953) and can presumably be neglected in the present case, as the ^{3}He and triton nuclei are more tightly bound structures than the deuteron. On the other hand, the gaussian wave functions and interactions employed lead to kernels $k_n(r, r')$ of too short a range and this may lead to an

underestimate of scattering at small angles. In the neutron–^{3}He collision the charge exchange reaction

$$n + {}^3He \rightarrow p + {}^3H$$

is possible at all energies and, therefore, the inclusion of an additional $p + {}^3H$ group in the resonating group function (5) may be of importance as the systems $n + {}^3He$ and $p + {}^3H$ will be strongly coupled. The D+D grouping and the influence of excited states of the alpha particle may also be of some importance. An investigation into the influence of the charge exchange reactions is being undertaken.

ACKNOWLEDGMENT

Some of the work described above was carried out as part of the research programme of the National Physical Laboratory and is published by permission of the Director.

REFERENCES

DE BORDE, A. H., and MASSEY, H. S. W., 1955, *Proc. Phys. Soc.* A, **68,** 769.
BRANSDEN, B. H., and MCKEE, J. S., 1954, *Phil. Mag.*, Ser. 7, **45,** 869.
CHRISTIAN, R. S., and GAMMEL, J. L., 1953, *Phys. Rev.*, **91,** 100.
COON, J. H., BOCKELMAN, C. K., and BARSCHALL, H. H., 1951, *Phys. Rev.*, **81,** 33.
HOCHBERG, S., MASSEY, H. S. W., ROBERTSON, H. H., and UNDERHILL, L. H., 1955, *Proc. Phys. Soc.* A, **68,** 746.
HOCHBERG, S., MASSEY, H. S. W., and UNDERHILL, L. H., 1954, *Proc. Phys. Soc.* A, **67,** 957.
ROBERTSON, H. H., 1956, *Proc. Camb. Phil. Soc.*, **52,** 538.
SWAN, P., 1953 a, *Proc. Phys. Soc.* A, **66,** 238; 1953 b, *Ibid.*, **66,** 740; 1955, *Proc. Roy. Soc.* A, **228,** 10.
WHEELER, J. A., 1937, *Phys. Rev.*, **52,** 1107.

Ionization Loss and the Range–Energy Relation for Low Energy Protons in Metals

By K. L. KAILA and N. K. SAHA
Physics Department, University of Delhi

Communicated by F. C. Auluck; MS. received 18th June 1956, and in revised form 14th August 1956

Abstract. In the absence of any precise theoretical treatment of the ionization loss of heavy charged particles at low energies, Bethe's original ionization loss formula has been modified empirically by introducing a multiplying factor $F=(Z_{\text{ett}}/Z)\{E^2/(E^2-E_0^2)\}$ which removes the zero of the logarithm at $2mv^2/I=1$ and passes to unity at high energy. The modified formula gives results showing reasonably good agreement with the experimental data of Madsen and of Warshaw on the ionization loss of protons in Al, Cu, Ag and Au down to approximately 50 kev and passes on smoothly to Bethe's original formula at medium and high energies. A modified range–energy relation for low-energy protons based on this formula is computed. Range–energy values are calculated from this relation for Al, Cu, Ag and Au. The results for Al and Cu show considerable departure from Livingston and Bethe's curves for protons at low energies.

§ 1. Bethe's Formula of Ionization Loss and its Limitations

Heavy charged particles like α-particles and protons continually lose energy, suffering ionization loss, in passing through a stopping medium by inelastic collisions with the bound electrons in the medium. The position regarding the theoretical calculations and experimental measurements of the ionization loss up to the end of 1951 has been admirably summarized by Bethe and Ashkin (1953) and that up to June 1953 by Allison and Warshaw (1953). Special mention should be made of the work of Warshaw (1950) on the measurements of ionization loss in Al, Ag, Cu and Au for protons of energy from 400 kev down to 50 kev and of Madsen (1953) in the energy region 2 Mev to 400 kev. Except for the low-energy region, the ionization loss of heavy charged particles is correctly represented by Bethe's formula (1930):

$$-\frac{dE}{dx}=\frac{4\pi e^4z^2}{mv^2}NZ\ln\frac{2mv^2}{I}, \qquad \ldots\ldots(1)$$

$$v\gg\frac{Ze^2}{\hbar} \quad \text{and} \quad E\gg\frac{M}{m}I \qquad \ldots\ldots(1\,a)$$

where v is the particle velocity, m the mass of the electron, M the mass of the proton and I the average ionization potential of the atoms in the medium.

The chief difficulty with Bethe's formula (1) is that the energy loss vanishes when $2mv^2/I=1$. Of course the usual binding corrections applied by Bethe do avoid the vanishing of the energy loss at $2mv^2/I=1$, but the treatment is quite complicated and also it does not solve the difficulty at very low energies. On the other hand, Lindhard and Scharff (1953) have recalculated the ionization loss

of charged particles on the Fermi–Thomas model of the atom. It has been admitted, however, that the apparent good agreement of their theory with experiment at low energies may not be justified, because when a more rigorous treatment is attempted on the Lenz–Jensen model, the agreement becomes much worse for low velocities. The problem is complicated at low velocities by the capture and loss of electrons which are difficult to treat theoretically, and have not been incorporated in any existing theory of stopping power.

In view of the difficulties of a purely theoretical approach to the low-energy problem, it seems possible to modify the simple Bethe formula empirically by introducing a multiplying factor F which would remove the zero of the logarithm and which would go to unity at high energies. The purpose of the present paper is to attempt this modification. Earlier a similar attempt was made by one of us (Kaila 1955) to explain the ionization loss of α-particles at low energies. By a careful analysis of the low-energy experimental data for protons in metals in the light of Bethe's formula we come to the following form of this factor:

$$F=\frac{Z_{\text{eff}}}{Z}\frac{E^2}{E^2-E_0^2}, \qquad \text{where} \qquad E_0=\frac{M}{4m}I.$$

Thus the modified ionization loss formula becomes

$$-\frac{dE}{dx}=\frac{2\pi Me^4z^2}{m}NZ_{\text{eff}}\frac{E}{E^2-E_0^2}\ln\frac{E}{E_0}. \qquad \ldots\ldots(2)$$

This modified formula can now be compared with the experimental results and its validity examined.

§ 2. Comparison with Experiment and Discussion

The results of the experiments on ionization loss at low energies (Warshaw 1950, Madsen 1953) are shown in figure 1, curve I, where the quantity

$$\frac{E}{NZ}\frac{dE}{dx}(\text{kev cm}^{-1})=\frac{AE}{Z}\frac{dE}{dx}(\text{kev cm}^2\text{ mg}^{-1})$$

is plotted against $\log_{10}(4mE/MI)$; E represents the particle energy $\frac{1}{2}Mv^2$ in kev and A is the mass number of the stopping element. The values of the ionization potential I for the various elements Al, Cu, Ag and Au which are used above are respectively 150, 279, 422 and 650 ev. The values for the first three elements are due to Bakker and Segrè (1951). For gold we have used the value 650 ev, which fits the experimental data quite well. Obviously, the validity of Bethe's formula requires the plot to be a straight line. The experimental points, however, clearly fall on a smooth curve considerably deviated from the expected straight line and approaching the latter only at medium energies corresponding to $\log_{10}(4mE/MI)\simeq 0{\cdot}8$. For the various elements Al, Cu, Ag and Au the critical energy below which the deviation sets in is approximately 500 kev, 750 kev, 1·3 Mev and 1·9 Mev respectively. To demonstrate the agreement of the experimental results with the modified formula (2) obtained after introducing the correction factor F, we have plotted $(AE/FZ)dE/dx$(kev cm^2 mg^{-1}) against $\log_{10}(E/E_0)$ for the various metals over the proton energy range of 2000 kev to 50 kev. The result is shown by curve II in figure 1, where the observed points for all the four metals are seen to fall very strikingly on a nearly smooth straight

line down to about 50 kev (for aluminium). The deviation of Bethe's original formula at low particle energies, therefore, vanishes in this modified form. In the plot of the curves in figure 1, Z the atomic number of the stopping element has been used as such instead of Z_{eff} and for all the four elements considered the points lie approximately on the single straight line II, which simply means that $Z_{eff} = \text{const. } Z$. The constant factor here can now be easily found by fitting the

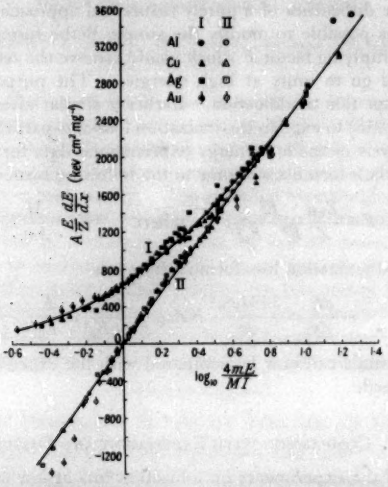

Figure 1. Plots of $(AE/Z)dE/dx$ (curve I) and $(AE/FZ)dE/dx$ (curve II) for protons against $\log_{10}(4mE/MI)$ in Al, Cu, Ag and Au.

observed dE/dx values for the various elements with the formula (2). Such a fitting gives us the relation $Z_{eff} = 0{\cdot}833Z$ and the nature of the fit is clearly seen from figure 2 (*a*) and (*b*) where the calculated values of dE/dx at various energies using formula (2) are plotted. The curves for Al, Cu, Ag and Au have been shown and for each of these metals the corresponding Bethe plots (using relation (1)) have been shown for comparison. In practically all the cases, the results calculated from formula (2) show a much better agreement with the experimental results than those from Bethe's formula. The fit for Al is the best, the average deviation between the calculated and experimental results being about 3 to 4%. For Cu and Ag, the fits obtained are within an average deviation of 7 to 8% from the experiment. In the case of gold the average deviation is somewhat larger (about 15%). This may be due to uncertainty in the value of the average ionization potential I for Au used by us or some uncertainty in the experimental data as mentioned by Green, Cooper and Harris (1955) who obtain experimental values about 25% higher than those of earlier workers. Thus there seems to be a doubtful situation so far as the experimental values of dE/dx for gold are concerned and an exact comparison with experiment as done by us is not quite satisfactory. Incidentally, it may be mentioned that the value $0{\cdot}833Z$ obtained by

us for Z_{eff} is quite close to the value $0{\cdot}85Z$ in Bloch's formula (1933) for the ionization potential I. Further we are using the same relation for Z_{eff} for all the metals in the whole range of energy, and for the same metal, the same value of I is used throughout the entire energy region. This may be considered consistent with the fundamental assumption of the validity of Bloch's theory for

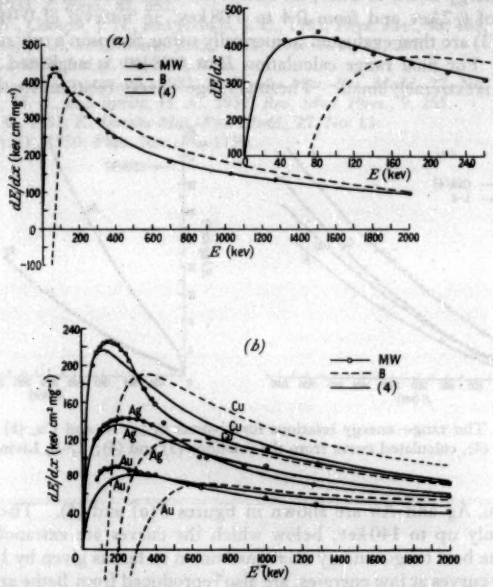

Figure 2. The plot of dE/dx (kev cm^2 mg^{-1}) values at various energies for protons in (*a*) Al, (*b*) Cu, Ag, Au. MW, experimental data of Madsen and of Warshaw; B, curve calculated from Bethe's formula (1); full curves calculated from formula (2) not (4).

ionization potential of elements at all energies. This is, however, unlike the procedure adopted by some earlier authors, Hirschfelder and Magee (1948), who tried to fit Bethe's original formula with the observed ionization loss at low energies by adjusting different values of Z_{eff} and I the average excitation potential at different small intervals of energies.

§ 3. The Range–Energy Relation for Protons at Low Energies

The range R of protons in the various metals can now be calculated from the usual definition of range and by using numerical integration over small intervals of energy between 0 and E. We have by definition

$$R=\int_0^E \frac{dE}{dE/dR}=\int_0^{0{\cdot}08\,\text{kev}} \frac{dE}{dE/dR}+\int_{0{\cdot}08\,\text{kev}}^{20\,\text{kev}} \frac{dE}{dE/dR}+\int_{20\,\text{kev}}^{E} \frac{dE}{dE/dR}. \quad \ldots\ldots(3)$$

For the ionization loss dE/dR we write from (2)

$$\frac{dE}{dR}(\text{kev cm}^2\ \text{mg}^{-1}) = 14{\cdot}42 \times 10^4 \frac{Z_{\text{eff}}}{A} \frac{E}{E^2 - E_0^2} \ln \frac{E}{E_0}. \quad \ldots\ldots(4)$$

where A is the mass number of the stopping element. The energy loss dE/dR is now calculated from (4) within energy intervals of 20 kev from E down to 20 kev. From this energy down to 2 kev, an interval of 1 kev is taken, from 2 to 0·4 kev, an interval of 0·2 kev and from 0·4 to 0·08 kev, an interval of 0·04 kev. The integrals in (3) are then evaluated numerically using Simpson's rule of numerical integration. For final range calculation R at 0·08 kev is neglected because its contribution is extremely small. The final range–energy relations for the different

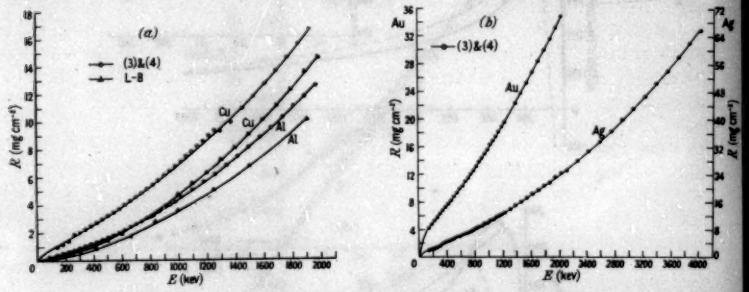

Figure 3 (a). The range–energy relations for protons in (*a*) Al and Cu, (*b*) Ag and Au. (3) and (4), calculated curve from the relations (3) and (4); L–B, Livingston-Bethe curve.

metals Al, Cu, Ag and Au are shown in figures 3 (*a*) and (*b*). The calculated points are only up to 140 kev, below which the curves are extrapolated. For Al and Cu the best range–energy relations known so far, as given by Livingston–Bethe (1937) curves at low energies, are also reproduced from Bethe and Ashkin's article (1953) for comparison. For Ag and Au no such range–energy relation exists at low energies.

§ 4. Conclusions

Of course, the main problem still remains to be solved, namely the exact mechanism for the capture and loss processes taking place in ionization phenomena. The solution of this alone will enable one to explain the peculiar form of the equation (2). However, since we have arrived at a definite form of the correction factor F which fits the experimental observations at low energies fairly well, and which brings about a smooth transition to Bethe's ionization formula at high energies, the nature of this factor may facilitate the understanding of the complicated mechanism of ionization loss at low energies.

Acknowledgments

Our thanks are due to Professor D. S. Kothari, Head of the Department of Physics, University of Delhi, for his kind encouragement and for providing all facilities to carry out this work.

References

ALLISON, S. K., and WARSHAW, S. D., 1953, *Rev. Mod. Phys.*, **25**, 779.
BAKKER, C. J., and SEGRÈ, E., 1951, *Phys. Rev.*, **81**, 489.
BETHE, H. A., and ASHKIN, J., 1953, *Experimental Nuclear Physics* (Ed. E. Segrè) Vol. I, (New York : Wiley; London : Chapman and Hall).
BETHE, H. A., 1930, *Ann. Phys. Lpz.*, **5**, 325.
BLOCH, F., 1933, *Z. Phys.*, **81**, 363.
GREEN, D. W., COOPER, J. N., and HARRIS, J. C., 1955, *Phys. Rev.*, **98**, 466.
HIRSCHFELDER, J. O., and MAGEE, J. L., 1948, *Phys. Rev.*, **73**, 207.
KAILA, K. L., 1955, *Ind. J. Phys.* **29**, 479.
LINDHARD, J., and SCHARFF, M., 1953, *K. Danske Mat.-Fys. Medd.*, **27**, No. 15.
LIVINGSTON, M. S., and BETHE, H. A., 1937, *Rev. Mod. Phys.*, **9**, 265.
MADSEN, C&B., 1953, *K. Danske Mat.-Fys. Medd.*, **27**, No. 13.
WARSHAW, S. D., 1950, *Phys. Rev.*, **76**, 1759.

The Nucleonic Component in Cosmic Ray Extensive Air Showers

By P. L. MARSDEN and G. A. DORAN†
Department of Physics, University of Leeds

Communicated by J. G. Wilson; MS. received 2nd July 1956 and in final form 8th October 1956

Abstract. The ratio β of the density of fast nucleons to that of electrons in extensive showers has been measured within 20 metres of the shower axis, the nucleons being detected through the evaporation neutrons arising from the interactions of these particles. It is shown that the ratio β decreases with increasing distance from the shower axis and also decreases with increasing shower size over a range defined by electron densities in the immediate neighbourhood of the axis of from 50 to 350 m^{-2}.

§ 1. Introduction

The nucleonic component of extensive air showers forms the initial structure of the showers from which the electronic and mesonic components are derived by the superposition of particles and cascades from a range of depths through the atmosphere. Near the shower axis the intensity of the nucleonic component is great enough for useful specific measurements to be made upon it, and measurements in this region may be expected to be of interest.

The two aspects of the N-component in extensive air showers which have been investigated most frequently are (1) the ratio β of the density of nucleonic particles to that of electrons (substantially, to that of all other ionizing particles) and (2) the variation of β with distance from the shower axis. The earlier experiments (Cocconi, Cocconi-Tongiorgi and Greisen 1949, McCusker 1950, Sitte 1950) were designed to determine the fraction of the 'penetrating particles' which caused nuclear interactions in absorbers (the nucleonic particles). The importance of shower size was not appreciated and many of these experiments appeared to be inconsistent. The variation of β with shower size has been demonstrated by Kasnitz and Sitte (1954), who concluded that the ratio of density of N-particles to that of the electrons decreases with increasing shower size, ranging in value from 0·62% for showers containing between 3×10^4 and 2×10^5 electrons to 0·43% for showers with more than 10^6 electrons.

The interpretation of experiments to investigate the variation of β with distance from the shower axis has only become effective with the application of core-selecting techniques. Thus Cocconi and Cocconi-Tongiorgi (1950) using a core selector at an altitude of 3260 m found that the intensity of N-particles to all other ionizing particles was about 1%, and that this value showed a tendency to diminish with distance from the shower axis. This result probably stands in spite of the fact shown by Greisen, Walker and Walker (1950) that nucleonic interactions themselves account for between 25% and 50% of the response of this core selector. At 3860 m altitude, Vavilov, Nikol'skij and Sarentsev (1955) using a different core-selecting technique showed that the intensity of N-particles is 0·3 to 0·5% of all ionizing particles and that this ratio decreases with increasing distance from the

† Now at the University of Birmingham.

core. At sea level Fujioka (1953), using apparatus similar to that of Cocconi has shown that the ratio of N-particles to ionizing particles does not change rapidly with distance from the core.

The present experiment was performed near sea level and the nucleonic component is, therefore, almost exclusively fast neutrons and protons. The nucleonic particles are detected by the evaporation neutrons they produce in a large absorber, and use has been made of a core-selecting device developed in the laboratory by E. W. Kellermann and his co-workers, the performance of which has been reported by Kellermann (1956) and will be described in detail elsewhere.

§ 2. The Apparatus

The arrangement of the detecting apparatus is shown in figure 1, and the component parts are described below. Two core selectors, CS_1 and CS_2, have been used with two nucleon detectors, N_1 and N_2. The relative positions of these four units were as indicated and they have thus given data for 2, 6, 12 and 20 m separations between core selector and N-detector.

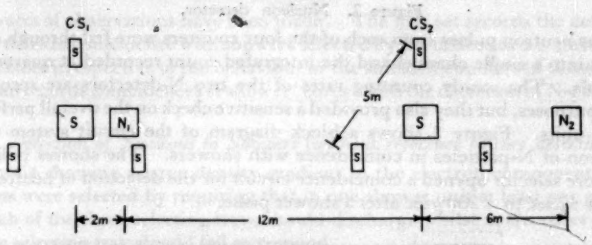

Figure 1. Arrangement of the detecting apparatus.

A core selector consisted of three trays s, each containing two unshielded counters of active area 140 cm^2, placed in a triangle about the shielded counters S. The shielded counters were placed at depths of 5 cm and 20 cm in a large lead pile. The minimum requirement for the detection of a shower was that at least one counter in each unshielded tray should be discharged simultaneously. Discharges amongst the shielded counters were used to detect a degree of cascade multiplication which, in coincidence with discharges in the shower trays s, was considered to indicate that the axis of the shower had fallen close to the core selector. The decoherence curves obtained between two such selectors show that it is possible to determine 'core criteria' which lead to approximately constant core selecting efficiency over a tenfold range of electron densities. Kellermann has also established from the decoherence curves that more than 50% of showers with detected cores will have axes falling within 3 m of the centre of the core selecting array.

Figure 2 gives a sectional drawing of one of the nucleon detectors. Four counters 41 cm long and 5 cm in diameter filled with $^{10}B F_3$ to a pressure of 40 cm Hg, were surrounded by paraffin wax blocks 1 in. thick which moderated the evaporation neutrons produced in the surrounding lead (6 in. thick). The background count due to evaporation and slow neutrons in the atmosphere was reduced by surrounding the lead by a further thickness of wax. For the N_1

detector this was 4in. thick and for the N_2 detector 8 in. thick. The detectors each contained about 2000 lb of lead and except for the difference of thickness of the external wax layer, which is of no account in the present work, were identical. The counters and immediate circuits, together with the moderating layer of wax, were sealed in a metal box containing a drying agent.

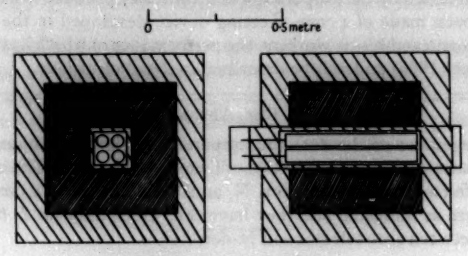

Figure 2. Nucleon detector.

The neutron pulses from each of the four counters were fed through a mixing circuit into a single channel and the integrated count recorded at quarter hourly intervals. The steady counting rates of the two N-detectors are recorded for other purposes, but they also provided a sensitive check on the overall performance of the units. Figure 3 shows a block diagram of the circuit system used for detection of N-particles in coincidence with showers. The shower pulses from each core selector opened a coincidence circuit for the detection of neutron pulses from $+5\,\mu$sec to $+200\,\mu$sec after a shower pulse.

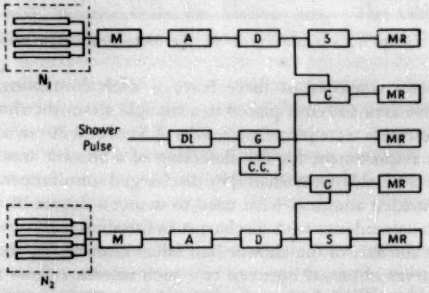

Figure 3. Circuit arrangement for detection of nucleons in coincidence with showers. M, Mixer; A, amplifier; D, discriminator; S, scaler; MR, message register; Dl, delay; C, coincidence unit; G, gate unit,; CC, Camera control.

The efficiency of detecting a nucleon which enters the lead of an N-detector must be determined if the observations are to lead to numerical values of β. Although the efficiency must be a function of nucleon energy, at this stage we do not attempt to determine this function but effectively introduce a lower energy cut-off below which we do not detect nucleons and above which we detect all nucleons with the same average efficiency ϵ. It is not possible to give a firm estimate of the cut-off energy, but this can hardly be less than 1 Gev. The efficiency ϵ is estimated

from the probability p of detecting a single evaporation neutron, the average number n of these neutrons derived from each incident nucleon in the lead absorber and the time interval ('gate') during which neutrons were detected after each prompt shower pulse. Following Cocconi a mean life of slow neutrons in our detector of 160 μsec has been adopted but the result is quite insensitive to this value in terms of the overall accuracy of the estimate of ϵ. Using the data of Tobey and Montgomery (1951) the rate of production of neutrons by N-particles in each of our units is $2{\cdot}2 \times 10^5\ h^{-1}$, the detected rate of the continuous neutron flux is $6900\ h^{-1}$, giving $p \sim 0{\cdot}03$. A concordant value of p was found by a direct measurement using a Ra–Be source of known neutron activity. The average multiplicity n is estimated to be 65 following the results of Cocconi, Cocconi-Tongiorgi and Widgoff (1950). These values of p, n and gate interval give $\epsilon = 0{\cdot}6$. Mainly on account of the uncertainty of the adopted value for n, this value of ϵ may be in error by as much as 30%, an uncertainty which extends through the whole of the results given below, but which does not affect comparisons made within the data.

§ 3. The Results

Two sets of observations have been made. The first set records the detection of N-particles in coincidence with showers selected by the unshielded s trays of the core selectors irrespective of the behaviour of the shielded counters of these units; the second records coincidences of shower 'cores' with the detection of N-particles.

3.1. *Detection of Nucleons in Showers (without reference to core detection)*

Showers showing a large density gradient in the electron component at the apparatus were selected by requiring that in one shower unit at least one counter from each of the three selecting trays should discharge whilst in the other unit at least one selecting tray should fail to respond.

Observations upon these showers are set out in table 1 in terms of the distance from that shower unit in which a shower response was observed to that N-detector in which a neutron was detected. The two N-detectors did not come into use at the same time; the total operating time for distances 2 and 12 m was 4871 hours and for the distances 6 and 20 m 3088 hours. The total numbers of shower–nucleon coincidences (s, n) are shown in line 3 of table 1. Line 4 shows the experimentally determined ratio (s, n)/(s).

The results are compared with the values of (s, n)/(s) calculated on the following assumptions : (*a*) that the lateral structure function of N-particles is the same as that for the electronic component. For this function the Bethe approximation of the Molière structure has been used, but Blatt (1949) has shown that analyses of this kind are not very sensitive to the form of structure function used; (*b*) that the number-spectrum of N-particles is of the same form as the number-spectrum of electrons:

$$S(N)\,dN = K\,N^{-(\gamma+1)}\,dN$$

where γ has been taken to be 1·5. These assumptions imply that β is independent of position in the shower and of shower size. The product $(\beta\epsilon)$ can be adjusted in the calculation to give the best fit with the observed values of (s, n)/(s). If this fit extends to all measured distances it provides evidence of the suitability of the assumptions.

The values of (s, n)/(s) calculated in this way are given in lines 5 and 6 for two values of $(\beta\epsilon)$ of which the first (line 5) is that giving the best fit with the observed ratio. The calculation, extended along well known lines, yields a value for $N_{1/2}$,

Table 1. Shower–Nucleon Coincidence Data

CS–N distance (m)	2	6	12	20
Total no. of showers (s)	8038	5095	8038	5095
No. of shower–nucleon coincidences (s, n)	594	341	266	115
Ratio (s, n)/(s)	$0{\cdot}047 \pm 0{\cdot}003$	$0{\cdot}067 \pm 0{\cdot}004$	$0{\cdot}033 \pm 0{\cdot}002$	$0{\cdot}023 \pm 0{\cdot}002$
Calc. (s, n)/(s)				
$(\beta\epsilon) = 0{\cdot}0069$	0·072	0·072	0·032	0·022
$(\beta\epsilon) = 0{\cdot}0050$	0·052	0·052	0·023	0·016
$N_{1/2} \times 10^{-5}$	1·1	1·3	1·4	2·0

the median shower size, and this is shown in the last line of the table. The estimate of $N_{1/2}$ is of very limited absoulte significance because of imperfect knowledge of the electronic structure function: it is of immediate value, however, in providing some indication of the uniformity of the shower size in our work for the various separations of the electron detectors and nucleon detectors.

For this calculation, which is rather insensitive to lateral structure, it appears adequate to assume that the lateral structure function of the nucleonic component is the same as that for the electrons. Then the best fit is obtained with $(\beta\epsilon) = 0{\cdot}0069$, where $(\beta\epsilon)$ is determined to a much greater precision than the efficiency ϵ is known. Since we consider that ϵ lies within 30% of 0·6, we conclude that β lies in the range $0{\cdot}008 < \beta < 0{\cdot}015$.

3.2. *Distribution of Nucleons in Showers with Located Cores*

The data used in this part of the work consist of records of coincidences between either nucleon detector and the particular response of the core-selecting units which is interpreted as due to a shower core falling in the immediate vicinity of a core unit. The records are classified according to shower density, measured in the unshielded counter trays of the core detectors, and according to the distance from the core selector to the nucleon detector involved. For small distances and for large showers, the probability of a core–neutron coincidence is so large that to estimate the corresponding density of incident nucleons account must be taken of 'overhitting', that is the probability that neutrons arising from more than one incident nucleon may be expected to be recorded in a single event.

Direct estimates of nucleon density at distances 2, 6, 12, 20 m from the core selector are given in table 2 for four (electron) density classes, the figures in brackets indicating the number of observations upon which each density estimate is based.

If the core selector located the strict axis of the shower, these figures would yield directly the lateral distribution of the detected nucleons. However, the uncertainty of location of cores is not negligible at least when compared with the smaller core selector–neutron detector separations, and it is preferable to interpret these densities in relation to electron densities measured with the same core-selecting system, and to the electron lateral structure observed in this way. The measured lateral structure was kindly communicated to us by Dr. Kellermann, and the calculation of the median electron density within each shower class (corresponding

Table 2. Nucleon Density $\Delta_n(m^{-2})$ as a function of Shower Class and of Distance from Core Selector

Shower Class	CS–N distance (m) 2		6		12		20	
3	1·01	(11)	0·34	(3)	0·40	(9)	0·21	(2)
4	1·48	(18)	0·89	(11)	0·49	(11)	0·14	(1)
5	2·21	(23)	1·36	(17)	0·52	(12)	0·22	(1)
6	2·67	(14)	1·47	(11)	0·83	(8)	0·76	(4)

to a particular response of the s counters) is straightforward. It must be noted that this median density is modified by the differing probabilities of occurrence of a nucleon coincidence over the range of shower densities comprising the shower class. This modification is not very sensitive to β and involves only a simple approximation.

In table 3 the values of β, corresponding to the neutron densities given in table 2, are shown; here also the number of nucleon–core coincidences in each case is shown in brackets, since the main uncertainty in the value of β arises from the small number of these coincidences which have been observed.

Table 3. Values of the Ratio β for various Electron Densities and Nucleon–Core Separations

Shower class	ρ_{el} (m^{-2})	CS–N distance (m) 2		6		12		20	
3	55	0·021	(11)	0·010	(3)	0·020	(9)	0·020	(2)
4	84	0·020	(18)	0·018	(11)	0·018	(11)	0·009	(1)
5	148	0·017	(23)	0·016	(17)	0·010	(12)	0·008	(1)
6	330	0·009	(14)	0·006	(11)	0·006	(8)	0·012	(4)

ρ_{el} = electron density at core selector.

While the table shows a tendency for β to decrease with increasing shower density and increasing distance from the shower core, the fluctuations are large. The data have, accordingly, been fitted to an expression of the form

$$\beta = \beta_0(1 - \alpha \log r)$$

where α is assumed the same for all shower classes investigated, and the best value of β_0 obtained for each class. The resulting constants of this expression are given in table 4.

Table 4. Values of β_0

Shower class	ρ_{el} (m^{-2})	α	β_0
3	55	0·2	0·023 ± 0·003
4	84	0·2	0·022 ± 0·003
5	148	0·2	0·017 ± 0·003
6	330	0·2	0·009 ± 0·003

ρ_{el} = mean electron density at core selector.

The fit is not sensitive to changes of α, but the results are not consistent with a negative value of α. On the other hand the values of β_0, and in particular the relative values, are not sensitive to change of α. For the data in tables 3 and 4, the median shower size, $N_{1/2}$ ranges from 5×10^4 in shower class 3 to 3×10^5 in shower class 6. As has already been stressed this quantity is open to grave objections when it is derived from a small sample of each shower, but it offers some indication of shower size which may be related to that of showers studied by other means.

§ 4. Discussion

The experiment on core-selected showers leads to the conclusion that the fraction β which the N-particles bear to all ionizing particles decreases with increasing distance from the shower axis, although the rate of decrease is not well determined. This conclusion is supported by a comparison of the results for the core selected and non-core selected showers, the average value of β for the former, 0·017, being significantly greater than that for the latter, 0·011. For the core-selected showers, the average distance from the nucleon detector to the shower axis is much less than 10 m; for the showers selected without core detection, on the other hand, this distance is certainly greater than 10 m.

This conclusion is not affected by the uncertainty of ϵ, the efficiency of nucleon detection. It establishes at sea level an effect already observed by Cocconi and Cocconi-Tongiorgi (1950) and by Vavilov, Nikol'skij and Sarentsev (1955) at mountain altitudes.

The near axial value β_0 of the ratio of N-particles to all charged particles is significantly greater than that at mountain altitudes (Vavilov *et al.*) by an amount which cannot be accounted for in terms of the uncertainty of the efficiency ϵ. It, moreover, decreases with increasing shower size (whether shower size is defined in terms of all particles, of electrons or of nucleons), in qualitative agreement with the mountain observations of Kasnitz and Sitte (1954).

Evidence has recently been assembled (Greisen 1956) which emphasizes the persistence of a nucleonic component of showers which in the lower part of the atmosphere governs the attenuation of the electronic component. This component must be concentrated very closely upon the shower axis, and the N-component described in this paper and the electronic component are both being continually reinforced by its interactions. From this view point the variation of β_0 with altitude and with shower size are in the direction to be expected, for the ratio of the electronic component to the observed N-component is a measure of the efficiency of meson production, and this is to be expected to diminish as the average energy of the sustaining axial nucleonic flux falls off, either with depth in the atmosphere or in a shower from a low energy primary as compared with that from a more energetic primary.

Acknowledgments

The authors wish to thank Professor J. G. Wilson for his encouragement and helpful discussion. The work was assisted by a grant from the Royal Society which defrayed the cost of counters.

One of us (G. A. D.) is indebted to the Department of Scientific and Industrial Research for a maintenance grant.

References

Blatt, J., 1949, *Phys. Rev.*, **75**, 1584.

Cocconi, G., and Cocconi-Tongiorgi, V., 1950, *Phys. Rev.*, **79**, 730.

Cocconi, G., Cocconi-Tongiorgi, V., and Greisen, K., 1949, *Phys. Rev.*, **76**, 1020.

Cocconi, G., Cocconi-Tongiorgi, V., and Widgoff, M., 1950, *Phys. Rev.*, **79**, 768.

Fujioka, G., 1953, *International Conference on Theoretical Physics, Japan* (Tokyo : Science Council of Japan).

Greisen, K., 1956, *Progress in Cosmic Ray Physics*, Vol. 3, Ch. 1 (Amsterdam : North-Holland).

Greisen, K., Walker, W. D., and Walker, S. P., 1950, *Phys. Rev.*, **80**, 535.

Kasnitz, H. L., and Sitte, K., 1954, *Phys. Rev.*, **94**, 977.

Kellermann, E. W., 1956, *Report of* 1955 *Guanajuato International Conference on Cosmic Rays*, to be published in Mexico.

McCusker, C. B. A., 1950, *Proc. Phys. Soc.* A, **63**, 1240.

Sitte, K., 1950, *Phys. Rev.*, **78**, 721.

Tobey, A. R., and Montgomery, C. G., 1951, *Phys. Rev.*, **81**, 517.

Vavilov, Iu. N., Nikol'skij, S. I., and Sarentsev, U. P., 1955, *Zh. Eksper. Teor. Fiz.*, **28**, (4), 505.

Directional Measurements on Extensive Air Showers

By P. ROTHWELL, B. WADE and A. GOODINGS
Imperial College of Science and Technology, London

Communicated by P. M. S. Blackett; *MS. received* 21*st August* 1956

Abstract. A search has been made for localized sources of high energy cosmic rays, by measuring the directions of arrival of the particles in extensive air showers with cloud chambers run in coincidence with a counter detecting system. An angular resolution rather better than 5° was achieved. No sources have been found between latitudes 10°N and 90°N on the celestial sphere for showers of average energy 8×10^{15} ev.

§ 1. Introduction

The only method available at present for the study of cosmic ray particles of energy, over about 10^{15} ev, is through the detection of extensive showers. Measurements in several laboratories (Cranshaw and Galbraith 1954, Auger *et al.* 1955, Cranshaw and Elliot 1956) have so far revealed no certain variation of these high-energy showers with time, which indicates a high degree of isotropy of the primary particles in space. However, the arrays of counters used for these measurements effectively collect extensive showers arriving throughout a large solid angle. If it were not for the atmosphere, this solid angle would be 2π. In fact, due to the absorption of the atmosphere the effective solid angle of collection at sea level lies between 1 and 2 steradians. Thus, though it is fully established that there is so far no detectable deviation from isotropy when the celestial sphere is scanned by a detecting apparatus with an aperture of 1–2 steradians, there always remains, in principle, the possibility of the existence of localized sources. Though there are reasons why the existence of such sources of high-energy cosmic rays is rather unlikely, it is important to make a direct experimental attack on the problem. To do this, one could use a cosmic-ray 'shower telescope' with a small aperture. This, however, is quite impracticable as the rate of events would be far too small. Consequently, it is necessary to measure the direction of arrival of every shower over the whole available solid angle permitted by the atmosphere.

This can be done in two ways : (*a*) by timing the delays between the arrival of the particles at different parts of the shower and deducing the direction from these times (Clark 1956), (*b*) by the direct but also more laborious method of measuring the particle directions in a cloud chamber.

Both these methods give comparable results, in that they have an angular accuracy of rather better than 5°. Thus, expressed in terms of solid angle, the direction of arrival of any shower can be determined to about a hundredth of steradian compared with 1–2 steradians of an ordinary counter array.

It is interesting to speculate on the possible ways in which some localized sources might originate.

(1) The present theory of isotropy of the cosmic rays depends on the assumption of the randomizing influence of interstellar magnetic fields, connected with the turbulent motion of interstellar gas. These fields might have some symmetry

characteristic which would allow high energy charged particles to arrive preferentially from certain directions.

(2) If a large nearby star emits very energetic charged particles, and the magnetic field between the star and the earth is either low in magnitude or parallel to the direction of the star, then a maximum intensity would be observed in that direction.

(3) It must not be completely excluded that stable neutral elementary particles might exist among the primary cosmic rays which would, therefore, be unaffected by magnetic fields and so would arrive directly from the source. It is even conceivable that high energy neutrons might arrive undecayed from nearby stars. For instance, a neutron of 10^{15} ev has a mean lifetime of about 30 years and so could travel 30 light years with only about 50% chance of decaying.

In this paper, an experiment is described which uses the cloud chamber method for determining the directions of arrival of extensive air showers, and it will be shown that no sign of localized sources has, in fact, been detected.

§ 2. Experimental Arrangement

The directions of arrival of shower particles have been measured in four cloud chambers, run in coincidence with a counter detecting system. A diagram of the apparatus is shown in figure 1. Two groups of counters were placed 20 metres

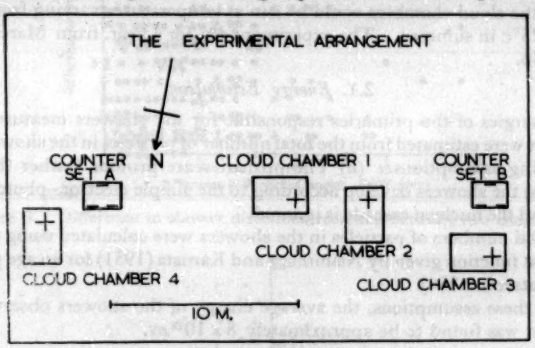

Figure 1. Experimental arrangement.

apart, roughly in the E–W plane. Each group consisted of 3 trays of 6 Geiger–Müller counters, $4 \times 40\,\text{cm}^2$, placed vertically so that their greatest area faced roughly North–South, on the corners of a triangle of side about 2 metres, and connected through a three-fold coincidence unit. The counter trays were placed on edge so that showers which arrived at an angle inclined to the vertical, and in which the number of particles were reduced owing to their greater path length through the atmosphere, had to some extent a compensatingly higher chance of detection. Those showers which came in inclined from the North–South direction saw greater counter area, while those which came in inclined from the East–West direction saw a shorter distance between counter sets. In this way, the effective opening angle of the apparatus was increased, so that as large an area as possible on the celestial sphere could be examined for point sources.

A double coincidence between the two groups of counters (i.e. a six-fold coincidence between the trays) provided a master pulse to trigger four cloud

chambers; two were placed halfway between the two counter sets, one facing North–South, the other East–West, and two were placed one near each counter set, also facing one N–S, and one E–W. The three-fold counting rates were about six per hour, and the six-fold, triggering, rate was 1·2 per hour. The cloud chambers expanded simultaneously on the master pulse from the counter sets, and a pair of stereoscopic photographs was taken of each, together with a plumb line, clock and date slip. Figure 2 (Plate) shows a large shower recorded in chambers I, II and IV (chamber III was not operating when this photograph was taken). The cloud chambers were of conventional design. They were filled with approximately 90% argon and 10% oxygen, saturated with an alcohol–water mixture (75% alcohol, 25% water). Chamber pressure was about 15 cm Hg above atmospheric, and the expansion ratio was approximately 1·08. The compressed position, determined by the air pressure between the piston and the back of the chamber, was controlled by a Nielsen valve. Illumination was provided by twenty-four 150 watt, 110 volt incandescent lamps, each with a 5 in. condenser lens, overrun at 230 volts, for the flash time of approximately 200 milliseconds. The cloud chamber dead time was about 3½ minutes.

All the apparatus was housed in thermostatically controlled huts on the roof of Imperial College, London. The temperature was usually set at approximately 20°c, but the cloud chambers could be run at temperatures varying from 15°c in winter to 25°c in summer. The experiment ran for a year, from March 1955 to March 1956.

2.1. *Energy Estimation*

The energies of the primaries responsible for the showers measured in this experiment were estimated from the total number of particles in the showers, under the following assumptions : (*a*) The primaries are protons (rather than heavy nuclei); (*b*) the showers develop according to the simple electron–photon cascade process, and the nucleon cascade is ignored.

The total numbers of particles in the showers were calculated using the lateral distribution function given by Nishimura and Kamata (1951) for an age parameter $S = 1{\cdot}2$ (Zatsepin 1956).

Under these assumptions, the average energy of the showers observed in the experiment was found to be approximately 8×10^{15} ev.

2.2. *Results*

The cloud chamber photographs for each day were examined, and events were selected in which four or more tracks looked reasonably parallel in any one chamber. About 25% of the events satisfied this criterion. The directions of the tracks in the N–S and E–W planes were then determined by projecting the stereoscopic photographs through the lenses of the camera which took the picture, on to a tilting screen. A further selection was then made of those events in which at least four tracks were parallel, first to within about 5° in any one chamber, and later to within 3°. This gave 1100 showers in the first class, and 685 in the second. These numbers are rather low, not so much because there was a wide scatter in the directions of particles in some of the showers, as that a number of events were rejected because of the quality of the cloud chamber photographs.

About 20% of the showers selected showed tracks in two or more chambers; a greater proportion would be expected to do so, but were not observed because the

cloud chambers did not operate equally well all the time. Comparison of the directions given by different chambers for the same shower gave agreement to within 5·2° standard deviation from the mean for the first group of showers and 3·2° for the second, so it was felt to be justifiable to rely upon directions given by single chambers and to include them in the analysis. Figure 3 shows the difference in shower directions recorded between two chambers.

Figure 4 shows 1100 shower directions plotted in laboratory coordinates. The projection in the N–S plane is plotted along the x-axis and the projection in the

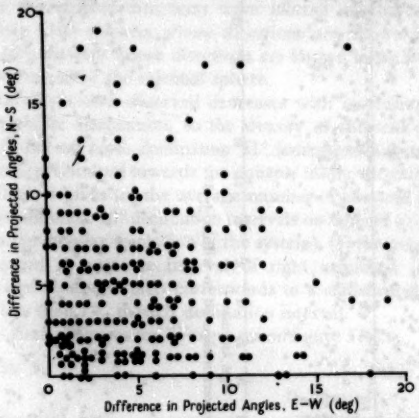

Figure 3. Difference in shower directions recorded between two chambers.

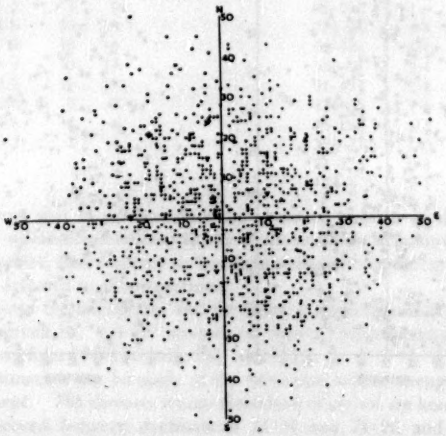

Figure 4. Shower directions in laboratory coordinates.

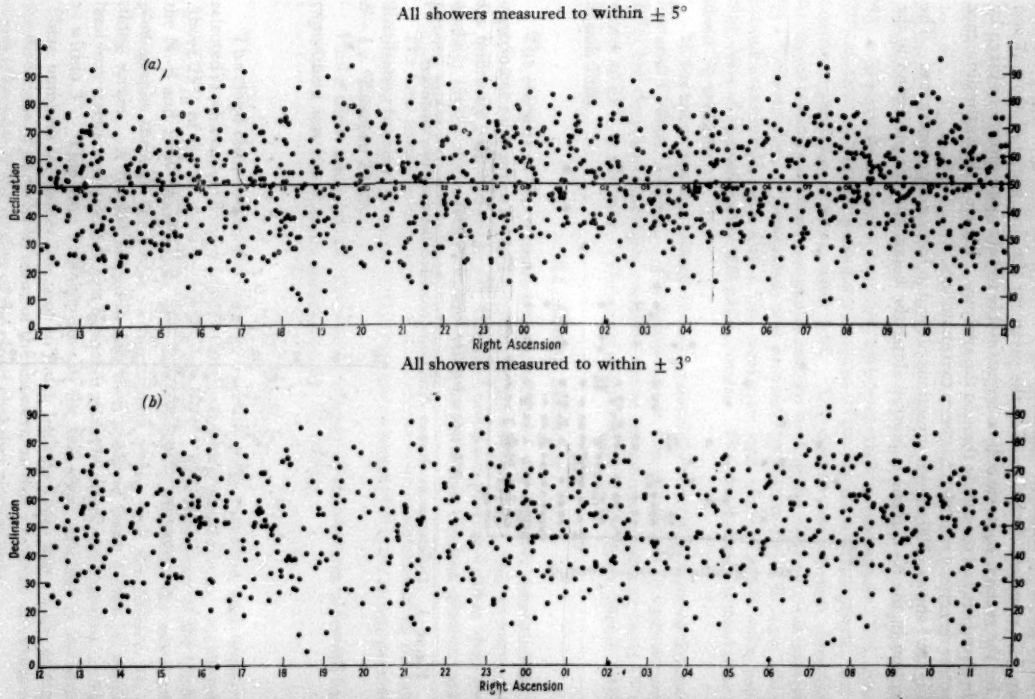

Figure 5 (*a*). 1100 showers measured to ± 5·2°, plotted on a mercator projection of the celestial sphere. (*b*) 700 showers measured to ± 3·2° plotted on a mercator projection of the celestial sphere.

E–W plane along the y-axis. The distribution is symmetrical about the vertical; most showers come in at small zenith angles, and the greatest angle from which a shower was recorded was 53°.

The 1100 showers were examined for a solar time variation. The film was usually removed and the cloud chambers checked in the morning, so a small spurious time variation was expected, with maximum in the early afternoon, just after the chambers had been reset. A small (~10%) variation was found, in fact, but statistically it was barely significant (χ^2 test gave a probability of 0·15), and since the experiment ran for a full year, no correction was made for this effect when the shower directions were plotted on the celestial sphere. Figure 5 (*a*) shows 1100 showers whose directions are known to within ±5°, and 5 (*b*) shows 685 showers whose directions are known to within ±3°, plotted on a mercator projection of the celestial sphere.

The numbers of showers observed decreases with increasing zenith angle, because of atmospheric attenuation, so the density of showers on the celestial sphere appears to fall off from declination 51° (corresponding to the direction vertically overhead in London) towards the equator in one direction and the pole in the other. Table 1 gives (*a*) the average number of showers per 40 minutes right ascension for different 10° declination intervals on figure 5 (*a*) (i.e. in squares corresponding to the angular resolution of the system), (*b*) the maximum number of showers observed in any one interval of right ascension at the different declinations, (*c*) the number which corresponds to a statistical fluctuation with a probability of less than 1% in each declination interval.

Table 2 gives similar figures for 7½° squares on figure 5 (*b*).

Table 1

Declination interval (deg)	(*a*)	(*b*)	(*c*)
90–81	0·9	4	6
81–71	3·3	7	9
71–61	4·8	10	14
61–51	5·9	10	14
51–41	5·7	10	14
41–31	5·5	10	14
31–21	3·3	8	9
21–11	0·8	4	6
11– 1	0·2	2	4

Table 2

Declination interval (deg)	(*a*)	(*b*)	(*c*)
88½–81	0·4	2	5
81–73½	1·0	3	7
73½–66	1·7	4	8
66–58½	1·7	5	8
58½–51	2·4	6	9
51–43½	2·2	7	9
43½–36	1·6	6	8
36–28½	1·5	4	7
28½–21	1·0	4	7
21–13½	0·4	3	5
13½–6	0·1	1	3

It can be seen that in no case does the observed number of showers reach the 1% level of significance, corresponding to the numbers in column (*c*) and it is concluded, therefore, that there are no localized sources of cosmic rays of sufficient strength to be detected in the experiment.

Figure 6 shows the histograms and the Poisson distributions of the numbers of showers observed in: (*a*) 10° squares on figure 5 (*a*) between 31° and 71°, (*b*) 7½° squares on figure 5 (*b*) between 28½° and 73½°.

A rough estimation can be made of the minimum source strength detectable in this experiment. 786 showers whose directions of arrival are known to within ±5° were observed between declinations 31° N and 71° N, and the average number per 10° square is 5·5. If 14 showers had been observed in any such

interval on this part of the celestial sphere, there would have been less than a 4% chance that it was due to a statistical fluctuation (see table 1). Taking 14 as the minimum number required to give any significant indication of a localized source, it follows that a source whose strength corresponds to $(14-5{\cdot}5)/786 = 1{\cdot}1 \times 10^{-2}$ of the background rate could have been detected in this experiment. A similar calculation made for the showers whose directions are known to within $\pm 3°$, between 28½° N and 73½° N, gives the minimum detectable source strength as $1{\cdot}2 \times 10^{-2}$ of the background rate.

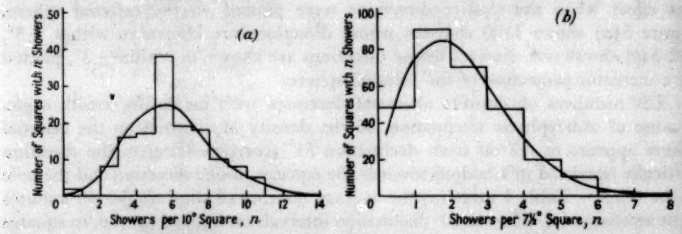

Figure 6 (*a*). Histogram and Poisson distribution of the numbers of showers observed per 10° square. (*b*) Histogram and Poisson distribution of the numbers of showers observed per 7½° square.

A rough upper limit to the intensity of any particular localized source of high energy particles which are not deflected by interstellar magnetic fields may also be deduced from these results.

Suppose that a certain source, distance R light years from the earth, emits N particles per second of energy greater than 8×10^{15} ev, which can travel to the earth's surface without decaying, and with less than 5° deflection. If the collecting area of the array for showers of this size is a circle of radius a cm, and the polar diagram of the apparatus has a half angle θ degrees, then the number of particles from the source detected by the array is

$$\frac{N}{4\pi} \frac{\pi a^2}{(R \times 10^{18})^2} \frac{2\theta}{360} \text{ sec}^{-1}.$$

The total number of showers actually measured to 5° accuracy in this experiment was 1100, and the rate of arrival of showers of energy greater than 8×10^{15} ev is about 1 per hour, so the effective observing time is 1100 hours. Taking $a \sim 25$ metres, and $\theta \sim 40°$, the number of showers received from a particular source during the course of the experiment is

$$n = \frac{N}{4R^2 \times 10^{36}} \times 6{\cdot}25 \times 10^6 \times \frac{80}{360} \times 1100 \times 60 \times 60 = \frac{N}{R^2} \times 1{\cdot}35 \times 10^{-24}.$$

The maximum number of showers observed in any one 10° square on the celestial sphere is 10, so taking $n = 10$, the upper limit to the intensity of any localized source is given by

$$N = 10 \times \frac{R^2}{1{\cdot}35 \times 10^{-24}} = 8 \times 10^{24} R^2.$$

For example, suppose the bright star Vega, right ascension 18h 35 min, declination 38° 44′ N, emits high energy cosmic ray particles. It lies 26 light

years from the earth, and the number of showers observed in the 10° square in that direction, $n=9$. Therefore

$$N=9\times\frac{26^2}{1{\cdot}35\times10^{-24}}=5\times10^{27}$$

i.e. the upper limit to the intensity of emission of particles of energy greater than 8×10^{15} ev which are not deflected by interstellar magnetic fields from Vega is 5×10^{27} sec^{-1}, which is approximately 10^{-3} of the total energy output of this star.

§ 3. Conclusion

No evidence has been found for the existence of localized sources of primary cosmic rays whose energies, according to conventional estimations, are of the order of 8×10^{15} ev. Sources of strength greater than 1% of the background counting rate could have been detected, if they existed. It is still possible that further experiments with better statistical accuracy or at higher energies may reveal some effect, but the results of this experiment imply that (*a*) interstellar fields do not have the shape or symmetry characteristics necessary to allow high energy charged particles to arrive preferentially from any particular direction at the earth's surface in numbers sufficient to be detected; (*b*) there are no localized sources of high energy cosmic rays, in the northern celestial hemisphere, between 10° N and 90° N, which emit particles undeflected by interstellar magnetic fields and of energy greater than 8×10^{15} ev, with an intensity greater than $8\times10^{24}R^2$ sec^{-1}, where R is the distance of the source from the earth, measured in light years.

Acknowledgments

The authors would like to thank Professor P. M. S. Blackett for providing the facilities for this work, and for his interest and encouragement, Dr. H. Elliot for many stimulating discussions, Dr. H. J. J. Braddick for designing the cloud chambers, Mr. D. Bryant for assistance in running the equipment, and Miss R. Roberts for much help in the analysis of the results. We are indebted to the Department of Scientific and Industrial Research for a grant covering the cost of the equipment, and for a maintenance grant to one of us (A. G.).

References

Auger, P., Cachon, A., Daudin, A., Freon, A., Mosykowski, C., 1955, *C. R. Acad. Sci., Paris*, **240**, 2407.

Clark, G., 1956, *Report of* 1955 *Guanajuato International Conference on Cosmic Rays*, in course of publication in Mexico.

Cranshaw, T. E., and Galbraith, W., 1954, *Phil. Mag.*, **45**, 1109.

Crawshaw, J. K., and Elliot, H., 1956, *Proc. Phys. Soc.* A, **69**, 102.

Nishimura, J., and Kamata, K., 1951, *Progr. Theor. Phys., Japan*, **6**, 628.

Zatsepin, G. T., 1956, *Report of Oxford Conference on Extensive Air Showers* (London: H.M.S.O.).

Inelastic Heavy Particle Collisions involving the Crossing of Potential Energy Curves IV. Ionic Recombination

By D. R. BATES and T. J. M. BOYD

Department of Applied Mathematics, The Queen's University of Belfast

MS. received 31*st July* 1956

Abstract. Calculations are carried out on the rate of simple ionic recombination between H^- ions and various positive ions $B^+(H^- + B^+ \rightarrow H + B)$. The coefficient describing the process is in general very high—at normal temperatures values of about 10^{-7} cm^3 sec^{-1} or more are to be expected. Dissociative ionic recombination $(A^- + CD^+ \rightarrow A + C + D)$ is also discussed. It may be extremely rapid.

§ 1. Introduction

Simple ionic recombination

$$A^- + B^+ \rightarrow A + B \qquad \ldots\ldots(1)$$

requires at least one transition between the potential energy curves associated with the initial and final systems. In general transitions occur mainly near the pseudo-crossings of these curves. The characteristics of the process have been discussed qualitatively by several authors (Magee 1940, 1952, Bates and Massey 1943, Massey 1952, Massey and Burhop 1952), and detailed calculations on

$$H^-(1s)^2 + H^+ \rightarrow H(1s) + H(2s, 2p, 3s, 3p \text{ and } 3d) \qquad \ldots\ldots(2)$$

have been performed (Bates and Lewis 1955). We present in this paper an account of an investigation concerned with the probable range of magnitudes of the rate coefficients for the cases in which the negative ion is that of atomic hydrogen. Some comments are also made on effects that arise with molecular ions. In particular dissociative ionic recombination is discussed.

§ 2. Recombination between H^- Ions and Atomic Positive Ions

2.1.

For simplicity we shall confine ourselves to the idealized case in which only a single pseudo-crossing of the potential energy curves is of importance. The occurrence of additional pseudo-crossings would tend to increase the rate coefficient.

Let R_x be the internuclear distance at the pseudo-crossing point, p the chance that the systems make the approach along the given potential†, E their initial energy of relative motion and ΔE the energy released by the recombination. Using the well-known Landau–Zener formula for the probability of a transition it may readily be shown (cf. Bates and Lewis 1955), that the cross section for the process is given approximately by

$$Q = 4\pi p R_x^2 \left(1 + \frac{\Delta E}{E}\right) F_3(\eta) \qquad \ldots\ldots(3)$$

† For the cases considered in § 2 p is unity.

where

$$F_3(\eta) = E_3(\eta) - E_3(2\eta); \quad E_3(x) = \int_1^\infty t^{-3} \exp(-tx)dt \qquad \ldots\ldots(4)$$

and

$$\eta = \frac{\pi^2 e^2 \overline{M}^{1/2}\{\Delta U(R_x)\}^2}{2^{1/2}h(E+\Delta E)^{1/2}(\Delta E)^2} \qquad \ldots\ldots(5)$$

$\overline{M}$ being the reduced mass of the colliding systems and $\Delta U(R_x)$ being the separation between the potential energy curves at the pseudo-crossing. In the derivation it is assumed that when R exceeds R_x the interaction between the ions may be taken to be coulombic (except in so far as it affects the value of R_x), and the interaction between the neutral atoms may be neglected. In the cases that are of interest R_x is so large that the assumption does not lead to serious error. If the assumption were not made the denominator of (5) would contain a certain additional factor differing only slightly from unity. This factor was included in the work reported in the earlier papers of the series (Bates and Moiseiwitsch 1954, Dalgarno 1954, Bates and Lewis 1955). We omit it here as we wish to keep the number of parameters as low as possible.

The ionic recombination coefficient α may be obtained by multiplying the cross section by the velocity of relative motion and averaging over the appropriate Maxwellian distribution. Putting

$$R_x = e^2/\Delta E \qquad \ldots\ldots(6)$$

in the external factor of (3), but not elsewhere, and inserting the values of the fundamental constants, we find that at a temperature of $T°$K

$$\alpha = \frac{0{\cdot}51p}{\overline{M}^{1/2}(\Delta E)^2 T^{3/2}} \int_{\Delta E}^\infty \exp[a(\Delta E - z)] F_3\left(\frac{\zeta}{z^{1/2}}\right) z\,dz (\mathrm{cm^3\,sec^{-1}}) \qquad \ldots\ldots(7)$$

where

$$a = 1{\cdot}16_1 \times 10^4/T \qquad \ldots\ldots(8) \qquad \zeta = \frac{247{\cdot}_2 \overline{M}^{1/2}\{\Delta U(R_x)\}^2}{(\Delta E)^2} \qquad \ldots\ldots(9)$$

$\Delta U(R_x)$ and ΔE being now in ev and $\overline{M}$ being on the ^{16}O-scale (and therefore being approximately unity if one of the ions is H^- and the other is relatively massive). The integral in (7) may be evaluated with the aid of the tables of Placzek (1946). Figure 1 shows plots of $\log[\overline{M}^{1/2}\alpha/p]$ against $\log\zeta$ for some chosen values of T and ΔE.

2.2.

With the exception of $\Delta U(R_x)$ the atomic parameters on which α depends may be readily determined provided the term values involved are known.

To add to the meagre information that is available on $\Delta U(R_x)$ it was judged desirable to compute this parameter for the pseudo-crossings associated with

$$H^-(1s)^2 + Li^+ \rightarrow H(1s) + Li(2s, 2p, 3s, 3p \text{ and } 3d) \qquad \ldots\ldots(10)$$

$$H^-(1s)^2 + Na^+ \rightarrow H(1s) + Na(3s, 3p, 4s, 3d \text{ and } 4p) \qquad \ldots\ldots(11)$$

and

$$H^-(1s)^2 + K^+ \rightarrow H(1s) + K(4s, 4p, 5s, 3d \text{ and } 5p). \qquad \ldots\ldots(12)$$

Let $\psi(\mathbf{r}_{a1}, \mathbf{r}_{a2})$ be the wave function of $H^-(1s)^2$, $\phi(\mathbf{r}_{a1}|1s)$ be that of H(1s) and $\phi(\mathbf{r}_{b2}|nl)$ be that of the valence electron of the alkali atom. Taking these

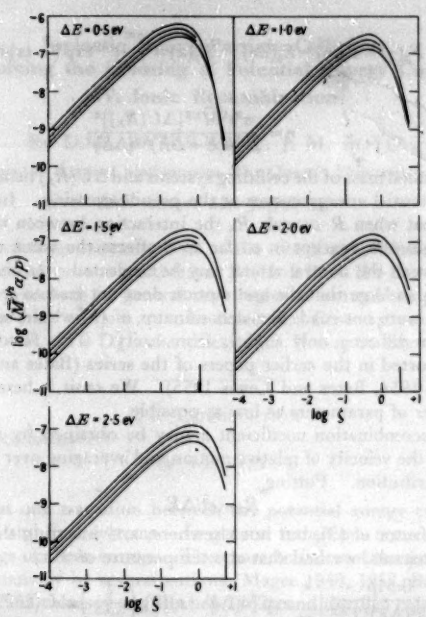

Figure 1. Dependence of recombination coefficient on parameter ζ defined in (9) of text. Predicted values of ζ are shown by the vertical lines: for $\Delta E = 0{\cdot}5$ ev the value is $-4{\cdot}6$ (which is off the scale). In each set the uppermost curve is for a temperature of 250°K, the lowest is for a temperature of 2000°K and the two intermediate are for temperatures of 500°K and 1000°K.

wave functions to be real and treating the electrons in the closed core as passive it may be shown from the standard quantal formula concerned (cf. Bates and Moiseiwitsch 1954), that

$$\Delta U(R_x) \simeq \frac{2\sqrt{2}}{(1-S^2)(1+s^2)^{1/2}} |\mathscr{I}| \text{(atomic units)} \qquad \ldots\ldots(13)$$

where

$$S = \sqrt{\left(\frac{2}{1+s^2}\right)} \iint \psi(\mathbf{r}_{a1}, \mathbf{r}_{a2}) \phi(\mathbf{r}_{a1} | 1s) \phi(\mathbf{r}_{b2} | nl) d\tau_1 \, d\tau_2 \qquad \ldots\ldots(14)$$

$$s = \int \phi(\mathbf{r}_a | 1s) \phi(\mathbf{r}_b | nl) d\tau \qquad \ldots\ldots(15)$$

and

$$\mathscr{I} = \iint \psi(\mathbf{r}_{a1}, \mathbf{r}_{a2}) \phi(\mathbf{r}_{a1} | 1s) \phi(\mathbf{r}_{b2} | nl) I d\tau_1 \, d\tau_2 \qquad \ldots\ldots(16)$$

with

$$\left.\begin{aligned} I &= \left(\frac{1}{r_{a1}} - \frac{1}{r_{a2}}\right) \qquad r_{a1} > r_{a2} \\ &= 0 \qquad\qquad\quad r_{a1} < r_{a2}. \end{aligned}\right\} \qquad \ldots\ldots(17)$$

In general S and s are small compared with unity so that it is only necessary to determine $\mathscr{I}$ accurately. Noting that $\phi(\mathbf{r}_{a_1}|1s)$ is a very compact wave function, it may be seen from (16) and (17) that $\mathscr{I}$ is not unduly sensitive to the form of $\psi(\mathbf{r}_{a_1}, \mathbf{r}_{a_2})$ and that it is controlled mainly by the amplitude of $\phi(\mathbf{r}_{b_2}|nl)$ at radial distances comparable with the internuclear distance at which the pseudo-crossing occurs. This is of considerable importance.

Representing $\psi(\mathbf{r}_{a_1}, \mathbf{r}_{a_2})$ by the approximation due to Löwdin (1953), and $\phi(\mathbf{r}_b|nl)$ by the Coulomb approximation (cf. Bates and Damgaard 1949), and using the exact $\phi(\mathbf{r}_a|1s)$ it is a simple task to express S, s and $\mathscr{I}$ in terms of the J-functions of Coulson (1942). The formulae are cumbersome and need not be presented.

With the detachment energy of the hydrogen negative ion taken to be 0·747 ev (Henrich 1943), and the polarizability to be 230 atomic units (Bates and Lewis 1955) R_x was found for each of the 15 pseudo-crossings being treated and $\Delta U(R_x)$ was then computed. The table gives the values obtained together with the corresponding values for the five pseudo-crossings investigated by Bates and Lewis (1955).

Basic Quantities relating to the Pseudo-crossings associated with $H^- + B^+ \rightarrow H(1s) + B(n, l)$

System B(n, l)	ΔE (ev)	R_x (A. U.)	$\Delta U(R_x)$ (ev)
Li (2s)	4·643	7·5	$6·07\times10^{-1}$
(2p)	2·796	10·6	$4·33\times10^{-1}$
(3s)	1·271	21·6	$5·36\times10^{-2}$
(3p)	0·810	33·7	$9·14\times10^{-3}$
(3d)	0·766	35·6	$4·53\times10^{-3}$
Na (3s)	4·390	7·7	$5·85\times10^{-1}$
(3p)	2·288	12·6	$3·20\times10^{-1}$
(4s)	1·200	22·9	$4·35\times10^{-2}$
(3d)	0·775	35·2	$4·86\times10^{-3}$
(4p)	0·639	42·6	$1·87\times10^{-3}$
K (4s)	3·592	8·8	$4·95\times10^{-1}$
(4p)	1·980	14·3	$2·42\times10^{-1}$
(5s)	0·986	27·7	$1·90\times10^{-2}$
(3d)	0·923	29·6	$1·23\times10^{-2}$
(5p)	0·530	51·4	$3·81\times10^{-4}$
H (2s)	2·652	11·1	$3·33\times10^{-1}$
(2p)	2·652	11·1	$4·07\times10^{-1}$
(3s)	0·763	35·6	$4·91\times10^{-3}$
(3p)	0·763	35·6	$6·40\times10^{-3}$
(3d)	0·763	35·6	$4·58\times10^{-3}$

All points on a $[\log(\Delta U(R_x)), \Delta E]$ plot cluster about a curve (cf. figure 2). This is as would be expected, for from what has been stated earlier it is apparent that $\Delta U(R_x)$ should be approximately proportional to the amplitude of the final wave function at the position of the H^- nucleus; and the amplitude depends mainly on R_x and on the effective principal quantum number both of which may be expressed in terms of ΔE.

Using (9) we may thus estimate ζ if ΔE is given. Relevant values are indicated in figure 1 by vertical lines. Figure 3 shows the $(\log\zeta, \Delta E)$ curve superimposed

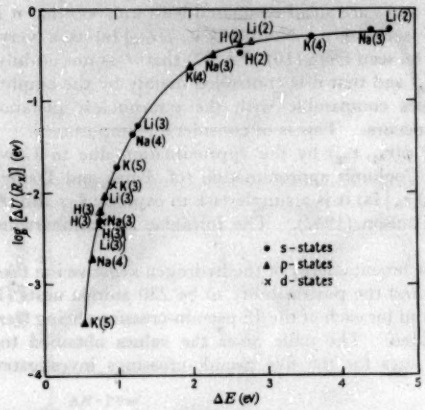

Figure 2. Calculated values of $\Delta U(R_x)$. Atom and principal quantum number of state entered as indicated.

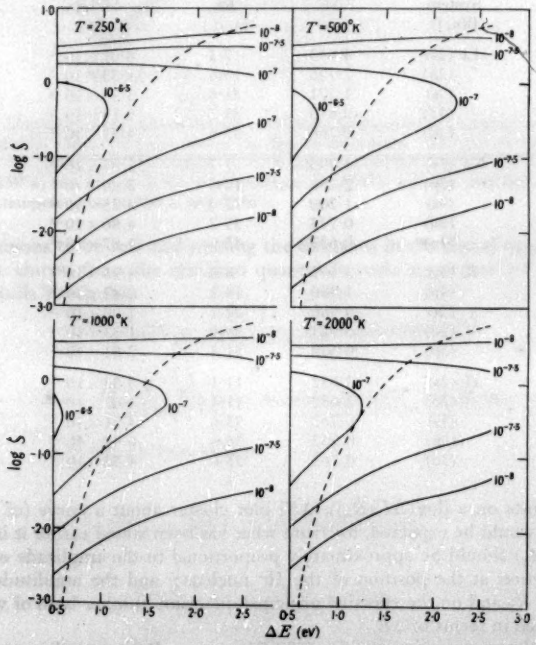

Figure 3. Full lines are contours of constant recombination coefficient (with values of $\overline{M}^{1/3}\alpha/p$ marked on each) : broken lines are the predicted (log ζ, ΔE) curves.

on a set of contours of constant α in $\log\zeta$–ΔE space. It is clear that the rate coefficient describing the recombination of H^- ions with positive ions of any species is very large indeed: thus in order that α/p should exceed 10^{-7} cm^3 sec^{-1} it is only necessary for ΔE for some interacting state to lie between the following limits (in ev): $0{\cdot}8_5$–$1{\cdot}6_5$ (250°K); $0{\cdot}9$–$1{\cdot}6$ (500°K); $1{\cdot}0_5$–$1{\cdot}4_5$(1000°K); —† (2000°K). For a particular species $\alpha T^{1/2}$ is approximately constant (cf. figure 1).

§ 3. Molecular Ions

3.1.

If one of the recombining ions is molecular account must be taken of the vibrational levels. Because of these we have, instead of pairs of interacting potential energy curves, networks of such curves. Provided it is small compared with the energy difference between neighbouring vibrational levels, the interaction energy at each pseudo-crossing in a network is simply the square root of the Franck–Condon factor connecting the vibrational levels concerned, multiplied by the value it would have for the same nuclear separation if there were no vibrational structure. In view of the great number of pseudo-crossings the ionic recombination coefficient must in all cases be large—with H^- ions values above 10^{-7} cm^3 sec^{-1} are to be expected at moderate temperatures.

The character of a band spectrum emitted as a result of ionic recombination is of interest in connection with upper atmospheric and other studies. It may be noted that the distribution amongst the rotational levels of the neutral molecules formed is essentially identical with the corresponding distribution for the original ions. The vibrational distribution may of course be very much changed. In general it is not the same as that ensuing from radiative electron recombination. If η is large compared with unity, transitions for which the Franck–Condon factors are low are favoured, while if η is small, transitions for which the Franck–Condon factors are high are favoured. The situation is complicated by the sensitivity of the interaction energy at a pseudo-crossing to the nuclear separation, $R_x(v_i, v_f)$, which is a decreasing function of v_i the initial vibrational quantum number, and an increasing functionof v_f the final vibrational quantum number. Other things being equal the transitions from a given v_i level which are favoured are those to high v_f levels for large η, and those to low v_f levels for small η.

3.2.

With molecular ions the electronic state entered may be repulsive so that dissociation takes place as in

$$A^- + CD^+ \rightarrow A + C + D. \qquad \ldots\ldots(18)$$

This type of process differs in two respects from the type already considered: the transition is into a continuum and if it occurs it is stabilized by the separation of the atoms forming the molecule. Using standard time-dependent perturbation theory (cf. Mott and Sneddon 1948) and representing the continuum wave functions as do Winans and Stueckelberg (1928), it may readily be shown that if electronic states other than those directly concerned are ignored, the cross section for dissociative ionic recombination is approximately

$$Q' = 2\pi p R_x^2 \left(1 + \frac{\Delta E}{E}\right) G_3(\eta) \qquad \ldots\ldots(19)$$

† The value at 2000°K approaches 10^{-7} cm^3 sec^{-1} if ΔE is close to 1·2 ev.

with

$$G_3(\eta) = E_3(0) - E_3(2\eta) \qquad \ldots\ldots(20)$$

where the notation is as before, except that $\Delta U(R_x)$, on which η depends (cf. (5)), is the interaction energy that would arise if the constituent atoms of the molecule were held fixed in their equilibrium relative positions. Modifying (7) in the obvious manner, we have at once that the recombination coefficient for the process is

$$\alpha' = \frac{0{\cdot}51p}{2\overline{M}^{1/2}(\Delta E)^2 T^{3/2}} \int_{\Delta E}^{\infty} \exp\left[a(\Delta E - z)\right] G_3\left(\frac{\zeta}{z^{1/2}}\right) z\, dz (\mathrm{cm^3\,sec^{-1}}). \qquad \ldots\ldots(21)$$

When $\zeta/\Delta E^{1/2}$ is much less than unity $G_3(\zeta/z^{1/2})$ is closely equal to twice $F_3(\zeta/z^{1/2})$ over the z-range of importance. Consequently α' does not differ appreciably from α in these circumstances. The left-hand portions of the curves in figure 1 therefore apply to dissociative ionic recombination as well as to simple ionic recombination.

Unlike $F_3(\zeta/z^{1/2})$, $G_3(\zeta/z^{1/2})$ is a monotonically increasing function of the variable. It is effectively equal to 0·5 when $\zeta/\Delta E^{1/2}$ is much greater than unity† so that (21) may be integrated to yield

$$\alpha' \simeq 1{\cdot}1 \times 10^{-5} (\overline{M}^{1/2} T^{1/2} \Delta E)^{-1} \left\{1 + \frac{1}{a\Delta E}\right\} (\mathrm{cm^3\,sec^{-1}}) \qquad \ldots\ldots(22)$$

where as usual $\overline{M}$ is on the ^{16}O-scale, T is in degrees Kelvin and ΔE is in ev. In contrast to α we thus see that α' is high when the interaction energy is large. It should, however, be noted that the path to the pseudo-crossing involved may be blocked by a non-dissociative pseudo-crossing which occurs at a greater nuclear separation but at which the interaction is still strong.

Acknowledgment

One of us (T. J. M. B.) wishes to thank Co. Antrim Education Authority and the Northern Ireland Ministry of Education for maintenance allowances.

References

Bates, D. R., and Damgaard, A., 1949, *Phil. Trans. Roy. Soc.* A, **242**, 101.
Bates, D. R., and Lewis, J. T., 1955, *Proc. Phys. Soc.* A, **68**, 173.
Bates, D. R., and Massey, H. S. W., 1943, *Phil. Trans. Roy. Soc.* A, **239**, 269.
Bates, D. R., and Moiseiwitsch, B. L., 1954, *Proc. Phys. Soc.* A, **67**, 805.
Coulson, C. A., 1942, *Proc. Camb. Phil. Soc.*, **38**, 210.
Dalgarno, A., 1954, *Proc. Phys. Soc.* A, **67**, 1010.
Henrich, L. R., 1943, *Astrophys. J.*, **99**, 59.
Löwdin, P., 1953, *Phys. Rev.*, **90**, 120.
Magee, J. L., 1940, *J. Chem. Phys.*, **8**, 687; 1952, *Disc. Faraday Soc.*, **12**, 33.
Massey, H. S. W., 1952, *Advanc. Phys.* (*Phil. Mag.* Suppl.), **1**, 395.
Massey, H. S. W., and Burhop, E. H. S., 1952, *Electronic and Ionic Impact Phenomena* (Oxford : Clarendon Press), p. 620.
Mott, N. F., and Sneddon, I. N., 1948, *Wave Mechanics and its Applications* (Oxford : Clarendon Press), p. 252.
Placzek, G., 1946, *The Functions* $E_n(x)$ (National Research Council of Canada; Chalk River).
Winans, S. G., and Stueckelberg, E. C. G., 1928, *Proc. Nat. Acad. Sci., Wash.*, **14**, 867.

† With H^- ions this occurs if ΔE exceeds about 2·5 ev (cf. figure 3).

The Reactions $^{12}C(\gamma, p)^{11}B$, $^{11}B(p, \gamma)^{12}C$ and $^{12}C(\gamma, 3\alpha)$ at 17.63 MeV Excitation

By A. K. MANN† and E. W. TITTERTON

Research School of Physical Sciences, The Australian National University, Canberra

MS. received 7th May 1956

Abstract. The absolute cross section for the reaction $^{12}C(\gamma, p)^{11}B$ at 17·63 MeV has been determined from a measurement of the ratio of the number of protons to the number of 'carbon stars' produced under the same experimental conditions, and utilization of the known cross section for $^{12}C(\gamma, 3\alpha)$. The value obtained is compared with that calculated by detailed balancing from data on the inverse reaction, $^{11}B(p, \gamma)^{12}C$, and shows that the measured values of the cross sections for $^{12}C(\gamma, 3\alpha)$ and $^{11}B(p, \gamma)^{12}C$ are consistent within their stated errors.

§ 1. Introduction

In this paper a measurement of the absolute cross section for the reaction $^{12}C(\gamma, p)^{11}B$ at 17·63 MeV is described which we believe to be of interest for the following reason. The cross section is obtained from a comparison of the number of protons with the number of three-particle 'carbon stars', each subject to appropriate energy criteria, produced in the same nuclear emulsion by the same incident photon flux, in conjunction with an absolute cross section for the $^{12}C(\gamma, 3\alpha)$ reaction at 17·63 MeV. It is possible also to compare the value so determined with that obtained by detailed balancing from data on the inverse reaction $^{11}B(p, \gamma)^{12}C$. Thus the present measurement of the (γ, p) reaction provides a direct and stringent test of the consistency of the cross sections for the two independent reactions $^{12}C(\gamma, 3\alpha)$ and $^{11}B(p, \gamma)^{12}C$.

§ 2. Experimental Method

2.1. *General Arrangement*

In the experiment the nuclear emulsions themselves furnish the target through the carbon content of the gelatine, and in addition detect the reaction products. The former function makes it possible to perform an experiment with poor irradiation geometry, and the method of detection eliminates in part, at least, the problems resulting from the low disintegration rates of the reactions under study. The emulsions also are well suited to recording the 1·5 MeV protons expected from $^{12}C(\gamma, p)$ at 17·63 MeV, measurement of which would present difficulties for other detection methods, especially in the presence of an intense background of energetic gamma rays.

2.2. *Resolution*

Ilford type E1 emulsions were chosen for the experiment since these are considerably less sensitive than type C2 so allowing a greater density of events to be achieved before general blackening of the plates makes the search process

† Fulbright Fellow, on leave from the University of Pennsylvania, Philadelphia, Pennsylvania.

difficult. Even with this low-sensitivity emulsion it is not possible to discriminate between protons and α-particles with ranges less than about 50 microns, or between α-particles and the residual recoil nuclei in the case of (γ, α) reactions. It was, therefore, necessary to measure the total range of all tracks having ranges in the vicinity of the expected $^{12}C(\gamma, p)$ peak at 26 microns and, in fact, a number–range distribution of all tracks in the interval 5 to 50 microns was determined. The resolution to be expected for 1·5 MeV protons in a type E1 emulsion was estimated from the data of Rotblat (1950) for C2 emulsions and the comparison of resolution of E1 and C2 emulsions for 2·1 MeV α-particles carried out by Titterton and Brinkley (1949); the total width of the proton peak at half height was computed as 250 keV which corresponds to 6·5 microns. This estimate is uncertain and is meant to be used primarily as a guide in the following discussion of background.

2.3. *Background*

In addition to the single photo-proton group from carbon (the 14·8 MeV component of the ^{7}Li capture radiation is below the proton threshold) and the 'carbon stars', there will be other groups produced by (γ, p) and (γ, α) reactions in the nitrogen and oxygen contained in the gelatine of the emulsions. Each of the latter reactions may terminate in any one of several energetically possible levels of the appropriate residual nuclei and, consequently, a spectrum of groups is to be expected from these disintegrations. Listed in table 1 are details of the

Table 1

Reaction	(1)	(2)	(3)	(4)
$^{12}C(\gamma, p)$	19·7	0	17·6	26
$^{14}N(\gamma, p)$	4·3	7·7 (doublet)	17·6	44
		8·4 (doublet)	17·6	26
		9·0	17·6	13
$^{14}N(\gamma, \alpha)$	4·3	0	17·6	19·7
		0·72	17·6	16·0
		1·74	17·6	12·0
		2·15	17·6	10·5
$^{16}O(\gamma, \alpha)$	10·7	0	17·6	43·8
		4·43	17·6	19·7
		7·65	17·6	7·1
$^{14}N(\gamma, \alpha)$	4·3	0	14·8	8·7
		0·72	14·8	7·0
$^{16}O(\gamma, \alpha)$	10·7	0	14·8	28·0
		4·43	14·8	8·1

(1) Percentage of atoms of element in emulsion; (2) state of residual nucleus (MeV); (3) γ-ray energy (MeV); (4) calculated total range.

photodisintegrations of ^{12}C, ^{14}N and ^{16}O which give rise to protons or α-particles with total ranges in the emulsion between 5 and 50 microns. It will be seen that there are only four possibilities in ^{14}N and ^{16}O leading to products with ranges between about 20 and 30 microns, the region of primary interest, and that three of them are the result of (γ, α) reactions.

The disintegration $^{16}O(\gamma, \alpha)^{12}C$ was reported by Wäffler and Younis (1949) to have a cross section at 17·63 MeV of $(1{\cdot}8 \pm 0{\cdot}6) \times 10^{-28}$ cm^2. In a later measurement

of the energy distribution of the α-particles, Nabholz, Stoll and Wäffler (1952 a) found that transitions involving absorption of 17·6 Mev radiation and leading to the ground state of ^{12}C were predominant: the number of α-particles produced both in transitions to the excited state of ^{12}C at 4·43 Mev and in transitions initiated by absorption of the 14·8 Mev gamma-ray component was given as only 25% of the number resulting from the favoured transition. They also confirmed the earlier cross section value. Millar and Cameron (1953) have investigated the reaction using bremsstrahlung and give an excitation function with a resonance centering on 17·5 Mev, of half-width about 5 Mev, and with peak value of $2{\cdot}6 \times 10^{-29}$ cm²; that is, values which are a factor of 10 smaller than those of the Swiss group. These are, however, regarded as lower limits because of the possibility of missing events in the emulsions employed. Stoll (1954), using bremsstrahlung of maximum energy 31 Mev, has obtained an excitation function with the values $0{\cdot}9 \times 10^{-28}$ cm² and $1{\cdot}5 \times 10^{-28}$ cm² at 14·8 and 17·6 Mev respectively.

From this evidence it appears that transitions to the 4·43 Mev state of ^{12}C from 17·6 Mev excitation of ^{16}O are small in number compared with transitions to the ground state of ^{12}C and with transitions induced by 14·8 Mev radiation. The major contribution from $^{16}O(\gamma, \alpha)$ to the interval 20 to 30 microns is thus due to absorption at 14·8 Mev; from Stoll's cross section value this contribution is roughly 3% of the peak expected from $^{12}C(\gamma, p)$, if the cross section for the latter reaction is taken as approximately 10^{-27} cm², as predicted from the inverse reaction data.

The cross section for $^{14}N(\gamma, \alpha)$ at 17·6 Mev has also been measured by Stoll (1954) who found the value $1{\cdot}1 \times 10^{-28}$ cm², which is compatible with evidence from the cloud chamber measurements of Wright *et al.* (1956). Hence the contribution of $^{14}N(\gamma, \alpha)$ to the background of the present experiment may be estimated as about 2% of the $^{12}C(\gamma, p)$ peak.

The background from the remaining reaction, $^{14}N(\gamma, p)$, is difficult to evaluate because at an excitation of 17·6 Mev transitions giving rise to protons of energy about 1·5 Mev permit subsequent decay by neutron emission. In fact, both of the reactions $^{14}N(\gamma, p)^{13}C(8{\cdot}4\ \text{Mev}) \rightarrow {}^{12}C + n$ and $^{14}N(\gamma, n)^{13}N(3{\cdot}5\ \text{Mev}) \rightarrow {}^{12}C + p$ may contribute protons to the background. The (γ, pn) cross section at 17·6 Mev may, however, be found as $1{\cdot}4 \times 10^{-27}$ cm² from a comparison of the (γ, n) excitation functions obtained by measuring residual radioactivity (Johns *et al.* 1951) and by measuring total neutron yields (Ferguson *et al.* 1954). Then, assuming equal probabilities of transitions to the several possible levels in the two intermediate nuclei, the total cross section for transitions through the 8·4 Mev level of ^{13}C and the 3·5 Mev level of ^{13}N is 4×10^{-28} cm². This is expected to be a generous estimate and, indeed is about four times larger than the value which may be determined from the data of Wright *et al.* if it is assumed that the fraction of (γ, pn) transitions in which 1·5 Mev protons are emitted does not change appreciably in going from a mean excitation energy of about 21 Mev to an excitation of 17·6 Mev. The average of these rough cross section estimates indicates a background from $^{14}N(\gamma, p)$ of about 5% of the peak expected from carbon.

The average total photo-proton cross section of the Ag and Br isotopes in nuclear emulsions has been measured for the lithium gamma rays by Wäffler (1953) who finds $(3{\cdot}6 \pm 1{\cdot}8) \times 10^{-27}$ cm². The energy distribution of the photo-protons shows a small excess (about 10% of the total) of protons near the maximum

possible energy, 10–12 Mev, while the remainder of the distribution is in rough agreement with an evaporation process. The latter process gives virtually no protons below about 2·5 Mev because of the Coulomb barrier. It thus appears unlikely that protons from Ag or Br contribute to the background in the present experiment. The (γ, α) reactions in these elements have been measured by Nabholz, Stoll and Wäffler (1952 b), who found a cross section of $(1{\cdot}2 \pm 0{\cdot}5) \times 10^{-28}$ cm² at 17·6 Mev, which is in approximate agreement with the prediction of statistical theory, assuming all particles arise from $Br(\gamma, \alpha)$ reactions. The observed spread in the α-particles' energies, in conjunction with the small total cross section, indicate a negligible contribution to the background of the present experiment from this source.

The final contribution to the background comes from naturally radioactive inclusions which all photographic emulsions contain and which give rise to α-particle tracks. This background was determined by employing control plates and corrections for it will be dicussed in a later section.

Excepting the last-mentioned background, the total background from competing reactions is thus estimated at 10% of the peak expected for $^{12}C(\gamma, p)$. In view of the possible presence of small contributions from certain reactions which have been considered to make negligible contributions it is to be anticipated that this value may be too small, but it is not likely, despite its very approximate character, to be in error by more than one-half of its magnitude.

2.4. *Irradiation and Search Procedures*

Irradiations were made at a proton bombarding energy of 480 kev using a thick lithium metal target. Six 3 in. × 1 in. type E1 plates were used, each being cut into halves; one half of each plate was kept as a control while the other halves were wrapped in black paper and arranged about the lithium target at approximately 2½ in. from the centre and with the plane of the emulsion as nearly as possible at right angles to the incoming γ-rays. Under these conditions an irradiation corresponding to an integrated target bombardment of 2500 microampere–hours yielded plates of optimum exposure—the compromise being between the requirements of reasonable event density and plates which were not too 'black'.

Five independent observers, using Cooke, Troughton and Simms model 4000 microscopes, searched the plates recording all carbon stars and measuring the total range of all tracks falling in the interval 5–50 microns. A typical number–range histogram is shown in figure 1 A where the group corresponding to the 1·5 Mev proton from the $^{12}C(\gamma, p)$ reaction (range 26 μ) is clearly resolved and, in this case, the total half-width is rather less than that corresponding to the estimate of 250 kev given previously. On completion of this work each of the observers measured a number–range distribution for single tracks in the half control plate corresponding to the irradiated half plate previously searched and the results were combined to yield the histogram of figure 1 B which represents the background due to radioactive material in the emulsions. Results were pooled since the radioactive inclusions in plates are not always uniformly distributed and an average was required. The histogram shows a group centering at 20 μ and corresponding to the well-known α-particle contaminant in all emulsions (Jenkner and Broda 1949). The background correction to the histogram of

figure 1 A (in terms of volume searched) is small and is indicated by the difference between the dotted and full lines.

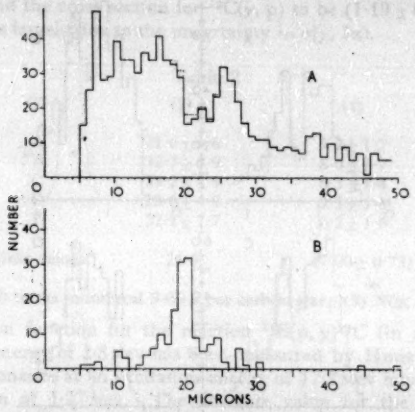

Figure 1. A. Number–range histogram for all linear tracks in an E1 emulsion irradiated with γ-rays from the $^{7}Li(p, \gamma)$ 440 kev resonance. Tracks of range below 20 μ are largely due to (γ, α) reactions. The clearly resolved group at 26 μ is due to the $^{12}C(\gamma, p)^{11}B$ reaction. B. Background of tracks in unexposed E1 emulsions due to natural radioactive inclusions. The volume of emulsion corresponding to B is far bigger than that yielding the spectrum of A. The corrected spectrum in A is given by full lines; the shape of the histogram in the relevant region before subtraction of the background is shown dotted.

§ 3. Results

The range measurements were converted to energy and number–energy histograms were plotted for the five independent sets of data. These are shown in figure 2 A, B, C, D, E and all except E show the 1·5 Mev group clearly resolved. The result of combining the five sets is given, with a change in ordinate scale, in figure 2F. The individual sets were fitted with gaussian curves centering on 1·5 Mev and having a half-width of 300 kev; this figure for the width was chosen because not all number–range histograms were as clean as that given in figure 1 A and the fit on the high-energy side of the $^{12}C(\gamma, p)$ peak taken over all the data is considerably better using 300 kev rather than the 250 kev mentioned in § 2.2. Comparison of the five independent observations shows them to be in good agreement within the expected statistical uncertainties. A total of 2947 complete tracks was measured and in the same volume of emulsion 110 complete carbon stars were observed. As a further check on the internal consistency of the work of the various observers the ratio of the tracks found in the range interval 5–50 microns to the number of carbon stars was determined and, as shown in table 2, agreement is good.

The number of tracks corresponding to the area contained by each gaussian in figure 2 was corrected for loss of tacks from the emulsions (Titterton 1955) and for the background from competing reactions discussed earlier to yield a

number $N(\gamma, p)$. The number of carbon stars in the same volume of emulsion, also corrected for loss, had to be further corrected since some are induced by

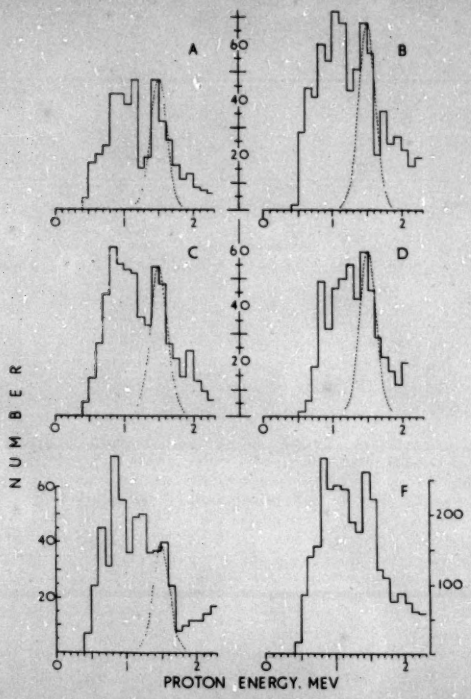

Figure 2. Corrected number–energy histograms derived for the five sets of data by treating all tracks as protons are shown in A, B, C, D, and E. The sum of all the data (with a change of scale) is shown in F. The proton peaks corresponding to the $^{12}C(\gamma, p)^{11}B$ reaction centre at 1·5 MEV.

14·8 MEV radiation; previous measurements in this laboratory showed that 90% of the carbon stars produced in emulsions are due to the 17·6 MEV line. If the corrected number of carbon stars is $N(\gamma, 3\alpha)$, then

$$\sigma(\gamma, p)_{17\cdot6} = \sigma(\gamma, 3\alpha)_{17\cdot6} \frac{N(\gamma,p)}{N(\gamma, 3\alpha)}. \qquad \ldots\ldots(1)$$

The values of $N(\gamma, p)/N(\gamma, 3\alpha)$ and their corresponding errors are given in table 2, the weighted mean being $7{\cdot}00 \pm 0{\cdot}73$ so that, in terms of the $^{12}C(\gamma, 3\alpha)$ cross section $\sigma_{17\cdot6}{}^{12}C(\gamma, p) = (7{\cdot}00 \pm 0{\cdot}73)\sigma_{17\cdot6}{}^{12}C(\gamma, 3\alpha)$.

§ 4. The Value of $\sigma_{17\cdot6}{}^{12}C(\gamma, p)^{11}B$ and Discussion of the Result

The reaction $^{12}C(\gamma, 3\alpha)$ has been studied intensively with both Li γ-rays and bremsstrahlung as sources of incident radiation. The wide spread of cross

section values which have been reported was discussed by Carver, Hay and Titterton (1955) and led these authors to remeasure the cross section at 17·6 MeV. They obtained $\sigma(\gamma, 3\alpha)_{17\cdot6} = (1\cdot70 \pm 0\cdot24) \times 10^{-28}$ cm^2, and using this value in equation (1) found the cross section for $^{12}C(\gamma, p)$ to be $(1\cdot19 \pm 0\cdot21) \times 10^{-27}$ cm^2, where the error is largely due to the uncertainty in $\sigma(\gamma, 3\alpha)$.

Table 2

(1)	(2)	(3)
A	$21\cdot6 \pm 4\cdot6$	$6\cdot7 \pm 1\cdot7$
B	$32\cdot7 \pm 6\cdot9$	$8\cdot0 \pm 1\cdot7$
C	$24\cdot2 \pm 4\cdot9$	$6\cdot3 \pm 1\cdot4$
D	$23\cdot0 \pm 4\cdot8$	$7\cdot3 \pm 1\cdot5$
E	$32\cdot1 \pm 7\cdot7$	$6\cdot3 \pm 1\cdot6$
Mean values	26·6	$(7\cdot00 \pm 0\cdot73)$ (weighted)

(1) Data; (2) tracks in interval 5–50 μ per carbon star; (3) $N(\gamma, p)/N(\gamma, 3\alpha)$.

The excitation function for the reaction $^{11}B(p, \gamma)^{12}C$ (in its ground state) up to a proton energy of 2·8 MeV has been measured by Huus and Day (1953) who found a resonance at an excitation energy of 17·2 MeV having a total width at half-maximum of 1·27 MeV. The absolute value for the cross section at the peak of the resonance was calculated by them under the assumption of an isotropic angular distribution. Gove and Paul (1955) have since determined the angular distribution to be anisotropic in the region of proton energies from 1·0 to 2·5 MeV, and also obtained a relative excitation function for the reaction which verifies the detailed shape of the broad resonance at 17·2 MeV. From these results it is possible using the principle of detailed balancing to compute the $^{12}C(\gamma, p)^{11}B$ cross section at 17·6 MeV as $(1\cdot09 \pm 0\cdot16) \times 10^{-27}$ cm^2 where the error is that of the $^{11}B(p, \gamma)$ absolute cross section.

The agreement between the two values of $\sigma(\gamma, p)$ is excellent and thus it appears that the measured cross sections for $^{11}B(p, \gamma)^{12}C$ and $^{12}C(\gamma, 3\alpha)$ are consistent within their stated errors.

Acknowledgments

We wish to thank Dr. F. C. Barker and Mr. I. F. Wright for a number of discussions and also members of the microscope group, Misses Lyons and Miller, Mesdames Nakunas, Strautmanis and Zsebehazy and Mr. T. A. Brinkley who carried out the larger part of the microscope work. One of us (A. K. M.) wishes to thank the U.S. Educational Foundation for the Fulbright Award which made his visit to Canberra possible.

References

Carver, J. H., Hay, H. J., and Titterton, E. W., 1955, *Phil. Mag.*, **46**, 841.
Ferguson, G. A., Halpern, J., Nathans, R., and Yergin, P. F., 1954, *Phys. Rev.*, **95**, 776.
Gove, H. E., and Paul, E. G., 1955, *Phys. Rev.*, **97**, 104.
Huus, T., and Day, R. B., 1953, *Phys. Rev.*, **91**, 599.
Jenkner, K., and Broda, E., 1949, *Nature, Lond.*, **164**, 412.
Johns, H. E., Horsley, R. J., Haslam, R. N. H., and Quinton, A., 1951, *Phys. Rev.*, **84**, 856.
Millar, C. H., and Cameron, A. G. W., 1953, *Canad. J. Phys.*, **31**, 723.

NABHOLZ, H., STOLL, P., and WÄFFLER, H., 1952 a, *Phys. Rev.*, **86**, 1043; 1952 b, *Helv. Phys. Acta*, **25**, 701.
ROTBLAT, J., 1950, *Nature, Lond.*, **165**, 823.
STOLL, P., 1954, *Helv. Phys. Acta.*, **27**, 395.
TITTERTON, E. W., 1955, *Progress in Nuclear Physics*, **4**, 1 (London: Pergamon Press).
TITTERTON, E. W., and BRINKLEY, T. A., 1949, *A.E.R.E. Report* No. G/R 326.
WÄFFLER, H., 1953, *Helv. Phys. Acta*, **26**, 785.
WÄFFLER, H., and YOUNIS, S., 1949, *Helv. Phys. Acta*, **22**, 616.
WRIGHT, I. F., MORRISON, D. R. O., REID, J. M., and ATKINSON, J. R., 1956, *Proc. Phys. Soc.* A, **69**, 77.

A Problem in Relativity Theory

By HERBERT DINGLE
104 Downs Court Road, Purley, Surrey

Communicated by Lord Halsbury; MS. received 20th June 1956 and in final form 22nd October 1956

Abstract. The paper analyses a form of the familiar 'clock paradox', in which two observers separate and re-unite, but in which the accelerations normally necessary at starting, reversing and stopping are eliminated, so that the problem lies wholly within the scope of the special theory of relativity.

The importance of the problem lies in the fact that it embodies all the essential principles of that theory, about which recent correspondence in *Nature* has shown much disagreement to exist. The points specially brought out are the following:

(1) The theory is not basically concerned with a comparison between different *observers* but between different *coordinate systems* which are available to a single observer.

(2) It is not basically concerned with a comparison between stationary and moving systems but between descriptions of a single system with respect to different arbitrarily chosen standards of rest.

(3) The familiar expression, 'time retardation', does not relate to a physical change experienced by a clock but to a comparison of times of an event by two clocks, at least one of which is not present at the event. When both are present the discrepancy vanishes. A similar remark applies to the 'Lorentz contraction' of moving rods.

In a recent correspondence in *Nature* (1956) the old problem of the 'clock paradox' was again discussed in relation to the recently recognized possibility that space travel at high velocities might become feasible some time in the future. It had been suggested by Sir George Thomson (1955), on the basis of a calculation by Professor W. H. McCrea (1951), that a traveller at uniform velocity to a star, on returning to the Earth, might find that he had 'aged' by $14\frac{1}{2}$ years, while terrestrial clocks would indicate that he had been absent for 17 years. I disputed McCrea's calculation and maintained that the traveller would have aged by the same amount as the terrestrial clocks indicated, except possibly for an infinitesimal amount which might be caused by the means adopted for accelerating him at the beginning, middle and end of his journey. The correspondence showed that it was very desirable to work out the problem in detail, but the space available in *Nature* was insufficient for this. This paper is, therefore, an attempt to do so on the basis of the special theory of relativity. It is hoped that it will make the essential nature of that theory clearer—a result which, whatever may be the truth of the matter, the variety of views expressed in the correspondence shows to be most necessary.

The essential part of McCrea's argument is as follows:

> "The observers R, M are initially at rest in an inertial frame F; R remains at rest; M moves directly away from R and travels for time T with uniform speed V in R's reckoning; M then comes to rest in F, remains at rest for time t, then returns to R, with the exact reverse of his

outward motion. The times during which M's speed is changing at the start and finish of his outward and return journeys, and the time t, are given and are independent of T. Whatever these times may be, we take T so great that they are negligible compared with T. Then the following statements can be made with negligible errors.

"At the event of M's completing the part of his outward journey performed with speed V, observer R plots M as at a distance $X(=VT)$ from himself. (We say 'plot' instead of 'see' to avoid complications about times of travel of light in the process of seeing.) Owing to the Lorentz contraction, M at the same event plots R as at distance αX from himself, when $\alpha=(1-V^2/\mathbf{c}^2)^{1/2}$. During the interval t when R, M are both at rest in F, they must each plot the other as at distance X. But as soon as M has again acquired uniform speed V, this time towards R, he again plots R as at distance αX.

"R's account of M's journey relative to himself is, still neglecting quantities small compared with X and T: M moves out and back through distance X at speed V; total time $2T$. On the other hand, M's account of R's journey relative to himself is: R moves out through distance αX at speed V, then R 'cheats' by rushing out to distance X and back again to distance αX in negligible time, and finally completes his return at speed V; total time $2\alpha T$. This is less than $2T$ and is the usual result.

"It does not matter which observer regards himself as at rest, and neither need know anything about inertial frames. All that is necessary is for an umpire to supply them with standard clocks and scales and to tell each to record a plot of the other's apparent motion. The whole point is that these plots will not be the same. There will be an unambiguous difference between the results which will involve no paradox."

McCrea, as will be seen, ignores the brief accelerations at the beginning, middle and end of the journey, and makes his calculations entirely in terms of formulae which are valid only when the motion is uniform. It would, therefore, seem that we are justified in considering this as a problem in special relativity only. Some, however, objected to this since the journey would not be possible without the accelerations, so I will substitute the following problem, suggested to me by Lord Halsbury, in which the uniform part of the motion is preserved without change, and the accelerations are not necessary and, in fact, do not occur.

Consider two clocks, A and B, situated respectively at the origins of the two coordinate systems assumed in the ordinary derivation of the Lorentz transformation formulae; i.e. they are in relative motion with uniform velocity V, and at the moment when they are at the same place they both read $t=0$; thereafter they recede from one another. A has an observer beside it, whom also we may call A without confusion; B is merely a clock. At some instant t_1 by A's clock he sends a beam of light (velocity $\mathbf{c}$) towards B and receives it back by reflection at a later instant t_3. It shows the reading of B at the instant when the light reaches B: call this t_2'. Now suppose a third clock, C, is approaching A from beyond B, and suppose that it reaches B at this instant t_2' and that it also reads t_2' at this instant, so that A sees this reading on the dials of both B and C. The problem is then: when C reaches A, will it agree with A or not?

Let us first of all consider the outward journey of B, from the time it leaves A to the time it meets C, as a problem by itself, and afterwards deal with the readings of C. We will consider this problem first from the pre-relativity point of view. At the instant t_1 let A be at A_1 and B at B_1. Now the course taken by the light will

depend on which of the two clocks is moving. If B is moving and A stationary, then the light will chase B, catch it at B_2, and return to A at A_1, so that its total path will be $2A_1B_2$. If, however, A is moving and B stationary, the light will reach B at B_1 and return to the retreating A at A_2, its total path being $A_1B_1 + B_1A_2$.

In case (1) the light travels, in time $t_2 - t_1$, a distance which B has travelled in time t_2 (t_2 is A's reading at t_2' by B, and $t_2 = t_2'$). Hence $(t_2 - t_1)/t_2 = V/\mathbf{c}$, whence

$$t_2 = t_2' = \frac{t_1}{1 - V/\mathbf{c}}, \qquad \ldots\ldots(1)$$

and

$$t_3 = t_1 + 2(t_2 - t_1) = t_1 \frac{1 + V/\mathbf{c}}{1 - V/\mathbf{c}}. \qquad \ldots\ldots(2)$$

In case (2) the light covers A_1B_1 in time $Vt_1/\mathbf{c}$, since $A_1B_1 = Vt_1$, so that

$$t_2 = t_2' = t_1(1 + V/\mathbf{c}). \qquad \ldots\ldots(1')$$

At this instant A is at a distance Vt_2 from B, so that by t_3 the light has to gain this distance over A. In unit time it beats him by $\mathbf{c} - V$, so it will do this in time $Vt_2/(\mathbf{c} - V)$. Hence

$$t_3 = t_2 + Vt_2/(\mathbf{c} - V) = t_1 \frac{1 + V/\mathbf{c}}{1 - V/\mathbf{c}}. \qquad \ldots\ldots(2')$$

We see, therefore, that while the light will return to A at the same time, no matter which clock is moving, the time it will show on B's dial will depend on which is the moving clock. This, in fact, would have been a perfectly good experiment to perform (if the practical difficulties were not insurmountable) to decide this point: it would have been the equivalent of the Michelson–Morley experiment in terms of clocks instead of measuring rods.

Now consider the problem in the light of the special theory of relativity. That theory rests first of all on the fact that the Michelson–Morley and all such experiments (and I do not think anyone will object to my including the one just described among these, although it has not actually been performed) do in fact fail to reveal which body is moving, but give the same result whatever motion we impose on the system as a whole. The first and most basic postulate of the theory, therefore, is that all observable phenomena connected with the relative motion of two bodies will be exactly the same however the motion may be supposed to be shared between them. In particular, if we suppose that one of them is at rest, then it does not matter which one that is; we must expect to observe exactly the same things in either case. But t_2' is an observable phenomenon, and the above discussion shows that, according to the ideas prevailing before 1905, its value must depend on whether it is A or B that is moving. Hence a second postulate is necessary in order to remove this requirement and justify the first postulate, that of the relativity of motion.

Einstein found scope for this second postulate in the fact, which he was the first to realize, that we had assumed without justification that the time at which a distant event occurred was something that had a meaning apart altogether from the means which we might adopt for discovering it; e.g., that t_2 was identical with t_2'. By denying the validity of this he gave himself the task of defining such a means, so as to satisfy the principle of the relativity of motion, i.e. he sought a definition of the means of timing an event, according to a clock which was not there, which would give the same result for all *observable* phenomena, however we supposed the relative motion of bodies to be shared between them. The foregoing calculation shows that this requires a definition in terms of t_1 and t_3, since these are the same whichever body we suppose to move, but the equivocal t_2 or t_2' must be excluded. Accordingly, Einstein's definition was this: Send a beam of light from the clock to the event and receive it back by reflection; then the time of its arrival at the event (or, in other words, the reading of an imaginary clock situated at the event and stationary with respect to the clock in question) is *defined* as the average of the times of its emission and return. If, then, you have two clocks in relative motion, and they are together when the light is emitted, they will not be together when it returns. They will receive it at different times, and so the times which they will assign to the event will be different.

This definition, therefore, made the time of an event, according to a clock not present at it, something which, *by definition*, depended on the motion of the clock, and since there was no way of giving an absolute meaning to the motion of a clock, there was no absolute meaning in the time of the event; it was always relative to the motion of the clock to whose time system it belonged. By a well-known calculation, which there is no need to repeat, this definition led to the Lorentz transformation equations and to the following rule for comparing the readings of relatively moving clocks: If two clocks are in relative motion you can divide the motion between them as you like, but each clock must then be regarded as running slow by the factor $\alpha=(1-V^2/c^2)^{1/2}$, where V is the velocity which you assign to it, as compared with a clock regarded as having no motion.

It is obvious from its derivation that this 'time retardation' or 'time dilatation', as it has been called, is not a physical change which a clock suffers. By changing your mind about the velocity of the clock (in technical language, changing the coordinate system) you automatically change its 'rate', because its 'rate', depending on its motion, must, like its motion, be a matter of arbitrary choice. There is no actual change of rate, but the convention for synchronizing clocks is such that the difference between the reading of a moving clock and that of an adjacent clock synchronized with a stationary one elsewhere is just what it would be if the moving clock had run slow. This was, of course, extremely startling at the time when it was first announced, but it did, in fact, achieve its object of making *observable* phenomena independent of your choice. The only prejudices that were violated were those which could not be tested by observation—not because they were too difficult to test but because a test was in the nature of things impossible. Let us apply the postulate to our clocks A and B.

We note first of all that the above diagram is now meaningless because we cannot distinguish A_1 from A_2 or B_1 from B_2 by any possible observation. We can, however, assume which clock we please to be at rest, so our previous calculations hold, provided that the clock which moves is supposed to run slow by the factor α. In case (1) (B moving), therefore, our calculation is correct for t_2, but

t_2', the time which the moving B shows for the same event, will be $t_2\alpha$, i.e.

$$t_2' = t_1\alpha/(1 - V/\mathbf{c}) = t_1\left(\frac{1+V/\mathbf{c}}{1-V/\mathbf{c}}\right)^{1/2}. \qquad \ldots\ldots(3)$$

In case (2) B will show the 'right' time, but to get that from A we must divide A's readings by α, so that for t_1 we must substitute t_1/α. Hence, from (1'),

$$t_2' = \frac{t_1}{\alpha}(1 + V/\mathbf{c}) = t_1\left(\frac{1+V/\mathbf{c}}{1-V/\mathbf{c}}\right)^{1/2}. \qquad \ldots\ldots(3')$$

Einstein's definition, therefore, does ensure that this experiment will not distinguish between the two cases, and requires that the reading of B which A will observe will be that given by (3) and (3'). I have no doubt that this would be verified if the experiment could be performed. The value of t_3 is not important, and to save space I will merely state (it can easily be verified) that in both cases it agrees with the pre-relativity value.

(It is of interest to note—the calculation is simple—that if this experiment had been performed before the relativity theory was thought of, and if the value of t_2' given by (3) had been obtained, the conclusion would have been that the bodies A and B would have been moving in opposite directions with equal velocity, if that velocity were small compared with $\mathbf{c}$. This would have been so in whatever direction the relative motion occurred, so the observers would have been faced by as great an *impasse* as that presented by the Michelson–Morley experiment. If the relative velocity were near $\mathbf{c}$, however, most of the motion would have been found to belong to B, and at $\mathbf{c}$ B would have been found to possess that velocity and A to be stationary. This would have agreed with the straightforward interpretation of the Michelson–Morley experiment, A being the Earth. It is fortunate that these experiments were not possible when the rivalry between the Ptolemaic and Copernican theories of celestial movements was a living question.)

Before proceeding to the second half of the problem I would point out two things. First, this calculation shows that the essential principles of relativity do not depend on comparing the readings of different *observers*. Only one observer has been assumed throughout. This conforms to the actual facts. In the Michelson–Morley experiment, for instance, we have only one observer—a terrestrial one—and this is true of all the relevant experiments. Secondly, it is not a matter of comparing two different situations, in one of which a clock is moving while in the other it is stationary. One single situation alone is in question, the difference in the two cases being merely in a *supposition*, namely, which clock we consider to have moved. Everything *observable* is the same in both cases; it is only in unobservable (i.e. purely conventional) distinctions that there is any difference.

This really settles the problem of the space traveller, for if his clock on return differs from the terrestrial clock, then something must have happened to one that did not happen to the other. But this analysis shows that the 'retardation' can be assigned to whichever we please without affecting anything observed. It cannot therefore, make one clock differ from the other.

It is most instructive, nevertheless, to consider the second part of the problem. I repeat that t_2—the time which a clock at B synchronous with A would show when B reads t_2'—is essentially unobservable. Its value can be determined only by applying our definition, and on doing so we find, as will be shown immediately,

that it requires that t_2 for B differs from the corresponding reading (let us call it T_2) for C, although B and C are at the same place and reading the same time, because one is receding from and the other approaching A. It requires further that T_2 shall be as much behind t_2' as t_2 is ahead of it; or, in other words, that at the moment when B and C are coincident, C is fast by the same amount as B is slow as compared with A. This, of course, would be impossible if t_2 and T_2 corresponded to anything objective in nature: the whole essence of Einstein's achievement is the realization that they do not. We can discover their values only by the process laid down. That this does indeed require that an approaching clock may be fast while a receding clock, at the same place and showing the same reading, is slow, may be seen by applying it.

Consider three clocks, B_1, C_1, D_1, which, at the common reading $t=0$, are together and such that, if D_1 is regarded as being at rest, B_1 and C_1 are moving in opposite directions, each with uniform speed V with respect to D_1. If these clocks are respectively at the origins of coordinate systems of which the x axes all lie along the line of motion and are positive in the direction towards which C_1 is moving, then these systems are related by the Lorentz transformation. There is a fourth clock A_1 at rest at the point $(x, 0, 0)$ in the D_1 system, and at the event $E_1' = (x, 0, 0, -x/\mathbf{c})$ in that system let it emit a beam of light which, on reaching D_1, is reflected back again to A_1, clearly reaching it at the event $E_2' = (x, 0, 0, x/\mathbf{c})$ in the D_1 system. By the Lorentz transformation, $E_1' = (x\beta, 0, 0, -x\beta/\mathbf{c})$ in the B_1 system and $(x/\beta, 0, 0, -x/\mathbf{c}\beta)$ in the C_1 system, where $\beta = [(1-V/\mathbf{c})/(1+V/\mathbf{c})]^{1/2}$, while $E_2' = (x/\beta, 0, 0, x/\mathbf{c}\beta)$ in the B_1 system and $(x\beta, 0, 0, x\beta/\mathbf{c})$ in the C_1 system. Hence, by Einstein's criterion, the time of the event E_2', at which the light falls on D_1, will be 0 in the D_1 system, $\frac{1}{2}(-x\beta/\mathbf{c}+x/\mathbf{c}\beta)$ in the B_1 system, and $\frac{1}{2}(-x/\mathbf{c}\beta+x\beta/\mathbf{c})$ in the C_1 system. Since D_1 is at rest with respect to A_1, D_1 is synchronized with A_1 if it actually reads 0 at this event. Let this be so. Then, by hypothesis, B_1, C_1 and D_1 will be coincident and will all read 0 at the event E_2'. Hence B_1 will be slow and C_1 fast by the same amount, viz. $x(1/\beta-\beta)/2\mathbf{c}$, at the event E_2'.

Now this corresponds to our problem, with A_1, B_1 and C_1 standing for A, B and C respectively. B and C both read the same when the light falls on them, and B, which is related with A by the Lorentz transformation, is slow, so C is fast by the same amount. Hence it must agree with A when the two clocks meet, for since it travels to A over the same distance (in the A system) and at the same speed as B travelled from A, it will lose the same amount on the journey, which is the amount by which it is fast at the beginning of that journey.

Some correspondents have objected to the discussion of the problem in terms of Einstein's original definition of synchronism, and have maintained that the whole thing becomes clear when the world-lines of the clocks are drawn in a Minkowski diagram. I, therefore, append such a diagram in which, in order to keep the axes rectangular, I have substituted $T=ict$ for the time axis throughout. The world-lines of the clocks A, B, C are then respectively OT_A, OT_B and $O'T_C$, and the axes of coordinates are (OX_A, OT_A), (OX_B, OT_B), $(O'X_C, O'T_C)$, where O′ is some point on the world-line of C which it is unnecessary to determine. Consider, then, the event P, which is the meeting of the clocks B and C. The clock reading of A which is simultaneous with this event is given in the A-system by OL, in the B-system by OM, and in the C-system by ON. It is obvious that LM = LN, i.e. that C will regard A as

being fast by the same amount that B will regard it as being slow. Reciprocally, of course, A will regard C as being fast by the same amount that he regards B as being slow. The symmetry of the diagram makes the rest of the argument obvious. This is certainly simpler than the algebraic treatment, but it is more mathematical and less physical, and, while agreeing that it should give the same result (as it does), I prefer the treatment in which one keeps the actual physical circumstances in sight all the time.

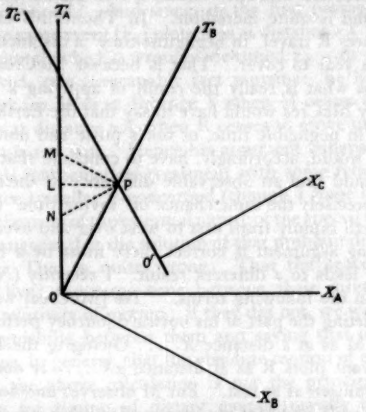

This fact, that two clocks which read the same at the same place may at that moment be respectively behind and ahead of a distant third clock, is one of the most surprising and least familiar consequences of Einstein's theory. It is utterly unintelligible if we suppose the times all to have an absolute meaning, and even when some of them are recognized to be conventional it is not easy to realize without an analogy that the phenomenon is really quite simple and natural. Unfortunately, a perfect analogy is hard to find, but a pretty close one is provided by the case of two identical travellers who set out at equal speeds along a parallel of latitude in opposite directions from the Greenwich meridian. When they reach the International Date Line their clocks, heart beats, etc, will show exactly the same advance over their starting values, but one will be a day ahead, and the other a day behind, the calendar date. When they meet again at longitude 0° they will find that in spite, or rather because, of the opposite changes which they have made in their calendars, the calendars still agree with those of their home-keeping friends, and that their clocks (assuming, of course, that they have not been altered) show the same number of hours to have elapsed during the journeys. The purely conventional calendar may be altered as we please in order to avoid confusion, but watches, clocks and human bodies are quite unaffected by such changes. The calendar change which we do make (or one of a number of trivial variations of it) is, in fact, the only one which would avoid confusion, and in the same way Einstein's conventional definition of distant times is probably the only one which would avoid confusion, but it remains a convention, and the apparently magical changes which occur are merely the results of applying the convention.

Whether it is Wednesday or Thursday at a certain place at a given moment depends on where we draw the Date Line, and this is at our choice; it is quite independent of what our clocks do.

The sudden change from being slow to being fast which occurs when we turn our attention from B to C (or, in McCrea's problem, when M turns round at the end of his outward journey) is the process which McCrea describes as 'cheating'. As a result of applying a convention it is intelligible, notwithstanding its surprising character, but McCrea's account violates a well-known requirement of special relativity theory and is quite incredible. In Thomson's example, for instance, it means that M sees R travel 'in negligible time' a distance which it would take light more than a year to cover. That is because McCrea wrongly regards as a physical process what is really the result of applying a convention. In the Date Line analogy McCrea would have to say that the Earth had suddenly made an extra rotation in negligible time, or one's pulse had done something equally startling, and he would, accordingly, have to conclude that when the travellers re-united they would find an observable difference in their physical condition. In fact, we have precisely the same chance of 'saving time' by space travel as by traversing the Earth rapidly from east to west over and over again.

If the foregoing argument is correct there must be a mistake in McCrea's calculation, for it leads to a different result. I recently (*Nature* 1956) pointed out this mistake in the following terms. "He [McCrea] writes: 'At the event [E_1] of M's completing the part of his outward journey performed with speed V, observer R plots M as at a distance X.... Owing to the Lorentz contraction, M at the same event plots R as at distance αX.... It does not matter which observer regards himself as at rest.' But M observes *another* event, E_2, at which R's uniform travel ends, and McCrea later confirms that it is at E_2 that R's distance is αX. Hence he connects R's estimate for one pair of events (E_0 and E_1, where E_0 is the event of R and M beginning their separation with velocity V) with M's for another (E_0 and E_2) by the 'Lorentz contraction', which is clearly wrong."

McCrea replied to this as follows (*Nature* 1956). "The pairs of events named by Dingle are not simultaneous in the reckonings of the respective observers and so are not pairs that can be directly connected by the Lorentz contraction; reference to my work will make it at once obvious that I did not apply the procedure directly to these pairs. On the other hand, if Dingle means merely that I used the contraction in the course of connecting these events, that is all right." The first sentence implies that only events which are simultaneous in the reckonings of different observers can be directly connected by the Lorentz transformation. The special theory of relativity, however, has the following requirements: (1) An event is uniquely characterized by four coordinates. (2) These coordinates vary from one coordinate system to another. (3) If two coordinate systems are in uniform relative motion the coordinates of an event, and the coordinate separations of specific pairs of events, in these two systems are directly connected by the Lorentz transformation, no matter whether the events concerned are simultaneous (i.e. have the same value for the fourth coordinate) or not. (4) The coordinate separations of *different* pairs of events are not connected by the Lorentz transformation, directly or indirectly.

My second comment, which is the really relevant one, concerns McCrea's statement that he did not apply the 'Lorentz contraction' directly to deduce

M's estimate of the space interval between E_0 and E_2 from R's estimate of the space interval between E_0 and E_1. The passage I have quoted shows that he gives the latter estimate as X. Later, in the same letter, he states: "M's account of R's journey relative to himself is: R moves out through distance αX at speed V, *then* [my italics] R 'cheats' by rushing out to distance X and back again to distance αX in negligible time". In other words, M plots R as at distance αX at the event which I have called E_2. If this value, αX, is not obtained by applying the 'Lorentz contraction' to R's distance X between E_0 and E_1, how is it obtained? And since, in the first passage quoted, McCrea states that "M at the same event [E_1] plots R as at distance αX", how is it possible to avoid the conclusion that he has wrongly identified E_2 with E_1? But, however the matter be viewed, this inescapable fact remains: he has not legitimately proved that if R reckons M as at distance X when M ceases to move uniformly, M will reckon R as at distance αX when R ceases to move uniformly. Nor can he do so, because it is not true. Hence his argument collapses.

I have given this mathematical treatment with some reluctance so far as the problem of the space traveller is concerned (though I hope it will help towards a much needed clarification of the essential nature of the special theory of relativity), because it tends to suggest that the solution of that problem depends on the result of the calculation. That is quite wrong. That the space traveller and the earthbound man 'live' the same time between their meetings is guaranteed by the principle of relativity of motion; if they did not, we would have a physical criterion for distinguishing between them and saying that one had moved and the other had not (or, in general, that the absolute motion of each was so-and-so). What is tested by the above calculation is not the principle of relativity but Einstein's criterion for timing of distant events (usually called the principle of the constancy of velocity of light), which, I repeat, is meant to ensure that no calculation shall lead us to expect a violation of the principle of relativity. To refute the principle of relativity we would need an *experimental* proof that the men had 'lived' different times, for the principle rests on universal experience, not on a mathematical theorem. It is satisfactory that Einstein's criterion has stood the test, but it has already received such abundant confirmation that we would be almost as much surprised if it ever failed as we would be if the Date Line device failed to reconcile the calendars of travellers who had chosen some peculiar routes round the Earth.

It may not be superfluous to add that it is now possible to put the special theory of relativity on a simpler axiomatic basis than that which, for historical reasons, naturally presented itself to Einstein. By generalizing the definition of length measurement from L (the length of a body as measured by a relatively stationary scale) to $L(1 - V^2/\mathbf{c}^2)^{1/2}$, where V is whatever velocity may be assigned to it, the whole theory follows. This I have tried to show elsewhere (Dingle 1940). The reason why this simplifies the theory is that length is the only completely independent measurement in Newtonian physics, all other measurements depending on it in some degree. A further advantage of this treatment is that when the theory is re-expressed in the Minkowski form, in terms of 'space–time', it at once becomes clear that the reason why space and time are so united in the theory is that the definition of time measurement implied (based on the constancy of the velocity of light) necessarily makes time measurement share the same generalization as space measurement in order to preserve this constancy. The

way then becomes open for a similar treatment of other essentially relative phenomena—e.g. temperature radiation—by a similar mathematical technique. There are rich harvests waiting here for those with the necessary mathematical attainments; but it will be necessary to understand the theory of the relativity of motion before they can be reaped.

References

DINGLE, H., 1940, *The Special Theory of Relativity*, 1st Edn. (London : Methuen)
MCCREA, W. H., 1951, *Nature, Lond.*, **167**, 681.
Nature, 1956, *Nature, Lond.*, **177**, 782, **178**, 680.
THOMSON, SIR GEORGE, 1955, *The Foreseeable Future* (Cambridge : University Press), p. 89.

A Problem in Relativity Theory : Reply to H. Dingle

By W. H. McCREA
Royal Holloway College, University of London

MS. received 16*th November* 1956

THE problem treated by Professor Dingle is an old one. The correct solution was published, for instance, by Ives (1951).

I have already replied to Dingle's criticisms (McCrea 1956 a, b). Here I need only call attention to their character. Dingle quotes a passage (McCrea 1951) in which I discuss what an observer would " ' plot ' instead of ' see ' to avoid complications about times of travel of light in the process of seeing ". Dingle criticizes my conclusion by applying it to Thomson's example as though it concerns what " M *sees* R " doing (my italics). Again, Dingle quotes a passage (McCrea 1956 b) in which I refer to events " that can be directly connected by the Lorentz contraction " and in which I was replying to his objection to my use of the *contraction*. In his present criticism he substitutes the Lorentz *transformation* for the contraction. His criticisms are thus based upon mis-readings.

References

IVES, H. E., 1951, *Nature, Lond.*, **168**, 246.
MCCREA, W. H., 1951, *Nature, Lond.*, **167**, 680; 1956 a, *Ibid.*, **177**, 784; 1956 b, *Ibid.*, **178**, 681.

RESEARCH NOTES

Many-Particle Systems : II

By H. R. POST

Department of Physics, Chelsea Polytechnic, London

MS. received 5th June 1956 and in final form 24th September 1956

In a previous publication (Post 1953) the many-identical-particle problem was solved in the case of a particular pair-force interaction. We now propose to deal with the general problem.

The general equation for n identical particles interacting by pair forces is (in suitable units)

$$-\left[\nabla^2-\sum_{i,j}{}' V_{ij}(x_i-x_j)\right]\psi\equiv H\psi=E\psi \qquad \ldots\ldots(1)$$

in one-dimensional laboratory space (or similarly in terms of $|\mathbf{r}_i-\mathbf{r}_j|$ for central forces in three-dimensional space) where V_{ij} is the pair potential between particles i and j and $\nabla^2\equiv\Sigma_i{}^n(\partial^2/\partial x_i{}^2)$; but $\nabla^2\equiv\Sigma_i{}^n(\partial^2/\partial\xi_i{}^2)$ where the ξ_i's are a set of normal coordinates including $\xi_1\equiv \mathrm{X}$, the centre-of-gravity coordinate, $\xi_2\equiv(1/\sqrt{2})(x_1-x_2)$ (for particles of equal masses, $m=1$), and

$$\xi_i\equiv\frac{1}{[i(i-1)]^{1/2}}\left\{\left(\sum_{r=1}^{r=i-1}x_r\right)-(i-1)x_i\right\}\text{ etc.} \qquad \ldots\ldots(2)$$

Then excluding the centre-of-gravity dependence we can write the equation (1)

$$-\left[\sum_2^n\frac{\partial^2}{\partial\xi_i{}^2}-\sum_{i,j}{}' V_{ij}\right]\psi=E\psi$$

or

$$-\int\psi^*\left\{\sum_2^n\frac{\partial^2}{\partial\xi_i{}^2}-\sum_{i,j}{}' V_{ij}\right\}\psi\,d\mathscr{V}=\min=E \qquad \ldots\ldots(3)$$

where $\mathscr{V}$ is the volume of integration over the whole of $\xi_2\ldots\xi_n$ coordinate space (the Jacobian with respect to x-space being unity, the transformation matrix being orthogonal).

Now

$$\int\psi^*V_{ij}\psi\,d\mathscr{V}\equiv\overline{V}_{ij}=V_{12}$$

for the symmetric problem (i.e. identical particles), but $V_{12}\equiv V_{12}\{\sqrt{2}\xi_2\}$; therefore

$$\overline{V}\equiv\sum\overline{V}_{ij}=\tfrac{1}{2}n(n-1)\overline{V}_{12}=\tfrac{1}{2}n(n-1)\int\psi^*V_{12}\{\sqrt{2}\xi_2\}\psi\,d\mathscr{V} \qquad \ldots\ldots(4)$$

but also

$$\overline{(\partial^2/\partial\xi_i{}^2)}=\overline{(\partial^2/\partial\xi_2{}^2)} \qquad \ldots\ldots(5)$$

for the symmetric problem (see Appendix I).

Hence we can write

$$-\overline{H}=(n-1)\,\overline{\frac{\partial^2}{\partial\xi_2{}^2}}-\tfrac{1}{2}n(n-1)\;\overline{V}_{12}(\sqrt{2}\xi_2) \qquad \ldots\ldots(6)$$

and the symmetric n-particle problem reduces to

$$-(n-1)\int \psi^* \left\{ \frac{\partial^2}{\partial \xi_2^2} - \tfrac{1}{2} n V_{12}(\sqrt{2}\xi_2) \right\} \psi \, d\mathcal{V} = E = \min$$

where $\mathcal{V}$ is the integration volume in $\xi_2 \ldots \xi_n$ space.

This reduction can similarly be carried out for three-dimensional laboratory space.

The admissible trial functions are restricted to those either totally symmetric or totally antisymmetric in particle indices (we are not introducing spin), i.e. to eigenfunctions of the operator

$$(1+P_{12})(1+P_{13}+P_{23})\ldots[\mathrm{S}] \quad \text{or} \quad (1-P_{12})(1-P_{13}-P_{23})\ldots[\mathrm{A}]$$

respectively.

Thus we can at once set a *lower* limit to the energy eigenvalue by evaluating the eigenvalue corresponding to the minimum of

$$-\int \psi^*(\xi)\Theta_\xi \psi(\xi)\, d\xi \quad \text{where} \quad \Theta_\xi \equiv (n-1)\left\{ \frac{d^2}{d\xi^2} - \tfrac{1}{2} n V_{12}(\sqrt{2}\xi) \right\}.$$

On the other hand, we can set an *upper* limit by evaluating the minimum of

$$-\int\int \ldots \int \psi^*(\xi_2^2+\xi_3^2+\ldots\xi_n^2)\Theta_{\xi_2}\psi(\xi_2^2+\xi_3^2+\ldots\xi_n^2)\, d\xi_2\, d\xi_3 \ldots d\xi_n$$

in the case of the totally symmetric problem. For the exact solution of the symmetric three-particle problem we have to restrict our trial functions to the space spanned by the set

even parity	odd parity
H_0^0	
$H_0^2+H_2^0$	$H_0^3-\sqrt{3}H_2^1$
$H_4^0+2H_2^2+H_0^4$	

and subsequent higher degree eigenfunctions of the S operator:

$$1+P_2\{\xi_2 \to \tfrac{1}{2}(\xi_2+\sqrt{3}\xi_3),\ \xi_3 \to -\tfrac{1}{2}(\xi_3-\sqrt{3}\xi_2)\}$$
$$+P_3\{\xi_2 \to \tfrac{1}{2}(\xi_2-\sqrt{3}\xi_3),\ \xi_3 \to -\tfrac{1}{2}(\xi_3+\sqrt{3}\xi_2)\}.$$

Here H_m^n denotes the mth (even) order Hermite function in ξ_2 and n denotes the direction of the Hilbert vector in ξ_3 space. [Thus H_m^n stands for $H_m(\xi_2)H_n(\xi_3)$.] These are a set of functions to be applied universally to all symmetric three-particle problems for any interaction potential.† (In any particular problem these functions may be expressed in terms of eigenfunctions ϕ of the problem $\Theta\phi = E\phi$ to facilitate the process of minimization.‡)

For the n-particle problem we can similarly choose to express the admissible functions in Hermite functions. In the antisymmetric case the first admissible function consists of terms whose Hermite indices each add up to $\frac{1}{2}n(n-1)$. The next higher degree is not admissible.

† The degree $n+m$ is invariant to S since there exists a symmetric operator with eigenvalues $n+m$. m must be even to fulfil 1–2 symmetry.

‡ It may be of interest that a many-body potential of the type

$$V\,|\,x_1+x_2-x_3-x_4\,|+V\,|\,x_1-x_2-x_3+x_4\,|+V\,|x_1-x_2+x_3-x_4\,|$$

leads immediately to ' shell structure '

$$\phi_r(x_1+x_2-x_3-x_4)\,\phi_s(x_1-x_2-x_3+x_4)\,\phi_t(x_1-x_2+x_3-x_4).$$

Shells, after all, do not necessarily imply separation in *individual* particle coordinates.

Appendix I

Proof of Relation (5)

The x-coordinate vector is transformed into the ξ-coordinate vector

$$\begin{bmatrix} \xi \\ . \\ . \\ . \\ . \end{bmatrix} \equiv (A) \begin{bmatrix} x \\ . \\ . \\ . \\ . \end{bmatrix}$$

by the matrix A, where A is an orthogonal matrix (the ξ's being normal coordinates) so that $A^{-1}=\tilde{A}$.

Moreover, the sum of the elements of any row (except the first) in A is zero (see equation (2)). This follows from the orthogonality to X. Hence the sum of the elements in any column (except the first) in A^{-1} is zero.

But this means that in the transformation

$$\frac{\partial^2}{\partial \xi_i^2} \equiv \sum_l \mathscr{A}_{li}^2 \frac{\partial^2}{\partial x_l^2} + \sum_{m,n}{}' \mathscr{A}_{mi}\mathscr{A}_{ni} \frac{\partial^2}{\partial x_m \partial x_n}$$

for $i>1$

$$\sum_l \mathscr{A}_{li}^2 = -\sum_{m,n}{}' \mathscr{A}_{mi}\mathscr{A}_{ni} \text{ since } \left(\sum_l \mathscr{A}_{li}\right)^2 = 0, \qquad \ldots\ldots(7)$$

so that

$$\overline{\frac{\partial^2}{\partial \xi_i^2}} = \overline{\frac{\partial^2}{\partial x_k^2}} - \overline{\frac{\partial^2}{\partial x_l \partial x_m}}$$

Thus $\overline{\partial^2/\partial \xi_i^2}$ is the same for all $i>1$, because the expectation values of all cross derivatives and of all second derivatives are independent of indices for symmetric (or antisymmetric) ψ's, and the total weight factors have been shown to be numerically equal, but of opposite sign, above (7), for the two types of sums (they are actually unity for all i since A is an orthogonal matrix).

Appendix II

We discuss some n-particle systems with interaction potentials $V_{ij}=x_{ij}{}^k$.

The case $n=3$, $k=4$, is soluble directly. Since there is one and only one translation invariant totally symmetric polynomial of degree four, we can see at once that $V \equiv V(r)$ where $r \equiv \xi_2{}^2+\xi_3{}^2$. This also shows that the energetically lowest state is totally symmetric in the spatial coordinates of the three particles (this becomes relevant when we go to the more general case introducing spin). For a given r-dependence of ψ the energy is, in fact, a monotonic function of l, characterizing the ϕ-dependence of the solutions, viz. $\cos 3l\phi$, where ϕ is $\tan^{-1}(\xi_2/\xi_3)$.

We can extend this to three dimensions by noting that the arguments are formally the same on replacing x_i by $\mathbf{r}_i$.

For $n=4$, $k=4$, we can regard the potential energy term as a superposition of the overall potential $V(r)$ resisting homogeneous expansion in the single scale argument $r \equiv \xi_2{}^2+\xi_3{}^2+\xi_4{}^2$, and the *uncoupled* potentials in the normal coordinates $x_1+x_2-x_3-x_4$ etc. (as in footnote p. 937‡), each, of course, of power 4.

The case $k=2$ has been solved previously (e.g. Post 1953). The case $k=-2$ is also separable, but does not lead to bound states (just as for $n=2$).

Reference

Post, H. R., 1953, *Proc. Phys. Soc.* A, **66**, 649.

On the Multiple Spin Wave Scattering of Neutrons in Ferromagnets

By R. J. ELLIOTT†, R. D. LOWDE‡ and W. MARSHALL‡
† Physics Department, Reading University
‡ Atomic Energy Research Establishment, Harwell

MS. received 27*th June* 1956

THIS subject was mentioned in an earlier paper (Elliott and Lowde 1955, hereafter called II, § 1.4) where the cross sections for single spin wave scattering were derived using the Holstein–Primakoff (1940) formalism. In discussing the experimental results (Lowde 1956) it was found desirable to have some further details of the multiple scattering process. Unfortunately it is very difficult to treat the Heisenberg model of a ferromagnet in an approximation which allows the cross sections for these processes to be calculated. The Holstein–Primakoff notation is not adequate for such a treatment (Marshall 1955). Nevertheless, provided we accept the validity of the concept of spin waves at the temperatures where multiple processes are important (but see Dyson 1956) it is possible to draw certain conclusions on quite general grounds.

In the notation of the earlier papers, $d_\lambda{}^*$ and d_λ are respectively the creation and destruction operators for a spin wave λ. The n-quantum scattering process is associated with terms in the interaction potential of order n in the d's, with some coefficient that we cannot trust the Holstein–Primakoff formalism to give correctly. The cross section for a particular process is readily obtained by the method of II and contains a factor $N_{\lambda_1}N_{\lambda_2}\ldots N_{\lambda_n}/N^nS^{n-2}$, N_{λ_n} being the number of spin waves λ_n. However, the number of processes contributing to the differential n-quantum cross section $\sigma(n)$ increases like N^n, so that $\sigma(n+1)/\sigma(n)\sim N_{\lambda_n}/S\sim T/T_c$. Thus at higher temperatures the sequence of differential cross sections does not converge very rapidly.

Furthermore, unlike the situation with multiple phonon scattering, the type of process which can take place in a simple Heisenberg ferromagnet is severely limited because the total Z component of spin must be conserved. If in the Hamiltonian other terms besides exchange are included this statement is still correct to order $(B_\lambda/A_\lambda)^2$ (see II, § 2). Thus, for example, the only two-quantum processes allowed to an appreciable extent are those of the type $d_\lambda{}^*d_\mu$ which involve one creation and one destruction; the permissible three-quantum processes—$d_\lambda{}^*d_\mu d_\nu$ and $d_\lambda{}^*d_\mu{}^*d_\nu$—are those which change the total number of spin waves by unity, and so on.

A study of the geometry of the processes involving multiple spin wave scattering shows that this limitation to certain allowed processes leads to scattering more diffuse than would otherwise be expected. For instance, in the two-spin wave case the scattering solids for $d_\lambda{}^*d_\mu$ and for $d_\lambda d_\mu$ processes are entirely different. Reflections of the former type, which are exceedingly diffuse, are allowed, while those of the latter type which are comparatively sharp are forbidden. With this geometrical factor it is, therefore, not possible to show that $\sigma(n)\gg\sigma(n+1)\gg\sigma(n+2)$ unless $T\ll T_c$. However, the diffuse nature of $\sigma(2)$, $\sigma(3)$, etc. means that $\sigma(1)$ will dominate at positions close to Bragg setting for larger values of T/T_c than might otherwise be expected.

Finally, it can be shown directly from the form $(\mathbf{s}.\mathbf{S}_l)-(\mathbf{e}.\mathbf{s})(\mathbf{e}.\mathbf{S}_l)$ of the interaction potential (Halpern and Johnson 1939, § 6) that the even-order processes coming from terms in S_l^z depend on the directions $\mathbf{x}$ of the magnetization and $\mathbf{e}$ of the scattering vector, like $1-(\mathbf{e}.\mathbf{x})^2$, while the odd-order processes coming from terms in S_l^x and S_l^y are like $1+(\mathbf{e}.\mathbf{x})^2$. Thus at low temperatures the single processes with a $1+(\mathbf{e}.\mathbf{x})^2$ dependence are dominant and this remains true at somewhat higher temperatures close to Bragg setting. The multiple processes probably have an overall dependence more like $1-(\mathbf{e}.\mathbf{x})^2$ than $1+(\mathbf{e}.\mathbf{x})^2$.

References

Dyson, F. J., 1956, *Phys. Rev.*, **102,** 1217, 1230.

Elliott, R. J., and Lowde, R. D., 1955, *Proc. Roy. Soc.* A, **230,** 46.

Halpern, O., and Johnson, M. H., 1939, *Phys. Rev.*, **55,** 981.

Holstein, T., and Primakoff, H., 1940, *Phys. Rev.*, **58,** 1098.

Lowde, R. D., 1956, *Proc. Roy. Soc.* A, **235,** 305.

Marshall, W., 1955, *Proc. Roy, Soc.* A, **232,** 69.

REVIEWS OF BOOKS

Kernmomente, by H. KOPFERMANN. 2nd Edn. Pp. xvi+462. (Frankfurt: Akademische Verlagsgesellschaft, 1956.) DM.54.

The first edition of this book appeared during the last war and is probably most widely known in the lithoprinted form in which it was republished by the U.S. government in 1945. Many physicists must have been eagerly looking forward to the publication of a further edition which would include the numerous important new developments in the field. The book in its new form, almost twice the size of the old one, will certainly not disappoint them. The author has done full justice to the new material by giving a thorough discussion of the underlying theories as well as the experimental methods. He has also used the opportunity of a new edition for improving and extending existing sections.

The theoretical treatment has, as far as possible, been based on a classical approach and the correspondence principle, but the essential steps in the rigorous, quantum-mechanical calculations are briefly and clearly described and, of course, their results given; only a very moderate knowledge of theoretical methods is thus required for the understanding of the text.

The first chapter deals with free atoms and is described by the author as the core of the book. It contains a survey of the theory of electrostatic and magnetic interactions in atoms and of transitions between the energy levels, describes atomic beam methods, optical methods of high resolution, the calculation of nuclear magnetic moments and quadrupole moments, and isotope effects.

The second chapter deals with investigations of nuclear moments from spectra of free molecules. The theory and term structure of diatomic and polyatomic molecules is described, including hyperfine structures and effects due to external magnetic and electric fields. Optical spectroscopy of molecules, microwave spectroscopy and molecular beam resonance methods are treated in considerable detail.

Investigations of nuclear moments in liquids and solids form the subject of the third chapter. The headings of the main sections are: nuclear resonance, quadrupole resonance, paramagnetic resonance.

The fourth chapter discusses the interpretation of nuclear moments and isotope shifts in terms of nuclear models. The theories of the individual particle model and of the collective model are outlined and compared with the experimental results.

Tables of nuclear spins, magnetic moments and quadrupole moments, and some tables of relativistic and diamagnetic corrections form a most useful appendix; there is an extensive list of references.

In writing this book Professor Kopfermann has made a further addition to his important contributions to the subject of nuclear moments; he has earned the gratitude of those working in the field and especially those who are entering it and are trying to acquaint themselves with the great variety of experimental techniques and theoretical methods. To those who are not familiar with the language it will be good news that an English translation is expected to appear shortly.

H. G. KUHN.

Atoms and the Universe, by G. O. Jones, J. Rotblat and G. J. Whitrow. Pp. 254. (London: Eyre and Spottiswoode, 1956.) 25*s*.

This is an interesting but strangely uneven book. It deals mainly with recent advances in the fields of nuclear physics and of astrophysics—with the almost unimaginably small and almost unimaginably vast. These are the two extremes of physics concerned with the behaviour of matter in conditions far removed from those of every-day events in our domestic physical world, yet they have much in common. The concept of bringing them together in one volume is original and stimulating.

The first five chapters are on Elementary particles, The atom breaks up, Smashing the atom, Energy from the atom and Cosmic radiation. The last four chapters deal with The solar system, The Milky Way, The size of the universe and The age of the universe. Both these sections are admirably up-to-date accounts of the kind one would hope for in an article in a first-rate encyclopaedia. They are sufficiently simple to be understood by the intelligent layman; they are sufficiently comprehensive to be read with interest and profit by the physicist who has not specialized in nuclear physics or astrophysics.

But one cannot help feeling that the book would have been better balanced if the authors had been content to restrict it to these two sections. The introduction, the chapters on Matter and its properties and From classical to modern physics, and the Appendix are scrappy and breathless in their haste. An attempt had been made to compress far too much into too small a space. One is reminded of the occasion when a lecturer realizes that he has only five minutes left of the appointed hour and finding he has not yet covered half of the matter which he had planned, attempts feverishly to race through the rest. The plan of the book is too ambitious; the nucleus and the universe are in themselves very considerable subjects. To try to include as well an account of the relation of physics to chemistry and biology, the methods of experimental science, relativity, the structure of matter, the quantum theory, a disquisition on theories and the role of mathematics, and laws, hypothesis and theories—no, the reader rebels. One cannot compress an account of the properties of matter into 24 pages, or of the philosophy of science into a few paragraphs and it would have been more artistic to refrain from the attempt.

In spite of these blemishes, it is a very readable book. It is hard to get a good general view of the various branches of science in these days of intense specialization, and one is grateful for this excellent summary of what the nuclear physicists and astronomers are discovering and thinking. W. L. Bragg.

Nuclear and Radiochemistry, by G. Friedlander and J. W. Kennedy. Pp. ix + 468. (New York: John Wiley; London: Chapman and Hall, 1955.) 60*s*.

The years 1940–46 brought many changes to the classical radiochemist, most of which arose in the atomic energy work of that time although a trend was apparent before this in the type of work undertaken by chemists in cyclotron studies. The changes have required that the chemist should have a considerable appreciation of nuclear physics. Seven years ago, Friedlander and Kennedy wrote

the first book of modern radiochemistry clearly showing the new bias. *Introduction to Radiochemistry* was an extremely timely and useful book but I enjoyed the revised version, *Nucelar and Radiochemistry*, even more. The revision consists of some rearrangement and expansion of the earlier framework to which is now added two new chapters. It is claimed that 65% of the material is new to this edition. Basically, the structure of the book remains the same, elementary radioactivity leading to atomic and nuclear structure, nuclear machines and reactions, modes of decay and the properties of nuclear radiation. Means of measurement of radiation are discussed in principle but not in practical detail as befitting a textbook of this kind. The chemical topics includes target chemistry, methods of radiochemical separation and tracers in chemical applications. In a work covering so much ground, no subject can be dealt with at great length, but a selected further reading list and a set of problems concludes every chapter.

The authors have continued in their admirable role of interpreters of nuclear physics in the additions made to bring the book up to date. These naturally include a considerable amount on shell structure and its ramifications in a simplified but very satisfactory form. Other topics in which there have been some progress include nuclear systematics in alpha-decay and spontaneous fission, gamma-scintillation counters and spectrometers.

The last two chapters are entirely new. The first discusses the basic elementary theory of slow neutron reactors and briefly describes several types which are in operation. I would have preferred, however, that fast and intermediate reactors had been included at the expense of chemical processing if something had to be omitted for reasons of space. The final chapter, Some Cosmic Problems, is very useful as a short summary of several physical problems of chemical interest, such as cosmic rays, geological dating, the genesis of the elements and energy production in stars.

This book will be of the greatest value to all nuclear chemists, and radiochemists will find in it all the background information needed to understand their technique. It is not intended for physicists but I find it hard to believe that they would find nothing of value in it, particularly in its chemical bias. As is typical of the publishing house, the binding, paper and presentation are first class.

G. B. C.

CONTENTS OF SECTION B

Page

Dr. P. Feltham. On the Mechanism of High-Temperature Creep in Metals . . . 1173

Dr. R. Street and Dr. J. C. Woolley. A Comparison of Magnetic Viscosity in Isotropic and Anisotropic High Coercivity Alloys 1189

Prof. L. F. Bates and Dr. A. Hart. Changes in Domain Structure accompanying Reduction in Depth of a Single Crystal of Silicon Iron 1200

Dr. J. M. Baker, Dr. B. Bleaney and Dr. K. D. Bowers. Paramagnetic Resonance in some Complex Cyanides of the Iron Group : I—Experimental Results . . . 1205

Dr. B. Bleaney and Dr. M. C. M. O'Brien. Paramagnetic Resonance in some Complex Cyanides of the Iron Group : II—Theory 1216

Mr. F. R.McKim and Dr. W. P. Wolf. The Susceptibility and Magnetic Specific Heat of Potassium Ferricyanide at Low Temperatures 1231

Dr. G. W. Jull. An Experimental Investigation of Characteristic Electron Energy Losses in Solids 1237

Dr. B. Donovan and Dr. N. H. March. Momentum Distribution of Electrons in Solids : II—Some General Results with an Application to Metallic Lithium 1249

Dr. K. W. Plessner. Ageing of the Dielectric Properties of Barium Titanate Ceramics . 1261

Mr. R. F. Broom and Dr. A. C. Rose-Innes. A Pulse Method for Measurement of Hall Coefficient at Low Temperatures : Some Results on Indium Antimonide . . . 1269

Dr. R. Bullough and Dr. B. A. Bilby. Continuous Distributions of Dislocations : Surface Dislocations and the Crystallography of Martensitic Transformations . . 1276

Dr. R. Cooper and Dr. A. A. Wallace. The Influence on Electric Strength of Mechanical Deformation caused by Application of Voltage to Potassium Chloride Crystals . . 1287

Mr. S. Pearson. Delayed Fracture of Sintered Alumina 1293

Dr. C. Carter. A Theoretical Study of Pentavalent Phosphorus 1297

Dr. M. F. Culpin and Dr. K. W. Kemp. The Orientation of the Structure of 6·6 Nylon Fibres 1301

Dr. H. G. Kuhn and Mr. S. A. Ramsden. The Phase Adjustment of the Double Etalon 1309

Miss S. M. Crawford. Some Elastic Properties of Organic Glasses in the Transition Region from Solid to Liquid at Ultrasonic Frequencies 1312

Mr. W. P. Osmond. Angles between Magnetic Spin Directions in Iron-Deficient Magnesium Manganese Ferrites 1319

Dr. P. B. Sherry and Prof. C. A. Coulson. The Vibrational Frequency Distribution of Graphite : I—Out-of-plane Modes of a Single Layer 1326

Research Notes :

Dr. G. G. E. Low. A Method of Evaluating Surface State Parameters from Conductance Measurements on Semiconductors 1331

Mr. C. H. Champness. The Statistics of Divalent Impurity Centres in a Semiconductor 1335

Dr. J. C. Woolley, Mr. B. A. Smith and Mr. D. G. Lees. Solid Solution in the GaSb–InSb System 1339

Mr. I. Brodie and Dr. R. O. Jenkins. Mixed Monolayers of Barium and Calcium on Tungsten 1343

Dr. B. K. Agarwal. On the Bose–Einstein Liquid Model for ^{3}He–^{4}He Solutions . 1345

Letters :

Prof. G. O. Jones and Dr. P. A. Walker. Specific Heats of Fluid Argon near the Critical Point 1348

Mr. D. Gerlich. Hole Injection at Metal–Semiconductor Point Contact . . . 1350

Dr. R. Cooper and Dr. D. T. Grossart. Time Lags in the Intrinsic Electric Breakdown of Solid Dielectrics 1351

Mr. T. B. Watkins. Slow Relaxation Phenomena in Junction Diodes 1353

Corrigendum : Dr. F. Berz 1355

Contents of Section A 1356

Subject Index, Section B, Vol. 69 1357

Index of Authors (with Titles), Section B, Vol. 69 1365

Index of Reviews of Books, Section B, Vol. 69 1375

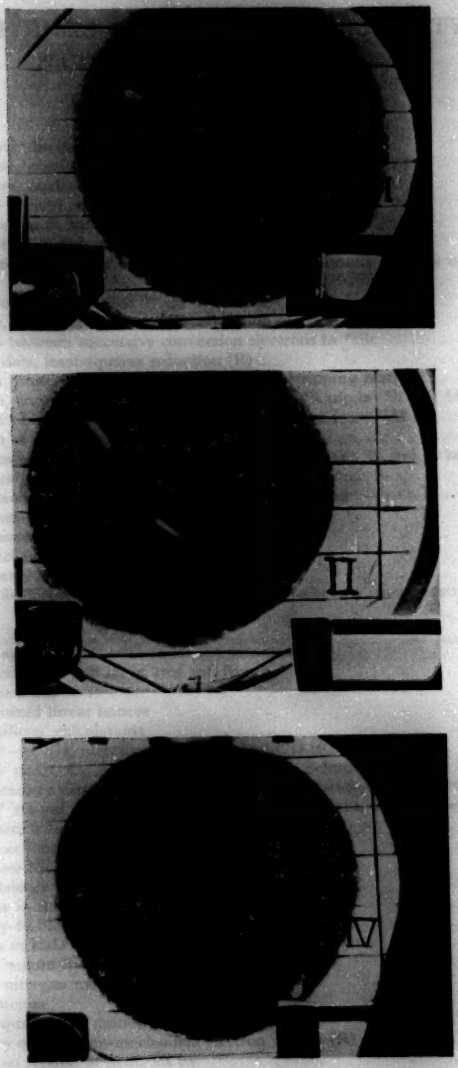

Figure 2. Photographs of a large shower recorded in chambers I, II and IV.

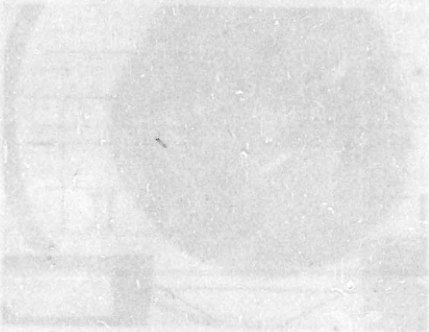

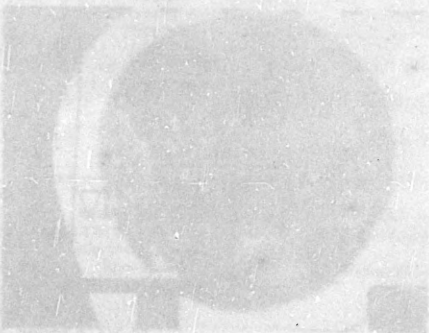

PROCEEDINGS OF THE PHYSICAL SOCIETY
SECTION A, 1956—VOLUME 69

SUBJECT INDEX

PAGE

Air showers, extensive, directional measurements 902
Air showers, extensive, energy spectrum 804
Air showers, extensive, nucleonic component 894
Alloys, de Haas–van Alphen effect 505
Alpha activity induced in Pt by bombardment with N ions (R) 862
Alpha-particle and shell models of nucleus 600
Alpha-particle counting behaviour of diamond conduction counters at fields up to 200 kv cm^{-1} 593
Aluminium 25, positron disintegration 624
Angular correlations, attenuated between K-conversion electrons in ^{197}Hg . . 566
Angular correlations between successive conversion electrons in ^{80}Br 453
Angular correlation data, least-squares reduction (R) 489
Angular correlations, proton–gamma, in ^{29}Si (d, pγ) ^{29}Si stripping reaction . . 705
Angular distribution, and yield, of neutrons from reaction $^{63}Cu(p, n)$ ^{63}Zn at 18Mev 447
Angular distribution of inelastically scattered deuteron groups from ^{27}Al (R) . 345
Angular distribution of neutrons from high energy fission 853
Angular distributions and cross section of D–D reactions between 40 and 90 kev . 265
Arcs and flames, band structure emitted by Sr and Ba 520
Atomic beam apparatus for hyperfine structure of radioactive Ag 581
Atomic beam experiments, shape of resonance curves. 588
Atoms at large separations, resonance forces 821
Atoms, Fermi or exchange hole in 734
Atoms, π-mesic, energy levels (R) 280
Auto-ionization probabilities calculation : III—Auto-detachment from negative H ion 65

Band intensities in system $b^3\Sigma^+ - a^3\Pi$ of carbon monoxide (R) 574
Band spectra emitted by Sr and Ba in arcs and flames 520
Band structure of bismuth 513
Band structure of mixed linear lattices 234
Band structure of silicon, calculations 548
Band system $B(^2\Sigma^+) - A(^2\Sigma^+)$, identification in OH and OD (R) 178
Band systems, CN violet, C_2 Swan, OH violet and O_2 Schumann–Runge, interpretation of intensity distribution by r-centroids and Franck–Condon factors . 741
Band systems, O_2^+ second negative, N_2 Lyman–Birge–Hopfield, and N_2 Vegard–Kaplan, r-centroids for (R) 713
Bands, electronic, *see* Electronic bands
Bands, molecular, *see* Molecular bands
Barium 131, high energy γ-ray in decay (R) 70
Benzene, intensities in Raman spectrum 375
Benzene, symmetry-forbidden electronic bands, intensities 245
Beta-disintegration of RaD 836
Binding energy of helium hydride ion (R) 868
Binding energy of nitrogen molecule 767
Bismuth, band structure 513
Bodies, rotating, equations of motion in general relativity 2
Bohm–Pines theory of quantum-mechanical electron plasma (R) 492
Boron, capture cross section of neutrons by 464

Carbon monoxide, band intensities in system $b^3\Sigma^+ - a^3\Pi$ (R) 574
Charge exchange and interaction energy between helium atoms and ions . . 653

	PAGE
Charge transfer and mobility of H^- ions in atomic hydrogen	615
Charged particles, *see* Particles, charged	
Cloud chamber, diffusion, π^+—p scattering in	798
Cobalt 56, 57, nuclear spins and magnetic moments (L)	353
Collisions, inelastic heavy particle, involving crossing of potential energy curves	910
Collisions, p–p, at 383 Mev positive pion production	691
Collisions, *see* also Radiation	
Cosmic-ray intensity at high energies, search for sidereal variation	102
Cosmic-ray transition curve, second maximum, liquid scintillator investigation	845
Cosmic-rays, *see also* Air showers	
Counter, scintillation, *see* Scintillation counter	
Counters, diamond conduction, α-particle counting behaviour up to 200 kv cm^{-1}	593
Cross section and angular distributions of D–D reactions between 40 and 90 kev	265
Cross section, capture, of neutrons by boron	464
Cross section, capture, of thermal neutrons in water	469
Decay of isomeric state of ^{198}Tl	541
Decay of ^{144}Pr, pseudoscalar interaction	789
Decay of τ and θ particles, isotopic spin changes	527
Deuterium atoms, fast neutral, ionization (L)	352
Deuteron groups inelastically scattered from ^{27}Al, angular distribution (R)	347
Deuteron induced reactions, *see* Reactions	
Deuterons, inelastically scattered, magnetic analysis and disintegration protons from deuteron bombardment of F	221
Diamagnetism and momentum correlation	441
Editorial	1
Eigenvalue problems, crystal augmented plane wave method	388
Elastic scattering, *see* Scattering	
Electron excitation functions of first negative bands of N_2^+	437
Electronic bands of benzene symmetry-forbidden, intensities	245
Electron impact and 1s–2s excitation of hydrogen (R)	422
Electron pair production, effect of finite nuclear size	135
Electron plasma, quantum-mechanical, Bohm–Pines theory (R)	492
Electrons, conversion, in ^{80}Br, angular correlations between	453
Electrons, fast, single scattering by atomic nuclei	196
Electrons, high energy, nuclear scattering of, on independent-particle model	205
Electrons, K-conversion, in ^{197}Hg attenuated angular correlations between	566
Electrons, neutron production by, in uranium and uranium–beryllium (R)	419
Electrons, *see* also Scattering	
Energy levels of ^{26}Al	335
Energy levels of π-mesic atoms (R)	280
Erbium 68, $M_{IV,\,V}$ spectra	93
Excitation curve for reaction ^{10}B (p, α)^{7}Be (R)	350
Excitation functions up to 980 Mev for proton induced reactions in ^{27}Al relative to ^{12}C(p, pn) ^{11}C	43
Extensive showers, density distribution (R)	875
Fermi or exchange hole in atoms	734
Ferromagnets, multiple spin wave scattering of neutrons in (R)	939
Fission, average number of neutrons from U and Bi under 147 Mev proton bombardment	330
Fission, high energy, angular distribution of neutrons from	853
Flames and arcs, band structure emitted by Sr and Ba	520
Force constants, evaluation from Raman effect data : molecules, radicals and groups of pyramidal XY_3 type (R)	180
Forces, long range, representation by series expansions	57

PAGE

Gamma radiation from various (p, γ) reactions, polarization 125
Gamma-ray beam, bremsstrahlung nuclear interactions of 110
Gamma ray, high energy, in decay of ^{131}Ba (R) 70
Gamma rays, elastic scattering 381
Gamma rays from ^{152}Eu, ^{154}Eu, ^{153}Sm and ^{165}Dy, precision wavelength and energy measurements (R) 415
Gamma rays from reactions ^{24}Mg(p, γ)^{25}Al and ^{12}C(p, γ)^{13}N 624
Gamma transition lifetimes, measurements by recoil methods: II—M1 transitions in ^{7}Li and ^{7}Be 165
Gamma transition lifetimes, measurements by recoil methods: III—E2 transitions in even–even nuclei 173
Gravitational field, quantized, two-body problem in theory of 189

de Haas–van Alphen effect in alloys 505
HeH^{2+}, oscillator strengths of various transitions 610
Helium, application of relativistic theory of specific ionization and stopping power . 318
Helium atoms and ions, interaction energy and charge exchange between . . 653
Helium atoms, metastable, destruction by collision-induced radiation . . . 271
Helium hydride ion, binding energy (R) 868
Hydrogen 1s–2s excitation by electron impact (R) 422
Hydrogen atom, application of Rayleigh–Schrödinger perturbation theory (L) . 784
Hydrogen atom, quadrupole moment in uniform field (R) 639
Hydrogen atom, quadrupole polarizability 777
Hydrogen, atomic, charge transfer and mobility of H^- ions 615
Hydrogen molecule, scattering of slow electrons by, use of variational methods . 659

Infra-red resonance lines of lutetium (L) 783
Interaction energy and charge exchange between helium atoms and ions . . 653
Interaction, pseudoscalar, in decay of ^{144}Pr 789
Interactions, nuclear, of 315 Mev bremsstrahlung γ-ray beam 110
Ionization loss and range–energy relation for low energy protons in metals . . 888
Ionization of fast neutral deuterium atoms (L) 352
Ionization, primary, and stopping power, relativistic theory and application in helium 318
Ions, rare-earth, structure of ground multiplets 157
Isomeric state of ^{198}Tl, decay 541
Isotopes, β-emitting, absolute standardization with liquid scintillation counter (R) . 865
Isotopic spin changes in τ and θ decay 527

Lattice, close packed hexagonal, of Ti, cellular method for (L) 185
Lattice, close packed hexagonal, spherical harmonics with symmetry of (L) . . 184
Lattices, mixed linear band structure 234
Liquid helium transition, nature (R) 630

Magnesium oxide, Raman spectrum (L) 426
Magnetic analysis for investigation of deuteron induced reactions: I—Experimental technique 16
Magnetic analysis for investigation of deuteron induced reactions: II—Results for ^{9}Be, ^{12}C, ^{14}N and ^{16}O 28
Magnetic analysis, for investigation of deuteron induced reactions: III—Results for neon and argon 310
Magnetic moments and nuclear spins of Co 56, 57 (L) 353
Magnetic moments and nuclear spins of ^{161}Dy, ^{163}Dy, ^{171}Yb and ^{173}Yb (L) . . 282
Magnetic moments of odd–odd nuclei (R) 635
Magnetic resonance, *see* Atomic beam
Many-particle systems: II (R) 936
Mesons, *see under* Atoms
Metals, range–energy relation for low energy protons in, and ionization loss . 888
Method of atoms in molecules: II—Intra-atomic correlation correction . . . 49

	PAGE
Method of atoms in molecules: III Ground state of HF	301
Mobility of H^- ions and charge transfer in atomic hydrogen	615
Molecular bands, average internuclear separations associated with	253
Molecular orbitals, approximate: IV—$3p\sigma_u$ and $4f\sigma_u$ states of H_2^+	285
Molecular orbitals, approximate: V—$1s\sigma$ and $2p\pi$ states of HeH^{2+}	480
Molecules, method of atoms in: II—Intra-atomic correlation correction	49
Molecules, method of atoms in: III—Ground state of HF	301
Moments, magnetic, *see* Magnetic moments	
Moments, quadrupole, of hydrogen atom in uniform field (R)	639
Momentum correlation and diamagnetism	441
Motion, equations of, for rotating bodies in general relativity	2
Multiplets, ground, structure in certain rare-earth ions	157
Mu-mesons, momentum spectrum at depth of 40 m.w.e.	725
Mu-mesons underground, star production by (L)	428
Neutron production by electrons in uranium and uranium–beryllium (R)	419
Neutrons, capture cross section by boron	464
Neutrons, from high energy fission, angular distribution	853
Neutrons, scattering of, *see* Scattering	
Neutrons, thermal, capture cross section in water	469
Neutrons, *see also* Angular distribution	
Nitrogen ions, bombardment inducing α-activity in Pt (R)	62
Nitrogen molecule, binding energy	767
Nitrogen, photodisintegration	77
Nitrogen, N_2^+, electron excitation function of first negative bands	437
Nuclear charge density distributions (L)	650
Nuclear energy levels, observed regularities (L)	354
Nuclear interaction, *see* Interaction	
Nuclear scattering of 0·4 and 0·5 Mev electrons in composite Al–U foils (R)	496
Nuclear size, finite, effect on electron pair production	135
Nuclear spins and magnetic moments of Co 56, 57 (L)	353
Nuclear spins and magnetic moments of ^{161}Dy, ^{163}Dy, ^{171}Yb and ^{173}Yb (L)	282
Nuclei, atomic, single scattering of fast electrons by	196
Nuclei, heavy, neutron–proton pairing interaction in	293
Nuclei, odd–odd, magnetic moments (R)	635
Nucleons, inelastic scattering by surface interaction	668
Nucleus, α-particle and shell models	600
Nucleus, optical model, calculations with	365
Optical model of nucleus, calculations with	365
Oscillator strengths of various transitions of HeH^{2+}	610
Oscillations, plasma-electron, spectroscopic study	696
Ozone, 9·6μ band, line widths in	530
Pairing, interaction, neutron–proton, in heavy nuclei	293
Paramagnetic resonance spectra of alkali superoxides and chlorine dioxide	556
Particles, fast charged, scattering: I—Single scattering of 13·5 Mev electrons in xenon	141
Particles, τ and θ, decay of, isotopic spin changes	527
Perturbation theory, equivalence of variational and perturbation calculations of small disturbances (R)	628
Perturbation theory, Rayleigh–Schrödinger, application to hydrogen atom (L)	784
Photodisintegration of nitrogen	77
Pion, positive, production in p–p collisions at 383 Mev	691
Polarizability, quadrupole, of hydrogen atom	777
Positron disintegration of ^{28}Al	624
Potential energy curves, crossing, and inelastic heavy particle collisions	910
Proportional counters, boron trifluoride, time delays in (R)	413

PAGE

Proton bombardment, 147 Mev, and average number of neutrons per fission from U and Bi . . . 330
Proton induced reactions, *see* Reactions
Proton–proton scattering at 134 Mev (R) . . . 645
Proton–proton scattering at 147 Mev (R) . . . 495
Proton synchrotrons, constant gradient, space charge and ionization phenomena . . . 153
Protons, disintegration, from deuteron bombardment of F, and magnetic analysis of inelastically scattered deuterons . . . 221
Protons, low energy, in metals, ionization loss and range energy relation . . . 888
Protons, 9·6 Mev, scattering by Mg . . . 686

Radiation, collision-induced, and destruction of metastable helium atoms . . . 271
Radioactive silver, hyperfine structure . . . 581
Radium D, β-disintegration . . . 836
Raman effect data, evaluation of force constants from : molecules, radicals and groups of pyramidal XY_3 type (R) . . . 180
Raman spectrum, *see* Spectrum
Range–velocity relationship for ^{7}Li ions in solids (R) . . . 345
Rare-earth ions, structure of ground multiplets . . . 157
r-centroids and Franck–Condon factors for interpretation of intensity distributions in CN violet, C_2 Swan, OH violet and O_2 Schumann–Runge band systems . . . 741
r-centroids : average internuclear separations associated with molecular bands . . . 253
r-centroids for O_2^+ second negative, N_2 Lyman–Birge–Hopfield, and N_2 Vegard–Kaplan band systems (R) . . . 713
Reactions ^{27}Al(p, γ)^{28}Si, ^{26}Mg(p, γ)^{27}Al, ^{23}Na(p, γ)^{24}Mg, polarization of γ-radiation from 125
Reactions ^{10}B(d, n)^{11}C and ^{11}B(d, n)^{12}C, investigation . . . 754
Reaction ^{10}B(p, α)^{7}Be, excitation curve (R) . . . 350
Reactions ^{12}C(γ, p)^{11}B, ^{11}B(p, γ)^{12}C and ^{12}C(γ, 3α) at 17·63 Mev excitation . . . 917
Reaction ^{13}C(α, n)^{16}O . . . 830
Reaction ^{63}Cu(p, n)^{63}Zn, yield and angular distribution of neutrons from, at 18 Mev . . . 447
Reactions, deuteron induced, investigation by magnetic analysis : I—Experimental technique . . . 16
Reactions, deuteron induced, investigation by magnetic analysis : II—Results for ^{9}Be, ^{12}C, ^{14}N and ^{16}O . . . 28
Reactions, deuteron induced, investigation by magnetic analysis : III—Results for neon and argon . . . 310
Reactions ^{24}Mg(p, γ)^{25}Al and ^{13}C(p, γ)^{13}N, γ-rays from . . . 624
Reaction ^{24}Mg(p, γ)^{25}Al (R) . . . 641
Reactions, proton, induced in ^{27}Al, excitation functions up to 980 Mev . . . 43
Recoil methods for measurement of γ-transition lifetimes : II—M1 transitions in ^{7}Li and ^{7}Be . . . 165
Recoil methods for measurements of γ-transition lifetimes : III—E2 transitions in even–even nuclei . . . 173
Relativistic theory of specific primary ionization and stopping power and application in helium . . . 318
Relativity, general, equations of motion of rotating bodies in . . . 2
Relativity theory . . . 925, 935
Resonance forces at large separations . . . 821
Resonance curves, shape, in atomic beam experiments . . . 588

Scattered deuterons, *see* Deuterons
Scattering, elastic, of gamma rays . . . 381
Scattering, elastic, of neutrons by tritons and ^{3}He . . . 877
Scattering, inelastic, of neutrons by uranium, experiments . . . 214
Scattering, inelastic, of nucleons by surface interaction . . . 668
Scattering, multiple spin wave, of neutrons in ferromagnets (R) . . . 939
Scattering, nuclear, of high energy electrons on independent-particle model . . . 205
Scattering, nuclear, of 0·4 and 0·5 Mev electrons in composite Al–U foils (R) . . . 496

	PAGE
Scattering of fast charged particles : I—Single scattering of 13·5 MEV electrons in xenon	141
Scattering of 9·6 MEV protons by Mg	686
Scattering of 130 MEV neutrons by protons	760
Scattering of slow electrons by hydrogen molecule, use of variational methods	659
Scattering, π^+–p, in diffusion cloud chamber	798
Scattering, proton–proton, at 134 MEV (R)	645
Scattering, proton–proton, at 147 MEV (R)	495
Scattering, single, of fast electrons by atomic nuclei	196
Scattering, *see also* Deuterons	
Scintillation counter, liquid absolute standardization of β-emitting isotopes (R)	865
Scintillator, liquid, for investigation of second maximum in cosmic ray transition curve	845
Series expansions, representation of long range forces by	57
Shell and α-particle models of nucleus	600
Showers, *see* Extensive showers	
Silicon, band structure, calculations	548
Silver, radioactive, hyperfine structure	581
Solids, range–velocity relationship for ^{7}Li ions in (R)	345
Spectra, infra-red resonance lines of lutetium (L)	783
Spectra, $M_{IV, V}$, of ^{68}Er	93
Spectra, paramagnetic resonance, of alkali superoxides and chlorine dioxide	556
Spectrum of AlO, supposed predissociation in (L)	356
Spectrum, Raman, of benzene, intensities	375
Spectrum, Raman, of magnesium oxide (L)	426
Spin changes, isotopic, in τ and θ decay	527
Star production by μ-mesons underground (L)	428
Stripping reaction, ^{28}Si(d, pγ)^{29}Si, proton–gamma angular correlations in	705
Synchrotrons, proton, *see* Proton synchrotrons	
Tellurium 198, decay of isomeric state	541
Titanium, close packed hexagonal, cellular method for (L)	185
Transition, 440 kev, in ^{23}Na (R)	858
Transitions, E2, in even–even nuclei	173
Transitions, M1, in ^{7}Li and ^{7}Be	165
Two-body problem in theory of quantized gravitational field	189
Uranium and uranium–beryllium, neutron production by electrons (R)	419
Uranium, inelastic scattering of neutrons by, experiments	214
Water, capture cross section of thermal neutrons in	469
Xenon, single scattering of 13·5 MEV electrons in	141
X-radiation, characteristic, intensity of emission	401

INDEX OF AUTHORS (WITH TITLES)

PAGE

Advani, M. K., Harihar, P., and Gatha, K. M. : Nuclear charge density distributions (L) . . . 650

Aikin, A. W. : Neutron production by electrons in uranium and uranium–beryllium (R) . . . 419

Allan, H. R., Govindjee, M., and Sarma, N. : Excitation curve for the reaction ^{10}B (p, α)^{7}Be (R) . . . 350

Allen, K. R., Lipsicas, M. M., Major, D., and Phillips, K. : The scattering of fast charged particles : I—On the single scattering of 13·5 MeV electrons in xenon . . . 141

Allen, K. W., Collinge, B., Hird, B., Maglić, B. C., and Orman, P. R. : The proton gamma angular correlations in the ^{28}Si (d, pγ)^{29}Si stripping reaction . . . 705

Alston, M. H., Crewe, A. V., Evans, W. H., and von Gierke, G. : A study of positive pion production in p–p collisions at 383 MeV . . . 691

Alston, M. H., Evans, W. H., Fidecaro, M., Newport, R. W., von Gierke, G., and Williams, P. R. : π^{+}–p scattering at 10–35 MeV in a diffusion cloud chamber . . . 798

Altmann, S. L. : Spherical harmonics with the symmetry of the close-packed hexagonal lattice . . . 184

Andersson, B. : Precision wavelength and energy measurements of gamma rays from ^{152}Eu, ^{154}Eu, ^{153}Sm and ^{165}Dy (R) . . . 415

Atkinson, J. R., Wright, I. F., Morrison, D. R. O., and Reid, J. M. : The photodisintegration of nitrogen . . . 77

Baker, J. M., Bleaney, B., Llewellyn, P. M., and Shaw, P. F. D. : Nuclear spins and magnetic moments of cobalt 56 and 57 (L) . . . 353

Barrow, R. F., and Downie, A. R. : The identification of a band system, B($^{2}\Sigma^{+}$) $-$A$^{2}\Sigma^{+}$, in OH and OD (R) . . . 178

Barrow, R. F., Gratzer, W. B., and Malherbe, J. F. : Intensities of bands in the system b$^{3}\Sigma^{+}$–a$^{3}\Pi$ of carbon monoxide (R) . . . 574

Barrow, R. F., Lagerqvist, A., and Lennart Nilsson, N. E. : One a supposed predissociation in the spectrum of AlO (L) . . . 356

Batchelor, R. : Experiments on the inelastic scattering of neutrons by uranium . . . 214

Bates, D. R., and Boyd, T. J. M. : Inelastic heavy particle collisions involving the crossing of potential energy curves . . . 910

Bennett, J. E., Ingram, D. J. E., and Schonland, D. : Paramagnetic resonance spectra of the alkali superoxides and chlorine dioxide . . . 556

Berenbaum, R., Towle, J. H., and Matthews, J. H. : The 440 kev transition in ^{23}Na (R) . . . 858

Bleaney, B., with Baker, J. M., Llewellyn, P. M., and Shaw, P. F. D. : Nuclear spins and magnetic moments of cobalt 56 and 57 (L) . . . 353

Booth, D. L., Preston, G., and Shaw, P. F. D. : The cross section and angular distributions of the D–D reactions between 40 and 90 kev . . . 265

Bovey, L. F. H., Steers, E. B. M., and Wise, H. S. : The infra-red resonance lines of lutetium (L) . . . 783

Boyd, T. J. M., with Bates, D. R. : Inelastic heavy particle collisions involving the crossing of potential energy curves . . . 910

Bransden, B. H., and Dalgarno, A. : The calculation of auto-ionization probabilities : III – Auto-detachment from the negative hydrogen ion . . . 65

Bransden, B. H., and McKee, J. S. C. : The 1s–2s excitation of hydrogen by electron impact (R) . . . 422

Bransden, B. H., Robertson, H. H., and Swan, P. : The elastic scattering of neutrons by tritons and ^{3}He . . . 877

Breitenberger, E. : Angular correlations between successive conversion electrons in ^{80}Br . . . 453

PAGE

Breitenberger, E.: Remarks on the least-squares reduction of angular correlation data (R) . . . 489

Breitenberger, E.: Attenuated angular correlations between K-conversion electrons in ^{197}Hg . . . 566

Broadbent, S. R.: An examination of observed regularities in nuclear energy levels (L) . . . 354

Brown, B., Matsukawa, E., and Stewardson, E. A.: The nuclear scattering of 0·4 and 0·5 MeV electrons in composite aluminium–uranium foils (R) . . . 496

Buckingham, A. D., Coulson, C. A., and Lewis, J. T.: The quadrupole moment of a hydrogen atom in a uniform field (R) . . . 639

Bunbury, D. St. P., Devons, S., Manning, G., and Towle, J. H.: Measurement of γ-transition lifetimes by recoil methods: II—M1 transitions in ^{7}Li and ^{7}Be . . . 165

Burcham, W. E., and Haywood, B. C.: The alpha activity induced in platinum by bombardment with nitrogen ions (R) . . . 862

Burhop, E. H. S.: The effect of finite nuclear size on electron pair production . . . 135

Burhop, E. H. S., and Marriott, R.: The destruction of metastable helium atoms by collision-induced radiation . . . 271

Burrows, H. B., Green, T. S., Hinds, S., and Middleton, R.: An investigation of deuteron induced reactions by magnetic analysis: III—Results for neon and argon . . . 310

Caine, C. A.: The magnetic moments of odd–odd nuclei (R) . . . 635

Calvert, J. M., with Maslin, E. E., and Jaffe, A. A.: An investigation of the reactions ^{10}B(d, n)^{11}C and ^{11}B(d, n)^{12}C . . . 754

Cassels, J. M.: Proton–proton scattering at 147 MeV (R) . . . 495

Chackett, G. A., Chackett, K. F., Reasbeck, P., Symonds, J. L., and Warren, J.: Excitation functions up to 980 MeV for proton-induced reactions in ^{27}Al, relative to ^{12}C(p, pn) ^{11}C . . . 43

Chackett, K. F., with Chackett, G. A., Reasbeck, P., Symonds, J. L., and Warren, J.: Excitation functions up to 980 MeV for proton-induced reactions in ^{27}Al, relative to ^{12}C(p, pn) ^{11}C . . . 43

Chalklin, L. P., and Fremlin, J. H.: The ionization of fast neutral deuterium atoms (L) . . . 352

Charton, M., and Gaydon, A. G.: Band spectra emitted by strontium and barium in arcs and flames . . . 520

Chick, D. R., Evans, W. W., Hancock, D. A., Hunt, S. E., and Pope, R. A.: An investigation of the γ-rays from the reactions ^{24}Mg(p, γ)^{25}Al and ^{12}C(p, γ)^{13}N, with a note on the positron disintegration of ^{25}Al . . . 624

Collie, C. H., Meads, R.E., England, C. J., and Weeks, G. C.: The capture cross section of thermal neutrons in water . . . 469

Collie, C. H., Meads, R. E., and Lockett, E. E.: The capture cross section of neutrons by boron . . . 464

Collinge, B., with Allen, K. W., Hird, B., Maglić, B. C., and Orman, P. R.: The proton–gamma angular correlations in the ^{28}Si(d, pγ)^{29}Si stripping reaction . . . 705

Cooke, A. H., and Park, J. G.: Nuclear spins and magnetic moments of ^{161}Dy, ^{163}Dy, ^{171}Yb and ^{173}Yb (L) . . . 282

Corinaldesi, E.: The two-body problem in the theory of the quantized gravitational field . . . 189

Coulson, C. A., and Stephen, M. J.: The quadrupole polarizability of the hydrogen atom . . . 777

Coulson, C. A., with Buckingham, A. D., and Lewis, J. T.: The quadrupole moment of a hydrogen atom in a uniform field (R) . . . 639

Crawshaw, J. K., and Elliot, H.: Search for a sidereal variation of the cosmic ray intensity at high energies . . . 102

Crewe, A. V., with Alston, M. H., Evans, W. H., and von Gierke, G.: A study of positive pion production in p–p collisions at 383 MeV . . . 691

Curr, R. M., with Damodaran, K. K.: Single scattering of fast electrons by atomic nuclei . . . 196

PAGE

Dalgarno, A.: Application of the Rayleigh–Schrödinger perturbation theory to the hydrogen atom (L) . . . 784
Dalgarno, A., and Lewis, J. T.: The representation of long range forces by series expansions: I—The divergence of the series; II—The complete perturbation calculation of long range forces . . . 57
Dalgarno, A., and Lewis, J. T.: Approximate molecular orbitals: IV—The $3p\sigma_u$ and $4f\sigma_u$ states of H_2^+ . . . 285
Dalgarno, A., and Lewis, J. T.: The equivalence of variational and perturbation calculations of small disturbances (R) . . . 628
Dalgarno, A., and Lynn, N.: Resonance forces at large separations . . . 821
Dalgarno, A., Lynn, N., and Williams, E. J. A.: The oscillator strengths of the $1s\sigma$–$2s\sigma$, $1s\sigma$–$3d\sigma$ and $2s\sigma$–$3d\sigma$ transitions of HeH^{2+} . . . 610
Dalgarno, A., and McDowell, M. R. C.: Charge transfer and the mobility of H^- ions in atomic hydrogen . . . 615
Dalgarno, A., with Bransden, B. H.: The calculation of auto-ionization probabilities: III—Auto-detachment from the negative hydrogen ion . . . 65
Dalitz, R. H.: Isotopic spin changes in τ and θ decay . . . 527
Damodaran, K. K., and Curr, R. M.: Single scattering of fast electrons by atomic nuclei . . . 196
Devons, S., Manning, G., and Towle, J. H.: Measurement of γ-transition lifetimes by recoil methods: III—E2 transitions in some even–even nuclei . . . 173
Devons, S., and Towle, J. H.: Range–velocity relationship for ^{7}Li ions in solids (R) 345
Devons, S., with Bunbury, D. St. P., Manning, G., and Towle, J. H.: Measurement of γ-transition lifetimes by recoil methods: II—M1 transitions in ^{7}Li and ^{7}Be 165
Dingle, H.: A problem in relativity theory . . . 925
Doran, G. A., with Marsden, P. L.: The nucleonic component in cosmic ray extensive air showers . . . 894
Downie, A. R., with Barrow, R. F.: The identification of a band system $B(^2\Sigma^+) - A^2\Sigma^+$ in OH and OD (R) . . . 178

El Bedewi, F. A.: Magnetic analysis of the inelastically scattered deuterons and disintegration protons from the deuteron bombardment of fluorine . . . 221
Elliot, H., with Crawshaw, J. K.: Search for a sidereal variation of the cosmic ray intensity at high energies . . . 102
Elliott, R. J., Lowde, R. D., and Marshall, W.: On the multiple spin wave scattering of neutrons in ferromagnets (R) . . . 939
England, C. J., with Meads, R. E., Collie, C. H., and Weeks, G. C.: The capture cross section of thermal neutrons in water . . . 469
Evans, W. H., with Alston, M. H., Crewe, A. V., and von Gierke, G.: A study of positive pion production in p–p collisions at 383 Mev . . . 691
Evans, W. H., with Alston, M. H., Fidecaro, M., Newport, R. W., von Gierke, G., and Williams, P. R.: π^+–p scattering at 10–35 Mev in a diffusion cloud chamber . . . 798
Evans, W. W., with Chick, D. R., Hancock, D. A., Hunt, S. E., and Pope, R. A.: An investigation of the γ-rays from the reactions $^{24}Mg(p,\gamma)^{25}Al$ and $^{12}C(p,\gamma)^{13}N$, with a note on the positron disintegration of ^{25}Al . . . 624

Farley, F. J. M., with Harding, G. N.: The angular distribution of neutrons from high energy fission . . . 853
Fidecaro, M., with Alston, M. H., Evans, W. H., Newport, R. W., von Gierke, G., and Williams, P. R.: π^+–p scattering at 10–35 Mev in a diffusion cloud chamber . . . 798
Fisher, P. S., and Knapp, V.: The decay of the isomeric state of ^{198}Tl . . . 541
Fremlin, J. H., with Chalklin, L. P.: The ionization of fast neutral deuterium atoms (L) . . . 352

PAGE

Gatha, K. M., with Advani, M. K., and Harihar, P.: Nuclear charge density distribution (L) . . . 650

Gaydon, A. G., with Charton, M.: Band spectra emitted by strontium and barium in arcs and flames . . . 520

George, E. P.: Observations of the nuclear interactions of a 315 MEV bremsstrahlung γ-ray beam . . . 110

George, E. P.: On star production by μ-mesons underground . . . 428

Ghoshal, S. N., and Saxena, A. N.: On neutron–proton pairing interaction in heavy nuclei . . . 293

von Gierke, G., with Alston, M. H., Crewe, A. V., and Evans, W. H.: A study of positive pion production in p–p collisions at 383 MEV . . . 691

von Gierke, G., with Alston, M. H., Evans, W. H., Fidecaro, M., Newport, R. W., and Williams, P. R.: π^+–p scattering at 10–35 MEV in a diffusion cloud chamber . . . 798

Goodings, A., with Rothwell, P., and Wade, B.: Directional measurements on extensive air showers . . . 902

Govindjee, M., with Allan, H. R., and Sarma, N.: Excitation curve for the reaction $^{10}B(p,\alpha)^7Be$ (R) . . . 350

Gratzer, W. B., with Barrow, R. F., and Malherbe, J. F.: Intensities of bands in the system $b^3\Sigma^+$–$a^3\Pi$ of carbon monoxide (R) . . . 574

Green, L. L., Singh, J. J., and Willmott, J. C.: The energy levels of ^{26}Al . . . 335

Green, T. S., and Middleton, R.: An investigation of deuteron induced reactions by magnetic analysis: I—Experimental technique . . . 16

Green, T. S., and Middleton, R.: An investigation of deuteron induced reactions by magnetic analysis: II—Results for ^9Be, ^{13}C, ^{14}N and ^{16}O . . . 28

Green, T. S., with Burrows, H. B., Hinds, S., and Middleton, R.: An investigation of deuteron induced reactions by magnetic analysis: III—Results for neon and argon . . . 310

Greenlees, G. W., and Souch, A. E.: The scattering of 9·6 MEV protons by Mg . . . 686

Gupta, R. K., and Jha, S.: A high energy gamma ray in the decay of barium 131 (R) . . . 70

Hancock, D. A., with Chick, D. R., Evans, W. W., Hunt, S. E., and Pope, R. A.: An investigation of the γ-rays from the reactions $^{24}Mg(p,\gamma)^{25}Al$ and $^{13}C(p,\gamma)^{14}N$, with a note on the positron disintegration of ^{25}Al . . . 624

Harding, G. N.: A measurement of the average number of neutrons per fission from uranium and bismuth when bombarded with 147 MEV protons . . . 330

Harding, G. N., and Farley, F. J. M.: The angular distribution of neutrons from high energy fission . . . 853

Harihar, P., with Advani, M. K., and Gatha, K. M.: Nuclear charge density distribution (L) . . . 650

Haywood, B. C., with Burcham, W. E.: The alpha activity induced in platinum by bombardment with nitrogen ions (R) . . . 862

Haywood, J. H.: The equations of motion of rotating bodies in general relativity . . . 2

Heine, V.: The de Haas–van Alphen effect in alloys . . . 505

Heine, V.: The band structure of bismuth . . . 513

Hellwarth, R. W., with Woodgate, G. K.: Hyperfine structure of radioactive silver $^{111}_{47}Ag$ . . . 581

Hellwarth, R. W., with Woodgate, G. K.: Shape of resonance curves in atomic beam experiments . . . 588

Hinds, S., and Middleton, R.: Angular distribution of some inelastically scattered deuteron groups from ^{27}Al (R) . . . 347

Hinds, S., with Burrows, H. B., Green, T. S., and Middleton, R.: An investigation of deuteron induced reactions by magnetic analysis: III—Results for neon and argon . . . 310

Hird, B., with Allen, K. W., Collinge, B., Maglić, B. C., and Orman, P. R.: The proton gamma angular correlations in the $^{28}Si(d, p\gamma)^{29}Si$ stripping reaction . . . 705

Hughes, I. S., and Sinclair, D.: The polarization of γ-radiation from the reactions $^{27}Al(p,\gamma)^{28}Si$, $^{26}Mg(p,\gamma)^{27}Al$, $^{23}Na(p,\gamma)^{24}Mg$. . . . 125

PAGE

Hunt, S. E., with Chick, D. R., Evans, W. W., Hancock, D. A., and Pope, R. A. : An investigation of the γ-rays from the reactions $^{24}Mg(p,\gamma)^{25}Al$ and $^{13}C(p,\gamma)^{13}N$, with a note on the positron disintegration of ^{25}Al 624
Hurley, A. C. : On the method of atoms in molecules : II—An intra-atomic correlation correction 49
Hurley, A. C. : On the method of atoms in molecules : III—The ground state of hydrogen fluoride 301
Hurley, A. C. : The binding energy of the nitrogen molecule 767
Hurley, A. C. : On the binding energy of the helium hydride ion (R) 868

Ingram, D. J. E., with Bennett, J. E., and Schonland, D. : Paramagnetic resonance spectra of the alkali superoxides and chlorine dioxide 556
Jaffe, A. A., with Maslin, E. E., and Calvert, J. M. : An investigation of the reactions $^{10}B(d,n)^{11}C$ and $^{11}B(d,n)^{12}C$. 754
Jarmain, W. R., with Nicholls, R. W. : r-centroids : average inter-nuclear separations associated with molecular bands 253
Jarmain, W. R., with Nicholls, R. W., Robinson, D., and Parkinson, D. : r-centroids for the O_2 second negative N_2 Lyman–Birge–Hopfield and N_2 Vegard–Kaplan band systems (R) 713
Jenkins, D. P. : Calculations on the band structure of silicon 548
Jha, A., with Gupta, R. K. : A high energy gamma ray in the decay of barium 131 (R) 70
Judd, B. R. : The structures of the ground multiplets of certain rare-earths ions . 157

Kaila, K. L., and Saha, N. K. : Ionization loss and the range–energy relation for low energy protons in metals 888
Kerner, E. H. : The band structure of mixed linear lattices 234
Khambátá, S. J. : Raman spectrum of magnesium oxide (L) 426
Knapp, V., with Fisher, P. S. : The decay of the isomeric state of ^{199}Tl 541
Kuper, C. G. : On the Bohm–Pines theory of a quantum-mechanical electron plasma (R) 492

Lagerqvist, A., Lennart Nilsson, N. E., and Barrow, R. F. : On a supposed predissociation in the spectrum of AlO (L). 356
Laubitz, M. J. : Pseudoscalar interaction in the decay of ^{144}Pr 789
Leigh, R. S. : The augmented plane wave and related methods for crystal eigenvalue problems 388
Lennart Nilsson, N. E., with Lagerqvist, A., and Barrow, R. F. : On a supposed predissociation in the spectrum of AlO (L) 356
Lewis, J. T., with Buckingham, A. D., and Coulson, C. A. : The quadrupole moment of a hydrogen atom in a uniform field (R). 639
Lewis, J. T., with Dalgarno, A. : The representation of long range forces by series expansions : I—The divergence of the series ; II—The complete perturbation calculation of long range forces 57
Lewis, J. T., with Dalgarno, A. : Approximate molecular orbitals : IV—The $3p\sigma_u$ and $4f\sigma_u$ states of H_2^+ 285
Lewis, J. T., with Dalgarno, A. : The equivalence of variational and perturbation calculations of small disturbances (R) 628
Lipsicas, M. M., with Allen, K. R., Major, D., and Phillips, K. : The scattering of fast charged particles : I—On the single scattering of 13·5 MeV electrons in xenon 141
Llewellyn, P. M., with Baker, J. M., Bleaney, B., and Shaw, P. F. D. : Nuclear spins and magnetic moments of cobalt 56 and 57 (L) 353
Lockett, E. E., with Collie, C. H., and Meads, R. E. : The capture cross section of neutrons by boron 464
Lowde, R. D., with Elliott, R. J., and Marshall, W. : On the multiple spin wave scattering of neutrons in ferromagnets (R) 939
Lynn, N., with Dalgarno, A. : Resonance forces at large separations 821
Lynn, N., with Dalgarno, A., and Williams, E. J. A. : The oscillator strengths of the $1s\sigma$–$2s\sigma$, $1s\sigma$–$3d\sigma$ and $2s\sigma$–$3d\sigma$ transition of HeH^{2+} 610

PAGE

McCormack, P. D. : A liquid scintillator investigation of the second maximum in the cosmic ray transition curve 845
McCrea, W. H. : A problem in relativity theory : Reply to H. Dingle 935
McDowell, M. R. C., with Dalgarno, A. : Charge transfer and the mobility of H^- ions in atomic hydrogen 615
Maglić, B. C., with Allen, K. W., Collinge, B., Orman, P. R., and Hird, B. : The proton gamma angular correlations in the $^{28}Si(d, p\gamma)^{29}Si$ stripping reaction . 705
Major, D., with Allen, K. R., Lipsicas, M. M., and Phillips, K. : The scattering of fast charged particles : I—On the single scattering of 13·5 MeV electrons in xenon 141
Malherbe, J. F., with Barrow, R. F., and Gratzer, W. B. : Intensities of bands in the system of $b^3\Sigma^+ - a^3\Pi$ of carbon monoxide (R) 574
Mann, A. K., and Titterton, E. W. : The reactions $^{12}C(\gamma, p)^{11}B$, $^{11}B(p, \gamma)^{12}C$ and $^{12}C(\gamma, 3\alpha)$ at 17·63 MeV excitation 917
Manning, G., with Bunbury, D. St. P., Devons, S., and Towle, J. H. : Measurement of γ-transition lifetimes by recoil methods : II—M1 transitions in ^7Li and ^7Be . 165
Manning, G., with Devons, S., and Towle, J. H. : Measurement of γ-transition lifetimes by recoil methods : III—E2 transitions in some even–even nuclei . 173
Marriott, R., with Burhop, E. H. S. : The destruction of metastable helium atoms by collision-induced radiation 271
Marsden, P. L., and Doran, G. A. : The nucleonic component in cosmic ray extensive air showers 894
Marshall, W., with Elliott, R. J., and Lowde, R. D. : On the multiple spin wave scattering of neutrons in ferromagnets (R) 939
Maslen, V. W. : The Fermi, or exchange, hole in atoms 734
Maslin, E. E., Calvert, J. M., and Jaffe, A. A. : An investigation of the reactions $^{10}B(d, n)^{11}C$ and $^{11}B(d, n)^{12}C$ 754
Massey, H. S. W., and Ridley, R. O. : Application of variational methods to the theory of the scattering of slow electrons by hydrogen molecules 659
Matsukawa, E., with Brown, B., and Stewardson, E. A. : The nuclear scattering of 0·4 and 0·5 MeV electrons in composite aluminium–uranium foils (R) . . 496
Matthews, J. H., with Berenbaum, R., and Towle, J. H. : The 440 kev transition in ^{22}Na (R) 858
Meads, R. E., England, C. J., Collie, C. H., and Weeks, G. C. : The capture cross section of thermal neutrons in water 469
Meads, R. E., with Collie, C. H., and Lockett, E. E. : The capture cross section of neutrons by boron 464
Messelt, S., and Storruste, A. : Elastic scattering of gamma rays 381
Middleton, R., with Burrows, H. B., Green, T. S., and Hinds, S. : An investigation of deuteron induced reactions by magnetic analysis : III—Results for neon and argon 310
Middleton, R., with Green, T. S. : An investigation of deuteron induced reactions by magnetic analysis : I—Experimental technique 16
Middleton, R., with Green, T. S. : An investigation of deuteron induced reactions by magnetic analysis : II—Results for ^9Be, ^{12}C, ^{14}N and ^{16}O 28
Middleton, R., with Hinds, S. : Angular distribution of some inelastically scattered deuteron groups from ^{27}Al (R) 347
Moiseiwitsch, B. L. : Interaction energy and charge exchange between helium atoms and ions 653
Moiseiwitsch, B. L., and Stewart, A. L. : Approximate molecular orbitals : V—The $1s\sigma$ and $2p\pi$ states of HeH^{2+} 480
Mohr, C. B. O., and Robson, B. A. : Calculations with the optical model of the nucleus 365
Moon, P. B. : Space charge and ionization phenomena in constant-gradient proton synchrotrons 153
Morrison, D. R. O., with Wright, I. F., Reid, J. M., and Atkinson, J. R. : The photodisintegration of nitrogen 77

PAGE

Murrell, J. N., and Pople, J. A. : The intensities of the symmetry-forbidden electronic bands of benzene 245

Nakajima, S. : A note on momentum correlation and diamagnetism 441
Nash, W. F., and Pointon, A. J. : The momentum spectrum of μ-mesons at a depth of 40 metres water equivalent 725
Newport, R. W., with Alston, M. H., Evans, W. H., Fidecaro, M., von Gierke, G., and Williams, P. R. : π^+–p scattering at 10–35 MEV in a diffusion cloud chamber 798
Nicholls, R. W. : The interpretation of intensity distributions in the CN violet, C_2 Swan, OH violet and O_2 Schumann–Runge band systems by use of their r-centroids and Franck–Condon factors 741
Nicholls, R. W., and Jarmain, W. R. : r-centroids : average inter-nuclear separations associated with molecular bands. 253
Nicholls, R. W., Robinson, D., Parkinson, W., and Jarmain, W. R. : r-centroids for the O_2 second negative, N_2 Lyman–Birge–Hopfield and N_2 Vegard–Kaplan band systems (R) 713
Nicholson, K. P. : Time delays in boron trifluoride proportional counters (R) . . 413
Norman, R. J. : The energy spectrum of extensive air showers 804

Orman, P. R., with Allen, K. W., Collinge, B., Hird, B., and Maglić, B. C. : The proton gamma angular correlations in the ^{28}Si(d, pγ)^{29}Si stripping reaction . 705

Park, J. G., with Cooke, A. H. : Nuclear spins and magnetic moments of ^{161}Dy, ^{163}Dy, ^{171}Yb and ^{173}Yb 282
Parkinson, D., with Nicholls, R. W., Robinson, D., and Jarmain, W. R. : r-centroids for the O_2 second negative, N_2 Lyman–Birge–Hopfield and N_2 Vegard–Kaplan band systems (R) 713
Perlman, H. S. : The relativistic theory of the specific primary ionization and stopping power and its application in helium 318
Perring, J. K., and Skyrme, T. H. R. : The alpha-particle and shell models of the nucleus 600
Phillips, K., with Allen, K. R., Lipsicas, M. M., and Major, D. : The scattering of fast charged particles : I—On the single scattering of 13·5 MEV electrons in xenon 141
Pointon, A. J., with Nash, W. F. : The momentum spectrum of μ-mesons at a depth of 40 metres water equivalent 725
Pope, R. A., with Chick, D. R., Evans, W. W., Hancock, D. A., and Hunt, S. E. : An investigation of the γ-rays from the reactions ^{24}Mg(p, γ)^{25}Al and ^{13}C(p, γ)^{13}N, with a note on the positron disintegration of ^{25}Al 624
Pople, J. A., with Murrell, J. N. : The intensities of the symmetry-forbidden electronic bands of benzene 245
Post, H. R. : Many-particle systems : II (R) 936
Prescott, J. R. : The density distribution of extensive showers (R) 870
Preston, G., with Booth, D. L., and Shaw, P. F. D. : The cross section and angular distributions of the D–D reactions between 40 and 90 KEV 265

Randle, T. C., Skyrme, D. M., Snowden, M., Taylor, A. E., Uridge, F., and Wood, E. : The scattering of 130 MEV neutrons by protons 760
Reasbeck, P., with Chackett, G. A., Chackett, K. F., Symonds, J. L., and Warren, J. : Excitation functions up to 980 MEV for proton-induced reactions in ^{27}Al, relative to ^{12}C(p, pn) ^{11}C 43
Reid, J. M., with Wright, I. F., Morrison, D. R. O., and Atkinson, J. R. : The photodisintegration of nitrogen 77
Ridley, R. O., with Massey, H. S. W. : Application of variational methods to the theory of the scattering of slow electrons by hydrogen molecules 659

PAGE

Robertson, H. H., with Bransden, B. H., and Swan, P. : The elastic scattering of neutrons by tritons and ^{3}He 877

Robinson, D., with Nicholls, R. W., Parkinson, W., and Jarmain, W. R. : r-centroids for the O_2 second negative, N_2 Lyman–Birge–Hopfield and N_2 Vegard–Kaplan band systems (R) 713

Robson, B. A., with Mohr, C. B. O. : Calculations with the optical model of the nucleus 365

Ross, M. A. S., with Stanners, W. : The β-disintegration of RaD 836

Rothwell, P., Wade, B., and Goodings, A. : Directional measurements on extensive air showers 902

Rusbridge, M. G. : On the reaction $^{13}C(\alpha, n)^{16}O$ 830

Saha, N. K., with Kaila, K. L. : Ionization loss and the range–energy relations for low energy protons in metals 888

Sarma, N., with Allan, H. R., and Govindjee, M. : Excitation curve for the reaction $^{10}B(p, \alpha)^7Be$ (R) 350

Saxena, A. N., with Ghoshal, S. N. : On neutron–proton pairing interaction in heavy nuclei 293

Schiff, B. : The cellular method for close-packed hexagonal titanium (L) . . 185

Schonland, D., with Bennett, J. E., and Ingram, D. J. E. : Paramagnetic resonance spectra of the alkali superoxides and chlorine dioxide 556

Shaw, P. F. D., with Baker, J. M., Bleaney, B., and Llewellyn, P. M. : Nuclear spins and magnetic moments of cobalt 56 and 57 (L) 353

Shaw, P. F. D., with Booth, D. L., and Preston, G. : The cross section and angular distributions of the D–D reactions between 40 and 90 kev 265

Sinclair, D., with Hughes, I. S. : The polarization of γ-radiation from the reactions $^{27}Al(p, \gamma)^{28}Si$, $^{26}Mg(p, \gamma)^{27}Al$, $^{23}Na(p, \gamma)^{24}Mg$ 125

Singh, J. J., with Green, L. L., and Willmott, J. C. : The energy levels of ^{26}Al . . 335

Skyrme, D. M., with Randle, T. C., Snowden, M., Taylor, A. E., Uridge, F., and Wood, E. : The scattering of 130 Mev neutrons by protons 760

Skyrme, H. R., with Perring, J. K. : The alpha-particle and shell models of the nucleus 600

Snowden, M., with Randle, T. C., Skyrme, D. M., Taylor, A. E., Uridge, F., and Wood, E. : The scattering of 130 Mev neutrons by protons 760

Souch, A. E., with Greenlees, G. W. : The scattering of 9·6 Mev protons by Mg . 686

Stanners, W., and Ross, M. A. S. : The β-disintegration of RaD 836

Steers, E. B. M., with Bovey, L. F. H., and Wise, H. S. : The infra-red resonance lines of lutetium (L) 783

Stephen, M. J., with Coulson, C. A. : The quadrupole polarizability of the hydrogen atom 777

Stewardson, E. A., and Wilson, J. E. : The $M_{IV, V}$ spectra of ^{68}Er 93

Stewardson, E. A., with Brown, B., and Matsukawa, E. : The nuclear scattering of 0·4 and 0·5 Mev electrons in composite aluminium–uranium foils (R) . . 504

Stewart, A. L., with Moiseiwitsch, B. L. : Approximate molecular orbitals : V—The 1sσ and 2pπ states of HeH^{2+} 480

Stewart, D. T. : Electron excitation functions of the first negative bands of N_2^+ . 437

Steyn, J. : Absolute standardization of beta-emitting isotopes with a liquid scintillation counter (R) 865

Sundaram, S., with Venkateswarlu, K. : Evaluation of force constants from Raman effect data : molecules, radicals and groups of pyramidal XY_3 type (R) . . 180

Swan, P., with Bransden, B. H., and Robertson, H. H. : The elastic scattering of neutrons by tritons and ^{3}He 877

Symonds, J. L., with Chackett, G. A., Chackett, K. F., Reasbeck, P., and Warren, J. : Excitation functions up to 980 Mev for proton-induced reactions in ^{27}Al, relative to $^{12}C(p, pn)^{11}C$ 43

Tassie, L. J. : Nuclear scattering of high energy electrons on the independent-particle model 205

Taylor, A. E., and Wood, E. : Proton–proton scattering at 134 Mev (R) . . . 645

PAGE

Taylor, A. E., with Randle, T. C., Skyrme, D. M., Snowden, M., Uridge, F., and Wood, E. : The scattering of 130 MeV neutrons by protons 760
Taylor, K. W. : α-Particle counting behaviour of diamond conduction counters at field strengths up to 200 kv cm^{-1} 593
Temperley, H. N. V. : New evidence about the nature of the liquid helium transition (R) 630
Thomson, D. M. : The yield and angular distribution of neutrons from the reaction $^{63}Cu(p, n)\ ^{63}Zn$ at 18 MeV 447
Thouless, D. J. : Energy levels of π-mesic atoms (R) 280
Titterton, E. W., with Mann, A. K. : The reactions $^{12}C(\gamma, p)^{11}B$, $^{11}B(p, \gamma)^{12}C$ and ^{12}C $(\gamma, 3\alpha)$ at 17·63 MeV excitation 917
Tomlin, S. G., and Worthington, C. R. : The intensity of emission of characteristic X-radiation 401
Towle, J. H., with Berenbaum R., and Matthews, J. H. : The 440 kev transition in ^{23}Na (R) 858
Towle, J. H., with Bunbury, D. St. P., Devons, S., and Manning, G. : Measurement of γ-transition lifetimes by recoil methods : II—M1 transitions in ^{7}Li and ^{7}Be . 165
Towle, J. H., with Devons, S. : Range–velocity relationship for ^{7}Li ions in solids (R) 345
Towle, J. H., with Devons, S., and Manning, G. : Measurement of γ-transition lifetimes by recoil methods : III—E2 transitions in some even–even nuclei . . 173

Uridge, F., with Randle, T. C., Skyrme, D. M., Snowden, M., Taylor, A. E., and Wood, E. : The scattering of 130 MeV neutrons by protons 760

Varma, J. : The reaction $^{24}Mg(p, \gamma)^{25}Al$ (R) 641
Venkateswarlu, K., and Sundaram, S. : Evaluation of force constants from Raman effect data : molecules, radicals and groups of pyramidal XY_3 type (R) . . 180

Wade, B., with Rothwell, P., and Goodings, A. : Directional measurements on extensive air showers 902
Warren, J., with Chackett, G. A., Chackett, K. F., Reasbeck, P., and Symonds, J. L. : Excitation functions up to 980 MeV for proton-induced reactions in ^{27}Al, relative to $^{12}C(p, pn)^{11}C$ 43
Weeks, G. C., with Meads, R. E., England, C. J., and Collie, C. H. : The capture cross section of thermal neutrons in water 469
Whiffen, D. H. : Intensities in the Raman spectrum of benzene 375
Williams, J. A., with Dalgarno, A., and Lynn, N. : The oscillator strengths of the $1s\sigma$–$2s\sigma$, $1s\sigma$–$3d\sigma$ and $2s\sigma$–$3d\sigma$ transitions of HeH^{2+} 610
Williams, P. R., with Alston, M. H., Evans, W. H., Fidecaro, M., Newport, R. W., and von Gierke, G. : π^+–p scattering at 10–35 MeV in a diffusion cloud chamber . 798
Willmott, J. C., with Green, L. L., and Singh, J. J. : The energy levels of ^{26}Al . 335
Wilson, J. E., with Stewardson, E. A. : The $M_{IV, V}$ spectra of ^{68}Er 93
Wise, H. S., with Bovey, L. F. H., and Steers, E. B. M. : The infra-red resonance lines of lutetium (L) 783
Wood, E., with Randle, T. C., Skyrme, D. M., Snowden, M., Taylor, A. E., and Uridge, F. : The scattering of 130 MeV neutrons by protons 760
Wood, E., with Taylor, A. E. : Proton–proton scattering at 134 MeV (R) 645
Woodgate, G. K., and Hellwarth, R. W. : Hyperfine structure of radioactive silver $^{111}_{47}Ag$ 581
Woodgate, G. K., and Hellwarth, R. W. : Shape of resonance curves in atomic beam experiments 588
Worthington, C. R., and Tomlin, S. G. : The intensity of emission of characteristic X-radiation 401
Wright, I. F., Morrison, D. R. O., Reid, J. M., and Atkinson, J. R. : The photo-disintegration of nitrogen 77

Yoshida, S. : The inelastic scattering of nucleons by the surface interaction . . 668

INDEX TO REVIEWS OF BOOKS

PAGE

Allen, C. W. : *Astrophysical Quantities* 72
Andrew, E. R. : *Nuclear Magnetic Resonance* 433

Bacq, Z. M., and Alexander, P. : *Fundamentals of Radiobiology* 500
Band, W. : *An Introduction to Quantum Statistics* 501
Barnard, G. P. : *Modern Mass Spectrometry* 187
Bartlett, M. S. : *An Introduction to Stochastic Processes, with Special Reference to Methods and Applications* 361
Bauer, R. : *Champs de vecteurs et de tenseurs* 723
Beckerley, J. G. (Ed.) : *Annual Review of Nuclear Science*. Vol. 3, 1953 . . . 578
Beckerley, J. G. (Ed.) : *Annual Review of Nuclear Science*. Vol. 5, 1955 . . . 502
Bethe, H. A., and de Hoffmann, F. : *Mesons and Fields*. Volume II—*Mesons* . 358
Boerner, H. : *Darstellung von Gruppen, mit Berücksichtigung der modernen Physik (Grundlehren der mathematischen Wissenschaften, Band 74)* 716
Brinkman, H. C. : *Application of Spinor Invariants in Atomic Physics* . . . 787

Curran, S. C. : *Luminescence and the Scintillation Counter* 430

Dumas, M. : *Les épreuves sur échantillon* 430

Ewald, H., and Hintenberger, M. : *Methoden and Anwendungen der Massenspektroskopie* 187

Feather, N. : *Nuclear Stability Rules* 577
Francis, G. E., Mulligan, W., and Wormall, A. : *Isotopic Tracers* 431

Goeppert Mayer, M., and Jensen, J. H. D. : *Elementary Theory of Nuclear Shell Structure* 73
Guggenheim, E. A., : *Boltzmann's Distribution Law* 74

Halliday, D. : *Introductory Nuclear Physics* (2nd Edn) 577

Imai, I. (Ed.) : *Proceedings of the International Conference of Theoretical Physics. Kyoto and Tokyo*, Sept. 1953 717
Ingram, D. J. E. : *Spectroscopy at Radio and Microwave Frequencies* . . . 718
Jeffreys, H., and Jeffreys, B. S. : *Methods of Mathematical Physics* (3rd Edn) . 577

Kaplan, I. : *Nuclear Physics* 363

Landé, A. : *Foundations of Quantum Theory* 359
Littler, D. J., and Raffle, J. F. : *An Introduction to Reactor Physics* . . . 74

Panofsky, W. K. H., and Phillips, M., : *Classical Electricity and Magnetism* . . 360
Pauli, W. (Ed.) : *Niels Bohr and the Development of Physics* 433
Peierls, R. E. : *Quantum Theory of Solids* 434
van der Pol, B., and Bremmer, H. : *Operational Calculus, based on the Two-sided Laplace Integral* (2nd Edn) 72

Rose, M. E. : *Multiple Fields* 361

Schweber, S. S., Bethe, H. A., and de Hoffmann, F. : *Mesons and Fields* . . 786
Sharpe, J. : *Nuclear Radiation Detectors* 432
Smith, K. F. : *Molecular Beams* 359
Smith, M. L. (Ed.) : *Electromagnetically Enriched Isotopes and Mass Spectrometry* . 875
Synge, J. L. : *Relativity : the Special Theory* 719

Vajda, S. : *The Theory of Games and Linear Programming* 723

White, H. E., : *Descriptive College Physics* 718